



SOLID STATE ABSTRACTS

*A reference journal devoted to the
theory, production and use of solid state materials and devices*

VOLUME 5

NUMBERS 5 - 6

PHYSICS
METALLURGY
ELECTRONICS

SEMICONDUCTORS
PHOSPHORS
MAGNETICS
DIELECTRICS
SUPERCONDUCTORS
METALS

SOLID STATE ABSTRACTS

VOLUME 5, NUMBERS 5-6

MAY - JUNE 1964

Abstracts 24,858-26,459

TABLE OF CONTENTS

Abstracts of the Solid State Literature

METALLURGY AND CHEMISTRY OF SOLIDS

GENERAL	249
THERMODYNAMIC PROPERTIES	249
General	249
Phase Diagrams	249
Changes of State	251
Solubility and Segregation	252
Phase Transitions (Transformations)	252
CRYSTAL STRUCTURE	254
General	254
Crystal Imperfections	260
Point Defects (Vacancies and Interstitials)	260
Dislocations	261
Grain Boundaries, Stacking Faults, etc.	263
Impurities	265
Impurity Diffusion	266
CRYSTAL GROWTH	268
General	268
Single Crystals	269
Growth of Thin Films	270
Growth of Whiskers (Dendrites)	271
CRYSTAL SURFACES	271
ENVIRONMENTAL EFFECTS	273

SOLID STATE PHYSICS

GENERAL	273
CRYSTAL PHYSICS	273
General	273
Crystal Fields	274
Energy Band Structure	274
Lattice Dynamics	276
ELECTRICAL PROPERTIES	277
General	277
Nuclear Quadrupole Effects	277
Dielectric Properties	278
Carrier Properties	280
Resistivity (Conductivity)	283
Superconductivity	286
Breakdown	292
Magnetoelectric (Galvanomagnetic) Properties	292
General	292
Magnetoresistivity	292
Hall Effect	293
Cyclotron Resonance	294
Noise	295
Electron Emission	295
MAGNETIC PROPERTIES	296
General	296
Ferro- and Ferrimagnetism	300
Ferro- and Ferrimagnetic Resonance	309
Antiferro- and Antiferrimagnetism	311
Paramagnetism	313
Paramagnetic Resonance	313
Diamagnetism	318
OPTICAL PROPERTIES	319
Absorption (Transmission)	319
Radiation and Luminescence	322
Photoelectronic Properties	325
Other Optical Properties	327
THERMAL PROPERTIES	328
Specific Heat	328
Thermal Conductivity	330

Thermal Expansion	331
Thermoelectric and Thermomagnetic Properties	331
MECHANICAL PROPERTIES	332
General	332
Deformation Properties	332
Sonic and Ultrasonic Properties	334

SOLID STATE DEVICES

GENERAL	337
RESISTORS and CAPACITORS	337
DIODES	338
TRANSISTORS	341
MAGNETOELECTRIC DEVICES	344
FERRITE DEVICES	345
MASERS AND LASERS	348
General	348
Theory	348
Characteristics	349
Laser Diodes	355
Associated Devices	358
Applications and Effects	360
THERMAL DEVICES	361
SUPERCONDUCTIVE DEVICES	363

BASIC SOLID STATE DEVICE CIRCUITS

GENERAL	365
Network Theory	365
Microcircuits	365
Circuit Aspects of Devices	367
AMPLIFIERS	369
OSCILLATORS	372
SWITCHING CIRCUITS	373
SIGNAL CONVERTERS	374
Modulators	374
Demodulators (Detectors)	375
Frequency Converters	375
WAVE GENERATORS	376
PULSE CIRCUITS	377
OTHER CIRCUITS	377
Filters	377

APPLICATIONS OF SOLID STATE DEVICES

GENERAL	378
Biomedical Applications	378
Automotive Applications	379
Navigation, Guidance and Ranging Applications	379
COMMUNICATIONS APPLICATIONS	380
Radio and TV	380
Telephony	381
Telemetry	382
Other Communications-Type Applications	382
COMPUTERS and OTHER DATA HANDLING SYSTEMS	383
Digital Computers	383
Analog Computers and Other Data Systems	387
POWER APPLICATIONS	388
CONTROL APPLICATIONS	390
INSTRUMENTATION	391
OTHER APPLICATIONS	394

SUBJECT INDEX	395
-------------------------	-----

AUTHOR INDEX	419
------------------------	-----

PUBLISHED BY

Cambridge Communications Corporation, 238 Main Street, Cambridge, Massachusetts 02142 Tel. 491-0710

Subscription Rate: U.S.A. and Canada — \$96. per year — Special 3 year rate — \$273.

Foreign — \$106. per year — Special 3 year rate — \$303.

Copyright 1964 by Cambridge Communications Corp. Printed in the U.S.A.

ABSTRACTS OF THE SOLID STATE LITERATURE

METALLURGY AND CHEMISTRY OF SOLIDS

GENERAL

24,858 ADVANCES IN ELEMENTAL SEMICONDUCTORS by C.G. Currin and E. Earleywine (Dow Corning); Semicond.Prod., Vol. 7, pp. 20-25, June 1964

Developments in elemental semiconductor materials and the parameters required for various devices are discussed. Emphasis is placed on the present state of the art. A table detailing comparative properties of today's two most generally used elemental materials, silicon and germanium, is included. Trends toward new forms of crystal growth, and other innovations that will permit easier and more economical processing techniques are also treated.

24,859 ADVANCES IN III-V AND II-VI SEMICONDUCTOR COMPOUNDS by P.M. Hamilton (Monsanto); Semicond.Prod., Vol. 7, pp. 15-20, June 1964

Advances in the semiconductor III-V and II-VI compounds over the past few years are discussed. Both properties and applications are treated. Some of the important properties of the semiconductor compounds are presented in table form. The correlation between properties and applications is studied. Finally, a brief look into the future is presented.

24,860 GALLIUM ARSENIDE DATA SHEETS by M. Neuberger (Hughes Aircraft); Contract AF33 616 8438, Nov. 1962, 97 pp., Rept. No. DS115; U.S. Gov. Res. Rep., Vol. 39, p. 81(A), June 20, 1964 AD 437 310 OTS \$8.60

24,861 LEAD SELENIDE DATA SHEETS by M. Neuberger (Hughes Aircraft); Contract AF33 616 8438, Dec. 1962, 48 pp., Rept. No. DS116; U.S. Gov. Res. Rep., Vol. 39, p. 81(A), June 20, 1964 AD 437 309 OTS \$4.60

24,862 LEAD TELLURIDE DATA SHEETS by M. Neuberger (Hughes Aircraft); Contract AF33 616 8438, Oct. 1962, 35 pp., Rept. No. DS113; U.S. Gov. Res. Rep., Vol. 39, p. 47(A), June 20, 1964 AD 437 311 OTS \$3.60

24,863 TELLURIDES OF LANTHANUM by E.I. Yarembash, E.S. Vigileva, A.A. Eliseev, and L.I. Antonova (Wright-Patterson AF Base); Nov. 29, 1963, 6 pp., FTD MT63 249, Trans. from Z. Neorgan. Khimii, AN SSSR, Vol. 8, No. 6, pp. 1542-1543, 1963; U.S. Gov. Res. Rep., Vol. 39, p. 18(A), June 5, 1964 AD434 972 OTS \$1.10

THERMODYNAMIC PROPERTIES

GENERAL

24,864 HIGH TEMPERATURE BEHAVIOR OF MoSi_2 and Mo_5Si_3 by G. Cherniack and A.G. Elliott (Lockheed); J. Am. Ceram. Soc., Vol. 47, pp. 136-141, Mar. 21, 1964

The high-temperature stability and behavior of MoSi_2 was studied by heating dense sintered specimens under a vacuum of 10^{-5} mm Hg from 1700 to 2000°C. The resulting material was examined using physical measurements, x-ray analysis, and metallographic techniques. The decomposition of MoSi_2 into Mo_5Si_3 is described. The Mo_5Si_3 - MoSi_2 eutectic temperature was determined as 1900°C, and the melting points of MoSi_2 and Mo_5Si_3 were determined as 1980° and 2085°C, respectively.

24,865 THERMODYNAMICS OF INTERSTITIAL SOLID SOLUTIONS AND REFRACTORY COMPOUNDS by L. Kaufman, H. Bernstein and A. Sarney (Manufacturing Labs.); Contract AF33 657 9826, Nov. 1963, 96 pp.; U.S. Gov. Res. Rep., Vol. 39, p. 142(A), May 20, 1964 AD 431 313 OTS \$2.25

The thermodynamics of interstitial solid solutions and non-stoichiometric compounds have been applied to analyses of the Ti-C, Zr-C, Hf-C, Nb-C, Ta-C, Ti-O, Zr-O, Ti-N, and Zr-N systems. The thermodynamic framework, based on the Schottky-Wagner model for non-stoichiometric phases has been applied to predict phase equilibria and vaporization data for these systems. Comparison with experimental thermodynamic, vapor pressure, and equilibria data available in the literature is very satisfactory. In addition, correlation between thermodynamic properties and vacancy concentration data where possible yields good agreement.

24,866 THE SYSTEM MAGNESIA-MAGNESIUM FLUORIDE-GERMANIA-LITHIUM FLUORIDE, 6.94 PERCENT LITHIUM FLUORIDE by G.R. McCormick (Bureau of Mines, Tenn.); 1964, 15 pp., BM-R1-6398; STAR, Vol. 2, p. 1193(A), May 8, 1964

Because several new and unusual synthetic minerals were found in the system $\text{MgO-MgF}_2\text{-SiO}_2$ with Li^+ or Na^+ , a similar system with GeO_2 replacing SiO_2 , plus Li^+ was investigated. In addition to the expected compounds of germanium, Ge-fluor-hectorite and a Ge-fluor-chrysotile were synthesized. Protoamphibole was not observed. Data are given for 69 compositions prepared in the system $\text{MgO-MgF}_2\text{-GeO}_2$ at 6.94-percent LiF.

PHASE DIAGRAMS

24,867 THE PHASE DIAGRAM FOR THE BINARY SYSTEM INDIUM-TELLURIUM AND ELECTRICAL PROPERTIES OF In_3Te_5 by E.G. Grochowski, D.R. Mason, G.A. Schmitt and P.H. Smith (U. Michigan); J. Phys. Chem. Solids, Vol. 25, pp. 551-558, June 1964

The phase diagram of the In-Te system has been redetermined by DTA, chemical, microscopic and X-ray analysis. Two new phases were found and the composition of three other phases have been determined more precisely. In_2Te (33.3 at.% Te) does not exist; the composition is In_9Te_7 (43 at.% Te) with a peritectic decomposition temperature of 462°C. InTe (50 at.% Te) has the composition $\text{In}_{30}\text{Te}_{31}$ (50.8 at.% Te) with a congruent melting point of 696°C. A new phase In_3Te_4 (57.0 at.% Te) has been found with a peritectic decomposition temperature of 650°C. In_7Te_3 (60 at.% Te) has the composition $\text{In}_{27}\text{Te}_{40}$ (59.7 at.% Te) with a congruent melting point of 667°C and a phase transition at 550°C. A new phase was observed at In_3Te_5 (62.5 at.% Te) with a peritectic decomposition temperature at 625°C and a phase transition at 463°C. In_2Te_5 (71.5 at.% Te) was prepared and has a large conductivity increase at its phase transition at 463°C.

24,868 A THERMODYNAMIC STUDY OF THE ZIRCONIUM-SULFUR SYSTEM IN THE REGION $\text{ZrS}_{1.49}$ TO $\text{ZrS}_{2.00}$ by A.H. Larson and A.W. Schlechten (Missouri School Mines); Trans. Met. Soc. AIME, Vol. 230, pp. 862-866, June 1964

Equilibrium H_2S/H_2 ratios were determined as functions of temperature (500° to 900°C) and composition in a hydrogen-circulation apparatus. Within the composition range studied there exists a two-phase region of " Zr_3S_4 " and " ZrS_2 ". The upper composition limit of this two-phase region is bounded by a disulfide phase and is practically constant over the temperature range investigated. The lower composition limit of this two-phase region is bounded by a " Zr_3S_4 " phase and varies appreciably with temperature. The upper composition limit of the homogeneous region of the disulfide phase is not definitely determined, but it appears to be bounded by the stoichiometric composition of ZrS_2 . The lower composition limit of the homogeneous region of the Zr_3S_4 phase could not be determined due to the extremely low values of the equilibrium H_2S/H_2 ratios. Various thermodynamic quantities are evaluated from the data.

24,869 THE CONSTITUTION OF COPPER-RICH COPPER-SILICON-ZINC ALLOYS by H. Pops (Mellon Inst.); *Trans. Met. Soc. AIME*, Vol. 230, pp. 813-820, June 1964

Isothermal sections in the copper-rich region of the Cu-Si-Zn alloy system have been determined at 847°, 760°, 600°, and 482°C by means of microscopic examination with confirmatory X-ray diffraction work. The stability of the bcc β phase decreases both with decreasing temperature and with increasing copper content. The silicon-rich β phase decomposes upon quenching from high temperatures either by a martensitic or by a "massive" transformation, depending upon the solute content. A two-phase equilibrium is found to exist in the Cu-Si-Zn system between the hcp ξ phase of the Cu-Si system and the bcc β phase of the Cu-Zn system. It is shown that the isothermal limits of the primary solid solution at 760°, 600°, and 482°C are in part affected by the intermediate phases which follow them in the ternary system. Possible electron-concentration and size effects upon phase boundaries are discussed.

24,870 PHASE EQUILIBRIA IN THE SYSTEM BORON CARBIDE-SILICON CARBIDE by D. Secrist (GE); *J. Am. Ceram. Soc.*, Vol. 47, pp. 127-130, Mar. 21, 1964

The system boron carbide-silicon carbide is quasi-binary and contains an eutectic of composition 70 wt pct. B_4C and 30 wt pct. SiC at a temperature of 2300°. The solid solubility of both B_4C in SiC and SiC in B_4C is less than 2 wt pct. at this temperature, based on metallographic and x-ray analyses. The SiC corresponds to the hexagonal (α) allotrope when the compositions contain more than 50 wt. pct. SiC . The cubic (β) form of SiC is stabilized in compositions which contain less than 50 wt. pct. SiC .

24,871 AN INVESTIGATION OF THE LEAD MOLYBDATE-BISMUTH MOLYBDATE PHASE DIAGRAM by D.F. Howard, G.P. Bowman, R.K. Saxer, and J.R. Myers (Wright-Patterson AF Base); *Trans. Met. Soc. AIME*, Vol. 230, pp. 850-853, June 1964

The phase diagram of the lead molybdate-bismuth molybdate salt system has been redetermined. Thermal analysis and X-ray methods were used to define the system. The diagram was found to be a simple eutectic type with an eutectic at 11 mol pct lead molybdate and 634°C. A maximum solid solubility of 6 mol pct was found at the lead molybdate end of the diagram. Solid solubility at the bismuth molybdate end of the diagram appeared to be quite limited and possibly nonexistent.

24,872 PHASE EQUILIBRIUM STUDIES IN THE SYSTEM $ThO_2-B_2O_3$ by D.E. Rose and G. Lane (Alfred U.); *J. Am. Ceramic Soc.*, Vol. 47, pp. 48-49, Jan. 1964

Phase equilibrium studies of the system $ThO_2-B_2O_3$ are reported. This system is characterized by one stable intermediate phase ThB_2O_5 and two eutectics. One eutectic occurs between ThB_2O_5 and B_2O_3 at about 98 mole % B_2O_3 and somewhat less than 325°C where ThB_2O_5 and B_2O_3 coexist with liquid. The other eutectic was between ThB_2O_5 and ThO_2 at about 19% B_2O_3 and slightly less than 1483°C. ThB_2O_5 existed only in the monoclinic structure, and no solid solution was found with either end member. Liquid immiscibility was clearly found.

24,873 THE SYSTEM $CaF_2-Ca(OH)_2-CaCO_3$ by J. Gittins and O. Tuttle (Penn. State U.); *Am. J. Sci.*, Vol. 262, pp. 66-75, Jan. 1964

Liquidus relations in the system have been studied at 1000 bars total pressure. The system $CaF_2-Ca(OH)_2$ has a simple eutectic at 32 CaF_2 -68 $Ca(OH)_2$ at 670°C. The system CaF_2-CaCO_3 has an eutectic at 36 CaF_2 -64 $CaCO_3$ at 880°C. The system $Ca(OH)_2-CaCO_3$ is characterized by an eutectic at 57 $Ca(OH)_2$ -43 $CaCO_3$ at 653°C. The liquidus of the ternary system has a stability field for each of the compounds, each field is separated by a boundary extending from the binary eutectics and joining at a ternary eutectic at 19 CaF_2 -36 $CaCO_3$ -45 $Ca(OH)_2$ at 575°C. The possibility that calcite-fluorite, calcite-fluorite-apatite, and calcite-fluorite-barite veins may represent differentiation from a fluorine-rich magma is considered as is the possibility that partial melting may promote the mobility of limestone in metamorphic terrains, application of the results to carbonatite flows is considered.

24,874 PHASE EQUILIBRIA AND MANGANESE-ACTIVATED LUMINESCENCE IN PORTIONS OF THE SYSTEM $Zn(PO_3)_2-Cd(PO_3)_2-Mg(PO_3)_2$ by J.J. Brown and F.A. Hummel (Penns. State U.); *J. Electrochem. Soc.*, Vol. 111, pp. 660-665, June 1964

The equilibrium relationships in the system $Zn(PO_3)_2-Cd(PO_3)_2$ have been established by quenching and solid state experiments. At 810°C α - $Cd(PO_3)_2$ inverted to β - $Cd(PO_3)_2$, which melted congruently at 896°C. Small regions of solid solution exist at the extremities of the system, involving the low and high temperature forms of $Zn(PO_3)_2$ and $Cd(PO_3)_2$. The most noteworthy feature of the system is the large region of intermediate solid solution which ranges from 35 to 90 mole % $Cd(PO_3)_2$ and has a distorted $Mg(PO_3)_2$ structure. Manganese-activated phosphors were prepared throughout the system $Zn(PO_3)_2-Cd(PO_3)_2-Mg(PO_3)_2$ and the cathodoluminescence emission peak and brightness values were obtained. The ternary system is dominated by a solid solution which has the $Mg(PO_3)_2$ structure. The phosphors are characterized by two emission peaks in the ranges 5950-5990 Å and 6200-6420 Å. Cadmium metaphosphate increases the intensity of the higher wavelength emission while $Zn(PO_3)_2$ and $Mg(PO_3)_2$ -rich compositions favor the lower wavelength emission.

24,875 THE 1010° AND 800°C ISOTHERMAL SECTIONS IN THE SYSTEM $Na_3AlF_6-Al_2O_3-SiO_2$ by D.F. Weill and W.S. Fyfe (U. Calif., Berkeley); *J. Electrochem. Soc.*, Vol. 111, pp. 582-585, May 1964

Isothermal sections at 1010° and 800°C have been determined in the system $Na_3AlF_6-Al_2O_3-SiO_2$ by the quenching technique. A determined solubility of 13-15 weight % for corundum in the $Na_3AlF_6-Al_2O_3$ system at 1010°C is in good agreement with recent revisions of that binary melting diagram. The steep nature of the corundum liquidus curve in the $Na_3AlF_6-Al_2O_3$ system is found to continue into the ternary system. Silica solubility which is less than 5% in molten Na_3AlF_6 at 1010°C increases rapidly with addition of Al_2O_3 to the system and reaches a maximum value of 69% at the invariant point. The refractive indices of quenched glasses plot smoothly against composition and vary from a maximum of 1.442 (at 17% Na_3AlF_6) to a minimum of 1.422 (at 50% Na_3AlF_6). Glasses richer than 50% in Na_3AlF_6 were difficult to quench. No evidence was found for liquid immiscibility or solid solution in the temperature range studied.

24,876 PHASE EQUILIBRIUM RELATIONS IN THE SYSTEM $CaMgSi_2O_6$ (diopside)- $NaAlSi_3O_8$ (nepheline)- $NaAlSi_3O_8$ (albite)- H_2O AT 1,000 kg/cm² WATER VAPOR PRESSURE by A.D. Edgar (U. Manchester, England); *Am. Mineralogist* J., Vol. 49, pp. 573-585, May/June 1964

Phase equilibrium relations for part of the system $CaMgSi_2O_6-NaAlSi_3O_8-NaAlSi_3O_8-H_2O$ have been determined at 1,000 Kg/cm² water vapor pressure. The minimum melting temperature in this system lies on the $NaAlSi_3O_8-NaAlSi_3O_8$ join at 835 ± 5°C at the composition $Ne_{27}Ab_{73}$. The size of the primary phase field of plagioclase, appearing at the liquidus surface, is considerably smaller at this water vapor pressure than it is under conditions of atmospheric pressure. A comparison between liquidus relations in this system and normative compositions of rocks of the nepheline syenite clan suggests that crystal-liquid equilibria have been involved in the genesis of many of these rocks.

24,877 EFFECT OF STARTING MATERIALS ON PHASE RELATIONS IN THE SYSTEM $CaO-Al_2O_3-H_2O$ by M. Crowley (American Oil); *J. Am. Ceram. Soc.*, Vol. 47, pp. 144-148, Mar. 21, 1964

Phase relations in the system $CaO-Al_2O_3-H_2O$ from 40° to 500°F have been determined by hydrothermal techniques. Very high purity starting materials must be used if the correct phase relations for this system are to be determined. A phase diagram made by using reagent grade $CaCO_3$ is compared with the diagram using luminescent-grade material. The general effect of introducing foreign ions into the system is to promote the formation of the dicalcium aluminate hydrate phase. The action of additives on calcium aluminate cements depends on such factors as the phase relations, nature of the hydrated alumina, and the interrelations of these factors with variable pH, foreign ions, and pressure-temperature variations.

24,878 URANIUM CORNER OF THE U-Al-Fe PHASE DIAGRAM by D.K. Khakimova, O.S. Ivanov and Yu.S. Virgil'yev; in *Structure and Properties of Uranium, Thorium and Zirconium Alloys*, Apr. 24, 1964, pp. 1-6; *STAR*, Vol. 2, p. 1501(A), June 23, 1964 JPRS-24347; OTS-64-31154; \$1.25

The joint solubility of aluminum and iron in uranium was determined. The microstructure of alloys quenched from various temperatures was investigated. Quenching of alloys was done in water at room temperature. At this time, the γ -phase was not fixed, and the γ to β or β to γ transformation was studied. Results of microstructure phase analysis were plotted on a concentration triangle, using data on solubility of aluminum and iron in binary systems of U-Al and U-Fe to construct isothermal sections of the U-Al-Fe system. Isothermal sections at 650°C, 690°C, 730°C, 760°C, 775°C, 800°C, 850°C, 970°C,

and 1,050°C were plotted. Identification of the precipitated phases j_1 (UAl_2) and j_2 (U_6Fe) was possible due to their behavior during electrolytic polishing with an electrolyte.

24,879 PHASE RELATIONS IN THE SYSTEM URANIUM-CARBON-OXYGEN by R. Stoops and J. Hamme (No. Carolina State Coll.); *J. Am. Ceram. Soc.*, Vol. 47, pp. 59-62, Feb. 21, 1964

The ternary system U-C-O has been investigated; a diagram is given expressing the phase relations in specimens which were reacted at 1800°C in vacuum or in inert atmospheres and furnace cooled. A U(C,O) single-phase area exists in this diagram. The limit of substitutional solid solution of oxygen atoms for carbon atoms in UC is 12.5 at.pct., which means that only 25 pct. of the carbon atoms in UC can be replaced by oxygen atoms. The oxygen-saturated UC phase, $U(C_{0.75}O_{0.25})$, has a lattice parameter of 4.953 ± 0.001 Å. The carbon monoxide partial pressures in equilibrium with this phase were determined for temperatures between 1705° and 1855°C.

24,880 PHASE RELATIONS IN THE SYSTEM UO_2 - UO_3 - Y_2O_3 by S. Bartram, E. Juenke, and E. Aitken (GE); *J. Am. Ceram. Soc.*, Vol. 47, pp. 171-175, Apr. 21, 1964

The phase relations in the systems UO_2 - UO_3 - Y_2O_3 have been examined by X-ray and chemical analyses of reacted powders heated at temperatures up to 1700°C. Four phases were identified; a rhombohedral phase oxidized to a second rhombohedral phase with composition $(U,Y)_8O_{15}$ at temperatures below 1000°C. This phase transformed to a FCC phase after heating in air above 1000°C. Solubility of UO_2 in the BCC phase is about 14 mol pct. between 1000° and 1700°C. Solubility of Y_2O_3 in the FCC phase ranges from 0 to 50 mol pct Y_2O_3 under reducing conditions and from 33 to 60 mol pct Y_2O_3 under oxidizing conditions at 1000°C. At temperatures above 1000°C, the FCC solution is limited by a filled fluorite lattice of composition $(U,Y)O_2$. A tentative phase diagram is presented and the change in lattice parameter and cell volume for solid solution phases is correlated with composition.

24,881 PROPOSED PHASE DIAGRAM FOR THE SYSTEM MAGNESIUM OXIDE - VANADIUM PENTOXIDE by A.J. Pollard (Naval Res. Lab.); Proj. SR007 08 04 0617, Feb. 14, 1964, 11 pp.; *U.S. Gov. Res. Rep.*, Vol. 39, p. 418(A), May 20, 1964 AD 432 318 OTS \$1.60

The liquidus-solidus regions of the system MgO - V_2O_5 were investigated over the entire composition range, with the following principal findings: There are two congruently melting compounds: $2MgO \cdot V_2O_5$ melting at 1128°C, and $3MgO \cdot V_2O_5$ melting at 1210°C. A third compound, $MgO \cdot V_2O_5$, is thought to have an incongruent melting point at 762°C. There are three eutectics: one at approximately 15 mole-percent V_2O_5 melting at 1192°C, one at approximately 30 mole-percent V_2O_5 melting at 1122°C, and one at approximately 75 mole-percent V_2O_5 melting at 658°C.

24,882 PHASE EQUILIBRIA IN THE SYSTEM MgO - $MgCr_2O_4$ by A.M. Alper, R.N. McNally, R.C. Doman, and F.G. Keihn (Corning Glass); *J. Am. Ceramic Soc.*, Vol. 47, pp. 30-33, Jan. 1964

The liquidus, solidus, and subsolidus in the system MgO - $MgCr_2O_4$ have been redetermined. It was found that at 2350°C, 47% Cr_2O_3 entered the periclase lattice in solid solution and approximately 5% MgO dissolved into the spinel lattice.

Phase Boundaries in:

H- and D-Pt-Pd - See 24,934

Fe-Zn Ferrites - See 24,946

CHANGES OF STATE

24,883 A HIGH TEMPERATURE DIFFERENTIAL CALORIMETER by C.V. Thomasson and D.A. Cunningham (Pilkington Brothers Ltd., Lancs); *J. Sci. Instr.*, Vol. 41, pp. 308-310, May 1964

A calorimetric method of determining the heats of reaction of materials in the solid state, at temperatures up to 1100°C, has been developed. The sample is heated at a rate of $10^\circ C \text{ min}^{-1}$ and the heat changes associated with reaction processes in the sample are measured. Values for the heats of decomposition of some carbonates have been determined. At the present stage only endothermic heats of reaction have been measured.

24,884 THERMODYNAMIC PROPERTIES OF SOLID VANADIUM-CHROMIUM ALLOYS by A.T. Aldred and K.M. Myles (Argonne Natl. Lab.); *Trans. Met. Soc. AIME*, Vol. 230, pp. 736-739, June 1964

The vapor pressure of chromium over solid V-Cr alloys has been measured by the torsion-effusion method in the temperature range 1450° to 1650°K. The chemical activities as well as the free energies, entropies, and enthalpies of formation of the alloys have been computed from the vapor-pressure data. The activities of both chromium and vanadium exhibit fairly small negative deviations from Raoult's law over the entire composition range. The values of the excess entropies and the enthalpies of formation found at 1550°K are considered in terms of the changes in the characteristic properties of vanadium and chromium that occur upon alloying.

24,885 HEAT OF FORMATION OF ALUMINUM CARBIDE by A.D. Mah (Bureau of Mines, Calif.); 1964, 8 pp., BM-RI-6415; *STAR*, Vol. 2, p.1242 (A), May 23, 1964

The heat of combustion of aluminum carbide (Al_4C_3), obtained directly by combustion calorimetry, was $\Delta H_{298,15} = -1,029.6 \pm 1.9$ kcal/mole. The heat of formation of aluminum carbide corresponding to this value was $\Delta H_{298,15} = -53.4 \pm 2.0$ kcal/mole.

24,886 THE HIGH TEMPERATURE VAPORIZATION PROPERTIES OF BORON CARBIDE AND THE HEAT OF SUBLIMATION OF BORON by H.E. Robson and P.W. Gilles (U. Kansas); *J. Phys. Chem.*, Vol. 68, pp. 983-989, May 15, 1964

The vaporization behavior of boron carbide solid solutions is shown to be the preferential loss of gaseous boron regardless of the sample composition. An invariant system consisting of a graphite crucible and a carbon-saturated boron carbide sample was used to measure the vapor pressure over the temperature range 2184-2522°K. The Knudsen technique employing condensation targets was used, and boron was specifically assayed by a coulometric titration of the mannitol complex. The derived third-law heats of sublimation in kcal/mole of boron are $\Delta H_0^B = 136.8 \pm 0.1$ and $\Delta H_{298}^B = 138.0 \pm 0.1$ for boron carbide and $\Delta H_0^B = 133.8 \pm 0.7$ and $\Delta H_{298}^B = 135.0 \pm 0.7$ for boron.

24,887 THE DECOMPOSITION PRESSURE OF BORON CARBIDE AND THE HEAT OF SUBLIMATION OF BORON by D.L. Hildenbrand and W.F. Hall (Philco); *J. Phys. Chem.*, Vol. 68, pp. 989-993, May 1964

The boron decomposition pressure over boron carbide, B_4C , has been measured by the torsion-effusion method in the range 2350 to 2615°K. A small "hole-size effect" indicates a condensation coefficient of roughly 0.07 for B(g) on $B_4C(s)$. The heat of dissociation of B_4C to B(g) and C(graphite) at 298°K has been derived as 138.7 ± 1.2 kcal/mole of boron from a third-law analysis of the vaporization data. From this result, the heat of sublimation of boron at 298°K has been evaluated as 135.7 ± 1.3 kcal/mole. An approximate value of 171 kcal/mole has been obtained for the heat of formation of $BC_2(g)$ at 298°K.

24,888 HIGH TEMPERATURE DECOMPOSITION OF BORON PHOSPHIDE by C. P'eng-nien and Mo. Chin-chi; in *Transl. on Communist China's Sci. and Technol.* No. 75, Mar. 19, 1964, pp. 48-56, No. 11, 1963, pp. 53-55; *STAR*, Vol. 2, pp. 1090-1091(A), May 8, 1964 JPRS-23767; OTS-64-21840; \$2.25

The carrier method was utilized to determine the thermal decomposition pressure of boron phosphide, using purified hydrogen gas as the carrier. The temperature range for the determination of the thermal decomposition pressure was 1,000° to 1,100°C. Hydrogen flow speed was in the range of 0 to 50 ml/min. The average molecular weight of the phosphorus vapor, at different temperatures, was calculated, and this average was used to determine the balanced decomposition pressure of the thermal decomposition of boron phosphide by Van Wazer's method.

24,889 EQUILIBRIUM VAPOR PRESSURE OF INDIUM ANTIMONIDE by M. Yamaguchi, Y. Mizushima and M. Toda (Nippon Tel. and Tel.); *J. Phys. Soc., Japan*, Vol. 19, pp. 580-581(L), Apr. 1964

The dissociation vapor pressure of InSb has been measured in the temperature range 783°-1243°K utilizing the "Dew point method." The vapor of InSb appears to consist of diatomic molecules with some tetra-atomic ones occurring. The equilibrium pressure of InSb at the melting point is 4×10^{-5} mm Hg.

24,890 THE VAPOR PRESSURES OF SILICON TETRACHLORIDE AND GERMANIUM TETRACHLORIDE BELOW THEIR MELTING POINTS by P. Balk and D. Dong (IBM, Yorktown); *J. Phys. Chem.*, Vol. 68, pp. 960-962, Apr. 1964

The temperature dependence of the saturated vapor pressures of $SiCl_4$ and $GeCl_4$ in the range from 0.01 to 0.5 mm has been studied. For both substances the pressures at the melting points are about 0.6 mm; thus in the pressure range of interest both substances are solids. Undercooling by about 20° was observed when attempting to freeze the substances, allowing an extension of liquid vapor pressure data. The data for both liquid and solid yield straight

lines when plotted as log pressure vs $1/T$. A least-square fit equation ($\log p$ (mm) = $-a/T + b$) is evaluated. Heats of vaporization and entropy are also calculated.

24,891 PARTIAL PRESSURES IN EQUILIBRIUM WITH GROUP IV TELLURIDES. Part I. OPTICAL ABSORPTION METHOD AND RESULTS FOR PbTe by R.F. Brebrick and A.J. Strauss (Lincoln Lab.); *J. Chem. Phys.*, Vol. 40, pp. 3230-3241, June 1, 1964

Results obtained by the optical absorption method for the partial pressures in the Pb-Te system are reported. Between 725° and 924°C, the maximum melting point of PbTe, the partial pressure of PbTe(g) in equilibrium with solid PbTe is given by $\log p$ (Torr) = $-11,430/T^\circ K + 10.612$, corresponding to a heat of sublimation of 52.3 ± 1.0 kcal/mole. The PbTe(g) partial pressure is independent of the composition of PbTe(c) within the limits of experimental error. The partial pressure of Te₂(g) varies strongly with the composition of the solid phase, as shown by data for Pb-saturated and Te-saturated PbTe. The maximum partial pressure of Te₂(g) in equilibrium with PbTe(c) is 12.5 Torr, which is attained between 796° and 832°C for Te-saturated PbTe. At these temperatures the partial pressures of Te₂(g) in equilibrium with Pb-saturated Te are about two orders of magnitude smaller. The partial pressures of PbTe(g) and Te₂(g) in equilibrium with PbTe(c) at its maximum melting point are 11.8 and 2.5 Torr, respectively.

24,892 MANGANESE VAPOR PRESSURES IN EQUILIBRIUM WITH MANGANESE-IRON-NICKEL SOLID SOLUTIONS by J.H. Smith (Ford Motor), H.W. Paxton, and C.L. McCabe (Carnegie Inst. Tech.); *J. Phys. Chem.*, Vol. 68, pp. 1345-1354, June 1964

The partial pressure of manganese gas in equilibrium with manganese-iron-nickel solid solutions was measured as a function of concentration at 1232°K by the Knudsen effusion technique coupled with a vacuum microbalance. The manganese-nickel system exhibits negative departures from an ideal solution with the exception of the β -phase alloys where the nonideality is slightly positive. These departures decrease as iron replaces nickel in solid solution. The Gibbs excess molal free energy was calculated for ternary concentrations from the ternary Gibbs-Duhem equation and estimated for the iron-nickel binary concentrations. Nonregular solution behavior exists in both binary and ternary concentrations.

24,893 ATOMIC VIBRATIONS AND THE MELTING PROCESS IN METALS by D. McLachlan, Jr. (U. Denver) and L.L. Chamberlain (Stanford Res. Inst.); *Acta Met.*, Vol. 12, pp. 571-576, May 1964

The Gruneisen equation for potential energy (as a function of distances between the atoms) provides for instability in the lattice of crystalline metals when the amplitude of vibration exceeds a critical distance, ($r_i - r_0$). Upon this basis the general theory is tested by comparing the experimental melting temperatures of thirty-one elements of the periodic table with those computed from the theory. A different equation is required for the close-packed structures than for the loose-packed structures.

24,894 THE OPTICAL CONTRAST BETWEEN SOLID AND LIQUID POTASSIUM IN TRANSMITTED ULTRA-VIOLET LIGHT by A.J. Forty (U. Bristol); *Philosophical Mag.*, Vol. 9, pp. 673-682, Apr. 1964

Transmission ultra-violet light microscopy can be used to study the melting and solidification of films of potassium. It is possible to differentiate between the solid and liquid phases by a form of optical contrast so that direct observations can be made on the structure of freezing and melting fronts and on the influence of microstructure on these processes. This paper is primarily concerned with the nature of the optical contrast. It shows how this depends on the change of refractive index of the metal during melting and the interference of multiple reflections from the surfaces of the film.

24,895 MELTING PROPERTIES OF KNO₃ UNDER HIGH PRESSURE by S.E. Bobb, Jr., and P.E. Chaney (U. Oklahoma); *Bul. Am. Phys. Soc.*, Vol. 9, p. 534(A), June 1964

Previous work of Owens has disclosed the possibility of KNO₃ possessing a maximum melting temperature at relatively moderate pressures. The melting curve of KNO₃ has been followed to 10,000 bar, using latent-heat sensing of melting. A broad maximum is present with approximate coordinates of 6400 bar and 355°C, the temperature value being uncorrected for the effects of pressure upon the emf of the thermocouple. By plotting the 1st derivative of the melting curve, it can be shown that no small 1st-order transitions have been overlooked in the vicinity of the maximum, and that a 2nd-order transition in this region is extremely improbable.

24,896 DIAGRAM OF FUSIBILITY OF THE SYSTEM Ni-Cr-NiAl by I.I. Kornilov and R.S. Mints (Wright-Patterson AF Base); *Trans. from Doklady Akade. Nauk SSSR*, 94:6, pp. 1085-1088, 1954; *FTD MT63 174*, Nov. 21, 1963, 11 pp.; *U.S. Gov. Res. Rep.*, Vol. 39, p. 92 June 5, 1964 AD 434 974 OTS 51.60

24,897 THE SOLUBILITY OF OXYGEN IN SILVER AND THE THERMODYNAMICS OF THE INTERNAL OXIDATION OF A SILVER-COPPER ALLOY by H.H. Padgurski and F.N. Davis (U.S. Steel); *Trans. Met. Soc. AIME*, Vol. 230, pp. 731-735, June 1964

In silver alloys containing less than 0.2 wt pct Cu, the reaction $\text{Cu} + 1/2 \text{O}_2 \rightleftharpoons \text{CuO(s)}$ was found to proceed to equilibrium between 700° and 808°C. From measurements of the equilibrium dissociation pressures of the CuO at several temperatures, the differential heat of solution and the activity coefficients for copper in silver were calculated. These values were found to be in reasonable agreement with those calculated from data appearing in the literature. A metastable "copper oxide" with an atom ratio of oxygen to copper as high as 1.7 was formed by internal oxidation at 300°C of these same dilute Ag-Cu alloys. No anomalous behavior was noted in the temperature dependence of oxygen solubility in silver. The solubility minima between 300° and 800°C reported several years ago can be accounted for, at least in part, by reactions with trace impurities, such as copper. Cold-worked silver exhibits an enhanced permeability to oxygen.

24,898 THE TEMPERATURE AND COMPOSITION DEPENDENCE OF THE SEGREGATION OF INTERSTITIAL IMPURITY ATOMS TO DISLOCATIONS by M.L. Rudee and R.A. Huggins (Stanford U.); *Acta Met.*, Vol. 12, pp. 501-504, May 1964

A relation for the equilibrium number of interstitial impurity atoms about dislocations is established. The effects of the temperature dependence of the impurity solubility in the matrix and the presence of sites of several energy levels around the dislocation are considered. It is shown that segregation will generally increase with increasing temperature. In the case of interstitial carbon in iron, it is shown that segregation to dislocations is not appreciable even though there is a significant binding energy. Nitrogen, with the same binding energy as carbon, will have a strong tendency to form atmospheres.

24,899 THE EFFECT OF ORIENTATION ON THE ELECTRICAL PROPERTIES OF EPITAXIAL GALLIUM ARSENIDE by F. Williams (Monsanto Chemical); *J. Electrochem. Soc.*, Vol. 111, pp. 886-888, July 1964

Data concerning the anisotropic segregation of impurities at a solid-vapor interface are presented. Epitaxial layers of gallium arsenide were deposited on seed crystals of gallium arsenide in various orientations. The electrical properties of the resultant layers were found to depend on orientation during crystal growth. These results tend to confirm the adsorption theory of Hall on the orientation dependence of segregation coefficients. It is concluded that purer GaAs can be produced by the Czochralski technique if the seed is oriented in the $\langle 100 \rangle$ or $\langle 110 \rangle$ direction.

24,900 THE SEGREGATION COEFFICIENT OF NAPHTHACENE IN ANTHRACENE by A. Matsui (Sanyo Electric); *J. Phys. Soc. Japan*, Vol. 19, p. 578, Apr. 1964

The segregation coefficient (κ) of naphthacene in anthracene has been determined by luminescence measurement. Calibration of intensity vs concentration of naphthacene is linear for powdered materials, enabling calculation of the segregation coefficient of doped crystals by use of the Pfann equation $C = C_0 \kappa (1 - p)^{\kappa-1}$. κ can be determined from the slope of a logarithmic plot or from the intercept; however, these values do not agree for all velocities of growth. Accounting for crystal imperfections, diffusion of naphthacene, trace impurities, and deposition of naphthacene, the most reliable value of κ is about 0.1.

Solubility of:

Zn in:

GaAs and GaP - See 25,073

InP - See 25,074

B₄C in SiC and SiC in B₄C - See 24,870

PHASE TRANSITIONS (TRANSFORMATIONS)

24,901 THE $\beta \rightarrow \alpha$ TRANSFORMATION IN TITANIUM by M.J. Bibby, and J.G. Parr (U. Alberta, Canada); *J. Inst. Metals*, Vol. 92, pp. 341-342(L), June 1964

Evidence is presented which indicates the martensitic transformation in pure titanium is isothermal. Transformation temperatures were determined for cooling rates up to 60,000 deg C/sec, starting from a soaking temperature of 1000°C. All samples cooled at rates greater than 200 deg C/sec showed a rumpled surface, characteristic of martensite formation. A plot of the $\beta \rightarrow \alpha$

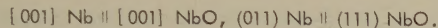
transformation temperatures against cooling rates yields a linear relation:

$$T = \frac{90}{60,000} \frac{dT}{dt} + 872.$$

Since M_5 is depressed as cooling rate increases, the transformation must have an isothermal component.

24,902 PHASE TRANSFORMATIONS IN NIOBIUM INVOLVING INTERSTITIALS by L. I. Van Tonne (Lawrence Radiation Lab.), and G. Thomas (U. Calif., Berkeley); *Acta Met.*, Vol. 12, pp. 601-615, May 1964

A homogeneous phase transformation b.c.c. Nb to a f.c.c. lattice, probably NbO but containing C + N also, has been observed by transmission electron microscopy both in thin foils and in bulk specimens containing ~ 0.5 at % interstitials after suitable aging treatments. The transformation proceeds in the following sequence: (a) ordering in Nb with interstitials taking $\frac{1}{2}\frac{1}{2}0, 00\frac{1}{2}$ sites (b) formation of a precipitate in alternate prisms of Nb and NbO (c) growth to perfect NbO structure (d) recrystallization of NbO above 1000°C. In thin foils the crystallographic features of the transformation are



The habit planes are four variants of $\{011\}$ but only those inclined at less than 90° to the foil surface operate. In bulk specimens the habit planes are observed to be $\{021\}$ which is in accord with the crystallographic theory for martensitic transformations. The difference between bulk and thin film behavior is attributed to the lack of constraints in the latter where the strains appear to be accommodated elastically. Conversely, in bulk specimens, dislocations are generated from the precipitate-matrix interfaces.

24,903 PHASE TRANSITIONS IN TELLURIUM AT HIGH PRESSURES by S. S. Kabalkina, L. F. Vereshchagin and B. M. Shulenin (Acad. Sci. USSR); *Soviet Phys. JETP*, Vol. 18, pp. 1422-1423(L), May 1964

The effect of high pressures on the crystal structure of tellurium has been studied up to a pressure of 100 kbar. It is found that at $p = 15$ kbar, tellurium undergoes a transition from the chain structure A8 to the laminar structure A7. In the new phase each tellurium atom has three nearest neighbors at a distance of 2.87 Å, three neighbors at a distance of 3.48 Å and six neighbors at a distance of 4.208 Å. The linear and volume compressibilities calculated up to 40 kbar agree with the results obtained by Bridgman.

24,904 POLYMORPHIC TRANSITIONS IN THE Fe-V ALLOY SYSTEM by T. R. Loree (Los Alamos Lab.); *Bull. Am. Phys. Soc.*, Vol. 9, p. 1534(A), 1964

The initial discovery of a polymorphic transition (now thought to be a transformation from bcc to hcp) at 130 kb in explosively shocked iron has led to dynamic-pressure investigations of several binary iron-alloy systems. Among these, the Fe-V system has proved to be remarkable in that the transition pressure rises sharply as the amount of alloying element is increased. At 10% vanadium (by weight), the transition pressure is up from 130 to about 250 kb. For this alloy, the normalized specific volume at the onset of the transition is 0.894. The volume change due to the transition itself is difficult to measure under dynamic conditions but seems to be above 5% for all alloys studied. Preliminary results have been obtained for higher vanadium-content alloys and indicate that, in the 20%-25% vanadium range, transition pressures will be in excess of 500 kb. For still higher vanadium contents, the pressure of the transformation is expected to level off, as these alloys no longer form in a pure bcc phase.

24,905 ORDER-DISORDER IN Co-V SIGMA PHASE by N. Marcone and J. Coll (Argentine AEC); *Acta Met.*, Vol. 12, pp. 742-744(L), June 1964

Hardness, dilatometric, and electrical resistivity measurements have been used to study the order-disorder transition in a sigma phase 50 at pct Co-50 at pct V alloy. Hardness determinations on specimens quenched from temperatures of 200-1200°C indicate a marked inflection in the temperature range of 400-600°C attributed to a disordering reaction. Characteristic points for dilatometric measurements indicate that the critical temperature for disordering is 550°C. The electrical resistivity of the Co-V sigma phase is of the order of 320 $\mu\Omega$ cm, decreasing with increased temperature, indicative of semiconductor behavior. Analysis of the electrical resistivity-temperature results indicate a disordering in the neighborhood of 550°C. This postulated disordering temperature agrees reasonably well with the Oriani hypothesis since the critical temperature-melting temperature ratio is found to be 0.53.

24,906 DILATOMETRIC INVESTIGATION OF THE ORDER-DISORDER TRANSITION IN Mg_3Cd by V. Hovi and P. Paalassalo (U. Turku, Finland); *Acta Met.*, Vol. 12, pp. 723-729, June 1964

The order-disorder transition in Mg_3Cd was investigated by means of a dilatometric precision method between 40°C and 190°C. Special attention was paid for making sure that the preparation had reached equilibrium during the measurements. The sample used for observations was made in a helium atmosphere. Its composition was 74.8 ± 0.2 at % Mg. Values for the specific volume were measured between 40°C and 190°C. On the basis of these data the value $149.5 \pm 0.5^\circ\text{C}$ was determined for the Curie point. No hysteresis in the thermal expansion near the Curie point was observed. The long range order parameter and the thermal expansion coefficient of Mg_3Cd were calculated as functions of temperature from the data measured for the specific volume.

24,907 ON THE KINETICS OF PRECIPITATION IN ALLOYS by F. E. Fujita (Brookhaven Lab.); *J. Phys. Soc. Japan*, Vol. 19, pp. 640-651, May 1964

From the analysis of experiments on the precipitation of carbon in α -iron, it is suggested that the idea of chemical rate process is applicable to precipitation in alloys. A set of fundamental equations to describe the whole process of precipitation in alloys is postulated on the basis of nucleation theory and first order kinetic theory for the growth process. Approximate solutions were found, and good agreement with the experimental results was obtained. Some physical foundations and application of the theory were also discussed.

24,908 PRECIPITATION OF AgCl IN NaCl (AgCl) SOLID SOLUTIONS by R. Hendricks, R. Baro, and J. Newkirk (Cornell U.); *Trans. Met. Soc. AIME*, Vol. 230, pp. 930-931(L), June 1964

Preliminary results are presented on a study of the kinetics of precipitation of AgCl from supersaturated solid solution of AgCl in NaCl containing trace amounts of divalent cation impurities. Growth kinetics of the precipitate particles were followed by small-angle x-ray scattering. For a specimen containing 21.0 at pct AgCl, the radius of gyration was measured as a function of aging time at room temperature. The result is consistent with the theory of Ham in which it is assumed that diffusion of solute atoms through the matrix is the rate limiting step in the precipitation process.

24,909 SOME OBSERVATIONS ON STRUCTURAL TRANSFORMATION OF Ag_2Se ALLOY FILMS by S. K. Sharma and G. L. Malthotra (Nat'l. Phys. Lab. India); *Phys. Lett. (Neth.)*, Vol. 9, pp. 218-219(L), Apr. 15, 1964

A transmission electron diffraction study of Ag_2Se alloy films is discussed. The films (200 to 500 Å thick) were formed by vacuum evaporation onto potassium chloride substrates kept at 30°C, and then homogenized by heating at about 150°C for a few hours. Single crystal films of α - Ag_2Se displayed the orthorhombic structure with lattice parameters $a = 7.05$ Å, $b = 4.325$ Å, and $c = 7.82$ Å. When the temperature was raised, the orthorhombic α - Ag_2Se structure changed to the body centered cubic β - Ag_2Se structure ($a = 4.98$ Å) at $166 \pm 2^\circ\text{C}$. When the β -phase was cooled at the rate of $2^\circ\text{C}/\text{min}$, this phase remained down to 107°C , below which it changed to the α -phase. The β -phase could be obtained again by heating to $166 \pm 2^\circ\text{C}$. The present data, and that of other workers, indicate that structural transformations occur at higher temperatures in thin films than in the bulk.

24,910 NMR STUDIES OF PHASE TRANSITIONS. Part II. NaCN by C. K. Coogan and H. S. Gutowsky (U. Illinois); *J. Chem. Phys.*, Vol. 40, pp. 3419-3425, June 1, 1964

The ^{23}Na nuclear magnetic resonance absorption has been observed in the cubic phase of polycrystalline NaCN between about 15° and 170°C , but could not be detected in the orthorhombic phase which forms below 10.5°C . The observed lineshape and its second moment S are compatible with a model in which $S = S_d + S_{q0} + S_q(T)$. The electric-field gradients (EFG) involved in $S_q(T)$ are attributed to the electric dipoles of the CN^- ions, and the temperature dependence, to the averaging out of the gradients by thermally activated reorientations of the CN^- ions. The reorientations are deemed responsible for the existence of a cubic phase. They are treated as a random-walk problem yielding algebraic expressions by means of which an activation energy of 6 kcal/mole is obtained from the experimental $S_q(T)$, and 5×10^8 cps at 10°C and 10^{10} cps at 150°C are estimated for ν_j , the CN^- reorientational jump frequency. A discussion is given of the relation between ν_j and the nucleation of the cubic to orthorhombic phase transition.

24,911 ON RADIATION INDUCED PHASE TRANSFORMATION OF BaTiO_3 [in German] by M. Schenk (Deutsche Akad. Wissen., Berlin); *Phys. Stat. Sol.*, Vol. 4, pp. K25-28, 1964

Radiation-induced phase transformations of BaTiO_3 from tetragonal to cubic symmetry has been investigated by an x-ray technique. Fast neutrons of flux 4.2×10^8 neutrons/cm² have been used for effecting such transformations on the basis of the high capture cross section properties of $^{22}\text{Ti}^{50}$ isotope for thermal neutrons; recoil displacement of $^{22}\text{Ti}^{51}$ is favored during irradiation. The point defects produced from such recoil displacement reactions are thought to be responsible for the observed phase transformations since such a transformation is known to proceed continuously.

24,912 THE THORITE → HUTTONITE PHASE TRANSFORMATION AS DETERMINED BY GROWTH OF SYNTHETIC THORITE AND HUTTONITE SINGLE CRYSTALS by C. Finch, L. Harris, and G. Clark (Oak Ridge Lab.); Amer. Mineralogist, Vol. 49, pp. 782-785, May-June 1964

The phase transformation, tetragonal ThSiO_4 (thorite) → monoclinic ThSiO_4 (huttonite) has been investigated using solution growth of the preferred modification of ThSiO_4 single crystals as a criterion for phase stability at a given temperature. Using alkali ditungstate or dimolybdate solutions, the data suggest the equilibrium transformation temperature to be 1225°C. The transformation is unique in that the denser modification, huttonite, is formed at higher temperatures. This method of studying sluggish phase transformations appears to be advantageous if solvents are available which do not contaminate the crystallizing phase.

Phase Transitions in:

In-Te - See 24,867

Be-Ti - See 24,953

CRYSTAL STRUCTURE

GENERAL

24,913 DISPERSIVE CORRECTIONS AND CRYSTAL STRUCTURE REFINEMENTS by J. Ibers and W. Hamilton (Brookhaven Lab.); Acta Cryst., Vol. 17, pp. 781-782, June 10, 1964

The relative merits of two methods of treating the effects of anomalous dispersion in x-ray crystal structure refinements are discussed. Both least-square and Fourier considerations for centrosymmetric and non-centrosymmetric crystals are included. The notation used is that of Paterson.

24,914 X-RAY DIFFRACTION FROM SMALL CRYSTALLITES by V.H. Tiensuu, S. Ergun, and L.E. Alexander (U.S. Bureau of Mines, Pittsburgh); J. Appl. Phys., Vol. 35, pp. 1718-1720, June 1964

The classical crystallographic equations used in deducing structure from peak positions, peak widths, and integrated intensities of x-ray scattering are facile enough, but they involve assumptions that are not valid for extremely small crystallites. An alternate approach more generally valid is to use the Debye interference function. These two different approaches have been compared, using as examples a diamond crystallite containing three unit cells on a side (~10.7 Å) and one containing ten unit cells on a side (~35 Å).

24,915 A NEW METHOD FOR NEUTRON DIFFRACTION CRYSTAL STRUCTURE INVESTIGATIONS by B. Buras and J. Leciejewicz (Inst. Nuc. Res. Swienki); Phys. Stat. Sol., Vol. 4, pp. 349-355, 1964

A neutron diffraction method for structure analysis of powdered specimens involving time-of-flight techniques is described. Calculated and measured structures are in good agreement for Al and Si.

24,916 RECEIVING APERTURE WIDTHS IN SINGLE CRYSTAL DIFFRACTOMETRY by L. Alexander and G. Smith (Mellon Inst.); Acta Cryst., Vol. 17, pp. 447-448(L), Apr. 1964

Attention is brought to a faulty assumption in an earlier paper by Alexander and Smith (Acta Cryst., 15, 983, 1962). Actually the critical angle β_0 can be precisely determined by minimizing the separation of the trailing edges of the diffracted rays and the receiving aperture. This is done by standard differential calculus. It is shown that the locations of aperture limits and diffracted beam edges are symmetrical about $2\theta_0$ and $\beta = 0$. The effect of the revised equations is actually very small; for aperture widths discussed, the maximum change is only 5%.

24,917 ILLUMINATION ATTACHMENT TO A TWO BEAM INFRA-RED SPECTROMETER FOR STUDYING SEMICONDUCTOR CRYSTALS AT LOW TEMPERATURES by E. Lotkova and A. Shustov (Acad. Sci., USSR); Cryogenics, Vol. 4, pp. 41-42(L); Feb. 1964

An illumination attachment to overcome many of the difficulties in two beam infrared spectroscopy of semiconductor crystals at low temperatures is described. This attachment permits focusing nearly the whole infrared flux from the source onto small specimens that are being held at low temperatures in a cryostat. The scheme is described in detail and an illustration of the improvement in the transmission spectrum of neutron irradiated n-type silicon is included.

24,918 ON "LATTICE IMAGE" IN ELECTRON MICROGRAPHS by S. Miyake, K. Fujiwara, M. Tokonami and F. Fujimoto (U. Tokyo); Japanese J. Appl. Phys., Vol. 3, pp. 276-285, May 1964

Assuming a plate-shaped crystal in which a lattice plane with the spacing d is perpendicular to the crystal surfaces and the potential varies according to the harmonic form $V(x) = 2V_1 \cos(2\pi x/d)$ in direction x perpendicular to the lattice plane, the lattice image of electrons on the exit surface was calculated by using the exact solution of Schrodinger equation for electron waves in the crystal. The values of d and V_1 were assumed to be 13.0 Å and 2.14 volts, respectively. These values are those approximately appropriate to (001) of Pt-Phthalocyanine. Calculation was made both for the case of normal incidence of primary electrons and the case in which Bragg condition is satisfied. Wavelength of electrons was assumed to be 0.0603 Å corresponding to the accelerating voltage 41.5 kv. A number of aspects of the lattice image which take place by the participation of higher order reflections were revealed. By the effect of higher order reflections, the peaks in the lattice image become much pronounced for the crystal thicker than about 300 Å, while, on the contrary, the intensity profile turns out to be rather flat for the crystal thinner than about 150 Å, in accordance with the trend expected from the phase grating theory.

24,919 USE OF THE INTERACTION OF THERMAL AND ULTRASONIC WAVES TO STUDY RADIATION-INDUCED DEFECTS IN QUARTZ by T.M. Fitzgerald, B.B. Chick, and R. Truell (Brown U.); J. Appl. Phys., Vol. 35, pp. 1639-1640, May 1964

Evidence is presented showing that the interaction of high-frequency stress waves with lattice vibration waves provides a means of studying crystal perfection. This discussion is concerned specifically with quartz single crystals, but the method has been found to apply to other materials as well.

24,920 THE INFLUENCE OF IMPURITIES ON THE FORMATION OF THE Cu_3Au -TYPE STRUCTURE FROM THE Cr_3Si -TYPE STRUCTURE by H. Von Philipsborn and F. Laves (Swiss Fed. Inst., Zurich); Acta Cryst., Vol. 17, pp. 213-214(L), Feb. 1964

The influence of impurities on formation of the Cu_3Au structure was investigated by melting stoichiometric amounts of Ti and Au in an argon furnace in the presence of oxygen, nitrogen or carbon to form Ti_3Au . The Cr_3Si -type structure (β phase) was obtained, as was a second phase having the ordered Cu_3Au structure (α phase). Total conversion of β to a Ti_3Au was obtained for 3.4 wt % oxygen. Nitrogen and carbon have the same influence, hydrogen none. The transformation is irreversible. Detailed intensity discussions indicate that oxygen atoms occupy the central octahedral hole in the Cu_3Au -type structure.

24,921 SURFACE STRUCTURE AND SURFACE MIGRATION OF GERMANIUM BY FIELD EMISSION MICROSCOPY by J.R. Arthur, Jr. (Bell Labs.); J. Phys. Chem. Solids, Vol. 25, pp. 583-591, June 1964

Field ion and electron microscopy were used to examine the structure of clean germanium surfaces. Both hydrogen and argon ion images were observed; however, the hydrogen produced a rapid field-induced etching of the surface. This etching process was useful in removing surface contamination without introducing impurities into the crystal. Argon ion and electron images showed that a clean germanium tip, smoothed by field evaporation, develops facets at the low index faces when annealed above 500°K. An activation energy of 31 kcal/mole for surface migration was measured in studies of the kinetics of annealing. The ion images failed to show much atomic ordering on field evaporated germanium; this may have been due to instability of the evaporated surface producing some reorientation of the surface atoms.

24,922 A DISTINCTION BETWEEN NATURAL AND SYNTHETIC EMERALDS by I. Sunagawa (Geological Survey of Japan); Amer. Mineralogist, Vol. 49, pp. 785-792, May-June, 1964

Comparative studies are reported on the surface structures of crystal faces of natural and synthetic emeralds. These emeralds can be easily distinguished under the reflection or phase contrast microscope since differences in growth conditions give rise to differences in the surface structure. Although spiral growth is the mechanism of growth for both natural and synthetic emeralds, distinct differences in the growth features can be observed. These differences are: 1) spacing of growth layers, 2) distortion (or lack of it) of the surface, 3) origin of the growth spirals, 4) morphology of the growth spirals, and 5) presence of impurity crystals on the surfaces of natural crystals. Conjectures are presented for the differences in growth conditions relative to the experimental observations.

24,923 EFFECT OF TEMPERATURE AND ENVIRONMENT ON THE STRUCTURE OF THIN SINGLE-CRYSTAL NICKEL FILMS by E. I. Alessandrini (IBM, Watson, Res. Ctr.); J. Appl. Phys., Vol. 35, pp. 1606-1610, May 1964

Single-crystal films of Ni have been epitaxially grown by vapor deposition on heated, freshly cleaved (100) faces of rocksalt, and annealing experiments

have been carried out in an electron diffraction instrument after the films had been floated off the rock salt and mounted on Ni grids. The diffraction patterns of the as-grown films indicated that the Ni was a {001}-oriented single crystal with faulting that resulted in streaking in all four [111] directions. The [111] faults were removed by annealing above 500°C for 1 h at less than 1×10^{-5} Torr. At 400°C and vacuum pressures controlled by leaking air into the diffraction unit, structural changes were observed. At 1×10^{-5} Torr, the film remained single crystal; at 3×10^{-5} Torr, the electron diffraction patterns indicated faults in the [111] directions; and as the pressure increased to 5×10^{-5} Torr, Ni plus the previously reported metastable Ni+O phase appeared. A new complex two-phase structure of Ni plus Ni + O occurred at 7×10^{-5} Torr; and at 1×10^{-4} Torr, only the equilibrium NiO phase was observed. At higher temperatures and a constant pressure of 3×10^{-5} Torr, there was an absence of any transition phases. Experiments were repeated with argon under similar conditions and no structural changes were observed. The changes are attributed to an increasing oxygen content in the film during the annealing conditions. The transformations are interpreted to be dependent upon a complex type of precipitation in which the oxygen fault interpretation postulated by Heidenreich et al. may be the first stage in the precipitation of NiO in the film.

24,924 VARIATION OF THE LATTICE PARAMETER OF SMALL SILVER CRYSTALS [in French] by T. de Plauta, R. Chez, and F. Piuze (EPUL Phys. Lab., Lausanne); *Helv. Phys. Acta*, Vol. 37, pp. 74-76, 1964

The contraction of lattice parameter for small particles has been studied on discontinuous thin films of silver utilizing electron diffraction techniques. The estimated error in values of a_0 is 2.4 to 5 pct. The change in a_0 as crystal size is reduced to diameters as low as 60° is a linear function which extrapolates to a value for massive silver of 4.0868 Å, slightly higher than the a_0 value tabulated for silver, 4.0856 Å. The reduction in a_0 with reduced grain size is possibly caused by a superficial constraint.

24,925 OBSERVATION OF LATTICE PLANES OF 2.35 Å SPACING WITH AN ELECTRON MICROSCOPE by T. Komoda (Hitachi Central Res. Lab.); *Japanese J. Appl. Phys.*, Vol. 3, pp. 122-123(L), Feb. 1964

Lattice planes have been observed with an electron microscope in Gold film specimens prepared by vacuum evaporation and epitaxial growth. The film plane was (111) and the film thickness as 40 Å, a quarter of the extinction distance. A Hitachi HU-11A operated at 100 kv accelerating voltage and a magnification of 210,000 times was employed. The electron beam was tilted so that the Bragg condition was satisfied for (111). An image of the (111) planes of gold is included.

Crystal Structure of Si Films - See 25,105

24,926 ON THE SYMMETRY OF PHASES IN THE RECIPROCAL LATTICE: A SIMPLE METHOD by E.F. Bertaut (Lab. d'Electrostat. et de Phys. du Metal, Inst. Fourier, Grenoble); *Acta Cryst.*, Vol. 17, pp. 778-779, June 10, 1964

A simple method of structure factor algebra used to find phase relations between structure factors is discussed. The method is based on the fact that to every symmetry operation $r \rightarrow r'$ there is a corresponding phase relation in reciprocal space.

24,927 INVESTIGATION ON AUSTENITE AND MARTENSITE SUBJECTED TO VERY LOW TEMPERATURE by J. Mazur (U. Wroclaw); *Acta Phys. Polonica*, Vol. 25, pp. 75-84, Jan. 1964

The variation of the lattice parameters of austenite and martensite and the breadth of their x-ray diffraction lines have been investigated after subjecting the metals to low temperature treatment in liquid air and liquid helium. From the breadth of the lines the average size of the crystal grains has been estimated. The broadening of the martensite lines is caused by two factors simultaneously: strain and small particle sizes.

24,928 THE CRYSTAL STRUCTURES OF NEW FORMS OF SILICON AND GERMANIUM by J.S. Kasper and S.M. Richards (GE Res. Lab.); *Acta Cryst.*, Vol. 17, pp. 752-755, June 1964

The structures of new dense forms of silicon and germanium, recovered from high pressure experiments, have been determined from their Debye-Scherrer patterns. For silicon, the space group is $Ia3(T_h)$, $a = 6.636 \pm 0.005$ Å, $Z = 16$, and there is one structural parameter corresponding to occupancy of 16 (c) positions, with $x = 0.1003 \pm 0.0008$. The measured and calculated density is 2.55 g cm^{-3} . The space group of germanium is $P4_32_1(D_2)$ with $a = 5.93 \pm 0.01$, $c = 6.98 \pm 0.01$ Å, and $Z = 12$. Two kinds of germanium atom occupy the 4(a), $xx0$, etc., and 8(b) xyz , etc., positions; x for 4(a) is 0.0912 ± 0.0060 , and for 8(b) $x = 0.1730 \pm 0.0037$, $y = 0.3784 \pm 0.0051$, $z = 0.2486 \pm 0.0048$. The measured density is 5.88 g cm^{-3} , the calculated 5.91 g cm^{-3} . The two structures represent two different ways of achieving higher density

relative to the diamond structure without change of coordination number and with little effect on interatomic distance. The angular distortions, particularly for germanium, are, however, appreciable.

24,929 CRYSTALLOGRAPHIC ANGLES FOR MERCURY, BISMUTH, ANTIMONY, AND ARSENIC by D.J. Bacon, F. Heckscher, and A. Crocker (Battersea Col. Tech. London); *Acta Cryst.*, Vol. 17, pp. 760, June 10, 1964

Data on the crystallographic angles of mercury, bismuth, antimony, and arsenic are presented. The structures are referred to face-centered rhombohedral cells, the axial angles used being $98^\circ 21.8'$ for mercury, $87^\circ 32.4'$ for bismuth, $87^\circ 25.4'$ for antimony, and $84^\circ 38'$ for arsenic.

24,930 DENSITIES AND LATTICE PARAMETERS OF TIN (INDIUM) SOLID SOLUTIONS by W. Helfrich and R. Dodd (U. Wisconsin); *Acta Met.*, Vol. 12, pp. 667-669(L), May 1964

New data on densities and lattice parameters of Sn (In) have been obtained to verify whether this system presents an exception to the expressed opinion that "structural vacancies do not occur in binary metallic primary solid solutions." Alloys containing 0-10 at.pct In were prepared by vacuum melting and by melting in evacuated Pyrex ampoules. Lattice parameters were calculated from x-ray powder photographs and densities calculated and measured by weighing in air and in 1,2 dibromoethane at 25°C. Theoretical and measured densities are in exact agreement. It is generally concluded from the newly generated data that no metallic primary solid solution has been shown to contain high vacancy concentrations due to Brillouin zone effects.

24,931 THE LATTICE PARAMETERS OF SOME δ - AND ϵ -PLUTONIUM ALLOYS by J.A.C. Marples (At. E. Res. Est. Harwell); *J. Phys. Chem. Solids*, Vol. 25, pp. 521-534, June 1964

A high temperature x-ray diffractometer has been used to measure the lattice parameters of δ - and ϵ -plutonium alloys with zirconium, hafnium, scandium and uranium. These results, and others reported in the literature, are presented as isothermal lattice parameter versus composition curves and show marked deviations from Vegard's law, zirconium even causing maxima in the curves for both δ - and ϵ -alloys. It is shown that solutes with valencies less than that of plutonium give positive deviations from Vegard's law while those with greater valencies give negative deviations. The effects of electronegativity and compressibility are considered and it is shown that these cannot explain the results. The lattice parameter versus temperature curves for some δ -phase plutonium-zirconium alloys have been fitted to an equation proposed by Rocher and Friedel which explains the form of the curves, suggesting that the negative expansion coefficient is caused by a thermally activated transition from one level to another. The activation energy is shown to increase more slowly with zirconium than with aluminium content as would be expected from their different valencies.

24,932 EFFECT OF TEMPERATURE ON THE LATTICE PARAMETER OF A 25% SILVER -75% PALLADIUM ALLOY by C. Nagabhushna Rao and K. Krishna Rao (Atomic Energy Est., India); *Philosophical Mag.*, Vol. 9, pp. 527-528(L), Mar. 1964

It has been suggested that Anomalous decreases in resistivity due to cold-work in silver-palladium alloys may be caused by the presence of a positive short-range order. This is indicated by negative heats of formation of the alloys. In the present investigation, lattice parameter changes were measured as a function of temperature for a 25 pct Ag-75 pct Pd alloy. A change in the slope indicates a local ordering transition temperature of about 430°C, consistent with the above hypothesis.

Lattice Parameters of Ag_2Se Films - See 24,909

24,933 LATTICE SPACING RELATIONSHIPS IN HEXAGONAL CLOSE-PACKED SILVER-ZINC-MANGANESE ALLOYS by B. Henderson (A.E. Res. Est., Harwell), and R.J.M. Willcox (U. Birmingham, England); *Phil. Mag.*, Vol. 9, pp. 829-846, May 1964

The lattice spacings of close-packed hexagonal ϵ -phase alloys in the ternary system silver-zinc-manganese have been determined as a function of alloy composition, using x-ray powder methods. The observed trends in the lattice spacing/composition curves are interpreted according to the established models for the interactions between the Fermi surface and the Brillouin zone faces. In particular the observation that the axial ratio of manganese-zinc alloys is less than 1.633 for all compositions is thought to be due to the (1010) zone faces being overlapped, while the reversal in slope of the c-spacing/composition curve at about 84 at.% zinc for silver-zinc-1% manganese alloys, is attributed to the onset of overlap of Fermi electrons across the (0002) zone boundaries. Effective valencies of metallic manganese in solid solution in these alloys have been deduced for alloys within the ternary phase field. It is suggested that in alloys having electron concentrations greater than 1.75,

manganese has a negative valency, i.e. manganese absorbs electrons from the valence band. The variations in valency are discussed in terms of the existence of virtual bound 3d states associated with the manganese atoms, and the transference of electrons to or from these states as a result of changes in the electron concentration or lattice spacings of the alloys.

24,934 LATTICE CONSTANTS AND THERMODYNAMIC PARAMETERS OF THE HYDROGEN-PLATINUM-PALLADIUM AND DEUTERIUM-PLATINUM-PALLADIUM SYSTEMS by A. Maeland and T.B. Flanagan (U. Vermont); *J. Phys. Chem.*, Vol. 68, pp. 1419-1426, June 1964

Absorption isotherms (25°) and thermodynamic parameters of absorption of deuterium by several platinum-palladium alloys have been determined. Relationships between the relative resistance of the alloys their deuterium content have been established (25°). Results have been compared to the previously obtained data on the hydrogen-platinum-palladium system. The experimental differences between the heats of absorption of deuterium and hydrogen in palladium and several platinum-palladium alloys have been compared to predicted values for these differences. Lattice constants of the f.c.c. platinum-palladium alloys have been determined as a function of both the hydrogen and deuterium content of the alloys. Phase boundaries have been established using x-ray diffraction techniques.

24,935 POWDER INDEXING AND LATTICE CONSTANTS FOR ThC_2 by P. Gantzel and N. Baldwin (Genl. Dynamics); *Acta Cryst.*, Vol. 17, pp. 772-773, June 10, 1964

A set of indices for the powder pattern of ThC_2 is presented. Lattice parameters are: $a = 6.691$, $b = 4.231$, $c = 6.744$ Å; $\beta = 103^\circ 51'$. The lattice constants were obtained from an x-ray pattern recorded with $\text{CrK}\alpha$ radiation in a 114.6 mm Straumanis-loading Debye-Scherrer camera filled with hydrogen. Data were refined by analytical extrapolation on an IBM 7090.

24,936 GADOLINIUM AND DYSPROSIUM INTERMEDIATE PHASES. Part III. THE STRUCTURES OF Gd_3Al_2 , Dy_3Al_2 , Gd_5Ge_3 , Dy_5Ge_3 , AND DyAl_3 by N. Baenziger and J. Hegenbarth (State U. Iowa); *Acta Cryst.*, Vol. 17, pp. 620-621(L), May 10, 1964

The structures of Dy_3Al_2 and Gd_3Al_2 have been determined by x-ray diffraction analysis of arc-melted single crystal chips. The tetragonal cell constants are:

$$\text{Gd}_3\text{Al}_2; a = 8.344, c = 7.656 \text{ Å}, Z = 4$$

$$\text{Dy}_3\text{Al}_2; a = 8.164, c = 7.560 \text{ Å}, Z = 4.$$

Possible space groups are $\text{P4}_2\text{nm}$, P4n2 , $\text{P4}_2/\text{mm}$. Atomic positions are calculated and presented. The structures of Gd_5Ge_3 and Dy_5Ge_3 were determined by a combination of single-crystal and powder methods. The hexagonal cell dimensions are:

$$\text{for } \text{Dy}_5\text{Ge}_3; a = 8.438, c = 6.336 \text{ Å},$$

$$\text{for } \text{Gd}_5\text{Ge}_3; a = 8.546, c = 6.410 \text{ Å}.$$

Powder diagrams of DyAl_3 were also indexed with a hexagonal unit cell with $a = 6.097$; $c = 9.534$ Å.

24,937 A NEW STRUCTURE IN THE MAGNESIUM-RICH REGION OF THE CERIUM-MAGNESIUM SYSTEM by Q.C. Johnson, G.S. Smith, D.H. Wood, and E.M. Cramer (Lawrence Rad. Labs.); *Nature*, Vol. 201, p. 600, Feb. 8, 1964

A structure determination was undertaken to investigate CeMg_9 which had been indexed as cubic and a mixture of two phases. Diffraction data revealed an orthorhombic structure with $a = b = 10.33$ Å, $c = 77.5$ Å, and $c/a = 13\sqrt{3}$. Extinction rules were found to be unusual and are presented. The exact atom positions determined by a Patterson function are given.

24,938 CRYSTAL STRUCTURE OF Ta_5Ga_3 by E.I. Gladyshevskii, V.S. Telegns, and V.Ya. Markiv (Franko L'vorsk State U.); *Soviet Phys. Cryst.*, Vol. 8, pp. 738-740(L), May-June 1964

X-ray diffraction data for the compound Ta_5Ga_3 are presented. It is found that Ta_5Ga_3 possesses tetragonal symmetry, corresponding to the W_5Si_3 structural type. The ratio c/a is equal to 0.501, and $a = 10.208 \pm 0.004$ Å, $c = 5.116 \pm 0.004$ Å.

24,939 THE CRYSTAL STRUCTURE OF BORON TRIFLUORIDE DIHYDRATE by W.B. Bang and G.B. Carpenter (Brown U.); *Acta Cryst.*, Vol. 17, pp. 742-745, June 1964

The crystal structure of boron trifluoride dihydrate has been determined at 3°C by x-ray diffraction. The crystals belong to the monoclinic space group $\text{P2}_1/\text{c}$

and have cell dimensions

$$a = 5.606, b = 7.438, c = 8.683 \text{ Å}; \beta = 90.45^\circ.$$

$\text{BF}_3 \cdot 2\text{H}_2\text{O}$ appears to have a structure with one water molecule bonded to boron to form the molecular addition compound $\text{F}_3\text{B} \cdot \text{OH}_2$; the other water molecule links these together by means of hydrogen bonds. However, the ionic formulation $[\text{H}_3\text{O}]^+ [\text{BF}_3\text{OH}]^-$ cannot be entirely excluded by the diffraction evidence.

24,940 THE UNIT CELL AND SPACE GROUP OF $\text{SF}_3 \cdot \text{BF}_4$ by L. Calvert and J. Morton (Natl. Res. Council, Canada); *Acta Cryst.*, Vol. 17, p. 613(L), May 10, 1964

Single crystal x-ray data have been obtained to assist in the interpretation of electron spin resonance spectra of radiation damaged crystals of $\text{SF}_3 \cdot \text{BF}_4$. The crystals are orthorhombic and have the possible space groups Pnma (D_{2h}^{16}) and Pn2_1 (C_{2v}^2). The axial lengths of the unit cell are $a = 9.63$, $b = 5.77$, $c = 8.99$ Å. X-ray density is 2.34 gm cm^{-3} . There is a strong similarity between the observed crystallographic data for $\text{SF}_3^+ \cdot \text{BF}_4^-$ and the data published for NH_4IO_3 .

24,941 LATTICE PARAMETERS AND LATTICE ENERGIES OF HIGH PRESSURE POLYMORPHS OF SOME ALKALI HALIDES by C.E. Wier and G.J. Piermorini; *J. Res. Natl. Bureau Stand. (A)*, Vol. 68(A), pp. 105-111, Jan.-Feb. 1964

Lattice parameters of the high-pressure forms of the alkali halides are discussed. The lattice parameters were used to compare the lattice energies of the NaCl and CsCl type structures at the transition pressure. An analysis of the effect of experimental uncertainties on the calculated lattice energies showed that in almost every instance the Born-Mayer theory adequately accounts for the lattice energy of the high-pressure structure. Experimental technique consisted of diffracting a collimated beam of Mo K α x-rays by a thin layer of material squeezed between the flat surfaces of two diamonds. Diffraction rings are recorded photographically.

24,942 LATTICE CONSTANTS OF SOME DOUBLE SULPHATES $\text{M}_2\text{Co}(\text{SO}_4)_2 \cdot 6\text{H}_2\text{O}$ by P. Hartman, and C. Woensdregt (Geolog. en Mineral. Inst. der Rijksuniversiteit, Leiden); *Acta Cryst.*, Vol. 17, pp. 779-780, June 10, 1964

A table of lattice constants for four isomorphous cobalt double sulphates $\text{M}_2\text{Co}(\text{SO}_4)_2 \cdot 6\text{H}_2\text{O}$ (with $\text{M} = \text{K}, \text{Rb}, \text{NH}_4, \text{Cs}$) determined from powder x-ray photographs is presented. The reference lines used were from potassium aluminum alum with unit cell edge of 12.157 Å.

24,943 CRYSTALLOGRAPHIC DATA ON VO_2WO_4 AND VO_2MoO_4 by E. Juenke and S. Bartram (GE); *Acta Cryst.*, Vol. 17, p. 618(L), May 10, 1964

Double oxides of uranium with tungsten or molybdenum were prepared by calcining mixtures of their oxides, forming only the compounds VO_2WO_4 and VO_2MoO_4 . Powder diffractometry established a monoclinic crystal structure for both compounds with the lattice constants:

	VO_2WO_4	VO_2MoO_4
a	7.205 Å	7.200 Å
b	5.482 Å	5.480 Å
c	13.57 Å	13.59 Å
β	$104^\circ 35'$	$104^\circ 36'$
Volume	518.59 Å^3	518.96 Å^3

The space group was determined to be $\text{P2}_1/\text{c}$ and calculated densities are 6.63 and 5.50 g cm^{-3} for VO_2WO_4 and VO_2MoO_4 respectively.

Lattice Parameters of UC - See 24,879

24,944 THE CRYSTAL STRUCTURE OF LITHIUM METABORATE by W.H. Zachariasen (Argonne); *Acta Cryst.*, Vol. 17, pp. 749-751, June 1964

Lithium metaborate, LiBO_2 , is monoclinic, space group $\text{P2}_1/\text{c}$, with four molecules in a cell of dimensions $a = 5.838$, $b = 4.348$, $c = 6.449$ Å, $\beta = 115.12^\circ$, and all atoms in general positions. Refinement of the structure gave $R = 0.046$ and a precision of 0.008 Å for Li-O, 0.006 Å for B-O bonds. The structure contains endless chains of BO_3 triangles with Li-O bonds between chains.

24,945 CRYSTAL STRUCTURE OF SILICON OXYNITRIDE, $\text{Si}_2\text{N}_2\text{O}$ by C. Brosset and I. Idrestedt (Swedish Inst. for Silicate Res.); *Nature*, Vol. 201, p. 1211, Mar. 21, 1964

A method of producing pure powder and single crystals of a silicon oxynitride has been developed by heating silicon and quartz powder in nitrogen at

1450°C. The crystals of $\text{Si}_2\text{N}_2\text{O}$ have orthorhombic symmetry, corresponding to the space group $\text{Cmc}2_1$. Unit cell dimensions are:

$$a = 8.843 \text{ \AA}, \quad b = 5.473 \text{ \AA}, \quad c = 4.835 \text{ \AA}.$$

The silicon atom is tetrahedrally surrounded by one oxygen atom and three nitrogen atoms. Si-O-Si bond angle is 147° and Si-O and Si-N bond distances are 1.62 Å and 1.71 Å, respectively.

24,946 THE LATTICE PARAMETER AND ALPHA PHASE BOUNDARY OF FERRITIC IRON-ZINC ALLOYS by G. Speich, L. Zwell, and H. Wriedt (U.S. Steel); *Trans. Met. Soc. AIME*, Vol. 230, pp. 939-940(L), June 1964

The lattice parameter and the boundary of the α -phase in Fe-Zn alloys have been measured in order to determine the degree of segregation accompanying cellular precipitation over a wide composition range, and to evaluate the free energy change accompanying the growth of cells. The lattice parameters of the ferritic solid solutions were measured by x-ray diffractometry. The α -phase boundary was determined by use of two phase ($\alpha + \gamma$) aged alloys; solubility of zinc was obtained by measurement of the lattice parameter of the α -phase in these alloys. Results of measurements are compared to earlier determinations by other researchers.

Lattice Parameters of:

In-Pb and In-Sn Superconductors - See 25,282

$\text{Mo}_3\text{Al}_2\text{C}$ Superconductors - See 25,280

$\text{Rb}_x\text{K}_{1-x}\text{NO}_3$ - See 24,189

Crystal Structure of Te - See 24,903

24,947 X-RAY AND NEUTRON STUDIES OF THE LINEAGE STRUCTURE IN LARGE ALUMINUM SINGLE CRYSTALS by A. Modzejewski and S. Szarras (Inst. Nucl. Res., Warsaw); *Phys. Stat. Sol.*, Vol. 5, pp. K23-26, 1964

X-ray and neutron diffraction studies of the substructure of four large Al single crystals grown by the Bridgman technique are reported. Neutron rocking curves for Al in the horizontal and vertical axis are found to be quite different. From these curves it is concluded that the position of the crystal influences broadening and the neutron intensity.

24,948 DIRECT OBSERVATION OF DOUBLE BRAGG REFLECTIONS IN X-RAY DIFFRACTION PATTERNS OF PYROLYTIC GRAPHITES by O.J. Guentert (Raytheon Res. Div.); *J. Appl. Phys.*, Vol. 35, pp. 1841-1847, June 1964

Several spurious peaks observed in the x-ray diffraction patterns of bulk specimens of pyrolytic graphites (PG) have been identified as double Bragg peaks. Their angular position is described by $2\theta_{hk\parallel} + 2\theta_{h'k'\perp}$, where $\theta_{hk\parallel}$ and $\theta_{h'k'\perp}$ are the Bragg angles of the participating single reflections. The intensity dependence of the peaks on the specimen shape and the specimen orientation is distinctly different from that of single Bragg reflections, but agrees well with predictions based on double Bragg reflections. The concentrations of doubly reflected power which give rise to the unexpected peaks are due to the highly preferential alignment of crystallites. It has been known for some time that double Bragg reflections from polycrystalline samples may be sufficiently strong to contribute significantly to the small-angle scattering of x-rays. The present study demonstrates that in favorably textured specimens they may even become strong enough to show up as peaks in normally recorded diffraction patterns. Techniques are described by which such peaks can be distinguished from single Bragg reflections.

24,949 STRUCTURAL FEATURES OF CARBON AND GRAPHITE by E.A. Kellert and H.P. Rooksby; *G.E.C. J.*, Vol. 31, pp. 28-36, No. 1, 1964

A number of aspects of the crystal structure of carbons and graphite are reviewed. Attention is drawn to the chief parameters which may be measured by x-ray diffraction and which are used in studies of graphitization phenomena. Thermal expansion of the graphite lattice has been investigated over a wide range of temperatures from -196°C to 2600°C . Changes in interlayer spacing follow a quadratic relation over the range 0° to 2600°C , and the rate of change is not noticeably affected by the disorder condition or p parameter. At low temperatures, the disorder parameter has some influence on the rate of change as well as on the limiting distance of approach of the layer planes. The much smaller thermal expansion and contraction parallel to the layer planes has also been measured, and notable behavior has been demonstrated. Results of measurements of the amplitude of vibration of carbon atoms perpendicular to the layer planes show that the amplitude increases with temperature at a greater rate than the interlayer spacing. Thus the mean free space between layers would appear to be progressively reduced as the temperature is increased and this could, in some measure, explain the increase of mechanical strength known to occur at high temperatures.

24,950 ON FORBIDDEN REFLECTION SPOTS AND UNEXPECTED STREAKS APPEARING IN ELECTRON DIFFRACTION PATTERNS FROM HEXAGONAL COBALT by S. Fujime, D. Watanabe and S. Ogawa (Tohoku U., Japan);

J. Phys. Soc. Japan, Vol. 19, May 1964

Using thin sections of hexagonal cobalt, the origin of the appearance of some of forbidden reflection spots and some of unexpected streaks has been studied by the selected area diffraction technique. The spots are forbidden by the space group symmetry and the streaks are not expected from stacking faults. The experimental results lead to the conclusion that the reflection spots in question which are forbidden also dynamically in the symmetrical case are observed because of bending of a specimen film and the streaks in question are caused by the dynamical interaction of other streaks due to stacking faults and normal reflections.

24,951 OBSERVATION OF SOLID NEON BY TRANSMISSION ELECTRON MICROSCOPY by M. Goringe and V. Valdre (Cavendish Lab., England); *Philosophical Mag.*, Vol. 9, pp. 897-900(L), May 1964

Observations by transmission electron microscopy and by transmission electron diffraction have been made on neon deposited on various substrates at temperatures as low as 10°K . During deposition of neon crystals on carbon, the flake-like crystals could be seen to grow and coalesce. Structure and lattice parameters deduced from a diffraction pattern agree with published results (fcc, $a = 4.54 \text{ \AA}$). However, diffraction rings do display extra 'hexagonal' rings, presumably due to the presence of stacking faults of both intrinsic and extrinsic nature.

24,952 SINGLE-CRYSTAL STUDIES OF $\beta\text{-F}_2$ AND $\gamma\text{-O}_2$ by T. Jordan, W. Streib, H.W. Smith, and W. Lipscomb (Harvard U.); *Acta Cryst.*, Vol. 17, pp. 777-778, June 10, 1964

X-ray diffraction studies of single crystal $\beta\text{-F}_2$ and $\gamma\text{-O}_2$ at 50°K are discussed. Both phases have the same structure type which makes untenable any description of $\gamma\text{-O}_2$ based on dimers of O_2 . Unit cell dimensions are $a = 6.67 \text{ \AA}$ for $\beta\text{-F}_2$ and $a = 6.38 \text{ \AA}$ for $\gamma\text{-O}_2$. There are eight diatomic molecules in the unit cell. Results indicate an orientationally disordered structure in space group $\text{Pm}3\text{n}$. The existence of a major transition from $\beta\text{-F}_2$ to $\alpha\text{-F}_2$ at 45.55°K was verified. Presence of infinite linear chains of O_2 molecules, consistent with the very short range interactions suspected by Kanda et al., was noted.

24,953 STRUCTURAL RELATIONSHIPS IN BERYLLIUM-TITANIUM ALLOYS by E. Gilliam, and H. Rooksby (GE, Wembley), and L. Brownlee (Assoc. Electric Ltd., Manchester); *Acta Cryst.*, Vol. 17, p. 762, June 10, 1964

Data on the structure of Be-Ti alloys are discussed. Be_{12}Ti is found to be tetragonal; $\text{Be}_{17}\text{Ti}_2$ is based on a similar primitive cell of hexagonal symmetry. Be_{12}Ti probably belongs to the space group I_4/mmm . It appears that the transition from Be_{12}Ti to $\beta\text{-Be}_{17}\text{Ti}_2$ is a simple one in which the $[010]_\text{T}$ direction becomes the $[0001]_\text{H}$ direction.

24,954 STRUCTURES IN CHROMIUM-NICKEL ALLOYS AT HIGH TEMPERATURE by D. Bare, E. Gibson, and O. Carlson (Iowa State U.); *Trans. Met. Soc. AIME*, Vol. 230, pp. 934-936(L), June 1964

An investigation of the equilibrium structures of Cr-Ni alloys at elevated temperatures has been conducted by x-ray diffractometry to elucidate the structures present in the system. Cr-27 at.pct Ni and C_{2-40} at.pct Ni alloys were prepared by inert gas arc melting. The only phases observed in either of these alloys in the temperature range 600° to 1260°C were a bcc and an fcc phase corresponding to a solid solution of nickel in chromium and chromium in nickel. Lattice parameters changes with temperature are discussed.

24,955 THE CRYSTALLOGRAPHY OF ANTHRACENE AT 95°K AND 290°K by R. Mason (Imperial Coll. Sci. and Tech., London); *Acta Cryst.*, Vol. 17, pp. 547-555, May 10, 1964

X-ray data, at both 290°K and 95°K , of high internal consistency, are reported together with the results of a number of detailed least-squares refinement analyses. The observed bond lengths, with an average estimated standard deviation of 0.008 Å, are compared with those predicted theoretically by a number of procedures and previous comparisons and suggestions are examined critically. The expansion coefficients of the crystal are markedly anisotropic and, together with the x-ray diffuse scattering, are discussed in relation to rigid body molecular vibrations and molecular reorientation in the lattice on cooling; this latter feature also provides an explanation for the temperature dependence of the principal crystal diamagnetic susceptibilities.

24,956 THE CRYSTAL STRUCTURE OF LITHIUM HYDRAZINIUM SULFATE by I.D. Brown (McMaster U.); *Acta Cryst.*, Vol. 17, pp. 654-660, June 1964

At room temperature, lithium hydrazinium sulfate, $\text{Li}(\text{N}_2\text{H}_5)\text{SO}_4$, is orthorhombic, space group $\text{Pbn}2_1$, with $a = 8.99$, $b = 9.94$, $c = 5.18 \text{ \AA}$, and $Z = 4$. The structure has been determined by x-ray diffraction and has been refined to give an R index ($\sum |F_o - F_c| / \sum |F_o|$) of 0.11. The lithium and sulfur atoms are at the centers of tetrahedra of oxygen atoms. The tetrahedra share apices to form a three-dimensional framework containing channels running parallel to

the c axis. The hydrazinium ions lie in these channels and are linked into infinite chains by hydrogen bonding between their NH_2 groups. The electrical properties of the crystal appear to be related to the movement of protons within this chain.

24,957 THE CRYSTAL STRUCTURE OF FERROELECTRIC LITHIUM HYDRAZINIUM SULFATE by J.H. Van Den Hende (Esso Res. and Engrg.) and H. Boutin (Brookhaven Lab.); *Acta Cryst.*, Vol. 17, pp. 660-663, June 1964

The crystal structure of lithium hydrazinium sulfate has been determined by the heavy atom method from 0kl, h0l and hk0 data. Bond lengths and angles based on three-dimensional data are given, esd 0.008 Å and 1° . The N-N distance found is 1.447 Å, which corresponds to previously reported values for the N_2H_5^+ ion. The nitrogen atoms form in the direction of the c axis an infinite hydrogen-bonded zigzag chain of the type NH-N with a distance of 3.018 Å. The length of one of the S-O bonds is 1.557 Å, which is considerably longer than the normally accepted value for that ion. That of another bond is 1.430 Å, which indicates a large amount of double bond character. The structure is held together by three-dimensional network of weak hydrogen bonds. Tentative positions of the hydrogen atoms are assigned.

24,958 THE CRYSTAL STRUCTURE OF SODIUM BROMIDE DIHYDRATE by W.R. Haaf and G.B. Carpenter (Brown U.); *Acta Cryst.*, Vol. 17, pp. 730-732, June 1964

$\text{NaBr} \cdot 2\text{H}_2\text{O}$ is monoclinic, $\text{P}2_1/\text{c}$, $Z = 4$, with $a = 6.575$, $b = 10.456$, $c = 6.776$ Å and $\beta = 113.38^\circ$. The structure agrees very well with that determined independently by Culot, Piret and Van Meersche (1962); the differences are attributed chiefly to different absorption errors.

24,959 COORDINATION OF COBALT IN DOPED NaCl, NaBr AND KCl CRYSTALS by M.E. Hills (U.S. Naval Ordn. Test Sta.); *J. Phys. Soc. Japan*, Vol. 19, p. 760, May 1964

Cobalt-doped KCl, NaCl and NaBr crystals have been grown by the Kyropoulos method in a helium atmosphere and their absorption in the visible region of the spectrum has been measured in an attempt to determine the nature of the lattice sites occupied by the cobalt ions. In both the cobalt-doped KCl and NaBr the absorption spectrum is characteristic of the respective tetrahedral ion. An examination of a lightly doped homogeneous NaCl:Co crystal revealed that it is not likely that an appreciable fraction of the cobalt present in the crystal is in the positions surrounded by a tetrahedral arrangement of chloride ions.

24,960 THE UNIT CELLS AND SPACE GROUPS OF SeCl_4 AND TeCl_4 by A. Cordes, R. Kruh, E. Gordon, and M. Kemp (U. Arkansas); *Acta Cryst.*, Vol. 17, p. 756, June 10, 1964

Data on SeCl_4 and TeCl_4 are presented. Selenium tetrachloride was prepared by the direct reaction of chloride with gray powdered selenium. Weissenberg photographs made with $\text{CuK}\alpha$ radiation indicate an orthorhombic unit cell with $a = 23.0$, $b = 16.5$, $c = 23.5$ Å. The experimental density is 2.7 gm cm^{-3} . The space group is either Bmb or Bb-b . Tellurium tetrachloride was prepared by the direct reaction of chlorine with tellurium metal: $a = 15.0$, $b = 10.0$, $c = 15.3$ Å; $\beta = 117^\circ$. The experimental density is 3.12 gm cm^{-3} . The space group is $\text{C}2/\text{c}$ or Cc .

24,961 A LEAST-SQUARES REFINEMENT OF THE CRYSTAL STRUCTURE OF TRICAESIUM PENTACHLOROCOBALT (II), Cs_3CoCl_5 by B.N. Figgis (U. Western Australia), and M. Gerloch and R. Mason (Imperial Coll., London); *Acta Cryst.*, Vol. 17, pp. 506-508, May 10, 1964

Bond lengths (esd 0.013 Å) and bond angles (esd 0.4°) are reported for the $[\text{CoCl}_5]^{2-}$ ion from a least-squares analysis of the three-dimensional x-ray data of Cs_3CoCl_5 . Axial distortions in the approximately tetrahedral ligand arrangement are discussed and compared with those in other transition metal complexes.

24,962 NEUTRON DIFFRACTION INVESTIGATION OF U_3O_8 by B.O. Loopstra (Reactor Centrum Nederland, Petten); *Acta Cryst.*, Vol. 17, pp. 651-654, June 1964

A polycrystalline sample of orthorhombic U_3O_8 has been investigated by neutron diffraction in order to resolve discrepancies between previous single-crystal x-ray and powder neutron investigations. The space group is $\text{Amm}2$ (C_{2v}^4). The uranium atoms are surrounded by six oxygen atoms in close contact at distances between 2.07 and 2.23 Å, with a seventh oxygen atom at 2.44 Å for the U(1) atom and at 2.71 Å for the U(2) atom.

24,963 THE CRYSTAL STRUCTURE OF URANYL DIHYDROXIDE, $\text{UO}_2(\text{OH})_2$ by R.B. Roof, Jr., D.T. Cromer and A.C. Larson (Los Alamos Lab.); *Acta Cryst.*, Vol. 17, pp. 701-705, June 1964

As a result of single-crystal structure analysis it has been determined that the material usually designated as uranium trioxide with one molecule of water of hydration, $\text{UO}_3 \cdot \text{H}_2\text{O}$, should be described chemically as uranyl dihydroxide, $\text{UO}_2(\text{OH})_2$. The orthorhombic unit cell has the dimensions

$$a = 5.635 \pm 0.007, b = 6.285 \pm 0.008 \text{ and } c = 9.919 \pm 0.008 \text{ Å.}$$

There are four formula units per unit cell and the space group was uniquely determined from the systematic extinctions to be Pbca . In the least-squares refinement of the structure, a secondary extinction parameter, real and imaginary portions of the anomalous dispersion, and anisotropic thermal parameters were used. The structure can be described as composed of layers that are hydrogen-bonded together, the hydrogen-bond distance being 2.69 Å. The layers are constructed by octahedra which share corners in order to build and expand the layer. Each octahedron contains a central uranium atom, two uranyl oxygen atoms and four hydroxyl oxygen atoms.

24,964 THE CRYSTAL STRUCTURE OF UF_4 by A.C. Larson, R.B. Roof, Jr., and D.T. Cromer (Los Alamos, Lab.); *Acta Cryst.*, Vol. 17, pp. 555-558, May 10, 1964

The crystal structure of UF_4 has been determined from single-crystal x-ray data. The monoclinic unit cell has the dimensions $a = 12.73$, $b = 10.75$, $c = 8.43$ Å and $\beta = 126^\circ 20'$; space group $\text{C}2/\text{c}$. It contains twelve formula units per unit cell. These cell dimensions are identical with those of Shankar, Khubchandani and Padmanabhan (1957). In the least-squares refinement of the structure a secondary extinction parameter and the real and imaginary portions of the anomalous dispersion corrections were used. Normal interatomic distances were observed. Uranium atoms have as neighbors eight fluorine atoms arranged in a slightly distorted antiprism configuration.

24,965 A METHOD FOR THE DETERMINATION OF COMPLEX CUBIC METAL STRUCTURES AND ITS APPLICATION TO THE SOLUTION OF THE STRUCTURE OF NaCd_2 by S. Samson (Calif. Inst. Tech.); *Acta Cryst.*, Vol. 17, pp. 491-495, May 10, 1964

Structures of intermetallic compounds of certain cubic space groups can be completely surveyed or determined with the use of a single map, the packing map, apparently irrespective of the size of the unit cell and the number of parameters involved. For certain cubic space groups two or perhaps three packing maps will have to be used. Sections through coordination polyhedra represented with transparent templates can be fitted together on the packing map which then guides the search for a reasonable structural motif. This technique is of particular value if the atomic arrangement is such as to render the interpretation of Patterson maps extremely difficult. The structure of NaCd_2 (cube edge $a_0 = 30.56$ Å, space group $\text{Fd}3\text{m}$ (O_h^7)) was derived with the use of a single packing map, avoiding the time-consuming construction of three-dimensional models.

24,966 THE ZnSb STRUCTURE; A FURTHER ENQUIRY by F.L. Carter and R. Mazelsky (Westinghouse Res. Lab.); *J. Phys. Chem. Solids*, Vol. 25, pp. 571-581, June 1964

A redetermination of the crystal structure of ZnSb was undertaken to resolve the question raised by a short Zn-Zn distance previously reported. The result (Zn-Zn distance = 2.81 Å) is in agreement with that found by Toman, who employed a diffractometer and a powder sample. From the bond distances a calculation of the bond orders and valences by the method of Pauling for intermetallic compounds leads to the interpretation of ZnSb as an electron transfer compound with Zn^{-1} having a valence of three and Sb^{+1} having a valence of four. The transference of approximately one electron from Sb to Zn permits better binding through the increased valence of both atoms. In the case of the Zn-Zn interaction it appears likely that a repulsive force exists between the atoms; however, it is not certain whether the force is that due to the close approach of nonbonded atoms or that of a bond in compression. With this uncertainty in mind the effects of normal twinning and polytype formation are discussed as a possible explanation of reported phase transformation. Using a single crystal and a modified powder camera the cell edges were determined at $28.4 \pm 2^\circ\text{C}$ to be $a_0 = 6.202$ Å, $b_0 = 7.742$ Å, $c_0 = 8.100$ Å.

24,967 THE ThAl_2 - ThMn_2 SYSTEM by J.H. Wernick and R.R. Soden (Bell Labs.); *J. Phys. Chem. Solids*, Vol. 25, pp. 449-450(L), Apr. 1964

Th is the only actinide element presently known not to form a Laves phase with Al. The intermediate phase ThAl_2 has the hexagonal AlB_2 structure-type although the reason for this formation is not clear. There is a close relationship between the AlB_2 structure-type and the Laves phases of the actinide elements; ThAl_2 and ThMn_2 (C-14) form a true ternary Laves phase with the MgCu_2 structure-type. Small amounts of Mn change the electronic structure of ThAl_2 to stabilize the C-15 structure. This stabilization probably arises through an electron transfer mechanism which effectively increases the size of Al and decreases the size of Th in ThAl_2 .

24,968 SOME TERNARY THALLIUM CHALCOGENIDES by C. Crevecoeur (U. Leyden, Netherlands); *Acta Cryst.*, Vol. 17, p. 757, June 10, 1964

Data on the structure of some ternary thallium chalcogenides are presented. The x-ray powder diagrams can be indexed on a cubic body-centered lattice containing two formula units Tl_2BX_4 per unit cell ($B = V, Nb, Ta$; $X = S, Se$). The space group is $I43m$ or one of its subgroups.

24,969 BISMUTH SUBSTITUTION IN YTTRIUM IRON ALUMINUM GARNETS by S. Geller, H.J. Williams, R.C. Sherwood, and G.P. Espinosa (Bell Labs.); *J. Appl. Phys.*, Vol. 35, pp. 1754-1756, June 1964

Magnetic, crystallographic, and preparative data are reported on the system $\{Y_{2.75}Bi_{0.25}\}Fe_5-xAl_xO_{12}$ for values of x to 1.50. For large x there appear to be differences in $0^\circ K$ magnetic moment between this system and the straight yttrium analog, which imply that the replacement of Y^{3+} by the larger Bi^{3+} ions favors occupation of the tetrahedral sites by the smaller Al^{3+} ions. The replacement of Y^{3+} by Bi^{3+} ions leads to the reduction of the preparation temperature of aluminum substituted iron garnets by about $350^\circ C$.

24,970 THE CRYSTAL STRUCTURES OF MAGNESIUM FORMATE DIHYDRATE AND MANGANOUS FORMATE DIHYDRATE by K. Osaki, Y. Nakai and T. Watanabe (Osaka U.); *J. Phys. Soc. Japan*, Vol. 19, pp. 717-723, May 1964

Magnesium and manganous formate dihydrates crystallize in the space group $P2_1/c$, with the unit cell dimensions:

$$a = 8.69, b = 7.18, c = 9.39 \text{ \AA}, \beta = 97.6^\circ \text{ (for the magnesium salt),}$$

$$a = 8.86, b = 7.29, c = 9.60 \text{ \AA}, \beta = 97.7^\circ \text{ (for the manganous salt).}$$

There are two kinds of magnesium (or manganous) ions in the unit cell. The first kind is surrounded by six carboxyl oxygen atoms and the second kind by two carboxyl oxygen atoms and four water molecules, both in a regular octahedral form.

24,971 THE STRUCTURAL ANALYSIS OF TWO DIMENSIONAL DEFECT ORDERED OD-STRUCTURE: THE STRUCTURES MEASUREMENT OF SODIUM TETRA METAPHOSPHATE $Na_2H_2P_4O_{12}$ [in German] by K. Dornberger-Schiff (Deutschen Akad. Wissensch., Berlin-Adlershof); *Acta Cryst.*, Vol. 17, pp. 482-491, May 10, 1964

X-ray diagrams of $Na_2H_2P_4O_{12}$ exhibit sharp reflexions as well as diffuse streaks or spots corresponding to diffuse platelets lying in parallel planes in reciprocal space and indicating two-dimensional disorder. The investigation started from the assumption that the structure may be classified as an OD-structure consisting of equivalent rods, the direction of periodicity of all rods being the same. One groupoid family was found to be consistent with the observed distribution (in reciprocal space) of diffuse planes and sharp points, the systematic absences and the symmetry of the intensity distribution of the sharp reflexions on the one hand, and of the maxima on the diffuse planes on the other hand. The sharpness of the maxima indicates the presence of regions corresponding to a structure of maximum degree of order. There are two alternative possibilities compatible with the known xy electron density projection and the atomic distances known approximately from other structures: phosphate rings of 4 tetrahedra and phosphate chains periodic after 4 tetrahedra. For each of these alternatives there are again two alternative possibilities for the prevalent structure of maximum degree of order. It is shown how the values of the intensity maxima on the diffuse platelets may be used to obtain generalized Patterson projections and electron density projections of a hypothetical structure which is closely related to the real structure. Thus a method for distinguishing between the four possibilities quoted and for further refinement of the structure is obtained.

24,972 PREPARATION AND CRYSTALLOGRAPHIC PROPERTIES OF $A^{2+}B_2^{3+}O_4$ TYPE CALCIUM AND STRONTIUM SCANDATES by J. Carter and R. Feigelson (Sperry Rand Res. Ctr.); *J. Am. Ceram. Soc.*, Vol. 47, pp. 141-144, Mar. 21, 1964

The compounds $CaSc_2O_4$ and $SrSc_2O_4$ have been synthesized by solid-state reaction of the component oxides at temperatures ranging from 950° to $1400^\circ C$. Both calcium and strontium monoscatates are orthorhombic and analogous to $CaFe_2O_4$. Lattice parameters for $CaSc_2O_4$ are $a_0 = 9.461$, $b_0 = 11.122$, $c_0 = 3.143$ and for $SrSc_2O_4$ are $a_0 = 9.698$, $b_0 = 11.302$, $c_0 = 3.185$. Based on four molecules per unit cell, the x-ray density for $CaSc_2O_4$ is 3.89 g cm^{-3} and that for $SrSc_2O_4$ is 4.59 g cm^{-3} .

24,973 AN ANOMALY IN THE CRYSTAL STRUCTURE OF Na_2CO_3 by E. Bruns, J. Visser, and P. de Wolff (Tech. Hog. Delft.); *Acta Cryst.*, Vol. 17, p. 614(L), May 10, 1964

Indexing the powder pattern of anhydrous sodium carbonate has proved to be uncommonly difficult. A C-centered monoclinic unit cell is indicated by powder diffractometry and single crystal rotation. About 20 pct of the powder

lines (mostly weak intensity) are not explained, even on the basis of a multiple cell. This anomaly is described for the single crystal pattern (weak extra satellite spots) in terms of reciprocal space. An investigation of the structures of higher temperature transition phases is in progress.

24,974 THE CRYSTAL STRUCTURE AND MAGNETIC PROPERTY OF $GdCoO_3$ by K. Aso and S. Miyahara (Hokkaido U.); *J. Phys. Soc. Japan*, Vol. 19, pp. 778-779, May 1964

The crystal structure and magnetic nature of $GdCoO_3$ have been determined. $GdCoO_3$ was found to have an orthorhombic structure with lattice parameters $a = 5.23 \text{ \AA}$, $b = 5.40 \text{ \AA}$ and $c = 7.45 \text{ \AA}$. Magnetic measurements made from liquid nitrogen to room temperature showed the Curie constant to be 7.9 per gram atom, implying that interactions between cations $Co^{3+} - Co^{3+}$, $Co^{3+} - Gd^{3+}$ and $Gd^{3+} - Gd^{3+}$ are unlikely. It was also concluded that Co^{3+} ion is nonmagnetic all magnetic properties coming solely from Gd^{3+} ions.

24,975 ELECTRON-DIFFRACTION STUDY OF THE CRYSTAL STRUCTURE OF $BiFeO_3$ by Yu. Ya. Tomashpol'skii, Yu. N. Venevsev and G.S. Zhdanov (Kar'pov Inst. of Phys. Chem.); *Soviet Phys. Doklady*, Vol. 8, pp. 1144-1145 (L), June 1964

The crystal structure of $BiFeO_3$ has been studied by the electron diffraction method. It is found that $BiFeO_3$ has a structure of perovskite type with rhombohedral distortion and Bi and Fe are displaced along a body diagonal in $BiFeO_3$. The diffraction pattern also indicates that this compound may be assigned to the space group $R3m$, and the oxygen atoms are at the centers of the faces in the perovskite cell.

24,976 ALKALI TITANONILOBATES: THE CRYSTAL STRUCTURES OF $KTiNbO_5$ AND KTi_3NbO_9 by A.D. Wadsley (C.S.I.R.O. Chem. Res. Lab., Melbourne); *Acta Cryst.*, Vol. 17, pp. 623-628, June 1964

Two orthorhombic alkali titanoniobates $KTiNbO_5$ and KTi_3NbO_9 have been prepared and described. The first, with the space group $Pnma$ and the unit-cell dimensions

$$a = 6.459, b = 3.792, c = 18.472 \text{ \AA},$$

is a layer structure, where each sheet consists of double zigzag strings of octahedra sharing corners. These are bonded through potassium ions in distorted cubic environments. A limited examination of KTi_3NbO_9 , which is isomorphous with $BaTi_4O_9$ (Lukaszewicz, 1957) gave the space group $Pnmm$ for the unit cell

$$a = 6.392, b = 3.785, c = 14.865 \text{ \AA}.$$

The crystal chemistry of the two compounds is discussed.

24,977 THE CRYSTAL STRUCTURE OF $CaPd_3O_4$ by R. Wnuk, T. Touw (IBM Poughkeepsie) and B. Post (Polytechnic Inst., Brooklyn); *IBM J. Res. and Dev.*, Vol. 8, pp. 185-186(L), Apr. 1964

Experiments to determine the crystal structure and electrical properties of an oxide of calcium and palladium, $CaPd_3O_4$, are described. X-ray powder data indicated a $Pm3n$ structure with 2Ca, 6Pd, and 8O atoms. A room temperature resistivity of about 0.2 ohm-cm was measured which increased with decreasing temperature to about 3 ohm-cm at liquid nitrogen temperature. The thermoelectric effect indicated that the current carriers were positive. The Hall coefficient could not be measured and thus was known to be below $3 \text{ cm}^3/\text{coulomb}$. These preliminary electrical measurements indicate that the new compound is a p-type semiconductor.

24,978 CRYSTAL STRUCTURE AND THE DIELECTRIC PROPERTIES OF $K_2O \cdot 2Ta_2O_5$ by E. Sawaguchi and A. Kikuchi (Sony Corp.); *J. Phys. Soc. Japan*, Vol. 19, p. 579, Apr. 1964

Several specimens of $K_2O \cdot nTa_2O_5$ were synthesized by firing a mixture of K_2CO_3 and Ta_2O_5 . Debye-Scherrer photographs indicate $2.5 > n \geq 1.8$. In order to determine the structure, single crystals were grown; these were tetragonal with lattice parameters $a = b = 12.574 \text{ \AA}$, $c = 3.969 \text{ \AA}$. The structure is shown to be the tungsten bronze type. The dielectric constant at 1 kc/sec was measured and is about 50 with almost no temperature dependence in the range 4° to $500^\circ K$.

24,979 NOTE ON CALCIUM-ORTHOVANADATE by L. Brixner, P. Flournoy, and K. Babcock (E.I. du Pont); *J. Electrochem. Soc.*, Vol. 111, pp. 873-874, July 1964

The properties of single crystal $Ca_3(VO_4)_2$ produced by the Czochralski technique are studied. Although polycrystalline $Ca_3(VO_4)_2$ is practically colorless, single crystals have a very light orange-yellow color indicating that the VO_4^{3-} group may be slightly colored intrinsically. X-ray examination of a section cut from a 10 cm crystal yielded: $a_0 = 8.35$, $b_0 = 10.77$, $c_0 = 7.00 \text{ \AA}$; $\beta = 95.0^\circ$. The most probable space group is $C_{2h}^2 C 2/c$; x-ray density determination yields 3.55 g ml^{-1} . Ca^{+2} can be easily introduced into the lattice of

$\text{Ca}_3(\text{VO}_4)_2$ if electrical neutrality is restored by compensation with Na^{+1} as in $\text{Ln}_x^{+3}\text{Na}_x^{+1}\text{Ca}_{3-2x}(\text{VO}_4)_2$. An intense fluorescence emission at 1.063μ is observed at -196°C from Na^{3+} doped $\text{Ca}_3(\text{VO}_4)_2$ when sodium compensation is used.

Crystal Structure of:

BaTiO_3 - See 25,090

BaTiO_3 and Ba-SrTiO_3 - See 25,250

CdTe-CdSe - See 25,168

CRYSTAL IMPERFECTIONS

POINT DEFECTS (VACANCIES AND INTERSTITIALS)

24,980 DISTRIBUTION FUNCTIONS FOR THE NUMBER OF DISTINCT SITES VISITED IN A RANDOM WALK ON CUBIC LATTICES: RELATION TO DEFECT ANNEALING by J.R. Beeler, Jr. (GE, Cincinnati); *Phys. Rev.*, Vol. 134A, pp. A1396-A1401, June 1, 1964

Distribution functions for the number of distinct sites $S(n)$ visited by a point defect executing a symmetric random walk of n jumps on two- and three-dimensional lattices were computed using the Monte Carlo method. The square planar, simple cubic, bcc, and fcc lattices were treated. In three dimensions, the normal distribution appears to describe $S(n)$ for $n > 10^4$ jumps and at 10^4 jumps the derivative $dS(n)/dn$ of the average number, $\bar{S}(n)$, of distinct sites is within 0.5% of the value given by Vineyard's exact asymptotic solution. The defect annealing rate was computed using the $S(n)$ distribution in a simple example and this result compared with an analog Monte Carlo solution. The comparison indicated that fluctuation in the initial defect concentration must be considered in computing the initial annealing rate and the mobile defect concentration as a function of time. After 500 jumps the annealing rate, but not the concentration, can be closely approximated without according for fluctuations in the initial concentration.

24,981 POINT DEFECT CONFIGURATIONS IN IRRADIATED IRON-CARBON ALLOYS by R.A. Johnson and A.C. Damask (Brookhaven Lab.); *Acta Metal.*, Vol. 12, pp. 443-445, Apr. 1964

Computer techniques have been applied to obtain information related to atomic configurations around point defects in irradiated Fe-C alloys. The calculations, which were based on minimization of the energy of an array of lattice atoms, yielded estimates of migration and binding energies for various configurations. These in turn allowed estimates of temperature of formation and dissociation and prediction of possible internal friction effects. The model of a split iron interstitial suggested by previous experimental work was further supported. A possible sequence of processes involved in migration and trapping of irradiation produced defects is outlined.

24,982 PRODUCTION OF DEFECTS IN CADMIUM SULPHIDE BY ^{60}Co GAMMA RAYS by G.F.J. Garlock, F.J. Bryant and A.F.J. Cox (The U., Hull); *Proc. Phys. Soc.*, Vol. 83, pp. 967-970, June 1964

Marked changes in the infra-red emission bands of cadmium sulphide phosphors have been observed after irradiation with ^{60}Co gamma rays. The computed number of displayed atoms by direct production of defects from the ordered lattice is much smaller than for electron bombardment experiments and suggests a Seitz mechanism for defect formation.

24,983 A RELATION BETWEEN DARK FIELD ELECTRON MICROGRAPHS OF LATTICE DEFECTS by C.J. Ball (U. Sheffield); *Philosophical Mag.*, Vol. 9, pp. 541-544, Apr. 1964

It is shown that at the Bragg angle in the two-beam approximation, dark field electron micrographs of deformed crystals with displacement functions $R(z)$ and $R_0 + R(t - z)$ are identical. Three examples of pairs of deformed crystals satisfying this relation are discussed.

24,984 OBSERVATION OF ELECTRON-IRRADIATION DAMAGES IN LiF SINGLE CRYSTAL BY ELECTRON MICROSCOPE by K. Tanaka, M. Mannami, K. Izumi, and O. Akisue (Kyoto U., Japan); *Japanese J. Appl. Phys.*, Vol. 3, pp. 164-165(L), Mar. 1964

Electron microscopic observation of LiF single crystals is discussed. It is concluded that lens-shaped voids considered to be a coagulation of point defects are produced by electron irradiation. These voids grow to be about 1000 Å in diameter when more than 5 Coulombs/cm² electrons are used. Electron micrographs are included.

Defects in GaSb - See 25,042

24,985 X-RAY OBSERVATION OF ZINC-INDUCED DEFECTS IN GALLIUM ARSENIDE SINGLE CRYSTALS by G.H. Schwuttke and H. Rupprecht (IBM Watson Res. Ctr.); *Bull. Am. Phys. Soc.*, Vol. 9, p. 543(A), June 1964

Gallium arsenide single crystals of [001] orientation have been investigated for perfection through x-ray-diffraction microscopy. The crystals were boat-grown (doped with Se or Te) and x-ray measurements were made before and after diffusion of high zinc concentration. Measurements indicate that such crystals are of high perfection, and that zinc diffusion generates a large number of defects in the crystals. The diffusion-induced defects form characteristic grid patterns; the grids are composed of lines in [110] and $[\bar{1}\bar{1}0]$ directions. The diffraction contrast of the defect lines is strongly reflection-dependent. The fault vectors are in $[1\bar{1}0]$ and $[110]$ directions, respectively. X-ray results are interpreted in terms of Lomer and Lomer-Cottrell dislocations.

24,986 STUDY OF DEFECT MOBILITY IN IRRADIATED SEMICONDUCTORS by P. Baruch et al (Ecole Nor. Sup., Paris); in *Radiation Damage in Semiconductors*, Contract AF 61(052)-543, pp. 11-13, July 23, 1963; *STAR*, Vol. 2, p. 1297(A), May 23, 1964 AFCRL-63-578; AD-433042

Radiation-induced defects in silicon can drift in the electric field of a p-n junction, as in germanium. At 288°K , there is drifting of defects with different charges, the acceptor type (negatively charged) being the slower. At 350°K , only acceptor type defects are seen to move, with a mobility of 2×10^{-14} cm²/v-sec.

24,987 INTERSTITIALS AND VACANCIES IN α IRON by R.A. Johnson (Brookhaven Lab.); *Phys. Rev.*, Vol. 134A, pp. A1329-1336, June 1, 1964

The migration energies and atomic configurations for mono- and di-interstitials and mono- and di-vacancies in α iron have been calculated using a classical model. About 530 atoms surrounding the defect were treated as individual particles, each with three degrees of freedom, while the remainder of the crystal was treated as an elastic continuum with atoms imbedded in it. A two-body central force was devised which matched the elastic moduli, was sharply repulsive at close separation, and which went to zero midway between the second and third neighboring atoms. Calculated activation energies for motion of mono- and di-interstitials and mono- and di-vacancies were 0.33, 0.18, 0.68, and 0.66 eV, respectively, and binding energies of di-interstitials and di-vacancies were 1.08 and 0.20 eV, respectively. The stable interstitial was a "split" configuration in which two atoms were symmetrically split in a $\langle 110 \rangle$ direction about a vacant normal lattice site, and the stable di-interstitial consisted of two parallel split interstitials at nearest-neighbor lattice sites with their axes perpendicular to the line joining their centers. In the vacancy configuration an atom was missing from a normal lattice site, and the divacancy consisted of two vacancies at second-nearest-neighbor lattice sites.

24,988 THE INFLUENCE OF VACANCIES ON THE DECOMPOSITION KINETICS DURING THE ZONE FORMATION IN ALUMINUM-MAGNESIUM-ALLOYS [in German] by K. Detert and L. Thomas (Tech. U., Berlin); *Acta Met.*, Vol. 12, pp. 431-441, Apr. 1964

The change of the electrical resistivity during aging of aluminum-magnesium-alloys was measured after quenching. The experimental parameters changed the rate of resistivity increase during aging, which indicates zone formation in the lattice. The quantity $\Delta R/\Delta R_{\text{max}}$ may be assumed proportional to the reaction turnover y for the decomposition. The curves of the form $y = 1 - \exp(-\sqrt{mt})$, which were found experimentally are interpreted by the growth model of thin plate shaped decomposition zones. The measured temperature dependences of the factor m describe the dependences of the diffusion coefficient of Mg in Al which are determined by the actual vacancy concentration and the position change probability of the Mg atoms with vacancies. The quantity $Q_1 = 0.74$ eV, deduced from quenching temperature dependence, may be assigned to the formation energy of vacancies in Al-Mg-alloys. The quantity $Q_2 = 0.51$ eV, deduced from the variation of the aging temperature, may be assigned to the activation energy for the position change of the magnesium atoms. No considerable association of vacancies and Mg-atoms occurs, and the migration of the Mg-atoms during zone formation and the annihilation of the excess vacancies take place simultaneously.

24,989 DETERMINATION OF LATTICE VACANCIES IN GRAPHITE by G.R. Hennig (Argonne Lab.); *J. Chem Phys.*, Vol. 40, pp. 2877-2882, May 15, 1964

Vacancies in graphite crystals can be rendered visible for electron microscopy by a technique which combines cleaving, etching, and decorating. The crystals are cleaved, and the vacant lattice sites in the exposed surface are attacked by a mixture of chlorine and oxygen, which expands these vacancies into monolayer loops of any desired diameter. These loops are decorated with

DISLOCATIONS

gold to enhance their contrast. Numerous tests have established that the loop concentration is a quantitative measure of the vacancy concentration. The method is capable of determining vacancies at concentrations at least as low as 10^{-10} per carbon atom. The relative chemical reactivities of carbon atoms surrounding a vacancy, of carbon atoms at the edges of layers and of carbon atoms within layers have been measured.

Vacancy Migration in Metals and Alloys - See 25,057

Vacancies in KCl - See 25,184

24,990 TEMPORARY BLEACHING OF THE M BAND IN KBr AND KCl by M. Ikezawa (Tohoku U.); *J. Phys. Soc. Japan*, Vol. 19, pp. 529-539, Apr. 1964

Temporary bleaching of color centers in additively colored KBr and KCl crystals has been investigated. The first and the second absorption bands of M center are bleached by F-light or M-light irradiation at 90°K. Accompanying the bleaching of the M band, two absorption bands grow at 555 mμ and 780 mμ in KBr and at 505 mμ and 690 mμ in KCl. These bands as well as the bleached M bands show dichroism when the original M band is dichroic. The oscillator strengths of these bands are determined with respect to the M band, and the nature of the bands is discussed.

24,991 OPTICAL-BLEACHING EFFICIENCY FOR F CENTERS IN KCl by R.W. Warren (Westinghouse Res. Lab.); *Bull. Am. Phys. Soc.*, Vol. 9, p. 543(A), June 1964

Measurements have been made of the bleaching of F centers in KCl, which is caused by light irradiation in the F band at room temperature. The quantum efficiency of both the bleaching of the F centers and the resulting growth of the aggregate centers M, R, N, etc., is found to be strongly dependent upon the intensity of I of the bleaching light. Over a range of 10^5 in light intensity, the bleaching rate is proportional to I^2 and the efficiency, therefore, to $I^{-2/3}$. A model for the bleaching process that predicts this dependence is discussed. The major assumptions made in constructing this model are that the F center is mobile at room temperature and is thermally stable, being destroyed only by collisions with other defects. A prediction of this model, that the room temperature photoconductivity of F centers is proportional to $I^{2/3}$, (*J. Phys. Chem. Sol.*, Vol. 22, p. 317) has found experimental confirmation.

24,992 DISTRIBUTION OF VACANCIES PRODUCED IN A SOLID BY IR-RADIATION [in French] by A. Corciovei and A. Babenco (Inst. de Phys. Atom., Bucharest), *Phys. Stat. Sol.*, Vol. 4, pp. K1-4, 1964

The distribution of vacancies in an irradiated solid has been studied by an analysis of the resistivity change due to single cascade, after taking into account the correlation between vacancies and interstitials in cascades through distribution functions for these defects. It has been found that the ratio between resistivity change due to the cascade and the "ideal" resistivity change, associated with the production of an equal number of independent interstitial vacancy pairs in the metal, decreases with an increase in number of cascade pairs. This result is suggested to be the reason for the discrepancy between data for resistivity change obtained by irradiation experiments and that obtained theoretically by summing the contribution from individual defects.

24,993 ANNIHILATION OF VACANCIES AT STACKING FAULTS IN FCC METALS by F. Schapink and M. de Jong (U. Amsterdam, Netherlands); *Acta Met.*, Vol. 12, pp. 755-757(L), June 1964

A simple model is presented for the rearrangement of atoms in a partial dislocation climb in an fcc lattice where the associated stacking fault climbs with the partial dislocation. Absorption of vacancies leads to the climb of an area of the stacking fault. Energetically, the vacancy absorption takes place more favorably near the Shockley partial bordering a stacking fault. Presumably a trivacancy is the smallest configuration which may act as a nucleus for climb of stacking faults in some fcc metals. A constant decrease of energy is obtained for each vacancy annihilated at such a nucleus.

24,994 INTERSTITIAL ATOMS IN NOBLE METALS by A. Seeger (Max Planck Inst. and Tech. Hochschule, Stuttgart); *Phys. Lett. (Neth.)*, Vol. 8, pp. 296-297(L), Mar. 1, 1964

The annealing stages of cold-worked irradiated, and quenched noble metals are discussed. Experimental results and models for these results are analyzed to determine in which annealing stage the free migration of interstitials occurs. All evidence indicates that stage III is due to the migration of isolated interstitial atoms.

Segregation of Interstitials - See 24,898

24,995 DIFFRACTION STUDIES OF DISLOCATIONS IN SILICON by J.C. Henderson (P.O. Engrg. Dept.); *Contemp. Phys.*, Vol. 5, pp. 293-295, Apr. 1964

X-ray projection topography has proved to be an almost ideal non-destructive method for observing dislocation structure in single crystal silicon wafers. The method relies on the fact that the localized strain fields associated with the individual dislocations can be rendered visible on a photographic film. By taking a series of topographs of reflections from different crystal planes, it is possible to find the direction of the Burgers vector of every segment of a dislocation line. Practically any single crystal material of not too high dislocation density can be studied using this technique.

24,996 SIMULTANEOUS OBSERVATION OF ETCH PITS AND DISLOCATIONS IN MgO SINGLE CRYSTALS BY TRANSMISSION ELECTRON MICROSCOPY by P.F. Stablein (Argonne Natl. Lab.); *Appl. Phys. Lett.*, Vol. 4, pp. 117-118(L), Apr. 1, 1964

Experimental evidence that pits revealed by dislocation etches are due to dislocations is discussed. Dislocations can be observed by transmission electron microscopy in a carefully thinned sample. If the sample is lightly etched after thinning, each etch pit produces a series of thickness extinction contours eccentric with the point at which the dislocation intersects the surface. Thus, both the dislocation and its etch pit can be observed simultaneously. This technique has been applied to single crystal MgO. Because of the different etching rates for the two dislocation types, pits are observed at the ends of screw dislocations, but not edge dislocations.

24,997 DIFFUSION-INDUCED DISLOCATIONS IN SILICON by J. Washburn and G. Thomas (Lawrence Radiation Lab.), and H.J. Queisser (Clevite Semiconductor); *J. Appl. Phys.*, Vol. 35, pp. 1909-1914, June 1964

Plastic deformation produced by phosphorus diffusion into a (001) silicon surface has been studied by transmission electron microscopy. The lattice parameter differences in regions of steep solute concentration gradient are accommodated by a crossed grid of edge dislocations having Burgers vector $a/2$ [110] and $a/2$ [110]. The long edge dislocations end at nodes, which suggests that they are formed by dislocation reactions between pairs of dislocations that can glide into the crystal on {111} planes.

24,998 DISLOCATION SOURCES AT INCLUSIONS IN ZINC by V. Damiano and N. Brown (U. Penn.); *Trans. Met. Soc. AIME*, Vol. 230, pp. 926-928(L), June 1964

A mechanism is proposed for dislocation multiplication at internal inclusions or cairties. A modification of the Frank-Read source, this mechanism differs in that the dislocation is nucleated by high stresses at the inclusion and the multiplication process depends on the mobility of the end points of the dislocation at the internal surface. Interfaces between precipitate and matrix are preferred nucleation sites for dislocations. If the ends of the dislocation climb or cross glide off the (0001) plane, the dislocation ends will not join and a helical dislocation may form. Numerous helical etch patterns suggest that this latter mechanism operates readily in zinc.

24,999 FACTORS AFFECTING DISLOCATION SUB-STRUCTURES IN DEFORMED COPPER by O. Johari and G. Thomas (Lawrence Radiation Lab.); *Acta Met.*, Vol. 12, pp. 679-682(L), May 1964

Electron microscopy investigations concerning the effects of grain size or strain rate on the substructure of 99.999 pct pure copper single crystals and polycrystals are described. Transmission electron micrographs show wide variations in substructure, but no quantitative correlation can be made between cell size and temperature, grain size (in polycrystals), strain rate, energy of cold work, or flow stress. Dislocation density for the same strain is much less for single crystal specimens than for polycrystalline specimens. It appears that cell formation is favored when two or more slip systems operate. Other qualitative observations are: (1) cell size decreases with increasing strain rate and for decreasing testing temperature, (2) for single crystals, dislocations tend to lie very close to the glide planes and (3) a uniform cell structure is observed after explosive deformation, unlike after static deformation.

25,000 METHOD OF REVEALING DISLOCATIONS IN GERMANIUM FILMS by A.A. Tikhonova, V.D. Vasil'ev and G.A. Kurov (Acad. Sci., USSR); *Soviet Phys. Cryst.*, Vol. 8, pp. 750-751(L), May-June 1964

The density and three-dimensional distribution of dislocations in the epitaxy films of germanium have been studied by the method of selective etching. It is found that the dislocation pits are mainly of three types. First, there are pits which grow through from the support to the film, and their density and

arrangement agree with the dislocation distribution in the support. The second type of pits owes its origin to dislocations formed at the film-support interface, due to the imperfection of the surface of the support. Finally, double pits may be observed in the body of the film, which are assumed to be generated by aggregation of vacancies in the process of growth and subsequent slow cooling of the film.

25,001 RELATIONSHIP BETWEEN NEUTRON-PRODUCED PRISMATIC DISLOCATIONS AND THE CHANGE IN VOLUME DURING ANNEALING IN COPPER by I.G. Greenfield and J.R. Demos (Franklin Inst. Lab.); *Phys. Rev.*, Vol. 134(A), pp. A1051-1058, May 18, 1964

Two groups of copper single crystals of various orientations were irradiated with neutrons between 50°C and 70°C; one group was exposed to 0.53×10^{18} nvt (total epithermal flux) and the other 1.1×10^{18} nvt (total epithermal flux). An irradiated and a nonirradiated crystal of each orientation were isothermally annealed in a dilatometer at temperatures ranging from 75°C to 350°C, and the irreversible differential changes in length were measured. In addition, electron microscope studies were made of the size distribution of irradiation-produced prismatic dislocations after several of the annealing treatments. These experiments revealed that (1) a direct relationship exists between the magnitude of shrinkage after annealing treatment and the total neutron exposure, (2) during annealing dislocation loops decrease in diameter until they disappear, (3) the decrease in dislocation density is related to the volume shrinkage, (4) the changes in loop distribution could be predicted by a line-tension-climb equation, and (5) the activation energy for the annealing of irradiation-produced loops lies between 2.08 eV and 2.10 eV. The results indicated that the annealing process in neutron-irradiated copper is not the same as observed in quenched metals although a self-diffusion mechanism appears to be the controlling factor.

Dislocations in Ag - See 25,262

25,002 THREE-DIMENSIONAL X-RAY TOPOGRAPHIC STUDIES OF INTERNAL DISLOCATION SOURCES IN SILICON by A. Authier and A.R. Lang (U. Bristol, England); *J. Appl. Phys.*, Vol. 35, pp. 1956-1959, June 1964

Stereo pairs of x-ray projection topographs have been used to elucidate the configuration of dislocations in a silicon bar lightly deformed at about 900°C. Dislocation reactions and interactions associated with a ten-turn Frank-Read spiral are described.

25,003 POSITION AND DENSITY OF GROWTH DEFECTS IN VAPOR PHASE GROWN CdS-CRYSTALS by W. Mohling, H. Peibst and L. Hildish (German Acad. Sci., Berlin); *Phys. Stat. Sol.*, Vol. 5, pp. 101-106, 1964

Lang x-ray diffraction micrographs of vapor phase grown CdS crystals have revealed high dislocation densities in the region of intergrowths with other crystals. Electron microscope studies of thin crystals confirm these observations. Screw dislocations responsible for spiral growth were not observed.

25,004 DISLOCATIONS IN RUBY LASER CRYSTALS by J.R. Janowski and H. Conrad (Aerospace Corp.); *Trans. Met. Soc. AIME*, Vol. 230, pp. 717-725, June 1964

A study of the dislocation structure of ruby crystals obtained from various sources is reported. Using KHSO_4 as an etchant, a detailed mapping of the dislocation structure on the (0001) and the (1120) planes was carried out. A less extensive study was made of the rhombohedral planes. The average dislocation density on the basal plane was 1.5 to $3 \times 10^4 \text{ cm}^{-2}$ and on the (1120) planes $\sim 5 \times 10^5 \text{ cm}^{-2}$. However, considerable variation existed between areas on a given plane. The subboundaries in the basal plane tended to lie along $[1\bar{1}00]$ type directions while those on the (1120) plane tended to lie: a) parallel to the basal plane, b) along traces of the $(1\bar{1}01)$ plane, and c) along normals to the traces of the (0001) planes. The orientations suggest that many of the dislocations lie on the (0001), $\{1\bar{1}01\}$, and $\{11\bar{2}0\}$ planes. A Laue back-reflection analysis of c-axis wander in one crystal revealed a gradual increase in misorientation from one end of the crystal to the other, with a maximum variation of $1^\circ 35'$. Slight etching of a mechanically polished crystal revealed numerous polishing scratches, suggesting the existence of a plastic flow layer.

25,005 DISLOCATION MOVEMENTS IN METALS by D. Kuhlmann-Wilsdorf and H. Wilsdorf (U. Virginia); *Science*, Vol. 144, pp. 17-25, Apr. 3, 1964

Dislocation motion in metals is reviewed. Plastic deformation is caused by the motion of dislocations; without mobile dislocations, all metals would be brittle. Dislocations in real crystals are line defects, thousands of angstroms long and possessing energies of many electron volts. They are not thermodynamically stable and cannot be propagated faster than the speed of sound in the same material. A dislocation cannot start on end inside a crystal, but dislocations can be joined, can branch and can form networks. The easiest kind of dislocation motion is on the slip surface. Forces inducing dislocation motion are glide forces and climb forces. These driving forces must be sufficient to over-

come frictional forces in order for dislocations to move. Three anchoring mechanisms impeding dislocation motion arise from impurity atoms, substitutional atoms and interstitial atoms. The force required to overcome the steepest gradient of the dislocation core energy (Peierls-Nabarro force) is the smallest force which will move a dislocation. Dislocation intersections, cross slip, and climb play a considerable role in the mechanism of plastic deformation.

25,006 THE EFFECT OF WORK HARDENING ON THE STRESS DEPENDENCE OF DISLOCATION VELOCITY by S. Floreen and T. Scott (Iowa State U.); *Acta Met.*, Vol. 12, pp. 758-759(L), June 1964

Experimental results of other researchers for silicon iron have been used to evaluate the effect of strain on m , an exponential factor on which dislocation velocity depends $[V = (\sigma/\sigma_0)^m]$ in order to determine the change in m , the term $\partial \ln N / \partial \ln \sigma$ must be evaluated as a function of strain. This is accomplished by utilizing the work-hardening expression $\sigma = K\epsilon^n$ and assuming the average distance the mobile dislocations move is proportional to the cell size d . Tabulated results show that m increases with increasing strain. It should be possible to estimate the values of m in work hardened alloys without difficulty.

25,007 DETERMINATION OF THE SENSE OF THE BURGERS VECTOR OF A DISLOCATION IN CdS OBSERVED BY X-RAY DIFFRACTION MICROSCOPY by J. Chikawa (NHK Tech. Res. Labs.); *Appl. Phys. Lett.*, Vol. 4, pp. 159-160(L), May 1, 1964

The use of Lang's camera to determine the direction of the Burgers vector of a dislocation in a CdS crystal is discussed. The orientation of the dislocation is obtained from a diffraction micrograph, and a rocking curve is obtained at a point remote from the dislocation. The crystal is then rotated either +7 or -7 sec of arc from the position of maximum intensity in the rocking curve, and is moved parallel to the c-axis so that the x-ray beam crosses the dislocation. Two separated intensity curves are obtained from angular shifts of +7 or -7 sec of arc, with the dislocation core located between the two peak positions. Rocking curves measured at the peaks of the diffracted intensity are also displaced to either side of the original rocking curve. The peak shifts of the rocking curves are attributed to the inclinations of the atomic planes on each side of the dislocation core, and indicate the sign of the Burgers vector.

25,008 DISLOCATIONS IN RECRYSTALLIZED ALUMINUM CRYSTALS by B. Basu and C. Elbaum (Brown U.); *Philosophical Mag.*, Vol. 9, pp. 533-536, Mar. 1964

Recrystallized specimens of aluminum were prepared by the strain-anneal technique. Using x-ray diffraction photographs, dislocation densities were observed under an optical microscope. Low (2×10^4 to $4 \times 10^4 \text{ lines/cm}^2$) and uniform densities are observed. Figures are presented showing the preferential alignment of dislocations along specific crystallographic directions. $\langle 110 \rangle$ is observed for each reflection while $\langle 112 \rangle$ and $\langle 113 \rangle$ are also frequent. The possibility of an equilibrium structure in the $\{113\}$ and/or $\{110\}$ planes is suggested because some $\langle 112 \rangle$ type dislocations do not lie in the same $\{111\}$ planes as their Burgers vectors.

25,009 DISLOCATION STRUCTURES IN SINGLE-CRYSTAL Al_2O_3 by D. Stephens and W. Alford (AF Cambridge Res. Labs.); *J. Am. Ceram. Soc.*, Vol. 47, pp. 81-86, Feb. 21, 1964

Chemical polishing and etching techniques were used to reveal the dislocation structures of sapphire and ruby crystals grown by the flame-fusion and flux techniques. The average density of edge dislocations lying in prism planes was $3.0 \times 10^5 \text{ per cm}^2$. An average basal dislocation density of $2.0 \times 10^6 \text{ per cm}^2$ decreased 35 to 80 pct on annealing. Crystal orientation (i.e. angle between c axis and growth axis) showed no effect on dislocation density, but a pronounced effect on sub-boundary arrangement and density. Principal observations included: (1) prismatic and basal slip on all as-grown crystals; (2) profuse basal slips; (3) dislocation densities of flux crystals lower than those of Verneuil crystals; and (4) a rare form of basal turning, composition plane $\{10\bar{1}0\}$, on all flux crystals.

25,010 DISLOCATIONS IN BENT SILVER CHLORIDE SINGLE CRYSTALS by M.T. Sprackling (Queen Elizabeth Coll., London); *Philosophical Mag.*, Vol. 9, pp. 739-747, May 1964

An etch-pit technique has been used to study the dislocation distribution in partially plastically bent silver chloride single crystals. A macroscopically uniform distribution of dislocations was found in the plastically deformed part except in a narrow strip containing the neutral plane of bending where the density of dislocations changed fairly sharply to a lower value in agreement with a model proposed by Nye et al.

25,011 DISLOCATION DAMPING DUE TO KINK MOTION by T. Suzuki and C. Elbaum (Brown U.); *J. Appl. Phys.*, Vol. 35, pp. 1539-1544, May 1964

The ultrasonic attenuation and velocity change that result from the damping due to motion of dislocation kinks have been calculated on the following assumptions: (1) the frequency of thermal creation of kinks is smaller than the frequency of the applied stress; (2) the frequency of thermal motion of the kinks is larger than the frequency of the applied stress. The characteristics of the attenuation calculated from the above assumptions differ from those of the string model for dislocation damping as follows. First, the resonance frequency depends on kink spacings and on the distance between pinning on the dislocation. Second, for strain amplitude in excess of a critical value given in terms of kink spacings and the distance between pinning points, the attenuation decreases with increasing strain amplitude.

25,012 THERMAL DISORDER IN A DISLOCATION CORE AND ITS EFFECT ON DAMPING by P.D. Southgate and K.S. Mendelson (IIT Res. Inst.); *Phys. Rev.*, Vol. 134A, pp. A1642-A1649, June 15, 1964

It is postulated that, at elevated temperatures, the core of a dislocation consists of a thermally disordered quasiliquid region, whose size increases with temperature. Calculations based on the effect of the disordering in relieving elastic stresses indicate that a flat strip core should be favored. A moving dislocation of this form will experience two distinct damping forces. One is thermodynamic, caused by the heat of disordering, and is analogous to the thermoelastic damping produced by the dislocation stress field; while the other is viscous, caused by the shear between the two sides of the strip. The calculated magnitudes of both of these damping forces in covalent and metallic crystals are comparable with those required to explain internal friction observations, although a positive demonstration of the validity of the mechanisms cannot be made on the basis of present data.

25,013 RELAXATION OF DISLOCATIONS IN GOLD-SILVER ALLOYS by F.M. Mazzolai (Inst. Naz. Ultracustica, Roma); *Nuovo Cimento*, Vol. 32, pp. 588-597, May 1, 1964

The dissipation of elastic energy has been measured as a function of temperature in some alloys of the binary system Ag-Au, with a small atomic percent of Ag. The height of the Bordoni peaks decreases monotonically with increasing atomic percent of Ag. The propagation velocity of the extensional elastic waves, computed from the measurements of the resonant frequency at different temperatures, increases monotonically with increasing concentration of Ag. A comparison has been made with the results obtained by Barducci in a similar series of alloys with a small atomic percent of Au. The obtained results can be explained by taking into account the lattice constants of gold and silver and the difference between their ionic diameters in the lattice.

25,014 THE EFFECT OF THE ANISOTROPY OF ELASTIC CONSTANTS ON DISLOCATIONS IN THE FERROELECTRIC BaTiO_3 PHASE [in French] by G. Fontaine (Fac. Sci., Orsay); *Phys. Stat. Sol.*, Vol. 5, pp. 203-206, 1964

An analysis of the elastic energy of a straight dislocation in BaTiO_3 single crystals for different orientation lines and Burger's vector is presented. The results of the analysis are used to study the crystalline directions for which the straight line is either unstable or metastable with respect to deformations in the slip plane.

25,015 FRICTIONAL STRESS ON DISLOCATIONS IN Cu_3Au CRYSTALS STRAINED IN TENSION by B.H. Kear (Pratt Whitney Aircraft); *Acta Met.*, Vol. 12, pp. 845-849(L), July 1964

Data on the dislocation frictional stress in deformed Cu_3Au crystals are presented, emphasizing the difference in slip behavior of the ordered and disordered phases. Crystals were grown from the melt by the Bridgman method and ordered or disordered structures were obtained by appropriate heat treatment. Interrupted stress-strain curves are presented for successively pre-strained samples. An anomalous reloading effect is presumably caused by some kind of diffusion controlled locking mechanism. By decreasing and subsequently increasing stress amplitude, the resulting anelastic loops have much smaller strain amplitudes than the original ones, a characteristic which is attributed to a dislocation locking mechanism. The dislocation frictional stress (τ_f) is found to increase on aging in the ordered and with pre-strain in the disordered crystal; τ_f does not change noticeably with prestrain in stages I and II.

25,016 INTERSTITIAL LOOPS IN NEUTRON-IRRADIATED MOLYBDENUM by J. Meakin (Franklin Inst. Lab.); *Nature*, Vol. 201, pp. 915-916, Feb. 29, 1964

Experimental evidence that large dislocation loops produced by neutron irradiation of molybdenum are interstitial in nature is presented. Samples consisted of a single crystal of three-pass zone-refined molybdenum cut into 0.5 mm sections which were then irradiated at 600°C to a total fast flux of 10^{18} nvt. Tilting experiments carried out in the manner of Groves and Kelly showed that all loops resulted from the aggregation of interstitials. Loop sizes varied from 100 Å to 2000 Å in diameter.

25,017 DISLOCATION CONFIGURATIONS IN ZONE-MELTED SINGLE CRYSTAL MOLYBDENUM by A. Lawley, H.L. Gaigher, and S. Schuster (Franklin Inst.); In *Deformation Characteristics of Thin Foils and Composites*, Contract Nonr-2992(00) AF - A2366, Jan. 1964, pp. 32-81; *STAR*, Vol. 2, p. 1195(A), May 8, 1964 AD 430 902

Single crystal molybdenum, deformed in tension at temperatures in the range of 4.2° to 300°K, was studied. It was found possible to correlate the bulk stress-strain behavior with the observed glide dislocation configurations. In addition to studying the glide dislocation configurations, a detailed examination was made of the grown-in networks and the effect of impurity segregations.

25,018 THE CRACKED DISLOCATION UNDER TENSION by R. Bullough (Atomic Energy Res. Est., Harwell); *Philosophical Mag.*, Vol. 9, pp. 917-925, June 1964

Appropriate distributions of infinitesimal dislocations are used to deduce the fracture criteria for dislocations or groups of dislocations with a crack either normal to or lying in their slip plane. The essential simplicity of the method of derivation is emphasized and the results are compared with previously published theoretical work by other authors. In addition the model, involving crack propagation in a slip plane containing a group of dislocations, is used to provide a new explanation of the observed orientation dependence of the fracture stress of zinc single crystals.

GRAIN BOUNDARIES, STACKING FAULTS, ETC.

25,019 ADDITIONAL OBSERVATIONS ON TWINNING IN SAPPHIRE ($\alpha\text{-Al}_2\text{O}_3$ CRYSTALS) DURING COMPRESSION by H. Conrad, K. Janowski, and E. Stofel (Aerospace Corp.); Apr. 10, 1964, 9 pp., ATN-64(9236)-16; *STAR*, Vol. 2, pp. 1385-1386(A), June 8, 1964

Twinning has been found to occur in 60° oriented sapphire rods at temperatures as high as 1,500°C. The temperature and strain-rate conditions for the two types of twins, (0001) and (0111), and for slip were established in detail.

25,020 TRANSMISSION ELECTRON-MICROSCOPIC STUDIES OF TWINNING IN Mo-Re ALLOYS by K. Ogawa and R. Maddin (U. Penn.); *Acta Met.*, Vol. 12, pp. 713-721, June 1964

Twins in Mo-35 at.% Re alloys deformed at room temperature and in Mo-18 at.% Re deformed at liquid nitrogen temperature were observed by transmission electron microscopy. Neither extended dislocations nor extended dislocation nodes were noted. Instead, a dislocation reaction between a slip dislocation and three twinning dislocations was often observed. Direct evidence of the operation of a pole mechanism for twinning was obtained. The present observations suggest that the critical stage of twinning is the dissociation of slip dislocations in $\{112\}$ planes into three twinning dislocations. Direct evidence of the existence of emissary type non-coherent twin boundaries was obtained. The fringe contrast observed in non-coherent twin boundaries in these bcc crystals is interpreted in terms of the kinematical theory of electron diffraction due to stacking faults. A new effect, oscillation of the intensities of electrons diffracted at non-coherent twin boundaries was found in the region where the absorption effect is prominent and the twinning dislocations are spaced closely. The effect of free surfaces upon the arrangement of dislocations was found to reach as deep as a few hundred Å.

25,021 GROWTH TWINNING IN GRAPHITE DENDRITES by M. Oron and I. Minkoff (Technion Israel Inst. Tech.); *Philosophical Mag.*, Vol. 9, pp. 1059-1062(L), June 1964

Lane photographs show parallel twin components in graphite dendrites grown from nickel-carbon solution. The composition plane of the turns is (0001). It was found that the angle of rotation of the boundary influences the direction of growth. A photomicrograph shows the leading edge of a dendritic crystal of graphite with a growth axis $\langle 25\bar{7}0 \rangle$, making an angle of 14° with the normal to the growth markings; it represents a compromise between the $\langle 1120 \rangle$ directions for each of the twin components. Graphite dendrites are shown to have a number of growth features similar to those observed in dendrites of diamond lattice materials. Crystals occasionally show development of side branching. Cavities, which originate from the splitting of the leading edge, are left in the graphite crystals.

25,022 GROWTH TWINS AND BRANCHING OF ELECTRODEPOSITED COPPER DENDRITES by F. Ogburn (Nat'l. Bu. Stand.); *J. Electrochem. Soc.*, Vol. 111, pp. 870-872, July 1964

Experimental evidence is presented supporting the hypothesis that electrodeposited dendrites, branched in only one plane, are due to the occurrence of growth twins with at least one twinning boundary extending through and

parallel to the plane of the dendrites. If the twinning boundary facilitates the growth of the deposit by providing a re-entrant groove, the dendrite should grow fastest close to the groove and form a platelet with the twinning boundary sandwiched between two thin layers of metal. X-ray diffraction and metallographic examinations of planar branched dendrites confirm the author's hypothesis.

25,023 PSEUDOPENTAGONAL TWINS IN ELECTRODEPOSITED COPPER DENDRITES by F. Ogburn, B. Paretzkin, and H. Peiser (Nat'l. Bu. Stand.); *Acta Cryst.*, Vol. 17, pp. 774-775, June 10, 1964

Pseudopentagonal twins in electrodeposited copper are investigated. The pseudopentagonal character arises from the fact that the angle $111^\circ 111'$ is $70^\circ 32'$ or nearly $360^\circ/5$. The copper $\langle 110 \rangle$ dendrites were grown at room temperature from a solution of $4 \text{ g} \cdot \text{l}^{-1}$ of $\text{CuSO}_4 \cdot 5\text{H}_2\text{O}$ (1/64M) and $0.4 \text{ g} \cdot \text{l}^{-1}$ of H_2SO_4 (1/256 M) on a crystalline copper wire about 0.8 mm in diameter and 3 cm long. Growth was primarily in the form of branched stalks perpendicular to the cathode surface.

25,024 TWIN INTERSECTIONS AND CAHN'S CONTINUITY CONDITIONS by R.E. Reed-Hill (U. Florida); *Trans. Met. Soc. AIME*, Vol. 230, pp. 809-813, June 1964

The shear continuity conditions under which one mechanical twin may cross another are considered. Twin intersections usually involve various types of slip deformation in addition to twinning. Because the shear of the crossing twin may be partly transmitted through the crossed twin by slip mechanisms, continuity of the twinning shear vectors is not required at a twin intersection. It is concluded that analyses based on twin intersections should be used as an independent method for deducing twinning elements in newly observed twinning modes.

25,025 EMISSARY DISLOCATION-TWIN INTERACTIONS AND TWIN GROWTH by A.W. Sleeswyk (Shell Int. Res., Amsterdam); *Acta Met.*, Vol. 12, pp. 669-673(L), May 1964

Twin intersections are described in the light of two recent findings: (1) shear deformation associated with $\{112\} \langle 111 \rangle$ twinning is in fact caused by the passage of $\frac{1}{2} \langle 111 \rangle$ "emissary" slip dislocations which precede the growing twins; and, (2) every $\frac{1}{2} \langle 111 \rangle$ slip dislocation in the bcc lattice can penetrate the coherent boundary of any $\{112\}$ twin lamella, if necessary by means of dislocation reactions at the boundary. Emissaries penetrating twin lamellae can be divided into three categories, depending on the orientations of the Burgers vectors of the emissary relative to the twin. If it is assumed that all partials created by emissaries traversing a twin lamella glide towards the twin tip, some sort of growth avalanche evidently may occur. Final twin thickness produced by this effect can be estimated. The mean twin thickness is approximately doubled during the first cycle, after which the growth rate rapidly decreases.

25,026 ON THE FORMATION OF A LARGE ANGLE GRAIN BOUNDARY DURING DEFORMATION OF METAL SINGLE CRYSTALS [in German] by O. Buck (Max Planck Inst., Stuttgart) and U. Essmann (Tech. Hoch., Stuttgart); *Phys. Stat. Sol.*, Vol. 4, pp. 143-149, 1964

The formation of large angle grain boundaries in Cu crystals during plastic deformation by tension at 4.2°K has been studied using a transmission electron microscope. The large angle grain boundary appears to a model example of recrystallization occurring in plastically deformed metals.

25,027 THE EFFECT OF SUBSTRUCTURE ON THE NUCLEATION OF GRAIN-BOUNDARY CAVITIES IN MAGNESIUM by A.E.B. Presland and R.I. Hutchinson (Intl. RD Ltd.); *J. Inst. Metals*, Vol. 92, pp. 264-269, May 1964

Transmission electron microscopy of magnesium has permitted the observation of grain-boundary cavities in thin foils prepared from suitably strained test-pieces. The intersection of a grain boundary by a sub-grain boundary has been identified as the principal cavitation site and a nucleation mechanism is proposed which accounts qualitatively for the available data on cavitation as a function of strain, strain rate, and temperature.

25,028 GRAIN BOUNDARY MIGRATION IN LiF BICRYSTALS by M. Davis and N. Tallan (Wright-Patterson AF Base); *J. Am. Ceram. Soc.*, Vol. 47, pp. 175-178, Apr. 21, 1964

Large scale grain-boundary movements have been observed in macroscopic LiF bicrystals. Bicrystals containing boundaries of varying orientations were prepared by sintering LiF single crystals at temperatures 20° to 30°C below their melting point. At these temperatures a boundary capable of large-scale movement formed rapidly. Subsequent heating at the same temperature resulted in boundary movements of 5 mm or more within 12 hours, frequency in a direction opposed to the radius of curvature. In some specimens boundary sliding and rotation, suggestive of the presence of an interfacial liquid layer, were observed.

25,029 THE STACKING-FAULT ENERGY OF GOLD AND SILVER by A. Seeger (Max Planck Inst.); *Philosophical Mag.*, Vol. 9, pp. 887-890(L), May 1964

It is reported that stacking fault energies can be obtained from the size of the observed stacking-fault tetrahedra which grow presumably, by the mechanism of vacancy absorption. By a suitable choice of experimental conditions, other researchers were able to obtain stacking-fault tetrahedra and other defects of widely different sizes in gold. Application of theory to their observations indicates that the specific energy of intrinsic stacking faults in gold in the temperature range $100\text{--}200^\circ\text{C}$ is $\gamma_{\text{Au}} = 1.5 \times 10^{-3} \text{ Gb}$ or $\gamma_{\text{Au}} = 12 \text{ ergs/cm}^2$. Under suitable conditions, tetrahedra are formed of such a size as to preclude formation by dislocation reactions indicating they grew as tetrahedra. The stacking-fault energy for silver is larger than that for gold; the upper limit is deduced as $\gamma_{\text{Ag}} = 5.1 \times 10^{-3} \text{ Gb} = 43 \text{ ergs/cm}^2$. Under suitable conditions both the dislocation reaction and the vacancy absorption mechanism may operate.

25,030 INFLUENCE OF OXIDIZING AND REDUCING TREATMENTS ON VACANCY CLUSTERING IN GOLD by R.L. Segall and L.M. Clarebrough (U. of Melbourne); *Philosophical Mag.*, Vol. 9, pp. 865-877, May 1964

The stacking-fault tetrahedra observed in specimens of gold, quenched from a reducing atmosphere, are found to be smaller by a factor of four than in specimens quenched from an oxidizing atmosphere. This result is discussed in terms of the different distribution of impurities after oxidation and reduction. The effect of the impurities on the measured stacking-fault resistivity is also examined. It has been observed that tetrahedra grow during isothermal annealing at 40°C . The results of experiments where quenched specimens are aged at different temperatures, between 40°C and 200°C , support the hypothesis that the initial tetrahedron nucleus is a small three-dimensional vacancy cluster. These experiments show that the proportion of clustered vacancy defects which are not tetrahedra, but dislocation loops, increases with increasing ageing temperature. In the specimens pre-treated in an oxidizing atmosphere, it was found that the stacking-fault tetrahedra commonly occur in rows along the $\langle 110 \rangle$ direction.

25,031 NUCLEATION AND GROWTH OF STACKING FAULT TETRAHEDRA IN GOLD by W. Westdorp, H. Kimura and R. Maddin (U. Penn.); *Acta Met.*, Vol. 12, pp. 995-500, May 1964

The formation of stacking fault tetrahedra in quenched gold foils was observed by transmission electron microscopy. The density of tetrahedra was found to be about $6 \times 10^{14} \text{ cm}^{-3}$ for quenches from 890°C and independent of the annealing time and temperature beyond the early stage of annealing. The growth of the tetrahedra was confirmed; their nucleation was found to be completed in the very early stages of annealing. These results imply that condensation of vacancies occurs, to some extent, during quenching and that the binding energy of a divacancy is about 0.4 ev.

25,032 THE EFFECT OF HYDROGEN ON THE STACKING FAULT PROBABILITY IN COPPER by M.L. Rudee and R.A. Huggins (Stanford U.); *Phys. Stat. Sol.*, Vol. 4, No. 3, pp. K101-K103, 1964

An investigation of the effect of hydrogen content on the stacking fault probability, α , in copper was made. Filings of hydrogen-saturated 99.999% pure copper were examined by a diffractometer using copper $K\beta$ radiation. A best-fit was made to counts near the peaks and a graph of α vs atomic percent hydrogen is presented. A value of 3.0×10^{-3} was found for α for outgassed copper. α increased with increasing atomic percent hydrogen.

25,033 FAULTS IN WURZITE TYPE CdS CRYSTALS by J. Chikawa, (NHK Tech. Res. Labs., Tokyo); *Japanese J. Appl. Phys.*, Vol. 3, pp. 229-230(L), Apr. 1964

Thin platelets of CdS with 25 wt pct GaCl_3 as an impurity were grown by the sublimation method. Stacking faults in the crystals were observed by transmission electron microscopy and identified by phase contrast in dark field images. It is shown that stacking faults connect with faults on non-basal planes and that images of faults with $1/3 \langle 10\bar{1}0 \rangle$ or $1/3 \langle 10\bar{1}0 \rangle + 1/2 \langle 0001 \rangle$ type fault vector are obtained. The fault structure was observed only along the $\{0001\}$ surface which grew faster (growth in the $\langle 0001 \rangle$ was asymmetric).

25,034 DISORDERING OF DEFECTS IN SINGLE CRYSTALS OF ZINC SULFIDE by L.T. Chadderton, A.G. Fitzgerald, and A.D. Yoffe (Cavendish Lab. J. Appl. Phys., Vol. 35, pp. 1582-1586, May 1964

Stacking faults are observed in zinc sulfide (wurtzite) single crystals on basal planes (0001) and on prismatic planes (1120) and (1210) to the growth surface. The degradation of these stacking faults in different environments is described. The loop contrast observed to form at stacking faults on prismatic planes when exposed to high electron beam intensities in the electron microscope is explained by a thermally activated mass-transport mechanism. Migration of vacancies or atoms occurs depending on whether the stacking fault is extrinsic

or intrinsic, respectively. Subjecting crystals to high pressures (about 60 kbar) results in an increase in the number of basal plane stacking faults. This is equivalent to a gradual phase change occurring over several atomic planes. Thermal etch figures observed by transmission electron microscopy in crystals annealed at 700° and 900°C are identified as a crystallographic polarity effect.

24,035 ORIENTATION OF STACKING FAULTS AND DISLOCATION ETCH PITS IN β -SiC by Liebmann (IBM Labs., Boeblingen, Germany); J. Electrochem. Soc., Vol. 111, pp. 885-886(L), July 1964

The relationship of stacking faults and dislocation etch pits in β -SiC to lattice planes is studied. In the zincblende structure, the lowest energy plane which can lead to a stacking fault or etch pit of opposite orientation from a {111} fault is the {311} plane. The formation of these etch pits can be interpreted using the same criterion that Sangster developed to determine the most favorable growth direction. This criterion predicts greatest etching rate in the direction normal to planes where the removal of individual atoms will not alter the net number of "dangling" covalent bonds.

25,036 CRACK NUCLEATION IN MgO SINGLE CRYSTALS by A.S. Argon and E. Orowan (MIT); Philosophical Mag., Vol. 9, pp. 1023-1039, June 1964

Three main types of crack formation in plastically deformed MgO crystals have been observed. All are due to internal stresses of macroscopic character resulting from the difficulty of mutual penetration of perpendicular dislocation bands and the consequent geometrical incompatibilities of plastic deformation. The accompanying internal stresses are strongly reduced by plastic deformation, mainly in the form of twinning; however, they often give rise to crack formation.

25,037 TWIN-INDUCED GRAIN BOUNDARY CRACKING IN BCC METALS by A. Gilbert, G. Hahn, C. Reid, and B. Wilcox (Battelle); Acta Met., Vol. 12, pp. 754-755(L), June 1964

Intercrystalline cracking in chromium, molybdenum, and tungsten can occur by the intersection of twins with grain boundaries. Photomicrographs of high strain rate, room temperature compression tests indicate that intercrystalline cracks were initiated at twin/grain boundary intersections. These cracks generally propagated a short distance along the grain boundaries and occasionally changed to transcrystalline cleavage. Twin/grain boundary intersections similarly gave rise to intercrystalline cracking for low strain rate tests at -196°C on similar specimens. Circumstantial evidence is given which indicates that grain boundary failures occurring in decarburized steel may have been initiated by this mechanism.

25,038 DAMAGED LAYERS IN ABRADED {111} SURFACES OF InSb by E.N. Pugh and L.E. Samuels (Australian Def. Sci. Service, Sydney); J. Appl. Phys., Vol. 35, pp. 1966-1969, June 1964

A metallographic investigation has been made of the nature and depth of the damaged layers in abraded {111} surfaces of InSb. It is shown that the damage consists of cracks which are associated with crack-like dislocation arrays of the type known to exist in abraded germanium and silicon surfaces. However, in InSb the damaged layer also contains glide dislocations and features which are thought to correspond to twins, both of which are absent in the elemental semiconductors. Contrary to previous reports by other workers, the depth of damage, taken as the depth of the deepest cracks, is found to be the same in surfaces terminating with In atoms and in those terminating in Sb atoms. In both cases, the glide dislocations and the twins extend to approximately half the depth of the deepest cracks.

25,039 DEFORMATION BY SLIP IN SINGLE CRYSTALS OF CALCIUM TUNGSTATE by B. Cockayne (Royal Radar Est., Great Malvern), and G.E. Hollox (U. Birmingham); Philosophical Mag., Vol. 9, pp. 911-916, June 1964

Plastic deformation of calcium tungstate single crystals has been observed to occur by slip on {100} <100> systems at temperatures in the range 800-1000°C. No plastic deformation has been observed below 800°C. The operation of these slip systems is correlated with the occurrence of low-angle dislocation boundaries parallel to <100> directions in crystals grown from the melt.

IMPURITIES

25,040 ELECTRON SPECTROSCOPY FOR CHEMICAL ANALYSES by S. Hagsstrom, C. Nordling, and K. Siegbahn (U. Uppsala); Phys. Lett. (Neth.), Vol. 9, pp. 235-236(L), Apr. 15, 1964

The application of electron spectroscopy to qualitative and quantitative chemical analysis of the elements, and to the determination of chemical valence state

is discussed. A qualitative analysis of the elements can be made from the positions of the lines of the photoelectron spectrum obtained when the material under study is irradiated by monochromatic x-rays. The intensities of the photoelectron lines are used for a quantitative analysis of the elements. The electron spectroscopic technique can be used throughout the periodic table of the elements. The method yields information about the composition of the surface. The chemical valence state of an element can be determined by the electron spectroscopic technique from the displacement of the photoelectron lines of the element in one compound with respect to the photoelectron lines from the element in another compound and in a different valence state.

25,041 THE APPLICATION OF A FLASH DISCHARGE LAMP TO THE DETERMINATION OF IMPURITIES IN THIN FILMS by W.G. Guldner (Bell Labs.); IEEE Trans., Vol. CP-11, pp. 9-12, June 1964

A xenon flash discharge lamp can be used for analysis of impurities in thin films of tantalum. A description of the apparatus and technique is presented. The discharge is used to vaporize the film from the substrate. Gases evolved as a result of the flash are collected and analyzed by gas chromatography. The method has been used to determine nitrogen content in sputtered films. A direct correlation is found with partial pressure of nitrogen in the sputtering chamber. The method can also be used to measure hydrogen, argon, and carbon monoxide.

25,042 AN INVESTIGATION INTO THE APPARENT PURITY LIMIT IN GaSb by D. Effer and P.J. Etter (Plessey Ltd.); J. Phys. Chem. Solids, Vol. 25, pp. 451-460, May 1964

Attempts have been made to reduce the high concentrations of acceptors found in all preparations of GaSb to date. No evidence of a significant concentration of impurities has been found but material of a reduced hole concentration has been grown from antimony rich melts. The best sample measured had a hole concentration of $9.2 \times 10^{15} \text{ cm}^{-3}$ and a Hall mobility of $5230 \text{ cm}^2/\text{v sec}$ at 77°K which compares with the best reported mobility at this temperature of $3570 \text{ cm}^2/\text{v sec}$. It is concluded that the p-type nature of GaSb is due to lattice defects rather than to impurities.

25,043 DETECTION OF HELIUM IN SILICON BY CLEAVAGE IN A HIGH VACUUM by T.A. Vanderslice and N.R. Whetten (GE Res. Lab.); J. Phys. Chem. Solids, Vol. 25, pp. 513-515, May 1964

Helium evolved during the cleavage of silicon crystals in a vacuum was detected using a sensitive mass spectrometer. The silicon had been boron-doped and neutron-irradiated. The amount of helium detected during the cleavage of the crystals was proportional to the original boron doping concentration of the crystals. Annealing the silicon at 930°C greatly increased the quantity of helium released on cleavage. Support is given for the hypothesis of Keesom and Seidel that at high temperatures the helium diffuses to defects in the crystal, forming clusters of helium atoms.

25,044 IMPURITY LINES OF BORON AND PHOSPHORUS IN SILICON by B. Pajot (Lab. Infrarouge, Orsay, France); J. Phys. Chem. Solids, Vol. 25, pp. 613-619, June 1964

From observations of the main infrared absorption lines of boron and phosphorus in silicon, with a grating spectrometer, their natural width and their temperature dependence have been determined. In boron-doped silicon a line was observed which cannot be related to the boron spectrum and might be due to phosphorus contamination of this could give rise to absorption. The results obtained show: the line widths observed are not purely instrumental; that the natural widths obtained are narrow ($8 \cdot 10^{-5} \text{ ev}$), and finally that temperature broadening increases much more quickly than expected by theory, suggesting a two process phenomenon.

25,045 THE GRAVIMETRIC DETERMINATION OF TRACE AMOUNTS OF CARBON IN SODIUM METAL by R.D. Gardner and W.H. Ashely (Los Alamos Lab.); Contract W-7405-ENG-36, Mar. 5, 1964, 15 pp., LA-3035; STAR, Vol. 2, p. 1089(A), May 8, 1964 OTS \$0.50

The classical combustion-gravimetric method for the determination of carbon has been modified and applied to the measurement of trace amounts of carbon in sodium metal. The sample, contained in an aluminum capsule, was reacted with a flux consisting of a mixture of boric anhydride and vanadium pentoxide and burned in a stream of purified oxygen at 1,100°C. An average recovery of 96% with a standard deviation of 10 ppm was obtained for the analysis of 40 samples containing known amounts of carbon in the 0 to 200 ppm range.

25,046 SEPARATION AND DETERMINATION OF RARE EARTH METALS IN ZIRCONIUM-RARE EARTH ALLOYS by E. Cogon (Bureau of Mines, Ore.); BMRI-6430, 1964, 11 pp.; STAR, Vol. 2, p. 1326(A), June 8, 1964

Equilibrium phase diagram studies of zirconium-rare earth metal alloys prompted the development of a rapid gravimetric method for determining rare earths in

zirconium in which the rare earths are absorbed from sulfuric acid solution of the alloys on a cation-exchange resin. The sample in 10-percent H_2SO_4 is introduced into the column, the zirconium is eluted with 10-percent H_2SO_4 , and the rare earths are eluted with $(\text{NH}_4)_2\text{SO}_4$ solution and precipitated with NH_4OH . A tracer technique was employed to determine the efficiency of the procedure. Y_2O_3 and europium 154 and 152 (Oak Ridge) were added to 10 g of zirconium and taken through the entire procedure. Recovery averaged 97.6 percent on 0.002 μg europium in the rare earth fraction. Rare earths were determined in the range 0.10 to 90 percent.

25,047 ON THE ULTIMATE DISTRIBUTION OF IMPURITY IN THE ZONE MELTING PROCESS by B. Velicky (Czech. Acad. Sci.); *Phys. Stat. Sol.*, Vol. 5, pp. 207-212, 1964

Ultimate impurity distribution in a finite ingot produced in the ideal zone melting process is analyzed. For the case of long ingots, the ultimate distribution at a distance from the end follows the form predicted by Pfann, irrespective of the freezing conditions of the last zone. However, these conditions affect quantities such as final purity and the absolute value of impurity concentration of the ingot. It is thought that the re-refining of a cropped ingot may lead to improved purification.

25,048 ON THE DISTRIBUTION OF IMPURITIES IN EPITAXIAL SILICON FILMS by T. Abe, T. Kato, and Y. Nishi (Tokyo Shibaura Electric); *Japanese J. Appl. Phys.*, Vol. 3, pp. 161-162(L), Mar. 1964

Measurements of impurities in epitaxial silicon films based on the generalized expression derived from the counter-current model $N(x) = N_0^* \exp(-\phi x) + A(1 - \exp(-\phi x))$ are discussed. $N(x)$ is the impurity concentration at x microns from the substrate-film. N_0^* , A , and ϕ are constants which vary with the film's growing conditions, but ϕ is independent of the doping elements. The significance and temperature dependence of ϕ are considered. Measurements were performed on six kinds of samples which were grown by means of hydrogen reduction of SiCl_4 .

25,049 EFFECT OF COPPER OR SILVER ON THE CLUSTERING IN Al-10 wt % Zn ALLOYS by M. Ohta and F. Hashimoto (Osaka City U.); *J. Phys. Soc. Japan*, Vol. 19, pp. 133-134(L), Jan. 1964

The effect of copper or silver on clustering in Al-10 wt % Zn alloys has been studied through resistivity measurements. Isothermal aging curves were found to be similar to the Al-Zn binary alloy. The energy of formation of vacancies and activation energy of clustering are not affected by 0.1 wt % Cu or Ag.

25,050 ALKALI ION DOPING OF SILICON by J. McCaldin and A. Widmer (N.A. Aviation); *Proc. IEEE*, Vol. 52, pp. 301-302(L), Mar. 1964

The introduction of donor sites at high concentrations in the surface layers of a silicon crystal by bombardment with alkali ions is discussed. It is proposed that the donor concentration profile produced in Si by alkali ion bombardment consists of two distinct regions, a heavily doped surface layer whose thickness is comparable to the penetration depths expected for the energetic ions and, underlying this surface layer, a region of much gentler concentration gradients. It is shown that either sodium or cesium ions impinging on a p^+ silicon crystal can produce a $p-n$ junction lying in the second region of the profile and having characteristics quite comparable to junctions prepared by conventional methods.

25,051 PURIFICATION OF CdS BY PARTIAL SUBLIMATION IN A GAS FLOW by A. Vecht, B.W. Ely, and A. Apling (AEI Ltd., Harlow); *J. Electrochem. Soc.*, Vol. 111, pp. 666-668, June 1964

A method of purifying cadmium sulfide by partial sublimation in a gas flow is described. Results of spectrographic and wet analysis are given.

IMPURITY DIFFUSION

25,052 SOLID STATE DIFFUSION IN METALS AND ALLOYS by S.D. Gertshteyn and I. Ya. Dekhtyar (AEC, Washington, D.C.); *Transl. from Diffuziya v Metallakh i Splavakh v Tverdoi Fazhe*, Moscow, Gos. Izd. Fiz-Mat. Lit., 1960, 564 pp.; *Apr. 1964*, 536 pp.; *STAR*, Vol. 2, p. 1531(A), June 23, 1964 AEC-tr-6313; OTS \$6.00

The use of radioactive isotopes in research on diffusion in metals made possible the understanding of the mechanism involved in the process, and permitted estimates of the fundamental significance of this process in a great variety of problems of solid-state physics. The principal results of the research proved that diffusion processes are governed by the character of the interatomic interaction in the metal and its structure. It is significant that the diffusion parameters, usually determined in high-temperature measurements, are of great importance in many processes that occur in metals and alloys at both high and normal temperatures.

25,053 AN EXPLANATION FOR THE EFFECT OF FERROMAGNETISM UPON ATOMIC DIFFUSION by R.J. Borg (Lawrence Radiation Lab.); *J. Appl. Phys.*, Vol. 35, pp. 567-569, Mar. 1964

The effect of ferromagnetism upon atomic diffusion is shown to depend upon the change in elastic properties corresponding to the degree of magnetic order. The unusual temperature dependence of D , the diffusion coefficient, in the vicinity of T_C , the Curie temperature, can be reconciled with recent measurements of the shear moduli by using the Zener model for diffusion.

25,054 IMPURITY ATOM DISTRIBUTION FROM A TWO-STEP DIFFUSION PROCESS by D. Kennedy and P. Murley (IBM); *Proc. IEEE*, Vol. 52, pp. 620-621(L), May 1964

A two-step diffusion process that is a combination of two more frequently used processes has been utilized in transistor fabrication. Impurity atom diffusion is analyzed by solving Fick's 2nd law of diffusion for plane-parallel geometrical configurations subject to a particular set of initial and boundary conditions. The two steps are separately solved and the solutions are combined to give the impurity atom distributions after the two-step process:

$$C_2(0, t; t_1) = \frac{2C_0}{\pi} \tan^{-1}(K)$$

where $K = D_1 t_1 / D_2 t_2$ and subscripts refer to the proper step. Results of the calculations are presented in a normalized form.

25,055 DISLOCATION PIPE DIFFUSION by G.R. Love (Oak Ridge Labs.); *Acta Met.*, Vol. 12, pp. 731-737, June 1964

A model is developed which attributes the observed enhanced diffusivity in dislocation arrays entirely to processes occurring in the dislocation core. If an atom is transferred from the edge of the inserted plane in an edge dislocation into the row of sites into which that plane might grow by negative climb, this creates a "vacancy" in the edge of the inserted plane and an "interstitial" in the line of sites adjacent to that plane. Motion of these defects along the dislocation core would give rise to a net flux parallel to the dislocation line. The effects of correlated motion of the defects (cf. Lothe), are discussed and it is demonstrated that motion of the interstitial is essentially uncorrelated in an edge dislocation. The model is consistent with available data on diffusion in edge dislocations in silver, accounts adequately for the observed difference between edge and screw dislocation diffusivities, and leads to qualitative predictions regarding the diffusivity along extended dislocations and solute diffusion in dislocations.

25,056 A STUDY OF THE EFFECT OF THE MUTUAL ORIENTATION OF CRYSTALS ON INTERCRYSTALLINE DIFFUSION AND INTERNAL ADSORPTION by V.I. Arkharov and A.A. Pentina (Wright-Patterson AF Base); In its *Invest. of Heat Resistant Alloys*, June 19, 1963, pp. 208-246, FTS-9848/1 + 2+4; *STAR*, Vol. 2, p. 1192(A), May 8, 1964

A study into the effects of the mutual orientation of crystals upon intercrystalline diffusion in pure metal and also in the same metal when it contains a porophyll additive is discussed. The study is divided into the following areas of interest: (1) structural inhomogeneities and their effect on physical properties; (2) effect of the mutual orientation of crystals on the amount of excess energy in intercrystalline transition zones and on intergranular diffusion; and (3) dependence of intercrystalline orientation on the penetration depth of the diffusing substance along intercrystalline boundaries.

25,057 ACTIVATION ENERGIES FOR DIFFUSION IN PURE METALS AND CONCENTRATED BINARY ALLOYS by L.E. Toth and A.W. Searcy (Lawrence Radiation Lab.); *Trans. Met. Soc. AIME*, Vol. 230, pp. 690-694, June 1964

A modification of Le Claire's microscopic model for self-diffusion is developed in a form suitable for prediction of activation energies for diffusion in disordered substitutional solutions as well as in pure metals. Bonding is considered as a localized interaction, and the energy of bonding between atoms of different types is taken as the arithmetic mean of the energies for in the pure elements. The activation energies for vacancy formation and migration in substitutional alloys are shown to depend on the empirical constants developed for self-diffusion when the equations are adjusted for the mole fractions of the two elements. The differences in activation energies between alloys and pure metals are calculated and compared with the experimental differences.

25,058 THE MEASUREMENT OF VOLUME DIFFUSION BY THE METHOD OF AUTORADIOGRAPHY by T.J. Renouf (U. Edinburgh); *Philosophical Mag.*, Vol. 9, pp. 781-795, May 1964

The application of autoradiography to the measurement of volume diffusion is limited because of the difficulty in interpreting the effects of the energy of the radiations, the scattering and absorption properties of the specimen and other complicating factors. A general method of interpretation is described in which the effects of these factors are suitably combined into a single function that is determined by one experiment. The method is applied by matching

the experimental density trace of the diffusion zone, with a density curve which is computed from a derived expression. As a trial of this treatment, the diffusion of ^{124}Sb into single crystals of copper has been studied over the penetration range $10\ \mu < (Dt)^{1/2} < 150\ \mu$ and in the temperature range 560°C to 896°C with specimens mounted singly and in a double sandwich-type arrangement.

25,059 DIFFUSION IN B.C.C. METALS by R.A. Wolfe and H.W. Paxton (Carnegie Inst. Tech.); Contract Nonr76008, Mar. 1, 1964, 28 pp.; U.S. Gov. Res. Rep., Vol. 39, p. 121(A), May 20, 1964 AD 432 969
OTS \$2.60

25,060 THERMAL DIFFUSION OF SUBSTITUTIONAL IMPURITIES IN COPPER, GOLD AND SILVER by D. Jaffe and P.G. Shewmon (Carnegie Inst. Tech.); *Acta Met.*, Vol. 12, pp. 515-525, May 1964

An investigation of impurity thermal diffusion (Soret effect) in dilute solid alloys of Co, Ge, Ag and Au in copper, Ag and Ti in gold, and Au in silver was carried out using radioactive tracer techniques. In addition, an investigation of self-diffusion of pure copper and gold in a temperature gradient was carried out using (surface) marker movement techniques. The tracer experiments showed that a measurable amount of impurity segregation occurred in all systems except Au in Ag. Of the systems that exhibited segregation, Co in Cu became enriched at the cold side and the other impurities became enriched at the hot side. Marker movement experiments showed that a new flow of atoms toward higher temperatures occurred in gold and (tentatively) in copper. Marker movement experiments with silver were unsuccessful because of excessive evaporation.

25,061 ANOMALOUS VOLUME DIFFUSION IN THE SURFACE LAYERS OF METALS by A.J. Mortlock (Austral. Natl. U.); *Acta Met.*, Vol. 12, pp. 675-677(L), May 1964

Recent measurements of diffusion of iron, cobalt, and nickel in silver are reported which yield values of D_0 and Q much lower than previous measurements and are not consistent with self-diffusion data. This divergence is reviewed and some possible explanations are examined. It appears that primary phase regions of both silver and aluminum which are adjacent to a moving boundary, may be characterized by impurity diffusion coefficients which are much smaller than those observed farther away in the bulk of the specimen. Apparently the presence of a phase boundary is not essential, nor do surface oxide layers seem to play an important role in explaining the unusually low D_0 's and Q 's. The original higher values of D_0 's and Q 's are probably not much in error, and represent lattice diffusion. Further experiments in which the penetration profiles are determined simultaneously in the surface zone and specimen bulk are needed.

25,062 DIFFUSION IN THE GOLD-INDIUM SYSTEM by G.W. Powell (Ohio State U.), and J.D. Braun (Monsanto); *Trans. Met. Soc. AIME*, Vol. 230, pp. 694-699, June 1964

Diffusion between gold and indium at two temperatures below the melting point of indium (155.4°C) was investigated. The major component of the diffusion zone was determined to be AuIn_2 ; the other intermediate phases in the system occur in much narrower layers. In order of decreasing layer width these are: Au_3In_4 , AuIn , Au_4In . Interdiffusion coefficients of the four intermediate phases and the terminal solid solutions lie in the range of 2.4×10^{-13} to 1.8×10^{-11} sq cm per sec.

25,063 A STUDY OF INTERGRANULAR DIFFUSION IN METALS AND ALLOYS by V.I. Arkharov, C.M. Klotzman, A.N. Timofeyev, and I.I. Rusakov (Wright-Patterson AFB); June 19, 1963, pp. 198-207, In its Invest. of Heat Resistant Alloys; *STAR*, Vol. 2, p. 1192(A), May 8, 1964 (FTS-9848/1 + 2 + 4)

Experiments carried out to determine the effect of small additions of antimony upon the parameters of intercrystalline diffusion of silver in copper are discussed. The study was carried out by making a radiometric study of the diffusion of silver in polycrystalline copper in an alloy of copper and 0.4% antimony. It was found that antimony accelerates the intragranular diffusion of silver and that the length of the protrusions on the diffusion front in copper alloyed with 0.4% silver is of an order greater than in pure copper.

25,064 INVESTIGATION OF DIFFUSION OF SILICON IN CERTAIN TRANSITIONAL METALS by G.V. Samaanov, M.S. Kovalchenko and T.S. Verkhoglyadova (Wright-Patterson AFB); July 12, 1963, 11 pp., Transl. from *Inzhenerno-Fizi. Z.*, No. 3, pp. 62-67, 1959; U.S. Gov. Res. Rep., Vol. 39, p. 92(A), June 5, 1964 AD 434 940 OTS \$1.60

Diffusion of Mg in Al - See 24,988

25,065 STUDY OF REACTION DIFFUSION IN A CHROMIUM-NITROGEN SYSTEM by V.I. Arkharov, V.N. Konev, and A.Z. Men'shikov (Wright-Patterson AFB); June 19, 1963, pp. 686-697, In its Invest. of Heat Resistant Alloys; *STAR*, Vol. 2, p. 1092(A), May 8, 1964 (FTS-9848/1 + 2 + 4)

Conclusions resulting from an investigation of the nitriding of chromium in an atmosphere of ammonia include the following: (1) Reaction diffusion in chromium-nitrogen system takes place at an appreciable rate at 700°C and obeys a parabolic time law over the whole temperature range studied (up to $1,200^\circ\text{C}$). (2) When the temperature rises, the diffusion rate in the chromium-nitrogen system at first increases slowly (below $1,030^\circ\text{C}$), and then (above $1,030^\circ\text{C}$) it becomes rapid. (3) Below $1,030^\circ\text{C}$ nitriding produces two layers on the chromium—an inner, thicker layer of Cr_2N and an outer, thinner layer of CrN . (4) No porosity, loosening, or separation is observed on the boundary between the Cr_2N layer and the chromium metal. (5) All the structural characteristics of nitride layers indicate that during reaction diffusion in the chromium-nitrogen system, the nitrogen diffuses into the metal from the outside through the nitride layers and that there is no appreciable diffusion at all of the metal in the opposite direction.

25,066 DIFFUSION IN NICKEL-BASE SOLID SOLUTIONS by Yu. F. Babikova and P.L. Gruzin (Wright-Patterson AFB); June 19, 1963, pp. 191-197, In its Invest. of Heat Resistant Alloys; *STAR*, Vol. 2, p. 1192(A), May 8, 1964 (FTS-9848/1 + 2 + 4)

The diffusion of chromium in nickel-chromium alloys (10% to 28%) was studied, and it was found that the self-diffusion coefficients of nickel and the diffusion coefficients of chromium for these alloys have approximately the same values in high-temperature zones. It was shown that intensive recovery in nickel-chromium alloys takes place at a diffusion level of the order of $10^{-13}\text{cm}^2\text{-sec}^{-1}$. The diffusion level of solid solutions corresponding to the diffusion coefficients of the basic elements of the given magnitude may be tentatively called the threshold level of the diffusion mobility of intensive recovery in heat-resistant alloys, intended for short-time service at high temperatures. A rough estimate can be made of the potential level of heat resistance of solid solutions from data obtained from the calculation of diffusion coefficients.

25,067 MEASUREMENT OF THE GRAIN BOUNDARY DIFFUSION OF NICKEL-63 IN NICKEL AND γ -IRON by A. Hässner and G. Mischer (Tech. U. Dresden); *Phys. Stat. Sol.*, Vol. 5, pp. 63-71, 1964

Grain boundary diffusion of Ni^{63} in Ni and γ -Fe over the temperature range of 850 to 1100°C and 940 to 1130°C is discussed. A residual activity method was used in the study. An Arrhenius-type equation statistically describes the temperature dependence of diffusion. The vacancy diffusion mechanism for large angle boundaries in Ni is described.

25,068 THE DIFFUSION OF CARBON IN IRON-COBALT-CARBON AUSTENITES by A.S. Appleton (U. Liverpool); *Trans. Met. Soc. AIME*, Vol. 230, pp. 893-898, June 1964

The diffusion of carbon in Fe-Co-C austenites was studied as a function of cobalt concentration up to 12 at. pct, using an autoradiographic technique. The diffusion coefficient was found to initially decrease and then increase with increasing cobalt concentration, the trends being more marked the higher the temperature of diffusion. These effects were paralleled by variations in the activation energy and the constant for diffusion which, however, were found to be dependent also on the carbon content. The results are compared with the previously available data and their significance is discussed in terms of the kinetics of solid-state reactions in this system.

25,069 EFFECT OF DISLOCATIONS ON THE DIFFUSION OF CADMIUM IN GALLIUM ARSENIDE by M.A. Benkik, R.L. Petrusevich and E.S. Sollertinskaya (Moscow State Sci. Res. Inst.); *Soviet Phys. Solid State*, Vol. 5, pp. 2375-2376, May 1964

The influence of dislocations on the depth and geometry of a p-n junction produced by diffusion of cadmium in gallium arsenide has been investigated. The experimental results show that the diffusion has a "slow" as well as a "fast" component, and the "fast" component is due to the dislocations. The depth of the p-n junction is found to increase with the increase of the dislocation density.

25,070 DIFFUSION OF Zn INTO GaAs UNDER THE PRESENCE OF EXCESS ARSENIC VAPOR by H. Rupprecht and C.Z. LeMay (IBM Watson Res. Ctr.); *J. Appl. Phys.*, Vol. 35, pp. 1970-1973, June 1964

The concentration dependence of the diffusion coefficient of Zn in GaAs has been measured under excess arsenic vapor pressure at 850°C . The diffusion coefficient varied under these conditions only from 10^{-11} to about $10^{-10}\text{cm}^2/\text{sec}$ as the zinc concentration increased from 10^{17} to 10^{20} zinc atoms/ cm^3 . These results are compared with diffusion coefficients found in the absence of excess arsenic by the authors and other workers. The observed difference can

be explained by means of an interstitial-substitutional equilibrium. The excess arsenic increases the substitutional component of the diffusion and suppresses the interstitial component. These results are in good agreement with the model first suggested by Longini. The activation energy of the substitutional diffusion coefficient is found to be about 2.8 eV.

25,071 RAPID IMPURITY DIFFUSION IN GaAs ESAKI DIODES by A. Shibata (Sony Res. Lab., Yokohama); *Solid-State Electronics*, Vol. 7, pp. 215-218, Mar. 1964

The rapid diffusion process of Zn in GaAs has been investigated experimentally by making use of the deterioration of GaAs Esaki diodes. Three diffusion processes were found responsible for the deterioration. The diffusion constants of these processes at an ambient temperature of 300°K were in the order of 10^{-20} cm²-sec⁻¹. This figure is about 10^{20} times larger than the thermal diffusion constant at the same temperature. This factor is approximately the value of $\exp(-E/kT)$ for $T = 300^\circ\text{K}$ and the forward bias voltage across a junction of 1.2 V observed in this experiment. The result obtained here confirms the deterioration mechanism proposed by Longini.

25,072 DIFFUSION MECHANISM OF Zn IN GaAs AND GaP BASED ON ISOCONCENTRATION DIFFUSION EXPERIMENTS by L.L. Chang and G.L. Pearson (Stanford U.); *J. Appl. Phys.*, Vol. 35, pp. 1960-1965, June 1964

Precise relationships between the diffusion coefficient D and the zinc concentration C are obtained from isoconcentration diffusion experiments performed at 900°C for zinc in GaAs and at 1000°C for zinc in GaP. It is found that D varies with C from a slightly less than cubic to a somewhat less than square dependence over the concentration range 10^{18} to 10^{20} cm⁻³. Possible mechanisms that result in concentration-dependent diffusion are discussed. Under the conditions given above, it is concluded that diffusion occurs by an interstitial-substitutional mechanism with the interstitial mode being dominant. The charge states of the various species involved in the diffusion are believed to be: (1) interstitial zinc atoms are doubly ionized donors; (2) substitutional zinc atoms are either neutral or singly ionized acceptors; and (3) gallium vacancies are neutral. A theoretical expression for D versus C , derived under these assumptions, fits the isoconcentration diffusion data over wide ranges of D and C through the use of only one adjustable parameter.

25,073 DIFFUSION AND SOLUBILITY OF IMPURITY ELEMENTS IN COMPOUND SEMICONDUCTORS by G.L. Pearson (Stanford U.); Rept. No. 63 147, Dec. 1963, 10 pp., Contract DA04 200ORD1087; U.S. Gov. Res. Rep., Vol. 39, p. 115(A), May 5, 1964 AD 430 994 OTS \$1.10

The diffusion of some impurity elements into III-V compounds is anomalous in that the diffusion coefficient is strongly concentration dependent. Careful measurements were made on the diffusion of Zn into both GaAs and GaP. A careful analysis of these results leads to the conclusion that diffusion occurs by an interstitial-substitutional mechanism, with the interstitial mode being dominant in the over-all process. The solubilities and distribution coefficients of Zn in these two semiconductors have been calculated as functions of temperature up to the melting point of the solvents. A sharp increase in the distribution coefficient near the melting point is accounted for by considering the transfer of neutral Zn from the liquid to the solid, where some Zn atoms become ionized acceptors.

25,074 DIFFUSION AND SOLUBILITY OF ZINC IN INDIUM PHOSPHIDE by L.L. Chang and H.C. Casey, Jr. (Stanford U.); *Solid State Electronics*, Vol. 7, pp. 481-485, June 1964

Radiotracer Zn⁶⁵ has been diffused into n-type indium phosphide single crystals from constant pressure vapor sources in closed, evacuated quartz ampoules. The solubilities and diffusion profiles have been obtained at temperatures between 600 and 900°C. Although retrograde solid solubility is expected at higher temperatures, the data below 900°C are an excellent fit to the relation $C = 1.4 \times 10^{25} \exp(-0.92/kT)$. The diffusion coefficient is found to be concentration dependent. The profiles drop steeply near the surface and have the same steep diffusion front that is found for Zn in GaAs. The diffusion is believed to occur by a parallel-mode mechanism involving both interstitial and substitutional zinc.

25,075 DIFFUSION OF GALLIUM IN INHOMOGENEOUS SILICON by B.I. Boltaks and T.D. Dzhaferov (Acad. Sci. USSR); *Soviet Phys. Solid State*, Vol. 5, pp. 2649-2651(L), June 1964

A study of the diffusion of gallium in silicon with a nonuniform distribution of antimony is reported. The results show that the presence of antimony raises the diffusion velocity of gallium and the rise increases with the decrease of the diffusion annealing temperature. It is suggested that this rise could be due to the oppositely directed concentration of the impurities, which may result when antimony evaporates from the test samples during the diffusion of gallium.

25,076 SELF-DIFFUSION STUDIES OF DELTA PLUTONIUM by R.E. Tate and E.M. Cramer; Appendix by A.S. Goldman (Los Alamos Lab.); *Trans. Met. Soc. AIME*, Vol. 230, pp. 639-644, June 1964

The diffusion coefficient for self-diffusion of plutonium in the temperature range 350 to 440°C has been measured by using Pu²³⁸ as the tracer isotope. Autoradiographic techniques were used to investigate the possibility of grain boundary diffusion but only evidence for volume diffusion was found. The least-squares fit of the data gives the following equation for the diffusion coefficient:

$$D = 4.5 \times 10^{-3} \exp \left[\frac{-23,800}{RT} \right] \text{ cm}^2/\text{sec}$$

The computer least-squares technique for fitting the nonlinear equations is outlined.

25,077 DIFFUSION OF XENON IN CERAMIC OXIDES by D.L. Morrison, T.S. Elleman, and D.N. Sunderman (Battelle Inst.); *J. Appl. Phys.*, Vol. 35, pp. 1616-1622, May 1964

Postirradiation measurements were made at 700° to 1500°C of the release of ¹³³Xe recoiled into single-crystal $\alpha\text{-Al}_2\text{O}_3$, BeO, MgO, and ZrO₂ crystals during neutron irradiation in contact with UO₂ powder. The release pattern from most of the specimens was identical: a high rate of loss of ¹³³Xe for several minutes followed by a slower release for which the cumulative fractional release was linear with the square root of the heating time. Diffusion coefficients for ¹³³Xe have been calculated from the slope of the release curve following the initial release. The magnitudes of the diffusion coefficients above 1100°C for $\alpha\text{-Al}_2\text{O}_3$, BeO, and MgO were nearly the same whereas the diffusion coefficients in ZrO₂ were ten to a hundred times larger. The activation energy for ¹³³Xe release from $\alpha\text{-Al}_2\text{O}_3$ above 1100°C was 64 kcal/g-mole. The xenon release behavior has been compared to anion diffusion in these oxides.

CRYSTAL GROWTH

GENERAL

25,078 CRYSTAL GROWTH TECHNIQUES by E.A.D. White; *GEC Journal*, Vol. 31, pp. 43-53, 1964

A critical review of modern techniques available for the growth of single crystals of oxides and refractory materials is presented. A novel classification of growth techniques with the relative advantages and disadvantages with regard to crystal quality and purity is given. The choice of an appropriate technique for any given material must be based on a number of factors of which the chemical stability, melting point and heat conductivity are particularly important.

25,079 ZONE-MELTING APPARATUS FOR ALKALI METAL CYANIDES AND ALKALI METAL HALIDES by T.J. Neubert (Illinois Inst. Tech.), and S. Susman (Argonne Lab.); *Rev. Sci. Instr.*, Vol. 35, pp. 724-727, June 1964

A zone-melting apparatus is described that can be largely assembled from commercially available components. Details of a technique are given for zone refining alkali metal cyanides and halides in reinforced, flexible metal boats.

25,080 ELECTRON BEAM FLOATING ZONE MELTING; AN IMPROVED BEAM DEFLECTION CAGE by R. Brownsword and J. Farr (U. Birmingham, G.B.); *J. Sci. Instr.*, Vol. 41, pp. 350-351(L), May 1964

A small electron focusing cage for use in electron bombardment floating zone melting is described. The design eliminates contamination of the specimen by the filament which is protected from material ejected by the molten zone, is not visible to the operator, and does not interfere with observation of the zone. A grid electrode has been used, which reduces the power required to form a given zone.

25,081 ELECTROMAGNETIC MIXING OF METALS AND ALLOYS by J.J. Schott (Bell Lab.); *Rev. Sci. Instr.*, Vol. 35, pp. 411-412, Mar. 1964

A method has been developed for improving the homogeneity of alloy blanks to be used in the growing of single crystals. The technique is particularly useful where widely different densities of the alloy components make uniform composition difficult to obtain. It involves premixing of the alloy charge by electro-magnetic stirring. The required apparatus is described in detail. X-ray analysis of bismuth-antimony alloys with antimony concentrations from 2-20 atomic percent showed macroscopic compositional variations of less than $\pm 5\%$ in Sb/Bi ratio over an 8 inch ingot. Electron microprobe analysis showed microscopic compositional fluctuations due to constitutional supercooling, but proper crystal growth techniques can effectively eliminate these fluctuations.

5,082 BACK DIFFUSION THROUGH THE CAPILLARY IN THE FLOATING CRUCIBLE TECHNIQUE OF CRYSTAL GROWTH by G. Blockwell (Brunel Coll. London); *Solid State Electronics*, Vol. 7, p. 105(L), Jan. 1964

An expression for the limiting length of the capillary to achieve no back diffusion is obtained from the equation for the impurity distribution which must exist during growth. The derived expression is $\exp(-vL/D) = 0$ where v = velocity of liquid flowing through the capillary, L = capillary length, and D = impurity diffusion coefficient. This condition is fulfilled if $L > 5D/v$; therefore, the capillary must be designed for the slowest pulling speed.

SINGLE CRYSTALS

5,083 GROWTH OF HIGH-PURITY COPPER CRYSTALS by E.M. Porbansky (Micro State Electronics); *Trans. Met. Soc. AIME*, Vol. 230, pp. 925-926(L), June 1964

A method for preparing very pure copper crystals by the Czochralski technique is described. A trace of oxygen in the helium atmosphere appears to be necessary for obtaining high-purity copper single crystals. A rotating polycrystalline copper rod is brought into contact with the melt. The seed is raised when equilibrium is obtained between the rod and melt, and temperature is controlled to reduce the crystal diameter. This reduces the number of crystals at the liquid-solid interface until only one crystal remains. Possible explanations of improved purity (as determined by resistivity ratios) compared with the starting material are improvement in crystal perfection, segregation, and oxidation of impurities. High purity copper crystals grown by this pulling technique make possible the acquisition of previously unobtainable information regarding the electron energy band structure.

Growth of:

$\text{Rb}_2\text{K}_1\text{-xNO}_3$ - See 25,189
 $\text{K}_2\text{O-nTi}_2\text{O}_5$ - See 24,978

5,084 GROWTH OF CUPROUS OXIDE (Cu_2O) CRYSTAL by T. Nakano, K. Ohnishi, A. Kinoshita, and T. Okuda (Tokyo Electrical Engrg. Coll.); *Japanese J. Appl. Phys.*, Vol. 3, p. 124, Feb. 1964

A method for growing Cu_2O crystals approximately 20 mm x 10 mm in area and 1 mm thick by successive oxidation of a Cu block is presented. Optimum results occur when the Cu is oxidized in air at 1020°C for 50 to 60 hours.

5,085 THE PRODUCTION OF LiF SINGLE CRYSTALS WITH SELECTED ISOTOPIC RATIOS OF LITHIUM by C.F. Weaver, R.G. Ross, B.J. Sturm, J.E. Morgan, and R.E. Thoma (Oak Ridge Lab.); Mar. 1964, 48 pp., Contract W-4405-ENG-26; *STAR*, Vol. 2, p. 1194(A), May 8, 1964 ORNL-3341 OTS 1,25

The purpose of this research was to develop the techniques and apparatus necessary to produce single crystals of LiF with selected ratios of the lithium isotopes containing not more than a few parts per million impurities. The starting material was prepared from purified aqueous solutions of LiOH and HF and was dehydrated in the molten state with anhydrous HF. The dehydrated LiF was then converted into a single crystal in a Stockbarger furnace. Crystals weighing several hundred grams and containing 99.99, 98.06, and 96.50 a/o lithium-7 have been produced as part of a sequence that will include 87.60, 92.28, 69.24, 50.77, and 0.7 a/o lithium-7. These crystals do not display birefringence under polarized light and do not show OH^- absorption of infrared radiation.

5,086 PRODUCTION OF LARGE FLOURITE CRYSTALS OF OPTICAL QUALITY by V. Prakash (U. Delhi); *Indian J. Tech.*, Vol. 2, pp. 46-48, Feb. 1964

The production of transparent single crystals of calcium fluoride suitable for use in optical systems is discussed. The crystals were produced by heating high quality natural flourspar (m.p. 1400°C) to 1600°C in a chemically clean graphite crucible and freezing it slowly under a high, constant, non-linear temperature gradient. It is found that the addition of 2% lead fluoride as a scavenger impurity improves the quality of the product. Construction details of the elevator type electric vacuum furnace with graphite heating element, and accessories employed, are described.

5,087 HYDROTHERMAL GROWTH OF LARGE SOUND CRYSTALS OF ZINC OXIDE by R.A. Laudise, E.D. Kohl, and A.J. Caporaso (Bell Labs.); *J. Am. Ceramic Soc.*, Vol. 47, pp. 9-12, Jan. 1964

Large macroscopically sound ZnO crystals were grown hydrothermally at rates of from 10 to 15 mils per day. Seven factors were found to be important in achieving good growth: (1) Base concentration of growth solution; (2) Temperature difference between dissolving and growth regions; (3) Presaturation of

growth solution; (4) Warm-up procedure; (5) Addition of Li^+ to growth solution to suppress dendrite formation; (6) Etching to remove seed damage; and, (7) An nutrient size. The effects of each factor are discussed.

25,088 RAISING-CRUCIBLE METHOD FOR SINGLE CRYSTAL GROWING by H. Sasaki and S. Kisaka (Matsushita Electric Ind., Ltd., Osaka); *Japanese J. Appl. Phys.*, Vol. 3, pp. 170-171(L), Mar. 1964

The technique of raising-crucible in a verticle furnace with appropriate temperature gradient for the preparation of a single crystal of volatile material is discussed. The experiment was conducted on HgS . A large single crystal required two weeks for growth. When finished, it contained small cracks probably due to phase transitions between hexagonal and cubic at about 335°C.

25,089 GROWTH OF SINGLE CRYSTALS OF BaTiO_3 BY EXAGGERATED GRAIN GROWTH by R. De Vries (GE); *J. Am. Ceram. Soc.*, Vol. 47, pp. 134-136, Mar. 21, 1964

Grain-growth experiments with steep temperature gradients and with polycrystalline aggregates seeded with single crystals have been carried out to explore the feasibility of growing large crystals of BaTiO_3 in the solid state. It is shown that both methods resulted in a large increase in size of crystals normally obtained by sintering but that the rapid grain-boundary motion resulted in high porosity. Definite orientation dependence of grain-boundary velocity is demonstrated, and growth in a $\langle 110 \rangle$ direction was found to be at least as fast as 2 mm per hour.

25,090 FLOATING-ZONE BaTiO_3 : PREPARATION AND PROPERTIES by F. Brown and W.H. Todt (Williams Coll.); *J. Appl. Phys.*, Vol. 35, pp. 1594-1598, May 1964

Single-crystal boules, 2.5 cm long by 0.32 cm diameter, of ferroelectric BaTiO_3 containing 1.5% SrTiO_3 have been grown by a floating-zone process. Since the use of a crucible to contain the molten material is avoided, high inherent purity is achieved. In addition boule shape permits studies not feasible with the earlier butterfly wing crystals of Remeika. Several of the ferroelectric and structural properties have been measured and are similar to those well known for crystals grown by other methods. X-ray rocking curves possessing double peaks have been observed, an effect which is ascribed to ferroelectric domains.

Growth of GaAs - See 24,899

25,091 THE PREPARATION OF SEMI-INSULATING GALLIUM ARSENIDE BY CHROMIUM DOPING by G. Cronin and R. Haisty (Texas Inst.); *J. Electrochem. Soc.*, Vol. 111, pp. 874-877, July 1964

The preparation of single crystal semi-insulating (10^4 - 10^{12} ohm-cm) GaAs is reviewed. Attempts to pull such crystals by oxygen doping are not uniformly successful because of the formation of oxides on the melt surface. Semi-insulating GaAs with a room temperature resistivity of 10^8 ohm-cm can be consistently pulled by doping with chromium. The amount of chromium used is not critical but must exceed the concentration of residual n-type impurities. Doping can be easily accomplished in vertical crystal pulling equipment allowing the production of single crystals of controlled orientation. Considerable discussion of the effects of chromium doping is included.

25,092 $\text{GaAs}_{1-x}\text{P}_x$ SYNTHESIS by R.N. Hall and T.J. Soltys (GE); In its *Semicond. Device Concepts*, Oct. 31, 1963, pp. 59-61; *STAR*, Vol. 2, p. 624(A), Mar. 8, 1964 AD 426 258

Growth of crystals from a gallium solution was studied as a method of preparing mixed crystals of gallium arsenide and gallium phosphate which are used to construct diodes. Runs were made to obtain these crystals; the procedure used is discussed; and the two compositions used for the runs are given. Diodes were made from the crystals obtained from the runs. The wavelengths of the radiation produced by the diodes indicate that the compositions of the crystals are reasonably close to the design value.

25,093 GROWTH OF GaP CRYSTALS AND p-n JUNCTIONS BY A TRAVELING SOLVENT METHOD by M. Weinstein and A.I. Mlavsky (Tyco Lab.); *J. Appl. Phys.*, Vol. 35, pp. 1892-1894, June 1964

A traveling solvent method has been used to grow GaP crystals from Ga solution. Growth rates of approximately 0.5 mm/h have been achieved at an average temperature as low as 850°C, from Ga zones 0.025 mm thick. Polycrystalline growth, 10 mm in diameter and 2 mm thick, has been achieved as a direct continuation of the crystal orientation in polycrystalline seeds. p-n junction structures have been grown by doping from a 2% Ge-Ga solvent zone. Some electrical characteristics of small diodes cut from polycrystalline crystals are described.

25,094 VAPOR PHASE GROWTH OF SINGLE CRYSTALS by P.S. Schaffer (Lexington Labs.); Contract AF19 628 2383, 47 pp., Jan. 1964; U.S. Gov. Res. Rep., Vol. 39, p. 161(A), May 20, 1964 AD 433 232 OTS \$4.60

A chemical vapor deposition process developed for epitaxial growth of sapphire single crystals is described. Apparatus was designed and constructed for use in the crystal growth process. Oriented crystals weighing up to five grams were grown at temperatures considerably below the melting point. The rate of growth for constant gas compositions and flow rates was found to increase with an increase in temperature. Etch pit studies showed an average dislocation density of 100 dislocations sq cm. Spectrochemical analyses indicated total impurity levels below 40 ppm.

25,095 PREPARATION OF URANIUM MONOCARBIDE SINGLE CRYSTALS by H. Nadler (Atomics Intl.); Contract AT(11-1)-GEN-8, 65 pp., Apr. 30, 1964; STAR, Vol. 2, pp. 1530-1531(A), June 23, 1964 NAA-SR-7465; OTS \$1.50

Single crystals of uranium monocarbide (UC), 1/4 in. in diameter by 2-in. long, were prepared from arc-melted rods of stoichiometric and off-stoichiometric compositions by a two-step process. An arc-melted rod was float-zone melted in an electron beam furnace to form a superstoichiometric two-phase structure, in which uranium dicarbide (UC₂) platelets precipitated along the (100) crystallographic planes of the UC matrix. Subsequent decarburization of the UC₂ platelets by hydrogen reduction produces a UC single crystal. Precise control of the decarburization process was required to achieve stoichiometry.

25,096 SINGLE-CRYSTAL GROWTH OF LaF₃ by P.F. Weller and J.A. Kucza (IBM Watson Res. Ctr.); J. Appl. Phys., Vol. 35, pp. 1945-1946, June 1964

Single crystals of LaF₃ have been grown by the Czochalski technique. Crystal clarity and perfection were strongly dependent on the amount of oxide impurity. Trivalent rare-earth doping was easily achieved, and divalent doping was possible with the easily reduced rare earths such as europium and samarium.

Growth of Bi₄Ti₃O₁₂ - See 25,187

25,097 SINGLE CRYSTALS OF LEAD ZIRCONATE-TITANATE SOLID SOLUTIONS by S. Fushimi and T. Ikeda (Nippon Tel. and Tel.); Japanese J. Appl. Phys., Vol. 3, pp. 171-172(L), Mar. 1964

Results of experiments aimed at obtaining single crystals of Pb(Zr-Ti)O₃ with KF-PbF₂ and PbO-PbF₂ as flux are reported. Raw materials were always powdered specimens prepared by the solid state reactions. Analytic procedures were employed to obtain distributions in resultant solid solutions since they often differ from the composition of starting materials. All crystals obtained were birefringent at room temperature and became optically isotropic above certain temperatures. Over certain composition ranges, no crystals could be obtained; it is postulated that these regions correspond to miscibility gaps in the phase diagram of the flux-PbTiO₃-PbZrO₃ system.

25,098 GROWTH OF BISMUTH-ANTIMONY SINGLE-CRYSTAL ALLOYS by D.M. Brown and F.K. Heumann (GE Res. Lab.); J. Appl. Phys., Vol. 35, pp. 1947-1951, June 1964

Homogeneous crystals of Bi-Sb solid solutions are difficult to grow, but are important for the basic understanding of the electron transport properties and band structure of these materials. The problems arise from (1) the low melting temperature (approximately 300°C) which makes it difficult to achieve a large thermal gradient at the crystal growing interface; (2) the small liquid diffusion coefficient which was estimated to be between 2 and 3 x 10⁻⁵ cm²/sec at 300°C; and (3) a segregation coefficient so large (5-10) as to favor growth of undesirable cellular substructure. Under existing theories of crystal growth, the conditions necessary for producing crystals with Sb compositions from 5% to 14% free of macro- and micro-inhomogeneity are described. A zone-melting technique was used to grow the crystals with temperature gradients in the molten zone about 60°C/cm and growth rates between 1.6 and 0.4 mm/h. The degree of homogeneity was determined by etching studies, chemical analysis, and electron beam microprobing. Preliminary electrical measurements show considerable difference from previous measurements, particularly for the higher Sb contents.

25,099 GROWTH AND PROPERTIES OF SINGLE CRYSTALS OF HEXAGONAL FERRITES by R.O. Savage and A. Tauber (USARDL); J. Am. Ceramic Soc., Vol. 47, pp. 13-18, Jan. 1964

The growth of single crystal hexagonal ferrites from the system NaFeO₂-Fe₂O₃-BaO-MeO (Me = divalent Zn, Co, Ni or Mg) is discussed. Reaction products were studied by x-ray diffraction and optical microscopy. Stability data for principal single products are given for initial compositions lying in quaternary planes. Four new hexagonal ferrite structures, derived from Ba₃Me₂Fe₂₄O₁₁ by

adding blocks of Ba₂Me₂Fe₁₂O₂₂, were discovered. Magnetization as a function of temperature and field was studied for crystals of two structure types.

GROWTH OF THIN FILMS

25,100 THICKNESS MEASUREMENTS OF THIN GOLD FILMS BY X-RAY SPECTROSCOPY by A. Tosaki, M. Saitoh, and A. Kinbara (U. Tokyo); Japanese J. Appl. Phys., Vol. 3, pp. 234-235(L), Apr. 1964

Samples of uniform gold films prepared by vacuum evaporation on quartz have been bombarded with neutron flux of 3 x 10¹¹ cm⁻² sec⁻¹ for one hour. The thickness of the thickest film was determined by multiple beam interferometry. The β -decay of Au¹⁹⁸ was followed with 410 keV γ -rays for all films and thickness was calculated for each by the ratio of the 410 keV photopeak to that of the thickest film. This method is much more accurate than interferometry for thicknesses below 100 Å. A discussion of inherent errors in the method is presented.

25,101 SPUTTERING OF POLYCRYSTALLINE COPPER AND SILVER BY 30-170 KEV ARGON IONS by C.E. Ramer, M.A. Narasimham, H.K. Reynolds, and J.C. Allred (U. Houston); J. Appl. Phys., Vol. 35, pp. 1673-1680, June 1964

Polycrystalline copper and silver have been sputtered by 30-170 keV singly ionized argon at various beam angles, and total yields (atoms/ion) have been measured as a function of energy and incident angle. Angular distributions of sputtered material about the target normal indicate a distribution approximately proportional to the cosine of the angle of emission, but with more material collected in the normal direction than for a strict cosine distribution. No significant variation of angular distribution with ion energy or with sputtering beam angle was observed. The yield appears to be independent of pressure, collector temperature, current, and current density. Erratic results were obtained when the target was not water cooled, and when the glass collector plates were not initially coated with a thin layer (~50 Å) of evaporated metal.

25,102 PREPARATION AND PROPERTIES OF GaAs-GaP, GaAs-Ge, AND GaP-Ge HETEROJUNCTIONS by M. Weinstein, R.O. Bell, and A.A. Menon (Tyco Lab.); J. Electrochem. Soc., Vol. 111, pp. 674-682, June 1964

Epitaxial films of GaAs and GaP have been deposited on GaAs, GaP, and Ge substrates by a vapor phase chemical reaction technique. The growth variables such as source temperature, seed temperature, crystal orientation, surface preparation, and gas flow rate, have been investigated. The optimum conditions for the growth of epitaxial films and the electrical characteristics of these films are reported. GaAs-GaP junctions grown by a solution growth technique (TSM) are abrupt, whereas junctions grown by the vapor phase technique are graded. Detailed measurements of the I-V characteristics and capacitance of GaAs-Ge, GaAs-GaP, and GaP-Ge abrupt heterojunctions are interpreted in terms of Anderson's model. Kinks in the I-V characteristic are explained by discontinuities in the valence and conduction bands.

25,103 VAPOR GROWTH OF GERMANIUM BY THE HYDROGEN REDUCTION OF GERMANIUM TETRAIODIDE by S. Iida and Y. Sugita (Hitachi Ltd.); Japanese J. Appl. Phys., Vol. 3, pp. 163-164(L), Mar. 1964

The epitaxial deposition of germanium by the hydrogen reduction of GeI₄ in "open tube" process is discussed. The deposition occurred in a two zone quartz reaction tube: the first zone, containing the GeI₄, was heated between 100° and 160°C; the second zone contained the germanium substrate. Deposition temperature was varied from 520° to 800°C. Hydrogen flow rate was 2 L/min. Crystal growth rate was found to increase with increasing GeI₄ concentration, peaking at a mole fraction of 0.0007 and then diminishing. From the temperature dependence at constant mole fraction (0.0002) the activation energy for the growth process was found to be 8.3 ± 0.7 kcal/mole.

25,104 EPITAXIAL DEPOSITION OF SILICON LAYERS BY PYROLYSIS OF SILANE by S.E. Mayer and D.E. Shea (Trancoa Chem.); J. Electrochem. Soc. Vol. 111, pp. 550-556, May 1964

The pyrolysis of silane diluted by a carrier gas in a horizontal-type system is described. Films of closely controlled thickness have been obtained. Control of the electrical resistivity of the films by admixture of suitable dopants is shown. The effect of various process parameters on growth rate is discussed. Experimental data on migration of dopant from the substrate to the grown layer are presented, and the mechanism involved is discussed. Some characteristics of devices using such layers are shown.

25,105 THE EPITAXIAL DEPOSITION OF SILICON ON QUARTZ by R.W. Bicknell, J.M. Charig, B.A. Joyce and D.J. Stirland (Plessey Ltd.); Philosophical Mag., Vol. 9, pp. 965-978, June 1964

pitaxial layers of silicon have been grown on single crystal quartz by a chemical reaction, the hydrogen reduction of trichlorosilane, at the substrate surface. Glancing angle electron diffraction has been used to determine the orientation dependence, which is {001} silicon parallel to {0001} quartz, and {100} silicon parallel to {1010} quartz. The growth process has been studied using electron microscope techniques, and found to be somewhat similar to that previously observed for vacuum condensed metal films. Transmission electron microscopy has also shown the presence of a very large number of defects in the films.

25,106 EPITAXIAL GROWTH OF SILICON CARBIDE by R.W. Brander (GE Ltd., Wembley); *J. Electrochem. Soc.*, Vol. 111, pp. 881-883, July 1964

The growth of single crystal layers on silicon carbide by simple vapor phase techniques is described. High quality growth can be achieved at rates of 0.5 μ /min if the vapor stream does not impinge on the growing face. Layers grown above 1900°C show perfect polytype reproduction. Low temperature may cause polycrystalline cubic material to nucleate. It was observed that opposite {0001} faces grow at markedly different rates under identical conditions.

25,107 ANODIC OXIDE FILMS FOR DEVICE FABRICATION IN SILICON. Part I. THE CONTROLLED INCORPORATION OF PHOSPHORUS INTO ANODIC OXIDE FILMS ON SILICON by P.F. Schmidt and A.E. Owen (Westinghouse Res. Lab.); *J. Electrochem. Soc.*, Vol. 111, pp. 682-688, June 1964

The preparation of phosphorus doped anodic oxide films on silicon is described. These oxide films can be used as phosphorus diffusion sources during heat treatment. The concentration and distribution of the phosphorus in the oxide film has been investigated by tracer techniques, the quality of the oxide film by electron microscopy. Oxide growth in the solutions and at the current densities investigated occurs preponderantly by cation migration. A novel method is described for measuring the amount of silicon converted into oxide per volt forming voltage. The density of the oxide can also be calculated by this method.

25,108 PbTe THIN FILM PREPARED BY VACUUM EVAPORATION ON MICA by Y. Mokino (Sony Corp.); *J. Phys. Soc. Japan*, Vol. 19, p. 580(L), Apr. 1964

Single crystal films of PbTe have been obtained by vapor deposition onto cleavage faces of mica. These films have parallel orientation over the entire specimen where the relation of orientation between PbTe and mica is (111) mica // (001) PbTe. Epitaxial growth of PbTe on mica is possible because; (1) the binding force between PbTe and mica is large, (2) nearly stoichiometric Pb and Te is deposited, and (3) thin layers of adsorbed gases on cleavage faces of mica may act to reduce misfit. Lattice constants, resistivity and Hall coefficient of these films were measured.

25,109 PREPARATION OF SINGLE-CRYSTAL FILMS OF PbS by R.B. Schooler and J.N. Zemel (U.S. Naval Ord. Lab.); *J. Appl. Phys.*, Vol. 35, pp. 1848-1851, June 1964

Thin single-crystal films of lead sulfide have been prepared by vapor deposition on heated rocksalt substrates in the 0.2-8.0- μ range. Electrical and optical measurements have established that the properties of the films compared favorably with the bulk material and are suitable for a large number of experimental investigations. The index of refraction for PbS is in good agreement with previously obtained bulk values. The various electrical properties of the films, particularly the Hall mobility, are in very good agreement with those of bulk material.

GROWTH OF WHISKERS (DENDRITES)

25,110 ELECTRON MICROSCOPIC EXAMINATION OF ROLE OF AXIAL DISLOCATIONS IN GROWTH OF AlN WHISKERS by C.M. Drum and J.W. Mitchell (U. Virginia); *Appl. Phys. Lett.*, Vol. 4, pp. 164-165(L), May 1, 1964

The role of axial dislocations in the growth of aluminum nitride (AlN) crystals from the vapor phase is discussed. Three types of whiskers were studied by transmission electron microscopy: (a) Blade-shaped filaments with large faces parallel to {1010} and with the growth direction along the C+2a or [2423] direction in this plane. Axial dislocations with Burgers vectors along C = [0001], at 52° to the dislocation line, were observed, (b) Blade-shaped filaments with large faces parallel to the basal plane (0001), with the growth direction along <1010> midway between two 2 vectors. In some of these crystals these were axial dislocations (with Burgers vectors along a \bar{a} direction at 30° to the dislocation line) along their entire length. (c) Dislocation free filaments of hexagonal cross section, with growth direction along <0001>.

The filaments of group (a) probably grow by means of a dislocations mechanism. However, the presence or absence of axial dislocations in crystals grown under identical conditions suggests that axial dislocations are not essential for the growth of AlN whiskers.

25,111 DENDRITE CRYSTALS OF METALLIC SELENIUM GROWN FROM VAPOR by N. Furuta (Tokyo Gakugei U.); *Japanese J. Appl. Phys.*, Vol. 3, pp. 237-242, May 1964

Dendrite crystals of metallic Se grown from the vapor with the supersaturation ratio maintained constant at 25 to 100 can be classified into five groups depending on the shape and crystal structure. The growth mechanism of these dendrite crystals, except for one group, relates to the twinning. The difference in the shape of these dendrite crystals comes mainly from the number of twin boundaries contained therein and the mutual relations between them. The growth of dendrite crystals containing two twin boundaries mainly starts at the steps and kinks formed by overlapping of two thin films originating from each boundary.

CRYSTAL SURFACES

25,112 THE DEPENDENCE OF THE INTERACTIONAL FORCES BETWEEN INERT GASES AND METAL SURFACES ON THE CRYSTALLOGRAPHICAL DIRECTIONS by K.F. Wojciechowski (U. Wroclaw); *Acta Phys. Polonica*, Vol. 25, pp. 255-263, Feb. 1964

On the basis of London's method, the interactional energy between inert gases and metal surfaces is computed and its dependence on the crystallographical direction is given. It is shown that for a metal with cubic body-centered lattice the surfaces with higher Miller indices adsorb inert gases more easily than those with lower indices. The calculations are in good agreement with the experimental results.

25,113 APPARATUS FOR STUDYING THE KINETICS OF OXIDATION IN METALS by P.M. Arzhanyi and N.N. Velichenko (Wright-Patterson AFB); in *Invest. of Heat Resistant Alloys*, June 19, 1963, pp. 643-646; *STAR*, Vol. 2, p. 1089(A), May 8, 1964 FTS-9848/1 + 2 + 4

Described is an apparatus for studying the kinetics of oxidation in metals, which automatically records weight variations while the specimens are still in the furnace. The apparatus consists of three major parts: the heating surface, a balance containing a photoelement, and the automatic recording instruments. In order to eliminate the influence of the furnace heat on the balance and to reduce convection currents, asbestos and testolite shields are placed between the platform containing the balance and the furnace.

25,114 THE EFFECT OF CRYSTALLOGRAPHIC ORIENTATION ON THE OXIDATION OF TIN by W.E. Boggs, R.H. Kachik, and G.E. Pellissier (US Steel); *J. Electrochem. Soc.*, Vol. 111, pp. 636-636, June 1964

The formation of oxide on five low-index faces of β -tin has been investigated in an attempt to determine the influence of the crystallographic orientation of the tin on the nucleation, growth, and orientation of the oxide. Orientation relationships between the metal and the oxide were determined using x-ray and electron diffraction. The number and size of the oxide particles formed in a given length of time under standard conditions of temperature and oxygen pressure were measured using an electron microscope. Crystallographic relationships were found to exist between the oxide and the metal; however, no simple over-all mechanism could be deduced that would explain the differences observed in the number or size of the oxide particles formed on the various tin crystal faces. Furthermore, there appeared to be little correlation between the number of oxide platelets and the number of different oxide orientations formed on each tin face. It is suggested that favorably oriented screw dislocations tend to increase the number of oxide platelets formed on certain tin faces. Crystal lattice matching between the metal and the oxide, in certain orientations, has an influence on the rate of oxidation.

25,115 THE OXIDATION OF IRON SINGLE CRYSTALS AROUND 200°C by P.B. Sewell and M. Cohen (Nat'l. Res. Council, Ottawa); *J. Electrochem. Soc.*, Vol. 111, pp. 501-508, May 1964

The oxidation of electropolished iron in the temperature region of 200°C is highly dependent on the surface orientation in respect to both the total thickness and phase composition of the oxide. In general, surface orientations close to the (001), (011), and (111) planes oxidize to give films with a large proportion of Fe_3O_4 . The thick oxide formed on the (001) surface has a thin outer layer containing a high percentage of $\gamma\text{-Fe}_2\text{O}_3$. Specimens with orientations remote from the above low index planes oxidize to form films containing a

smaller percentage of Fe_3O_4 . On the (112) surface, $\alpha\text{-Fe}_2\text{O}_3$ develops in the outer layer of the oxide at an earlier stage than on the (001). No discrete phase boundaries exist between the oxide phases. These trends are also shown at higher temperatures. Thin films of Fe_3O_4 (up to about 100Å) on the (001) and (112) surfaces behave differently with regard to cathodic reduction, with mainly formation of Fe^{++} from magnetite on the (001) surface, and a mixed reaction with a large amount of reduction to metallic iron on the (112) surface. A change in surface preparation can change the distribution of phases in the oxide.

25,116 THE KINETICS OF ANODIC OXIDATION OF IRON IN NEUTRAL SOLUTION. Part I. STEADY GROWTH REGION by N. Sato and M. Cohen (Natl. Res. Council, Ottawa); *J. Electrochem. Soc.*, Vol. 111, pp. 512-519, May 1964

Iron has been anodically oxidized under both potentiostatic and galvanostatic conditions. It was found that the rate of film growth could be expressed by the over-all equation $i = k' \exp(\beta E - Q_T/B)$ where Q_T is the film thickness, E the potential, and k' , β , and B are constants. A model is proposed based on a "place-exchange" mechanism in which all the M-O exchanges in a given row take place simultaneously. β is then related to the transfer of oxygen from the OH^- in the solution to the oxide and B is related to the activation energy for an equivalent ion-pair exchange. The activation energy for a single place exchange was calculated to be 3.5 kcal. This mechanism would lead to an increase of activation energy with thickness and a probable change of mechanism at some finite thickness.

25,117 THE KINETICS OF ANODIC OXIDATION OF IRON IN NEUTRAL SOLUTION. Part II. INITIAL STAGES by N. Sato and M. Cohen (Natl. Res. Council, Ottawa); *J. Electrochem. Soc.*, Vol. 111, pp. 519-522, May 1964

When passive iron is oxidized galvanostatically, a potential arrest is observed in the initial region. Polarization curves obtained using the arrest potentials at different current densities lead to an equation of the form

$$i = a' \exp(\beta' E_i)$$

The value of β' decreases with increasing film thickness and is smaller than that observed in the steady state region. Cathodic reduction experiments show that the ratio of iron in the outer layer of the film to charge passed is considerably smaller in the initial region than in the following steady growth region. It is concluded that in the initial region the charge passed is used in the formation of iron-ion vacancy-electron pairs and the transfer of oxygen from the solution to the outer layer of the oxide. The extent of this reaction depends on the film thickness in that the latter determines the distribution of the potential drops between the metal and the solution.

25,118 ON THE OXIDATION MECHANISM OF TITANIUM by D.I. Lainer, A.S. Bai (Redstone Arsenal); Transl. from *Fizika Metallor i Metallovedeniye*, 14:2, 1962, 10 pp., Feb. 14, 1964; *U.S. Gov. Res. Rep.*, Vol. 39, p. 113(A), May 20, 1964 RSIC 135 AD 431 576 OTS \$1.60

25,119 THE OXIDATION KINETICS OF ZIRCONIUM IN THE TEMPERATURE RANGE 400°-600°C by R.J. Hussey and W.W. Smeltzer (McMaster U.); *J. Electrochem. Soc.*, Vol. 111, pp. 564-568, May 1964

The oxidation kinetics of zirconium have been determined in the temperature range 400°-600°C at subatmospheric pressures for exposure times of 650 hr at 400°C to 160 hr at 600°C by a microbalance technique. From scale thickness measurements, it was shown that at temperatures between 500°-600°C the amount of oxygen in the metal varies from 14 to 23% of the total oxygen consumption respectively. Further both the oxidation kinetics and the oxygen distribution between the metal and the oxide were found to be independent of changes of oxygen pressure from 0.25 to 50 cm Hg. The kinetics were fitted to a parabolic rate relation after an initial deviation. In the parabolic range, oxidation behavior approximated to a model in which the oxidation rate was determined by oxygen diffusion in both the oxide and metal.

25,120 OXIDATION OF PYROLITIC CARBON 1000° TO 1500°C AND OXYGEN PRESSURES OF 2 TO 38 TORR by E. Gulbransen, K. Andrew, and F. Brassart (Westinghouse); *J. Electrochem. Soc.*, Vol. 111, pp. 626-627(L), May 1964

It is shown that pyrolytic and a spectroscopic grade of graphite oxidize at nearly identical rates in the gas diffusion region of the oxidation process. The rate of weight loss by oxidation in the temperature range 1000°C to 1500°C can be expressed as

$$\frac{dw}{dt} = Kp^{0.32}$$

where K is a constant and P is pressure. Interpretation of experimental data indicates that two different types of oxidation exist, chemical and gas-diffusion controlled. The chemical controlled region has not been determined for pyrolytic carbon. It is expected that pyrolytic graphite should oxidize at a lower rate under conditions of chemical control.

25,121 RATES OF FORMATION OF THERMAL OXIDES OF SILICON by H.C. Evitts, H.W. Cooper, and S.S. Flaschen (Motorola); *J. Electrochem. Soc.*, Vol. 111, pp. 688-690, June 1964

Oxidation growth rates of SiO_2 have been studied using as variables Si conductivity types, crystal growing methods, and bulk resistivity. Rates were determined in closed systems of both dry O_2 and steam over a temperature range of 800°-1300°C. The conclusion is drawn that the only factors controlling oxide growth rate are time, temperature, and ambient. Results reported include a study of the optical properties of the oxide films.

25,122 RESEARCH INTO THE CHEMICAL BEHAVIOUR OF SURFACES OF SINGLE-CRYSTALS AND BI-CRYSTALS UNDER OXIDIZING AND REDUCING CONDITIONS by P. Spinedi (Bologna U., Italy); Contract DA91 591EUC2744 28 pp., Jan. 31, 1964; *U.S. Gov. Res. Rep.*, Vol. 39, p. 143(A), May 5, 1964 AD 430 457 OTS \$2.60

Research activities concerning chemical behaviour of single- and bi-crystals under oxidizing and reducing conditions are summarized. They are (1) behavior of Sn single- and bi-crystal surfaces under controlled oxidizing conditions; decoration of Sn single- and bi-crystal surfaces by pure Zn or Cd, from vapour phase; (3) Ge single-crystal surfaces under controlled oxidizing conditions; (4) decoration of single- and bi-crystal surfaces by organic substances; (5) controlled etching of single-crystal; (6) new devices; (7) penetration of a liquid metal or alloy along the grain boundary of a bi-crystal; and (8) review of research in the field of controlled reduction of oxide crystals.

25,123 THE CONTROLLED OXIDATION OF SINGLE CRYSTALS OF UO_2 TO U_4O_9 by W. Van Lierde and L. De Jonghe (S.C.K.-C.E.N., Belgium); *Solid State Commun.*, Vol. 2, pp. 129-131, May 1964

A simple and reliable method is presented for the controlled oxidation of UO_2 which allows the preparation of single crystals with a composition between UO_2 and U_4O_9 starting from a stoichiometric crystal. The principle of the method is the equilibration of the oxygen dissociation pressures of UO_2 and U_3O_8 heated together in vacuum. The practical applications are shown.

Nitridation of Cr - See 25,065

Absorption Isotherms in H- and D-Pt-Pd - See 24,934

25,124 LOW-ENERGY ELECTRON DIFFRACTION STUDIES OF GAS ADSORPTION ON PLATINUM (100), (110), AND (111) SURFACES by C.W. Tucker, Jr. (GE Res. Lab.); *J. Appl. Phys.*, Vol. 35, pp. 1897-1905, June 1964

A low-energy electron diffraction apparatus has been built and used to study the adsorption of simple gases on platinum (100), (110), and (111) faces. Some simple structures formed on various faces are described. Adsorption of oxygen on the (110) face is shown to lead to a rearrangement of the top layer of Pt atoms. On the basis of single scattering it is shown that the adsorbate-substrate combination leads to reflections to be expected from each lattice considered separately. When double scattering is permitted, reflections appear in positions given by the sums and differences of the reciprocal lattice vectors of the separate lattices. This double scattering or multiple reflection is shown to play an important role in low-energy electron diffraction. In particular, two sets of complex diffraction patterns formed by oxygen on the Pt (100) face are shown to have an easy interpretation in terms of multiple reflection. The simple oxygen structures formed are rotated with respect to the Pt substrate but form coincidence lattices with it.

25,125 HYDROGEN ADSORPTION ON SILVER, GOLD, AND ALUMINUM STUDIES OF PARAHYDROGEN CONVERSION by S.J. Holden and D.R. Rossington (Alfred U.); *J. Phys. Chem.*, Vol. 68, pp. 1061-1067, May 1964

The para-ortho hydrogen conversion has been investigated in order to study aspects of hydrogen adsorption on silver, gold, and aluminum films. The pressure dependence of the first-order rate constant for the conversion obeys a Langmuir isotherm on silver and aluminum. From the temperature dependence of the ratio of the Langmuir adsorption-desorption rate constants, heats of adsorption of hydrogen were calculated. Values of -2.5 kcal/mole in the range 363-413°K on silver and -7.7 and -8.4 kcal/mole in the range 308-358°K on aluminum were obtained. No pressure dependence for the conversion on gold was observed in the range 2-20 mm. The normal compensation effect between activation energy and frequency factor for the conversion on the metals was obtained. Calculated values for the activation energies and frequency factors fell on the experimentally obtained line. By comparing the experimentally obtained entropy change upon adsorption with the calculated entropy changes for adsorption into mobile and immobile layers, it is concluded that the adsorbed hydrogen film on silver, in the temperature range studied, is mobile.

Adsorption of O and CO on Cu_2O Films - See 25,381

126 DESORPTION OF CO AND O⁺ FROM POLYCRYSTALLINE MO
 SURFACES BY SLOW ELECTRON IMPACT by P.A. Redhead (Nat'l. Res.
 Canada); *Appl. Phys. Lett.*, Vol. 4, pp. 166-167(L), May 1, 1964

desorption of carbon monoxide and oxygen ions from polycrystalline molybdenum surfaces at 300°K by normally incident 0-300 eV energy electrons is discussed. For 100 eV energy incident electrons the ion yield (only the O⁺ ion released) from a fully covered surface had a maximum value of 3×10^{-7} electrons/ion. If ions are produced from all adsorbed states, the coverage is 10^{-14} molecules/cm² and the ionization cross section $\sigma^+ = 6 \times 10^{-22}$ cm². Only the σ^+ state is involved. The coverage is about 2×10^{13} molecules/cm² and $\sigma^+ = 1.5 \times 10^{-20}$ cm². The O⁺ ion energy distribution from adsorbed carbon monoxide is very similar to that from carbon monoxide in the gas phase. The cross section, σ , for the desorption of neutrals (carbon monoxide molecules) and ions was estimated to be $\sigma_{\max} = 10^{-16}$ cm² for $V_e = 100$ V, and less for $V_e = 200$ V. Electron desorption occurs predominantly from the gas phase or a second adsorbed layer. The ratio of neutrals to ions desorbed is about 10^5 .

127 ETCHING OF TOPAZ CLEAVAGES by A.R. Patel and K.N. Goswami (Mardar Vallabhbhai Vidyapeeth, India); *Acta Cryst.*, Vol. 17, pp. 569-573, May 10, 1964

Topaz cleavages have been etched in potassium hydroxide at various temperatures. Three distinctive types of distribution of etch-pits, (a) individual isolated pits, (b) random distribution of micro-pits and (c) rectilinear etch patterns have been observed. The structures of the individual isolated pits are of two types: (a) point-bottomed and (b) curl-bottomed. From the asymmetry of the point bottoms of the point-bottomed pits, it is established that these pits nucleate at linear dislocation lines inclined to the cleavage face at an angle of about 25°. It is conjectured that curl-bottomed pits nucleate at screw dislocations. By etching matched cleavage faces, correspondence in regard to number, shape, size, position and structure of the pits has been established. Correspondence exists even in the etch patterns on the opposite sides of thin flakes of topaz. The rectilinear etch patterns show a considerable amount of displacement when crossing large cleavage steps. The rectilinear traces are on faces of planes inclined at an angle of about 45° with the cleavage face. It is therefore, conjectured that they may be the traces of (111) planes which make an angle of about 45° with the (001) cleavage face. The correspondence of the rectilinear etch patterns on the two sides of a thin flake shows that these planes go right through the body of the crystal.

128 THERMAL ETCHING OF COPPER SINGLE CRYSTALS IN VACUUM by A. Ponslet and D. Bariaux (U. Brussels); *Acta Met.*, Vol. 12, pp. 593-597, May 1964

Copper single crystals thermally etched in vacuum, show a hill and valley surface topography, formed by facets which correspond to (100) and (111) planes. The surface structure formed by these two facets is complemented by a third facet of high indices which is in general bent. The orientation of these facets has been determined by examination in the electron microscope of double replicas and by interpretation of x-ray diagrams. The formation of these facets is ascribed to an anisotropy of the oxygen adsorption on the different crystalline faces. The geometrical equilibrium of the topography is obtained from the minimum of the total free energy of the surface. Experimental results show a value $\gamma_{100}/\gamma_{111} = 1.08$. The influence of the oxygen partial pressure on the growth kinetics of the facets has also been studied.

129 THERMAL ETCHING ON ICE CRYSTALS by L. Levi, S.M. de Micheli and L. Lubart (Inst. Phys. Atmos., Buenos Aires); *Phys. Stat. Sol.*, Vol. 4, pp. 63-70, 1964

Etch pits on ice surfaces arising from thermal etching of pure ice and NaCl-doped ice have been studied. Features of thermal etching of ice and of metals are compared. Etch pits limited by low index planes were observed on the surface of pure ice; for NaCl-doped ice, the surface was mostly smooth except for occasional small cells unrelated to the symmetry of the crystals.

130 ELECTROPOLISHING OF PYRITE by E. Ehlers and J. Birle (Ohio State Univ.); *Amer. Mineralogist*, Vol. 49, pp. 800-804, May-June 1964

An electropolishing technique has been developed for pyrite during a study of oxidation processes. The crystal is immersed in an appropriate solution and an electric potential is placed across the crystal and solution making the crystal anodic. The relationship between applied voltage and current density is critical for electrical polishing results when current density is constant during voltage change. Viscosity, temperature, concentration, and agitation of the solutions tend to vary polishing characteristics. The formula for the best electropolishing solution is described. The mechanism of the polishing reaction for pyrite is not examined in detail.

ENVIRONMENTAL EFFECTS

Kinetics of Defect Annealing - See 24,980

Annealing of Interstitials in Noble Metals - See 24,994

Dislocation Annealing in Cu - See 25,001

Irradiation:

Produced Vacancies - See 24,992

Effects on the Dielectric Properties, Conductivity and Adsorption of NaNO₂ - See - 25,177

SOLID STATE PHYSICS

GENERAL

25,131 SEMICONDUCTING OXIDE GLASSES by J.D. Mackenzie (Rensselaer Polytech.); NASA Grant NsG-100-60, 52 pp., 1964; *STAR*, Vol. 2, p. 1181(A), May 8, 1964 NASA CR-53199; OTS: \$5.60 pH, \$1.76 mf

A general principle for the preparation of oxide glasses that are electronic conductors (semiconducting) is described. Various methods for proving electronic conduction in some of the glasses are discussed. The electrical conductivity and thermo-electric power of known semiconducting glasses, particularly glasses in the V₂O₅-P₂O₅-RO systems, are reviewed. Also included is a summary of possible applications of this type of semiconductor.

Advances in:

Elemental Semiconductors - See 24,858

II-VI and III-V Compounds - See 24,859

Data Sheets on:

GaAs - See 24,860

PbSe - See 24,861

PbTe - See 24,862

Tellurides of La - See 24,863

CRYSTAL PHYSICS

GENERAL

25,132 THE METHOD OF NEUTRAL PSEUDO-ATOMS IN THE THEORY OF METALS by J.M. Ziman (CSIRO, Sydney, Austr.); *Adv. in Phys.*, Vol. 13, pp. 89-138, Jan. 1964

Treatment of a metal as if it were an assembly of neutral atoms is used as a model attempting to show that a unifying and simplifying principle may be discerned in recent theoretical and experimental work on the properties of metals. The method of pseudo-atoms extends the validity of the free-electron model. It is mathematically simple and physically realistic and is a starting point for more exact calculations. All questions of screening and charge shift can be avoided since each ion is assumed to carry its screening charge with it. Most important, the method avoids treating the ions as a continuum of positive charge. Detailed discussion of phase shifts, band structure, interatomic forces, resistivity of liquid metals, electron-phonon interactions, vacancies, interstitials, dislocations, and impurities are given relative to the model.

25,133 ON THE THEORY OF THE d-ELECTRON COVALENCY IN IONIC CRYSTALS by E. Simanek (Czech. Acad. Sci.); *Phys. Stat. Sol.*, Vol. 4, pp. 251-259, 1964

The covalency parameter λ is calculated for the (NiF₆)⁴⁻ complex with reference to the unrestricted Hartree-Fock method. This method of calculation leads to much smaller values of λ than those obtained by using the maximization of the anti-bonding orbital energy. An approximate treatment of the self-consistency is developed, introducing delocalization of σ -orbitals into the one electron Hamiltonian. The modifications introduced by such a treatment are found to be significant in the maximization of anti-bonding orbital energy.

CRYSTAL FIELDS

25,134 COVALENCY IN CRYSTAL FIELD THEORY: KNiF_3 by R.E. Watson (Bell Labs.) and A.J. Freeman (Nat'l. Magnet Lab., MIT); Phys. Rev., Vol. 134, pp. A1526-A1546, June 15, 1964

The theory of covalency in crystal field phenomena is examined using the NiF_6 complex in KNiF_3 . The Hund-Mulliken-Van Vleck molecular orbital-linear combination of atomic orbitals treatment is followed. The role of the antibonding and bonding electrons in the complex is discussed from a multi-electron point of view. The exact self-consistent one-electron Hamiltonian is discussed. Emphasis is placed on elucidating the source and nature of the covalent effects appropriate to the various physical phenomena. The covalent mixing of those bonding electrons having no antibonding partners contribute to all experimental observables (including the crystal field splitting $10 Dq$, transferred hyperfine interactions, neutron magnetic form factors, and superexchange interactions). This view of covalency differs from the one followed by Sugano and Shulman, in that the covalency of the antibonding electrons, which are assigned the sole role in their approach, is totally irrelevant. Quantitative numerical estimates (using approximations to the exact Hamiltonian) are given for the two models of the covalent effects in KNiF_3 , i.e., "unpaired" bonding and antibonding; they are shown to differ strongly. The relative roles of overlap and covalency are discussed; covalency is found to play an important but by no means dominant role. Numerical agreement between the present inexact cluster theory and experiment is found to be poor.

25,135 CONFIGURATION INTERACTION IN CRYSTAL-FIELD THEORY by B.G. Wybourne (Argonne Lab.) and K. Rajnak (Lawrence Lab.); Bull. Am. Phys. Soc., Vol. 9, p. 501(A), Apr. 1964

The effect of configuration interaction on the validity of the usual method of expanding the crystal-field potential in terms of spherical harmonics was examined using 2nd-order perturbation theory. It was found that for a configuration of equivalent electrons $1N$ most mechanisms of configuration interaction lead to a simple scaling of the crystal-field parameters B_k^N . However, 1-electron excitations either from the $1N$ shell to unfilled orbitals or from closed shells into the $1N$ shell result in a scaling of the Slater integrals F^k and in overt effects that cannot be accommodated by the parameters alone. As a result, the crystal-field parameters can be expected to vary from one multiplet to another, even in the limit of Russell-Saunders coupling.

25,136 EFFECTIVE FIELDS IN CUBIC LATTICES WITH EXTENDED CHARGES by R.F. Guertin (Yale U.) and F. Stern (IBM Watson Res. Ctr.); Phys. Rev., Vol. 134, pp. A427-433, Apr. 20, 1964

The effective field in cubic lattices is calculated for a simple model in which the electrons have spatially extended charge distributions. For simple cubic, body-centered cubic, and face-centered cubic lattices in which the electrons in each primitive cell are infinitesimally displaced from rigid cores, the effective field can be written

$$E_{\text{eff}} = E + (4\pi/3)\gamma P,$$

where E is the average electric field in the medium, and P is the polarization. The coefficient γ varies from zero for very extended electronic charge distributions to 1 for the limit of point charges. Values of γ for Gaussian distributions of intermediate width are given. Effective fields are also calculated for the rocksalt, zincblende, and cesium chloride structures. These results involve an additional coefficient γ' which also varies between 0 and 1. For moderate overlaps between electronic charge distributions of next-nearest neighbors the effective fields differ appreciably from the Lorentz field $E + (4\pi/3)P$.

25,137 THE MAGNETIC BEHAVIOR OF GADOLINIUM TRICHLORIDE HEXAHYDRATE AT LOW TEMPERATURES by P.M. Levy (Lab. Electrostat. et Phys. Métal, France); J. Phys. Chem. Solids, Vol. 25, pp. 431-435, Apr. 1964

From the susceptibility data on $\text{GdCl}_3 \cdot 6\text{H}_2\text{O}$ the crystalline field about the Gd^{3+} ions can be described by the potential (between $T = 2$ and 20°K)

$$V = -0.06 [S_x^2 - 1/3 S(S+1)] + 0.02 (S_y^2 - S_z^2) \text{ cm}^{-1}.$$

This field produces an overall splitting of about 1 cm^{-1} in the ground state $^8S_{7/2}$, and is consistent with the analysis made at the Néel point. The exchange interaction and dipole-dipole coupling give only subordinate contributions to the susceptibility and specific heat.

25,138 CORRECTION AND EXTENSION OF EVJEN'S METHOD FOR EVALUATING CRYSTAL POTENTIALS BY MEANS OF LATTICE SUMS by J.P. Dahl (MIT); Contract Nonr-1841(34); NSF Grant 24908 NSF Grant 10821; STAR, Vol. 2, p. 1418(A), June 8, 1964 AD 429 325

Evjen's sum is set up for a general lattice. By solving Poisson's equation, with well-defined boundary conditions, it is shown how to obtain the proper constant of integration and correction to the Evjen potential. The method is illustrated by using as examples NaCl structure and CsCl structure.

ENERGY BAND STRUCTURE

25,139 FURTHER EVIDENCE FOR THE 2-VALENCE BAND MODEL IN SnTe by B.B. Houston and R.S. Allgaier (US Naval Ord. Lab.); Bull. Am. Phys. Soc., Vol. 9, p. 293(A), Mar. 1964

A two-band model has been used by several investigators (the authors, Bull. Am. Phys. Soc., Vol. 6, p. 436, 1961; Sager and Miller, Proc. Int. Conf. Semicon. Phys. Exeter (1962), p. 653; Brebrick and Strauss, Phys. Rev., Vol. 131, p. 104, 1963 - SSA No. 20, 429) to explain transport in p-type SnTe . Thermoelectric power (α) decrease to values of $0.5 \mu\text{V}/^\circ\text{C}$ at 200°K as p^* decreases from 9 to $2 \times 10^{20} \text{ cm}^{-3}$ was observed by the latter two investigators. Sager and Miller concluded that the conduction band was contributing to α ; hence with further decrease in p^* , α should continue to decrease and become negative. Measurements at 300°K on pure SnTe show that α is a minimum ($4 \mu\text{V}/^\circ\text{C}$) at $p^* = 2.2 \times 10^{20} \text{ cm}^{-3}$ and increases to $14 \mu\text{V}/^\circ\text{C}$ at $p^* = 0.8 \times 10^{20} \text{ cm}^{-3}$. Hall-coefficient measurements at lower p^* show that R_{25}/R_{77} is a maximum of 1.45 at $p^* = 2.3 \times 10^{20} \text{ cm}^{-3}$ and decreases to 1.25 at $0.8 \times 10^{20} \text{ cm}^{-3}$. Both results are consistent with a model in which the Fermi level at 0°K enters the 2nd valence band at $p^* = 2 \times 10^{20} \text{ cm}^{-3}$. The low value of α at $p^* = 2 \times 10^{20} \text{ cm}^{-3}$ may be due to interband scattering of the higher-kinetic-energy holes in the region of overlap between the 2 bands.

Valence States in Transition Metals - See 25,434

Surface States in PbS Films - See 25,263

25,140 ENERGY BAND CALCULATIONS BY THE AUGMENTED PLANE WAVE METHOD by J.C. Slater (MIT); Contract Nonr-1841(34); STAR, Vol. 2, p. 1418(A), June 8, 1964 AD 429 325

The augmented plane-wave method was investigated. Results indicate that it shares with the Green-function method the distinction of being the most accurate procedure available for calculating energy bands in the type of periodic potential found in a solid. The errors involved in the particular type of potential assumed, namely one that is spherically symmetrical in spheres surrounding each atom and constant between, are small.

25,141 RELATIVISTIC CORRECTIONS TO THE BAND STRUCTURE OF TETRAHEDRALLY BONDED SEMICONDUCTORS by F. Herman, C.D. Kuglin, K.F. Cuff, R.L. Kortum (Lockheed Res. Lab.); Phys. Rev. Lett., Vol. 11, pp. 541-545, Dec. 15, 1963

Estimates of the magnitudes of the relativistic mass-velocity and Darwin corrections for a wide variety of crystals are presented. Three successive corrections are applied to the relativistic and spin-orbit coupling terms of the free atoms, following and extending the ideas of Kane. Correction "A" compensates for inadequacies in the perturbation treatment of the free atom corrections, corrections "B" and "C" account for wave function renormalization effects in the crystal. The relativistic corrections are shown to have a sizable effect on the band structure of the crystals considered.

25,142 RELATIVISTIC EFFECTS IN THE BAND STRUCTURE OF PbTe by L.E. Johnson, J.B. Conklin, G.W. Pratt, Jr. (MIT); Phys. Rev. Lett., Vol. 11, pp. 538-540, Dec. 15, 1963

Preliminary results of calculations of the influence of the inclusion of relativistic terms in the one-electron Hamiltonian on the (111) band edge of PbTe are reported. It is shown that the inclusion of the mass-velocity term $(-1/2 mc^2)(E + e\phi)^2$ and a term $-(7\mu_0/2 mc) \times \vec{e} \cdot \vec{p}$ in the Hamiltonian have a very large effect on the energy band structure, energy gaps, and effective masses. A perturbation method is used to consider the $\vec{e} \cdot \vec{p}$ term in an augmented plane wave investigation of the PbTe band structure for several ionicities. The results are compared with relativistic shifts of isolated Pb and Te as found by Herman and Skillman.

25,143 BAND STRUCTURE AND THE MECHANISM OF ELECTRICAL CONDUCTION IN TRANSITION METAL COMPOUNDS by W. Albers and C. Haas (Philips Res. Labs.); Phys. Lett. (Neth.), Vol. 8, pp. 300-302(L), Mar. 1, 1964

The band structures of the Tx chalcogenides ($x = \text{S}, \text{Se}, \text{Te}$) and pnictides ($x = \text{P}, \text{As}, \text{Sb}, \text{Bi}$) of the 3d-transition metals are discussed. The electrical resistivity of these compounds was measured as a function of temperature, and the spin disorder resistivity was determined by subtracting the residual resistivity

and lattice scattering from the measured value. Analysis of the results indicates that all the compounds, except MnTe, are broad band metallic conductors. Band structures for these compounds are given. MnTe is a semiconductor with a large energy gap and holes moving in a broad band. Band structures for this compound are also given.

25,144 ELECTRONIC SPECTRA OF CRYSTALLINE GERMANIUM AND SILICON by D. Brust (Argonne Lab.); *Phys. Rev.*, Vol. 134, pp. A1337-A1353, June 1, 1964

A detailed calculation of the energy bands of Ge and Si has been performed by use of the pseudopotential method. The first three potential coefficients have been determined empirically, and all higher ones set equal to zero. This potential was used to compute the energy eigenvalues at $\sim 50,000$ points throughout the Brillouin zone. By use of this sample, the imaginary part of the dielectric constant in the optical and near ultraviolet where direct transitions between the valence and low-lying conduction bands dominate the response was calculated. Photoelectric yield curves were obtained for comparison with recent experiments. In all cases agreement of theory and experiment was reasonable. Energy contours were constructed in several of the principal symmetry planes. These were used to explain the structure in the optical properties of Ge and Si in terms of transitions near certain important critical points. Effective masses and the static dielectric constant were also computed.

25,145 BAND STRUCTURE OF GALLIUM PHOSPHIDE FROM OPTICAL EXPERIMENTS AT HIGH PRESSURE by R. Zallen and W. Paul (Harvard U.); *Phys. Rev.*, Vol. 134, pp. A1628-A1641, June 15, 1964

The effect of hydrostatic pressure on the following optical properties of GaP has been measured at room temperature: the fundamental absorption edge (region from 2.2 to 2.7 eV, an infrared absorption band appearing in n-type material at 0.3-0.5 eV, peaks in the reflectivity spectrum at 2.8 and 3.7 eV, and recombination radiation in forward-biased p-n junctions at 1.7-2.3 eV. The results have been interpreted by means of a proposed energy band structure in which the conduction band states X_{1c} , X_{3c} , Γ_{5c} , Γ_{15c} are located at energies of 2.2, 2.5, 2.8, 3.7 eV, respectively, above the valence band maximum at Γ_{15v} . The following pressure coefficients have been measured (the transition involved is given in parenthesis), where energy is expressed in eV and pressure in 10^6 bars: E_G ($\Gamma_{15v} \rightarrow X_{1c}$) = $2.22 - 1.1P$; E_0 ($\Gamma_{15v} \rightarrow \Gamma_{1c}$) = $2.78 + 10.7P$; E_0' ($\Gamma_{15v} \rightarrow \Gamma_{15c}$) = $3.71 + 5.8P$; ΔE_2 ($X_{1c} \rightarrow X_{3c}$) = $0.3 + 1P$. The coefficients of E_G and E_0' are close to those for the corresponding transitions in Si; that of E_0 is close to the corresponding coefficient in Ge. The weak reflectivity peak at 2.8 eV, the direct gap, shifts with temperature at a rate of about -4.6×10^{-4} eV/ $^\circ$ K, compared to a value of about -5.2×10^{-4} eV/ $^\circ$ K for the 2.2 eV indirect gap.

25,146 BAND STRUCTURE OF GREY TIN by S. Gooves and W. Paul (Harvard U.); *Phys. Rev. Lett.*, Vol. 11, pp. 194-196, Sept. 1, 1963

A new model for the band structure of α -Sn which is compatible with observed values of magnetoresistance and pressure dependence of conductivity and Hall coefficient is described. The Γ_2^- state is located 0.3 eV below the Γ_3^+ states, implying zero energy gap at all temperatures and pressures. This yields plausible interpretations of the transport and pressure measurements; quantitative effects are discussed. Reasonable assumptions for the carrier concentration and mobility in each of the three bands permit a better fit with experimental data between 0 and 160 $^\circ$ K.

25,147 DEPENDENCE OF THE FORBIDDEN ENERGY GAP WIDTH OF GERMANIUM ON FREE CARRIER CONCENTRATION by V.M. Asnin and A.A. Rogachev (Acad. Sci. USSR); *Soviet Phys. Solid State*, Vol. 5, pp. 1257-1259 (L), Dec. 1963

25,148 LOCALIZED STATES IN CRYSTALS WITH TWO KINDS OF ATOMS by A.T. Amos and S.G. Davison (Manchester Coll. Sci. Tech.); *Physica*, Vol. 30, pp. 905-913, Apr. 1964

The localized end states of a one-dimensional crystal with two kinds of atoms are discussed using the molecular orbital method with the tight-binding approximation. An extra parameter has to be introduced to allow for the different potentials at the two kinds of atoms and this complicates the theory. In certain cases the conditions for the existence of localized states can be more favourable in mixed crystals but this may also depend on which one of the two types of atom is at the end. The theory is also extended to include localized impurity states in a three-dimensional crystal by using a Green's matrix method and similar results are found.

25,149 THE DENSITY OF STATES OF A HIGHLY IMPURE SEMICONDUCTOR by S. Edwards and Y. Gulyaev (U. Manchester); *Proc. Phys. Soc.*, Vol. 83, pp. 495-496(L), Mar. 1964

Using the Feynman representation of quantum mechanics it is possible to derive the exact density of states of non-interacting electrons in the presence of impurities as their density becomes very large.

Energy Gap of Sn Superconductors - See 25,789

Temperature Effects on the Band Gap of Bi - See 25,269

Energy Gap of:
Bi₂S₃ - See 25,709
BP - See 25,617

25,150 FERMI LEVEL POSITION AT METAL-SEMICONDUCTOR INTERFACES by C.A. Mead (Calif. Inst. Tech.) and W.G. Spitzer (U. Southern Calif.); *Phys. Rev.*, Vol. 134, pp. A713-716, May 4, 1964

The position of the Fermi level at a metal-semiconductor interface relative to the conduction band has been found to be a constant fraction of the semiconductor band gap for all but 3 of the 14 group IV or III-V semiconductors studied. In all cases, the position was essentially independent of the metal work function. This general result is not inconsistent with the limited theories of surface state energies now available. The three exceptional cases can be understood in terms of a first-order perturbation to the surface state energies correlated with a similar perturbation observed in the energy gap at the (111) zone edge. Experiments are also reported on Ga(As-P) alloys, and two II-VI materials showing distinctly different behavior.

25,151 THE FERMI SURFACE OF LEAD by J.R. Anderson and A.V. Gold (Iowa State U.); Contract W-7405-ENG-82, 237 pp., Jan. 1, 1964; STAR, Vol. 2, p. 1184(A), May 8, 1964 IS-762; OTS:\$3.00

An apparatus has been designed and constructed to extend magnetic fields to 200 kg. With the aid of these higher fields, many new features of the Fermi surface in lead have been determined quantitatively. The shape of the Fermi surface can be explained in terms of an orthogonalized-plane-wave model using only two parameters, the two Fourier components of the pseudopotential, V_{111} and V_{200} . Although the orthogonalized-plane-wave approach is successful in describing the shape of the Fermi surface, the calculated cyclotron masses are too small by a factor of order two. The theoretical implications of this are discussed briefly. De Haas-van Alphen oscillations have been observed in iron whiskers—the first time that the effect has been observed in a ferromagnetic metal. Preliminary results show that the saturation magnetization in iron must be taken into account in order to determine the true periods of the oscillations.

25,152 FERMI SURFACE OF NICKEL FROM GALVANOMAGNETIC MEASUREMENTS by W.A. Reed and E. Fawcett (Bell Labs.); *J. Appl. Phys.*, Vol. 35, pp. 754-759, Mar. 1964

Measurements of the high-field galvanomagnetic properties of nickel show that one electron-sheet of its Fermi surface is multiply connected, and touches the {111} faces of the Brillouin zone as does the Fermi surface of copper. In magnetic fields up to 80 koe applied in a nonsymmetry direction, the magnetoresistance saturates and the transverse voltage is linear, the Hall constant corresponding to one electron per atom within the experimental accuracy. The last result strongly suggests that nickel is uncompensated, and if so it is a direct consequence of the removal of the spin degeneracy of the d bands by the ferromagnetic exchange interaction. According to this explanation, one, and only one, sheet of the Fermi surface in a spin zone (i.e., a half-band consisting of the states of a single sign of spin) of the 3d bands has an electronic character. The alternative explanation that the d bands contain only holes with a mobility at least two orders of magnitude smaller than the s-band electrons, cannot yet be conclusively ruled out but seems most unlikely. This study of nickel has shown that the experimental methods used to investigate the Fermi surfaces of nonmagnetic metals may be taken over directly to determine the Fermi surfaces of the ferromagnetic metals.

Fermi Surface of Ni - See 25,604

25,153 FURTHER RESULTS ON THE FERMI SURFACE OF BERYLLIUM by T.L. Loucks (North Am. Aviation, Tulsa); *Phys. Rev.*, Vol. 134, pp. A1618-A1620, June 15, 1964

Following the methods presented in an earlier paper, the conduction eigenvalues for beryllium at the equivalent of over 80,000 points in the first Brillouin zone (all in the immediate vicinity of the Fermi surface) were calculated. The constant energy surfaces were constructed for several values of the energy near the Fermi energy. The hole and electron volumes were calculated for each case, and the Fermi energy was determined by the requirement that the two volumes be equal. This is the first time that this well-known result has actually been used to determine the Fermi energy in a band calculation. The corresponding Fermi surface was defined by about ten cross sections perpendicular to the [0001] direction. The agreement between these results and experiment is generally good and slightly improved over the previous results.

Fermi Surface of:
Al - See 25,355
Cu - See 25,356, 25,603
Cd - See 25,605

- 25,154 LATTICE DYNAMICAL STUDIES USING ABSOLUTE MEASUREMENTS OF THE LAMB-MÖSSBAUER RECOIL-FREE FRACTION by W.A. Steyert and R.D. Taylor (Los Alamos Lab.); *Phys. Rev.*, Vol. 134, pp. A716-722, May 4, 1964

Absolute values of the recoil-free fraction f of the 14.4-keV γ rays of Fe^{57} are reported at temperatures from 4 to 1050°K. Co^{57} , the parent of Fe^{57} , is a dilute impurity in Au, Cu, Ir, Pd, Pt, Rh, and Ti. For intermediate temperatures the measured f is consistent with the calculations of Visscher, and Maradudin and Flinn when the impurity-host coupling constant is taken to be about the same as the host-host coupling constant. At the highest temperatures, the f 's of Au, Cu, and Pd fall off faster than simple theory would predict due to diffusion and anharmonicities. The results are compared with the anharmonic lattice theory of Maradudin and Flinn. Chemical and temperature-shift data are also reported.

- 25,155 LATTICE DYNAMICS AND PHASE TRANSITIONS OF STRONTIUM TITANATE by R.A. Cowley (Cavendish Lab.); *Phys. Rev.*, Vol. 134, pp. A981-A997, May 18, 1964

The crystal dynamics of strontium titanate has been studied both experimentally and theoretically. The frequency versus wave-vector dispersion curves for some of the normal modes propagating along the $[0,0,1]$ direction have been measured by neutron spectrometry at 90 and 296°K. The temperature dependence of the transverse optic mode of the lowest frequency has been found to be in agreement with the temperature dependence of the dielectric constant, as predicted by Cochran. The experimental results have been used to obtain the parameters of several models, more than one of which gives reasonable agreement with the experimental results. It is suggested that the anomalous behavior of the elastic properties and the phase transition at 110°K are associated with an accidental degeneracy of two branches of the dispersion curves; the longitudinal acoustic branch and the transverse optic branch of lowest frequency. The origin of the temperature dependence of this transverse optic mode and the relevance of lattice dynamics to the phase transitions in other perovskites are discussed.

- 25,156 FREQUENCY SPECTRA OF BODY-CENTERED CUBIC LATTICES by B.C. Clark (GM Res. Lab.), D.C. Gazis (IBM Res. Ctr.) and R.F. Wallis (US Naval Ord. Res. Lab.); *Phys. Rev.*, Vol. 134, pp. 1486-1491, June 15, 1964

A Born-von Karman model has been used to determine the frequency spectrum for a body-centered cubic lattice. The model used contains noncentral angular stiffness forces as well as central forces between nearest and next-nearest neighbors. Frequency distributions have been calculated for vanadium and compared with experimental frequency distributions available from slow neutron experiments. Qualitative agreement was found between the shapes of the experimental and theoretical distributions. The calculated maximum frequency for vanadium was within 2% of that derived from the experimental frequency distribution. Dispersion curves for iron were also calculated, and were found to be in good agreement with experiment.

- 25,157 QUANTUM RELAXATION, THE SHAPE OF LATTICE ABSORPTION AND INELASTIC NEUTRON SCATTERING LINES by M. Lax (Bell Labs.); *J. Phys. Chem. Solids*, Vol. 25, pp. 987-503 May 1964

The fundamental optical lattice vibrations are treated as the system, the remaining lattice vibrations as the reservoir, and the anharmonic interactions as the coupling in a general density matrix theory of relaxation processes. An immediate result of this theory are expressions for frequency dependent level shifts and damping coefficients as well as corresponding frequency dependent coupling coefficients between the optical modes. If the coupling coefficients are neglected, and if in our expressions for the shift and damping coefficients anharmonic interactions in the reservoir are neglected our expressions simplify to those obtained by Wallis and Maradudin by summing an infinite ladder of diagrams. By treating an arbitrary mode as the system and using the fluctuation-dissipation theorem, the relation between the lifetime and shift of the mode and its contribution to the one-phonon inelastic neutron scattering line shape are derived. The relaxation theory used is based on a systematic improvement of the Hartree approximation in which the system and reservoir are treated in a symmetric fashion.

- 25,158 A NEW SAMPLING METHOD FOR CALCULATING THE FREQUENCY DISTRIBUTION FUNCTION OF SOLIDS by C. Gilat and G. Dolling (Chalk River Nucl. Labs.); *Phys. Lett. (Neth.)*, Vol. 8, pp. 304-306(L), Mar. 1, 1964

The calculation of the frequency distribution function $g(\nu)$ of the normal modes of vibration of a solid from the frequency-wave vector relation $\nu(\vec{q})$ by an extrapolation sampling method is discussed. The method is outlined, and some

of its features including the accuracy of the method, are considered. The method is illustrated by application to sodium. The $g(\nu)$ obtained is in good agreement with that obtained by the sampling method used by Dixon et al.

- 25,159 PROGRAMS FOR CALCULATING RELATIVE INTENSITIES IN THE VIBRATIONAL STRUCTURE OF ELECTRONIC BAND SYSTEMS by R. N. Zare (Lawrence Rad. Lab.); Contract W-7405-ENG-26, 62 pp., Nov. 19, 1963; STAR, Vol. 2, p. 1177(A), May 8, 1964 UCRL-10925; OTS \$1.50

Source-deck listings of two computer programs are given for the calculation of relative intensities in the vibrational structure of an electronic transition. The first program finds turning points of an electronic potential-energy curve by direct numerical evaluation of the Klein action integrals in the RKR procedure. The second program uses these turning points to construct an effective potential for the molecule with rotational quantum number J . The radial Schrödinger equation then is solved for this potential to yield vibrational-rotational wavefunctions from which the program calculates Franck-Condon factors, r -centroids, and relative intensities.

Lattice Vibrations in Metals - See 24, 893

- 25,160 LATTICE DYNAMICS OF NIOBIUM by Y. Nakagawa and A.D. Woods (Atomic Energy of Canada); *Phys. Rev. Lett.*, Vol. 11, pp. 271-274, Sept. 15, 1963

The frequency/wave-vector dispersion relation in Nb for symmetry directions was measured by neutron inelastic scattering at 296°K. Curves for four directions are presented; the $[00\bar{1}]$ "T" and "L" branches cross over in spite of the absence of a symmetry requirement and a significant departure from the Debye spectrum is observed. The experimental curves were fitted using the Born-von Karman model in the 8-neighbor approximation. The latter was used to calculate the frequency distribution function $g(\nu)$. The results are discussed in connection with analogous ones obtained for V.

- 25,161 NORMAL VIBRATIONS OF NICKEL by R.J. Birgeneau, J. Cordes, G. Dolling, and A.D.B. Woods (Chalk River Nucl. Lab.); *Bull. Am. Phys. Soc.*, Vol. 9, p. 413(A), Apr. 1964

The frequency/wave-vector relation $\nu(\vec{q})$ for normal modes propagating along the $[00\bar{1}]$, $[\bar{1}\bar{1}0]$, $[\bar{1}\bar{1}\bar{1}]$, and $[1\bar{1}0]$ high-symmetry directions in a single crystal of nickel has been determined at 296°K by means of coherent inelastic neutron scattering. The frequencies (units 10^{12} cps) of selected modes are $(0, 0, 1, 0)$ L 8.55 ± 0.13 and T 6.27 ± 0.10 ; $(0.5, 0.5, 0)$ L 7.63 ± 0.20 , T_1 (polarization vector $\hat{\epsilon} \parallel \hat{x}$) 4.36 ± 0.08 and T_2 ($\hat{\epsilon} \parallel \hat{\Delta}$) 6.15 ± 0.12 ; $(0.5, 0.5, 0.5)$ L 8.88 ± 0.17 and T 4.24 ± 0.08 . The results were analyzed in terms of the Born-von Karman theory. A good fit between theory and experiment was obtained for a model involving interactions out to 4th nearest-neighbor atoms. A numerical computation of the frequency distribution function $g(\nu)$, based on this force model, has been carried out by means of a new sampling method. The calculated $g(\nu)$ is in qualitative agreement with that determined experimentally by means of incoherent inelastic neutron scattering.

- 25,162 LATTICE VIBRATIONAL SPECTRA OF BERYLLIUM, MAGNESIUM, AND ZINC by J.A. Young and J.U. Koppel (John Jay Hopkins Lab.); *Phys. Rev.*, Vol. 134, pp. A1476-1479, June 15, 1964

The lattice vibrational spectra of Be, Mg, and Zn have been obtained using the root sampling method. The force constants used in the calculations were those determined from measurements of the dispersion relations by slow neutron scattering techniques. Calculations of the specific heat of each metal show good agreement with measured values.

Lattice Vibrations in:

C and Graphite - See 24, 949

$(\text{NH}_4)_2\text{SO}_4$, RbHSO_4 , $\text{NaH}_2(\text{SeO}_3)_2$ and $\text{LiH}_3(\text{SeO}_3)_2$ - See 25, 634

- 25,163 ON THE MEAN FREE PATH OF LOW ENERGY PHONONS IN SINGLE CRYSTAL QUARTZ by H.J. Maris (Imperial Coll., London); *Phil. Mag.*, Vol. 9, pp. 901-910, June 1964

The attenuation of mechanical waves in single crystal quartz at low temperatures and at frequencies in the range 600 Mc/s to 1110 Mc/s has been measured. The results are interpreted in terms of collisions between the low energy phonons, constituting the sound wave, and thermal phonons.

- 25,164 THE DEBYE-WALLER FACTORS OF SODIUM CHLORIDE by W.J.L. Buyers and T. Smith (U. Aberdeen); *J. Phys. Chem. Solids*, Vol. 25, pp. 483-486, May 1964

The Debye-Waller factors in sodium chloride have been worked out from the normal mode data of Karo and Hardy. It is found that the values for the two ions are almost equal, and considerably greater than recent experimental

determinations. The values obtained are determined essentially by the value of the compressibility, but significant changes are found if the deformability of the ions is ignored. Anharmonic contributions to the Debye-Waller factors are discussed.

ELECTRICAL PROPERTIES

GENERAL

25,165 ALUMINUM OXIDE DATA SHEETS by J. T. Milek (Hughes Aircraft); Contract AF33 615 1235, 169 pp., Mar. 1964; U.S. Gov. Res. Rep., Vol. 39, p. 67, June 5, 1964 AD 434 173 OTS \$12.00

A compilation of the electrical properties of a wide range (80-100%) Aluminum oxide ceramic composition is presented. Included are Sapphire, Sintered single crystal and Polycrystalline material. Detailed electrical properties for the individual Alumina material data sheet include dielectric constant, dielectric strength, dissipation factor, electrical conductivity, electrical resistivity, loss factor and Te value. Each property is compiled over the widest possible range of temperatures and frequencies from references obtained in a thorough literature search. The crystal structure, applications and phase diagrams are briefly reviewed.

25,166 SEMIMETALLIC PROPERTIES OF $\text{Co}_{1-x}\text{Fe}_x\text{Si}$ SOLID SOLUTIONS by S. Asanabe, D. Shinoda, and Y. Sasaki (Nippon Electric, Tokyo); *Phys. Rev.*, Vol. 134, pp. A774-779, May 4, 1964

The electrical resistivity, Hall coefficient, and thermoelectric power have been measured over the temperature range from 4.2 to 800°K on $\text{Co}_{1-x}\text{Fe}_x\text{Si}$ solid solutions, with x varying from 0 to 1. The specimens are n -type near $x = 0$. In the purest specimen of CoSi the electron mobility reaches 800 $\text{cm}^2/\text{volt}\cdot\text{sec}$ at 4.2°K. With increasing x , hole conduction becomes predominant. Anomalies are observed for intermediate compositions. The temperature range over which the Hall coefficient and the thermoelectric power take opposite signs is unusually wide compared with ordinary p -type semiconductors. Detailed analysis of the Hall coefficient and thermoelectric power based on a two-carrier model leads to the conclusions: (1) The upper and the lower bands overlap in energy for $\text{Co}_{1-x}\text{Fe}_x\text{Si}$ solid solutions. (2) By substitution of one iron atom for one cobalt atom in the solid solutions, approximately one hole is produced. For CoSi the best fit to the data is obtained with the overlap energy of 0.02 eV, with the electron effective mass of $2 m_0$, with the hole effective mass of $4 m_0$ and with the electron-to-hole mobility ratio of 5. For the solid solutions, the observed data are qualitatively interpreted assuming that the overlap energy and the hole effective mass increase with x , but the mobility ratio and the electron effective mass remain unchanged. It is also suggested that interband scattering becomes predominant in passing from CoSi to FeSi.

25,167 ELECTRICAL PROPERTIES OF SINGLE CRYSTALS OF SOLID SOLUTIONS OF TELLURIUM IN BISMUTH IN THE TEMPERATURE RANGE 77-300°K by G. A. Ivanov (Gertsen State Pedagogical Inst.); *Soviet Phys. Solid State*, Vol. 5, pp. 2322-2325, May 1964

Measurements of the Hall effect and resistivity of single crystals of solid solutions of tellurium in bismuth are reported. The concentration and mobility of electrons in these alloys are determined from the experimental data. It is shown that the relaxation time has considerable anisotropy $\tau_1 : \tau_2 : \tau_3 = 0.8 : 9.5 : 1.0$, which is easily explained by the anisotropy of the effective mass in the case of isotropic mean free paths.

25,168 ELECTRICAL AND THERMAL PROPERTIES OF ALLOYS OF CdTe AND CdSe by A. D. Struckes (Royal Coll. Adv. Tech.) and G. Farrell (AEI Res. Lab.); *J. Phys. Chem. Solids*, Vol. 25, pp. 477-482, May 1964

The CdTe:CdSe system has been investigated in order to assess its thermoelectric properties. A series of alloys was made ranging from 10 mol.% CdSe in CdTe to 30:70 CdTe:CdSe. Those containing up to 30 mol.% CdSe were found to have a zinc blende structure while the 30:70 CdTe:CdSe alloy had a wurtzite structure. At the equimolecular composition the structure was dominantly cubic but converted to hexagonal on doping with iodine. The material was of small grain size, extremely brittle, and thermally unstable above 250°C. A wide variation in electrical conductivity (from 54 to 740 $(\Omega\text{cm})^{-1}$) was found, giving rise to a large spread in mobility, which was probably due to the poor structure of the material. Measurements of electrical conductivity, Hall constant, thermoelectric power and thermal conductivity were carried out above room temperature, within the limits of thermal stability. Thermoelectric power decreased with increasing CdSe content and increased linearly with increasing temperature up to 400°C. Thermoelectric figures of merit were a little greater than for iodine doped CdTe, the best achieved being that for the 70:30 CdTe:CdSe alloy.

25,169 ELECTRICAL AND THERMAL PROPERTIES OF ALLOYS OF InAs AND CdTe by A. D. Struckes and R. P. Chasmar (AEI Res. Lab.); *J. Phys. Chem. Solids*, Vol. 25, pp. 469-476, May 1964

The InAs-CdTe system has been studied and a range of solid solution crystallizing with a zinc blende structure found for alloys containing up to 35 mol.% CdTe in InAs and up to 38 mol.% InAs in CdTe, the intermediate region being two phase. The electrical and thermal properties of alloys containing up to 20 mol.% CdTe were investigated up to 400°C. Ingots were all n -type with an electron concentration of about $10^{19}/\text{cm}^3$ and a mobility which decreased as the CdTe content was increased, to a value of 1000 cm^2 per V sec at the 80:20 InAs:CdTe composition. The carrier concentration was found to be dependent upon the pressure of Cd vapor maintained over the melt during crystallization and the constant value obtained was due to the technique of preparation. The electrical conductivity and Hall constant of the n -type alloys were practically invariant up to 400°C for all samples. The lattice thermal conductivity had a minimum value at the 50:50 composition of 0.005 cal $(\text{cm sec}^\circ\text{C})^{-1}$ and was almost constant for this alloy up to 400°C. A solubility limit for Tellurium in InAs was found to be about $4 \times 10^{19}/\text{cm}^3$.

NUCLEAR QUADRUPOLE EFFECTS

25,170 LOW-ENERGY EXPANSION OF THE SCATTERING AMPLITUDE FOR LONG-RANGE QUADRUPOLE POTENTIALS by T. F. O'Malley (Joint Inst. for Lab. Astrophysics); *Phys. Rev.*, Vol. 134, pp. A1188-A1197, June 1, 1964

For static potentials which are proportional asymptotically to $qP_2(\cos\theta)/r^3$, the low-energy expansion of the scattering amplitude is found through terms of $O(k)$, using a modification of the method developed by Levy and Keller for central potentials. The resulting expansion to lowest order in k is found to be

$$f(\theta, \varphi) \sim -A + (q/3)P_2(\cos\theta) + O(k),$$

where A is the scattering length and θ_K is the coordinate of the momentum transfer vector. Applications are attempted first to electron-atom elastic scattering where results are somewhat more complicated than for the potentials above, secondly to transitions between magnetic quantum states of atoms caused by slow electrons.

25,171 NUCLEAR QUADRUPOLE MOMENT OF VANADIUM by H. Nagasawa, S. K. Takeshita and Y. Tomono (U. Tokyo); *J. Phys. Soc., Japan*, Vol. 19, pp. 764-765(L), May 1964

The nuclear quadrupole moment of V was re-evaluated to give a value of 0.73×10^{-2} barn, 1/40 smaller than previous values reported. The new value is consistent with NMR of V alloys. Nuclear resonance measurements were made on V_2O_5 .

25,172 ^{23}Na QUADRUPOLE COUPLING IN ROCHELLE SALT by N. C. Miller and P. A. Casabella (Rensselaer Polytech.); *Bull. Am. Phys. Soc.*, Vol. 9, p. 503(A), Apr. 1964

The nuclear quadrupole-coupling constant of ^{23}Na in Rochelle salt has been determined by studying the splitting of the nuclear magnetic resonance in a single crystal. Complete rotation patterns were obtained at 28°C, in the high-temperature paraelectric phase, and at 3°C in the ferroelectric phase. In both phases, 4 sets of satellite resonances were observed corresponding to the 4 sodium positions in the unit cell. In the high-temperature phase, all 4 of these positions give rise to the same quadrupole-coupling constant which is 1323 ± 30 kc/sec, with an asymmetry parameter of 0.796 ± 0.035 . The crystal was then fixed at one orientation, and the resonance was studied as the temperature was raised from 3° to 28°C. Over a small temperature range about the Curie temperature of 24°C, the resonance pattern was observed to change continuously from the low-temperature to the high-temperature pattern. This behavior is quite different from that observed in potassium niobate.

25,173 DEPENDENCE OF NUCLEAR QUADRUPOLE RELAXATION TIMES IN IONIC CRYSTALS ON THE PHONON SPECTRUM by S. K. Joshi, R. Gupta (U. Allahabad, India) and T. P. Das (U. Calif. Riverside); *Phys. Rev.*, Vol. 134, pp. A693-700, May 4, 1964

Nuclear quadrupole relaxation times are calculated for the halogen and alkali nuclei in a number of alkali halides using lattice phonon density curves computed by Karo. The calculated values of T_1 at room temperature are generally lower than those obtained using the Debye model and in better agreement with experiment. The variation of T_1 with temperature has also been calculated over the range 20°K to room temperature for Na^{23} and I^{127} nuclei in NaI. Excellent agreement is obtained with the experimental data on the temperature variation of T_1 when use is made of the Karo distribution function. The Debye model gives a temperature variation comparable with experimental above 70°K but a relatively slower variation below 70°K.

25,174 FERROELECTRIC BIBLIOGRAPHY SUPPLEMENT by R.D. Hall (Elec-tronic Def. Lab.); Contract DA36 039AMC00088E, 90 pp., Aug. 23, 1963; U.S. Gov. Res. Rep., Vol. 39, p. 66, June 5, 1964 AD 433 653 OTS\$8.10

25,175 HIGH TEMPERATURE FERROELECTRIC MATERIALS by R.W. Ohlweiler (Wright-Patterson AFB); Mar. 1964, 26 pp., Proj. 7371, Task 737101; U.S. Gov. Res. Rep., Vol. 39, p. 81(A), June 20, 1964 AD 437 307 OTS\$0.75

Published data on high temperature ferroelectric materials are reviewed. Ap-plicable terms are defined and general characteristics of this type of material are given. High temperature ferroelectric materials studied were: lead meta-niobate, lithium tantalate, potassium niobate, lead titanate, sodium tantalate, and lead metatantalate. Other ferroelectric materials with less supporting data are discussed also.

25,176 AN EXTENSION OF THE Te_{01n} RESONATOR METHOD OF MAKING MEASUREMENTS ON SOLID DIELECTRICS by D.T. Paris (Georgia Tech.); IEEE Trans., Vol. MTT-12, pp. 251-252(L), Mar. 1964

The possibility that dielectric measurements may be made on materials other than those having low loss characteristics is demonstrated, and an improvement in experimental procedure which eliminates the necessity of performing the usual quality-factor measurements is suggested. A sketch of the resonant cavity is presented and the measuring problem is discussed. Maxwell's Equations, with the appropriate boundary conditions, are introduced, and the solutions are dis-cussed in terms of both large and small cavity losses.

Ferroelectric Properties of $BaTiO_3$ - See 25,090

25,177 THE EFFECT OF GAMMA-RAY IRRADIATION ON THE DIELECTRIC PROPERTIES OF SINGLE CRYSTALS OF SODIUM NITRITE by K. Gesi and Y. Takagi (Japan Atomic Energy Res. Inst.); J. Phys. Soc. Japan, Vol. 19, pp. 632-639, May 1964

Single crystals of sodium nitrite were irradiated with Co^{60} gamma-ray and radiation-induced change in dielectric properties were measured. The de-pression of the Curie temperature, the decrease of the maximum dielectric con-stant, the increase of the coercive field, the appearance of weak double hysteresis loop, the increase of the electrical conductivity and the change in its activation energy were observed as the results of the irradiation. The optical absorption spectrum of the irradiated specimen showed a broad band about 400 m μ which was assigned to neutral nitrite.

25,178 ON THE IMMERSION METHOD OF MEASURING THE DIELECTRIC PERMITTIVITY OF SOLIDS, AS COMPARED TO OTHER METHODS by M. Jezewski, T. Morstin and M. Wierzbicki (Inst. Physics, Cracow); Acta Phys. Polonica, pp. 187-192, Feb. 1964

The dielectric permittivity of glass samples was determined, applying a con-denser of special construction consisting of two coaxial cylindrical condensers in a single vessel. Results obtained by various methods were compared. Those yielded by the immersion method when using the Authors' condenser were found to be more correct and more easily obtained, provided the powder was properly dried and the liquids dehydrated.

25,179 A STUDY ON THE DIELECTRIC CONSTANT AND RESISTIVITY OF AMORPHOUS, POLYCRYSTALLINE AND MONOCRYSTALLINE SELENIUM AT 24 GHz by R. Lilja and T. Stubb; Acta Polytech. Scand. Physics Incl. Nucl. Series No. 28, Helsinki 1964, 32 pp.

Resistivity and dielectric constant of thin semiconductor samples have been measured by means of a microwave bridge. Necessary calculations are based on a perturbation theory. Measurements have been carried out on amorphous, polycrystalline and single crystal selenium. Results indicate that the resistivity of crystalline selenium has a positive temperature coefficient at the measuring frequency, 24.029 GHz. The dielectric constant ϵ_r of single crystal selenium, measured parallel to the crystal c-axis was found to be 20 at $\pm 20^\circ C$, increasing to 28 at $\pm 183^\circ C$.

25,180 DIELECTRIC CONSTANT OF FERROMAGNETIC $CrBr_3$ ABOVE THE ABSORPTION-BAND EDGE by W. Jung (Bell Lab.); Bull. Am. Phys. Soc., Vol. 9, p. 463(A), Apr. 1964

The dielectric constant $\epsilon = \epsilon_1 - i\epsilon_2$ was measured at room temperature by re-flection techniques, using an ellipsometer. The room-temperature data provide information on the dielectric behavior in the unmagnetized state and, hence, on the diagonal elements of the polarizability tensor. The quantity ϵ_1 varies from 6.47 at 14,300 cm^{-1} up to 10.6 at 22,000 cm^{-1} , and shows a pronounced

anomalous dispersion between 22,000 and 28,000 cm^{-1} . A distinct peak in ϵ_2 corresponding to this transition is found at 25,000 cm^{-1} with $(\epsilon_2)_{max} = 7.9$. The data yield $g = 0.185$ for the dimensionless parameter of the transition.

25,181 DIELECTRIC CONSTANT OF A SUPERCONDUCTOR by R.E. Prange (Maryland U.); Grant AF AFOSR62 46, 37 pp., Oct. 1962; U.S. Gov. Res. Rep., Vol. 39, p. 141(A), June 20, 1964

The longitudinal dielectric constant was calculated for the Bardeen-Copper-Schrieffer model of a superconductor. An explicit formula is obtained which has been evaluated numerically. The competition between collective and single particle effects is pronounced, so that the dielectric function differs remarkably from the most elementary approximations to it. However, the dielectric function of the superconductor does not differ greatly from that in the normal metal in either the high frequency or static limit, regardless of the wavelength. This prevents the modifications due to superconductivity from being readily observed. In particular, the shift in the static polarizability should cause very small shifts in the phonon speed, so small that no effect on the lattice specific heat should be observed.

Dielectric Constant of:

$K_2O \cdot nTa_2O_5$ - See 24,978

ZnSe - See 25,224

Ge and Si - See 25,144

25,182 DIELECTRIC BREAKDOWN OF SINGLE-CRYSTAL STRONTIUM TITANATE by H.H. Barrett (Raytheon Res. Div.); J. Appl. Phys., Vol. 35, pp. 1420-1425, May 1964

Measurements of the intrinsic dielectric breakdown strength of single-crystal strontium titanate over a temperature range from -195° to $+100^\circ C$ and under both pulse and dc conditions are described; dc breakdown at $+100^\circ C$ is thermal in origin. At room temperature and at $-40^\circ C$ the breakdown strength is inde-pendent of duration of applied field and of sample configuration and hence may properly be termed intrinsic. At $-80^\circ C$ and $-195^\circ C$, both the values of break-down strength and the scatter of the data depend strongly on sample configura-tion. The breakdown strength unexpectedly decreases with increasing tempera-ture. Current-voltage curves show an anomalous saturation effect at low temperature. These effects may be qualitatively explained by postulating that the high electrostrictive stress causes the creation of electron trapping centers.

Breakdown in Dielectric Films - See 25,330

Polaron Effects in CdS - See 25,225

Ferroelectric Transitions in $(NH_4)_2SO_4$, $RbHSO_4$, $NaH_3(SeO_3)_3$ and $LiH_3(SeO_3)_2$ - See 25,634

25,183 EFFECT OF THERMAL TREATMENT AND PLASTIC DEFORMATION ON DIELECTRIC LOSSES IN $KCl-CaCl_2$ CRYSTALS by A.S. Bagdanovich, Yu. A. Sikorskii and P.A. Yurachkovskii (Polytech. Inst.); Soviet Phys. Solid State, Vol. 5, pp. 2586-2589, June 1964

It is shown that the location and half-width of the relaxation peak of dielectric losses in $KCl-CaCl_2$ crystals are sensitive to the thermal and mechanical treat-ments. As a result of deformation and heating, the set of relaxation times is increased and is accompanied by a broadening of the loss peak.

25,184 INTRINSIC DIELECTRIC LOSS IN POTASSIUM CHLORIDE by N.A. Economou (U. Illinois); Bull. Am. Phys. Soc., Vol. 9, p. 491(A), Apr. 1964

A dielectric loss that is described by the Debye equations has been found in potassium chloride at high temperature by Sastry and Srinivasan (Phys. Rev., Vol. 132, p. 2445, 1963 - SSA No. 21,836). Their data yield a heat of formation and a reorientation energy for the dipoles that are in good agreement with the theoretical results for vacancy pairs. The concentration of vacancy pairs that is obtained from the data is, however, more than 10 times larger than is reasonable. Dielectric-loss measurements have been made on potassium chloride containing strontium chloride in concentrations between 4×10^{-5} and 20×10^{-5} mol fraction. These data, which were obtained in the extrinsic ranges of conductivity and temperature, yield the same results as obtained from pure potassium chloride. Since the addition of strontium chloride to potassium chloride changes the cation- and anion-vacancy concentrations but leaves the vacancy-pair concentration unaltered, the results indicate that the observed loss is not due to Schottky defects and provide additional evidence that it is due to vacancy pairs.

25,185 DIELECTRIC CONSTANT AND LOSS MEASUREMENTS ON HIGH-TEMPERATURE MATERIALS by W.B. Westphal (Lab. Insul. Res. MIT); Contract AF33 616 8353, 47 pp., Oct. 1963; U.S. Gov. Res. Rep., Vol. 39, p. 87(A), May 20, 1964 AD 432 446 OTS\$4.60

Dielectric measurement techniques for frequencies of 100 to 2.5×10^{10} and temperatures to 1650°C are described. Apparatus employed are bridges, resonant circuits, and resonant cavities. Data on Al_2O_3 , Cr_2O_3 , MgO , LaAlO_3 , ZrO_2 single crystals; Al_2O_3 , BeO , MgO , Mg_2SiO_4 , Ta_2O_5 , ThO multicrystals; glass ceramics, silica glass and BN are presented for lower frequency and temperature ranges. Pyrolytic BN has a low loss tangent (0.0004 at 1375°C, 4.8×10^{-9} cps) and a low temperature coefficient of dielectric constant. Some aluminas and silicas exhibit loss tangents of ca. 0.0006 at 1000°C in the microwave region. Microwave losses are due partly to the charge transfer responsible for low-frequency conductivity and to the vibration spectra of infrared absorption. Both losses are increased by the addition of impurities.

25,186 DIELECTRIC PROPERTIES OF STRONTIUM-BISMUTH TITANATES by V.V. Bogdanov (Acad. Sci. USSR); *Soviet Phys. Solid State*, Vol. 5, pp. 2489-2493, June 1964

The dielectric properties of $\text{SrTiO}_3\text{-Bi}_2\text{O}_3\cdot 3\text{TiO}_2$ (SBT) is discussed on the basis of the model proposed by Skanavi. It is proposed that the relaxation polarization is caused by titanium ions relaxing within oxygen octahedra distorted by the existence of vacant sites in the strontium part of the lattice. The resultant quadrupole concentration is high, their activation energy distribution function is asymmetric and there is strong dipole-dipole interaction. This model permits a qualitative explanation of the principal properties of SBT and shows that SBT represents a new class of materials occupying an intermediate position between true ferroelectrics and materials in which classical ion relaxation occurs.

25,187 PRODUCTION OF BISMUTH TITANATE SINGLE CRYSTALS AND SOME OF THEIR PROPERTIES by D.A. Tambovtsev, V.M. Skorikov and I.S. Zheludev (Acad. Sci. USSR); *Soviet Phys. Cryst.*, Vol. 8, pp. 713-716, May-June 1964

The growth of $\text{Bi}_4\text{Ti}_3\text{O}_{12}$ crystals by crystallization from the melt and their dielectric properties are described. Results are given of measurements of the dielectric constant and piezoelectric modulus of the crystals produced. The temperature dependence of the spontaneous polarization P_0 , coercive field E_c , coefficient of nonlinearity and resistivity have also been studied. The results show that P_0 and E_c depend only slightly on the temperature, and the logarithm of resistivity has a discontinuity at temperature 643°C.

25,188 SOLID SOLUTIONS IN ANTIFERROELECTRIC REGION OF THE SYSTEM $\text{PbHfO}_3\text{-PbTiO}_3\text{-PbSnO}_3\text{-PbNb}_2\text{O}_6$ by C. Hall, R. Dungan, and A. Stark (Sandia Corp.); *J. Amer. Ceramic Soc.*, Vol. 47, pp. 259-264, June 1964

Dielectric, ferroelectric, and piezoelectric properties were investigated for compositions in the high-lead hafnate region of the system $\text{PbHfO}_3\text{-PbTiO}_3\text{-PbSnO}_3\text{-PbNb}_2\text{O}_6$. Phase diagrams were prepared that show the existence of a ferroelectric-to-antiferroelectric phase transition with increasing temperature. Five phases were shown to exist in the portion of the system investigated: two ferroelectric phases, two antiferroelectric phases, and one paraelectric phase. Ferroelectric-antiferroelectric phase transitions induced by temperature, electric field, and pressure were investigated. The highest spontaneous polarization measured was approximately 25 $\mu\text{Coul per cm}^2$.

25,189 FERROELECTRICITY IN $\text{Rb}_x\text{K}_{1-x}\text{NO}_3$ MIXED CRYSTALS by U. Kawabe, Y. Yanagi and S. Sawade (Tokyo Inst. Tech.); *J. Phys. Soc. Japan*, Vol. 19, pp. 767-768(L), May 1964

Dielectric properties and the lattice parameters for the $\text{Rb}_x\text{K}_{1-x}\text{NO}_3$ system have been measured at room temperature for the whole range of compositions. The melt growth method of producing the mixed crystals is described. The crystals obeyed Vegard's law in the molar ratio 0 to 0.52. Above 0.56 the KNO_3 pattern was clearly seen to be superimposed upon those of the mixed crystals, suggesting a mixing limit of somewhere between 0.52-0.56. The phase diagram shows a hysteresis loop upon cooling but not upon heating. A temperature dependence in the dielectric constant was also observed along the c-axis.

25,190 INFRARED INVESTIGATION OF THE PHASE TRANSITION IN NaNO_3 by Y. Sato, K. Gesi and Y. Takagi (Japan Atomic Energy Res. Inst.); *J. Phys. Soc. Japan*, Vol. 19, pp. 449-453, Apr. 1964

Absorption spectra of a combination mode $\nu_1 + \nu_4$ of NaNO_3 single crystal are studied over the temperature range between 26°C and 297°C with a polarized infrared radiation. It is found that as temperature rises half-band width markedly broadens as the temperature approaches the transition point of 275°C. The band shape in the high temperature phase is in good agreement with the relative intensity distribution curve calculated on an assumption that the NO_3 ions are rotating freely around the three-fold axis. The broadening of the band at any temperature can be explained satisfactorily if the two contours of the band observed at 26°C and 275°C, respectively, are superposed with an appropriate intensity ratio.

25,191 DIELECTRIC PARAMETERS OF RUBIDIUM NITRATE by A. Ya. Dantsiger and E.G. Fesenko (Rostov-on-Don State U.); *Soviet Phys. Cryst.*, Vol. 8, pp. 717-720, May-June 1964

Dielectric and thermal expansion measurements of RbNO_3 monocrystals from room temperature to the melting point (314°C) are reported. The results indicate that the $\text{II} \rightarrow \text{III}$ transition (at about 200°C) is from an antiferroelectric state to a paraelectric state, and the $\text{III} \rightleftharpoons \text{II}$ transition is of a first-order. The nature of $\text{IV} \rightarrow \text{III}$ transition is not clear and the phase IV is possibly ferroelectric.

25,192 THERMODYNAMIC THEORY OF DOMAIN WALLS IN FERROELECTRIC MATERIALS WITH THE PEROVSKITE STRUCTURES by L.N. Bulaevskii (Acad. Sci. USSR); *Soviet Phys. Solid State*, Vol. 5, pp. 2329-2332, May 1964

An analysis of the 180° and 90° domain walls in the tetragonal phase of ferroelectric materials with the perovskite structure is presented. All solutions are obtained for the polarization in the domain wall, and the conditions under which these solutions apply are indicated. Numerical estimates for the barium titanate show that only one solution without the rotation of the polarization vector is possible. The thickness and surface energy of domain walls in barium titanate are calculated.

25,193 ORIGIN OF THE VISIBILITY OF THE ANTIPARALLEL 180° DOMAINS IN BARIUM TITANATE by J. Kobayashi, N. Yamada (Waseda U., Tokyo), and T. Nakamura (U. Tokyo); *Phys. Rev. Lett.*, Vol. 11, pp. 410-414, Nov. 1963

The antiparallel 180° domains observed by Miller and Savage in BaTiO_3 under crossed polaroids are investigated. Using optical means of inspecting the zones it is concluded that these domains exhibit birefringence when viewed along the ferroelectric axis. The amount of birefringence is proportional to the speed with which the domain moves in the applied field. By means of x-ray diffraction methods it has also been shown that the crystal structure of the zones changes from tetragonal to some lower symmetry under the applied electric field. The "switching" entails a considerable relaxation time.

25,194 QUANTUM EFFECTS IN FERROELECTRIC MATERIALS WITH HYDROGEN BONDS by V. Kh. Kozlovskii (All-Union Res. Inst.); *Soviet Phys. Solid State*, Vol. 5, pp. 2411-2415, May 1964

Equations for the determination of the quantum states of anharmonic oscillators are formulated. Using these equations, an analysis is made of an oscillator whose potential curve exhibits two maxima. Its state and polarization are investigated. In the analysis of the ferroelectric crystals, an equation for the polarization is derived and certain quantum effects are discussed. It is predicted that a ferroelectric crystal can be formed by means of the isotopic substitution in nonferroelectric crystals with hydrogen bonds.

25,195 SWITCHING BEHAVIOR IN FERROELECTRIC POTASSIUM NITRATE by R. Dork, N. Schubring, and J. Nolte (GM Res. Labs.); *J. Appl. Phys.*, Vol. 35, pp. 1984-1985(L), June 1964

Total switching time and peak switching current density of KNO_3 have been measured as a function of applied field and temperature. Linearity at high fields is evident and the ferroelectric dipoles are seen to switch faster at higher temperatures. Rapid change in switching time occurs at low temperatures followed by a leveling off at higher temperatures. Peak switching is also larger at higher temperatures because the ferroelectric dipoles can reverse in a shorter time interval. Linearity at high fields indicates the element may be approximated by a resistance in series with a voltage bias.

25,196 MICROSCOPIC DIELECTRIC SUSCEPTIBILITY OF GERMANIUM by W. Cochran (Crystallographic Lab., England) and J.C. Phillips (U. Chicago); *Phys. Rev.*, Vol. 134, pp. A1402-A1406, June 1, 1964

The microscopic dielectric susceptibility $\epsilon(q)$ is calculated for germanium using the shell model. It is found that except at $q = 0$ the longitudinal and transverse susceptibilities differ and are anisotropic. The results agree qualitatively with Penn's isotropic quantum model based on the random-phase approximation. It is suggested that the quantitative differences may in part represent shortcomings of the RPA in treating the stiffness of covalent bonds.

25,197 ANOMALOUS DISPERSION OF COERCIVE FIELD AT VERY LOW FREQUENCIES AND A JERKY WALL MOTION IN ROCHELLE SALT by R. Abe (Nagoya U.); *Japanese J. Appl. Phys.*, Vol. 3, pp. 243-249, May 1964

An optical method was used to study the dependences of coercive field on temperature and frequency of very low frequency regions. From the analysis of the data following conclusions are obtained. (1) The dependence of coercive field on frequency at 0°C can be explained satisfactorily if the velocity of the wall motion is assumed to be proportional to $\exp(-a/E)$, where E is an applied field. The value of a was determined to be about 190 volt/cm from the

experimental data. (2) The temperature at which the coercive field is maximum decreases with the decrease of frequency and it becomes finally about 2°C at 0.004 cps. This dependence of coercive field on frequency and temperature can be explained by assuming that a certain Schottky defect, probably the defect of H_2O molecule, prevents the faster movement of the domain wall.

25,198 DYNAMICAL THEORY OF RIGID LATTICES OF ANTIFERROELECTRICS by V.K. Kozlovskii (All-Union Sci. Res. Inst.); *Soviet Phys. Cryst.*, Vol. 8, pp. 659-664, May-June 1964

Phase transition in antiferroelectrics, consisting of the splitting of the crystal's translation lattice into two identical sublattices displaced in opposite directions is discussed by means of dynamical equations for anharmonic vibrations of rigid lattices. The crystal's phases, as well as the temperature ranges of their existence and stability, are determined. It is shown that stable existence of both the antiferroelectric and ferroelectric phases is possible at low temperatures.

25,199 MAGNETIC AND ELECTRICAL PROPERTIES OF FERROELECTRIC YTTRIUM AND YTTERBIUM MANGANATES by V.A. Bokov, G.A. Smolenskii, S.A. Kizhaev and I.E. Myl'nikova (Acad. Sci. USSR); *Soviet Phys. Solid State*, Vol. 5, pp. 2646-2647(L), June 1964

Investigations of the magnetic and electrical properties of YMnO_3 and YbMnO_3 are reported. It is found that all crystals investigated exhibit a dielectric hysteresis loop, and in the majority of the crystals saturation is reached only at room temperature. The sample capacitance increases monotonically with the increase of temperature and no maximum is found up to 500°C . The magnetic susceptibility of YMnO_3 between 475 and 950°K obeys the Curie-Weiss law; in the case of YbMnO_3 the Curie-Weiss law is obeyed in the range 190 - 950°K . It is concluded that YMnO_3 and YbMnO_3 are ferroelectric antiferromagnets with high ferroelectric Curie points and low Néel points.

25,200 PIEZOELECTRICITY IN SALICYLIDENE ANILINE CRYSTALS by A. Aharoni and D. Sapozhnikov (Weizmann Inst. Sci., Rehovoth, Israel); *J. Appl. Phys.*, Vol. 35, pp. 1906-1909, June 1964

The resonance frequencies of various single crystals of salicylidene aniline were measured for different modes of vibration, and the velocities of sound waves in these materials were deduced. Values are given for the electric equivalent circuit parameters and elastic constants in such crystals.

25,201 PRIMARY PYROELECTRIC EFFECT IN THE PZT 95/5 CERAMIC by J.L. Wentz and L.Z. Kennedy (Sandia); *J. Appl. Phys.*, Vol. 35, pp. 1767-1770, June 1964

An expression of the thermodynamic potential is examined in terms of the primary and secondary pyroelectric coefficients of a poled ferroelectric ceramic. Anisotropic expansion and zero electric field conditions are assumed. The pyroelectric coefficient is applied to the composition, $\text{Pb}(\text{Zr}_{0.95}\text{Ti}_{0.05})\text{O}_3$ (PZT 95/5) with 1 wt.% of Nb_2O_5 , for which a complete set of elastic, piezoelectric, thermoelastic, and pyroelectric coefficients were determined. A value of $-26.8 \times 10^{-9} \text{ C/cm}^2\text{-}^{\circ}\text{C}$ was found for the total pyroelectric coefficient of which $+3.77 \times 10^{-9}$ was contributed towards the piezoelectric or secondary effect; therefore, $-30.6 \times 10^{-9} \text{ C/cm}^2\text{-}^{\circ}\text{C}$ is reported for the primary pyroelectric coefficient for this material over the temperature range 25° - 50°C .

CARRIER PROPERTIES

25,202 EXCITON NEAR THE SURFACE OF A HOMOPOLAR CRYSTAL by M.F. Diegen and M.D. Glinchuk (Acad. Sci. USSR); *Soviet Phys. Solid State*, Vol. 5, pp. 2377-2382, May 1964

An exciton of the Mott type near the surface of a crystal is studied by the effective mass method. It is concluded that a "dead" layer, in which the exciton is very unlikely to remain, exists near the surface of a semiconductor. The width of the layer is of the order of one hundred angstroms in the case of a homopolar crystal with dielectric constant $\epsilon \approx 10$. This conclusion is in agreement with data given in the literature, which indicates the existence of similar "dead" layers near the surface of a crystal.

25,203 TRANSPORT THEORY FOR ELECTRON-PHONON INTERACTIONS IN METALS by R.E. Prange (U. Maryland) and L.P. Kadanoff (U. Illinois); *Phys. Rev.*, Vol. 134, pp. A566-580, May 4, 1964

By extending Migdal's approximation for electron-phonon interactions in metals to the nonequilibrium case, it is possible to derive a set of transport equations which are exact to order $(m/M)^{1/2}$. This coupled set of equations for the electron and phonon distribution functions is correct even in the situation in which the electronic excitation spectrum has considerable width and structure

so that one might not expect a priori that there would be well-defined quasiparticles. Nonetheless, one of the forms of the electronic transport equation is identical to the transport equation suggested by Landau for the case in which the quasiparticle energy is well defined. The transport equations may be written in two different forms: In the first the electronic distribution function is labeled by a momentum vector; in the second, the labels are excitation energy and the position on the Fermi surface. Despite the width in the spectrum, the momentum-space form is identical with the Landau quasiparticle theory. The energy space form is slightly simpler because no wave function renormalization constants appear in the definition of the energies or in the scattering matrix elements. In fact, in the case in which there is space dependence but no time dependence this form of the transport equations looks identical to the weak-coupling Boltzmann equations.

25,204 ON THE BLOCH-REPRESENTATION OF ELECTRON-ELECTRON INTERACTION [in German] by W. Brauer (German Acad. Sci., Berlin); *Phys. Stat. Sol.*, Vol. 5, pp. 139-144, 1964

The general expressions for the Bloch representation of the electron-electron interaction in the reduced zone scheme is used to develop a relationship between the matrix element considered and the matrix element of an electron-phonon interaction, regardless of normal-or Umklapp-type processes. A special study is made of the behavior of the matrix element for small wave vector differences on the assumption that a center of inversion exists.

25,205 THE ENERGY SPECTRUM OF A DEGENERATE SEMICONDUCTOR WITH AN IONIC LATTICE by L.V. Keldysh and Yu. V. Kopoev (Acad. Sci. USSR); *Soviet Phys. Solid State*, Vol. 3, pp. 1026-1030, Nov. 1963

It is shown that electron interaction with longitudinal, optical phonons in a degenerate semiconductor leads to characteristic peculiarities in the energy spectrum. At the Fermi surface, the velocity approaches infinity logarithmically, while the density of states approaches zero. The results obtained enable an explanation to be made for the maxima in the conductivity of type AlV_{BV} tunnel diodes, and also for the frequency dependence of the coefficient of the self-absorption of light of these crystals in the vicinity of the threshold.

25,206 INTERACTION OF ELECTRON ON THE DONOR CENTER WITH THE CRYSTAL LATTICE IN GERMANIUM AND SILICON by A. Myszkowski and S. Gómulka (Warsaw U., Poland); *Phys. Rev.*, Vol. 134, pp. 1102-1106, May 18, 1964

The diagonal matrix element of interaction of the bound electron with longitudinal acoustic phonon, squared and averaged over all directions of the phonon wave vector, was calculated for n-type Ge and Si assuming a single-deformation-potential constant. The donor wave functions have been taken in the ellipsoidal form. Some simple integrals containing the squared and averaged matrix element are given and are used, as an example, to get the one-phonon transition rate in the impurity conduction by "hopping" and the relaxation energy of the lattice deformed by interaction with the donor electron. Appreciable differences are found between the case of ellipsoidal and spherical donor wave functions.

25,207 PHONON AND ELECTRON DISTRIBUTIONS IN HIGH ELECTRIC FIELDS by E.M. Conwell (Genl. Tel. and Electronics Lab.); *J. Phys. Chem. Solids*, Vol. 25, pp. 593-601, June 1964

The coupled Boltzmann equations for the electron and acoustic phonon distributions in high electric fields are set up. Similar in form to the disturbed electron distribution, the disturbed phonon distribution should be well approximately by a sum of two terms, the first, $N_0(\epsilon_p)$, dependent on phonon energy only, while the second, $q_x q_p(\epsilon_p)$, represents an excess of phonons with q in the direction of carrier drift. Solutions are obtained for the case in which the deviation of the phonon distribution from its thermal equilibrium value is small, although that of the electrons need not be. These are evaluated for a lattice temperature such that equipartition is valid for the thermal equilibrium distribution. It is found that the disturbance is proportional to carrier concentration and phonon lifetime, and should be measurable in n-Ge at 30°K in properly chosen samples. For a given q it increases strongly with field, starting from zero field, but reaches a peak at fairly low fields after which it is steady or declines with field. The disturbance also decreases monotonically with increasing q of the phonons. The effect on carrier transport of the disturbance is opposite for the two terms mentioned. The increase of N_0 over the thermal equilibrium value gives an increase in scattering, which of course tends to decrease mobility. The $q_x q_p$ term produces a phonon drag effect that tends to increase mobility. At very low fields the latter would predominate.

25,208 EXCESS CARRIER CONCENTRATION IN A BULK SEMICONDUCTOR ILLUMINATED BY A PULSE OF LIGHT by D. Homes and D. Feucht (Carnegie Inst. Tech.); *Proc. IEEE*, Vol. 52, p. 630(L), May 1964

Transient behavior of the excess carrier density of a semiconductor illuminated by light pulses is of special interest in microwave lifetime measurements. A

transient solution for the excess carrier density is derived from the diffusion equation for excess carrier concentration, considering semi-infinite geometry, for all time t measured from the onset of the light pulse. When the result for the excess carrier concentration, $\Delta p(x, t)$, is integrated, the total number of excess carriers contained in the waveguide is dependent upon the parameters α , the optical absorption coefficient and t_0 , the light pulse duration.

25,209 ON THE VALIDITY OF THE BOLTZMANN BOUNDARY CONDITIONS AT SEMICONDUCTOR INTERFACES by R. Lade and C. Poncelet (North Carolina State); *Proc. IEEE*, Vol. 52, pp. 629-630(L), May 1964

A rapid method, in terms of curves depending on doping levels only by which the degree of validity of the Boltzmann relation can be ascertained for any injection level is described. Using general carrier relations applicable at semiconductor interfaces, equations describing the excess carrier densities \bar{p}_1 and \bar{p}_2 are developed. Similar results are obtained for both \bar{p}_1 and \bar{p}_2 :

$$\bar{p}_1 = \gamma n_{10} (e^{V'} - 1),$$

Plots of γ as a function of the voltage V' are shown for various doping levels to illustrate deviations from the Boltzmann boundary conditions.

25,210 EFFECTS OF EXCITED STATES IN RECOMBINATION STATISTICS by V.V. Voronkov (Moscow State Sci. Res. Inst.) *Soviet Phys. Solid State*, Vol. 5, pp. 2292-2293, May 1964

The statistics of recombination at a multiply charged center are extended to cover the case in which there exist excited states. It is shown that if the internal transitions predominate over the processes of capture and ejection of carriers, the effect of excited states reduces to a generalization of the capture coefficients in the formulas of the ordinary statistics of recombination at a multiply charged center.

25,211 ANALOGUE COMPUTATION OF DIFFUSION CONTROLLED RECOMBINATION EQUATIONS by H.J. Wintle (Royal Military Coll. Sci.); *J. Sci. Instr.*, Vol. 41, pp. 178-179, Mar. 1964

The role of radiation-induced electrical conductivity in the carrier recombination mechanism is discussed. An equation is developed to assess the behavior of the time-dependent 'rate' constant when various interaction potentials exist between the carriers and the recombination centers. Solution for dc operation of a tapered RC line analog shows that steady state recombination rate is approached approximately as $t^{-1/2}$. Results indicate that there is no extended time period during which the rate constant is proportional to t^{-m} for which m differs appreciably from $1/2$. Extension to other potential functions is possible and it is clear that a tapered line can serve as a very useful function generator in dc as well as ac operation.

25,212 A SIMPLE PHOTOELECTRIC BRIDGE METHOD FOR DETERMINING THE LIFETIME OF INJECTED CURRENT CARRIERS IN SEMICONDUCTORS by T. Figielski (Polish Acad. Sci., Warsaw) and Z. Wieckowska (Warsaw U.); *Acta Phys. Polonica*, Vol. 24, pp. 675-680, Nov. 1963

A new stationary, photoelectric method for determining the current carriers lifetime is proposed. The method can be successfully used for germanium or silicon samples with $\tau \geq 10 \mu s$.

25,213 DETERMINATION OF CARRIER LIFETIME, DIFFUSION LENGTH, AND SURFACE RECOMBINATION VELOCITY IN SEMICONDUCTORS FROM PHOTO-EXCITED INFRARED ABSORPTION by N.G. Nilsson (Royal Inst. Tech., Stockholm); *Solid-State Electronics*, Vol. 7, pp. 455-463, June 1964

The mean carrier lifetime τ , diffusion length L , and surface recombination velocity s have been determined from the absorption by photo-injected carriers in the infrared. No electrical connections to the specimens were necessary. With light for carrier injection that was modulated, at a variable frequency, an infrared detector could be used whose time constant was longer than the carrier lifetime. The measuring method is described, and measurements with germanium are shown. For the one-dimensional case an expression in closed form has been derived for the effective lifetime as a function of τ , L , and s . These parameters may be determined from measurements with three or more sample thicknesses.

25,214 ELECTRICAL MEASUREMENTS ON PHOTOGRAPHIC GRAINS CONTAINING CADMIUM by L.E. Brady and J.F. Hamilton (Eastman Kodak); *J. Appl. Phys.*, Vol. 35, pp. 1565-1569, May 1964

Ionic conductance and electron lifetime measurements have been made on emulsion grains containing cadmium. The reduction in the concentration of interstitial silver ions because of the divalent cationic impurity, decreases the ionic conductivity, correspondingly increases the electron lifetimes in the grains, and introduces a high-intensity, reciprocity-law failure in the emulsion.

These results confirm the conclusion that silver ions are the dominant carriers of ionic current and that these same silver ions play a major role in the initial trapping of photoelectrons during latent-image formation. Moreover, they strongly suggest that the silver ions responsible for ionic conductance in grains with no impurity additions are interstitials generated at kink sites on the grain surface and moving in a space-charge layer within the grains.

25,215 CdTe HOLE LIFETIME FROM THE PHOTOVOLTAIC EFFECT by D.A. Cusano and M.R. Lorenz (GE Res. Lab.); *Solid State Comm.*, Vol. 2, pp. 125-128, Apr. 1964

A direct determination of the minority carrier lifetime for n-type semiconducting CdTe is described. The value of 5×10^{-10} sec is obtained from the spectral response of photovoltaic heterojunctions. These junctions are formed on highly-doped single crystals so that minority carrier production and transport occur principally in field-free regions. This value for hole lifetime differs substantially from earlier estimates for the II-VI compounds.

25,216 METHOD FOR DETERMINATION OF THE PARAMETERS OF TRAPPING LEVELS IN CdS-TYPE CRYSTALS by K. Kirov (Acad. Sci. Bulgarian SSR); *Soviet Phys. Solid State*, Vol. 5, pp. 1267-1269(L), Dec. 1963

25,217 CARRIER LIFETIME STUDIES IN ELECTRON-(10-55 Mev) AND PROTON-(25-110 Mev) IRRADIATED GERMANIUM by J.E. Fischer and J.C. Corelli (Rensselaer Polytech.); NASA Grant NsG-290, 41 pp., 1964; *STAR*, Vol. 2, pp. 1528-1529(A), June 23, 1964 NASA CR-53782; OTS:\$4.60 ph

Samples of single-crystal germanium were irradiated at room temperature with electrons of energies from 12 Mev to 55 Mev, and with protons of energies from 25 Mev to 109 Mev. Measurements of the minority carrier lifetime as a function of flux and of initial carrier concentration suggest that: (1) More than one recombination level is introduced into the forbidden gap by the defects created during electron and proton bombardment, with the multilevel effect being greater for the proton-irradiated specimens. (2) Nonlinearity of the defect introduction rates of two-proton irradiated samples may be due to the closing of channels and the resulting decrease in the number and range of "stenons" (channeled knockons). (3) The carrier lifetime change with increasing proton energy does not decrease as sharply as predicted by Rutherford scattering and the Kinchin-Pease model. (4) The energy dependence of carrier lifetime change in the case of electron bombardment is complicated by a nonconstant contribution of multiple levels to the recombination process in the electron-energy range studied.

25,218 EFFECT OF OXYGEN ON RECOMBINATION IN SILICON SUBJECTED TO HEAT TREATMENT by V.N. Mordkovich and L.E. Gartsera; *Soviet Phys. Solid State*, Vol. 5, pp. 1081(L), Nov. 1963

25,219 TRAPPING OF CHARGE CARRIERS IN HEAT-TREATED SILICON by K.D. Glinchuk and N.M. Litovchenko (Acad. Sci. USSR); *Soviet Phys. Solid State*, Vol. 5, pp. 2305-2308, May 1964

It is shown from a study of the intrinsic photoconductivity in heat-treated Si that heat treatment of the n- and p-type Si in the temperature range 800-1300°C leads to formation of effective trapping centers for electrons and holes. The nature of the trapping centers is analyzed. The impurity atoms in Si either occupy interstitial positions or form complexes and may thus be in different charge states. It is possible that some of these may act as the trapping centers.

25,220 CARRIER TRAPPING IN PHOTOCONDUCTING ANTHRACENE by S.Z. Weisz, R.C. Jarnagin, M. Silver (U. North Carolina), M. Simhony and J. Balberg (Hebrew U. Jerusalem); *J. Chem. Phys.*, Vol. 40, pp. 3365-3369, June 1, 1964

The techniques of transient space charge limited photocurrent have been employed to observe hole trapping in monocrystalline anthracene. Two trapping processes are clearly evident. One corresponding to fast trapping with time about $10^2 \mu sec$ and a relatively slow process with time about $10^4 \mu sec$. The fast process is shown to be associated with traps whose density is reducible by simple crystal annealing. Evidence is presented which suggest these traps to be molecules in distorted positions in the crystal lattice.

25,221 THERMALLY STIMULATED CURRENTS AND CARRIER TRAPPING IN ANTHRACENE CRYSTALS by H. Kokado and W.G. Schneider (Natl. Res. Council); *J. Chem. Phys.*, Vol. 40, pp. 2937-2945, May 15, 1964

Thermally stimulated currents in anthracene single crystals have been investigated. A fairly large current peak observed at a temperature near 0°C, is shown to be characteristic of anthracene and corresponds to a carrier trap level of depth 0.76 ± 0.05 ev. The effects of temperature, applied voltage, and the time of illumination with uv light on trap filling were investigated. Illumination at low temperatures, with or without an applied field, generates charge carriers which are localized in the crystal. Below -60°C the rate of carrier release and/or recombination appears negligibly small, permitting

charge storage for indefinitely long periods of time. In addition to thermal detrapping, it was found that carrier detrapping could also be brought about by optical radiation with wavelengths in the visible and near infrared region. The resulting optically stimulated currents depended linearly on the intensity of the long wavelength light. The results suggest that on uv illumination at low temperatures ion pairs are generated at dissociation centers, the electron being deeply trapped by the center. The liberated holes (majority carriers) are partially mobile at low temperatures and are eventually localized in traps. The observed thermally stimulated currents are attributed to thermal release of the majority carriers.

Trapping in Se - See 25,694

25,222 A FAST RECOMBINATION MECHANISM AT THE SURFACE OF CdS SINGLE CRYSTALS by V.E. Lashkarev, G.I. Golynnya and M.K. Sheinkman (Acad. Sci. USSR); *Soviet Phys. Solid State*, Vol. 5, pp. 2511-2515, June 1964

The phenomenological quantum yield of the photocurrent in CdS crystals and the spectral characteristics of the photocurrent in the presence of a transverse electrical field have been investigated. The results obtained confirm the concept of an effective fast recombination mechanism in the bulk and at the surface of the crystals, which acts in parallel with the usual slow recombination mechanism.

Recombination Radiation from:

Diodes - See also Laser Diodes

GaAs Diodes - See 25,657

GaP Junctions - See 25,145

25,223 MEASUREMENT OF THE CONDUCTIVITY EFFECTIVE MASS IN SEMICONDUCTORS USING INFRARED REFLECTION by H.A. Lyden (MIT); *Phys. Rev.*, Vol. 134, pp. A1106-A1112, May 18, 1964

There exist various approximate relationships between the conductivity effective mass of free carriers m_c and the angular frequency ω_0 of the reflectivity minimum in the infrared arising from the free-carrier dispersion. A detailed analysis of the reflectivity equation shows that it is possible to obtain a relationship between m_c and ω_0 when in addition one has a knowledge of the free-carrier concentration, the drift mobility, and the dielectric constant of the semiconductor at very high frequencies. This relationship is shown to yield a value of $m_c^* = 0.145$ for n-type germanium at room temperature using data presented in the literature. This value compares well with the value of $m_c^* = 0.15$ obtained using a combination of reflection and transmission measurements. The experimental work required to obtain accurate values for m_c using this relationship is considerably less than that required by other techniques, such as cyclotron resonance, magnetoplasma, and combined infrared reflection and transmission measurements, which are presently used. Moreover, this procedure can be applied over very broad ranges of temperature and of free-carrier concentration.

Effective Mass:

of Ge and Si - See 25,144

in PbTe - See 25,252

25,224 ELECTRON EFFECTIVE MASS IN ZnSe by D.T.F. Morple (GE Res. Lab.); *J. Appl. Phys.*, Vol. 35, pp. 1879-1882, June 1964

Infrared reflectance and Faraday rotation data were obtained for pure and for highly Al-doped n-type ZnSe crystals. Comparison of these data gave the free-carrier contribution to the dielectric constant and Faraday rotation, which, in turn, yielded the electron effective mass and carrier concentration. The result for the effective mass ratio, $m^*/m = 0.17 \pm 0.025$, agrees satisfactorily with previous estimates. The Hall scattering constant r was obtained from the optically measured carrier concentration and Hall effect data on the optical samples. The result, $r \approx 1.4$, for $N \approx 0.7 N_{\text{deg}}$, is consistent with values found in other II-VI compounds.

25,225 PIEZOELECTRIC POLARON EFFECTS IN CdS by G.D. Mahan and J.J. Hopfield (U. Calif.); *Phys. Rev. Lett.*, Vol. 12, pp. 241-243(L), Mar. 9, 1964

Cyclotron resonance measurements of conduction mass in CdS are discussed. Cyclotron resonance measurements yield values of $m_{\text{tr}}^* = 0.177$ and $m_{\text{h}}^* = 0.157$, while other experiments have given values $m_{\text{tr}}^* \approx m_{\text{h}}^* = 0.20$ (or 0.19). It is shown that polaron effects from piezoelectric electron-phonon interactions cause the mass shift of the cyclotron resonance values of conduction mass in CdS.

25,226 ELECTRON MOBILITY IN GERMANIUM ABOVE ROOM TEMPERATURE by O.A. Golikova (Acad. Sci. USSR); *Soviet Phys. Solid State*, Vol. 5, pp. 1276-1277(L), Dec. 1963

25,227 MINORITY CARRIER HALL MOBILITY by M.G. Buehler and L. Pensak (Duke U.); *Solid-State Electronics*, Vol. 7, pp. 431-438, June 1964

An experimental technique has been devised to measure the Hall mobility of minority carriers in semiconductors. The minority carrier Hall mobility has been measured in p-type germanium at room temperature and the value obtained is in qualitative agreement with the theory given by Prince. Experimental observations are based on the injection of a narrow stream of minority carriers into a bar of semiconductor and on the measurement of the deflection angle of the stream in a magnetic field. The experimental structure lends itself to the measurement of not only the minority carrier Hall mobility but also the (majority carrier) Hall mobility and drift mobility. Comparison of these mobilities over a range of temperatures is expected to be of value in studying such transport properties as scattering mechanisms, relaxation times and ambipolar drag effects.

25,228 HALL MOBILITY OF ELECTRONS IN KBr, KI, KCl, AND NaCl AT LOW TEMPERATURES by R.K. Ahrenkiel and F.C. Brown (U. Illinois); *Bull. Am. Phys. Soc.*, Vol. 9, p. 492(A), Apr. 1964

The mobility of electrons in alkali-halide crystals down to the temperature of liquid helium was discussed. Optical-mode scattering with mobility dependence upon $\exp(\Theta/T)$ was generally observed above 40°K. The Debye temperature Θ can be compared with the optical-mode frequency of the material, where the magnitude of the scattering can be used to estimate band and polaron parameters. Mobilities as high as 15,000 cm²/V·sec, depending upon F-center density, were observed for lightly colored crystals of KBr at 7°K. Similar high mobilities were found for KI and a sample of zone-refined KCl, but the largest mobility observed in NaCl was 1200 cm²/V·sec. The low-temperature mobility in KBr could be reduced an order of magnitude by optically converting F centers (neutral defects) to F' and a centers (charged defects). The original mobility could then be restored by illumination in the F' band at low temperature.

Mobility in Se - See 25,347

25,229 THEORY OF SCATTERING IN SOLIDS by J. Callaway (U. Calif., Riverside); *Bull. Am. Phys. Soc.*, Vol. 9, p. 412(A), Apr. 1964

A Green's-function method was used to determine the amplitude for the scattering of excitations in solids by localized imperfections. An electron wave function was expanded in Wannier functions. The coefficients in this expansion satisfy an equation analogous to the Lippmann-Schwinger equation of scattering theory. If the matrix elements of the potential on the basis of Wannier functions $V(R_n, R_m)$ are zero for R_n and R_m sufficiently large, the equation can be solved exactly. A partial-wave expansion of the scattering amplitude is possible in which contributions are classified according to irreducible representations of the point group of the crystal. Bound states and scattering resonances are obtained from poles of the scattering amplitude. In the case of a resonance the imaginary part of the energy at the pole determines the width. An expression was derived for the change in the density of states produced by the defect.

Electron-Atom Scattering - See 25,170

25,230 INTERVALLEY SCATTERING BY DONOR IONS IN GERMANIUM by P.J. Price and R.L. Hartman (IBM Watson Lab.); *J. Phys. Chem. Solids*, Vol. 25, pp. 567-570, June 1964

A contribution to the intervalley scattering rate in n-germanium is the direct transition induced by the donor-ion potential, U . The scattering rate for this process is calculated to lowest order in U , using the relation between the intervalley matrix elements of U and the singlet-triplet splitting of the donor ground state. The predicted scattering rate for Arsenic agrees with the experimental results of Weinreich, Sanders and White for the intervalley scattering due to donor ions, above 40°K.

Scattering in:

PbTe - See 25,252

GaAs, GaP, GaSb, and InP - See 25,615

25,231 INVESTIGATION OF THE SATURATION OF THE DRIFT VELOCITY OF HOT CARRIERS IN p-TYPE GERMANIUM by E.M. Gershenson and L.B. Litvak-Gorskaya (Lenin State Pedagogical Inst.); *Soviet Phys. Solid State*, Vol. 5, pp. 1074-1075(L), Nov. 1963

25,232 IONIZATION RATES OF HOLES AND ELECTRONS IN SILICON by C.A. Lee, R.A. Logan, R.L. Batdorf, J.J. Kleimack, and W. Wiegmann (Bell Labs.); *Phys. Rev.*, Vol. 134, pp. A761-773, May 4, 1964

The ionization rates of charge carriers in silicon have been measured and fit to the recent theoretical calculations of Baroff; in contrast, none of the existing published data could be fit to these theoretical curves. The study has been

made using microplasma-free junctions of demonstrably high, uniform local multiplication. A new and considerably simplified approach to the problem of extracting the ionization rates from the multiplication data has been used. By employing much more precise control of the electron and hole currents used to initiate the multiplication process, the hole ionization rate at electric fields less than 300 kv/cm is found to be more than an order of magnitude smaller than any previously published measurements. Hole and electron ionization rates have been measured in the same junction and consequently in the identical scattering environment. The threshold energy is determined to be $E_g \leq E_i < 1.5 E_g$, and the mean free path for scattering of high-energy electrons is $50 \text{ \AA} \leq \lambda_e \leq 70 \text{ \AA}$ and for energetic holes $30 \text{ \AA} \leq \lambda_h \leq 45 \text{ \AA}$. Measurement of ionization rates at various temperatures substantiates the assumption that the energy-loss mechanism is the emission of optical phonons. In addition, significant differences of the electrical breakdown characteristics of microplasma-free junctions are discussed as well as their preparation.

RESISTIVITY (CONDUCTIVITY)

25,233 COMPONENTS OF THE TWO-BAND RESISTIVITY TENSOR IN SEMI-CONDUCTORS by R.G. Moore and J.A. Stamper (Texas Instr.); *J. Appl. Phys.*, Vol. 35, pp. 1545-1549, May 1964

The components of the two-band resistivity tensor are determined as functions of the two single-band carrier concentrations and mobilities to yield the general equations for the two-band resistivity and Hall coefficient. The conductivities which usually appear in the two-band formulas for Hall coefficient and "conductivity" are reciprocals of the components of the resistivity tensors and are not components of the conductivity tensor. The two-band equations reduce to those of Kurnick and Zitter for semiconductors by assuming (1) that a time of relaxation for the carriers exists and that it is energy independent or (2) that the magnetic field is sufficiently large.

25,234 THEORY OF ELECTRICAL RESISTIVITY OF FERROMAGNETIC METALS by S.H. Liu (IBM Watson Res. Ctr.); *J. Appl. Phys.*, Vol. 35, pp. 1087-1088, Mar. 1964

A brief account of a new calculation of the electrical resistivity of ferromagnetic metals on the s-d or s-f exchange model is presented. It points out that the conventional treatment of the problem taking the s-d interaction as a small perturbation to a system of free electrons and ferromagnetically coupled spins is basically inconsistent with the indirect exchange theory. The consistent formulation of the problem is then given with the help of the Kubo method of electrical conductivity. The correlation functions involved in the Kubo formula are evaluated by the equation of motion method for many body problems. The hierarchy of equations of motion is terminated at a finite order by the decoupling approximation. The resulting equations are solved and the solutions are used to calculate the conductivity. A new result that comes out of this theory is that the low-temperature electrical resistivity is proportional to the density of spin waves and has a $T^{3/2}$ dependence on the temperature T . This result is in quantitative agreement with the experimental findings of Kondorsky et al.

25,235 ON THE PROBLEM OF THE EFFECTIVE CONDUCTIVITY TENSOR OF A POLYCRYSTALLINE MIXTURE, IN CONNECTION WITH THE THEORY OF METALS IN HIGH MAGNETIC FIELDS by H. Stachowiak (Low Temperature Lab., Wrocław); *Acta Phys. Polonica*, Vol. 24, pp. 651-661, Nov. 1963

In polycrystalline mixtures, the particular components form connected areas, to be referred to henceforth as agglomerations. For the properties of the mixture it is essential whether the agglomerations of a component of lower concentration are isolated within a medium constituted by a component of high concentration. If the agglomerations of a component are so large as to reach to the opposite sides of the sample, the component cannot be considered to be a small admixture, quite independently of its concentration, which may be relatively small. The present paper gives, in a first approximation neglecting the correlations between different "side-branches" of an agglomeration, the greatest value of the concentration of a component in a two-components mixture for which the dimensions of the agglomerations are still finite, on the assumption that the crystals of various components have the same geometrical properties and that there is no correlation between their positions. For special simplified models of the polycrystal, numerical results are obtained. This subject is of interest for the theory of metals in high magnetic fields.

25,236 STOCHASTIC PROCESSES IN POLYCRYSTALLINE MIXTURES AND THE PROBLEM OF THE EFFECTIVE CONDUCTIVITY by H. Stachowiak (Low Temperature Lab., Wrocław); *Acta Phys. Polonica*, Vol. 24, pp. 749-762, Dec. 1963

Polycrystals consisting of crystals of different kinds are considered. Crystals of the same kind form connected areas, called agglomerations, within the polycrystal. An agglomeration as such is a stochastic process. The purpose of this paper is to find how large the concentration of a given component must be in order that agglomerations of this component shall be infinitely extended (in an

infinite polycrystalline sample). A method of finding this critical concentration is evolved for simplified models of polycrystals. It is found that a concentration of about 30% is sufficient in the three-dimensional case for the existence of infinite agglomerations (in the two-dimensional case a concentration of 50% is required).

25,237 THE ELECTRICAL RESISTIVITY OF SOLID AND MOLTEN FUSED SILICA IN THE TEMPERATURE RANGE 1000-2480°C by R.D. Veltri (United Aircraft); *Phys. Chem. Glasses*, Vol. 4, pp. 221-228, Dec. 1963

Resistivity of fused silica has been measured by two different techniques in the temperature range of 1000 to 2480°C. Between 1000 to 1800°C, solid fused silica rods with electrodes attached to their ends were used; a tungsten conductivity cell was used in the 1540 to 2480°C range. Resistivity data for temperatures lower than 1600°C show good accord with results from earlier work. The activation energy for conduction was found to be 23.1 kcal/mole. At higher temperatures the activation energy went to 86.7 kcal/mole. However, rod samples exposed to 1800°C gave a variety of energies upon cooling and subsequent reheating. Values ranged between 23.1 to 86.7 kcal/mole in such cases.

25,238 A SURVEY OF CONDUCTION MECHANISMS IN VERY THIN FILMS by N.M. Bashara (U. Nebraska); *IEEE Trans.*, Vol. CP-11, pp. 4-9, Mar. 1964

Conduction mechanisms in thin films, both metals and dielectrics, in the thickness range between 10^{-6} and 10^{-5} cm and generally under $2-3 \times 10^{-6}$ cm are surveyed. Conduction in metals with an island structure is discussed in terms of a thermally-activated process based on a model suggested by Frenkel. The model makes it possible to interpret the behavior qualitatively. Dielectrics exhibit a tunneling-like behavior and/or a Schottky-like behavior depending on thickness and temperature. Anomalous effects such as the negative resistance sandwich structure and gap structures with low work functions are also discussed.

25,239 CONDUCTION IN VERY THIN FILMS AT HIGH ELECTRIC FIELDS by N.M. Bashara and L. Weitzenkamp (U. Nebraska); *J. Appl. Phys.*, Vol. 35, pp. 1983-1984(L), June 1964

A saturation effect is observed for $\ln(\sigma/\sigma_0)$ vs E/E_0 curves of thicker gold films measured at fields up to 55,000 volt cm^{-1} . A possible cause for this saturation is that an appreciable fraction of metal particles have given up electrons for conduction at high fields. Predictions of the slope of curves based on particle size influence on effective internal field are confirmed; a steeper slope is observed for thicker films. Experimental data confirm the relation:

$$\ln \sigma/\sigma_0 = \frac{2(e^3 E_g/k)^{1/2} - re E_g}{kT}$$

where k is dielectric constant, r is particle size, and E_g is electric field between particles.

25,240 FOUR-POINT PROBE MEASUREMENT OF NON-UNIFORMITIES IN SEMICONDUCTOR SHEET RESISTIVITY by L.J. Swartzendruber (Nat'l. Bur. Stand.); *Solid-State Electronics*, Vol. 7, pp. 413-422, June 1964

Equations and graphs are presented to aid in the evaluation of resistivity non-uniformities when measured by use of the four-point probe. Both the in-line and square array four-point probes are considered. To enable a circular disc to be probed for non-uniformities, correction factors for a displaced probe are given for an in-line array displaced with points on a diameter, for an in-line array displaced with points perpendicular to a diameter, and for a displaced square array.

25,241 FOUR-POINT METHOD FOR MEASURING THE ANISOTROPY OF RESISTIVITY by P. Schnabel (Philips); *Philips Res. Rep.*, Vol. 19, pp. 43-52, Feb. 1964

A simple four-point method is described for measuring the anisotropy ratios $\nu_{ij} = \rho_i/\rho_j$ ($i, j = 1, 2, 3$) of the resistivity of a crystal. In pairs and opposite to each other four probes are placed on the top and the bottom face of a plane-parallel sample. Two contacts are current leads, the other two are potential probes. Two resistances are measured the ratio r of which is a function of ν_{ij} . This function is evaluated. The main feature of the method is that the resistivity perpendicular to the parallel faces of the sample can be obtained without using probes along this direction.

25,242 THICKNESS CORRECTIONS TO RESISTIVITY MEASUREMENT BY Q-METER by A.C. Brown (Standard Tel. and Cables Ltd.); *J. Sci. Instr.*, Vol. 41, pp. 335-336, May 1964

A method is described by which resistivity meters (of the Q-meter type) can be calibrated for sample thickness as well as for resistivity. This may be of assistance in fields where the sample thickness is less than the theoretical skin thickness for the frequency used.

25,243 INDUCTION MEASUREMENT OF SEMICONDUCTOR AND THIN-FILM RESISTIVITY by T. Poehler and W. Liben (Applied Phys. Lab.); Proc. IEEE, Vol. 52, pp. 731-732(L), June 1964

Experiments have been conducted in measuring semiconductor resistivity and thin film resistance by placing samples at the end of an RF solenoid. The change in Q of the coils upon insertion of a sample can be related to the power loss in the solenoid. For correct geometric configurations, this power loss is inversely proportional to the sample resistivity. For the expression to be valid, skin depth must be greater than the sample dimensions. Dependence of ΔQ on frequency is illustrated for a 500 Ω /square chromium film. Reasonable agreement between the simple expression for power loss and experimental results for both C_r film and Si wafers is obtained over a rather limited range of σd .

Resistivity-Vacancy Relationships - See 24,992

25,244 RESIDUAL RESISTANCE RATIO, DIAMETER EFFECT AND CURRENT DEPENDENCE OF RESISTANCE RATIO OF ZONE REFINED TUNGSTEN AT LOW TEMPERATURES [in German] by K.H. Berthel (German Acad. Sci., Dresden); Phys. Stat. Sol., Vol. 5, pp. 159-168, 1964

A low temperature resistivity study of electron beam zone refined single crystal W shows that the extrapolated residual resistance ratio ranges from 3 to 65 $\times 10^{-6}$ over the temperature range of 1.4 to 27°K. The magnetic field of the sample current increases the resistivity of the sample in the temperature range. Resistivity ratio vs diameter was measured. The product of the mean free path (λ) and the bulk resistance ratio (γ_{∞}) was 3.8×10^{-6} cm.

25,245 ELECTRICAL PROPERTIES OF SOME BINARY TERMINAL SOLID SOLUTIONS OF SILVER by D.D. Pollock (Douglas Aircraft, Santa Monica); Trans. Met. Soc. AIME, Vol. 230, pp. 753-757, June 1964

The resistivity, temperature coefficient of resistance, and absolute thermoelectric properties of some binary terminal solid solutions of silver were determined. Equations are given which permit the calculation of these properties.

25,246 THE ELECTRICAL RESISTIVITY OF PYROLYTIC BETA MnO_2 by J.S. Wiley and H.T. Knight (Fransteel Metallurgical Corp.); J. Electrochem. Soc., Vol. 111, pp. 656-660, June 1964

In an investigation of the role of MnO_2 in the "solid electrolytic" tantalum capacitor, a technique was developed to produce samples of pyrolytic β - MnO_2 which could be used for electrical resistivity measurements without the necessity of grinding and pressing into pellets. The samples were prepared by repeatedly filling a test tube with $Mn(NO_3)_2$ solution and pyrolyzing it. The residue of MnO_2 in the tube was then used for resistivity measurements. The resistivity of such samples was approximately 0.1 ohm-cm which is two to three orders of magnitude below previously reported values from MnO_2 compacts. The effect of the addition of certain doping agents to the samples and the variation of resistivity with temperature was also studied. The only dopant of those studied which produced a lower resistivity was a vanadium-containing compound, ammonium vanadate. Two activation energies for conduction were found over the temperature range of -55°-185°C. The more recently published values for resistivity and activation energies are summarized and compared with the present work.

25,247 ROOM-TEMPERATURE RESISTIVITY OF Mo-Nb and Mo-Re ALLOYS CONTAINING ONE PERCENT IRON by M.P. Sarachik (Bell Labs.); J. Appl. Phys., Vol. 35, pp. 1094-1095, Mar. 1964

The room temperature resistivity has been measured for a series of molybdenum-niobium and molybdenum-rhenium alloys, with and without 1% iron as solute. A maximum in the scattering due to the iron is found near the alloy composition for which a localized moment first appears. The results are interpreted in the light of current theories of localized moments.

Resistivity of:

Al-Mg - See 24,988

Co-V - See 24,905

FeAl - See 25,438

25,248 RESIDUAL RESISTANCE DUE TO GOLD IN AN ALLOY CONTAINING 2 At.% GOLD IN NICKEL by L.D. Roberts, F.E. Obershain, R.L. Becker (Oak Ridge Lab.) and J.O. Thomson (U. Tenn.); Bull. Am. Phys. Soc., Vol. 9, p. 398(A), Apr. 1964

The electrical resistances of nickel and of an alloy of nickel with 2 at.% Au have been measured in the temperature range 4.2-1240°K. The difference in resistance $\Delta\rho$ between the 2 samples rises from a value of 0.76 $\mu\Omega \cdot \text{cm}$ at 4.2°K to a highest measured value of 3.3 $\mu\Omega \cdot \text{cm}$ near the Curie point. At temperatures above the Curie point, $\Delta\rho$ first falls sharply and then decreases slowly to a value near 1.2 $\mu\Omega \cdot \text{cm}$ at 1240°K. The sharp rise of $\Delta\rho$ below the

Curie point may be associated with magnetic scattering while the relatively constant value for $\Delta\rho$ above the Curie point, as well as the value at 4.2°K, may be related to the Au-impurity scattering.

25,249 RESISTANCE MINIMA AND MAXIMA IN DILUTE ALLOYS OF RARE-EARTH METALS by T. Sugawara, R. Soga and I. Yamase (U. Tokyo); J. Phys. Soc. Japan, Vol. 19, p. 780(L), May 1964

Resistivity measurements have been made on dilute alloys of Y-Ce and Ag-Gd. A resistivity minimum was found in Y-Ce and was dependent on Ce concentration. The minimum occurred at 15°K for a 1% Ce alloy. In Ag-Gd a sharp maximum occurred; this maximum was attributed to the onset of magnetic ordering since the magnetic susceptibility shows a shape change in slope at the temperature of the maximum.

Anisotropy of Conductivity in TiO_2 - See 25,352

25,250 SEMICONDUCTING BARIUM AND STRONTIUM TITANATES WITH POSITIVE TEMPERATURE COEFFICIENTS OF RESISTIVITY by G.N. Tekster-Proskuryakova and I.T. Sheftel'; Soviet Phys. Solid State, Vol. 5, pp. 2542-2548, June 1964

The electrical properties and the crystal structure of semiconducting $BaTiO_3$ and $(Ba, Sr)TiO_3$ have been studied. On the basis of the data concerning the temperature dependences of conductivity and thermoelectric coefficient, it is suggested that the anomalous increase in the resistivity with temperature in the region of the tetragonal-cubic phase transition is related to a decrease in the carrier mobility. At room temperature, the x-ray investigation shows that $BaTiO_3$ possesses a tetragonally distorted perovskite structure and the transition temperature to the cubic modification is at 123°C.

25,251 OPTICAL ABSORPTION AND ELECTRICAL PROPERTIES OF N-TYPE α -SiC by G.N. Violina, L.H. Yeh and G.F. Kholuyarov (Ul'yanov Leningrad Electrotech. Inst.); Soviet Phys. Solid State, Vol. 5, pp. 2500-2505, June 1964

Measurements of the optical absorption, resistivity and Hall effect of samples of n-type α -SiC doped with nitrogen are reported. The nitrogen concentration lies in the range from 10^{17} to $2 \cdot 10^{19} \text{ cm}^{-3}$. When the nitrogen concentration is increased, the thermal activation energy of the donor diminishes, the electron mobility decreases and the absorption in the impurity region drops. In samples with a nitrogen concentration greater than 10^{18} cm^{-3} , there is a marked shift of the fundamental absorption band toward the lower energy. Calculation based on electrical measurements shows a tendency toward compensation; there is a rise in the number of acceptors as the donor concentration increases.

25,252 THE SEEBECK COEFFICIENT AND ELECTRICAL RESISTIVITY OF N-TYPE PbTe BETWEEN 20°C AND 550°C by G.W. Johnson (AEI Res. Lab.); J. Electronics Control, Vol. 16, pp. 497-507, May 1964

A technique is described for measuring the Seebeck coefficient and electrical resistivity of small samples of thermoelectric materials over the temperature range 20°C to 550°C. The sample is encapsulated to minimize evaporation and a graphical method of presenting the measurements allows for thermocouple mis-match and enables errors in the temperature measurements, due to poor thermal contact between the thermocouples and sample, to be assessed. Results are given of measurements on a range of n-type PbTe samples. The rapid rise of Seebeck coefficient and electrical resistivity with temperature at variance with conventional theory, is interpreted as being due to an increase of effective mass, m^* , with temperature given by the approximate relation:

$$m^* \propto T^{0.6} \rightarrow 0.7$$

At low doping levels comparison of results and theory suggests that there is appreciable impurity scattering.

Conductivity of In_3Te_5 - See 24,867

25,253 ELECTRIC PROPERTIES OF MONOCRYSTALLINE AND POLYCRYSTALLINE LAYERS OF LEAD SULFIDE by R. Ya. Berlaga, I.V. Vinokurov and P.P. Konorov (Leningrad State U.); Soviet Phys. Solid State, Vol. 5, pp. 2523-2525, June 1964

The conductivity, Hall effect and the thermo-emf of monocrystalline and polycrystalline layers of PbS have been investigated. The monocrystalline layers show a relatively high mobility, which indicates the possibility of practical applications of such layers. The thermo-emf of polycrystalline layers does not change on illumination, which agrees with the barrier theory of photoconductivity. The height of the potential barrier was found to be 0.12-0.14 eV.

Ionic Conductivity of Cd Emulsion Grains - See 25,214

25,254 IONIC CONDUCTIVITY OF KI COLORED WITH I_2^* by H.L. Forbes and D.W. Lynch (Iowa State U.); J. Phys. Chem. Solids, Vol. 25, pp. 21-627, June 1964

When V_2 and V_3 bands are present in KI crystals additively colored with iodine, the ionic conductivity in the region from 90 to 200°C is found to be enhanced, but with an unchanged activation energy. A stoichiometric excess of iodine presumably gives rise to two cation vacancies and two holes per excess iodine molecule. The enhanced conductivity indicates that not all of the vacancies introduced are bound in the V centers. Some of them are free. The V_2 and V_3 center models of Seitz are not compatible with this result, but those of Hersh and Effenberger are, although the addition of one vacancy to their models would also be consistent with the conductivity increase. An interpretation of several earlier experiments on V centers is made in terms of the above models.

25,255 ELECTRICAL EFFECTS DUE TO THE F CENTER IN THE POTASSIUM HALIDES by J.N. Maycock (RIAS, Martin); J. Appl. Phys., Vol. 35, pp. 1512-1515, May 1964

The electrical conductivity of the additively colored potassium halides has been investigated as a function of color density and temperature. These studies show that the crystals have a conductivity lower than that of the pure crystals for temperatures outside the intrinsic range. The experimental thermal dissociation energy of an F center is compared with the theoretical values.

25,256 PROPERTIES OF CADMIUM ANTIMONIDE DOPED WITH GOLD by M.M. Pilat and L.I. Anatyshuk (Chernovtsy State U.); Soviet Phys. Solid State, Vol. 5, pp. 2653-2654(L), June 1964

Measurements of the conductivity and Hall coefficient of CdSb single crystals doped with gold in the temperature range 100-400°K are reported. Samples of stoichiometric composition have p-type conduction at all temperatures and their Hall coefficient is positive. It is found that the introduction of gold alters strongly the nature of the temperature dependence of the conductivity and Hall coefficient. The experimental results suggest that gold gives rise to donor levels near the valence band and acceptor levels in the middle of the forbidden band.

Temperature Dependence of the Resistivity of Se - See 25,179

25,257 INVESTIGATION OF THE DEPENDENCE OF THE GALVANOMAGNETIC EFFECTS IN GRAPHITE ON TEMPERATURE AND PRESSURE by A.I. Likhter and V.V. Kechin (Acad. Sci. USSR); Soviet Phys. Solid State, Vol. 5, pp. 2246-2252, May 1964

Measurements of the resistance, Hall coefficient and magnetoresistance of natural graphite flakes at pressures up to 9000 atm. in the temperature range 290-420°K are reported. The results confirm the theory of galvanomagnetic properties of graphite developed by Arkhipov et al. The carrier scattering law for graphite is unaffected by the pressure up to 10,000 atm. On increase of pressure, the extreme point of the interaction of the Fermi surface with an edge of the Brillouin zone does not approach the boundary of the zone.

Irradiation Effects on the Conductivity of NaNO_2 - See 25,177

Resistivity of:

CoPd_3O_4 - See 24,777

US - See 25,333

$\text{Bi}_4\text{Ti}_3\text{O}_{12}$ - See 25,187

25,258 PIEZORESISTIVITY OF MANGANIN by D. Bernstein and D.D. Keough (Stanford Res. Inst.); J. Appl. Phys., Vol. 35, pp. 1471-1474, May 1964

The change in resistance of a class of alloys called Manganin has been measured as a function of peak shock-wave pressure up to 190 kbar. The pressures are obtained from explosively generated plane shock waves in a material of known Hugoniot equation of state. The Hugoniot of Manganin, which has been measured up to 359 kbar, is used with the resistance measurements to calculate the change in resistivity with volume. The results are compared with previous measurements.

25,259 PIEZORESISTANCE OF GERMANIUM by V.S. Shadrin and A.F. Goroedetskii (Novosibirsk Electrical Engr. Inst.); Soviet Phys. Solid State, Vol. 5, pp. 2257-2261, May 1964

Measurement of the piezoresistance of n- and p-type samples of germanium containing various amounts of impurities in the temperature range from 77 to 600°K is reported. The nature of the temperature dependence of the piezoresistance of degenerate n-type Ge does not change on passing from low to high temperatures, which indicates that the contribution of intervalley scat-

tering to the piezoresistance is slight, and the temperature dependence of the piezoresistance of degenerate p-type Ge indicates a more complex carrier scattering mechanism than in n-type degenerate Ge, in which the carriers are scattered by ionized impurities. The piezoresistance of nondegenerate p-type germanium changes sign in the intrinsic-conduction range of temperatures.

25,260 EFFECT OF PRESSURE ON THE ELECTRICAL RESISTANCE OF BIS-MUTH TELLURIDE by E.S. Itskevich, S.V. Popova and E. Ya. Atabaeva (Acad. Sci. USSR); Soviet Phys. Doklady, Vol. 8, pp. 1086-1088(L), May 1964

The effect of pressure on the resistance of Bi_2Te_3 has been studied up to pressure 15,000 bar. It is found that the resistance decreases with increasing pressure. For p-type samples the resistance has a semiconducting character, while for n-type samples, the resistivity is metallic in character in the whole range of pressures. The forbidden energy gap E_g for p-type samples has been calculated from the temperature dependence of the resistance. The result shows that E_g decreases with the increase of pressure above 25 kbar with an averaged rate about -6×10^{-6} eV/bar.

25,261 PRESSURE EFFECT OF RESISTIVITY OF $\text{Ga}(\text{As}_{1-x}\text{P}_x)$ by G.E. Fenner (GE Res. Lab.); Phys. Rev., Vol. 134, pp. A1113-A1118, May 18, 1964

The change of resistance of n-type $\text{Ga}(\text{As}_{1-x}\text{P}_x)$ samples under hydrostatic pressure up to 15,000 atm. was measured between 190 and 363°K. Large pressure-dependent resistance changes were observed for samples with $x \approx 0.35$. These observations are consistent with the presence of another conduction band edge of much lower mobility presumably along $k = (100)$ into which electrons are transferred when the relative energy separation between the two edges is lowered by pressure. The measured results are compared with calculations based on the model proposed by Ehrenreich. The agreement between theory and experiment is found to be good if certain parameters are varied in a systematic way. For lightly doped material the mobility ratio of electrons in the light mass band to those in the heavy mass band is found to be large and to decrease rapidly with increasing temperature. At higher carrier concentrations both the magnitude of the mobility ratio as well as its variation with temperature are substantially reduced. At 300°K the (000) and (100) minima are found to cross at $x \approx 0.44$ if we assume Vegard's law to be valid. The experimental data are best explained if it is assumed that the separation between the two sets of minima changes at a rate of $> 1 \times 10^{-4}$ eV/°K.

25,262 RESISTIVITY CHANGES IN SILVER DUE TO PLASTIC DEFORMATION by I. Kovacs, E. Nagy (Loránd Eötvös U., Budapest), and P. Feltham (Brunel Coll., London); Philosophical Mag., Vol. 9, pp. 797-801, May 1964

The excess resistivity induced in high purity silver wires by torsion at shear strains of up to 250% at 77-293°K is shown to be a linear function of the square of the flow stress. A discontinuity in this relation at the transition from the linear, second stage of hardening to the third stage of work-hardening was not observed; but it is well defined by a sharp change of slope on curves relating the excess resistivity and the shear strain. The results show that the resistivity increases linearly with the density of dislocations, and suggest that a proportionality exists between the concentration of vacancies and the density of dislocation produced in the course of isothermal plastic deformation. The resistivity per centimeter of dislocation line in silver was estimated to be close to 2×10^{-19} ohm cm.

25,263 INVESTIGATION OF THE FIELD EFFECT IN THIN LAYERS OF LEAD SULFIDE by B.A. Nesterenko, Yu.A. Pasechnik, O.V. Snitko and O.S. Frolov (Acad. Sci. USSR); Soviet Phys. Solid State, Vol. 5, pp. 2341-2346, May 1964

The effect of an external electric field on the conductivity of thin layers of lead sulfide has been investigated, and the fast and slow relaxation of the field effect is discussed. It is shown that there are two types of slow relaxation: one decreases with time and the other increases with time. The relaxation time of the fast surface levels is less than 5×10^{-5} sec. Two models for the surface layers are proposed. a) in the case of chemical layers, a surface carries a thin insulating oxide film; b) in the case of physical layers a surface carries a semiconducting oxide film. The existence of an oxide film results in a creation of fast and slow surface layers with a concentration in excess of 10^{12} cm $^{-2}$.

25,264 ELECTRICAL CONDUCTIVITY OF FERROUS OXIDE AT HIGH TEMPERATURES by S.M. Ariya and B. Ya. Brach (Leningrad State U.); Soviet Phys. Solid State, Vol. 5, pp. 2565-2567, June 1964

A study of the dependence of the conductivity and thermo-emf of ferrous oxide on its composition at high temperatures is reported. The results confirm the idea that the conductivity is due mainly to the process of electron exchange between iron atoms of different valence.

25,265 TEMPERATURE AND PRESSURE DEPENDENCE AND ACTIVATION ENERGY OF THE SLOW SURFACE CONDUCTIVITY RELAXATIONS ON Ge by S. Koc (Zech. Acad. Sci.); Appl. Phys. Lett., Vol. 4, pp. 151-152(L), Apr. 15, 1964

The temperature and pressure dependence of slow conductivity relaxations on germanium surfaces are discussed. The "time constant" of the slow relaxations decreased with increasing pressure, and by extrapolation would become zero at ~ 400 torr of moist air. A strong dependence ΔE , the activation energy of the rate limiting process, on the partial pressure of water vapor was observed. ΔE has a maximum value of about 0.79 eV in vacuum; it decreases with increasing pressure to about 0.2 eV at 200-250 torr of moist air. The parameter $\tau = \tau_0 \exp(\Delta E/kT)$ changes by 9-10 orders of magnitude over the pressure range 0-200 torr. The present results agree with those of Pilkuhn for the magnitude of τ_0 in vacuum; however, τ_0 increases as the pressure of the moist ambient air increases. The opposite is expected from Pilkuhn's ion migration model, which can not explain the observed slow surface conductivity relaxations. These can be explained by an electron transport process.

25,266 SURFACE CONDUCTIVITY OF GERMANIUM DOPED WITH GOLD by G.A. Katrich and O.G. Sarbei (Acad. Sci. UkrSSR); Soviet Phys. Solid State, Vol. 5, pp. 2432-2433(L), May 1964

Surface conductivity of gold-doped germanium when it is fractured has been investigated. It is found that the fracture produces an enormous increase of the sample conductivity at the liquid nitrogen temperature. This increase in conductivity may be due to the fact that as a result of the fracture some of the impurity atoms will appear on the surface and have an ionization energy considerably lower than in the interior, thus giving rise to larger surface conductivity.

25,267 SURFACE CONDUCTANCE AND FIELD-EFFECT ON THE SURFACE CONDUCTANCE OF {111} AND {111} SURFACES OF InSb by S. Kawaji (Gakushuin U., Japan); Surface Science, Vol. 1, pp. 122-124(L), Jan. 1964

Surface conductance and field effect on surface conductance of the {111} and the {111} surfaces were measured for p-type InSb crystals with dislocation density of about $10^4/\text{cm}^2$. Conventional dc potentiometer methods were used to measure conductance at liquid nitrogen temperatures whereas an ac method was used to measure field effect on conductance. Field effect mobility, μ_{FE} , change in surface conductance, ΔG , and surface potential, u_s , are reported for {111} surfaces terminating with In and Sb atoms. Field-effect patterns show that alcohol adsorbed from the ambient liquid onto the InSb surface introduces excess positive charge. Two types of surface states on surfaces terminate with In atoms. One located near the middle of the forbidden gap, and the other near the bottom of the conduction band.

25,268 PHOTOCONTROLLED SURFACE CONDUCTANCE IN ANODIZED InSb by R.K. Mueller and R.L. Jacobson (Litton Sys.); J. Appl. Phys., Vol. 35, pp. 1524-1529, May 1964

Anodized p-type InSb, cooled to the extrinsic conduction range in the dark, was found to have an n-type inversion layer at the surface. Illumination changes the n-type inversion layer to a p^+ accumulation layer; any intermediate surface condition can be obtained by controlled exposure. A method for determining the surface conductance of the inversion layer is described. This method utilizes a high-impedance grain boundary barrier to avoid shunting of surface conduction by bulk conduction. The highest surface conductance on unilluminated anodized samples was found to be 100 $\mu\text{mhos}/\text{square}$. Spectral response measurements show that photons in the energy range 0.8 to 3.5 eV are effective. The effect is believed due to photoemission of electrons from the InSb into the oxide. Transient response measurements for light on and off conditions on n- and p-surfaces support this model.

25,269 NEGATIVE TEMPERATURE COEFFICIENT OF RESISTANCE IN BISMUTH I by P.C. Sovers and G. Jura (U. Calif.); Science, Vol. 143, pp. 467-469, Jan. 31, 1964

Measurements of electrical resistance of bismuth at pressures between 15 and 35 kilobars, and at temperatures between 77.4° and 120°K have been made. Above 150°, the temperature coefficient of resistance is positive, as in a metal; below 150°K, the coefficient is negative, as in a semiconductor. The energy gap is calculated by the exponential resistance formula and is plotted as a function of temperature. At room temperature, the energy gap is not visible because thermal excitation populates the conduction band and metallic behavior is the result. It is concluded that the observed behavior is due to an energy gap rather than a decrease in carrier mobility.

25,270 INVESTIGATION OF SOME PROPERTIES OF GOLD-DOPED GERMANIUM by V.I. Stafeyev (Acad. Sci. USSR); Soviet Phys. Solid State, Vol. 5, pp. 2267-2274, May 1964

It is found that illuminated gold-doped Ge at low temperatures ($T = 77^\circ\text{K}$) displays a sublinear relationship between current and electric field intensity.

At field intensities higher than 10^3 V/cm, the current decreases with the increase of the electric field intensity up to the commencement of the avalanche injection. The sublinearity and the n-type negative resistance result from the decrease in mobility and lifetime with the increase of the electric field intensity. In gold-doped germanium diodes, a magnetic field weakly affects the reverse current in the diode but considerably reduces the current up to and after cut-off, and the cut-off voltage increases linearly with the magnetic field.

25,271 FURTHER PROPERTIES AND A SUGGESTED MODEL FOR NIOBIUM OXIDE NEGATIVE RESISTANCE by W. Bean and A. Armstrong (Rensselaer Polytech.); Proc. IEEE, Vol. 52, pp. 300-301(L), Mar. 1964

A negative resistance phenomenon in thin amorphous anodic oxides of niobium is described. The properties in the phenomenon are reported as well as a simple theory which agrees well with observation. The negative resistance phenomenon is explained by postulating a single carrier injection mechanism that may be either Schottky emission, and/or tunneling. Further studies are expected to resolve some questions still existing.

SUPERCONDUCTIVITY

25,272 PERTURBATION EXPANSIONS AND FUNCTIONAL INTEGRALS IN THE THEORY OF SUPERCONDUCTIVITY by J.S. Langer (Carnegie Inst. Tech.); Phys. Rev., Vol. 134, pp. 553-565, May 4, 1964

A functional integral representation of the partition function for a superconductor is derived by conventional perturbation-theoretic techniques. The derivation involves a generalization of the ladder diagram expansion by means of a trick due to Gaudin, and the result turns out to be a variation of the functional integral derived by Hubbard. A saddle-point approximation then leads to the usual Bardeen-Cooper-Schrieffer (BCS) equations. Although this approximation is mathematically unjustified, its predictions seem to be accurate. In particular, a very literal interpretation of the saddle-point method is supported by flux-quantization experiments.

25,273 MECHANISMS FOR SUPERCONDUCTIVITY IN THE TRANSITION METALS by J.W. Garland (U. Chicago); Phys. Rev. Lett., Vol. 11, pp. 111-114, Aug. 1, 1963

The compatibility of the experimental data on superconductivity in transition metals with the BCS theory and the idea of phonon-induced superconductivity is discussed. A two-band model for the electronic structure is constructed, where the d band is associated with a sub-band at the Fermi surface, and it is assumed that the surface is separable into distinct s- and d-region. It is shown that "clean" and "dirty" states should be experimentally distinguishable and that impurity scattering must be included theoretically. Additionally, the single gap theory proves most appropriate, which, assuming Cooper pairing, leads to the conclusion that superconductivity arises from exchange of virtual phonons.

25,274 AN EMPIRICISM FOR ESTABLISHING THE TRANSITION TEMPERATURES OF SUPERCONDUCTING ALLOYS AND COMPOUNDS by L. Gold (Kennecott Copper); Phys. Stat. Sol., Vol. 4, pp. 261-265, 1964

An empirical parameter, based upon an isotope law, is suggested to establish guidelines in the search for alloys with critical temperatures higher than Nb_3Sn . A prediction is made from such empirical studies that Nb_3Si would have a higher critical transition temperature than Nb_3Sn on the assumption that it could be synthesized and would have β -tungsten crystal structure. Theoretical calculations are presented for Nb_3In and Nb_3Ga and it is suggested that experimental values of transition point would require slight revision.

25,275 A FIELD-THEORETICAL METHOD IN THE THEORY OF SUPERCONDUCTIVITY-II by G. Pocsik and A. Zawadowski (Cen. Res. Inst. for Phys.-Budapest); Nuovo Cimento, Vol. 32, pp. 1110-1112(L), May 16, 1964

Exact equations of the various simple correlation functions in the pole approximation lead to the usual superconducting equations. By pole approximation, it is meant that only one stable excited state contributes to the correlation functions. The present note extends the method for more realistic interactions by examining the equation of motion assuming that the potential V depends only on the coordinate differences. The results of the treatment show that the equations satisfied by the correlation functions $K^{(+)}$, $F^{(+)}$ are very similar to Valatin's (Nuovo Cimento, Vol. 7, p. 843, 1958). The ground energy $\langle H \rangle$ and the chemical potential E_0 are also studied using the pole approximation.

25,276 ON ONE MODEL OF A SUPERCONDUCTOR WITH PAIRS IN THE p-STATE by A.V. Svidzinskii; Soviet Phys. Doklady, Vol. 8, pp. 1197-1199 (L), June 1964

On the basis of the model of superconductors with pairs in the p-state, a necessary and sufficient condition is formulated for obtaining a physically meaningful solution of the problem. It is shown that the solution is asymptotically exact as the volume approaches infinity, and the isotropic solution corresponds to a lower energy than any anisotropic solution.

25,277 THE SUPERCONDUCTIVITY AND MAGNETISM OF THE ACTINIDE METALS by G.T. Meaden (U. Grenoble, France); *Cryogenics*, Vol. 4, pp. 105-107(L), Apr. 1964

Low temperature magnetic and superconducting behavior is reported for the actinides, lanthanide and transition metals. As one passes along the actinide series in the periodic table from actinium to plutonium comparing the various properties, the metals become less transition-like and more lanthanide-like. Considerations of chemical and physical similarities indicate superconductivity in lanthanum, and uranium is consistent with the d-transition elements. Since actinium and protactinium are likely to have a virtual F-level in the same way as lanthanum and uranium, superconductivity in actinium and protactinium is also expected.

25,278 PAIR CORRELATIONS IN SUPERCONDUCTING TANTALUM by L. Meyers and W. Little (Stanford U.); *Phys. Rev. Lett.*, Vol. 11, pp. 156-157, Aug. 15, 1963

The existence of higher-order pair correlations in superconducting tantalum is investigated. Such correlations would have been indicated by a periodicity in T_c equal to hc/ne , where n is an even integer > 2 . A cylindrical sample of zone-refined tantalum was deposited upon a glass fibre of 1.5 microns diameter. The observed periodicity of the field between 2.4°K and 2.2°K was 12.1 gauss. The calculated value assuming only pair correlations, was 11.6 gauss, whence the higher-order correlations may be rejected.

25,279 BULK SUPERCONDUCTIVITY IN DILUTE HEXAGONAL TITANIUM ALLOYS by F. Heiniger and J. Muller (Fed. Inst. Tech., Zurich); *Phys. Rev.*, Vol. 134, pp. A1407-A1409, June 15, 1964

The superconductivity, the low-temperature specific heat, and the paramagnetic susceptibility have been investigated in a series of dilute hexagonal titanium alloys. In the solid solutions with V or Nb, both the transition temperature and the density of states are strongly increased and the entire volume exhibits superconductivity. A similar study of Ti-Fe alloys suggests either an incomplete volume transition or a different entropy variation in the superconducting state.

25,280 SUPERCONDUCTIVITY OF $\text{Mo}_3\text{Al}_2\text{C}$ by J. Johnston, L. Toth, K. Kennedy, and E. Parker (U. Calif.); *Solid State Commun.*, Vol. 2, p. 123, Apr. 1964

A new superconductor, $\text{Mo}_3\text{Al}_2\text{C}$, has been discovered. The compound has a superconduction transition of 10.0°K and crystallizes in the β -Mn(Al_3) structure. The lattice parameter for the β -Mn cubic cell wall was $a = 6.867\text{\AA}$. The occurrence of superconductivity in $\text{Mo}_3\text{Al}_2\text{C}$ and $\text{Nb}_3\text{Al}_{0.5}\text{Ge}_{0.5}$ which has a transition temperature of 12.6°K indicates that the β -Mn structure is favorable for the occurrence of superconductivity at relatively high temperatures.

25,281 TRANSIENT ELECTRODYNAMIC PHENOMENA IN SUPERCONDUCTING NIOBIUM-TIN by W.H. Cherry (RCA); *Bull. Am. Phys. Soc.*, Vol. 9, p. 454(A), Apr. 1964

Surge magnetic fields up to 250 kg and pulsed conduction-current densities up to 10^6 A/cm^2 have been impressed upon samples of vapor-deposited niobium-tin. The potential differences along the specimens as recorded from oscilloscope traces show very complex variations with time, even though the surge and pulse shapes are quite simple. These observations are categorized as (1) inductive effects of current, including fluctuations of what may be a transient intermediate state, (2) effects of Joulean heat generated by current, (3) transient magnetic-field effects, including both sudden and semicontinuous, large-scale flux movements in and out of the material, and (4) interactions between current and field, including (a) possible transitions from surface current flow to bulk flow, (b) admission and expulsion of field flux as controlled by the conduction current, possibly giving evidence of a Meissner effect in the 100-kg range, and (c) strongly oscillatory flux motion.

25,282 BRILLOUIN EFFECTS, SUPERCONDUCTIVITY, AND FERMI SURFACE OF INDIUM ALLOYS by M.F. Merriam (U. Calif., La Jolla); *Phys. Rev. Lett.*, Vol. 11, pp. 321-323, Oct. 1, 1963

Measurements of superconducting properties and lattice parameters of solid solutions of In-Sn and In-Pb as functions of the atom percent composition of the alloys are reported. The curves of critical temperature vs composition exhibit discontinuities in dT_c/dx at about 8% Sn or Pb, respectively. By measuring the lattice parameters it is shown that the lattice first expands, then

contracts, and finally expands again in this region. The effect is explained by means of an analysis proposed by B. Goodenough as an interaction between Fermi surface and Brillouin zone boundary.

25,283 MECHANISM FOR SUPERCONDUCTIVITY IN LANTHANUM AND URANIUM by D. Hamilton and M. Jense (U. Calif.); *Phys. Rev. Lett.*, Vol. 11, pp. 205-206, Sept. 1, 1963

A mechanism for superconductivity in La and U which entails a modification of Matthias rule is proposed. Lu is interchanged in the table with La, consequently the favored values of " n " for superconductivity are reduced to "5" and "7", consistent with other related properties. Symmetry about $n = 6$ is thereby reinforced. Anomalous superconductivity in La and U is attributed to their lack of occupied 4f or 5f electrons, respectively, in the solid state.

25,284 CORRECTIONS TO THE PAIRING INTERACTION IN SUPERCONDUCTIVITY by E.M. Henley, L. Willets (U. Washington); *Phys. Rev. Lett.*, Vol. 11, pp. 326-328, Oct. 1, 1963

Second order corrections of the generalized integral equation for the energy gap parameter are investigated. By means of a Monte-Carlo technique successive solutions to the integral equation are calculated numerically. The expansion parameter is the "effective" pair interaction parameter G . It is concluded that, in contrast to Bogoliubov's original assumption, second order terms are not small. The correction terms tend to reduce the gap when the interaction is attractive.

25,285 A STUDY OF SUPERCONDUCTING TIN BY THE TUNNEL EFFECT by N.V. Zavaritskii (Acad. Sci. USSR); *Soviet Phys. JETP*, Vol. 18, pp. 1260-1267, May 1964

The width of the energy gap in superconducting tins has been studied by the tunnel effect method. Depending on the crystallographic orientation, the gap width changes from $2\Delta/kT_c = 2.7$ to 4.3. The anisotropy of Δ is of a complicated type. Together with large regions in which the change of Δ does not exceed 2%, regions are observed in which there is a sharp change of Δ , amounting to 20% in intervals of $\sim 5^\circ$. It is suggested that anisotropy of such a type is related to the structure of the Fermi surface of tin. The relative change of the gap width with temperature is close to that implied by the theory of superconductivity.

25,286 ENERGY GAP OF THE HIGH FIELD SUPERCONDUCTOR NbZr by I. Dretrich (Siemens and Halske); *Phys. Lett. (Neth.)*, Vol. 9, pp. 221-222 (L), Apr. 15, 1964

Energy gap measurements in the superconductor NbZr are discussed. From the measured tunneling characteristic of a Nb 75 Zr 25 - $\text{Nb}_x\text{Zr}_{1-x}\text{O}_2$ - Pb sandwich, two energy gaps, resulting from crystals of slightly different alloy ratios, were observed. For peak 1, $2\epsilon_0 = 3.62\text{ kT}_c$; for peak 2, $2\epsilon_0 = 3.90\text{ kT}_c$. The average value of the constant relating the energy gap to the transition temperature in NbZr is 3.75, in relatively good agreement with the value of 3.5 given by the BCS theory.

Energy Gap of Sn Superconductors - See 25,789

25,287 CRITICAL CURRENT AND CRITICAL MAGNETIC FIELD IN HARD SUPERCONDUCTORS by V.V. Shmidt (Baikov Inst. Metal.); *Soviet Phys. JETP*, Vol. 18, pp. 1368-1376, May 1964

The distribution of the critical current over the cross section of a superconductor and its dependence on the density of filaments n and on the external magnetic field are discussed on the basis of the filamentary model of hard superconductors. If no external magnetic field is present, the critical current is distributed uniformly over the cross section for n much less than a certain characteristic density n_0 , for $n \gg n_0$, the critical current is concentrated near the middle region. The dependence of the critical current on n is characterized by the fact that the critical current reaches its maximum value for $n > n_0$. It is shown that the calculated dependence of the critical current on the magnetic field is in good agreement with experiment.

25,288 SUPERCONDUCTING-TO-NORMALLY CONDUCTING TRANSITIONS IN STRIP TRANSMISSION LINE STRUCTURES by A.R. Sass (Lewis Res. Ctr) and F.J. Friedlaender (Purdue U.); *J. Appl. Phys.*, Vol. 35, pp. 1494-1500, May 1964

A theoretical and experimental investigation of superconducting-to-normally conducting transitions in strip transmission line structures is presented. The theoretical analysis is based on a macroscopic model, which is the transmission line analog of the Pippard model. It is assumed that during the transition a superconducting-normally conducting (S-N) interface propagates along the transmission line structure. This situation is treated theoretically as a moving boundary value problem. The S-N interface propagation velocity is determined

explicitly in terms of the current that induces the transition, the operating temperature, and the superconductive penetration depth. Experimental results indicate that the model is useful for predicting the transition time of a strip transmission line structure.

25,289 EFFECT OF FAST-NEUTRON-INDUCED DEFECTS ON THE CURRENT CARRYING BEHAVIOR OF SUPERCONDUCTING Nb_3Sn by G.W. Cullen and R.L. Novak (RCA); *Appl. Phys. Lett.*, Vol. 4, pp. 147-149(L), Apr. 15, 1964

Direct measurements of neutron irradiation-produced increases in the critical current density of superconducting Nb_3Sn are discussed. The specimens (Nb_3Sn strips formed by vapor deposition on a ceramic substrate) were irradiated by fast neutrons at 50°C. Relatively large changes in I_c were observed, particularly for the case where the current in the specimen is normal to the applied field. According to the Lorenz model of Kim et al the current density $J_c = \alpha/H + B_0$, where α and B_0 are constants. The constant α , the value of which can be shown to be directly proportional to the defect density, is increased by irradiation. Thus, increases in α may be due to an increase in the number of defects as a result of neutron bombardment. These changes result in an increased critical current carrying capacity of the superconductor.

25,290 CRITICAL ALTERNATING CURRENTS IN SUPERCONDUCTORS by F.J. Young and H.L. Schenk (Westinghouse); *J. Appl. Phys.*, Vol. 35, pp. 980-981, Mar. 1964

Critical alternating currents were studied in 0.96-cm (3/8 in.) lengths and coils of superconducting wire. Critical current density vs frequency were measured for three short Nb-25% Zr wires having the same amount of cold work. For the 5-, 10-, and 20-mil (125-, 250-, and 500- μ) specimens, the critical ac density varies from 290 to 170 ka/cm², 200 to 110 ka/cm², and 107 to 54 ka/cm², respectively, as the frequency is varied from 0.02 to 4.5 kc/sec. A short length of Nb-Ti wire 9 mils in diameter has a critical ac density that varies from 260 to 130 ka/cm² as the frequency ranges from 0.01 to 4.5 kc/sec. In a 15-mil Nb_3Sn specimen, the critical ac density is constant at 90 ka/cm² from 0.01 to 4 kc/sec. In a tightly wound Nb-25% Zr coil, the critical ac density is found to vary inversely with the one-fourth power of frequency. In a very loosely wound coil of the same material, the critical ac density varies inversely with the cube root of frequency. In all cases investigated, except for pure niobium, the exponent on the frequency varies from -0.25 to -0.36. In a Nb coil, no variation of critical ac density is observed below 200 cps. Above 200 cps, it behaves in the same way as the other coils tested. The data indicate that the critical ac density occurs such that the coil or short wire always becomes normal at the same level of power dissipation.

25,291 MAGNETIC AND CALORIC EFFECTS IN A HARD SUPERCONDUCTOR by S. Goedemodt, C. van Kolmeschate, D. de Klerk and C. Gorter (Kammerlingh Onnes Lab., Netherlands); *Physica*, Vol. 30, pp. 1225-1228(L), June 1964

Magnetization curves have been obtained at temperatures between 1.03°-4.2°K for a sample of impure niobium. Values for the upper critical field, H_{c2} , were obtained by extrapolation, yielding a linear relation for H_{c2} vs T , leading to $T_c = 8.9^\circ\text{K}$. Temperature of the sample was observed during variation in magnetic field, showing that flux jumps seen in the magnetization curves are accompanied by pronounced fluctuations in temperature. Total amount of heat generated during magnetization was calculated by considering temperature curves to be equilibrium curves. Applying the first law of thermodynamics, it was possible to calculate values for the magnetocaloric effect, $T\Delta S$, and H_c at 4.2°K.

25,292 SOME REMARKS ON THE UPPER CRITICAL FIELD OF THE SUPERCONDUCTIVITY OF NIOBIUM by G. Van den Berg and H. Van Rongen (Kammerlingh Onnes Labs., Netherlands); *Physica*, Vol. 30, pp. 1229-1230 (L), June 1964

Experiments between 4° and 0.5°K were performed with impure niobium (99.5 pct.) and electron beam zone refined niobium (99.992 pct purity) to investigate the following: 1) slope of the curve for upper critical field as a function of temperature at 0°K; 2) shape of such a curve; and 3) difference between upper critical field values measured magnetically or electrically. Results suggest that the curve for H_{c2} vs T will have a slope zero at 0°K. For the impure wire H_{c2} at 4°K is 0.51 times the H_{c2} at 1°K and for the purer wire this ratio is 0.73. The upper critical field for the purer niobium at 0°K measure electrically is about 18 koe is twice the value at 0°K obtained for the same niobium by extrapolation of magnetization results.

25,293 MICROWAVE OBSERVATION OF SUPERCONDUCTIVITY ABOVE THE UPPER CRITICAL FIELD by M. Cardona and B. Rosenblum (RCA Labs.); *Phys. Lett. (Neth.)*, Vol. 8, pp. 308-309(L), Mar. 1, 1964

Measurements of the real part of microwave surface impedance R at 23 BM_c in a $\text{Pb}_{0.5}\text{Ti}_{0.5}$ alloy are discussed. When the applied magnetic field was

perpendicular to the sample surface, R increased approximately linearly to its normal value R_n at the upper critical field H_{c2} . When the magnetic field was applied parallel to the surface, the surface impedance increased rapidly at the lower critical field H_{c1} , changes slope at H_{c2} , and attained its normal state value at a higher field, which has been identified with the field H_{c3} proposed by Saint-James and Gennes. H_{c3} varied from 1.4 H_{c2} to 1.9 H_{c2} , depending on the condition of the surface. The ratio of H_{c3} to H_{c2} was found to be independent of temperature, and no dependence of surface impedance on surface current was observed. Mechanisms for microwave absorption are discussed.

25,294 ANGULAR DEPENDENCE OF THE SUPERCONDUCTING NUCLEATION FIELD by M. Tinkham (Faculte des Sciences, Orsay); *Phys. Lett. (Neth.)*, Vol. 9, pp. 217-218(L), Apr. 15, 1964

Critical nucleation fields H_0 measured as a function of the angle θ between the applied magnetic field direction and the plane of Pb-Tl films and foils are discussed. The measured values of H_0 are in very good agreement with those given by a formula proposed by Tinkham for interpolating between the parallel and perpendicular critical fields of a thin film. This agreement is explained.

25,295 THE SUPPRESSION OF EDGE EFFECTS IN SUPERCONDUCTING FILMS by A.R. Tyler and P.A. Walker (Intl. Computers and Tabulators Engng.); *Phys. Lett. (Neth.)*, Vol. 9, pp. 226-227(L), Apr. 15, 1964

The thickness of the silver film required to obtain a minimum magnetic transition width ($\Delta H/H$) of tin films by the proximity effect is discussed. The silver film thickness for minimum transition width is temperature dependent, and the shape of the magnetic field transition changes with temperature. Above an optimum operating temperature the edges of the tin film switch at lower applied fields than the bulk of the film, and there is a toe to the transition. As the temperature is reduced, the toe decreases until the minimum transition width is obtained at the optimum operating temperature. Below the optimum temperature the edges of the film switch at fields higher than the bulk of the film, causing the magnetic field transition $\Delta H/H$ to increase and a high-field tail to appear on the transition. These changes with temperature have been experimentally observed for tin films 800 to 10,000 Å thick, on top of which were deposited silver films between 30 and 120 Å thick. Transition widths $\Delta H/H = 3\%$ have been obtained.

25,296 SPECIFIC HEAT AND MAGNETIC SUSCEPTIBILITY OF SUPERCONDUCTIVE, BINARY COMPLEX PHASES OF TRANSITION METALS [in German] by E. Bucher, F. Heiniger and J. Müller (Tech. Hoch. Zürich); *Phys. Cond. Matter*, Vol. 2, pp. 210-240, Apr. 1964

Measurements of the electronic specific heat in the normal and superconducting state of 15 superconducting binary complex phases of the σ - and X-structure are presented. The alloys have been prepared under high vacuum in an electron-beam melting apparatus described in detail. In the investigated range between 6 and 7 valence-electrons, the obvious correlation between T_c , the superconducting critical temperature, and γ , the coefficient of the electronic specific heat, leads to agreement with the empirical rules, found by Matthias. Recently, Morel and Anderson and Garland have calculated the values of the deviation of the normal isotope-effect. With these values it is possible to relate the observed T_c -data for most of the transition metal alloys investigated so far to the density of states at the Fermi level and to a systematically varying electron-phonon interaction parameter. In the superconducting state, an exponential dependence of the electronic specific heat on $1/T$ is found in the range between $T_c/2$ and $T_c/6$. However the parameters are somewhat different from those predicted by theory. The values of γ observed also account for the lack of any correlation between the total magnetic susceptibility and the superconducting critical temperature for these phases.

25,297 ISOTOPE EFFECT IN SUPERCONDUCTIVITY by J.W. Garland (U. Chicago); *Phys. Rev. Lett.*, Vol. 15, pp. 114-119, Aug. 1, 1963

The isotopic effect of the average atomic mass of a superconductor upon the transition temperature is investigated theoretically. The qualitative difference in the effect for transition metals ($\xi \geq 0.3$) and that in simple metals ($\xi \sim 0.1$) is shown to follow from elementary consideration of band structure. A 2-band model for the transitional metals and an isotropic free-electron model for the simple metals are chosen. The maximum error in determining the "reduced-isotope effect" coefficient is 40%. Substantial improvements in accuracy compared to experimental values result from considering band structure effects and a more exact treatment of the Coulomb contribution.

25,298 INDUCEMENT OF SUPERCONDUCTIVITY BY VARIATION OF STRUCTURAL PARAMETERS by A. Arrhenius, et al (U. Calif., San Diego); *Phys. Rev. Lett.*, Vol. 11, p. 313, Oct. 1, 1964

The transition temperatures of BaAu_5 for a wide range of homogeneous samples ranging from $\text{BaAu}_{3.5}$ to $\text{BaAu}_{6.3}$ (at 700°C) and to $\text{BaAu}_{5.3}$ (at 360°) were investigated experimentally. The transition temperatures vary between 0.7°K

and 0.35°K (lower limit of detectability) depending on the structural state of Au in the system. The transition temperature of pure Au is estimated by extrapolation to be finite, but not above the millidegree range. This estimate is based on similar behavior of other AB₅ compounds like YIr₅.

25,299 SUPERCONDUCTIVITY OF TITANIUM by R.L. Falge, Jr. (US Naval Res. Lab.); *Phys. Rev. Lett.*, Vol. 11, pp. 248-250, Sept. 15, 1963

The effect of Mn content upon the critical temperature of Ti-Mn alloys is investigated. The range from 0-1% Mn was given particular emphasis. Contrary to earlier results based upon extrapolation to 0% Mn, T_C for Ti-Mn alloys is first reduced by small quantities of Mn and only for larger dosages does it exhibit a monotonic increase with Mn concentration. The T_C for bulk, pure Ti is given as 0.42°K and

$$H_C = 56 [1 - (T/0.42)^2].$$

It was not possible to definitively ascribe the initial depression of the value of T_C to the Mn itself, rather than to some associated impurity.

25,300 CAN PRESSURE DESTROY SUPERCONDUCTIVITY IN ALUMINUM, by M. Levy, J.L. Olsen (Swiss Fed. Inst. Tech. Zurich); *Solid State Commun.*, Vol. 2, pp. 137-139, May 1964

It is found that the relation between T_C and the superconducting transition temperature, and pressure is non-linear. At 21,000 atmospheres, the maximum pressure achieved, T_C was lowered from 1.170° to 0.687°K. An analysis of the data indicates that pressures larger than 500,000 atmospheres, most likely infinite pressures, would be required to quench superconductivity in aluminum.

25,301 SUPERCONDUCTIVITY OF SOLID SOLUTIONS OF TaC AND NbC by M. Wells, M. Pickus, K. Kennedy, and V. Zackay (U. Calif.); *Phys. Rev. Lett.*, Vol. 12, pp. 536-538(L), May 11, 1964

Measurements of the critical temperatures of solid solutions of TaC and NbC are discussed. The critical temperature has a broad maximum in NbC-rich compositions. At a given composition the transition from normal to superconducting behavior occurs over a range of three to four degrees. The linearity of the variation of the lattice parameter with composition in the system TaC-NbC suggests that the maximum in critical temperature cannot be the result of a variation in combined carbon. The analogous superconducting system HfN-ZrN, on the other hand, does not exhibit a maximum in the critical temperature. The available data indicate that parameters such as electron-to-atom ratio or electrons per unit volume can not be related to the critical temperature of transition metal-interstitial element compounds.

25,302 INTERMEDIATE STATE OF AN INCLOSED SUPERCONDUCTOR by R.I. Gayley (State U. N.Y., Buffalo); *Bull. Am. Phys. Soc.*, Vol. 9, p. 455(A), Apr. 1964

The intermediate state of coupled superconductors was discussed. In particular, a superconducting rod enclosed by a coaxial superconducting shell of higher transition temperature is considered. If the system is cooled in the presence of an axial magnetic field, the effect of the outer shell can be accounted for by assigning an effective demagnetizing coefficient to the rod. If the cylinder is cloffitting the demagnetizing coefficient will be quite large and we can point to 3 major advantages of this system. The 1st is that the enclosed superconductor combines large demagnetizing coefficient with cylindrical symmetry so that it is ideally suited to quantitative tests of theories of the intermediate state. The 2nd is that specimens of small cross section are very sensitive to weak magnetic fields, the depression of the transition temperature of the rod being proportional to the square of the applied field. The 3rd is that this depression is inversely proportional to the square of the sum of the penetration depths of the 2 superconductors. Thus, the system can be used as a magnetometer or for measurements of penetration depth.

25,303 METASTABLE RESISTANCE STATES IN THE INTERMEDIATE REGION OF SUPERCONDUCTORS by B. Lalevic (Franklin Inst. Lab.); *J. Appl. Phys.*, Vol. 35, pp. 1785-1789, June 1964

The present report extends resistance fluctuation studies in the current-induced intermediate state to the intermediate state induced by the application of an external magnetic field. Evidence for the existence of resistance levels is again found for both directions of the superconducting transition. The resistance levels are interpreted in terms of superconducting domains. The number of levels consequently represents the number of superconducting domains present and the difference ΔR between the two successive resistance levels correspond to a spread of the normal phase over a length Δl of a specimen. The transition time between two successive resistance levels is identified as the time of collapse of a domain. The observed transition times for soft superconductors are compared with theory of propagation of a normal phase boundary and some conclusions on the structure of the intermediate state are presented.

25,304 TORQUE MEASUREMENTS ON SUPERCONDUCTORS IN THE INTERMEDIATE STATE by S.L. Wipf (Westinghouse Res. Lab.); *Bull. Am. Phys. Soc.*, Vol. 9, p. 453(A), Apr. 1964

A thin superconducting disk is placed in a magnetic field (parallel to the plane of the disk) that can be rotated around the axis of the disk. The intermediate-state pattern does not align itself to a new field position but produces a torque on the disk that is measurable by a sensitive torque balance. For an ideal superconductor, only a transient torque is expected, but measurements show nondecaying torques (towards the field direction) of the order of 1 dyn-cm/deg for disks of 7 mm in diam and 1 mm thick. Measurements in Ta disks of different thicknesses indicate that the torques are proportional to the volume up to the bulk critical field, above which towards higher fields the torques tail off and are proportional to the surface area of the specimens. Measurements in several other metals, including superconductors of both kinds, and the effect of annealing are discussed. A simple model is sufficient to determine from these measurements the force per unit area with which the n-s interphase surface is held in place. Assuming that these forces are caused by local variations of the surface energy, the treatment can be extended to superconductors of the second kind.

25,305 OBSERVATION OF SURFACE SUPERCONDUCTIVITY ABOVE THE THERMODYNAMIC CRITICAL FIELD IN TYPE I SUPERCONDUCTORS by B. Rosenblum and M. Cardona (RCA Lab.); *Phys. Lett. (Neth.)*, Vol. 9, pp. 220-221(L), Apr. 15, 1964

Surface superconductivity observed above the thermodynamic critical field (H_C) in the type I superconductors Pb_{0.99}Tl_{0.01}, more dilute alloys, and pure Pb is discussed. The surface superconductivity occurs only when the magnetic field is parallel to the surface and persists up to a field H_{C3} = cv₂ K H_C. Measurements of the real part of the microwave surface impedance R as a function of magnetic field indicated that when the field is parallel to the surface, R remains very small up to the field H_C and then rises rapidly, reaching its normal value at a field H_{C3}. The increase in surface resistance above H_C is attributed to decreasing order parameter in the surface layer as the magnetic field is increased to H_{C3}. It is shown that the Ginzburg-Landau parameter K of type I superconductors can be determined from measurements of surface superconductivity.

25,306 ALTERNATING CURRENT RESISTANCE OF NONIDEAL SUPERCONDUCTORS by J.L. Zar (Avco-Everett Res. Lab.); *J. Appl. Phys.*, Vol. 35, pp. 1610-1615, May 1964

A direct electrical measurement is made of the resistance of nonideal superconductors at power and audio frequencies, at 4.2°K and in zero applied field. The resistance of short samples of several Nb-Zr and Mo-Re alloys is found to be independent of the composition and of impressed current. The resistivity is found to depend on $\rho^{0.5}$ above 1000 cps and on $\rho^{1.7}$ for frequencies f below 500 cps. The resistance is also independent of wire diameter for some sizes near 0.25 mm. Three explanations are considered to account for resistance at low frequencies. Relaxation time effects are ruled out by the observed frequency dependence at high frequencies. Inductive coupling between the magnetic fields of the normal and the superconducting currents leads to a resistance effect six orders of magnitude lower than the observed ones, and an $\rho^{2.0}$ dependence. Trapping of flux within the superconductor leads to an upper bound for the resistance that agrees with the experimental results in being independent of the wire diameter and the current, and giving the approximately correct resistance values, although an $\rho^{1.0}$ dependence. The measurements suggest that the ac resistance may result from eddy currents induced in normal regions near the surface of heavily cold-worked superconductors.

25,307 SUPERCURRENT DISSIPATION by G.M. Foster (Pomona Coll.); *Phys. Rev. Lett.*, Vol. 11, pp. 122-124, Aug. 1, 1963

The attenuation of applied ac fields measured at the center of cylinders is investigated. An apparently anomalous current behavior, below the transition temperature, was observed. This exhibited a dissipative character more appropriate to the normal state. The applied frequencies varied between 23 cps and 25 kc/sec; field amplitudes ranged between 1 and 250 milligauss. When the field amplitude was less than a few percent of bulk initial field, the attenuation was nearly independent of applied amplitude, whereas for higher fields a non-linear, switching effect was observed. The plot of log attenuation against Δ/kT (Δ is the BCS energy gap normed to 1.0) is a straight line with slope = 18 indicating a T⁻¹ dependence and suggesting an ohmic dissipation. The effect, however, exhibits some frequency dependence.

25,308 RESISTIVE TRANSITION AND CURRENT DENSITY CHARACTERISTICS IN SUPERCONDUCTING NIOBIUM CONTAINING DISSOLVED GASES by W. DeSorbo (GE Res. Lab., Schenectady); *Phys. Rev.*, Vol. 134, pp. A1119-A1135, June 1, 1964

Oxygen and nitrogen as interstitial solutes in niobium cause the metal in transverse field to exhibit anomalous resistance minima or critical current maxima

(peak effect). The anomaly appears at H_{C2} , the upper critical field of these Type II superconductors. The resistance in the mixed state is decreased by exceeding the solubility limit, by cold working and by strain aging at 170°C, masking out the anomaly. Rapidly quenching from the solution temperature decreases the anomaly. The results suggest that the anomaly is strongest at some intermediate stage of the process of segregation and precipitation at dislocations. Resistance in the mixed state is increased by introducing more solute, by quenching, and by etching. Structural changes brought about by cold working, strain aging, and rapid quenching responsible for large changes in $J_c(H)$ or $R(H)$ in the mixed state also cause changes in the region $H_{C2} < H < H_{C3}$. In this latter region, field orientation effects and observed H_{C3}/H_{C2} ratios are roughly consistent with the concept of a superconducting surface sheath as recently proposed by Saint-James and de Gennes. Pure niobium, however, tends to exhibit consistently higher ratios.

25,309 QUANTIZED FLUX PENETRATION THROUGH THIN SUPERCONDUCTORS by J.E. Mercereau and L.T. Crane (Ford Sci. Lab.); Phys. Rev. Lett., Vol. 11, pp. 107-108, Aug. 1, 1963

An experimental confirmation of the critical magnetic field normal to a thin superconductor is reported. Both the penetration depth (λ) and the critical field were measured. A 350°A tin film, was evaporated onto Pyrex substrate at 10^{-6} mm Hg, and λ was determined from measurements of the magnetic shielding in an alternating axial field. The magnitude of λ is almost independent of the theoretical model. The critical field is almost three times the bulk initial field. The results are not essentially changed by employing films of different thicknesses.

25,310 SUPERCONDUCTING PENETRATION DEPTH OF NIOBIUM by W.L. McLean and B.W. Maxfield (Rutgers U.); Bull. Am. Phys. Soc., Vol. 9, p. 454(A), Apr. 1964

The change in the resonant frequency with temperature of a tank circuit, the coil of which contained a niobium core has been measured. The measurements were carried out at 3 mc/sec by the "active" method and at 80 mc/sec by the "passive" method. From these, the rate of change of the penetration depth λ with $y = (1 - t^4)^{-1/2}$, where t is the reduced temperature, has been found. Above $y = 2$, $d\lambda/dy$ does not vary greatly and is about 400 Å. As y decreases towards 1, $d\lambda/dy$ increases more than predicted by the BCS theory in contrast to tin, indium, and aluminum, where the increase is less than predicted. The trend is, however, in accordance with the temperature dependence of the ultrasonic attenuation in niobium found by Dobbs and Perz.

25,311 THE PENETRATION DEPTH IN SEVERAL HARD SUPERCONDUCTORS by T.J. Greytak and J.H. Wernick (Bell Labs.); J. Phys. Chem. Solids, Vol. 25, pp. 535-542, June 1964

The magnetic penetration depth in the superconducting intermetallic compounds V_3Si , V_3Ga , V_3Ge and V_3Pt and in tantalum was studied by means of a coil whose inductance was made to depend on this parameter. Difficulty was experienced in finding samples of the intermetallic compounds with sharp enough superconducting transitions to allow quantitative measurements to be made. However, quantitative results were obtained for V_3Si and tantalum which showed that below the transition region, in the temperature range studied, the magnetic field penetration depth varied linearly with $y = (1 - (T/T_c)^4)^{-1/2}$. For V_3Si the slope of this line, λ_0 , is found to be 2,300 Å to an accuracy ± 10 and ± 30 per cent. For tantalum, λ_0 is 1,500 Å ± 50 per cent. From these figures, the BCS theory is used to find a zero temperature penetration depth $\lambda(0)$, and a coherence distance, ξ_0 . The relative values of $\lambda(0)$ and ξ_0 confirm that these materials are hard superconductors in the negative surface energy sense.

25,312 EXPERIMENTAL EVIDENCE FOR DELAYED ENTRY OF FLUX INTO A TYPE-II SUPERCONDUCTOR by A.S. Joseph and W.J. Tomasch (N.American Aviation); Phys. Rev. Lett., Vol. 12, pp. 219-222(L), Mar. 2, 1964

The behavior of H_T in Pb-Tl foils and films is discussed. H_T is the field at which the ratio τ/H (τ is torque in a field H) departs from its initial linear dependence on H . The latter can be ascribed to flux penetration. Foils exhibited H_T values approximately equal to H_{C1} (bulk), and flux trapping was observed only when H_T was exceeded. In as-deposited, annealed alloy films, H_T was always higher (up to three times greater) than H_{C1} (bulk). Flux trapping occurred only after H was well above H_T . In a film scored to form an array of small, isolated squares H_T was nearly equal to H_{C1} (bulk) at 4.2°K. Flux trapping at $H = 0$ was observed only when H_T was exceeded. It is suggested that in unscored films flux penetration is inhibited by a surface barrier, with the high values of H_T resulting from the low concentration of surface irregularities. Scoring the film creates flux injection centers which facilitate flux entry once H_{C1} (bulk) is exceeded.

25,313 HOMOGENIZATION OF A TRAPPED MAGNETIC FIELD by W.L. Williams, M.J. Stephen and C.T. Lane (Yale U.); Bull. Am. Phys. Soc., Vol. 9, p. 455(A), Apr. 1964

An analytic form for the trapped magnetic field near the center of a superconducting cylinder has been obtained. In the simplest case of a circular hole of radius a in an otherwise infinite sheet of superconductor of thickness $2l$, one finds that near the center of the cylinder the departure of the field from uniformity is proportional to $\exp[-3.8l/a(1-z/l)]$, where z is the axial coordinate measured from the center of the cylinder. For $l/a = 3$ (approximately the value used here), the field will be uniform to 100 ppm for $z/l < 1/4$. This may be improved by choosing a larger l/a ratio. Longitudinal trapped-field configurations were observed in a Sn cylinder 13.5 cm in length and 4 cm i.d. with Pb guard rings 3.81 cm in length at a central field of approximately 220 g with an NMR probe. The guard rings eliminated intermediate-state effects and the trapped field was found to be homogeneous over an axial distance of 4-5 cm to at least 400 ppm. The error in the measurement arises from the limited sensitivity obtainable with the small NMR sample volume and the low value of the magnetic field.

25,314 FLUX MIGRATION AND INSTABILITIES IN HARD SUPERCONDUCTORS by C.R. Wischmeyer (William Marsh Rice U.) and Y.B. Kim (Bell Labs.); Bull. Am. Phys. Soc., Vol. 9, p. 439(A), Apr. 1964

Power is dissipated in hard superconductors as flux lines pinned to structural defects creep by thermal activation. With increased power dissipation, flux creep often turns into turbulent flow, causing a catastrophic breakdown of flux structure or a flux jump. For a thin-walled tube (radius $a \gg$ wall thickness w) the critical-state relation $J_c(B + B_0) = a_c$ with $H \approx H' \gg B_0$ leads to a power dissipation

$$P = 10^{-8} (J_w/2\pi a) (d\pi a^2 H/dt) = 10^{-8} (aw/2) (a_c/H) (dH/dt)$$

in a volume bounded by unit surface area. In qualitative conformity with this expression, we observe more flux jumps by increasing any one of the 5 variables in P ; but the overall temperature rise in the sample is not sufficient to cause such instabilities. Flux-creep pulses observed in pickup coils indicate that, in reality, power dissipation is localized to isolated spots and instabilities grow out of these spots.

25,315 FLUX FLOW IN TYPE II SUPERCONDUCTORS by A.R. Strnad, C.F. Hempstead, and Y.B. Kim (Bell Labs.); Bull. Am. Phys. Soc., Vol. 9, p. 438(A), Apr. 1964

Well-annealed Nb-Ta samples have been used to study the flux-flow phenomenon in type II superconductors. In the presence of transport current J (H), flux lines undergo viscous flow and generate an electric field $E = (\phi_0/\eta c^2) JH$, where ϕ_0 is the flux quantum and $\eta(H, T)$ is the viscosity coefficient. Experimentally, η is determined by measuring the resistivity $\rho = \Delta E/\Delta J$ at fixed H . For $H > H_{C1}$, ρ increases with H and reaches ρ_H at $H = H_{C2}$. Numerically, the viscosity coefficient is given by $\eta = 2 \times 10^{-16} H(G)/\rho(\Omega \cdot cm)$, η reflects the bulk superconducting properties: it decreases with increasing H and increases with decreasing T . Its relation to other bulk parameters is discussed.

25,316 FLUX JUMPING IN Nb + 25% Zr WIRE by M.S. Lubell and G.T. Mallick (Westinghouse Res. Lab., Pittsburgh) and B.S. Chandrasekhar (Western Reserve U.); J. Appl. Phys., Vol. 35, pp. 956-958, Mar. 1964

Flux jumping has been investigated in both cold-worked and heat-treated Nb + 25% Zr wire wound into solenoids and noninductive coils. The measurements taken at 4.2°K were: (1) The induced voltage pulses vs applied magnetic field with both $I = 0$ and a preset transport current. (2) The induced voltage pulses vs coil current for $H = 0$ and with a preset uniform external field. For the case with no transport current in the coil ($I = 0$) when the external field was increased smoothly from zero, a sequence of very sharp voltage pulses (flux jumps) were induced in the coil. These flux jumps had the following general characteristics for all the cases discussed: (1) Starting from well defined initial conditions, the pulse always appeared at about the same place in the field sweeping cycle. (2) The polarity of the pulses is reversed when the direction of field changes is reversed. (3) The pattern of these pulses was essentially unchanged when the field sweep rate was increased from 7 to 340 g/sec. The flux jumps are interpreted according to an extension of a model proposed by both Bean and London.

25,317 MAGNETIZATION AND ASSOCIATED "FLUX-JUMPING" OF Ti-V ALLOYS by R.D. Blaugher, (Westinghouse); Bull. Am. Phys. Soc., Vol. 9, p. 422(A), Apr. 1964

Magnetization measurements were performed on a series of 8 Ti-V alloys across the entire bcc phase region. Every alloy exhibited nonideal second-type superconducting behavior, i.e., a nonreversible magnetization with a large frozen-in moment. The temperature dependence of H_{C1} , the lower penetration field, was investigated for each alloy. For a given reduced temperature ($t = 0.56$), H_{C1} peaks around 25 at.% titanium at approximately 3.6 kg, which is consistent with upper critical-field measurements by Berlincourt and Hake. Well-defined flux-jumping was observed in the lower Ti-concentration alloys.

The frequency and actual occurrence of flux-jumping decreased for increasing titanium concentration. Flux-jumping in some cases could be induced by mechanical vibration of the system, indicating a "metastable" situation.

25,318 FLUX-JUMPING IN TYPE-2 SUPERCONDUCTING TIN FILMS by R.E. Glover III and A. Rodolakis (U. Maryland); Bull. Am. Phys. Soc., Vol. 9, p. 423(A), Apr. 1964

Flux-jumping was observed through superconducting Sn films. A magnetic field varying sinusoidally with time was applied perpendicularly to the disk-shaped film and the change of flux penetrating the sample observed with a pickup coil. The arrangement is similar to that described by van Lint. Tin films roughly 1000 Å thick were condensed in vacuum on glass substrates at room temperature. Resistivity measurements indicated that they were type-2 superconductors. Magnetic flux was observed to come through the film in bursts, each containing several hundred "flux quanta". Near the transition temperature, the field necessary to initiate flux penetration was found to be a function of temperature, going through a maximum in the case of a driving frequency of 300 cps. On the other hand, at reduced temperatures below 0.7 the initiating field was frequency- and temperature-independent. There was considerable spread in the amplitudes of the pickup pulses. The maximum observed heights were roughly independent of the frequency and amplitude of the applied field but increased rapidly with decreasing temperature.

25,319 NEW QUANTIZED VORTEX PHENOMENA IN THIN SUPERCONDUCTORS by J.M. Mochel and R.D. Parks (U. Rochester); Bull. Am. Phys. Soc., Vol. 9, p. 438(A), Apr. 1964

Quantized vortex effects have been observed in thin superconducting films with microconstrictions approximately 1 μ wide. Ac measurements in the frequency range 10 cps-100 kc/sec reveal structure in the resistance versus magnetic-field curves similar to that observed in narrow superconducting strips by the authors. In dc measurements, abrupt voltage signals across the constrictions are observed at unique values of the applied magnetic field. Because of the correlation of these signals with the size of the constrictions, it is believed that they are due to the motion of vortices, each containing 1 flux quantum, past the constriction. The results of measurements of time effects associated with the motion of individual vortices are discussed.

25,320 EVIDENCE FOR QUANTIZED VORTICES IN A SUPERCONDUCTING STRIP by R.D. Parks, J.M. Mochel (U. Rochester); Phys. Rev. Lett., Vol. 11, pp. 354-357, Oct. 15, 1963

Preliminary results of a study of the reduced resistivity r/r_N of 1 μ wide superconducting tin films (≈ 1000 Å thick) in a perpendicular magnetic field near the transition temperature are reported. The r/r_N versus field strength curves exhibit minima which show agreement with a theory of Tinkham postulating quantized current vortices in thin superconductors in a perpendicular field. The vortices have a radius $R^2 = n\phi_0/\pi H$, filling the entire width of the film. If the width of the film is made smaller than $2R$ as in these experiments, resistive anomalies are to be expected. Various vortex distributions in such narrow strips are proposed to explain the experimental results.

25,321 EFFECT OF ANISOTROPY ON THE PROPERTIES OF SUPERCONDUCTORS by B.T. Geilikman and V.Z. Kresin (Moscow State Pedagogical Inst.); Soviet Phys. Solid State, Vol. 5, pp. 2605-2611, June 1964

The effect of anisotropy on the gap and thermodynamic properties of superconductors is discussed for two types of Fermi surfaces: closed and open. Formulas are obtained for describing the dependence of the gap on direction and for various thermodynamic quantities. A general expression is also given, which relates the current and vector potential and does not depend on the specific form of the dispersion law.

25,322 CRITICAL FIELDS OF SnIn THIN FILMS by J.P. Burger, G. Deutscher, E. Gyuon and A. Martinet (Fac. Sci., Orsay); Solid State Commun., Vol. 2, pp. 101-103, Apr. 1964

Thin hollow cylinders of SnIn alloys (type II superconductors) have been studied in the field range $H_{c2} < H < H_{c3}$ where the superconductivity is restricted to a surface layer. With these cylinders both H_{c2} and H_{c3} are determined independently by resistive and by magnetic measurements. The transitions are much sharper than in the corresponding bulk samples. The resulting H_{c3}/H_{c2} ratio is in good agreement with the theoretical value. Preliminary results on the angular dependence of the upper limiting field have also been obtained.

25,323 SUPERCONDUCTIVITY IN SUPERIMPOSED THIN FILMS OF Al AND Sn by D.S. Schreiber (Northwestern U.) and W.D. Knight (U. Calif., Berkeley); Bull. Am. Phys. Soc., Vol. 9, p. 423(A), Apr. 1964

Nuclear-magnetic-resonance (NMR) and resistivity measurement: were used to study the superconducting behavior in several alternating superimposed layers

of Sn and Al down to 1.5°K. In most of the samples (a large number with a varying number and thickness for the layers) studied, a single undepressed, superconducting transition temperature very near that of pure Sn, ($T_c = 3.75^\circ K$), was observed. The remainder exhibited two transitions, one around 3.75°K, the second, about 1.76°K, which are interpreted in terms of a 2-component globular film structure. The NMR of Al and Sn are characteristic of the pure metals and reveal no evidence for the formation of solid solutions or compounds of any kind. Furthermore, the Al resonance shows no change in its shift below the Sn transition temperature, whereas pure, single, superconducting Al films do. The results suggest that the superconducting properties of the Sn are not affected by intimate contact with a metal in its normal state, nor is Al affected above its normal transition temperature.

25,324 PULSE INDUCED SUPERCONDUCTING TO NORMAL TRANSITIONS IN THIN FILMS by E.M. Hartlin, R.M. Wertheimer, and G.M. Graham (U. Toronto); Canadian J. Phys., Vol. 42, pp. 1282-1289, June 1964

The superconducting to normal transition in thin films of Al, Sn, In, and Pb has been studied by applying square voltage pulses to a coaxial line terminated by the film and observing the reflected pulse shape. Interest has centered on the nearly isothermal transitions which could be induced below the lambda temperature of liquid helium. The results have been analyzed in terms of the nucleation and growth of normal domains. The use of very rapidly rising pulses has allowed an estimation of the nucleation time of a normal domain as not more than 3×10^{-10} second. The number of nucleation sites was a sensitive function of the current density in the film. The subsequent growth of normal domains proceeded with a velocity characteristic of the material, of the order of the velocity of transverse sound waves in the bulk metal. Roughly the same velocity was deduced for normal domain growth both parallel and perpendicular to the direction of the current in the film. Growth velocities smaller than these have not been observed, but the "pinning" of domain boundaries by defects in the film has been encountered.

25,325 PHONON-ASSISTED TUNNELING IN SUPERCONDUCTORS by M. Fibich (U. Maryland); Bull. Am. Phys. Soc., Vol. 9, p. 454(A), Apr. 1964

Excess tunneling current has been observed, by Taylor and Burstein, in some superconductor-superconductor junctions at voltages below $eV_0 = \Delta + \Delta'$ are the BCS energy gaps of the 2 superconductors, and has been interpreted as phonon-assisted tunneling. Theoretical calculations of the phonon-assisted current show that the current arises from the electron/thermal-phonon interactions, which gives rise to a nonvanishing imaginary part of the gap function and thus to a finite density of states inside the gap. This theory, unlike a recently proposed one by Kleinman, is essentially correct to all orders in the electron-phonon coupling and has no dependence on the thickness of the superconducting films. Comparison with experiment at 2.86°K for Pb-Pb junction results in a fairly good agreement.

25,326 ANOMALOUS DENSITY OF STATES IN THICK SUPERCONDUCTING LEAD FILMS by P. Townshend and J. Sutton (Plessey Co., England); Phys. Rev. Lett., Vol. 11, pp. 154-156, Aug. 15, 1963

The fine structure in the voltage-current characteristic of a superconductor/barrier/lead tunneling junction is investigated. The thickness dependence of the phenomenon is ascribed to deviations from a BCS density of states; transition occurs when the electron mean free path $\sim 1.2\mu$. Two energy gaps are calculated for the thick film, whereas the single gap in the thin film is the mean of the first two. The phenomenon is discussed with reference to several models and associated complications in the Fermi structure for lead.

25,327 INFLUENCE OF TRANSPORT CURRENT ON THE MAGNETIZATION OF A HARD SUPERCONDUCTOR by M.A.R. LeBlanc (Stanford U.); Phys. Rev. Lett., Vol. 11, pp. 149-152, Aug. 15, 1963

The influence of transport current upon the magnetization of cold-worked Nb-Zn wire in a transverse field at 4.2°K was investigated. The curve of magnetic moment versus transport current is multiple valued. This behavior can be qualitatively explained, with and without transport current, by Bean et al's model of a hard superconductor. Both paramagnetic and diamagnetic cases are discussed, and it is indicated that critical magnetization curves can be derived from the I_c -H curves and vice versa. Anomalous behavior is observed below 3 kg due to resistive transitions.

25,328 MAGNETIZATION OF SUPERCONDUCTING NIOBIUM-ZIRCONIUM ALLOYS by J.P. McEvoy, Jr., and R.F. Decell (RCA Appl. Res.); J. Appl. Phys., Vol. 35, pp. 982-983, Mar. 1964

The magnetization of hollow cylinders of niobium-25 at.% zirconium has been measured at 4.2°K. The experimental results can be described by a model in which the magnetization is derived from an induced supercurrent density given by $J_c = \alpha/B_0 + H$, where H is the transverse magnetic field. This relationship has been verified for Nb-25% Zr with a microstructure varied by mechanical deformation. The values of α and B_0 for several samples cold worked from

25% to 65% have been determined. Extrapolation of the functional dependence of these parameters to negligible cold work (annealed samples) and maximum cold work (heavily strained wire) are shown to be in agreement with previously reported results on cylinders and wires. The current density in the absence of the Lorentz force, ($H = 0$) is found to be somewhat independent of the cold working, implying that the constant $J(0) = \alpha/B_0$ may be related to bulk electronic parameters.

Magnetic:

Properties of Superconducting Sheets - See 25,453

Moment in Sn Superconducting Cylinders - See 25,548

Paramagnetic Moments in Nb-Zr Superconductors - See 25,549

Knight Shift in Superconductors - See 25,599

Magnetocalorie Effect in Nb-Zr Superconductors - See 25,750

Specific Heat of Nb Superconductors - See 25,719, 25,720

Thermal Conductivity of Superconductors - See 25,733

Effect of Magnetic Fields on the Thermal Conductivity of Sn, In and Pb Films - See 25,734

Dielectric Constant of Superconductors - See 25,181

Ultrasonic Absorption in Sn Superconductors - See 25,789

BREAKDOWN

25,329 LOW-TEMPERATURE BREAKDOWN IN p-TYPE GERMANIUM SUBJECT TO UNIAXIAL COMPRESSION by B.M. Vul and I.V. Kucherenko (Acad. Sci. NaukSSSR); *Soviet Phys. Doklady*, Vol. 8, pp. 1191-1193(L), June 1964

The effect of uniaxial compressive stress on the breakdown voltage in p-type germaniums is discussed. The breakdown voltages measured as a function of the pressure along the [111] and [100] axes show a decrease with increasing pressure in the relatively low pressure region (up to about 20 kg/mm²), and vary slightly at higher pressures. The ionization potential and the shear deformation potential constant d deduced from several methods are given. It is found that d is of the order of -10 eV.

25,330 THICKNESS INFLUENCE IN BREAKDOWN PHENOMENA OF THIN DIELECTRIC FILMS by F. Forlani and N. Minnaja (Olivetti); *Phys. Stat. Sol.*, Vol. 4, pp. 311-324, 1964

The influence of film thickness on the breakdown of dielectric films has been examined, using an ionization avalanche theory. The ionization avalanche probability is derived using current relations involving the electron-lattice scattering mechanism and electron behavior in the conduction band of the dielectric. Current density is evaluated by considering the tunnel effect injection of electrons at the negative bias contact. It is suggested that breakdown occurs when the current density at some point within the dielectric layer exceeds a critical value that varies with different materials. A correlation between breakdown field strength and thickness is described.

25,331 MODEL FOR THE ELECTRICAL BEHAVIOR OF A MICROPLASMA by R.H. Haitz (Shockley Lab., Clevite); *J. Appl. Phys.*, Vol. 35, pp. 1370-1376, May 1964

The complex current fluctuation observed in connection with microplasma breakdown can be explained by a simple model containing two constants: extrapolated breakdown voltage V_b and series resistance R_s ; and two continuous probability functions: turnoff probability per unit time $p_{10}(I)$ as a function of pulse current I and turn-on probability per unit time p_{01} . Experimental methods allowing an accurate measurement of these four quantities are described. The new concept of an extrapolated breakdown voltage V_b is discussed based on two independent measurements: one of secondary multiplication and the other of instantaneous current, both as a function of voltage. Within the experimental accuracy of 20 mV both methods extrapolated to one and the same breakdown voltage. The turnoff probability $p_{10}(I)$ is determined by a new combination of experimental techniques to cover the current range from 5 to 70 μ A with a variation of 11 decades for $p_{10}(I)$. The observation of a narrow turnoff intervals is explained quantitatively.

Dielectric Breakdown in SrTiO₃ - See 25,182

MAGNETOELECTRIC (GALVANOMAGNETIC) PROPERTIES

GENERAL

25,332 GALVANOMAGNETIC EFFECTS IN n-TYPE GERMANIUM by W.E. Krog and M.C. Brown (Lincoln Lab.); *Phys. Rev.*, Vol. 134A, pp. A779-787, May 4, 1964

The galvanomagnetic coefficients of n-type Ge have been calculated theoretically and compared with previously published experimental data. Calculations have been made for material containing from 10^{11} to 10^{18} impurity centers per cm³, and comparisons were made with samples having free-carrier concentrations from 5×10^{13} to 2×10^{17} per cm³. The calculations were made primarily at 77 and 300°K, but also as functions of temperature. A solution of the Boltzmann transport equation with a collision time which was anisotropic, energy-dependent, and which depended on the impurity content was used. In the expressions Herring and Vogt's equations were used for the acoustic lattice scattering, the Brooks-Herring equation modified by Ham's calculation of the anisotropy was used for the ionized impurity scattering, and the Erginsoy formula for neutral impurity scattering was used to account for the energy-independent scattering. It is shown that even though a constant mean collision time can be used to qualitatively predict the dependence of the coefficients on the magnetic field, the quantitative agreement with experiment is considerably improved when a more realistic form of the collision time is used for the calculations. Scattering functions which take the temperature dependence of the scattering and the presence of ionized impurities into account enable quantitative predictions of the behavior of the galvanomagnetic coefficients to be made quite successfully.

25,333 GALVANOMAGNETIC PROPERTIES OF FERROMAGNETIC URANIUM MONOSULFIDE by M.A. Kanter and C.W. Kazmierowicz (Argonne Lab.); *J. Appl. Phys.*, Vol. 35, p. 1053, Mar. 1964

Uranium monosulfide has been found to be ferromagnetic with a Curie point at 180°K and a saturation magnetic moment of 1.02 Bohr magnetons per atom at 0°K. Between 4.2°-360°K. The resistivity was found to be about a hundred times larger in US than in the common ferromagnetic metals but the temperature dependence was similar showing an abnormal decrease below the Curie point. The magnetoresistance was found to be negative with a sharp minimum at the Curie point. Two Hall coefficients could be identified as in the transition metals. The extraordinary Hall coefficient related to the magnetization was found to vary as the 2.1 power of the resistivity in reasonable agreement with previous theories. The ordinary Hall coefficient related to the applied field was found to be positive and temperature-dependent with a maximum at the Curie point. The effective carrier concentration evaluated from the ordinary Hall coefficient is 0.45 holes per U atom at absolute zero. These results can be correlated with a band picture based on overlapping 7s and 5f bands, where the states in the broad 7s band contribute the major conductivity whereas the magnetic behavior is due to the unpaired spins of electrons in the narrow 5f band.

25,334 PROPERTIES AND DEVICE APPLICATIONS OF EVAPORATED InSb FILMS by H.H. Wieder (US Naval Ord. Lab.); in *ONR Solution to Navy Probl. through Adv. Tech.*, (1963), pp. 206-226, ONR-16, Vol. 1; *STAR*, Vol. 2, p. 916(A), Apr. 8, 1964 OTS \$5.00

The galvanomagnetic properties of evaporated intermetallic semiconductor films of indium antimonide are investigated and are presented with emphasis on their application to devices employing the Hall effect. The design and construction of a magnetometer based on the pulsed operation of a thin-film Hall generator are described in detail. The magnetometer is capable of resolving dc or alternating magnetic fields of the order of 10^{-4} gauss. Operation of either dc- or pulse-driven analog multipliers, dividers, square root computers, and function generators based on the Hall effect in InSb films are discussed and compared to similar devices using bulk crystalline materials.

MAGNETORESISTIVITY

25,335 OSCILLATORY MAGNETORESISTANCE IN GRAY TIN by E.D. Hinkley and A.W. Ewald (Northwestern U.); *Phys. Rev.*, Vol. 134A, pp. A1261-1267, June 1, 1964

The oscillatory component of magnetoresistance has been measured for single crystals of n-type gray tin at liquid-helium temperatures. The period of oscillation is independent of magnetic field direction, confirming an isotropic effective mass and, therefore, a conduction-band edge at the center of the

lloin zone. Oscillations were also observed in a polycrystalline specimen. Carrier concentrations deduced from the oscillatory period are in reasonably good agreement with values obtained from the Hall coefficient over a range of almost two orders of magnitude in this parameter. An electron effective mass $0.024 m_0$ was obtained from the field and temperature dependence of the oscillatory amplitude for samples having carrier concentrations on the order of 10^{16} cm^{-3} . Nonthermal damping of the oscillation is attributed mainly to inhomogeneities in the impurity distribution. The experimental results are compared with theory.

25,336 EMPIRICAL CHARACTERIZATION OF LOW-TEMPERATURE MAGNETORESISTANCE EFFECTS IN HEAVILY DOPED Ge AND Si by H. Roth, J.D. Straub, W. Bernard (Raytheon) and J.E. Mulhern Jr. (U. New Hampshire); *Phys. Rev. Lett.*, Vol. 11, pp. 328-331, Oct. 1, 1963

Positive anomalous magnetoresistive effects in p-type germanium and negative and positive anomalous effects in heavily doped n- and p-type silicon have been observed. The resultant curves can be described by an equation

$$\frac{\Delta \rho}{\rho_0} = aH^c + bH^2$$

The field strength H has been varied between 0 and 20 koe. The parameters a and b which are functions of T were determined by a least square fit technique from the experimental values. The authors advance the hypothesis that the positive and negative effects arise from the same physical mechanism.

25,337 MAGNETORESISTANCE OF DEGENERATE n-TYPE GERMANIUM AND SILICON by D.G. Andrianov and V.I. Fistul (State Scientific-Res. and Des. Inst.); *Soviet Phys. Solid State*, Vol. 5, pp. 1077-1079(L), Nov. 1963

25,338 MAGNETORESISTANCE OF THE CORBINO DISK AT MICROWAVE FREQUENCIES by C.B. Burckhardt (Bell Labs.), M.J.O. Strutt (Swiss Fed. Inst. Tech., Zurich) and F.K. von Willisen (GE Electronics Park, Syracuse); *Solid-State Electronics*, Vol. 7, pp. 343-355, May 1964

The behavior of a Corbino disk of InSb in a static transverse magnetic field and a high frequency electric field is investigated. Measurements and analysis show that, owing to an internal magnetic field effect, the impedance of the Corbino disk shows a frequency dependence already at microwave frequencies. Measurements performed on rectangular samples show the same effect even more pronounced. It is concluded that in the case of medium to high Hall angles this effect may determine an upper frequency limit of Hall effect devices, which is considerably lower than the dielectric relaxation frequency or the reciprocal average collision time.

25,339 NEGATIVE MAGNETORESISTANCE IN PYROLYTIC CARBONS AND GRAPHITE BROMINE by G.A. Saunders (Imperial Coll.); *Appl. Phys. Lett.*, Vol. 4, pp. 138-140(L), Apr. 15, 1964

Negative magnetoresistance observed in pyrolytic carbon and in the bromine-graphite compound $C_{700}\text{Br}$ is discussed. Negative magnetoresistance in pyrolytic carbons can be the direct result of boundaries separating regions of differing crystallite size and orientation, and differing carrier concentration. A direct correlation between the Hall coefficients and the magnetoresistances of defective graphites has been observed. This and the observed temperature dependence of magnetoresistance in pyrolytic carbons agree with the expression for magnetoresistance derived by Bate et al. The negative magnetoresistance is proportional to H^x , with x lying between 1.5 and 2.0. Negative magnetoresistance also occurs in the bromine-graphite "residue" compound $C_{700}\text{Br}$, probably because of the existence of regions of graphite and bromine separated by distinct boundaries. A voltage reversal along the a -axis of this compound was observed at -196° and -77°C on the application of a sufficiently large magnetic field.

25,340 NEGATIVE MAGNETORESISTANCE OF n-TYPE INDIUM ARSENIDE AT LOW TEMPERATURES by N.V. Zotova, T.S. Lagunova and D.N. Nasledov (Acad. Sci. USSR); *Soviet Phys. Solid State*, Vol. 5, pp. 2439-2440(L), May 1964

Measurements of the conductivity, Hall constant and the change of resistance in a transverse magnetic field of indium arsenide specimens with electron concentrations from 1.2×10^{16} to $4 \times 10^{16} \text{ cm}^{-3}$ are reported. At low temperatures, the resistivity decreases with magnetic field, and the magnitude of this effect increases with decreasing electron concentration. The dependence of the negative magnetoresistance on the field intensity is quadratic in weak fields, and saturation tends to take place in strong fields. The Hall constant exhibits a maximum in the nitrogen temperature range and is independent of the magnetic field intensity over the entire range $0-1.3 \times 10^4 \text{ oe}$.

25,341 HIGH-FIELD MAGNETORESISTANCE OF MOLYBDENUM AND TUNGSTEN by E. Fawcett and W.A. Reed (Bell Labs.); *Phys. Rev.*, Vol. 134A, pp. A723-727, May 4, 1964

The transverse magnetoresistance of high-purity samples of Mo and W was measured in magnetic fields up to 83 koe. No deviation from the quadratic magnetoresistance characteristic of a compensated metal was observed, which shows that the Fermi surfaces of these metals support less than 10^{-4} open cyclotron orbits per atom for Mo and 10^{-7} per atom for W. The numbers of electrons and holes in W differ by less than 0.07%, which indicates that to this accuracy the number of quasiparticles in a many-body scheme is equal to the number of particles in a one-electron scheme.

25,342 MAGNETORESISTANCE AND HALL-VOLTAGE MEASUREMENTS ON SINGLE-CRYSTAL Ni AND Ni-Fe THIN FILMS by V.A. Marsocci (New York U.); *J. Appl. Phys.*, Vol. 35, pp. 774-775, Mar. 1964

Measurements were taken at room temperature and at liquid-nitrogen temperature of the magnetoresistance of nickel and nickel-iron alloy thin films. The transverse magnetoresistance data, with current in a $[110]$ direction, of $\Delta\rho/\rho_0$ vs θ , where θ is the angle between the plane of the film and the direction of the magnetic field, show marked anisotropies with large lobes at values of θ corresponding to the magnetic field perpendicular to a $\langle 111 \rangle$ direction of the crystal structure. Similar measurements performed on a polycrystalline film show quite an isotropic behavior. With the films at the low temperature (77°K) the graphical plot of $\Delta\rho/\rho_0$ shows the same general shape as that for the room-temperature data, except that for the nickel films $\Delta\rho/\rho_0$ is reduced in magnitude. No corresponding anisotropies were observed, however, in the Hall-voltage measurements which were taken at room temperature. The anisotropies observed in the magnetoresistance data for the nickel-iron alloy films were of the same general character as those observed for the nickel films.

25,343 LOW-TEMPERATURE MAGNETORESISTANCE IN MAGNESIUM AND ALUMINUM CONTAINING SMALL CONCENTRATIONS OF MANGANESE OF IRON by F.T. Hedgcock and Y. Muto (Franklin Inst. Lab.); *Phys. Rev.*, Vol. 134A, pp. A1593-A1599, June 15, 1964

Magnetoresistance measurements in magnetic fields up to 21 koe have been made on Mg-Mn, Mg-Cd, Mg-Al, Al-Mn, and Al-Fe alloys in the temperature region of liquid helium. Magnesium alloys containing more than 0.1 at. % Mn which exhibit a resistance maximum and minimum in zero field, show a negative magnetoresistance, whereas the more dilute samples (0.001-0.1 at. % Mn) show a positive magnetoresistance, the magnitude of which decreases with decreasing temperature. The magnesium alloys containing nontransition element impurities, as well as the aluminum alloys containing transition metal impurities, are found to obey Kohler's rule. From an analysis of these data it is found that the magnetoresistivity of a dilute alloy of magnesium containing manganese, can be considered as the sum of a normal positive magnetoresistivity (obeying Kohler's rule) and an anomalous term which is negative in sign, does not obey Kohler's rule and is presumably due to a magnetic scattering of the conduction electrons. Using values of the s - d exchange integral and the Coulomb scattering integral derived from an analysis of the zero-field resistivity permits an explanation of the magnetoresistivity based on Kasuya's theory, at temperatures near the Néel point.

HALL EFFECT

25,344 BIBLIOGRAPHY ON THE HALL-EFFECT THEORY AND APPLICATIONS by A. Clawson and H. Wieder (US Naval Ord. Lab.); *Solid-State Electronics*, Vol. 7, pp. 387-396, May 1964

A bibliography listing 297 references from current literature pertinent to the theory and application of Hall effect devices up to July 1, 1963 is presented. This list was taken from readily available articles in English, German, and Russian. A reference guide, which classifies the Hall effect literature by subject, follows the main bibliography.

25,345 HALL-EFFECT STUDIES IN DEPOSITED CdS THIN FILMS by R.S. Muller and B.G. Watkins (U. Calif.); *Proc. IEEE*, Vol. 52, pp. 425-426(L), Apr. 1964

Hall effect measurements taken as a function of temperature on deposited thin film of CdS are discussed. Resistivity variations as a function of temperature are noted with different methods of fabrication of the CdS crystal. Measurements techniques are stated. The most striking behavior observed in all the films studied is an exponentially increasing Hall mobility with increases in temperature. An attempt is made to explain this phenomenon, and contemporary theories on the subject are discussed.

25,346 THEORY OF THE FERROMAGNETIC HALL EFFECT by L.E. Gurevich and I.N. Yassievich (Acad. Sci. USSR); *Soviet Phys. Solid State*, Vol. 5, pp. 1914-1918, Mar. 1964

It is shown that the terms independent of the presence of scatterers but dependent on interband transitions of the carriers under the action of an electric field are absent from the ferromagnetic Hall current. This current is determined by the diagonal part of the density matrix and the diagonal matrix elements of the velocities of the electrons, and is related to the asymmetric scattering of polarized carriers.

25,347 THE PHOTO-HALL EFFECT IN VITREOUS SELENIUM by J. Dresner (RCA Lab.); *J. Phys. Chem. Solids*, Vol. 25, pp. 505-513, May 1964

The photo-Hall effect has been measured in the insulating vitreous form of selenium. The high mobility holes predicted by Spear have not been found; rather, under intense illumination, the material shows n-type conductivity. The mobility for electrons $\mu_{\text{on}} = 0.32 \pm 0.1 \text{ cm}^2 \text{ V}^{-1} \text{ sec}^{-1}$ at 20°C . The mobility for holes μ_{op} is estimated to be very close to the drift mobility $\mu_{\text{DP}} = 0.15 \text{ cm}^2 \text{ V}^{-1} \text{ sec}^{-1}$.

Hall Coefficient of Semiconductors - See 25,233

25,348 ANALYSIS OF 2-BAND HALL-COEFFICIENT BEHAVIOR AT HIGH CARRIER DENSITIES, WITH APPLICATION TO p-TYPE PbTe by R.S. Allgaier, (US Naval Ord. Lab.); *Bull. Am. Phys. Soc.*, Vol. 9, p. 479(A), Apr. 1964

The analysis of Aukerman and Willardson was restricted to classical statistics; at higher carrier densities, the Hall-coefficient behavior evolves in a characteristic fashion best described in terms of the 0-degree Fermi level E_{F_0} , the band-edge separation E_{G} , and kT , rather than in terms of carrier concentrations and effective masses. In particular, when E_{F_0} and $E_{\text{G}} \gg kT$, but

$$E_{\text{G}} - E_{\text{F}_0} \approx kT, \Delta R/R_0 \propto T^{1/2}.$$

This behavior has been observed in p-type PbTe at $p^* (= 1/R_{77}^0/e) = 1.5 \times 10^{20} \text{ cm}^{-3}$. When E_{F_0} exceeds E_{G} , a sharp kink in a Hall ratio (e.g., R_{25}^0/R_{77}^0) vs carrier-density curve should occur. Such a kink is seen in SnTe but not in PbTe. Previously, an Aukerman-Willardson analysis on p-type PbTe gave $E_{\text{G}} = 0.14 \text{ eV}$. The present extension leads to the conclusions that (a) at low temperature, there are no carriers in a 2nd valence band for $p^* < 1.5 \times 10^{20} \text{ cm}^{-3}$ and (b) the 1st valence band is significantly nonparabolic.

Hall:

Effect in SiC - See 25,251

Coefficient of CdSb:Au - See 25,256

Effect in PbS Layers - See 25,253

25,349 HALL EFFECT IN NICKEL OXIDE by V.P. Zhuze and A.I. Shelykh (Acad. Sci. USSR); *Soviet Phys. Solid State*, Vol. 5, pp. 1278-1280(L), Dec. 1963

25,350 THE HALL EFFECT IN SEMICONDUCTING GLASSES by W.F. Peck, Jr. and J.F. Dewald (Bell Labs.); *J. Electrochem. Soc.*, Vol. 111, pp. 561-563, May 1964

Hall effect measurements on semiconducting glasses from the systems, arsenic-tellurium-iodine and arsenic-tellurium-bromine, are reported. The Hall field is linear in the drift field up to 4.6 v/cm and in the magnetic field up to 70 kilogauss. The sign of the Hall effect in these systems indicates n-type semiconductors which is in apparent contradiction with the sign of the thermoelectric effect which indicates p-type conductivity. The carrier mobilities are of the order of $0.05 \text{ cm}^2/\text{volt-sec}$, with only small temperature dependence.

25,351 THE HALL EFFECT-SEEBECK EFFECT SIGN ANOMALY IN SEMICONDUCTING GLASSES by A. Pearson (Bell Labs.); *J. Electrochem. Soc.*, Vol. 111, pp. 753-755(L), June 1964

An anomaly between the sign of the Hall effect and Seebeck effect in semiconducting glasses has been investigated using a series of arsenic-tellurium-iodine glasses. Although other possible sources for this anomaly may exist, electron microscopic studies indicate the source is probably a small amount of a n-type crystalline which has precipitated in a p-type glassy matrix. In a Seebeck effect measurement, the low thermal conductivity of the glass causes it to support the temperature gradient and thus give a positive result. However, the relatively high carrier mobility of the crystalline phase causes it to dominate over the glassy matrix in a Hall effect measurement thus giving an n-type result.

25,352 ANISOTROPY OF THE HALL EFFECT IN PARTIALLY-REDUCED SINGLE-CRYSTAL RUTILE (TiO_2) by V.N. Bogomolov and V.P. Zhuze (Acad. Sci. USSR); *Soviet Phys. Solid State*, Vol. 5, pp. 2404-2408, May 1964

Measurements of the conductivity and Hall effect in oriented specimens of slightly reduced single-crystal rutile are reported. The anisotropy of the conductivity is found due to the anisotropy of the current carrier mobility. It is

shown that the chemical binding in rutile is mixed and the crystal can not be considered as purely ionic. A qualitative consideration of the scattering mechanism shows that the "natural" scattering mechanism is determined by a combined scattering by acoustic and optical phonons.

25,353 FERROMAGNETIC HALL EFFECT AT OPTICAL FREQUENCIES AND INNER EFFECTIVE MAGNETIC FIELD OF FERROMAGNETIC METALS by G. Krinchik (Moscow State U.); *J. Appl. Phys.*, Vol. 35, pp. 1089-1092, Mar. 1964

The results of magneto-optical measurements on Fe, Co, and Ni over a wide range of frequencies, varying from infrared to ultraviolet, have been analyzed. It is suggested that the magneto-optical phenomena in ferromagnetic metals are caused by the influence of the inner effective magnetic field H_i (which is responsible for the static ferromagnetic Hall effect) on the motion of the current carriers. The previously detected infrared magneto-optical resonance in Ni is interpreted according to this theory as the cyclotron resonance of the current carriers in the field H_i . A quantitative correlation of the static electrical conductivity and the ferromagnetic Hall constant is obtained by comparison of the magneto-optical data with the results of direct measurements. The conclusion may lead to a change in the commonly accepted point of view of the origin of ferromagnetism in transition metals.

CYCLOTRON RESONANCE

25,354 FERMI-LIQUID EFFECTS IN CYCLOTRON RESONANCE by P.M. Platzman and K.C. Jacobs (Bell Labs.); *Phys. Rev.*, Vol. 134A, pp. A974-A978, May 18, 1964

The steady-state properties of transverse circularly polarized waves propagating along a static magnetic field in a uniform plasma (metal) are considered. Using the Landau theory of Fermi liquids, the effect of correlations on the reflection properties of a semi-infinite metallic plasma are computed. The expressions are numerically evaluated and discussed for a range of parameters pertinent to the alkalis.

25,355 CYCLOTRON RESONANCE INVOLVING CURRENT SHEETS IN ALUMINUM by C.C. Grimes (Bell Labs.), A.F. Kip and F. Strong (U. Calif., Berkeley), R.A. Stradling (Oxford U.), and P. Pincus (U. Calif., LA); *Phys. Rev. Lett.*, Vol. 11, pp. 455-457(L), Nov. 15, 1963

Limiting point resonances due to charge carriers on parts of the Fermi surface tangent to the magnetic field in Al have been observed. These resonances are attributed to the helical orbits of holes on the spherical caps (with axes along the $\langle 111 \rangle$ and $\langle 100 \rangle$ directions) of the second Brillouin zone. A theoretical explanation is proposed to explain the following observed discrepancies with the theory of Azbel'-Kaner: (1) the cyclotron mass is too large by a factor of 2; (2) the resonances are observed for angles greater than 5° between specimen and field; and (3) the surface impedance derivatives are of opposite sign with respect to field.

25,356 SOME NEW ASPECTS OF CYCLOTRON RESONANCE IN COPPER by J.F. Koch, R.A. Stradling and A.F. Kip (U. Calif., Berkeley); *Grant AFOSR62 127*, 40 pp., June 12, 1963; *U.S. Gov. Res. Rep.*, Vol. 39, p. 149(A), May 5, 1964 AD 430 971 OTS \\$3.60

The development of improved techniques has made possible a new series of cyclotron resonance experiments on Cu which gives more accurate and extended information on electron cyclotron masses. New orbits which have been observed are measured include a limiting point orbit, orbits extending through three and four Brillouin zones, orbits whose centers are neither at the center nor edge of the zone, and orbits observed with the magnetic field tipped at large angles (up to 80 degrees) with respect to the crystal surface. The neck orbit has been observed and measured with the field along the 111 direction. The cyclotron mass ratio for this orbit is 0.46. Certain discrepancies and puzzling aspects of earlier data have been clarified and the present data are in excellent accord with the Haas-van Alphen and magnetoacoustic data on the geometry of the Fermi surface.

25,357 ANALYSIS OF CYCLOTRON ABSORPTION IN LEAD TELLURIDE by H. Numata and Y. Vemura (U. Tokyo); *Phys. Lett. (Neth.)*, Vol. 9, pp. 227-228(L), Apr. 15, 1964

An analysis of cyclotron resonance absorption in n- and p-type PbTe is discussed. Theoretical results were obtained under classical skin effect conditions, with a set of $\langle 111 \rangle$ ellipsoids of revolution assumed for both the conduction and valence bands. Field strengths vs field direction, and the derivative of power absorption vs magnetic field have been calculated and compared with experimental values. The calculated values of penetration depth vs magnetic field has also been compared with the variation of cyclotron radius r_c with magnetic field. The good agreement obtained between the theoretical

cles and the experimental results of Nii indicate that the absorption peaks correspond to dielectric anomalies and that both conduction and valence band minima have $\langle 111 \rangle$ ellipsoid of revolution energy surfaces.

Electron Resonance in CdS - See 25, 225

NOISE

25,358 ON THE NOISE CAUSED BY DIFFUSION AND SURFACE RECOMBINATION by K.M. Van Vliet (U. Minn.); *Physica*, Vol. 30, pp. 1092-1106, June 1964

Various theories concerning noise in semiconductors resulting from surface generation and recombination of carriers and the associated diffusion to and from the surface are discussed. It is shown that critique by Champlin on the earlier papers by Hyde and by van Vliet and van der Ziel is unjustified and that the one dimensional geometry, used both by Champlin and by Lax and Langert, complete agreement is established with the aforementioned earlier papers.

25,359 1/F NOISE IN THIN FILMS OF SEMICONDUCTORS by K.M. Kiser (Res. Lab.); *J. Electrochem. Soc.*, Vol. 111, pp. 556-560, May 1964

Measurements have been made of the 1/f noise produced by thin films of indium oxide on a gelatin substrate and of thin films of copper iodide on a polycarbonate substrate. Only the audiofrequency range was examined. For relatively small d-c currents the noise power for the indium oxide films is directly af^{-1} . This proportionality is preserved at the higher current levels but anomalies appear in these spectra. The noise power decreases slightly with temperature and increases somewhat when oxygen is removed. Moisture has a large effect on the 1/f noise. In the case of the copper iodide films, the noise apparently has two components, a f^{-1} component detectable at low frequencies and high currents, and a single time constant component

$$\propto [1 + \omega^2 \tau^2]^{-1}$$

detectable at high frequencies and low currents.

ELECTRON EMISSION

25,360 NOTE ON ELECTRON AND ION EMISSION FROM LASER-HEATED KIDIE CATHODES by G.C. Dalman (Cornell U.); in *Invest. of New Concepts for Microwave Power Gen. Laser Studies*, Dec. 1963, 17 pp.; *STAR*, Vol. 2, p. 626(A), Mar. 8, 1964 AD 427 115

An exploratory study of the emission of electrons and ions from a cold barium oxide cathode surface was made to assess the usefulness of the conventional oxide cathode as a high-density current source. It is indicated that a laser-activated oxide-coated cathode does not seem practical, since the coating rapidly breaks down. However, advantage may be taken of this effect to produce a pulsed source of high-density positive or negative ions.

25,361 AN INVESTIGATION OF ELECTRON EMISSION FROM A TUNGSTEN SURFACE INDUCED BY A LASER BEAM by L.A. Mac Kenzie (Cornell U.); in *Invest. of New Concepts for Microwave Power Gen. Laser Studies*, Dec. 1963, 81 pp.; *STAR*, Vol. 2, p. 626(A), Mar. 8, 1964 AD 427 115

The emission of electrons and ions from a metallic cathode when the surface is heated by a pulsed laser beam was investigated experimentally. The incident energy of the laser beam on the cathode ranged from 0.1 joules to 3 joules per a 300- μsec pulse. A very large electron emission density was found under ordinary thermionic emission conditions. Also, a plasma discharge was obtained, which contained a large volumetric electron density. Some initial theoretical work is described as support for the experiments reported.

25,362 PRELIMINARY STUDIES OF ELECTRON EMISSION FROM TUNGSTEN INDIRECTLY HEATED BY A PULSED LASER by G.C. Dalman (Cornell U.); in *Invest. of New Concepts for Microwave Power Gen. Laser Studies*, Dec. 1963, 10 pp.; *STAR*, Vol. 2, p. 626(A), Mar. 8, 1964 AD 427 115

An experimental and theoretical investigation of the emission of electrons, ions, and vertical particles from a tungsten cathode which is "surface-heated" by a laser beam is described. Principal emphasis is given the phenomenon of electron emission because of the interest in its application to the formation of a very dense electron beam. Two different experimental approaches are taken in obtaining electron emission. The first approach is to collect electrons which are "boiled off" the surface the laser beam strikes, whereas the second approach is to use a very thin tungsten ribbon to collect electrons from the surface opposite to the laser beam strikes.

25,363 ELECTRON AND ION EMISSION FROM A TUNGSTEN MONO-CRYSTAL by J.L. Coggins (MIT); in *New Concepts in Energy Conv.*, pp. 19-22, Cont. AF 33(616)-1083; *STAR*, Vol. 2, p. 1280(A), May 23, 1964

The growth and emission properties of single crystal W filaments is described. The crystal was grown in a projection tube by heating the filament at 2,000°K for several hours. Vacuum measurements were taken in a tube with a rotating slit which subtended an angle of 4.2° on the filament. The parameters varied are filament temperature, anode bias voltage, collector bias voltage and direction. Both the anode and collector are run at a positive potential with respect to the filament. A typical collector bias curve and the emission map of collector current vs azimuth. This map gives an indication of how work function varies with crystallographic direction.

25,364 EFFECT OF AN EXTERNAL ELECTRIC FIELD ON PHOTOSTIMULATED EXOELECTRON EMISSION FROM ADDITIVELY COLOURED NaCl INTO A GASEOUS ATMOSPHERE (II) by S. Gasior, W. Stepniowski (Medical Acad., Wroclaw) and B. Sujak (Wroclaw U.); *Acta Phys. Polonica*, Vol. 25, pp. 247-253, Feb. 1964

The dependence of photostimulated exoelectron emission from NaCl single crystals coloured additively in sodium vapour was investigated versus the accelerating voltage. The measurements yielded graphs of the decay curves of the photostimulated emission with time, at constant values of the voltage; analysis of the graphs led to three relationships between the decay constants λ_1 , λ_2 , λ_3 and the accelerating voltage applied, U:

$$\begin{aligned}\lambda_1 &= 1.3-93 \times 10^{-3} \sqrt{U} & \text{for } 0 < U \leq 190 \text{ V,} \\ \lambda_2 &= 0.09-25 \times 10^{-7} U^2 & \text{for } 0 < U \leq 190 \text{ V,} \\ \lambda_3 &= 0.0089-15 \times 10^{-8} U^2 & \text{for } 0 < U \leq 250 \text{ V.}\end{aligned}$$

In measurements with accelerating voltages exceeding approximately 200 V (distance 0.5 cm), λ_1 assumed negative values causing the photostimulated exoelectron emission intensity to increase with time during the initial phase of observation.

25,365 SURFACE EFFECT IN SECONDARY AND PHOTOELECTRIC EMISSION by I. Adawi (Battelle Inst.); *Phys. Rev.*, Vol. 134A, pp. A1649-1654, June 15, 1964

The secondary emission yield of metals by the surface effect δ is expressed in terms of the surface photoelectric yield $y(\omega)$ for a radiation of frequency ω and angle of incidence of $\cos^{-1} \frac{1}{2} (5\frac{1}{2})$ which is about 52°. It is shown that

$$\delta \sim (2\pi\alpha E_p)^{-1} \int_{\omega_1}^{\omega_2} y(\omega) d\omega/\omega,$$

where E_p is the primary energy in atomic units, $\alpha = 1/137$, ω_1 is the threshold frequency, and ω_2 depends on the energy of the primary and may be replaced by ∞ . For a square-well potential model for a metal, $\delta \sim 10^{-3}/E_p$ with a relative error of order $(E_F/E_p) \ln(E_F/E_p)$, where E_F is the Fermi energy.

25,366 DOUBLE-QUANTUM PHOTOELECTRIC EMISSION by G. Wolga and H. Bowers (Cornell U.); in *Invest. of New Concepts for Microwave Power Gen. Laser Studies*, Dec. 1963, 8 pp.; *STAR*, Vol. 2, p. 626(A), Mar. 8, 1964 AD 427 115

A theoretical study of double photon-induced photoelectric emission from single zinc crystals was made, and an experiment was designed to observe such emission. The double-photon absorption process leading to this photoelectric emission is a second-order process in the conventional perturbation treatment of the interaction of free, metallic electrons with electromagnetic radiation; therefore, a ruby laser was used as a source of light in order to obtain the high fields necessary to produce this emission in measurable quantities. A detailed study of thermionic emission was made to distinguish the second-order photoelectric emission from simultaneously occurring thermionic emission. It was revealed that a high-frequency modulation of the laser light impinging on the crystal might well make the second-order effect observable. The quantum mechanical effects of this modulation on the second-order photoeffect were studied in detail along with the thermionic emission response to this modulation. The modulation is accomplished by means of the longitudinal Pockel's effect in KDP.

25,367 CALCULATION OF HIGH-ENERGY SECONDARY ELECTRON EMISSION by J.A. Sawyer (AF Weapons Lab., Albuquerque) and V.A.J. Van Lint (Genl. Dynamics); *J. Appl. Phys.*, Vol. 35, pp. 1706-1711, June 1964

The emission of high-energy secondary electrons from thin targets of low atomic number has been calculated. The targets are assumed to be bombarded with 25-mev electrons, 600-kvp x rays, and prompt fission gamma radiation. The results give maximum efficiency of high-energy secondary electron emission of 8% for 25-mev electrons, 0.30% for prompt fission gamma radiation, and 0.05% and 600-kvp x rays.

25,368 ON THE THEORY OF SECONDARY ELECTRON EMISSION OF TRANSPORT PROCESSES. Part I. FORMULATION OF PROBLEM [in German] by H. Puff (Phys. Tech. Inst., Berlin); *Phys. Stat. Sol.*, Vol. 4, pp. 125-138, 1964

A formal, theoretical approach to the transport of excited electrons arising from secondary emission effects is presented. The inadequacy of earlier approaches that used Boltzmann's equation to describe transport of excited electrons is discussed and a new approach assuming that excited electrons may be regarded as free is presented. The whole transport problem is converted to an integral equation.

25,369 ON THE THEORY OF SECONDARY ELECTRON EMISSION OF TRANSPORT PROCESSES-II ELEMENTARY SCATTERING MODELS [in German] by H. Puff (Phys. Tech. Inst. Berlin); *Phys. Stat. Sol.*, Vol. 4, pp. 365-382, 1964

The theoretical formalism developed in an earlier paper (SSA No. 25,368) is applied to the interaction with optical phonons (forward scattering) and to the interaction with electrons (isotropic scattering).

25,370 KINETIC SECONDARY ELECTRON EJECTION FROM TUNGSTEN BY CESIUM IONS by S.H. Bosch and G. Kuskevics (Electro-Optical Sys.); *Phys. Rev.*, Vol. 134A, pp. A1336-A1358, June 1, 1964

Initial measurements of the number of electrons ejected per incident ion, γ_i , have been made for medium-energy (1-21 kev) cesium ions at normal incidence on a clean polycrystalline tungsten surface. The residual gas pressure was $< 5 \times 10^{-9}$ Torr. The tungsten surface was cleaned by prolonged bakeouts and by flashing before each measurement. A dc ion-beam pulse method of measurement was used to prevent cesium coverage of the tungsten surface. In the energy range of 3-21 kev γ_i is a linear function of the ion kinetic energy with $\partial \gamma_i / \partial E \approx 0.04$ electron per ion per kev. At 3 and 21 kev γ_i is 0.02 and 0.74, respectively. If the data are extrapolated to $\gamma_i = 0$, a threshold energy of 2.5 kev is obtained. Below this energy the measured values of γ_i were equal to zero within the accuracy of the measurement. The change of γ_i with cesium adsorption on the tungsten was also recorded.

25,371 FIELD EMISSION FROM THIN FILM CATHODES [in German] by A. Möschwitzer and S. Wagner (U. Dresden); *Phys. Stat. Sol.*, Vol. 4, pp. 357-364, 1964

Field emission from thin films of Al-Al₂O₃-Al and Ta-Ta₂O₅-Al is discussed.

MAGNETIC PROPERTIES

GENERAL

25,372 MAGNETISM IN ONE-DIMENSIONAL SYSTEMS — THE HEISENBERG MODEL FOR INFINITE SPIN by M.E. Fisher (Rockefeller Inst.); *Am. J. Phys.*, Vol. 32, pp. 343-346, May 1964

It is observed that the free-energy, susceptibility, and correlation functions for a linear chain of N spins with nearest-neighbor isotropic Heisenberg coupling can be calculated explicitly in the (classical) limit of infinite spin. The results are compared briefly with those for Ising and Heisenberg chains of spin $\frac{1}{2}$.

25,373 ON THE DYSON METHOD IN THE THEORY OF MAGNETISM by S.T. Dembinski (U. British Columbia); *Physica*, Vol. 30, pp. 1217-1224, June 1964

A simple derivation of various correspondence formulae between the angular momentum operators and the harmonic oscillator operators is given. Some of the possible equivalent representations of the Heisenberg antiferromagnetic exchange Hamiltonian are listed. In this connection a criticism is presented of the general validity of a transformation recently introduced by Oguchi.

25,374 MAGNETIC TRANSLATION GROUP by J. Zak (Nat'l. Magnet Lab., MIT); *Phys. Rev.*, Vol. 134A, pp. A1602-1606, June 15, 1964

A group-theoretical approach to the problem of a Bloch electron in a magnetic field is given. A magnetic translation group is defined and its properties, in particular its connection with the usual translation group, are established.

25,375 MAGNETIC TRANSLATION GROUP II. IRREDUCIBLE REPRESENTATIONS by J. Zak (Nat'l. Magnet Lab., MIT); *Phys. Rev.*, Vol. 134A, pp. A1607-1611, June 15, 1964

The physical irreducible representations of the magnetic translation group (M.T.G.) defined previously have been found. From these a set of solutions of Schrödinger's equation for a Bloch electron in a magnetic field has been constructed. In general the M.T.G. is non-Abelian. However, when the magnetic flux through areas enclosed by any vectors of the Bravais lattice become multiples of an elementary "fluxon" hc/e , the M.T.G. becomes isomorphic to the usual translation group.

25,376 SPIN WAVE SCATTERING OF NEUTRONS by R.D. Lowde (AE Res. Estab., Harwell); *Prog. 10th Ann. Conf. Magnetism and Magnetic Materials*, Nov. 1964 (to be publ. in *J. Appl. Phys.*)

A review is given of the problems and possibilities in this field. Special features of the neutron scattering technique as applied to spin-wave studies are the use of bulk material and the comparative ease with which attention can be turned from wavelengths measured in hundreds of Å to wavelengths of a few Å. Thus the effects due to dipolar, exchange and other interactions which normally contribute in different degree at different wavelengths and energies can often be singled out. The three principal experimental techniques employ (a) conventional neutron energy analysis to determine the dispersion law, (b) analysis of the angular distribution of scattered intensity, and (c) small-angle scattering. (b) and (c) were evolved especially to deal with the very low cross-sections encountered in this work; they exploit various general aspects of spin-wave dispersion and relate exchange parameters to certain easily detected scattering effects. Other areas of interest in which neutron techniques have much to offer are discussed.

25,377 A METHOD OF MEASURING MAGNETIC PROPERTIES OF FERRO-MAGNETIC AND OTHER SUBSTANCES by A.K. Mukerjee and N.G. Sutradhar (Indian Assoc. Cultivation of Sci., Calcutta); *Indian J. Phys.*, Vol. 37, pp. 616-624, Dec. 1963

In connection with the study of the magnetic properties of Indian minerals, meteorites and various semiconductors which may be Ferro-, Antiferro-, Ferri-, Para- or Dia-magnetic at various temperatures, a horizontal translation type balance has been designed and constructed here. This balance is particularly suitable for measurements at high temperatures as convection disturbances are eliminated by having a horizontal oven. Description and working of the balance are given in the paper.

25,378 MODIFIED SHAPE FACTOR NMR METHOD FOR MEASURING MAGNETIC SUSCEPTIBILITY by L. Mulay and M. Haverbusch (Penn. State U.); *Rev. Sci. Instr.*, Vol. 35, pp. 756-757(L), June 1964

A modification of an NMR technique (*J. Chem. Phys.*, Vol. 37, p. 1891, 1962) is introduced which circumvents the cumbersome adjustment of the Y-gradient of the steady magnetic field. This modification utilizes a reference liquid of known susceptibility in the assembly. Due to large volume diamagnetic susceptibility, the splittings are large and easily measured. From the observed splitting and reference susceptibility, the volume susceptibility of a sample can be calculated. Excellent agreement is obtained for results of hemoglobin solutions with those reported in the literature.

25,379 EFFECT OF AN ENERGY-DEPENDENT RELAXATION TIME ON THE MAGNETIC SUSCEPTIBILITY OF CONDUCTION ELECTRONS by W.B. Muir (Franklin Inst. Lab.); *Bull. Am. Phys. Soc.*, Vol. 9, p. 434(A), Apr. 1964

The anomalous temperature dependence of the amplitude of the de Haas-van Alphen effect, in an alloy exhibiting a resistance minimum, can be explained by assuming that the conduction-electron relaxation time τ was such that $\tau = \tau_0$ everywhere, except where $E_0 - kT \Delta \leq E \leq E_0 + kT \Delta$ when $\tau = 0$, where E_0 is the Fermi energy. The effect of this relaxation time was extended to the nonoscillatory terms in the susceptibility. The effect on the diamagnetism was shown to be negligible. The paramagnetic term χ_p is given by $\chi_p = \chi_0 (1 - T \Delta / 2T + T \Delta / T)$, where χ_0 is the Pauli paramagnetism of a free-electron gas. The 2nd term in the square brackets is due to the gap induced in the "effective density of states" by the energy-dependent relaxation time. The 3rd term is due to the assumption that the electrons displaced from the gap are bound. Typically, $T \Delta$ is of the order of 1°K, which means that the paramagnetic susceptibility would increase by about 10 per cent at 5°K.

Magnetic Susceptibility of Pt - See 25,602

25,380 MAGNETIC PROPERTIES OF NEARLY FREE ELECTRONS. NON-OSCILLATORY MAGNETIC SUSCEPTIBILITY by M.L. Glasser (Battelle Inst.); *Phys. Rev.*, Vol. 134A, pp. A1296-1299, June 1, 1964

The partition function is derived for a gas of electrons in the presence of a weak periodic potential and uniform magnetic field. From it the steady terms

the free energy and the zero-field-zero-temperature total electronic magnetic susceptibility are calculated. The results are applied to the alkali metals. The non-additivity of the paramagnetic and diamagnetic susceptibilities and the inadequacy of the effective mass approximation are discussed.

25,381 EFFECT OF HYDROSTATIC PRESSURE ON THE MAGNETIC SUSCEPTIBILITY OF COPPER-ZINC FERRITES by N.N. Sirota and Yu.M. Khachikyan (Acad. Sci. BSSR); *Soviet Phys.-Solid State*, Vol. 5, pp. 2278-2279, May 1964

The dependence of the magnetic susceptibility of copper-zinc ferrites on the hydrostatic pressure has been investigated. It is found that the pressure produces an essentially reversible effect on the magnetic susceptibility of ferrites, and the magnetic susceptibility is very sensitive to the change in pressure.

25,382 MAGNETIC SUSCEPTIBILITY AND MÖSSBAUER STUDIES OF DIHYDRATED FORMATES by S. A. Friedberg, S. de S. Barros, G. R. Hoy and F. de S. Barros (Carnegie Inst. Tech.); *Prog. 10th Ann. Conf. Magnetism and Magnetic Materials*, Nov. 1964 (to be publ. in *J. Appl. Phys.*)

Several dihydrated formates, including $\text{Ni}(\text{HCOO})_2 \cdot 2\text{H}_2\text{O}$ and $\text{Co}(\text{COO})_2 \cdot 2\text{H}_2\text{O}$ crystallize in a monoclinic structure whose unit cell contains two each of two inequivalent types of metal ions. The temperature variation of the powder susceptibility, χ_p , of the Ni^{++} salt suggests that those ions on one type of site become cooperatively ordered near 15.7°K while the rest remain essentially independent even at 1.3°K. χ_p for the Fe^{++} salt exhibits a huge peak at 3.68°K associated apparently with the long-range ordering of moments on sites of both types. Mössbauer experiments at 300°K on the Fe^{++} salt clearly distinguish ions on the two sites, the ratio of the effective electric field gradients being ~ 5 to 1. The smaller field gradient is assumed to characterize the site (type 1) approximately octahedrally coordinated by oxygens from the formate groups. The Mössbauer spectrum near the transition point differs from those measured at 300°K, 77°K, 20°K, and 4°K.

25,383 LOW-TEMPERATURE MAGNETIC SUSCEPTIBILITIES OF THE HYDRATED NICKEL NITRATES by L. Berger and S. A. Friedberg (Carnegie Inst.); *Prog. 10th Ann. Conf. Magnetism and Magnetic Materials*, Nov. 1964 (to be publ. in *J. Appl. Phys.*)

When measured along the a -axis, the zero-field susceptibility of monoclinic single crystals of the dihydrate $\text{Ni}(\text{NO}_3)_2 \cdot 2\text{H}_2\text{O}$ has a large, sharp, peak at 4.20°K, where it reaches 1.5 CGS/mole. It drops to vanishing values at lower temperatures. The susceptibility in the bc plane reaches only 0.3 CGS/mole, and is nearly isotropic. It drops little below 4.20°K. This behavior is similar to that of FeCl_2 , or FeCO_3 , and suggests the existence of two magnetic sub-lattices, with strong ferromagnetic interactions within each sub-lattice, and weaker antiferromagnetic interactions between one sub-lattice and the other (metamagnetism). A spin Hamiltonian with $S = 1$ and uniaxial one-ion anisotropy gives results in fair agreement with the experimental data, using the molecular field approximation. The best fit corresponds to $g = 2.25$, $D/k = 0.650^\circ\text{K}$, $n_1 = +0.32$ mole/CGS, $n_2 = -2.12$ mole/CGS, where n_1 and n_2 are respectively the anti- and ferromagnetic molecular field constants.

25,384 MAGNETIC SUSCEPTIBILITY CHANGES DURING THE ADSORPTION OF OXYGEN AND CARBON MONOXIDE ON CUPROUS OXIDE by J. D. Cotton and P. J. Fensham (U. Melbourne, Australia); *J. Phys. Chem.*, Vol. 68, pp. 1052-1055, May 1964

Measurements of the magnetic susceptibility of cuprous oxide films on copper powder have been made during the adsorption of oxygen and carbon monoxide. A paramagnetic form of ionized oxygen appears and reaches an equilibrium coverage which is less than a monolayer. No change in susceptibility occurs when carbon monoxide adsorbs on an evacuated surface of the oxide, but on a previously oxygenated surface, carbon monoxide adsorbs and reacts with some of the oxygen and at the same time the paramagnetism is destroyed. The implications of these results for the nature of the absorbed species are discussed.

25,385 MAGNETIC SUSCEPTIBILITIES OF TRANSITION ELEMENTS IN HOST CRYSTALS. Part II. Ni^{2+} IN ZnO AND CdS by W. H. Brumage and C. C. Lin (U. Oklahoma); *Phys. Rev.*, Vol. 134A, pp. A950-957, May 18, 1964

The susceptibilities of Ni^{2+} -doped ZnO and CdS crystals have been measured along and perpendicular to the trigonal crystalline axes from 28-500°K. The susceptibilities of both crystals approach constant values at low temperature and decrease more rapidly with increasing temperature at $T > 60^\circ\text{K}$. An unusually large magnetic anisotropy is observed for $\text{Ni}^{2+}:\text{ZnO}$. The non-Curie behavior can be explained on the basis that the ground state of Ni^{2+} is non-magnetic (A_1) and the temperature-dependent susceptibility arises mainly from the ions in the first two excited states (A_2 and E). By fitting the theoretical susceptibilities to the experimental values, the spin-orbit coupling constant of $\text{Ni}^{2+}:\text{ZnO}$ is obtained as $-175 \pm 25 \text{ cm}^{-1}$ and the trigonal field splitting of the $T_1[{}^3\text{F}]$ state (the lowest T_1 state) as $100 \pm 10 \text{ cm}^{-1}$. The corresponding quantities for $\text{Ni}^{2+}:\text{CdS}$ are $-170 \pm 10 \text{ cm}^{-1}$ and $10 \pm 4 \text{ cm}^{-1}$. In both crystals the A_2 component of the $T_1[{}^3\text{F}]$ state lies below the E level.

25,386 THEORY OF THE ELECTRONIC SUSCEPTIBILITIES OF STOICHIOMETRIC RUTILE (TiO_2) by A. R. Ruffa (Nat'l. Bureau Standards); *Phys. Rev.*, Vol. 133A, pp. A1418-1426, Mar. 2, 1964

A theoretical analysis of the symmetry properties of crystalline rutile is made, leading to the conclusion that the isotropic solution of the local field equations for this material is correct. This conclusion is supported by the experimentally determined isotropic nature of the magnetic susceptibility of rutile. The isotropic solution of the local field equations yields a value for the electronic polarizability of the titanium ion of $\alpha_T = 2.2 \text{ Å}^3$, an order of magnitude greater than the free-ion values usually assigned to the Ti^{4+} ion. This result is supported by a correlation of the ionic sizes as obtained from the electron-density map of rutile determined by X-ray analysis with the polarizabilities. This conclusion is in good quantitative agreement with a theoretical prediction made previously of the effect of the crystalline potential on the cation polarizability. The results of this study give a specific example of a conclusion arrived at in an earlier work to the effect that a cation polarizability in a crystal may be many times its free-ion value.

25,387 STUDY OF MAGNETIC PROPERTIES OF THE ACTINIDE METALS: $\text{Th}_{1-x}\text{U}_x\text{Pd}_3$ by J. H. Wernick, H. J. Williams, D. Chaltiel and R. C. Sherwood (Bell Lab.); *Prog. 10th Ann. Conf. Magnetism and Magnetic Materials*, Nov. 1964 (to be publ. in *J. Appl. Phys.*)

ThPd_3 forms with UPd_3 a continuous series of solid solutions. These two intermetallic compounds have the DO_{24} structure. The magnetic susceptibilities of 11 $\text{Th}_{1-x}\text{U}_x\text{Pd}_3$ alloys ($0 < x < 1$) have been studied at temperatures from 1.4°K to 300°K in fields up to 15 kgauss and at 4.2°K in fields up to 80 kgauss. ThPd_3 is diamagnetic and shows a temperature independent susceptibility, but the addition of U, even in small amounts, gives rise to a strongly temperature dependent paramagnetic susceptibility. The data analyzed in terms of T against $1/\chi - \chi_\infty$ gives a Curie-Weiss behavior in the high temperature region with $3.1 \mu\text{B}$ per U atom at low U concentrations; decreasing to $2.3 \mu\text{B}$ for UPd_3 . A deviation from a Curie law at around 100°K for all U concentrations is attributed to crystal field splitting of the U-5f levels. It is apparent that the U-5f electrons form a localized moment for low U concentrations.

25,388 CRYSTAL GROWTH AND MAGNETIC SUSCEPTIBILITIES OF SAMARIUM AND EUROPIUM GALLIUM GARNETS by M. Schieber and L. Holmes (Harvard U.); *Prog. 10th Ann. Conf. Magnetism and Magnetic Materials*, Nov. 1964 (to be publ. in *J. Appl. Phys.*)

Magnetic susceptibilities at low temperatures of SmGaG and EuGaG single crystals are reported. The crystals were grown by the flux method and the susceptibilities were measured with a Foner-type magnetometer. The susceptibilities of EuGaG and, at high temperatures, of SmGaG follow Van Vleck's formula for free Eu^{3+} and Sm^{3+} , with splittings of 400°K and 1340°K, respectively, between the lowest two energy levels. At low temperatures the susceptibility of SmGaG is smaller than that of the free Sm^{3+} ion and can be represented by the formula

$$\chi_{\text{Sm}} = \frac{\left(\frac{0.0212}{T} + \frac{0.136}{\Delta}\right) + \left(\frac{0.110}{T} - \frac{0.136}{\Delta}\right) e^{-\Delta/T}}{1 + 2 e^{-\Delta/T}}$$

Magnetic Susceptibility of:

$\text{CuCl}_2 \cdot 2\text{H}_2\text{O}$ - See 25,520

$\text{Ce}_2\text{O}_3 \cdot 2.67 \text{ P}_2\text{O}_5$ - See 25,715

Al-V-Tc - See 25,601

25,389 THE THEORY OF MAGNETOELASTIC EFFECTS IN FERROMAGNETISM by W. F. Brown, Jr. (U. Minnesota); *Prog. 10th Ann. Conf. Magnetism and Magnetic Materials*, Nov. 1964 (to be publ. in *J. Appl. Phys.*)

Standard magnetostriction theory constructs a free energy from three terms: the energy of a rigid magnetized body, the energy of a nonmagnetic elastic body, and the volume integral of an interaction energy-density linear in the strains. This procedure is open to three criticisms. First, strains invalidate the magnetization calculation; in particular, the magnetostatic self-energy is strain-dependent. Second, magnetization invalidates the elastic calculation; the stresses (whose definition is somewhat arbitrary) need not be symmetric or even constitute a tensor. Third, small-strain formulas, valid only to the first order of small quantities, are being used in energy terms that must be correct to the second order and that are linear in the strains. Previous studies make possible a rigorous treatment, by finite-strain theory, and a small-strain approximation with assumptions explicitly stated. The mechanical equilibrium equations contain the usual terms plus others; the "form effect" is a special case.

25,390 MEASUREMENT OF THE MAGNETOELASTIC COUPLING CONSTANT IN CYLINDRICAL MAGNETIC FILMS by N. Goldberg (UNIVAC, Sperry Rand); *Prog. 10th Ann. Conf. Magnetism and Magnetic Materials*, Nov. 1964 (to be publ. in *J. Appl. Phys.*)

Two experimental methods of determining the magnetoelastic coupling constant of cylindrical polycrystalline magnetic films of cubic material have been developed, and the results related to the single crystal constants. H. Callen has shown that the magnetoelastic energy of a polycrystalline film is $B \sum a_n \epsilon_{nm}$, where $B = (2B_1 + 3B_2)/5$, B_1 and B_2 are the magnetoelastic coupling constants of the single crystal material, the a 's are the direction cosines of the magnetization direction, and the ϵ 's are the strains. For a film with an easy axis in the circumferential direction (labeled 1), the effect of applying a tension in the axial direction (labeled 2) and introducing a strain, ϵ_{22} , is to change H_k . B is related to this change by $B = \Delta H_k M / 2(1 + \sigma) \epsilon_{22}$, where M is the magnetization and σ is Poisson's ratio of the wire substrate.

25,391 LOSS ASSOCIATED WITH MAGNETOELASTIC WAVES IN YTTRIUM IRON GARNET by W. Strauss (Bell Labs.); *Prog. 10th Ann. Conf. Magnetism and Magnetic Materials*, Nov. 1964 (to be publ. in *J. Appl. Phys.*)

Room temperature magnetoelastic waves have been observed in yttrium iron garnet from L-band to X-band. From insertion loss measurements it is possible to deduce the transmission loss and the loss for conversion from electromagnetism to magnetoelastic energy. Preliminary results show that the transmission loss increases approximately linearly with frequency from about 6 db/ μ sec at 1.6 Gc/sec to about 14 db/ μ sec at 6.1 Gc/sec; results at X-band are incomplete. The smallest observed insertion loss, which includes both transmission and conversion loss, was 15 db for a 1 μ sec delay at 1.6 Gc/sec. These data also yield the lowest conversion loss (~ 4.5 db); nevertheless, experimental conversion loss figures exceed the theoretical values due to Schlömann and Joseph by about an order of magnitude.

25,392 MAGNETOSTRICTION OF POLYCRYSTALLINE AGGREGATES by H.B. Callen and N. Goldberg (UNIVAC, Sperry Rand); *Prog. 10th Ann. Conf. Magnetism and Magnetic Materials*, Nov. 1964 (to be publ. in *J. Appl. Phys.*)

The problem of calculating the magnetostriction constant of a randomly oriented aggregate of cubic microcrystals is reviewed. The magnetostriction constant of the polycrystal λ_s can be written as a linear combination of the constants of the cubic crystallites: $\lambda_s = a_{100} + (1-a) \lambda_{111}$. The almost universally used approximation $a = 2/5$ is a poor one. It is based on the assumption of uniform stress through the aggregate (analogous to the Reuss lower bound for the polycrystalline shear modulus). We have calculated λ_s on the basis of uniform strain (analogous to the Voigt upper bound of the shear modulus), obtaining $a = 2\gamma/(2\gamma+3)$ where $\gamma = 2c_{44}/(c_{11}-c_{12})$ is a measure of the elastic anisotropy of the microcrystals. Empirical data is shown to favor the latter formula over the former. However, both limits lie outside more stringent elastic case (although the magnetostrictive analogues have not been calculated).

25,393 MONITORING THE MAGNETOSTRICTION OF THIN FILMS DURING VACUUM DEPOSITION by C.H. Tolman, P.E. Oberg and S.M. Rubens (UNIVAC); *Rev. Sci. Instr.*, Vol. 35, pp. 738-741, June 1964

A device has been constructed which monitors the magnetostriction of magnetic films prepared by vacuum deposition techniques. The substrate upon which the film is deposited is stressed mechanically during deposition, thereby applying alternate tensile and compressive states of strain to the depositing film. A localized alternating magnetic field is employed as an anisotropy orienting field and is used also to switch the state of magnetization of the film. The substrate is strained at a low repetition rate, and the depositing film is switched magnetically at a high rate. The periodic stress application to the film and the associated strain-induced anisotropy modulate the flux reversal output; the resulting signal is detected by a pickup coil. The phase and amplitude of the modulated signal are a function of the magnetostriction and the corresponding film composition.

25,394 THE FORCED MAGNETOSTRICTION IN NICKEL by J.A.J. Lourens and L. Alberts (U. Orange Free State, South Africa); *Solid State Commun.*, Vol. 2, pp. 141-143, May 1964

A careful determination of the magnetostrictive behavior of a single crystal of nickel in high fields, at room temperature, revealed that the volume magnetostriction is positive and has a value of $0.78 \pm 0.15 \times 10^{-10}$ oe $^{-1}$. The normal magnetostriction constants also show a field dependence viz. $h_1^0 = -0.84 \times 10^{-10}$ oe $^{-1}$ and $h_2^0 = -0.33 \times 10^{-10}$ oe $^{-1}$.

25,395 "FORCED" MAGNETOSTRICTION OF Gd SINGLE CRYSTALS by A.S. Pavlovic and W.E. Coleman (West Virginia U.); *Bull. Am. Phys. Soc.*, Vol. 9, p. 435(A), Apr. 1964

The temperature and magnetic-field dependence of the magnetostriction of single-crystal gadolinium have been measured from 77°-325°K in magnetic fields up to 20 koe. Expressing the magnetostriction as a power series in the a 's, the experimental data can be fitted by the expansion

$$\lambda = R_0 + R_1 \beta_3^2 (R_2 + R_3 \beta_3^2) (1 - a_3^2) + [R_4 a_3 \beta_3 + R_5 (a_1 \beta_1 + a_2 \beta_2)] (a_1 \beta_1 + a_2 \beta_2),$$

where a_j and β_j are the direction cosines of the magnetization and the measurement direction, respectively, with the crystal axes. R_0 and R_1 are related to the strain dependence of the exchange interaction. R_2, \dots, R_5 , the spontaneous magnetostriction constants, are related to the strain dependence of the anisotropy energy. It is found that above 11 koe, R_0 and R_1 may be represented by $A(T)H^n$, where n is determined by a log-log plot.

25,396 POSSIBLE MAGNETIC STRUCTURES IN CRYSTALS HAVING THE SYMMETRY OF HEXAGONAL CLOSEST PACKINGS FOR THE MAGNETIC ATOMS by O.V. Kovalev (Acad. Sci. UkrSSR); *Soviet Phys.-Solid State*, Vol. 5, pp. 2315-2321, May 1964

All the possible cases of space symmetry of the magnetic-moment density function have been found for crystals in which the magnetic atoms form hexagonal close packings. The calculation is based on the irreducible representations of the group D_{6h} and Landau's thermodynamic theory of second-order phase transitions.

25,397 ON THE DETERMINATION OF MAGNETIC ORDERING FROM HIGH-TEMPERATURE EXPANSIONS by T.A. Kaplan, H.E. Stanley, K. Dwight and N. Menyuk (Lincoln Lab.); *Prog. 10th Ann. Conf. Magnetism and Magnetic Materials*, Nov. 1964 (to be publ. in *J. Appl. Phys.*)

A class of functions $\phi(\underline{c}, T) = N^{-1} \sum_{n,m} c_n^* c_m \langle S_n \cdot S_m \rangle_T$, where N is the number of sites, \underline{c} is a set of complex numbers c_n satisfying $\sum_n |c_n|^2 = N$, and

$\langle S_n \cdot S_m \rangle_T$ is the static correlation function between spins at sites R_n and R_m are investigated. It is argued that if the set $\underline{c}^{(0)}$ maximizes $\phi(\underline{c}, T)$, then $\phi(\underline{c}^{(0)}(T), T) \rightarrow \infty$ as $T \rightarrow T_c$, the critical ordering temperature, whereas $\phi(\underline{c}(T), T)$ is bounded as $T \rightarrow T_c$ for $\underline{c}(T)$ orthogonal to $\underline{c}^{(0)}(T)$. Thus a divergence to infinity of $\phi(\underline{c}^{(0)}(T), T)$ indicates the location of T_c , and the form of $\underline{c}^{(0)}(T_c)$ contains information about the type of order. E.g., ferromagnetic ordering is predicted for $c_n^{(0)}(T_c) = 1$, and a sinusoidal or spiral ordering of wave vector k_0 is predicted for $c_n^{(0)}(T_c) = \exp(ik_0 \cdot R_n)$.

25,398 MAGNETIC STRUCTURE OF Cr_2O_3 by L.M. Corliss, J.M. Hastings, R. Nathans and G. Shirane (Brookhaven Lab.); *Prog. 10th Ann. Conf. Magnetism and Magnetic Materials*, Nov. 1964 (to be publ. in *J. Appl. Phys.*)

Pratt and Bailey have recently explained the optical and anomalous magnetic properties of Cr_2O_3 by means of a model consisting of the basic Cr_2O_3 antiferromagnetic structure with moments canted away from the c -axis and forming some kind of a spiral. Our neutron powder diffraction data confirm the original Brockhouse moment configuration but indicate that the c -axis component of the Cr moment is eight percent lower than the spin-only value. This result can be interpreted as supporting the canted model of Pratt and Bailey. A careful search has been made, using single crystals, to find evidence for an ordered or spiraling perpendicular component. Polarization studies establish that there is no magnetic contribution to the fundamental reflections other than that arising from the C -Axis components. A survey of reciprocal space revealed extra spots at forbidden positions, but these could be accounted for semi-quantitatively in terms of double Bragg scattering.

25,399 EFFECT OF OXYGEN ON THE MAGNETIC AND LONG-RANGE ORDERING PROPERTIES OF Ni_3Fe by B.W. Batterman, E.A. Nesbitt, L.D. Fullerton, and A.J. Williams (Bell Labs.); *Prog. 10th Ann. Conf. Magnetism and Magnetic Materials*, Nov. 1964 (to be publ. in *J. Appl. Phys.*)

Previously, it was shown that oxygen is a factor in the magnetic annealing of permalloy (Ni-Fe alloys) and permivar (Ni-Fe-Co alloys). Electron diffraction studies indicated that oxygen caused impurity faults by condensing on the (111) planes of the crystal. An intimate connection between the presence of these impurity faults and the ability to respond to heat treatment in a magnetic field was established. However, the orientation of these faults were not observed to be directly related to the direction of the field heat treatment. In the present work on single crystals of 76% Ni-24%Fe, it was found that those crystals which were heat treated in a purified hydrogen atmosphere did not respond to the magnetic annealing treatments, whereas those that were heat treated in a slightly oxidizing atmosphere did respond.

25,400 EXCHANGE ANISOTROPY AND LONG-RANGE MAGNETIC ORDER IN THE MIXED INTERMETALLIC COMPOUNDS, $(\text{Mn}, \text{Fe})_3\text{Sn}$ by J.S. Kouvel (G.E. Res. Lab.); *Prog. 10th Ann. Conf. Magnetism and Magnetic Materials*, Nov. 1964 (to be publ. in *J. Appl. Phys.*)

Magnetization and neutron diffraction studies have been made of hexagonal (DO_{19}) pseudo-binary compounds of compositions intermediate between Mn_3Sn (which is antiferromagnetic below 420°K) and Fe_3Sn (ferromagnetic below 850°K). For compositions close to $\text{Mn}_{2.5}\text{Fe}_{0.5}\text{Sn}$ (having Curie points as low as 300°K), a complex magnetization-field-temperature behavior was observed, suggestive of a mixed ferromagnetic-antiferromagnetic state of the type previously proposed for Cu-Mn and several other disordered alloys. This hybrid magnetic state was further demonstrated by displaced hysteresis loops produced by cooling to low temperatures in a magnetic field; unidirectional anisotropies over 10^6 erg/g were computed from these loops.

25,401 MAGNETIC STRUCTURE OF Mn_2Ge_3 NEAR THE CURIE POINT by R. Ciszewski (Inst. Nuc. Res., Warsaw); *Phys. Stat. Sol.*, Vol. 4, pp. 199-202, 1964

The magnetic structure of Mn_2Ge_3 near the Curie point has been studied using neutron diffraction. The structure remains unaltered when the samples are cooled below the Curie point.

25,402 MAGNETIC STRUCTURE OF RARE EARTH-COBALT (RCO_2) INTER-METALLIC COMPOUNDS by R.M. Moon and W.C. Koehler (Oak Ridge Lab) and J.J. Farrell (U. Pittsburgh); *Prog. 10th Ann. Conf. Magnetism and Magnetic Materials*, Nov. 1964 (to be publ. in *J. Appl. Phys.*)

Saturation magnetization and neutron diffraction measurements have been performed on cubic Laves phase compounds RCO_2 in which R is Nd, Tb, Ho, and Er. The low temperature patterns are of the ferromagnetic or ferrimagnetic type, with large magnetic intensities superimposed on the nuclear peaks. For the compounds of Tb, Ho and Er, the rare-earth atoms show the full moment expected for the free tri-positive ion and the cobalt moment is about one Bohr magneton. The rare-earth moments are coupled parallel to each other, but anti-parallel to all the cobalt moments. For $NdCo_2$, the observed Nd moment of 2.6 ± 0.2 Bohr magnetons is smaller than the free ion value of 3.27 Bohr magnetons, and it is coupled parallel to the cobalt moment of 0.8 ± 0.2 Bohr magnetons. In the Nd ion, the spin is opposite to the moment ($J = L - S$), while for the heavier rare earths the spin is parallel to the total moment ($J = L + S$).

25,403 MAGNETIC ORDERING IN DILUTE SOLID SOLUTIONS OF IRON IN GOLD by R.J. Borg, R. Booth, C.E. Violet (Lawrence Rad. Lab.); *Phys. Rev. Lett.*, Vol. 11, pp. 464-467 (L), Nov. 15, 1963

Dilute solid solution foils of Fe in Au have been studied by means of the Mössbauer effect at low temperatures. The preliminary magnetization measurements show that ferromagnetic behavior is present. Four Au foils containing .84 to 11.5 atom % Fe were used; temperatures ranged from 80 to 2.2°K. At low temperatures the six-line magnetic hyperfine Mössbauer spectrum was observed, demonstrating magnetic ordering. The dependence of Curie temperature as a function of Fe concentration is discussed and a mechanism of indirect exchange that must produce the magnetic ordering is described.

25,404 LOW-TEMPERATURE MAGNETIC TRANSITIONS IN DILUTE Au-BASED ALLOYS WITH Cr, Mn, AND Fe by O.S. Lutes and J.L. Schmit (Honeywell Res. Center); *Phys. Rev.*, Vol. 134 A, pp. A 676-683, May 4, 1964

The low-temperature magnetic behavior of gold-based solid solutions containing transition metals in dilute concentration has been studied. Of particular interest are Au-Cr, Au-Mn and Au-Fe, for which solid solutions of higher concentration have been found by other workers to undergo antiferromagnetic (Cr) and ferromagnetic (Mn and Fe) transitions. The present results show that for alloys of about 1 at. % there occur low-temperature magnetic transitions which are similar for all three solutes. The main features of the transitions, as in dilute Cu-Mn alloys, are a susceptibility maximum and, below the temperature of the maximum, a saturable remanent magnetic moment which increases with decreasing temperature in a characteristic manner. The temperature of the maximum increases nearly in proportion to concentration and also depends on the identity of the solute, being about 12, 4, and 8°K/at. %, respectively, for Cr, Mn, and Fe.

Magnetic:

Structure of:

$MnSO_4$ - See 25,541

Fe_2As - See 25,540

Transitions - See 25,170

25,405 MECHANISM OF THE FERRIMAGNETIC TO ANTIFERROMAGNETIC TRANSITION IN $Mn_{2-x}Cr_xSb$ by H.S. Jarrett (du Pont); *Phys. Rev.*, Vol. 134A, pp. A 942-950, May 18, 1964

The mechanism of the first-order ferrimagnetic to antiferromagnetic transition (exchange inversion) in $Mn_{2-x}Cr_xSb$, $x < 0.41$, was investigated by exchange magnetostriction. A second-order term has been included in the strain energy which gives an effective elastic constant dependent on magnetization and magnetic ordering. It also introduces a discontinuous change in the magnetization at the transition and hence a contribution to the entropy change in addition to that caused by the change of lattice dimension. For $Mn_{2-x}Cr_xSb$, the effect of this term is small but necessary to obtain the qualitative behavior of the discontinuous change in lattice dimension and the shift in the Curie temperature with composition.

25,406 MAGNETIC STRUCTURE VERSUS ELECTRON NUMBER FOR SOME RARE EARTH INTERMETALLIC COMPOUNDS by J.W. Cable, W.C. Koehler and H.R. Child (Oak Ridge Lab.); *Prog. 10th Ann. Conf. Magnetism and Magnetic Materials*, Nov. 1964 (to be publ. in *J. Appl. Phys.*)

Neutron diffraction measurements were made on a series of rare earth compounds in the Tb (Pd, Ag) and Tb (Ag, In) systems. Most of these compounds exhibit the CsCl type of crystal structure and, for these, magnetic structure determinations were made in order to relate the type of magnetic structure to the number of valence electrons. Two types of antiferromagnetic structures were observed: the $(\pi\pi\pi)$ type consisting of an antiparallel array of ferromagnetic (110) planes of moments, and the $(\pi\pi\sigma)$ type with ferromagnetic (100) planes of moments alternating in direction. On the basis of 0, 1, 3 and 3 valence electrons for Pd, Ag, In and Tb, respectively, the $(\pi\pi\sigma)$ structure is found in the region of 3.5 to 4 valence electrons per unit cell and the $(\pi\pi\sigma)$ structure in the region of 5 valence electrons per unit cell.

25,407 INVESTIGATION OF THE MAGNETIC STRUCTURE OF $ErMn_2$, $TmMn_2$, $TbNi_2$ BY NEUTRON DIFFRACTION by G.P. Felcher, L.M. Corliss and J.M. Hastings (Brookhaven Lab.); *Prog. 10th Ann. Conf. Magnetism and Magnetic Materials*, Nov. 1964 (to be publ. in *J. Appl. Phys.*)

Magnetic measurements by H.J. Williams et al. ($ErMn_2$ and $TmMn_2$), and Wallace ($TbNi_2$) have shown that these compounds are magnetically ordered at low temperatures with a moment per formula unit lower than that of the free rare-earth ion. Neutron diffraction powder patterns have been used to determine the actual magnetic structure. $ErMn_2$ and $TmMn_2$ crystallize with the hexagonal Laves phase structure (C-14 type). $ErMn_2$ is ferromagnetic, with a moment of 7.79 μ_B per Er atom at 4.2°K aligned along the c-axis. No detectable moment on Mn is observed. $TmMn_2$ is almost completely ferromagnetic, with a moment of 4.95 μ_B per Tm atom at 2.1°K aligned along the c-axis, and essentially zero moment for Mn. A faint additional line at low angle seems to indicate a weak antiferromagnetic contribution. $TbNi_2$ crystallizes with the cubic Laves phase structure (C-15 type). At 4.2°K, strong ferromagnetic lines as well as weak additional peaks appear in the diffraction pattern.

25,408 THE MAGNETIC PROPERTIES OF RARE EARTH METALS AND ALLOYS by W. C. Koehler (Oak Ridge Lab.); *Prog. 10th Ann. Conf. Magnetism and Magnetic Materials*, Nov. 1964 (to be publ. in *J. Appl. Phys.*)

A review of neutron diffraction studies of the magnetic properties of rare earth metals and alloys is presented. For each of the pure metals, Tb, Dy, Ho, Er, and Tm, a transition at a temperature T_N to an oscillatory antiferromagnetic configuration (helical or linear oscillator type) is observed. At lower temperatures, further transitions to ferromagnetic, ferromagnetic spiral, or antiphase domain type configurations are observed. For Gd, only the ferromagnetic configurations at low temperatures approach the values expected from the corresponding free tripositive ions. In the first half of the series, only Nd has been studied by single crystal methods, but Ce, Pr, and Eu have now been investigated with polycrystalline samples. The data for Ce are complicated by the existence of several allotropic forms, but a complex antiferromagnetic structure appears to be associated with the hexagonal form at low temperatures. For Nd and Pr, oscillatory antiferromagnetic configurations are observed at very low temperatures.

Magnetic Moment of YAlG:Bi - See 24,969

25,409 INTERNAL FIELDS AT IRON IN FePd ALLOYS by G. Bemski and X. A. da Silva (Cen. Brasil. Pesq. Fis., Rio de Janeiro); *J. Appl. Phys.*, Vol. 35, March 1964

Mössbauer absorption of gamma rays by Fe nuclei in FePd alloys indicates that the internal field at iron is about the same for iron concentrations between 4 and 100 per cent. This field is identical to that in metallic iron. A temperature-dependent isomeric shift has also been observed for temperatures between 120° and 350°K.

25,410 MAGNETIC MOMENTS AND UNPAIRED SPIN DENSITIES IN THE Fe-Rh ALLOYS by G. Shirane, R. Nathans (Brookhaven Lab.) and C.W. Chen (Westinghouse Res. Lab.); *Phys. Rev.*, Vol. 134A, pp. A1547-1553, June 15, 1964

The distribution of magnetic moments in the Fe-Rh system has been investigated by the neutron diffraction technique in the composition range between 35 and 50 at. % Rh. These alloys have chemical order of CsCl type; the body-corner positions are occupied by Fe I atoms and the body centers by Rh and Fe II atoms. The magnetic moments in ferromagnetic alloys containing 35, 40 and 48% Rh are $\mu_{FeI} = 3.1 \mu_B$, $\mu_{FeII} = 2.5 \mu_B$, and $\mu_{Rh} = 1.0 \mu_B$ at 25°C. The moment of the Fe I atom in the 50% Rh alloy, which is antiferromagnetic at room temperature, increases to 3.3 μ_B . A detailed study of the unpaired spin density distribution in the 48% Rh alloy was made by the polarized beam technique. While the Fe I atom has a nearly spherical density distribution, that of the Rh atom shows a strong tendency towards e_g symmetry. The coherent nuclear scattering amplitude of Rh was determined to be $0.585 \pm 0.005 \times 10^{-12}$ cm.

25,411 MAGNETIZATION OF THE RARE EARTH MANGANESE COMPOUNDS R_2Mn_{23} by B.F. DeSavage, R.M. Bozorth and F.E. Wang (U.S. Naval Ord. Lab.); Prog. 10th Ann. Conf. Magnetism and Magnetic Materials, Nov. 1964 (to be publ. in *J. Appl. Phys.*)

Compounds of the type R_2Mn_{23} , where R is a rare-earth metal, have been shown by Wang et al to be of the fcc ($Fm\bar{3}m$) Th_2Mn_{23} structure with an octahedron of the heavy elements surrounded by 50 manganese atoms on the faces, edges, and corners of the octahedron. Determination of the saturation moments of these compounds of Mn with nine of the rare-earths (Sm to Lu) shows that with one exception the rare-earths and the manganese are antiparallel; only in the gadolinium compound is there complete ferromagnetic coupling. From the moment of Lu_2Mn_{23} one derives the moment per Mn atom of $0.4 \mu_B$, in agreement with previous work. The moments of the other compounds agree closely with those expected for this moment of 0.4 for Mn and the normal moments of gJ for the rare-earth atoms. The results of this system may be contrasted with those for the garnets and the R_2Ir_{17} type compounds in that some of the moments of the rare-earths in both of the latter two series deviate considerably from gJ.

25,412 STUDIES ON ORTHOFERRITES AT THE WEIZMANN INSTITUTE OF SCIENCE by D. Treves (Weizmann Inst. Sci.); Prog. 10th Ann. Conf. Magnetism and Magnetic Materials, Nov. 1964 (to be publ. in *J. Appl. Phys.*)

The Curie point, lattice constants, sublattice magnetization, spontaneous magnetic moment, susceptibility and the nonlinear susceptibility has been measured on the compounds $RFeO_3$ with R Yttrium or a rare earth. The main conclusions from these measurements are: 1) The rare earth ions' contribution to the magnetic properties of these materials at relatively high temperature is mainly through the geometrical effect of ionic radii; 2) the ratio of iron sublattice to the weak ferromagnetic moment shows that the canting angle is temperature dependent; 3) between liquid air temperature and the Curie point, the rare earth ions behave like a paramagnet in an effective magnetic field of the iron ions. This field is of the order of a few thousand gauss of either sign; 4) from measurements of the spontaneous moment, the susceptibility and the nonlinear dependence of the magnetization on applied fields, it appears that the antisymmetric exchange interaction is responsible for the weak ferromagnetism of these materials.

25,413 MAGNETIC PROPERTIES OF CuF_2 by R.J. Joenk and R.M. Bozorth (IBM Watson Res. Ctr.); Prog. 10th Ann. Conf. Magnetism and Magnetic Materials, Nov. 1964 (to be publ. in *J. Appl. Phys.*)

The susceptibility of a pressed powder sample of monoclinic CuF_2 has been measured from 1.3 to 293°K for $H_0 = 10$ and 20 koe, and the moment at 4.2°K in fields up to 25 koe. $\chi(T)$ indicates an AFM transition at about 70°K. After choosing a correction for temperature independent susceptibility which forces the Curie constant to agree with $J = \frac{1}{2}$ and $g \approx 2.03$ as determined by paramagnetic resonance, Θ was found to equal $-190^\circ K$. T_N and Θ are consistent with magnetic ordering of the first kind and indicate AFM exchange interactions J_1 (corner-*bc*) $-32^\circ K$ and $J_2 = -20^\circ K$. At low T , χ was also corrected for paramagnetic impurities ($\leq 1\%$). Weak ferromagnetism of anisotropic exchange origin is expected on grounds of symmetry proportional to the monoclinic distortion from tetragonal structure. The measured ferromagnetic moment is small, $\mu_0 \leq 1$ emu/mole, corresponding to a canting angle $\phi \leq 0.01^\circ$.

25,414 AN INTERPRETATION OF THE MAGNETIC PROPERTIES OF $LaCoO_3$ by C.S. Naiman, R. Gilmore (Mithras) and A. Linz (MIT); Prog. 10th Ann. Conf. Magnetism and Magnetic Materials, Nov. 1964 (to be publ. in *J. Appl. Phys.*)

Susceptibility measurements have been carried out on single crystal $LaCoO_3$ in the temperature range of 4.2°K to 300°K. An effective magnetic moment squared that agrees with Heikes et al at 300°K, but which falls more rapidly with decreasing temperature to a value of about 2.7 at 25°K and 0.9 at 4.2°K was found. Paramagnetic resonance measurements at 4.2°K, 77°K, and 300°K have ruled out the presence of modest quantities of paramagnetic cobalt, leaving only the possibilities of diamagnetic or highly concentrated paramagnetic Co^{3+} . (Large concentrations of other cobalt valencies are ruled out for chemical reasons). Using a model found successful by Goodenough for $(La_{1-x}Sr_x)CoO_{3-\lambda}$, we assume that Co^{3+} is near the cross-over point, with the 1A_1 state lowest. A calculation including spin orbit effects but assuming cubic symmetry for the 300°K to 4.2°K range, gives essentially a linear variation for the energy difference between the 1A_1 and center of gravity of the 5T_2 states.

25,415 MAGNETIC CHARACTERISTICS OF GADOLINIUM, PRASEODYMIUM, AND THULIUM NITRIDES by D.P. Schumacher and W.E. Wallace (U. Pittsburgh); Prog. 10th Ann. Conf. Magnetism and Magnetic Materials, Nov. 1964 (to be publ. in *J. Appl. Phys.*)

Bulk magnetic measurements were made on GdN, PrN, and TmN over the range 4.2 to 300°K. GdN is ferromagnetic with $T_c = 69^\circ K$ and a saturation moment of $7.03 \mu_B$ ($gJ = 7.00$). Results obtained in the paramagnetic region give: for GdN $\mu_{eff} = 7.86 \mu_B$ ($g \sqrt{J(J+1)} = 7.94$), $\theta_p = 75^\circ K$; for PrN $3.57 \mu_B$ (3.58), $-11^\circ K$; for TmN $7.32 \mu_B$ (7.56), $-21^\circ K$. These nitrides all occur in the NaCl structure. Under the influence of the cubic crystal field the $2J+1 - fold$

degenerate multiplet is decomposed so that Pr and Tm have singlet (non-magnetic) ground states. Thus if the crystal field splitting exceeds the exchange interaction, no cooperative magnetic phase is expected at low temperatures. The measurements indicate this to be the case for TmN, supporting neutron diffraction work by Child et al, and apparently this is also true for PrN. The possibility cannot be excluded, however, that PrN is a weak ferromagnet.

25,416 EXCHANGE INVERSION IN TERNARY MODIFICATIONS OF IRON RHOIDIUM by P.H.L. Walter (du Pont); *J. Appl. Phys.*, Vol. 35, pp. 938-939, Mar. 1964

The effect of various transition metal modifiers on the magnetic properties of iron-rhodium alloys was studied. The exchange inversion temperature T_S , residual magnetization, and maximum magnetization are dependent on the nature of the modifier and on the degree of substitution. As little as 2 at.% of Co, Ni, Cu, Nb, Mo, Ta, or W eliminates the exchange inversion transition, while addition of Ru, Os, Ir, or Pt increases T_S over that for the comparable binary alloy, and addition of Pd, V, Mn, or Au decreases T_S . For the series of alloys $FeRhIr_x$, T_S increases as x increases from 0-0.25; for the series $FeRhPd_x$, T_S decreases as x increases. The range of composition over which exchange inversion is observed is quite narrow.

25,417 DILUTE FERROMAGNETIC ALLOYS by J. Kanamori (Serv. Phys. Sol., Orsay (S et O), France); Prog. 10th Ann. Conf. Magnetism and Magnetic Materials, Nov. 1964 (to be publ. in *J. Appl. Phys.*)

Theoretical discussions about the magnetic and electric properties of dilute alloys of Ni, Co, and Fe with nonmagnetic elements such as Cu, Zn, Al and transition elements such as Cr, V as solute are presented. It is well known that nonmagnetic atoms cause in Ni and Co alloys a decrease of magnetization whose magnitude per solute atom is related closely to the valence of solute. On the other hand, Fe alloys do not show such a dependence on the valence of impurity atom. A microscopic picture of the electronic distribution around an impurity atom in these alloys will be discussed on the basis of a model Hamiltonian in which the mixing of the valence orbitals of the impurity atom with the d and s bands of host metal as well as the perturbing potential energies on the impurity atom of the d and s bands is included. The calculation is an extension of Anderson and Wolff's treatments of impurity state. A reasonable interpretation of various features of the phenomena is given by this calculation.

Magnetic Properties of $GdCoO_3$ - See 24, 974

FERRO- AND FERRIMAGNETISM

25,418 A PROOF THAT THE FREE ENERGY OF A SPIN SYSTEM IS EXTENSIVE by R.B. Griffiths (U. Calif., La Jolla); Cont. Nonr2216 11, 29 pp., Jan. 1, 1964; U.S. Gov. Res. Rep., Vol. 39, p. 134(A), May 5, 1964 AD 429 544 OTS \$3.60

The free energy obtained from the canonical partition function for a finite spin system possesses a certain convexity property, of which theorems by Peierls and Bogoliubov are particular applications. This property is used in proving the following result: the free energy of a spin system in a regular lattice, divided by the number of spins, converges to a definite limit as the system becomes infinite (in such a way that the surface to volume ratio goes to zero). The limit is not influenced by certain common types of boundary conditions. A similar result, but with convergence understood in a weaker sense, holds for derivatives of the free energy such as entropy, magnetization, and specific heat. In the proof it is necessary to assume that the Hamiltonian has the translational symmetry of the spin system, and that long range interactions decrease sufficiently rapidly with the distance r between spins.

25,419 SPIN-WAVE THEORY OF MAGNETOPLUMBITE FERRITES by L. Kowalewski (Adam Mickiewicz U., Poznań); *Acta Phys. Polonica*, Vol. 24, pp. 583-589, Nov. 1963

The theory of spin waves in ferrites having the magnetoplumbite structure is presented. The approximation of the magnetic quasisaturation is used. The spin-wave spectrum consists of five branches. The dispersion formulas have great uniaxial anisotropy.

25,420 REMARKS ON THE OGUCHI TRANSFORMATION by R.A. Tahir-Kheli and H.B. Callen (U. Penn.); Cont. Nonr551 36, 8 pp., May 1963; U.S. Gov. Res. Rep., Vol. 39, p. 149(A), May 5, 1964 AD 430 972 OTS \$1.10

It is shown that the Oguchi transformation in the theory of ferromagnetism is a low temperature spin wave approximation, the validity of which depends on the implicit assumption that the kinematical interaction can be ignored. This limitation has the consequence that the theory of Oguchi and Honma, if accepted at higher temperatures, predicts an infinite Curie temperature.

25,421 RENORMALIZED SPIN WAVES IN FERRIMAGNETS by R.E. Mills, R.P. Kenan and F.J. Milford (Battelle); *Prog. 10th Ann. Conf. Magnetism and Magnetic Materials*, Nov. 1964 (to be publ. in *J. Appl. Phys.*)

The two-time Green's function theories of Heisenberg ferromagnets have been generalized to treat ferrimagnets with arbitrary numbers of sublattices. Anti-ferromagnets are clearly included as special cases. The generalized theory appears to be capable of dealing with non-nearest-neighbor exchange interactions and anisotropy fields without further modification, but no numerical results are available for such cases. The Tyablikov method of decoupling has been followed. A theorem due to Callen has been used to simplify the theory and as an aid to obtaining a physical interpretation of the results. The renormalized sublattice magnetizations are expressed as the solutions to a coupled set of implicit equations. A second such set of equations determines a common Curie temperature for the sublattices of the ferrimagnet. Either set of equations can be solved numerically by iterative procedures which yield self-consistent solutions.

25,422 INTRINSIC LIFETIME OF SPIN WAVES IN AN IDEAL METAL by E.D. Thompson (Case Inst. Tech.); *Prog. 10th Ann. Conf. Magnetism and Magnetic Materials*, Nov. 1964 (to be publ. in *J. Appl. Phys.*)

The spin wave state, being an eigenstate of the approximate Hamiltonian only within the adiabatic approximation, has a finite lifetime in a metal. This lifetime is here calculated within the molecular field model (local and non-local fields) for long wavelength spin waves and is shown to be negligible. The dominant process in determining this lifetime is the forward scattering of the d-electrons out of the Fermi sea with the consequent reduction in the momentum and energy of the spin wave. The Pauli exclusion principle is responsible for this long lifetime by restricting this scattering process to those d-electrons with energies near the Fermi surface. The intrinsic lifetime is found to be proportional to the sixth power of the wavelength of the spin wave.

25,423 BOUND STATES IN THE HEISENBERG FERROMAGNET by J. Hanus (MIT); *Phys. Rev. Lett.*, Vol. 11, pp. 336-338(L), Oct. 1, 1963

The existence and some consequences of bound states in a Heisenberg ferromagnet are shown theoretically. The interactions of spin waves are studied following a method developed by Van Kramendonk. A complete solution to the problem of two reverse spins in a crystal lattice of otherwise parallel atomic spins has been found. A hard-core interaction has been introduced in the Hamiltonian to prevent these reversed spins from being localized on the same atomic site. As in the linear chain, for some eigenstates of this system, it is found that the two reversed spins are bound together in a stable complex which travels through the crystal.

25,424 SPIN WAVE-SPIN WAVE SCATTERING IN A HEISENBERG FERROMAGNET by R.G. Boyd and J. Callaway (U. Calif.); *Phys. Rev. Lett.*, Vol. 12, pp. 540-541(L), May 11, 1964

An exact expression for the scattering cross section of two spin waves in a simple cubic Heisenberg ferromagnet is derived. The expression is obtained by solving the Lippmann-Schwinger equation by the scattering method previously described by Callaway. The total cross section, in the long-wavelength limits, $\sigma \approx (\vec{k} \cdot \vec{k}')^2 / 8\pi S^2$, where S is the spin, and \vec{k} and \vec{k}' are spin-wave vectors. This result agrees with that obtained by Dyson.

25,425 SCATTERING OF SPIN WAVES BY MAGNETIC DEFECTS by J. Callaway and R. Boyd (U. Calif., Riverside); *Phys. Rev.*, Vol. 134A, pp. A1655-1662, June 15, 1964

A previous calculation of the scattering amplitude for the scattering of spin waves by magnetic defects in a simple cubic lattice is simplified and extended to body-centered and face-centered cubic lattices. Expressions are given for the mean free path, and the thermal resistivity due to defect scattering is calculated by a method which takes some account of spin-wave interactions.

25,426 SPIN WAVE SCATTERING OF POLARIZED NEUTRONS FROM Co AND Ni by T. Riste, G. Shirane (Brookhaven Lab.), H. Alperin and S.J. Pickart (U.S. Naval Ord. Lab.); *Prog. 10th Ann. Conf. Magnetism and Magnetic Materials*, Nov. 1964 (to be publ. in *J. Appl. Phys.*)

The polarized neutron technique provides a very powerful method of distinguishing ferromagnetic spin wave scattering from other elastic and inelastic intensity components. Following the qualitative measurements by Ferguson and Saenz, this technique was successfully applied to magnetite by Samuelsen, Riste, and Steinsvoll. The measurements have been extended to cobalt and nickel. The cobalt crystal used is in the face-centered cubic phase with a composition of $\text{Co}_{0.92}\text{Fe}_{0.08}$. In determination of the magnon dispersion relations, the diffraction method in which the size of the scattering surface was measured as a function of crystal offset from the Bragg angle is employed. In nickel only the exchange integral and the general shape of the dispersion curve is presented.

25,427 STANDING SPIN WAVE MODE (SSWM) SPECTRA IN PERMALLOY FILMS PREPARED AT PRESSURES NEAR 10^{-7} TORR by M. Nisenoff and R. W. Terhune (Sci. Lab., Ford Motor); *Prog. 10th Ann. Conf. Magnetism and Magnetic Materials*, Nov. 1964 (to be publ. in *J. Appl. Phys.*)

The field spacings between the SSWM in Permalloy films prepared in an ion diffusion pump vacuum system at pressures near 10^{-7} Torr obey the predicted quadratic dependence on order number (l) for the magnetic field in the plane of the film (H_{\parallel}) as well as normal to the plane of the film (H_{\perp}). The spacings and intensities of the modes suggest that, with H_{\parallel} , the modes are nearly unpinned while, with H_{\perp} , the modes are pinned with an effective film thickness $\sim 140\text{Å}$ greater than for H_{\parallel} . At some specific intermediate angle, the modes appear to be completely unpinned. This type of pinning can be explained qualitatively by assuming that the film is uniformly magnetized throughout the interior, but that there are surface layers five to ten lattice spacings thick which exhibit lower values of M and A/M than the bulk, where M is the saturation magnetization and A is the exchange constant.

25,428 SPIN-WAVE SPECTRA IN THIN MAGNETIC FILMS by T. D. Rossing, R. Thern, D. Larson, and R. Heppner (St. Olaf Col.); *Prog. 10th Ann. Conf. Magnetism and Magnetic Materials*, Nov. 1964 (to be publ. in *J. Appl. Phys.*)

Spin-wave spectra have been studied in Permalloy films of varying thickness. In some of the films, the low-lying spin peaks exhibit the uniform spacing and slowly decreasing intensities associated with a parabolic variation in magnetization through the film, whereas the higher modes show the quadratic spacing and rapidly decreasing intensities associated with spin-pinning at the surface. The transition between these two regions depends on the amplitude of the variation in magnetization and the film thickness, or, in other words, the depth and width of the parabolic "well." When the angle of the applied field is changed with respect to the film, the lowest modes are virtually unchanged, but the transition moves to a lower mode number. This is probably because the parabolic well appears shallower as the field approaches the "critical" angle at which the resonance frequency is independent on the magnetization.

25,429 ANALYSIS OF HIGH-POWER EFFECTS IN FERRIMAGNETICS FROM THE POINT OF VIEW OF ENERGY TRANSFER. Part I. FIRST-ORDER INSTABILITIES by G. Kemanis (Hughes Aircraft) and S. Wang (U. Calif., Berkeley); *J. Appl. Phys.*, Vol. 35, pp. 1465-1470, May 1964

Spin-wave instabilities in ferrimagnetics in the past have usually been analyzed by considering the perturbed equations of motion of the normal variables of the spin system. The spin-wave behavior is analyzed without the use of the normal mode development. The properties of the k th spin-wave — its energy and the phases and amplitudes of its transverse magnetization components — are derived using real variables exclusively. Then the criteria for all the first-order instability thresholds are derived from the power balance of the spin system. The physical processes which lead to spin-wave instabilities are discussed.

25,430 THE SPIN ARRANGEMENT OF THE HIGH TEMPERATURE MAGNETIC PHASE IN CHROMIUM by P.J. Brown, C.R. Wilkinson (Cavendish Lab.), J. B. Forsyth and R. Nathans (AERE, Harwell); *Prog. 10th Ann. Conf. Magnetism and Magnetic Materials*, Nov. 1964 (to be publ. in *J. Appl. Phys.*)

Experiments with unpolarized neutrons on random domain single crystals are unable to distinguish between a simple spiral model and a transverse sinusoidal spin arrangement for the Cr magnetic structure above the low temperature transitions. Using a Cr single crystal which had been cooled through the Néel point in a strong magnetic field, the polarization of the diffracted beams was analyzed from the $\{100\}$ satellites on the three-crystal polarized beam spectrometer. The polarizations of the reflected beam in the various satellites predicted by the simple spiral model, independent of domain distribution, were not observed. To the contrary observations are consistent with each domain containing two transverse sinusoidal spin arrangements with unequal populations each oriented along a $\{100\}$ direction.

25,431 A STUDY OF STANDING SPIN WAVES IN THIN PERMALLOY FILMS AT RADIO AND ULTRAHIGH FREQUENCIES by T.E. Hasty (Texas Instr.); *J. Appl. Phys.*, Vol. 35, pp. 1486-1493, May 1964

Standing spin waves in thin Permalloy films in the frequency range 50-4200 Mc/sec have been studied with a dc magnetic field applied perpendicular to the film surface. The purpose of the experiment was to study the behavior of the spin-wave absorption lines at fields just above saturation and to investigate the possibility of exciting standing spin waves at fields below saturation. It proved possible to excite one spin-wave line when the field was less than that required for saturation. Comparison of the field separating this line from the main absorption line with the separation of the spin-wave lines when the dc field is above saturation indicates that this line is the $N=1$ line. Further study based on the concept of dynamic pinning demonstrates that the surface spins are not pinned in this unsaturated region and that this $N=1$ line is excited only by an inhomogeneous field. An expression for the rf susceptibility and the general boundary conditions are derived in the Appendix.

25,432 MAGNETIC PROPERTIES OF MnCr_2S_4 by N. Menyuk, K. Dwight (Lincoln Lab.) and A. Wold (Brown U.); Prog. 10th Ann. Conf. Magnetism and Magnetic Materials, Nov. 1964 (to be publ. in J. Appl. Phys.)

The neutron diffraction pattern of MnCr_2S_4 at room temperature shows it to be a normal cubic spinel. The magnetization of this material was measured from 4.2°K through the Curie temperature. It was then determined, on the basis of a molecular field calculation, that the shape of the magnetization curve requires a large and ferromagnetic B-B interaction such that $J_{BB}/J_{AB} \sim -4$. This is in general accord with Lotgering's conclusion, which was based on paramagnetic susceptibility data, and indicates that the material should have a simple Néel (collinear) spin configuration. This expectation was confirmed by a 4.2°K neutron diffraction investigation which also established the cation moments to be $3\mu_B$ per chromium ion and $4.7\mu_B$ per manganese ion, in agreement with the measured net magnetization of $1.3\mu_B$. Furthermore, the 4.2°K diffraction pattern clearly indicates that the reduction of the manganese moment below its spin-only value cannot be attributed to A-site canting.

25,433 THE SPIN-WAVE THEORY OF MnF_2 IN THE RANDOM PHASE APPROXIMATION by H.R. Carleton (Sperry Rand Res. Ctr.), R. Brout (Free U., Brussels), and R. Stinchcombe (Clarendon Lab.); Prog. 10th Ann. Conf. Magnetism and Magnetic Materials, Nov. 1964 (To be Publ. in J. Appl. Phys.)

In order to extend the validity of ferromagnetic spin-wave theory to higher temperature, Englert used the Random Phase Approximation (RPA), in which the spin-wave interactions are represented by a model in which the number of spin-wave excitations are related self-consistently to the magnetization through a sum rule. A theoretical study of the Heisenberg antiferromagnet in the linked-cluster expansion indicates that a similar relation exists between the sublattice magnetization and the spin-wave spectrum. The validity of this approximation is examined by calculating the dispersion relation for antiferromagnetic spin-waves, including corrections for anisotropy and next-neighbor interactions.

25,434 EFFECT OF CORRELATION ON THE FERROMAGNETISM OF TRANSITION METALS by M. C. Gutzwiller (IBM Zurich Res. Lab.); Phys. Rev., Vol. 134, No. 4A, pp. A923-941, May 18, 1964

The wave function for the electrons is investigated when a set of narrow bands (valence states) has its energies within a wide band (conduction states). The valence states are linear combinations of localized states which are attached to each lattice site. The intra-atomic Coulomb and exchange integrals for the localized states are much larger than the bandwidths of the valence states. Some of the narrow bands are neither completely empty nor completely filled. The wave function is therefore expected to be correlated, because it is disadvantageous for the electrons to crowd into the same lattice site, or take up some configuration contrary to Hund's rule. This correlation is important in transition metals, where it is considered to be the cause of ferromagnetism. The correlated wave function is obtained by applying to the uncorrelated antisymmetrized product of Bloch functions an operator which provides each configuration of localized valence states with an appropriate amplitude and phase factor.

Ferromagnetic EuS - See 25,726

25,435 THE EFFECTS OF RADIATION ON FERRITES by S. Taimuty and J. Mills (Stanford Res. Instr.); Commun. and Electronics, No. 66, pp. 305-308, May 1963

The effects of reactor exposures in the range of 10^{16} - 10^{18} fast neutrons per square centimeter (cm^2) on the magnetic properties of 16 polycrystalline ferrites and garnets are presented. Measured properties included coercive force, remanence, saturation induction, complex permeability, and FMR (ferromagnetic resonance) linewidth. It was found that the hysteresis properties and FMR linewidth were slightly affected by exposures of 10^{18} neutrons per cm^2 . Complex permeability was effected by exposures as small as 10^{16} neutrons per cm^2 . The magnitudes of the observed changes were small and it is likely that the operation of devices incorporating these materials will not be significantly affected by such changes.

25,436 INVESTIGATION OF THE EFFECT OF O_2 , N_2 AND H_2O ON NICKEL THIN FILMS by J.F. Freedman (IBM Watson Res. Ctr.); Prog. 10th Ann. Conf. Magnetism and Magnetic Materials, Nov. 1964 (To be Publ. in J. Appl. Phys.)

The role of impurities adsorbed during the evaporation process was investigated for nickel films grown on room temperature glass substrates. The effects of oxygen, nitrogen and water vapor have been determined by bleeding controlled amounts of those gases into the evaporation chamber. Ferromagnetic resonance, torque magnetometer and vibrating sample magnetometer measurements were made on the samples. A change in pressure from 10^{-10} to 10^{-7} Torr oxygen caused a marked shift in the resonance field and the perpendicular anisotropy. This shift could be accounted for by an increase in internal stress from 5×10^9 dynes/ cm^2 at 10^{-10} Torr to 2×10^{10} dynes/ cm^2 at 10^{-7} Torr. The wall motion coercive force also increased with increasing pressure, ranging from 50 to greater than 200 oe. Samples made in pressures as high as 1×10^{-5} Torr nitrogen appeared identical to films made in residual vacuum of 10^{-10} Torr.

25,437 HARD MAGNETIC FILMS OF IRON, COBALT, AND NICKEL by D.E. Speltiotis, G. Bate, J. K. Alstad, and J. R. Morrison (IBM); Prog. 10th Ann. Conf. Magnetism and Magnetic Materials, Nov. 1964, (to be publ. in J. Appl. Phys.)

Thin films of Fe, Co, and Ni were prepared by vacuum deposition onto glass substrates at room temperature. The angle of incidence was varied from 0° to 80° for the explicit purpose of changing the anisotropy and producing very high coercivities. Increasing the angle of deposition from the substrate normal had a dramatic effect on the magnetic properties of the films. The maximum effect was observed in Fe, where easy axis coercivity exceeded 100 oe at angles approaching 90°, while, at normal incidence, it was only 20 oe. Next was Co with maximum coercivity of 900 oe and Ni with maximum coercivity of 300 oe. This order is what would be expected on the basis of shape anisotropy of elongated particles formed on account of the oblique incidence of the vapor flux. The ratio of remanence to saturation intensity along the easy axis increases slightly as the angle of deposition increases, while along the hard axis it decreases markedly.

25,438 ALLOYS WITH LOW REMANENCE AND LOW COERCIVE FORCE IN THE REGION OF 9% ALUMINUM IRON by D. Pavlovic and K. Foster (Westinghouse); Prog. 10th Ann. Conf. Magnetism and Magnetic Materials, Nov. 1964 (to be publ. in J. Appl. Phys.)

A material combining low remanence with a low coercive force has been developed by applying a high temperature heat treatment to alloys in the region of 9 wt. % aluminum iron. This material displays a large grain size with a predominantly (111) texture in the plane of the sheet. Epstein strips as well as rings of 9% aluminum iron had a remanence of 1.66 to 2.68 kilogausses and a coercive force of 0.25 to 0.3 oersteds. Other typical properties were maximum permeability of 2,700, inductions of 12.9 kilogausses at 10 oersteds and 16.1 kilogausses at 100 oersteds, electrical resistivity of 90 microhm-cm, and Rockwell B hardness of 87. The low coercive force of this material is most likely a result of the large grain size obtained with the high temperature heat treatment. The low remanence appears to be a result of preferred orientation in the material which might be expected for an orientation composed largely of (111) grains.

25,439 MAGNETIZATION, RESONANCE AND OPTICAL PROPERTIES OF THE FERROMAGNET, CrI_3 by J.F. Dillon, Jr. (Bell Lab.) and C.E. Olsen (Los Alamos Sci. Lab.); Prog. 10th Ann. Conf. Magnetism and Magnetic Materials, Nov. 1964 (to be publ. in J. Appl. Phys.)

CrI_3 , noteworthy as one of the few insulating ferromagnets, is one of a series of presumably isomorphous compounds (CrCl_3 , CrBr_3 and CrI_3) which show similar or closely related magnetic ordering. Magnetization measurements of the powder were made at several fields up to 15,300 oe over the range 1.5 to 300°K. In addition, $M(H)$ was plotted at 4.2°K up to 70,000 oe. The ferromagnetic Curie temperature is 68°K, and the paramagnetic Curie temperature is 70°K. The low temperature saturation magnetization is $3.10 \mu_B/\text{Cr}^{+++}$, corresponding to $4\pi M = 2690$ gauss. The field for ferromagnetic resonance was measured at 86, 91 and 99 Gc/sec. The spectroscopic splitting factor $g = 2.07$, and the anisotropy field $2K/M = 28.6$ koe at 1.5°K. Optical transmission measurements on CrI_3 single crystals showed a very strong absorption band down to a band edge near $10,000 \text{ cm}^{-1}$.

25,440 EUROPIUM ORTHOSILICATE, A NEW TRANSPARENT FERROMAGNET by M. Shafer, T. McGuire and J. Suits (IBM); Phys. Rev. Lett., Vol. 11, pp. 251-252(L), Sept. 15, 1963

The discovery of a new ferromagnetic europium compound which is optically transparent in bulk is reported. These Eu_2SiO_4 powders were prepared by a solid-state reaction between EuO and SiO_2 . The magnetization curves at 4.2°K are presented. Low values of C_M and M_0 suggest the presence of trivalent Eu with $J = 0$. Strong anisotropy is observed. The Verdet constant equals (20°C) minus 2.5 min/oe/cm, and the Faraday rotation tentatively is in the range of 7600 deg/cm at a saturation magnetization of 175 emu (4.2°K).

25,441 LORENTZ MICROSCOPIC EXAMINATION OF POLYCRYSTALLINE FILMS WITH BIAXIAL PROPERTIES by Y. Gondo, B.E. Gran and R.J. Prosen (Honeywell Res. Ctr.); Prog. 10th Ann. Conf. Magnetism and Magnetic Materials, Nov. 1964 (To be Publ. in J. Appl. Phys.)

Three types of polycrystalline Permalloy films with biaxial magnetic properties have been examined by Lorentz microscopic techniques. Type I films consist of an array of discrete small squares. The stable configuration for these films is a simple arrangement of four domains with complete flux closure and 90° walls along the diagonals. The stability of this closure structure is a function of the dimension of the square. Type II films are composed of discrete thick squares superimposed on an isotropic continuous thin film. The closure configuration of the squares influences the domain configuration of the continuous film to produce biaxial properties with low coercive forces and the easy axis along the diagonal. Type III films are produced by etching an array of square voids from a continuous polycrystalline film. The biaxial properties of these films are similar to the Type II films.

25,442 MAGNETIC ANNEALING OF THIN PERMALLOY FILMS by S. Greenberg (USN Air Dev. Ctr.) and E. Korostoff (U. Penn.); *J. Appl. Phys.*, Vol. 35, pp. 1653-1654(L), May 1964

Observations have been made on the effects of magnetic annealing and cooling in the anisotropy field of 80-20 Permalloy thin films. Annealing was done in an argon-hydrogen atmosphere in a magnetic field of 35 oe. Changes produced in H_C and H_R by short-term annealing at temperatures up to 350°C in a transverse field could be reversed by a subsequent anneal in a longitudinal field. Above 350°C, the film became isotropic and the reversibility property was lost. It was also observed that annealing caused a substantial change in H_C for films deposited on room temperature substrates, but little change for films deposited at 300°C.

25,443 A FORTRAN III (IBM 7090) PROGRAM FOR THE CALCULATION OF THREE-SUBLATTICE MAGNETIZATIONS by G. Heiche (Naval Ord. Lab.); Task FR30 NOL TR63 32, M35, Jan. 16, 1964, 29 pp.; U.S. Gov. Res. Rep., Vol. 39, p. 142(A), June 5, 1964 AD 434 924 OTS \$2.60

An IBM 7090 program for calculating the total and partial magnetizations for a given set of molecular field coefficients as a function of temperature is presented. It is assumed that the molecular field coefficients vary linearly with temperature. Up to 1000 values can be calculated for each magnetization at equidistant temperatures. A complete listing of the subroutines and an example are included.

25,444 SPONTANEOUS MAGNETIZATION IN THE NEIGHBORHOOD OF THE CURIE TEMPERATURE by E. Callen (Naval Ord. Lab.) and H.B. Callen (U. Penn.); *Prog. 10th Ann. Conf. Magnetism and Magnetic Materials*, Nov. 1964 (To be Publ. in *J. Appl. Phys.*)

Near a ferromagnetic transition the magnetization $M \sim (T_C - T)^f$ and susceptibility $\chi \sim (T - T_C)^{-p}$. While Landau theory suggests $f = 1/2$ and $p = 1$, Padé approximations gives $p = 4/3$, and Tahir-Kheli's interpolation scheme then implies $f = 1/3$. P. Heller's precise measurements of EuS confirm $f = 1/3$ for $0.85 T_C < T < 0.99 T_C$. An accurate numerical analyses of the thermodynamic properties of a two-spin cluster theory and of two forms of Green function theory has been made. With the Charap-Boyd exchange constants of EuS, the cluster theory accurately predicts T_C and the observed λ -like discontinuity of C_V . $f = 1/2$ in the immediate vicinity of T_C , rapidly changing to $f = 1/3$ shortly below T_C and remaining so to $.7 T_C$. The slope of the M^3 vs T straight line agrees within 4% with Heller's, and the extrapolated intercept deviates from T_C by only 3%.

25,445 MAGNETIC PROPERTIES UNDER PRESSURE OF SOME TRANSITION METAL ALLOYS by D. Bloch and R. Pauthenet (Lab. d'Electrostat. et Phys. Metal, Grenoble); *Prog. 10th Ann. Conf. Magnetism and Magnetic Materials*, Nov. 1964 (to be publ. in *J. Appl. Phys.*)

The variation of the spontaneous magnetization, σ_s , and the Curie temperature, T_C , of several transition metals and some of their solid solutions have been studied as a function of the pressure up to 5,000 bars and in magnetic fields up to 30,000 oe. The measurements were carried out between 77 and 700°K. In the system Ni-Si, $d\sigma_s/dp$ is $0.32 \times 10^{-3} \cdot \text{K bar}^{-1}$ for pure nickel, and decreases by $0.033 \times 10^{-3} \cdot \text{K bar}^{-1}$ per 1 per cent of Si dissolved. In the system Ni-Cu, $d\sigma_s/dp = 0.14 \times 10^{-3} \cdot \text{K bar}^{-1}$ for Ni-20 at. per cent Cu, and decreases by $0.01 \times 10^{-3} \cdot \text{K bar}^{-1}$ per 1 per cent of Cu dissolved. For polycrystalline cobalt, $(1/\sigma_s) \times (d\sigma_s/dp)$ at 293°K is equal to $-10 \pm 1.5 \times 10^{-7} \text{ bar}^{-1}$. In a molecular field model, the molecular field coefficient, n , i.e. the numerical value of the exchange integral, varies with the volume.

Magnetization of Hexagonal Ferrites - See 25,099

25,446 LORENTZ MICROSCOPY OF SMALL FERROMAGNETIC PARTICLES by M.S. Cohen (Lincoln Lab.); *Prog. 10th Ann. Conf. Magnetism and Magnetic Materials*, Nov. 1964 (To be Publ. in *J. Appl. Phys.*)

Using special techniques, specimens have been prepared which contain discrete islands of NiFe on a nonmagnetic substrate. Each specimen contained islands (usually circularly shaped) about 300 Å thick with a wide range of diameters (~ 1 to 50μ). The islands were thus two-dimensional analogues of Kittel's three-dimensional particles. Lorentz microscopy gave direct evidence of the configurations predicted by Kittel for uniaxially anisotropic particles: a) a circular magnetization configuration, b) a 180° domain wall separating oppositely-directed domains, c) a single domain, uniformly-magnetized particle (this state could not be observed for circular islands, but only for elongated islands). The transition for state b to a was noted below a critical island diameter, D_c , if all other parameters were fixed; theoretical estimates of D_c were made. In addition, the distortion of all three states in the presence of fields was observed and is discussed.

25,447 SPATIAL VARIATION OF THE MAGNETIZATION ACROSS A FERROMAGNETIC THIN FILM IN THE BETHE-PEIERLS-WEISS APPROXIMATION by J.J. Pearson (Lockheed Res. Labs.); *Prog. 10th Ann. Conf. Magnetism and Magnetic Materials*, Nov. 1964 (to be publ. in *J. Appl. Phys.*)

The variation of the magnetization across a ferromagnetic film as a function of temperature and film thickness has been calculated in the Bethe-Peierls-Weiss approximation. In this approximation the Heisenberg exchange interaction between a given spin and the shell consisting of its nearest neighbors is treated exactly. The interaction of this shell with the rest of the sample is treated approximately, as an interaction with a molecular field. The extension to thin films was made by allowing this molecular field to vary across the film in the manner used by Valenta for the molecular field approximation. The finite thickness of the film had little effect on the temperature variation of the magnetization, reducing the Curie temperature by only a few per cent from the bulk value even for films as thin as eight layers. The spatial fall-off of the magnetization at the surface was even more abrupt than in the molecular field case and almost independent of film thickness.

25,448 FERROMAGNETIC CURIE TEMPERATURE IN CUBIC LATTICES WITH NEXT NEAREST NEIGHBOR INTERACTION by R.A. Tahir-Kheli and H.S. Jorrett (U. Penn.); Contract Nonr55136, Tech. Rept. No. 13, 13 pp., Mar. 1964; U.S. Gov. Res. Rep., Vol. 39, p. 127(A), June 20, 1964 AD 435 886 OTS \$1.60

25,449 MAGNETIC BEHAVIOR OF GADOLINIUM NEAR THE CURIE POINT by C.D. Graham, Jr. (GE Res. Lab.); *Prog. 10th Ann. Conf. Magnetism and Magnetic Materials*, Nov. 1964 (To be Publ. in *J. Appl. Phys.*)

Magnetization curves have been measured on a single crystal of gadolinium in fields up to 29 koe and over a range of temperatures from below the Curie point to 350°K. Plots of σ^2 vs H/σ define the Curie temperature as $292.5 \pm 0.5^\circ\text{K}$ and the data above the Curie point lead to $1/\chi_0 = 1.9 (T - T_C)^{4/3}$. The $4/3$ exponent is significantly different from the unity exponent predicted by the molecular field model, but in good agreement with the experimental results for nickel and with recent theoretical work. These results apply when the field is parallel to the easy crystallographic direction of the sample; because the crystal anisotropy of Gd is not zero at the Curie temperature, the results with the field applied perpendicular to the easy direction are somewhat different.

25,450 EFFECTS OF LOCAL ATOMIC ORDER ON MAGNETIC PROPERTIES OF Au-25 At.% Fe by R. Sundahl, J. Sivertsen and T. Chen (U. Minn.); *Prog. 10th Ann. Conf. Magnetism and Magnetic Materials*, Nov. 1964 (To be Publ. in *J. Appl. Phys.*)

Changes in magnetic properties of a Au-25 at.% Fe alloy with heat treatment have been studied. Measurements were made on samples quenched from 900°C and on samples subsequently annealed 10⁵ minutes at 75°C. Magnetizations were determined as a function of T (77° - 320°K) and H (9 - 18.5 koe). The Curie temperatures of the two states were determined from plots of H/M vs M^2 . Values of M (18.5 koe) were plotted vs $T^{3/2}$ and extrapolated to 0°K. The local atomic order parameters were determined from x-ray diffuse scattering measurements. The Curie temperatures obtained were $283 \pm 5^\circ\text{K}$ for the quenched state and $308 \pm 5^\circ\text{K}$ for the aged state. The magnetizations at 0°K and 18.5 koe were $23.7 \pm 0.3 \text{ emu/g}$ and $24.6 \pm 0.3 \text{ emu/g}$ for the quenched and aged alloys.

Curie Point of US - See 25,333

25,451 TIME DECREASE OF THE REVERSIBLE PERMEABILITY IN NICKEL UNDER STRESS by E. Klugmann and Z. Rozkwilski (Tech. U., Gdansk); *Acta Phys. Polonica*, Vol. 25, pp. 155-159, Feb. 1964

The time decrease effect in polycrystalline nickel wire under compressive stress is discussed. The time decrease characteristics were plotted after change of stress at constant temperature. The ratio $[\mu(0) - \mu(\infty)]/\mu(0)$ attains its maximum in the region of elastic limit for samples annealed in hydrogen. The after-effect is presumably due to excess vacancies generated owing to deformations. All measurements were carried out by means of an ac bridge.

25,452 PERMEABILITY OF DENSE NICKEL-ZINC FERRITES IN POLARIZING FIELDS by J. Verweil (Philips); *Philips Res. Rep.*, Vol. 19, pp. 29-42, Feb. 1964

Polycrystalline nickel-zinc ferrites with a porosity considerably smaller than 1 per cent have recently been made. These materials have a high resistivity, a high initial permeability, a small coercive force and a small line width. The permeability in a perpendicular polarizing dc field can be 20 or more with a small loss angle. This permeability is essentially independent of frequency up to about 3000 Mc/s. Because it depends on the dc field it can be used for magnetic tuning of cavities.

25,453 CALCULATION OF THE CURRENT AND FIELD DISTRIBUTION AND THE MAGNETIZATION CURVES FOR HIGH-FIELD, SUPERCONDUCTING MATERIALS IN THE FORM OF SHEET by H. Riemersma (Westinghouse Res. Labs.); *J. Appl. Phys.*, Vol. 35, pp. 1802-1806, June 1964

The field and current distribution in a high-field, superconducting material in sheet form, where the applied magnetic field is parallel to the sheet, is determined. The distributions are obtained from a critical state equation and Maxwell's equations, and determined for the two cases of absence or presence of a net transport current in the material. The field distributions are used to determine the magnetization of the material as a function of applied magnetic field, with the short-sample current-carrying capacity as a parameter. The zero transport current magnetization curves show good agreement in general shape with those experimentally observed. The analysis indicates a reduction in magnetization with increasing transport current.

25,454 MAGNETIC AFTEREFFECTS IN Fe-Al ALLOYS by R.E. Maringer (Battelle Inst.); *Prog. 10th Ann. Conf. Magnetism and Magnetic Materials*, Nov. 1964 (to be publ. in *J. Appl. Phys.*)

Measurements of the decay of magnetic permeability with time after demagnetization have been performed on several Fe-Al alloys. Measurements were obtained over the range of 350 to 450°C, with a wire specimen acting as the core of an open-end transformer. The decay curves could be separated analytically into two components, with relaxation times differing by about a factor of six. Relaxation times for the shorter of the two components agree well with relaxation times calculated from observations of the Zener peak (by internal-friction methods) in these alloys. Thus, as is the case for carbon in alpha-iron, this component results from an ordering process which can be either stress- or magnetically induced. The activation energy for this process is about 56 kcal/mole. The longer of the two relaxation processes, which also has an activation energy of about 56 kcal/mole, apparently involves directional ordering alone.

25,455 MAGNETIZATION CREEP IN THIN NICKEL-IRON FILMS by A. L. Olson and E.J. Torok (UNIVAC, Sperry Rand); *Prog. 10th Ann. Conf. Magnetism and Magnetic Materials*, Nov. 1964 (to be publ. in *J. Appl. Phys.*)

The initial magnetization creep threshold of vacuum deposited thin nickel-iron films has been investigated as a function of film thickness, film composition, magnitude of the anisotropy field and the amount of "negative" anisotropy present. The creep threshold, normalized to the transverse field where the probability density function is a maximum, shows a large improvement as the anisotropy field is decreased by uniformly straining the film; this process makes "negative" anisotropy regions appear. For isotropic films this normalized creep threshold is inversely proportional to the film thickness for thicknesses above 200 Å. The creep threshold for anisotropic films also decreases with increasing thickness, except for a dip in the thickness range where cross tie walls appear, 200-800 Å. Because the B-N-B transition occurs at larger transverse fields for thicker films, this mechanism is rejected.

25,456 MAGNETIZATION RIPPLE AND ARCTIC FOXES by H.B. Callen, R. L. Coren and W.D. Doyle (UNIVAC, Sperry Rand); *Prog. 10th Ann. Conf. Magnetism and Magnetic Materials*, Nov. 1964 (to be publ. in *J. Appl. Phys.*)

It has been observed previously that the magnetization in polycrystalline Permalloy films exhibits a longitudinal "ripple" with a wavelength of the order of four times the crystallite size (for $a < 2500$ Å). This observation has encouraged the exploration of mechanisms leading to sinusoidal variation. It is suggested that no such mechanism exists, but that the ripple is analogous to the famous three-year periodicity in the population of arctic foxes. In that case various ecological feedback theories were obviated with the observation that purely random numbers exhibit a pronounced apparent periodicity, with a wavelength of three units.

25,457 QUANTITATIVE CALCULATION OF THE MAGNETIC RIPPLE OF UNIAXIAL THIN PERMALLOY FILMS by H. Hoffmann (U. München); *J. Appl. Phys.*, Vol. 35, pp. 1790-1798, June 1964

The magnetic ripple of thin films with uniaxial anisotropy is calculated for the field and the magnetization lying along the easy and the hard direction of the uniaxial anisotropy. Its solutions (cylindrical functions) describe the two-dimensional magnetic ripple of the films. Along the mean direction of the magnetization the fluctuations of the magnetization vector are much greater than perpendicular to it. In the first case these fluctuations are coupled by exchange forces, and in the second case by the stray field. The theory is able to explain the image of the ripple observed by the electron microscope and to explain the variation of the ripple quantitatively, if the applied field is varied. The estimation of the mean magnetization dispersion agrees with the experimental data of Fuller and Hale.

25,458 THE DEPENDENCE OF THE MAGNETIZATION FLUCTUATION ON THE DOMAIN WIDTH AND DISPERSION OF THE EASY DIRECTION FROM THE LAYER PARAMETERS OF UNIAXIAL PERMALLOY FILMS [in German] by H. Hoffmann (U. München); *Phys. Stat. Sol.*, Vol. 5, pp. 187-202, 1964

The mean value of the fluctuation of magnetization is calculated from the general equation of magnetic ripple in a thin Permalloy film. The mean value has a close relation to the mean crystallite size. The width of domain splitting in magnetization reversal in the hard direction has been calculated from the mean wavelength of the ripple for decreasing field. The dispersion of the easy axis has also been calculated from the ripple.

25,459 EFFECT OF CRYSTALLITE SIZE AND ORIENTATION ON THE MAGNETIZATION RIPPLE IN PERMALLOY FILMS by A. Baltz and W.D. Doyle (Franklin Inst.); *J. Appl. Phys.*, Vol. 35, pp. 1814-1818, June 1964

Permalloy films of composition 83 per cent Ni 17 per cent Fe ranging from polycrystalline to monocrystalline were prepared by evaporation. Conventional electron micrographs, selected area diffraction patterns, and Lorentz electron micrographs were taken to study the average magnetic ripple wavelength (λ_0) as a function of the average crystallite size (a) of the film. Below a critical crystallite size, polycrystalline films showed a linear increase of the ripple wavelength with increase in crystallite size. It was found that $\lambda_0 = 4a$ in agreement with the maximum probable wavelength predicted theoretically by Rother. Films with preferred orientation showed similar behavior with $\lambda_0 = 10a$. A plateau was reached ($\lambda_0 = 9000$ Å, $a = 2000$ Å, $\lambda_0 = 12,000$ Å, $a = 1160$ Å, respectively) after which an increase in crystallite size had no effect on the ripple wavelength. Monocrystalline films did not exhibit ripple structure and it is concluded that in these films $\lambda_0 = \infty$.

25,460 TORQUE AND ROTATIONAL HYSTERESIS IN FCC SINGLE CRYSTAL COBALT FILMS by W.D. Doyle (Franklin Inst.); *Cont. AF19 628 2415*, 11 pp., Dec. 1963; *U.S. Gov. Res. Rep.*, Vol. 39, p. 157(A), May 20, 1964 AD 432 825 OTS \$1.60

The Stoner-Wohlfarth coherent rotation model is extended to the case of biaxial anisotropy. The rotational hysteresis integral W equals 1.54. Measurements on fcc single crystal Co films ($-k = 4-6 \times 10^5$ ergs/cc) prepared by epitaxial evaporation onto the (100) face of single crystal MgO slabs held at 400°C yield results in wide disagreement with theory. While the expected angular symmetry of the torque is observed the model does not correctly predict the magnitude of the torque nor the fields at which specific types of angular dependence will be observed. The magnetization reversal process in single crystal Co films is not coherent and that as in the case of polycrystalline films noncoherent rotations or wall motions must be investigated.

25,461 MOLECULAR FIELD MODEL AND THE MAGNETIZATION OF YIG by E.E. Anderson (U.S. Naval Ord. Lab.); *Phys. Rev.*, Vol. 134A, pp. A1581-1585, June 15, 1964

The susceptibility and magnetization of YIG of high purity have been measured from 4.2 to 650°K by means of a precision vacuum balance. The spontaneous magnetization has a saturation value of 37.90 emu/g at 4.2°K and 27.40 emu/g at 292°K. The Curie point is at 559°K as determined by both the vanishing of the spontaneous moment and the discontinuity in the susceptibility curve. Using a program written for the IBM 7090, the molecular field coefficients were determined by fitting the experimental total magnetization curve. The sublattice magnetizations and the exchange interactions are calculated and compared with other results. On the basis of the molecular field model the intrasublattice interactions must be larger than previously supposed.

25,462 ON THE USE OF MAGNETOSTATIC MODES FOR MEASURING SATURATION MAGNETIZATION OF FERRIMAGNETIC MATERIALS by B.R. Capone (AF Cambridge Res. Labs.); *AFRL 64 49, Proj. 5621*, 17 pp., Jan. 1964; *U.S. Gov. Res. Rep.*, Vol. 39, p. 125(A), June 20, 1964 AD 435 617 OTS \$1.60

The use of magnetostatic modes as a research tool has been suggested. Attempts to utilize this phenomenon for measuring the saturation magnetization of pure YIG samples and gallium substituted YIG samples show this method to be quite accurate for the narrow line width pure YIG material. However, in the measurement of gallium substituted YIG samples, difficulties were encountered in mode identification and interpretation of data.

25,463 REMANENCE AND APPROACH TO SATURATION OF $\text{Au}_{0.95}\text{Fe}_{0.05}$ by W.E. Henry (Lockheed Res. Lab.); *Phys. Rev. Lett.*, Vol. 11, pp. 468-469(L), Nov. 15, 1963

Magnetization measurements on $\text{Au}_{0.95}\text{Fe}_{0.05}$ by a sample displacement method in fields up to 95,000 gauss and at temperatures as low as 1.5°K have been performed. At temperatures of 4.2°K and lower, remanence and saturation ef-

ects are found. At 295°K the magnetization is $M = 9.17 \times 10^{-6}$ H [Bohr Magnetrans], at 77.4°K the magnetization curve is still linear and $M = 47.4 \times 10^{-6}$ H [Magnetrans]. From this a Curie temperature of $\theta = +23^\circ\text{C}$ is inferred indicating a ferromagnetic behavior of the alloy. From the remanence measurements some indication of antiferromagnetism at very low temperatures is obtained.

25,464 SWITCHING BY AN AVALANCHE OF DOMAIN NUCLEATIONS IN MAGNETIC THIN FILMS by E. Tatsumoto, M. Nomura and M. Goto (Hiroshima U.); *J. Phys. Soc. Japan*, Vol. 19, p. 761, May 1964

The switching mechanisms of magnetic thin films were investigated using the magnetoresistance effect. The three regions of the switching curve were explained as follows: region 1 is of the type of wall motion which follows a small rotation even at $H_L = 0$; region 2 is of the type of wall motion rather than non-uniform rotation as has previously been reported. This effect is explained by a theory of local switchings producing many domain walls and their subsequent motion. A switching mechanism similar to nonuniform rotation is thought to be the cause of region 3.

25,465 SPIN-WAVE EFFECTS IN MAGNETIC-FILM SWITCHING by K.J. Harte (Lincoln Lab.); *Prog. 10th Ann. Conf. Magnetism and Magnetic Materials*, Nov. 1964 (to be publ. in *J. Appl. Phys.*)

The nonlinear reaction of dispersion-induced spin waves on the uniform mode \vec{m}_0 has been calculated for a thin film undergoing rapid rotational magnetization reversal. It is found that if \vec{m}_0 rotates faster than longitudinal spin waves ($\vec{k} \parallel \vec{m}_0$) can relax, the magnetization goes through a transient state of high magnetostatic energy. If the pulse switching field H_p is less than a critical field H_{pc} , the energy of this intermediate state is greater than the energy available for switching and the uniform mode becomes locked at some point in the reversal process; rotational switching cannot proceed until initially longitudinal spin waves have relaxed into components propagating in the instantaneous direction of \vec{m}_0 . Such a highly damped process is suggestive of the non-coherent (intermediate-speed) reversal mode observed in thin films. For $H_p > H_{pc}$, reversal is found to occur by a modified uniform rotation; H_{pc} may therefore be identified as the threshold field for coherent rotation.

25,466 MAGNETIZATION SWITCHING TIME AT LOW TEMPERATURES by A. Hirsch (Israel Inst. Tech.); *Physica*, Vol. 30, pp. 563-564(L), Mar. 1964

A new experimental method for the investigation of low temperature magnetization switching time, based on the study of dynamic magnetoresistance hysteresis (MRH), is described. Peaks in the MRH loops which appear at the critical field H_c correspond to states in which the specimen is demagnetized. For a linearly applied magnetic field, the switching time τ can be expressed as: $\tau = (H_c - H_0)/r$, where r is the rate of rise in the applied field. Calculated data for τ are presented for a cold-rolled Ni sample in the temperature range of 4.2-297°K. This method may also be used for the investigation of thin film switching properties.

25,467 TWO PEAK OUTPUT WAVE FORMS IN UNIFORM ROTATION SWITCHING OF THIN FILMS by A.A. Toppeto (U. Detroit) and D.M. Grimes (U. Michigan); *Prog. 10th Ann. Conf. Magnetism and Magnetic Materials*, Nov. 1964 (to be publ. in *J. Appl. Phys.*)

A theoretical model for high-drive switching of a thin-film, finite length, ferrite, cylindrical shell or toroid is developed from Gilbert's equation. The equation of uniform magnetization reversal includes terms which result from an arbitrary applied field and terms due to the axial demagnetizing field. Machine solution of the equation shows the existence of two peaks in the output wave form which are directly traced to the axial demagnetizing field. The dependence of these peaks on the applied field is also shown. Comparison with published data on a thin-walled toroid is made. A physical description of the reversal mechanism which leads to the two peaks as they result from the axial demagnetizing field is included.

25,468 CREEP REVERSAL IN COUPLED FILM STRIPS by J.M. Daughton and H. Chang (IBM Watson Res. Ctr.); *Prog. 10th Ann. Conf. Magnetism and Magnetic Materials*, Nov. 1964 (to be publ. in *J. Appl. Phys.*)

Creep reversal of the magnetization in coupled film strips is examined theoretically and experimentally. The structure is a conductor strip sandwiched between two permalloy strips having their easy-directions across the strips. If a train of current pulses of sufficient amplitude pass through the conductor strip, the permalloy layers may be switched around the conductor in either of two senses depending on the polarity of the current. Criteria are presented for coupling (that is, that the two layers remain essentially oppositely magnetized as a function of width of the strip, thickness of the permalloy, coercivities of the films, and thickness of the intermediate conductor area. It is found that coupling may breakdown either if the strip is too narrow or too wide. For strips which are coupled and have relatively thin intermediate conductor layers,

the multiple-pulse field necessary to switch the film strip is about the average of the coercivities of the two permalloy layers. For thicker conductor layers, this field is reduced by a geometric factor accurately predicted by a model

25,469 THICKNESS DEPENDENCE OF CREEP SWITCHING IN MAGNETIC FILMS by G.P. Gagnon and T.S. Crowther (Lincoln Lab.); *Prog. 10th Ann. Conf. Magnetism and Magnetic Materials*, Nov. 1964 (to be publ. in *J. Appl. Phys.*)

The dependence of creep switching on film thickness has been measured in permalloy magnetic films 200 Å to 2000 Å thick. No creep was observed in films thinner than 400 Å. With a 1 oe. D-C easy axis field present, the transverse threshold field for many-pulse disturbing decreases an order of magnitude between 400 Å and 600 Å. Between 600 Å and 2000 Å, this creep threshold remains essentially constant. The practical significance in limiting the word line density in magnetic film memories and providing a writing mode for a non-destructive memory are discussed.

25,470 MAGNETIC AFTER EFFECTS IN NEUTRON IRRADIATED IRON, NICKEL AND COBALT by P. Moser, P. Peretto, D. Dautreppe and P. Vigier (CEN, Grenoble); *Prog. 10th Ann. Conf. Magnetism and Magnetic Materials*, Nov. 1964 (to be publ. in *J. Appl. Phys.*)

After neutron irradiation of iron at 78°K, four magnetic after effect zones were observed in the following temperature ranges: Zone 1, 78°K-93°K; Zone 2, (superimposed on zone 1) 78°K-178°K; Zone 3, 180°K-230°K and Zone 4, 230°K-370°K. Some of these have a fine structure showing the presence of different defects with closed activation energies. All of these zones annealed out in different temperature ranges corresponding to the well known stages of recovery in neutron irradiated iron. If the sample is annealed during 30 minutes at 500°C after an irradiation at 78°K, a new magnetic after effect zone appears between -40°C and +40°C. The different characteristics of each zone (activation energy for reorientation, spectrum width, defects symmetry, etc.) have been studied. A model concerning the nature of the defects responsible for these magnetic after effects is proposed.

25,471 COUPLING EFFECT BETWEEN THE MAGNETIZATIONS OF TWO THIN LAYERS SEPARATED BY A THIN NON-MAGNETIC METALLIC LAYER by J.C. Bruyere, G. Clerc, O. Massenet, R. Montmory, L. Neel, D. Paccard and A. Yelon (Lab. Electrost. et Phys. Metal, Grenoble); *Prog. 10th Ann. Conf. Magnetism and Magnetic Materials*, Nov. 1964 (to be publ. in *J. Appl. Phys.*)

The interaction phenomenon between the magnetizations of two thin ferromagnetic layers separated by a non-magnetic metal such as Ag, Au, Cr, Pd, of thickness less than a few hundred Å has been studied. This interaction tends to align the magnetizations of the two layers parallel. One of the two magnetic layers is Permalloy and the other is a ternary alloy of FeNiCo or pure Co. The interaction energy between 90°K and 520°K varies according to the nature of the intermediate layer; these variations are small, in the order of a few per cent, for Ag, Au and Cr while for Pd they are much greater. The influence of the substrate temperature during evaporation (lying between 300°K and 620°K) is negligible for intermediate layers of Au and Ag but for Cr the interaction decreases with decreasing temperature.

25,472 MAGNETIZATION BEHAVIOR OF A COPPER-CADMIUM FERRITE IN PULSED FIELDS UP TO 200 koe by V.E. Rode, A.V. Vedyayev and B.N. Krainov (Lomonosov Moscow State U.); *Soviet Phys.-Solid State*, Vol. 5, pp. 1277-1278(L), Dec. 1963

25,473 BARKHAUSEN EFFECT IN IRRADIATED PURE IRON AND NICKEL by S.I. Taimuty and J.B. Swedlund (Stanford Res. Inst.); *Cont. Nonr361500*, 44 pp., Feb. 28, 1964; *U.S. Gov. Res. Rep.*, Vol. 39, pp. 108-109(A), June 5, 1964 AD 433 849 OTS \$4.60

The effect of electron and neutron irradiation on the Barkhausen effect and coercive force of pure iron and nickel were investigated. The investigation was designed to establish whether (1) the Barkhausen effect can provide a sensitive indication of the presence of large radiation-induced defect clusters and whether (2) study of the Barkhausen effect could provide meaningful information about behavior of such defects. Results indicate that the Barkhausen effect is a more sensitive indicator of radiation damage in magnetic materials than is the coercive force. However, the smallness of the effect after neutron irradiation is puzzling. Based on estimates of the number of high-energy primary recoils produced by neutrons, the observed changes were several orders of magnitude too small.

25,474 DYNAMIC PULSE HYSTERESIS OF MAGNETIC DEVICES by C.H. Ste (IBM Watson Res. Ctr.); *Prog. 10th Ann. Conf. Magnetism and Magnetic Materials*, Nov. 1964 (to be publ. in *J. Appl. Phys.*)

An experimental technique has been developed to measure the dynamic pulse hysteresis loop which displays the instantaneous flux behavior with applied

field at nanosecond rise times. By utilizing the time stretching characteristic of sampling techniques, measurement of flux reversal in the order of 10^{-12} webers is realizable. Since the field is applied through a transmission line in these techniques, the device is measured with all its environmental effects such as demagnetization and flux trapping. By observing the ϕ -H relationship during the rise time, the necessary parameters for transmission line calculation can be obtained. The experimental and theoretical pulse hysteresis loops for a thick Permalloy film (10,000 Å) are presented along with the measurement techniques. The pulse hysteresis loop is compared with the low frequency hysteresis loop.

25,475 SQUARE-LOOP PROPERTIES OF MATERIALS IN THE SYSTEM NiFe_2O_4 - Fe_3O_4 - MnFe_2O_4 by H.B. Im and D.G. Wickham (Ampex Computer Prod.); *J. Appl. Phys.*, Vol. 35, pp. 1442-1445, May 1964

Toroids composed of polycrystalline materials of a number of compositions in the system NiFe_2O_4 - Fe_3O_4 - MnFe_2O_4 exhibit rectangular magnetic hysteresis loops. The squareness ratios, switching coefficients, and coercivities, and their temperature coefficients demonstrate the usefulness of these materials as the storage elements in coincident-current computer memories. The square hysteresis loops in this system can be explained with the aid of existing knowledge of the magnetocrystalline and stress anisotropies.

25,476 Ni-Fe-Nb-Ag, A NEW SQUARE-LOOP ALLOY FOR MAGNETIC MEMORY ELEMENTS by E.M. Tolman (Bell Labs.); *Prog. 10th Ann. Conf. Magnetism and Magnetic Materials*, Nov. 1964 (to be publ. in *J. Appl. Phys.*)

In some memory designs, it is essential that magnetic storage elements in flat-tened wire form have a coercive force in the 1 oe range and a rectangular hysteresis loop. For such applications, it was decided to investigate the reduction in coercive force and accompanying loss of loop squareness which results from annealing Ni-base Permalloys in the cold worked state (6-8 oe). Flattened wire samples of 78.5 Ni-Fe Permalloy did not possess square hysteresis loops even before anneal. When similarly prepared samples of 4-79 Mo Permalloy were annealed, a loss of loop squareness coincided with a drop in coercive force. The addition of 1 per cent Ag to this alloy allowed the material to be annealed to 2 oe before an appreciable loss of squareness. The substitution of Nb for Mo in the ternary 4-79 alloy produced a material in the cold worked state with a truly rectangular loop which was retained when it was annealed.

25,477 DOMAIN ORIENTATION IN Mo PERMALLOY AND 65 Ni-Fe BY ELECTRON IRRADIATION AT 100°C by R.S. Sery and D.I. Gordon (U.S. Naval Ord. Lab.); *Prog. 10th Ann. Conf. Magnetism and Magnetic Materials*, Nov. 1964 (to be publ. in *J. Appl. Phys.*)

A variety of effects have been observed in flat-ring polycrystalline samples of 5-80 Mo Permalloy and 65 Ni-Fe irradiated by 2 Mev electrons at temperatures within the range of 70 to 170°C. For the Mo Permalloy samples, application of a 0.22 oe field during irradiation to 1.10×10^{17} e/cm² resulted in square hysteresis loops with B_r as high as 6500 (possibly a record high) but with little or no increase in H_c . In zero applied field, H_c increased and B_r and μ_m decreased in all cases, but loop shapes were either rectangular, constricted, tri-stable, or conventional. The tri-stable loops, which appeared after a run in which the beam was interrupted several times, resemble those theorized by Kaya for the case of a material having two dominant anisotropy axes. Irradiation of 65 Ni-Fe with a 1 oe field and a dose of 7×10^{17} e/cm² resulted in increases of ~100% in B_r and μ_{\max} but accompanied by a 50% increase of H_c .

25,478 THE INFLUENCE OF STATIC PRESSURE ON THE COERCIVE FORCE OF BARIUM FERRITE POWDER by R.K. Tenzer (Indiana Genl.); *Prog. 10th Ann. Conf. Magnetism and Magnetic Materials*, Nov. 1964 (to be publ. in *J. Appl. Phys.*)

In recent studies of ferrite powders, changes of the intrinsic coercive force (H_{ci}) have been ascribed to lattice defects and to particle size reduction which occur during milling. In order to test the two interpretations, the H_{ci} of barium ferrite powder (ball milled to 0.02-0.5 μ) was measured under static pressure. The coercive force increased with increasing pressure, reached a maximum at 800 psi, and then decreased. This behavior is easily understood on the basis of an increase of the effective particle size due to more contact between the particles at higher pressure. Increasing pressure reduced the effect of thermal fluctuations, thus increasing the coercive force. At pressures above 8000 psi multidomain behavior becomes a predominant factor in lowering the H_{ci} .

25,479 VERY HIGH COERCIVITY CHEMICALLY DEPOSITED Co-Ni FILMS by J.S. Judge, J.R. Morrison and D.E. Speliotis (IBM, Poughkeepsie); *Prog. 10th Ann. Conf. Magnetism and Magnetic Materials*, Nov. 1964 (to be publ. in *J. Appl. Phys.*)

Films of Co-Ni, varying in composition from 30% Co to 100% Co, and ranging in thickness from 250 Å to 2500 Å were prepared by chemical deposition.

Their crystallographic and magnetic properties were studied as a function of composition and thickness. The coercivity for a particular thickness increased as the Ni content of the films increased, reaching a peak of about 1300 oe at 20 to 30% Ni depending on the thickness. In this range, the cubic phase is clearly coexistent with the hexagonal phase. Beyond it, the coercivity decreased rapidly to a value of 200 oe, as the Ni content of the films increased to 70%. In the Co films the coercivity decreases markedly with increasing thickness. This dependence on thickness becomes less and less pronounced as Ni is introduced, until the coercivity becomes independent of thickness in the vicinity of 20% Ni. Thereafter, the coercivity increases with increasing thickness, and this effect becomes more evident at higher Ni contents.

25,480 COERCIVE FORCE OF SINGLE CRYSTAL GdIG AS A FUNCTION OF TEMPERATURE by J.P. Hanton and A.H. Morrish (U. Minn.); *Prog. 10th Ann. Conf. Magnetism and Magnetic Materials*, Nov. 1964 (To be Publ. in *J. Appl. Phys.*)

The intrinsic coercive force (H_c) of single crystal gadolinium iron garnet (GdIG) has been measured as a function of temperature and orientation ([100] [110] [111]) in the temperature range of 77°K to 323°K. These data are compared to data taken on a specially prepared GdIG polycrystalline sample. Both samples were found to exhibit a single peak in H_c at the magnetization compensation temperature (T_{CM}) with the single crystal having a temperature width, measured at the $1/2H_c$ points, of 1.5°K and the polycrystalline sample of 8°K. The maximum value of H_c varied with orientation for the single crystal but was approximately 50 oe while for the polycrystalline sample it was 225 oe. Measurements were made at temperature intervals (ΔT) of $0.01^\circ\text{K} < \Delta T < 0.05^\circ\text{K}$ in the neighborhood of the compensation temperature in order to study the fine details of the curve.

25,481 GREEN FUNCTIONS IN THE THEORY OF A UNIAXIAL AND CUBIC FERROMAGNETIC ANISOTROPY [in German] by W. Haubenreisser and E. Jäger (German Acad. Sci., Jena); *Phys. Stat. Sol.*, Vol. 5, pp. 33-46, 1964

The renormalized energy spectrum and the magnetization of a ferromagnet are calculated for uniaxial, dipolar and quadrupolar anisotropy. The validity of the results are limited to low temperatures due to the decoupling of the Green functions. A derivation of the relation between the constants of anisotropy and the magnetization is also presented.

25,482 THE ORIGIN AND EFFECTS OF LOCAL REGIONS OF COMPLEX BIAXIAL ANISOTROPY IN THIN FERROMAGNETIC FILMS WITH UNIAXIAL ANISOTROPY by E.J. Torok (UNIVAC); *Prog. 10th Ann. Conf. Magnetism and Magnetic Materials*, Nov. 1964 (to be publ. in *J. Appl. Phys.*)

Inhomogeneity in the magnitude and direction of the anisotropy field of a thin polycrystalline ferromagnetic film arises from the magnetocrystalline anisotropy of the crystallites, their shape anisotropy, the shape anisotropy of the film at the edge, and from the locally anisotropic strains on the crystallites. The mechanism is described by which the inhomogeneities of large magnitude in crystallite-sized areas appear instead as inhomogeneities of smaller magnitude over domain-sized regions. Neither the size, location, nor local anisotropy field of the domain-sized regions remains fixed in a given film, but varies as a function of applied field. These perturbation anisotropy fields have both uniaxial and biaxial characteristics. It is shown that local regions of complex biaxial anisotropy can arise from the interaction of strongly coupled adjacent areas of the film with different uniaxial anisotropy fields as well as from magnetocrystalline anisotropy.

25,483 EXCHANGE COUPLING OF UNIAXIAL MAGNETIC THIN FILMS by W.T. Siegle (Rensselaer Polytech.); *Prog. 10th Ann. Conf. Magnetism and Magnetic Materials*, Nov. 1964 (to be publ. in *J. Appl. Phys.*)

The properties of two uniaxial magnetic films in intimate contact have been investigated. It is shown that when the uniaxial easy axes of the two films are orthogonal, and the magnitude of the uniaxial anisotropy the same in each film, uniaxial anisotropy in the composite film vanishes, to be replaced by a field-dependent biaxial anisotropy. The theoretical analysis relates this biaxiality to exchange coupling between the two halves of the composite film. Experimental measurements on several films are compared with the theory and imply for A, the exchange coupling constant, an average value of 2.0×10^{-6} erg/cm in a 66-34 Ni-Fe alloy film. The possibilities of using this structure as a practical biaxial element are considered.

25,484 KERR EFFECT AND BITTER PATTERN MEASUREMENTS OF EASY AXIS DISTRIBUTIONS IN UNIAXIAL PERMALLOY FILMS by D.B. Dove and T.R. Long (Bell Labs.); *Prog. 10th Ann. Conf. Magnetism and Magnetic Materials*, Nov. 1964 (to be publ. in *J. Appl. Phys.*)

Measurements on small regions (1 mil²) of magnetic films have been made with a Kerr magneto-optic apparatus that utilizes a laser light source and employs narrow band detection techniques. Bitter patterns have been recorded during the course of an angular distribution fall back experiment. The pictures have

been assembled sequentially as a motion picture showing the remanent domain state developed throughout the experiment. Dynamic Kerr effect observations show that significant domain wall rearrangements occur near zero transverse field. The direction of M in small regions of single domain films have been determined to 0.1° using an MH alignment technique, and hence an alternative estimate of the angular distribution of easy axes is obtained. Strong transverse magnetostatic coupling between regions are of importance in both the full back and MH alignment measurements.

25,485 INDUCED MAGNETIC ANISOTROPY IN FERRITE SINGLE CRYSTALS by E. Gyorgy and F. Schnetter (Bell Labs.); *J. Appl. Phys.*, Vol. 35, pp. 1648-1649(L), May 1964

The behavior of induced anisotropy in single crystals is shown to be different from the Jahn-Teller distortion model and directional ordering model. Using a general argument based on cubic lattice symmetry, which characterizes the theory of induced anisotropy, expressions are derived for coefficients of the energy at a site or orientation. Experimental results available in the literature for manganese and nickel ferrite were compared to these relations. Although the directional ordering model can be modified to fit specific experimental results, the available experiments are not consistent with this model. The experimental results can, however, be readily explained by attributing the induced anisotropy to localized Jahn-Teller distortions.

25,486 MAGNETIC ANNEALING EXPERIMENTS IN SOME Cu-Ni-Fe AND Cu-Ni-Co ALLOYS by J.J. Becker (GE Res. Lab.); *Prog. 10th Ann. Conf. Magnetism and Magnetic Materials*, Nov. 1964 (To be Publ. in *J. Appl. Phys.*)

It is sometimes stated that Cu-Ni-Fe and Cu-Ni-Co alloys do not respond to magnetic annealing. Usually this means that no significant difference in reluctance and coercive force parallel and perpendicular to the field direction is found. However, torque measurements provide a much more sensitive indication of the development of uniaxial anisotropy. In these experiments, a number of Cu-Ni-Fe and Cu-Ni-Co alloys were solution treated, quenched, and annealed in a magnetic field for various times and temperatures. The field was applied along a diameter of the disk-shaped specimens. Torque curves were then measured. None of the Cu-Ni-Fe alloys developed uniaxial torque. However, all three Cu-Ni-Co alloys investigated did. The largest value of K_u attained was in an alloy of composition 50% Cu, 20% Co, and 30% Ni by weight. For this alloy, K_u reached a value of 5×10^4 erg/cm³ after 250 minutes at 650°C or 800 minutes at 600°C in a field of 1000 oersteds.

25,487 THE EFFECTS OF UHV AND SUBSTRATE TEMPERATURE ON THE MAGNETIC ANISOTROPY OF PERMALLOY THIN FILMS by G.I. Lykken and E.N. Mitchell (U. North Carolina); *Prog. 10th Ann. Conf. Magnetism and Magnetic Materials*, Nov. 1964 (to be publ. in *J. Appl. Phys.*)

In order to determine the extent to which trapped impurity atoms (oxygen in particular) affect the magnetic anisotropy observed in Permalloy thin films a specific, oil-free vacuum system was developed which allowed rapid, simultaneous deposition (1000 Å per min) of 82% Ni-18% Fe onto two glass substrates, one usually at liquid helium temperature, the other at selected temperatures above liquid helium, with a deposition pressure better than 2×10^{-9} mm Hg. In all cases the films deposited onto the heated substrates appeared anisotropic while those deposited onto the cold substrates appeared isotropic at liquid helium, intermediate and room temperatures (when examined in UHV with a hysteresis loop tracer). It was found that anisotropy could be introduced into the isotropic films by low temperature annealing.

25,488 THE CAUSES OF THE INHOMOGENEITY IN THE MAGNITUDE OF THE ANISOTROPY FIELD IN THIN NICKEL-IRON FILMS by H.N. Oredson and E.J. Torok (UNIVAC, Sperry Rand); *Prog. 10th Ann. Conf. Magnetism and Magnetic Materials*, Nov. 1964 (to be publ. in *J. Appl. Phys.*)

The inhomogeneity in the magnitude of the anisotropy field of vacuum deposited nickel-iron films has been determined as a function of film composition. The contributions from the magnetocrystalline anisotropy of the randomly oriented crystallites, and from local uniaxial strains has been determined for various substrate temperatures and sources. For example, for evaporation from a ring source onto a substrate at 300°C, $(5H_k)^2 = (2.87 \times 10^{-10})n^2 + (1.25 \times 10^{-8})K_1^2 + 0.133$. The constant term is attributed to shape anisotropy due to film surface roughness and to the edge of the film and to variations in the magnitude of the anisotropy field due to temperature variations across the film during deposition. The contribution due to magnetocrystalline anisotropy and that due to magnetostriction plus local strain are roughly equal.

Magnetic Anisotropy of Ni₃Fe - See 25,399

25,489 DEPENDENCE OF MAGNETIC FIELD INDUCED ANISOTROPY IN NICKEL-IRON FERRITES ON NICKEL CONCENTRATION [in German] by K. Motzke (Inst. Mag. Werkstoff, Jena); *Phys. Stat. Sol.*, Vol. 4, pp. K13-K16, 1964

The dependence of the magnetic field induced anisotropy (K_u) in Ni-Fe ferrites ($Ni_x Fe_{3-x} O_p$) on Ni concentration in the range of x up to 0.43 has been studied. Earlier experiments have established that field induced magnetic anisotropy for this material is characterized by two distinct temperature regions. K_u was found to be proportional to p and the relaxation time was found to be independent of p . The lower temperature region extended from 0 to 100°C, the higher region from 200 to 350°C. The dependence reversed in the higher temperature region, where K_u was proportional to x^2 ($2-x$)², in agreement with Neel's theory. At the lower region, K_u was proportional to $p(2-x)$.

25,490 FIELD INDUCED ANISOTROPY IN Fe-Co EVAPORATED THIN FILMS by F.B. Humphrey and M. Takahashi (Calif. Inst. Tech.); *Prog. 10th Ann. Conf. Magnetism and Magnetic Materials*, Nov. 1964 (to be publ. in *J. Appl. Phys.*)

Field induced uniaxial magnetic anisotropy has been observed in vacuum evaporated thin Fe-Co films over the entire composition range. A uniaxial anisotropy, with the easy axis parallel to a field during evaporation, was observed with a torque magnetometer. The observed value of K_u as a function of film composition showed only a slight indication of long range order in the bcc solid solution range for the FeCo and Fe₃Co composition. The maximum value of K_u is at 60 per cent Co for a substrate at 300°C with a value of 35×10^3 ergs/cm³. The anisotropy constant for films made with the substrate at 20°C, $K_u(20^\circ C)$, is greater than $K_u(300^\circ C)$ for Fe rich and for Co rich alloys as was expected. An anomalous inversion was observed in the composition range 25 per cent to 70 per cent Co where $K_u(20^\circ C) < K_u(300^\circ C)$.

25,491 ROLL INDUCED ANISOTROPY IN A Co-Fe ALLOY by A.R. Von Neida and G.Y. Chin (Bell Lab.); *Prog. 10th Ann. Conf. Magnetism and Magnetic Materials*, Nov. 1964 (To be Publ. in *J. Appl. Phys.*)

The development of magnetic anisotropy induced by cold rolling of a Co-Fe alloy was studied with the aid of magnetic torque measurements and x-ray pole figures. In the annealed strip the texture is principally $\{311\}$ $[112]$, with the torque dependence of the magnetization showing "easy" axes both parallel and transverse to the rolling direction. With rolling the torque curves are converted to mainly a uniaxial behavior with the easy axis transverse to the roll direction. After 95% reduction the texture is found to be $\{110\}$ $[112]$. Measurements of the intensity of $\{110\}$ planes lying in the plane of the strip show the texture to sharpen linearly with true strain. The torque maximum associated with the transverse direction, which is a measure of the strength of the induced easy axis, is likewise linear with true strain. Theoretical torque curves based on magnetocrystalline anisotropy energy were computed from the texture data.

25,492 STRIPE MAGNETIC DOMAIN AND ROTATABLE ANISOTROPY IN IRON FILMS by Y. Sugita, H. Fumiwara and N. Saito (Hitachi Central Res. Lab.); *J. Phys. Soc. Japan*, Vol. 19, p. 782(L), May 1964

The interaction between stripe magnetic domains and rotatable anisotropy in pure Fe films is discussed. Strain and negative magnetostriction play decisive roles in producing stripe domains. The uniaxial anisotropy with its easy axis normal to the film was created by the magnetostriction. The symmetry of torque curves at low fields unidirectional; at higher fields, a large uniaxial anisotropy appears with its easy direction parallel to the previously applied saturation field. When the measuring field is high enough to rotate the stripe, the uniaxial anisotropy disappears.

25,493 UNIAXIAL ANISOTROPY DUE TO MAGNETOELASTIC ENERGY IN CONSTRAINED POLYCRYSTALLINE FILMS by F.G. West (Texas Instr.); *J. Appl. Phys.*, Vol. 35, pp. 1827-1840, June 1964

A possible mechanism for uniaxial anisotropy in ferromagnetic films is the magnetoelastic energy W_λ which results from the constraint imposed on the film by the substrate. This constraint energy is examined and it is shown that earlier calculations are not correct. Maximum values for W_λ at room temperature are 4.2, 1.8 and 42 (10^3 erg cm⁻³) in Ni, Fe, and Co, respectively. The temperature dependence of W_λ in Ni films is in agreement with the reported experimental behavior when annealing of the constraint is allowed for.

25,494 ON THE MAGNETIC ANISOTROPY OF Fe₃Ge₅ by Y. Tawara (Matsushita Elec. Indus. Co.); *J. Phys. Soc. Japan*, Vol. 19, pp. 776-777, May 1964

The magnetic anisotropy of a plane disk of Fe₃Ge₅ cut and ground so as to include both the a- and c-axis of the hexagonal lattice is described. It was found that the easy direction of magnetization lay on the a-axis in the present geometry of the specimen. The amplitude of the torque curve was also found to increase with external field. The explanation for the observation is offered. The anisotropy energy caused by the magnetic dipolar interaction of the crystal was also calculated and its deviation from measured values explained by mechanisms such as spin-orbit interaction.

25,495 MAGNETIC EXCHANGE ANISOTROPY IN MIXTURES OF BARIUM, STRONTIUM, OR LEAD FERRITE WITH POTASSIUM FERRITE by W.L. Roth and F.E. Luborsky (GE Res. Lab.); *J. Appl. Phys.*, Vol. 35, pp. 966-967, Mar. 1, 1964

Some new systems $F_{1-x}A_x$, showing exchange anisotropy at room temperature and above are described. F is ferrimagnetic lead (P), barium (M), or strontium (S) ferrite, all with the magnetoplumbite structure, $PbFe_{12}O_{19}$, $T_C = 455^\circ C$. A is antiferromagnetic potassium ferrite ($KFe_{10}O_{17}$, $T_N = 530^\circ C$) which crystallizes in the closely related β -alumina structure. Mixtures $F_{1-x}A_x$ were prepared with $0 < x < 1$. Specimens were cooled from above $600^\circ C$ to room temperature in a field of 4 koe and measurements made of the magnetic saturation σ_s , intrinsic coercive force H_{ci} , torque L , and rotational hysteresis W_r , from -197° to $480^\circ C$.

25,496 ON THE MAGNETIC ANISOTROPY OF A Fe-Ge ALLOY by J.J. Becker and E.M. Symes (GE Res. Lab.); *Prog. 10th Ann. Conf. Magnetism and Magnetic Materials*, Nov. 1964 (To be Publ. in *J. Appl. Phys.*)

A number of investigators have measured the saturation magnetization and Curie temperature of the iron-germanium β phase, which extends from about 36 to 45 atomic per cent germanium and has a modified NiAs structure. Tawara (*J. Phys. Soc. Japan*, Vol. 19, p. 776, 1964) investigated the magnetocrystalline anisotropy of a single crystal disk of Fe_3Ge_5 and found the c axis to be the hard direction, with $K_1 = -9 \times 10^6$ erg/cm³ at $77^\circ K$ but did not investigate the variation in the base plane. In the present experiments, an alloy of composition 57% Fe + 43% Ge by weight (68.6 atomic per cent Fe) was prepared and found by x-ray diffraction to be single phase. This brittle alloy could be ground into a powder consisting of individual single crystallites. These were then aligned by a magnetic field and held in a binder. It could then be established by x-ray diffraction that $\langle 11\bar{2}0 \rangle$ is the direction aligned parallel to the field.

25,497 MAGNETOCRYSTALLINE ANISOTROPY OF GALLIUM IRON OXIDE by J.H. Schelleng (U.S. Naval Res. Lab.); *Prog. 10th Ann. Conf. Magnetism and Magnetic Materials*, Nov. 1964 (to be publ. in *J. Appl. Phys.*)

Magnetocrystalline anisotropy measurements have been made on a sample of ferromagnetic and piezoelectric $Fe_xGa_{2-x}O_3$ (x being near unity) using a torque method. Torque curves in the ac plane on an X-ray oriented single crystal indicate a large uniaxial anisotropy of the form $E = K \sin^2\theta$, where θ is the angle between M_s and the preferred (c) axis. As the anisotropy field ($2K/M_s$) is larger than the external field presently available (11 koe) the anisotropy values were obtained from measurements in which the angle between the external field and the c direction was small. Preliminary results obtained with this method show that $2K/M_s$ is +23 koe at $77^\circ K$ and +13 koe at $196^\circ K$. These directly measured values are to be compared with the values of 300 koe and 16 to 23 koe deduced from energy gap and susceptibility measurement, respectively. The small-angle measurements yield magnetization values which are in substantial agreement with those previously reported.

25,498 MAGNETIC PROPERTIES OF SINGLE CRYSTALS OF COBALT SUBSTITUTED NICKEL FERRITE by R. Krishnan and H. Makram (Lab. Magnétisme et Phys. Sol., C.N.R.S., Bellevue); *Prog. 10th Ann. Conf. Magnetism and Magnetic Materials*, Nov. 1964 (to be publ. in *J. Appl. Phys.*)

The contributions of Co to the anisotropic energy and the resonance linewidth in Co substituted Ni ferrite has been studied. The effect of Co substitution in Ni ferrite has been studied in comparison with the results obtained by other authors with Co substitution in magnetite and Mn ferrite. Concerning the anisotropy, it is seen that at room temperature the effect of Co in the Ni ferrite is less than that of the magnetite but greater than that of the Mn ferrite. An explanation is given based in part on the fact that the Ni^{2+} ions in the octahedral sites destroy the trigonal symmetry of these sites which in turn decreases the spin-orbit coupling of Co ions, thus reducing their contribution to the anisotropic energy.

25,499 UNIAXIAL-ANISOTROPY ACTIVATION ENERGIES IN PERMALLOY FILMS by D.O. Smith and G.P. Weiss (Lincoln Lab.); *Prog. 10th Ann. Conf. Magnetism and Magnetic Materials*, Nov. 1964 (to be publ. in *J. Appl. Phys.*)

Permalloy films vacuum deposited in a dc field $H_{||}$ develop uniaxial anisotropy commonly described by an anisotropy field H_k which is due to several structural effects with different activation energies. These effects can be separated by: (1) deposition in $H_{||}$ on a substrate at temperature T_s ; (2) annealing in either a dc field H_{\perp} perpendicular to $H_{||}$ or a circular rotating field H_r for specified time intervals; (3) quenching by water-cooled coils. One result of such experiments has been the identification of a contribution H_p to H_k due to oriented pairs of lattice vacancies. In 83-17 Permalloy, with $100 < T_s < 350^\circ C$, $H_p \sim 2.5$ oe and U_p the activation energy for reorientation ~ 0.2 ev. After exposure to oxygen at room temperature H_p is unchanged but U_p increases to ≥ 1 ev. The increase in U_p is attributed to the filling of lattice vacancies by oxygen atoms.

25,500 SINGLE CRYSTAL MAGNETIZATION DATA FOR ANISOTROPIC RARE-EARTH IRON GARNETS AT LOW TEMPERATURES by F.W. Harrison, J.F.A. Thompson and G.K. Lang (Mullard Res. Labs.); *Prog. 10th Ann. Conf. Magnetism and Magnetic Materials*, Nov. 1964 (to be publ. in *J. Appl. Phys.*)

Measurements were made on selected single crystal spheres of TbIG, DyIG, HoIG and ErIG as well as YIG, SmIG, GdIG and YbIG, in the temperature range $4^\circ K$ - $300^\circ K$ and applied fields up to 17,000 oe in one or more of the principal crystallographic directions. Appreciable differences from Pauthenet's original results were found in the region below $100^\circ K$ particularly for TbIG, where at $20^\circ K$ compared with the Pauthenet value of $26.3 \mu_B$ the saturation magnetization extrapolated to zero field at temperature T is $35 \mu_B$ in the $[111]$, easy direction, and $19.6 \mu_B$ in the $[100]$, hard direction due to unsaturation. The easy and hard direction σ -T curves straddle the Pauthenet curve up to about $100^\circ K$ where the three curves merge.

25,501 ON THE APPARENT AFTER-EFFECT ANOMALY NEAR THE MAGNETIC ANISOTROPY COMPENSATION POINT by A. Braginski and J. Kulikowski (Polfer Res. Lab., Warsaw); *Phys. Stat. Sol.*, Vol. 4, No. 3, p. K129, 1964

A previous report (*Phys. Stat. Sol.*, Vol. 4, p. K9, 1964) of an anomaly in the magnetic disaccommodation curve near the compensation point in cobalt-substituted nickel-iron ferrites was found to be incorrect. Thermocouple measurements showed temperature changes in the sample due to alternating current demagnetization. The disaccommodation anomaly resulted from insufficient heat exchange between the sample and the thermostatic bath.

25,502 ON BLOCH WALLS IN CUBIC FERROMAGNETIC LATTICES. Part I. VARIATIONAL PRINCIPLES by W. Zietek (U. Wroclaw); *Acta Phys. Polonica*, Vol. 25, pp. 117-138, Jan. 1964

All the types of ideal stable and metastable Bloch walls which exist in cubic ferromagnetic lattices are examined on the basis of a uniform theory developed earlier. In order to facilitate the calculations, a phenomenological operator for the magnetic anisotropy energy is used, in correspondence to classical theories. The influence of a uniform external magnetic field is considered. The variational principles for the Bloch walls in body-centered and face-centered cubic lattices are derived. The solutions of the corresponding Euler equations are given and the energies and widths of the Bloch walls are calculated and discussed.

25,503 DOMAIN INDUCED APPARENT ROTATION OF THE ANISOTROPY AXIS by D.J. Frantsvog (Concordia Coll.), C.S. Comstock and A.V. Pohn (Iowa State U.); *Prog. 10th Ann. Conf. Magnetism and Magnetic Materials*, Nov. 1964 (to be publ. in *J. Appl. Phys.*)

Hysteresis loop and Bitter pattern measurements have been made on 80-20 Permalloy films of approximately 1000 and 2000 Å thickness which exhibited an "apparent" rotation of the easy axis as first described by Hart. The dispersion in the films varied from approximately 2° to 10° . When an alternating near transverse field was applied to determine the hard direction, no apparent rotation of the easy axis occurred. However, when a single polarity near transverse field was applied, an apparent rotation of the easy direction from 1° to 10° was observed. The magnitude of the apparent rotation depended on the amplitude of the applied field. A detailed examination by Bitter technique revealed that the apparent rotation of the uniaxial anisotropy axis was induced by the formation of strip domains typically 10 to 30μ wide separated by Néel walls even with zero applied fields.

25,504 SMOOTH CONTROLLABLE WALL MOTION IN THIN Ni/Fe/Co FILMS by R.J. Sapin and H.I. Jauvitis (LFE); *Prog. 10th Ann. Conf. Magnetism and Magnetic Materials*, Nov. 1964 (to be publ. in *J. Appl. Phys.*)

Techniques which permit the smooth controlled motion of domain walls in thin Ni/Fe/Co films while avoiding the spontaneous nucleation of extraneous domains have been applied to a planar thin film geometry in which the easy anisotropy axis is parallel to the narrow film dimension and displacement of the walls is produced in a perpendicular direction. It is this case for which the stray field from the film edges presents the greatest difficulty to achieving the desired wall motion properties. Appropriate film edge taper, in addition to higher cobalt concentrations in zero-magnetostriction Ni/Fe/Co films, are found to effectively inhibit the formation of unwanted domains as reversed magnetization. The film edges are shown to have a pronounced effect upon the shape of a domain wall put into motion by an applied field as a result of the stray field from the edges and an increase in coercive force within the tapered regions. The "stiffness" of a domain wall is also discussed as it applies to dynamic wall properties.

25,505 DETERMINATION OF THE FERROMAGNETIC EXCHANGE ENERGY CONSTANT IN FERROMAGNETIC Ni AND Ni-Cu FILMS BY MEANS OF DOMAIN WALL WIDTH MEASUREMENTS by P.M. Hemenger (Armco Steel)

and H. Weik (U. Cincinnati); Prog. 10th Ann. Conf. Magnetism and Magnetic Materials, Nov. 1964 (to be publ. in J. Appl. Phys.)

A method for measuring the ferromagnetic exchange energy constant "A" has been proposed. From "A" the exchange integral "J", which is the energy due to exchange coupling between nearest neighbors, can also be determined. The method depends upon relating "A" to the image width of a Néel-type domain wall observed in an electron microscope by Lorentz microscopy. An expression was found which relates the constants of the film (the exchange energy constant "A", the saturation magnetization "M_s" and the anisotropy constant "K") to the domain wall width. Measurements were made in an electron microscope on vacuum deposited films of 200 Å thickness. Values of "A" and "J" for pure Ni were found to be $A = 0.45 \times 10^{-6}$ ergs/cm and $J = 7.5 \times 10^{-14}$ ergs. Due to a rapid decrease in wall image contrast as Cu was added, observations were made only up to 3.7 wt. per cent Cu.

25,506 WALL TRANSITIONS IN COUPLED FILMS by F.J. Friedlaender and J.F. Silva (Purdue U.); Prog. 10th Ann. Conf. Magnetism and Magnetic Materials, Nov. 1964 (to be publ. in J. Appl. Phys.)

Two coupled Permalloy films of 81% Ni-19% Fe composition separated by a layer of silicon monoxide were used to study domain wall interactions. Néel walls were observed in 900 Å coupled film segments with 300 Å film separation. Since the separation layer is an insulator, the interaction is thought to be magnetostatic. The films were prepared in a step fashion on a single substrate so that uncoupled and coupled portions of a film, prepared in the same evaporation, could be observed simultaneously using Bitter powder pattern technique. Multiple-step coupled structures of varying film thickness with constant separation and varying separation with constant film thickness were prepared with thicknesses chosen in the region of Néel-Bloch transition. An analysis, based on an extension of Middelhoek's work, treats the coupled domain walls as elliptic cylinders arranged in a minimum magnetostatic energy configuration and shows that coupled Néel walls have less energy than coupled Bloch walls up to film thicknesses of 760 Å with 300 Å film separations.

25,507 ELECTRON-MICROSCOPIC OBSERVATION OF "STRIPE" OR "DENSE-STRIPED" MAGNETIC DOMAINS IN NICKEL-RICH PERMALLOY FILMS by J. Koikeda, K. Suzuki and S. Chikazumi (U. Tokyo); Appl. Phys. Lett., Vol. 4, pp. 160-162(L), May 1, 1964

Stripe magnetic domains observed by transmission electron microscopy in an evaporated 5% Fe-95% Ni film are discussed. When the specimen was placed several millimeters above the upper edge of the objective lens, the stripe domains were observed by slightly defocusing the transmitted electron beam. The stripe domain patterns have been explained by the variation of spin. The film exhibited a rotatable anisotropy, and its easy axis was rotated by a field higher than 200 oe. If the film is saturated by a field higher than 1000 oe, well defined parallel stripe domains occur parallel to the remanent magnetization. They disappear when a field higher than 200 oe is applied perpendicular to the stripes, and will appear again, perpendicular to the original direction, if the applied field exceeds 500 oe. These results indicate that the rotatable anisotropy is caused by stripe domains, and that the easy axis is parallel to the stripe domains.

25,508 FERROMAGNETIC DOMAINS IN THIN SINGLE-CRYSTAL NICKEL PLATELETS by R.W. De Blois (GE Res. Lab.); Prog. 10th Ann. Conf. Magnetism and Magnetic Materials, Nov. 1964 (to be publ. in J. Appl. Phys.)

Single crystal nickel platelets ranging from 600 Å to about 10 microns in thickness have been grown non-epitaxially by the hydrogen reduction of the bromide. Because their perfection is close to that of metal whiskers, the intrinsic coercive force for domain wall motion is minute (< 0.01 oe). Thus the ferromagnetic domain configurations, observed by electron microscope and Bitter techniques, are in stable or metastable equilibrium. For platelets less than 0.9 μ thick the magnetization lies in the plane along [110] directions, these being the projections of the [111] direction of minimum anisotropy energy. Echelons form the common closure structure near the edges. At a thickness of 0.9 μ a dense-banded or striped powder pattern appears within the planar domains, with a 0.6 μ spacing between bands. With increasing thickness the bands become coarser and are generally not parallel to the planar component of magnetization.

25,509 METAMAGNETISM OF SOME RARE-EARTH COPPER COMPOUNDS WITH CeCu₂ STRUCTURE by R.C. Sherwood, H.J. Williams and J.H. Wernick (Bell Lab.); J. Appl. Phys., Vol. 35, pp. 1049-1050, March 1964

Magnetic moments of the series of rare-earth copper (RCu₂) intermetallic compounds have been measured at temperatures from 1.4° to 300°K. These compounds have an orthorhombic crystal structure and are isostructural with CeCu₂. The susceptibility at high temperatures of most of the compounds followed the Curie-Weiss law giving effective moments close to those of the trivalent rare-earth ions. Eu and Yb appeared to be divalent. At low fields antiferromagnetic behavior was indicated in some of these compounds by peaks in the curves of

moment vs temperature, and by a lack of remanence. Metamagnetic behavior was observed when measurements were made at 4.2°K and with fields up to 80,000 oe. For example, the moment of TbCu₂ increased abruptly at a critical field, and at 80,000 oe, although not yet saturated, had a moment of 6.2 Bohr magnetons. The moments of EuCu₂ and GdCu₂ increased gradually, and at 80,000 oe reached moments of 5.7 and 6.0 Bohr magnetons, respectively.

25,510 METAMAGNETISM AND EXCHANGE IN FERROUS BROMIDE by I.S. Jacobs and P.E. Lawrence (GE Res. Lab., Schenectady); J. Appl. Phys., Vol. 35, pp. 996-997, March 1964

The highly anisotropic behavior of several ferrous ion antiferromagnets (FeCl₂, FeCO₃) has suggested Ising-model behavior. Sharp field-induced (metamagnetic) transitions to a ferromagnetic (or nearly saturated paramagnetic) configuration have been observed. This transition in a single crystal of anhydrous FeBr₂ occurs at a field of 31.5 koe at 4.2°K. The spontaneous magnetization per Fe²⁺ ion is 4.05 ± 0.2 Bohr magnetons. A differential molar susceptibility between 70 and 200 koe of $0.8 \pm 0.2 \times 10^{-2}$ is interpreted as a Van Vleck "temperature-independent" paramagnetism in qualitative agreement with expectation. Susceptibility-temperature measurements along the c axis reveal an asymmetric shape characteristic of recent Ising-model calculations. In the region just above the Néel point (11°K), the magnetization shows an initial upward concavity with field and a subsequent inflection point. This destruction of residual intermediate range order had also been predicted in Ising-model calculations.

25,511 NUCLEAR MAGNETIC RESONANCE STUDIES IN ANTIFERROMAGNETIC CrCl₃ by A. Narath (Sandia); J. Appl. Phys., Vol. 35, p. 838, Mar. 1964

The metamagnetic properties of CrCl₃ have been investigated by studying the temperature and field dependences of the Cr⁵³ nuclear magnetic resonance in the temperature range 0.39° to 11.5°K. The large field-dependent perpendicular susceptibility arises from the small value of the antiferromagnetic interlayer exchange energy. Low-temperature magnetic properties are shown to approximate those of a two-dimensional Heisenberg ferromagnet. Intensity enhancement of the Cr⁵³ resonance in zero field indicates the resonance is driven by the appropriate antiferromagnetic resonance mode. Observable splittings of the nuclear resonance occurring when the driving field is parallel to the steady field are a result of the expected strong field dependence of the sublattice magnetizations.

25,512 METAMAGNETIC BEHAVIOR OF FERROMAGNETIC LINEAR CHAIN IN CoCl₂·2H₂O by H. Kobayashi and T. Haseda (Tohoku U.); J. Phys. Soc. Japan, Vol. 19, pp. 765-767, May 1964

The magnetic behavior of a ferromagnetic linear chain in CoCl₂·2H₂O was studied. Below 17.6°K, CoCl₂·2H₂O was found to be antiferromagnetic with the axis of easy magnetization parallel to the b axis. The magnetization as a function of external field parallel to the b axis showed two steep increases, explained by assuming that the superexchange interaction within a chain is ferromagnetic. The first jump was evidently caused by a spin flopping; the second by a breaking of the weak antiferromagnetic coupling among the different chains.

FERRO- AND FERRIMAGNETIC RESONANCE

25,513 QUANTUM STATISTICAL THEORY OF FERROMAGNETIC RESONANCE by O.A. Ol'khov and B.N. Provotorov (Acad. Sci. USSR); Soviet Phys.-Doklady, Vol. 8, pp. 922-924(L), Mar. 1964

A quantum statistical theory of ferromagnetic resonance, which is valid for all temperature ranges, is presented. The resonance equations are derived using the density matrix technique. It is shown that in the temperature range $T \gg T_c$ (Curie temperature), the derived equations reduce to equations of the Bloch type.

25,514 FERROMAGNETIC RESONANCE MEASUREMENTS IN Ni-Fe FILMS AT 2-100 Mc by F. Vescial, T.J. Hutchings, R.H. Durrett, E.D. Jacobs, J. Winocur and W.L. Zingery (Autonetics); Prog. 10th Ann. Conf. Magnetism and Magnetic Materials, Nov. 1964 (to be publ. in J. Appl. Phys.)

The anisotropy field distribution in both magnitude and direction has been investigated in Ni-Fe thin films through the frequency range of 2.4 to 100 Mc using RF ferromagnetic resonance. Measurements were centered around the region of field values near H_k where the theory of Smit and Beljers predicts extreme angular sensitivity of FMR. Linewidths and line shapes at the lower frequencies agree with Hasty, but at higher frequencies the observed linewidth does not follow the expected w^2 dependence. Assuming that the double valued line separation follows this theory, the results indicate a line broadening with

increasing frequency. Curves are presented which show excessive line broadening at higher frequencies. Vibrating sample magnetometer anisotropy dispersion measurements are also presented. Data taken at high and low power levels with two different spectrometers were in agreement.

25,515 FERROMAGNETIC RESONANCE IN MULTIDOMAIN THIN FILMS by T.E. Hasty (Texas Instr.); *J. Appl. Phys.*, Vol. 35, pp. 1434-1441, May 1964

A thin Ni-Fe film, having a uniaxial magnetic energy of the form $E_K = K \sin^2 \theta$, usually exists as a single domain. If a magnetic field of sufficient magnitude is placed perpendicular to the easy axis of magnetization and then removed, the film splits into a large number of 180° domains. When this simple multidomain structure occurs, it is theoretically possible to excite two ferromagnetic resonance modes by applying a small magnetic field perpendicular to the easy axis. The first of these, a low-frequency mode (0-10 Mc/sec) is excited by an RF field perpendicular to the domain walls; and the second, a high-frequency mode (0-25 Gc/sec) is excited by an RF field parallel to the domain walls. The high-frequency mode has been observed in a number of films having anisotropy fields from 3-5 oe. The experimental results are compared with theoretical relations for frequency as a function of applied field. In addition, it is possible to estimate the domain wall separation from measurements of the high-frequency mode.

25,516 FERROMAGNETIC RESONANCE IN CALCIUM FERRITE CONTAINING Gd^{3+} by N. Ichinose, S. Chiba and K. Kurihara (Tokyo Shibaura Electr. Co.); *Japanese J. Appl. Phys.*, Vol. 3, pp. 235-236(L), Apr. 1964

Ferromagnetic resonance experiments are reported for single crystals of calcium diferrite ($CaFe_2O_7$) containing 3 mol pct. Gd_2O_3 . The crystals are of the ferropilgrane type with Curie temperature of 393°K, and saturation magnetization of 205 gauss and 102 gauss at 77°K and 296°K, respectively. Observed linewidth when the crystal was magnetized in the easy direction at 296°K was 240 oe. With the applied field in the hard direction, resonance fields H_1 and H_2 are 1950 oe and 6600 oe, respectively. The magnetic anisotropy H_a is 1290 gauss, and γ is 2.85.

25,517 MAGNETIC RESONANCE IN DYSPROSIUM METAL by F.C. Rossol and B.R. Cooper (Harvard U.); *Prog. 10th Ann. Conf. Magnetism and Magnetic Materials*, Nov. 1964 (to be publ. in *J. Appl. Phys.*)

Magnetic resonance has been observed at 37.7 Gc in a hexagonal platelet of dysprosium metal at temperatures from 79°K to 138°K. The variation of microwave absorption with dc field has been observed with dc field along both hard and easy axes of the planar anisotropy, with RF field both perpendicular and parallel to dc field. A resonance width on the order of one kilogauss was observed over the entire temperature range investigated for the spiral structure with the dc and RF fields perpendicular and the dc field along a hard direction of the planar anisotropy. Near the transition temperature from ferromagnetic to spiral the resonance field was about two thousand gauss above the critical field and became equal to the critical field at the highest part of the temperature range investigated. This behavior is to be expected according to the theory of Cooper and Elliott. The spin waves in the ferromagnetic region lie at quite high energies.

25,518 INDUCED MAGNETIC ANISOTROPY IN SPINEL FERRITE SINGLE CRYSTALS AT LOW TEMPERATURES by R.P. Poplawsky, R.E. Michel and F.W. Chapman (Genl. Motors Res. Lab.); *Prog. 10th Ann. Conf. Magnetism and Magnetic Materials*, Nov. 1964 (to be publ. in *J. Appl. Phys.*)

Magnetic resonance measurements have been made at 9.5 Gc/s on two ferrite single crystals $Ni_{0.78}Fe_{0.16}^{2+}Fe_{0.06}^{3+}O_4$ and $Mg_{0.88}Fe_{0.22}^{2+}Fe_{0.00}^{3+}O_4$ in the temperature range 4°K to 20°K. Both samples exhibit induced anisotropy when cooled from above 10°K in a magnetic field. The associated shifts in the field for resonance indicate an induced uniaxial anisotropy energy in both samples of the form $K' \frac{1}{2} \alpha_1^2 \beta_1^2$, where α_1 and β_1 are the direction cosines of the magnetization at the measuring temperature and the annealing temperature respectively. The shifts in resonance fields due to the anneal, decrease smoothly as the measuring temperature is raised and disappear above 10°K. The similarity of the induced anisotropy for both samples irrespective of the difference in compositions suggests that the source is the same and is associated with the Fe^{2+} . The observed symmetry could arise from the proposed directional ordering of the interstitial cations.

25,519 EXCHANGE EFFECTS IN THE SPIN-LATTICE RELAXATION OF IMPURITIES IN THULIUM GARNETS by R.W. Bierig and L. Rimal (Raytheon Res. Div.); *Prog. 10th Ann. Conf. Magnetism and Magnetic Materials*, Nov. 1964 (to be publ. in *J. Appl. Phys.*)

Preliminary data on exchange enhanced relaxation processes have been reported for Fe^{3+} ; similar effects observed in the spin-lattice relaxation of Yb^{3+} in TmAl and TmGa garnets are reported. It was found that $1/T = 275/T + 1.6 \times 10^7 e^{-41/T}$ 0.1% Yb^{3+} :TmAl garnet and $1/T = 550/T + 8.9 \times 10^6 e^{-75/T}$ 0.1%

Yb^{3+} :TmGa garnet while Svare has previously reported $1/T_1 = 33/T + 1.8 \times 10^{-7} T^9$ for Yb^{3+} in the isomorphic, diamagnetic host YGa garnet. A discussion of the matrix elements involved in the observed two phonon relaxation process is presented. In addition, the dynamic exchange effects contributions to the one phonon relaxation mechanism at low temperatures and to Raman relaxation at high temperatures and the connection of the preceding results with the ferrimagnetic relaxation of rare earth doped YIG are also discussed.

25,520 SPIN-FLOPPING RELAXATION TIME IN $CuCl_2 \cdot 2H_2O$ by C.S. Naiman and T.R. Lawrence (Mithras); *Prog. 10th Ann. Conf. Magnetism and Magnetic Materials*, Nov. 1964 (to be publ. in *J. Appl. Phys.*)

The relaxation time associated with the spin-flopping transition in $CuCl_2 \cdot 2H_2O$ has been measured and found to be $(0.70 \pm 0.15) \times 10^{-7}$ sec. at 2.4°K. The measurements also yield the susceptibility and temperature dependence of the critical field, H_c , in good agreement with previous data. The crystal was placed in a coil and in a constant magnetic field, H , so that the a-axis of the crystal, the axis of the coil, and H , were all parallel. The r.f. inductance and resistance of the coil were measured with $H \neq H_c$, then with $H = H_c$. The inductive and resistive components of the critical field susceptibility, χ_c^i and χ_c^r , obtained from the observed shifts in inductance and resistance, as a function of frequency, fit a dispersion curve of the form $\chi_c^i/\chi_c^r = 1/[1 + (\omega t_{sf})^2]$, where, at a temperature of 2.4°K, $2\pi\eta\chi_c^r = 3.2 \times 10^{-3}$ (η is the filling factor of the crystal in the coil) and $t_{sf} = 0.7 \times 10^{-7}$ sec.

25,521 FERRIMAGNETIC RESONANCE LINEWIDTH IN RARE EARTH DOPED YIG AT LOW TEMPERATURES by B.H. Clarke (Mullard Res. Labs.); *Prog. 10th Ann. Conf. Magnetism and Magnetic Materials*, Nov. 1964 (to be publ. in *J. Appl. Phys.*)

The longitudinal mechanism of relaxation is now well established in explaining the observed linewidths, ΔH , in YIG doped with certain rare earth ions, particularly in the temperature range of the linewidth maximum. In order to test the theory at lower temperatures, linewidths were measured in [111] directions at $\omega = 9.3$ Gc/s in YIG doped with 5 per cent Yb, 2.6 per cent Er and 1 per cent Nd, from 1.5-100°K. The longitudinal mechanism, in which the iron sublattice is relaxed through its anisotropic exchange with rare earth ions having a doublet ground state, predicts that $\Delta H \propto [\omega \tau kT \cosh^2(\delta/2kT)]^{-1}$ at low temperatures where $\omega \tau \gg 1$ (i.e. below the linewidth maximum). It was assumed that in [111] directions the doublet splitting, δ , is the same for the different rare earth sites. At very low temperatures when $kT < \delta$, the temperature dependence of ΔH becomes very strong, viz. $\Delta H \propto [1/\tau T] \exp(-\delta/kT)$.

25,522 FERROMAGNETIC RELAXATION IN EUROPIUM IRON GARNET by R.C. Le Craw, W.G. Nielsen, J.P. Remick (Bell Labs.) and J.H. Van Vleck (Harvard U.); *Phys. Rev. Lett.*, Vol. 11, pp. 490-493(L), Dec. 1, 1963

The variation of ΔH vs T at 9980 Mc/sec in single crystal spheres of EuIG is reported. It is found that (1) $g_{eff} = g(YIG) M_s(EuIG)/M_s(YIG)$ in the range of 1.5°-300°K and for frequencies of 9600 Mc/sec - 12,300 Mc/sec. (2) $\Delta H \propto \exp(-370/T^\circ)$ for 50°-100°K. (3) $\Delta H \propto \omega$ for 6000 Mc/sec - 18,320 Mc/sec and for 45°-300°K. (4) Temperature for ΔH_{max} at 9980 Mc/sec is 210°K. (2) to (4) are explained by a modified longitudinal ("slow") relaxation mechanism. The results could, however, also be brought into agreement with a transfer ("fast") mechanism if the relaxation time $\leq 10^{-13}$ sec.

25,523 ON THE THEORY OF SPIN-WAVE RESONANCE IN THIN FILMS by E. Schlomann (Raytheon Res. Div.); *Prog. 10th Ann. Conf. Magnetism and Magnetic Materials*, Nov. 1964 (to be publ. in *J. Appl. Phys.*)

A new theory of spin-wave resonance, based upon the assumption that the saturation magnetization varies linearly across the thickness of the film, is described. The characteristic equation for the normal modes has been solved both for free and for strongly pinned surface spins. According to this theory the lower order modes are approximately equally spaced, their separation in magnetic field being given by $\delta H \approx 1.5 (H_0')^{2/3} D^{1/3}$, where H_0' is the field gradient and $D = 2A/M_0$ a phenomenological exchange constant (A = Landau-Lifshitz constant, M_0 = saturation magnetization). The theory agrees remarkably well with the experimental data of Nisenoff and Terhune on Permalloy films.

25,524 PARALLEL PUMPED INSTABILITIES IN MAGNETIC METAL FILMS by J.B. Comly and R.V. Jones (Harvard U.); *Prog. 10th Ann. Conf. Magnetism and Magnetic Materials*, Nov. 1964 (to be publ. in *J. Appl. Phys.*)

Study of the unstable growth of parallel pumped microwave spin waves has proved uniquely capable of revealing fine details of spin relaxation processes in ferrimagnetic insulators. These instabilities were observed in a metallic system - viz. thin films of the nickel-iron alloy, Permalloy. Measurements are made at 16.7 Gc with the microwave and dc magnetic fields parallel to each other and in the film plane. Estimates of the relaxation parameter, ΔH_k , of spin waves can be made from the threshold power for microwave instability. For a fixed alloy composition threshold values indicate that damping parameters for short wavelength spin waves are independent of film thickness in con-

contrast with considerable thickness variations in the resonance damping parameter, ΔH_r (at half frequency). For the alloy 83% Ni:17% Fe we find $\Delta H_k = 80$ oe, $\Delta H_r = 104$ oe, for 1700 Å films and $\Delta H_k = 84$ oe, $\Delta H_r = 226$ oe, for 4900 Å films.

25,525 PARALLEL PUMPING IN NARROW LINEWIDTH PLANAR Mn-ZnY by G.S. Dixon, Jr., A. Tauber and R.O. Savage, Jr. (USAEL); Prog. 10th Ann. Conf. Magnetism and Magnetic Materials, Nov. 1964 (to be publ. in J. Appl. Phys.)

Single-crystal samples of ZnY with substituted manganese have been studied under perpendicular and parallel pumping. Highly polished spheres were measured with RF and dc fields applied in the easy plane of the material. Single-crystal specimens were grown from BaO/B₂O₃ flux with substituted Mn ranging from 0 to 6.2 wt.%. The dc magnetization at room temperature decreases almost linearly as a function of increasing Mn substitution. The ferrimagnetic resonance linewidth at 9.0 kMc and room temperature decreases with increasing Mn to a minimum of 3.9 oe. This represents the lowest reported value for planar hexagonal ferrites. Pumping experiments were carried out on minimum linewidth samples. For perpendicular pumping an h_{crit} of 6×10^{-2} oe was obtained at 17.2 kMc and room temperature. Parallel pump measurements were made at the same frequency and temperature.

25,526 NUCLEAR MAGNETIC RELAXATION OF THE IMPURITY NUCLEUS IN DILUTE FERROMAGNETIC ALLOYS by R.L. Streever (Nat'l. Bur. Stand.); Phys. Rev., Vol. 134A, pp. A1612-1617, June 15, 1964

The nuclear relaxation times T_1 and T_2 for 1% Ni⁶¹ in 99% iron, 1% Ni⁶¹ in 99% cobalt, and 0.5% Co⁵⁹ in 99.5% nickel have been observed at several temperatures using the pulsed-free precession method. The relaxation curves are generally nonexponential and power-dependent. The signals at low-power levels are from nuclei in domain walls and T_1 is due to thermal fluctuations of the domain walls. At high-power levels, where the signal is mainly from nuclei in domains, the longest measured relaxation times T_1 are lower limits for relaxation times for nuclei in domains. The longest T_1 's are found to be inversely proportional to temperature with $T_1 T = 1.0$ sec°K for 1% Ni⁶¹ in cobalt, $T_1 T = 1.2$ sec°K for 1% Ni⁶¹ in iron, and $T_1 T = 0.3$ sec°K for 0.5% Co⁵⁹ in nickel, and are believed to be due to conduction electron relaxation.

25,527 NUCLEAR MAGNETIC RELAXATION IN FERROMAGNETIC TRANSITION METALS by T. Moriya (U. Tokyo); J. Phys. Soc. Japan, Vol. 19, pp. 681-687, May, 1964

The spin-lattice relaxation rates associated with the nuclear magnetic resonance in ferromagnetic transition metals, Fe, Co and Ni, are studied theoretically. Thermal fluctuations of the internal magnetic field at a nucleus associated with the spin wave excitation and the individual excitations corresponding to s- and d-bands are considered. The effect of the coupling between the spin waves and the conduction electrons is also considered. The d-band electrons are treated in a tight binding approximation. The predominant nuclear spin relaxation mechanism in all of these metals is shown to come from the fluctuation of the orbital current of the d-band electrons. The other possible mechanisms are shown to make smaller contribution than this by one to two orders of magnitude, except for the Fermi contact interaction of the s-band electrons in Fe and Co, which can possibly make a significant contribution, though not of primary importance.

25,528 THE ACOUSTIC PROPERTIES OF MAGNETITE AS A FUNCTION OF TEMPERATURE/ AND CATION VACANCIES by W.B. Suiter and R. Blair (Bell Lab.); Prog. 10th Ann. Conf. Magnetism and Magnetic Materials, Nov. 1964 (to be publ. in J. Appl. Phys.)

The acoustic loss and resonant frequency have been measured in magnetite spheres from 4.2°K to 780°K. The acoustic frequency was of the order of 1 Mc. The cation vacancies were varied from .001 to .007 per formula unit by firing in the appropriate atmospheres as given by the phase diagram of Darken and Gurry. Previous work on magnetite by Gibbons was limited to the temperature range of 4.2 to 160°K and to samples of unknown vacancy content. The samples with .007 vacancies had a small loss peak at 40°K. This loss peak was not observed for the samples with .001 vacancies. All the samples had a large loss peak centered at 100°K. This peak is associated with the first order transition in magnetite. An additional loss peak was observed near 660°K, which decreased in amplitude and shifted to slightly lower temperatures with decreasing vacancy content.

25,529 MICROWAVE MAGNETO-ELASTIC RESONANCES IN A NONUNI-FORM MAGNETIC FIELD by T. Kohane and E. Schlomann (Raytheon Res. Div.); Prog. 10th Ann. Conf. Magnetism and Magnetic Materials, Nov. 1964 (to be publ. in J. Appl. Phys.)

A new magneto-elastic resonance effect has been observed in the course of an investigation on an experimental delay line. A dc magnetic field was applied in the long direction of YIG slabs (1 cm long, 0.5 cm wide, and 0.1 or 0.07 cm high) each end of which was inserted in a stripline cavity. Under appropriate

conditions a pulse of microwave power applied to one cavity resulted in a pulse in the second cavity delayed by several μ sec. Small variations were observed in the amplitude of the delayed pulse as the dc field was varied. Similar variations with the same periodicity (~ 1 oe) were also observed in the undelayed reflection from the input cavity. The amplitude variation is attributed to the excitation of magneto-elastic resonances near the end face of the sample. Because of the strong coupling between spin waves and elastic waves, the turning point (at which $k_{spin\ wave} = 0$) and the end face of the sample define a magneto-elastic quasi-cavity whose resonances give rise to the effect noted.

25,530 A STUDY OF NEW ACOUSTIC AND MAGNETIC PROPERTIES OF YIG AND YAG WITH SMALL Mn AND Ni ADDITIONS by D.B. Fraser, E.M. Gyorgy, R.C. LeCraw, J. Remeika, F.J. Schnettler and L. Van Uitert (Bell Lab.); Prog. 10th Ann. Conf. Magnetism and Magnetic Materials, Nov. 1964 (to be publ. in J. Appl. Phys.)

The resonant frequency and Q of the acoustic modes of YIG and of YAG spheres have been investigated as a function of temperature at ~ 1 Mc. The samples studied were YIG with 0.25% and 1.0% Mn and YAG with 0.15% Mn and 0.06% Ni additions. For all these samples the resonant frequency of the shear modes ($f_0 \propto d^{-1} \sqrt{c_{44}/\rho}$) has a maximum as a function of temperature. For pure YIG and YAG this maximum is not observed and the resonant frequency increases monotonically with decreasing temperature. For the YIG with 1.0% Mn the frequency maximum occurs at 330°K. At 40°K, f_0 has decreased by 11% from its peak value. Below 30°K, such a large increase in loss is observed that the complete low temperature behavior cannot be determined at present. For the YIG with 0.25% Mn the frequency maximum occurs at 130°K.

ANTIFERRO- AND ANTIFERRIMAGNETISM

25,531 THE GREEN FUNCTION METHOD IN THE THEORY OF ANTIFERRO-MAGNETISM by A.C. Hewson and D. Ter Haar (Clarendon Lab., Oxford); Physica, Vol. 30, pp. 890-898, Apr. 1964

A Green function calculation for the susceptibility of a Heisenberg antiferromagnet is presented. In the random phase approximation the susceptibility at the Néel point has the molecular field value and the perpendicular susceptibility is independent of temperature. These results are modified in the generalized Callen approximation which is also considered. Spin-flopping is briefly mentioned and an expression for the temperature dependence of the critical field is given.

25,532 SIMPLIFIED MOLECULAR FIELD THEORY APPLIED TO CUBIC ANTIFERROMAGNETIC LATTICES by L. Adamowicz (Tech. U., Warsaw); Acta Physica Polonica, Vol. 24, pp. 591-600, Nov. 1963

Molecular field theory as developed for isotropic exchange interactions is used to find from the complete set of geometrically possible Gersch-Koehler superstructures the most stable ones and to determine the intervals of their existence. It is shown that within the molecular field approach the antiferromagnetic collinear superstructures may be considered as a composition of two equivalent ferromagnetic sublattices when the requirement of the same numbers of like and unlike neighbours for each spin is satisfied. This requirement allows to obtain the general expression for the Néel temperature in very simple algebraic form similar to that for the net interaction energy. A simplified discussion for the first- and second-nearest neighbour interactions, based on a comparison of the Néel temperatures, is performed for all Gersch-Koehler superstructures of cubic magnetic lattices and the intervals of existences of the most stable superstructures are determined.

25,533 ANTIFERROMAGNETIC LINEAR CHAIN WITH SPIN 1/2 by T. Oguichi (Carnegie Inst. Tech.); Phys. Rev. Lett., Vol. 15, pp. 266-268(L), Sept. 15, 1963

A perturbation method for calculating the energy of an antiferromagnetic linear chain (spin = 1/2) at 0°K is described. The Hamiltonian of the Heisenberg model is used, ignoring the quartic terms in the first approximation, because of the low exciton population at low temperatures. The Hamiltonian is diagonalized, using appropriate transformations, yielding $E_0 = -0.716 N|J|$. In the second approximation, the quartic terms are retained, the diagonalizing transformation modified and the resulting non-diagonal quartic terms neglected, yielding $E_0 = -0.862 N|J|$.

25,534 MÖSSBAUER STUDIES OF SPIN FLOP IN ANTIFERROMAGNETIC HEMATITE by N. Blum, A.J. Freeman and J.W. Shaner (Nat'l. Magnet Lab., MIT) and L. Grodzins (MIT); Prog. 10th Ann. Conf. Magnetism and Magnetic Materials, Nov. 1964 (to be publ. in J. Appl. Phys.)

The antiferromagnetic sublattice magnetizations below the Morin transition temperature, $T_M = 250^\circ\text{K}$, are parallel and antiparallel to the trigonal axis of

rhombohedral α - Fe_2O_3 . Experiments at 80°K using the Mössbauer technique together with high external magnetic fields on both polycrystalline and single crystal samples show that the directions of the sublattice magnetizations flop from along the trigonal axis for the applied field $H_0 < H_c$ to perpendicular to the trigonal axis for $H_0 > H_c$; H_c is found to be 67.5 ± 3 koe. In the polycrystalline sample this behavior is exhibited through the occurrence of a maximum in the width of the outer lines of the Mössbauer spectrum plotted as a function of H_0 .

25,535 NÉEL TEMPERATURES OF CHROMIUM-VANADIUM ALLOYS FROM NMR MEASUREMENTS by R.G. Barnes and T.P. Graham (Iowa State U.); Prog. 10th Ann. Conf. Magnetism and Magnetic Materials, Nov. 1964 (to be publ. in J. Appl. Phys.)

The antiferromagnetic transition temperature, T_N , of chromium-rich Cr-V alloys has been investigated by means of the V^{51} and Cr^{53} NMR in these alloys. The intensity of the NMR signal decreases rapidly in a relatively narrow temperature range just above T_N and vanishes at T_N . Measurements on both natural and Cr^{53} -enriched chromium yield $T_N = 39.0 \pm 0.5^\circ\text{C}$, in excellent agreement with neutron diffraction results. T_N decreases roughly linearly with V content, falling below 4.2°K at 3.5 per cent V. Identical results are obtained from both the V^{51} and Cr^{53} resonances, and the extinction of the V^{51} resonance shows T_N to be field-independent within the range 3–13 koe. In all cases, the resonance intensity follows the empirical behavior, $I = I_0 \tanh K(1 - T_N/T)$, where $K \approx 15$.

25,536 A GRAPHICAL CORRELATION OF THE NÉEL TEMPERATURES OF CHLORIDES, BROMIDES AND IODIDES OF DIVALENT 3d TRANSITION METAL IONS by L.G. Van Uitert, H.J. Williams, R.C. Sherwood and J.J. Rubin (Bell Lab.); Prog. 10th Ann. Conf. Magnetism and Magnetic Materials, Nov. 1964 (to be publ. in J. Appl. Phys.)

Indirect exchange in isostructural compounds of divalent Mn, Fe, Co and Ni increases with the electron affinities of the cations and the polarizabilities of the anions. Spin-orbital coupling can increase T_N (for Fe) in a strong trigonal field, and decrease T_N in a cubic field. In either case T_N decreases with the crystal field. Exchange interactions in the chlorides, bromides and iodides take place via double anions. As a result a higher threshold cation electron affinity is required to effect spin alignment than for single anion intermediaries. A graphical comparison of the T_N values of the chlorides, bromides and iodides as a function of the ionization potentials of the cations demonstrates the consistency of these data with those of cubic oxides and fluorides and with simple principles.

25,537 A REVISED ANALYSIS OF MAGNETIC ANISOTROPY IN ANTIFERROMAGNETIC Cr_2O_3 by J.O. Artman (Carnegie Inst. Tech.), J.C. Murphy (Johns Hopkins U.) and S. Foner (Nat'l. Magnet Lab., MIT); Prog. 10th Ann. Conf. Magnetism and Magnetic Materials, Nov. 1964 (to be publ. in J. Appl. Phys.)

In antiferromagnetic crystals the results of AFMR, when combined with other data, yield the anisotropy K . By subtracting the magnetic dipolar anisotropy K_{MD} from K , the fine structure anisotropy K_{FS} is found. For Cr_2O_3 , the K_{MD} computation of Tachiki and Nagamiya, $0.059 \text{ cm}^{-1}/\text{ion}$, had been accepted as a basis for further analyses. However, in the course of computing K_{MD} by modern machine methods for various sesquioxide antiferromagnets, this value was found to be inappropriate. The Shull magnetic structure (c) to which Cr_2O_3 belongs is one in which the magnetic geometry effectively is almost cubic! The computed K_{MD} value thus is sensitive to small changes in lattice geometry.

25,538 MAGNETIC PROPERTIES OF THE Pd_3Mn_2 ALLOY by H. Yamauchi (Tohoku U.); J. Phys. Soc. Japan, Vol. 19, pp. 652–657, May 1964

The structure, magnetic properties and thermal properties of the η -phase and μ -phase of the Pd_3Mn_2 alloy were investigated. The ξ -phase has a b.c.c. lattice with the CsCl-type superstructure, while the μ -phase has a modified form of the ξ -phase superstructure. Both phases are antiferromagnetic, but in the μ -phase the susceptibility below the Néel point is strongly dependent on the field strength. The excess heat absorption at the Néel point is 510 cal./mol. (Pd_{15}Mn) for the μ -phase, 890 cal./mol. (Pd_{13}Mn) for the ξ -phase, and the heat of transformation from μ to ξ is 180 cal./mol. ($\text{Pd}_{10}\text{CrMn}_{10}$). These results are discussed on the basis of the two sublattice model of an antiferromagnet.

Antiferromagnetism of:

FeBr_2 - See 25,435

Rare Earth-Cu Compounds - See 25,509

CrCl_3 - See 25,436

Antiferromagnetic Properties of YMnO_3 and YbMnO_3 - See 25,199

25,539 RESONANCE OBSERVATION OF ANTIFERROMAGNETIC ORDERING IN RbMnCl_3 , CsMnCl_3 , and KMnCl_3 by R.W. Kedzie, J.R. Shane, M. Kestian and W.J. Croft (Sperry Rand Res. Ctr.); Prog. 10th Ann. Conf. Magnetism and Magnetic Materials, Nov. 1964 (to be publ. in J. Appl. Phys.)

Paramagnetic and antiferromagnetic resonances have been observed as a function of temperature in KMnCl_3 , CsMnCl_3 and RbMnCl_3 at 25 Gc. The linewidth (ΔH) of the nearly cubic KMnCl_3 [$\Delta H(297^\circ\text{K}) = 24$ gauss] remains essentially constant in the paramagnetic region. The ordering temperature (T_N) is sharply defined and can be determined to better than 0.5°K but it is found to vary from 103°K to 98°K depending upon crystal perfection. At $T = T_N$ the resonance abruptly and simultaneously broadens and splits into four anisotropic components. The AFMR move rapidly to zero applied magnetic field and then back up to 9.5 kG as the temperature is lowered. In contrast, the PMR linewidth of CsMnCl_3 [$\Delta H(297^\circ\text{K}) = 40$ gauss] does not remain constant but rises rapidly from 62 gauss at 100°K to 240 gauss at 77°K ($T_N \approx 70 \pm 5^\circ\text{K}$). A resonance line in the $g = 2$ region is visible down to a temperature of 35°K .

25,540 MAGNETIC STRUCTURE OF Fe_2As by H. Katsuraki and K. Suzuki (Nippon Tel. and Tel., Ibaraki); Prog. 10th Ann. Conf. Magnetism and Magnetic Materials, Nov. 1964 (to be publ. in J. Appl. Phys.)

Magnetic structure of single crystals of Fe_2As which corresponds to C38 type of crystal structure, the same as that of Mn_2Sb , has been determined by neutron diffraction methods. The crystal is antiferromagnetic with Néel temperature of approximately 50°C . A series of 00 l type reflections at room temperature reveals magnetic superstructure reflections at 001/2, 003/2, 005/2 and 007/2. These reflections disappear when the temperature of the specimen is elevated to 50°C , whereas the main reflections do not show any changes within the experimental error. The 003/2 reflection is considerably weak relative to 005/2. From these results it can be concluded that, as far as the components of the magnetic moments perpendicular to the [001] are concerned, this crystal has such an antiferromagnetic arrangement that Fe(II), Fe(I) and Fe(II) atoms, each on three successive layers parallel to the (001) plane, form a group in which the magnetic moments are parallel to one another, and these moments are anti-parallel to those of the neighboring groups.

25,541 THE CYCLOIDAL SPIN CONFIGURATION OF ORTHORHOMBIC MnSO_4 by G. Will, B.C. Frazer, G. Shirane, D.E. Cox and P.J. Brown (Brookhaven Lab.); Prog. 10th Ann. Conf. Magnetism and Magnetic Materials, Nov. 1964 (to be publ. in J. Appl. Phys.)

The magnetic structure of antiferromagnetic MnSO_4 has been determined from neutron diffraction data. At 4.2°K additional peaks of magnetic origin are observed which are slightly displaced from the positions expected on the basis of the original unit cell, or any simple multiple cell. Complete indexing of the magnetic peaks can be achieved only on the basis of a cone spiral arrangement related to a simple antiferromagnetic structure of CrVO_4 type, in which ferromagnetic (001) sheets are coupled antiparallel to adjacent sheets. The propagation vector of the spiral is along the a -axis, with a periodicity of 30 Å (almost 6a). The spin plane of the spiral component is the a - b plane. It is believed that this is the first case in which a spiral has been observed in an orthorhombic compound and it is of particular interest that the spiral is cycloidal.

25,542 PHASE TRANSITIONS AND ANTIFERROMAGNETIC RESONANCE IN UNIAXIAL ANTIFERROMAGNETS by H.B. Callen (U. Penna.); Prog. 10th Ann. Conf. Magnetism and Magnetic Materials, Nov. 1964 (to be publ. in J. Appl. Phys.)

The spin-flop transition, the transition to the paramagnetic state, AFMR, sublattice magnetization, and susceptibility in the various phases for a simple Heisenberg antiferromagnet with uniaxial anisotropy have been studied. The various effects are sensitive to the temperature dependent renormalization of spin-wave energies, and this renormalization is analyzed in some detail by a Green function analysis. The second-order transition from spin-flop to paramagnetic phases is directly proportional to the renormalization factor, and it is found that this varies as $(1 - 2aT^{3/2} + \dots)$ at low temperatures. In contrast to the ferromagnet (in which the magnetization varies as $1 - aT^{3/2}$) the kinematical and dynamical-kinematical interactions add rather than cancel; the physical interpretation will be discussed. In the antiferromagnetic phase two renormalizations (of spin-wave energies and of spin-wave moments) compete.

25,543 ANTIFERROMAGNETIC RESONANCE IN CoCl_2 AND FeCl_2 by I.S. Jacobs, S. Roberts and P.E. Lawrence (GE Res. Lab.); Prog. 10th Ann. Conf. Magnetism and Magnetic Materials, Nov. 1964 (to be publ. in J. Appl. Phys.)

The dichlorides of cobalt and iron are hexagonal layer antiferromagnets with ordering temperatures, T_N , at 24.7°K and 23.5°K respectively. The resonances were observed using a grating monochromator with Czerny-Turner optics. Their frequencies at 4.2°K are $\nu = 19.2 \pm 0.4 \text{ cm}^{-1}$ (CoCl_2) and $16.5 \pm 0.3 \text{ cm}^{-1}$ (FeCl_2); ν decreases slowly and the line broadens with increasing temperature, disappearing at T_N . CoCl_2 : The resonance condition contains a strong anisotropic exchange term taking the role usually played by phenomenological anisotropy.

25,544 LOW TEMPERATURE ANTIFERROMAGNETIC RESONANCE IN $\alpha\text{Fe}_2\text{O}_3$ by S. Foner and S.J. Williamson (Nat'l. Magnet Lab., MIT); Prog. 10th Ann. Conf. Magnetism and Magnetic Materials, Nov. 1964 (to be publ. in J. Appl. Phys.)

Antiferromagnetic resonance (AFMR) has been observed with 35, 70, and 120 cps radiation in single crystal synthetic and natural $\alpha\text{Fe}_2\text{O}_3$ from 4.2°K to 780°K. These measurements thus extend from far below the spin reorientation transition temperature T_M (about -10°C) to well above T_M . The usual low field AFMR as well as the spin-flop resonance mode were observed with pulsed magnetic fields applied parallel to the c-axis. The low temperature value of $(\Delta K)^{1/2}$ is approximately 65 gauss and decreases as T_M is approached. The anisotropy over the temperature range examined is much less than expected from magnetic dipolar or fine structure contributions. The high field (spin-flop) resonance mode ($T > T_M$) high frequency mode, whereas the usual AFMR mode abruptly terminates at $T = T_M$.

PARAMAGNETISM

25,545 DERIVATION OF SPIN HAMILTONIANS BY TENSOR DECOMPOSITION by W.J.C. Grant (Bell Lab.) and M.W.P. Strandberg (MIT); J. Phys. Chem. Solids, Vol. 25, pp. 635-639, June 1964

The spin Hamiltonian of a paramagnetic system is derived from the decomposition of spherical tensors having appropriate symmetry properties. Although the explicit use of group theory is involved, the Hamiltonian obtained is similar to that derived from purely group theoretical methods. Since perturbation theory is not invoked, the derivation applies regardless of the relative magnitude of the interactions, regardless of whether the lowest state of the free ion is an S-state, and regardless of whether the interaction of interest is linear, quadratic or of higher order.

25,546 DIFFUSE PARAMAGNETIC NEUTRON SCATTERING IN CHROMIUM SPINELS by K. Dwight, N. Menyuk and T.A. Kaplan (Lincoln Lab.); Prog. 10th Ann. Conf. Magnetism and Magnetic Materials, Nov. 1964 (to be publ. in J. Appl. Phys.)

The diffuse neutron diffraction attributable to the paramagnetic state in normal, cubic spinels is described. The elastic neutron scattering is calculated from the high-temperature expansion of the correlation function $\langle S_i \cdot S_j \rangle$ as a power series in inverse temperature, the pertinent coefficients being evaluated explicitly for a Heisenberg Hamiltonian with both nearest-neighbor A-B and B-B interactions. After normalization to the nuclear diffraction pattern, the computed diffuse scattering is compared with the experimental findings for both MnCr_2O_4 and MnCr_2S_4 . Excellent agreement exists in both cases, despite the striking qualitative difference between these two patterns. This agreement supports the calculational model, and thereby answers earlier speculation concerning the origin of the liquid-type diffraction peaks observed in the room-temperature diffraction patterns of most chromium spinels. It is shown that these peaks are not directly related to any spin canting in the ground state.

25,547 SOME MEASUREMENTS OF EXCHANGE ENERGIES BY PARAMAGNETIC NEUTRON INELASTIC SCATTERING by M.F. Collins and R. Nathans (AERE, Harwell); Prog. 10th Ann. Conf. Magnetism and Magnetic Materials, Nov. 1964 (to be publ. in J. Appl. Phys.)

A twin-rotor neutron spectrometer has been used to determine energy spectra for the paramagnetic scattering of slow neutrons. The second moment of the energy transfer for scattering at large angles gives the sum over all atoms of the square of the exchange constant J . This relationship is exact. Measurements for KMnF_3 assuming interactions to first neighbors only give an exchange constant of -0.43 ± 0.03 Mev. From a measurement of the paramagnetic Néel temperature a value of -0.39 Mev can be derived for J , again with first neighbor interactions only, while Smart, using the Bethe-Peierls-Weiss method, has obtained values of -0.26 Mev and -0.31 Mev from measurements of the Néel temperature and the susceptibility at the Néel temperature respectively. The discrepancy between these different values is surprisingly large and suggests that perhaps the assumption of interactions between nearest neighbors only is incorrect.

25,548 ON THE PARAMAGNETIC EFFECT IN SUPERCONDUCTORS IN TRANSVERSAL MAGNETIC FIELD by E. Trojnar (Low Temperature Lab., Wrocław); Acta Phys. Polonica, Vol. 24, pp. 801-808, Dec. 1963

The magnetic moment of the tin superconducting cylinder carrying current in transversal magnetic field has been measured. When the cylinder was in the intermediate state its magnetic moment obtained a paramagnetic sign, i.e., opposite to the sign of magnetic moment in completely superconducting state. It has been found that, likewise the case of longitudinal field, the minimal current required for the appearance of the effect is, for tin, 1.2 amperes. It has

been stated that this paramagnetic effect was a result of circular superconducting currents, circulating in the plane perpendicular to the direction of external magnetic field.

25,549 TRANSVERSE PARAMAGNETIC EFFECT IN A HARD SUPERCONDUCTOR by M.A.R. LeBlanc (Aerospace Corp. and U. Southern Calif.); Bull. Am. Phys. Soc., Vol. 9, p. 453(A), Apr. 1964

From an analysis of the induction in a hard superconductor of the Bean-Anderson type carrying a transport current in the presence of an external transverse field, Riemersma predicted the occurrence of a transverse paramagnetic effect. Observations of this phenomenon in a Nb-Zr wire are presented. The excess flux threading the sample is determined by the heat-pulse ballistic technique. The behavior of the effect shows good qualitative and semiquantitative agreement with calculations based on the Bean-Anderson model for an infinite slab // to the applied field H_a . When $4\pi I_c / 10H_a < 1$; (i) the transverse paramagnetic moment $\Delta\mu_0 / H_a^3$ at the critical current density I_c and (ii) upon introducing a transport current I after cooling in a field, $\Delta\mu_0(I/I_c)^3$.

25,550 PARAMAGNETIC SUSCEPTIBILITY OF FERRIMAGNETIC AND ANTIFERRIMAGNETIC SYSTEMS. Part II. DISCUSSION by B. Fehner (Mickiewicz U., Poznan); Acta Phys. Polonica, Vol. 25, pp. 61-69, Jan. 1964

The expression for the temperature dependence of the paramagnetic susceptibility derived is applied to manganese ferrite and comparison with experimental data is performed. The possibility of evaluation of the three phenomenological exchange interaction coefficients is discussed. It is proved that they may be chosen in such a way as to get a satisfactory agreement between theory and experiment for high temperatures. The expression for the susceptibility is compared also with formulae resulting from other theories. This leads to the conclusion that: (1) The Néel formula for the inverse susceptibility, based on molecular field theory, is an asymptotic expression valid only in the limit when the exchange interactions become very long range; otherwise it is exact only up to the zero power term of its expansion in $1/T$. (2) The formula for the inverse susceptibility given by the cluster theory of Bethe-Weiss, when expanded in $1/T$, is rigorously valid up to the square power term.

Paramagnetic Susceptibility of:

$\text{Th}_{1-x}\text{U}_x\text{Pd}$ - See 25,387

Superconducting Ta-V and Ta-Nb - See 25,279

25,551 PARAMAGNETISM OF Ti^{3+} IN TRIGONAL CRYSTALLINE FIELDS by T.H.E. Cottrell and C.R. Quade (U. Delaware); Bull. Am. Phys. Soc., Vol. 9, p. 502(A), Apr. 1964

The paramagnetic properties of Ti^{3+} in a crystalline field of trigonal symmetry have been calculated. If the behavior of the electronic-energy levels in a trigonal field is normal, then for Ti^{3+} the ground state should be magnetically inert to 1st order. However, after inclusion of the 2nd-order terms, the theoretical values for the g factors are $g_{\parallel} = 4[(\lambda + 30\gamma - 60\tau)^2 + 2\lambda^2]^{1/2} / \Delta_c$ and $g_{\perp} = 0$, where λ is the spin-orbit constant, γ and τ the trigonal-field parameters, and Δ_c the separation of the 2T_2 and 2E levels by the cubic field. The experimental g factors for Ti^{3+} in Al_2O_3 have been reported to be $g_{\parallel} = 1.067$ and $g_{\perp} < 0.1$, which also show the anomalous anisotropy. If it is assumed that $\Delta_c \sim 20,000$, $\lambda \sim 100$, $\gamma \sim -85$, and $\tau \sim 45 \text{ cm}^{-1}$, then the calculated value is $g_{\parallel} \sim 1.0$. The assumed parameters are not unique, but at the same time are consistent with those for other transition ions in crystalline fields.

25,552 OBSERVATION OF SUPERPARAMAGNETISM BY MÖSSBAUER EFFECT by W.J. Schuele (Franklin Inst.), S. Shtrikman (U. Penna.) and D. Treves (The Weizmann Inst. Sci., Rehovoth); Prog. 10th Ann. Conf. Magnetism and Magnetic Materials, Nov. 1964 (to be publ. in J. Appl. Phys.)

Mössbauer spectra in Fe^{57} in ultrafine NiFe_2O_4 and CoFe_2O_4 were studied as a function of crystallite size. A transition from 6-line to a doublet was observed with decreasing size with a corresponding change of the hyperfine field from about 0.5 to 0 mg. At room temperature, the transition occurred for a size of 170 and 130 Å for NiFe_2O_4 and CoFe_2O_4 , respectively. The transition was interpreted as a "motional narrowing" due to onset of superparamagnetism. A lower limit of 10^9 cps could be estimated for f_0 in the relation for the electron-spin-relaxation time, $\tau = (\exp K_v / kT) f_0$. Here, K is the anisotropy per unit volume, v crystallite volume, k Boltzman's constant, and T absolute temperature. As expected, the transition size was found to decrease at liquid-air temperature.

PARAMAGNETIC RESONANCE

25,553 QUANTUM THEORY OF TRANSITION PROCESSES IN PARAMAGNETIC RESONANCE (EFFECTIVE SPIN 1, EQUIDISTANT SPECTRUM) by A.R. Kessel' (Moscow State Sci. Res. Inst.); Soviet Phys.-Solid State, Vol. 5, pp. 2285-2291, May 1964

The equations describing the motion of the unfilled electron shells of paramagnetic particles with effective spin 1 and an equidistant spectrum are derived quantum-mechanically under the action of external alternating fields. Solutions are found for the equations for the case of a short-pulse of an external alternating field, for the process of returning to the equilibrium when the external field is turned off, and for the case under stationary condition. The possibility of observing the effects of electric dipole and quadrupole interaction is discussed.

25,554 AN ANALYSIS OF THE SHAPE OF ELECTRON PARAMAGNETIC RESONANCE SIGNALS FROM SAMPLES CONTAINING RANDOMLY ORIENTED PARAMAGNETIC CENTERS by V. S. Korolkov and A. K. Potapovich; *Optics and Spectroscopy*, Vol. 16, pp. 251-253, Mar. 1964

A simple method is suggested for the approximate analytical description of the shape of the first derivative of an EPR spectrum. Various methods for analyzing asymmetric lines are evaluated. The spectra of a number of compounds are analyzed, as examples.

25,555 ZEEMAN EFFECT OF THE PRINCIPAL EMISSION LINE IN A $\text{CaF}_2\text{-Tm}^{2+}$ CRYSTAL by B. P. Zakharchenya, V. P. Makarov, A. V. Varfolomeyev and A. Ya. Ryskin; *Optics and Spectroscopy*, Vol. 16, pp. 248-250, Mar. 1964

The Zeeman splitting of the narrow intensive emission line at 1.116μ in a $\text{CaF}_2\text{-Tm}^{2+}$ crystal has been investigated both experimentally and theoretically. It has been found that the line results from the magnetic dipole transitions $(^2F_{5/2})^2 \Gamma_7 \rightarrow (^2F_{7/2})^2 \Gamma_7$.

25,556 PARAMAGNETIC RESONANCE AND RELAXATION OF TRIVALENT RARE-EARTH IONS IN CALCIUM FLUORIDE. Part I. RESONANCE SPECTRA AND CRYSTAL FIELDS by M. J. Weber and R. W. Bierig (Raytheon Res. Div.); *Phys. Rev.*, Vol. 134A, pp. A1492-1503, June 15, 1964

The energy level structures arising from the crystal-field splitting of the free-ion ground states of trivalent rare-earth ions in CaF_2 are determined from a survey of the optical and electron paramagnetic resonance spectra. The predicted ground states are in agreement with existing paramagnetic resonance data. Estimates are made of the magnitude of the cubic crystal-field parameters and their variation throughout the rare-earth series. Axial crystal fields of tetragonal and trigonal symmetries, due to nearest-neighbor charge compensation, are found to cause large perturbations on the cubic-field energy levels. The paramagnetic resonance spectra of all rare-earth ions are reviewed and new resonances for Ce^{3+} , Sm^{3+} , Er^{3+} , and Yb^{3+} are reported. Expressions for the calculation of crystal-field matrix elements in terms of 3-j and 6-j symbols and their relationship to the operator equivalent approach are given in an Appendix.

25,557 SPLITTING OF THE PARAMAGNETIC RESONANCE LINES OF Cr^{3+} IONS IN RUBY IN AN EXTERNAL ELECTRIC FIELD by A. I. Rimus and A. A. Manenkov (Acad. Sci. USSR); *Soviet Phys.-Solid State*, Vol. 5, pp. 2634-2636, June 1964

A study of the splitting of the EPR lines of Cr^{3+} ions in ruby by an external electric field parallel to the trigonal crystal axis is reported. By comparing the experimental data with calculation, it is shown that the action of the external electric field is equivalent to a change in a constant D in the spin Hamiltonian. The mechanisms of splitting of the EPR lines and the R luminescence lines by an external electric field are shown to be the same.

25,558 ON DEHMELT'S EXPERIMENT by E. B. Alexandrov and V. A. Khodov (Acad. Sci. USSR); *Quantum Electronics-III*, pp. 299-300, Columbia U. Press, 1964

The results of Dehmelt's experiment (*Phys. Rev.*, Vol. 105, p. 1487, 1957) on the spin relaxation time of optically oriented free Na atoms are re-evaluated. It is suggested that Dehmelt's results were correct, but his explanation of the phenomenon was wrong. A new model to explain these results is presented and experiments to support it are reported.

25,559 SPIN RELAXATION OF ACCEPTOR STATES IN SILICON by Y. Yafet (Bell Labs.); *Bull. Am. Phys. Soc.*, Vol. 9, p. 502(A), Apr. 1964

The relaxation rates for the $3/2 \rightarrow 1/2$ and $3/2 \rightarrow -1/2$ transitions in the ground state of an acceptor in silicon have been calculated in the limits of ∞ and 0 spin-orbit coupling λ . Schechter's wavefunctions and measured values of the deformation potentials are used to obtain numerical values. The 2 limiting cases $\lambda = \infty$ and $\lambda = 0$ give comparable transition rates. For the $3/2 \rightarrow 1/2$ transition of a boron acceptor the following was found: (a) a 1-phonon process $(1/\tau) \sim H^2 T$ having a value of $\sim 2 \times 10^8 \text{ sec}^{-1}$ for $H = 30 \text{ kg}$ and $T = 1.2^\circ \text{K}$; (b) a Raman process $(1/\tau) \sim H^0 T^5$, which becomes comparable to the 1-phonon process at $T \sim 11^\circ \text{K}$; (c) an Orbach process via the lowest excited acceptor state 350°K above the ground state, which becomes dominant about 35°K .

25,560 INTENSITY OF ALLOWED AND FORBIDDEN ELECTRON PARAMAGNETIC RESONANCE LINES OF Mn^{2+} IN SrCl_2 by G. L. Bir and L. S. Sochava (Acad. Sci. USSR); *Soviet Phys.-Solid State*, Vol. 5, pp. 2637-2645, June 1964

An experimental study of the angular dependence of the intensity of the allowed and forbidden EPR lines in the axial spectrum of Mn^{2+} in SrCl_2 is reported. The data obtained are compared with the calculations based on Bir's theory. It is shown that the theory agrees very satisfactorily with experimental data. The results show that the reduction in the intensity of the allowed lines is related only to the increase in the intensity of the forbidden lines.

25,561 GENERAL THEORY OF CROSS RELAXATION. Part I. FUNDAMENTAL CONSIDERATIONS by W. J. C. Grant (Bell Labs.); *Phys. Rev.*, Vol. 134A, pp. A1554-1564, June 15, 1964

A statistical analysis is made of spin transitions induced by dipole interactions which change the total magnetization while exactly conserving energy. The first-order effect of the dipole operator can be described by a function $\Phi(\omega)$, which is related to the level broadening observed in resonance lines. The second-order effect leads to a function $\chi(\omega)$ which represents the power spectrum of the dipole operator. The cross-relaxation probability $W_{CR}(\omega)$ is given by the convolution of these two functions. W_{CR} is calculated explicitly in various approximations, without appeal to moments. For single-spin flips in magnetically dilute systems, the magnitude of W_{CR} depends linearly on the concentration n . There is a very sharp peak at $\omega = 0$ with a width proportional to the geometric mean of the resonance width and of the nearest-neighbor dipole energy.

25,562 GENERAL THEORY OF CROSS RELAXATION. Part II. HIGHER-ORDER PROCESSES by W. J. C. Grant (Bell Labs.); *Phys. Rev.*, Vol. 134A, pp. A1565-1573, June 15, 1964

The theory of part I is extended to multiple spin processes. The lowest order two-spin process yields a cross-relaxation probability W_{CR} whose principal characteristics are the same as those of W_{CR} for single spin flips. Higher order two-spin processes occur with much lower probability and this probability is not sharply peaked at harmonic coincidence. Three-spin and higher multiple K-spin processes yield functions $W_{CR}(\omega)$ whose width becomes progressively larger and less dependent on the concentration, and whose magnitude depends on the concentration n as n^K . The effects of short-range forces (exchange) are easily embodied in the theory, but in the absence of such forces special attention must be paid to the dipole fields of near neighbors, which are then likely to dominate the cross-relaxation process.

25,563 GENERAL THEORY OF CROSS RELAXATION. III. APPLICATION TO EXPERIMENT by W. J. C. Grant (Bell Lab.); *Phys. Rev.*, Vol. 134A, pp. A1574-1581, June 15, 1964

The theory developed in parts I and II is applied to the classical experiments of Mims and McGee, and Pershan. The predictions of the theory regarding the dependence of W_{CR} on the energy imbalance $\hbar\omega$ on concentration and on the exchange radius, as well as the prediction of the actual magnitude of W_{CR} , are confirmed in the Mims and McGee experiment on ruby. The crucial significance of near-neighbor dipole interactions, in particular, the effect of the associated power spectrum, which is quite broad and quite sensitive to crystal direction, is illustrated by application of the theory to Pershan's experiments on LiF.

25,564 NONERGODIC BEHAVIOR IN RUBY CROSSRELAXATION by R. L. Kyhl and B. D. N. Rao (MIT); *Bull. Am. Phys. Soc.*, Vol. 9, p. 502(A), Apr. 1964

A detailed study of the electron spin resonance in 0.05% ruby has been made at various crossrelaxation orientations at 8 kMc/sec. The 2-quantum cross-relaxation near 4400 G and an angle of 27° between c axis and magnetic field, and the two 3-quantum processes near 3100 G and 33° were examined for 4 concentrations: 0.005%, 0.02%, 0.05% and 0.1%. The crossrelaxation decay for the 3-quantum processes is a good exponential and the time constants vary approximately as the inverse 1.6 power of concentration. The 2-quantum process shows a t^{-2} -type decay. The inhomogeneous broadening of the EPR lines could provide a distribution of time constants in the decay, but the spin diffusion within the resonance is observed with a time constant $\sim 5 \mu\text{sec}$, which is much smaller than the crossrelaxation times. This indicates that the spin diffusion is nonergodic.

25,565 SPIN-LATTICE RELAXATION TIME OF CONDUCTION ELECTRONS IN SODIUM METAL by F. Vescial, N. S. VanderVen and R. T. Schumacher (Carnegie Inst. Tech.); *Phys. Rev.*, Vol. 134A, pp. A1286-1290, June 1, 1964

The temperature dependence of the spin-lattice relaxation time T_1 in sodium metal from 14 to 77°K has been measured. Results agree with those of Feher and Kip, and Levy, in the range 20 to 40°K , but disagree with Feher and Kip

above 40°K. As a consequence, marked deviation from the relation T_1T_2 -constant is found even at the highest temperatures. The temperature dependence lends strong support to the recent calculation of Yafet in the temperature range 5 to 77°K.

25,566 PARAMAGNETIC-RESONANCE-RELAXATION STUDIES AT MILLIMETER WAVELENGTHS WITH THE USE OF PULSED MAGNETIC FIELDS by R. Rimai, B.D. Silverman and R.W. Bierig (Raytheon Res. Div.); *Bull. Am. Phys. Soc.*, Vol. 9, p. 502(A), Apr. 1964

Paramagnetic resonance of a number of impurities in ionic-crystal hosts has been investigated, and observed relaxation effects have been interpreted to give field information about spin-lattice relaxation processes. For rare earths, with Kramers doublet ground state well-separated from the higher energy states, the field dependence of the direct-process relaxation rate follows the law $T_1^{-1} \propto H^5 \coth(g\beta H/2kT)$. The relaxation times observed at X band are shorter than the preceding relation predicts, which indicates that at the smaller splittings the relaxation due to the thermal modulation of the crystal field is dominated by other mechanisms. For cases where the crystal-field splitting cannot be considered large as compared with the Zeeman splitting of the ground Kramers doublet, one expects deviations from the above field dependence.

25,567 HIGH-TEMPERATURE ELECTRON SPIN RELAXATION OF THE F CENTER by E.L. Wolf (Cornell U.); *Bull. Am. Phys. Soc.*, Vol. 9, p. 492(A), Apr. 1964

The spin-relaxation-time product T_1T_2 of the F electron in additively colored KCl crystals has been measured by the saturation technique for temperatures between 20° and 550°C. Up to about 350°C, the rate $(T_1T_2)^{-1}$ increases approximately as T^2 and shows noticeable dependence on the thermal history of the sample. Above about 400°C, the relaxation rate is well-defined and increases exponentially: $(T_1T_2)^{-1} = 3 \times 10^{23} e^{-2U/k} \text{ sec}^{-2}$, where $U = 0.85 \pm 0.1 \text{ eV}$. For F concentrations of 5×10^{17} to 2×10^{18} per cc. The high-temperature relaxation process was tentatively interpreted as the exchange of the F electron for a conduction electron having antiparallel spin. The conduction electrons, in ionization equilibrium with F centers were assumed to have short T_1 . The exchange cross section was estimated to be $\sim 10^{-13} \text{ cm}^2$ for KCl, giving agreement with the measured $(T_1T_2)^{-1}$ at 550°C for conduction-electron concentration $n \sim 10^{12}$ per cc.

25,568 PARAMAGNETIC RESONANCE AND RELAXATION OF TRIVALENT RARE-EARTH IONS IN CALCIUM FLUORIDE. Part II. SPIN-LATTICE RELAXATION by R.W. Bierig, M.J. Weber and S.L. Warshaw (Raytheon Res. Div.); *Phys. Rev.*, Vol. 134A, pp. A1504-1516, June 15, 1964

The temperature dependence of the spin-lattice relaxation time T_1 of trivalent rare-earth impurities in CaF_2 has been measured at 9.6 kMc/sec. The rare earths investigated include Kramers ions (Ce^{3+} , Nd^{3+} , Dy^{3+} , Er^{3+} , Yb^{3+}), one non-Kramers ion (Tb^{3+}), and one S-state ion (Gd^{3+}). The relaxation of ions in lattice sites of cubic, tetragonal, and trigonal crystal-field symmetries have been studied and are different. At liquid-helium temperatures the relaxation usually exhibits a T^{-1} temperature dependence; however, the magnitudes are approximately two orders-of-magnitude shorter than estimated single-phonon relaxation times based upon the orbit-lattice interaction. Measurements of the Ce^{3+} relaxation in five samples containing from 0.08 to 1.6 per cent Ce combined with results from other ions show that T_1 decreases with increasing rare-earth concentration. Multiple exponential recoveries from saturation are observed at low temperatures.

25,569 MAGNETIC RELAXATION IN RARE EARTH SALTS by A.H. Cooke and E.J. Daintree (Clarendon Lab.); *Cont. AF61 052 677*, 11pp., Sept. 20, 1963; U.S. Gov. Res. Rep., Vol. 39, p. 144(A), May 5, 1964
AD 430 574 OTS \$1.60

Experiments have been made on spin-lattice relaxation in rare earth salts in the helium range of temperatures. It is found that at the lowest temperatures, at which relaxation by the 'direct' one-phonon process would be expected to predominate, the relaxation time derived from measurements by the Casimir-Du Pre low frequency method departs in several ways from the predictions of theory, and in particular increases with magnetic field. It is shown that these features can be accounted for if allowance is made for variations of the temperature of the phonons in contact with the spin system, due to a 'phonon bottleneck,' of the type postulated by Scott and Jeffries.

25,570 SPIN-LATTICE INTERACTION IN RUBY by P.L. Donoho and R.B. Hemphill (Rice U.); *Repr. from Proc. Intern. Conf. on Low Temp. Phys.*, pp. 294-295; *STAR*, Vol. 2, p. 1297(A), May 23, 1964 NASA Grant NsG-6-59

The spin-lattice interaction in ruby containing 0.05% Cr^{+++} was investigated by measuring the effect of uniaxial stress on the electron-spin-resonance spectrum. Line shifts proportional to the applied stress have been observed at a frequency of 10.1 Gc for all observable transitions and for various directions of the stress. The observed shifts and the components of the magnetoelastic tensor computed from the observed line shifts agree quite well with the work of others. The spin-lattice relaxation time for direct one-phonon transitions can be computed from knowledge of the magnetoelastic tensor G . Crude computation of the relaxation time indicates that exchange interactions should be negligible for extremely small chromium concentrations, and that the direct one-phonon process should dominate, although cross relaxation is still important.

25,571 ELECTRON-SPIN RESONANCES IN GAMMA-RAY-IRRADIATED ALUMINUM OXIDE by F.T. Gamble, R.H. Bartram, C.G. Young and O.R. Gilliam (U. Connecticut) and P.W. Levy (Brookhaven Lab.); *Phys. Rev.*, Vol. 134A, pp. A589-595, May 4, 1964

Single crystals of α -aluminum oxide were subjected to gamma-ray irradiation at 77°K. A single, asymmetric, paramagnetic-resonance absorption was produced with $g_{\parallel} = 2.012 \pm 0.002$ and $g_{\perp} = 2.008 \pm 0.002$, where \parallel and \perp are with respect to the c axis. The line width is about 50 G at 300 and 77°K. The absorption line has been analyzed as a superposition of three Gaussian lines with the isotropic g values: $g_1 = 2.020 \pm 0.003$, $g_2 = 2.006 \pm 0.003$, $g_3 = 2.006 \pm 0.003$. The component lines are tentatively attributed to two types of centers: a trapped hole localized on an anion adjacent to a cation site which is deficient in positive charge, and an electron trapped at an anion vacancy. The cation site may be vacant, or may contain a monovalent or divalent substitutional impurity.

25,572 ISOTOPIC SHIFT IN THE ELECTRON-SPIN-RESONANCE ABSORPTION SPECTRUM OF Cr^{3+} IN MAGNESIUM OXIDE by S.A. Marshall, J.A. Hodges and R.A. Serway (IITRI); *Bull. Am. Phys. Soc.*, Vol. 9, p. 502(A), Apr. 1964

The fine- and hyperfine-structure spectra of trivalent ^{52}Cr ($I=0$) and ^{53}Cr ($I=\frac{3}{2}$) located substitutionally for magnesium in magnesium oxide at sites of axial symmetry, where the axial distortion is along a crystal [100] direction, have been reexamined at 3 cm wavelength. Spectral constants for both these isotopes have been measured with a precision equivalent to determining absorption-line field positions to within ± 20 mOe. From measurements taken at 77°K, it is concluded that the D value for ^{52}Cr is (0.20 ± 0.01) oe greater than that for ^{53}Cr , which corresponds to a relative shift in D of 2.3×10^{-4} . The g values for the 2 isotopes exhibit no measurable differences. From similar data taken over the range 4.2° to 273°K, it was found that the isotopic shift in the D value measurably decreases with increasing temperature over this temperature range.

25,573 INVESTIGATION OF NARROW LINE PARAMAGNETIC RESONANCE ABSORPTION SPECTRUM IN SINGLE CRYSTAL CALCITE by S.A. Marshall (ITT Res. Inst.); *Cont. AF30 602 2912*, 55pp., Mar. 1964; U.S. Gov. Res. Rep., Vol. 39, p. 107(A), June 5, 1964 AD 433 680 OTS \$5.60

Results of a program of study on the narrow line paramagnetic resonance absorptions in single crystals of calcite are presented. These include an analysis carried out on the spectrum of the trivalent iron isotopes, Fe^{54} , Fe^{56} , and Fe^{57} in calcite and the spectral shifts associated with these isotopes, an analysis of the spectrum of the molecular ion CO_2 and finally the superhyperfine structure in the divalent manganese ion spectrum due to the magnetic interaction of the C^{13} isotope with the manganese ion.

25,574 ELECTRON PARAMAGNETIC ABSORPTION IN IRRADIATED POLY-CRYSTALLINE $\text{Hg}_2(\text{NO}_3)_2 \cdot 2\text{H}_2\text{O}$ by I. Bójko (Polish Acad. Sci.); *Acta Phys. Polonica*, Vol. 24, pp. 281-282(L), Aug. 1963

Electron paramagnetic absorption in γ -irradiated $\text{Hg}_2(\text{NO}_3)_2 \cdot 2\text{H}_2\text{O}$ is discussed. From a study of the absorption spectrum it is concluded that changes are due to the hyperfine structure of the spectrum, derived from the interaction between electrons and nuclear magnetic moments of spin $I=1$. One of the paramagnetic products of decay of $\text{Hg}_2(\text{NO}_3)_2 \cdot 2\text{H}_2\text{O}$ is Nitrogen Peroxide.

25,575 COMMENT ON g-SHIFT IN THE ELECTRON PARAMAGNETIC RESONANCE OF F-CENTERS by F. Hughes (U.S. Naval Res. Lab.); *Phys. Stat. Sol.*, Vol. 5, pp. 55-61, 1964

g-shift calculations for the electron paramagnetic resonance of F-centers arising from nuclear hyperfine interactions are discussed. The calculated g-shift is found to be too small to be of interest for instances solely requiring the use

of the contact hyperfine term of the first nuclei shell. For F-centers with large anisotropic hyperfine interaction constants, the concept of a hyperfine induced g-shift is meaningful solely in terms of an electron-nuclear double resonance experiment. Under such circumstances, the experimentally observed hyperfine g-shifts are comparable to the shifts induced by spin-orbit effects.

25,576 SOME SATURATION EFFECTS ON THE EPR SPECTRUM OF F CENTERS IN KCl AT 4°K by G.A. Noble (IITRI); *Bull. Am. Phys. Soc.*, Vol. 9, p. 491(L), Apr. 1964

When a portion of the electron spin resonance of the F center in KCl is saturated, the width of the saturated region is greater than that expected for low concentrations. The same magnetic field and microwave frequency that saturates symmetrically about the center of the line will produce a greater saturation of the part of the resonance that is at a lower field if the power is increased. The results also depend on the duration of the application of the saturation power. The experimental results indicate that the nuclear-spin environment of the F centers possibly changes during the application of power.

25,577 EPR OF EXCHANGE-COUPLED PAIRS OF Eu^{2+} IN CaO AND SrO by B.A. Calhoun and J. Overmeyer (IBM Watson Res. Ctr.); *J. Appl. Phys.*, Vol. 35, pp. 989-990, Mar. 1964

The EPR spectra of isolated Eu^{2+} ions have been studied in crystals of CaO and SrO . In SrO , there is no crystal field splitting of the $^8S_{7/2}$ level of the Eu^{2+} . The g values and hyperfine constants are the same in both crystals. Crystals of CaO and SrO containing 1%-2% Eu exhibit in addition a large number of weak lines at both lower and higher fields than the single ion spectra observed in more lightly doped crystals. These resonances arise from coupled pairs of Eu^{2+} ions, and their analysis provides direct information about the exchange interactions between the Eu^{2+} ions. The temperature dependence of these intensities shows that the nearest neighbor exchange interaction J_{nn} is ferromagnetic and its magnitude is approximately 1° . In the [100] direction, some of the resonances due to next-nearest neighbor pairs have been identified. This exchange interaction J_{nnn} is very small, less than 0.1° . Its sign cannot be determined from the temperature dependence of the intensities of the resonances.

25,578 PARAMAGNETIC CENTERS IN IRRADIATED NaClO_3 AND NaBrO_3 by C. Ramasastry, S.B.S. Sastry, Y.V.G.S. Murthy and J. Sobhadhri (Indian Inst. Tech.); *J. Phys. Soc. Japan*, Vol. 19, pp. 770-771, May 1964

Paramagnetic resonance observed in X-ray irradiated NaClO_3 and NaBrO_3 crystals are interpreted in light of their optical absorption. Peaks were found for O_3 , Cl^{35} , Cl^{37} , ClO_2 , and ClO_3^- in NaClO_3 . In NaBrO_3 optical absorption has shown the presence of only the non-paramagnetic BrO . After a partial thermal bleaching the residual ESR signal consisted of a single peak of gaussian shape.

25,579 ELECTRON PARAMAGNETIC RESONANCE OF Fe^{3+} IN THE STRONG AXIAL FIELD OF PbTiO_3 HOST by D.J.A. Gainon (Clevite, Cleveland); *Phys. Rev.*, Vol. 134A, pp. A1300-1301, June 1, 1964

An electron paramagnetic resonance investigation has been made of single crystals of tetragonal PbTiO_3 . A spectrum attributed to Fe^{3+} was found which can be described by the spin Hamiltonian: $\mathcal{H} = g_{\parallel}\beta H_z S_z + g_{\perp}\beta(H_x S_x + H_y S_y)$ with $S = \frac{1}{2}$, $g_{\parallel} = 2.009 \pm 0.005$ and $g_{\perp} = 5.97 \pm 0.02$ at room temperature. These values are explained in terms of a strong tetragonal component of the crystal-line field.

25,580 ELECTRON SPIN RESONANCE ON INTERACTING DONORS IN SILICON by D. Jérôme and J.M. Winter (CEN, Saclay); *Phys. Rev.*, Vol. 134A, pp. A1001-1007, May 18, 1964

The value of the exchange integral J between pairs of donor centers in silicon has been investigated by looking at the ENDOR spectrum of phosphorus-doped silicon in a range of concentration of the order of 8×10^{16} per cc. The microwave field is saturating the cluster electronic line. The line shape of the ENDOR lines gives an unambiguous determination of the sign of this exchange integral which turns out to be antiferromagnetic. It is also possible to determine an order of magnitude of J and to have an idea about its distribution for two samples. All the features of the ENDOR spectrum are explained in a qualitative way by calculating all the energy levels using a second-order perturbation calculation. A line coming from an ionized phosphorus center, weakly coupled to a pair of neutral phosphorus is also identified.

25,581 ELECTRON SPIN RESONANCE STUDIES WITH SUPERCONDUCTING MAGNETS: THE SPECTRUM OF Dy^{3+} AND Sm^{3+} IN CaF_2 by W. Low (Nat'l. Magnet Lab., MIT); *Phys. Rev.*, Vol. 134A, pp. A1479-1482, June 15, 1964

An electron spin resonance spectrometer has been constructed using strong magnetic fields up to 46,000 G generated by a superconducting magnet. It is being used for the measurement of the magnetic properties of transition elements in ionic crystals such as (a) small g factors, (b) energy level separations up to 20 cm^{-1} , (c) isotropic and anisotropic exchange terms in spectra of pairs of paramagnetic ions, (d) spin-lattice relaxation times at high magnetic fields. The method is illustrated in the measurements of (1) the energy level separation of $\Gamma_8 - \Gamma_7$ levels of Dy^{3+} in CaF_2 which is found to be $7.35 \pm 0.2 \text{ cm}^{-1}$; (2) the g factors of the tetragonal spectrum of Sm^{3+} in CaF_2 which are found as $g_{\parallel} = 0.907 \pm 0.01$, $g_{\perp} = 0.544 \pm 0.015$.

25,582 PARAMAGNETIC RESONANCE OF CHROMIUM IN CdTe by G.W. Ludwig and M.R. Lorentz (GE); in *Res. on CdTe* (1963), Cont. AF 33(616)-8264, 15 pp.; *STAR*, Vol. 2, p. 1298(A), May 23, 1964 AD 404 859

The paramagnetic properties of chromium in the $3d^5$ configuration in cadmium telluride are discussed. Sample preparation, properties, and the resonance spectrum are described. A description is presented of an electron-nuclear double-resonance technique used to examine samples in order to gain information on the hyperfine interactions with Cr^{53} and with the magnetic Cd isotope. Results of the study are discussed.

25,583 ELECTRON SPIN RESONANCE OF Mn^{4+} ION IN MgO by M. Nakado, K. Awazu, S. Ibuki and M. Date (Osaka U.); *J. Phys. Soc. Japan*, Vol. 19, p. 78(L), May 1964

Electron spin resonance of Mn^{4+} in MgO has been studied by using optical luminescence measurements at liquid He temperatures. The g value was found to be 1.99 ± 0.002 and $|A| = (72.0 \pm 0.4) \times 10^{-4}$. These values were compared with the Mn ion in TiO_2 .

25,584 PARAMAGNETIC RESONANCE OF Yb^{3+} IN CaWO_4 by U. Ranon (Israel AEC) and V. Volterra (Hebrew U.); *Phys. Rev.*, Vol. 134A, pp. A1483-1485, June 15, 1964

Paramagnetic resonance of Yb^{3+} has been observed in single crystals of CaWO_4 at 20°K and 3 cm. A tetragonal as well as two rhombic spectra were found. The tetragonal spectrum is fitted to an axial spin Hamiltonian with $g_{\parallel} = 1.058 \pm 0.002$, $g_{\perp} = 3.920 \pm 0.005$, $|^1A| = (77 \pm 1) 10^{-4} \text{ cm}^{-1}$, $|^1B| = (285 \pm 1) 10^{-4} \text{ cm}^{-1}$, $|^1E| < 2.10^{-3} \text{ cm}^{-1}$, $|^1A| = (279 \pm 3) 10^{-4} \text{ cm}^{-1}$, $|^1B| = (1034 \pm 3) 10^{-4} \text{ cm}^{-1}$. The rhombic spectra have the y and z axes in the {110} planes. One has the z axis at $6^\circ \pm 1^\circ$ to the crystallographic c axis and $g_x = 3.012 \pm 0.005$, $g_y = 4.788 \pm 0.005$, $g_z = 0.975 \pm 0.003$. The other has the z axis at $7^\circ \pm 1^\circ$ to the c axis and $g_x = 4.155 \pm 0.005$, $g_y = 3.704 \pm 0.005$, $g_z = 1.155 \pm 0.003$. The spectra arise from Yb^{3+} ions at Ca^{2+} sites and the rhombic symmetry is caused by charge compensation at next-nearest-neighbor Ca^{2+} sites. The possibility of W^{6+} substitution is discussed.

25,585 SELECTION RULES AND ANGULAR DEPENDENCE IN PARAMAGNETIC ACOUSTIC RESONANCE by W.I. Dobrov (Lockheed Res. Lab.); *Phys. Rev.*, Vol. 134A, pp. A739-742, May 4, 1964

The problem of spin transitions between magnetic sublevels under ultrasonic excitation is treated by considering perturbation terms $\beta H_0 \cdot h \cdot S$ (dipolar) and $S \cdot d \cdot S$ (quadrupolar). When the tensors h and d are expanded in acoustic strains, the resulting expansion coefficients form a magnetoelastic matrix which describes the spin-phonon coupling. For the quadrupolar term which is dominant for $S > \frac{1}{2}$, the magnetoelastic matrices are obtained for all crystal classes with the assumption that they are not necessarily symmetric. By using the transformation of spin operators, which includes the case of anisotropic g factors, general expressions for acoustic transition probabilities in dipolar and quadrupolar cases are derived in terms of h_i and d_i . It is shown how the acoustic absorption coefficients are obtained for any direction of polarization and wave propagation, for arbitrary direction of the external magnetic field, and for all crystal classes.

Paramagnetic Resonance in RbMnCl_3 , CsMnCl_3 and KMnCl_3 - See 25,539

25,586 NUCLEAR MAGNETIC RESONANCE OF La^{139} AND Al^{27} AND ELECTRON PARAMAGNETIC RESONANCE OF Fe^{3+} IN LANTHANUM ALUMINATE by K.A. Mueller (IBM Zurich Res. Lab.), E. Brun, B. Derighetti, J. E. Drumheller and F. Waldner (U. Zurich); *Phys. Lett., Neth.*, Vol. 9, pp. 223-224(L), Apr. 15, 1964

Measurements of the nuclear magnetic resonance (NMR) of La^{139} and Al^{27} and the electron paramagnetic resonance (EPR) of Fe^{3+} in lanthanum aluminate are

discussed. Electric nuclear quadrupole effects were found in the NMR spectra of La^{139} and Al^{27} in crystals grown by the Verneuil process. Systematic measurements of the angular dependence of the quadrupolar split lines have provided evidence for the existence of an axial field gradient tensor with respect to the deformation axis in the temperature range from 77° to 300°K. The quadrupolar coupling constants eQV_{ZZ}/h were determined using the usual Hamiltonian. Comparison of experimental results indicates that for the temperature range studied V_{ZZ} for Al^{27} and D for Fe^{57} are proportional to each other and are almost linearly dependent on the rhombohedral distortion angle $\Delta\beta$.

25,587 NUCLEAR MAGNETIC RESONANCE IN BISMUTH METAL AT 4.2°K by R.R. Hewitt and B.F. Williams (U. California); *Phys. Rev. Lett.*, Vol. 12, pp. 216-217(L), Mar. 2, 1964

The nuclear magnetic resonance (NMR) spectrum of pure bismuth metal powder at 4.2°K is discussed. Analysis of the spectrum measured at the resonant frequency ν_R of 16 Mc indicates that the splitting of the $(\frac{1}{2}-\frac{1}{2})$ transition $\Delta\nu_{HL}$ is given by $\Delta\nu_{HL}/\nu_R = 25b/9\nu_R^2 - 5/3a$, where $b = 1/16 \nu_Q^2 [I(I+1)-3/4]$, $a = K_{ax}/(1+K_{iso})$, and $\nu_Q = 3e^2qQ/2I(2I-1)h$. From the plot $(\Delta\nu_{HL}/\nu_R^{-1})$ vs ν_R^{-2} , $K_{ax} = 2.7$ per cent and $\nu_Q = 2.40$ Mc, and from the extremum positions ν_H and ν_L , the isotropic Knight shift $K_{iso} = -0.3 \pm 0.2$ per cent. In an independent measurement (based on the separation of pairs of corresponding satellites), a value of $\nu_Q = 2.44 \pm 0.07$ Mc was obtained. The quadrupole coupling e^2qQ/h of 58.5 ± 2 Mc is higher by a factor of about two than the value estimated from specific heat data.

25,588 ABSENCE OF PRONOUNCED QUADRUPOLE EFFECTS IN THE NUCLEAR MAGNETIC RESONANCE OF In^{115} IN A NONCUBIC ENVIRONMENT by L.H. Bennett and R.J. Snodgrass (Nat'l. Bur. Stand.); *Phys. Rev.*, Vol. 134A, pp. A1290-1293, June 1, 1964

The nuclear magnetic resonance of In^{115} has been observed throughout the cubic phase of Pb-In alloys, at 77 and 300°K. The Knight shift is 0.87 per cent and is essentially unchanged with composition. The linewidths increase rapidly with In concentration, probably mostly due to pseudodipolar interaction. The average electric field gradient at a In^{115} nucleus for any configuration of Pb neighbors is about $q \sim 3 \times 10^{22} \text{ cm}^{-3}$, about 20 times smaller than for Cu having a Zn second neighbor in the fcc Cu lattice. The small value of the field gradient is discussed in terms of the behavior of the charge oscillations, and is related to the small change in Knight shift for Pb^{207} in these same alloys.

25,589 NUCLEAR MAGNETIC RESONANCE IN LEAD ALLOYS by R.J. Snodgrass and L.H. Bennett (U. Maryland); *Phys. Rev.*, Vol. 134A, pp. A1294-1295, June 1, 1964

The Pb^{207} nuclear magnetic resonance has been measured in a series of lead base primary solid solutions containing Cd, In, Sn, Sb, Hg, Tl, and Bi as solutes. The central resonance frequency of Pb^{207} shifts in proportion to the solute concentration and in the opposite direction to be explained by impurity charge screening of the Thomas-Fermi type. The fractional change in Knight shift for all solutes is small $\Delta k/k \approx 0.05$ c. The important parameter in determining the change in Knight shift seems to be the difference in valence between the impurity atoms and the lead atoms. The absorption linewidths broaden rapidly upon the addition of solute. In the absence of a quantitative calculation it is not possible to determine if the small shifts, large widths, and small quadrupole effects in In^{115} are consistent with the theory of long-range oscillations of electronic charge.

25,590 NUCLEAR MAGNETIC RESONANCE IN INTERMETALLIC COMPOUNDS by G.W. West (U. Melbourne, Australia); *Philosophical Mag.*, Vol. 9, pp. 979-991, June 1964

The nuclear magnetic resonance absorption of aluminum and cobalt has been studied in the intermetallic compounds NiAl, CoAl, FeAl, Al_2NiCo , Al_2FeCo , Al_2FeNi and CoTi. The intensity measurements indicate a high degree of order in all the compounds studied, particularly NiAl and CoAl. The relatively large values of intensity at compositions appreciably different from the equiatomic value for these two series of compounds is accounted for by assuming that a large volume of the material remains ideally ordered and that the excess atoms, or vacancies, are not distributed at random. The Knight shift for ^{27}Al in the equiatomic compounds NiAl, CoAl and FeAl is $+0.063 \pm 0.003\%$, $+0.034 \pm 0.003\%$, and $-0.390 \pm 0.005\%$ respectively, and for ^{59}Co in CoAl and CoTi the values are $+0.110 \pm 0.003\%$ and $+2.250 \pm 0.003\%$. The Knight shift is independent of composition in the β' phase region for NiAl and FeAl, but varies in CoAl becoming negative at lower values of aluminum content.

25,591 NUCLEAR MAGNETIC RESONANCE OF H^1 AND Nb^{93} IN THE NI-BIUM-HYDROGEN SYSTEM by D. Zamir and R.M. Cotts (Cornell U.); *Phys. Rev.*, Vol. 134A, pp. A666-675, May 4, 1964

The nuclear magnetic resonance of H and Nb⁹³ have been observed in the NbH_x system as a function of hydrogen concentration and temperature. It is shown that line narrowing of the steady-state absorption resonance is limited at high temperatures by inhomogeneous broadening due to a distribution of fields caused by bulk paramagnetism of the samples. A sharp, though not discontinuous, change of hydrogen diffusion is observed at temperatures that range from 60 to 100°C and that depends on hydrogen concentration. Niobium resonance linewidth and intensity changes indicate that sharp change in proton diffusion is associated with the phase transition to the high-temperature cubic phase of the hydrides. The activation energy of NbH_{0.7} is $E_a = 5$ kcal/mole in the low-temperature (orthorhombic) phase and $E_a = 3.7$ kcal/mole in the high-temperature (cubic) phase. The niobium resonance is observable at all hydrogen concentrations.

25,592 SENSITIVE DETECTION OF PURE QUADRUPOLE SPECTRA OF NUCLEI (10^{15} TO 10^{18} cm^{-3}) NEAR IMPURITIES IN NaCl by R.E. Slusher and E. L. Hahn (U. California); *Phys. Rev. Lett.*, Vol. 12, pp. 246-248(L), Mar. 9, 1964

The detection of the nuclear magnetic resonance of Na and Cl nuclei located at noncubic sites (b spins) in impure NaCl is discussed. The magnetic resonance of these low concentration nuclear moments (10^{15} to 10^{18} cm^{-3}) is detected by their effect on the more abundant nuclear moments of Na and Cl nuclei located at cubic sites (a spins). The noncubic sites result from lattice distortions caused by isolated impurities. The Na and Cl nuclei at the cubic sites come into contact with the nuclei at the noncubic sites through the spin-spin diffusion process, following adiabatic demagnetization of the sample from an initial magnetic field.

25,593 MOTIONAL NARROWING OF NUCLEAR MAGNETIC-RESONANCE LINES IN MANGANESE-DOPED LITHIUM FLUORIDE by T.G. Stoebe, T.O. Ogurtani and R.A. Huggins (Stanford U.); *Phys. Rev.*, Vol. 134A, pp. A963-964, May 18, 1964

Nuclear magnetic-resonance experiments have been performed between 25 and 550°C in LiF powder doped with manganese. Motional narrowing of the Li^7 resonance line occurred somewhat below 400°C. Resonance absorption lines were not observable in the temperature range 200-390°C, probably because an effective loss of paramagnetic relaxation centers increased the spin-lattice relaxation time. Electron spin-resonance experiments verified that the paramagnetic manganese does cluster upon heating above 200°C. A method of analysis is developed which eliminates errors due to constant linewidth contributions in the analysis of motional narrowing data in terms of diffusion activation energies. The activation energy for motion of Li ion vacancies in LiF is found to be 0.74 ev.

25,594 Mn^{55} NUCLEAR MAGNETIC RESONANCE IN MnO by E.D. Jones (Bell Labs.); *Prog. 10th Ann. Conf. Magnetism and Magnetic Materials*, Nov. 1964 (to be publ. in *J. Appl. Phys.*)

The Mn^{55} NMR has been observed in the paramagnetic state of the antiferromagnet MnO. A hyperfine interaction of the form $\mathbf{A} \cdot \mathbf{I} < \mathbf{S} >$ gives rise to a Mn^{55} NMR frequency shift $(\Delta\nu/\nu)$. The observed frequency shift is temperature dependent, varying from about -10.9% to -9.2% in the range 150°K to 300°K. The temperature dependence of the Mn^{55} frequency shift agrees, within experimental error, with the observed temperature dependence of the O^{17} frequency shift in MnO. From the observed linear dependence of the frequency shift on the magnetic susceptibility, the hyperfine coupling constant A^{55} is evaluated for MnO and compared with the value for A^{55} determined by EPR on $\text{Mn}^{2+}:\text{MgO}$. The separation between the absorption derivative extreme of the Mn^{55} NMR is $\Delta H \approx 340$ gauss, in satisfactory agreement with the predictions of exchange narrowing of hyperfine broadened nuclear magnetic resonances in paramagnetic media.

25,595 NUCLEAR MAGNETIC RESONANCE IN NICKEL-FLUOSILICATE BETWEEN 0.15°K AND 4.2°K by K. Kume and T. Sugawara (U. Tokyo); *J. Phys. Soc. Japan*, Vol. 19, pp. 688-694, May 1964

Proton and fluorine nuclear resonance in nickel-fluosilicate were studied in the paramagnetic region of temperatures between 0.15°K and 4.2°K. Temperatures below one degree were obtained by the magnetic cooling of the sample itself. From the temperature dependence of the shift, the sign of the exchange interaction between Ni^{++} ions was found to be ferromagnetic. The order of magnitude of the observed shift was well explained by the dipolar field alone. The signals disappeared when the temperature went below the Curie point.

25,596 NUCLEAR MAGNETIC RESONANCE IN SINGLE CRYSTALS OF CdS by T. Kushida and A.H. Silver (Ford Motor Sci. Lab.); *Bull. Am. Phys. Soc.*, Vol. 9, p. 446(A), Apr. 1964

The ^{111}Cd and the ^{113}Cd NMR lines in CdS single crystals were studied at 4.2°K. The spin-lattice relaxation time T_1 of high-resistivity samples is strongly affected by optical illumination. A typical value of T_1 for a sample cooled in the dark, 2.4×10^3 min, was decreased to 30 min while the sample was being illuminated with white light. T_1 did not return to the original value but remained at about 4×10^2 min after the light was turned off as long as the sample was kept cold and in the dark. T_1 of the thus-treated sample was returned to 1.4×10^3 min by shining with red light. The lifetime of the nuclear-spin polarization in a rotary frame T_r was measured as a function of RF-field strength H_1 under various illumination conditions. T_r decreases very sharply, when H_1 is decreased below 1 G. The light-created trapped centers are mainly responsible for these light effects. The local field seen at the neighboring nuclei of the trapped centers was studied using a double-resonance technique in the rotary frame.

25,597 NUCLEAR MAGNETIC RESONANCE OF Fe^{57} IN GALLIUM-SUBSTITUTED YIG by R.L. Streever and G.A. Uriano (Natl. Bur. Stand.); *Bull. Am. Phys. Soc.*, Vol. 9, p. 464(A), Apr. 1964

The nuclear magnetic resonance of ^{57}Fe has been studied in the system $3\text{Y}_2\text{O}_3 \cdot (5-x)\text{Fe}_2\text{O}_3 \cdot x\text{Ga}_2\text{O}_3$ in the concentration range from $x = 0$ to $x = 2.0$ at 77°K and from $x = 0$ to $x = 1.0$ at room temperature. The resonance was studied in polycrystalline powders in 0 external field, using spin-echo equipment. At $x = 2.0$, the 77°K resonance frequency for the (a) site has shifted from its value in pure YIG (75.7 Mc) to about 65 Mc, while the (d)-site frequency decreases from the pure-YIG value (64.3 Mc) to about 58 Mc. The shifts are mainly due to the decrease in the component of electronic spin along the magnetization direction. The faster drop in the resonance frequency on the (a) site is a consequence of the large (a)-(d) interaction and the strong preference of gallium for the (d) site.

25,598 NUCLEAR MAGNETIC RESONANCE IN GADOLINIUM IRON GARNET by J.I. Budnick (Fordham U.); *Bull. Am. Phys. Soc.*, Vol. 9, p. 464(A), Apr. 1964

A single very weak resonance has been observed in several samples of gadolinium iron garnet at 4.2°K. This resonance is about 0.6 Mc in width and is centered at a frequency of about 45.9 Mc. This line is attributed to the Gd^{155} resonance.

25,599 THE MAGNETIC PROPERTIES OF SUPERCONDUCTORS WITH $\ell \neq 0$ PAIRING. THEORY OF THE KNIGHT SHIFT by I.A. Privorotskii; *Soviet Phys.-JETP*, Vol. 18, pp. 1346-1350, May 1964

A theory of the Knight shift in superconductors is developed in which formation of pairs with nonzero angular momentum is taken into account. It is found that for pairing in the triplet state the Knight shift at $T = 0$ does not vanish. The theoretical predictions are in good agreement with the experimental data.

25,600 SOLUTE KNIGHT SHIFTS IN Cu AND Ag BASE SOLID SOLUTIONS by T.J. Rowland (U. Illinois) and F. Borsa (Iowa State U.); *Phys. Rev.*, Vol. 134A, pp. A 743-747, May 4, 1964

Measurements of the Knight shift of Al, P, Ga, Cd and Sn in Cu base solid solutions, and of Cu, Ga, Cd and Sn in Ag base solid solutions are reported. The change in solute Knight shift with composition and the dependence of linewidth on composition and external field strength are also discussed for selected alloys. The difference in the rate of change of relative Knight shift with composition for Sn and Ag in the Ag-Sn alloys indicates a tendency for the Sn atoms to avoid being nearest neighbors.

25,601 KNIGHT SHIFT χ_{V} , χ_{Tc} , AND χ_{Al} AND MAGNETIC SUSCEPTIBILITIES IN THE BCC REGION OF THE V-Tc-Al TERNARY ALLOY SYSTEMS by D.O. Von Osternburg, D.J. Lam, H.D. Trapp and D.W. Pracht (Argonne Natl. Lab.); *Phys. Rev. Lett.*, Vol. 11, pp. 352-353(L), Oct. 15, 1963

The magnetic susceptibilities and Knight shifts in $\text{Al}_{50-55}\text{V}_{45-45}\text{Tc}_x$ alloys with x varying from 0 to 0.50 are experimentally investigated. The susceptibility decreases with increasing Tc content. Compared to the binary V-Tc system it is shown that the magnitude of the Knight shift in Al is very small, while the shifts of V^{51} and Tc^{99} are of the same magnitude and concentration dependence as in the binary systems. The results suggest that the electrons contributing to the V^{51} and Tc^{99} shifts enter a common band, while the Al conduction electrons have little or no interaction with transition elements.

25,602 INTERPRETATION OF KNIGHT SHIFTS AND SUSCEPTIBILITIES OF TRANSITION METALS: PLATINUM by A.M. Clogston, V. Jaccarino and Y. Yafet (Bell Labs.); *Phys. Rev.*, Vol. 134A, pp. A650-661, May 4, 1964

Measurements of the magnitude, sign, and temperature dependence of the Knight shift and susceptibility in platinum are used to determine the contributions to each arising from the spin paramagnetism of the s and d bands, the orbital paramagnetism and the core diamagnetism. A complete expression for the orbital contribution to the Knight shift in a transition metal is derived, including spin-orbit coupling. It is shown that in the tight-binding limit, as in the free ion, a simple relation exists between the orbital susceptibility and the orbital hyperfine field. The relation of the enhancement of the d-spin susceptibility over its specific heat value to the possible occurrence of superconductivity is discussed.

NMR Study of Phase Transitions in NaCN - See 24,910

DIAMAGNETISM

Diamagnetic Susceptibility of:

$\text{Th}_{1-x}\text{U}_x\text{Pd}$ - See 25,387

Anthracene - See 24,955

de Haas-van Alphen Effect in Fe Whiskers - See 25,151

25,603 LOW-FIELD DE HAAS-VAN ALPHEN EFFECT IN COPPER by A.S. Joseph and A.C. Thorsen (N.A. Aviation); *Phys. Rev.*, Vol. 134A, pp. A979-980, May 18, 1964

The de Haas-van Alphen effect has been observed in a copper single crystal by means of a null-deflection torsion balance technique. Detailed measurements have been carried out which provide an accurate determination of the topology of the Fermi surface necks in copper. Effective mass values are found to be in excellent agreement with cyclotron resonance results. Unusual behavior observed in the angular dependence of the amplitude of the oscillatory torque is attributed to the spin-splitting factor in the theoretical expression for the magnetization.

25,604 DE HAAS-VAN ALPHEN EFFECT AND FERMI SURFACE IN NICKEL by A.S. Joseph and A.C. Thorsen (Atomics International); *Phys. Rev. Lett.*, Vol. 11, pp. 554-556(L), Dec. 15, 1963

De Haas-van Alphen oscillations in nickel monocrystals which were suspended in magnetic fields of up to 40 kG were studied. The variation of the period of the oscillation as a function of the field orientation in the (001) and (110) planes indicate that the (111) axis is a symmetry axis for the Fermi surface segment responsible for the oscillations. Preliminary conclusions indicate necks in the Fermi surface protruding in the (111) direction. The minimum diameter of the electrons' orbits around these necks is, 0.18Å^{-1} , subtending an angle of $6.8^\circ \pm 0.2^\circ$ from the Γ at the center of the Brillouin zone. This is in excellent agreement with data by Fawcett and Reed.

25,605 THE DE HAAS-VAN ALPHEN EFFECT AT HIGH MAGNETIC FIELDS IN CADMIUM by D.C. Grassie (Royal Soc. Mond Lab., Cambridge); *Philosophical Mag.*, Vol. 9, pp. 847-863, May 1964

The de Haas-van Alphen effect in cadmium has been studied by the pulsed high-field method. The extremal cross-sectional areas of the Fermi surface thus derived can in many instances be plausibly associated with those of the almost-free-electron model suggested by Harrison when the competing effects of spin-orbit coupling and magnetic breakthrough are taken into account.

OPTICAL PROPERTIES

ABSORPTION (TRANSMISSION)

25,606 THEORY OF OPTICAL AND MICROWAVE ABSORPTION LINE

SHAPE by U. Kh. Kopvillem and V. P. Nagibarov (Acad. Sci. USSR); *Soviet Phys.-Solid State*, Vol. 5, pp. 2154-2160, Apr. 1964

The dislocation broadening of optical and magnetic resonance lines has been investigated. A relationship between the line form of magnetic and optical resonance absorption is established, and conditions under which narrow optical absorption lines can be observed are formulated.

25,607 ON DETERMINATION OF THE OPTICAL ABSORPTION COEFFICIENT

IN T, PART II by A. Kahan (A. F. Cambridge Res. Labs.); Dec. 1963, 125pp.; S. Gov. Res. Rep., Vol. 39, p. 125(A), June 20, 1964
435 620 OTS 10.10

The equation for the optical absorption coefficient α in terms of the average measured reflection and transmission coefficients r and T is derived. A set of tables of αd , where d is the sample thickness, as a function of T in intervals of 0.2% for parameters of r in 0.5% is included. Both r and T values range between 0 and 100%. In addition, tables for the bulk reflectivity R as a function of r and T are given.

25,608 OPTICAL ABSORPTION IN AN ELECTRIC FIELD by J. Callaway

and J. L. Hilco (Newport Beach); *Phys. Rev.*, Vol. 134A, pp. A998-1000, May 18, 1964
The previous calculation of the effect of an external, uniform electric field on the optical absorption associated with a direct transition between bands is extended. The absorption is shown to consist of a series of steps whose width is determined by the separation of the discrete levels produced by the field.

25,609 INFRARED ABSORPTION IN HIGHLY DOPED GERMANIUM by L. V.

Udysch and G. P. Proshko (Acad. Sci. USSR); *Soviet Phys.-Solid State*, Vol. 6, pp. 2481-2488, June 1964

The infrared absorption in highly doped germanium has been measured. It is found that the edge of the absorption band is displaced toward longer wavelengths and the displacement is very different for direct and indirect transitions. The peculiarities of the intrinsic absorption can be qualitatively explained by taking into account the difference in the effective masses corresponding to direct and indirect transitions.

25,610 THE INTRINSIC ABSORPTION EDGE OF HEAVILY DOPED N- AND

P-TYPE GERMANIUM by S. Munesue and T. Arai (Nippon Tel. and Tel.); *Japanese J. Appl. Phys.*, Vol. 3, pp. 269-275, May 1964

Measurements of the infrared absorption spectrum of heavily doped p- and n-type germanium in the free carrier concentration range of 4×10^{17} to 9×10^{19} cm⁻³ are reported. Both the indirect and the direct absorption edge in the impure samples of both types differ strongly from that in pure germanium. The shift of the indirect absorption edge is larger than the shift of the direct absorption edge in both types. The shift of the direct absorption edge is almost the same in both cases, but the shift of indirect absorption edge in n-type is about twice as large as that in p-type. The absorption due to indirect transitions increases more rapidly with photon energy in the impure samples of both types than in pure germanium. The highest absorption value in the direct absorption region is less than that in the pure sample.

25,611 ENERGY DEPENDENCE OF THE ABSORPTION SPECTRUM IN THE

VICINITY OF THE INTRINSIC ABSORPTION BAND IN HEAVILY DOPED GERMANIUM AND SILICON by G. B. Dubrovskii (Acad. Sci. USSR); *Soviet Phys.-Solid State*, Vol. 5, pp. 2467-2471, June 1964

The absorption spectrum in the vicinity of the intrinsic absorption band in heavily doped Ge and Si is calculated taking into account the departures from the quadratic form of the dispersion law for electrons in the valence band. A method is proposed for analyzing the experimental data relating to the edge of the intrinsic absorption band so as to evaluate the energy dependence of the probability of a direct transition and the degree to which the valence band departs from a parabolic form.

Infrared Absorption in Si - See 25,044

25,612 ABSORPTION IN SILICON DOPED WITH ZINC by B. V. Kornilov;

Soviet Phys.-Solid State, Vol. 5, pp. 2420-2424, May 1964
Absorption in p- and n-type silicon containing zinc impurity over the wavelength region from 1 to 5 μ at temperatures 90° and 290°K has been investigated. Two acceptor levels in silicon determined from the absorption curve are located at 0.33 eV in p-type silicon and at 0.55 eV in n-type silicon. It is

found that the cross section for absorption of a photon by a neutral zinc atom with excitation of a hole from the 0.33 eV level to the valence band is $2 \cdot 10^{-16}$ cm², and the cross section for capture of a photon by a singly negative-charged zinc atom with excitation of a hole from the 0.55 eV. Level to the valence band is $2 \cdot 10^{-15}$ cm²

25,613 ABSORPTION DATA OF LASER-TYPE GaAs at 300° and 77°K by W. J. Turner and W. E. Reese (IBM Watson Res. Ctr.); *J. Appl. Phys.*, Vol. 35, pp. 350-352, Feb. 1964

Optical absorption coefficients have been determined at 300° and 77°K for samples of GaAs which were doped to concentrations comparable to those present in the n, p, and p⁺ regions of the GaAs injection laser. n-Type GaAs doped with Te to 3×10^{17} cm⁻³ and 9.6×10^{17} cm⁻³ have absorption coefficients of 20 cm⁻¹ and 10 cm⁻¹, respectively, at 1.475 eV and 77°K. Free carrier and deep-level absorptions contribute approximately 5 cm⁻¹ to these values. At 77°K, p-type Zn-doped samples with $N_A - N_D$ equal to 1.6×10^{10} cm⁻³ exhibit in the spectral region of laser emission an absorption that increases exponentially with photon energy and probably results from transitions of electrons in acceptor states to levels in the conducting band or conduction band tail. At 1.475 eV and 77°K, the absorption coefficient of this p-type material is 225 cm⁻¹ to which free carrier absorption contributes only 3 cm⁻¹. For heavier Zn-doped p⁺ material, e.g., 7×10^{10} cm⁻³, the value of K at 77°K and 1.475 eV is 250 cm⁻¹ and is entirely due to free carrier absorption. For both n and p materials, a Burstein shift of the edge to higher energies is observed for the heavily doped materials in agreement with the observations of others.

25,614 FREE AND BOUND EXITONS IN GaP CRYSTALS by E. F. Gross, N. S. Kochneva, and D. S. Nedzvetskii (Acad. Sci. USSR); *Soviet Phys.-Doklady*, Vol. 8, pp. 1103-1106(L), May 1964

The absorption and luminescence spectra of GaP crystals are discussed. It is found that there are several absorption steps in the absorption spectrum, which are interpreted as indirect transitions from the valence band to the free exciton levels with the participation of phonons. In the luminescence spectrum, two narrow lines ν_0' and ν_0'' were found, which are shown to be two independent lines. If the minimum of the conduction band and the maximum of the valence band occur at different values of k , then ν_0' and ν_0'' are assumed to be induced by bound excitons. The binding energies at $T = 77.3^\circ$ K are found to be 0.11 eV and 0.013 eV, respectively.

Pressure Effects on Absorption Edge of GaP - See 25,145

25,615 FREE-CARRIER INFRARED ABSORPTION IN III-V SEMICONDUCTORS III. GaAs, InP, GaP, and GaSb by E. Haga and H. Kimura (Nagoya U.); *J. Phys. Soc. Japan*, Vol. 19, pp. 658-669, May 1964

The free carrier absorption data for n-GaAs, -InP, -GaP, and -GaSb are analyzed in order to investigate the scattering mechanism of electrons. The magnitudes of the deformation potential constant E_1 are found to be ~ 6 eV for GaAs, ~ 0 eV for InP, ~ 55 eV for GaP, and ~ 60 eV for GaSb. It is found from this that, among acoustic and optical phonon scatterings, the former is predominant in GaP and GaSb, and the latter predominant in GaAs and InP. The impurity concentration is found to be very large compared with the electron concentration, for the samples of GaAs and InP with low carrier concentrations. This suggests the presence of some additional scatterers different from the ordinary ones, that is, lattice vibrations and ionized impurities. From the present analysis, it is inferred that the absorption coefficient due to additional scatterers have a wavelength dependence very similar to the one due to ionized impurities.

25,616 OPTICAL ABSORPTION EDGE OF GaS and GaSe SINGLE CRYSTALS by F. I. Ismailov, E. S. Guseinova, and G. A. Akhundov (Acad. Sci. AzSSR); *Soviet Phys.-Solid State*, Vol. pp. 2656-2657(L), June 1964

Measurements of the temperature dependence of the optical absorption edge of GaS and GaSe in the range 280-580°K are reported. The forbidden band widths found from the absorption edge at room temperature are 2.53 eV for GaS and 1.97 eV for GaSe. The temperature coefficients of the band width are -7.2×10^{-4} and -8×10^{-4} eV/°K for GaS and GaSe, respectively.

25,617 OPTICAL ABSORPTION, ELECTROLUMINESCENCE, AND THE BAND GAP OF BP by R. J. Archer, R. Y. Koyama, E. E. Loebner, and R. C. Lucas (HP Assoc.); *Phys. Rev. Lett.*, Vol. 12, pp. 538-539(L), May 11, 1964

Measurements of injection electroluminescence and optical absorption in BP and of the photoelectric response of an Au-BP surface barrier are discussed. The electroluminescence peaks at 1.97 eV, a value which suggests a phonon-assisted optical transition. The magnitude of the absorption coefficient at the high energy side of the absorption edge agrees with that of GaP and SiC. This suggests that the edge corresponds to an indirect band-to-band excitation. A band gap of 2 eV and phonon-assisted optical transitions are also indicated by the plot obtained for $\alpha^{1/2}$ vs $h\nu$ and the photoelectric yield of an Au-p-type BP contact. The latter measurements yield a value of 2.02 eV for the room temperature band gap of BP.

Temperature Dependence of Absorption in ZnS - See 25,707

25,618 OPTICALLY ACTIVE PHONON PROCESSES IN CdS and ZnS by R. Marshall and S. S. Mitra (IIT Res. Inst.); Phys. Rev., Vol. 134A, pp. A1019-1025, May 18, 1964

Transmission spectra of thin (10 to 30 μ) CdS single-crystal samples have been recorded in the hitherto uninvestigated region of 250 to 400 cm^{-1} . A number of new absorption maxima are located which necessitated a new phonon assignment with considerably lower values of the acoustic modes. Some 30 absorption peaks are attributed to multiphonon combinations of the following Brillouin zone-edge frequencies: $\text{LO}=295\text{ cm}^{-1}$, $\text{TO}_1=238\text{ cm}^{-1}$, $\text{LA}=149\text{ cm}^{-1}$, $\text{TA}_1=79\text{ cm}^{-1}$, and $\text{TA}_2=70\text{ cm}^{-1}$. The transmission spectrum of hexagonal ZnS is obtained for the first time in the region 300 to 750 cm^{-1} . Again some 27 absorption maxima are assigned to multiphonon combinations of $\text{LO}=346\text{ cm}^{-1}$, $\text{TO}_1=318\text{ cm}^{-1}$, $\text{TO}_2=297\text{ cm}^{-1}$, $\text{LA}=181\text{ cm}^{-1}$, $\text{TA}_1=92\text{ cm}^{-1}$, and $\text{TA}_2=73\text{ cm}^{-1}$. The phonon assignment for the optical lattice absorption in cubic ZnS due to Deutsch is shown to be inconsistent with the requirements of the Brout sum rule and other regularities expected for the zincblende-type semiconductors. Two new assignments ($\text{LO}=339\text{ cm}^{-1}$, $\text{TO}=298\text{ cm}^{-1}$, $\text{LA}=155\text{ cm}^{-1}$, and $\text{TA}=93\text{ cm}^{-1}$, and $\text{LO}=339\text{ cm}^{-1}$, $\text{TO}=298\text{ cm}^{-1}$, $\text{LA}=190\text{ cm}^{-1}$, and $\text{TA}=115\text{ cm}^{-1}$) only slightly different from each other are proposed. The characteristic phonon frequencies are discussed in terms of structure and effective ionic charge.

25,619 FIELD INDUCED SHIFT OF THE ABSORPTION EDGE IN CdS by E. Gutsche (Phys. Tech. Inst., Berlin) and H. Lange (Huboldt U., Berlin); Phys. Stat. Sol., Vol. 4, pp. K21-24, 1964

The field induced absorption edge in CdS has been studied. A linear log relation was observed between the shift in the edge and the applied field strength for light polarized parallel as well as perpendicular to the c-axis. The shift is proportional to the square of the electric field, in agreement with an earlier prediction of Franz. A field of 2×10^5 v/cm accounts for a shift of $\sim 100\text{ \AA}$.

Absorption in SiC - See 25,251

25,620 NEW ABSORPTION BANDS ASSOCIATED WITH THE N-CENTER IN THE ALKALI HALIDES by J. N. Maycock and D. E. Grabenstein (RIAS, Baltimore); Solid State Commun., Vol. 2, Pergamon Press, pp. 97-99, Apr. 1964

The new absorption bands in the near infrared have been observed in optically bleached, additively colored alkali halides. These bands are attributed to directional absorption by the N_1 and N_2 centers. Three of the now four bands associated with the N-centers are believed to arise from absorptions by the N_1 -center, the remaining band being associated with the N_2 -center.

25,621 OCCURRENCE OF NEW COLOR CENTER ABSORPTIONS IN KCl by J. Ring and L. Grossweiner (Illinois Inst. Tech.); J. Appl. Phys., Vol. 35, pp. 2257-2258(L), July 1964

New color center absorptions have been observed in KCl after suitable optical bleaching at 100°C . In studying the effects of bleaching, three basic wavelength regions were utilized. The new absorption peaks were observed on samples irradiated by white light followed by "F+N" light—550-560 m μ and 950-1000 m μ wavelength. Occurrence of the peaks is at 891, 836, and 988 m μ wavelength. These new bands are due to one or more specific F-aggregate color centers of unknown structure.

25,622 LINE INTENSITY OF INFRARED ABSORPTION BY IMPURITY VIBRATIONS by D. N. Mirlin and I. I. Reshina (Acad. Sci. USSR); Soviet Phys. Solid State, Vol. 5, pp. 2458-2459(L), May 1964

Measurements of the temperature dependence of the line intensity of infrared absorption by impurity vibrations in KCl and KBr crystals with Cl^- and Br^- ions substituted by H^- ions are reported. It is found that the line intensity remains almost constant as a function of temperature, in contrast to Shaefer's results for alkali halide crystals. The temperature dependence of the half-width approximately follows the T^2 law.

Color Center Absorption in KBr and KCl - See 24,990

25,623 THEORY OF THE β -BAND IN THE ABSORPTION SPECTRUM OF A NaCl CRYSTAL by A. A. Kiselev (Leningrad State U.); Soviet Phys.-Solid State, Vol. 5, pp. 1269-1270(L), Dec. 1963

Irradiation-Anneal Effects on Absorption in NaCl - See 25,754

Absorption in:

NaBr:Co, NaCl:Co and KCl:Co - See 24,959

NaI and NaI:TI - See 25,680

Irradiation-Anneal Effects on Absorption in LiF - See 25,752

25,624 F-BAND SHAPE IN THE CsCl STRUCTURE UNDER PRESSURE by D. B. Fitchen (U. Illinois); Phys. Rev., Vol. 134A, pp. A1599-1602, June 15, 1964

Color Centers have been formed by x irradiation of RbCl above the polymorphic transition pressure, and the shape of the new F band at 509 m μ in this CsCl-type structure has been examined under a pressure of 6200 atm at liquid-helium temperature. The band shows no evidence of the multiplet structure observed in the cesium halides, thus indicating that the lattice structure is not responsible for this effect. The F band in CsCl has also been formed and studied under pressure at helium temperature, and the triplet components show the usual relative intensity and the characteristic F-band shift. No evidence of K' bands was observed for these hydrostatic pressures.

25,625 SPECTRUM OF TRIVALENT ERBIUM ION IN THE MATRIX OF CALCIUM FLUORIDE by S. A. Pallack (TRW Space Tech. Lab.); J. Chem. Phys., Vol. 40, pp. 2751-2767, May 15, 1964

The absorption and emission spectra of $\text{CaF}_2:\text{Er}^{3+}$ are presented, discussed, and analyzed phenomenologically. The crystalline states are listed and identified with the free ion quantum numbers by comparison with the states of erbium chloride. The oscillator strengths are determined from the absorbance spectrum and compared with the oscillator strengths reported in the literature. The study of the emission properties of the erbium ion in CaF_2 includes identification of transition schemes for the major emission groups from their excitation spectra, measurements of relative intensities, decay times of fluorescence, and quantum efficiencies. By combining data obtained from the absorption and emission spectra at 77° and 4°K , the crystalline field splitting of the ground $^4\text{I}_{15/2}$ multiplet was determined. The wavelengths of all emission lines at 77°K are presented. The effects of temperature and ion concentration are discussed. All pertinent data are given in a table form. The important features of the absorption and emission spectra are amply illustrated by figures, graphs, and tables. In addition to the purely spectroscopic properties of $\text{CaF}_2:\text{Er}^{3+}$, its properties as a potential laser material are considered and discussed.

25,626 ANOMALOUS DEPENDENCE OF THE INTENSITY OF ABSORPTION ON THE THICKNESS OF CuCl SINGLE CRYSTALS by M. S. Brodin and A. S. Krochuk (Acad. Sci. Ukr. SSR); Soviet Phys. Solid State, Vol. 5, pp. 2647-2649(L), June 1964

The fundamental absorption of CuCl crystals has been investigated. The dependence of the optical density on the thickness indicates a departure from the Lambert-Bouguer law. On moving away from the maximum of the absorption band toward longer wavelengths, the magnitude of the departure decreases. Increase of temperature also "smooths out" the non-monotonic dependence, at room temperature there is practically no departure from the Lambert-Bouguer law. These results indicate an interaction of complex nature between the light wave and the crystal when the excitons are excited.

25,627 VISIBLE ABSORPTION SPECTRA OF CADMIUM IN CADMIUM HALIDES AND LEAD CHLORIDE AND IN LEAD BROMIDE by J. Greenberg (NASA Lewis Res. Ctr.); J. Chem. Phys., Vol. 40, pp. 3126-3127, May 15, 1964

Spectrophotometer measurements were made on cadmium halides, lead chloride, and lead bromide in the visible and in the infrared. No specific infrared absorption bands were observed to 15μ wavelength in any of the materials. Increasing temperature broadened the bands and shifted the peak to longer wavelengths. The absence of absorption continua in the visible spectrum and dependence of band position on anion indicate the metallic species exist as cations rather than as metal atoms. A mechanism accounting for band shift due to changing anion species is suggested.

25,628 INFRARED SPECTRUM OF DIBORON TETRAFLUORIDE IN THE GASEOUS AND SOLID STATES by J. N. Gayles and J. Self (Oregon State U.); J. Chem. Phys., Vol. 40, pp. 3530-3539, June 15, 1964

Infrared spectra of B_2F_4 are reported over the range 2.5 to 50μ at small grating resolution for both the gaseous and polycrystalline states. Examination of band envelopes for the gas and of differences between gas and solid spectra indicates that a structural difference exists between gaseous and solid B_2F_4 . It is suggested that the alteration is analogous to that observed for B_2Cl_4 with the V_d or staggered configuration applying in gas and the V_h or planar configuration applying in the solid. Rough estimates are made for some of the principal potential constants.

25,629 OPTICAL ABSORPTION SPECTRUM OF NiF_2 by M. Balkanski and P. Moch (Ecole Norm. Sup., Paris), and R. G. Shulman (Bell Labs.); J. Chem. Phys., Vol. 40, pp. 1897-1901, Apr. 1 1964

The optical absorption spectrum of NiF_2 is reported for the paramagnetic and antiferromagnetic states. A prominent satellite appears in the $^3\text{A}_2 \rightarrow ^1\text{E}$ transition below the Neel temperature. This new line is explained in terms of the interaction of the excited Ni^{2+} ion with its six antiparallel Ni^{2+} neighbors.

Infrared Transmittance of KMgF_3 and MgF_3 - See 25,708

Paramagnetic Curie Temperature of CrI_3 - See 25,439

Transmission of CrI_3 - See 25,439

Infrared Absorption in NaNO_3 - See 25,190

Absorption Edge in Niobates and Tantalates - See 25,650

25,630 X-RAY K ABSORPTION SPECTRA OF Cu-Ni ALLOYS by L. V. Azaroff and B. N. Das (Illinois Inst. Tech.); *Phys. Rev.*, Vol. 134A, pp. A747-751, May 4, 1964

Copper and nickel K absorption spectra have been measured in the pure metals and in four alloys, respectively, containing 17.2, 26.0, 43.3, and 65.6 at. % copper. Variations in the absorption-edge fine structure of both metals were observed in the nickel-rich solid solutions. These variations are interpreted by considering the electronic configurations of the individual absorbing atoms and how they are altered by alloying. It is proposed that the K absorption spectrum of each constituent should be different and should not reflect a common density-of-states distribution for the alloy. It is also shown that this model can be applied to explain the x-ray emission spectra observed by others.

25,631 X-RAY ABSORPTION SPECTRA OF Cu-Ni ALLOYS by L. V. Azaroff and B. Das (Illinois Inst. Tech.); *Cont. Nonr* 1406 07, 14 pp., Dec. 1963; *U.S. Gov. Res. Rep.*, Vol. 39, May 5, 1964 AD 429 486 OTS \$1.60

Copper and Nickel K absorption spectra have been measured in the pure metals and in four alloys containing 17.2, 26.0, 43.3 and 65.6 at. % copper. Variations in the absorption-edge fine structure of both metals were observed in the nickel-rich solid solutions. These variations are interpreted to indicate progressive sharing of copper 4s electrons with nickel, in accord with the collective-electron model. The specific interpretation of the x-ray spectra, however, requires the consideration of atomic electron configurations as they exist in the crystal field of each alloy. It is also shown that this interpretation can be applied to explain the x-ray emission spectra observed by others.

25,632 FAR-INFRARED SPECTRUM OF $\text{Fe}(\text{CO})_5$ by K. R. Loos (MIT); *J. Chem. Phys.*, p. 3741, June 15, 1964

The far-infrared spectrum of $\text{Fe}(\text{CO})_5$ from 35 to 120 cm^{-1} was investigated using the spectrometer of Lord and McCubbin adapted for vacuum operation. Studies were made on liquid at room temperature and on the solid phase at liquid-nitrogen temperatures. A broad band was found in liquid phase at $111 \pm 1\text{ cm}^{-1}$ and an additional band was observed at $80 \pm 1\text{ cm}^{-1}$ in the solid. No other bands were found, although there was considerable generalized absorption in both liquid and solid samples below 60 cm^{-1} .

25,633 INFRARED ABSORPTION OF Mg_2Sn Single Crystals by H. G. Lipson (AF Cambridge Res. Labs.); *AFCRL* 63 534, Nov. 1963, 36 pp.; *U.S. Gov. Res. Rep.*, Vol. 39, p. 146(A), May 5, 1964

Infrared transmission and reflection measurements of n- and p-type semiconducting Mg_2Sn single crystals of different impurity concentrations were made between 2 and 30 microns at temperatures ranging from 18 to 296°K . At energies of 0.22 eV and above, the rapid increase in absorption is attributed to the intrinsic edge. From the energy dependence of absorption in the edge region, the mechanism of indirect transitions between the valence and conduction bands can be established. The energy axis intercepts of the straight lines representing phonon emission decrease with temperature, indicating a negative temperature variation of the absorption edge. A band in the 0.10 to 0.22 eV energy range present at all temperatures in n-type and above 196°K in p-type samples suggests transitions between two conduction minima separated by 0.62 eV at 18°K . The presence of a fundamental lattice vibration band has been indicated from transmission and reflection measurements at longer wavelengths. The absorption spectrum of Mg_2Sn is similar in character to those reported for other semiconducting intermetallic compounds of the II-IV series.

25,634 LOW-FREQUENCY ABSORPTION SPECTRA OF SOME FERROELECTRICS by T. Myasnikova and I. Arefev; *Optics and Spectros.*, Vol. 16, pp. 293-294, Mar. 1964

Preliminary results on the investigation of the absorption spectra in the $55\text{--}170\text{ cm}^{-1}$ region at room temperature are reported for four ferroelectric materials: $(\text{NH}_4)_2\text{SO}_4$, RbHSO_4 , $\text{NaH}_2(\text{SeO}_3)_2$, and $\text{LiH}_3(\text{SeO}_3)_2$. The work was performed in conjunction with a search for optical lattice vibrations associated with ferroelectric phase transitions, the frequency of which should diminish to very small values at the Curie point. The complex structure of the crystals studied, and consequently the large number of lattice vibrations, make the interpretation of the spectra obtained very difficult. Elucidation of the "ferroelectric modes" is expected to be considerably easier when the temperature dependence of infrared spectra in the low frequency range is investigated.

25,635 VIBRATIONAL SPECTRUM OF SODIUM AZIDE SINGLE CRYSTALS by J. I. Bryant (USAERDL); *J. Chem. Physics*, Vol. 40, pp. 3195-3203, June 1, 1964

The infrared and Raman spectra of a single crystal of sodium azide have been intensively investigated at 298° and 90°K using grating spectrometers. Selection rules for internal and lattice vibrations are determined by application of the unit cell (factor group) method of Bhagavantam and Venkatarayudu. The unit cell modes of the crystal belonging to irreducible representations of the unit cell group have been constructed to within a good approximation. Spectra in the infrared are characterized by the occurrence of medium-strength absorptions symmetrically spaced about the principal bands of the spectrum with a separation of 122 cm^{-1} . The observation of the Raman-active rotatory lattice mode at this frequency confirms the assignment of the medium-strength bands as sum and difference frequencies involving rotational motion of the azide ion as a rigid unit. Tentative assignments were made for all bands observed in the spectra and deduced frequencies for unobserved infrared lattice modes are presented. The spectra were found to be in good agreement with the accepted structure as described by the space group $\text{D}_{3d}^5\text{--R}\bar{3}\text{m}$.

25,636 INFRARED SPECTRA OF ICES Ih AND Ic IN THE RANGE 4000 TO 350 cm^{-1} by J. E. Bertie and E. Whalley (Nat'l. Res. Council, Ottawa); *J. Chem. Phys.*, Vol. 40, pp. 1637-1645, Mar. 15, 1964

The infrared spectra of Ice Ih made from H_2O , D_2O , a mixture of 95% H_2O and 5% D_2O , and a mixture of 5% H_2O and 95% D_2O , and of Ice Ic made from H_2O , D_2O , and a mixture of 95% H_2O and 5% D_2O , have been recorded in the region 4000 to 350 cm^{-1} . The Ice Ic was made by transformation of Ices II and III, and was authenticated by its X-ray diffraction powder pattern. The spectra of Ices Ih and Ic are identical within experimental error. The spectra of Ice Ih, while similar in their main features to those reported by earlier workers, differ significantly in detail, probably largely because much of the previous work, particularly on D_2O ice, has been done with partly vitreous ice. The usual interpretation of the bands in terms of the ν_1 , ν_2 , and ν_R vibrations of isolated molecules is greatly oversimplified because intermolecular coupling is important. There are at least six (five infrared and one Raman) bands due to O-D stretching vibrations in the spectrum of D_2O Ice I, but the detailed origin is unknown. The breadth of the O-H and O-D stretching bands of HDO in dilute solution in D_2O and H_2O is interpreted as indicating a disarrangement of the oxygen positions due to the disorder of the hydrogen atoms.

25,637 INFRARED SPECTRA OF ICES II, III, AND V IN THE RANGE 4000 TO 350 cm^{-1} by J. E. Bertie and E. Whalley (Nat'l. Res. Council, Ottawa); *J. Chem. Phys.*, Vol. 40, pp. 1646-1659, Mar. 15, 1964

The infrared spectra of Ices II, III, and V between 4000 and 350 cm^{-1} have been obtained. The ices were made at appropriate pressures and temperatures, cooled under pressure to liquid-nitrogen temperature, and removed from the pressure vessel. The spectra of ices made from H_2O , D_2O , 5% H_2O in D_2O , 5% D_2O in H_2O , and, for Ices II and III, 1% D_2O in H_2O were obtained. The spectra of pure H_2O and D_2O Ices II, III, and V are similar to those of Ice I. For most bands there is a shift of frequency from that in Ice I towards the vapor frequencies, but the shift is small compared with the shift between Ice I and the vapor. Ices II, III, and V are therefore essentially fully hydrogen bonded and are probably four coordinated. This agrees with a proposed structure for Ice III. In Ices II and III the bands due to the O-H and the O-D stretching vibrations of HDO in dilute solution in D_2O and H_2O , respectively, show a good deal of fine structure, and are quite narrow, the half-width of the O-D bands being about 5 cm^{-1} . These are by far the sharpest O-H (or O-D) stretching vibrations of hydrogen-bonded O-H---O groups so far observed. Clearly, breadth is not inherent in the O-H stretching bands of O-H---O. There is also a good deal of fine structure in the bands due to rotational vibrations of water molecules in Ices II and III, and much of this fine structure broadens and weakens when a small amount of H_2O is added to D_2O , and of D_2O to H_2O . The only simple explanation of this, and of the fine structure of the O-H stretching bands, is that the hydrogen atoms in Ices II and III are ordered.

25,638 POLARIZED ABSORPTION SPECTRUM OF A SINGLE CRYSTAL OF PYRENE-TETRACYANOETHYLENE COMPLEX by H. Kuroda and H. Acamatu (U. Tokyo); *J. Chem. Phys.*, Vol. 40, pp. 3748-3749, June 15, 1964

The polarized absorption spectrum of pyrene-tetracyanoethylene complex single crystals show multiple charge transfer bands. The complex is monoclinic with cell dimensions $a = 14.58\text{ \AA}$, $b = 7.34\text{ \AA}$, $c = 8.09\text{ \AA}$, and $\beta = 92.4^\circ$ and belongs to the $\text{P}2_1/\text{a}$ space group. The unit cell of pyrene-tetracyanoethylene contains 4 molecules, 2 of pyrene and 2 of TCNE. Spectra of b polarization and c polarization were observed. The maxima at 510 and $830\text{ m}\mu$ were charge-transfer bands and were not associated with excitation of free molecules.

25,639 THE ABSORPTION AND FLUORESCENCE SPECTRA OF TRIVALENT EUROPIUM IN SILICATE GLASSES by C. R. Kurkjian, P. K. Gallagher, W. R. Sinclair and E. A. Sigety (Bell Labs.); *Phys. Chem. Glasses*, Vol. 4, pp. 239-246, Dec. 1963

A room temperature study of the absorption and fluorescence spectra of tri-valent europium in silicate glasses is reported. The absorption and fluorescence intensities in this system are interpreted on the basis of a model that uses the wavelength shift of the $^5D_0 - ^7F_0$ fluorescence transition as a measure of Eu-O interaction strength.

Absorption in $Y_2O_3:Er^{3+}$ - See 25,671

25,640 RESULTS OF MAGNETO-OPTICAL INVESTIGATION OF RARE-EARTH IRON GARNETS by G. S. Krinchik and G. K. Tjutneva (Moscow State U.); *J. Appl. Phys.*, Vol. 35, pp. 1014-1017, Mar. 1964

The fine structure of the $^7F_0 \rightarrow ^7F_4$ absorption line of the Eu^{3+} ion in single crystals of europium iron garnet has been studied. The magneto-optical method allows us to evaluate the contributions of magnetic and electric dipole transitions to the absorption coefficient of the garnet. Anisotropy in the structure of the line was observed, the intensities of individual components depending on the relative orientation of the plane of the polarized light and on the magnetization vector of the crystal. The main components of the line are shown to arise from an exchange Zeeman effect. From the magnitude of the splitting the exchange field acting on the Eu^{3+} ion is found to be 220,000 oe. Certain components of the fine structure are interpreted in terms of combination lines involving spin-wave modes in the garnet. Measurements of the Faraday rotation in europium, dysprosium, terbium, and samarium garnet in the infrared are described and used to calculate the g factor for the ground state of the rare-earth ion.

25,641 SPECTRA AND QUANTUM STATES OF EUROPIUM β -DIKETONE CHELATES IN POLYMETHYLMETHACRYLATE by N. McAvoy, N. Filipescu, R. Kagan and F. A. Serafin (Melpar); *J. Phys. Chem. Solids*, Vol. 25, pp. 461-468, May 1964

An analysis of the absorption spectra of different Eu β -diketone chelates led to a detailed spectroscopic investigation of Eu tris (4,4,4-trifluoro-1,2-thienyl-1,3-butanedione) chelate dissolved in polymethylmethacrylate and other hosts, at different temperatures and concentrations. The mechanism responsible for the line fluorescence is attributed to an intramolecular energy transfer from the triplet states of the organic chelate of the 5D_0 and 5D_1 resonance energy levels of the central europium ion. The concentration, temperature and host dependent fluorescence spectrum of Eu chelate have been investigated and interpreted. The absorption and phosphorescence spectra of the identical gadolinium chelate in different hosts were related to the overall transfer mechanism and the lowest-lying triplet states. The "molecular field splitting" effects are observed at low temperatures for the $^7F_0 \rightarrow ^5D_2$ transition and interpreted based on structural criteria. The intramolecular energy transfer has been tentatively formulated based on the admixture of the biradical triplet state of the chelate with the emitting levels of the europium ion.

25,642 ABSORPTION SPECTRA OF URANIUM (IV) IN OCTAHEDRAL COORDINATION by R. Pappalardo and C. K. Jorgensen (Cyanamid European Res. Inst., Geneva); *Helv. Phys. Acta*, Vol. 37, No. 2, pp. 79-103, 1964

Optical absorption spectra of crystals containing octahedrally coordinated U^{4+} ions in triphenylphosphonium complex salts are reported for the region 2.5 μ to 0.3 μ , both at RT and 78°K. Vibrational frequencies for the $\langle UCl_6 \rangle^{2-}$ and $\langle UBr_6 \rangle^{2-}$ groups have been found superimposed on to the electronic transitions. General properties of the spectra in connection with the $5f^2$ energy levels are discussed.

RADIATION AND LUMINESCENCE

25,643 EMISSION SPECTRUM OF $MgCl$: A NEW DOUBLET SYSTEM by V. S. Rao and P. T. Rao (Andhra U.); *Indian J. Phys.*, Vol. 37, pp. 640-644, Dec. 1963

A new doublet system of bands attributed to $MgCl$ molecule has been observed in the visible region $\lambda 5000 - \lambda 4550$ in the high frequency discharge. From the vibrational analysis of the system it is concluded that the lower state of this system is the same as the first excited $A^2 \Pi$ state of $MgCl$ with a doublet separation of 55 cm^{-1} . The approximate vibrational constants of the upper state are estimated as $\omega_e' = 563 \text{ cm}^{-1}$ and $x_e' \omega_e' = 5.5 \text{ cm}^{-1}$. The electronic structures of the ground and excited states of $MgCl$ are discussed in relation to those of BeF and MgF .

Emission Spectra of $CaF_2:Er^{3+}$ - See 25,625

25,644 HIGHER ORDER COHERENT RAMAN EFFECTS by C. L. Tang (Raytheon Res. Div.); *Phys. Rev.*, Vol. 134A, pp. A1166-1173, June 1, 1964

With the recently available very intense coherent maser light, interesting higher order coherent Raman effects have been observed in solids, liquids, and

gases. Garmire, Pandarese, and Townes have given a phenomenological theory of these higher order coherent Raman effects. A somewhat more detailed theory of these effects is given. The analysis is based on a perturbation solution of the Boltzmann equation for the density matrix of the Raman active medium. General expressions for all the relevant induced dipole moments and absorbed or emitted Stokes and anti-Stokes radiations in the ordinary or higher order coherent Raman processes are given. These cover a great variety of possible experimental situations. Several specific simple examples are studied in some detail and the results of the phenomenological theory are reproduced from the general results given here.

25,645 RAMAN SPECTRA OF ICES Ih, Ic, II, III, AND V by M. J. Taylor and E. Whalley (Nat'l. Res. Council, Ottawa); *J. Chem. Phys.*, Vol. 40, pp. 1660-1664, Mar. 15, 1964

The Raman spectra at 77°K of ices Ih, Ic, II, III, and V made from H_2O and D_2O have been obtained. The spectra in the O-H and O-D stretching region were obtained both photographically and photoelectrically using Hg 4358 Å as the exciting radiation, and the low-frequency spectra were obtained photographically using Hg 2537 Å as the exciting radiation. In the O-H stretching region, the spectra of ices Ih and Ic are identical, and the spectra of ices II, III, and V are similar except that the frequencies are higher than in ice I. Ices II, III, and V appear to be essentially fully hydrogen bonded, as was concluded from the infrared spectra. In the low-frequency spectrum there is one band or sometimes two bands in all the ices, and they are probably due to translational vibrations of the molecules.

25,646 LUMINESCENCE IN SOLIDS by G. F. J. Garlock (U. Hull); *Science Progress*, Vol. 52, pp. 3-25, Jan. 1964

The basic processes in luminescence, conditions for luminescence in solids, luminescence "centers," phosphorescence, electron trap phenomena, and electro- and thermo-luminescence are discussed. Basically, luminescence is the emission of light other than that produced thermally when energy is absorbed from ultraviolet light, fast electrons, other particles, or from an electric field. In most cases, emission takes place from specific atomic sites known as luminescence centers. Additional references are cited for a more thorough discussion of the separate topics.

25,647 THEORY OF THE SHAPE, WIDTH AND SHIFT OF LUMINESCENCE LINES OF IMPURITY CENTERS IN IONIC CRYSTALS by B. F. Malkin (Ul'yanov-Lenin Kazan State U.); *Soviet Phys.-Solid State*, Vol. 5, pp. 2262-2266, May 1964

The effect of electron-phonon interaction on the shape, width and shift of luminescence lines of impurity ions of the transition group elements in ionic crystals is discussed in the harmonic approximation. An analysis is made of the optical line broadening caused by adding a background. The calculated width of the luminescence lines of ruby as a function of temperature is in good agreement with experimental data.

25,648 LUMINESCENT SULFUR CENTERS IN ALKALI HALIDES AND OTHER INORGANIC SOLIDS by J. H. Schulman and R. D. Kirk (U.S. Naval Res. Lab.); *Solid State Commun.*, Vol. 2, pp. 105-108, Apr. 1964

Luminescent centers are formed by heating alkali halides in sulfur vapor. The similarity between their emission spectrum and the spectrum attributed to O_2^- in alkali halides suggests that the centers are S_2^- molecule-ions. From the structure in the emission spectrum the ground state vibrational frequency is found to be $1.74 \times 10^{13} \text{ sec}^{-1}$.

Luminescence of GaP - See 25,614

25,649 COPPER-ACTIVATED ALKALINE-EARTH PHOSPHATE PHOSPHORS by R. C. Ropp (Sylvania); *J. Electrochem. Soc.*, Vol. 111, pp. 538-541, May 1964

Spectral properties of the alkaline earth pyrophosphates and a condensed strontium phosphate, all activated by copper, are described. Of the pyrophosphates, only $\alpha\text{-Ca}_2P_2O_7$, $\beta\text{-Ca}_2P_2O_7$, and $\delta\text{-Ba}_2P_2O_7$ produce moderately intense emission when activated by copper. In the condensed phosphate systems, only $Sr_3(P_3O_{10})_2:Cu$ produces intense luminescence. An explanation in terms of d-electron interaction or coupling is proposed.

25,650 SELF-ACTIVATED LUMINESCENCE OF M^{2+} NIOBATES AND TANTALATES by A. Wachtel (Westinghouse); *J. Electrochem. Soc.*, Vol. 111, pp. 534-538, May 1964

Among 22 compounds examined for photoluminescence, only $Mg_4Nb_2O_9$, $CaTa_2O_6$ and the metaniobates of Mg, Ca, Zn, and Cd show appreciable room temperature emission. With the exception of $Mg_4Nb_2O_9$, all of these have the columbite structure; moreover, the only essentially nonluminescent columbite-type compound noted was $ZnTa_2O_6$. The absorption edges of the luminescent niobates lie at shorter wavelengths than those of otherwise similar compositions.

This indicates a relationship between luminescence and the separation of energy states within the Nb-O bond, as influenced by structure.

25,651 LUMINESCENCE OF SOLID SOLUTIONS $\text{CaWO}_4\text{-PbWO}_4$ ACTIVATED BY SAMARIUM by Y. Koteva and T. Sekine (Govt. Chem. Ind. Res. Inst., Tokyo); *J. Phys. Chem. Solids*, Vol. 25, pp. 353-354(L), Mar. 1964

Mixtures of precipitated calcium tungstate, lead tungstate, and a samarium compound were fired at 1100°C for one hour in air. The resulting solid solutions obey Vegard's law in the whole range of the calcium-lead tungstate system. At room temperature under 2537 Å excitation, the samarium-activated solid solution has an emission composed of a broad blue band and a band in the red and infrared region showing fine structure. The red emission is due to samarium and emission intensity varies with amount of lead present. This composition dependence may be associated with the movement of the absorption edge and the energy transfer from the host structure to Sm^{3+} .

25,652 LUMINESCENCE OF KNO_3 IRRADIATED WITH γ RAYS by Yu. A. Kulyupin and A. F. Yatsenko (Acad. Sci. UkrSSR); *Soviet Phys.-Solid State*, Vol. 5, pp. 2443-2445(L), May 1964

Luminescence of NO_2^- impurities in KNO_3 has been investigated. It is found that the halfwidth of the bands of the spectrum remains almost constant as the temperature is increased from 20 to 77°K, which indicates the existence of a local mechanism of the impurity luminescence. The slight displacement (25 cm^{-1}) of the impurity luminescence spectrum to the short-wavelength side relative to the spectrum of KNO_2 indicates that NO_2^- in the KNO_3 lattice has more freedom, compared with its state in KNO_2 .

25,653 INVESTIGATION OF THE LUMINOUS EFFICIENCY OF ELECTROLUMINESCENT CAPACITORS by F. M. Pekerman and L. N. Petoshina; *Optics and Spectrosc.*, Vol. 16, pp. 269-271, Mar. 1964

The luminous efficiency of electroluminescent capacitors was measured by an oscilloscopic method, and its dependence on excitation conditions, on the properties of the electroluminescent phosphor, and on the method of preparing the capacitors was investigated. It is shown that the luminous efficiency decreases less than the brightness during "aging" of electroluminescent capacitors.

25,654 ELECTROLUMINESCENCE OF ORGANIC DIELECTRICS by H. Armstrong and J. Hancock (Queen's U., Canada); *Can. J. Phys.*, Vol. 42, pp. 823-824(L), Apr. 1964

Electroluminescence has been found to occur in several organic dielectric materials such as vaseline, paraffin wax, toluene, and polyvinylidene chloride. Cells for studying electroluminescence were prepared and excited by application of an alternating voltage at 60 cps. The brightness is roughly proportional to $\exp(-a/V^{1/2})$ where a is a constant and V the applied voltage. Most of the dielectrics show some emission of visible light under ultraviolet light. Results do show that the material in which a phosphor is imbedded, as well as the phosphor itself, may contribute to electroluminescence.

25,655 ELECTROLUMINESCENCE OF AN EVAPORATED ZnS-Mn PHOSPHOR EXCITED BY UNIPOLAR ELECTRIC PULSES by V. Korsun and S. Kostylev (Acad. Sci. USSR); *Optics and Spectrosc.*, Vol. 15, pp. 448-449, Dec. 1963

A study of ZnS-Mn phosphors, which can be excited by both alternating and constant electric fields, is described. Electroluminescence was excited by rectangular, unipolar pulses of 50-2000 μsec duration at repetition rates of 20-50 cps. The rise time of the luminescence was faster than the fastest pulse used; the results indicate a fast rise, constant value proportional to the applied voltage and near exponential decay with a time constant.

25,656 THE ROLE OF HOLES IN THE ELECTROLUMINESCENCE KINETICS OF ZnS-Cu , Al , Cl PHOSPHORS by E. E. Bukke, L. A. Vinokurov and M. V. Fok; *Optics and Spectrosc.*, Vol. 16, pp. 266-268, Mar. 1964

Ignition and extinction are investigated under the influence of infrared light following photo- and electroexcitation. It is shown that with electroexcitation some of the holes leave the interior of the crystal for the surface, and return during the afterglow period.

Electroluminescence of BP - See 25,617

Tapping Luminescence of CdS - See 25,687

25,657 LONG-WAVELENGTH EDGE OF THE PHOTOEFFECT AND RECOMBINATION RADIATION OF GaAs p-n JUNCTIONS by A. A. Gutkin, M. M. Kozlov, D. N. Nasledov and V. E. Sedov (Acad. Sci. USSR); *Soviet Phys.-Solid State*, Vol. 5, pp. 2654-2656(L), June 1964

The mechanism of the recombination radiation of GaAs p-n junctions is discussed. It is found that the position of the long-wavelength radiation maximum coincides with the beginning of the step in the spectral distribution of the photosensitivity, and it is concluded that the long-wavelength maximum of the re-

combination radiation is due to transitions involving impurity centers, not due to the indirect interband transitions.

Cathodoluminescence of $\text{Zn(PO}_3)_2\text{-Cd(PO}_3)_2\text{-Mg(PO}_3)_2$ - See 24,874

25,658 TIME CONSTANT OF CATHODE LUMINESCENCE IN GaAs by H. Flicker and J. A. Baicker (RCA Labs.); *Bull. Am. Phys. Soc.*, Vol. 9, p. 446(A), Apr. 1964

N-type GaAs wafers were irradiated with pulses of high-energy electrons from a Van de Graaff accelerator. The time of decay of recombination radiation from the injected carriers has been measured after the pulse is deflected off the sample. An RCA 7102 photomultiplier was used as detector, and interference filters were used to examine the spectral distribution. Although the electron beam is deflected off the sample in less than 10^{-9} sec, the detector circuits have a rise time of 10^{-8} sec, which constitutes the lower limit of measurable time constants. Several nondegenerate n-type samples had a large 1.1 eV emission with a time constant of 10^{-6} sec. This emission corresponds to a recombination center approximately 0.3 eV from the valence-band edge that captures a hole in a time less than the minority-carrier lifetime ($< 10^{-9}$ sec) and an electron some time thereafter. The emission at 1.4 eV near the band edge was quite weak and had a time constant of less than 10^{-8} sec. Samples of p-type GaAs emitted light of short time constant, at 1.4 eV.

25,659 PHOTOLUMINESCENCE OF Mn- AND Cr-DOPED GaAs by W. J. Turner and G. D. Pettit (IBM Watson Res. Ctr.); *Bull. Am. Phys. Soc.*, Vol. 9, p. 269(A), Mar. 1964

Photoluminescence data on Mn- and Cr-doped GaAs have been obtained as a function of temperature. Mn, an acceptor in GaAs , produced a 77°K recombination peak at 1.39 or 0.12 eV from the valence band. At higher temperatures, the probability of recombination at the Mn center decreases and other shallower centers dominate, presumably due to a shift in the Fermi level. GaAs doped with Cr has a high resistivity at room temperature, viz., $\rho \approx 10^8 \Omega\cdot\text{cm}$. This material exhibits a 0.82-eV luminescence peak at 77°K due to recombination at the Cr.

25,660 PHOTOLUMINESCENCE OF EXCITON COMPLEXES IN 21R SiC by W. J. Choyke, D. R. Hamilton and L. Patrick (Westinghouse); *Bull. Am. Phys. Soc.*, Vol. 9, p. 270(A), Mar. 1964

Polytype 21R SiC has an indirect energy gap of 2.86 eV at 4°K, and has a large unit cell with 7 inequivalent Si or C sites. The low-temperature edge luminescence can be attributed to exciton complexes, which are formed, under uv irradiation, by the capture of excitons by neutral nitrogen (the most common donor in SiC). Since there are 7 inequivalent nitrogens and 42 phonon branches, the spectrum could have 301 lines, including the non-phonon lines. Only about 40 lines are clearly resolved. These can be arranged in 6 series (of an expected 7), with only the phonons at the edge of the extended zone boundary giving rise to strong lines. These phonons have energies of 46, 77, 95, and 104 MeV, in good agreement with zone-boundary phonons in 6H and 15R SiC .

25,661 A THEORY OF THERMOLUMINESCENCE OF FLUORITE ($\text{CaF}_2\text{:Y}$). RADIATIVE RECOMBINATION FROM HIGHLY ASSOCIATED ELECTRON-HOLE PAIRS by J. R. O'Connor (Lincoln Lab.); *Appl. Phys. Lett.*, Vol. 4, pp. 126-128(L), Apr. 1, 1964

The thermoluminescent spectra of electron-irradiated, YF_3 - and Y_2O_3 -doped CaF_2 single crystals over the temperature range 77° to 273°K are discussed. The spectra previously reported for fluorite are the same as those for Y-doped CaF_2 and the position of the emission lines depends on the charge compensation method. The spectra can be explained by radiative recombination of highly associated pairs of Y^{3+} and a compensator ion (either substitutional O^{2-} ions or interstitial F^{-1} ions). When the system is exposed to ionizing radiation, Y^{3+} is reduced to $\text{Y}^{2+}(4d^1)$. Subsequent reduction in the concentration of Y^{2+} is probably due to hole hopping.

25,662 THERMOLUMINESCENCE AT LOW TEMPERATURE IN CRYSTAL OF LiF by J. Tournon and P. Berge (CENS, France); *Phys. Stat. Sol.*, Vol. 5, pp. 117-121, 1964

The thermoluminescence of γ -irradiated LiF crystals, excited in the F-center band at 78°K, is discussed. Peaks were observed at 100°K and 150°K. The thermoluminescence depends upon the time of γ -irradiation, excitation time and the number of thermoluminescent experiments performed.

25,663 LOW-TEMPERATURE EMISSION SPECTRUM OF O_2^- IN ALKALI HALIDES by J. Rolfe (Nat'l. Res. Council, Ottawa); *J. Chem. Phys.*, Vol. 40, pp. 1664-1670, Mar. 15, 1964

The fluorescence emission spectrum of the O_2^- molecule-ion has been measured at 4.2°K in the alkali halides NaF , NaCl , NaBr , KCl , RbCl , KBr , RbBr , and KI . The most intense peaks in the emission spectra are shown to be due to transitions to vibrationally excited levels of the ground state of O_2^- . The vibration-

al properties of O_2^- in its ground state can be represented by an anharmonic oscillator with a vibrational constant (ω_0) of approximately 1170 cm^{-1} , and an anharmonicity (ω_{ex0}) of 8.5 cm^{-1} . The cause of the fine structure which appears around these intense peaks is not known, but the fine structure for the alkali halides NaF, KCl, and RbBr, which have almost equal anion and cation masses, is quite different from the other alkali halides NaCl, NaBr, KBr, and KI.

25,664 THE LIFETIME OF THE EXCITED F_A CENTRE IN KCl(Li) by G. Gramm (Tech. Hochs., Stuttgart); *Phys. Lett., Neth.*, Vol. 8, pp. 157-158(L), Feb. 1, 1964

Measurements of the emission lifetime of excited F_A centers in KCl crystals doped with Li are discussed. The F_A center is formed by replacing one of the K^+ ions surrounding an F center with an Na^+ or Li^+ ion. In KCl(Li) crystals at low temperatures (near 0°K), the measured total lifetime was $85 \times 10^{-9}\text{ sec}$ \pm 10 per cent and the radiative lifetime $\tau_R(F_A)$ was $3.4 \times 10^{-7}\text{ sec}$. The F_A (Li) center has a higher radiative transition probability than the F center. The radiative transition of the F_A (Li) center to the ground state can be explained as an allowed transition.

25,665 FLUORESCENCE AND PHOTOCONDUCTIVITY OF EXCITON IN CuCl CRYSTAL by T. Goto and M. Veta (Tohoku U.); *J. Phys. Soc. Japan*, Vol. 19, pp. 774-775(L), May 1964

The excitation spectrum for fluorescence and absorption of CuCl at 4°K has been studied. The fluorescence spectrum consisted of a strong narrow band at $390.6\text{ m}\mu$ and three broad bands extending to $490\text{ m}\mu$. The excitation spectrum of thick film showed two sharp peaks at 387.5 and $378.5\text{ m}\mu$. The efficiency of fluorescence excitation in the band to band region was five times smaller than that in the exciton band region. This leads to the conclusion that the narrow band fluorescence arises from exciton annihilation and not from electron-hole recombination.

25,666 UNUSUAL INFRARED FLUORESCENCE IN $\text{PrCl}_3(\text{Nd}^{3+})$ CRYSTALS by F. Varsany (Bell Labs.); *Phys. Rev. Lett.*, Vol. 1, pp. 314-315(L), Oct. 1, 1963

A very sharp fluorescence line at $2.54\text{ }\mu$ has been observed in anhydrous PrCl_3 : Nd^{3+} under black body radiation. The linewidth is less than .2 of a wave number and the decay time is in the order of 50 msec. The radiation is identified as the $X_1 \rightarrow Z_1$ fluorescence of Nd^{3+} , where $X_1: \text{Nd}^{3+} 4f_{13/2}$, $\mu = \pm 1/2$ and $Z_1: \text{Nd}^{3+} 4f_{5/2}$, $\mu = \pm 5/2$. The identification is aided by high resolution Zeeman experiments. Absorption measurements using an illuminating monochromator were also made.

25,667 THE FLUORESCENT DECAY OF CsI(Tl) EXCITED BY CHARGED PARTICLES by E.A. Womack, A.J. Lazarus and M. Joseph (MIT); *IEEE Trans.*, Vol. NS-11, pp. 24-26, June 1964

The fluorescence from a CsI(0.08 per cent Tl) scintillator excited by charged particles which come to a stop within the scintillator has been measured for alpha particles, deuterons, and protons. In the region 0.1 to 0.6 microseconds after its initial rise, the fluorescent decay can be accurately described by a simple exponential. The characteristic time for this exponential decay has been measured at several energies up to 28.7 Mev for alpha particles and 7.2 Mev for protons. A linear relationship was found between this decay time and the log of the particle energy, $\tau = k \ln E + \tau_0$, where k and τ_0 are constants which are characteristic of the type of stopping particle.

25,668 IMPROVED FLUORESCENCE DECAY-TIME MEASURING APPARATUS by I.B. Berlman and O.J. Steingraber (Argonne Lab.); *IEEE Trans.*, Vol. NS-11, pp. 27-28, June 1964

An apparatus has been assembled which is capable of detecting and reproducing the fluorescence pulse contours from scintillation materials. Two areas of our work are emphasized: The recent modifications in the apparatus and the presentation of preliminary data. A comparison is made between the fluorescence decay time of ordinary and deuterated compounds. Preliminary results also indicate that in a series of similar type molecules each with a high quantum yield, the longer the molecule the shorter the fluorescence decay time.

25,669 DOUBLE ACCEPTOR FLUORESCENCE IN II-VI COMPOUNDS by R. E. Halsted and B. Segall (GE Res. Lab.); in *Res. on CdTe*, 1963, 6 pp., Cont. AF 33(616)-8264; *STAR*, Vol. 2, p. 1298(A), May 23, 1964 AD 404 859

An attempt is made to show that the unique characteristics of a radiative recombination process can be examined in terms of the properties of a native double-acceptor defect, recently identified in electrical transport measurements. The fluorescent emission characteristic of this defect is studied in terms of the native double acceptor, which has a doubly ionized level close to the conduction band. From the study, it is seen that the specific concept of a doubly ionized native-acceptor level near the conduction band, coordinating transport and fluorescence measurements, provides a basis for a detailed understanding of the characteristics of emission in group II-VI compounds.

25,670 FLUORESCENCE AND ENERGY TRANSFER IN $\text{Y}_2\text{O}_3:\text{Eu}^{3+}$ by J.D. Axe and P.F. Weller (IBM Watson Res. Ctr.); *J. Chem. Phys.*, Vol. 40, pp. 3066-3069, May 15, 1964

Experimental evidence for nonradiative resonant energy transfer between Eu^{3+} and other trivalent rare-earth ions in Y_2O_3 is presented and possible interaction mechanisms are examined. It is concluded that coupling via overlap of near zone quadrupolar fields is important. Measurements on the transient behavior of the Eu^{3+} fluorescence are also discussed.

25,671 SPECTRUM OF Er^{3+} IN SINGLE CRYSTALS OF Y_2O_3 by P. Kisliuk and W.F. Krupke (Aerospace), and J.B. Gruber (U. Calif., Los Angeles); *J. Chem. Phys.*, Vol. 40, pp. 3606-3610, June 15, 1964

The spectrum of Er^{3+} in single crystals of Y_2O_3 has been examined from 0.225 to $2.4\text{ }\mu$ in absorption and fluorescence, and energy levels have been assigned. The Slater integrals and spin-orbit coupling parameter have been determined, which give the best over-all agreement between the centers of gravity of the observed groups of levels and the $4f^{11}$ SLJ energy levels of the "free" Er^{3+} ion; they are $F_2 = 429.583\text{ cm}^{-1}$, $F_4 = 65.012\text{ cm}^{-1}$, $F_6 = 7.136\text{ cm}^{-1}$, $\zeta = 2383.17\text{ cm}^{-1}$. Of the two inequivalent cation sites, C_2 and C_{3j} , one can with consistency demonstrate that the site without inversion symmetry (C_2) gives rise to the entire observed spectrum.

25,672 STIMULATED AND FLUORESCENT OPTICAL EMISSION IN RUBY FROM 4.2 TO 300°K : ZERO-FIELD SPLITTING AND MODE STRUCTURE by I.J. D'Haenens and C.K. Asawa (Hughes Res. Lab.); *Quantum Electronics III*, pp. 796-804, Columbia U. Press, 1964

Spectroscopic and stimulated emission experiments have been performed on ruby. The observed temperature dependence of the ruby R_1 fluorescent linewidth can be used to study the effect of transition linewidth on stimulated emission. It is shown that the crystal field splitting of the $4A_2$ ground level can be resolved spectroscopically at temperatures lower than 100°K , which in turn allows the study of stimulated emission for competing transitions that have a common upper level.

Fluorescence of:

$\text{Ca}_3(\text{VO}_4)_2$ - See 24,979

Eu Chelates in Hosts - See 25,641

Silicate Glass:Eu - See 25,639

25,673 NOTE ON THE MÖSSBAUER EFFECT OBSERVED IN UO_2 SINGLE CRYSTALS by M. DeCoster, L. Mewissen and M. Verschueren (S.C.K. Mol, Belgium); *Phys. Lett., Neth.*, Vol. 8, pp. 293-294(L), Mar. 1, 1964

A Mössbauer effect study of Co^{57} -doped VO_2 single crystals is discussed. The Mössbauer spectrum was measured after the sample preparation, and nine months later, during which it was stored at room temperature and half of the Co^{57} had decayed. The former spectrum suggests that the iron present in the VO_2 crystal is Fe^{+++} . A larger value of Γ found for the peak of the first spectrum than for the components of the latter five-peak pattern is attributed to slight deviations in the environment of the Fe^{+++} in the disordered specimen. A magnetic field was observed at the Fe nucleus. At room temperature, this cannot be due to antiferromagnetism. Likewise it cannot be attributed to the formation of Fe_2O_3 . It is suggested that the internal field may be caused by a reordering of interstitial oxygen around the Fe ion.

Mössbauer Effect in:

FePd - See 25,409

Au:Fe Foils - See 25,403

Mössbauer Study of:

Superparamagnetism in Ni Ferrite - See 25,552

Spin Flop in Hematite - See 25,534

25,674 COPPER-ACTIVATED THORIUM PHOSPHATE PHOSPHORS by W.F. Schmid and R.W. Mooney (Sylvania); *J. Electrochem. Soc.*, Vol. 111, pp. 668-673, June 1964

Eight different copper-activated thorium phosphate phosphors were prepared, identified, and their fluorescence properties measured. The brightest phosphors, with their fluorescence maxima, are: $\text{Th}_3(\text{PO}_4)_4$:0.045 Cu, 440 nm and 540 nm; $\text{Th}_3(\text{PO}_4)_4$:0.48 Cu, 590 nm; $\text{Th}_2(\text{PO}_4)_3$, 590 nm; $\text{Th}_2\text{Li}(\text{PO}_4)_3$:0.04 Cu, 455 nm; and $\text{Th}_2\text{Ag}(\text{PO}_4)_3$:Cu, 565 nm. The copper concentration has a pronounced effect on the fluorescence color and phosphor composition. All the phosphors except $\text{Th}_2\text{Ag}(\text{PO}_4)_3$:Cu have good temperature dependence. If the proper coating technique is used, these phosphors are highly efficient in high pressure mercury vapor lamps.

25,675 LASER PHENOMENA IN EUROPIUM CHELATES. Part I. SPECTROSCOPIC PROPERTIES OF EUROPIUM BENZOYLACETONATE by H. Samelson, A. Lempicki, V.A. Brophy and C. Brecher (Genl. Tel. and Electronics Lab.); *J. Chem. Phys.*, Vol. 40, pp. 2547-2558, May 1, 1964

The absorption and fluorescence emission spectra of solutions of the chelate europium benzoylacetonate (EuB), the fluorescence decay times of these solutions, and the fluorescence emission spectrum of the solid chelate are described in detail. From this information an energy-level structure for the lower states of the ground multiplet is obtained for the solid and for the solutions and the room temperature radiative lifetime of the europium fluorescence in solutions of the chelate has been determined. The temperature dependence of the intensity and lifetimes of the fluorescence reveals that the efficiency of the intramolecular energy transfer must decrease as the temperature increases.

25,676 FLUORESCENCE OF PURE ZINC SULFIDE IN CORRELATION WITH DEVIATION FROM STOICHIOMETRY by I. Uchida (Nippon Electric); J. Phys. Soc. Japan, Vol. 19, pp. 670-674, May 1964

Studies were carried out on the correlation between the B and SAL emission bands of pure ZnS phosphors and the deviation from the stoichiometry in the phosphors. SAL is observed in the phosphors having excess zinc, while it disappears in the phosphors having excess sulfur. The SAL center may be caused by a sulfur vacancy. B grows in either case that the phosphors are fired in the atmosphere of zinc or sulfur. The peak of B of the phosphors having excess sulfur is located at 347 mμ, while that of the phosphors having excess zinc at 357 mμ. These facts suggest that the so-called B band is composed of two bands of B_I and B_{II}. It may be reasonably concluded that the center of B_I is formed by an interstitial sulfur atom and that the center of B_{II} is caused by an interstitial zinc atom or a sulfur vacancy having the value of charge different from that of the center of SAL.

25,677 DURATION OF PHOSPHORESCENCE. Part II by H.E. Millson (Jordan Mfg., Philadelphia) and H.E. Millson, Jr. (Hoffman-LaRoche, Nutley, N.J.); J. Optical Soc. Am., Vol. 54, pp. 638-640, May 1964

Phosphorescence of calcite and fluorite, exposed for a few minutes to 2537° ultraviolet light from a low-pressure cold quartz mercury vapor lamp, persisted for 18 years. Emission was detected by placing the phosphorescing minerals on black-and-white and Kodachrome film, to obtain "phosphorographs" of the glowing areas. The rate of emission depends on temperature; the color of the phosphorescence has not changed; these confirm the results of other tests that prove that radioactivity is not involved. The patterns of growth of a crystal, and changes of its environment during formation, are clearly shown by the variegated colors in its phosphorograph.

25,678 YELLOW AND RED EMITTING ZnS:Cu PHOSPHORS by M. Presland, R. Marshall and J. Franks (AEL, Ltd.); J. Electrochem. Soc., Vol. 111, p. 628(L), May 1964

The preparation and properties of intense yellow and red emitting ZnS:Cu phosphors are described. The phosphors are prepared by firing a slurry in an Ar atmosphere and quenching directly in deionized water. Red and yellow photoluminescence are observed after drying at room temperature. Low temperature annealing causes a conversion of yellow emission to red and subsequently complete destruction of the red. Further annealing causes a reversion to the more usual blue or green.

25,679 THE SCINTILLATION PROCESS IN ALKALI HALIDE CRYSTALS by J.B. Birks (U. Manchester, England); IEEE Trans., Vol. NS-11, pp. 4-11, June 1964

The scintillation process in impurity-activated alkali halide crystals is considered by analogy to that in binary solid organic solutions. A general relation is proposed for the differential scintillation efficiency dL/dE as the product of the efficiencies of the primary and secondary scintillation processes. The primary efficiency is influenced by electron-hole recombination and ionization quenching and is a function of the specific energy loss dE/dr . The secondary efficiency is influenced by host-activator energy transfer and concentration quenching and is a function of the activator concentration c . Experimental data in support of the model are cited. An extension of the model is proposed to account for the temperature dependence of the scintillation efficiencies and decay times of pure and impurity-activated alkali halides, and this is compared with experimental data.

25,680 THE SCINTILLATION MECHANISM IN THALLIUM ACTIVATED SODIUM IODIDE by I. Cooke and R. Palser (U. Manitoba, Canada); IEEE Trans., Vol. NS-11, pp. 15-19, June 1964

The emission and transmission of both pure and Tl activated NaI crystals have been studied as functions of wavelength and plastic deformation in the sample. The results show an increase in emission at 0.42 micron for the NaI(Tl) phosphor, and a probable decrease for the pure NaI specimen. In pure NaI three emission bands, located at 0.33, 0.375 and 0.42 micron, were observed. The 0.42 micron band in both NaI(Tl) and NaI is associated at least in part with chemical contamination of the surface. Some reduction in absorption in both the activated and pure crystals was observed upon increasing the dislocation density.

25,681 ELECTRON RESPONSE OF NaI(Tl) AND A COMPARISON WITH ANTHRACENE AND PILOT B by I.S. Sherman, M.S. Freedman, F.T. Porter and F. Wagner, Jr. (Argonne Lab.); IEEE Trans., Vol. NS-11, pp. 20-23, June 1964

The relative response of NaI(Tl) to electrons over an energy range of 6 kev to 1 Mev has been studied. The light output at 6 kev is quite sensitive to the nature of the exposed surface. The results are given for the two best cleaved NaI(Tl) crystals and compared to the electron response deduced from photon data. There is good agreement above 20 kev, where little sensitivity to changes in surface condition was observed. Similar measurements were made for anthracene and Pilot B. The relative light output per unit energy is shown for all three scintillators. Their merit as low energy electron detectors was found to be significantly affected by the amount of backscattering and the intensity and duration of long lived excitation states arising from ionizing events.

25,682 BISMUTH ARSENATE PHOSPHORS ACTIVATED BY RARE EARTH IONS by T. Sekine and Y. Koteva (Govt. Chem. Ind. Res. Inst., Tokyo); J. Phys. Chem. Solids, Vol. 25, pp. 354-357, Mar. 1964

Efficient phosphors have been obtained by activating bismuth arsenate by rare earth ions which appear to substitute trivalent cations in the host lattice. X-ray patterns showed that all samples were monoclinic with Huttonite structure. An excitation spectrum indicated the phosphor would be efficiently excited by 3650 Å. Excitation and emission spectra of the phosphors are different from those of tungstate or molybdate phosphors activated by the same rare earth ions, presumably because of the difference of crystal field between the arsenate and tungstate or molybdate.

PHOTOELECTRONIC PROPERTIES

25,683 PHYSICAL PRINCIPLES OF PHOTOCONDUCTIVITY. Part I. BASIC CONCEPTS: CONTACTS ON SEMICONDUCTORS by L. Heijne (Philips); Philips Tech. Rev., Vol. 25, pp. 120-131, No. 5, 1963-1964

Elementary concepts and hypotheses of photoconductivity that involve energy band scheme, differences between metals, semiconductor and insulators, intrinsic and extrinsic semiconductors, donor and acceptor centers, electron and hole conduction, and lifetime and mobility are discussed. Photoconductivity occurs when the absorption of light quanta causes electrons to be raised from the valence band or from impurity centers into the conduction band. Finally, the properties of photoconductors provided with metal contacts are dealt with at some length. These properties are governed by the relative situation of the Fermi levels. If that of an N-type photoconductor is higher than that of the metal, a boundary layer forms in the semiconductor which is greatly depleted in charge carriers. The contact then has a rectifying action. In the other case Ohm's law is more or less obeyed, provided the photocurrent is not too high.

25,684 A NONTHRESHOLD PHOTOCONDUCTIVE EFFECT IN METALS WITH INTERSECTING BANDS by M.I. Kaganov and I.M. Lifshitz (Acad. Sci. UkrSSR); Soviet Phys.-JETP, Vol. 18, pp. 655-659, Mar. 1964

The electric conductivity due to the interaction with the electromagnetic field of electrons located near the degenerate points in the Brillouin zone is calculated for metals with intersecting bands. Various cases of the frequency dependence of the conductivity near threshold are discussed. It is shown that the real part of the conductivity tensor is proportional to ω^3 in relatively broad frequency and temperature ranges.

25,685 PHOTOCONDUCTIVITY SPECTRUM OF SEMICONDUCTORS FOR THE CASE OF ADDITIVE ABSORPTION by R.A. Titov (Acad. Sci. USSR); Soviet Phys.-Solid State, Vol. 5, pp. 2553-2556, June 1964

An analytical expression for the spectral distribution of the photoconductivity of a semiconductor in the presence of two absorption mechanisms is obtained. The form of the photoconductivity spectrum is calculated for a number of cases and the results are presented graphically. Conditions are established under which the structure of the photoconductivity spectrum will coincide with the maxima in the absorption spectrum.

25,686 REACTION KINETIC INVESTIGATIONS ON THE INFLUENCE OF TRAP SPECTRA ON THE PHOTOCURRENT-LIGHT INTENSITY CHARACTERISTICS OF PHOTOCONDUCTING PHOSPHORS by J. Voigt (Humboldt U.); Phys. Stat. Sol., Vol. 5, pp. 123-138, 1964

A reaction kinetic model has been developed to understand the light intensity and temperature dependence of conduction electron concentration. The model is based on a minimal model for photoconducting phosphors and has been extended to include an arbitrary number of trap groups or distributions. A closed approximative solution is found without assuming quasiequilibrium and for conditions that are valid for n-type photoconductors. Detailed study of the effect of various trap distributions on the dependence of electron concentration on

light intensity — especially in the superlinear region of electron concentration-light intensity characteristic — is outlined. Trap distributions for a single trap level, homogeneous distributions and Gaussian distributions are compared.

Photocurrents in CdS — See 25,222

25,687 ELECTRICAL PROPERTIES OF CdS CRYSTALS by B.A. Kulp (Aerospace Res. Lab.); *Bull. Am. Phys. Soc.*, Vol. 9, p. 248(A), Mar. 1964

Certain crystals of CdS have been shown to emit green luminescence when struck a blow with a hard object at low temperature. Many of these crystals show unusual electrical properties. When cooled in dark, the conductivity goes to very low values, $10^{-12} \Omega \cdot \text{cm}^{-1}$ or less; then, upon exposure to light of wavelength less than 6900 Å, the conductivity increases irreversibly to values as high as $10^{-3} \Omega \cdot \text{cm}^{-1}$. The defect structure of these crystals has been studied by the technique of thermally stimulated currents in the temperature range 80° to 300°K. Five current peaks are observed with different intensities in different crystals. When the crystal is illuminated with light of wavelength shorter than 6900 Å, the traps noted above can be filled without changing the conductivity of the crystal. The energy of the traps can be determined by the threshold wavelength of light required to fill the various levels with electrons from the level located 6900 Å (1.79 eV) from the conduction band, as well as by the position of the Fermi level when the traps are being emptied.

25,688 EFFECT OF CHEMISORBED OXYGEN ON PHOTOVOLTAIC AND PHOTOCONDUCTIVE PROCESSES IN RUTILE by R. Keezer (U. Michigan); *J. Appl. Phys.*, Vol. 35, pp. 1866-1867, June 1964

Absorbed oxygen increases both the response and the response time for the photovoltaic effect in rutile. The model for the effect of chemisorbed oxygen on the photoconductivity has been modified to take into consideration the effect of oxygen pressure. The conductance of rutile, measured as a function of oxygen pressure, agrees with the modified model. The increase in the photovoltaic response and response time with exposure to oxygen has been explained in terms of the barrier layer formed by chemisorbed oxygen.

25,689 NATURE OF LOCALIZED CENTERS WITH DEEP-LYING ENERGY LEVELS IN HIGH-ENERGY ELECTRON-IRRADIATED SILICON by V.D. Tkachev, A.F. Plotnikov and V.S. Vavilov (Acad. Sci. USSR); *Soviet Phys.-Solid State*, Vol. 5, pp. 2333-2337, May 1964

The photoconductivity of silicon single crystals doped with copper and gold and irradiated by high-energy electrons is analyzed. It is postulated that as a result of the interaction of atomic defects with the impurity atoms, the latter become electrically active centers. The results of this investigation suggest that irradiation by fast electrons can be used as a method of detecting certain impurities which are present in a crystal with small concentrations.

25,690 PHOTOELECTRIC PROPERTIES OF GALLIUM ARSENIDE by N.M. Voronkova, D.N. Nasledov and S.V. Slobodchikov (Acad. Sci. USSR); *Soviet Phys.-Solid State*, Vol. 5, pp. 2383-2386, May 1964

The photoconductivity of partially compensated p-type GaAs samples has been investigated in the temperature range 78-295°K. It is found that the photosensitivity increases with temperature in high resistivity samples, and decreases with temperature in low resistivity samples. Energy levels are found at 0.09, 1.0 and 0.7 eV above the top of the valence band. An energy diagram of these levels which shows the principal transitions among them is constructed with the help of the photoconductivity spectra.

Photocurrents in Anthracene — See 25,220

25,691 RUBY-LASER EXCITED PHOTOCURRENTS IN ANTHRACENE by K. Hasegawa and W.G. Schneider (Nat'l. Res. Council, Ottawa); *J. Chem. Phys.*, Vol. 40, pp. 2533-2537, May 1, 1964

Photocurrents in anthracene single crystals excited by the 6943-Å ruby laser line have been studied. At room temperature (and at higher temperatures) the currents are proportional to the square root of the intensity of exciting light, as reported previously. As the temperature is lowered this changes progressively to a linear dependence at -25°C. In the vicinity of 0°C the photocurrent pulses exhibit long decay times following termination of the laser pulse. These are interpreted in terms of carrier-trapping effects. The observed photocurrents are attributed mainly to single photon excitation of localized anthracene ions or trapped carriers. The enhanced currents observed in experiments using pre-illumination with uv light support this interpretation.

25,692 GAMMA-RAY PHOTOCONDUCTIVITY DECAY IN ORGANIC DIELECTRIC MATERIALS by S.E. Harrison (Sandia); SCR-671, 20 pp., June 1963, Pres. Summer Gen. Meeting IEEE, Toronto, June 1963; *STAR*, Vol. 2, p. 1263 (A), May 23, 1964

From experimental data it has been determined that gamma-ray photoconductivity decay in a number of organic dielectric materials can be characterized

to good approximation by

$$\frac{\sigma(t)}{\sigma_0} = \sum_{i=1}^n K_i e^{-t/\tau_i}$$

where $\sigma(t)$ is the conductivity as a function of time during the decay, σ_0 the conductivity at time zero immediately prior to removal of the gamma-ray intensity, n the number of decay time constants in the decay, τ_i the magnitude of the i th decay time constant, and K_i the weighting factor associated with the i th decay time constant. Experimental values for n , τ_i , K_i , and σ_0 were measured for Teflon, polyethylene, polyvinylchloride, polystyrene, Kel-F, and nylon.

25,693 OSCILLATIONS IN THE INTRINSIC PHOTOCONDUCTIVITY OF InSb by C.R. Stannard, Jr. and H.J. Stocker (Syracuse U.); *Bull. Am. Phys. Soc.*, Vol. 9, p. 478(A), Apr. 1964

The photoconductive response of p-type InSb shows oscillatory behavior as a function of incident-photon energy in the case of both acceptor-impurity to valence-band transitions and valence-band to conduction-band transitions. Intrinsic photoresponse measurements vs temperature indicate that the magnitude of the oscillations is largest below $T \sim 20^\circ\text{K}$ and disappears at $T \sim 60^\circ\text{K}$. The intrinsic threshold shifts toward lower energies with higher temperature and the positions of the minima shift with it, but the relative spacing remains the same. The positions of the minima were found to be independent of electric-field strength, but the oscillations become shallower at fields greater than a few v/cm. It is shown that the minima of the oscillations are related to both the energy of the LO phonon and the band structure of InSb. Up to 17 oscillations have been observed between photon energies of 0.24 and 0.70 eV.

25,694 VOLTAGE DECAY MEASUREMENT OF PHOTOEXCITATION AND TRAPPING OF CARRIERS IN SELENIUM by P.J. Regensburger (Zerex); *J. Appl. Phys.*, Vol. 35, pp. 1863-1865, June 1964

The trapping range of holes and electrons in amorphous selenium layers has been measured with a voltage decay technique. Values of 1.1 to $7.8 \times 10^{-8} \text{ cm}^2/\text{v}$ were obtained for holes. This agreed well with values obtained by the pulse method. An electron range of 5.0 to $8.3 \times 10^{-8} \text{ cm}^2/\text{v}$ was measured. Quantum efficiencies for photoexcitation of holes and electrons ranged from 7.5×10^{-4} to 1.0 , depending on the wavelength of the incident light.

25,695 THE EFFECTS OF TEMPERATURE AND ELECTRIC FIELD FOR THE PHOTO-GENERATION OF FREE CARRIERS IN ANTHRACENE by I. Nakada (U. Tokyo) and Y. Ishihara (Gakushuin U.); *J. Phys. Soc. Japan*, Vol. 19, pp. 695-701, May 1964

In order to study the generation of free carriers in an anthracene crystal, the measurement of the pulsed photoconduction has been performed. The number of free holes and electrons produced in a crystal after a flash illumination has been found to depend both on the temperature and the electric field. The number of generated holes increases exponentially with the rise of the temperature. At the higher temperatures it shows a tendency of saturation. The temperature dependency is not so remarkable for electrons. The number of holes and electrons increases with the field strength; yet in the higher field region the tendency of the saturation appears. The mobility of holes at the room temperature is $0.8 \text{ cm}^2/\text{v.s}$ and decreases as the temperature is raised. The mobility of electrons at the room temperature is $0.4 \text{ cm}^2/\text{v.s}$ and its variation with temperature is small. A model of energy levels is proposed for the carrier generation.

25,696 PHOTOGENERATION OF CHARGE CARRIERS IN ANTHRACENE BY A SINGLE EXCITON PROCESS by D.R. Kearns (U. Calif.); *J. Chem. Phys.*, Vol. 40, pp. 1452-1453(L), Mar. 1964

The rate at which carriers may be generated by the spontaneous ionization of singlet-state excitons is calculated and compared with the calculated rate for the double singlet exciton generation of charge carriers and some relevant experimental results. Domination of the double-exciton mechanism is predicted only when the mole fraction of excited singlet-state molecules in the crystal, M_{S^*} , is greater than $\sim 10^{-3}$. Experimental results using anthracene show a much lower mechanism transition, $M_{S^*} \leq 10^{-10}$. The discrepancy is most likely due to the assumption in calculations that the energy of an excited singlet-state molecule is sufficient to cause ionization. It is concluded that the minimum energy to generate charge carriers in pure anthracene is larger than the energy required to produce the lowest excited singlet-state of anthracene (3.1 eV).

25,697 STRONG PHOTO-EMF IN MONOCRYSTALLINE FILMS OF CdTe by F.T. Novik (Leningrad State U.); *Soviet Phys.-Solid State*, Vol. 5, pp. 2300-2304, May 1964

Measurement of the photo-EMF in monocrystalline films of CdTe is reported. It is found that the photovoltaic properties of such films result from the presence of the hexagonal CdTe phase with thin alternating layers of the cubic phase parallel to the {111} planes. The magnitude and the polarity of the photo-EMF depends on the degree of the orientation of the polar axes of crystallites composing the films. This orientation depends on the selective properties of the sul-

strate. It is concluded that the electrons move from the metalloid to the metal during the photoexcitation of CdTe.

25,698 HIGH-VOLTAGE PHOTO-EMF IN Sb_2S_3 FILMS by I.A. Karpovich and M.V. Shilova (Lobachevskii Gor'kov State U.); Soviet Phys.-Solid State, Vol. 5, pp. 2612-2617, June 1964

Investigation of the photovoltaic properties of Sb_2S_3 films in the temperature range $90^\circ\text{--}350^\circ\text{K}$ is reported. The results on the temperature dependence of the photo-EMF, short-circuit current, spectral distribution and some other characteristics show that the high-voltage photo-EMF is created by the barrier mechanism.

25,699 PHOTOVOLTAIC EFFECTS IN RUTILE by R. Keezer, J. Modar and D.E. Brown (U. Michigan); J. Appl. Phys., Vol. 35, pp. 1868-1870, June 1964

The ultraviolet photovoltaic response of barrier-layer cells formed from single-crystal rutile has been investigated. Typical samples have response maxima at 3200 Å, a D^* of 10^9 cm $\text{cps}^{1/2}/\text{W}$, and time constants of 100 μsec . Variations in time constant over several orders of magnitude have been observed, dependent largely on preparative technique. The effect of surface treatment on cell characteristics is discussed.

25,700 SLOW CHANGES OF THE PHOTOELECTROMAGNETIC EFFECT IN GERMANIUM by L.I. Kolesnik and Yu.A. Kontsevoi; Soviet Phys.-Solid State, Vol. 5, pp. 2454-2455(L), May 1964

The photoelectromagnetic effect (PEM) in n- and p-type plastically deformed germanium samples with a dislocation density about 8×10^5 to 8×10^6 cm $^{-2}$ has been investigated. The lifetime τ_{PEM} was calculated from measured values of the PEM EMF for two cases: (1) Cooling of the sample in darkness, (2) Cooling in the presence of illumination and long holding time. In the "nonstationary" state (case 1), the dependence of PEM EMF on the illumination I is nonlinear according to $\tau_{\text{PEM}} \sim I^\alpha$ with $\alpha = 1$ or 2. In the "stationary" state $\alpha = 0$. It is found that if a specimen initially cooled in darkness is illuminated and measurement is made after certain time intervals, then the PEM EMF increases, and if this specimen is again heated to room temperature and cooled in darkness, then the PEM EMF decreases back to the values as in case 1. The relaxation of the PEM EMF is shown not to relate to the recombination rate and the minority carrier lifetime τ_{min} .

OTHER OPTICAL PROPERTIES

25,701 OPTICAL CONSTANTS IN THE X-RAY RANGE by H.R. Philipp (GE Res. Lab.) and H. Ehrenreich (Harvard U.); J. Appl. Phys., Vol. 35, pp. 1416-1419, May 1964

In conjunction with X-ray transmission data, the integral relationship between the refraction index and the absorption coefficient can be employed to extend the range over which optical constants have been determined by Kramers-Kronig analysis of reflectance data. The procedure is applied to measurements on aluminum and the optical constants are determined for the energy range 10^{-3} to 10^5 eV. The results are useful in testing some general sum rules. They also permit a comparison of the behavior of the dielectric constant for energies above the K absorption edge with the expected asymptotic behavior.

25,702 OPTICAL PROPERTIES OF THE NOBLE METALS by M. Suffczynski (Polish Acad. Sci.); Phys. Stat. Sol., Vol. 4, pp. 3-29, 1964

Recent experimental data, methods of interpretation of such data, and problems involving the optical constants of the noble metals are reviewed. The optical properties of multivalent elements (Ni and Al) and alloys (brass) are compared with those of the noble metals. The electronic band structure is computed and it is considered probable that the multivalent elements exhibit weaker short-wavelength interband transitions in contrast to the behavior of noble metals.

25,703 A SIMPLE METHOD FOR THE DETERMINATION OF THE THICKNESS AND OPTICAL CONSTANTS OF SEMICONDUCTING AND DIELECTRIC LAYERS by S. Lyashenko and V. Miloslavskii (Acad. Sci. USSR); Optics and Spectrosc., Vol. 16, pp. 80-81, Jan. 1964

A method is proposed to determine the thickness and optical constants N and R of semiconducting and dielectric layers by measuring transmission T over a wide spectral range. Necessary conditions for application of the method include uniform thickness, no scattering, and smaller spectral width of the spectrophotometer than the half-width of the interference maximum. The advantage of this method is the simplification of experimental procedure, but it is pointed out that the usual interferometric method for thickness determination is more accurate.

25,704 A COMPUTER PROGRAM FOR A KRAMERS-KRONIG TRANSFORMATION OF THE OPTICAL REFLECTIVITY by R.J. Esposito, F. Rothwarf, R.M. Robbins, J.N. Brown and E.R. Thilo (Frankford Arsenal); 22 pp., Dec. 1963; U.S. Gov. Res. Rep., Vol. 39, p. 145(A), May 5, 1964 AD 430 722 OTS \$2.60

Relations involving the frequency-dependent optical constants give information on the electronic properties of solids. Power reflectivity measurements at normal incidence over a wide frequency region can be utilized in obtaining the optical constants by means of a general integral transformation known as the Kramers-Kronig transformation. A computer program based on this integral transformation has been constructed in Fortran II, version 9000, language for a Remington Rand Solid State 90 computer. The program converts experimental reflectivity measurements into parameters containing the optical constants. A brief presentation of the electronic quasiparticle and collective excitation modes is given in terms of the optical constants.

25,705 REFLECTION IN THE LONG-WAVELENGTH REGION OF SEMICONDUCTION FILMS OF SILICON MONOXIDE CONTAINING SILVER AND GOLD by V. Kryzhanovskii, A. Kuznetsov and L. Pafomova (Acad. Sci. USSR); Optics and Spectrosc., Vol. 15, pp. 447-448(L), Dec. 1963

The infrared reflectivity of $\text{SiO}_2\text{:Ag,Au}$ films is discussed. The films have high transmission in the visible together with a high reflection coefficient (80-95 per cent at 4-14 μ) in the infrared. The reflection coefficient increases with the increasing magnitude of the electric conductivity.

25,706 OPTICAL REFLECTION OF PbS AND PbSe SINGLE CRYSTALS IN THE 6-1.5 eV REGION by M.L. Belle (Acad. Sci. USSR); Soviet Phys.-Solid State, Vol. 5, pp. 2401-2403, May 1964

The single and double optical reflection spectra have been obtained for PbS and PbSe single crystals. Several maxima were found in the visible and ultraviolet regions due to transitions between energy bands. The splitting of the main reflection peak of PbS and PbSe observed is identified to be due to the spin-orbit splitting of the valence band.

25,707 TEMPERATURE DEPENDENCE OF THE REFLECTION SPECTRA OF ZINC SULFIDE SINGLE CRYSTALS OF VARIOUS STRUCTURAL FORMS by K.V. Shalimova and N.K. Morozova; Optics and Spectrosc., Vol. 16, pp. 261-262, Mar. 1964

The temperature dependence of the reflection and absorption spectra of zinc sulfide single crystals has been studied in the spectral region 300-370 m μ and in the temperature range from 77°K to room temperature for cubic and hexagonal forms with and without chlorine activation and also for crystals with growth defects.

25,708 FAR-INFRARED REFLECTANCE AND TRANSMITTANCE OF POTASSIUM MAGNESIUM FLUORIDE AND MAGNESIUM FLUORIDE by G.R. Hunt, C.H. Perry (MIT) and J. Ferguson (Bell Labs.); Phys. Rev., Vol. 134A, pp. A688-691, May 4, 1964

The room-temperature transmittance of KMgF_3 and MgF_2 have been measured from 800 to 70 cm^{-1} . Reflectance measurements were made over a wider range in the far infrared and the data have been analyzed using the Kramers-Kronig relationship to obtain the dielectric dispersion of these materials. Three resonances were observed for KMgF_3 and four were observed for MgF_2 as required by standard group theory and these have been related to presumed normal modes of vibration of the crystals.

Pressure Effects on Reflectivity of GaP - See 25,145

Infrared Reflectivity of:

Semiconductors - See 25,223

ZnSe - See 25,224

Mg $_2$ Sn - See 25,633

25,709 OPTICAL PROPERTIES OF Bi_2S_3 NEAR THE ABSORPTION EDGE by L.R. Loewenstern and N. Ginsburg (Carrier Corp. and Syracuse U.); Bull. Am. Phys. Soc., Vol. 9, p. 447(A), Apr. 1964

Transmission and reflection spectra were observed between 0.6 and 2.0 μ of single crystals of orthorhombic Bi_2S_3 . Measurements were made using polarized light with polarization parallel to each of the 3 crystallographic axes. Evaluation of the transmission and reflection measurements on a single crystal gives the indices of refraction and the absorption coefficients parallel to each of the 3 crystallographic axes. Determination of the orientation of the optic axes of the biaxial Bi_2S_3 are made from the values of the indices of refraction. The indices of refraction are $n_a = 5.2$, $n_b = 5.7$, and $n_c = 6.3$. Each of the optic axes makes an angle of 150° with the Z axis. The value of the energy gap parallel to each crystallographic axis and type of transition are found from the absorption coefficient. The energy gaps are $E_a = 1.22$, $E_b = 1.21$, and $E_c = 0.70$ eV and are identified as direct forbidden transitions.

25,710 REFRACTIVE PROPERTIES OF BARIUM FLUORIDE by I.H. Malitson (Nat'l. Bur. Stand.); *J. Optical Soc. Am.*, Vol. 54, pp. 628-632, May 1964

Refractive properties of barium fluoride are discussed. The refractive index, n , was determined at 25°C for 46 measured wavelengths from 0.2652 μ in the ultraviolet to 10.346 μ in the infrared. The dispersion equation

$$n^2 - 1 = \frac{0.643356\lambda^2}{\lambda^2 - (0.057789)^2} + \frac{0.506762\lambda^2}{\lambda^2 - (0.10968)^2} + \frac{3.8261\lambda^2}{\lambda^2 - (46.3864)^2},$$

where λ is expressed in microns was found to fit the measured values with an average absolute residual of 1.91×10^{-5} . A tentative average thermal coefficient of index dn/dT for the measured spectral range is $-12 \times 10^{-6}/^\circ\text{C}$. Dispersive quantities which indicate the expected relative dispersion, chromatic aberration, and the effect of index on resolution are graphically presented. A review of transmittance data from the literature is also presented.

25,711 AN INTERFEROMETRIC MEASUREMENT OF INDEX OF REFRACTION by M.S. Shumate (Calif. Inst. Tech.); *Contr. AF19 604 8052*, 77 pp., Mar. 13, 1964; U.S. Gov. Res. Rep., Vol. 39, p. 145(A), June 20, 1964 AD 437 768 OTS \$7.60

Of the several common methods for measurement of the index of refraction of solid optical materials, only one, the minimum deviation method, can conveniently be used for materials whose refractive index exceeds 1.8. The minimum deviation method requires that a large prism of the optical material be constructed; this is not always possible or feasible for some crystalline optical materials that are of current interest. A method for measurement of index of refraction is presented which requires a thin flat plate of the optical material and is unlimited in the range of refractive index it can cover. The method uses a two-beam interferometer to determine the optical path length through the flat plate by tipping away from normal incidence through a measured angle. It may be used in the visible portion of the spectrum directly, or extended to other spectral regions with the use of a suitable detector.

25,712 INDEX OF REFRACTION MEASURED BY DOUBLE-SLIT DIFFRACTION OF COHERENT LIGHT FROM A GAS LASER by R. Aagard, D. Chen, and G. Otto (Honeywell Res. Ctr.); *Appl. Optics*, Vol. 3, pp. 643-644(L), May 1964

A method for determination of the refractive index of a material using the He-Ne gas laser as a light source, particularly useful when the quantity desired is the average index of a bulk material, is described. Interference of the coherent light from two slits yields a diffraction pattern from which the index of refraction can be calculated. Accuracy of the index of refraction using this method is about $\pm .003$.

25,713 NONLINEAR OPTICAL FREQUENCY POLARIZATION IN A DIELECTRIC by E. Adler (IBM Watson Lab.); *Phys. Rev.*, Vol. 134A, pp. A728-733, May 4, 1964

A perturbation calculation of optical frequency polarization quadratic in the Maxwell field is made for a dielectric in which the electrons are localized on units of the crystal. The result is expressed in a power series in $K\langle r \rangle \sim 10^{-3}$ where $\langle r \rangle$ is the size of the unit and K is the wave number of the field. The term of zeroth order is the electric-dipole term which vanishes in a crystal with a center of symmetry. The term first order in $K\langle r \rangle$ is separated into electric-quadrupole and magnetic-dipole contributions by introducing a special gauge for the electromagnetic potentials. Higher power terms are neglected.

Faraday Rotation in ZnSe - See 25,224

25,714 FARADAY ROTATIONS OF DIVALENT RARE-EARTH IONS IN FLUORIDES. Part III by Y.R. Shen (Harvard U.); *Phys. Rev.*, Vol. 134A, pp. A661-665, May 4, 1964

A large rotatory power for Eu^{2+} in cubic fluoride lattices has been observed in the visible range. At frequencies sufficiently removed from the absorption bands, the rotation is proportional to the magnetization. This suggests that the upper levels in the allowed optical transitions are of the P_J character. Measurements on CaF_2 and SrF_2 crystals doped with very low concentrations of Eu (~ 0.005 per cent) also suggest some possible structure for the strong, sharp characteristic line of Eu^{2+} near 4000 Å. The rotatory powers of several other divalent rare-earth ions in fluorides have also been measured.

25,715 A COMPARISON OF THE OPTICAL FARADAY ROTATION AND MAGNETIC SUSCEPTIBILITY OF CERIOUS PHOSPHATE GLASS by S.B. Berger and C.B. Rubinstein (Bell Labs.); *J. Appl. Phys.*, Vol. 35, pp. 1798-1801, June 1964

The optical Faraday rotation and magnetic susceptibility of cerous phosphate glass of concentration $\text{Ce}_2\text{O}_3 \cdot 2.67 \text{ P}_2\text{O}_5$ has been studied as a function of temperature. The Verdet constant exhibits the same temperature dependence as the magnetic susceptibility, consistent with the theory formulated by Van Vleck and Hebb.

Faraday Rotation in Dy-, Eu-, Sm-, and Tb-Garnets - See 25,640

25,716 REVERSAL IN OPTICAL ROTATORY POWER - "GYROELECTRIC" CRYSTALS AND "HYPERGYROELECTRIC" CRYSTALS by K. Aizu (Hitachi Cent. Res. Lab.); *Phys. Rev.*, Vol. 133A, pp. A1584-1588, Mar. 16, 1964

A crystal is provisionally referred to as being "gyroelectric," when its optical rotatory power or gyration is nonzero at no biasing electric field and can be reversed in sign by means of a suitable biasing electric field. The gyroelectric crystals must be ferroelectric. It is found that, of the 19 kinds of regular ferroelectrics, only 9 kinds are gyroelectric. It is further shown that the other 10 kinds are divided into 5 "hypergyroelectric" and 5 optically inactive kinds. The rate of change of the gyration with the biasing electric field at zero value of the biasing electric field is provisionally referred to as the "electrogyration." The hypergyroelectric crystals are, somewhat roughly speaking, those crystals whose electrogyration is nonzero and can be reversed in sign by means of a suitable biasing electric field. Also, as a first step in the investigation of the properties of the gyroelectric and hypergyroelectric crystals, a theoretical inference is made into the change with temperature T of the gyration G_s at no biasing field and electrogyration η of the gyroelectric and hypergyroelectric crystals in the neighborhood of their Curie temperature T_0 . On some assumptions, the following are presumed. In the gyroelectrics, G_s changes like $(T_0 - T)^{1/2}$ with T below T_0 and vanishes above T_0 . In the hypergyroelectrics, G_s changes linearly with T both below and above T_0 , but breaks at T_0 . In the gyroelectrics, η changes like $(T_0 - T)^{-1}$ below T_0 and changes like $2(T - T_0)^{-1}$ above T_0 . In the hypergyroelectrics, η changes like $(T_0 - T)^{-1/2}$ below T_0 and vanishes above T_0 .

25,717 EFFECT OF PRESSURE ON THE OPTICAL ROTATORY POWER AND ROTATORY DISPERSION OF A QUARTZ by M.B. Myers and K. Vedam (Penn. State U.); *Bull. Am. Phys. Soc.*, Vol. 9, p. 447(A), Apr. 1964

The effect of pressure on the optical rotatory power and rotatory dispersion of a quartz has been studied to 10 kbar at 25°C. The measurements were made with an uniaxial pressure device employing Bridgman-type opposed anvils, formed from single-crystal sapphires, with the light-propagation direction along the optic axes of the sapphire anvils and the α -quartz sample. The variation of rotatory dispersion with pressure has been studied in the visible region of the spectrum. The uniaxial-pressure measurements are coordinated with isostatic-pressure measurements utilizing fluid-pressure media, with the results in good agreement. The optical rotatory power of a quartz decreases on the application of a uniaxial pressure of 10 kbar by an amount greater than 60 per cent of its initial value for λ -5893 Å.

THERMAL PROPERTIES

SPECIFIC HEAT

25,718 ELECTRONIC SPECIFIC HEATS OF DILUTE SOLID SOLUTIONS by H. Jones (Oklahoma State U.); *Phys. Rev.*, Vol. 134A, pp. A958-962, May 18, 1964

The partition function of an electron gas in the presence of scattering centers, such as exist in a dilute solution, is obtained by using the method first introduced by Matsubara. It is shown that the electronic specific heat at low temperatures, in such a case, contains a term arising from virtual electron scattering. If the Fermi limit in the pure metal lies just beyond a sharp peak in the density-of-states curve, this term increases the specific heat. Comparison with the observations by Rayne on the dilute solid solutions of zinc and germanium in copper indicate that the effect discussed is probably the explanation of the observed initial increase in the low-temperature specific heat at small concentrations.

Specific Heat of:

Transition Metal Superconducting Compounds - See 25,296
Superconducting Ta-V and Ta-Nb - See 25,279

25,719 SUPERCONDUCTING AND NORMAL SPECIFIC HEATS OF A SINGLE CRYSTAL OF NIOBIUM by H.A. Leupold and H.A. Boorse (Columbia U.); *Phys. Rev.*, Vol. 134A, pp. A1322-1328, June 1, 1964

The anomalous specific heat found in a polycrystalline sample of niobium and previously reported from this laboratory by Hirshfeld, Leupold, and Boorse (HLB) prompted complete remeasurements both in the normal and superconducting phases on a single crystal with lower tantalum content. The thermal constants of the single crystal show only small differences from the polycrystal in the same temperature range, the single-crystal values being $T_c = 9.20^\circ\text{K}$ and $\theta = 241^\circ\text{K}$ between about 10° and 3°K . The normal-state single-crystal measurements agree with measurements on the HLB polycrystal made both in this

laboratory and by van der Hoeven and Keesom at Purdue University. The latter measurements were carried to about 0.4°K in a field of 17 kg. As a result of their investigation, they report a Debye θ of 275°K in the region below 3°K. With this value of θ , the anomaly in the specific heat disappears. As both the single-crystal results and the van der Hoeven and Keesom values agree in the mutually measured ranges, θ is taken to be 275°K. The corresponding value of γ is found to be 7.80 mJ/mole deg². The usual exponential behavior of the electronic specific heat $C_{es}/\gamma T_C = ae^{-bT_C/T}$ with $a = 8.21$ and $b = 1.52$, is observed over a restricted temperature range. Below $t = 5$ the data exhibit larger values than predicted by the exponential in agreement with a number of other superconductors. The value of the energy gap at 0°K was found to be 3.69 kT_C. Overall comparisons are made with the BCS theory and a modification due to Swihart.

25,720 SPECIFIC HEAT OF NIOBIUM BETWEEN 0.4 AND 4.2°K by B.J.C. van der Hoeven, Jr. and P.H. Keesom (Purdue U.); Phys. Rev., Vol. 134A, pp. A1320-1321, June 1, 1964

Below 3.3°K, the normal-state specific heat of niobium, measured in a magnetic field at 17 kg, can be represented by $C_N = 7.79T + 0.094T^3$ mJ/mole deg. This corresponds to a value of the Debye parameter at 0°K, $\theta(0)$, of 275°K. The specific heat in the superconducting state does not appear to be anomalous, as has been reported.

25,721 SPECIFIC HEAT OF THULIUM METAL BETWEEN 0.38 AND 3.9°K by O.V. Lounasmaa (Argonne Lab.); Phys. Rev., Vol. 134A, pp. A1620-1624, June 15, 1964

The specific heat C_p of thulium metal has been measured. Between 0.38 and 3.9°K $C_p = 2.839T^3 + 17.94T + 23.43T^{-2} - 1.79T^{-3} - 0.066T^{-4}$ (in mJ/mole °K). The last three terms represent the nuclear specific heat C_N . On the basis of earlier estimates, $C_L = 0.243T^3$ and $C_E = 10.5T$ for the lattice and electronic specific heats, respectively. According to the simple spin-wave theory, the magnetic specific heat C_M is proportional to T^3 for a ferrimagnetic metal; experimentally $C_M = 6.2T^{3/2}$ for thulium, which has a rather complicated ferrimagnetic structure. Further, there seems to be no evidence in C_M for an exponential factor, to be expected because of magnetic anisotropy. All conclusions on C_M are tentative, however, until data at temperatures between 4 and 20°K become available. C_N does not fit to the simple picture as given by Bleaney. Since $I = \frac{1}{2}$ for the only stable thulium isotope Tm^{169} , quadrupole interactions are zero and there are only two nuclear energy levels, their separation being determined by the magnetic hyperfine constant a' . This would give a nuclear specific heat with even powers of T only, with a' determining the values of the coefficients. The observed C_N cannot be fitted into an equation of this type which indicates that other interactions, probably nuclear exchange interactions, are present. Formally, the experimental situation may be expressed by writing $a' = a_0 - b/T$, instead of treating a' as a constant. Our results are in good agreement with recent Mössbauer data by Kalvius et al. who found 22.9 for the coefficient of the T^{-2} term.

Grüneisen Constant of Ge - See 25,739

25,722 A CALCULATION OF THE GRÜNEISEN PARAMETERS, $\gamma(n)$, FOR INERT GAS SOLIDS by G.M. Graham (U. Toronto); Can. J. Phys., Vol. 42, pp. 563-568(L), Mar. 1964

An algebraic derivation of the moments of the frequency distribution for a cubic lattice and numerical calculations of $\gamma(n)$ for a fcc lattice with $n = -3, 0, 1, 2, 4, 6, 8$ are presented. The method makes use of the fact that sums over the Brillouin zone obey the relation:

$$\sum_q \sum_L e^{iq \cdot L} f(L) = N f(0) \delta_{L0}$$

where L is a lattice vector, N is the total number of atoms, and δ_{L0} is the Kronecker delta. Functional dependence of Γ_0 , the mean square frequency in the lattice and Q_i , the i^{th} moment about the mean of the square frequency distribution, is obtained for the fcc lattice. Results of calculations are tabulated and it is noted that values of $\gamma(n)$ rise monotonically with n .

25,723 SPECIFIC HEAT OF SOLID NEON by H. Fenichel and B. Serin (Rutgers U.); Bull. Am. Phys. Soc., Vol. 9, p. 455(A), Apr. 1964

The specific heat has been measured in the temperature range 1.7° to 12°K. For a Debye temperature at 0°K, $\theta_0 = 74.4 \pm 0.5^\circ\text{K}$. This value, and the values of θ_0 for argon and krypton, when considered as a function of the de Boer parameter, are in good agreement with the theoretical treatment of Bernardes. For neon, the Debye temperature $\theta(T)$ decreases parabolically in the temperature range $0 < T/\theta_0 < 0.06$ and then more slowly as the temperature is increased. $\theta(T)/\theta_0$ is, within experimental error, the same function of T/θ_0 for neon, argon, and krypton in the temperature range $0 < T/\theta_0 < 0.1$.

25,724 HEAT CAPACITIES OF SOLID DEUTERIUM (33.1% - 87.2% PARA) FROM 1.5°K TO THE TRIPLE POINTS. HEATS OF FUSION AND HEAT CAPACITY OF LIQUID by G. Grenier and D. White (Ohio State U.); J. Chem.

Phys., Vol. 40, pp. 3015-3030, May 15, 1964

The heat capacities of a number of deuterium samples enriched in para content have been measured in the temperature range 1.5° to 22°K. The variation of the triple points and heats of fusion as a function of ortho-para composition have also been measured. All the heat capacities of the solid show anomalies due to the quenching of the molecular rotation of the $J = 1$ species present in the mixtures. For para compositions above 60 per cent para-D₂ a sharp λ transition is observed. A linear dependence of the transition temperature with para content is observed. The high-temperature heat capacities of the solid show a dependence on ortho-para composition, suggesting a structural dependence on composition. A calculation of the entropy from the data shows that the three-fold degeneracy of the $J = 1$ species is completely removed at the absolute zero. An analysis of the anomalies resulting from the removal of the degeneracy confirm Nakamura's conclusions that the quenching of the molecular rotations is principally a result of quadrupolar interactions. The anomalous heat capacities of the solid, at sufficiently high temperatures, are expressed by the relation $CT^2/R = \alpha x + \beta x^2$ just as in the case of hydrogen. The ratio of the experimental β 's for the two isotopes is in excellent agreement with the theoretical ratio. This ratio is a measure of quadrupolar interactions in the two isotopic solids.

Debye Temperature of Al - See 25,757

25,725 HEAT CAPACITY OF SOLID HD by G. Grenier and D. White (Cryogenic Lab., Ohio State U.); J. Chem. Phys., Vol. 40, pp. 3451-3452, June 1, 1964

The heat capacity, C_s , of solid HD along the saturation curve was measured from 2.5° to 15°K by calorimetry. The results obtained do not agree with others covering a narrower temperature range. The Debye temperature and constants in the expression for the temperature dependence of C_s are given. The Debye temperatures of H₂ and D₂ are listed for comparison and the differences evaluated. An experimentally observed rapid rise of C_s/T^3 with decreasing temperature is discussed. It is believed due to a rotational anomaly due to quenching of rotations of $J = 1$ species by $J = 1 - J = 0$ interactions.

25,726 HIGH-TEMPERATURE HEAT CAPACITY OF FERROMAGNETS HAVING 1st- AND 2nd-NEIGHBOR EXCHANGE: APPLICATION TO EuS by P.J. Wojtowicz (RCA Labs.); J. Appl. Phys., Vol. 35, pp. 991-993, Mar. 1964

The derivation of exact power series expansions of the high-temperature magnetic-heat capacity of Heisenberg ferromagnets having both first- and second-neighbor exchange interactions is described. The calculations employ the general diagrammatic techniques developed by Rushbrooke and Wood as extended by Wojtowicz and Joseph to include the second-neighbor interaction. All mixed coefficients for terms through the fifth power of the inverse temperature have been computed for arbitrary spin and general lattice structure. The series expansions have been used to obtain certain information on the nature of the exchange interactions in ferromagnetic EuS. By the use of a spin-wave analysis Charap has been able to deduce a set of values for the exchange interactions which simultaneously fit the low-temperature magnetization and heat capacity data. It has been found that these same values substituted into the present theory are capable of reproducing the high-temperature heat capacity data of Moruzzi and Teaney. This result lends considerable support to the hypothesis that EuS is very nearly an ideal Heisenberg ferromagnet.

25,727 THERMODYNAMIC PROPERTIES OF SODIUM BROMIDE AND SODIUM IODIDE AT LOW TEMPERATURES by T.E. Gardner and A.R. Taylor, Jr. (Bureau of Mines); BMRI-6435, 12 pp., 1964; STAR, Vol. 2, p. 1384(A), June 8, 1964

Heat capacity measurements were made on sodium bromide and sodium iodide in the temperature ranges of 7° to 300°K, and 56° to 300°K, using an adiabatic calorimeter. Smooth values of heat capacity, entropy, enthalpy function, and free-energy function were calculated from the heat capacity data at 10°K intervals and at 273.15° and 298.15°K. Entropy and free energy of formation values at 298.15°K also were calculated for the two compounds using entropy values determined in this study and other data reported in the literature. The entropy values calculated at 298.15°K were 20.75 ± 0.06 entropy units (eu) for sodium bromide and 23.55 ± 0.07 eu for sodium iodide.

25,728 AN X-RAY DETERMINATION OF THE DEBYE TEMPERATURE OF SILVER IODIDE by G. Burley (Nat'l. Bur. Stand.); J. Phys. Chem. Solids, Vol. 25, pp. 629-634, June 1964

The characteristic temperature of silver iodide has been calculated both from the Debye-Waller temperature exponent derived from the variation of single crystal intensities of the hexagonal phase with Bragg angle at constant temperature and also from the ratio of the intensities of a powder reflection of the cubic phase in the range from 20° to 120°K. The θ_D values calculated by these two methods are 119° and 116°K, respectively. This compares to $\theta_D = 116^\circ\text{K}$ calculated from published specific heat data and $\theta_D = 107^\circ\text{K}$ calculated from elastic moduli determined at 25°C.

25,729 HEAT CAPACITY OF MnCl_2 FROM 1.3° TO 4.2°K WITH MAGNETIC FIELDS TO 50 KILOGAUSS PARALLEL TO THE b MAGNETIC AXIS by R.A. Butera and W.F. Glaue (U. Calif., Berkeley); *J. Chem. Phys.*, Vol. 40, pp. 2379-2389, Apr. 15, 1964

The heat capacity of single-crystal manganous chloride has been measured in constant magnetic fields stabilized at exactly 0, 5000, 7500, 10,000, 18,000, 25,000, and 50,000 G. The measurements which cover the range from 1.3° to 4.2°K, extend the results of Murray who made measurements to 7.25 kilogauss. All of the measurements have been made with the field parallel to the a crystallographic axis (b magnetic axis) as were those of Murray. Except at fields high enough to approach paramagnetic saturation the heat-capacity curves have double maxima, but at about 8000 G the maxima at the lower temperatures are below 1.3°K, the lowest temperature of observation. The heat capacity maxima in zero field were found to be at 1.815° and 1.945°K. The loci of the maxima curve at the higher temperature has temperature increasing with field as found by Murray; however, near 12 kilogauss and 2.03°K, it has been found that a reversal takes place and the field increases as the temperature decreases. The curves for the loci of both sets of maxima evidently approach zero values of dH/dT at 0°K. The heat capacity maxima are not high compared to those of adjacent temperature regions and we do not believe they can be identified as "transition points" but rather are merely regions of somewhat accelerated ordering to some ultimate arrangement of magnetic moments, such as the general type suggested by Wilkinson et al. on the basis of neutron diffraction.

25,730 RECENT STUDIES OF THERMODYNAMIC PROPERTIES OF BERYLLIUM SPECIES by T.B. Douglas (Nat'l. Bur. Stand.); in JPL Proc. 1st Meeting ICRPG Working Group on Thermochem., New York, Nov. 1963, Vol. 1, Feb. 1964, pp. 87-99; Cont. N0W-62-0604-C; *STAR*, Vol. 2, p. 1348(A), June 8, 1964 CPlA-44, Vol. 1 AD 435 000

The heat capacity of a crystalline sample of BeF_2 from 7° to 300°K was measured by adiabatic calorimetry, and the relative enthalpy from 273° to approximately 1200°K was measured by drop calorimetry. A number of qualitative and quantitative mass-spectrometric studies were carried out on the BeF_2 , the BeO-BeF_2 , BeOAl_2O_3 , and $\text{BeO-Al}_2\text{O}_3$ systems. Methods for determining the physical properties of the various polymorphic forms of BeF_2 are discussed.

25,731 HEAT CAPACITY OF PLUTONIUM MONOCARBIDE FROM 400° TO 1300°K by O.L. Kruger and H. Savage (Argonne Lab.); *J. Chem. Phys.*, Vol. 40, pp. 3324-3328, June 1, 1964

The heat content of PuC above 298°K was measured with an isothermal drop calorimeter. No discontinuities were observed in the heat-content-vs-temperature curve, which is described by the equation

$$H_T - H_{298} = -5035 + 13.08T + 5.718 \times 10^{-4}T^2 + 3.232 \times 10^{-5}T^3$$

The equation for the heat capacity

$$C_p = 13.08 + 11.44 \times 10^{-4}T - 3.232 \times 10^{-5}T^2$$

was derived from the calculated enthalpy equation. Values of the change in enthalpy, heat capacity, and entropy increments are given up to the melting point of PuC. Corrections of the enthalpy data for the self-heating of plutonium and the defect structure of PuC are described.

25,732 THERMODYNAMIC STUDIES AT LOW AND HIGH TEMPERATURES by R.A. McDonald, F.L. Oetting, and H. Prophet (Dow Chemical); in JPL Proc. 1st Meeting ICRPG Working Group on Thermochem., New York, Nov. 5-7, 1963, Vol. 1, Feb. 1964, pp. 213-245; *STAR*, Vol. 2, p. 1350(A), June 8, 1964 AD 435 000

Heat capacity curves for the following materials are presented along with a discussion of methods used in obtaining the data: lithium chloride and phosphorus pentoxide (both up to 320°K); boron and boron nitride (both up to 1700°K); ZrF_4 (between 300 and 1200°K); aluminum chloride (up to 500°K); boron phosphate and lithium metaborate (both up to 1200°K); beta beryllium chloride (up to 700°K); aluminum oxide (between 500 and 2000°K); beryllium oxide, titanium nitride, titanium diboride, zirconium diboride, and zirconium carbide (all up to 2200°K); boron nitride (between 500 and 2300°K); titanium diboride, tungsten monoboride, and tungsten pentaboride (all between 300 and 2200°K); and tantalum carbide, niobium carbide, hafnium carbide, and tungsten carbide (all between 1000 and 2200°K).

THERMAL CONDUCTIVITY

25,733 THEORY OF THE ELECTRONIC THERMAL CONDUCTIVITY OF SUPERCONDUCTORS WITH STRONG ELECTRON-PHONON COUPLING by V. Ambegaokar (Cornell U.) and L. Tewordt (Bell Labs.); *Phys. Rev.*, Vol. 134A, pp. A805-815, May 18, 1964

The electronic thermal conductivity of superconductors is discussed without recourse to the quasiparticle approximation. The Kubo formula for the thermal conductivity is used as the starting point. This is first examined in the Hartree-

Fock approximation in the Nambu space. It is shown that in the Eliashberg approximation of neglecting the momentum dependence of the electronic self-energy, the calculation of the thermal conductivity is reduced to a quadrature, involving however the complex energy gap and renormalization functions which are solutions of the Eliashberg gap equations at finite temperatures. These equations are given in an Appendix. The problem is also considered in the ladder approximation in the Nambu space, and a generalized Boltzmann equation is derived which includes corrections to the Hartree-Fock approximation corresponding to the replacement of the scattering by the transport cross section. It is shown that the standard Boltzmann equation for superconducting quasiparticles is obtained in the weak-coupling limit. No numerical calculations are performed in this paper, but a clear scheme for such calculations is outlined. Reasons for believing that such calculations will explain the anomalous drop in the electronic thermal conductivity of superconducting lead are given.

25,734 EFFECT OF MAGNETIC FIELD ON THERMAL CONDUCTIVITY AND ENERGY GAP OF SUPERCONDUCTING FILMS by D.E. Morris and M. Tinkham (U. Calif., Berkeley); *Phys. Rev.*, Vol. 134A, pp. A1154-1166, June 1, 1964

The change in the thermal conductivity of superconducting tin, indium, and lead films upon application of a magnetic field in the plane of the film has been measured. Within the range of temperatures available (0.35 T_c to 0.65 T_c) the thermal conductivity of indium and tin films increases nearly as H^2 . In films of thickness $d \geq 2800 \text{ \AA}$ the thermal conductivity jumps at H_c to the normal state value, indicating a first-order phase transition in thin films, consistent with the Ginzburg-Landau (GL) theory. If the effect of a field upon the superconducting state can be adequately represented as a change of the ϵ_0 of BCS, the theory of Bardeen, Rickayzen, and Tewordt may be used to compute $\epsilon_0(H)$ from the data. At $T = 0.65 T_c$, $\epsilon_0(H)/\epsilon_0(H=0) = [1 - (H/H_c)^2]^{1/2}$ in agreement with the GL prediction. At $T = 0.35 T_c$ however, $\epsilon_0(H)/\epsilon_0(0) = 1 - (H/H_c)^2$ provides a more satisfactory fit to the data. Orientation of the field \perp and \parallel to the direction of heat flow produces the same effect on the thermal conductivity to ± 1 per cent. This is interesting in view of Bogoliubov's prediction of a $\text{PF} \cdot V_{\text{drift}}$ term in the excitation spectrum of a current-carrying superconductor. When the field is not parallel to the surface of the film the thermodynamic transition is still sharply defined, but H_c is reduced. Thin lead films gave results similar to those of indium and tin films except that at low fields the field-dependent conductivity increased more slowly than H^2 at low temperatures.

Spin Wave Calculations on Thermal Resistivity - See 25,425

25,735 THERMAL CONDUCTIVITY AND LORENTZ FUNCTION OF GADOLINIUM BETWEEN 5° AND 310°K by S. Araj and R.V. Colvin (U.S. Steel); *J. Appl. Phys.*, Vol. 35, pp. 1043-1044, Mar. 1964

The thermal conductivity (λ) of a polycrystalline gadolinium sample, having an electrical resistivity of 2.41 $\mu\Omega \text{ cm}$ at 4.18°K, has been studied as a function of temperature (T) between 5° and 310°K. The thermal conductivity has a maximum value of 0.333 $\text{W cm}^{-1} \text{ }^\circ\text{K}^{-1}$ at 16.5°K. Changes in the slope of the λ vs T curve occur at 230° and 270°K. The former is believed due to the rapidly varying easy cone of magnetization. The second anomaly is associated with the ferromagnetic-paramagnetic transformation. The Lorenz function, from measured thermal conductivity and electrical resistivity data on the same sample, has been calculated as a function of temperature. This function clearly indicates that in addition to the electronic thermal conductivity there is considerable phonon and possibly some magnon heat transport.

25,736 DEPENDENCE OF THE THERMAL CONDUCTIVITY OF THE CRYSTAL LATTICE ON THE DEGREE OF IONICITY OF COMPOUNDS by A.V. Ioffe (Acad. Sci. USSR); *Soviet Phys.-Solid State*, Vol. 5, pp. 2446-2447(L), May 1964

Measurements of the lattice thermal conductivity of an isoelectronic series of compounds, crystallizing in the zincblende structure and exhibiting covalent bonding with different degrees of ionicity are reported. It is found that the lattice thermal conductivity of compounds decreases with increasing degree of ionicity of bonding and as going from light compounds to heavier compounds. The nature of the thermal conductivity observed by Eucken for alkali halide crystals does not exist in the case of crystals having covalent bonding.

25,737 THERMAL CONDUCTIVITY OF SILICON AND GERMANIUM FROM 3°K TO THE MELTING POINT by C.J. Glassbrenner and G.A. Slack (GE Res. Lab.); *Phys. Rev.*, Vol. 134A, pp. A1058-1069, May 18, 1964

The thermal conductivity K of single crystals of silicon has been measured from 3 to 1580°K and of single crystals of germanium from 3 to 1190°K. At all temperatures the major contribution to K in Si and Ge is produced by phonons. The phonon thermal conductivity has been calculated from a combination of the relaxation times for boundary, isotope, three-phonon, and four-phonon scattering, and was found to agree with the experimental measurements. Above 700°K for Ge and 1000°K for Si an electronic contribution to K occurs, which agrees quite well with the theoretical estimates. At the respective melting points of Si and Ge, electrons and holes are responsible for 40 per cent of the total K

and phonons are responsible for 60 per cent. The measured electronic K yields values for the thermal band gap at the melting point of 0.6 ± 0.1 eV for Si and 0.26 ± 0.08 eV for Ge.

25,738 THERMAL CONDUCTIVITY OF SELENIUM by G.B. Abdullaev, G. M. Aliev and K.G. Borkinkhoev (Acad. Sci. AzSSR); *Soviet Phys.-Solid State*, Vol. 5, pp. 2651-2652(L), June 1964

Measurements of the thermal conductivity, λ , of amorphous selenium in the temperature range 85-300°K and of crystalline selenium in the range 85-450°K are reported. The thermal conductivity of amorphous selenium increases with the increase of temperature and can be described by the empirical formula $\lambda = 0.37 \times 10^{-5} T$ in the range of temperature investigated. The data obtained for crystalline selenium samples in the temperature range from liquid-nitrogen to room temperature can be described by $\lambda = a/T$, but beyond 350°K, λ deviates from this dependence. It is shown that this deviation is due to the transport of heat by electromagnetic radiation.

Thermal Conductivity of:

InSb-CdTe - See 25,169

CdTe-CdSe - See 25,168

THERMAL EXPANSION

25,739 A CALCULATION OF THE THERMAL EXPANSION OF GERMANIUM by A. Bienenstock (AERE, Harwell); *Philosophical Mag.*, Vol. 9, pp. 755-766, May 1964

The Grüneisen parameters, γ_i , for a number of the acoustic modes of vibration of Ge have been calculated. The method of calculation is an approximate one which uses the volume dependence of the elastic constants, plus an adjustable parameter which tends to simulate the results of a shell model calculation. The resulting γ_i for the transverse modes are rapidly varying functions of the wave vector, q . They are positive for small q and negative near the Brillouin zone surface. Optical modes are treated in the Einstein approximation. The calculated γ is in good agreement with experiment at all temperatures when optical modes are included. The optical modes contribute appreciably to γ at temperatures where their contribution to C_V is negligible.

25,740 EFFECT OF IMPURITIES ON THE COEFFICIENT OF THERMAL EXPANSION OF p-Ge by V.V. Zhdanova (Acad. Sci. USSR); *Soviet Phys.-Solid State*, Vol. 5, pp. 2450-2451(L), May 1964

Measurement of the thermal expansion coefficient α of germanium crystals doped with gallium is reported. The results show that above 400°K the coefficients of thermal expansion are the same for all samples regardless of the concentration of impurities. Below 400°K, the thermal expansion coefficient of p-Ge is greater with higher impurity concentrations. The maximum difference in α between pure and "dirty" samples occurs in temperatures between 125 and 200°K. The results of the measurement confirm the assumption that the addition of impurities leads to a weakening of the covalent bonds and thus increasing of α .

Thermal Expansion of:

C and Graphite - See 24,949

Anthracene - See 24,955

25,741 THERMAL EXPANSION OF ANISOTROPIC METALS AT LOW TEMPERATURES by G.K. White (CSIRO); *Phys. Lett., Neth.*, Vol. 8, pp. 294-295(L), Mar. 1, 1964

Measurements of the thermal expansion (α) at temperatures down to 1.5°K both parallel and perpendicular to the major symmetry axes of magnesium, zinc, bismuth, and tin are discussed. In magnesium above 50°K, values of $\alpha_{||}$ are slightly larger than those for α_{\perp} , and agree with earlier measurements. Below 30°K, $\alpha_{||}$ is smaller than α_{\perp} . Below 10°K $\alpha_{||} = (1.0 \pm 0.2) \times 10^{-9} T + (2.1 \pm 0.2) \times 10^{-11} T^3 \text{ deg K}^{-1}$ and $\alpha_{\perp} = (1.3 \pm 0.2) \times 10^{-9} T + (3.3 \pm 0.2) \times 10^{-11} T^3 \text{ deg K}^{-1}$. Below 60°K, α_{\perp} of zinc is more negative than the values reported by Meyerhoff and Smith, and $\alpha_{||}$ is smaller. The present results for bismuth disagree with earlier work, particularly in the observation that α_{\perp} is greater than $\alpha_{||}$. In tin α_{\perp} is negative between 2° and 20°K, but the volume coefficient and $\alpha_{||}$ are positive at all temperatures, except in superconducting (S) state. Below 2°K, α_{\perp} for tin in the normal state is very small but appears to be positive. In the s-state, both linear expansion coefficients are negative. The pressure dependence of the critical field $(dH_c/dp)_T$ was determined to be $-5.7 \times 10^{-3} \text{ oe bar}^{-1}$ at 2°K and $-7.2 \times 10^{-3} \text{ oe bar}^{-1}$ at 3°K.

Thermal Expansion of RbNO₃ - See 25,191

THERMOELECTRIC AND THERMOMAGNETIC PROPERTIES

25,743 THERMOELECTRIC POWER IN METALS AT NORMAL TEMPERATURES - REPLY TO A QUERY by F.J. Blatt (Tech. Hoch., Zurich); *Proc. Phys. Soc.*, Vol. 83, pp. 1065-1068, June 1964

Two questions relating to this subject were raised by MacDonald and Pearson in 1961. The first concerns the need to take specific account of normal and Umklapp processes even at high temperatures in calculating the phonon drag thermoelectric power S_g . The other discusses why the phonon drag contribution to the thermopower is always negligible compared with the diffusion contribution at ordinary temperatures. The first question is considered by both Bailyn and Ziman. The answer to the second is that theoretical estimates based on an assumed Debye spectrum very grossly overestimate both normal S_g^N and Umklapp S_g^U contributions to S_g at ordinary temperatures although at low temperatures such estimates are probably reasonably good. It is concluded that the unexpectedly small values of S_g at room temperature are, therefore, not the result of some curiously general and nearly precise cancellation between S_g^N and S_g^U .

25,744 PHONON-DRAG SEEBECK EFFECT IN A TRANSVERSE MAGNETIC FIELD by T. Ohta (Defense Acad.); *J. Phys. Soc. Japan*, Vol. 19, pp. 769-770, May 1964

A theoretical expression for the ratio of the phonon-drag thermoelectric power at magnetic field B to that at magnetic field zero is derived in the lower range of the transverse magnetic field where $\hbar\omega_c \leq kT$ (ω_c = cyclotron frequency). An experimental curve for Ge in the temperature range 15°K to 70°K is presented and the theoretically derived expression fitted to that region where $\hbar\omega_c < kT$, the higher region being fitted to the rule found by Gurevich et al.

25,745 TRANSMITTED PHONON DRAG EFFECT IN GERMANIUM AT VERY LOW TEMPERATURES by E.J. Walker and R.W. Keyes (IBM); *Phys. Rev. Lett.*, Vol. 12, pp. 217-219(L), Mar. 2, 1964

Measurements of the phonon drag contribution to the thermoelectric power in degenerate germanium at very low temperatures are discussed. The transmitted phonon drag effect of Hubner and Shockley, which permits measurement of the phonon contribution to the Peltier coefficient independently of the electronic contribution, was used. The magnitude of the transmitted phonon drag effect is a measure of the momentum carried by phonons in the degenerate n-type germanium of the n-p-n structures used. Analysis of phonon momentum flow in these structures yields the phonon Peltier coefficient $\Pi_0 = (6vt/\mu)(E_0/E_i)$, where t is the thickness of the n-layer, v is the phonon velocity, and E_0/E_i is the ratio of output to input voltages.

25,746 CONTRIBUTION OF MAGNON DRAG TO THE THERMOELECTRIC POWER OF ANTIFERROMAGNETIC MnTe by J.D. Wasscher and C. Haas (NV Philips); *Phys. Lett., Neth.*, Vol. 8, pp. 302-304(L), Mar. 1, 1964

The anomalous temperature dependence of the thermoelectric power (α) of p-type MnTe near its Néel temperature (310°K) is discussed. This temperature dependence is shown to result from the magnon drag contribution to the thermoelectric power which arises primarily from the strong temperature dependence of τ_{em} (the relaxation time for scattering of the charge carriers at the ion-spins) just below T_N . The relaxation time τ_m (the relaxation time for the processes in which the magnon system loses its surplus crystal momentum) near T_N (4×10^{-12} sec) corresponds to a mean free path of the magnons of 120 Å, about twice their wavelength.

25,747 THERMOELECTRIC POWER OF LATTICE VACANCIES IN GOLD by R.P. Huebener (Argonne Lab.); *Bull. Am. Phys. Soc.*, Vol. 9, p. 397(A), Apr. 1964

The change ΔS in the thermoelectric power of high-purity gold wires due to quenched-in lattice vacancies was measured between 4.2° and 220°K. The vacancy concentration c was determined from the quenched-in electrical resistance at 4.2°K. From the value of ΔS at 200°K, where phonon-drag effects are negligible, the electronic part ΔS_e of ΔS was calculated as a function of the temperature, using the Friedel theory. The phonon-drag part ΔS_g was obtained from the equation $\Delta S_g = \Delta S - \Delta S_e$. Vacancies were found to cause a reduction of the electronic part and of the phonon-drag part of the thermoelectric power. $|\Delta S_e|$ and $|\Delta S_g|$ reach a maximum at low temperatures. At 40°K, the relations $\Delta S_e/c = 3.6 \mu\text{V}/^\circ\text{K}$ and $\Delta S_g/c = -7.9 \mu\text{V}/^\circ\text{K}$ at.% were obtained. The phonon-scattering cross section of vacancies, as estimated from ΔS_g assuming a pure Rayleigh-type scattering mechanism, is in qualitative agreement with the value calculated from the theory of Klemens.

25,748 SEMICONDUCTING ORGANIC POLYMERS DERIVED FROM NITRILES. THERMOELECTRIC POWER AND THERMAL CONDUCTIVITY MEASUREMENTS by J.E. Katon and B.S. Wild (Monsanto Chem.); *J. Chem. Phys.*, Vol. 40, pp. 2977-2982, May 15, 1964

The thermal conductivities and thermoelectric powers of two previously re-

ported polymeric organic semiconductive materials are reported. One system, thought to be a form of oxidized polyphthalocyanine, shows very complex behavior on heating in the presence of oxygen. The thermoelectric power is very sensitive to this treatment but the electrical resistivity, although changing slightly, is relatively insensitive. Two different oxygen-polymer effects, one reversible and one irreversible, appear to be superimposed in this system.

25,749 MAXIMUM THERMOMAGNETIC FIGURE OF MERIT OF TWO-BAND, MULTIVALENCE SEMICONDUCTORS by R. Simon (Battelle Inst.); *Solid-State Electronics*, Vol. 7, pp. 397-412, June 1964

The general equations are derived for the transport of electrical charge and energy in an anisotropic multiband, multi-energy-extremum semiconductor or semimetal. These are applied to compute the transverse thermomagnetic figure of merit for two-band (one conduction plus one valence band) material. The dimensionless adiabatic thermomagnetic figure of merit, Z_{ad}^T , approaches a maximum value of about $10-20\beta_y$ for an intrinsic semimetal with about a 0-5 kT overlap of the conduction and valence band as the magnetic-field strength increases indefinitely. The quantity β_y is a generalized Chasmar and Stratton type of dimensionless material parameter that is a function of the density-of-states masses of electrons and holes, the lattice thermal conductivity, the partial mobilities associated with transport in the principal directions of the constant-energy ellipsoids in the neighborhoods of the various band extrema in wave-number vector space, and the orientations of the principal axes of the various ellipsoids with respect to the rectangular coordinate system corresponding to the case of mutually orthogonal magnetic field, electric current and temperature-gradient directions. Criteria for improved thermomagnetic materials are discussed.

Seebeck Coefficient of PbTe - See 25,252

Thermal EMF of PbS Layers - See 25,253

Thermoelectric Power of:

SnTe - See 25,139

CdTe-CdSe - See 25,168

Thermoelectric Properties of Ag Solid Solutions - See 25,245

25,750 MAGNETOCALORIC EFFECT IN SUPERCONDUCTING Nb-Zr ALLOY by N.H. Zebouni, A. Vankataram, G.N. Rao and J.M. Reynolds (Louisiana State U.); *Bull. Am. Phys. Soc.*, Vol. 9, p. 453(A), Apr. 1964

In the course of study of the thermal properties in a rod of Nb-31.2% Zr, large magnetocaloric oscillations were observed at 1.5°K. Below 1000 G, the temperature of the sample was independent of field. In the range 1000 to 2500 G, the temperature underwent 4 successive sawtooth oscillations. Above 2500 G, the temperature again became independent of field. The amplitude of the oscillation was 38 mdeg. The effect was reproducible, provided the sample was heated to the normal resistive state between each field sweep.

Composition Dependence of Thermal EMF of FeO - See 25,264

Thermoelectric Power of $\text{Co}_{1-x}\text{Fe}_x\text{Si}$ - See 25,166

Thermal-Induced Currents in Anthracene - See 25,221

Hall Effect-Seebeck Anomaly in Glasses - See 25,351

Thermoelectric Coefficient of BaTiO_3 and Ba-SrTiO_3 - See 25,250

MECHANICAL PROPERTIES

GENERAL

25,751 HIGH-PRECISION DENSITY DETERMINATION OF NATURAL DIAMONDS by R. Mykolejwicz, J. Kalnajs and A. Smakula (MIT); *J. Appl. Phys.*, Vol. 35, pp. 1773-1778, June 1964

Densities of 35 diamonds have been determined by an improved high-precision flotation method. The density varies from $\rho_{25} = 3.51477-3.51554 \text{ g/cm}^3$. The average density of 35 samples is $\rho_{25} = 3.51532 \text{ g/cm}^3$. The type I diamonds have higher density and narrower range than type II. Comparison with density computed from the lattice constant shows that type II diamonds contain either vacancies (voids) or impurities of lower atomic weight than carbon, or both, and that type I are contaminated by impurities of higher atomic weight than carbon. Computed nitrogen impurity concentration is in excellent agreement with that found by Kaiser and Bond.

25,752 LOW-TEMPERATURE ANNEALING OF THE X-RAY-INDUCED VOLUME EXPANSION AND COLORATION OF LiF by S. Mascarenhas (U. Sao Paulo, Brazil), D.A. Wiegand (Carnegie Inst. Tech.) and R. Smoluchowski

(Princeton U.); *Phys. Rev.*, Vol. 134A, pp. A485-491, Apr. 20, 1964

It has been shown previously that both $\Delta V/V$ and the density of F centers produced by x irradiation of LiF at 80°K anneal out partially near 130°K. Upon reirradiation at 80°K the F band quickly recovers while $\Delta V/V$ does not recover. In the present study, an additional annealing stage of $\Delta V/V$ and the F band was found near 270°K. Upon reirradiation at 80°K after annealing at 270°K, neither $\Delta V/V$ or the F band recover in contrast to the recovery after annealing at 130°K. The irreversibility of the 270°K annealing of the F band indicates vacancy annihilation which apparently does not occur at 130°K. The formation of M centers at the higher temperature suggests vacancy motion. The fractional annealing at 130°K was found to be smaller than in previous work, presumably because of different sample perfection before irradiation.

25,753 VOLUME EXPANSION AND COLOR CENTER BEHAVIOR OF NaCl X-RAY IRRADIATED AT LOW TEMPERATURE by S. Mascarenhas (U. Sao Paulo, Brazil), D.A. Wiegand (Carnegie Inst. Tech.) and R. Smoluchowski (Princeton U.); *Phys. Rev.*, Vol. 134A, pp. A481-485, Apr. 20, 1964

Volume expansion of X-ray irradiated NaCl was measured in the range 15-90°K and its optical behavior was analyzed from 15 to 300°K. An improved photoelastic method showed that strain profiles agree with the shape predicted by the linear theory and that slow cooling (10°C per h) is essential to minimize background strain. Twenty-four hours of irradiation by 45 kv, 30 ma X-rays at 15°K produces $\Delta V/V$ of the order of 10^{-5} which does not anneal below 80°K while, in contrast, the F band shows in this range one-stage annealing. Growth curves of the F band and of the 343-m μ band were made at 15°K. Annealing at 80°K followed by reirradiation at 15°K indicates that these bands recover quickly and a comparison with results on KCl and KBr suggests that the F centers are annihilated by hole capture. It follows also that in the range 15 to 80°K electronic changes in these centers do not lead to volume changes greater than the experimental error, $\Delta V/V \approx 10^{-6}$. Heat-treated crystals presented a different behavior of thermal annealing of the F band with several annealing stages between 15 and 80°K.

25,754 VOLUME EXPANSION AND COLORATION IN X-IRRADIATED SODIUM CHLORIDE by M.F. Merriam (U. Calif., San Diego), D.A. Wiegand (Carnegie Inst. Tech.) and R. Smoluchowski (Princeton U.); *J. Phys. Chem. Solids*, Vol. 25, pp. 273-292, Mar. 1964

The growth and thermal annealing of the volume expansion produced in NaCl by prolonged exposure to penetrating X-rays at room temperature has been studied by a photoelastic technique. Growth and annealing of the visible optical absorption bands were also measured. The growth curves for volume expansion and coloration are mutually consistent, within experimental error and theoretical uncertainties. The latter are, however, too large to permit unambiguous determination of the types of defects generated by irradiation. The F-center growth curve is of the type reported for KCl, that is, it contains an inflection point. The M- and F-band absorption constants are quadratically related in a manner consistent with previous evidence for the double F-model of the M-center. Annealing of the volume expansion and the optical absorption is in general agreement with the earlier results of Kobayashi on NaCl bombarded with high energy protons but in our case better resolution is obtained. The annealing is highly structure sensitive and details of the annealing curves were not completely reproducible. Kinetic analyses indicate that the annealing of volume expansion is limited initially (200-250°C) by diffusion of negative ion vacancies or by close pair vacancy-interstitial recombination. An interesting after effect in the annealing of the volume expansion may be connected with radiation enhanced impurity precipitation. Profiles of the photoelastically measured strain as a function of distance from the crystal midplane were obtained experimentally and compared with those calculated from the one dimensional theory.

25,755 EXPANSION OF ANNEALED PYROLYTIC GRAPHITE by S. McKay (U. New Hampshire); *J. Appl. Phys.*, Vol. 35, pp. 1992-1993(L), June 1964

Swelling of pyrolytic graphite has been studied by leaching in a mixture of concentrated H_2SO_4 and HNO_3 . Ordinary pyrolytic graphite swelled rapidly in the "c" direction and delaminated after leaching for 30 seconds. The same leaching mixture produced a different effect on pyrolytic graphite vacuum annealed at 3000°C. This material swells on leaching and changes its color to black. Upon baking at 500°C, the leached graphite expands in the "c" direction as much as eighty times as thick as the original piece. The expanded graphite is soft and compressible and much less dense than ordinary pyrolytic graphite.

DEFORMATION PROPERTIES

25,756 STRESS-WAVE PROPAGATION IN ALUMINUM by R.N. Waser, J. L. Rand and J.M. Marshall (Naval Ord. Lab.); *NOL TR63 141*, BRR 107, 27 pp., Mar. 11, 1964; *U.S. Gov. Res. Rep.*, Vol. 39, p. 135(A), May 5, 1964 AD 429 735 OTS \$3.60

The one-dimensional theory of stress-wave propagation has been found to adequately represent a three dimensional experimental situation in both the elastic and plastic regimes. An air gun was used to accelerate a rod and impact it against a stationary test rod to produce a force pulse. The strain resulting from this pulse was recorded at various positions along the test rod. The deviation between the theoretical and experimental values of maximum stress was less than 11.5 per cent.

25,757 ELASTIC CONSTANTS OF ALUMINUM by J. Vallin, M. Mongy, K. Salama and O. Beckman (Uppsala U., Sweden); *J. Appl. Phys.*, Vol. 35, pp. 1825-1826, June 1964

The adiabatic elastic constants of aluminum have been measured with an ultrasonic pulse technique at liquid-helium, liquid-nitrogen, and room temperatures. The values of the elastic constants at 4°K are $c_{11} = 11.63$, $c_{12} = 6.48$, and $c_{44} = 3.09$ in units of 10^{10} N/m². The Debye characteristic temperature calculated from these figures is $\theta = 425^\circ\text{K}$ in good agreement with the value obtained from specific heat data. The shear elastic constants $\frac{1}{2}(c_{11}-c_{12})$ and c_{44} are discussed with reference to the theory given by Leigh.

25,758 ELASTIC CONSTANTS OF TELLURIUM BETWEEN 100°K AND 300°K [in French] by J.L. Malgrange, G. Quentin and J.M. Thuillier (Ecole Norm. Sup., Paris); *Phys. Stat. Sol.*, Vol. 4, pp. 139-141, 1964

The six independent coefficients of the elastic stiffness matrix of Te have been measured by an ultrasonic echo method between 100°K and 300°K. The coefficients, in 10^{11} cgs units are: $c_{11} = 3.76 - 1.65 \times 10^{-3}T$, $c_{12} = 0.924 - 0.23 \times 10^{-3}T$, $c_{13} = 2.88 - 1.29 \times 10^{-3}T$, $c_{14} = 1.43 - 0.645 \times 10^{-3}T$, $c_{33} = 7.85 - 2.10 \times 10^{-3}T$ and $c_{44} = 3.55 - 1.43 \times 10^{-3}T$.

25,759 THE EFFECT OF NEUTRON IRRADIATION ON THE ELASTIC MODULI OF GRAPHITE SINGLE CRYSTALS by C. Baker and A. Kelly (U. Cambridge); *Philosophical Mag.*, Vol. 9, pp. 927-951, June 1964

The resonant frequency in transverse vibration of natural single crystals of purified Ticonderoga graphite has been measured as a function of neutron dose. The resonant frequency increases on irradiation by a factor of two and saturates at a dose of $\sim 4 \times 10^{17}$ n.v.t. Annealing reduces the resonant frequency again. The indentation hardness of the crystals has been measured and an electron microscopic investigation of the dislocation distribution in irradiated crystals carried out. The increase in resonant frequency on irradiation is shown to be due to a reduction of the strain produced by dislocation motion. Experimental values for $1/S_{44}$ and $1/S_{11}$ for graphite are derived.

25,760 THE ELASTIC CONSTANTS OF POLYCRYSTALLINE CARBONS AND GRAPHITES by B.T. Kelly (U.K. AEA, Warrington); *Philosophical Mag.*, Vol. 9, pp. 721-737, May 1964

An attempt is made to produce a model for the small strain elastic constants of polycrystalline carbons and graphites in terms of the dislocations present in the crystallites constituting the material. The model is mainly based on the effects of fast neutron irradiation on the moduli of reactor graphites and carbons, but a wide variety of evidence is discussed and reviewed, and explanations suggested for the observations.

25,761 COMMENT ON PAPER, "RELATION OF SINGLE-CRYSTAL ELASTIC CONSTANTS TO POLYCRYSTALLINE ISOTROPIC ELASTIC MODULI OF MgO" (*J. Am. Ceramic Soc.*, Vol. 46, No. 9, pp. 452-457, 1963) by R. Colombo (FIAT, Sezione Energia Nucleare, Italy); *J. Am. Ceramic Soc.*, Vol. 47, p. 255(L), May 1964

Reported results for metals and alloys indicate striking departures from a relation for polycrystalline aggregates derived from moduli of isotropic single crystals. In this case, the difference between the Voigt and Reuss moduli should be small and the measured value should be closely related to the Voigt-Reuss-Hill approximation. For this approximation the relation

$$\vec{S} \cdot \vec{E} = \int_V \vec{\sigma} \cdot \vec{\epsilon} dV$$

should be valid where \vec{S} and \vec{E} are macroscopic stress and strain in an aggregate of volume V and $\vec{\sigma}$ and $\vec{\epsilon}$ are microscopic stress and strain. Extensive data for metals are presented which show that the Voigt-Reuss-Hill modulus differs from the measured modulus.

25,762 ELASTIC CONSTANTS OF SINGLE CRYSTAL UCd₁₁ AT 300°K by M. Shepard and J. Smith (Iowa State U.); *Acta Met.*, Vol. 12, pp. 744-745(L), June 1964

Pulse-echo techniques have been used to measure the elastic constants of single crystals of UCd₁₁, the only intermetallic compound in the U-Cd binary system. Crystals were cut so that sonic waves could be propagated in the [110] direction. Mean values for the elastic constants of single crystalline UCd₁₁ are $c_{11} = 10.07$, $c_{12} = 3.59$ and $c_{44} = 3.235$ in units of 10^{11} dyn/cm². These values indicate the single crystal bulk modulus to be 5.75×10^{11} dyn/cm². It appears that the bulk moduli of intermetallic phases of this type can be approximated from the bulk moduli of the constituent elements.

25,763 ELASTIC CONSTANTS OF SINGLE-CRYSTAL BENZENE by J.C.W. Hesselstine, W. Elliott and O.B. Wilson, Jr. (U.S. Naval Postgrad. School, Monterey); *J. Chem. Phys.*, Vol. 40, pp. 2584-2587, May 1, 1964

The elastic coefficients of benzene are determined from sound velocities measured with the use of an ultrasonic pulse technique over a temperature range of 170° to 250°K. At 250°K the results are (in units of 10^{10} dyn/cm²): $c_{11} = 6.14$; $c_{22} = 6.56$; $c_{33} = 5.83$; $c_{44} = 1.97$; $c_{55} = 3.78$; $c_{66} = 1.53$; $c_{12} = 3.52$; $c_{13} = 4.01$; $c_{23} = 3.90$. These elastic coefficients generally increase as the temperature is lowered. The observed absorption coefficients are relatively large, thus confirming data reported by L.N. Liebermann. However, it was found that the absorption is not isotropic and that the absorption for shear waves is comparable with that for longitudinal waves. Some of the experimental techniques used are described.

Elastic Constant of Salicylidene Aniline - See 25,200

Plastic Deformation of CaWO₄ - See 25,039

25,764 INFLUENCE OF THERMAL AND MECHANICAL HISTORY ON YOUNG'S MODULUS AND DAMPING ANOMALIES NEAR 40°C IN CHROMIUM by M. Klein, A. Clauer, and R. Maringer (Battelle Inst.); *J. Appl. Phys.*, Vol. 35, pp. 1994-1995(L), June 1964

Results are presented which show the influence of plastic deformation and heat treatment on the Young's modulus and damping in chromium. Observations prove that internal strains cause a decrease in the strength of the anomalous discontinuity in Young's modulus at about 40°C. Results of heat treatment studies indicate that the broad, shallow modulus and damping profiles obtained by quenching from 1150°C, become progressively sharper as annealing temperature is raised. It is believed that residual quenching strains are responsible for this behavior.

25,765 MECHANICAL PROPERTIES OF VACUUM-DEPOSITED GOLD FILMS by J.M. Blakely (Harvard U.); *J. Appl. Phys.*, Vol. 35, pp. 1756-1759, June 1964

Experiments were performed to investigate the tensile properties of gold films of thickness ranging from 2000 to 50,000 Å, deposited on rocksalt cleavage surfaces at temperatures from 40°-300°C. The grain size, which varied from about 200 Å to single crystals, has little influence on the early stages of the stress-strain curve which is characterized by an extremely high work-hardening rate and small total strain at fracture. The extent of plastic deformation is greater in monocrystalline films than in fine-grained polycrystalline ones. It is inferred that surface defects play an important role in determining the observed fracture stresses of the films.

25,766 YIELDING IN COPPER SINGLE CRYSTALS HAVING DIAMETERS IN THE RANGE 50 μ TO 150 μ by P. Barton, E. Hughes, and A. Johnson (Mats. Res. Corp.); *J. Phys. Soc. Japan*, Vol. 19, pp. 407-408(L), Mar. 1964

Single crystals of copper (99.999 pct) having a (100) orientation and diameters in the range 50 μ to 150 μ were prepared by a strain anneal technique followed by chemical polishing. Load-elongation curves of these crystals gave information about yield stresses, but not about work hardening characteristics. The yield stresses can best be described by the equation $\sigma = A + B\epsilon^{-1/2}$ where $A = .25$ kg/mm² and $B = .38$ kg/mm². Presumably the strong size effect is due to surface phenomena such as an oxide film or the interaction of dislocations with their surface image forces.

Fracture of Zn - See 25,018

25,767 FATIGUE LIMIT OF BODY-CENTERED IRON by P. Kettunen (Inst. Tech., Finland); *Philosophical Mag.*, Vol. 9, pp. 713-717(L), Apr. 1964

Specimens for fatigue and tensile tests were prepared from spectroscopically pure iron (99.999 pct). No yield point is obtained in the stress-strain curve, indicative of very high purity. In fatigue tests, the stress vs number of cycles curve of the "pure" iron is uninterrupted, as those reported for fcc pure materials. The most likely reason for this behavior is precipitation of epsilon carbides eliminating the possibility of formation of Snoek atmospheres around moving dislocations. When dislocations have escaped from Cottrell atmospheres, they can glide and continuously multiply. The most important obstruction is then due to the dislocations themselves, thus resulting in the smooth S-N curve characteristic of fcc pure materials.

25,768 NUCLEATION OF TWINNING AND FRACTURE by F. Hamer and D. Hull (The University, Liverpool); *Acta Met.*, Vol. 12, pp. 682-684(L), May 1964

It is reported that fracture of silicon iron can occur with no observable plastic deformation since the crack is nucleated by a very rapid burst of plastic deformation, indistinguishable from fracture on a stress strain curve. Observations in polycrystalline 3.25 pct silicon iron of the nucleation of twinning and fracture have been made by straining for a time t to a stress σ , and allowing the load to relax. Plastic strain can be measured as a function of both time and applied stress in this manner. Experimental observations show conclusively that, in this material, some dislocation motion occurs before fracture and twinning. Close agreement between the stress levels and time intervals required for delayed twinning and fracture provides further evidence that deformation twins can nucleate cracks.

25,769 EFFECT OF GASEOUS ENVIRONMENT ON FRACTURE BEHAVIOR OF Al_2O_3 by A. Mountvala and G. Murray (Matls. Res. Corp.); *J. Am. Ceramic Soc.*, Vol. 47, pp. 237-239, May 1964

The effect of various gaseous atmospheres (nitrogen, hydrogen, and water vapor) on the fracture strength of single-crystal and polycrystalline Al_2O_3 was investigated. Sapphire specimens exposed to hydrogen and nitrogen at elevated temperatures and subsequently tested at room temperature did not become brittle or lose strength. Sapphire specimens exposed to moisture in a specific temperature range showed a definite impairment of strength in subsequent room-temperature bend tests. The strength was recovered when the moisture-exposed specimens were heated to 400°C. It is suggested that the loss of strength and the recovery are due to the formation and decomposition of a surface precipitate, presumably a hydrate of some type. Polycrystalline alumina (Lucalox) did not show any significant loss in strength when exposed to moisture.

25,770 YIELDING AND FLOW OF SAPPHIRE ($\alpha-Al_2O_3$ CRYSTALS) IN TENSION AND COMPRESSION by H. Conrad, G. Stone and K. Janowski (Aerospace); *Cont. AT(11-1)-GEN-8*, ATN-64(9236)-15, 37 pp., Apr. 15, 1964; *STAR*, Vol. 2, p. 1504(A), June 23, 1964

The available data on the dynamics of plastic flow of sapphire indicate that the deformation rate $\dot{\gamma}$ in the temperature range from 900° to 1700°C can be expressed either as (1) $\dot{\gamma} = A/T(\tau^*)^n \exp[-(H_0/RT)]$, or (2) $\dot{\gamma} = \nu \exp[-(H(\tau^*)/RT)]$, where A , n , and ν are constants. In Eq. (1), n is of the order of 3 to 7 and H_0 is 90 to 125 kcal/mole. In Eq. (2), H is 120 kcal/mole and $\nu^* = -dH/d\tau^*$ is $110b^3$ at $\tau^* = 1$ kg/mm², decreasing with stress. Assuming the presence of an excess of oxygen ion vacancies, Eq. (1) is in accord with Weertman's dislocation climb mechanism, whereas the results based on Eq. (2) support overcoming the Peierls-Nabarro stress as the rate-controlling mechanism. It is concluded that the available data are in better accord with Eq. (2) and the Peierls-Nabarro mechanism.

25,771 EXPERIMENTAL DEFORMATION OF QUARTZ SINGLE CRYSTALS AT 27 TO 30 KILOBARS CONFINING PRESSURE AND 24°C by J. Christie, H. Heard, and P. LaMori (U. Calif.); *Am. J. Sci.*, Vol. 262, pp. 26-55, Jan. 1964

Oriented cylindrical samples cored from clear untwinned quartz crystals were deformed in compression in a piston and cylinder device. Many samples were deformed to failure at 27 kb; values of VTS show a high degree of consistency. Strengths of samples compressed parallel to the c-axis are significantly higher than those of crystals compressed in other directions. The samples failed by rupture along "faults" in planes of high shear stress; the faulting is apparently a fracture phenomenon. Thin zones of isotropic material, with lower refractive index than quartz, are present along many faults. Some of these zones contain minute amounts of crystalline material, with higher indices and lower birefrin-

gence than quartz, probably coesite. Faulting takes place at lower shear stress on the base than on the unit rhombohedra, and on the unit rhombohedra than on the prism planes. Shear strengths along different planes are unrelated either to the bond density across these planes, the shear moduli, or the theoretical strengths. Critical shear stresses for slip appear to vary in the same way for the base, unit rhombohedra, and prism planes as those for faulting. It is suggested that faulting is initiated by small amounts of slip on the planes which gives rise to submicroscopic cracks which become large enough to propagate, causing brittle fracture.

25,772 TENSILE BEHAVIOR OF Mo POLYCRYSTALS UNDER ULTRAHIGH VACUUM by S. Feuerstein, L. Rice and H. Conrad (Aerospace); *Appl. Phys. Lett.*, Vol. 4, pp. 154-155(L), Apr. 15, 1964

The stress-strain behavior of bulk molybdenum polycrystals under ultrahigh vacuum is discussed. For specimens tested either at atmospheric pressure or under ultrahigh vacuum, at any constant strain rate, the upper yield point, lower yield point, Lüders region, and strain hardening regions are almost invariant. Specimens tested under vacuum exhibited about a 30 per cent increase in strain to fracture over fracture strains observed under atmospheric conditions. No significant contribution of strain rate to ductility was observed over the range investigated. There is a possible correlation between surface desorption during early stages of the vacuum deformation and the increased ductility.

25,773 GENERAL RESEARCH: MECHANICAL BEHAVIOR OF SAPPHIRE by H. Conrad (Aerospace); ATN-64-(9236)-14, 40 pp., Mar. 23, 1964; *STAR*, Vol. 2, p. 1506(A), June 23, 1964

The present state of knowledge on the mechanical behavior of sapphire is reviewed. Sapphire deforms plastically at temperatures above 900°C, the most common mode of deformation being slip on the basal plane in the $\langle 11\bar{2}0 \rangle$ direction; under certain conditions, slip may occur on prism planes or twinning may occur. A yield point is often observed. This is related to the multiplication of dislocations by a mechanism controlled by the motion of dislocations through the lattice, rather than by the tearing of dislocations from an impurity (or defect) atmosphere. The dynamics of yielding and flow is similar and can be expressed by either of two thermally activated equations. Fracture generally occurs on a plane approximately normal to the tensile stress, and the fracture surface is conchoidal. From 1100° to 1500°C, the tensile fracture stress decreases with increase in plastic strain, independent of temperature and strain rate. The mechanism of failure in this case is the interaction of edge dislocations with preexisting cracks.

25,774 ANISOTROPIC EFFECT OF IRRADIATION ON DEFORMATION OF ZINC SINGLE CRYSTALS by O. A. Troitskii (Acad. Sci. USSR); *Soviet Phys.-Cryst.*, Vol. 8, pp. 726-730, May-June, 1964

The anisotropic effects of radiation on the deformation of zinc single crystals have been investigated. Under optimum conditions, the radiation, oriented along the glide elements $\{001\}$, causes dynamic facilitation of the gliding. It is shown that the anisotropy of the radiation effect increases with decreasing speed of deformation under irradiation, and the bombardment by heavy particles is more effective than irradiation by light particles.

25,775 CREEP, STRENGTH, EXPANSION, AND ELASTIC MODULI OF SINTERED BeO AS A FUNCTION OF GRAIN SIZE, POROSITY, AND GRAIN ORIENTATION by R. Fryxell and B. Chandler (GE); *J. Am. Ceramic Soc.*, Vol. 47, pp. 283-291, June 1964

Physical properties are presented for extruded and sintered BeO from 25° to 1400°C as a function of porosity (0 to 15 per cent), grain size (5 to 100 μ), and grain orientation (random to 80 per cent preferred). The elastic constants and linear thermal expansion are sensitive to the degree of preferred grain orientation. Measurements on polycrystalline specimens permitted calculation of the anisotropy in single crystals of BeO for these properties. Modulus of rupture data are treated in terms of the Knudsen equation, and compressive creep data have been used to estimate the diffusion coefficient controlling strain rate at 1200°C.

SONIC AND ULTRASONIC PROPERTIES

25,776 DISLOCATION CONTRIBUTION TO ULTRASONIC HARMONIC GENERATION by A. Brailsford (Ford Motor); *J. Appl. Phys.*, Vol. 35, pp. 2256-2257(L), July 1964

A theoretical model is derived which describes the nonlinear effects associated with the propagation of sound waves in solids. For a solid containing dislocations, the stress-strain relation is described and substituted into the equation of motion yielding a nonlinear relation describing the propagation of shear waves. The predictions of this theory are favorably compared with experimental evidence for variation of the second-harmonic generation, and the accompanying change in attenuation of the fundamental, in single crystal aluminum.

25,777 ULTRASONIC WAVE PROPAGATION IN DOPED n-GERMANIUM AND p-SILICON by W.P. Mason and T.B. Bateman (Bell Labs.); *Phys. Rev.*, Vol. 134A, pp. A1387-1396, June 1, 1964

The effect of doping germanium with n-type material and silicon with p-type material is to increase the attenuation and decrease the elastic moduli. The decrease in the c_{44} elastic modulus for n-type germanium agrees fairly well with theoretical predictions. However, the modulus decrease in p-type silicon is much larger and varies with temperature much faster than predicted by any present theory. It is suggested that there is a temperature-induced change in hole population along the energy surfaces. The intervalley relaxation time, which determines the added attenuation, becomes independent of the doping for high dopings with the antimony time being about 100 times that for arsenic. This result indicates that the relative values are determined by the square of the triplet singlet separation which occurs near the impurity atoms. For p-type silicon the relaxation time at low temperatures increases very markedly indicating an activation-energy effect. The energies agree well with the energies measured by infrared techniques for the largest excited state orbits around the impurity atoms. The relaxation times measured at high temperatures indicate that the hole is transported $1/3$ cycle from one $\langle 111 \rangle$ position to the next.

25,778 ANOMALOUS SOUND PROPAGATION IN CdS by H. Kroger, E. Prohofsky and R. Damon (Sperry Rand, Sudbury); *Phys. Rev. Lett.*, Vol. 11, pp. 246-248(L), Sept. 15, 1963

An acoustic wave which propagates with anomalously slow velocity under acoustic gain conditions in CdS crystals is discussed. Observations were made at 10, 15, 20, 30, and 60 Mc. The observed pulse is neither the spontaneously generated sound reported by McFee, nor the "trailing-pulse" phenomenon described by Redwood. It is proposed that the observations are explained by a collective propagation of momentum within the phonon field. The velocity appears to be consistent with this hypothesis.

25,779 THEORY OF THE PARALLEL FIELD MAGNETOACOUSTIC EFFECT by J. Quinn (RCA); *Phys. Rev. Lett.*, Vol. 11, pp. 316-318(L), Oct. 1, 1963

A theoretical treatment of the attenuation of longitudinal sound waves propagating parallel to the magnetic field is presented. It is based upon the observations of magnetoacoustic resonances of MacKinnon et al. The conductivity tensor is presented assuming with MacKinnon that the effect is associated with deviations from a spherical Fermi surface. It is shown that the parallel field resonances are semi-classical in nature and arise in the same way as in the normal magnetoacoustic effect. An expression for the attenuation maxima is given.

25,780 ULTRASONIC ATTENUATION IN CADMIUM SULPHIDE ABOVE ROOM TEMPERATURE by R. Truell, C. Elbaum and A. Granato (Brown U.); *J. Appl. Phys.*, Vol. 35, pp. 1483-1485, May 1964

The temperature dependence of the attenuation of 30-Mc/sec longitudinal ultrasonic waves has been measured from room temperature to 380°C in CdS. The observed attenuation is in good agreement with the theory of Hutson and White and with the temperature dependence of the resistance measured on the same specimen.

25,781 ULTRASONIC ATTENUATION IN MnF_2 NEAR THE NÉEL TEMPERATURE by J.R. Neighbors, R.W. Oliver and C.H. Stilwell (U.S. Naval Postgrad. School); *Phys. Rev. Lett.*, Vol. 11, pp. 125-129(L), Aug. 1, 1963

Ultrasonic attenuation in MnF_2 near the Néel temperature has been investigated. A frequency dependent attenuation peak was observed for longitudinal waves [110] with a maximum at $67.35 \pm 0.02^\circ K$. The attenuation is essentially unaffected by the magnetic field and no change in the elastic constant was observed. Any change in the modulus is attributable only to thermal expansion.

25,782 ULTRASONIC ATTENUATION IN Al_2O_3 by B. Desilets and R. Meister (Catholic U.); *Bull. Am. Phys. Soc.*, Vol. 9, p. 491(A), Apr. 1964

Measurements of ultrasonic attenuation have been made in Al_2O_3 doped with 0.05 per cent iron (Fe^{3+}), using the pulse-echo technique. The measurements were made over a temperature range from 4° to 300°K and a frequency range of 100 to 3000 Mc/sec. The attenuation was found to vary less than 20 per cent over the temperature range and to vary linearly with frequency. Both 0° and 90° orientations were studied. A scattering mechanism involving defects is used to account for the losses.

Ultrasonic Attenuation in Quartz - See 25,163

25,783 ULTRASONIC RELAXATION LOSS IN SiO_2 , GeO_2 , B_2O_3 , AND As_2O_3 GLASS by R.E. Strakna and H.T. Savage (U.S. Naval Ord. Lab.); *J. Appl. Phys.*, Vol. 35, pp. 1445-1450, May 1964

Measurements of the temperature dependence of the longitudinal and shear ultrasonic attenuation from 5 to 50 Mc/sec were made in SiO_2 , GeO_2 , B_2O_3 , and As_2O_3 glass. In each case a relaxation loss with a distribution of relaxation times was found. The median activation energy of the relaxation process is about 500 cal/mole in SiO_2 , 2500 cal/mole in GeO_2 , 5400 cal/mole in As_2O_3 , and 6300 cal/mole in B_2O_3 . The results are interpreted in terms of a two-bond-length model of glass where the relaxation loss is associated with bridging oxygen atoms which have two stress-sensitive equivalent equilibrium positions. A relationship between the relaxation loss mechanism and the viscosity of these glasses is assumed in this study. A calculation of the activation energies based upon this assumption agrees well with the values determined experimentally.

25,784 ULTRASONIC ATTENUATION AND VELOCITY IN THREE TRANSFORMATION PRODUCTS IN STEEL by E.P. Papadakis (Bell Labs.); *J. Appl. Phys.*, Vol. 35, pp. 1474-1482, May 1964

Ultrasonic attenuation measurements were made from 2 to 100 Mc/sec in the pearlitic-plus-ferritic, bainitic, and martensitic transformation products in SAE 4150 steel, a low-alloy, 0.5 per cent carbon variety. Measurements were also made in the martensitic specimen after tempering. Ultrasonic velocity measurements were made at 10 Mc/sec in each case. The attenuation can be expressed as $Af^4 + Cf^2$, where f is frequency. The first term is Rayleigh scattering and the second may be from dislocation damping, atomic relaxations, or magnetic domain boundary effects. Both A and C are strong functions of microstructure. Both coefficients decrease in the order pearlite-plus-ferrite, bainite, martensite, tempered martensite. On tempering, A decreased in the ratio 3:2 while C decreased 3:1. In pearlite-plus-ferrite, A is larger by a factor of 225 than it is in tempered martensite, and C is larger by a factor of 10. The ratio C_T/C_L (T = transverse waves, L = longitudinal waves) was a constant independent of microstructure and equal to 2.4. This suggests either dislocation damping, an atomic relaxation, or a magnetic effect. The large change in C on tempering (with C_T/C_L = constant) indicates that the interstitial carbon is involved. The ultrasonic velocity measurements showed an increase in velocity on tempering the martensite. Pearlite-plus-ferrite has the highest velocities and density, while raw martensite has the lowest. The differences in velocities arise primarily from differences in the elastic moduli of the transformation products, not from the density differences.

25,785 ULTRASONIC ATTENUATION IN A Nb-25% Zr ALLOY TO 110 kg by L.J. Neuringer and Y. Shapira (Nat'l. Magnet Lab., MIT); *Bull. Am. Phys. Soc.*, Vol. 9, p. 454(A), Apr. 1964

The attenuation of 9-Mc/sec shear waves in a Nb-25% Zr alloy was measured at 1.7°, 4.2°, and 77°K in a magnetic field up to 110 kg. The direction of the magnetic field was parallel to the direction of propagation. At 4.2° and 1.7°K, a sharp increase (~ 5 kg in width) in the attenuation is observed at high magnetic fields, followed by a gradual rise as the magnetic field is increased further. The abrupt transition in the attenuation at 4.2°K occurred at 69 kg, while at 1.7°K it was observed at 83 kg. These fields appear to be correlated with those necessary to destroy the superconducting currents, as measured by the resistance method. No hysteresis effects in the attenuation were observed at liquid-helium temperatures. At 77°K, no abrupt change in the attenuation was observed over the full range of magnetic field.

25,786 ULTRASONIC ABSORPTION MEASUREMENTS IN SINGLE CRYSTALS OF NAPHTHALENE AND p-DICHLOROBENZENE by S.S. Yun and R.T. Beyer (Brown U.); *J. Chem. Phys.*, Vol. 40, pp. 2538-2546, May 1, 1964

The attenuation of ultrasonic waves has been measured in single crystals of naphthalene and p-dichlorobenzene at frequencies from 5 to 95 MHz for the former crystal, and 5 to 65 MHz for the latter. The absorption coefficients of

the crystals were proportional to the square of the acoustic frequency. The change in absorption coefficient for the temperature range from 30°C down to -70°C was very small to about -40°C; a slight decrease was observed below this point. There was no appreciable change in the absorption coefficient within the limit of experimental error, up to a (uniaxial) pressure of 4.25×10^6 dyn/cm² applied in a direction perpendicular to the direction of propagation of the acoustic wave. From these results, it is concluded that any contributions of dislocation damping and thermal conduction in the crystals to the total acoustic absorption were negligibly small. The sound velocity was determined for these same crystals at room temperature. This velocity was to be found to be a linear function of the temperature, with negative slope, and shows approximately the same temperature coefficient in both cases.

Paramagnetic Acoustic Resonance - See 25,585

Acoustic Velocity of Salicylidene Aniline - See 25,200

25,787 THEORY OF SOUND ABSORPTION IN SOLIDS by M. I. Kaganov and V. G. Peschanskii (Physicotech. Inst.); *Soviet Phys.-Solid State*, Vol. 5, pp. 2353-2358, May 1964

The effect of thermal conductivity on sound absorption in pure dielectrics and metals over a wide range of temperatures is discussed. It is shown that the effect is very important on the sound absorption in dielectrics of low temperatures, and in the case of metals thermal conductivity is important principally at high temperatures and very low acoustic frequencies. The effect of heat transfer between electrons and phonons on the sound absorption coefficient is examined. It is found that the frequency dependence of the absorption coefficient due to the effects of heat transfer is complex in character in the extremely low frequency region.

25,788 "GIANT" QUANTUM OSCILLATIONS OF THE ACOUSTIC ABSORPTION COEFFICIENT IN BISMUTH by A. P. Korolyuk (Acad. Sci. UkrSSR); *Soviet Phys.-Solid State*, Vol. 5, pp. 2433-2435(L), May 1964

The acoustic absorption coefficient in bismuth irradiated with sound along a twofold axis C_2 has been investigated. The crystal was oriented so that the magnetic field could be rotated in the plane of the twofold axes, thus varying the angle θ . The "giant" oscillations of the absorption of sound for various angles θ and ϕ are shown (ϕ is the angle between C_2 and the magnetic field). All the features of the "giant" oscillations may be explained by considering the fact that the areas of the cross sections of the Fermi surface cut by the planes $p_z = \text{const}$ vary with the angle θ according to $p_z = p_{z0} \cos \theta$. The experimental result agrees satisfactorily with the theory of Gurevich, Skobov and Firsov.

25,789 ANISOTROPY OF THE ENERGY GAP IN SUPERCONDUCTING TIN by A. G. Shepelev (Acad. Sci. UkrSSR); *Soviet Phys-JETP*, Vol. 18, pp. 1423-1424(L), May 1964

A study of the absorption of longitudinal ultrasound in the frequency range 100-250 Mc in single crystals of tin at temperatures of 1-4°K is reported. It is found that the anisotropy of the energy gap in superconducting tin is not less than 50 per cent.

25,790 HYPERSONIC ABSORPTION IN QUARTZ AT TEMPERATURES BELOW 30°K by R. Nava, R. Azrt, I. Ciccarello and K. Dransfeld (U. Calif., Berkeley); *Phys. Rev.*, Vol. 134A, pp. A581-589, May 4, 1964

Earlier absorption measurements between 500 and 10,000 Mc/sec have been extended to temperatures below 30°K where the mean free path of thermal phonons is likely to be larger than the ultrasonic wavelength. The absorption of transverse waves follows in magnitude, as well as in the dependence on temperature and frequency, as expected for a three-phonon process. However, the measured absorption per cm for longitudinal waves depends only slightly on frequency in contrast to the expectations for a four-phonon process; instead it supports a different absorption mechanism discussed here in detail. Finally, experiments with imperfect and neutron-irradiated quartz are reported in which strong additional absorption appears, which may be related to the absorption in fused quartz.

25,791 ULTRASONIC ABSORPTION AT MICROWAVE FREQUENCIES AND AT LOW TEMPERATURES IN MgO AND Al₂O₃ by I. S. Ciccarello and K. Dransfeld (U. Calif., Berkeley); *Phys. Rev.*, Vol. 134A, pp. A1517-1520, June 15, 1964

Measurements are presented of the ultrasonic absorption in MgO and Al₂O₃ for

transverse and longitudinal waves in the low-temperature region. In contrast to some theoretical expectations, the absorption of longitudinal waves is not negligible but even stronger than for transverse waves. In the theoretical discussion it is shown that this strong longitudinal absorption probably is caused by three-phonon processes.

25,792 PHONON MASER PICTURE OF ACOUSTIC AMPLIFICATION: A SIMPLE EXAMPLE by H. Spector (IIT Res. Inst.); *Philosophical Mag.*, Vol. 9, pp. 1057-1058(L), June 1964

A simple calculation is presented in which the phonon maser picture of acoustic amplification clearly emerges. Using a previous calculation of the absorption coefficient for phonons in crossed electric and magnetic fields in a semimetal, it is assumed that such strong magnetic fields exist that all the electrons are in the lowest Landau level with $n = 0$. In this extreme quantum limit, the real part of the conductivity tensor σ is:

$$\text{Re } \sigma_{11} = \frac{3\omega_p^2 \omega \omega_c}{4(qv_F)^2 q_x v_F} \exp\left(-\frac{\hbar q_y^2}{4m\omega_c}\right) \{f_0(\epsilon_{k0}) - f_0(\epsilon_{k0} + \hbar\omega\mu)\}.$$

The phonon maser aspect of the acoustic amplification manifests itself in the terms in brackets. The first term in the brackets is the number of electrons which can absorb phonons while the second term is the number of electrons which emit phonons. As long as $\mu > 0$, the first term predominates and phonons are absorbed. However, when the drift velocity is greater than the sound velocity, electron distribution is shifted in such a way that phonon emission is more probable than absorption.

25,793 ULTRASONIC HARMONIC GENERATION IN CADMIUM SULFIDE by B. Tell (Bell Labs.); *Bull. Am. Phys. Soc.*, Vol. 9, p. 478(A), Apr. 1964

Harmonic generation has been achieved in photoconducting CdS due to the electron/ultrasonic-wave interaction, which produces amplification in piezoelectric semiconductors. Data were taken at crossover (where the electron-drift velocity is equal to the sound velocity) for various light levels in a 7-mm crystal at a fundamental shear-wave frequency of 30 Mc/sec. The largest 2nd harmonic produced was 15 db below the fundamental for an acoustic-power density of approximately 2 w/cm. This harmonic was greater than 30 db above its ordinary anharmonic dark value, and considerably larger generation can be achieved in the amplifying region. The results are interpreted by using the theory of Hutson, and are compared with ordinary anharmonic theory.

25,794 ULTRASONIC AMPLIFICATION CHARACTERISTICS AND NONLINEARITY IN CdS by T. Ishiguro, I. Uchida and T. Suzuki (Nippon Electric); 1964 IEEE Intl. Conv. Rec., Part 2, pp. 93-101

Studies are carried out on the gain and the nonlinear characteristics of ultrasonic amplification in CdS in the frequency range 15-195 Mc. A gain of 94 db at 135 Mc is obtained. Saturation characteristics and generation of higher harmonics up to 405 Mc are observed. The observed relation between the gain and the drift field is unsymmetric with respect to the drift field and the plots of the maximum gain versus frequency do not agree with the theory developed by White. When the conductivity of the crystal is low, these disagreements become considerable. A modified expression for the gain is developed taking into account the effects of phase shift between the space charge waves formed by conduction electrons and by trapped electrons.

25,795 EFFECT OF TRAPPING OF FREE CARRIERS IN CdS ULTRASONIC AMPLIFIER by I. Uchida, T. Ishiguro, Y. Sasaki and T. Suzuki (Nippon Electric); *J. Phys. Soc. Japan*, Vol. 19, pp. 674-680, May 1964

Bunched electron waves in CdS ultrasonic amplifiers are formed by two kinds of space charge waves, that is, mobile electron waves due to free electrons and bound electron waves at trapping centers. When the product of the relaxation time of electron trapping and the angular frequency of sound is an order of unity, the phase difference between the mobile and the trapped waves becomes appreciable, and the fraction, f , which gives the ratio between the mobile and the total space charges, takes a complex form. Under this condition the dependence of amplification factor, a' , deduced by use of the complex f , on the applied dc voltages becomes considerably unsymmetrical about a certain value of the dc voltage at which $a' = 0$. Further, the frequency characteristics of a'_{max} should deviate from the theory derived by Hutson and White.

SOLID STATE DEVICES

GENERAL

25,796 SEMICONDUCTOR TECHNOLOGY by D.M. Van Winkle (Continental Device); Electronic Ind., Vol. 23, pp. 68-71, June 1964

Manufacturing techniques and associated problems, possible improvements and cost lowering measures of semiconductor device technology are presented. A short history of semiconductor experimentation and materials development is given, and the growth and present extent of device technology with some needed scientific gains are reviewed. The industry itself is discussed with respect to the quality improvements it must maintain to equal present growth and success.

25,797 NOMOGRAPH FOR DETERMINING EQUIVALENT NOISE GENERATORS FOR SEMICONDUCTOR NOISE MEASUREMENT by T.F. Prosser (Amelco Semiconductor); Solid State Design, Vol. 5, pp. 36-42, June 1964

Nomographs for determining the rms value of noise voltage and noise current generated by a resistor at 25°C are presented. The concept of noise figure is defined and explained, and an equation is developed that allows one to find the noise figure of a device if certain constants and device characteristics are known. The nomograph is designed for use when the equation, because of changing values of the source resistance, R_g , becomes unwieldy and tedious.

25,798 THE COOL WORLD OF COMPONENTS by R.J. Allen and E. Niehenke (Bunker-Ramo); Electronics, Vol. 37, pp. 75-79, June 15, 1964

Performance data for resistors, capacitors, diodes, transistors and complete circuits are given for operation at a temperature of 77°K. The carbon composition resistor is shown to have a larger change in resistance than the carbon-film types, which seem to show great promise for low temperature applications. No mechanical or electrical failure was noted for capacitors subjected to extreme cold except for the cracking of the phenolic case on the large wet electrolytics. Transistors in general suffered from incomplete ionization of donors at low temperatures, but FET and tunnel diode circuits showed improved operation.

25,799 CORRELATION OF PROTON TO NEUTRON AND ELECTRON TO PHOTON RADIATION DAMAGE IN TRANSISTORS AND DIODES by G.L. Keister (Boeing, Seattle); Doc. no. D2 90407, 21 pp., Apr. 22, 1963; U.S. Gov. Res. Rep., Vol. 39, p. 145(A), June 20, 1964 AD 437 754
OTS \$2.60

The correlation of proton, neutron, electron and photon radiation damage in semiconductor devices is in reality one part of a much more comprehensive concept which is being considered by many investigators in the field of radiation damage. This concept is the establishment of some means whereby a general correlation (or equivalence) of radiation damage can be established. In discussing the correlation of proton, neutron, electron and photon radiation damage in semiconductor devices, the results of work which has been done at Boeing and selected results of other investigators in the context of this overall problem are presented and some generalized statements are made which might help ASTM members establish standards for a uniform method of handling the radiation problem.

25,800 THE RADIATION ENVIRONMENT AND COMPONENT SELECTION; Electronic Design, Vol. 12, pp. 36-45, June 8, 1964

The influence of prompt, initial, steady-state and residual nuclear radiation on military equipment design and corresponding component selection is discussed. Prompt radiation, generally gamma rays, is emitted from explosions as an intense microsecond burst; initial radiation consists of gammas and neutrons delayed in transit compared to the "prompt" energy - (the two most harmful forms of nuclear radiation), and may effect transient as well as permanent damage to semiconductor components. Charts are presented which rate semiconductor components and circuits, resistors, varistors, thermistors and capacitors, as well as elastomeric and plastic materials, in terms of either permanent or degrading dosage rates of radiation.

25,801 SHIELDING REQUIREMENTS FOR ELECTRONIC COMPONENTS IN RADIATION ENVIRONMENTS by A.J. Beck and E.L. Divita (Martin); Proc. Nat. Electronics Conf., 1963, Vol. 19, pp. 588-602

Data on the natural and artificial radiation environment have been surveyed. Realistic radiation environmental models are selected for use with radiation shielding analyses programmed for the digital computer. These programs evaluate the radiation levels in shielded compartments resulting from 1) primary protons, 2) primary electrons, and 3) secondary radiations produced in the protective shielding such as neutrons, gamma rays and bremsstrahlung. Radiation levels computed by means of these programs are presented for flights in the

natural and artificial radiation belts and for missions exposed to typical solar flare events and galactic cosmic radiation. As an example, the unshielded and shielded radiation fluxes incident on solar cells are evaluated for orbital flight in the artificial radiation belt and solar flare radiation. An estimate of the degradation of output power is determined as a function of time in the assumed radiation environment.

25,802 STEADY-STATE RADIATION EFFECTS ON ELECTRONIC COMPONENTS AND CIRCUITS by R.M. Magee (Bendix Systems Div.); Proc. Nat. Electronics Conf., 1963, Vol. 19, pp. 603-618

Recent work on nuclear radiation effects on electronic components from steady-state radiation environments is reviewed. Much of this work relates to semiconductor devices, which are the most radiation-sensitive components usually encountered in electronic systems. Emphasis is placed on: 1. Variation of radiation effects with particle energy for neutrons, protons, and electrons. 2. Relative effects of different kinds of radiation, including neutrons, protons, electrons and gamma rays. 3. Radiation-induced surface effects in transistors. 4. Reliability predictions based on statistical analyses of effects. The use of this kind of component information in circuit design applications is discussed. Various techniques, such as derating, redundancy and feedback, may be used to increase the radiation-tolerance of circuits.

25,803 COMPUTER SCREENING TECHNIQUE FOR HIGHER RELIABILITY by L.V. Ingle (Delco Radio); IEEE Trans., Vol. CP-11, pp. 251-257, June 1964

A computer program has been developed that can be applied to screening potential failures from any group of components using an outlier technique. The program features flexibility in that the user can request any frequency cell size for the 16 three digit parameter positions available. It is equally possible to attempt screening from either high or low values for each parameter. A general cost model is presented which utilizes the computer output in determining the optimum economic screening level.

25,804 FAILURE PATTERNS OF COMPONENTS by T.R.W. Bushby (Amalgamated Wireless (Australasia)); Proc. IREE, Austr., Vol. 25, pp. 290-295, Apr. 1964

Many components have failure-patterns that conform to the Gaussian law. If individual lifetimes be recorded, the test for conformity, and the determination of the mean life and standard deviation is easy. If this be impracticable, as occurs when the data consist of total failures in given time-intervals, mathematical models are necessary for such determination. Conversely, if individual lifetimes be recorded, the determination of total failures in given time-intervals is useful for stock-estimating. The solution of the models reveals some unsuspected variations in successive time-intervals, which might cause alarm and stock-estimating difficulties, if not foreseen. Such variations may also occur when a reliability-improvement project, resulting in an increased lifetime, is instituted. When an improvement by other means is not possible, a mandatory replacement of the faulty component at a determined time can reduce the failure-rate. The data are then used to prescribe the optimum replacement time. An example of the use of this technique is given.

RESISTORS and CAPACITORS

25,805 A NEW PRECISION FILM RESISTOR EXHIBITING BULK PROPERTIES by F. Zandman (Vishay Instr.), and S.J. Stein (EMC); IEEE Trans., Vol. CP-11, pp. 107-112, June 1964

A resistor combining the small size and high frequency properties of the evaporated film technique with the accuracy, precision and stability of wire-wound construction is described. Its size permits application in printed circuit technology, while its accuracy adapts it for use in half and full bridge use. Design concepts and principles of construction are given. Although the finished product does have the desired features above, the resistance ranges are limited to 100,000 Ω maximum. Additional long term and larger scale test data is required to give more information on reliability and failure rate performance.

25,806 AUTOMATIC SPUTTERING OF TANTALUM FILMS FOR RESISTOR AND CAPACITOR FABRICATION by W.L. Shockley, E.L. Geissinger, and L.A. Svach (Collins Radio); IEEE Trans., Vol. CP-11, pp. 34-37, June 1964

As a step toward achieving high volume, low-cost production of tantalum film circuits a continuous tantalum sputtering chamber has been designed and tested. This device yields up to 800 high quality tantalum coated substrates per day, depending upon the film thickness desired. Output can be increased by increasing sputtering power. The system features automatic feed of substrates into and out of the vacuum chamber without breaking the vacuum, thereby eliminating the inefficiencies of batch-type operation. Evaluation of sample substrates indicates a uniformity of sheet resistivity which is better than one percent across the surface of a given substrate. The sheet resistivity varies a maximum of ten percent between substrates.

25,807 A CRITICAL EVALUATION OF TANTALUM NITRIDE THIN FILM RESISTORS by R.W. Berry, W.H. Jackson, G.I. Parisi and A.H. Schafer (Bell Lab.); IEEE Trans., Vol. CP-11, pp. 86-96, June 1964

An extensive evaluation program has been carried out on newly developed tantalum nitride thin film resistors that were specifically prepared for this purpose and which included several levels of four manufacturing variables, namely substrate material, film thickness, line width and anodizing voltage. Resistors were subjected to a series of non-destructive screening tests followed by severe environmental evaluation tests. Preliminary test results indicate that tantalum nitride thin film resistors with a high degree of reliability and stability can be commercially manufactured.

25,808 DEVELOPMENTS IN TANTALUM NITRIDE RESISTORS by D.A. McLean, N. Schwartz and E.D. Tidd (Bell Lab.); 1964 IEEE Int. Conv. Rec., Part 9, pp. 128-138, Mar. 23-26, 1964

The use of tantalum nitride films produced by sputtering tantalum in the presence of a low and closely controlled nitrogen partial pressure to make resistors with negative temperature coefficients of the order of 50-100ppm/°C is described. The resistor, with only an anodic film protection, is stable on accelerated load aging and exhibits no electrochemical erosion. Precisions down to about 0.02% to 0.10% can be obtained, depending on resistance level. Noise levels and parasitics are low.

25,809 THE GLAZE RESISTOR - ITS STRUCTURE AND RELIABILITY by E.H. Melan and A.H. Mones (IBM Components Div.); IEEE Trans., Vol. CP-11, pp. 76-85, June 1964

Certain features of the microstructure of the palladium-silver-glass glaze resistor are described. Experimental evidence given indicates PdO to be a controlling factor in the conduction process. The effect of process variables on resistivity, TCR, and drift behavior under environmental stress are also discussed.

25,810 NOISE IN SILICON CARBIDE NON-LINEAR RESISTORS by A.G.J. Holt, P.L. Bainbridge and F.W. Stephenson (U. Newcastle upon Tyne); Radio and Electronic Eng., Vol. 27, pp. 381-383, May 1964

This paper deals with the noise arising in excess of thermal noise when a steady current is passed through a silicon-carbide non-linear resistor. Curves are given showing the variation of excess noise with current for four different resistors. Pulses of an amplitude considerably greater than the r.m.s. value of the excess noise are found to occur. These are photographed and their amplitude is measured.

25,811 STABLE, HIGH-RANGE Cr/SiO FILM RESISTORS by R. Wagner and M. Merz (Intl. Resistance); IEEE Trans., Vol. CP-11, pp. 97-100, June 1964

The development of a process compatible with standard commercial processes for the deposition of Cr/SiO films on ceramic substrates at a resistance level of 750Ω/□ and with a temperature coefficient of resistance less than 50ppm/°C. The process is described, and the effects of experimental parameters are discussed. The flash evaporation technique and the Cr/SiO system are capable of producing the desired resistor. The upper range of commercially available evaporated film resistors should be extended to at least 7.5KΩ/□ and probably to 20KΩ/□.

25,812 FOIL TYPE SOLID ELECTROLYTE TANTALUM CAPACITORS by A.L. Jenny (GE); IEEE Trans., Vol. CP-11, pp. 182-186, June 1964

Results of recent work on solid electrolyte tantalum foil capacitors rated at 150 volts and 250 volts DC and capable of full operation at an ambient temperature of 85°C are given. Considerations of construction details, cleaning, etching and anodizing foil, and final application of the solid electrolyte are discussed. Electrical characteristics of microfarads/sq. in. vs. anodizing voltage for plain and etched foils of various thicknesses are presented in graphical form.

25,813 METHOD OF PRODUCING A SOLID ELECTROLYTIC CAPACITOR by J. Von Bonin (Intl. Standard Elect.); U.S. Pat. 3,123,894, Issued Mar. 10, 1964

A method of manufacturing solid electrolytic tantalum capacitors which consistently provide a good insulation between the anode lead-in and the semiconductor layer is described. Due to the lower temperature of the process used to produce a manganese dioxide semiconducting layer on the tantalum slug it is possible to use insulating lacquers now available to isolate the anode lead-in effectively. A firmly adhering layer of manganese dioxide is produced by immersing the slug in a solution of manganese-II salts, reacting these salts with ammonia gas and oxidizing the resultant product in oxygen at 150° to 250°C. The silicone rubber insulating material, applied in the form of a solution or an emulsion is hardened but not destroyed by the application of these low temperatures.

25,814 SiO₂ THIN FILM CAPACITOR [in Japanese] by A. Morio, S. Sakurai, T. Saitô, S. Watabe and H. Amari (Elect. Commun. Lab.); J. IEE, Japan, Vol. 84, pp. 136-144, Jan. 1964

The preparation and properties of SiO₂ thin film capacitors are discussed. The films were prepared by the thermal decomposition of tetra ethoxy silane on Ni plates at 700-800°C. Capacitors produced from such films have a dissipation factor less than 10×10^{-4} with a temperature coefficient of $+10 \sim +50$ ppm/°C.

DIODES

25,815 γ-RADIATION DAMAGE IN p-i-n JUNCTIONS by J.A. Coleman (Bell Lab.); Bull. Am. Phys. Soc., Vol. 9, p. 492(A), Apr. 1964

The effect of radiation damage by ⁶⁰Co γ-rays in 1- and 2-mm-thick lithium ion-drifted silicon p-i-n junctions has been studied. Variations of particle-detection characteristics were measured using particles from an ²⁴¹Am source. A significant decrease of collection efficiency and an increase of pulse rise-time and capacitance occur at radiation doses of the order of 10⁵ R, an amount that is considered negligible for damage in normal p-n junctions.

25,816 LOWERING THE BREAKDOWN VOLTAGE OF SILICON p-n JUNCTIONS BY STRESS by A. Goetzberger and R.H. Finch (Shockley Res. Lab.); J. Appl. Phys., Vol. 35, pp. 1851-1854, June 1964

A reversible reduction of breakdown voltage is observed when mechanical stress is applied to silicon p-n junctions. This effect can best be investigated in junctions exhibiting uniform avalanche breakdown. When uniaxial stress is applied the normalized reduction of breakdown voltage $\Delta V/V_B$ is proportional to stress, the proportionality constant being of the order of 10^{-12} dyn⁻¹ cm². When stress is applied by means of a flat stylus, $\Delta V/V_B$ is proportional to the load, when a spherical stylus is used, $\Delta V/V_B$ is proportional to the cube root of load. It can be shown that the relative current change for a given force is to a first approximation independent of diode area and breakdown voltage V_B . It is proposed that the effect is caused by reduction of the energy gap.

25,817 ANISOTROPIC STRESS EFFECT OF SILICON pn JUNCTIONS by Y. Matukura (Nippon Elect.); Japanese J. Appl. Phys., Vol. 3, pp. 256-261, May 1964

The effect of large anisotropic stress on shallow silicon pn junctions is investigated. Anisotropic stresses are applied perpendicularly to four types of junction planes, each having an orientation of (100), (110), (211) or (111). The current through the region stressed increases exponentially with the increasing stress, and its dependence on the applied voltage is similar to that of a normal pn junction. Current under the stressed condition is shown empirically as follows:

$$I_s = (1 - \alpha)I + \alpha A J_0 \exp(W/W_0) [\exp(qV/mkT) - 1]$$

W_0 is the characteristic weight, which can be a measure of the sensitivity to the increased current. The characteristic weight is found to be minimum for the (100) pn junction and maximum for the (111). An influence of the spreading resistance on the current through the stressed region has been considered, and possible explanations of the anisotropic stress effect are given.

25,818 ANISOTROPIC STRESS EFFECT OF Ge pn JUNCTIONS by Y. Matukura (Nippon Elect.); Japanese J. Appl. Phys., Vol. 3, pp. 304-305, May 1964

The effect of anisotropic stresses on the V-I characteristics of Ge pn junctions is discussed. Qualitatively, the effect of a perpendicular stress to a shallow pn junction is an extreme increase in current through the junction in both the forward and reverse directions. The exact analytical behavior is also given. Mera-type pn junctions with an area of 2.42×10^{-4} cm² are subjected to stresses of up to 4000 dynes applied perpendicularly to the junction. The effect is entirely reversible in the measured stress range.

25,819 TWO-CARRIER SPACE-CHARGE-LIMITED CURRENT IN GaP by R.A. Logan, H.G. White, P.W. Foy and C.J. Frosch (Bell Lab.); Solid State Electronics, Vol. 7, pp. 473-479, June 1964

Junctions have been made in GaP which become p⁺-i-n⁺ structures at low temperatures. At high forward bias, the current voltage characteristic may be ascribed to two-carrier space-charge-limited current. This interpretation permits estimates of the electron mobility, the electric field at which the electron drift velocity saturates, the recombination kinetics and trapping effects. The techniques necessary to provide good ohmic contact to both n- and p-type GaP are described. These contacts permit measurement of the diode characteristics at high current levels and low temperatures.

25,820 DIFFUSION OF p-n PAIRS THROUGH A JUNCTION by M. Green (Burroughs); Bull. Am. Phys. Soc., Vol. 9, p. 479(A), Apr. 1964

Holes and electrons diffuse together in the steady state. The important parameter in the diffusion is the characteristic (or attenuation) length $\lambda = (kT\mu_n\mu_p/\sigma\alpha)^{1/2}$. The symbols are conventional (α is the recombination coefficient of p-n pairs). (Only for extrinsic material is λ equal to the diffusion length of minority carriers.) Generally, λ will have its maximum value where σ is a minimum, so that the concentrated product np in the diffusion of p-n pairs is least attenuated at a junction. The other important parameter in the diffusion of the pairs is the characteristic current $\Gamma = enp(\alpha\mu_n\mu_p kT/\sigma)^{1/2}$. In a pn (concentration product) gradient, p-n pairs tend to pile up in passing through regions where Γ is small, and to flow easily through where Γ is large.

25,821 HIGH ELECTRIC FIELD EFFECTS IN P-N JUNCTIONS FAST BREAK-DOWNS by L. van Biljon (U. Illinois); Cont. Nonr1834 15, 70 pp., Jan. 20, 1964; U.S. Gov. Res. Rep., Vol. 39, p. 138(A), May 5, 1964 AD429 903 OTS \$6.60

The transit time of electrons across a p-n junction in which an electric field of 10 times v/m is present is investigated and proven to be about 1 picosecond. It is shown that carrier distribution adds about 25 per cent to this time when a pulse is considered and that increasing the applied voltage does not necessarily decrease the transit time. The energy exchange between electric field, carriers and lattice is investigated and a cause of random pulse formation suggested from the results. Experimental results are presented, obtained on Si junctions in which breakdowns occur. It is suggested that small breakdowns are established at speeds too fast for conventional oscilloscopes of sufficient sensitivity. It is proposed that the experimental technique of photon stimulation used here be further refined to allow the display of the true waveshape in time of microplasma breakdown.

25,822 MICROPLASMA INTERACTION IN SILICON P-N JUNCTIONS by R. H. Haitz (Shockley Lab.); Solid State Electronics, Vol. 7, pp. 439-444, June 1964

An interaction between several microplasmas of a silicon diode is experimentally established. This interaction consists of a considerable enhancement of the pulse rate of an unstable microplasma after another microplasma on the same diode has switched to its conducting state. Infrared emission from a conducting microplasma provoking turn-on by preferential infrared absorption at crystal defects, e.g. microplasma sites, is proposed as the interaction mechanism. Evidence for such a mechanism is shown in a separate experiment and is in agreement with quantitative estimates. Apparent multistable microplasmas are interpreted as adjacent, mutually interacting microplasmas with approximately the same breakdown voltage.

Microplasma Breakdown in Junctions - See 25,331

Breakdown in Microplasma-Free Junctions - See 25,232

Recombination Radiation from:

GaAs Diodes - See 25,657

GaP Junctions - See 25,145

25,823 ANISOTROPIC STRESS EFFECT ON THE EXCESS CURRENT IN TUNNEL DIODES by W. Bernard, W. Rindner and H. Roth (Raytheon Res. Div.); J. Appl. Phys., Vol. 35, pp. 1860-1862, June 1964

The existence is reported of large reversible changes in the excess current of germanium, silicon and gallium arsenide tunnel diodes subjected to highly localized stress. The relationship of this effect to the anisotropic stress effect recently reported by Rindner and Braun in conventional p-n junctions is discussed. It is suggested that both effects may arise from deep-lying electronic states associated with strain-induced lattice defects in the junction region. A consistent interpretation is presented of the tunnel diode excess current in terms of strain-induced intermediate tunneling states, and of the conventional diode current in terms of strain-induced generation-recombination centers.

25,824 TECHNOLOGY OF TUNNEL DIODES [in French] by J. Fraleux (Lab. d'Electron. et Phys. Appl., Paris); Acta Electronica, Vol. 7, pp. 223-234, July 1963

After recalling some theoretical points concerning tunnel diodes to make clear the more fundamental parameters, the different operations of realization are described. It is then shown how to control the different parameters so that the necessary properties demanded for the application of these diodes in various fields can be obtained.

25,825 MEASUREMENTS OF THE CHARACTERISTIC PARAMETERS OF TUNNEL DIODES [in French] by G.E. Zaijier (Lab. Electron. et Phys. Appl., Paris); Acta Electronica, Vol. 7, pp. 235-244, July 1963

The necessary precautions to be taken for measuring separately each parameter of a tunnel diode and the methods employed to obtain the best results are

discussed. Two experimental units designed for the rapid measurement of negative resistance and capacity are described in detail.

25,826 MEASUREMENT OF THE SPOT NOISE OF GERMANIUM, GALLIUM ANTIMONIDE, GALLIUM ARSENIDE AND SILICON ESAKI DIODES by B.G. King and G.E. Sharpe (Bell Lab.); IEEE Trans., Vol. ED-11, pp. 273-285, June 1964

The spot (band-limited) noise of Ge, GaSb, GaAs and Si Esaki diodes was measured at 297°K for diodes having a peak current between 1 ma and 5 ma. The measured results are presented in terms of an equivalent noise current I_{EQ} which, flowing in a thermionic diode, would produce the same noise as the Esaki diode at each measure point. At zero bias, I_{EQ} was found in every case to equal the noise produced by a resistor having the same conductance as the diode and was, to a first approximation, related to the peak bias current and voltage, and the temperature. For small forward biases, I_{EQ} was in reasonably good agreement with the value calculated from $I_B \coth(qV/2kT)$, where I_B is the bias current. The bias current can be decomposed into a forward and reverse current by a linear combination of I_{EQ} and I_B . The forward current reached a peak near the peak of bias current and then declined to a value greater than the excess current in the valley. The reverse current declined rapidly from its value at zero bias and instead of tailing out often showed an inflection or anomalous peak. The noise figure and gain of a linear amplifier using Esaki diodes is strongly affected by the measure of noise $I_{EQ}/|GD|$. The diode materials were rank ordered according to this ratio with GaSb the quietest, followed by Ge, Si and GaAs. In all cases the measure of noise was reduced by cooling.

25,827 DIRECT TUNNEL-CURRENT NOISE IN TUNNEL DIODES FOR SMALL BIASES by B.E. Turner and R.E. Burgess (U. British Columbia); Canadian J. Phys., Vol. 42, pp. 1046-1057, June 1964

The Esaki theory describing the current components arising from direct inter-band tunneling in tunnel diodes has previously been used to predict a relation between the noise spectrum of direct-tunneling currents and the p-n junction voltage (Pucel 1961). Experimental confirmation of this relation is presented which provides a sensitive test of the Esaki formulation for tunneling currents and indicates as well, that the noise spectrum is independent of the band structure of the semiconductor and that the two oppositely flowing tunnel currents are uncorrelated. These facts form a basis for examining the extent to which the Esaki formulation can be generalized, and the relation independent of band structure, between the direct tunnel-current noise spectrum and the applied junction voltage.

Deterioration of GaAs Tunnel Diodes - See 25,071

25,828 DETERIORATION OF GaAs ESAKI DIODES by A. Shibata (Sony Res. Lab., Yokohama); Japanese J. Appl. Phys., Vol. 3, pp. 262-268, May 1964

The deterioration of GaAs Esaki diodes is caused by the rapid diffusions of interstitial impurities. Among the diffusion processes involved, the electric-field-assisted diffusion of interstitial Zn which acts as a donor is the most important one. The migration of impurities produces intermediate states and a defect level or levels, most probably a trap level, in the forbidden band. This defect level is then responsible for the second peak at about 0.5V found in deteriorated samples. Vacancies at and in the vicinity of a junction act against deterioration. It is found that a quantity C/nI_p , where C is the junction capacitance measured at the valley in pf, $n=I_p/I_v$, I_p and I_v the peak and the valley currents in ma is a useful measure of deteriorability of GaAs Esaki diodes. A GaAs Esaki diode with $C/nI_p < 0.35$ deteriorates significantly while a unit with $C/nI_p > 0.8$ will not.

25,829 CHARACTERISTICS OF GERMANIUM TUNNELING JUNCTIONS WITH PEAK-TO-VALLEY RATIOS OF ONE OR LESS, UNDER HYDROSTATIC PRESSURE by M. M. Cohen and L. Horn (Harry Diamond Lab.); Bull. Am. Phys. Soc., Vol. 9, pp. 557-558(A), June 1964

Tunnelling junctions have been fabricated in arsenic-doped germanium of resistivity 0.001Ω-cm. The excess and injection currents have been greatly magnified via high-temperature alloying and increased alloying times. This magnification leads to peak-to-valley ratios of 1 or less at room temperature and to the appearance of a negative-resistance characteristic, only at low temperatures. This type of flat, characteristic 2-terminal device is useful as a variable-range pressure gauge by making use of the pressure dependence of the tunneling current and as a constant-current device. These devices are superior to ordinary tunnel diodes, which must satisfy the rigid stability requirements of the amplifier mode when used in this manner. Much higher peak-current devices are now useful. The forward-bias characteristic of diodes, with peaks up to 25 mA, have been tested under hydrostatic pressures up to 10,000 psi, and the change in peak current with pressure has been found to be comparable to that of ordinary Esaki diodes. When used as a pressure gauge, gauge factors of 350 have been achieved.

25,830 METHOD OF MAKING SILICON CARBIDE NEGATIVE RESISTANCE DIODE by I. Berman (AF Cambridge Res. Lab.); U.S. Pat. 3,724,454, Issued Mar. 10, 1964

A silicon carbide tunnel diode structure capable of operating under non-linear characteristics at approximately 0.05 to 0.6 volts and 1 to 3 ma of current after starting the device by heating to between 500° and 700°C with excess current is described. The device consists of a platelet of highly doped silicon carbide of 10^{-1} to 10^{-2} ohm-cm resistivity and 1 mm thick, on top of which was placed a ring of rhenium for an ohmic contact and on the bottom a disc of aluminum. The diode was alloyed in an argon atmosphere at 1800°C for 20 seconds. The operating temperature range of the device is considerably greater than the 500° to 700°C used to start the operation of the device.

25,831 CONTROLLED ETCHING OF TUNNEL DIODES by A. Goodman (RCA Lab.); Rev. Sci. Instr., Vol. 35, pp. 642-644(L), May 1964

A technique has been developed for reproducibly etching tunnel diodes to a desired peak current value. It is usually convenient to fabricate a diode with larger junction area than desirable and electrolytically reducing the junction area (and peak current) to the final value. For electrolytic etching, the diode is immersed in an electrolyte as an anode. The diode is braised by a constant current and as etching progresses, the operating point shifts; this shift is used to terminate the etching action. Difficulties in use of the etching control circuit are described and their solutions given. With the described technique, tolerances of ± 1 pct. of a desired peak current value is possible for etched tunnel diodes.

25,832 A POINT-CONTACT DIODE FOR HIGHER-ORDER HARMONIC GENERATION OF MILLIMETER WAVES, UTILIZING SHALLOW DIFFUSED JUNCTIONS by C.A. Burrus (Bell Lab.); Solid State Electronics, Vol. 7, pp. 219-223, Mar. 1964

Point-contact diodes suitable for the harmonic generation of millimeter and sub-millimeter wave frequencies from 8-12 mm fundamental sources have been fabricated. The diodes were made by establishing a point contact to the surface of silicon into which a shallow diffusion had produced a p-n junction about 0.1-0.2 μ below the surface. When used as harmonic generators at frequencies to 365 Gc, the 15th harmonic of K-band, the performance of these diodes was found to approximate that obtained with the widely used point-contact diodes made on silicon prepared by the more complicated and difficult ion-bombardment techniques of R. S. Ohl. A simple process for the preparation of the requisite thin diffused surface layer is described.

25,833 VARACTOR DIODE IMPEDANCE MEASUREMENTS by R.B. Smith (College of North Wales); J. Electronics and Control, Vol. 16, pp. 901-906, Apr. 1964

A comparison is made between impedance data obtained by two different methods for a coaxially encapsulated varactor diode. In one of these the impedances are normalized to the series resistance of the diode and in the other to the characteristic impedance of the measuring line. The agreement between the two sets of data is good.

25,834 HIGH-FREQUENCY PROPERTIES OF EPITAXIAL SILICON p-n JUNCTIONS AT LOW TEMPERATURES by H.J. Fink (Bell Lab.); J. Appl. Phys., Vol. 35, pp. 1883-1889, June 1964

Variable reactance epitaxial silicon p-n junctions with approximately constant impurity gradients were investigated at 5.85 Gc/sec, 1 Mc/sec and dc between room temperature and 2°K. The p-n junctions were B-P and B-As doped. The units with breakdown voltages larger than 11V (at 300°K) showed an exponential freeze-out of the carriers at 5.85 Gc/sec when the temperature was lowered. The units with less than 7.7 V breakdown voltage showed clearly impurity band conduction at low temperatures. The maximum change of the reactive component between large forward currents and the breakdown voltage was temperature independent within $\pm 10\%$ for all the wafers. The cutoff frequencies of the wafers at 300°K were between 190 and 320 Gc/sec. The units with large breakdown voltages (> 14 V) had a negative differential resistance in the dc forward voltage-current characteristics at low temperatures. From an extrapolation of the present experiments one would expect, when the impurity gradient at the junction is increased to such a value that the breakdown voltage is about 5.5 V, that epitaxial silicon variable reactance p-n junctions will operate at microwave frequencies and liquid-helium temperatures with approximately the same losses as at room temperature.

25,835 GALLIUM ARSENIDE VARACTOR DIODES by H. Kressel, A. Solomon, G. Kupsky and H. Lee (RCA); Cont. NObsr87405, 88 pp., Aug. 26, 1963; U.S. Gov. Res. Rep., Vol. 39, p. 36(A), June 29, 1964

Three types of devices for high efficiency power conversion between 12Gc and 24 Gc were designed. The first type was designed to yield 40% conversion efficiency, with a minimum of 25mw power input. The others were designed to handle a minimum 100mw and 250mw input power, respectively. High cut-off diodes require an optimum combination of breakdown, series resistance,

and junction capacitance. The use of p⁺nn⁺ epitaxial structures, with closely controlled n-region properties, offer the best means of achieving this goal. A number of excellent devices were fabricated with such material. Mechanical means of controlling the diode base thickness were also investigated.

25,836 ALLOY-JUNCTION SEMICONDUCTORS AND METHODS FOR MAKING THE SAME by S. Matlow (Hoffman Electronics); U.S. Pat. 3,124,493, Issued Mar. 10, 1964

A method of producing a mechanically strong alloy junction in a semiconductor device having a high Zener breakdown voltage is described. An aluminum wire doped with boron, in a concentration between approximately .25% and 2%, is pressed onto a piece of n-type silicon and heated until the wire melts and is then allowed to cool. When plain aluminum wire is used, (111) crystal planes appear in the recrystallized silicon. These planes lead to a low Zener breakdown voltage and must be completely etched away thereby reducing the mechanical strength of the junction. However the (111) plane can be eliminated by making the eutectic with silicon richer in silicon. Boron is the only group III element with a melting point high enough to yield a eutectic richer in silicon. When the aluminum is doped with boron, the resulting eutectic is richer in silicon and the geometry is hemispherical thereby reducing the necessary etching time and preserving the mechanical strength of the junction.

Microwave Diode Switches - See 26,208-26,211

25,837 JUNCTION CAPACITANCE SWITCHES by G. Adam (Stand. Tel. and Cables); IEEE Trans., Vol. ED-10, pp. 51-58, Jan. 1963

The design of junction capacitance switches consisting of a combination of abrupt junctions is considered. Theoretical characteristics are calculated for ideally abrupt junctions. The possibilities of fabrication by alloying and epitaxial growth are briefly discussed.

25,838 THE RESEARCH AND DEVELOPMENT OF HIGH CURRENT AND HIGH VOLTAGE SILICON CONTROLLED RECTIFIERS (GE, Auburn, N.Y.); 111 pp., Dec. 31, 1963; U.S. Gov. Res. Rep., Vol. 39, p. 51(A), May 5, 1964

Research concerned the development of high-current, high-voltage silicon controlled rectifiers. The design, development, optimization, fabrication and characterization of a 155 amp, 1300 volt device are described and discussed in detail, along with a description of process steps and component parts.

25,839 SILICON RECTIFIER CONTROLS POWER IN EITHER DIRECTION by J. Lüscher, H.C. Voorrips and B. Zega (Battelle); Electronics, Vol. 36, pp. 63-65, Dec. 20, 1963

A controlled bidirectional power switch constructed from semiconductor junctions having backward rectifier characteristics is discussed. The device has an n- π -n structure, with a central region of high resistivity p-type silicon, terminated on both sides by alloyed degenerate p-type layers. Each of these junctions acts as an ohmic contact to its N zone in a conventional PN π N structure when the device is polarized in its direction. Switching is controlled by contacts on the N-layers which are driven with respect to the degenerate p-zone, working as an emitter, by negative voltage pulses. Analogous to the conventional four-layer switch, the device can be switched on by light. The device is constructed by submitting the n-doped layers of the basic n- π -n structure to electrolytic etching. The etched surfaces are then coated with an aluminum-boron film which is alloyed into the n-type layers to form the degenerate p-type junction. The control contacts are thereby produced simultaneously on the degenerate parts of the n-type layers. Different device characteristics are obtained by choosing different doping levels at the emitter junctions and different resistivities and widths of the π -layer.

25,840 BIDIRECTIONAL SOLID STATE SWITCH USING BACKWARD RECTIFIER JUNCTIONS by J. Lüscher, H. Voorrips and B. Zega (Battelle); Proc. IEEE, Vol. 52, pp. 610-611, May 1964

A silicon controlled bidirectional medium-power switch using the characteristic properties of backward rectifier junctions has been developed. The device consists basically of a symmetrically diffused n-p-n sandwich made by conventional processes, the central p layer of which has a high resistivity, whereas the surface concentration of the n layers is of the order of 10^{19} cm⁻³. Backward-rectifier junctions are formed on the n layers by alloying an aluminum boron layer. In this way a symmetrical P⁺-N- π -N-P⁺ structure is obtained. The characteristics of this five layer device are very nearly equal to those of two identical pnpn switches connected in parallel but in opposite directions. Typical medium power units have breakover voltages of 300 volts and maximum current rating of 8 amperes. The turn-on current is about 25 ma and the average voltage drop in the turn-on condition is 1 volt at 50 ma, increasing to 1.5 volts at maximum current rating.

25,841 CHARACTERISTICS AND UTILIZATION OF BACKWARD DIODES FOR UHF DETECTION [in French] by H. Derooy and P. Leclerc (CSF Co.); Ann.

Radioelect., Vol. 19, pp. 21-29, Jan. 1964

The rapidity of the passage of electrons by tunnel effect into the space charge of a junction allows the use of inverse diodes on UHF to be envisaged. Among all the possible applications, the study of square law detection brings out the fundamental physical parameters of diodes and permits direct comparison with conventional crystals. This study shows that the efficiency of detection due to tunnel effect is high. But frequency response is limited by the stray elements of the equivalent circuit, the magnitude of which is imposed by the technology applied. In its present state the performance of the inverse diode is comparable to that of UHF crystals, except in those applications where the absence of $\frac{1}{f}$ noise is an advantage.

25,842 SEMICONDUCTOR DEVICES by T. Sylvan (GE); U.S. Pat. 3,124,703, Issued Mar. 10, 1964

A four-layer, four electrode semiconductor switching device is described. Alternate layers of p-type and n-type material are stacked so as to form a plurality of p-n junctions. Two main current carrying electrodes are connected to the top n-type and bottom p-type regions. An additional control junction is formed. When one main electrode is biased in one polarity with respect to the other terminal, the two p-n junctions nearest the main electrodes become, or tend to become, reverse biased and the center p-n junction becomes forward biased; thus a high impedance is presented between the electrodes. When the main electrodes are biased in the other polarity, the two p-n junctions nearest the main electrodes become, or tend to become, forward biased and the center p-n junction becomes reverse biased; thus a high impedance is again seen between the terminals. However, if the potential applied between the main electrodes is increased, or if control current of suitable magnitude and direction is applied, even the center p-n junction breaks down, polarization is reversed, and a very low impedance is present between the main terminals.

Growth of Junctions in GaP - See 25,093

25,843 VAPOR-DEPOSITED, THIN-FILM HETEROJUNCTION DIODES by R.S. Muller (U. Calif., Berkeley) and R. Zuleeg (Hughes Semicond. Div.); J. Appl. Phys., Vol. 35, pp. 1550-1556, May 1964

Deposited heterojunctions between semi-insulating CdS thin films and insulating materials have been fabricated, and their characteristics studied. Excellent rectification properties are obtained in which contact-field emission from the heterojunction carries the forward currents. Field emission of this type exhibits several characteristics which differ from the Schottky field emission. These differences stem from the nondegeneracy of the electron source in the heterojunction case. Correspondence between the theoretical predictions for the behavior of such emission, as derived in this paper, with observed temperature and voltage dependence is very good. The theory developed may account for the low value for the Richardson factor obtained experimentally for oxide-coated vacuum emitters. The structures studied consist of Al contacting a film of deposited CdS roughly 1 μ in thickness. Three different insulating materials CdTe, Al₂O₃ and SiO_x were used to form the thin insulating film between the CdS and the metallic counter electrode.

25,844 LOW TEMPERATURE PASSIVATION OF SILICON DEVICES USING EVAPORATED LEAD FILM by T. Tokuyama (Hitachi); Proc. IEEE, Vol. 52, pp. 723-724, June 1964

A lower temperature passivating process producing stable and water resistant oxide glass films on silicon substrates is described. The method consists of evaporating lead films on the silicon substrates and heating them in an oxidizing atmosphere. Evaporated lead film reacts with oxygen and turns to lead oxide, which accelerates the oxidation reaction of the silicon surface and forms PbO/SiO₂ glass on the substrate surface. Processing temperature is 500°C to 800°C, and requires from a few minutes to about half an hour. Low temperature and short processing time makes this method useful for passivating devices, in the stage of raw wafers, and after they are completed junction structures.

TRANSISTORS

25,845 PROTON DAMAGE IN SEMICONDUCTOR DEVICES by D.M. Arnold, J.A. Baicker, H. Flicker, D.A. Gandolfo and J.R. Parker (RCA); NASA Cont. NAS1-1654, 73 pp., Apr. 1964; STAR, Vol. 2, p. 1420(A), June 8, 1964 NASA CR-40 OTS \$2.00

Changes in transistor electrical characteristics are interpreted in terms of fundamental changes in the semiconductor crystal structure and, the effects of proton bombardment are predicted. Emphasis is placed on lattice displacements, but transmutations and ionization are also considered. Proton and neutron displacement production rates are calculated. These are used in conjunction with neutron irradiation data and an assumed similarity of defect clusters to determine the effects of protons on transistors. Reasonable agreement with

experiment is obtained. The expected lives of transistors in satellites orbiting in the inner Van Allen belt are given.

Radiation Effects on Transistors - See 25,802

25,846 ACCELERATED RELIABILITY TESTS ON TRANSISTORS by H. Koschel and A. Jäger; Nachr.-Techn. Z., Vol. 17, pp. 237-244, May 1964

Transistor tests with overloading in incremental steps provide the manufacturer with important information on failure mechanisms depending on volume, surface and capsulation and offers important suggestions for further technical developments. Design and operation of test equipment required for this purpose are described. Test results from germanium mesa and alloy transistors are quoted and compared with data on the operational reliability in communication equipment.

25,847 TESTING TRANSISTORS IN-CIRCUIT by A.T. Ashby, T.R. Shaifer and H.R. Hegner (IIT Res. Inst.); Electronics, Vol. 37, pp. 53-56, June 1, 1964

An in-circuit tester that measures transistor leakage current I_{CBX} (the collector current when both the collector and emitter junctions of the transistor are reverse-biased) is described. The unit is battery powered for portable field use. The test connections are explained, and the heart of the testing device, the differential d-c amplifier is discussed. A sample testing procedure is given.

25,848 MEASURING INPUT AND OUTPUT CAPACITANCES OF HIGH-FREQUENCY TRANSISTORS by E. Gottlieb (GE); Electronic Design, Vol. 12, pp. 64-67, June 8, 1964

Methods of accurately measuring input and output capacitances of UHF transistors are presented. An analysis of inter-element UHF transistor capacitances is given, and a mathematical expression is derived for the quantity C_{ob} . A two-terminal and three-terminal bridge test setup and procedure is described, and the three-terminal method is formed to be superior in terms of proximity capacitance elimination.

25,849 SOME EFFECTS OF LOCALIZED STRESS ON SILICON PLANAR TRANSISTORS by R. Edwards (Bell Lab.); IEEE Trans., Vol. ED-11, pp. 286-294, June 1964

When local compressive stress is applied to the emitter surface of a silicon planar transistor, increases in collector and base currents are observed. From the relationship between these currents and the base-to-emitter junction potential, it is inferred that changes in minority-carrier current occur in the stressed material. The effects described are consistent with a decrease in energy gap of a few tenths of an electron volt at compressive stresses of the order of 10^{11} dynes cm^{-2} . It is shown that the influence of stress on the current gain of a transistor depends on the strain distribution in the material. When the stress is applied over a relatively large area using a blunt stressing element, the increased minority-carrier current causes a rise in common-emitter current gain at low currents. In the case of the stress pattern produced by a sharper stressing element, a decrease in current gain is observed over a wide current range. It is proposed that this decrease results from a degradation in emitter efficiency caused by the stress concentration in the emitter region.

Parameters of Transistors - See 26,167

25,850 COMPARISON OF LARGE SIGNAL MODELS FOR JUNCTION TRANSISTORS by D.J. Hamilton and F.A. Lindholm (U. Arizona) and J.A. Narud (Semiconductor Prod.); Proc. IEEE, Vol. 52, pp. 239-248, Mar. 1964

The Ebers-Moll, charge control, and Linvill lumped models are systematically derived from a common mathematical origin. Approximations are discussed in detail, and the models are compared on the basis of their ability to represent physical processes, the ease with which they lend themselves to analysis, and the degree of approximation involved. It is shown that all three models are equivalent with regard to over-all degree of approximation, and therefore yield the same results in the solution of large-signal transient problems. However, the lumped model best portrays physical processes and lends itself most easily to intuitive understanding.

25,851 TRANSIENT RESPONSE OF JUNCTION TRANSISTOR TO BASE CURRENT PULSE by L.J. Giacoletto (Michigan State U.); Proc. IEEE, Vol. 52, pp. 627-628(L), May 1964

A general solution for the transient operation of transistors has been obtained, subject to arbitrary terminal voltages and currents. Curves are calculated for the collector and base voltages, using typical n-p-n silicon transistor properties, and curves for the associated emitter and collector minority carrier densities are shown. Analytical results yield time constants of interest in the transient response to a base current pulse. The results are modified by feedback via the collector-to-base transition capacitance; such modification indicates that the

presence of the fixed feedback capacitor is significant only when the collector voltage is changing rapidly.

25,852 TRANSISTOR CHARACTERIZATION AND DERATING FOR SECOND BREAKDOWN by B. Reich and E. B. Hakim; Solid State Design, Vol. 5, pp. 24-28, May 1964

Two modes attributing to secondary breakdown in transistors have been found—the current and voltage modes. Localized spots due to current constriction as a result of either mode causes an exponential rise in thermal resistance prior to secondary breakdown. These localized secondary breakdown spots have been calculated to be between 900–110°C in silicon. The study indicates that the maximum secondary breakdown power is a function of the device design and should be considered in light of other device performance requirements.

25,853 SECONDARY BREAKDOWN IN TRANSISTORS by H. Melchior, 2nd, and M.J.O. Strutt (Swiss Feder. Inst. of Tech.); Proc. IEEE, Vol. 52, pp. 439-440(L), Apr. 1964

Theoretical discussions and experimental results of the secondary breakdown effect in transistors are given. Models for the breakdown phenomenon are presented. It is shown that p-n junctions with a low breakdown voltage have a high secondary breakdown trigger temperature, and junctions with a high breakdown voltage have a low secondary breakdown trigger temperature. A plot of time to achieve secondary breakdown vs. applied pulse power with case temperature as a parameter is useful to determine how long a given pulse power may be applied to the transistor without causing secondary breakdown.

25,854 AN APPRAISAL OF TRANSISTOR THERMAL RESISTANCE AND JUNCTION TEMPERATURE by B. Reich and E.B. Hakim (AERDA); AERDL TR2364, 23 pp., Nov. 1963; U.S. Gov. Res. Rep., Vol. 39, p. 42(A), May 5, 1964 AD 430 144 OTS \$2.60

The current state-of-the-art of pulsed thermal resistance measurements is reviewed. Some of the reasons are presented for the apparent lack of correlation in thermal measurements when these techniques are used. Two techniques of continuous thermal resistance measurements are presented and possible sources of error indicated. Some preliminary data is presented which indicates that thermal resistance measurements made by the continuous h_{FE} technique is the most sensitive method currently known.

25,855 AN EXPERIMENTAL STUDY OF 1/f NOISE IN TRANSISTORS by M.J. Wiggins (Martin, Orlando); 1964 IEEE Intl. Conv. Rec., Part 2, pp. 102-110

An experimental approach for the determination of optimum operating point and source impedance for transistor circuits in applications where 1/f noise predominates is described. Results of a number of tests which measure the noise spectrum as a function of operating point and source impedance are described. Results of such tests are presented as parametric plots of noise factor versus frequency, and conclusions are drawn as to the choice of parameters for optimum noise performance at low frequencies. A description of the special measurement techniques is included. A procedure is developed for rapid determination of the entire noise spectrum of a transistor for practical design purposes.

25,856 INTERNAL OSCILLATIONS IN P-N-P-M TRANSISTORS by N.A. Shekhtsov, E.D. Prokhorov and B.V. Safronov (Wright-Patterson AFB); 9 pp., Feb. 19, 1964, Trans. from Radiotekh. i Elektron., Vol. 8, No. 10, pp. 1783-1786, 1963; U.S. Gov. Res. Rep., Vol. 39, p. 28(A), June 5, 1964 AD 433 541 OTS \$1.10

It is shown that the complex dependence of the coefficient of amplification in accordance with the current alpha of transistors of the type p-n-p-m is to be explained by the occurrence of inner oscillations. There are presented some results of experimental investigation of the internal oscillations and the proposed mechanism of their formation.

25,857 A UNIJUNCTION TRANSISTOR STRUCTURE USING SPREADING RESISTANCE MODULATION by V.A. Bluhm and T.P. Sylvan; Solid State Design, Vol. 5, pp. 26-31, June 1964

Unijunction transistors made using the conventional bar geometry have higher values of peak point current, valley point current, saturation voltage and turn-on time than is desirable in many applications. A new structure using the spreading resistance of a small area ohmic contact has overcome the geometrical restrictions of the bar structure and made possible a significant improvement in many of the electrical characteristics. An additional benefit of the new unijunction transistor is the reduction in manufacturing costs made possible by simplifications in processing and elimination of the need for a ceramic pellet mount.

25,858 A SURVEY OF HOT-ELECTRON AND THIN-FILM TRANSISTORS by J.M. Lavine (Raytheon Res. Div.); Solid State Tech., Vol. 7, pp. 17-23,

May 1964

For some time, the need for an amplifying device fabricated by techniques compatible with thin-film microcircuit passive elements has been clearly evident. Efforts to fabricate bipolar transistors have failed mostly because of the difficulty in preparing semiconductor grade materials by evaporative techniques. Unipolar transistor studies have shown possibility, again, somewhat restricted by the semiconductor materials technology. The thin-film transistor developed by Weimer makes use of evaporated CdS films, one of the few to show useful semiconducting properties. This device is at present the only thin-film device capable of exhibiting a useful gain-bandwidth product. The recently proposed hot-electron devices have not yet exhibited unambiguous evidence of power-gain capability or reduction to thin-film form. The present, however, a potentially useful area for the development of such devices as well as representing a new amplifying concept, and are fully treated in this survey. One consequence of the several studies on the metal-interface amplifier was to point out the possibility of obtaining an improved geometry for the depletion-layer transistor proposed by Gärtner, a geometry with potential for reduction to thin-film form.

25,859 THE EFFECTS OF RECTIFYING CONTACTS ON THE CHARACTERISTICS OF THE TFT by W. Gutiérrez and H.L. Wilson (Melpar); Proc. IEEE, Vol. 52, p. 607, May 1964

An explanation for a two-level current saturation condition ("double pinch off") that has been observed in the I-V characteristics of numerous CdSe thin-film transistors (TFT) with aluminum, gold or nichrome as the source-drain electrodes is presented. The existence of rectifying metal-semiconductor contacts at the source and/or drain electrodes explain this phenomena. As the drain voltage is increased, one of the contact diodes is forward biased and the other, reverse biased. The reverse biased diode limits the amount of current through the channel. This leakage current of the reverse biased diode is then modulated by the gate potential and constitutes the current of the first lower saturation level. If the drain voltage is increased beyond the reverse breakdown of the blocking diode, the blocking contact is eliminated and a larger current is allowed through the channel. This current will then become saturated by the drain voltage and will be modulated by the gate potential as in normal TFT operation, and constitute the second or higher saturation level.

25,860 A p-TYPE TELLURIUM THIN-FILM TRANSISTOR by P. Weiner (RCA); Proc. IEEE, Vol. 52, pp. 608-609, May 1964

Preliminary results with evaporated tellurium films yielding high performance p-type thin-film transistors (TFT) are described. The gold source and drain electrodes were deposited directly on the substrate, followed in order by the tellurium, the insulator and the gate. Successful units were also made with coplanar source, gate and drain deposited in different sequences. A typical source-drain gap was 0.4 to 0.8 mil by 100 mils long. Silicon monoxide and calcium fluoride films are suitable for the insulation. The transconductance (gm) of such units has ranged up to 40,000 μ mho. This device demonstrates that well-saturated "enhancement" mode characteristics are possible with a narrow band-gap semiconductor (0.34 eV) whose resistivity is no more than a few tenths ohm-cm. This is accomplished by using a semiconductor layer so thin that the depletion layer produced by the gate in the neighborhood of the drain extends almost completely through the semiconductor layer (about 150 Å in this case).

25,861 AGING CHARACTERISTICS OF FIELD EFFECT THIN FILM ACTIVE DEVICES by K.K. Reinhartz, V.A. Russel, D.L. Stockman, W.J. van der Grinten and W.L. Willis (GE Electronics Lab., Syracuse); IEEE Trans., Vol. CP-11, pp. 27-33, June 1964

The aging characteristics of thin film field effect triodes have been studied under humidity, temperature and electrical stress. The device characteristics are very sensitive to humidity. In dry argon at room temperature the device characteristics did not change within six months. At constant elevated temperature between 50°C and 121°C the transconductance of thin film triodes is almost constant for at least 50 days. The gate voltage at constant drain current and voltage increases during the first few days until it reaches a constant level again. Devices under electrical stress showed a similar behavior but the increase of the gate voltage continued for about 20 days. A tentative model is proposed for some of the failure modes.

25,862 LOW-FREQUENCY OPERATION OF FOUR-TERMINAL FIELD-EFFECT TRANSISTORS by D.C. Latham (Martin), F.A. Lindholm and D.J. Hamilton (U. Arizona); IEEE Trans., Vol. ED-11, pp. 300-305, June 1964

Interesting and useful behavior is obtained by operating a two-gate field-effect transistor as a four-terminal device. Important aspects of the low-frequency four-terminal behavior of a transistor with symmetrical geometry are considered. The functional dependence of the drain current upon gate bias voltages and material and structural constants is determined, and four general modes of operation of the device are defined. For each mode the dependence of relevant transconductances on gate biases is calculated. Special cases of interest are analyzed, including that in which the transconductance exhibits a linear variation with gate bias voltage. Experimental results are in good agreement

with the theory.

25,863 PINCH OFF IN INSULATED-GATE FIELD-EFFECT TRANSISTORS by C. Goldberg (Westinghouse); Proc. IEEE, Vol. 52, pp. 414-415(L), Apr. 1964

A current saturation effect beyond the pinch-off point of the insulated gate field-effect transistor previously discussed by Hofstein and Heiman is described. Their first order theory is invalid beyond the pinch-off point, and therefore cannot predict saturation. If the theory incorporates the idea that current carriers are always present, however, it is mathematically shown that saturation phenomena are predicted. Analogous theories can be used to explain current saturation in the depletion-type insulated-gate, thin film and junction-gate field-effect transistors.

25,864 SPACE-CHARGE EFFECTS IN THE INSULATED-GATE FIELD-EFFECT TRIODE by J. Winslow (Electro-Optical Systems); Proc. IEEE, Vol. 52, p. 618(L), May 1964

Space charge plays an important role in the operation of the insulated-gate field-effect triode when the drain voltage approaches or exceeds the gate voltage. An analysis is presented which accounts for space charge and agrees well, over a wide range of drain voltages, with measured drain characteristics of the field-effect triode. Comparison is made between the present analysis and a previous one not accounting for space charge. Good agreement is evident for cases where the drain potential is less than the gate potential; i.e., drain voltages where space charge effects are not prominent.

25,865 EFFECT OF TEMPERATURE ON FET CHARACTERISTICS by L.J. Sevin (Texas Instr.); Electro-Technology, Vol. 73, pp. 103-107, Apr 1964

A formula for biasing field effect transistors (FETs) used in dc amplifiers which compensates for the unusual variations of drain characteristics with temperature is derived. Even the sign of the temperature coefficient of I_{DSS} (zero bias drain current) may differ from published data. Assuming only a square-law behavior for FETs and considering mobility, contact potential, and forward transfer characteristics yields

$$\frac{I_{DQ}}{I_{DO}} = \frac{4T_0 N_T^2 N}{N_A^2 V_{PO}} \left[\frac{3K}{q} (1 + \ln T) + 0.28 \times 10^{-3} \right]^2$$

which tells how to bias FETs for temperature-independent dc gain. I_{DO} is the reference temperature (T_0) value of I_{DSS} where the rate of change of gate bias voltage is zero, n is 1.5 for electrons and 2.3 for holes in silicon, K is 8.616×10^{-5} eV/degree Kelvin, and q is 1.6×10^{-19} coulombs. V_{PO} (the pinch-off voltage) is $2I_{DSS}/g_{MAX}$ where g_{MAX} is the low frequency zero-bias transconductance. Eight graphs illustrate this derivation.

25,866 CONDITIONS FOR A TEMPERATURE COMPENSATED SILICON FIELD EFFECT TRANSISTOR by J. Hoemi and B. Weir (Amelco Semiconductor); Proc. IEEE, Vol. 51, pp. 1058-1059(L), July 1963

A method of producing a silicon field effect transistor (FET) with a zero temperature coefficient for the source to drain current (I_{DSS}) is described. There are two independent temperature dependent parameters which are made to oppose each other and thus stabilize the operating point of the device in a common source amplifier. The resistivity of the silicon in the channel increases, due to scattering processes, with increasing temperature at about 0.8 per cent/°C tending to decrease I_{DSS} . The diffusion voltage has a negative temperature coefficient of about 2.5 mV/°C thereby narrowing the depletion layer and widening the channel thus tending to increase I_{DSS} . For zero temperature coefficient of I_{DSS} , it is calculated that $gm/I_{DSS} = K/V_P$; where $K = 3$ for step junctions, $K = 5/2$ for a graded junction and V_P is the device pinch-off voltage. The expression derived is seen to be satisfied experimentally.

25,867 DESIGN THEORY OF A SURFACE FIELD-EFFECT TRANSISTOR by H.K.J. Ihanola (Inst. Tech., Helsinki, Finland) and J.L. Moll (Stanford U.); Solid State Electronics, Vol. 7, pp. 423-430, June 1964

The design theory of insulated gate, surface field-effect transistors is presented. It is shown that for similar dimensions the surface field-effect transistor has frequency response comparable to other field-effect transistors. It is found to be quite simple to trade capacitance and transconductance in the surface field-effect transistor. The static input resistance of the surface field-effect transistor is just the leakage of the insulator, so that this device may be used in electrometers and similar equipment. In addition, the construction on the surface of a semiconductor crystal offers interesting possibilities as an element of an integrated circuit.

25,868 DESIGN CALCULATIONS FOR MOS FIELD EFFECT TRANSISTORS by C.D. Root (Raytheon) and L. Vadasz (Fairchild Semiconductor); IEEE Trans., Vol. ED-11, pp. 294-299, June 1964

Design equations for the Metal-Oxide-Semiconductor Field Effect Transistor are developed. Approximate solutions for static characteristics, transconduct-

ance and frequency cutoff are presented for the case of a very high resistivity substrate. Specific sets of static characteristics from computer calculations are presented graphically to illustrate the effects of oxide thickness and various substrate resistivities.

25,869 COMPOSITE FIELD EFFECT TRANSISTOR by R. Bockemuehl (Genl. Motors); U.S. Pat. 3,135,926, Issued June 2, 1964

A semiconductor device having unitary construction but multiple element function is described. The device acts as a field effect transistor with one portion of the crystalline body acting as a light transducer and another as an amplifying region. An impedance matching region may also be incorporated.

25,870 A MODIFIED PRESENTATION FOR THIN-FILM TRIODES by D. Abraham and T.O. Poehler (Appl. Phys. Lab.); Proc. IEEE, Vol. 52, pp. 416-417(L), Apr. 1964

Thin-film field effect "enhancement mode" triodes and an expression published by Borkan and Weimer characterizing the thin-film triode with pentode-like properties are discussed. Weimer's expression is given and it is stated that such a voltage-current relationship cannot properly describe the behavior of a TFT "triode," and only represents the TFT "pentode" up to saturation. A modified voltage-current relationship for the TFT "triode" is presented and discussed in the light of experimental evidence.

25,871 FIELD EFFECT TRANSISTOR HAVING GRAIN BOUNDARY THEREIN by W. Shockley (Clevite); U.S. Pat. 3,126,505, Mar. 24, 1964

An improved unipolar or field effect transistor in which the channel length is comparable to the channel width and in which the gate regions are formed along a grain boundary extending across the channel is described. Diffusion regions of the opposite type (for example p-type if the main body of semiconductor material is n-type) are formed at the grain boundary and extended in a wedge shape deeper into the body at the boundary. Thus there is formed a channel which is relatively short since the gate regions converge along a sharp edge. The procedure for producing this device is outlined and utilizes the fact that in a small angle grain boundary (composed of edge dislocations in the crystal structure along the boundary), diffusion proceeds most readily in the direction of the edge dislocations.

25,872 FABRICATION TECHNIQUES FOR A DIFFUSED PLANAR PNP TRANSISTOR by G. Bradshaw and C.H. Taylor; Brit. Commun. and Electronics, Vol. 11, pp. 248-251, Apr. 1964

The processes and techniques necessary to fabricate a planar PNP silicon transistor are described. A silicon slice approximately 0.875 in. diameter and 0.013 thick and 1 to 5 Ω/cm is first lapped and etch-polished. Then an oxide film is grown on one side and etched into patterns with photolithographic techniques. Boron and phosphorus are next selectively diffused into the silicon to produce an array of PNP transistor structures; contact areas are then metallized and the slice cut into chips containing individual transistors. These are finally mounted on a header and connections made to the header pins by thermo-compression bonding fine wires. Transistors mounted and tested gave a wide variety of gains depending on base widths. Current gains (β) of up to 300 were obtained under dc conditions and I_{CO} was less than 10^{-7} A at room temperatures. A typical value of common-base cut-off frequency was 70 Mc/s.

25,873 HIGH GAIN MICROPOWER TRANSISTORS by M. Guilliano, R.M. McLouski, C.Z. Leinkram and E. Goins (Westinghouse); Proc. IEEE, Vol. 52, p. 712, June 1964

Surface effects which greatly affect the low-current alpha for double-diffused n-p-n transistors are described. The large effects of the surface recombination component of base current have been seen empirically and are here described. A comparison of collector and base current as a function of emitter-base voltage for standard process transistors and transistors which have been annealed in hydrogen prior to metallizing is presented. The hydrogen heat treatment greatly increases the transistor gain. The hydrogen-annealed transistor exhibits useful gain down to extremely low current levels (e.g. $h_{FE} = 33$ with $I_C = 1$ nanoampere). The nonhydrogen treated transistor exhibits normal high gain in the usual region of operation ($I_C > 10 \mu\text{A}$), but h_{FE} drops rapidly below this level. The hydrogen treatment used on these silicon wafers is accomplished by heating for 10 to 30 minutes at a temperature from 600 to 800°C.

25,874 CONTACT STRUCTURES FOR LARGE TRANSISTORS by H. Armstrong (Pacific Semicond.); U.S. Pat. 3,124,640, Issued Mar. 10, 1964

An improved method of making closely-spaced large-area electrical contacts to semiconductor devices is described. These contacts have efficient heat transfer characteristics and are capable of producing transistors that can operate at high-current densities. The transistor itself is produced in the usual planar geometry with interleaving combs of emitter and base regions over the collector region. Contact is made to these regions by sets of similarly shaped but somewhat smaller and narrower conducting electrodes or fins, placed on their ap-

appropriate regions of conductivity and either alloyed or gold bonded on. Details of conducting fin materials and bonding procedures are outlined.

MAGNETOELECTRIC DEVICES

Bibliography on Hall Effect Devices - See 25,344

25,875 THE HALL GENERATOR AND ITS APPLICATION [in German] by H. Weiss (Siemens-Schuckertw., Erlangen); *Solid State Electronics*, Vol. 7, pp. 279-289, May 1964

The basic phenomena connected with the design of a Hall effect device and the parameters of efficiency, Hall voltage, linearity and temperature of the device are discussed. Many applications require a careful design of an appropriate magnetic circuit. With Hall generators made of InAs or InSb it is possible to construct contactless sensors and multipliers for a great number of industrial applications.

25,876 NOISE IN HALL-EFFECT SENSORS by M. Epstein (IIT Res. Inst.); 1964 IEEE Intl. Conv. Rec., Part 8, pp. 84-90, Mar. 1964

The sensitivity of Hall-effect magnetometers for the measurement of very small magnetic field fluctuations depends on the noise at the Hall terminals of the sensor. A study of this noise indicates that its power spectrum is similar to that of the conventional current noise in the specimen. An analytical model was assumed in which the specimen was divided into mutually uncorrelated elements of resistance fluctuation. The noise generated at the Hall terminals was then obtained by summing the contributions of the individual resistance elements. The potential fluctuations at the Hall terminals are due to both the resistance fluctuations of the individual elements and the associated current redistribution in the sensor. Comparison of the experimental results with computed values of the analytical model for generation-recombination noise indicates that the mutually uncorrelated elements of resistance fluctuation are squares of sides equal to four diffusion lengths of the excess carrier density. The analytical model was utilized to evaluate the signal-to-noise ratio in Hall-effect sensors. The results, obtained for sensors made of intrinsic germanium indicate that the optimum signal-to-noise ratio is acquired for a Hall-effect sensor of width-to-length ratio of one half.

25,877 HALL GENERATORS: WHAT, WHY AND HOW MUCH? by S. Rubin (NBS); 1964 IEEE Intl. Conv. Rec., Part 8, pp. 74-83, Mar. 1964

A brief tutorial introduction to the galvanomagnetic effects, the Hall effect and the magnetoresistive effect is presented. The characteristics of the Hall effect of interest in engineering applications are outlined, and a list of applications is given. Standards of terminology and measuring methods being evolved are discussed. The concept of linearity error as the departure of the actual characteristic of a device from the straight line graph is fully discussed. An example of its application in a magnetic flux density (magnetic induction) measuring application is given. The common sensitivity index for Hall generators, the product sensitivity, is discussed, and two additional indices, the current and magnetic sensitivities, are introduced. The relations between the three and the advantages of each are considered. Equations are presented which allow the derivation of either one of the other two, if one of the three indices is known.

25,878 DEVELOPMENT OF IMPROVED HALL EFFECT SENSORS by L.J. Greenstein and M. Epstein (IIT Res. Inst.); Cont. NObsr85057, 165 pp., Dec. 1963; U.S. Gov. Res. Rep., Vol. 39, p. 27(A), May 5, 1964

The results of various studies on the development of highly sensitive Hall effect probes, and the incorporation of these probes in the design of a portable, low frequency, magnetic field spectrum analyzer are presented. Several of the subtasks performed on the program resulted in the enhanced capability of magnetic field instrumentation utilizing Hall effect probes. Among the results obtained are (a) the development of a simple technique for achieving predetection magnetic field filtering; (b) the development methods for suppressing carrier frequency components at the outputs of ac-biased Hall sensors; and (c) the optimization of Hall output transformer circuits for dc-biased magnetometers. These results have been utilized in the design of the magnetic field spectrum analyzer, as well as in the development of a three-axis magnetometer. In addition, an investigation has been conducted concerning the possible utilization of magnetoresistive effects in semiconductors, with particular applications to magnetic field detection and true rms metering.

25,879 HALL-EFFECT DEVICES FOR LOW LEVEL MAGNETIC DETECTION by N.P. Milligan and J.P. Burgess (Ohio Semicond. Div. of Tecumseh Prod.); *Solid State Electronics*, Vol. 7, pp. 323-333, May 1964

The design and performance of improved low-level magnetic detection devices combining optimized Hall plates and magnetic concentrators are described.

The factors relating to the fabrication of a high gain concentrator are presented and a Hall effect device compatible with this magnetic structure is then developed. Wide band width, stable operation, shock and vibration, output voltage, power requirements and optimum semiconductor selection materials, all relative to low level performance, are considered. Performance data from several devices are presented and operational characteristics discussed. The relationships of concentrator length and air gap of Hall plate thickness are utilized to provide magnetic gains of over 100 times that of the ambient magnetic field. Indium arsenide, indium antimonide and other III-V compound semiconductor devices are shown to be ideally suited for this application due to the combination of high mobility, high purity and temperature characteristics. Exceptional performance is achieved in one sensor designed for operation at -196°C. This sensor exhibits an overall sensitivity of over 3000 V/A kG as well as exceptional stability. Finally, a method is outlined which will cancel any distortion the concentrator would have created in respect to the source field which is being measured.

25,880 HALL-EFFECT VECTOR-PRODUCT GENERATORS by W. Saraga and R.K.P. Galpin (AEI); *Solid State Electronics*, Vol. 7, pp. 335-342, May 1964

Whereas conventional Hall multipliers make no use of the vectorial aspect of the Hall effect, the devices discussed here are genuine vector-product generators, able to accept vectorial input signals and to produce an output signal in the direction of, and proportional to, the vector product of the input-vectors. The devices generate either an output vector of fixed direction from two rotating input vectors, or a rotating output vector from one rotating and one fixed-direction input vector (the rotation occurring at constant angular frequencies). In the first case an output signal containing either the sum or the difference of the input frequencies is obtained. In the second case separate vectorial output components, rotating in the same plane and at the same angular frequency but in different directions, can be extracted; in this way positive frequency differences can be distinguished from negative differences. Possible applications of such devices to telecommunication problems are indicated. The validity of the new principle was confirmed with a cube-shaped Hall-element with low efficiency, and with a cruciform element with improved efficiency (a thin-plate version, possessing the efficiency of conventional Hall multipliers is also discussed).

25,881 A SILICON HALL ELEMENT FOR APPLICATION IN AN ANALOG MULTIPLIER by O.J. Mengali and T.S. Shilliday (Battelle); *Solid State Electronics*, Vol. 7, pp. 379-385, May 1964

A Hall element with characteristics suitable for application in an analog multiplier has been designed and developed. General multiplier specifications call for inputs to ± 2 mA and $\pm 10^4$ G maximum. Stability and circuitry considerations led to the selection of silicon for the element material. Using approximately 150 Ω -cm n-type silicon, the resulting elements exhibited outputs of 1.6-1.7 volts at maximum input current and magnetic field and outputs of about 1 mV at maximum input current and zero magnetic field. Error in element output is generally less than ± 0.5 per cent of full scale range at room temperature over the full range of input parameters.

25,882 NON-LINEAR HALL-EFFECT TERNARY LOGIC ELEMENT by C.F. Kooi and J.L. Weaver (Lockheed Res. Lab.); *Solid State Electronics*, Vol. 7, pp. 311-321, May 1964

Ternary logic appears to offer advantages over binary logic. In order to realize the potential advantages, a basically ternary device of simple and inexpensive construction must be available. It must also form by itself or with other logic elements, a functionally complete set of logic elements. In addition, it must have as many of the commonly useful properties of logic elements as possible. A ternary-logic device utilizing the non-linear magneto-conductivity tensor in a high mobility semi-metal (bismuth) has been constructed and operated. Together with its complementary element formed by reversal of the output leads, it forms a functionally complete set. The device also exhibits other desirable properties and a few undesirable properties. These are discussed in some detail. Excellent agreement is obtained between theoretical operation of the device and actual laboratory operation.

25,883 ON THE THEORY OF HALL-EFFECT ISOLATORS FOR TUNNEL DIODE AMPLIFIERS by H. Kroemer (Varian Assoc.); *Solid State Electronics*, Vol. 7, pp. 291-310, May 1964

Hall isolators are four-terminal semiconductor devices similar to Hall generators that permit unidirectional signal transmission, like ferrite isolators. Compared to the latter they are inherently broad-banded, including dc operation, but also lossy. Losses below 10 dB can easily be achieved. The impedance of Hall isolators can easily be made to match that of tunnel diodes. By combining the two devices the diodes can be operated closely to critical matching, producing amplification large compared to the insertion loss of the isolator and resulting in substantial overall unidirectional gain, combined with excellent stability. The amplifiers are frequency limited primarily by the tunnel diodes provided the isolator is kept thin compared to the skin depth. Because of the

Faraday rotation thick isolators are impractical. For most practical applications one must compensate for the temperature dependence of the mobilities in the isolator. This can be done by using heavily doped isolators with partial impurity scattering, by self-heating of the isolator to a desired temperature, and by changing the dc operating point of the tunnel diodes.

25,884 MULTIPLYING ACTION OF THE MAGNETORESISTANCE EFFECT IN SEMICONDUCTORS AND ITS APPLICATION TO POWER MEASUREMENT by S. Kataoka (Electrotech. Lab., Tokyo); 1964 IEEE Intl. Conv. Rec., Part 8, pp. 91-98, Mar. 1964

A theory has been developed on the multiplying action of the magnetoresistance effect in comparison with that of the Hall effect. The multiplication sensitivity in the same semiconductor is practically the same for both effects; it may be enhanced several times by redesigning the magnetoresistive element. Experiments were made on the multiplication characteristics of polycrystal InAs and InSb and satisfactory agreement with theory was obtained. Applications to power measurement were demonstrated at DC, AC and microwave frequencies and the temperature dependence, influences of power factor and bias instability were investigated. Application results show good performance in linearity and voltage gain with some advantages over Hall effect devices.

Magnetoresistivity of InSb Corbino Disks - See 25,338

Hall Effect Device of InSb Films - See 25,334

FERRITE DEVICES

25,885 HEXAGONAL FERRITE ISOLATORS by D.R. Taft (Sperry Microwave); J. Appl. Phys., Vol. 35, pp. 776-778, Mar. 1964

Waveguide bandwidth isolators requiring virtually no externally applied magnetic field have been developed for the millimeter wave frequency range. These ferrimagnetic resonance-type devices utilize highly anisotropic uniaxial hexagonal ferrites. The specific ferrite compounds used are from the two families $\text{BaO} \cdot 2\text{NiO} \cdot \Delta\text{Al}_2\text{O}_3 \cdot (8-\Delta)\text{Fe}_2\text{O}_3$ and $\text{SrO} \cdot \delta\text{Al}_2\text{O}_3 \cdot (6-\delta)\text{Fe}_2\text{O}_3$ denoted $\text{Ni}_2\text{W}(\Delta\text{Al})$ and $\text{SrM}(\delta\text{Al})$, respectively. The substitution variables Δ and δ were adjusted to yield different materials whose effective magnetic anisotropy fields were appropriately spaced over the range 16 to 30 koe. This spacing permitted their use in isolator designs throughout the frequency range 50 to 90 Gc/sec. Five materials from the $\text{Ni}_2\text{W}(\Delta\text{Al})$ family were used to cover the frequency range 50 to 60 Gc/sec and 12 materials from the $\text{SrM}(\delta\text{Al})$ family covered the range 60 to 90 Gc/sec. Pertinent electrical properties of these materials are reported as well as techniques essential to their successful application in the isolator structure. Waveguide bandwidth isolators using these materials were developed for the bands 50 to 75 and 60 to 90 Gc/sec.

25,886 A BROAD-BAND TAPERED FIELD RESONANCE ISOLATOR by J.H. Collins and T.M. Heng (The University, Glasgow); Electronic Engrg., Vol. 36, pp. 250-252, Apr. 1964

The design of a broad-band resonance isolator using a transversely varying external dc magnetic field is described. A simple theory for the required magnetic field taper is given. This is compared with the field gradient obtained from the fringing field between the poles of a magnet. A ratio of reverse to forward loss of 80 has been achieved experimentally, over the frequency range 7.5 Gc/s to 11.5 Gc/s, with a 0.300in by 0.100in by 3.25in F5X magnesium-manganese ferrite slab mounted in standard X-band waveguide.

25,887 USE OF SINGLE CRYSTAL FERRIMAGNETIC GARNETS AT UHF by A.J. Marriage (Philips Elect. Ind.); Proc. IRE, Austral., Vol. 25, pp. 90-95, Feb. 1964

The performance and low frequency limits of typical nonreciprocal UHF devices using polycrystalline yttrium iron garnet (YIG) are described. A comparison is made of the magnetic properties of polycrystalline YIG and single crystal material. The use of single crystal YIG as a magnetically tunable resonator element is described and theoretical predictions are made of the possible performance of various materials in the UHF and microwave band. The necessity of a reduced saturation material for use at UHF is shown and also the desirability of using an ellipsoidal shape. A description is given of the equivalent circuit of the composite resonator and coupling circuit and also of the methods used to determine the unloaded Q, the external Q and the loaded Q of the composite circuit. Measurements have been made on resonator circuits using aluminium substituted YIG to find the variation of Q with frequency, the orientation of crystallographic axes and the coupling parameter.

25,888 A NOVEL FERRITE QUARTER-WAVE PLATE by J. Helsen (Sylvania); Radio and Electronic Engrg., Vol. 27, pp. 955-958, June 1964

Coupled-wave theory is applied to make an adjustment to the length of an elliptical Faraday rotator to obtain a ferrite quarter-wave plate with non-

reciprocal properties. A ferrite rotator can be interposed between two such quarter-wave plates and matrix algebra used to obtain a new reciprocal ferrite phase shifter. A pulsed 180° non-reciprocal phase shifter is also described.

25,889 SOME UNIQUE DESIGNS OF MICROWAVE FERRITE PHASE SHIFTERS by H. Jones and F. Reggia (Harry Diamond Lab.); HDL TR 1189, 21 pp., Dec. 30, 1963; U.S. Gov. Res. Rep., Vol. 39, p. 37(A), Apr. 20, 1964 AD 428 429 OTS \$1.60

Several unique types of microwave ferrite phase-shifter designs are described. Each type offers certain distinct advantages when used in the laboratory and in microwave systems. The most salient feature of these low-loss devices is the design compactness, consistent with optimum electrical performance. The electrical characteristics of these phase shifters and their components are given. These characteristics show that as much as 500° of phase shift can be achieved in x-band with a one-in. spacing between input and output ports. In each case, only a small magnetic field strength is required to obtain the desired phase shift. Other features of these ferrite devices include simplicity in construction, low cost and small physical size.

25,890 A RECIPROCAL FERRITE PHASE SHIFTER by G. Buchta (Philips Res. Lab., Germany); Proc. IEEE, Vol. 52, pp. 304-305(L), Mar. 1964

A reciprocal phase shifter with a thin slab of ferrite asymmetrically fixed against the side wall and magnetized parallel to the broad wall of the waveguide is described. That this structure was a reciprocal phase shifter was verified by experimental investigations in the x-band. High power handling capabilities are a result of the thermal contact between the ferrite and the metal waveguide wall permitting forced cooling. Measured curves for phase shift and insertion loss of a MnMg-ferrite slab (9mm x 3mm cross section, 135mm over-all length, ends conically tapered over a length of 35mm) at 9.1 kMc are shown. The insertion loss is less than 0.4db and a shift of up to 300 degrees for an applied magnetic field of 670 oersteds was seen.

25,891 DEVELOPMENT OF A FERRITE MATERIAL FOR A HIGH-POWER PHASE SHIFTER AT S-BAND (Airtex); Cont. NObsr87388, 123 pp., Jan. 15, 1964; U.S. Gov. Res. Rep., Vol. 39, p. 30(A), June 5, 1964

Data obtained on gallium and aluminum substituted nickel ferrite are presented. The material which seemed best capable for use in a phase shifter had a total aluminum plus gallium substitution of 0.975 moles. The composition was $\text{Ni}_{0.98}\text{Mn}_{0.02}\text{Ga}_{0.30}\text{Al}_{0.674}\text{Fe}_{1.02504}$. This material had a Curie temperature of 200°C, a 20Mc tan delta of approximately 0.003, a saturation magnetization of approximately 970 gauss, and a χ'' at resonance of approximately 4.0 at 930 gauss. This material when hot pressed did not show any decrease in relative susceptibility at power levels as high as 2000 KW, whereas magnesium manganese ferrite showed non-linear effects at a power level of 20 KW.

25,892 ISOLATORS, RADIO FREQUENCY REFLECTION CU- ()/U DU- PLEXERS CU ()/U AND HIGH POWER CIRCULATORS (Sperry Microwave); Cont. AF30 602 1630, 139 pp., Mar. 1964; U.S. Gov. Res. Rep., Vol. 39, p. 47(A), June 20, 1964 AD 437 300 OTS \$11.00

A series of ferrite duplexers and isolators were developed for operation in the 400 to 2000 mc region. The first phase was a feasibility study at low power levels in which ferrite material processing techniques and microwave performance capabilities were investigated. The second phase utilized the information generated in the first phase to develop additional components for high power applications. Differential phase shift duplexers in WR-1800 and WR-975 waveguide, and an octave bandwidth resonance isolator in 7/8-in. coaxial line were developed in connection with the feasibility study of Phase I. Additional differential phase shift duplexers in WR-975 and WR-2100 waveguide were designed in Phase II, along with WR-650, WR-975 and WR-1500 resonance isolators.

25,893 ON SOLID STATE CIRCUITS by S. Hamilton, W.W. Heinz, S. Okwit, E.W. Sard and K. Siegel (Airborne Instr.); Cont. AF30 602 2699 Iv, Oct. 1963; U.S. Gov. Res. Rep., Vol. 39, p. 35(A), May 5, 1964 AD 429 724 OTS \$10.10

Results are presented of a study program to advance the state of the art in UHF limiters, octave-band ferrite circulators, and low-noise receivers having linear phase response suitable for pulse-compression applications. Two practical varactor limiters were developed -- a broad-band configuration (octave range) using a PN diode, and a low threshold ultra-dynamic range configuration. The broad-band limiter was successfully tested at high pulse powers using a 1-megawatt radar. Its burnout energy was in excess of 87,000 ergs, provided 30 db of protection, had a recovery time of 0.5 μsec, and did not exhibit any spike leakage. The low-threshold limiter had a limiting level of less than -20 dbm, an insertion loss of less than 2 db, and a dynamic range of about 70 db. A comprehensive theoretical and experimental technique was developed that was applied to the design and development of octave-wide Y-junction ferrite circulators. These circulators had isolations of greater than 20 db, SWR's of less than 1.4, and insertion losses of about 0.5 db over the

complete octave range.

25,894 DEVELOPMENT OF C-BAND BEACON FERRITE DUPLEXER PHASE III (Sperry Microwave); Cont. DA36 039sc89158, 1v., Oct. 1963; U.S. Gov. Res. Rep., Vol. 39, p. 49(A), Apr. 20, 1964 AD429 315 OTS \$8.10

Several possible approaches to the required C-band duplexer-limiter package were considered to meet the stringent electrical and mechanical requirements. Two principal designs were evaluated: (1) a four-port junction circulator used in conjunction with a high power coaxial load and broadband fixed-tuned gyro-magnetic coupling limiter, and (2) the same circulator and load but with a low-threshold subsidiary resonance limiter followed by a varactor limiter. In the course of the program the latter configuration was chosen as the most promising approach. Both approaches are discussed to the extent to which they were investigated.

25,895 BIASED FERROMAGNETIC MULTI-PORT MICROWAVE CIRCULATOR by C. Bowness (Raytheon); U.S. Pat. 3,136,962 Issued June 9, 1964

A nonreciprocal N port microwave circulator is described. This circulator can be matched in all arms, and all ports are symmetrical about a common geometrically central axis. Ferrite material is placed axially symmetric about the axis within the circulator, and a magnetic field is supplied along the axis.

25,896 A FAST-SWITCHING HIGH POWER C-BAND FERRITE CIRCULATOR by L.M. Silber and A. Weis (Polytechnic Inst Brooklyn); 1964 IEEE Intl. Conv. Rec., Part 2, pp. 32-36, Mar. 1964

A differential phase shift circulator for C band has been developed using non-reciprocal transverse field ferrite elements of novel configuration. In this configuration the non-reciprocal phase shifters are constructed using ferrite toroids with a wire running axially inside the ferrite to magnetize it to remanence. This configuration realizes two advantages. First, the magnetizing coil is inside the waveguide rather than outside and it is not necessary to propagate the switching pulse through the waveguide walls. Second, the ferrite toroids form a closed magnetic path. This allows the ferrite, once magnetized, to remain at remanence without having to maintain the magnetizing current. The circulator uses two 90° differential phase shift sections (gyrators), a magic tee, and a short-slot hybrid coupler. The switching pulse is supplied by a line pulser which would supply current pulses of alternate polarity at the required current (30 amperes). The circulator operated over a frequency range of 4.9 KMc/sec to 5.6 KMc/sec, with insertion loss of 1.3 db or less, and isolation of 20 db or more, at peak powers up to 550 KW, average power 100 to 200 watts. The device switched at all peak powers up to 550 KW, in 20 nano seconds or less.

25,897 RECIPROCAL FERRITE SWITCH BASED ON A SLOT BRIDGE by V.S. Averbakh and Yu. M. Zhidko; In News of Higher Educational Inst. Min. of Higher and Secondary Specialized Educ., USSR, Radio Eng. Ser., pp. 98-113, Dec. 4, 1964; STAR, Vol. 2, p. 404(A), Feb. 23, 1964 JPRS 22132 OTS 63-41289 \$4.00

An analysis is presented of the operation of a ferrite switch, consisting of a power divider, two ferrite phase shifters and a slot bridge. The influence of the errors in the individual units of the switch on its operation as a whole is estimated. Results are presented of an experimental investigation of a ferrite switch, designed to operate over a wide frequency range.

25,898 AUTOMATIC OPTIMIZATION OF CHARACTERISTICS OF A FERRITE SWITCH by V.V. Koshelev and V.I. Talanov; In News of Higher Educational Inst., Min. of Higher and Secondary Specialized Educ., USSR, Radio Eng. Ser., pp. 224-233, Dec. 4, 1963; STAR, Vol. 2, p. 405(A), Feb. 23, 1964 JPRS 22132 OTS 63-41289 \$4.00

A model of an automatic tuning system is described. The system was investigated in order to ascertain the possibility of automatic optimization of the characteristics of the ferrite switch by variation of the ferrite parameters. Automatic tuning of the ferrite switch was obtained by variations in the signal frequency although the circuit could not be used with excessively low levels of a high frequency signal.

25,899 A FERRITE SLOW-WAVE STRUCTURE FOR BACKWARD-WAVE APPLICATIONS by J.H. Collins and T.M. Heng (U. Glasgow); J. Electronics and Control, Vol. 16, pp. 241-255, Mar. 1964

The propagation of electromagnetic energy through a small diameter cylindrical waveguide partially filled with a ferrite medium is analysed by a quasi-static approx. based on Maxwell's equations and the Polder permeability tensor. It is shown that for the passband where the diagonal component of the permeability tensor is negative, a slow HE₀₁ mode can exist which exhibits characteristics suitable for backward-wave applications. The design parameters are reviewed and an example is given pertinent to a possible S-band backward-wave oscillator.

25,900 RADIATION FROM A FERRITE CYLINDER by J.C. Palais (U. Mich.); J. Appl. Phys., Vol. 35, pp. 779-781, Mar. 1964

A theoretical and experimental investigation has been made of a ferrite in the aperture of a rectangular waveguide. This problem is representative of a general class of problems where an anisotropic obstacle is superimposed on an isotropic discontinuity. In the example treated by the diffraction approach, a simple solution has been obtained which predicts and explains the observed phenomena. A modified aperture is especially interesting because it offers good opportunity for directly measuring the effects of ferrite obstacles on rf fields. It also has the practical advantage of serving as a scanning antenna. The analysis of this radiating structure is also shown to apply to circulators that use cylindrical ferrites. In general, the theory shows that the energy in the far fields is directed at some angle ϕ with respect to pure forward scatter. A corresponding asymmetry is also present in the field plots inside the ferrite. The field displacement within the material is shown to explain this far field beam shift. Experimentally, continuous scanning from a waveguide was obtained over $\pm 30^\circ$ with a MgMn ferrite post 0.297 in. (0.754 cm) in diameter and with applied fields of less than 300 G. The frequencies were from 9.0-10.3 Gc/sec. The low reflection coefficients obtained make this a practical antenna. Beam patterns are presented, as are curves comparing the theoretical and experimental results.

25,901 MILLIMETER WAVE GENERATION USING FERROMAGNETIC MATERIALS by G.L. Heiter (Stanford U.); Cont. DA36 039AMC00041E, 228 pp., Oct. 1963; U.S. Gov. Res. Rep., Vol. 39, p. 134(A), May 5, 1964 AD 429 717 OTS \$16.00

Generation of millimeter waves with ferromagnetic materials by using pulsed magnetic fields as the energy source is discussed. Two specific types of generators were studied. The first utilized an external (low microwave frequency) rf magnetic field applied to a spherical yttrium iron garnet (YIG) sample to establish the initial precession angle in a conventional ferromagnetic resonance experiment. Successful operation of this generator was obtained in the K-band range and V-band range, yielding peak pulsed powers of about 700 mW and 25 mW, respectively, with pulse widths in the order of 10 nsec in both cases. The second type generator, which uses crystalline anisotropy to achieve the initial precession angle, was originally proposed for cubic materials. A more detailed quasistatic analysis of its operation is presented, together with attempts to verify the performance of this scheme experimentally.

25,902 RECENT DEVELOPMENTS IN PERMANENT MAGNETISM by M. McCaig (Permanent Magnet Assoc., Central Res. Lab., Sheffield, England); J. Appl. Phys., Vol. 35, pp. 958-965, Mar. 1964

The properties of permanent magnets together with their theoretical background are reviewed. The study of micromagnetics has shown that because of processes such as fanning, buckling, and curling, the high energies once predicted for elongated single domain particle magnets are unlikely to be obtained by shape anisotropy alone. There may be a better chance of obtaining high energies from materials with crystal anisotropy or if displaced loops due to exchange anisotropy could be produced in a practical material at room temperature. The properties of barium ferrite are due to crystal anisotropy, but its magnetization is low. Other materials with high crystal anisotropy at present require expensive materials or manufacturing processes. The properties of Alnico V and related alloys can be explained in terms of shape anisotropy due to two-phase structure. Progress has been made in a group of high coercivity alloys containing more than 4% Ti and 29% Co. A single crystal of one of these alloys has given the highest (BH)_{max} so far obtained, but it is only recently that it has been discovered that small additions of S or Se enable these alloys to be made columnar by simple methods.

25,903 A REVIEW OF THE PROBLEM OF FINE-PARTICLE INTERACTIONS WITH SPECIAL REFERENCE TO MAGNETIC RECORDING by E.P. Wohlfarth (Imperial Coll.); J. Appl. Phys., Vol. 35, pp. 783-790, Mar. 1964

The problem of interactions between the fine iron oxide particles used in the coatings of magnetic recording tapes is reviewed. Particular attention is paid to the factors influencing the initial susceptibility of the anhysteretic remanence curve which is related to the sensitivity of the tape under high-frequency biasing conditions. As a satisfactory discussion of particle interactions and the anhysteretic process is not possible, it is necessary to rely on a number of theoretical models which are considered critically. For pairs of particles interacting positively or negatively a complete discussion is, however, possible, and this introduces the concept of anhysteresis as a growth process. This concept is then extended as far as possible to assemblies, where it is seen to be necessary to modify the usual Preisach model in a number of essential ways. The characteristic properties of several different recording tapes, namely the reduced saturation remanence and the initial anhysteretic susceptibility, are tabulated and discussed. Results for some other hard magnetic materials are also considered.

25,904 COUPLED BIAXIAL FILMS by H. Chang (IBM Watson Res. Ctr.); J. Appl. Phys., Vol. 35, pp. 770-771, Mar. 1964

Biaxial films were proposed by Pugh for storage elements of a noncoincident memory. In this paper, it is demonstrated that two identical uniaxial films with their easy axes at a right angle and driven by interposed striplines that carry currents also exhibit biaxial properties.

25,905 OPTIMIZATION OF MAGNETIC PARAMETERS IN THIN FILMS DRO STORAGE ELEMENTS by R. J. Petschauer, W. V. Rausch and P. L. Morawetz (Fabri-Tek, Hopkins, Minn.); J. Appl. Phys., Vol. 35, pp. 766-767, Mar. 1964

The digit current margins of a DRO magnetic film memory are determined by the disturb and writing or restoring thresholds. In an actual memory these thresholds will vary with both the film parameters and the drive line configuration. The effect of the magnetic parameters of the storage elements on these thresholds is determined by measuring the digit current margins of storage element arrays of varied magnetic parameters in a test apparatus simulating the memory operations and drive line configuration. A figure of merit calculated from these margin measurements is introduced and is used to determine the optimum film parameter values. To illustrate the effectiveness of the technique, data obtained during the experimental determination of optimum array coercivity are presented and the resultant figure of merit is discussed. Results indicate that array coercivities of 2.5 to 2.6 Oe yield maximum digit current margins. Interpretation of results of restore current measurements in terms of skew and dispersion currents is also presented.

25,906 THE FERREED by A. Feiner and R. L. Peek, Jr. (Bell Labs Rec.); Vol. 42, pp. 71-74, Feb. 1964

The development and operation of the Ferreed electromechanical switching capsule are discussed. This device consists of two magnetic reeds sealed in a glass tube which make contact when acted on by a magnetic field. In addition to the reeds, the Ferreed contains one or more remanent magnetic members whose magnetization can be changed by current in associate coils. These magnets supply the "operate" and "release" pulse which make and break the reed contacts. The Ferreed has been used in two and four wire crosspoint arrays, and is also applicable wherever short pulse operation of metallic contacts is desirable.

25,907 MAGNETIC CORE DEVICE by F. L. Post (IBM); U.S. Pat. 3,126,530, Issued Mar. 24, 1964

Multiperture cores requiring only one wire through each hole are detailed. Hole geometry is such that a proper sequence of winding excitation will switch the core's flux patterns and cause an appropriate voltage in the sense winding. One version, a square shape with rounded corners, has a center hole and a hole at each corner. Current flows through a wire passing through two adjacent holes in a clockwise sense with respect to the center opening. A read-write wire passes through the center, an inhibit conductor through another aperture and a sense element through the last. The first wire is continuously energized except when reading or writing is performed.

25,908 MAGNETIC MEMORY DEVICE WITH ORTHOGONAL INTERSECTING FLUX PATHS by C. L. Wanlass, Jr. (Ford); U.S. Pat. 3,134,964, Issued May 26, 1964

A memory device adapted for construction as a sanitary package for plug-in use is described. It is comprised of a block of magnetic material having at least three conductors passing through it, the read and write conductors are parallel to each other and the sense conductor is perpendicular to the read and write wires. The device utilizes fanning sheets of magnetic material for ease of wiring that can be closed for insertion in the computer. An increase in operating speed by a factor of 100 is obtained.

26,909 AN APPROACH TOWARDS BATCH FABRICATED FERRITE MEMORY PLANES by E. A. Bartkus, J. M. Brownlow, W. A. Crapo, R. F. Elfant, K. R. Grebe and O. A. Gutwin (IBM, Yorktown); IBM J. Res. Dev., Vol. 8, pp. 170-176, Apr. 1964

A technique for the batch fabrication of ferrite memory arrays in which wire, previously coated with a thermoplastic, is formed into two orthogonally disposed sets of parallel wires is described. These grids are oriented between opposing molds having matched grooves filled with a fluid mixture of ferrite powder and thermosetting resin, in such a manner that one set of parallel wires coincides with the groove axes. After suitable curing this structure is released and heat treated to pyrolyze the organic materials and sinter the ferrite. A yield study on 108 memory arrays produced in this manner resulted in a yield of 72.2% on pulse testing under simulated operating conditions and an overall process yield of 36.1%. The electrical characteristics of the arrays are tabulated and the applicability of the technology to various modes of operation and its potential for high-speed (250 nsec magnetic cycle time) operation are briefly discussed.

25,910 CONTROL OF PROPERTIES OF MAGNETIC THIN FILMS FOR SHIFTING REGISTER by A. C. Tickle (Intl. Computers and Tabulators Ltd.); J. Appl. Phys., Vol. 35, pp. 768-769, Mar. 1964

Domain wall motion, thick film (>2000 Å), Shift registers of Ni-Fe-Co alloys are described. Operation depends on the fact that the critical threshold field H_s required to introduce a reverse domain into a saturated, uniaxial, anisotropic, magnetic film is greater than the critical threshold field H_0 required to move walls of already existing domains. The nucleation factor $\eta = H_s/H_0$ must be large to obtain a wide tolerance in the shifting field, H , as $H_0 \leq H \leq H_s$, and to obtain high speed since wall velocity varies as $H-H_0$. Kerr effect measurement of domains in a register show a tendency for domains to nucleate at film edges when shifting fields are applied, the nuclei growing to represent spurious information. This is prevented by reducing film thickness at the edges. Another difficulty involves remanent nuclei that remain unshifted when domains are propagated along the film. This may be prevented by applying biasing fields of about 10e to erase the remanent nuclei. Shift registers with a packing density of 40 bits/in, cycle times of 1 μ sec, shifting fields of 14 oe and biasing fields of 10e have been fabricated.

25,911 INTERACTION BETWEEN MAGNETIC FILM STORAGE ELEMENTS by P. L. Bonyhard (Intl. Computers and Tabulators Ltd.); J. Appl. Phys., Vol. 35, pp. 764-765, Mar. 1964

The effect of the dimensions and relative separations of storage elements upon interaction is considered in a plane geometry, word-organized, ferromagnetic thin-film computer store. Interaction consists of the switching of a fraction of the magnetization of the storage element and may result in the loss of stored information. Interaction between adjacent digits of the same word (digit interaction) and that between corresponding digits of adjacent words (word interaction) are distinguished. Interaction is measured by the reduction of the output voltage of the storage element. An experiment is described in which interaction is measured using strip-line conductor patterns of different widths and pitches to define storage element in the same area of continuous magnetic film. The results show how word interaction increases as the pitch of the word lines is reduced and that digit interaction reduces as the word line width is reduced. The interaction between elements in a continuous magnetic film is compared to that between discrete rectangles of film produced by etching or by masked evaporation. Discrete elements are found to give less word interaction especially if the film thickness is over about 800 Å. Films varying in thickness from a few 100 Å to a few 1000 Å are examined and the properties relevant to storage, and interaction in particular, are compared. Although there is not obvious correlation between interaction and film thickness for thinner films, both word and digit interaction increases with film thickness for thicker films.

Switching in Magnetic Films - See 25,467-25,469

25,912 VARIABLE AXIS MAGNETIC FILMS by A. Schmeckenbecher (Sperry Rand); U.S. Pat. 3,124,490, Issued Mar. 10, 1964

The fabrication and characteristics of Fe and Ni magnetic films having variable magnetization axes are described. The films rapidly reverse their magnetization direction under alternating magnetic fields, the perpendicular easy and hard axes exchanging places. Application of a high field pulse changes the threshold field. These two effects introduce two new parameters for computer logic components. The films obtain their new properties by the association of a small amount of an interstitial element (C or N). The diffusion of the interstitials from one set of sites to another and the presence of single ferromagnetic domain areas separated by carbide, etc. phases provide an explanation of film behavior.

25,913 THE EFFECT OF CONDUCTING SUBSTRATES ON THE SWITCHING OF FERROMAGNETIC THIN FILMS by P. L. Bonyhard (I.C.T. Ltd.); J. Electronics and Control, Vol. 16, pp. 339-347, Mar. 1964

The use of conducting substrates in a ferromagnetic thin film computer store alters the switching behaviour of storage elements. The effect of the conducting substrate can be calculated by solving the equation for the diffusion of eddy currents into the substrate. The solution is outlined for the case of a drive field due to a current in a strip line conductor, and for the case of a stray field due to an inhomogeneous distribution of magnetization in the thin film. Values of field are enumerated by approximation for the former case. For fast switching the effect of the conducting substrate is to double all tangential fields and this gives rise to an increase of the apparent value of the anisotropy field, H_k . This effect is demonstrated by an experiment where the storage element configurations, corresponding to conducting and non-conducting substrates, respectively, are compared directly.

Magnetic Hysteresis Properties of Ni-Mn Ferrite Toroids - See 25,475

25,914 WIDE-TEMPERATURE-RANGE FERRITE CORES FOR COMPUTER MEM-

ORIES by H.P. Lemaire, H. Lessoff and E. Fortin (RCA Electronic Comp.); RCA Rev., Vol. 25, pp. 308-318, June 1964

The operating temperature range of a ferrite memory is determined primarily by the temperature coefficients of the break current and the output of the cores. The break-current and output characteristics of the new lithium-ferrite cores are relatively independent of temperature, and the use of these types of cores will substantially increase the operating range of memory devices over that obtainable with conventional types. Experimental data are given to show, as a function of temperature, the typical response characteristics of practical wide-temperature-range cores of two different sizes; one has an outside diameter of 50 mils and an inside diameter of 30 mils, the other an outside diameter of 30 mils and an inside diameter of 18 mils. The techniques used to design a core for operation in a specific temperature range are described. The performance characteristics of a memory plane that consists of a square array of 4096 wide-temperature-range cores are summarized.

25,915 FERRITE CORE STORAGE DEVICES by W.J. Bartik (Sperry Rand); U.S. Pat. 3,124,787, Issued Mar. 10, 1964

The effect of temperature on the operating characteristics of ferrite cores is discussed. The signal to noise ratio was found to increase with temperature for a constant drive current. The drive current, however, was found to decrease with temperature. An optimum operating temperature of 125°F was determined and a thermostat-heating unit capable of being enclosed within the storage matrices and of maintaining the temperature at 125°C is described.

25,916 OFFSET MAGNETIC CORE by R.J. Foster (Goodyear Aerospace); U.S. Pat. 3,127,591, Issued Mar. 31, 1964

A solution is offered for the thermal activity of the standard matrix of toroidal magnetic cores. Each flux change in a core generates heat. Rapid switching may thus cause the magnetic properties of a magnetic core to be temporarily modified. Furthermore, the heat is distributed unequally throughout the matrix. It is recommended that cores of a nonstandard shape should be used. Offset cores consisting of a base portion and a diametrically opposed and longitudinally spaced top portion connected by two side portions, with surfaces normal to the longitudinal axis of the core, would alleviate the problem. A thermoconductive means engaging the parallel surfaces would result in a compact, thermally stable matrix.

25,917 ELECTRON BEAM MACHINING OF FERRITES by R.A. Shahbender (RCA Lab.); Proc. Natl. Electronics Conf., 1963, Vol. 19, pp. 545-553

Electron beam machining of ferrites with square loop characteristics to provide storage elements which are orders of magnitude smaller than those achieved using conventional fabrication techniques is described. The reduced size of the storage element poses some difficulties in effecting the required interconnections for memory operation. These interconnections may be partly completed by electron beam machining techniques. Data is presented showing the high degree of uniformity attained in the physical size of electron beam machined elements. This uniformity is partly achieved in the magnetic characteristics of the elements.

MASERS and LASERS

GENERAL

25,918 MASERS AND LASERS (SUPPLEMENT). A DDC REPORT BIBLIOGRAPHY by M.F. Aukland (Def. Doc. Ctr.); Mar. 1964; U.S. Gov. Res. Rep., Vol. 39, p. 146(A), May 20, 1964 AD 431 800 OTS \$2.25

25,919 LASERS AND MASERS by T.H. Maiman (Korad); Industrial Res., Vol. 6, pp. 52-59, June 1964

Present developments in the technology of lasers and masers is reviewed. The field has not reached its full potential for lack of better materials and processes. Practical requirements for any proposed application of lasers and masers are listed, and new developments in this technology are described. The injection laser is described as the most important advance since the birth of the field; other developments including the silicon carbide laser, a miniature helium-neon gas laser, and laser instruments are described.

25,920 REVIEW OF SOLID STATE LASERS by G.G.B. Garret (Bell Lab.); Quantum Electronics III, pp. 971-982, Columbia U. Press, 1964

The developments in the field of optically excited solid state lasers from the summer of 1960 are reviewed. Physical principles of laser operation, the

orders of magnitude involved, materials used in optical maser experiments, luminescent centers involved, different host lattices used and output characteristics of solid state lasers are discussed. Among output characteristics of laser beam, the power, the spectral distribution, near and far field patterns and spiking are the factors that have been examined.

THEORY

25,921 UNIFIED THEORY OF STEADY STATE CAVITY MASERS by D.E. McCumber (Bell Lab.); Quantum Electronics III, Columbia U. Press, 1964, pp. 95-100

A theoretical study of the properties governing specific performance criteria of steady state masers is presented. The properties are generally characterized in terms of the set of phonon autocorrelation functions which lend themselves to an unambiguous interpretation in terms of simple thought experiments. Each phonon function depends on relatively few correlation properties of the subsystems from which the maser has been constructed. The susceptibility function, based on the driven maser ensemble, reflects certain inherent nonlinearities.

25,922 STEADY STATE POPULATION DISTRIBUTIONS IN QUANTUM MECHANICAL SYSTEMS by W.A. Barker and J.D. Keating (McDonnell Aircraft); Quantum Electronics III, Columbia U. Press, 1964, pp. 741-749

The determination of steady state population distributions in a number of quantum mechanical systems is described. The systems involved are: (1) the three level microwave maser; (2) the three level optical maser; (3) the four level optical maser; (4) the four level push-push and push-pull microwave maser; and (5) dynamic nuclear polarization by the Overhauser effect. Expressions for the inversion condition, signal power output, and pump power absorbed for the microwave and optical maser are presented.

25,923 QUANTUM FLUCTUATIONS IN MASERS WITH LOSS by W.H. Louisell (Stanford U.); Quantum Electronics III, Columbia U. Press, 1964, pp. 65-69

A theoretical study has been made of quantum fluctuations (phonons) in a single mode of a cavity in thermal equilibrium at a positive temperature (T_L) and simultaneously coupled to a large number of $\frac{1}{2}$ spin particles in thermal equilibrium at a negative temperature ($-T_m$). The model used takes into account the effects of a finite cavity Q or load in a self-consistent quantum mechanical way. It is shown how the average number of noise quanta may be estimated and that it approaches a steady state value in agreement with the value of Planck.

25,924 OSCILLATION CHARACTERISTICS AND ITS TEMPERATURE DEPENDENCE OF A PULSED RUBY MASER by F. Saito (Nippon Elect.); Quantum Electronics III, Columbia U. Press, 1964, pp. 937-941

The relation between oscillation characteristics and relaxation processes in a pulse ruby maser at temperatures of 1.6 - 20°K is discussed. The preliminary experimental results have been interpreted qualitatively. A rigorous theory of maser oscillations cannot be realized without further experimental data over 20°K.

25,925 MULTIMODE OSCILLATIONS IN SOLID-STATE MASERS by H. Statz and C.L. Tang (Raytheon Res. Div.); J. Appl. Phys., Vol. 25, pp. 1377-1383, May 1964

Previous work by the authors on the effects of slow spatial cross relaxation is extended in two directions. First, off-axis modes are included in the calculations, and thus it becomes possible to calculate the number of oscillating off-axis modes as a function of the various laser parameters. In this way the expected beam angle of a laser can be predicted. Second, a more detailed analysis of the spiking behavior is given; both regular and irregular spiking trains may be obtained depending upon the laser parameters and the pump power.

25,926 MULTIMODE OSCILLATIONS IN SOLID STATE MASERS by H. Statz and C. Tang (Raytheon); Cont. AF19 628 3226, 29 pp., Oct. 1963; U.S. Gov. Res. Rep., Vol. 39, p. 162(A), May 20, 1964 AD 433 282 OTS \$2.60

Previous work on the effects of slow spatial cross relaxation is extended in two directions. First, off-axis models are included in the calculations, and it becomes possible to calculate the number of oscillating off-axis modes as a function of the various laser parameters. The expected beam angle of a laser can be predicted. Second, a more detailed analysis of the spiking behavior is given. Both regular and irregular spiking trains may be obtained, depending upon the laser parameters and pump power.

25,927 THEORY OF AN OPTICAL MASER by W.E. Lamb, Jr., (Yale U.); *Phys. Rev.*, Vol. 134(A), pp. A1929-1950, June 15 1964

A theoretical model for the behavior of an optical maser is presented in which the electromagnetic field is treated classically, and the active medium is made up of thermally moving atoms which acquire nonlinear electric dipole moments under the action of the field according to the laws of quantum mechanics. The corresponding macroscopic electric polarization of the medium acts as a source for an electromagnetic field. The self-consistency requirement that a quasi-stationary field should be sustained by the induced polarization leads to equations which determine the amplitudes and frequencies of multimode oscillation as functions of the various parameters characterizing the maser. Among the results obtained are: threshold conditions, single-mode output as a function of cavity tuning, frequency pulling and pushing, mode competition phenomena including frequency locking, production of combination tones, and population pulsations. A more approximate discussion of maser action using rate equations is also given in which the concept of "hole burning" plays a role.

25,928 THEORY OF RELAXATION SPIKES IN TWO-LEVEL LASER AMPLIFIERS by H.A. Trenchard (Westinghouse); *Quantum Electronics III*, Columbia U. Press, 1964, pp. 1089-1096

The theory concerning the origin of relaxation spikes in two-level laser amplifiers is discussed. The time-dependent Schroedinger equation is solved for a two-level electric dipole system acted on by an electromagnetic wave tuned to the frequency of the two level system. It is observed that this solution is exact, if spontaneous emission were to be neglected. The equation governing the change in intensity of an electromagnetic wave travelling through this medium is then obtained from above results. A numerical solution attempted for the above equation is shown to indicate the appearance of spikes generally encountered in ruby laser outputs.

25,929 CRITERIA FOR OPTICAL MASER AMPLIFIERS AND OSCILLATORS by J. Jacobs, D. Holmes, L. Hatkin and F. A. Brand (U.S. Army); *Quantum Electronics III*, Columbia U. Press, 1964, pp. 1071-1077

The output intensity for multiple internal reflection in a medium with a negative attenuation factor is discussed. The criteria for oscillations are given and an equivalent circuit for the laser amplifier is formulated. It is shown that there is a specific length for a given value of the attenuation constant for power (a) in the laser amplifier which corresponds to the maximum amplification conditions. At that point the power gains for the forward and backward waves are nearly the same. It is speculated that a backward wave amplifier can be developed and the conditions for oscillations in this hypothetical device are described.

CHARACTERISTICS

25,930 INFLUENCE OF SOME OPTICAL PROCESSES ON POPULATION INVERSION IN A THREE-LEVEL MASER by J. Glowacki (High School of Pedagogy, Gdansk Poland); *Acta Phys. Polonica*, Vol. 25, pp. 301-302, Feb. 1964

A method of enhancing the metastable level population in lasers with active organic substances is described. Under the influence of diamagnetic substances, the probability of intercombination transitions from an excited level, F , to a metastable level M increases. Owing to non-radiative transitions $F \rightarrow M$, the intensity of slow fluorescence is enhanced. It is therefore possible that in the presence of non-absorbing foreign diamagnetic molecules in active substances the power emitted due to stimulated emission will increase or the generation threshold can be lowered.

25,931 THE COHERENCE BRIGHTENED LASER by R.H. Dicke (Princeton U.); *Quantum Electronics III*, Columbia U. Press, 1964, pp. 35-54

A mirrorless coherence brightened laser which utilizes the Brownstew (Photo Correlation Effect) is described. Though formidable problems exist in the development of such a laser, the extremely short pulses that may be produced warrant the effort.

25,932 MEASUREMENT OF FACTORS AFFECTING THE THRESHOLD OF A CONTINUOUSLY OPERATING RUBY OPTICAL MASER by D.F. Nelson and D.E. McCumber (Bell Lab.); *Quantum Electronics III*, Columbia U. Press, 1964, pp. 1037-1043

The measurement of threshold populations of the metastable levels by studying the nonlinearity of the fluorescence versus the optical pumping power is described. The nonlinearity is used to deduce the fractional population of the levels. A major difficulty with this approach is the absorption of fluorescent intensity on pumping power for different viewing directions. The population at 77°K has been calculated, taking this difficulty into account, and has been compared to the experimental value.

25,933 VARIATION OF REFRACTIVE INDEX DURING LASER OPERATION by J.R. Izatt, H.A. Daw and R.C. Mitchell (New Mexico State U. Agricul., Eng. and Sci.); *Cont. Nonr* 3531 04, 22 pp., Jan. 1964; *U.S. Gov. Res. Rep.*, Vol. 39, p. 63(A), Apr. 5, 1964 AD 427 725 OTS \$7.75

The refractive index of a laser in the region of anomalous dispersion surrounding the active laser frequency should vary as the relative population of states changes. The behavior of the multimode cavity depends on the index of refraction of the laser material, and hence this effect influences the temporal evolution of the mode structure in the cavity. Variation in refractive index as a function of the distribution of population among pertinent energy states can be studied experimentally. The latter is optically pumped to achieve a sequence non-Boltzmann population distribution, and an interferometric technique is employed to determine refractive index as a function of frequency for each distribution. Several items of equipment are described which were designed and constructed to partially fill the optical pumping and temperature control requirements of the experiment. A unique cast-plastic optical-pump cavity is described which has displayed high optical efficiency in addition to being durable and economical.

25,934 DYNAMIC LIMITATIONS ON THE ATTAINABLE INVERSION IN RUBY LASERS by W.R. Sooy, R.S. Congleton, B.E. Dobratz and W.K. Ng (Hughes Aircraft); *Quantum Electronics III*, Columbia U. Press, 1964, pp. 1103-1112

Dynamic limitations in ruby lasers have been studied in terms of depumping mechanisms. Of the various depumping mechanisms possible only internal modes are thought to present a problem with current laser types. For future development of high gain devices, spontaneous decay, super-radiance, pre-lasing and lateral depumping should be considered. A combination of immersion, selective filtering and end wall canting are suggested to eliminate limitations arising from internal modes, pre-lasing and lateral depumping. Spontaneous decay and super-radiance cannot be eliminated by the above techniques since the two effects are intrinsic limitations.

25,935 FRUSTRATED TOTAL INTERNAL REFLECTION AND APPLICATION OF ITS PRINCIPLE TO LASER CAVITY DESIGN by I.N. Court and F.K. von Willisen (GE Electronics Lab.); *Appl. Optics*, Vol. 3, pp. 719-726, June 1964

A general treatment of the phenomenon of frustrated total internal reflection is presented and numerical results are given which are related to cavity resonator design parameters. A minimum loss, minimum alignment requirement resonator is described offering a maximum of versatility. Experimental results of quasi-cw and single-pulse Q switching with a ruby optical maser are presented.

25,936 LASER DEVICES EXPLORATORY INVESTIGATION (Hughes Res. Lab.); *Cont. AF33 657 11650*, 82 pp., Jan. 31, 1964; *U.S. Gov. Res. Rep.*, Vol. 39, p. 137(A), May 5, 1964 AD 429 856 OTS \$7.60

Pinhole mode selectors have been successfully analyzed by a theory which does not depend on the assumption of differences in propagation angle between different transverse modes. The frequency spacing between transverse modes was determined to be 160 ± 40 Mc in a 1-in. ruby, agreeing with effectively-curved-reflector resonator theory. Regular spiking in a Hughes Model 200 laser appears to be correlated with simultaneous excitation of many transverse modes. Experiments intended to decrease the emission line width of chromium in spinel by varying the host composition have not yet been successful. The optical spectroscopy of Pr^{3+} -doped LaF_3 was studied; the microwave spectrum of LaF_3 doped with terbium indicated the presence of Tb^{4+} .

25,937 A LASER WITH A MULTIHOLE DIAPHRAGM by T. Morokuma (NBS); *J. Res. NBS*, Vol. 68C, pp. 25-34, Jan.-Mar. 1964

The properties of a laser with a multihole diaphragm are theoretically and experimentally examined. This "multibeam laser" produced laser action in the optical paths defined by the position of the holes and the cavity configuration. Interference fringes were observed on one of the cavity mirrors. A wavelength dependent interaction among the beams was also observed. It is believed that the wavelength of a beam can be stabilized by the intensities of the other beams.

25,938 TIME DEPENDENCE OF RUBY LASER EMISSION AT 78°K by A. Szabo (Nat'l. Res. Council, Canada); *J. Appl. Phys.*, Vol. 35, pp. 2263-2264(L), July 1964

The time delay for the oscillation onset of the $\bar{E} \leftrightarrow 3/2 \text{ } ^4\text{A}_2$ transition has been confirmed. Direct time delay measurements were made by simultaneous monitoring of line intensities. The dependence of the time delay on pump power agrees with observations made during optical pumping experiments. Paramagnetic absorption sharply decreases and then increases; the sudden increase is associated with the oscillation of the $\pm 1/2$ line.

25,939 STIMULATED OPTICAL EMISSION FROM RUBY AT LIQUID NITROGEN TEMPERATURE by V.K. Konjukhov, L.A. Kulevsky and A.M. Prokhorov (Acad. Sci. USSR); Quantum Electronics III, Columbia U. Press, 1964, pp. 1067-1070

A spectral characteristics of a ruby laser at $T=77.4^\circ\text{K}$ are reported. At threshold pumping the laser beam had only a short wave component corresponding to the transition to the sublevel $\pm 3/2$. With increased pumping, a second long wave component corresponding to sub level $\pm 1/2$ was observed. Above threshold pumping the contribution of the long wave components reached 0.21 ± 0.01 from the short wave component energy and it was found to be independent of the total energy. Component intensity varied sharply with time. The component $\pm 3/2$ was observed to oscillate beyond 0.5 ± 0.8 msec; the time increased as the pumping became larger. The component $\pm 1/2$ oscillated at 0.15 ± 0.1 msec and decreased with pumping energy increase.

25,940 CORRELATION OF LASER THRESHOLD WITH THE OPTICAL QUALITY OF RUBY by C.M. Kellington, M. Katzman and S.K. Poultney (USAERDL); 12 pp., Dec. 1963; U.S. Gov. Res. Rep., Vol. 39, p. 141(A), May 20, 1964 AD 431 243 OTS \$7.60

Measurements of the threshold for laser action and of the optical quality of fabricated ruby are presented. The correlation between the two is displayed.

25,941 INFLUENCE OF OPTICAL QUALITY ON RUBY LASER OSCILLATORS AND AMPLIFIERS by D. Bortfeld, R. Congleton, M. Geller, R. McComas, L. Riley, W. Sooy and M. Stitch (Hughes Aircraft); J. Appl. Phys., Vol. 35, pp. 2267-2269(L), July 1964

Availability of a ruby cylinder with nearly perfect optical properties has made it possible to study the effects of optical quality on laser performance. Experimental measurements have shown that the optical quality is critically important where beam divergence or radiance are important, i.e., wherever power and energy density in the far field must be high. Optical quality does not influence energy extraction in amplifiers, but small-angle scattering is deleterious in oscillators. An essentially diffraction limited beam was observed from a high quality ruby in a nonmode-selected, giant pulse oscillator.

25,942 SOME THEORETICAL ASPECTS OF A PROPOSED DOUBLE QUANTUM STIMULATED EMISSION DEVICE by P.P. Sorokin and N. Braslau (IBM Yorktown); IBM J. Res. and Dev., Vol. 8, pp. 177-181, Apr. 1964

A double quantum stimulated emission device with some operating characteristics and relevant systems of materials is discussed. The device presented is realizable under assumptions compatible with current knowledge and state of the art regarding optically pumped solid state lasers. Requirements for triggering and time development of the giant pulse needed are theoretically presented. A possible triggering scheme uses silicate glass rods doped with either Ho^{+3} or Tm^{+3} . These ions lase around 2μ ; the exact frequency will be a function of the selective reflectance of multiple dielectric layers.

25,943 PARALLEL THETA-PINCH PUMPING OF A LASER OSCILLATOR-AMPLIFIER by J. Hitt and J. Feldman (Carnegie Inst. Tech.); Proc. IEEE, Vol. 52, pp. 616-617(L), May 1964

The high luminosity theta-pinch optical pump has been modified so that a single capacitor can simultaneously drive two parallel ring discharges. The resulting pair of optical pumps has been employed to excite two laser rods arranged as an oscillator-amplifier combination. The apparatus and experimental procedure are described. An additional amplifier rod improves the rise time, peak power and total energy output.

25,944 INJECTION-LUMINESCENCE PUMPING OF A $\text{CaF}_2:\text{Dy}^{2+}$ LASER by S. Ochs and J. Pankove (RCA Lab.); Proc. IEEE, Vol. 52, pp. 413-414, June 1964

The successful pumping of a $\text{CaF}_2:\text{Dy}^{2+}$ laser by injection luminescence is reported. $\text{GaAs}_x\text{P}_{1-x}$ diodes were used at pumped-helium temperatures to provide optical pumping for durations of up to 0.2 seconds. The absorption spectrum of divalent dysprosium in CaF_2 is due to a transition promoting one of the 4f electrons to the 5d state. The lasing fluorescence takes place at 2.36μ between two 4f levels. The most intense absorption band occurs at about 7200 Å (1.72 eV). This corresponds to the emission spectrum of a forward biased p-n junction in a $\text{GaAs}_{0.73}\text{P}_{0.27}$ alloy at 77°K . One hundred of these diodes were arranged in an array around the laser rod to pump it. Oscillograms of the pumping current and laser output are presented.

25,945 CATHODOLUMINESCENCE FOR $\text{CaWO}_4:\text{Nd}$ LASER PUMPING by J.W. Ogland, C.W. Baugh and W.E. Horn (Westinghouse); Appl. Phys. Lett., Vol. 4, pp. 133-134(L), Apr. 1, 1964

Laser pumping of a Nd-doped calcium tungstate crystal by means of cathodoluminescence is discussed. The pump consists of a phosphor-coated quartz tube surrounded by an assembly of four thermionic electron emitters. The phos-

phor was coated with an aluminum film, to provide electrical connection and to trap most of the light within the quartz tube. The phosphor-coated quartz tube is cooled by nitrogen gas passed through a T-shaped quartz tube in which the laser rod is inserted. The cooled gas passes by the laser rod and returns in the space between the two tubes. The efficiency of a cathodoluminescent pump is dependent on the optical coupling for phosphor radiation of the coated cavity and the laser crystal. For the equipment in which these measurements were performed, the optical coupling is about 55%. This value can be raised by improvements in the reflectivity of the phosphor and reduction of the non-reflecting cavity area.

25,946 CONTROL OF LASER PERFORMANCE by G.E. Danielson, Jr. and A.J. DeMaria (United Aircraft); Mar. 31, 1964. 18 pp.; U.S. Gov. Res. Rep., Vol. 39, p. 112(A). June 5, 1964 AD 434 166 OTS \$1.60

Investigations on a research program relating to the control of laser output are described. Studies of the effect on laser output control of varying the refractive index of a medium in a laser cavity are being carried out with ultrasonic, electric, or magnetic means. The following experimental results were obtained: 1. Initial tests of the glass prism light shutter were conducted with a visible He-Ne laser beam which was mechanically chopped at approximately 83 cps to facilitate modulation percentage measurements. Experimental results showed that approximately 80% modulation was obtained. 2. Gating of a $3 \times 1/4$ in. dia. Nd^{3+} doped glass laser rod with one megacycle transducers bonded to the ends produced an increase in peak and total output power. 3. Recent investigations of ultrasonic cell configurations have disclosed that an improved ultrasonic standing wave can be obtained with the use of one complete cylindrical transducer instead of two 180 degree focusing sections which were previously proposed.

25,947 A REVIEW OF OPTICAL-ULTRASONIC INTERACTION WITH ILLUSTRATIVE APPLICATIONS TO COHERENT LIGHT PHENOMENA by V. Suprunowicz and A.J. DeMaria (United Aircraft); Proc. Nat. Electronics Conf., 1963, Vol. 19, pp. 564-568

The preoccupation of most investigators with laser modulation methods which make use of the wide bandwidths available in the optical region of the electromagnetic spectrum has tended to overshadow the considerable utility of narrow bandwidth modulation schemes. Narrow band modulation systems utilizing optical-ultrasonic interaction have been demonstrated as holding considerable promise as identification "markers" for light beams, voice modulators of light, a means of deflecting light, etc. These functions are performed with extremely simple apparatus which as a consequence are quite inexpensive and highly reliable. Following a presentation of the history and theory of optical-ultrasonic interaction as applied to incoherent sources, the application of such methods as a means of controlling lasers are discussed.

25,948 MULTIMODING IN LASERS by R.H. Pantell (Standard Telecommun. Lab., Ltd.); J. Appl. Phys., Vol. 35, pp. 1404-1408, May 1964

It is well established that multimoding occurs in lasers within the homogeneous linewidth of the active medium. The oscillations at more than one frequency can be explained on the basis of the spatial or time dependence of the population difference. A threshold condition for multimoding is obtained in terms of the maximum power density from the laser with a single frequency output.

25,949 NEW MODES OF OPTICAL OSCILLATION IN CLOSED RESONATORS by R.J. Collins (Inst. Def. Anal.) and J.A. Giordmaine (Bell Lab.); Quantum Electronics III, Columbia U. Press, 1964, pp. 1239-1246

New modes of optical oscillation in closed resonators have been studied. Small nonuniformities in surface reflectivity or volume may cause interaction among certain degenerate modes having unique propagation directions and may produce new modes of higher Q and lower oscillation threshold, thus providing a mechanism for mode selection. Nonuniform reflectivity may provide a mechanism for axial emission from circular rods and off axial bouncing-ball emission.

25,950 OPTICAL MASERS by W. Culver (Res. Corp., N.Y.); U.S. Pat. 3,136,959, Issued June 9, 1964

Mode enhancing techniques involving the use of reflectors having varying patterns of reflectivity are discussed. One mode of oscillation has a higher Q than other modes and coherence is thereby increased.

25,951 OPTICAL MASER by P. Kisliuk and D. Kleinman (Bell Lab.); U.S. Pat. 3,134,837, Issued May 26, 1964

An optical maser with a well defined output line which is suitable for communications applications is described. Mode suppression is obtained by the addition of another reflective surface to the Fabry-Perot resonator structure. The additional reflector discriminates against undesirable modes by increasing their losses relative to losses in other modes.

25,952 CHARACTERISTICS OF RUBY LASER MODES IN A NOMINALLY PLANE PARALLEL RESONATOR by V. Evthuv and J.K. Neeland (Hughes Res. Lab.); Quantum Electronics III, Columbia U. Press, 1964, pp. 1405-1414

The characteristics of transverse modes in a ruby laser are discussed. The modes are similar to those of a resonator with curved but not necessarily spherical end plates. Most ruby lasers operate in such modes or a superposition of them rather than in modes of a truly plane-parallel resonator. Laser action is likely to start at areas of greatest effective end plate curvature for rubies of large cross section, since the modes in such areas have the lowest losses. However, it is not known whether the effective end-plate curvature during laser action is the same as that of an unpumped sample. In the far field the ruby laser output consists of a central spot resulting from superposition, interference of excited modes and Fabry-Perot rings, believed to be unrelated to the true mode.

25,953 THE EFFECTS OF TEMPERATURE ON RUBY OPTICAL MASER MODE SEQUENCES by M.C. Adamson, T.P. Hughes and K.M. Young (AEI Res. Lab.); Quantum Electronics III, Columbia U. Press, 1964, pp. 1459-1467

Oscillation modes of a ruby laser were observed at temperatures between 77 and 290°K. Lowering the temperature narrowed the R_1 line profile and restricted the number of allowed longitudinal modes in the splitting of the R_1 line when observed at 113°K. Oscillation occurred first in the large wavelength component and then in the other component. The output consisted of spikes from small active areas of the crystal face at temperatures down to 77°K. Occasionally more than one longitudinal mode was observed in a single spike. At regions close to oscillation threshold and at lower temperatures the spikes were found to be less intense; and increase in pumping power increased the spike intensity and numbers so that the output appeared continuous. Changes in transverse mode numbers produced measurable changes in wavelength because of the small active area dimensions. Transverse mode patterns were relatively insensitive to temperature variations.

25,954 COMPETITION BETWEEN INTERNAL AND EXTERNAL MODES OF A RUBY LASER by A. Korpel and J. Free (Zenith Radio); Proc. IEEE, Vol. 52, pp. 619-620(L), May 1964

A convenient and simple way to investigate in detail mode competition in lasers is described. Far field distribution, measurement of the threshold for external lasing as a function of neutral density, and monitoring the time-varying output in both modes simultaneously were utilized to study the mode competition. It is shown that the external mode is the first to set in, although its presence does not prevent the internal mode from setting in some time later. As the neutral density increases, the time difference between the onset of these two modes decreases at a neutral density of 0.8, the external mode virtually disappears.

25,955 RESONATOR INFLUENCE ON TEMPORAL CHARACTER OF LASER OUTPUT by M. Katzman and J.W. Strozyk (USAERDL); Proc. IEEE, Vol. 52, pp. 433-434(L), Apr. 1964

The results of an experiment designed to demonstrate that the temporal character of a laser output is strongly influenced by the resonator length for a resonator composed of spherical mirrors are given. The laser medium is ruby which is inserted in a spherical mirror resonator formed by two mirrors. The experiment consists of varying the mirror spacing D in increments of 1 cm from the concentric position of 20 cm beyond the concentric. At a mirror spacing of $D + 5$ cm, the distinct regions in the laser output disappear leaving a random spiking with a reduced pulse length and average amplitude. The oscillation at $D + 9$ cm closely resembles the usual output when a ruby in a Fabry-Perot is pumped close to threshold.

25,956 OSCILLATORY CHARACTER OF $\text{CaWO}_4:\text{Nd}^{3+}$ LASER OUTPUT by E. Brenal, J. Ready and D. Chen (Honeywell); Proc. IEEE, Vol. 52, pp. 7710-7711, June 1964

Some results of a study of the oscillatory character of a pulsed $\text{CaWO}_4:\text{Nd}^{3+}$ laser are described. The output consists of a regularly spaced train of spikes (relaxation oscillations) with decreasing amplitudes. The train of oscillations develops from a single spike at threshold with additional spikes appearing one at a time as the pumping energy is increased. The lack of a beat note when the spiking behavior is regular indicates oscillation in a single longitudinal mode. Complete numerical solutions were obtained by computer to the full rate equations. These solutions had regularly spaced spikes which have exponentially decaying amplitudes. The agreement between theory and experiment is good with respect to spike spacing, spike width, number of spikes, relative amplitude of the spikes and development of the train of oscillations with increasing pump energy.

25,957 STUDY OF LASER OUTPUT PARAMETERS AND MEASUREMENT TECHNIQUES by E.R. Schineller, H.M. Heinemann, H.W. Reslien and R. A. Kaplan (Wheeler Lab.); Cont. AF30 602 3132, 163 pp., Feb. 1964; U.S. Gov. Res. Rep., Vol. 39, p. 160(A), May 20, 1964 AD 433 174

OTS \$12.00

A detailed study was made of the laser parameters associated with system applications involving both energy and information transfer. The approach to the study included a discussion of the fundamental properties of EM radiation, independent of specific laser types, the determination of system parameters, and their relation to these fundamental properties. The specific output parameters of the solid state, gaseous, and diode lasers were computed theoretically and finally measurement principles were reviewed. The study resulted in definitions of a wide variety of parameters needed to describe the many different properties of laser radiation in space and time. However, the parameters have been grouped with respect to applications to provide unification and simplification. The results are presented in a set of tables of indicated system parameters, system relations and the applicable laser parameters.

25,958 CRITERIA FOR THE STABILITY OF RUNNING WAVES IN LASERS by J.A. White (Natl. Bur. Stand.); Bull. Am. Phys. Soc., Vol. 9, p. 560(A), June 1964

Suppose that 2 waves of the same polarization and angular frequencies ($\omega_1 \approx \omega_2$) propagate in opposite directions through an amplifying medium of fixed atoms with the single atomic frequency ω_{atom} and decay constant γ . At saturation, the waves should be stable against the growth of one at the expense of the other if $|I(x, y)I(y, x)| < 1$, where $I(x, y) = \frac{1}{2}[4 + x^2 + y^2 + 2xy^3 - y(x^2 - 1)X(x + 2y)](1 + y^2)^{-1}[1 + (x - y)^2]^{-1}$, with $xy = \omega_1 - \omega_{\text{atom}}$, $\gamma\gamma = \omega_2 - \omega_{\text{atom}}$. Coexistence of the 2 waves should be unstable, in particular, for stationary radiation for all $x = y$ if the amplifying medium is at rest, or if $\omega_1 = \omega_2 = \omega_0$ and the medium is moving uniformly so the $\omega_{\text{atom}} = \omega_0(1 \pm v/c)$ for $x^2 = y^2 < 1/5$. For a dilute gas of randomly moving atoms, coexistence becomes stable in the limit of large Doppler broadening for $[1 + (\omega - \omega_0)^2/\gamma^2]^{-1} < 1$. Here, $\omega = (\omega_1 + \omega_2)/2$. In a laser, with 3 mirrors adjusted to reflect light around the edges of a triangle, oppositely directed waves with the same frequency and polarization may coexist for gaseous but normally not for solid amplifying media.

25,959 SPECTRAL ANALYSIS, SPATIAL AND TEMPORAL RESOLUTION OF PULSES EMITTED BY A RUBY OPTICAL MASER [in French] by J.C. Vienot and J. Bulabois (Fac. Sci., Besancon); Quantum Electronics III, Columbia U. Press, 1964, pp. 1469-1475

Laser emission studies utilizing high speed continuous photographs of Fabry-Perot rings are discussed. High intensity pulses of 10^{-8} sec. duration followed by spike sequences of longer duration, periodic over 15 cycles, were observed. The spectral profile was as limited as that observed by static photography.

25,960 COHERENCE, SPECTRA TIME SCANNING AND PULSATIONS OF LASER EMISSION by Z. A. Chizhikova, M.D. Galanin, V.V. Korobkin, A.M. Lenotovitch and V.N. Smortchkov (Akad. Sci. USSR); Quantum Electronics III, Columbia U. Press, 1964, pp. 1483-1491

The time dependence of excitation of the axial modes excited in each pulsation of laser emission and coherence and spectra time scanning of laser emission at temperatures of +20 to -165°C have been observed in a ruby laser. Michelson interferometric studies of emission interference at -165°C revealed interference fringes that were less sharp. Data obtained from a Fabry-Perot interferometer and a high speed mirror camera are also discussed.

25,961 DIFFUSION OF RESONANCE RADIATION IN RUBY by F. Saito (Nippon Elect.); J. Phys. Soc. Japan, Vol. 19, p. 759(L), May 1964

The presence of radiation diffusion and imprisonment in solids has been confirmed. The temperature dependence of $1/B$, the radiative decay time of a cylindrical sample, can be described by a modified diffusion equation with the boundary condition being a 3-dimensional extension of Milne's theory.

25,962 THE EFFECTS OF SATURATION AND REGENERATION IN RUBY LASER AMPLIFIERS by J.I. Davis and W.R. Sooy (Hughes Aircraft); Appl. Optics, Vol. 3, pp. 715-718, June 1964

An analytic expression which relates the input and output energies of a ruby laser amplifier has been derived for the general situation in which both saturation and regeneration are present. The solution also includes all other special cases (e.g., weak signal and/or no regeneration) which have been independently treated in the past. The results obtained from the analysis have been compared with those obtained by numerical integration of the nonlinear partial differential equations governing the amplification process, and the agreement is excellent. The majority of situations encountered in practice fall within the limits of the assumptions made in the analysis.

25,963 THE DETERMINATION OF OPTICAL BANDWIDTH FROM PHOTO-ELECTRIC MIXING EXPERIMENTS WITH RUBY LASERS by M. Lipsett (Perkin-Elmer) and L. Mandel (Imperial College, G.B.); Appl. Optics, Vol. 3, p. 643(L), May 1964

The ambiguity between the photoelectric spectrum of radiation from coupled atomic systems or from a system would not arise in a photoelectric mixing

experiment using light beams from two independent ruby lasers. Observations have been made of beats in such an experiment made with ruby crystals that exhibit the phenomenon of spiking. Beat notes were observed, indicating a coherence time ξ of order 0.5 μ sec. For pulses shorter than 0.5 μ sec, ξ is presumably limited by the pulse width. Operation of the ruby laser quasi-continuously with pulse durations of some hundreds of μ sec. led to beats which did not have a common geometry.

25,964 DISTRIBUTION OF RADIATION FROM A RECTANGULAR LASER ROD (RUBY) by H. Hora, B. Kronast and H. Kunze (Inst. Plasma Phys., Garching, Germany); Proc. IEEE, Vol. 52, pp. 611-612, May 1964

The distribution of emission from a truncated rectangular ruby crystal which is totally reflecting at one end, (i.e., ground and polished in the shape of a wedge) is described. Emission was seen to start in the truncated corners of the crystal just above threshold, and spread inwards from the corner until the whole face emitted as pump power was increased. The possibility that this behavior was due to a mode mechanism was eliminated by changing the resonator length without appreciable change in the emission behavior pattern. It was established by calculation of the internal light intensities that this behavior was due to the geometry of the rod, since greater light intensity, and therefore pumping action occurs in the corners.

25,965 BEAM ANGLE AND OUTPUT ENERGY OF RUBY LASER IN EXTERNAL MIRROR ALIGNMENT by P.H. Kim and S. Namba (Inst. of Phys. Chem. Res.); Japan J. Appl. Phys., Vol. 3, pp. 305-306, May 1964

Beam angle and output energy of the ruby laser using the plane or hemispherical mirror as a method of mode selection are reported. The ruby rod used is 63mm long and 6.3mm in diameter. The reflector was installed at 20cm, 40 cm, and 60cm away from the output end of the ruby and aligned parallel to it. The beam angle is experimentally found to decrease as the distance between the output end surface of the ruby and the external reflector increases, and the output energy also decreases nearly inversely proportional to the square of the beam angle.

25,966 TEMPORAL COHERENCE BETWEEN SUPERPOSED LIGHT BEAMS FROM TWO RUBY OPTICAL MASERS by M.S. Lipsett and L. Mandel (Imperial College, U.K.); Quantum Electronics III, Columbia U. Press, 1964, pp. 1271-1276

An experimental set up for the measurement of temporal coherence between superposed light beams from two ruby lasers is described. Results obtained show that transient coherence may exist between independent ruby lasers for periods of the same order as the spike widths and that the line widths for certain components are a few Mc.

25,967 STUDIES OF THE COHERENCE TIME FOR PULSED RUBY LASER EMISSION by D.A. Berkeley and G.J. Wolga (Cornell U.); Quantum Electronics III, Columbia U. Press, 1964, pp. 1097-1101

Studies have been made on the coherence time of pulsed ruby laser emission. One objective was to determine whether temporal coherence extended from pulse to pulse so that fringes could be observed when one pinhole was illuminated by a particular laser while another was illuminated by a pulse that preceded or followed it. Such interference fringes have been observed for delay lengths as large as 2520 cm; fringe visibility was poor for delay lengths of 3000 cm. Coherence time corresponding to delay lengths of 3000 cm was estimated at 0.1 μ sec. A simple model for a laser emission pulse has been developed to account for the experimental results. The coherence time should be measured for each parameter of the physical detail of the laser such as geometry, temperature, etc, since the time need not be the same for different configurations.

25,968 CW SOLID STATE OPTICAL MASER (LASER) (Bell Lab.); Cont. DA36 039sc89068, 44 pp., July 15, 1963; U.S. Gov. Res. Rep., Vol. 39, p. 143(A), May 20, 1964 AD 431 601 OTS \$4.60

The following topics are discussed: (1) High gain traveling-wave optical amplifier, (2) Pumping-light energy distribution in ruby rods, (3) Ruby oscillation linewidth, (4) Investigations of rare-earth spectra in yttrium aluminum garnets, (5) Nonlinear dielectric properties of KTaO_3 near its Curie point, (6) the Diffraction-limited oscillator.

25,969 POWER-DEPENDENT SPLITTING OF THE R_1 DOUBLET IN RUBY LASERS AT 77°K by T.L. Stocker and M. Birnbaum (Aerospace); Bull. Am. Phys. Soc., Vol. 9, p. 499(A), Apr. 1964

Operation of ruby lasers at 77°K has shown that near threshold the splitting of the R_1 doublet agrees closely with the 0-field splitting determined by microwave methods (11.49 Gc/sec). Increasing the power decreases the doublet separation. At power levels about a factor of 3 above threshold for a rod of 0.6 cm diam and 7.5 cm length, splitting of about 10.60 Gc/sec has been observed. A model that considers the R_1 doublet to be a pair of over-

lapping Lorentzian lines is used to calculate the dependence of the splitting upon the power level. Saturation effects alter the contribution to the gain of the neighboring line, which results in a shift in the frequency at which the gain attains its maximum value. The predicted variation in the splittings agrees with the observed values.

25,970 PHOTON-PHONON INTERACTION IN GIANT-LASER PULSES by A. Bramley (Bramley Consult.); Bull. Am. Phys. Soc., Vol. 9, p. 500(A), Apr. 1964

A high-intensity coherent light beam can be sharply focused to produce a region L in which ∇E^2 becomes large. A solution of Maxwell's equations indicates that the propagation constant is markedly reduced and the field vectors modified by the existence of a longitudinal component. Furthermore, the electromagnetic energy density in region L may exceed its value averaged over the cross section of the light beam by a considerable factor. Another consequence of this high electromagnetic energy density is the change in the susceptibilities of the medium through which the beam is propagated. For field-dependent susceptibilities, classical electrodynamics predicts an optical force exerted on the medium. Inserting the field-dependent susceptibilities in Maxwell's equations, this force can be proved to be equivalent to the Lorentz force on the charge induced by the electromagnetic field, a charge apparently propagated with the light beam. A calculation based on a phenomenological approach, closely analogous to generation of Cerenkov radiation, predicts the generation and amplification of phonon waves by the charge distribution induced in region L by the electromagnetic field.

25,971 ON INTERFERENCE EFFECTS IN LASER SYSTEMS by V. Strizhetskii (USSR Acad. Sci.); Optics and Spectroscopy, Vol. 16, pp. 92-94, Jan. 1964

Some properties of interference phenomena in lasers are treated as a result of the multiple reflection of the light beam. For a fixed excess population in the upper states, the treatment is analogous to the theory of the linear light-wave amplifier. Consideration is given to a laser system with an active medium in the form of a homogeneous isotropic cylindrical rod. The formula arrived at wherein interference rings are visible in vacuum has been experimentally verified. Reasons for the broadening of interference rings include scattering on different inhomogeneities, finite line-width and nonlinear optical phenomena.

25,972 AN INTERFERENCE EXPERIMENT WITH TWO INDEPENDENT BEAMS OF RUBY LASER LIGHT by G. Mappay and L. Mandel (Imp. Col., U.K.); Quantum Electronics III, Columbia U. Press, 1964, pp. 1247-1252

Interference between two independent ruby laser beams is discussed and the fringes obtained are recorded. The experiment on interference is the spatial analog of optical beat experiments which have been performed with independent beams. Equations are derived for fringe visibility and the positions of fringe maxima and minima. The experimental set up uses an electronically gated image tube to photograph the fringes. Seven fringes were recorded, all having visibility below 10% due to a large difference between the center of frequencies and V_1 and V_0 of the beams.

25,973 SCATTERING OF STIMULATED EMISSION IN LASER MATERIALS by W.R. Mallory (GE); Appl. Optics, Vol. 3, pp. 727-729, June 1964

An important consideration in the determination of threshold for laser oscillation and of laser efficiency is the scattering and diffraction losses which are present in the resonant optical cavity. Previous techniques for measuring such losses include: (1) conventional techniques for small-angle scattering, and (2) variation of the cavity loss in a known manner [Collins and Nelson, Proc. on Opt. Instr. and Tech., K.J. Habell, ed. (Wiley, New York, 1963)]. The first technique leaves uncertain the acceptance angle of the resonant cavity for scattered radiation. This paper describes the extension of the second method to permit measurement of losses effective in prohibiting laser oscillation in materials which are not operative as laser oscillators. Thus, the technique discussed is useful in evaluating otherwise promising laser materials. Scattering losses in some potential organic laser materials are obtained using the technique described.

25,974 SIZE-DEPENDENT SPONTANEOUS ENERGY LOSS IN LASERS DUE TO SELF-STIMULATED EMISSION by T. Waite (North Am. Aviation Sci. Ctr.); J. Appl. Phys., Vol. 35, pp. 1680-1682, June 1964

Laser amplifiers when pumped to a significant degree of population inversion undergo decay via (1) natural spontaneous emission of radiation from individual excited atoms, and (2) a size-dependent decay due to self-amplification of the spontaneously emitted radiation which passes through a large fraction of the amplifier length before escaping. This latter effect has a definite size threshold near which the decay rate changes several orders of magnitude. The decay rate is roughly independent of size except near the threshold.

25,975 LOSS FACTORS AFFECTING RUBY LASER SYSTEMS by J. Masters, J. Ward and E.M.E. Murray (Tech. Ops.); Jan. 31, 1964, 76 pp.; U.S. Gov. Res. Rep., Vol. 39, p. 142(A), June 20, 1964 AD 437 608 OTS \$2.00

Efficient high-power output performance of ruby lasers depends largely on reducing the effect of two basic types of loss: (1) storage losses, or losses of atoms from the excited state that occur during the pumping phase, and (2) internal propagation loss suffered by stimulated emission; both are strongly dependent on geometric parameters. Internal propagation losses were found to be significant in ruby. Storage loss due to non-linear de-excitation during pumping is important. Preliminary measurements of the nonlinear de-excitation due to spontaneous emission amplification were performed under nonstandard operating conditions and found to be as large as 50% inversion loss for a large, cooled ruby sample. The limitations of simple physical models of ruby laser systems are discussed. Studies are reported of the important influence of mode coupling and mode selection upon the threshold condition for oscillation in ruby lasers.

25,976 PULSE PROPAGATION IN A LASER AMPLIFIER by J.P. Wittke (RCA) and P.J. Warter (Princeton U.); J. Appl. Phys., Vol. 35, pp. 1668-1672, June 1964

Pulse propagation in maser-type traveling-wave amplifiers with a homogeneously broadened transition is treated by a formalism analogous to the Bloch equations. Phenomenological dephasing (T_2) and recovery (T_1) times are defined, and a linear (nonsaturable) loss mechanism is included. In the numerical calculations, only the case of negligible excitation during the time it takes a pulse to pass is considered. When pulses are allowed to grow until the amplifier is "saturated", steady-state pulses having a unique shape and intensity independent of the initial pulse are found. The parameters of these steady-state pulses depend only on the ratio of the linear loss and gain coefficients. Steady-state pulses have a peak intensity that decreases monotonically from infinity to zero as the linear loss coefficient varies from zero to the gain coefficient, while the pulse width correspondingly varies from zero to infinity, and the pulse energy varies from a finite value to zero. Steady-state pulses propagate at a velocity less than that of the small signal velocity in the medium.

25,977 FILLING FACTOR AND ISOLATOR PERFORMANCE OF THE TRAVELLING-WAVE MASER by F.S. Chen and W.J. Tabor (Bell Lab.); Bell Sys. Tech. J., Vol. 43, pp. 1005-1033, May 1964

In designing a large gain and simultaneously large instantaneous band-width travelling-wave maser (TWM), the filling factor and the isolator performance should be optimized. The filling factor is a measure of the efficiency of interaction between the spin system of the maser material and the RF magnetic fields of the slow wave structure. For the TWM using the 90° operation of ruby and the comb as the slow-wave structure, the c axis of the ruby should be parallel to the z axis of the structure (the direction of the signal wave propagation) for the largest filling factor. The improvement of the filling factor by the proper orientation of the c axis of the ruby is larger at the lower signal frequencies because the transition probability of ruby is more nearly linear at those frequencies. An analysis of the filling factor and isolator performance and its comparison with measurements was made. Although the discussion is centered on the comb-type ruby TWM, the data provided also apply to other type slow-wave structures using different active crystals.

25,978 THEORY OF INTERMODULATION AND HARMONIC GENERATION IN TRAVELLING-WAVE MASERS by E.O. Schulz-DuBois (Bell Lab.); Proc. IEEE, Vol. 52, pp. 644-656, June 1964

Under high power conditions, a nonlinear response in the spin system of a maser is predicted by an analysis based on the density matrix formalism or the Bloch equations of motion. The coupling of the nonlinearities to the traveling-wave maser circuit is considered and the measurable power output at intermodulation and second harmonic frequencies is computed. For a typical traveling-wave maser with ruby maser material and a comb slow-wave structure, the computation yields

$$P(2\omega_1) = 2P(\omega_1) - 103.5$$

and

$$P(2\omega_1 - \omega_2) = 2P(\omega_1) + P(\omega_2) - 92$$

where, for example, $\omega_1 = 2\pi \times 4140$ Mc, $\omega_2 = 2\pi \times 4110$ Mc and the respective power levels are measured in dbm. These levels are well below noise under most conceivable operating conditions for masers used as low-noise receiver preamplifiers and, in this sense, the maser is a "better linear amplifier" than others. The theoretical predictions are in satisfactory agreement with experimental results.

25,979 MEASUREMENT OF INTERMODULATION AND A DISCUSSION OF DYNAMIC RANGE IN A RUBY TRAVELLING-WAVE MASER by W.J. Tabor, F.S. Chen and E.O. Schulz-DuBois (Bell Lab.); Proc. IEEE, Vol. 52, pp. 656-663, June 1964

Measurements of intermodulation in a ruby traveling-wave maser are reported.

The power level at frequency $2f_2 - f_1$ was measured when strong signals at frequencies f_1 and f_2 were applied to the maser. In agreement with theoretical predictions, the intermodulation level was found to be extremely weak. Results of the measurement can be expressed as

$$P(2f_2 - f_1) = 2P(f_2) - P(f_1) - 95$$

where $f_1 = 4110$ Mc, $f_2 = 4140$ Mc and the powers are measured in dbm. The pertinent characteristics of traveling-wave masers are summarized in a concluding section.

25,980 A TRAVELLING WAVE MASER FOR SATELLITE COMMUNICATIONS SYSTEMS by J.C. Walling and F.W. Smith (Mullard Res. Labs.); Quantum Electronics III, Columbia U. Press, 1964, pp. 923-930

Physical and operational features of a ruby travelling wave maser for satellite communication systems are described. Improvements for increasing the operating life and bandwidth to greater than 40 Mc before the net gain falls below 26 db are noted. The application of a superconducting magnet to overcome the effects of center frequency drift and for field stabilization is discussed.

25,981 INCREASE OF EFFICIENCY OF A TRAVELLING-WAVE RUBY MASER by V.B. Steinschleiger and G.S. Mizezhnikov (Acad. Sci. USSR); Quantum Electronics III, Columbia U. Press, 1964, pp. 957-961

The possibility of increasing the operation temperature of a traveling wave ruby maser by increasing the filling factor value, the group velocity slowing factor and the inversion ratio is discussed. A slow wave structure 115mm long that was loaded on both sides with 0.03% Cr-doped ruby gave an electronic gain of 40 db and a net gain of 28 db with a band width of 20 Mc; electronic gain is maximum at 0.03% Cr, the optimum concentration. The structure operated at $T=4.2^\circ\text{K}$ with pumping between the 1-4 levels.

25,982 TRAVELLING WAVE RUBY OPTICAL MASER by L.A. Kulevsky, P.P. Pashinin and A.M. Prokhorov (Acad. Sci. USSR); Quantum Electronics III, Columbia U. Press, 1964, pp. 1065-1066

A maser system with operating conditions similar to those of a ruby ring has been constructed to obtain information on the differences between the non-spiked output of a ruby laser and the usual spiked output of other lasers. This behavior is connected with the fact that positions of nodes and loops of radiation are not fixed in a crystal.

25,983 HIGH GAIN, HIGH POWER PULSED RUBY OPTICAL AMPLIFIERS by J.E. Geusic and H.E.D. Sconl (Bell Lab.); Quantum Electronics III, Columbia U. Press, 1964, pp. 1211-1220

The high gain and high power capabilities of a pulsed ruby travelling wave optical maser are described. A pulsed ruby oscillator may obtain output powers of 10^2 to 10^3 megawatts in a single mode. Applications of such a device would be in microdrilling, optical radar, and dielectric studies.

25,984 A HYDROGEN-LINE TRAVELLING-WAVE MASER, USING CHROMIUM-DOPED RUTILE by K.S. Yngresson (Chalmers Inst. Tech., Sweden); Quantum Electronics III, Columbia U. Press, 1964, pp. 899-910

A rutile maser operating at 1400 Mc and using a pump frequency of 45 kMc is described. Various means for obtaining a high inversion at such high pump-to-signal frequency ratios are discussed and it is shown that rutile compares favorably with ruby, although the inversion level is not as high as expected. The rutile maser has a Karp type slow wave structure and employs a garnet isolator suitable for low field (400-1000 G) operation.

25,985 TRAVELLING-WAVE MASERS EMPLOYING IRON-DOPED RUTILE by L.C. Morris and D.J. Miller (RCA); Proc. IEEE, Vol. 52, p. 410(L), Apr. 1964

The characteristics of a travelling-wave maser loaded with iron doped rutile are described. Amplification was achieved from 3 to 7 Gc with maximum gain of 20 db/inch measured at 4.2°K . The frequency response of the gain is plotted from 5 to 6 Gc. It is concluded that iron is superior to ruby as a maser material since it accommodates very low magnetic fields at nominal pump frequencies.

25,986 PROPOSAL FOR OBTAINING LASER BEAT FREQUENCY RADIATION IN THE FAR INFRARED BY THE SMITH-PUCELL EFFECT by A.J. Fox and N.W. Smith (Mullard); Proc. IEEE, Vol. 52, pp. 429-430(L), Apr. 1964

The use of a Smith-Pucell coupler to obtain coherent radiation in the far infrared is described. This coupler avoids the charging-up difficulties associated with the Cerenkov coupler. The coupler is based on the effect that visible radiation is produced when an electron beam is projected parallel to the surface of a metallic diffraction grating. The wavelength of the radiation varies with beam velocity and observation angle. Experimental verification requires a modulated electron beam produced by 2 coherent light sources of slightly different frequencies, each capable of delivering 4mw of power.

25,987 SOLID STATE X-RAY MASERS by L. Gold (Kennecott Copper); Quantum Electronics III, Columbia U. Press, 1964, pp. 1155-1160

The feasibility of developing solid state x-ray masers capable of producing intense, well-collimated, coherent, monochromatic x-irradiation is discussed. The pumping power for the maser might easily exceed the megawatt mark. Uncertainties related to details of the x-ray levels and their fine structure, and the probable relaxation mechanisms make it difficult to ascertain whether or not amplification via stimulated emission would occur at x-ray levels.

25,988 THE PHONON MASER by E. B. Tucker (GE); Quantum Electronics III, Columbia U. Press, 1964, pp. 1787-1800

Amplification and oscillation in a phonon maser using an electromagnetic pump and a pink (c-axis) ruby rod are described. The output of this maser was found to consist of beats corresponding to those between normal modes of the ruby and a low frequency beating that has not yet been accounted for. It is thought that phonon maser with its relatively low velocity will permit properties of induced emission systems such as the build-up of coherence, to be studied more readily. However, the importance of the phonon maser as a source of vibrational energy can not be assessed until a better understanding of the spurious modulations and the ways to increase power output are realized.

25,989 RAMAN LASER WITH LOW EXCITING POWER by H. Takuma and D. A. Jennings (Natl. Bur. Stand.); Bull. Am. Phys. Soc., Vol. 9, p. 499(A), Apr. 1964

Raman-laser action for benzene Stokes line (990 cm^{-1}) is observed using an ordinary ruby laser without using Q-spoiling technique. A 4-in.-long Raman cell is inserted in the resonant cavity of a ruby laser with a ruby rod of excellent optical quality. Dielectric coatings with more than 99% reflectivity are used as the resonator of the laser. The peak output power of the Stokes line of benzene is measured to be of the order of 50 W when the input power is 1.2 times the threshold of the Raman laser. The threshold exciting power of the ruby laser is estimated to be about 200 kW. The Raman-laser output consists of a sharp spike that has a short rise up time of less than 5 nsec and decays exponentially with a time constant of about 10 nsec.

25,990 THE COUPLED-CAVITY TRANSMISSION MASER-ANALYSIS by T.R. O'Meara (Hughes Res. Lab.); IEEE Trans., Vol. MTT-12, pp. 336-398, May 1964

A maser amplifier structure consisting of a cascade of iris-coupled $\pi/2$ cavities intermixed with isolators is analyzed. Starting from the basic media susceptibility, narrow-band equivalent networks and matrix representations are derived for maser and isolator cavities. A rational function approximation to the over-all gain function is thereby derived by matrix methods. From one viewpoint, the over-all amplifier may be regarded as a negative-resistance inverse-feedback amplifier. The key design parameter is shown to be the isolator round-trip attenuation. Excess isolation yields an overly rounded gain-frequency characteristic, while deficient isolation yields a characteristic with excess ripple or instability in the extreme cases. The feedback effects associated with intermediate "optimum" values of isolation reduce the effective gain per cavity below the normal gain of a single cavity, but in return one obtains a reduced gain sensitivity which may be reduced to a value comparable to or lower than that of the pure traveling-wave maser.

25,991 THE COUPLED-CAVITY TRANSMISSION MASER-ENGINEERING DESIGN by F.E. Goodwin, J.E. Kiefer and G.E. Moss (Hughes Res. Lab.); IEEE Trans., Vol. MTT-12, pp. 349-358, May 1964

The experimental design of an X-band microwave maser amplifier which uses a new type of slow-wave circuit is described. The slow-wave circuit consists of a cascade of iris-coupled ruby resonators separated by garnet isolators. The microwave properties of the solid ruby resonator are treated in detail, and the passive bandwidth of the single transmission cavity and its relation to the iris susceptance are shown. Experimental techniques involved in obtaining and measuring precise iris susceptance are presented. A step-by-step procedure for designing an amplifier having a given gain and tuning range is also presented. Typical performance characteristics include a gain of 30 db, instantaneous bandwidth of 25 Mc, and a noise temperature of 15°K. An electronic tuning range of 200 Mc has been achieved in one configuration with a 20 db gain and a 25 Mc bandwidth. The weight of the maser-dewar unit, filled with 6 liters of helium for 24 hours of operation is less than 40 pounds. The design of the dewar enables the cryogenic system to work over a wide range of vertical angles, thus facilitating the use of the maser at the feed of a large steerable antenna.

25,992 LASER PUMPED MASER by D.P. Devor, I.J. D'Haenens and C.K. Asawa; Quantum Electronics III, Columbia U. Press, 1964, pp. 931-936

The advantages and disadvantages of an optically pumped ruby microwave maser by use of a ruby laser pump are discussed. Design criteria and laser emission characteristics are described. The time resolution spectroscopy of the emission of the refrigerated laser yields information as to the utility of the laser as an intense spectral source in maser pumping. The spectral sweep of the

laser is found to reduce the requirements of exact optical spectroscopy, but it also limits the amount of energy which can be matched to the maser pump transition. Little success has been achieved in obtaining maser gain at reduced laser emission energy. Poor thermal coupling of the laser ruby to the cryogenic bath account for the persistent difficulties.

25,993 STUDIES ON THE REALIZATION OF S-BAND MASER [in French] by M. Bidault (French Thomson-Houston Co.); Quantum Electronics III, Columbia U. Press, 1964, pp. 883-898

A ruby, S-band maser with a pump frequency in the Ku-band is described. The energy levels, the corresponding eigenstates of the Cr ions and the transition probabilities between levels have been calculated by studying the spin Hamiltonian. The magnetic field, H_0 , (~ 2750 G), crystal orientation (90° between crystal axis and H_0 direction), and the optimum polarization of the signal and pump fields have been determined. Cavity characteristics, spin-spin relaxation and susceptibility are also discussed.

25,994 LARGE ZINC TUNGSTATE CRYSTALS FOR MICROWAVE MASER APPLICATIONS by J.J. Rubin, W.G. Nilsen and L.G. van Uitert (Bell Lab.); Quantum Electronics III, Columbia U. Press, 1964, pp. 825-831

Growth of large zinc tungstate (ZnWO_4) crystals (containing Cr^{3+} or Fe^{3+} ions) by Czochralski technique and their use as active materials for comb structure masers are described. Comparisons of the properties of Cr^{3+} containing zinc tungstate crystals to those of pink ruby ($\text{Al}_2\text{O}_3:\text{Cr}_{0.005}$) are made. The zero field splitting of Cr^{3+} in zinc tungstate is reported to be 51.6 Gc/sec compared to that of 11.5 Gc/sec in ruby. Because of the higher zero field splitting, ZnWO_4 crystals are recognized to have higher inversions at equal frequencies and volume concentrations and are useful over larger frequency ranges than pink ruby crystals. The spin lattice relaxation time of Cr^{3+} in ZnWO_4 are also to be shorter by a factor of about one hundred. Which accounts for the increase in the dynamic range of a travelling wave maser and shortens the time required for it to recover its gain after a saturating pulse. Despite the above advantages, the shorter spin-lattice relaxation time is thought to increase the pump power requirements. The problems connected with crystal growth of ZnWO_4 are also discussed.

25,995 PROPERTIES OF MATERIALS FOR SUBMILLIMETER MASERS by W.S.C. Chang and R.F. Rowntree (Ohio State U.); Quantum Electronics III, Columbia U. Press, 1964, pp. 677-684

The operating conditions and measured properties of the host lattice and cavities used for the development of a solid state submillimeter maser are discussed. Successful development depends on the selection of an active material having a Q_{abs} factor = 10^3 (i.e., a resonant absorption coefficient $\sim 1\text{ cm}^{-1}$) or better, with a population inversion ratio of 10%. This may be interpreted to mean that any material in which an electric dipole transition does not occur will be unsuitable for maser application at submillimeter frequencies. A number of materials have resonant absorption coefficients of 1 cm^{-1} ; the major obstacle is realization of the inversion ratio.

25,996 DEVELOPMENT OF MILLIMETER AND SUBMILLIMETER MASER DEVICES by W.E. Hughes (Westinghouse Def. and Space Ctr.); Cont. AF33 657 10472, 30 pp., Jan. 31, 1964; U.S. Gov. Res. Rep., Vol. 39, p. 49(A), May 20, 1964 AD 432 597 OTS \$2.60

Iron doped (Fe^{3+}) zinc tungstate (ZnWO_4) is discussed as a possible new quantum amplifier material. The solutions to the spin Hamiltonian have been obtained so that identification of energy levels is possible, and a computer program for the solution of radiation-induced transition probabilities has been established. Since the dielectric constant of the zinc tungstate is considerably lower than that of the materials used previously, it has been necessary to make several changes in the experimental apparatus.

25,997 GENERATION OF MILLIMETER WAVES IN OPTICALLY PUMPED RUBY by G.M. Zverev, A.M. Prokhorov and A.K. Shevchenko (Moscow State U.); Quantum Electronics III, Columbia U. Press, 1964, pp. 963-966

A ruby laser pumped ruby millimeter wave maser operating at 35-50 kMc is described. The pump was cooled to liquid nitrogen temperatures. The ruby crystal employed had a Cr concentration of $\sim 0.05\%$. Maximum energy of generation was calculated at ~ 2.5 ergs. The maximum power observed from 150 μsec pulses was ~ 1.7 mw. Thermal relaxation accounts for the difference.

25,998 CONTINUOUS SUN-PUMPED ROOM TEMPERATURE GLASS LASER OPERATION by G.R. Simson (Am. Optical); Appl. Optics, Vol. 3, pp. 783-784, June 1964

Continuous laser oscillation at $1.06\text{ }\mu$ and 30°C with 6.25 wt. % Nd_2O_3 -doped barium crown glass pumped by the sun and a carbon sun simulator is described. Solar operation was attained on a day when a high, thin cirrus cloud coverage existed. Operation was approximately 15% above threshold with sun and 50% above using the carbon arc simulator. No provisions were made for cooling the laser cavity, so operation was limited to 0.5 sec by use

of a hand-operated dowser situated just in front of the refracting elements. An exposure in excess of 5 sec resulted in the silver on the exposed laser facet burning off.

25,999 TRANSVERSE MODE PATTERNS IN NEODYMIUM GLASS AND RUBY by E.S. Dayhoff (U.S. Naval Ord. Lab.); Quantum Electronics III, Columbia U. Press, 1964, pp. 1445-1451

Glass:Nd and ruby lasers are discussed and a model is developed for describing scattering phenomena. The differences observed in the primary mode pattern is a general property of the glass and is a measure of scattering at very small angles.

26,000 INTERACTIONS BETWEEN TWO Nd³⁺ GLASS LASERS by C.J. Koester, R.F. Woodcock and E. Snitzer (Am. Optical), and H.M. Teager (MIT); Quantum Electronics III, Columbia U. Press, 1964, pp. 1703-1710

The laser quenching effect arising from the interactions between the outputs of two coupled lasers is described. It is shown that quenching of laser oscillation can be accomplished by using the output of another laser having the same emission wavelength. The effect is observed to be at least as fast as 1 μsec. This quenching effect is known to occur when the intensity of light from the first laser is sufficiently great to reduce the inversion in the second laser below that required for oscillation. Using first order theory, the rate at which inversion is depleted is thought to be proportional to the product of three factors; the intensity of incident light, the transition probability, and the instantaneous value of the inversion. By employing high intensity signal pulses, quenching times less than 1 μsec may be realized.

26,001 HAIR-TRIGGER OPERATION OF A NEODYMIUM LASER by D.L. Caskey (Nav. Ord. Lab.); 74 pp., Mar. 4, 1964; U.S. Gov. Res. Rep., Vol. 39, p. 136(A), June 20, 1964 AD 436 893 OTS \$8.10

A laser system has been devised which provides a preselected number of laser bursts at controlled intervals, by shaping the output of the optical pump light in a suitable manner. Two techniques were used. A system was constructed to demonstrate the principle. The working model provides up to three 15 micro-second laser bursts per firing, while the time between bursts is controlled by preselected delays of from 50 to 500 microseconds. The peak power output is several kilowatts. Although the model employs a 2'' x 1/4'' Neodymium-doped glass laser, the method is applicable to a wide variety of laser materials and sizes.

26,002 RESEARCH ON VITREOUS LASER MATERIALS (Ctr. Natl. D'Etud. des Telecommun., France); 23 pp., Dec. 31, 1963; U.S. Gov. Res. Rep., Vol. 39, p. 80(A), May 20, 1964 AD 431 679 OTS \$2.60

A systematic study was made of vitreous materials which would possibly exhibit better performances in laser action than the silicate, borate and boro-silicate glasses. About 150 samples were prepared of phosphate and fluoride glasses of different composition, doped in general with 2% of neodymium by weight. Neodymium doping was chosen because it has a four level energy system and therefore exhibits laser action at room temperature. Series of simple alkaline phosphate glasses of different mole ratios had been prepared, as well as series of bivalent cation phosphate glasses, equally of different mole ratios. The influence of fusion time and temperature had been studied by preparing different samples of a phosphate glass of the same composition, at different fusion temperatures and for different fusion times. In order to investigate the influence of the neodymium concentration on the optical properties, a series of phosphate glasses of a given composition had been doped with various quantities of neodymium.

26,003 NEODYMIUM GLASS LASER by E. Switzer (Am. Optical); Quantum Electronics III, Columbia U. Press, 1964, pp. 999-1019

The spectroscopic properties and energy configurations of Glass:Nd lasers are discussed and the potential of fiber lasers is reviewed. The threshold for a fiber a few mils in diameter or smaller is substantially lower than that of a solid rod. It is suggested that the properties of glass lasers under high pumping conditions are best studied with fiber configurations.

26,004 LASER OSCILLATIONS AT 0.918, 1.057 AND 1.401 MICRONS IN Nd³⁺-DOPED BORATE GLASSES by A.D. Pearson, S.P.S. Porto and W.R. Northover (Bell Lab.); J. Appl. Phys., Vol. 35, pp. 1704-1706, June 1964

Borate glasses doped with Nd³⁺ have been prepared in small (70 g) batches, and rods of sufficiently high optical quality for laser oscillations have been pulled directly from the melts. Laser action occurs in three groups of wavelengths, the strongest emission being at 0.918, 1.057 and 1.401 μ. Plots of the threshold for oscillation at 1.057 μ are given as a function of both Nd₂O₃ concentration and base glass composition.

26,005 SOLID STATE MASER RESEARCH (OPTICAL) by J.E. Geusic, J. Konigstein, H.E.D. Scovil and W.P. Unruh (Bell Lab.); Cont. DA36 039 AMC02333E, 39 pp., Nov. 14, 1963; U.S. Gov. Res. Rep., Vol. 39, p. 22 (A), June 5, 1964 AD433 775 OTS \$3.60

Part I gives a brief report on the first successful demonstration of pulsed and CW optical maser oscillations in Nd:YAG. Part II is a rather detailed discussion of crystal field calculations for some of the states of trivalent rare-earth ions in YAG. Particular emphasis is given to a discussion of the Nd³⁺ spectrum in YAG.

26,006 SPECTRUM OF Er³⁺ IN SINGLE CRYSTALS OF Y₂O₃ by P. Kisliuk and W.F. Krupke (Aerospace) and J.B. Gruber (U. Calif.); Bull. Am. Phys. Soc., Vol. 9, p. 560(A), June 1964

The spectrum of Er³⁺ in Y₂O₃ has been examined from 0.225-2.4 μ in absorption and fluorescence, and energy levels have been assigned. The spin-orbit coupling parameter and radial integrals have been determined, which give a satisfactory fit to the mean positions of the Stark levels of the "free" electron states. Of the 2 unequivalent cation sites, the one without inversion symmetry gives rise to the entire observed spectrum, since its Stark levels are sufficient to account for all of the observed lines. The lifetime of the ⁴S_{3/2} state, which is the initial state of the strong green fluorescence, is 80 μsec at room temperature and 100 μsec at 77°K. The merit of this substance for possible applications to lasers is discussed.

CaF₂:Er³⁺ as Laser Material - See 25,625

26,007 THE CaF₂:Tm²⁺ AND THE CaF₂:Dy²⁺ OPTICAL MASER SYSTEMS by Z.J. Kiss (RCA); Quantum Electronics III, Columbia U. Press, 1964, pp. 805-815

Laser transitions in CaF₂:Tm²⁺ and CaF₂:Dy²⁺ are identified and the energy levels including crystal field symmetries of the states are presented. The divalent rare earth - CaF₂ system shows a narrow magnetic dipole 4f-4f transitions; in the CaF₂ host lattice the divalent rare earth replaces the divalent Ca in a cubic site and the resulting spectrum is not complicated by the familiar distortions due to charge compensation present in the trivalent rare earth:CaF₂ system. Photoreduction of all trivalent rare earth ions to the divalent state (excluding Pm) in CaF₂ is discussed. Operation of the CaF₂:Ho²⁺ and CaF₂:Er²⁺ systems were unsuccessful due to unfavorable characteristics of the broader line-widths of the 4f-4f fluorescent transitions and fluorescent reabsorption by atoms in the emitting state.

26,008 LOW LYING ENERGY LEVELS AND COMPARISON OF LASER ACTION OF U³⁺ in CaF₂ by S.P.S. Porto and Y. Yariv (Bell Lab.); Quantum Electronics III, Columbia U. Press, 1964, pp. 717-723

Electron paramagnetic resonance (EPR) has been used to study the low lying energy levels of U³⁺ in CaF₂ and to explain laser action in this system. The studies reveal that the crystals contain different ions in different sites of the lattice; U³⁺ was found in sites of 4-fold symmetry (tetragonal sites) in which the excess positive charge is compensated by an F⁻ ion in the nearest intersite; U⁴⁺ was found in sites of trigonal symmetry in which charge compensation is obtained via the replacement of two nearest F⁻ ions along the <111> direction by two O²⁻ ions; U³⁺ was also found in orthorhombic sites due to charge compensation by an F⁻ ion in the next nearest intersite. The relative amounts and spectra of the U ions were isolated by using the EPR data. The low lying energy levels were then constructed and the sites responsible for various laser frequencies were established. Preliminary work on SrF₂:U³⁺ and BaF₂:U³⁺ show a similar behavior. Laser actions were selectively pumped in the green and the 0.9 μ regions.

26,009 LASER CHARACTERISTICS OF THE NdNbO₄/CaMoO₄ LASER SYSTEM by P.A. Flournoy, J.G. Forsythe, E.S. Mayo and L.H. Brixner (DuPont Exp. Station); Bull. Am. Phys. Soc., Vol. 9, pp. 559-560(A), June 1964

Neodymium-doped calcium molybdate was first demonstrated to lase by Johnson, but he observed high thresholds due to poor crystal properties. Brixner developed a procedure for purifying and stabilizing calcium molybdate to improve its growing characteristics and produce large single crystals of excellent optical quality. In the present study, the fluorescence and stimulated emission characteristics of neodymium-doped calcium molybdate were presented, and the advantages of calcium molybdate over calcium tungstate as a host for rare-earth ions were discussed.

LASER DIODES

26,010 THE SEMICONDUCTOR OPTICAL MASER by C. Hilsum (Baldock Lab.); Sci. Prog., Vol. 52, pp. 91-97, Jan. 1964

Semiconductor radiation and the process of light amplification are explained and the characteristics of a semiconductor optical maser are discussed. The semiconductor laser is not considered a replacement or alternative to the gaseous or crystal laser; each device has its distinctive merits which suggests the possibility of combination of the devices rather than replacing one by the other. Examples of future prospects here are the use of a semiconductor as a light amplifier for the gas laser thus raising the mean power available, and also as a light source for pumping the crystal laser to improve the efficiency.

26,011 IMPURITY STATE IN SEMICONDUCTING MASERS by H.J. Zeiger (Lincoln Lab.); *J. Appl. Phys.*, Vol. 35, pp. 1657-1667, June 1964

A formalism is developed for computing negative conductivities for inverted populations involving impurity states in semiconductors. General expressions are obtained for three classes of systems: class (1), transitions between states belonging to the same band edge; class (2), direct transitions between states belonging to two different band edges; and class (3), indirect transitions between states belonging to two different band edges. The expressions for negative conductivities are simplified by using the effective mass approximation. The results are then applied to an example of each of the three classes of processes. Class (2) is represented by a model of the GaAs diode laser. It is concluded for this model that at low temperatures, with an acceptor concentration $N_a \sim 10^{18}/\text{cc}$, and an effective acceptor radius of $\sim 20 \text{ \AA}$, population inversion of donor states relative to acceptor states yields a greater negative conductivity than inversion of donor states relative to the valence band. A brief discussion is presented of the threshold conditions for diode lasers.

26,012 CONDITIONS FOR COHERENT EMISSION AND SUPERRADIANT NARROWING IN p-n INJECTION LASERS by A. Yariv and R.C.C. Leite; *Quantum Electronics III*, Columbia U. Press, 1964, pp. 1873-1878

An expression for the onset of spectral narrowing and start oscillation in the recombination radiation from p-n junctions is derived. The exact nature of the physical mechanisms involved in the recombination radiation need not be known for the development of a phenomenological laser theory. Narrowing due to coherent laser oscillation is a direct consequence of the inversion of population and is distinct from spectral narrowing due to recombination radiation arising from onset of laser action. The superradiant narrowing process is not limited to p-n junctions; the formalism developed for narrowing conditions may be applied to any medium with inverted population.

26,013 CURRENT DEPENDENCE OF INJECTION LUMINESCENCE by P.N. Keating (Tyco Lab.); *Bull. Am. Phys. Soc.*, Vol. 9, p. 270(A), Mar. 1964

It is well-known that the injected carrier density for diffusion-controlled injection processes is almost exactly proportional to the current density J at high levels. However, the high-level injected carrier density for a drift-controlled (i.e., bulk) injection process is proportional to the applied voltage and thus to J^2 , respectively. This difference gives rise to different theoretical variations of spontaneous electroluminescence (EL) with current in the two cases. In the diffusion-controlled case, bimolecular electroluminescence varies as J^2 and monomolecular EL is linear in current. In the drift-controlled case, however, they vary as J and J^2 , respectively. The latter interpretation can account for some previously unexplained results of EL from germanium, cadmium sulfide, and silicon carbide.

26,014 SEMICONDUCTION INJECTION LASERS by P.S. Newman; *Brit. Commun. and Electronics*, Vol. 11, pp. 252-255, Apr. 1964

The mechanism of light emission in injection lasers is discussed. The radiation from such a P-N junction generally arises from one particular scheme of recombination of electrons or holes, injected as minority carriers into the P or N regions respectively on each side of the junction. Whether the radiation is intense enough for outside detection depends on the relative occurrence of radiative and non-radiative recombinations, the absorption of the radiation within the semiconductor, and reflection at the semiconductor boundary. The first factor depends on the impurity of the semiconductor, while the second depends partly on the intrinsic properties of the semiconductor and partly on impurities. To obtain coherent emission of radiation, there must be an inverted population as well as a high density of radiation. Since the observation of laser action in GaAs, it has also been observed in InP, InAs, $\text{GaAs}_{1-x}\text{P}_x$ (with x up to about $\frac{1}{2}$), and InSb; no laser action has been observed in pure GaP or GaSb. However, it has recently been shown that silicon carbide may produce what is almost the ideal injection laser - a device that will emit continuous, coherent light in the visible region of the spectrum, with a conversion efficiency (light output/pump power) approaching 100 per cent, all operated at room temperature.

Recombination Radiation from GaAs Diodes - See 25,657

26,015 MICROWAVE MODULATION OF A GaAs INJECTION LASER by B. Goldstein and J. Welch (Lincoln Lab.); *Proc. IEEE*, Vol. 52, p. 715, June 1964

The modulation of a GaAs laser at 2 Gc is reported. A 0.1 μsec , 12.5 ampere video pulse was used to drive the GaAs diode into the lasing mode. A microwave modulator produced 1 watt peak 0.1 μsec pulses synchronized with the video pulses and the sum was fed into the laser mounting termination. The laser crystal was made by diffusing Zn into Te doped GaAs with a net impurity concentration of $3 \times 10^{17} \text{ cm}^{-3}$. The crystal was cleaved along the (110) plane. The junction area is $2 \times 10^{-3} \text{ cm}^2$ and the lasing threshold is 10.5 amperes ($5.25 \times 10^3 \text{ a/cm}^2$).

26,016 LIGHT EMISSION AND ELECTRICAL CHARACTERISTICS OF EPITAXIAL GaAs LASERS AND TUNNEL DIODES by N.N. Winogradoff and H.K. Kessler (IBM, Fed. Sys. Div.); *Solid State Commun.*, Vol. 2, pp. 119-122, Apr. 1964

Lasing characteristics of epitaxially formed GaAs p-n junctions are compared with those of Zn diffused lasers. Abrupt epitaxially formed junctions only lased when a high concentration of donors was deliberately added to the p-type side. This result supports Nelson's et al band filling model of the GaAs laser and relates the impurity band in this model to the n-type dopant.

26,017 COOPERATIVE EFFECT IN GaAs LASERS by A. Fowler (IBM); *J. Appl. Phys.*, Vol. 35, pp. 2275-2276(L), July, 1964

Cooperative effects in GaAs lasers distinguished by a lowering of current density threshold and an absence of enhanced mode selectivity are discussed. For lasers connected end-to-end, the spectrum of the pair was predominantly that of one of the units. For pairs where one laser was much longer than the other, current density at threshold for the short laser was 1.2 times that of the long laser. The two lasers do not act as a pair of coupled oscillators, but rather the emission from the long laser is amplified by the short laser.

26,018 EFFECT OF TEMPERATURE ON THE STIMULATED EMISSION FROM GaAs p-n JUNCTIONS by M.H. Pilkuhn and H. Ruprecht (IBM Watson Res. Ctr.); *Bull. Am. Phys. Soc.*, Vol. 9, pp. 269(A), Mar. 1964

The temperature dependence of the threshold current density was examined for a series of GaAs injection lasers with different lengths but otherwise identical structure. From a plot of threshold current density as a function of reciprocal length at constant temperature, the gain and loss factor can be calculated. The laser losses exhibit only a small temperature dependence in the range from 4.2° to 300°K. The reciprocal gain factor, however, has the same temperature dependence as the threshold current density j_t . The detailed nature of the temperature dependence of j_t for diodes of different lengths (different gain at threshold) is compared with theoretical results obtained by Lasher and Stern.

26,019 DELAY BETWEEN CURRENT PULSE AND LIGHT EMISSION OF A GALLIUM ARSENIDE INJECTION LASER by K. Konnerth and C. Lanza (IBM); *Appl. Phys. Lett.*, Vol. 4, pp. 120-121(L), Apr. 1, 1964

Measurements of the time delay between the application of a current pulse and the emission of light from a gallium arsenide injection laser at 77°K are discussed. A delay, attributed to the time necessary to inject sufficient carriers to create the population inversion required for coherent emission, was observed when the laser was driven with pulses of about 2 nsec duration. From a simple model of the delay mechanism, the spontaneous recombination lifetime τ was calculated to be 2 nsec. The measured stimulated emission rise time suggests that cw modulation at frequencies in the gigacycle per second region are possible.

26,020 ON THE FORWARD V-I CHARACTERISTICS OF THE GaAs LASER DIODE by Y. Nannichi (Nippon Elec.); *Japanese J. Appl. Phys.*, Vol. 3, pp. 233-234(L), Apr. 1964

The forward V-I characteristics were measured for both lasing and non-lasing GaAs diodes. Optical and electrical properties were also measured at liquid nitrogen temperatures. It was determined that lasing diodes generally display discontinuities at the critical currents for laser action, presumably due to the increase of conductivity of bulk GaAs. Non-linearity in the high current region is probably caused by decrease of the mobility of the carrier due to the high electric field.

26,021 SHAPED ELECTROLUMINESCENT GaAs DIODES by A.R. Franklin and R. Newman (Sperry Rand Res. Ctr.); *J. Appl. Phys.*, Vol. 35, pp. 1153-1155, Apr. 1964

Electroluminescent GaAs diodes have been shaped as truncated cones with the p-n junction at the apex to direct a large fraction of the radiation toward the base of the cone within the critical angle for transmission. Devices having an efficiency at 77°K of 8% have been fabricated. Efficiency is defined here as the radiant power out of the base per unit electrical power input. It is calculated that improved devices of this type will have efficiencies of about 18%.

26,022 CHARACTERISTICS OF A CONTINUOUS HIGH-POWER GaAs JUNCTION LASER by W.E. Engeler and M. Garfinkel (GE Res. Lab.); *J. Appl. Phys.*, Vol. 35, pp. 1734-1741, June 1964

The construction details and output characteristics of a high-power GaAs junction laser are described. With the diode cooled to 20°K, continuous coherent optical power outputs up to 3.1 W have been obtained. This output was achieved with power efficiency of 46%. The coherent spectral output at several power levels well above threshold is shown. High resolution measurements of the spectral output place an upper limit of 310 Mc/sec upon the laser linewidth.

26,023 EFFICIENCY MEASUREMENTS ON GaAs ELECTROLUMINESCENT DIODES by S.V. Galginaitis (GE Res. Lab.); *J. Appl. Phys.*, Vol. 35, pp. 295-298, Feb. 1964

An integrating sphere was adapted to measurement of external efficiencies of GaAs injection lasers. External efficiencies rise rather sharply with current once the laser threshold is reached, attaining ultimate values of about 35% at 77°K for the more efficient diodes, as high as 60% at 20°K. On the basis of a highly simplified model, the observed external efficiencies indicate junction efficiencies near unity.

26,024 INJECTION LASER STUDY by G.J. Lasher, F. Stern and K. Weiser (Watson Res. Ctr.); *Cont. DA36 039AMC02349E*, 58 pp., Nov. 30, 1963; *U.S. Gov. Res. Rep.*, Vol. 39, p. 145(A), May 5, 1964

A bistable device, whose two stable states are a lasing state and a state with only spontaneous emission, both for the same current through one of two separated contacts to the p-type side of a p-n junction, was shown to be feasible. Calculations for several models of absorption and emission spectra show the device to be bistable when the area of the low-current contact is greater than the area of the high-current contact. An approximate method for determining the far-field emission pattern perpendicular to the junction plane for the lasing modes has been found. Lasing has been seen for the first time in double-diffused Mn- and Zn-doped GaAs diodes, whose negative resistance was reported previously. The threshold densities at 77°K were 5000A/cm sq and higher.

26,025 ELECTRICALLY BISTABLE Mn- AND Zn-DIFFUSED GaAs INJECTION LASER by G.J. Lasher, F. Stern and K. Weiser (IBM); *In Injection Laser Study*, Contract DA-36-039-AMC-02349(E), pp. 33-41, 1963; *STAR*, Vol. 2, p. 1295(A), May 23, 1964 AD 430696

The electrical and optical properties of GaAs diodes prepared by subsequent diffusions of Mn and Zn into n-type GaAs are discussed. Such diodes exhibit a negative resistance over part of their I-V characteristics, and have interesting electroluminescent properties. Laser action was obtained in these structures. The achievement of lasing action is believed to be the result of improved diffusion techniques, which result in very straight diffusion fronts. Lasing thresholds, mode structures, directionality, and near-field patterns of a number of these diodes were examined. At 77°K, the most striking difference between these and ordinary lasing diodes is the fact that lasing action was found to occur some 10 microns away from the p-n junction. There are also indications of a different temperature dependence of the threshold current from that found for ordinary lasers; however, the experiments underlying the observation are preliminary.

26,026 PROPOSED BISTABLE INJECTION LASER by G.J. Lasher, F. Stern and K. Weiser (IBM); *In Injection Laser Study*, pp. 6-28, 1963; *STAR*, Vol. 2, p. 1295(A), May 23, 1964 *Cont. DA 36 039 AMC 02349(E)* AD 430 696

The possibility of constructing a bistable injection laser from a single, semi-conducting crystal diode is analyzed. A GaAs diode that emits recombination radiation from electrons injected into an active layer on the p-side of the junction is considered. The bistability depends upon nonlinear absorption of light by a portion of the p-side of the junction. Its operation is somewhat analogous to a bistable microwave maser recently constructed by Gerritsen. The analysis is made for the liquid-helium temperatures, assuming the recombining electrons are in the exponential tail of the conduction band. Bistability is predicted, assuming either a constant or a square-root dependence of the density of states in the valence band on energy. For liquid-nitrogen temperature, the numerical results of Lasher and Stern, which refer to parabolic conduction and valence bands, are used.

26,027 OSCILLATIONS IN GaAs SPONTANEOUS EMISSION IN FABRY-PEROT CAVITIES by M. Nathan, A. Fowler and G. Burns (IBM); *Phys. Rev. Lett.*, Vol. 11, pp. 152-154, Aug. 15, 1963

Oscillations in the spectra of GaAs injection lasers at levels below the threshold current for single mode operation have been observed. The level varies from 0.025 at 2°K to 0.0002 at 77°K. They merge into equally spaced spectral lines as the threshold current is increased and are independent of stimulated emission. Internal loss of the laser and the behavior of the refractive index

near the absorption edge are determined by the analysis of the current dependence of the oscillations.

26,028 LIGHT EMITTING CHARACTERISTICS OF A GaAs DIODE HAVING NEGATIVE RESISTANCE by T. Yamamoto (Shizuoka U.); *Proc. IEEE*, Vol. 52, pp. 409(L), Apr. 1964

The construction and performance of a GaAs diode exhibiting negative resistance for generation of infrared light beams are described. The intensity of the resultant beam from the negative resistance diode is found to be about one-fourth that of the usual light-emitting GaAs diode at liquid oxygen temperature. The signal or pulse transfer characteristics with which it can emit infrared beams and tune on another negative resistance diode is another feature of this device. The infrared characteristics of both types and the V-I characteristics of the negative resistance diode are presented.

26,029 TRIANGULAR INJECTION LASERS by J. Marinace, A. Michel and M. Nathan (IBM); *Proc. IEEE*, Vol. 52, pp. 772-723, June 1964

Gallium arsenide injection lasers having an equilateral triangle geometry which exhibit highly directional beams and a rapid increase in quantum efficiency at threshold (similar to Fabry-Perot lasers) are described. Diffused GaAs wafers were fabricated into triangular structures by cleaving along the three (110) planes perpendicular to the (111) plane. Some of the lasers exhibit non-directional beam properties and do not increase their quantum efficiency at threshold; their spectrum is similar to non-directional rectangular parallelepipeds with four cleaved sites.

26,030 LOW-LEVEL ELECTROLUMINESCENCE IN GaAs p-n JUNCTIONS by M. I. Nathan, G. Burns and A.E. Michel (IBM Watson Res. Ctr.); *Bull. Am. Phys. Soc.*, Vol. 9, pp. 269(A), Mar. 1964

The electroluminescence of diffused GaAs p-n junctions with n-type substrate-carrier concentrations between 7×10^{15} and 6×10^{18} cm⁻³ has been measured as a function of current density between 2° and 77°K. The emissions observed near the absorption edge are: (1) Line 1. The photon energy of the peak $h\nu_1$ satisfies $h\nu_1 = eV$, the applied voltage, with a small correction that depends on temperature. This behavior has previously been reported in heavily doped diodes. (2) In diodes where $n > 2 \times 10^{17}$ cm⁻³, line 2. The photon energy of its peak satisfies $h\nu_2 > eV$. Line 2 is observed only at low-current density where the quantum efficiency is small ($\approx 10^{-4}$). At higher current density, it is obscured by line 1. $h\nu_2$ is independent of V and is close to the value that $h\nu_1$ has at a current density near the threshold for stimulated emission. It has been shown that the extra energy for line 2 ($h\nu_2 - eV$) does not come from thermal excitation; thus, it must come from the applied voltage.

26,031 LIGHT EMISSION FROM REVERSE-BIASED GaAs p-n JUNCTIONS by A.E. Michel and M.I. Nathan (IBM Watson Res. Ctr.); *Bull. Am. Phys. Soc.*, Vol. 9, pp. 269(A), Mar. 1964

The emission of infrared radiation from reverse-biased GaAs p-n junctions has been observed at 77° and 2°K. The junctions studied were zinc-diffused into n-type substrates with electron concentrations between 2×10^{17} and 2×10^{18} cm⁻³. In addition to the broad spectral band reported for other semiconductors, the emission usually exhibits a strong narrow line ($\Delta E \leq 0.04$ eV) just below the energy gap of pure material. In contrast to the forward-biased luminescence, the spectral distribution of reverse-biased emission is independent of current. Its peak is close to that of the forward-biased emission near the threshold for stimulated emission and to that of the photoluminescence of p-type material. The light output varies linearly with reverse current and the quantum efficiency is of the order of 10^{-4} . The spatial distribution of the light is similar to the avalanche breakdown "spots" reported in Si. The spectra of some units also exhibit other emissions. Some show a broad line at lower photon energy, while others have a line at about 1.50 eV.

26,032 RECOMBINATION RADIATION EMITTED BY GALLIUM ARSENIDE by R.J. Keyes and T.M. Quist (Lincoln Lab.); *Quantum Electronics III*, Columbia U. Press, 1964, pp. 1825-1831

The electrical properties and incoherent radiation characteristics of GaAs diodes are discussed. Various mechanisms are proposed to explain the 8400 Å emission. Electrical properties covered are: I-V characteristics of a Zn-diffused GaAs diode at 77°K and 298°K; diode emission intensity as a function of photon energy at 77°K and 29.8°K; and emission intensity at 77°K for the 1.47 eV line as a function of diode current. The mechanism involving transitions from donor to valence level is preferred in explaining emission at 8.400 Å or 1.47 eV.

26,033 LIGHT EMISSION FROM GaAs_xP_{1-x} DIODES by M.H. Pilkuhn and H. Rupprecht (IBM Watson Res. Ctr.); *Trans. Soc. AIME*, Vol. 230, pp. 282-286, Mar. 1964

The junction luminescence of GaAs_xP_{1-x} diodes containing up to 47 pct GaP

was studied. Diodes were prepared by diffusing zinc into n-type material which was either boat- or vapor-grown. Observations concerning the energy and the line shape of the spontaneous emissions are presented and discussed; in particular the influence of inhomogeneous phosphorus distribution is considered. The role of reabsorption of the junction radiation is pointed out. With increasing current, the peak emission shifts to higher energy. This is also true in cases where slow line narrowing occurs simultaneously. The length dependence of the threshold current density for lasing at 77°K was examined for lasers made from the same material. It was found that longer lasers have lower threshold current densities. Estimates of the characteristic laser losses are given. Data concerning the range of GaP concentration in which stimulated emission was observed are presented.

26,034 HIGH-ENERGY LIGHT EMISSION FROM JUNCTIONS IN $\text{GaAs}_{1-x}\text{P}_x$ DIODES by N. Ainslie, M. Pilkuhn and H. Rupprecht (IBM Watson Ctr.); *J. Appl. Phys.*, Vol. 35, pp. 105-107, Jan. 1964

Spontaneous and stimulated emission from junctions in diodes made of silicon-doped, melt-grown $\text{GaAs}_{1-x}\text{P}_x$ alloys have been studied. Variations of the emission spectra as a function of current and of composition ranging up to 40 mole % GaP were examined both at room temperature and 77°K.

26,035 THE RED-BLACK EFFECT IN $\text{Ga}(\text{As}_{1-x}\text{P}_x)$ by N. Holonyak, Jr., (U. Illinois) and S. Beracqa (GE); *Solid State Electronics*, Vol. 7, p. 488(L), June 1964

The red-black effect frequently can be used to select laser quality material for $\text{Ga}(\text{As}_{1-x}\text{P}_x)$ crystals with a composition of 40 pct. or more phosphorus. When a strongly Se doped crystal of this composition is sliced into wafers, the saw-blade coolant may "bleed" one or the other of these two colors, red or black. $\text{Ga}(\text{As}_{1-x}\text{P}_x)$ wafers from "black regions" can be readily fabricated into laser junctions; those in "red regions" cannot. It is likely that the red-black color effect is caused by fluctuation in composition near the "direct-indirect" transition.

26,036 LUMINESCENT P-N JUNCTIONS IN GALLIUM PHOSPHIDE by W. Glässer, H.G. Grimmeiss and H. Scholz (Philips, Aachen Lab.); *Philips Tech. Rev.*, Vol. 25, pp. 20-21, 1963/1964

The fabrication of GaP light-sources of relatively high intensity is described. A significant advance has been made using a polycrystalline wafer of GaP doped with certain activators, in which all crystallites grow in the [111] direction. Two contacts are alloyed into this wafer from the (111) face, one of tin and the other (ohmic) of gold (+ 4% zinc). The result is a readily reproducible P-N junction which runs mainly parallel with the surface and which, at about 2V and 10 mA, emits fairly intense light of 7000Å wavelength. The effect is illustrated by a colour photo. A diode fabricated in this way also has excellent electrical properties.

26,037 EFFECT OF PRESSURE ON THE RECOMBINATION RADIATION OF GaSb DIODES by T. Deutsch, (Raytheon) and B. Kosicki (Harvard U.); *Bull. Am. Phys. Soc.*, Vol. 9, pp. 60-61, Jan. 1964

The effect of hydrostatic pressure on the recombination radiation of forward-biased GaSb diodes has been measured. Junctions made by diffusing zinc into n-type substrates were measured at 77°K. The radiation peaks E at atmospheric pressure were between 0.69 and 0.75 eV for different units. The pressure coefficient of the peak varied between 8 and 15×10^{-6} eV/bar, and decreased as E increased. The radiation intensity usually showed a maximum near 5kbar. Alloy junctions on p-type substrates were also examined; E was about 0.78 eV at 77°K. For these units, the pressure coefficients, measured to 9 kbar at 77° and 300°K, varied between 13.5 and 15×10^{-6} eV/bar. The intensity decreased with pressure. The results are considered in light of the fact that the (111) conduction minima, lying about 0.050 eV above the (000) minimum at 77°K and atmospheric pressure, probably become equal in energy to the (000) minimum within the pressure range used. The large spread in pressure coefficient for the diffused units is to be contrasted with the results of similar measurements on GaAs units.

26,038 STIMULATED LIGHT EMISSION FROM INDIUM PHOSPHIDE by K. Weiser and R.S. Levitt (IBM), *Appl. Phys. Lett.*, Vol. 2, pp. 178-179(L), May 1, 1963

The light intensity measured as a function of the wavelength for InP diodes at 77° and 4.2°K is discussed. At 77°K, the threshold current beyond which the stimulated emission begins is 1.5A. At 4.2°K, the threshold current is reduced to about 350 mA. The evidence for the stimulated emission is the narrow spike which appears on the low energy side of the spontaneous line.

26,039 SPONTANEOUS AND STIMULATED INFRARED EMISSION FROM INDIUM PHOSPHIDE ARSENIDE DIODES by F.B. Alexander, V.R. Bird, D.R. Carpenter, G.W. Manley, P.S. McDermott, J.R. Peloke, H.F. Quinn, R.J. Riley and L.R. Tetter (IBM); *Appl. Phys. Lett.*, Vol. 4, pp. 13-15(L), Jan. 1, 1964

Spontaneous infrared emission from $\text{In}(\text{P}_{0.49}\text{As}_{0.51})$ diodes at 77°K are discussed. The mean peak ($\lambda_p = 2.287\mu$) of the spontaneous spectra of the four $\text{In}(\text{P}_{0.18}\text{As}_{0.82})$ diodes agrees with the value 2.210μ computed for this composition on the assumption of a linear band gap variation with composition between InP and InAs at 77°K. No stimulated emission was observed in these diodes up to a current density of $100,000 \text{ A cm}^{-2}$, probably because of high losses from free carrier absorption. All five $\text{In}(\text{P}_{0.49}\text{As}_{0.51})$ diodes exhibited both spontaneous and stimulated emission, with threshold current densities for stimulated emission ranging from 6.42 to 12.60 kA cm^{-2} . The mean value of λ_p for the stimulated emission corresponds to a band gap of 0.800 eV compared to 0.867 eV calculated from the assumption of a linear variation of the band gap with composition.

26,040 STIMULATED EMISSION OF 100μ RADIATION FROM Bi-Sb P-N JUNCTIONS by R. Sehr (Korad); *Proc. IEEE*, Vol. 52, pp. 725-726, June 1964

The feasibility of a 100μ laser, operating on the principle of carrier injection across a p-n junction of p- and n-doped Bi-Sb alloy is discussed. In alloys between approximately 15 per cent to 25 per cent Sb, the optical interband transition is direct. The corresponding absorption coefficient is at least one order of magnitude larger than for an indirect transition. This fact, together with the large carrier mobility found in these alloys, and the large index of refraction, makes stimulated emission by injection feasible at around 100μ . The bandgap of $\text{Bi}_{85}\text{Sb}_{15}$ is approximately 1.5×10^{-2} eV at 10°K. A quantitative evaluation of the $\text{Bi}_{85}\text{Sb}_{15}$ free carrier absorption coefficient, interband absorption coefficient, and transmission loss coefficient shows that a sufficient condition for stimulated emission by carrier injection is satisfied. Likewise a necessary condition on the material's quasi Fermi levels, relaxation time and recombination time is also seen to be satisfied.

ASSOCIATED DEVICES

26,041 AN INTERFEROMETRIC OPTICAL MODULATOR by D.L. Fried, W.S. Reed and D.B. Pollock (NA Aviation); *Appl. Optics*, Vol. 3, pp. 697-701, June 1964

A modulator for collimated monochromatic light is described. The arrangement of components is similar to that of a Twyman-Green interferometer. The two mirrors, however, are replaced by piezoelectric disks with a reflective coating. Thus the optical path length of each leg of the interferometer can be adjusted electrically to achieve modulation. Theoretical analysis is presented concerning bandwidth, required voltage, and power dissipation. It is shown that modulation bandwidths up to 20 Mc/sec are possible with nearly 100% depth of modulation, that the required driving voltages are less than 100-V rms and that power dissipation in the modulator is a fraction of a watt. Experimental results are presented.

26,042 PHASE MODULATION OF LASER LIGHT BY MOVING DIELECTRICS by L.E. Follis and T.J. Carroll (Bendix Radio Div.); *Bull. Am. Phys. Soc.*, Vol. 9, p. 501(A), Apr. 1964

If a sheet of glass is placed between a laser and a photomultiplier tube, the optical pathlength of the transmitted laser beam can be made to change with time by a uniform rotation of the glass about an axis perpendicular to the laser beam. An audiotone can be heard in the output and photographed on an oscilloscope. The maximum audiofrequency seems to occur at the angle of incidence at which the rate of change of the phase is maximum. First experimental results on the audiofrequency produced and the incidence angle of maximum frequency can be related by simple theoretical ideas to the plate thickness and rotation rate.

26,043 MODES IN CONFOCAL GEOMETRIES by G.D. Boyd (Bell Lab.); *Quantum Electronics III*, Columbia U. Press, 1964, pp. 1173-1186

The theory of multimode resonators and periodic transmission systems that function at optical and millimeter wavelengths is reviewed. Major points are: (1) A resonator formed by two curved reflectors separated by almost any distance up to twice their curvature will work as a high Q optical resonator; (2) the absence of side walls is necessary for optical resonators to limit the number of modes with high Q's; and (3) the application of the Fox and Li concept of a self-consistent field for defining a mode, recognition of the large number of equivalent possibilities and the large number of useful combinations that still are to be evolved, point to the development of new devices such as mode filters, harmonic generators and couplers.

26,044 ANOMALOUS DISPERSION OPTICAL MODULATOR AND DEMODULATOR by P. Parzen (RCA); *Quantum Electronics III*, Columbia U. Press, 1964, pp. 1711-1715

The physical characteristics and theory of operation of two solid state devices - one a reflection resonance modulator and the other a reflection resonance

AM-FM detector - are described. Both the devices use a dielectric crystal in the anomalous dispersion range and operate similarly. The modulator varies optical signals at microwave rates, without destroying the narrowness of the laser beam. The demodulator detects both AM and FM optical signals at microwave modulation rates with low noise properties. It is observed that optical powers of a milliwatt with modulation band width of hundreds of megacycles could be detected and a modulation index of 30% with similar bandwidths could be obtained. The principle behind these devices is that every dielectric crystal is inherently a parametric device with the necessary pump cavity supplied by the crystal itself in its resonant absorption frequency region. The laser element itself, with modified doping to control the resonant frequency and its line width is thought to be an appropriate system to use. Any other material that absorbs strongly at the optical frequency is also considered suitable for this application.

26,045 A MICROWAVE ELECTRO-OPTIC MODULATOR WHICH OVERCOMES TRANSIT TIME MODULATION by S.M. Stone (Gen. Tel. and Electronics Lab.); Proc. IEEE, Vol. 52, pp. 409-410(L), Apr. 1964

The performance of a specially designed resonant cavity microwave electro-optic modulator using KH_2PO_4 crystals is described. The design is based on a maximum crystal length criterion requiring the optimum length to be equal to the distance light will propagate in the crystal in one-half microwave period. The intensity modulation index vs. the square root of peak cavity input power is plotted for both the single and double crystal cavity. It is anticipated that the use of multicrystal cavities will enable one to achieve depths of modulation unobtainable at the present time with single crystal cavities

26,046 ELECTRO-OPTIC FREQUENCY MODULATION IN OPTICAL RESONATORS by A. Yariv (Lockheed); Proc. IEEE, Vol. 52, pp. 719-720(L), June 1964

The use of the electro-optic Pockel's effect to control internal feedback in an optical resonator to provide electrical rather than electro-mechanical or magneto-mechanical tuning of optical resonators is described. The optimum arrangement, using KDP crystals, is one in which the external electric field is applied in the Z direction, the light in the Y' (or X') direction, with polarization in the X' (or Y') direction. Applications involve frequency modulation, longitudinal mode suppression and frequency stabilization of lasers.

26,047 FAST InSb PEM DETECTORS FOR OPTICAL MASER STUDIES TO 7μ by R.N. Zitter (Bell Lab.); Rev. Sci. Instr., Vol. 35, pp. 594-596, May 1964

An indium antimonide photoelectromagnetic (PEM) detector, operating at room temperature, has shown capabilities as a fast demodulator for optical maser studies at wavelengths up to 7μ , well beyond the spectral range of phototubes and Ge or Si photodiodes. The detector responds to modulation frequencies of at least 150 Mc, and the use of more highly doped material could result in speeds up to 1 kMc. Construction is simple, no bias current is required, and detector response should be linear even for large incident intensities; the main disadvantage is the relatively small amount of output power and the consequent necessity of low noise amplifiers. An important application is the study of the high gain transitions in xenon and neon lasers.

26,048 DETECTION OF COHERENT LIGHT BY HETERODYNE TECHNIQUES USING SOLID STATE PHOTODIODES by G. Lucovsky, R.B. Emmons, B. Hanned and J.K. Powers (Philco); Quantum Electronics III, Columbia U. Press, 1964, pp. 1731-1738

Parameters are developed to describe the operating characteristics of solid state photomixer diodes as heterodyne detectors for coherent light. The parameters of interest are: (1) the quantum efficiency; (2) the current collection efficiency; (3) the conversion gain; and (4) the noise figure. Conditions for measuring these parameters are outlined and measurements relating to the performance of InSb , Ge, Si and GaAs photo cathodes are presented. Experimental results indicate that neither photomixer diodes nor existing laser sources are optimized for superheterodyne junction detection. However, the figure of merit parameters indicate that this detection technique has considerable promise for yielding a low noise optical frequency superheterodyne system.

26,049 A NEW PRINCIPLE IN THE DESIGN OF A MILLIMETRIC PHOTO-ELECTRIC LASER MIXER by A.L. Cullen and P.N. Robson (U. Sheffield); Quantum Electronics III, Columbia U. Press, 1964, pp. 1741-1750

A theoretical study regarding establishment of a new principle in the design of a millimetric photoelectric laser mixer is described. When two laser beams of different frequency are incident on a photoemissive surface, the transverse electron current wave drawn from the surface will have a wide range of phase velocities depending on the direction of two beams with respect to the surface. With an appropriate choice of laser frequencies, the beat frequency will be in the millimetric or submillimetric range. Several configurations of potential interest in the design of a practical mixer have been examined. Possible drawbacks in this system concerning the alignment accuracy

required and the small tolerance on the divergence of the laser beams are pointed out.

26,050 INTERFEROMETER LASER MODE SELECTOR by S.A. Collins and G.R. White (Sperry Gyroscope), Quantum Electronics III, Columbia U. Press, 1964, pp. 1291-1300

A laser mode selector formed from a Fabry-Perot etalon placed inside the laser and tipped with respect to the laser axis cavity is described. Frequency rejection has been observed arising from the mode selector's frequency transmission characteristics. A decrease in beam angle caused by tilting the mode selector etalon as well as an increase in peak photometric intensity has also been observed.

26,051 ATTENUATION OF LASER LIGHT BY A DIFFRACTION GRATING by R. Gerharz; Proc. IEEE, Vol. 52, p. 438(L), Apr. 1964

A technique for performing an intensity analysis of laser radiation previously used only for intensity measurements of spectrum lines is described. The principle element of the apparatus is a coarse diffraction grating which attenuates the laser beam and produces a large number of diffraction orders n of known intensity I_n . The experiment employed a precision photo-etched grating with a grating constant of 3.85 lines/cm. n should be large to attain high attenuation numbers. A calibrated incandescent secondary-standard light source and comparative densitometry of any selected I_n will provide the output energy of any individual laser pulse.

26,052 EXCITING A LIGHT SOURCE WITH A COMMON AXIS PULSE LASER by H. Chi-jen, C. Tsun-k'uei et al.; In Trans. on Communist China's Sci. and Tech., No. 75, pp. 29-40, Mar. 19, 1964, Trans. into English from K'uo Hsueh T'ung Pao (Peking), No. 11, pp. 39-41, 1963; STAR, Vol. 2, p. 1194(A), May 8, 1964 JPRS 23767; OTS 64 21840 \$2.25

A new, common-axis, cylindrical, xenon flash lamp for exciting a light source for a ruby light, quantum oscillator is described. The lamp is designed to match a 4-cm-long and 0.5-cm-diameter ruby rod. The lamp tube is made of "Pa-li-k'o-ssu" glass or crystal material. The input energy of the glass lamp is up to 800 Joules, whereas that of the crystal lamp can be raised to more than 3,000 Joules. Pure nickel is used as the electrodes. The lamp was observed to have the following advantages: (1) It provided high flash power and high efficiency without an axial magnetic field. (2) The energy was higher than that of a linear tube lamp with the same electrode interval. (3) The structure was tight. (4) It is an ideal tool for theoretical study.

26,053 NOVEL LASER Q-SWITCHING MECHANISM by J. Wents (Westinghouse); Proc. IEEE, Vol. 52, pp. 716-717(L), June 1964

Q-switching using KDP crystals is described. Switching is accomplished without passing the laser beam through transparent electrodes and occurs at half-wave voltages substantially less than 1000 volts. Q-switching results from a 90° oriented laser rod that will only oscillate in a linearly polarized mode when the pump energies is kept below a critical value. Altering the beam polarization results in a suppression of oscillation. Laser pulses of 50 nsec duration and 1 megawatt per power have been generated using the Q-switch with a driving voltage of 400 volts.

26,054 ANALYSIS OF SPHERICAL SECTOR RESONATORS FOR THE PRODUCTION OF A FOCUSED LASER BEAM by C.Y. She and H. Heffner (Stanford U.); Appl. Optics, Vol. 3, pp. 703-708, June 1964

The analysis of the modes of a spherical sector resonator reveals that with a simple change of variable, the results of previous Fabry-Perot mode calculations of cylindrical resonators can be applied. The focusing action is shown to be equivalent to that of a corresponding cylindrical resonator and an associated lens. The diffraction limit at the focus for the lowest order mode is shown to be approximately the Fraunhofer diffraction limit of a focused uniformly illuminated circular aperture. In an appendix, a new method is presented for solving the integral equation for the mode description.

26,055 AN INTERNALLY REFLECTING OPTICAL RESONATOR WITH CONFOCAL PROPERTIES by D.F. Holsouser (U. Illinois), Quantum Electronics III, Columbia U. Press, 1964, pp. 1453-1458

The configuration for an internally reflecting surface, exhibiting properties of a spherical mirror, is described and experimental results obtained with a semi-confocal optical maser using this configuration are presented. An analytic expression for the internally reflecting surface that satisfies confocal requirements is derived. It is observed that the most obvious use for such an internally reflecting confocal configuration is with isotropic solid state optical masers with large indices of refraction. However, the use of such a configuration is not ruled out for gas or other masers possessing low index of refraction. Fabrication and testing of a semi-confocal optical maser is also described.

26,056 LASER ENERGY MEASURING DEVICE by J. Ackerman (Aircraft Armaments); Appl. Optics, Vol. 3, pp. 644-645(L), May 1964

A simple calorimetric energy measuring device has been developed which is easy and inexpensive to construct and offers several advantages over the usual conical configuration. The device consists merely of a stack of one hundred stainless-steel injector-type razor blades, a bridge circuit and reference stack. Measurement of the total energy output of pulsed lasers is possible by evaluation of the temperature-time curves obtained using this device. Good agreement exists between experimental and calculated curves up to the point in time when effects due to the finite extent of the actual device come into play.

26,057 DIRECT OBSERVATION OF AXIAL MODE BEATING IN Q-SWITCHED RUBY LASERS by L. Waszak (TRG); Proc. IEEE, Vol. 52, p. 428(L), Apr. 1964

The performance and component parts of a special phototube assembly to directly observe axial mode beating in Q-switched lasers are described. The system shown schematically, consists of an ITT FW-114 in a wide-band structure with a 519 Tektronix traveling-wave oscilloscope. First-order axial mode beating in a typical Fabry-Perot resonator takes place at frequencies within the bandwidth of the detector, approximately 1.59 Gc. Rise times are observed that are less than .292 nanosec and therefore at the point where rise time limitations are set by the scope.

LASER APPLICATIONS AND EFFECTS

26,058 LASERS AND THEIR EFFECTS by J. H. Burkhalter (Martin-Marietta); Cont. DA49 193MD2456, 54 pp., Apr. 1, 1964; U.S. Gov. Res. Rep., Vol. 39, p. 16(A), May 20, 1964 AD 433 218 OTS \$5.60

The biological effects of lasers and laser radiation are described. Design and construction of a research laser and associated instrumentation is included. Important problems investigated for various biological researchers and the approaches used are discussed.

26,059 PROTECTION OF THE HUMAN EYE FROM LASER RADIATION by H. W. Straub (Harry Diamond Lab.); HDL TR1153, 11 pp., July 10, 1963; U.S. Gov. Res. Rep., Vol. 39, p. 95(A), June 20, 1964 AD436 705 OTS \$1.60

Various possibilities for protecting the human eye from blinding through laser radiation have been considered. Of the investigated selectively absorptive and/or selectively reflective (dielectric) optical filters, some have to be disregarded for a variety of reasons. The Schott BG-18 type filter glass, in a thickness of approximately 4.3 mm, appears to provide adequate protection in the low and medium energy pulse range and in a spectral range between 0.69 and 1.2 microns, covering the ruby as well as the Nd-doped glass and CaWO₄ lasers. The calculations are based on the assumption of equality of the burn sensitivities of the human and of the rabbit retina.

26,060 PRESENCE OF FREE RADICALS IN LASER IRRADIATED BIOLOGICAL SPECIMENS BY ELECTRON-SPIN RESONANCE by V. E. Derr (Martin), E. Klein (Roswell Park Memorial Inst.) and S. Fine (Northeastern U.); Appl. Optics, Vol. 3, pp. 786-787, June 1964

The results of studies conducted on the interactions of laser radiation with biological materials ranging from subcellular structures to intact organisms are presented. Although conclusive experiments have not as yet been conducted, the deep wounds produced by laser beams in mouse and rabbit tissue are indicative that laboratory workers must exercise great caution to prevent exposure. Experiments were performed to determine if free radicals are produced by laser irradiation in white and black mouse skin, mouse liver and preparations of the enzymes homolysin and collangenase.

26,061 APPLICABILITY OF LASER TECHNIQUES by W. S. Litchman (ITT Commun. Sys.); Cont. AF19 628 3358, 80 pp., Mar. 13, 1964; U.S. Gov. Res. Rep., Vol. 39, p. 114(A), June 5, 1964 AD 434 378 OTS \$7.60

Laser communication techniques that can be integrated into the AIRCOM System to satisfy unmet current and estimated future AF requirements are described. The advent of the laser has aroused great interest among communication engineers because it affords use of a new spectrum millions of megacycles wide. Although the laser will have a great impact in certain areas of communications technology, its potential in any specific area must be carefully evaluated.

26,062 X-BAND MASER RECEIVER COMPLEX (Collins Radio); Cont. AF33 657 8604, 161 pp., Jan 1964; U.S. Gov. Res. Rep., Vol. 39, p. 24(A), May 5, 1964 AD430 101 OTS \$12.00

A maser receiving complex is described. The system was designed to study the capability and performance using a belt of orbiting resonant dipoles as reflectors for microwave communications. A twin cavity maser preamplifier is used to obtain low-noise performance at 7750 and 8350 mc. The measured equivalent noise temperature of the receiver is approximately 50°K. A 13.5-foot parabolic reflector is used, having a high F/D ratio. This resulted in extremely low side-lobe gains, thereby increasing the system signal-to-noise ratio. The antenna is mounted upon a modified SCR-584 radar mount. The system local oscillator has a short-term stability of 1×10^8 , permitting accurate signal frequency determination. The oscillator stability is obtained by the use of crystal oscillator and varactor multipliers.

26,063 ANALYSIS AND OPTIMIZATION OF LASER RANGING TECHNIQUES by G. W. Flint (Martin); IEEE Trans., Vol. MIL-8, pp. 22-28, Jan. 1964

The general criteria for the operational performance of laser ranging systems are considered in quantitative terms with emphasis being placed on the optimization of systems which must meet specific operational requirements. The entire range-determining process is discussed on a statistical basis and the target detection capabilities of a system are defined in terms of the relative probabilities of recording real and false targets. Within this analysis appears a detailed discussion of all contributing noise sources, these being reduced to a fundamental noise source for two specific systems which transmit at different frequencies. A comparison is then made between the relative power requirements of the two systems performing the same task. In the case of some pulsed gas lasers, the pulse duration is somewhat long, thus necessitating a compromise between range resolution and maximum range capability. The relationship between these parameters is discussed in detail. In addition, a technique is proposed whereby the resolution is varied as a function of target return. This technique employs a multiple pulse transmitter and automatically optimizes its resolution and range capabilities.

26,064 FEASIBILITY OF A LUNAR OPTICAL RANGING EXPERIMENT by R. L. Iliff and M. S. Tavenner (AFC Res. Lab.); AFCRL 63 908, 24 pp., Dec. 1963; U.S. Gov. Res. Rep., Vol. 39, p. 117(A), June 5, 1964 AD 434 586 OTS \$2.60

A lunar ranging experiment using a high energy pulsed laser is discussed giving special attention to the required minimum return signal, interfering radiation, detector devices, and pulse length.

26,065 A CLOUD SURVEILLANCE RADAR UTILIZING A MASER AS A LOW-NOISE PREAMPLIFIER by E. Frost and M. Katzman (AERDA); AERDL TR 2399, 12 pp., Sept. 1963; U.S. Gov. Res. Rep., Vol. 39, p. 8(A), Apr. 5, 1964

The application of an X-band maser as a preamplifier for a weather radar is described. It was desirable to increase the sensitivity of the radar in order to observe greater cloud detail in addition to achieving greater range. The possible ways of accomplishing increased sensitivity include increasing transmitter power, optimizing bandwidth and signal processing to the information rate, shifting the operating frequency, and optimizing antenna design. The application of a low-noise preamplifier was chosen for this investigation. The results of this application are presented, and the system, consisting of a traveling wave ruby maser and the AN/MPS-34 radar, is described.

26,066 ROTATION DETECTION WITH A RING LASER by P. G. R. King (Services Electronics Res. Lab.); Contemp. Phys., Vol. 5, pp. 280-283, Apr. 1964

A ring laser scheme, able to detect very small angular rotations, with possible applications in inertial guidance systems is described. Rotation detection is done by frequency comparison of two light beams that travel in opposite directions around the ring. Radiation propagating around the ring against mechanical rotation has its frequency increased. If samples of this and the oppositely directed radiation are suitably superimposed on a photo detector, the output from the detector is modulated at a frequency equal to the difference between the two oscillation frequencies, which is directly proportional to the absolute rotation rate.

26,067 RING LASER ROTATION RATE SENSOR by W. M. Macek, D. T. M. Davis, Jr., R. W. Othius, Jr., J. R. Schneider and G. R. White (Sperry Gyroscope); Quantum Electronics III, Columbia U. Press, 1964, pp. 1313-1317

The sensing of rotation rate with respect to an inertial frame of reference using a CW He-Ne gas travelling wave ring laser is described. The sensor requires no external references, has no moving parts and may be rigidly mounted on the object to be monitored.

26,068 DETERMINATION OF THE VELOCITY OF LIGHT USING THE LASER AS A SOURCE by D. Sinclair and M.P. Givens (U. Rochester); J. Optical Soc. Am., Vol. 54, pp. 795-797, June 1964

A measurement has been made of the velocity of light using the laser as a light source. The beating between the modes of the laser provided intensity fluctuations which made it unnecessary to modulate the beam artificially.

26,069 GENERATION OF ACOUSTIC SIGNALS IN LIQUIDS BY RUBY LASER-INDUCED THERMAL STRESS TRANSIENTS by E.F. Carome, N.A. Clark and C.E. Moeller (John Carroll U.); Appl. Phys. Lett., Vol. 4, pp. 95-97(L), Mar. 15, 1964

The use of optical impulses from a Q-spoiled ruby laser to generate acoustic signals in liquids of high optical absorptivity is discussed. A laser beam illuminated a 1.3 cm diameter area on top of the sample (various concentrations of ferric ferrocyanide, Prussian blue, in wafer). A piezoelectric transducer was mounted flush with the bottom of the sample holder and coaxial with the laser beam. Measurements were made with and without a glass backing plate in contact with the illuminated interface to study the effect of altering the acoustic boundary conditions. With the backing plate the stress consists of a unidirectional compressive impulse; without the plate it is a compression followed by a rarefaction. The peak amplitude of the impulse decreases and the duration increases as the optical absorptivity is reduced. These results indicate that the acoustic signals are produced by transient heating.

26,070 POLARIZATION OF LASER LIGHT SCATTERED BY GASES by N.J. Bridge and A.D. Buckingham (U. Oxford); J. Chem. Phys., Vol. 40, pp. 2733-2734, May 1, 1964

A device is described which produces the parallel monochromatic light beam required for accurate determination of the polarization of light scattered by gases. Apparatus for collection and analysis of scattered polarized light is also described. Required corrections for use of gases of different molecular form are discussed. Observed anisotropy, κ , for H_2 is compared with some former theoretical and experimental results.

26,071 ON THE POSSIBILITY OF SIMULATING METEOROID IMPACT BY THE USE OF LASERS by W.J. Rae and A. Hertzberg (Cornell Aeronautical Lab.); NASA Cont. NAS3-2536, 44 pp., Apr. 1964, STAR, Vol. 2, p. 1476(A), June 23, 1964 NASA CR 54029; CAL-AT-1821-A-1 OTS \$4.60

This report discusses the possibility of studying the problem of meteoroid damage by using a laser to simulate the conditions of high-speed impact. The characteristics of the light output from a laser allow a strongly focused pulse of energy to impinge on the target surface. The principal content of the report is a critical examination of the extent to which such irradiation simulates the conditions of impact by a solid projectile. The present state of knowledge concerning meteoroid-impact damage is briefly reviewed, and the capabilities of a laser are examined.

26,072 MEASUREMENT OF CONTINENTAL DRIFT AND EARTH MOVEMENT WITH LASERS by W. Honig (Honig Lab.); Proc. IEEE, Vol. 52, p. 430(L), Apr. 1964

A method of experimental determination of a theoretical continental drift of 1-2 inches per year using helium-neon cw lasers is described. An experimental setup to measure doppler shift with lasers is shown, and sites for possible observation of the drift, the Straits of Gibraltar and the Straits of Aden, are given. Problems of operation are either solvable or will not detract from the usefulness of the method.

Photoemission from Laser Heated Zn - See 25,366

Emission from Laser Heated:

BaO Cathodes- See 25,360

W Cathodes- See 25,361, 25,362

Laser Induced Photocurrents in Anthracene - See 25,692

26,073 EFFECTS OF THE LASER BEAM by D. V. Missio (Raytheon); Proc. Natl. Electronics Conf., Vol. 19, pp. 569-573, 1963

Pulsed ruby lasers have been used to perforate various targets. The relationship between various parameters of the laser device and the nature of the target and the resulting hole is discussed. Some of the parameters found to influence the drilling capability are peak power, pulse length and power density. The importance of the focusing effects of off-axis modes will be indicated along with steps taken to reduce off axis radiation. Typical examples of work done at the Laser Advanced Development Center laboratory include the penetration of 0.25 inches of brass with 130 joules and the penetration of 0.002 inches of brass with a few millijoules to produce a hole 0.0002 inches in diameter.

26,074 SOME DYNAMIC ASPECTS OF THEORETICAL LASER MICROMACHINING LIMITATIONS by J. Rothstein (LFE); Proc. Natl. Electronics Conf., Vol. 19, pp. 554-563, 1963

This paper questions the following: (a) that lasers are inherently incapable of micromachining to dimensions less than the diffraction limit, and (b) that opacity of materials to be machined need limit working depth to small values (as could be the case in welds where pitting is objectionable). In both cases change in material properties during heating is decisive, and though (a) is possibly trivial, (b) is probably significant. The physical conditions in the working region are examined, and it is shown that the solid matter is transformed into a transparent superheated gas or plasma. The chief mechanism for energy removal is by convection as kinetic energy of the resulting plasma jet. Other mechanisms (radiation, conduction) are examined and their magnitude assessed. Effects of condensation, melting, surface tension and turbulence are examined, machining, welding and soldering briefly compared, and some remarks made on practical problems, open questions, and the comparison between light and particle beams.

26,075 LASER WELDING FOR MICROELECTRONIC INTERCONNECTIONS by H. Rischall and J.R. Shackleton (Hughes Aircraft); IEEE Trans., Vol. CP-11, pp. 145-151, June 1964

The ability to join dissimilar materials having markedly different thicknesses (ratio of 50:1) is shown to be possible using a laser. The feasibility of welding to thin films has been demonstrated by metallurgical examination of the welded connection. Welds were evaluated by visual inspection, macrosection and microsection. Preliminary results of substrate studies indicate that unglazed alumina is a satisfactory material. Laser welding, having been demonstrated as a useful interconnection method, can be developed through additional investigation for extensive application to microelectronic circuitry.

THERMAL DEVICES

26,076 NEW WAYS IN THERMOELECTRICITY by D.A. Wright (U. Durham); Brit. J. Appl. Phys., Vol. 15, pp. 217-227, Mar. 1964

The conditions necessary for thermoelectric refrigeration and generation are discussed, and are related with the properties of semiconductors. The best materials available give a performance which is adequate for numerous small scale applications but not for the conversion of significant amounts of power. The present state of the subject is described, and it is concluded that significantly better thermoelectric materials are unlikely to be discovered. It is shown that some advantage, though not very much, may be obtained by the application of a magnetic field. The Nernst and Ettingshausen effects may be useful in semiconductors which are intrinsic at the operating temperature and in which the thermal conductivity is low and electron and hole mobilities are both large. Nernst-effect generation will probably require fields exceeding 10^5 oe, but the Ettingshausen effect may be more readily applied to refrigeration.

26,077 THE COEFFICIENT OF PERFORMANCE OF THERMOELECTRIC COOLING DEVICES by W.M. Pritchard (Old Dominion College); Proc. IEEE, Vol. 52, pp. 442-443(L), Apr. 1964

A procedure for calculating and optimizing the coefficient of performance of thermoelectric cooling devices including the effects of electrical junction resistances and ac ripple in the electrical power supply is given. The objective of the optimizing procedure is to maximize the coefficient of performance with respect to the cross-sectional area of the n leg of the coupling device and the applied voltage. AC power supply ripple is introduced into the calculations through the ripple

factor $\lambda = 1 + \Theta^2$, where Θ is the rms value of the AC current component divided by the average direct current.

26,078 THE INFLUENCE OF THE THOMSON EFFECT ON THE PERFORMANCE OF A THERMOELECTRIC POWER GENERATOR by J.E. Sunderland (Knolls Atomic Power Lab., GE); Solid State Electronics, Vol. 7, pp. 465-471, June 1964

Closed form analytical solutions are given for the temperature distribution, thermal efficiency, and power output of a fully insulated thermoelectric power generator. The influence of the Thomson effect on performance of thermoelectric power generators is studied for various values of the Thomson coefficient. To facilitate the study, a logarithmic expression for the Seebeck coefficient is introduced. This expression for the Seebeck coefficient makes it possible to study the performance of devices made of materials with different Thomson coefficients, but the same average Seebeck coefficient. The results show that for positive Thomson coefficients, the Thomson effect increases the power output and decreases the thermal efficiency. The thermal efficiency increases and the power output decreases due to negative Thomson coefficients. The results of a numerical example show that serious analytical errors can result by neglecting the influence of the Thomson effect when calculating the performance of a thermoelectric power generator.

26,079 APPROXIMATE ANALYSIS OF THE OPERATION OF THERMOELECTRIC GENERATORS WITH TEMPERATURE DEPENDENT PARAMETERS by J.M. Borrego (Centro de Investigación y Estud. Avanzados del I.P.N.); IEEE Trans., Vol. AS-2, pp. 4-9, Feb. 1964

An approximate analysis of the operation of thermoelectric generators with temperature dependent parameters is presented. Expressions for the optimum current and optimum area to length ratio are obtained for the cases of maximum efficiency and of maximum power output per unit volume. The principal assumption made in the analysis is that the temperature distribution along the legs of the generator is determined, to the first order of approximation, by the thermal conductivity of the material. The equations derived in the analysis are applied to a particular solvable case, and the approximate results obtained from them are compared with the exact results.

26,080 SILICON-GERMANIUM THERMOCOUPLE DEVELOPMENT by V. Raag (RCA); In Army Signal Res. and Dev. Lab., Proc. 17th Ann. Power Sources Conf., pp. 34-37, 1963; STAR, Vol. 2, p. 1086(A), May 8, 1964

The silicon-germanium alloys and their applications as thermocouples are discussed. These alloys have a high figure of merit, possess excellent electrical and mechanical stability over a large temperature range, and can be operated unprotected in air or vacuum. Representative thermoelectric properties of these alloys are discussed. A 50-watt air-operated, silicon-germanium alloy thermoelectric generator that has exhibited negligible deterioration in prolonged operation is given as an example of the application of these alloys.

26,081 OPERATIONAL PERFORMANCE CHARACTERISTICS OF PYROLYTIC GRAPHITE THERMOCOUPLES by C.A. Klein and M.P. Lepie (Raytheon Res. Div.); Solid State Electronics, Vol. 7, pp. 241-252, Apr. 1964

Output and sensitivity of thermoelectric units made up of boron Pyrographalloy (PGB) and Pyrographite (PG) rods assembled in a layer-plane configuration are discussed. Primary consideration is given to the following operational features: (a) e.m.f. enhancement as a result of heat treatment, (b) e.m.f. variation with boron content of the alloy leg, and (c) e.m.f. stability under severe thermal cycling conditions. The PG-0.7 per cent B/PG combination is shown to exhibit desirable characteristics from the standpoint of potential temperature-sensing applications. Up to about 2000°C, the thermoelectric behavior of these couples can be described in terms of a parabolic zero-gap two-band model, provided that exact Fermi-Dirac statistics are used. At ultra-high temperatures, the PGB/PG systems investigated so far develop less TEP than predicted. The reasons for this are not yet known: It may reflect intrinsic limitations of graphite thermocouples, or it may be a consequence of difficulties inherent in calibrating at very high temperatures.

26,082 DEVELOPMENT OF AN ULTRA-HIGH TEMPERATURE PYROLYTIC GRAPHITE THERMOCOUPLE by C.A. Klein, M.P. Lepie, W.D. Straub and S.M. Zalar (Raytheon); Cont. AF33 657 10332, 93 pp., Jan. 1964; U.S. Gov. Res. Rep., Vol. 39, p. 141(A), May 20, 1964 AD 431 203 OTS \$8.60

Electrical and galvanomagnetic effects along the layer planes of three classes of pyrolytic graphites (heat-treated, as-deposited, and boron-doped) are investigated in the temperature range from 0 to 1000°C. It is shown that the

simple two-band model with symmetrical upper and lower π bands and zero-gap configuration provides an adequate description of the charge-transport mechanism. Carrier concentrations and mobilities substantiate previous conclusions derived from low-temperature work, and permit assessment of crystallite sizes on an independent basis. Theoretical evaluations of the Seebeck coefficient are performed in the framework of a formation presumed rigorous for semimetals. Critical information on the scattering parameter of pyrolytic graphite is thus deduced. Experimental Seebeck-coefficient results confirm the main features of the analysis, in particular the type reversal that occurs in turbostratic graphites at temperatures of about 500°C. Thermocouple-design feasibility studies reveal that PGB/PG systems are capable of operation at least up to 2800°C.

26,083 EXPERIMENTAL RESEARCH ON THERMOELECTRIC CONVERTER [in Japanese] by S. Fujimoto (Fukui U.); J. IEE Japan, Vol. 83, pp. 2080-2088, Dec. 1963

The principles and performance of a thermoelectric converter are described. A ferroelectric has a large capacitance, C_1 , at a temperature T_1 near the Curie point and a smaller capacitance, C_2 , at a higher temperature T_2 . If the ferroelectric is charged by voltage V_1 at T_1 and heated to T_2 , the voltage at T_2 , V_2 is $V_2 = V_1 C_1 / C_2$ while the change in energy is $\Delta W = (C_1 / C_2 - 1) C_1 V_1^2 / 2$. (Ba + Ca + Sr)TiO₃ ceramics have been used to fabricate converters; the Curie point of all the materials is about 22°C. Static experiments on the device heated with an infrared lamp for 3.5 sec. from $T_1 = 23^\circ\text{C}$ to $T_2 = 94^\circ\text{C}$ gave a voltage increase of $V_1 = 10\text{v}$ to $V_2 = 75\text{v}$. Rotating the converter between a heater and cooler gave a dynamic characteristic of 4.2 mW output (0.1%) for a rotating period of 15.4 sec. across a load resistance of 10 M Ω when $V_1 = 250\text{V}$ and the temperature amplitude is $96-23^\circ\text{C}$.

26,084 REFINED TREATMENT OF THE THEORY PERTAINING TO OPERATING CHARACTERISTICS OF ANISOTROPIC NERNST-ETTINGSHAUSEN DEVICES by J.M. Honig and B.M. Tarmy (MIT); J. Appl. Phys., Vol. 35, pp. 722-723, Mar. 1964

A refinement of the theory dealing with the operating characteristics of anisotropic Nernst-Ettingshausen devices is presented. This treatment resembles that of the Lockheed group and Riddiford concerning galvanomagnetic (GTM) devices. It applies to the case of arbitrary orientations of anisotropic device materials.

26,085 EXPERIMENTS ON ROOM TEMPERATURE NERNST-ETTINGSHAUSEN REFRIGERATORS by T.C. Harman, J.M. Honig, S. Fischler, A.E. Paladino and M.J. Button (Lincoln Lab.); Bull. Am. Phys. Soc., Vol. 9, pp. 216(A), Mar. 1964

Cooling experiments with a Nernst-Ettingshausen (NE) refrigerator, using oriented and shaped crystals of pure bismuth were reported. By cooling the hot-junction T_h of the refrigerator with flowing water, the cold-junction temperature T_c was reduced below 200°K. The cooling achieved with shaped samples as a function of electric current and magnetic field is shown. The following features are noteworthy: (a) imposing a heat load on the device by operating in air rather than vacuum increased the cold-junction temperature only a few degrees; and (b) the steady-state cold-junction temperature was closely approached in a few seconds after the current was turned on. These experiments illustrate some of the following advantages of the NE over the standard Seebeck-Peltier refrigerators: (a) the need for only one type of material for the active element, i.e., Bi in the intrinsic-conduction range; (b) the separation of the heat-flow direction from the current-flow direction; (c) the ability to use shaped arms to enhance the temperature difference; and (d) the larger ultimate figure of merit that can be anticipated.

26,086 FIGURE OF MERIT FOR ETTINGSHAUSEN COOLING by R.T. Delves (Royal Radar Estb., Malvern); Brit. J. Appl. Phys., Vol. 15, pp. 105-106(L), Jan. 1964

Measurement of the parameters of Ettingshausen cooling is discussed. The apparently divergent results obtained by various experimenters are attributed to differences in starting assumptions. The particular device under discussion is a long rectangular bar with electric current J in the 3-direction, magnetic field H in the 2-direction, and temperature gradient in the 1-direction. It is shown mathematically that a proper choice of parameters leads to measurements which are consistent.

26,087 UNICRYSTALLINE SILICON CARBIDE THERMISTOR by H.D. Batha and P.E. Carroll (Carborundum); IEEE Trans., Vol. CP-11, pp. 129-134, June 1964

The development of a uniaxial silicon carbide thermistor with a combina-

tion of unique properties is described. The device has a useful operating range from -100°C to $+300^{\circ}\text{C}$. The stability, retraceability and reproducibility which have been achieved recommend this sensor for some entirely new areas of application for thermistors.

SUPERCONDUCTIVE DEVICES

26,088 THE PRODUCTION OF MAGNETIC FIELDS BY SUPERCONDUCTORS by D.A. Watt (AE Res. Est., (Harwell); 30 pp., 1963; STAR, Vol. 2, p. 609 (A), Mar. 8, 1964 AERE-M-1207 HMSO: 4s

Summaries of information on the properties of superconductors and their application to the production of magnetic fields are given, with use of a wide selection of recent papers.

26,089 THE DESIGN OF A SUPERCONDUCTING MAGNET FOR A TRAVELING WAVE MASER USING A HELMHOLTZ PAIR by J.D.A. Day and J.W. Orton (Mullard Res. Lab.); Quantum Electronics III, Columbia U. Press, 1964, pp. 947-956

A superconducting magnet designed for use with a S-band traveling wave maser is described.

26,090 SUPERPOSITION OF SEMI-INFINITE SOLENOIDS FOR CALCULATING MAGNETIC FIELDS OF THICK SOLENOIDS by G.V. Brown and L. Flax (Lewis Res. Ctr.); J. Appl. Phys., Vol. 35, pp. 1764-1767, June 1964

A simple method is given for calculating the magnetic field components in or around any thick finite solenoid by superposition of fields of semi-infinite solenoids with zero inner radius. Equations and graphs are presented for the field components of such semi-infinite solenoids. From these graphs, the fields of solenoids of practical interest can be obtained with errors of less than a few percent. Greater accuracy is possible if numerical tables are used instead of graphs.

26,091 FIELD ENERGY REMOVAL FROM A SUPERCONDUCTING SOLENOID by M.W. Dowley (IBM San Jose Res. Lab.); Cryogenics, Vol. 4, pp. 153-165, June 1964

The necessity for protective circuitry or special fabrication techniques (copper coating of wire) for large superconducting solenoids is pointed out. The advantages of significant energy removal from a quenching solenoid are stressed. Three methods, (1) the parallel resistor method, (2) the oscillating circuit method, (3) the transformer method, of removing a large fraction of the field energy are discussed. Their advantages and disadvantages are stated and their performance evaluated. A composite method involving (2) and (3) is suggested for very large solenoids. Experimental results for methods (1) and (2) are presented. The success of these two methods depends largely on a high power, fast acting relay. Methods (1) and (2) are more efficient for coils with a long natural time constant for decay, i.e. copper coated coils, whereas the transformer method (3) is more efficient when the time constant for natural decay of the solenoid is short. Finally, methods (1) and (2) provide a means of rapidly and smoothly switching a high magnetic field to zero.

26,092 TRAINING IN SUPERCONDUCTING SOLENOIDS by M.S. Lubell and G.T. Mallick (Westinghouse); Bull. Am. Phys. Soc., Vol. 39, p. 253(A), Mar. 1964

A method has been discovered for inducing and annihilating training in superconducting solenoids. The experiments were performed on solenoids of approximate dimensions: I.D.=0.3 cm, o.d.=1.2 cm and length=2.6 cm, wound with both cold-worked and heat-treated (1 h at 700°C) 0.025-cm-diam Nb+25% Zr wire. Training was induced by cycling a uniform external magnetic field to some minimum value $-H_T$ parallel to the axis of the test solenoid in a direction opposite to the self-field of the solenoid. With the preset saturated diamagnetic moment, the solenoid exhibited training with the first quench $\rightarrow I_T \sim I_C/2$. The training can be removed by cycling the external field to $+H_T$ creating saturated paramagnetic moments, any place during the training cycle. X-Y recorder traces of flux-jump pulses V vs H_{ex} (with $I=0$) and V vs I (with $H_{ex}=$

0) were made and show that there are flux jumps without training after pre-sweeping with $+H_{ex}$ but no major flux jumps until the quench at the lowest trained value I_T after presweeping with $-H_{ex}$. A method that predicts the trained value of critical current for understanding the sequence of small steps in the trained condition was described.

26,093 SUPERCONDUCTING MAGNETS by N.S. Freedman (RCA); In RCA, Direct Energy Conversion, pp. 36-39, 1963; STAR, Vol. 2, p. 1516(A), June 23, 1964

Superconductivity allows the design of very-high-field magnets that can be started by low-voltage storage batteries and then operated with little or no further current input because of the zero loss in the windings. The process discussed for producing niobium-tin ribbon results in a unique, practical superconductor. Modular designs using this ribbon have an excellent chance of providing breakthroughs in the technology of large superconducting magnets.

26,094 NON SELF-DESTRUCTIVE 100,000-G SUPERCONDUCTING SOLENOID by H.T. Coffey, D.K. Fox, J.K. Hulm, R.E. Span and W.T. Reynolds (Westinghouse Res. Lab.); Bull. Am. Phys. Soc., Vol. 9, p. 454(A), Apr. 1964

A superconducting solenoid consisting of an outer section wound from niobium-zirconium wire and an inner section wound from niobium-titanium wire has been operated up to 100,000 G at 4.2°K . The solenoid is approximately 7 in. o.d., 4 in. long, and had an access hole of 0.125 in. in diam. Copper plate of 1 mil thickness was used to protect the windings from high-voltage damage, in contrast to an earlier solenoid constructed from Nb_3Sn that achieved 100,000 G once but then seriously damaged itself upon normalization and had to be scrapped. The solenoid has been driven normal a large number of times in the range between 90,000 and 100,000 G without damage to the windings. Some training effects were observed in the present coil and as many as 3 repeated normalizations have been necessary in the range between 94,000 and 100,000 G in order to achieve the maximum field. It is concluded that ductile alloys are useful for magnet construction in the range up to 100,000 G.

26,095 SOME EXPERIMENTAL RESULTS OF SUPERCONDUCTING SOLENOIDS by G. Pasotti, N. Sacchetti, G. Sacerdoti and G. Sanna (Com. Naz. Nuc., Frascati (Italy); 16 pp., Nov. 11, 1963; STAR, Vol. 2, p. 733 (A), Mar. 23, 1964 Its Nota interna 217; LNF-63/67

Experimental results indicate that it is impossible, in the design stage, to predict the performance of a superconducting coil because of the difference in behavior of a piece of wire and the same wire wound in a coil. A lack of reproducibility of the performance of the coils in a given series of trials, as well as in successive trials, was found. Among the causes of nonreproducibility were the "training," local annealing of the wire caused by transitions to the normal state, residual fields, etc. It was not possible to exclude the effect of various phenomena, such as mechanical vibrations and shocks, electrical oscillation caused by the high inductance, the high stray capacitance, and the very low resistance of the circuit. Results indicate that a considerable quantity of magnetic energy is concentrated in a small volume, and that rough calculations for magnets near transition show that this stored energy is of the order of magnitude of the total energy necessary to make the superconducting electrons go into the normal state.

26,096 A SUPERCONDUCTING MAGNET WITH INDUCTIVE EXCITATION by V. Karasik, R. Akchurin and S. Akhmedov (Acad. Sci., USSR); Cryogenics, Vol. 4, p. 44(L), Feb. 1964

The specifications, limitations and construction details of a superconducting magnet with inductive excitation are discussed. A field is induced in niobium windings by current flowing in surrounding copper windings. The magnet is then lowered to liquid helium temperatures and the current in the copper coils shut off, "freezing-in" 90% of the field obtained in this manner.

26,097 FABRICATION OF Nb_3Sn SUPERCONDUCTING ELEMENT by E. Buehler and J. Kunzler (Bell Lab.); U.S. Pat. 3,124,455, Issued Mar. 10, 1964

The fabrication of Nb_3Sn superconducting solenoids capable of current densities of 100,000 amp/cm² at fields of 88 k Gauss is described. Winding wires are produced by successive cold rolling of metallic tubes filled with powdered Nb_3Sn or Nb and Sn.

26,098 FAST-ACTING SUPERCONDUCTING POWER SWITCHES by D.L. Ameen and P.R. Wiederhold (Ion Physics); *Rev. Sci. Instr.*, Vol. 35, pp. 733-737, June 1964

Superconducting switches operating on the basis of superconducting-to-normal transitions are considered as a means of initiating high power pulsed discharges from inductive energy storage systems. An analysis of transition times, power losses, and design techniques is presented. Thermally and magnetically activated switches, consisting of long, noninductively wound 0.005-in. Nb-25% Zr wires, with normal resistances in the kilohm region, have been tested. A linear representation of the reappearance of resistance during a superconducting-to-normal transition yielded values up to $10^5 \Omega/\text{sec}$. A mathematical analysis, which is in good agreement with experimental results, is given. Factors influencing the rate of increase of resistance are reviewed.

26,099 CRYOGENIC FLUX PUMP SWITCHES HIGH CURRENTS by T.A. Buchhold (GE); *Electronics*, Vol. 37, pp. 61-63, Mar. 23, 1964

A flux pump that could handle thousands of amperes of current without heavy conductors is described. A saturable reactor is used to switch a modified cryotron unit on or off to make it superconducting. It resembles a controlled rectifier, which is made conductive by a gate signal, and offers very high resistance to reverse currents; all circuits suitable for controlled rectifiers can be used also for controlled reactor cryotrons. The main difference between this new reactor cryotron and the conventional small-current computer cryotrons is its different geometry and much larger dimensions.

26,100 SUPERCOOLED COILS PROMISE INDUCTIVE ENERGY STORAGE by P.R. Wiederhold and D.L. Ameen (Ion Physics); *Electronics*, Vol. 37, pp. 75-79, Mar. 13, 1964

Inductive storage of energy in superconducting coils which provide more than 10^7 joules/m³ is described. The coil can be charged over a long period of time with a low-voltage power supply. Once stored, the energy can be kept in storage for indefinite periods at 4.2°K since the persistent current encounters no resistance. Short discharges in the millisecond range are possible, provided that a suitable superconducting switch is available. An experimental supercooled energy store has delivered 350 joules with efficiencies up to 90 percent.

26,101 SUPERCONDUCTING PULSE POWER SUPPLY by P. Wiederhold (Ion Physics); *IEEE Trans.*, Vol. MTT-12, p. 386(L), May 1964

The storage of large quantities of electrical energy in superconducting coils operating at liquid He temperatures is described. The stored energy can be released in the form of a high power pulse of short duration. Switching of the stored energy is accomplished by the superconducting-to-normal transition. A 1200 joule-storage coil has an efficiency greater than 90%.

26,102 EVALUATION OF A SUPERCONDUCTING ROTATING ELECTRIC GENERATOR by C.J. Oberhauser, E.F. Doyle and R.L. Mela (Dynatech); *Contr. AF33 657 11062*, 30 pp., Jan. 1964; *U.S. Gov. Res. Rep.*, Vol. 39, p. 30(A), May 5, 1964 AD 430 128 OTS \$2.60

Research was continued on a program to determine the feasibility of the application of superconductor technology to the generation of electrical power by rotating electromagnetic devices. Since the anticipated use of such a generator is for long missions, a refrigerator with associated equipment must be part of the package. The work includes analytical and design studies of both electrical and mechanical components. The program is divided into three parts: initial design study, supporting tests, and second-round design. Results of supporting tests and initial second-round design are discussed.

26,103 A SUPERCONDUCTING DC DYNAMO DRIVEN BY A ROTATORY MAGNETIC FIELD by D. van Houwelingen, P.S. Admiraal and J. van Suchtelen (Philips Res. Lab.); *Phys. Lett. (Neth.)*, Vol. 8, pp. 310-311 (L), Mar. 1, 1964

A superconducting dc dynamo in which the movement of a normal spot is obtained by a moving pattern of a magneto field, rather than by a rotating magnet, is discussed. The moving field pattern has been obtained from the

stator field of a 0.01 hp, 3000 rpm, 50 cps, 220 v three-phase squirrel cage motor, fitted with an iron yoke for dc superposition. A superconducting foil consisting of a vacuum-deposited Pb layer on 0.1 mm brass cylindrical substrate, with a slit parallel to the axis, was used. A dc voltage of 0.01v has been obtained at liquid helium temperature. When a superconducting circuit of small self-inductance was connected to the lead foil, a current of 85A was obtained almost immediately. After the rotatory ac field was switched off there was a persistent current of about 70A in the circuit. Redesign of the magnetic circuit will improve the emf and maximum current levels.

26,104 THREE-PHASE SUPERCONDUCTING MOTOR by J.D. Jones and P.W. Matthews (U. British Columbia); *Rev. Sci. Instr.*, Vol. 35, pp. 630-633, May 1964

A three-phase motor is described which has one or more loops of superconductor for its rotor and uses superconducting field coils. The theory of the motor is outlined, including the case when flux is frozen into the rotor. The predictions of the theory are compared with the experimentally observed torque produced by the motor.

26,105 HIGH-FIELD Nb₃Sn SUPERCONDUCTING MAGNETS BY MAGNETIC-FIELD STABILIZATION by E.R. Schrader and N.S. Freedman (RCA) and J.C. Fakan (NASA); *Appl. Phys. Lett.*, Vol. 4, pp. 105-106(L), Mar. 15, 1964

A superconducting Nb₃Sn magnet which can achieve central fields up to 92 k/gauss at 4.2°K is discussed. The superconducting coils in the magnet consisted of a 5-to-8μ thick coating of Nb₃Sn vapor deposited on a stainless steel substrate, with an equal thickness of copper on all surfaces. Preliminary studies indicated that copper plating of an Nb₃Sn tape increased the maximum critical currents attainable in both coils and short samples, with a significant increase in stability, and that high background fields increased the coil critical current and self field. A high central field (coil self field plus background field) results. A magnet constructed of three physically independent, axially aligned coils had central field values in excess of 85 k/gauss at 4.2°K, with a maximum of 92 k/gauss. The current in each coil when tested independently was only 60 to 80 A; with a background field of 10 k/gauss provided by the outer coil, the inner and central coils had critical currents of 120 A.

26,106 SUPERCONDUCTIVE DEVICE UTILIZING A FERROMAGNETIC SUPERCONDUCTIVE ELEMENT by J.L. Rogers (Space Tech. Lab.); *U.S. Pat.* 3 125,688, Issued Mar. 17, 1964

A thin film superconductive gating device featuring high switching speed while preserving signal gain is described. The device is comprised of control elements and a superconducting gate, a thin layer of material that exhibits ferromagnetic properties at the same temperature at which it exhibits superconductive properties. The resulting increased permeability of the element leads to a higher gain of the overall device than can be achieved with non-ferromagnetic materials. A memory unit is also described which stores information by use of the remanent magnetization of the gating element.

26,107 LONG SUPERCONDUCTIVE DELAY LINES by R.J. Allen (Martin); *Proc. IEEE*, Vol. 52, pp. 615-616(L), May 1964

Superconductive delay lines with appreciable storage capacity over a μsec delay and at 100 Mc or better clock rates are described. The lines were constructed from a 15 mil Nb center conductor, a 51 mil FEP teflon dielectric to give 50 Ω impedance and a heavy lead jacket. Pulse storage in a 1 μsec line clocked at 250 Mc phase rate is illustrated, storing a 1011 code randomly in six locations.

Tunneling in Superconducting Pb Junction - See 25,326

BASIC SOLID STATE DEVICE CIRCUITS

GENERAL

NETWORK THEORY

- 26,108 A METHOD OF TIME-DOMAIN APPROXIMATION FOR ARBITRARY INPUTS by B. Liu (Princeton U.), and H.E. Meadows (Columbia U.); 1964 IEEE Int. Conv. Rec., Part 1, pp. 338-343, Mar. 23-26

A method for solving the time-domain approximation problem directly, without recourse to the frequency domain is presented. Such a direct approach avoids the cumbersome process of actually taking the transforms of real signals, a process difficult to instrument simply. Using the concept and techniques of signal decomposition into orthogonal exponential functions, the proposed method provides the desired impulse response of the network by determining the coefficients of its orthonormal expansion. These coefficients can be determined simply and straightforwardly. Furthermore, the method has the added merit that it may be easily implemented.

- 26,109 CUT-SET MATRICES AND THE CEDERBAUM ALGORITHM by F.T. Boesch (Bell Labs.); 1964 IEEE Int. Conv. Rec., Part 1, pp. 257-262, Mar. 23-26

The relation between a fundamental cut-set matrix and the nodepair admittance matrix is discussed. The main contribution lies in a simplified derivation and utilization of the Cederbaum algorithm, which relates the realization of cut-set matrices to the synthesis of resistor networks. The Cederbaum algorithm was based on two theorems which are entirely algebraic in nature, and they were originally derived from the algebraic properties of total unimodular matrices. A considerable simplification is provided by a network derivation of these two theorems. The algorithm itself is also simplified by network concepts.

- 26,110 MATRIX ANALYSIS OF NETWORK SENSITIVITIES by L.P. Huelsman (U. Arizona); Proc. Natl. Electronics Conf. 1963, Vol. 19, pp. 1-5

The designer of any passive or active network is intimately concerned with the problem of sensitivity, i.e., the effect that changes in the characteristics of individual network components may have on the overall characteristics of a network. A general method is presented whereby all the sensitivity information for a given network may be expressed in matrix form. The method consists of three steps. In the first step, a relation is developed between the changes in the pole and zero locations of the network function and the changes in the coefficients of the denominator and numerator polynomials. In the second step, a relation is developed between the changes in the coefficients of the polynomials and the changes in the values of the network components. Finally, a matrix expression is written for the sensitivity relations, and appropriate normalizations are made. The result is a complete sensitivity description of the network. Application of the technique is made to an active network situation, and the effects of approximations are illustrated.

- 26,111 MATRICES FOR BASIC TWO-PORT NETWORKS by E.H. Kopp (Los Angeles State Coll.); Electro-Tech., Vol. 73, pp. 34-39, Mar. 1964

The six basic matrices for the sixteen most used networks are given. First two-port matrices for the basic networks (series and shunt impedance, T and pi circuits, and the ideal transformer) are presented. A table defines and names the general z , y , h , g , a , and b open and short circuit parameters (4 each). A second table lists the same 24 parameters for these networks; series element, shunt element, T circuit, pi circuit, symmetric lattice, general transmission line, lossless transmission line, ideal transformer, negative-impedance inverter, ideal gyrator, voltage and current controlled v and i sources, and negative impedance converter. Active networks are carefully defined and the classification of networks as active vs passive and reciprocal vs non-reciprocal is discussed.

- 26,112 A TOPOLOGICAL TEST FOR THE REALIZABILITY OF A CLASS OF RESISTIVE n -PORTS by K.K. Nambiar and L.N. Kanal (Philco Res. Lab.); 1964 IEEE Int. Conv. Rec., Part 1, pp. 263-269, Mar. 23-26

A simple topological procedure, requiring no computation is presented for testing the realizability of an open-circuit resistance matrix of order n satisfying the relation

$$r_{ij} = r_{ji}, \quad i, j = 1, 2, \dots, n,$$

for some value of the index j . The method described is applicable to matrices of arbitrary order and an example is presented using a 20×20 matrix. It is also shown that three matrices which require considerable computation before their realizability or non-realizability can be decided by known methods, become very simple exercises for the topological method described here.

- 26,113 COMPUTER GENERATION OF EQUIVALENT NETWORKS by D.A. Calahan (U. Calif., Berkeley); 1964 IEEE Int. Conv. Rec., Part 1, pp. 330-337, Mar. 23-26

The theory of continuously equivalent networks is extended to the state equations and to include a scaling option. The theory is then applied to the classical problem of the design of low- and band-pass filters with loss in inductors only. The alignment problem in active filters is also approached from an equivalence viewpoint.

- 26,114 DISTRIBUTED CIRCUIT DESIGN by M. Kohn (Sprague Electric); Electro-Tech., Vol. 73, pp. 93-96, May 1964

The criteria leading to a predictable performance distributed network design which allows reduced component count and enhanced performance, but not trial and error substitution advantages over conventional circuitry are presented. The general problem is the description of a circuit that consists of a generator, its impedance, a distributed network, and a load impedance. Approximation methods, including approximation by lumped equivalents are presented, and an explicit calculation of a series-resistance, shunt-capacitance distributed network is made. A computer is recommended for calculation leading to the synthesis of an optimum distributed network.

MICROCIRCUITS

- 26,115 INTEGRATED CIRCUITS TODAY AND TOMORROW by C.L. Hogan (Motorola); Electron Indus., Vol. 23, pp. 58-67, June 1964

The development pattern in integrated circuit technology is summarized and future growth predicted. The basic microminiature techniques used today are given and component construction of the integrated circuit method is reviewed. Labor and material costs are compared among the various technologies, and the problem of high speed, high frequency limitation in the monolithic silicon circuit is discussed at length. The capacitor as a part of an integrated circuit is examined with respect to construction methods and cost. State-of-the-art packaging techniques are presented.

- 26,116 INTEGRATED CIRCUITS by P.E. Haggerty (TI), C.L. Hogan (Motorola), R.N. Noyce (Fairchild), L.C. Maier (GE), J.E. Brown (Zenith), and C.H. Knowles (Westinghouse); IEEE Spectrum, Vol. 1, pp. 62-82, June 1964

An edited version of a 1964 IEEE Intl. Convention symposium is presented. Various types of available integrated circuits including thin films, multiple chip, monolithic silicon, hybrid and magnetic are discussed with relation to comparative manufacturing processes, performance and costs. The impact of integrated circuitry in government and consumer as well as industrial equipment is reviewed. The field of research and development in integrated circuitry is described, and the economic effect of integrated circuitry on the entire electronics industry is summarized.

- 26,117 CURRENT TECHNICAL STATUS AND PROBLEMS IN MICROELECTRONICS by J.S. Kilby (Texas Instr.); The Impact of Microelectronics, McGraw-Hill, 1963, pp. 75-87

The areas in which semiconductor microelectronic circuits may be produced, may equal or exceed the performance of conventional components and may be produced at attractive prices are outlined.

- 26,118 ULTIMATE LIMITS OF MICROELECTRONICS by J.T. Wallmark (RCA Labs.); The Impact of Microelectronics, McGraw-Hill, 1963, pp. 89-101

Economic and technological considerations are invoked in estimating the maximum packing density and maximum justifiable complexity which can be expected in microelectronics. Limiting factors considered include cosmic rays, doping variations, inaccuracies in fabrication, heat generation, and power supply and other peripheral equipment.

- 26,119 ELECTROCOMPATIBILITY ASPECTS OF MICROELECTRONICS by R.B. Schulz, and R.L. Clapsaddle (Boeing); IEEE Trans., Vol. EMC-6, pp. 37-46, Jan. 1964

The effects (relative to conventional design) of microminiaturization on the mutual compatibility among various portions of systems are considered. Major factors such as power levels, sizes of radiators and pick-ups, spacing among them and function trends toward solid-state switching and greater use of digital

operations are discussed. From these, compatibility relationships are developed, and the relative severity of the compatibility problem is estimated. Problems of corrective measures to enhance electrocompatibility are discussed, such as common use of heat paths as electromagnetic shields, filter utilizing effective or apparent inductance from semiconductor functions, and shielding effectiveness of flat cables and microminiature connectors. Conclusions are that RF susceptibility to magnetic fields is reduced, but susceptibility to electric fields is increased with respect to conventional construction. The larger parasitic parameters of the Semiconductor Integrated Circuits (ASIC) approach will degrade electro-compatibility. An anticipated trend toward digitized circuits will also degrade electrocompatibility.

26,120 RELIABILITY IN MICROELECTRONICS by E.R. Jervis (ARINC Res.); The Impact of Microelectronics, McGraw-Hill, 1963, pp. 103-114

Two aspects of microelectronics reliability are discussed, the problem of predicting reliabilities and the possibilities opened up by the reliability of microelectronics. The performance-spread and the product-rule prediction methods have both been incorporated into a computer program which now awaits testing. Mean times between failures for typical 1000-active-unit Systems are 10 to 100 times longer for microelectronic circuits than for comparable conventional equipment; this may greatly reduce if not eliminate maintenance organizations.

26,121 EXPERIMENTAL INVESTIGATION OF SIMULATED SPACE PARTICULATE RADIATION EFFECTS ON MICROELECTRONICS by E. Rind and F.R. Bryant (NASA Langley Res. Ctr.); 1964 IEEE Int. Conv. Rec., Part 7, pp. 57-63, Mar. 23-26

Microelectronics, like their more conventional solid-state counterparts, are adversely affected by radiation environments such as those found in outer space. These space radiation environments are briefly summarized. Proton irradiation data at 22, 40, 128, and 440 mev are presented for typical macroelectronic components such as low-, medium, and high-frequency transistors and compared with similarly irradiated discrete- and integrated- circuit type of microcomponents. Damage tends to vary inversely with energy. Integrated flux levels of approximately 10^{11} protons/cm² are needed before the radiation effects become noticeable. Integrated circuits appear to be slightly more resistant to radiation but this finding may not be significant on a statistical basis. A typical experimental setup and circuit which were actually used in the tests are illustrated and described.

26,122 MONOLITHIC INTEGRATED CIRCUITS by A.B. Phillips (Motorola); IEEE Spectrum, Vol. 1, pp. 83-101, June 1964

Using a typical monolithic digital integrated circuit as an illustrative example, the steps involved in translating this circuit design into a final monolithic circuit are described. The highlights of integrated circuit theory, design relationships, processes, and parameters are developed, covering most contemporary applications of monolithic circuits to digital computers. Parasitic capacitances introduced during monolithic construction are analyzed, and a new parasitic-less integrated circuit design is announced. DTL circuit performance comparisons are made between the monolithic and hybrid or discrete circuit.

26,123 INTEGRATING LINEAR CIRCUITS by D. Bailey (Motorola); Electronic Products, Vol. 7, pp. 50-51, 91-95, June 1964

The design procedure for creating integrated circuits from a black box requirement for both hybrid and monolithic types is given. Application criteria for hybrid, monolithic, and monolithic compatible silicon circuits, including performance, quantity, initial cost considerations and flexibility. Monolithic transistor, resistor and capacitor characteristics are presented, and some exceptional monolithic component characteristics such as matched transistor temperature tracking are discussed. The hybrid technology is explained and the nature of circuit design described.

26,124 BLACK BOXING YOUR INTEGRATED CIRCUIT by D. Bailey (Motorola); Electronic Design, Vol. 12, pp. 74-77, June 22, 1964

A design approach compatible with the problem of the wide variety of parameters in integrated circuits is proposed. The design engineer may either keep himself thoroughly informed on the latest technical developments so that he can provide the integrated circuit manufacturer with a complete set of device specifications and a workable schematic, or he can provide the semiconductor manufacturer with complete "black box" terminal specifications to which the final device must be manufactured and guaranteed. A flow chart of integrated circuit manufacture with typical time breakdown for design and fabrication is given, and the limitations of monolithic construction are discussed. A summary in the form of a check list of black-box specifications is presented.

26,125 THREE WAYS TO INTEGRATE A FREQUENCY DIVIDER by E.R. de Atley (Fairchild Camera Instr. Corp.); Electronic Design, Vol. 12, pp. 78-81, June 8, 1964

A 100:1 frequency divider for an experimental radar demonstrating reduction in power and size required by integrated circuitry is examined. The evolution of the system from a 27.5-sq. in. printed circuit board unit having 167 components with power dissipation of 700 mw. To a 3.75 sq. in. board with three TO-5 cans and 18 interconnections is described. System and circuit diagrams as well as photographs of completed units are presented.

26,126 CAPACITIVE INTERACTIONS IN FILM-TYPE CIRCUITS by J.B. Compton and W.W. Happ (Arizona State U.); Proc. Natl. Electronics Conf., 1963, Vol. 19, pp. 721-729

Conformal mapping techniques such as the Schwartz-Christoffel transformation are utilized to derive interfilm capacitances for a wide range of commonly used geometries. Design techniques to minimize interelectrode capacitive effects on circuit performance were developed. Commercially available prototypes were studied to determine quantitatively parasitic capacitive effects such as spurious oscillations and undesired feedback. Design charts and practical examples illustrate the power and directness of the techniques. Approximation methods for conformal mapping and tables of transforms suitable for engineering calculations are presented with a view to assist the circuit designer in analyzing integrated and film-type structures.

26,127 PHOTOETCHING THIN FILM CIRCUITS by C.W. Skaygs (Bunker Ramo Corp.); Electronics, Vol. 37, pp. 94-98, June 15, 1964

A method of photoetching which promises better quality with less cost and time than that required with the mechanical masking technique is described. The conductive bonds and resistive parts of the thin films circuit pattern are made by selective chemical etching, using Kodak Photo-Resist and photographic techniques. The apparatus for the process including the vacuum system and the source selector is described along with representative parts of the process itself, composite and conductor etching, bonding assembly and sweating.

26,128 WILL MOLECULAR STRUCTURES MAKE MICROCIRCUIT INDUCTORS? by H.G. Dill (Hughes Aircraft); Electronic Design, Vol. 12, p. 82, Mar. 16, 1964

Inductive elements using coil-like organic structures are described. They hold particular promise as resonant elements in vhf thin-film circuits. From x-ray measurements of one molecule, the inductance L of a whole element with many coiled molecules in parallel would be 4×10^{-15} h and the Q factor would be 2.4×10^{14} . The development of metal-organic polymers should increase L and reduce the losses by building into the organic structure copper, silver, gold and aluminum for low resistivity, and iron, cobalt and nickel for high permeability. Such a development may produce devices that can be used as molecular resonant elements in the mm-wave region.

26,129 INTERCONNECTION TECHNIQUES FOR MICROCIRCUITS by F.Z. Keister, R.D. Engquist, and J.H. Holley (Hughes Aircraft); IEEE Trans., Vol. CP-11, pp. 33-41, Mar. 1964

The problem of how to interconnect today and tomorrow's microminiature electronic circuit packages is one which is growing increasingly complex in view of the ever-diminishing size factor. Twelve interconnection techniques, ranging from the relatively-simple soft soldering technique to highly-advanced methods, such as electron beam welding and laser welding are described. An attempt has been made to present not only the mechanics of the various techniques, but to emphasize the materials, processes and equipment involved in each specific microcircuit interconnection method.

26,130 NEW INTERCONNECTION METHODS FOR MICRO CIRCUITS by J.B. Northrop and C.L. Zachry (Autonetics); IEEE Trans., Vol. CP-11, pp. 152-156, June 1964

New microbonding techniques involving a method of attacking conductive lead to thin metal films on substrates without changing the electrical properties of the components deposited on the substrates are discussed. A split tip bonder is described with its special electrodes, a split tip nailhead, a momentarily heated bushing insert nailhead, and a momentarily heated wedge insert. Tensile and torque tests show that the nailhead bond has a high resistance to peeling stresses. A Metallography and microprobe analysis is also conducted.

26,131 A NEW CONCEPT FOR MICROMINIATURE INTERCONNECTIONS by M.E. Peel (Burndy Corp.); IEEE Trans., Vol. CP-11, pp. 173-181, June 1964

A design in microminiature connections which features a broad system applicability and maximization of contact density while maintaining minimum weight and space, satisfactory performance characteristics, design flexibility and structural stability at an adequate reliability level is presented. Material selection criteria, reflection-permanent set, and deflection-normal force characteristics are studied to reveal the optimum design. The microminiature

checkerboard connector is introduced with claims that this concept can save space by 20-60%, reduce weight by 20-60%, and at the same time double the contact density.

26,132 A NEW INTERCONNECTION TECHNIQUE FOR INTEGRATED CIRCUITS by D. Grabbie (Photocircuits Corp.); 1964 IEEE Int. Conv. Rec., Part 9, pp. 105-111, Mar. 23-26

A technique for interconnecting integrated circuits with printed wiring which allows the use of conventional resistance welding equipment and does not require bending the leads of modules in flat or wafer packages is described. The technique consists of inserting weldable pins into plated-through holes in multilayer printed circuit boards and forming a continuous metal alloy between the pin and the plated-through hole by a diffusion process. Integrated circuits can be welded directly to the pins which can be set at any desired height above the surface of the board. Defective modules can be removed and replaced without damage to the printed circuit board.

26,133 INTERCONNECTION OF INTEGRATED CIRCUIT FLAT PACKS IN AUTONETICS IMPROVED MINUTEMAN PROGRAM by E.F. Harmon (North Am. Aviation); IEEE Trans., Vol. CP-11, pp. 135-144, June 1964

Design studies for the Improved Minuteman computer reveal the necessity for advanced microcircuit interconnection techniques in order to capture the potential advantages of integrated circuits. The development of a unique multilayer board concept is described in terms of such factors as design procedures, masking techniques, and fabrication, test and rework methods. With reliability as the dominant factor in all trade-off studies the significance of physical and electrical parameters is discussed as well as the influence of considerations of producibility, yield, and system constraints.

26,134 VERSATILE INTERCONNECTION - PACKAGING SYSTEM FOR INTEGRAL ELECTRONICS USING ELECTRON BEAM TECHNIQUES by E.H. Miller (Wright-Patterson AFB) and D.J. Garibotti (Hamilton Standard); Proc. Natl. Electronics Conf. 1963, Vol. 19, pp. 519-534

The progressive reduction in size of electronic circuits as typified by semiconductor and thin films microcircuits requires drastic changes in existing interconnection - packaging manufacturing processes to maintain high reliability standards at reasonable cost. Electron beam techniques offer reliable as well as high speed automated processes. An automated electron beam system comprising an electron beam machine with both micro-welding and scribing capability coupled with tape programmers and beam deflection function generators is in an advanced stage of development. This facility permits the automatic interconnection and packaging of integral devices in a rapid and reliable manner. An interconnection matrix - packaging system with extremely high horizontal and vertical interconnection capability and flexibility has been defined. Exceptional thermal dissipation and volumetric efficiency in addition to compatibility with cases and uncased integral devices and auxiliary components are achieved with the proposed multilayer beryllia or alumina structure.

26,135 SUBSTRATES FOR THIN-FILM CIRCUITRY by T.C. Macavoy and S.A. Halaby (Corning); IEEE Trans., Vol. CP-11, pp. 15-22, Mar. 1964

The properties of available glass, ceramic and other substrate materials are reviewed in the light of requirements imposed by current practice in thin-film circuitry. Special substrate glasses and glazed high thermal conductivity ceramics appear to be best suited to the majority of applications. Techniques for evaluation of the smoothness of substrate surfaces are reviewed and procedures for cleaning glass and glaze surfaces are recommended.

26,136 DIELECTRIC FORMULATIONS FOR USE IN PROCESSING SCREENED CERAMIC MICROCIRCUIT SUBSTRATES by R.L. Stermer, Jr. (Langley Res. Ctr.); 1964 IEEE Int. Conv. Rec., Part 9, pp. 47-53, Mar. 23-26

Two principal dielectric types for use in the screened thin-film process are described. The first dielectric material is for use in the fabrication of minimum stray capacitance conductor crossovers. The second material is designed for application in high-Q, high-capacitance devices which are compatible with normal substrate areas. Material formulation, processing, and firing techniques are discussed. Pertinent electrical characteristics of the materials are presented. These materials have been used in the fabrication of practical circuits and the advantage of their application is discussed.

26,137 A PRACTICAL APPROACH TO THIN FILM CIRCUITS by P.L. Kirby (Welwyn Electric Limited, England); Brit. Commun. and Electronics, Vol. 11, pp. 242-246, Apr. 1964

Microminiaturization, the importance of the substrate, micro-circuit geometry, and pattern production are discussed. Of the many materials which are electrically insulating, ceramics and glasses are the most appropriate for substrates. A high alumina ceramic with its high strength and thermal conductivity would be preferable were it not for its normal surface condition. Two advan-

tages of a polished surface are improved reproducibility of a deposition process and improvements in final stability and, therefore, in performance of the deposited film. A wide choice of suitable substrates should become available. In many circuits the absolute accuracy required for individual elements is appreciably less exacting provided a given relationship is maintained between them, as when several elements are deposited simultaneously. A mere variation of the overall magnitude of a pattern affects both length and width equally and provides no means of varying the final value of a meandered resistor.

26,138 THE MICRO-CIRCUIT-MODULE, A UNIVERSAL INTERCONNECTION - PACKAGING SYSTEM by D.J. Garibotti and L.R. Ullery (United Aircraft); IEEE Trans., Vol. CP-11, pp. 163-172, June 1964

An interconnection - packaging system -- Micro-Circuit-Module -- has been developed which is compatible with thin film as well as semiconductor integrated circuits. The system has evolved through the developmental stages and is now in the pilot production stage. The assembling and hermetic sealing of the module are carried out by automatic electron beam processes and associated transfer-indexing machines.

26,139 STANDARDS PUSHED FOR MICROELECTRONIC PACKAGING by staff; Electronic Design, Vol. 12, pp. 86-87, Mar. 16, 1964

Registration systems and packaging standards for microelectronic circuits are discussed. A straight listing type of registration currently used with transistors, simplifies the task of handling large numbers of devices but conveys no information about them. The opposite is true for a coding system of the type now used for vacuum tube numbering, which uses the first digit to indicate the type of integrated logic circuit, an alphabetic letter next for the element function, the third character for the power dissipation per mode, and the final digit for the propagation delay per stage through a logic ring over the entire operating temperature range. Flat package configurations that have been developed thus far may be covered by three specifications--for packages with eight, fourteen and sixteen leads. Such structures as Signetic's all-glass package and Motorola's ceramic packages easily fit into this system.

26,140 NEW DEVELOPMENTS IN MICROCIRCUIT PACKAGING by D.E. MacElroy (Intl. Resistance); Electronics Indus., Vol. 23, pp. 57-60, Apr. 1964

The Micromodule, Dot, Hybrid, and Integrated System methods of microcircuit packaging are described. The Micromodule system uses stacks of component wafers with soldered interconnections. The Dot method uses pellet shaped elements fitted into a prepunched insulation board. A conducting pattern sprayed on completes the process. Both the micromodule and dot systems offer automation production possibilities. Hybrid circuits employ both film and discrete elements and provide a rugged, low cost, versatile unit. The integrated circuit is the smallest of these miniature systems in terms of physical size, and potentially the most reliable, although the present state of the art includes disadvantages such as high tooling costs and difficulty of testing individual elements.

CIRCUIT ASPECTS OF DEVICES

26,141 EMPIRICAL PARAMETER VARIATION ANALYSIS FOR ELECTRONIC CIRCUITS by S. Klapp (SCM Corp.); IEEE Trans., Vol. R-13, pp. 34-40, Mar. 1964

Procedures for empirical parameter variation analysis are presented which should be useful in practical programs of design analysis and reliability improvement for electronic circuits. The objective of the technique is to estimate the effect that drifts in component-part parameters will have upon circuit performance. This estimate is obtained by application of formal statistical and/or worst-case analysis methods in conjunction with systematically made circuit "breadboard" measurements and data from component-part test programs. The mathematical basis for the technique is presented, along with a description of methods to simulate part-parameter drifts and other suggestions for conducting the required breadboard measurements.

26,142 THE DESIGN ENGINEER APPLIES RELIABILITY TECHNIQUES by D. Shuda (Sylvania); Solid State Design, Vol. 5, pp. 29-32, May 1964

Reliability can be successfully incorporated by a design engineer into an electronic circuit at the very start of a design effort. However, reliability techniques are usually applied to a circuit design effort only after the design has been firmed up (a posteriori) so that it will meet the technical specifications governing functional performance. At this point, the design is analyzed for its ability to meet the reliability objective by reliability specialists during circuit design reviews. The current trend, however, especially in companies heavily committed to the design of highly-reliable electronic systems for on-

board use in missiles and satellites, is to encourage the design engineer to use reliability techniques at the start of his design effort (a priori). Reliability techniques are readily applied during the early design effort and that such techniques, when properly applied, invariably lead to an efficient and cost-saving design.

26,143 ANALYTICAL METHODS FOR PREDICTING TRANSIENT NUCLEAR RADIATION EFFECTS OF ELECTRONIC CIRCUITS AND DEVICES (Boeing); Contract AF29 601 5238, 255 pp., July 1963; U.S. Gov. Res. Rep., Vol. 39, p. 52(A), May 20, 1964 AD 432 940 OTS \$16.50

This method employs generalized radiation equivalent circuits for each component of the circuit or system. The component equivalent circuits are combined for circuit and system prediction using standard electrical engineering methods of circuit analysis, and the resulting circuit equations are solved on either an analog or digital computer. Four component equivalent circuits have been developed for use in circuit analysis. Detailed component equivalent circuits and their associated constants and circuit equations are presented for use in analyzing the behavior of these circuits in a generalized radiation environment. This method has been applied to the prediction of the response of four guidance and control circuits for flash x-ray, linac, and nuclear weapon environments, and of a simple servo loop for the flash x-ray and linac environments. The results of the prediction were compared with experimental results in the same environments. Within the scope of present knowledge of the component and environment variations, this comparison has resulted in excellent agreement for both the real time pulse shapes and the signal amplitude for radiation rates up to 10^9 r/sec.

Radiation Effects on Devices - See 25,799, 25,802

Properties of Tunnel Diodes - See 25,824, 25,825

26,144 ABOUT TUNNEL DIODES [in French] by A. Schmitz and N.V. Philips; *Acta Electronica*, Vol. 7, pp. 199-206, July 1963

After recalling and explaining tunnel effect, tunnel diode behavior is dealt with and the equivalent circuit and methods for its elements measurements are surveyed. In conclusion, technological problems are discussed.

26,145 TUNNEL-DIODE STABILIZATION by I.P. MacFarlane (Postmaster-General Department); *Proc. IREE, Australia*, Vol. 25, pp. 323-324, May 1964

A method of tailoring a tunnel-diode's parameters to enable stable operation in a non-switching circuit at low frequencies is described.

26,146 STABLE AND UNSTABLE WORKING CONDITIONS OF TUNNEL DIODES [in French] by J. Revuz (Lab. Electronique et Phys. Appl., Paris); *Acta Electronica*, Vol. 7, pp. 207-222, July 1963

The working conditions of series and parallel tunnel diode circuits are examined. The two modes of working conditions related to the two distinct types of instability, commutation and relaxation oscillations, are separated after recalling stability conditions. A geometrical method is used to indicate the current variations as a function of the voltage.

26,147 STABILITY CRITERIA FOR TUNNEL-DIODE CIRCUITS by B.W. Nelson and R. Masens (ITT Federal Labs.); *Electro-Tech.*, Vol. 73, pp. 52-58, June 1964

Using broadband and narrowband tunnel diode amplifiers as models, stability criteria for a large variety of tunnel diode circuits in terms of network parameters and tunnel diode characteristics are developed. Prerequisites for stability are listed, and a method for determining the roots of the characteristic equation using the Nyquist stability criterion is given. Stability plots of phase and attenuation vs frequency are then introduced. Examples of a UHF and narrow band amplifier are discussed and a straightforward general method of determining stability is presented.

26,148 A NORMALIZED STABILITY PLOT FOR TUNNEL-DIODE CIRCUITS by H. Gruenberg (Syracuse U.); *Proc. IEEE*, Vol. 52, p. 733, June 1964

A normalized stability plot is proposed which shows graphically the boundaries of the region of stable operation of a tunnel diode in terms of dimensionless parameters. This plot is derived by consideration of an equivalent circuit of the diode which includes a shunt capacitance representing the packaging capacitance of the diode and a tuning inductance. The characteristic equation for this equivalent circuit is solved in terms of dimensionless parameters and stability boundaries are derived for specific constraints.

26,149 GETTING INSIDE THE TRANSISTOR WITH LUMPED PHYSICAL MODELS - Part I by D.J. Hamilton and F.A. Lindholm (U. Arizona); *Electronic Design*, Vol. 12, pp. 54-61, Mar. 16, 1964

Lumped model analysis of transistor circuit behavior is discussed. The actual physical processes within the transistor are represented by lumped elements, interconnected in the model to form a network. The designer may then analyze the transistor much as he would a conventional circuit. The model gives a continuous awareness of the influence of device properties on terminal behavior. The model is particularly useful for the analysis of switching circuits because it can represent transistors under all possible conditions of bias. The three basic lumped elements are the thermal generator, representing thermal sensitivity, the combination, representing electron-hole pair recombination, and the diffusion, representing carrier diffusion. These elements are used to illustrate α derivation, non-linear current leakage, and the conditions of low saturation voltage.

26,150 THE THIN-FILM TRANSISTOR (TFT) AS A CIRCUIT ELEMENT by H.G. Dill and R. Zuleeg (Hughes Aircraft); Dec. 9, 1963, 57 pp.; *STAR*, Vol. 2, p. 1333(A), June 8, 1964

The linear and nonlinear circuit application of the insulated gate field effect transistor operating in the enhancement mode is discussed. The operating mechanism of the TFT is briefly described and is related to temperature and ambient effects on parameters that determine the stability of the device. Results obtained with cadmium sulfide (CdS) films outline the present status of the TFT and emphasize certain future directions for research and development. Circuitry performance of the TFT in special circuits, not possible with other known transistor types, is demonstrated and supported by laboratory measurements.

26,151 THE FIELD-EFFECT TRANSISTOR—ITS CHARACTERISTICS AND APPLICATIONS by V. Radeka (Brookhaven Lab.); *IEEE Trans.*, Vol. NS-11, pp. 358-364, June 1964

The characteristics of the junction gate field-effect transistor and the basic relations among its parameters are described. Some figures of merit are derived in terms of its physical parameters and the limitations considered. Applications in nuclear instrumentation are discussed. Some advantages of field-effect transistors are in high input impedance, low noise at very low and medium frequencies, and a wide operating temperature range (-200°C to $+100^{\circ}\text{C}$). In addition, the field-effect transistor represents a new circuit element — voltage (charge) controlled conductance with fast response. Field-effect transistors are particularly suitable for low noise amplifiers at low and medium frequencies, for high input impedance amplifiers (as for integrators), for charge-sensitive amplifiers, and for analogue multipliers. They can also be applied as controllable feedback elements.

26,152 THE UNIJUNCTION TRANSISTOR IN RELAXATION CIRCUITS by B. Crawford and R.T. Dean (Texas Instr.); *Electro-Tech.*, Vol. 73, pp. 40-45, Mar. 1964

The unijunction transistor and its circuit applications are discussed. The following circuit applications were described: (1) a variable frequency (800-6 kc), variable slope (7×10^4 to 7×10^5 v/sec) ramp function generator; (2) a staircase generator and counter with an adjustable number of steps (5-24), a frequency range of 100 cps to 10 kc and operable from 0 to 100°C ; (3) an astable multivibrator; (4) a 30 kc ring counter operating in the decimal system and able to drive Nixie readouts directly; (5) a 15v pulse generator with rise and fall times of 1 μsec ; (6) a voltage comparator sensitive to 2 mv changes; (7) a motor control circuit with power output roughly the inverse of speed; (8) an ac power control; and (9) a voltage regulator which changes only 0.1v (0.4%) for a 100% input voltage change and 0.2v over 0 to full load.

26,153 AVALANCHE CIRCUITS ARE MORE VERSATILE THAN YOU THINK by B.H. Bell (Nat'l. Semiconductor); *Electronic Design*, Vol. 12, pp. 56-63, June 8, 1964

Advances in avalanche circuits, illustrated by practical circuits, in areas of pulse generation, where rise times of less than 1 μsec at peak powers in excess of 500 w are obtainable, and in voltage comparators, which, with nanosecond delay time, large power gains and high sensitivities, make the avalanche effect one of the few means available for determining rapidly varying voltage levels are described. A method of increasing the repetition rate by a factor of 100 is given. A selection of avalanche circuits is presented with a detailed explanation of design and operation criteria.

26,154 LARGE SIGNAL THEORY OF AVALANCHE TRANSISTOR CIRCUIT OPERATION by J.S. T. Huang and A.A. Pandiscio (Harvard U.); Contract Nonr1866 16, 1v, Sept. 16, 1963; U.S. Gov. Res. Rep., Vol. 39, May 6, 1964 AD 429 805 OTS \$12.00

The transient analysis of avalanche transistor pulse circuits from which fast current pulses are obtained is presented. The transistor, when properly biased in the avalanche mode, is seen to exhibit a negative resistance at the collector-emitter terminals. The existence and significance of a reactive element associated with such negative resistance are thoroughly discussed.

26,155 CAPACITOR CHARGE SETS TRANSISTOR BIAS POINT by C.G. Dorn (US Naval Ord. Lab.); Electronics Design, Vol. 12, p. 105, Mar. 16, 1964

A single transistor output stage capable of generating its own bias and operating without distortion in Class A using a $16\text{-}\Omega$ load is described. The collector is connected in series to a capacitor and resistor back to base. Polarity is maintained positive by a diode connected to ground. As the input increases, the output on the collector also increases with the voltage across the capacitor proportional to the input. Bias is therefore maintained proportional to the input, helping to keep excessive dc current out of transformer primaries.

26,156 THERMISTOR AS A CIRCUIT ELEMENT IN LOW FREQUENCY SYSTEMS by K. Kraus (Ejovice 96 u Plzne, Czech.); J. Sci. Instr., Vol. 41, pp. 384-385, June 1964

The properties of a polarizing thermistor that arise from the fact that the thermistor acts as a negative resistance to low-frequency signals have been investigated and a method of measuring the thermistor impedance has been devised. To illustrate the use of a polarizing thermistor three simple networks have been designed.

AMPLIFIERS

26,157 ANALYSIS AND SYNTHESIS OF AMPLIFIER CIRCUITS by L. Ya. Nagornyy (Wright-Patterson AFB); Transl. from Gosudarstvennoye Izdatel'stvo Tech. Lit., Kiyev, pp. 1-244, 1963, Feb. 10, 1964, 316 pp.; U.S. Gov. Res. Rep., Vol. 39, p. 43(A), May 20, 1964 AD 432 069 OTS \$19.75

The development of a general method of analysis and synthesis of electron-tube and transistor circuits operating in the linear range are presented. The method is based on the generalized methods of node potentials and loop currents and makes it relatively easy to determine expressions for the basic parameters of the amplifier, to determine their relative change with variation of several parameters of the circuit elements, to investigate the final expression of the basic characteristics of the amplifier depending on variation of any parameter of the element of the circuit for the case where all of them are complex numbers, etc. The basic calculating formulas expressed in terms of the determinant of the circuit matrix and its cofactor are presented in tables which to a significant degree facilitate their use in the analysis and synthesis of amplifiers. The book is intended for radio engineers and is also of interest to scientific workers dealing with the development and application of methods of electronic circuit analysis.

26,158 USING BARRETERS FOR STABILIZING AN OUTPUT STAGE BY APPLICATION by W. Folder (Tung-Sol Electronics); Electronic Design, Vol. 12, p. 68, June 8, 1964

The use of barreters (positive temperature coefficient, low current drain electric lamps) as stability control and protective circuit elements in output stages of transistorized amplifiers is discussed. When used in the emitter circuit, the barreter stabilizes the circuit by emitter feedback, and can react with a time constant of approximately 500 msec. A particular application of this device in a Knight-Kit model KG-60 stereo amplifier is described. Life-time and fuse effects are also examined.

26,159 PARAMETRIC AMPLIFIERS AND CONVERTERS WITH PUMPED INDUCTANCE AND CAPACITANCE by D.G. Tucker and K.L. Hughes (U. Birmingham); Radio and Electronic Engr., Vol. 27, pp. 435-439, June 1964

It is shown that when both inductance and capacitance are pumped in a parametric amplifier or converter, a special kind of resonance involving only the variable parts of the L and C may occur and produce null responses. An equivalent circuit has been devised for the up-converter, in which an idealized frequency-converter appears. Double-sideband converters are also briefly considered.

26,160 A THEORY OF A UNILATERAL PARAMETRIC AMPLIFIER USING TWO DIODES by J. Hamasaki (Bell Labs.); Bell Sys. Tech. J., Vol. 43, pp. 1123-1147, May 1964

The theory of a unilateral parametric amplifier which contains two variable-capacitance diodes separated by a quarter wavelength at the signal frequency and a half wavelength at the idler frequency is described. It is shown that a broadband signal circuit is essential in order to obtain unilateral gain, and that matching conditions are obtainable even with a high gain. The optimum noise figure is slightly worse than that of a single-diode reflection-type amplifier; however, this amplifier has advantages if it is refrigerated at liquid helium temperature, because it does not require a circulator in front of its

input port. The amplifier usually requires an isolator at its output port, since it does not have substantial loss in the reverse direction.

26,161 A BROADBAND BALANCED IDLER CIRCUIT FOR PARAMETRIC AMPLIFIERS by J.D. Pearson and K.S. Lunt (Ferranti Ltd.); Radio and Electronic Engr., Vol. 27, pp. 331-335, May 1964

The bandwidth of the idler circuit of a parametric amplifier is discussed, and reductions in bandwidth associated with stray reactances of the diode encapsulation and filter networks required to complete the idler circuit are described. A balanced idler circuit using two diodes is shown to approach the theoretically maximum idler bandwidth. A 3000 mc/s amplifier is described having a 10% bandwidth at 20 db gain.

26,162 ON THE PASSIVE CIRCUIT ADJUSTMENT OF PARAMETRIC AMPLIFIERS INCORPORATING VARACTOR DIODES by T. Buckley (Royal Radar Est., Great Malvern); J. Sci. Instr., Vol. 41, pp. 333-334, May 1964

A time-saving method of adjusting the signal input circuit of a parametric amplifier to have any desired value of coupling ratio and to be resonant at a given frequency and diode bias voltage is described. The principle of the method is the sweeping of the bias voltage of the varactor diode at a low frequency and is a development of the method suggested by Kurokawa in an earlier paper.

26,163 NON-RECIPROCAL PARAMETRIC AMPLIFIERS: THEORY AND INSTRUMENTATION by H.B. Henning (LFE Lab.); 1964 IEEE Int. Conv. Rec., Part 2, pp. 83-92, Mar. 23-26

The theory of non-reciprocity is discussed and is applied to two single-varactor paramps. One paramp operates in a CW mode, the other is superregenerative. Both units will (a) provide down-conversion and (b) accommodate signal frequencies which exceed the nominal value of the pump. Design constraints and performance characteristics are discussed.

26,164 PARAMETRIC AMPLIFIER USING PHOTO-CELL REACTANCE by W.W. Goerther and W.G. Matthei (Dept. Army); U.S. Pat. 3,132,258, Issued May 5, 1964

An efficient, high sensitivity, parametric amplifier, capable of detecting and converting an intensity-modulated light beam and suitable for system control applications, is described. A reference frequency and a modulated light beam presented to a surface barrier photo diode induce capacitance variation which generates the difference frequency. The system may function as a demodulator, differential amplifier, or upper (or lower) sideband four frequency up (or down) converter.

26,165 A MAGNETIC FILM LOW FREQUENCY PARAMETRIC AMPLIFIER by G.E. Fanslow (Iowa State U.); Proc. Natl. Electronics Conf., 1963, Vol. 19, pp. 448-452

A thin magnetic film is used in a balanced modulator configuration to investigate the application of magnetic films in the amplification of low level, low frequency signals. The theoretical gain is shown to be dependent upon the coupling between the output and the input windings. As the coupling improves the power gain approaches the ratio of the output frequency to the input frequency. A Thevenin equivalent impedance is derived which shows that the output impedance is relatively small (about 200 ohms for the experimental model) and that it is not frequency dependent.

Parametric Amplifiers - See 26,234

26,166 COMPLEMENTARY AMPLIFIER OFFERS HIGH INPUT IMPEDANCE; by L.J. Ernst (Genl. Magnetics); Electronics, Vol. 37, pp. 92-93, May 18, 1964

A negative feedback amplifier which obtains 220,000 ohms input impedance, 61 ohm output impedance and ambient stability from -55° to $+100^{\circ}\text{C}$ by using a pair of high-gain, silicon planar transistors in complementary operation is described. The output is 0 to 7 volts rms. Input impedance and voltage gain expressions are given.

26,167 TRANSISTOR LOW DRIFT DC AMPLIFIERS by J.J. Pinto (S. Smith and Sons); Electronic Engr., Vol. 36, pp. 304-308, May 1964

The variations of the dc parameters of transistors, important in the design of low drift dc amplifiers are described. The conventional long-tailed pair and the modifications necessary for improved performance are described and the results assessed. A new, balanced, mirror-image amplifier is then described and its performance and capabilities are discussed. Finally, the latest trends in direct coupled amplifier design and development are indicated.

26,168 DRIFT COMPENSATION IN DC AMPLIFIERS by P.J. Beneteau, G.M. Riva, B. Murari and G. Quinzio (Fairchild, Italy); Solid State Design, Vol. 5, pp. 19-23, May 1964

In dc amplifiers built with silicon planar transistors, the drift encountered as a function of temperature is generally linear over some temperature range. A linear compensation circuit can therefore be used to reduce this drift. Various compensation circuits are proposed and any one of these reduces the drift by about one order of magnitude over a temperature range of about 0 - 100°C; lesser improvement is obtained over wider ranges. Drifts referred to the input of the order of $1/\mu\text{V}/^\circ\text{C}$ can now be obtained without difficulty and without using any choppers.

26,169 LOW VOLTAGE, HIGH INPUT IMPEDANCE HYBRID AMPLIFIER CIRCUITS by F.H. Laishley (Joseph Lucas Ltd.); Electronic Engrg., Vol. 309-311, May 1964

A family of hybrid dc coupled amplifier circuits is described. The circuits operate from low voltage supplies and have very high input impedances. The technique used is to employ a single valve requiring a low anode voltage in the input stage of each of the circuits and to follow this stage with conventional semiconductor circuits. This allows simple high impedance circuits to be obtained of small physical size and of low power consumption. The circuits were initially developed for measuring voltages stored on low value capacitors.

DC Amplifiers - See 26,303

26,170 SIMULTANEOUS AMPLIFICATION AND PARAMETRIC FREQUENCY MULTIPLICATION IN VHF POWER TRANSISTORS by J. Pulfer and A. Lindsay (Nat'l. Res. Coun. Canada); Proc. IEEE, Vol. 52, p. 212(L), Feb. 1964

A single transistor circuit that may simultaneously amplify and provide variable reactance frequency multiplication is described. A 2N1709 transistor operates as an amplifier at 60 mc and a quadrupler from 60 to 240 mc. The amplifier is a conventional common emitter circuit with the output tap on the emitter tank adjusted for optimum coupling of the 240 mc. Component from the transistor to the load. A power output of 1.25 w at 240 mc has been obtained.

26,171 A MICROWAVE CERAMIC TRIODE AMPLIFIER by J.R. Kay (Redstone Arsenal); AMC RA RE TR63 32, 34 pp.; U.S. Gov. Res. Rep., Vol. 39, pp. 39-40(A), May 20, 1964 AD 431 828 OTS \$3.60

The development and design of a broadband, low-noise microwave amplifier using ceramic triodes is presented. After the feasibility of ceramic triodes in microwave amplifiers was proven by initial experiments with single-stage and two-stage amplifiers, a four-stage broadband amplifier with approximately 33 db gain was designed. Experiments were made using the GE Z-2869 and 7768 ceramic triodes; the Z-2869 gave better results and was used in the final four-stage amplifier. Bandwidth was measured at the 1 db points. Noise figure was 11.5 db or better across the band and maximum gain variation across the band was 0.7 db. No phase measurements were taken; however, phase characteristics of this amplifier are being investigated in conjunction with another project.

26,172 BROADBANDING WITH TRANSISTORS by H. Klink (Tech. Hoch. Braunschweig); Archiv. Elektrischen Über., Vol. 350-354, June 1964

It has been shown, that for gain-peaking of broadband amplifiers, whose upper frequency limit lies in the UHF region and in the vicinity of the transit frequency of the chosen transistors, a transmission line with a wave impedance of several hundred ohms may be used as coupling element. A procedure for dimensioning the transmission line is derived and applied to a sample problem. A three-stage amplifier with transmission line coupling is described which has a gain of 19.5 ± 1.5 db between 170 and 640 mc/s.

26,173 THE DESIGN OF BROAD-BAND TUNNEL DIODE AMPLIFIERS by J. Lepoff (Electronic Def. Labs.); Contract DA36 039AMC00088E, 31 pp., Oct. 21, 1963, Rept. No. M583; U.S. Gov. Res. Rep., Vol. 39, May 5, 1964 AD 430 257 OTS \$3.60

An analytic method for designing broad-band tunnel diode amplifiers is presented. A stabilizing circuit is added to a basic double-tuned circuit in order to prevent out-of-band oscillations. Amplifiers were designed for 1-gc and 2-gc bandwidths at C band. Models were built with greater than 10-db gain and less than 5-db noise figure over a 1-gc band.

26,174 WIDE-BAND TRANSISTOR AMPLIFIERS AND PROBES FOR OSCILLOSCOPES by G.A. Rigby (U. Melbourne); Proc. IREE, Australia, Vol. 25, pp. 234-239, Apr. 1964

The factors limiting the bandwidth of oscilloscopes are briefly reviewed and it is pointed out that the cathode-ray tubes in most conventional instruments have bandwidths considerably in excess of the vertical amplifier bandwidths. The design of transistor amplifiers and probes to fully utilize the vertical bandwidth

of high-quality tubes is discussed. A design example is given of a vertical amplifier with a gain of 30 db and a bandwidth of 120 mc/s, and of a probe with an input impedance of 6 k Ω across 2 pf and a bandwidth of 110 mc/s. Both units are designed around cascades of alternate shunt- and series-feed-back stages.

26,175 A WIDEBAND AMPLIFIER USING MICRO-POWER PLANAR TRANSISTORS by Sylvania Semiconductor Division; Solid State Design, Vol. 5, pp. 14-17, Apr. 1964

A two stage wideband amplifier was designed and constructed to demonstrate the capabilities of the 2N2784 Micro-Power Planar transistor in a high frequency amplifier circuit. Design criteria include selection of a DC operating point to best utilize the 2N2784's ft, direct interstage coupling, and, from AC considerations, feedback from the second collector stage to the first emitter stage, as well as some local series feedback in the first stage. Values of feedback components are varied, and a plot giving tradeoffs between voltage gain and frequency is shown. Two possible gain-bandwidth combinations are 23 db at 100 mc and 13 db at 150 mc.

26,176 TWO STAGE TRANSISTOR AMPLIFIER WITH BROAD-BAND GAIN-EQUALIZING FEEDBACK by R.S. Dahlberg (Philco); U.S. Pat. 3,124,759, Issued Mar. 10, 1964

Miniature transistor amplifiers for application in signal transmission lines to compensate for signal attenuation incident to transmission are described. Two transistors are arranged in common base, common emitter cascade and may be powered from the transmission line. Negative feedback is used to ensure uniform response with 0.5 db from 300 cps to 150 kc.

26,177 ELEMENTS OF TRANSISTOR PULSE CIRCUITS by T.D. Towers (Newmarket Transistors, Ltd.); Wireless World, Vol. 70, pp. 74-80, Feb. 1964

The design of linear pulse amplifiers is discussed. Methods of approaching linear pulse amplifier design include consideration of the response of the amplifier to a square-wave input, specifying performance in terms of pulse gain, rise time and droop; and examination of its response to a cw sine input specifying performance by midband gain, and upper and lower half power bandwidth limits. Both high and low frequency compensation techniques are given with the appropriate equivalent circuit models.

26,178 SHUT-OFF IS NOT REQUIRED IN SCR PULSE AMPLIFIER by A.J. Fishman (EGG, Boston); Electronic Design, Vol. 12, pp. 107-108, Mar. 16, 1964

A SCR circuit is described which acts as a low impedance pulse amplifier without a shut-off mechanism wherever only the leading edge of a pulse is needed. The steady-state current through the SCR is limited below the holding current so that it remains off under normal conditions. When a low-level pulse is applied at the input, a capacitor between the SCR and ground appears as low impedance to the SCR, so that it turns on. The capacitor recharges to B+ (+ 60v dc) in 2-msec, causing the SCR to turn off again and is ready for the next pulse. It is necessary to ac-couple the load in order to prevent dc current, which would be drawn by the load, from holding the SCR on. The pulse period is 8-msec long.

26,179 ANALYSIS OF A FEEDBACK AMPLIFIER by C.D. West (U. Liverpool); Electronic Engrg., Vol. 36, pp. 326-329, May 1964

The analysis of a pulse amplifier circuit is presented. The circuit, which has a low temperature coefficient of gain, consists of a dc coupled difference amplifier and a common emitter stage. Component values are given for an amplifier with a gain of 10 and a temperature coefficient of $50 \times 10^{-6}/^\circ\text{C}$. Several stages may be cascaded.

26,180 ELECTRICAL APPARATUS by J.A. Dever (Minn.-Honeywell); U.S. Pat. 3,127,524, Issued Mar. 31, 1964

A polarity-decision amplifier for detecting instantaneous polarity of a signal having a rapidly fluctuating polarity is described. An output gating circuit is selectively operated in relation to an input gating circuit, applying the output signal to a bistable circuit for polarity sensing.

26,181 TRANSISTOR AMPLIFIER WITH VARIABLE PEAK CLIPPING ANG AGC by J. Dijkstra (N.A. Philips); U.S. Pat. 3,124,760, Issued Mar. 10, 1964

Low power amplifiers suitable for application in hearing aids are described. The peaks of oscillation are clipped by symmetrical over-excitation of the last transistor in the amplifier to ensure that sensitivity of the automatic gain control remains constant with adjustment to a lower clipping level.

26,182 A LOW-NOISE CHARGE-SENSITIVE PREAMPLIFIER WITH A FIELD-EFFECT TRANSISTOR IN THE INPUT STAGE by T.V. Blalock (Oak Ridge Lab.); *IEEE Trans.*, Vol. NS-11, pp. 365-372, June 1964

The application of field-effect transistors in charge-sensitive configurations is discussed. The preamplifier has a junction field-effect transistor in the input stage. The field-effect transistor is connected in cascade with the second stage bipolar transistor which has its collector load bootstrapped by a White follower. The bias stabilization is adequate for normal operation of the preamplifier over an FET temperature range from room temperature to liquid nitrogen temperature. Measured values of the preamplifier noise line-width as a function of pulse-shaping time constants, total input capacitance, and temperature are presented. Formulas are included for the theoretical determination of the noise line-width. Application of the formulas requires knowledge of the parameters of the preamplifier and pulse-shaping circuitry and the noise characteristics of the FET. The FET noise characteristics are shown as experimentally determined graphs of narrow-band equivalent noise resistance versus frequency, temperature, and bias point. Preamplifier noise line-widths less than 1.6 kev fwhm for silicon detectors (189 rms electronic charges) and slopes less than 0.06 kev/pf (7.1 rms electronic charges per pf) were obtained when the FET was cooled to the optimum temperature which was approximately 125°K.

26,183 APPLICATIONS OF FIELD-EFFECT TRANSISTORS IN LOW-NOISE WIDEBAND VOLTAGE AND CHARGE-SENSITIVE PREAMPLIFIERS by T.V. Blalock and J.F. Pierce (U. Tenn.); *Proc. Natl. Electronics Conf.* 1963, Vol. 19, pp. 407-420

The design and performance characteristics of two voltage-sensitive and two charge-sensitive preamplifiers using field-effect transistors in the input circuits are described. The better voltage-sensitive preamplifier has an input impedance greater than 10 megohms, an input capacity less than 3 picofarads, a rise time of 350 nanosec, a gain of 540, and an equivalent noise input of $5.2 \text{ nanovolts}/(\text{cps})^{1/2}$. The better charge-sensitive preamplifier has a noise resolution of less than 7 kev fwhm for a detector capacitance of 10 pf.

26,184 HOW TO DESIGN MICROPOWER TRANSISTOR AMPLIFIERS: Part I by J.D. Meindl, R.A. Gilson, O. Pitzalis, and W.F. Kiss (US AERDL); *Electronics*, Vol. 37, pp. 73-78, May 18, 1964

A worst-case load-line technique which determines component values for a 25 microwatt linear broadband transistor amplifier with 25 db gain and provides 0.18 volt peak ac voltage in the range -50°C to +100°C is described. Multi-chip fabrication reduces parasitic capacitances and produces a compact, light unit for portable and space applications. Parameters for several micropower transistors are given. Special micropower problems are dc bias point instability, dynamic range restriction, sensitivity to component tolerances, and poor high-frequency transistor response. Bandwidth beyond 10 to 25 kc is obtained by increasing collector current or by adding the cascade stage of the concluding article.

26,185 HOW TO DESIGN MICROPOWER TRANSISTOR AMPLIFIERS: Part II by J.D. Meindl, R. Gilson, O. Pitzalis, and W. Kiss (US Army Electronics and Dev. Labs.); *Electronics*, Vol. 37, pp. 48-52, June 1, 1964

The problem of obtaining large amplifier bandwidths at microwatt power levels is discussed and the over-all performance of both common-emitter and cascade amplifiers, designed according to the first article of the series is examined. Amplifier ac characteristics are examined and a design example is given. A detailed characteristic listing is given for each of the four broadband micropower amplifiers; the basic common-emitter amplifier, feedback worstcase, and cascade design, and the design are compared.

26,186 A LOW-NOISE TRANSISTORIZED SEISMIC AMPLIFIER by S.N. Thanos (Columbia U.); *Bull. Seismol. Soc. Am.*, v. 54, pp. 347-368, Feb. 1964

The use of transistors for the amplification of fractional microvolt signals at extremely low frequencies is illustrated in the design of an amplifier developed for use in a lunar seismograph. The amplifier has an equivalent input noise voltage of 0.2 microvolts, p-p, with a source impedance of 2,000 ohms and a 3-db bandwidth of 0.035 cps to 22 cps. The nominal input impedance is 1,700 ohms. It is completely transistorized and performs satisfactorily over a specified temperature range of -20° to +100°C. Low power requirements, high reliability, and capability for remote calibration and gain change make this amplifier especially suitable for any field or remote operation under extreme environmental conditions. This amplifier is presently being used in ocean bottom seismographs and magnetic variometers.

26,187 SOME RESULTS ON THE USE OF A TUNNEL-DIODE AMPLIFIER ON A RADIO ASTRONOMY RECEIVER by T.V. Seling (U. Mich.); *Proc. IEEE*, Vol. 52, pp. 423-424(L), Apr. 1964

The performance of a tunnel diode amplifier (TDA) installed on the broadband radio astronomy receiver of the University of Michigan's 85 foot radio tele-

scope is described. Amplifier operation is simple, requiring only application of bias to the diode, as is amplifier service, entailing a periodic change of battery and occasional bias potentiometer adjustment. The noise temperature of the over-all receiver before and after addition of the TDA are 2900°K and 1700°K. Further improvement of temperature (to 1300°K) is obtained by placing the TDA at the focus directly following the RF switch. No problems have been encountered with the TDA after a year's operation.

26,188 OPERATION OF TUNNEL DIODE AMPLIFIERS BEYOND CUTOFF FREQUENCY by J.O. Scanlan (U. Leeds); *Proc. IEEE*, Vol. 52, pp. 435-436(L), Apr. 1964

A theoretical explanation of the possibilities of oscillation beyond the resistive cutoff frequency specified by the equivalent circuit of the tunnel diode is given. Gain and bandwidth of the diode when used as an amplifier are theoretically investigated. The feature brought out by the analysis is that operation is possible with improved performance at frequencies approaching the cutoff frequency. Experimental verification of the effect has not yet been attempted.

Hall Effect Isolators for Tunnel Diode Amplifiers - See 25,883

26,189 COMPLEMENTARY TWO-STAGE AMPLIFIERS by B. Crawford (Texas Instr.); *Electro-Tech.*, Vol. 73, pp. 48-53, May 1964

The characteristics and design features of complementary two-stage amplifiers are discussed. Bias stability, including leakage and V_{BE} stability in each stage, is explained and analytically examined in terms of a basic complementary amplifier circuit. A design example is presented along with an appendix giving further mathematical discussion. The performance is in dependent of transistor parameter values, but theoretical analysis did not include temperature variations in other circuit components, which effect dc and bias point operation.

26,190 DARLINGTON DESIGN FOR HIGH STABILITY AT ELEVATED TEMPERATURE by J. Comer (Gulton Indus. Inc.); *Systems Design*, Vol. 6, pp. 36-37, June 1964

Two methods of achieving thermal stability in the Darlington transistor connection are presented. The addition of a diode in the forward direction from the base to emitter of the input transistor provides a leakage path that will shunt the current through the base to the emitter and eliminate the h_{FE} multiplication factor, but can only be used with a square wave input having fast rise and fall times. Resistor stabilization, on the other hand, sacrifices a little overall circuit gain (from 1600 to 1350 in the example) but input signals are not limited, as in the diode case.

26,191 SMALLER, BETTER MAGNETIC AMPLIFIERS FOR POWER AND CONTROL CIRCUITS, special ed. rep; *Electronics*, Vol. 37, pp. 69-73, June 29, 1964

Several relatively light, rugged, stable magnetic amplifiers for power and control circuits which combine improved magnetic materials with semiconductor devices are described. Magamps, saturable reactors with a diode in each gate winding, achieve ten to one volume economics, operate at 5 and even 10 kc, have rise times near a millisecond, and are temperature stable to one microvolt per degree C or better. Other features are low-level dc operation, electrical isolation, noise immunity, overload tolerance, and high power capacity. Magamps are valuable in modulation, amplification, telemetry, and power conversion and regulation systems and in space electronics.

26,192 MAGNETIC AMPLIFIER WITH SHUNT LOAD AND AMPLITUDE CONTROLLED OUTPUT VOLTAGE by E.W. Manteuffel (GE); U.S. Pat. 3,129,381, Issued Apr. 14, 1964

A lightweight magnetic amplifier employing small saturable reactors and switching elements comprising silicon controlled rectifiers in parallel with a capacitor is described. The flux swing within the cores of the reactors is regulated in a manner which permits the use of the amplifier as a variable voltage source. The level of the flux swing is controlled by means of a control winding supplied with a unidirectional signal. The firing sequence is controlled by the gating action of the saturable reactors on the SCR's.

26,193 TWO-TERMINAL MAGNETIC AMPLIFIER APPARATUS by J. Marlow; U.S. Pat. 3,136,941, Issued June 9, 1964

An amplifying and control circuit using variable impedances having two terminals (thermistors, photocells, or infrared detectors, etc.) is discussed. These variables are considered better than the power-consuming three-terminal devices which are often used. The circuit arrangement provides a full-wave saturating magnetic amplifier using a single current rectifier controlled by the two-terminal device mentioned, and operates by means a change in electrical power flowing in the circuit as a result of a phase variation proportional to the

controller impedance changes. The impedance of the controller is isolated from the circuit's power supply. This kind of circuit is often used in maintaining a certain controlled condition at a level determined by the setting of one or more elements in the reactive circuit.

High Impedance Amplifiers - See 26,151

Low Noise Amplifiers - See 26,151

OSCILLATORS

26,194 MATRIX ANALYSIS OF THE COLPITTS' OSCILLATOR by G. Zelinger (De Havilland Aircraft of Canada, Ltd.); Electronic Engrg., Vol. 36, pp. 394-398, June 1964

The basic design problems of Colpitts' oscillators are examined and solved by means of matrix analysis. Practical oscillator circuits are considered which utilize either transistors or valves as the active element. It is shown that the complete oscillatory system can be synthesized from an active and passive two-port, each in turn described by an admittance matrix. Design equations are derived for the oscillating frequency and conditions of oscillation in terms of the fundamental circuit parameters.

26,195 MEASUREMENT OF PHASE STABILITY OF QUARTZ CRYSTAL OSCILLATORS FOR AIRBORNE RADAR APPLICATIONS by J.R. Buck, D.J. Healey, III, and M. Meiseles (Westinghouse Aerospace); 1964 IEEE Int. Conv. Rec., Part 8, pp. 34-42, Mar. 23-26

A technique used to measure the spectrum at the output of the HF oscillator prior to frequency multiplication in a high frequency oscillator designed for carrier frequency generation in airborne radar sets is described. Results of the measurement of the phase spectrum of two crystal oscillators are given which indicate the feasibility of isolating the quartz crystal unit so that negligible degradation of the spectrum occurs when the oscillator is subjected to the aircraft environment. An appendix is included which mathematically discussed the derivation of sensitivity through measurement apparatus.

26,196 PHASE LOCKED OSCILLATOR by J.E.R. Harrison (Genl. Dynamics); U.S. Pat. 3,132,310, Issued May 6, 1964

A simple, all-transistor, RF oscillator which is fairly accurate and utilizes inexpensive crystals is described. A feedback correction signal is obtained by mixing the crystal oscillator output with multipoles of a single accurate frequency standard. Zener clipping diodes in the feedback loop keep oscillator output constant without applying switched capacitors or tuned circuits. Uncorrected generation continues in the event of control circuit breakdown.

Relaxation Oscillators - See 26,238

26,197 MICROWAVE GENERATION BY THE USE OF TRANSISTORS SWITCHING IN THE AVALANCHE MODE by R.J. Vilmur and K. Ishii (Marquette U.); Proc. Natl. Electronics Conf. 1963, Vol. 19, pp. 421-435

An extremely simple transistor relaxation oscillator circuit has been developed as a source of microwave output. A high of 15.8 microwatts at 11,153 mc has been generated. The relaxation oscillator circuit consists of a transistor, a resistor, and power supply. The transistor switches in the avalanche mode giving current pulses with rise times of less than one nanosecond. The extremely fast rise time current pulses contain a large amount of microwave energy that can be coupled into a propagating medium. The transistor relaxation oscillator can have repetition rates from the high kilocycle range out to a measured 118 mc. The generation method offers the possibility of producing any frequency from the circuit's lowest repetition rate out to at least 12,000 mc. Low cost and simplicity can be included in the advantages of this new generation method.

26,198 DIGITAL COMPUTER ANALYSIS OF THE TUNNEL DIODE RELAXATION OSCILLATOR by A.L. Riemenschneider (U. Wyoming) and C.W. Cox (S. Dakota School of Mine and Tech.); Electronic Engrg., Vol. 36, pp. 382-385, June 1964

A digital computer method for obtaining the solution to the tunnel diode relaxation oscillator is described. Equations for analyzing the tunnel diode relaxation oscillator in the phase plane using Lienard's construction are selected. These equations are used to develop computer programs which accurately yield the oscillator output response directly from the complete diode characteristic and circuit parameters of a second order system. The method faithfully reproduces response waveforms with an accuracy limited only by the accuracy with which the characteristics of the non-linear element is known and is easily within the limits of normal component drift.

26,199 NON-LINEAR OSCILLATIONS IN TUNNEL DIODES by L.L. Svasand (Norwegian Def. Res. Est.); Contract AF61 052 484, 28 pp., Apr. 16, 1963; U.S. Gov. Res. Rep., Vol. 39, p. 51(A), May 5, 1964 AD 430 775 OTS \$2.60

The high frequency operation of a tunnel diode oscillator has been studied through approximative analytical solutions of the characteristic non-linear differential equation of the oscillator. Special attention has been given to the case of quasi-harmonic oscillations. For this certain characteristics phenomena of non-linear resistance oscillators, such as amplitude quenching and hard oscillations, are shown to exist.

26,200 WIDE-RANGE GARNET-TUNED TUNNEL-DIODE OSCILLATOR by M.L. Wright (Airborne Instr. Lab.); Proc. IEEE, Vol. 52, p. 631(L), May 1964

The performance of a tunnel-diode oscillator over a multi-octave frequency range is described. A gallium-doped yttrium-iron-garnet (YIG) sphere is used as the tuning element and is coupled to a strip-transmission line tunnel-diode circuit. The tuning range for this oscillator is limited by the low-frequency limit of the YIG, the high frequency resonance of the tunnel-diode capacitance, and the YIG coupling inductance. Operation has been possible over a two-octave range (600 to 2400 mc) using a selected high-cutoff-frequency diode.

26,201 OCTAVE RANGE VOLTAGE-TUNED TUNNEL-DIODE OSCILLATOR by M.L. Wright (Airborne Instr. Lab.); Proc. IEEE, Vol. 52, p. 442(L), Apr. 1964

The performance of a miniature tunnel-diode oscillator that can be tuned from 900-1800 mc, and tuned by varying the bias voltage between the values of 216 to 450 mv. is described. Erratic behavior occurs as oscillation stops when an increase of bias voltage above the upper limit lowers the frequency to about 1800 mc. The oscillator occupies a volume of approximately 1/6-cubic in. and uses an RCA 40062 gallium-arsenide tunnel diode. Power output to a matched load varies from 0.2 to 0.6 mw over the normal operating range.

26,202 WIDE-BAND VARACTOR-TUNED TUNNEL-DIODE OSCILLATORS by M.M. Fortgang and H.J. Hindin (Airborne Instr. Lab.); Proc. IEEE, Vol. 52, pp. 419-420(L), Apr. 1964

The performance of a miniature tunnel diode oscillator that can be tuned electrically over wide frequency bands is described. Tuning is accomplished by varying dc bias on a given varactor diode. Specifically, a MA4652 gallium-arsenide diode and a MA5037 varactor resulted in a frequency range of 2600-4000 mc, whereas a range of 1800-4000 mc was obtained by changing to an MS1541 diode. The size of the unit was about one cubic inch with a weight of several ounces, although it is possible to make it 30 per cent smaller.

26,203 TEMPERATURE COMPENSATION OF ASTABLE MULTIVIBRATORS by I.R. Marcus and A.D. Smith (Harry Diamond Labs.); Jan. 20, 1964, 36 pp.; U.S. Gov. Res. Rep., Vol. 39, p. 46A, May 20, 1964 AD 432 255 OTS \$3.60

The limits to which the frequency of astable multivibrators could be stabilized against temperature and power-supply voltage variations so that they could be used as a time base in electric time fuses and programmers are determined. The temperature range was -55 to +75°C, and the voltage variation was $\pm 20\%$. The frequency was about 100 cps. Four different circuits are developed. One circuit yielded $\pm 0.06\%$ frequency stability over the temperature and voltage range.

26,204 TRANSISTOR MULTIVIBRATOR WITH SATURABLE CORE TIMING MEANS by J.C. Freeborn (Minn.-Honeywell); U.S. Pat. 3,127,575, Issued Mar. 31, 1964

A low frequency, stable, transistor-tunnel diode-magnetic oscillator is described. A saturable core reactor is connected between the bases of the transistors and switching occurs when the core saturates; timing is adjusted by means of a variable resistor in the emitter circuit.

26,205 VARIABLE FREQUENCY MAGNETIC MULTIVIBRATOR by S. Pauli (NASA); U.S. Pat. 3,128,389, Issued Apr. 7, 1964

An improved variable frequency magnetic-coupled multivibrator circuit in which the frequency of the output signal is continuously variable over a predetermined range is described. Features of the system include electronic on-off gating, improved magnetic-coupled feedback control, and a temperature compensated full wave frequency control circuit for providing stable operation over a wide temperature range. The resulting output signal is free of radiation variations for periods during each half cycle of operation.

26,206 MULTIVIBRATOR EMPLOYING TWO-TERMINAL NEGATIVE RESISTANCE DEVICES by O.E. DeLange (Bell Labs.); U.S. Pat. 3,124,702, Issued Mar. 10, 1964

Multivibrators employing negative resistance devices to obtain greater speed and to decrease the number of component parts are described. One specific embodiment of the invention employs two negative resistance diodes in a multivibrator which can be converted from monostable to bistable operation by a simple shift of the magnitude of the bias current. Another embodiment of the invention adds a third negative resistance diode and a capacitor to the circuit described above to form a unique amplifying and differentiating circuit in the output branch of the multivibrator.

SWITCHING CIRCUITS

26,207 TRANSISTOR CURRENT-SWITCHING CIRCUITS by Y.N. Bapat (Indian Inst. Tech., Bombay); Radio and Electronic Engr., Vol. 27, pp. 353-364, May 1964

An analysis and dc design criteria with experimental results for high-speed current-switching circuits are presented. Some improved forms of the basic current-switching circuits have been suggested. These modified circuits considerably ease the stringent tolerance requirements of the components and the power supplies of the original circuits in addition to reducing the number of components and power supplies used in the basic building block of the circuit. DC circuit analysis is presented for the modified single-transistor-type and also for the modified complementary-transistor-type circuits. Design equations and the pyramiding factors for various types of circuits have been discussed. Transient processes in current-switching circuits are considered in detail. It is shown that the major factors limiting the minimum delay per stage obtained is the emitter-base transition capacitance in addition to the rise-time and hence the inherent frequency response of the transistors. A half-adder circuit and a wave-form generating circuit using current-switching mode are described.

26,208 ATC RADAR BEACON SLS CRYSTAL DIODE SWITCH (Am. Electronics Labs.); Contract ARDS464, 17 pp., Sept. 30, 1963; U.S. Gov. Res. Rep., Vol. 39, p. 34(A), May 5, 1964 AD 429 510 OTS \$2.60

The development of a crystal diode microwave switch with coaxial input and output connectors is described. The switch was designed for alternately switching the RF output pulses of an ATC Radar Beacon System transmitter from a rotating directional antenna to an omnidirectional antenna. The switch is a fast-acting solid-state switch that has relatively high power handling capability, low insertion loss and high isolation between the output channels. The solid-state switch driver is also described. The switch meets all design specifications. Field replacement of crystal diodes is not recommended in the model delivered but should be a design goal for future production model switches. The acceptance test procedure and test results are included.

26,209 HIGH SPEED MICROWAVE SWITCHES USING SILVER-BONDED DIODES IN THE Li-Gc REGION by K. Miyauchi and O. Veda (Electrical Commun. Lab., Japan); IEEE Trans., Vol. MTT-12, pp. 368-369(L), May 1964

A high speed switch with a switching time of 0.5 nsec in the 11-Gc region employing silver-bonded diodes, originally developed as variable capacitance elements for use in parametric amplifiers, is described. Static switching characteristics include insertion losses of about 1 db, isolation as large as 20 db, handling power as large as 10 mw, and a required controlling voltage of 5v. Reflection-type switches were also examined. Their switching rise time was dependent on the static bias current. Results for this latter switch exhibited hole storage effects.

26,210 A LOW INPUT VSWR COAXIAL DIODE SWITCH FOR THE UHF BAND by W.L. Ecklund (Natl. Bur. of Stds.); IEEE Trans., Vol. MTT-12, p. 359(L), May 1964

A SPDT coaxial diode switch comprising a system of outer conductor reducers, special blocking capacitors and a series of tuning screws to attain an input VSWR of less than 1.07 over a broad frequency band centered at 1000 mc is described. The same construction technique should work well for any coaxial frequency, particularly 500 mc and higher. The characteristic impedance of the switch is 50 Ω , the isolation in one arm is greater than 63 db, the insertion loss is 1.5 db, the switching time is 20 nsec, and the cw power capability is 3 w.

26,211 SEMICONDUCTOR SWITCHING AND LIMITING USING 3 db SHORT-SLOT (HYBRID) COUPLERS by V.J. Higgins (USAERL); IEEE Trans., Vol. MTT-12, pp. 258-259(L), Mar. 1964

Shunt mode switching and limiting in the frequency range of 9.0 to 9.6 Gc using silver-bonded Gc diodes and a 3db short-slot (hybrid) coupler are discussed.

26,212 A MORE ACCURATE METHOD OF DESIGNING TRANSISTORIZED SCHMITT TRIGGERS by R.A. Jensen (IBM); Electronic Design, Vol. 12, pp. 68-70, Mar. 16, 1964

A new design procedure for the accurate selection of Schmitt trigger switching levels is presented. Most previous expressions assume that the triggering levels are the levels at which each of the two transistors saturates—an assumption often correct for ac-coupled Schmitt triggers but incorrect for dc-coupled triggers where the triggering levels may be one-half or more of the supply-voltage. A detailed analysis is given with both circuit and wave-form parameters.

26,213 A SINGLE TRANSISTOR FLIPFLOP CIRCUIT by C. Isborn (Beckman Instr.); 1964 IEEE Int. Conv. Rec., Part 8, pp. 104-108, Mar. 23-26

Certain transistor oscillator circuits have two stable conditions; one oscillatory and the other quiescent. The nature of this bistability is investigated and circuits are devised which switch readily and reliably from one stable state to the other. These circuits are utilized to perform Schmitt trigger and flip-flop functions with only one transistor instead of the usual two. This technique will make possible a significant reduction in the number of active elements in certain digital instruments and data systems with consequent improvements in reliability at lower cost.

26,214 FLIP-FLOP OPERATION AT VERY HIGH SPEEDS by P. Danzei (Lockheed Electronics); Proc. IEEE, Vol. 52, p. 738(L), June 1964

The results obtained in a study of the use of conventional flip-flop circuits at very high speeds are described. Useful counting action at trigger speeds up to and including 500 Mc are reported. The transistor used for the flip-flop is a germanium device with a specified $\beta = 4$ at 400 Mc and a MAS of 12 db at 16 c. The key to the system appears to be the selection of the transistor operating point and careful fabrication. Special attention point and careful fabrication. Special attention was paid to symmetry, lead length and balanced ground capacity, with a resulting trigger capacity in excess of that normally expected.

Bistable Multivibrators - See 26,206

26,215 BISTABLE TRIGGER CIRCUIT by R.L. Welken and L.M. Lambert, Jr. (Ford Motor Co.); U.S. Pat. 3,132,265, Issued May 5, 1964

Efficiency and speed of a bistable transistor flip-flop circuit are increased by replacing the usual regeneration circuits with a diode and transformer binary trigger which controls both flip-flop transistors with a single pulse source.

26,216 BISTABLE TRANSISTOR MULTIVIBRATOR USED AS A GATING CIRCUIT by S. Pure (US Navy); U.S. Pat. 3,128,393, Issued Apr. 7, 1964

A transistorized gating circuit in which the conductive states of a bistable multivibrator determine the gating interval during which clock pulses are passed by the multivibrator acting as an electronic gate is described. The system is particularly adaptable for use in interval timing circuits where the signal transmitted may comprise a clock signal supplied from an oscillator. The system may be caused to assume each of the two stable conductive states with applications of triggering pulses operable in response to the occurrence of the two events.

26,217 BROADBAND GATE COMPRISING TWO BALANCED BRIDGES CANCELING BIAS VOLTAGES AT OUTPUT AND ATTENUATING WHEN OFF by A.J. Giger (Bell Labs.); U.S. Pat. 3,127,564, Issued Mar. 31, 1964

A broadband gate capable of passing signals ranging from dc to high frequency without interference from the gate control signals is described. In the ON state the gate appears as a low-loss, balanced T pad having an impedance equal to the characteristic impedance of the transmission lines connected at input and output. In the OFF state the gate appears as high loss network for signal attenuation.

26,218 DYNAMIC PULSE COMPARATOR USING SWITCHED TRANSFORMER SECONDARIES AND TRANSFORMER PRIMARY AS PLURAL INPUTS by N. Lentz (Bell Labs.); U.S. Pat. 3,134,946, Issued May 26, 1964

A single logic circuit for binary signal pulse systems of the comparator or disparity recognizer type is described. The circuit uses a transistor, transformer and three diodes and resistors. In a system which already includes a flip-flop circuit having outputs which are opposite to one another in phase, the circuit permits ready comparison of the state of one of the flip-flop outputs with the state of a separate input pulse channel. The input pulses are applied to the

primary winding of a transformer having a pair of oppositely phase secondary windings; each flip-flop is used to switch one of the secondary windings to a common output lead. The switching controlled by the flip-flop output combines with the relative phasing of the transformer secondary winding to provide one indication on the common output lead when the compared signals are alike and another when they are different.

26,219 TUNNEL-DIODE AMPLITUDE COMPARATOR by L. Goodstein (AEK Res. Est., Denmark); *IEEE Trans.*, Vol. EC-13, pp. 309-310(L), June 1964

A single tunnel diode amplitude comparator capable of quick transfer from one side of "zero" to the other without the need for a latch each time is described. E_i values for low-to-high and high-to-low switching can be made arbitrarily small. Switching speed is a function of diode characteristic curvature, diode capacitance, location of operating points and the magnitude of switching signals.

26,220 LOW IMPEDANCE SWITCHING CIRCUIT UTILIZING ZENER DIODE GATE by J.A. Baudin (ITT); U.S. Pat. 3,136,899, Issued June 9, 1964

A Zener diode-transistor switching circuit capable of low impedance switching is described. The circuit was developed to provide an inexpensive, transformer-less, circuit having input isolation and low impedance. Previous difficulties in realizing such circuits involved high power blanking while maintaining proper impedance matching.

SIGNAL CONVERTERS

MODULATORS

26,221 A PULSE MODULATOR THAT CAN BE USED AS AN AMPLIFIER, A MULTIPLIER, OR A DIVIDER by J.A. Rosenthal (Lawrence Radiation Lab.); 1964 *IEEE Intl. Conv. Rec.*, Part 8, pp. 129-136, Mar. 23-26

A pulse modulator that offers several useful features is introduced. Some of its desirable features are that it can respond without delay to a change in input signal and that it is of very simple construction. The modulator can be used as an amplifier, a multiplier, or a divider. It can also be used to control either proportional or on-off systems.

26,222 A SINGLE VALUED TIME TO PULSE HEIGHT SYSTEM USING TUNNEL DIODES by H.L. Weisberg and S. Berko (Brandeis U.); *IEEE Trans.*, Vol. NS-11, pp. 406-408, June 1964

Several aspects of interest in a new delayed coincidence apparatus are described. A tunnel diode time to pulse height converter has been built having an inherently single-valued response, rather than the usual double-valued one. The circuit built has an inherent time resolution (full width at half maximum) of 40 psec. The method used to obtain an accurate time calibration and detect small non-linearities in the system response is discussed. A pile-up detector, consisting of a univibrator, an integrator, and a biased diode discriminator is also discussed. Using Naton 136 plastic scintillators, RCA 7850 photomultipliers, zero-crossing triggers and pulse height compensation, Co⁶⁰ resolution curves having a fwhm of 250 psec and covering more than four decades are obtained.

26,223 A VERSATILE SOLID-STATE TIME-TO-PULSE-HEIGHT CONVERTER by R.G. Roddick and F.J. Lynch (Argonne Lab.); *IEEE Trans.*, Vol. NS-11, pp. 399-405, June 1964

A time-to-pulse-height converter has been developed for use in delayed-coincidence as well as pulsed-beam experiments. It embodies advantages of both start-stop and overlap converters with a single-valued output. A constant current flows into a capacitor only when a fast bistable element is in the "on" condition. In the pulsed-beam mode of operation, the "start" pulse from the detector turns the bistable element on and the "stop" pulse derived from the rf chopping signal turns it off. In the delayed-coincidence mode, the "start" pulse turns the bistable element on only if a "ready" pulse from a second detector is present, and it is turned off by the termination of the "ready" pulse, whose duration is determined by the length of a coaxial line shorted at one end. A means of gating the timing pulses by a fast integral gate is provided to reduce the duty cycle.

Pulse Modulators - See 26,244

26,224 ARRANGEMENT FOR CONVERTING A CONTROL POTENTIAL INTO PULSE-WIDTH-MODULATED RECTANGULAR IMPULSES by R. Schraierogel; U.S. Pat. 3,136,961, Issued June 9, 1964

A method of creating impulses having durations proportional to a certain modulating voltage is described. Initially, short pulses with given repetition rates and time durations are amplitude-modulated; these pulses before modulation have a small, constant, ratio of a/T , where a = width and T = period. The pulses are converted to amplitude-modulated sawtooth waves by means of charging a condenser. A transistor is made to conduct at a certain point on each sawtooth wave, and since these vary in amplitude, a series of pulses is then created varying in width proportional to the modulation. To square the pulses, which retain some slope despite clipping, a Schmitt trigger or other electronic means may be used. One major advantage of the method lies in the comparatively high input impedance of the input modulating transistor.

26,225 PULSE WIDTH MODULATOR by H.D. Ausfresser (Westinghouse Electric Co.); U.S. Pat. 3,135,960, Issued June 9, 1964

Comparison with a prior modulator (US Pat. 2,780,782) is made and certain improvements in its operation is cited. Modulators of the earlier kind generally used a saturable magnetic core with three windings wherein the direct current control voltage applied to one winding controls saturation, and by this means controls pulse width output. Generally in this configuration on resistance is used to limit current flow after saturation; however, this may increase rise and fall time. Fall time is further limited by hysteresis curve-rounding before saturation, and by voltage drop produced in the resistance mentioned. These and other drawbacks are eliminated by adding a fourth winding on the saturable core and applying its voltage to a transistor in the reset part of the circuit to control its conductivity and in turn control the application of reset voltage in such a way as to properly restore saturation. Three circuit configurations are given in which these principles are maintained and further corollary advantages cited.

26,226 A PULSE MODULATOR by J. Kontos (Nucl. Res. Ctr.); *Proc. IEEE*, Vol. 52, pp. 726-727, June 1964

A simply constructed modulator that produces constant-amplitude pulse trains, time modulated by the input signal, is described. The output of the modulator is a pulse train whose repetition frequency and pulse duration both vary with the input signal. The circuit is based on a low-output impedance Schmitt trigger. The output of the trigger is fed back to the base of the input transistor through a two-stage RC filter. This feedback forces the mean level of the output rectangular pulses to vary in proportion to the input voltage. Since the switching levels of the output are kept constant, the duty cycle of the output is forced to vary in proportion to the input voltage.

Pulse:

Duration Modulators - See 26,311

Width Modulators - See 26,242, 26,243

Code Modulators - See 26,312

26,227 CODE CONVERTING ARRANGEMENTS FOR PULSE CODE MODULATION SYSTEMS by A.T. Starr (Intl. Stand. Electric); U.S. Pat. 3,136,988, Issued June 9, 1964

Improvements on the operation of a pulse modulator (U.S. Pat. 2,954,550) which allow amplitude compression and expansion plus code translation are described. Two-condition trigger devices with magnetic cores are employed to convert a signal into groups of digit pulses.

26,228 WIDE DEVIATION FREQUENCY MODULATION SIGNAL GENERATOR by L.J. Kabell (Ampex); U.S. Pat. 3,129,391, Issued Apr. 14, 1964

A frequency modulated signal generator capable of large frequency derivation and responsive to modulation frequencies close to the carrier frequency is described. The generator utilizes semiconductor components to achieve good frequency stability and modulation sensitivity with a minimum of video feed through or amplitude modulation. An output transformer coupled in balanced fashion to the output transistor stages prevents the tendency of the video input signal to mix with the output waveform.

26,229 BACKWARD DIODES IMPROVE LOW-LEVEL CIRCUITS by R.N. Riggs (Aircraft Arm.); *Solid State Design*, Vol. 5, pp. 32-34, June 1964

Unique characteristics of the new backward diodes permit significant improvements in some low-level circuits. The design of an RF balanced modulator and a low-level video detector utilizing backward diodes is discussed. Performance data are given and compared with some results obtained with conventional diodes. Properties of conventional, tunnel and backward diodes are compared which predict usefulness of the backward diode in detectors, modulators and limiters.

DEMODULATORS (DETECTORS)

26,230 CIRCUIT FOR DETECTING THE FREQUENCY DIFFERENCE OF SIMULTANEOUSLY APPLIED ALTERNATING CURRENT SIGNALS AS A DIRECT CURRENT SIGNAL by N.W. Bell (Bell and Howell Co.); U.S. Pat. 3,136,900, Issued June 9, 1964

A means for generally improving frequency discriminator apparatus, which previously had employed two separate discriminators and summing networks, by means of a unified configuration using six diodes is discussed. A dc voltage directly proportional to the sum or difference of the frequencies applied to the unit is measured. Since the principle of the circuit is basically to generate dc indicating voltages from ac input, the input frequencies must be regulated closely so that amplitude changes will not cause false readings. This is accomplished by use of double anode breakdown diodes in each input. The square waves produced are then discriminated, rectified, and depending upon whether sum or difference readings are wanted, read either series aiding or series opposing respectively.

26,231 COMPENSATED PULSE WIDTH DEMODULATOR by N.E. Maestre (Vector); U.S. Pat. 3,129,385, Issued Apr. 14, 1964

A device for converting pulse width or time intervals into a direct current voltage signal which employs the principle of linearly charging a capacitor for a time interval accurately controlled by the width of the pulse is described. The ratio of direct current signal output to the pulse or time duration may be controllably varied; the dc output at zero input time duration may also be independently varied. Transistor and solid state components reduce the size, weight and power consumption from previous models employing vacuum tube as active elements.

26,232 SCR DEMODULATOR HANDLES HIGH POWER EFFICIENTLY by R.C. Howard (Giannini Cont. Corp.); Electronic Design, Vol. 12, p. 102, Mar. 16, 1964

A phase-sensitive, synchronous, full-wave demodulator using SCR's is described. It is an updated version of the ring demodulator, having improved stability and a wide dynamic range of 1 in 10,000. It also has a high peak power output of 16 watts with a reduced power input. Four SCR's are used to obtain a polarity-reversible, phase-sensitive, full-wave output. A schematic is provided.

FREQUENCY CONVERTERS

26,233 DOUBLE-SIDEBAND PARAMETRIC CONVERSION USING NON-LINEAR RESISTANCE AND CAPACITANCE by K.L. Hughes and D.P. Howson (U. Birmingham); Radio and Electronic Engr., Vol. 27, pp. 417-424, June 1964

The power gain of a double-sideband up-converter using both non-linear resistance and capacitance is found. With the assumption that the second-harmonic components of resistance and capacitance are zero, it is shown that if the elements are pumped in quadrature the forward gain can be made arbitrarily high with 'cold' tuning while the reverse gain is zero. It is also shown that unidirectional operation with arbitrarily high forward gain can be achieved for any up-conversion frequency ratio. Expressions are also derived for the bandwidth and noise figure of the device. Arbitrarily high forward gain and unidirectionality appear possible when the second-harmonic components of resistance and capacitance are non-zero.

26,234 PARAMETRIC UP-CONVERSION BY THE USE OF NON-LINEAR RESISTANCE AND CAPACITANCE by D.P. Howson and A. Szerlip (U. Birmingham); Radio and Electronic Engr., Vol. 27, pp. 425-434, June 1964

The power gain of parametric up-converters using both nonlinear resistance and capacitance is found for the condition of conjugate matching at the output termination only. It is shown that for the elements pumped in quadrature it is possible to obtain input impedances with a negative real part, and that under these conditions the gain may be arbitrarily large in principle for any value of pump frequency greater than zero. It is also shown that the device may be used as a negative-resistance parametric amplifier in which the pump frequency is lower than the signal frequency. Previous results showing that the up-converters may be made unidirectional in operation are confirmed, and it is shown that the gain under these conditions may be optimized by suitable adjustment of the mark/space ratio of the resistance variation. Attempts are made on physical grounds to explain both the unidirectional operation and also the high gain possible with r-c converters.

26,235 PARAMETRIC FREQUENCY CONVERTERS WITH NONLINEAR CAPACITANCE AND RESISTANCE by D.P. Howson (U. Birmingham); Proc. IEEE, Vol. 52, p. 425(L), Apr. 1964

A discussion of the effect of the relative phase shift, θ , between the pumps of parametric converters on the power gain of a noninverting converter is presented. The complete mathematical proof is so complicated that gross approximations are made in order to establish some simple results. Special cases of $\theta = \pi/2$ and $\theta = -\pi/2$ are discussed briefly.

26,236 THE PROPERTIES OF PARAMETRIC FREQUENCY MULTIPLIERS WHICH ARE DRIVEN BY MODULATED SIGNALS [in German] by P. Birgels; Nachr.-Techn.Z., Vol. 17, pp. 225-229, May 1964

The properties of parametric frequency multipliers which are driven by modulated signals are investigated. The considerations refer to amplitude modulation since frequency modulation and its derivatives are not affected by ideal frequency multipliers. Statements relating to the harmonic distortion factor and the intermodulation distortion factor are given for two possible modes of operation — controlled and fixed operating point. The results are to a large extent confirmed by practical results.

Parametric Converters — See 26,159

26,237 STUDY OF FREQUENCY MULTIPLIERS USING VARIABLE CAPACITANCE DIODES [in French] by D.J. Roulston and M. Schwindenhammer (CSF); Ann. Radioelect., Vol. 19, pp. 30-39, Jan. 1964

A theory for calculating the performance of a frequency multiplier using a varactor is presented. The internal diode is examined with a view to determining the optimum conditions for the physical parameters, taking the circuits used into consideration. Considering the overall efficiency and the converted power an optimum value of the exponent of non-linearity, γ , is obtained. The results are given by curves of efficiency and converted power for various circuits; the theory is followed by the discussion of some spurious or stray effects, and results obtained in practice are given.

26,238 4-TERMINAL CONTROLLED SWITCH DIVIDES FREQUENCIES BY 10 by R.J. Wold (U. Wisc.); Electronics, Vol. 37, pp. 81-82, June 15, 1964

An accurate relaxation oscillator frequency divider using two stages of division in each stage consisting of a four-terminal silicon-controlled switch, resistor and capacitor is described. Synchronization of the oscillator is achieved by applying a positive pulse to the base of the input switch. Synchronization pulses raise the frequency to a synchronous frequency that is higher than the oscillator's natural frequency. The output of the circuit is a sawtooth waveform, and with periods of up to one minute, a fairly linear waveform is produced, thus making the circuit useful as a sawtooth generator.

26,239 DESIGN OF X-BAND VARACTOR DIODE FREQUENCY MULTIPLIERS by C. Hoffins (AC Spark Plug); Proc. IEEE, Vol. 52, pp. 742-743, June 1964

A varactor frequency multiplier designed to multiply the 1k Mc output of a crystal controlled secondary standard to 10 k Mc is described. The varactor diode mount consists of a coaxial transmission line in which the diode is placed in series with the center conductor. The end of the line is shorted one half wavelength from the diode at 1k Mc placing the diode at the high current point for this frequency. The transmission line is coupled to an x-band waveguide (RG-52/U) at the diode location. Impedance matching is provided by tapered waveguide and tapered transmission line. The diode used has a cutoff frequency of 89 k Mc and a C_{jmin} of 0.653 pf operated at zero bias. The multiplier is able to multiply by a factor of 10 times in a single stage with a relatively high efficiency, providing useful output power at x-band from a UHF crystal controlled source. Outputs from 7 to 12 k Mc can be obtained for a 1 k Mc input without any appreciable change in the one-half per cent efficiency.

26,240 STABILIZED 400-CYCLE-OPERATED MAGNETIC FREQUENCY MULTIPLIER by W.A. Geyger (US Naval Ord. Lab.); Proc. Natl. Electronics Conf., 1963, Vol. 19, pp. 219-236

Design information and performance characteristics of a phase-multiplier-type frequency transformer which meets the requirements of (1) stabilization of the 2000-cps, 2800-cps, or 3600-cps output voltage against large variations of the 400-cps supply voltage, (2) application of single-phase supply instead of the generally used three-phase supply, and (3) current-limiting protection from current overloads and external short-circuit are presented. By providing 5, 7, and 9 saturating-core transformers with multiple, series-star connected primary windings and series-aiding connected secondary windings, the need for additional phase-changing transformers is eliminated. Furthermore, by combining the primary circuits of these transformers with three power-factor-correcting shunt capacitors and linear reactors this magnetic frequency multiplier has the properties of ordinary ferroresonant constant-voltage transformers. Measured total efficiency (watts out divided by watts in) of the described miniaturized systems (maximum output power: about 10 watts) is 60 to 70 percent with a purely resistive load.

26,241 HARMONIC GENERATION BY AN ARRAY by D.D. King, F. Soble, and J.W. Dozier (Electronic Commun. Inc.); *IEEE Trans.*, Vol. MTT-12, p. 256, Mar. 1964

A diode array as a millimeter wave source having adequate power handling capacity is described. Such an array, while feasible, is uneconomical with presently available diodes. A schematic drawing and photograph of the completed 10 element harmonic array are given. The array was constructed for $f_0 = 25$ Gc and had conversion and coupling losses of 20 db and 6 db respectively.

Integrated Frequency Dividers - See 26,125

Photo-Modulated Converters - See 26,164

WAVE GENERATORS

26,242 GENERATOR PERMITS INFINITE PULSE WIDTH VARIATION by T. Hart (Collins Radio); *Electronic Design*, Vol. 12, pp. 68-71, June 22, 1964

An infinitely variable pulse-width generator having a zero to 100 percent duty cycle and consisting of a standard clamp circuit followed by a properly biased two-stage dc amplifier is described. The input may be any waveform, but for the pulse-width output to be a linear relationship to the positive of the control input potentiometer, the input should be a linear ramp function or a sawtooth. If this control input adjustment is replaced by a dc voltage from any type transducer, the output pulse width would be proportional to the dc voltage at the control input with respect to ground.

26,243 ADJUSTABLE WIDTH SQUARE WAVE PULSE GENERATOR CIRCUIT PRODUCING FAST RISE PULSES by F. Eagle (US Navy); U.S. Pat. 3,135,878, Issued June 2, 1964

A transistorized pulse generator capable of producing square output pulses of fast rise and fall times with the leading edge coincident with that of the input pulse and the trailing edge adjustable to vary output pulse width independent of the input pulse is described. Input pulses are applied through an emitter follower transistor to trigger a grounded emitter transistor having its collector in common coupling with a third holding circuit grounded emitter transistor. The common coupling of the second and third grounded emitter transistors is coupled to one base of a pair of grounded emitter switching transistors, the base of the other switching transistor being coupled to an adjustable delay line. The common-coupled collector output of the switching transistors is coupled through a pair of driving transistors arranged in a complementary circuit manner to produce the output square waves. Adjustment of the delay line will vary the pulse width by charging the trailing edge with respect to the leading edge of the output pulse.

26,244 DELAY GENERATOR HAVING FIRST AND SECOND RESONANCE CIRCUITS CONTROLLING DELAY INTERVAL AND PULSE DURATION RESPECTIVELY by M. Fischman (Genl. Tel. and Electronics Lab.); U.S. Pat. 3,135,877, Issued June 2, 1964

A time delay generator in which the delay interval and pulse duration are controlled by the time constants of two resonant circuits is described. Upon application of an input signal to the delay generator the first inductor is connected in series with a charged capacitor, resulting in a half cycle of sinusoidal current at the frequency of the first resonant circuit. When the current through the capacitor goes to zero at the end of the half cycle, switching circuits initiate the output pulse while simultaneously disconnecting the first inductor from the circuit and coupling a second inductor in series with the capacitor. A sinusoidal current at the frequency of the second resonant circuit then flows through the capacitor and the second inductor. When this current goes to zero, the output pulse is terminated by the switching circuits and the second inductor is disconnected from the circuit. Thus the first and second resonant circuits control the delay interval and the duration of the output pulse respectively.

26,245 GENERATING TWO RECTANGULAR WAVES by R.W. Maine (Dyna-electron Corp.); *Electronics*, Vol. 37, pp. 82-83, June 15, 1964

A means of accurately generating two separate rectangular waveforms, a 50-millisecond positive pulse and a 125-millisecond positive pulse both occurring at 0.5 cps, using a minimum of components, is described. The pulses have rise and fall times of less than one microsecond and the amplitude of the pulse voltage ranged from 14 to 17 volts. Stability for the time periods was ± 5 milliseconds. The operating temperature range is 0° to 55° . Circuit diagrams and operation explanation are given.

26,246 THE GENERATION OF RANDOM-TIME PULSES AT AN ACCURATELY KNOWN MEAN RATE AND HAVING A NEARLY PERFECT POISSON DISTRIBUTION by G. White (AE Res. Est.); *J. Sci. Instr.*, Vol. 41, pp. 361-364, June 1964

It is shown that the individual microplasma breakdowns in silicon p-n junctions may be used in the generation of pulses which have a random time distribution. A practical instrument has been constructed in which the mean output pulse rates are accurately defined at rates between 100 and 10,000 pulses per sec. Much lower rates may be obtained if required.

26,247 FIELD EFFECT TRANSISTOR CONTROLS PULSE OSCILLATOR by T.C. Ross (Infrared Indus., Inc.); *Electronics*, Vol. 37, p. 80, June 15, 1964

A field effect transistor used as a voltage-controlled non-linear resistor in a pulse oscillator to provide a circuit with greater reliability than a conventional multivibrator is described. The basic configuration and subsequent alteration and circuit operation of the pulse amplifier is presented. The frequency of the completed circuit is plotted against the control voltage of the FET.

26,248 POWER PULSE GENERATOR by J. Cole and L. Newlin (Continental Oil Co.); U.S. Patent 3,136,896, Issued June 9, 1964

A power pulse generator circuit employing two silicon controlled rectifiers is described. The advantages of this circuit over other SCR circuits are low average current through the SCR's, since both are operated in the normally cut off state, and a novel method of accurately controlling pulse width.

26,249 2000-A PULSE GENERATOR by N.A. Sullivan (Lincoln Lab.); *Rev. Sci. Instr.*, Vol. 35, p. 639-640, May 1964

A pulse generator designed to supply pulses of up to 2200-A amplitude and 50-nsec duration to injection lasers presenting an extremely low impedance to these pulses is described. When a 0.5 Ω load is used, the peak current is 4000 A with a slightly distorted pulse due to the line mismatch. Operation above 5 kv was not attempted, although it is expected that peak currents of over 10,000 A may be realized at higher voltages. The results above were obtained with a pulse rate of 50 pps; the generator is operable up to 1000 pps with reduced peak currents.

26,250 LINEAR MAGNETIC SWEEP GENERATOR by K.E. Wood (Westinghouse); U.S. Pat. 3,129,355, Issued Apr. 14, 1964

A new and improved linear magnetic sweep generator in which a Hall generator device is utilized to provide a feedback voltage directly proportional to the magnetic flux in the deflection coil is described. Since the Hall device is characterized by an output voltage proportional to current times the field strength transverse to the current direction, a constant current will make the output voltage dependent upon the field strength. The circuit also employs a linear flux sweep with time by using the feedback voltage to control the current in the deflection coils.

26,251 SAWTOOTH WAVEFORM GENERATOR EMPLOYING MONOSTABLE CIRCUIT TO CONTROL RESET by D.L. Alexander; U.S. Pat. 3,124,706, Issued Mar. 10, 1964

A sawtooth generator with input trigger "holdoff" is described. Spurious triggers are prevented during a predetermined time after a given cycle is started.

26,252 SQUARE WAVE GENERATOR EMPLOYING REVERSE-BIASED DIODES AT TRANSISTOR INPUT TO PRODUCE SYMMETRICAL OUTPUT by R.A. Greiner (Gisholt Machine Co.); U.S. Patent 3,128,395, Issued Apr. 7, 1964

A transistorized squaring circuit which maintains a zero cross-over point at the output over a wide ratio of maximum to minimum input signals is described. Reverse biased diodes at the input are symmetrically located between the coupling capacitor and the input transistor; the reverse bias allows very small current flow in the transistor immediately adjacent to the zero crossover point. One important operating criterion is that the bias of the diodes be accurately established, for errors may lead to zero circuit gain or capacitor loading, hence a shift in transistor bias.

Sawtooth Generators - See 26,238

PULSE CIRCUITS

Pulse Generators - See Wave Generators

26,253 TRANSISTOR COUPLING CIRCUITS FOR THE Z504S STEPPING TUBE by G.C. Chappell and G.F. Jeynes (Mullard Appl. Res. Lab.); Mullard Tech. Commun., Vol. 7, pp. 310-322, May 1964

A transistor pulse shaping circuit for coupling stepping tubes at speeds up to 400 pps, and a 4000 pps blocking oscillator input circuit is described. In addition, two alternative light-sensitive input circuits are described, using ORP60 and RPY15 cadmium sulphide cells, for operation at counting speeds up to 25 pps and 13 pps respectively. The ORP60 operates satisfactorily with a drop in intensity of illumination from 2000 to 10 lux while the RPY15 requires 1000 lux falling to 10 lux. Auxiliary circuits for power supplies and resetting are also discussed.

25,254 PULSE SHAPER USING CARRIER STORAGE DIODES by K.B. Magleby (Hewlett-Packard); U.S. Pat. 3,132,259, Issued May 5, 1964

A transformer-isolated pulse shaping circuit capable of producing pulses with rise and fall times below a nsec from conventional pulses is described.

26,255 PULSE FORMING CIRCUIT UTILIZING TRANSISTOR AVALANCE CHARACTERISTICS by J.G. Dill (Hughes Aircraft); U.S. Pat. 3,126,489, Issued Mar. 24, 1964

A pulse forming circuit utilizing transistors having avalanche characteristics to form pulses of a selected width and polarity is described. Output pulses in the range of 1 to 2 msec may be developed using the transistors in avalanche mode operation. The circuit includes first and second avalanche transistors biased in the avalanche multiplication region with their base to emitter junctions reverse biased. Trigger pulses applied through a variable delay to the bases of the transistors initiate the avalanche breakdown operation. Current pulses are formed in response to the trigger signals and have an opposite flow direction through the load which cancel except between application of trigger pulses. Pulse width is determined by the time delay between trigger pulses.

26,256 TRANSISTOR'S STORED CHARGE CONTROLS PULSE DELAY by R.H. Blumenthal and F.E. Williams (Sperry Gyroscope); Electronics, Vol. 37, pp. 52-53, June 29, 1964

Variable output pulse widths and time delays in the range 0.58 to 4.65 microsec are obtained using the storage charge phenomena of four saturated low alpha cutoff germanium transistors. Impedance matching and input pulse width regulation are necessary. Performance of several transistors are given. Operation is reliable at pulse repetition rates between 50 and 5000 pulses per second and temperatures between 50 and 5000 pulses per second and temperatures between -55° and +55°C.

26,257 RELAY CIRCUIT DELIVERS DELAYED PULSE OUTPUT by I. Karmin (Loral Electronics); Electronic Design, Vol. 12, p. 108, Mar. 16, 1964

A relay circuit which allows a short, single delayed pulse out after a long pulse input is described. The circuit uses a sensitive relay, a 50- μ f capacitor and a 0.5-megohm resistor. The relay contact closes 0.5 sec after the 24-v dc input, and opens 1 sec after that. Circuit timing is controlled by the capacitor, relay inductance and relay sensitivity.

Pulse Delay Circuits - See 26,244

26,258 REDUNDANT PULSE HEIGHT DISCRIMINATOR by R.H. Wagner (Bendix Res. Labs.); IEEE Trans., Vol. NS-11, pp. 308-313, Jan. 1964

A semiconductor pulse-height discriminator and driver amplifier was developed which will operate reliably for long periods of time aboard unattended space craft. Adequate threshold stability under variable temperature and supply voltage conditions is provided by a new tunnel-diode circuit. Active parallel circuit redundancy is employed to enhance reliability. The resulting circuit tolerates opens or shorts in any of the semiconductors with little performance degradation.

26,259 BEHAVIOR OF TUNNEL DIODE AMPLITUDE DISCRIMINATORS by F. Pandarese (Brookhaven Lab.); IEEE Trans., Vol. NS-11, pp. 16-23, Apr. 1964

The dependence of the output of a tunnel diode amplitude discriminator on the excess over threshold is analyzed; the input pulse is assumed to be from a scintillation counter. An approximate formula for the maximum delay introduced is given. The results of numerical integration are summarized in a diagram, allowing the calculation of the delay introduced for various values of excess over threshold and of circuit time constants.

26,260 TUNNEL DIODE DISCRIMINATOR CIRCUIT by Q.A. Kerns (AEC); U.S. Pat. 3,136,902, Issued June 9, 1964

A detector and discriminator for high energy particles is described. The circuit uses standard scintillators and photomultipliers to feed a negative pip for each particle to either a shorted concentric line or an LCR circuit, producing zero-crossing signals. Weak, unwanted signals are rejected by a biased tunnel diode. A bridge is unbalanced by signals extending to the negative resistance region of the diode and the output from the bridge is discriminated and amplified, and the negative pips removed, leaving a positive pulse train. The threshold for the input is variable. For one LCR configuration, the dynamic amplitude range was 100:1 between the unbalance bridge condition and saturation. Dead time is less than 25 msec. Time definition of the original photomultiplier pulse is better than 0.5 nsec over a 20:1 dynamic output range.

26,261 SYNCHRONIZED SINGLE PULSE CIRCUIT PRODUCING OUTPUT OF PREDETERMINED LENGTH FROM DELAY LINES HAVING DISSIMILAR PERIODS by H.J. Gray, Jr. (Sperry Rand); U.S. Pat. 3,124,705, Mar. 10, 1964

Circuits which permit the production of a single synchronized output pulse in response to a non-synchronous input signal are described. A number of transistorized logic circuits and two delay lines of dissimilar periods are employed. The circuits are capable of converting an asynchronous input signal of any duration to a single 0.5 microsecond pulse which is synchronized with a clock pulse.

Pulse Rate Counters - See 26,273

OTHER CIRCUITS

FILTERS

26,262 DESIGN OF FILTERS AND NETWORKS by E. Pezirtoglou (Ampex); Oct. 1963, 212 pp.; U.S. Gov. Res. Rep., Vol. 39, p. 41(A), May 5, 1964 AD 430 092 OTS \$14.50

A handbook is presented on filter designs. The problem of filter design is the synthesis of networks having prescribed amounts of discrimination between the wanted and the unwanted bands of the frequency spectrum. Existing textbooks on filters, however, concentrate on theoretical principles and give comparatively little attention to the needs of the practical designer. The present work is an attempt to provide practical approaches.

26,263 INTRODUCTION TO FILTERS by A.I. Zverev (Westinghouse); Electro-Tech., Vol. 73, pp. 61-90, June 1964

A basic treatment of filter theory is presented. The use and functions of a filter design are described and the types of filters to fit these uses are given. Filter design techniques, the image-parameter method and the polynomial synthesis method, are described and compared. Butterworth, Chebyshev and Cauer-parameter filter synthesis procedures are discussed with simple polynomial as well as multipole filter realization. The narrow band approximation is explained, and some physical problems of filter design are listed. Appendices are given for mathematical understanding of the synthesis techniques.

26,264 AN ITERATIVE APPROXIMATION PROCEDURE FOR AUTOMATIC FILTER SYNTHESIS by B.R. Smith and G.C. Temes (Northern Electric R and D Labs.); 1964 IEEE Intl. Conv. Rec., Part 1, pp. 270-281, Mar. 23-26

The design of m-derived image parameter filters, as well as the synthesis of Butterworth or Chebyshev passband insertion loss parameter filters with prescribed frequency-dependent minimum stopband attenuation, normally involves the use of graphical methods to find the necessary number and location of the attenuation poles. These methods are tedious and inaccurate. An iterative approximation process, somewhat similar to Remez's second method, for the synthesis of lowpass and bandpass filters is described. The process is very fast and its programmed version (containing numerous options) fits into a 40,000 position computer memory. A brief analysis of the optimality and convergence of the procedure is included. Finally the actual computer programs are described and some examples given.

26,265 TUNABLE FILTER FOR LOW FREQUENCIES USING OPERATIONAL AMPLIFIERS by H. Sutcliffe (Royal Coll. of Advanced Tech.); Electronic Engrg., Vol. 36, pp. 399-403, June 1964

The design of tunable narrow band filters for frequencies down to 0.1 cps, using active elements and RC networks, is complicated by the requirements of

trimming and ganging. A principle is described whereby the difficulties are overcome and a method is given for obtaining a 'constant Q' filter equivalent to a critically coupled pair. The design of the associated operational amplifiers, using transistors, forms a substantial part of the article. Details are given of a filter suitable for the frequency range 1 to 1000 cps.

26,266 THEORY OF SIMULATED-SKIN-EFFECT FILTERS A THIN FILM APPROACH TO EMI by H.M. Schlicke (Allen-Bradley Co.); *IEEE Trans.*, Vol. EMC-6, pp. 47-54, Jan. 1964

The theory of a new, ceramic low-pass filter, highly effective at very high frequencies, is discussed. Its excellent performance is based on simulation of the skin effect whereby the VHF, UHF and microwave currents are forced along a thin, electrically permeable resistive film deposited inside a high-dielectric tube while a large dc current may flow through the coaxial conductor. Theory and experiment are in excellent agreement. In several respects these filters are better than cascaded filters (ferrites and dielectrics combined) which were considered the best available. The simulated-skin-effect filter shows great promise of becoming a significant means in combatting conducted electromagnetic interference.

26,267 A SOLUTION TO THE APPROXIMATION AND REALIZATION PROBLEMS FOR CRYSTAL LADDER FILTERS by J.D. Schoeffler (Case Inst. Tech.); 1964 *IEEE Intl. Conv. Rec.*, Part 1, pp. 282-288, Mar. 23-26

The standard elliptic or equal-ripple filter functions are not realizable in the form of a ladder network whose elements are all piezoelectric resonators. A solution to the approximation problem is derived which gives a transmission function with equal ripple in both pass and stop bands and which is realizable by a ladder network of resonators. The accuracy problem associated with realization of band pass filters on a digital computer are circumvented by carrying out the realization with a transformed frequency variable, resulting in a design time of a few seconds. Examples are presented which indicate that reasonable resonator parameters may be obtained from the designs.

26,268 A DISSIPATIVE COAXIAL RFI FILTER by P. Schiffrès (Paradynamics, Inc.); *IEEE Trans.*, Vol. EMC-6, pp. 55-61, Jan. 1964

A lossy coaxial filter has been developed to protect electroexplosive devices from accidental detonation by stray high-power RF fields. The characteristics of a coaxial transmission line, filled with dielectromagnetic material, are analyzed in terms of various proposed filter configurations. The design concept for the prototype filter is chosen so as to provide a maximum stop-band attenuation. Measured results are presented to show that the filter provides an insertion loss of about 90 db from 5 Mc to at least 10 k Mc. Furthermore, it is shown that the use of a lossy filter guarantees a minimum value of insertion loss regardless of the terminating impedances.

26,269 TUNING A THIN-FILM NOTCH FILTER; *Electronic Products.*, Vol. 7, pp. 52-53, June 1964

A tantalum RC network comparing favorably in terms of precision for tuning, temperature coefficient and long-term stability with conventional component networks is presented. The filter, which is used as a frequency-selective circuit, has an initial frequency accuracy of ± 0.02 percent. The physical size of the filter is about 0.65 in. by 0.65 in. The photoetched film is anodized to produce the capacitor dielectrics and adjust the resistance values. Evaporated gold is used as the capacitor counter electrodes.

APPLICATIONS OF SOLID STATE DEVICES

GENERAL

BIOMEDICAL APPLICATIONS

26,270 WHAT'S AHEAD IN BIOMEDICAL MEASUREMENTS? by L.E. Slater (Case Inst. Tech.); *ISA J.*, Vol. 11, pp. 55-60, Feb. 1964

A survey of microminiature transducers for use in biomedical instrumentation is presented. The report covers both pick-up and implanted devices and provides a brief description of each device. A tabular list of solid-state transducers for biomedical applications itemizes devices available to measure specific physical parameters. The suggestion is made that future transducers may utilize nuclear magnetic resonance and electron spin resonance to map biological molecules by their magnetic behavior.

26,271 DYNAMIC BIOTELEMETRY by V.V. Rozenblat; Transl. into English from *Usp. Sovrem. Biol.* (Moscow), v. 56, No. 3(6), 1963, pp. 341-364; *STAR*, Vol. 2, p. 1227(A), May 23, 1964 JPRS-23910; OTS-64-21918; OTS \$1.00

A general survey of the use of radiotelemetry in medicobiological investigation is presented with particular emphasis on dynamic biotelemetry. After a brief history of the development biotelemetry, the working classification of biotelemetry (onboard, dynamic, endoradioprobe, retranslation or relay, and stationary) are defined. Dynamic biotelemetry deals with the remote recording of physiological data by radio during unrestricted physical movement of the subject. The general characteristics of the transmitting and the receiving-recording apparatus for dynamic biotelemetry are discussed. The applications of dynamic biotelemetry considered include: sport physiology; with particular emphasis on cardiac function; work physiology, especially during physical labor; and clinical physiology, particularly for diagnostic evaluation. The future prospects of dynamic physiology are seen to depend upon close cooperation between design engineers and physiologists, the use of existing facilities mainly for applications that cannot be investigated in other ways, and increased production of biotelemetric apparatus.

26,272 A PERSONALIZED RADIO TELEMETRY SYSTEM FOR MONITORING CENTRAL NERVOUS SYSTEM AROUSAL IN AEROSPACE FLIGHT by D.G. Simons and W. Prather (Brooks AFB); *IEEE Trans.*, Vol. BME-11, pp. 40-51 Jan.-Apr. 1964

Simultaneous analysis of four measures, Electroencephalogram (EEG), Base Skin Resistance and Galvanic Skin Response (BSR/GSR), Electrocardiograph (ECG), and respiration, were employed to detect changes in the level of Central Nervous System (CNS) arousal. In the original configuration, a 6-channel personalized telemetry unit transmitted all measures except EEG. A separate transmitter was used for EEG. Subsequently an outboard subcarrier oscillator unit was developed to incorporate the EEG on the common RF carrier. Problems of electronic interaction through body contact electrodes, insulation leakage of sensors, a single-ended system, and excessive subcarrier drift were encountered. Solutions to these problems were found. Analyses included the conversion of EEG to units of activation, beat-by-beat rate analysis of ECG, breath-by-breath rate analysis of respiration, and a slow writeout of base skin resistance. Sample results of data obtained from the personalized telemetry are presented, and the appearance of analyzed records included. Major changes in levels of CNS arousal were generally identifiable in any one measure. Subtle changes are frequently clearly demonstrable employing this system for simultaneous presentation of analyzed multiple physiological measures.

26,273 PULSE PERIOD METER WITH SHORT RESPONSE TIME, APPLIED TO CARDIOTACHOMETRY by P.A. Tove and J. Czepakewski; *Electronic Engrg.*, Vol. 36, pp. 290-295, May 1964

A method of measuring pulse repetition rate with fast response to frequency changes has been developed. The principle is to measure intervals between pulses by alternate charging of two capacitors during successive pulse intervals. The voltage on that capacitor which is not being charged is indicated on a meter or oscilloscope and is a measure of the length of the last period. Direct scale indication of pulse interval length or frequency is achieved and the possibility of obtaining linear and logarithmic frequency-scales is discussed. It is shown that simple exponential charging of the capacitors approximates the desired scale shapes over limited frequency regions. Methods of obtaining linear and logarithmic scales over large regions are described. Practical circuits are described for medical applications in cardiachometry and registration of respiratory frequency where it is essential to have fast response to changes in pulse rate. Another application is in information transmission systems using pulse length modulation.

26,274 AN INSTRUMENT FOR RECORDING THE FETAL PULSE RATE by J.B. Cornwall and F.G. Tattam (Scientific and Indus. Res. Lab.); *IEEE Trans.*, Vol. BME-11, pp. 24-28, Jan.-Apr. 1964

An instrument is described for recording the fetal heart rate using a microphone strapped onto the abdomen. Special precautions have been taken to reduce the effects of extraneous noise received by the microphone. The electronic system incorporates a narrow passband amplifier, a rapidly responding automatic gain control circuit, and a ratemeter in which the intervals between successive pulses are compared so that pulses which are unlikely to be genuine can be disregarded. The equipment is suitable for operation by nontechnical personnel and has been used regularly in a maternity hospital for a period of eighteen months.

26,275 NEW IMPROVEMENTS IN BELL SYSTEM'S ARTIFICIAL LARYNX; *Bell Labs. Rec.*, Vol. 42, p. 39, Jan. 1964

The use of a smaller head (1 inch dia.), in the Bell System's electronic larynx is discussed. Held against the throat, this device transmits sound waves which are passed up the throat and formed into words by lip and tongue movements as in normal speech.

Electrometers for Medical Applications - See 26,422

Laser Applications in Biology - See 26,058, 26,060

AUTOMOTIVE APPLICATIONS

26,276 GROWTH OF SEMICONDUCTOR BUSINESS IN AUTOMOBILES by D.I. Van Blois and L.J. Giacoletto (Mich. State U.); IEEE Trans., Vol. IECI-11, pp. 39-43, Feb. 1964

The various uses of semiconductor devices in automobiles, radios, alternators, ignition systems, and miscellaneous applications are examined in terms of past and present dollar volume. These performances are totaled and extrapolated into the future. The total growth curve shows a very steep rise for the next five years.

26,277 THE FUTURE FOR SEMICONDUCTOR BUSINESS IN AUTOMOBILES by D.I. Van Blois, L.J. Giacoletto, and T.A. Faulkner (Mich. State U.); 1964 IEEE Intl. Conv. Rec., Part 4, pp. 119-123, Mar. 23-26

The automotive industry has become a significant user of semiconductors. The growth rate has been spectacular due, in great measure, to the recent reductions in prices of semiconductor devices. The reduced prices, together with greater reliability, and in most cases, improved operating properties has accelerated the switch from heretofore standard to new manufacturing. The various segments of the semiconductor uses in automobiles; radios, alternators, regulators, ignition systems, and miscellaneous applications, have been examined individually in terms of present dollar volumes. These performances are then totaled and extrapolated into the future with suitable weightings for probable prices, probable percentage adoption, and probable total automobile sales. The resulting total growth curve shows a very steep rise for the next five years with a volume of \$30 million by 1965 and a likely volume of \$65 million by 1970.

26,278 A CHALLENGE FOR INNOVATION—THE USE OF SEMICONDUCTOR DEVICES IN THE AUTOMOTIVE INDUSTRY by M. Caserio (Delco); IEEE Trans., Vol. IECI-11, pp. 13-16, Feb. 1964

The applications of semiconductors in the automotive field are reviewed.

26,279 CHARACTERISTICS OF IGNITION TRANSISTORS by G.M. Ford (GM); IEEE Trans., Vol. IECI-11, pp. 7-12, Feb. 1964

The factors which enter into the selection of a transistor ignition switch are considered and the benefits to be gained from transistor switching are reviewed. Frequent adjustment is rendered unnecessary and the output voltage of the coil does not fall off at high engine speed when transistors are employed in auto ignitions. The inductive discharge circuit and the prevention of its principle failure mode, secondary breakdown, are discussed. Prevention of secondary breakdown commonly takes one of three forms: 1) The transistor is clamped to less than its avalanche voltage by a zener diode. 2) A transistor is biased in such a way that it can absorb the full energy of the coil in the avalanche condition without breaking down. 3) A very high voltage transistor or a string of transistors is used, making clamping unnecessary.

26,280 AN ELECTRONIC METHOD OF IGNITION ADVANCE FOR AUTOMOBILES by A.R. Hayes (Royal Coll. of Advanced Tech.); Electronic Engrg., Vol. 36, pp. 369-373, June 1964

The full load ignition requirements of a particular engine are described by an algebraic equation which, when applied to a proposed basic scheme, indicates the type of circuit needed to control ignition timing electronically. As an illustration, a possible circuit is given whose performance compares favourably with the present mechanical system.

26,281 TRANSISTOR CAR IGNITION SYSTEM by J.H. Willis; Wireless World, Vol. 70, pp. 151-152, Mar. 1964

The operation, construction, installation and testing of a two transistor circuit linking the contact breaker and ignition coil of a 12 volt, positive ground car ignition system are described. With the circuit installed the contact breaker only has to break 10 ma flowing through a resistor, as against approximately 4 amps through the coil in the normal direct link system. Thus contact breaker point erosion is practically eliminated.

26,282 TYPE IGNITION CIRCUIT CONDENSER DISCHARGE by H.P. Quinn (Tung-Sol); U.S. Pat. 3,131,327, Issued Apr. 28, 1964

An ignition circuit that generates a high voltage pulse without drawing excessive current through the breaker points is described. The circuit provides increased spark plug life and reduction of misfiring of fouled plugs by producing a single high voltage pulse across the spark plug terminals. Spark

plug voltage is obtained by discharging a capacitor which has been charged by a transistorized current amplifier and an inductor which stores the energy of the input current pulses. The capacitor is discharged through a unidirectional device and the primary winding of an output transformer, the secondary connected to the spark plugs through the distributor.

26,283 TRANSISTOR-SWITCHED IGNITION SYSTEMS by J. Nawracaj (Amphenol Borg Electronics); Electro-Tech., Vol. 73, pp. 112-113, May 1964

The operation and advantages of a transistorized ignition system are discussed. An experimental transistor-assisted ignition system is described. A fully transistorized system comprising a pulse distributor, pulse amplifier and special coil and requiring no breaker points is also discussed.

26,284 VEHICLE ELECTRICAL SYSTEM INCLUDING SEMICONDUCTOR REGULATOR AND SWITCH MEANS by L.J. Raven and R.L. Larson (GM); U.S. Pat. 3,129,378, Issued Apr. 14, 1964

An electrical system suitable for use in motor vehicles employing a transistorized field circuit which is not subject to vibration effects and has no moving parts. A very small control switch circuit is required so that no appreciable voltage drop occurs in the control or ignition switch circuit. With this system the battery will not discharge through the regulator and field or contact winding while the circuit between the dc power sources and the regulator is open. A manual electronic switch for the transistor circuit is employed.

26,285 MULTIPLE THERMISTORS MONITOR CAR COMFORT by N. Hunter; Control Engrg., Vol. 11, p. 125, May 1964

A three thermistor monitor for automatic air conditioning of automobiles is described. The temperature is automatically maintained between 65 to 85°F. The thermistors are placed on the dashboard, at the outside air duct, and at the inside air discharge duct; they combine to act upon an expander-contractor transducer attached to a servo to regulate temperature.

NAVIGATION, GUIDANCE AND RANGING APPLICATIONS

Laser Ranging Systems - See 26,063, 26,064

26,286 POSITIONING SERVO FOR NAVIGATIONAL COMPUTER by L. Smith; U.S. Pat. 3,135,900, Issued June 2, 1964

A positioning servo for a navigational computer which is extremely accurate, simple and reliable is described. The system automatically indicates the number of degrees the aircraft is off course without having a left-right and a to-from meter to indicate direction. The positioning servo is comprised of an iron core upon which coils are mounted for receiving reference and variable phase voltages, and amplifiers for providing constant impedances for reference and variable phase voltages and a constant output voltage across the varying impedances of the coils. The amplifiers are of either tube or transistor design. When an error signal is obtained it is amplified and connected to the rotor of an ac motor designed to run at the frequency of the reference voltage. The ac motor is connected to a phase shifter by a gear train and will rotate the phase until a null is obtained.

26,287 DOPPLER DIFFERENCE COLLISION WARNING SYSTEM by E. Lakatos (Thompson Ramo Wooldridge); U.S. Pat. 3,134,100, Issued May 19, 1964

A two position reception Doppler radar system capable of providing collision warning relatively unaffected by the acceleration of the colliding vehicle to the system is described. The system provides a comparison of a difference between the Doppler shifts of two receivers to provide an angular velocity vector of the line of sight from the system transmitter to the intruder vehicle. A feature of the invention is a signal threshold below which the magnitude of the signal is considered dangerous. An array of antennas used in pairs provides the difference input.

26,288 A COMPASS USING A THIN MAGNETIC FILM COMPONENT by P.S. Castro (Lockheed Res. Labs.); IEEE Trans., Vol. CP-11, pp. 19-26, June 1964

The design and development of an all-electronic device which indicates bearing from local magnetic north is reported. The sensing element of the compass consists of two thin magnetic films each of which contains a pumping coil and an output coil. When an ac current is applied to the pumping coil, an ac voltage is developed in the output coil whose frequency is harmonically related to that of the pumping current and whose amplitude varies as $H \cos \theta$, where H is the magnitude of an externally applied magnetic field and θ is the

angle between the external field and the axis of the output coil. By placing the two magnetic films in space quadrature and shifting the phase of the output voltages of the units so that the outputs are also in time quadrature, the output voltage of one unit will vary as $H \cos \theta \sin \omega t$ while that of the other will vary as $H \sin \theta \cos \omega t$. The sum of these voltages will produce an ac voltage whose phase shift depends upon θ , according to the trigonometric identity:

$$\cos \theta \sin \omega t + \sin \theta \cos \omega t = \sin (\omega t + \theta).$$

Detecting the phase shift of this signal will thus produce an output voltage proportional to the bearing of the magnetic field sensing element with respect to the external magnetic field.

26,289 NAVY TRIES SOLID STATE COMPASS by C.M. Wiley; *Electronics*, pp. 57-58, Feb. 19, 1964

A Motorola engineered Hall-effect magnetic compass is briefly described. The sensors, two orthogonal positioned Hall elements, are fed 90 degrees apart by a battery powered transistor oscillator at 2.5 to 5 kc. Combined Hall voltages go to a bistable multivibrator which delivers a pulse proportional to the compass's rotation angle. The device has a 10 millisecond time constant. A variable frequency output varying from 28 kc to 32 kc. may also be obtained. The new compass is more sensitive and will avoid the problem of lubricant congealing in Arctic environs.

26,290 MAJORITY VOTING PROTECTS AIRCRAFT AND PILOT by H. Moreines, R. Worthington, and F. Thomas (Eclipse-Pioneer Div., Bendix); *Electronics*, Vol. 37, pp. 85-91, May 18, 1964

A fail-operative, failure-detecting, solid state aircraft control system utilizing redundancy and logic methods is described. A passive element intermediate-amplitude selective gate, or voter, instantly rejects an erroneous signal from among the outputs of triply duplicated control circuitry. Cascading of voters and triplication of power supplies protects in case of voter or power supply failures. Offline monitors indicate subsystem failures and are fail-safe due to differential amplifier symmetry. Previous signal amplitude comparison methods disconnected failed subsystems too slowly.

26,291 MARINE AUTOPILOT by P.J. Sokson (Genl. Prec.); U.S. Pat. 3,129,686, Issued Apr. 21, 1964

An aircraft or small boat autopilot employing electrical feedback for automatic steering control and power steering for manual control is described. An electrical signal is emitted by the compass set on the boat heading and a control element produces an error signal representing the divergence of the craft from true course. This signal corrects the rudder setting and consequently sends back a rudder neutralization signal to stabilize the operation. Provisions are made for automatic neutralization of rudder bias caused by the use of a single propeller.

COMMUNICATIONS APPLICATIONS

Laser Communications Systems - See 26,061

Maser X-Band Maser Communications Systems - See 26,062

RADIO AND TV

26,292 SELF-QUENCHED SUPER-REGENERATIVE CIRCUIT UTILIZING VARIABLE IMPEDANCE DIODE IN QUENCHING CIRCUIT by H. Lenk (Avco); U.S. Pat. 3,135,921, Issued June 2, 1964

A very high frequency super-regenerative transistorized amplifier and detector circuit having constant self-regulating power gain characteristics for variable input signal levels is described. The automatic power gain characteristic is a result of incorporating a variable impedance diode in the self quenching circuit. The impedance of the diode is made to vary inversely with the magnitude of the super-regenerative oscillation current in the transistor emitter-collector circuit. This variable impedance changes the discharge rate of a bias capacitor and thus charges the self quenching. Since the quench varies inversely with transistor conduction, and hence input signal level, the output power is maintained substantially constant for varying input signal levels. The super-regenerative stage is utilized as an amplifier and/or detector by employing a tuned filter and a low pass filter in the transistor collector stage.

26,293 SELECTIVE CALL SYSTEMS by O.B. Sneath; U.S. Pat. 3,124,658, Mar. 10, 1964

A system in which one or more of a large number of receivers can be selectively called by transmitting a corresponding call signal, received by means of low frequency magnetic, or electrostatic induction is described. Forms of the invention provide for an audio tone or one way code or voice communication immediately upon activation of the receiver by the call signal. Each receiver is operated by two or more pulses of a certain frequency sent out in succession, comprising a train of oscillations, and a different receiver operated according to the order, as well as the combination, of the frequencies sent out. Each receiver consists essentially of an electromagnetic pick-up device, such as a coil wound on a ferrite rod, followed by an amplifier, terminating in a limiter stage, which will be loaded up by any signal receiver, followed by two or three frequency-selective filters. In the case of the two-pulse receiver, the first pulse is passed by one of the filters to open a gate, which stays open for a short interval and while open allows a signal from the second filter to operate a signalling device.

26,294 FREQUENCY MODULATION RECEIVER by A.J. DeVries (Zenith); U.S. Pat. 3,129,288, Issued Apr. 14, 1964

The features of a frequency modulation receiver which may be employed for the reception of monophonic or stereophonic broadcast programs are described and a novel detecting arrangement for demodulating a suppressed-carrier amplitude-modulated signal is detailed. The receiver comprises an F-M detector responsive to the received carrier for deriving a composite signal representing the modulation of that carrier. The A-M detector uses two basic schemes, the simpler of which develops two cleanly separated audio signals using only one transistor.

26,295 MATCHING OF A WHIP AERIAL TO A TRANSISTORIZED V.H.F. RECEIVER by D. Nederlof (Philips, Eindhoven); *Electronic Appl.*, Vol. 24, pp. 25-40, Apr. 1964

At present it is common practice to provide portable v.h.f. receivers with a single whip aerial having a length of roughly one quarter wavelength, the metal chassis of the receiver acting as a counterpoise. Matching such an aerial so that the most favourable signal-to-noise ratio is obtained is more important than matching for maximum sensitivity, since loss in sensitivity can easily be compensated in the subsequent stages of the receiver, but the signal-to-noise ratio of the i.f. signal depends almost exclusively on the aerial matching and on the noise introduced by the first stage. The signal and noise are calculated with the view to providing sufficient data for designing the coupling circuit in such a way that matching is optimum as regards the signal-to-noise ratio. These calculations are supplemented by an investigation of the influence of the radiation temperature. In an Addendum the matching of two impedances by means of a short length of cable and one reactance is discussed in brief. Moreover, details are given of an automatic noise figure meter which has proved to be a most useful accessory for adjusting v.h.f. aerial circuits.

26,296 PHOTO-CELL GENERATOR SYSTEM FOR CHARGING STORAGE DEVICES by R.C.T. Stead; U.S. Pat. 3,127,552, Mar. 31, 1964

A light-powered generator capable of producing low power output suitable for driving transistor radio receivers is described. The generator employs 12 photo-cells, series connected, and a Ni-Cd storage battery. During illumination, the battery is charged; in darkness, reverse current is prevented by the polarity arrangement of the solar cells.

26,297 NOISE REDUCING SYSTEM by J. Germain, J. Battin and J. Mitchell (Motorola); U.S. Pat. 3,126,514, Issued Mar. 24, 1964

An impulse noise plunger circuit for operation in the radio frequency portion of communications receivers is described. When integrated into a radio receiver the circuit detects noise disturbances above the carrier signal level and responds by applying blanking pulses to a stage of the radio frequency portion of the receiver, which turn off that stage during the occurrence of the noise disturbance. The noise blanking system operates within the r.f. portion of the receiver to provide blanking action before noise disturbances are stretched in subsequent tuned circuits, and thereby provides maximum blanking efficiency by minimizing the loss of usable carrier signal. Signals are applied directly from the receiver antenna circuit to an r.f. amplifier and then detected so that impulse noise disturbances above the carrier level are translated into pulses. A diode gate passes detected noise pulses only above a predetermined level and those pulses are filtered through a high pass filter to strip off undesired signals within the pass band range of the receiver. The filtered pulses are amplified, stretched a predetermined time duration, and utilized to turn off an r.f. stage in the receiver for the duration of the applied pulse.

26,298 CIRCUIT SYSTEM FOR PREVENTING INTERFERENCE RADIATION FROM TRANSISTOR SUPERHETERODYNE RECEIVERS by Y. Kondo, M. Takahashi, and A. Ichikawa (Japan Broadcasting Co.); U.S. Pat. 3,130,370, Issued Apr. 1964

TELEPHONY

A highly effective and stable circuit for preventing local oscillation radiation from the superheterodyne transistor receiver tunable over a wide frequency band is described. The method applies a part of the local oscillation voltage taken from the bias circuit of the frequency conversion transistor through a small capacitance to the first high frequency amplification stage. The phase of the signal is inverted by the use of a high frequency transformer, thereby cancelling the interfering voltage effect.

26,299 AN UNDERWATER ACOUSTIC TELEPHONE FOR FREE-SWIMMING DIVERS by B.K. Gazey and J.C. Morris (U. Birmingham); Electronic Engrg., Vol. 36, pp. 364-368, June 1964

A frequency-modulated acoustic carrier telephone system has been developed for the use of free-swimming divers. Operating at a carrier frequency of 120 kc/s and transmitting approximately 1w of acoustic power, it has been tested at ranges of up to 500 yards. The system is described briefly and details of the experimental trials are given.

26,300 SOLID STATE TRANSMITTER READY FOR UHF TELEMTRY by N. Downs and B. van Sutphin (Electronic Commun.); Electronics, Vol. 37, pp. 76-80, June 1964

A 3 watt, modular, 2.2-2.3 Gc solid state transmitter is described. The transmitter is cooled by thermal conduction through the module case to a heat sink. The unit accommodates a wide variety of modulating signal inputs and may be operated from either dc or ac primary sources without supplemental power supply modules. The system is discussed in terms of its components, the FM modulator, RF generator, power amplifier, and power supply. The complete transmitter occupies less than 50 in.³ and weighs less than 47 oz.

26,301 GETTING TRANSISTORS INTO SINGLE SIDEBAND AMPLIFIERS by R.C. Hejhall (Motorola); Electronics, Vol. 37, pp. 72-75, June 1, 1964

A 30 Mc SSB amplifier capable of delivering 15 to 20 watts of peak envelope power r-f output, with all odd-order distortion products at least 30 decibels below the desired signal in a two-tone single-sideband test is described. The transistor used is a 2N3297 npn silicon, and is bolted to the chassis for heat sinking. Greater peak power can be obtained at the expense of linearity; at 30 w. pep the signal distortion ratio is reduced to 22 db. The techniques of this design are applicable not only to SSB, but to any communications receiver in which intelligence is imposed or the r-f carrier prior to the power amplifier stages.

26,302 MINIATURE RADIO TRANSMITTER by R.H. Walker (Motorola); U.S. Pat. 3,128,431, Issued Apr. 7, 1964

A transistorized miniature radio transmitter having an all plastic housing in which the complete circuitry of the transmitter is provided as an integral unit, and in which the power amplifier transistor is temperature compensated is described. Thermal feedback is produced by a low inductance heat sink which reduces the output of the driver stage with increasing temperature, cutting the operating current of the output transistor. The low inductance characteristic of the heat sink an efficient ground path for radio frequency signals.

26,303 HIGH-GAIN DC AMPLIFIER DRIVES CRT DISPLAY by F.J. Murphee and J.H. Hammond, Jr. (US Navy Mine Def. Lab.); Electronics, Vol. 37, p. 53, June 29, 1964

A cathode ray tube horizontal deflection drive amplifier with dc voltage gains up to 35 to 45 db and 28 volt supply voltage is presented. Gain is one-half the amplification factor of a field-effect transistor which loads a field effect transistor amplifier stage. Two transistor types amplify 0.6 volt peak-to-peak input to 9 to 15 volt output.

26,304 TRANSISTOR VERTICAL DEFLECTION CIRCUITS by L.A. Freedman (RCA); U.S. Pat. 3,134,928, Issued May 26, 1964

A transistorized circuit for generating vertical deflection signals for an electromechanical CRT deflection yoke of a television receiver is described. The circuit uses a drive and switching transistor as principal components. The collector-to-emitter path of the switch transistor is connected across a charging capacitor to discharge it during retrace time. Feedback in the circuit maintains self oscillation and provides immunity against noise signals that may accompany the vertical deflection synchronizing signals applied at the base of the switching transistor.

Deflection Sweep Generators - See 26,250

Video Detectors - See 26,229

26,305 HANDSETS WITH TRANSISTOR AMPLIFIERS by K.E. Hammer (Bell Labs.); Bell Labs. Rec., Vol. 42, pp. 159-164, May 1964

Three transistorized, amplifying handsets (G6A, G7A, G8A) are described. The G6A is intended primarily for persons with impaired hearing and has receiver gain; the G7A is intended for persons with weak speech facilities, the G8A is designed for improved reception and transmission in noisy locations. Circuit schematics, frequency response curves, and photographs of prototypes are presented and the frequency characteristics are compared with those of previous models.

26,306 QUASI-ELECTRONIC TELEPHONE SWITCHING SYSTEM HE-60 by H. Schönmeyer (Stand. Elektrik Lorenz AG); Electrical Commun., Vol. 39, No. 2, pp. 244-259, 1964

A telephone switching system to provide simultaneous connections between many subscribers for the required lengths of time, operable on either time, space, or frequency division, and employing hermetically sealed contacts in the form of reed switches is described. Control, reliability, system features and mechanical design are presented. The HE-60 system uses only 2 voltages to supply power, -36 v and + 24 v. Augmented service includes push-button subscribers stations, abbreviated dialing to frequently called subscribers, operator or subscriber-controlled switching to absentee and changed number systems, and announcement services.

26,307 CURRENT-PULSE TRANSMISSION SYSTEM EMPLOYING POTENTIAL RESTORATION MEANS ALONG THE TRANSMISSION PATH by D. Leakey (The Genl. Electric Co., London); U.S. Pat. 3,136,859, June 9, 1964

A current pulse transmission system employing potential restoration means along the transmission path is described. Since current is utilized, rather than potential pulses, pulse transfer stages in the transmission path have low input impedances compared with the output impedance of the immediately preceding stage. Connected to each section of the transmission path are resistances to restore that section to a predetermined level after the passage of a current pulse. The circuits described are primarily for telephone exchange use.

26,308 TOLL CHARGE COMPUTER by H.J. McCreary (Auto. Elect. Lab.); U.S. Pat. 3,124,651, Issued Mar. 10, 1964

The substitution of solid state for electromechanical devices in automatic telephone toll charge computers is advocated and some of the essential circuits for this change are presented. The necessary information about a call can be obtained and recorded by a tabulator which is connected when a subscriber dials a toll access code. This information includes the subscriber's zone, the called zone, and duration. The tabulator submits this information to a computer for calculation of the toll charge. Each zone in the system is represented by a column and by a row in a matrix of magnetic cores. If the column corresponding to the called zone and the row corresponding to the calling zone are each raised to half of saturation potential, the core at the junction of the row and column, representing the given connection, is saturated. At the moment of saturation a pulse is induced in any wire passing through the center of the core. All of the cores have wires threaded through them representing different amounts; connections with the same toll rate share a common bundle of wires. Of the several wires passing through the saturated core, only the one corresponding to the proper duration is connected to the toll registers, which determine the associated cost physically by the manner of the connection and then send the cost back to the tabulator. Transistor switches in the bundles of wires are set by the tabulator information about duration so that only the proper circuit is left conductive.

26,309 ELECTRONIC LINE CIRCUIT by D.F. Seemann (ITT); U.S. Pat. 3,129,289, Issued Apr. 14, 1964

Line circuits used in telephone systems and in electronic line circuits to determine whether subscriber stations are off-hook and to mark idle subscriber lines available to switching equipment are described. The line circuits may be used with either electromechanical or electronic switching means, and include provisions for the inclusion of lockout facilities. A memory device, consisting of a four layer diode and relay is provided to "remember" the occurrence of an off-hook or calling condition.

26,310 LINE CIRCUIT FOR TELEPHONE SYSTEM by J. Kolbinger (Bradley Tel. Sales and Ser. Co.); U.S. Pat. 3,134,857, Issued May 26, 1964

A line circuit for connecting a telephone to a link circuit at the exchange is described. The line circuit is adapted to be disconnected from the talking wires after the connection between the telephone and the link circuit is made. In the conventional line circuit, relays are employed in the line circuit loop for

disconnecting the loop after the talking connection is made through the link circuit. This circuit utilizes two low voltage diodes to accomplish the same result. Circuits for testing the connection between the talking wires and the link circuit are also described.

TELEMETRY

26,311 A NEW PULSE LENGTH TELEMETERING SYSTEM by J.H. Keillar, G.J. Powell and A.H. Spinks; *ATE J.*, Vol. 20, pp. 32-40, Jan. 1964

A new pulse length telemetering system using time-division multiplexing for transmitting 16 analog or two-state signals over a bandwidth of 120 cps is discussed. The hardware is in unit form to maximize its versatility. Dry reed relays, driven by binary circuitry, operate as scanners and distributors. Synchronization occurs in a 300 ms. period preceding the 16 50 ms. data periods. Representative circuits for both scanner and distributor are given. The theory, circuits, and waveforms for the 16-channel transmitter and receiver are presented. The stameter, which produces a continuous output proportional to the magnitude of an input which is only periodically available is similarly treated. These circuits are best as two-state circuits as for alarms or valve position detectors and operate on 50, 24, or 12 vdc.

26,312 A HIGH SPEED, COMPANDED, NEGATIVE RESISTANCE PCM ENCODER by F. Selber (US A.E. R and D Labs); *1964 IEEE Intl. Conv. Rec.*, Part 5, pp. 1-5, Mar. 23-26

Negative resistance encoding is discussed as a new technique for analog-to-digital conversion in pulse code modulation systems. An explanation of the general characteristics of negative resistance circuits is included and their properties are presented in light of their contributions to the operation of the encoder. A new switching circuit is discussed and a digital companding scheme was developed that works with the encoder. Special features such as ruggedized circuitry and component economy are also mentioned and the method is shown to have many applications.

26,313 EXPERIMENTAL 24-CHANNEL P.C.M. SYSTEM FOR JUNCTION CIRCUITS. Part II. LINE TRANSMISSION EQUIPMENT by B.S. Helliwell (Brit. Telecommun. Res. Ltd.); *ATE J.*, Vol. 20, pp. 25-31, Jan. 1964

The accurate transmission of pulse trains, repeater requirements, and cross-talk problems at 1.6×10^6 bits/sec are discussed. Alternating pulse polarity for transmission avoids dc drift problems, concentrates signal power at 800 kc where crosstalk is reduced, and simplifies error detection. Repeater design, including preamp, timing circuit, and regeneration is described for individual error rates of 1 in 10^7 and system error rates of 1 in 10^6 . Basic formulas for near-end crosstalk are derived and far-end crosstalk is estimated. The transmission and crosstalk properties of both star-quad and unit-twin cables are discussed.

26,314 SWEEPING CARRIER SIGNALS THROUGH INTERFERENCE by W.H. Chiles and H.G. LaFuse (Bendix); *Electronics*, Vol. 37, pp. 94-96, May 18, 1964

A wide band audio communications system using frequency slope modulation to prevent narrow band interference from other systems is described. A c-band klystron sweeps signal frequency in a 33.3 kc sawtooth; the slope of the signal frequency in a cycle codes the momentary voice modulation level. Any portion of the uniform energy bandwidth contains the desired information. Addition of carrier and delayed carrier signals converts from frequency slope modulation to FM in the receiver.

26,315 EXPERIMENTAL 24-CHANNEL P.C.M. SYSTEM FOR JUNCTION CIRCUITS. Part I. TERMINAL MULTIPLEXING EQUIPMENT by R.F. Purton (Brit. Telecommun. Res. Ltd.); *ATE J.*, Vol. 20, pp. 17-24, Jan. 1964

The terminal equipment for quantizing, encoding and decoding voice signals and generating synchronizing and timing arrangements is described. 24 speech channels are sampled at 8 kc and produce 7 bits per channel transmitted at 1.6 bits/sec. Non-linear encoding with a logarithmic characteristics produces small steps only for low speech levels. Six attenuators encode the signal. The transmitted signals are stored in capacitors, detected by attenuators, and expanded to the original speech signals. The 25th channel provides eight bits of sync to lock input and output together. A "flywheel effect" initiates correction only if two successive sync bursts are in error. Three systems were built showing quantizing noise ratios of 33 db and interchannel crosstalk at -70 db.

26,316 TIME DIVISION MULTIPLEXING FOR INDUSTRIAL APPLICATIONS by J.L. Haynes; *Instr. and Control Sys.*, Vol. 37, pp. 98-102, Apr. 1964

A time division multiplex system (TDM) for the transmission of multiple on-off signals over a single channel or cable pair is described. The system uses

balanced input wiring, input transient protection, an optimum modulation-index FM-transmission scheme — with continual scan but no synchronization loss — and error-detecting code formats. Latching reed-relay outputs avoid false outputs during periods of abnormal environment.

26,317 TEN SIGNALS AT A GLANCE by J.E. Russell (Avco); *Electronics*, Vol. 37, pp. 54-57, June 29, 1964

A segmented-sweep time multiplexing system for displaying up to 18 subchannels in FM/FM telemetry is described. Simultaneous observation enables a controller to note previously hard-to-detect system characteristics and malfunctions such as intermittently noisy channels. An electronic commutator and clock generator provide pulses to a ring counter composed of flip-flop circuits. The resulting operation gates and displays each particular signal as the scope trace passes through the scope face section preassigned to display that signal.

OTHER COMMUNICATIONS-TYPE APPLICATIONS

26,318 NOISE-MODULATED OPTICAL RADAR by H. Band (Concord Rad. Lab.); *Proc. IEEE*, Vol. 52, pp. 306-307(L), Mar. 1964

A noise-modulated CW optical radar for nonambiguous distance measurement is proposed. Artificially produced random noise with a suitably shaped power spectrum is impressed as amplitude, frequency or phase modulation on a suitable steady-state optical carrier of coherent or non-coherent nature. The noise might possibly be the random magnitudes of a quantity generated by a computer. The radar echo signal is cross-correlated with a delayed portion of the transmitted signal. The delay is varied until the cross-correlation signal is a maximum, at which time the delay gives the distance traveled by the emitted signal, hence the radar range.

Masers in Radar — See 26,065

Doppler Radar Systems — See 26,287

26,319 CODE SELECTOR by R.C. Clark (GE); U.S. Pat. 3,134,961, Issued May 26, 1964

An code selector which will sample the code to determine if the received code is the desired code and will also compare the input conditions to determined errors in the code transmission is described. The code selection is intended for use in paging doctors or other persons who move from place to place and who otherwise could not be contacted. A two tone binary code is featured which improves device reliability by using one tone to represent the "1" state and another tone to represent the "0" state.

26,320 MAGNETIC RECORDING by H. Rosenberg (Burroughs); U.S. Pat. 3,126,547, Issued Mar. 24, 1964

A magnetic recording system providing an improved signal to noise ratio is described in detail. A high frequency erasing current with a wavelength less than or equal to the write-head air gap is applied to the head. This signal puts the magnetic material in an essentially zero magnetic remanent state. It will thus be relatively insensitive to noise such as may be caused by material defect or scratches in the magnetic medium. Binary ones are recorded upon the material in the form of square wave pulses, each occurring at a predetermined time between when the erase signal is between 90 and 270 degrees. Schematics and a block diagram of a practical system are presented.

26,321 MAGNETIC TAPE RECORDING AND REPRODUCING OF ATMOSPHERIC NOISE WITH A WIDE DYNAMIC RANGE by E.C. Bolton (Nat'l. Bur. Stand., Boulder); *Rev. Sci. Instr.*, Vol. 35, pp. 377-380, Mar. 1964

To properly evaluate the performance of radio systems in the presence of atmospheric noise, it is necessary to be able to reproduce atmospheric noise of various known amplitude distributions whenever necessary. However, conventional tape recording techniques cannot be used because of the large dynamic range of atmospheric noise. This paper describes a tape recording and reproducing system which has been developed that can record and reproduce atmospheric noise with a dynamic range of 90 db. The frequency range is 1 to 25 kc with a one-half octave bandwidth and, by using frequency conversion, frequencies from 25 to 500 kc may be recorded with a maximum bandwidth of 10 kc.

Hearing Aid Amplifiers — See 26,181

COMPUTERS and OTHER DATA HANDLING SYSTEMS

DIGITAL COMPUTERS

- 26,322 A THEORY OF NONLINEAR AUTONOMOUS SEQUENTIAL NETS USING Z TRANSFORMS by J. Gaudiosi and K. Fukunaga (Mitsubishi); IEEE Trans., Vol. EC-13, pp. 310-312(L), June 1964

Nonlinearity of logical nets is linearized by increasing the number of variables. If the nonlinear net is autonomous, it can be replaced by an equivalent linear net and the behavior of this equivalent sequential net can be expressed by difference equations which can in turn be solved by using z transforms. This method is applied to solve for a sequential net which has p inputs, q outputs, and r delay elements.

- 26,323 HOW IMPORTANT ARE COMPONENT TOLERANCES? by J.G. Curtis (Corning Glass); Electronic Design, Vol. 12, pp. 60-65, June 22, 1964

By use of worst-case analysis, the initial economy realized from the use of high-tolerance components in diode-logic design and the advantages, including greater over-all economy possible with the use of low tolerance components are contrasted. The AND gate is analyzed both in saturated and cutoff conditions, and the worst case design equation is solved. The OR gate is similarly observed in saturation considering both fan-in and fan-out configurations. Permissible gate combinations are plotted as a function of design tolerance, and it is seen that the higher design tolerances dramatically reduce complexity.

- 26,324 THE DESIGN OF ADDERS USING NOR GATES by C.D. Todd (Hughes Aircraft); Semiconductor Prod., Vol. 23-30, May 1964

Binary addition is a major function in many computer and control circuits. Logic requirements for binary full and half adders are discussed and the realization of the logic utilizing the NOR gate as a basic component is presented. Electrical requirements are described and design information is substantiated with measured results of a full adder operating at 500 kc and a complete 3-bit adder operating at clock rate of 100 kc.

- 26,325 A FERRITE PARITY-DETERMINING DEVICE CAPABLE OF PERFORMING PARALLEL CODING OPERATIONS by E.N. Belland (Lockheed); 1964 IEEE Intl. Conv. Rec., Part 1, pp. 12-21, Mar. 23-26

A ferrite device capable of doing the 'exclusive-or' function, or parity determination, on twelve variables has been operated. At the same time the parity of any contiguous subgroup of bits can also be determined. The device is a hollow ferrite cylinder into which slots have been cut. The input variables control windings threading these slots. Flux injected at one end of the cylinder is 'steered' along a path determined by the input variables. This device is discussed in connection with a Hamming code, a Reed-Muller code, and a low-density code; being used for encoding, decoding, and error correction information.

- 26,326 COMPLEMENTARY TRANSISTORS REDUCE EXCLUSIVE OR SIZE by J.L. Shagena (Bendix); Electronic Design, Vol. 12, p. 102, Mar. 16, 1964

Two complementary transistor EXCLUSIVE OR circuit are described. When both inputs are at logical zero (-6 v), both transistors are turned off, when one of the inputs goes to logical one (ground), both turn on. The output level changes from a logical zero to a logical one. With both inputs at logical one, only one of the transistors turns on.

- 26,327 NOR/NAND LOGIC by C.F. Hill; Control Engrg., Vol. 11, pp.81-83, May 1964

A simplified solution to the problem of converting the Boolean expression of control logic into a minimum-circuit configuration is described. The disadvantages of synthesizing such a network with present methods are: (1) manipulation of cumbersome algebraic expressions; (2) redundant elements in original synthesis that must be removed by additional operations, and (3) continued reference to a previously developed table of equivalent AND, OR, and NOT circuits. The advantages to the method described are; a step-by-step procedure that permits checking each stage as it is completed; no redundant elements in the synthesis; complementation; negation, as the only required Boolean algebraic operation; and applicable to both NOR and NAND logic. With the use of diagrams and an example the theory and applying NOR logic is described. The conditions for NAND logic, the conversion of NOR, are presented.

- 26,328 CURRENT OPERATED DIODE LOGIC GATES by H. Reineck, Jr, R.W. Hofheimer and K.E. Perry; U.S. Pat. 3,124,708; Issued Mar. 10, 1964

Current-operated diode logic circuits which represent binary information by the direction of current flow are described. Voltage-operated gates cannot be cascaded to many levels without insertion of a gain device to reestablish voltage levels; furthermore, the use of common grounds creates a coupling problem at high switching speeds. Circuits are given for logic gates which perform the logical functions "AND", "INCLUSIVE OR", and "EXCLUSIVE OR". Complementation of a binary variable is obtained by reversing the polarity of the connections. Since the outputs of one stage may be used as the inputs of the next stage, and since the given functions are an adequate set of connectives, any logical function may be obtained.

- 26,329 LOGICAL AND MEMORY CIRCUITS UTILIZING TRI-LEVEL SIGNALS by H.B. Baskin (IBM); U.S. Pat. 3,129,340, Issued Apr. 14, 1964

Multivalued switching circuits that embody ternary logical and memory functions are described. The circuits use transistorized binary switches to obtain ternary logic. The circuit configurations for ternary inversion, storage, AND and OR devices are presented and the truth tables for each are given. The mathematical approach to the problem of synthesizing ternary logical functions is discussed.

- 26,330 LOGIC INVERTER CIRCUITS by E.H.P. Bigo and P. Pleshko (ITT); U.S. Pat. 3,124,704, Issued Mar. 10, 1964

Logic inverter circuits employing tunnel diodes are suggested. Any device which operates at low resistance initially and can be switched to a high resistance state by a given current may be used. One of these "negative resistance" devices is used in each of two paths, each in series with a fixed resistance. The input is the application of a voltage to a junction at one end of the two paths; whereupon the voltage appears substantially across the fixed resistance of the second path and the output node is at a first potential. The alternative input is the application of the same voltage to the same junction, with means for switching the first negative resistance device to its high resistance state. This causes increased current in the second path which switches the second device. Now the voltage difference in the second path appears substantially across the negative resistance device, and the output node is at a different potential. These two different potentials can be interpreted as the two different states of the binary logic, and can easily be modified to an acceptable form for input.

- 26,331 INTEGRATED MICROPOWER CIRCUITS by R.A. Tietsch (Sperry Rand); NASA Contract NAS1-2619, 124 pp., 1963; STAR, Vol. 2, pp. 1474-1475(A), June 23, 1964 NASA CR-53512; OTS \$10.10 ph

Investigations of various digital gate circuits were made using similar design conditions to determine relative performance characteristics over a wide range of power drains. Care was taken to obtain comparative performance by using the same semiconductor devices throughout the investigation. The most promising configurations were T²L (direct coupled), DTL (single-transistor gate), and complementary RDTL (two-transistor complementary gate). Each family of configurations (gates, flip-flops, etc.) were investigated in detail over the temperature range of interest to further investigate comparative performance characteristics. Integrated component characteristics and the effect of various integration techniques on circuit performance were evaluated. Of the circuit configurations investigated, complementary RDTL offered the best overall performance characteristics.

- 26,332 INTEGRATED MICROPOWER CIRCUITS by R.A. Tietsch, D.S. Dunavan and V.J. Capano (Sperry Rand); NASA Contract NAS1-2619, 16 pp., 1964; STAR, Vol. 2, p. 1475(A), June 23, 1964 NASA CR-53511; OTS: \$1.60 ph

A circuit configuration that uses complementary RDTL logic is discussed. The considerations of a flip-flop dc set or reset, and ac sets and resets, are outlined. The possible use of a universal flip-flop and shifting accumulator is also considered. Power supply variations as a function of uniform and nonuniform nickel-cadmium battery drain discharge and their effect on circuit performance are considered. The effect of externally induced noise on the power supplies and circuit resistance variations is also discussed. The packaging requirements for a universal flip-flop and a NAND and NOR gate in a 10-in flat package are considered.

- 26,333 APPLICATION OF THE TRANSISTOR CHARGE CONTROL MODEL TO PREDICT RTL AND DTL TRANSIENT RESPONSE by P.M. Ansbro; Solid State Design, Vol. 5, pp. 19-25, June 1964

The charge control theory is applied to predict the transient behavior of a basic logic circuit under actual operating conditions. RTL and DTL are chosen as examples of this application since the former represents a simple basic logic form while the latter represents a more complex logic form. Since the form of

analysis is similar, only RTL is considered in detail. Equations are presented for both logic forms that allow the circuit designer to specify an upper limit on the transient response of a logic inverter under "worst-case" operating conditions.

26,334 COMPOSITE SYNCHRONOUS-SYNCHRONOUS LOGIC CIRCUITS FOR NANOSECOND COMPUTING by J.F. Krzy and C.V. Ramamoorthy (Honeywell-EDP); *Proc. Natl. Electronics Conf.* 1963, Vol. 19, pp. 173-182,

Composite logic circuits suitable for various functional units are described. The iterative circuit approach within the units combines the useful features of both synchronous and asynchronous operations. Hybrid, tunnel diode-transistor circuit techniques are employed to achieve fast switching speed and to ease component and power supply tolerance requirements. The use of the tunnel diode circuits permits nanosecond signal propagation between synchronous clock pulses. In addition to their threshold property and fast switching speed, the inherent storage capability of the tunnel diodes is also used to advantage. The functional nature of the units permits optimization of the performance/cost ratio with respect to the number of asynchronous logic levels between synchronous clock pulses, circuit-speed, input-output fan, tolerances, and timing. The logical organization, and the operation and design criteria of the circuits are described in conjunction with the following functional units: 1) a reversible binary counter which can establish a new count in a flip-flop reversal time, 2) a binary full adder capable of adding two 48 bit operands in 175 nsec., 3) a combined decoder-encoder in which the bilateral nature of the tunnel diode is utilized.

26,335 THE CASE FOR MAGNETIC LOGIC by J. Rogers and J. King (Sperry Gyroscopes); *Electronics*, Vol. 37, pp. 40-47, June 1, 1964

The capabilities and performance characteristics of magnetic elements as memory and logic devices are discussed. Reliability is the greatest advantage obtained by employing magnetic devices; inherent disadvantages are due to loop and coercive force problems. The properties of tape wound cores are examined and compared to those of ferrites. Logic concepts, including four phase inhibit logic, are shown to be applicable to magnetic systems. Other applications are in timing systems, sequential switch circuits and current steering memory addressing.

26,336 COINCIDENCE MAGNETIC GATE by H.R. Burns, Jr. (IBM); U.S. Pat. 3,124,700, Issued Mar. 10, 1964

A circuit for magnetic storage of binary information is presented. The major drawback of previous systems is that switching a bistable core from one state to another induces current in the windings. Blocking these induced currents requires diodes, delay circuits, or inhibit windings. The circuit consists of two bistable magnetic cores having a set winding, a reset winding, and an output winding in common. One of the cores also has a sampling winding. A pulse applied to the sampling winding resets only the associated core to the "0" state. A change in state of one or both cores induces a pulse in the output winding; but since this winding has opposite polarity on the two cores, the output pulse will cancel whenever both cores are being switched in the same manner. On the other hand, if only one core is switched from the "1" state to the "0" state, the output pulse will be positive or negative, depending on which core had been made to change its state. A third core may be added to provide an additional output pulse. If the set and reset windings are continued on the third core with the same polarity opposite to the output winding on the core with the sampling winding, and furthermore if the sampling winding is continued with the same polarity, then both a positive and a negative output can be produced by a sampling pulse. The second output will provide additional information in other cases as well.

26,337 MAGNETIC CORE SWITCHING SYSTEM by J.H. Hohl (IBM); U.S. Pat. 3,129,337, Issued Apr. 14, 1964

A magnetic core switching system using groups of bistable cores is described. Alternate groups of cores are preset to one stable state while other groups are preset to opposite stable states. Transfer circuits couple a core in an odd group to a core in an even group. Data contained in one group is progressively advanced to succeeding groups in order by sequentially energizing the transfer circuits with opposite polarity pulses.

26,338 THE DESIGN OF MODULAR 250-MC COMPUTING CIRCUITRY by B.E. Sear (Martin); *Proc. Natl. Electronics Conf.* 1963, Vol. 19, pp. 158-163

The possibility that 250-megacycle circuits can be built using standard sized components and a modular packaging construction is discussed. The modules are attached to a motherboard which can be plugged into a standard connector, enabling the backboard to be wired with miniature coax (in much the same way as 20-megacycle modules using twisted pair). The tunnel diode charge transformer, TDCT, circuits are discussed, and difficult design areas are pointed

pointed. Finally, the problems in clock generation and distribution for nanosecond circuits are outlined and a solution for these circuits is given.

26,339 LOGIC IMPLEMENTATION USING MECL INTEGRATED CIRCUIT LOGIC BLOCKS; *Systems Design*, Vol. 8, pp. 40-41, June 1964

High speed emitter coupled monolithic logic devices having an average propagation delay of 6 nanosecond and a power dissipation of 35 milliwatts, and packaged in a modified 10-5 can with 10 terminal pins are described. Schematics are shown for the half-adder and flip-flop modules, and descriptions as well as system diagrams are presented for the full adder, shift register, and serial adder logic circuits.

26,340 A NANOSECOND PARALLEL-PARALLEL BINARY ADDER IMPLEMENTED WITH CURRENT MODE LOGIC BUILDING BLOCKS by W.C. Seelbach and K.E. Lampathakis (Motorola); *Proc. Natl. Electronics Conf.* 1963, Vol. 19, pp. 311-340

Current mode logic digital circuits offer a great number of advantages for logic implementation. They are extremely fast and insensitive to many device and circuit parameters and provide the complement in addition to the regular output. They can incorporate powered outputs which increase their driving capabilities. Costwise they compare very favorably with other logic digital circuit families at the integrated circuits level. A six-bit parallel adder, with look ahead logic scheme for carry generation was implemented, using Motorola MECL current mode logic building blocks. The high speed (38-4 nsec delay per stage) building blocks used in this implementation consisted of three and five input gates, expander modules capable of expanding the three input gate fan-in increments of 5, half adders, R-S type flip-flops and bias drivers. The system was packaged using a unique multilayer printed wiring logic board technique.

26,341 SWITCHING MATRICES WITH PROTECTION AGAINST SHORT-CIRCUIT IN THE GATES AT THE CROSSING by T.M. Schurings and W. Smit (NA Philips); U.S. Pat. 3,127,519, Issued Mar. 31, 1964

A self-checking safety circuit for a switching matrix is described. The matrix consists of several inputs each connected to each of several outputs through gates. For m inputs and n outputs there would be mn gates. A short circuit could occur in some of these gates, so that they would conduct at all times instead of only when activated by controls. The safety circuit uses another device called a storing pulse generator. This device will deliver an output pulse only if a current pulse of proper polarity and amplitude has been delivered to the so-called setting terminals and subsequently a current pulse of proper polarity and amplitude is delivered to the firing terminal. The safety circuit uses a cycle of eight phases. The input signal is delivered to the switching matrix in the first phase, and sets a storing pulse generator as well. Other phases of the cycle test parts of the circuit; the presence or absence of pulses at specified times, detected by the behavior of the storing pulse generator, indicated whether the tested part of the circuit is behaving normally or has malfunctioned. For example, if a gate has a short circuit, it will conduct a pulse which sets the storing pulse generator at a time when the setting circuit should be nonconductive. Other malfunctions will be detected in similar ways.

26,342 MAGNETIC CORE MEMORY CIRCUITS by J.H. McGuigan (Bell Labs); U.S. Pat. 3,126,527, Mar. 24, 1964

A magnetic storage cell capable of storing an information bit and retaining that bit during the interrogating (read) operation, (thus eliminating the need for a re-write operation), and memory matrices utilizing these storage cells as basic units are described. The non-destructive read-out feature is realized by using two standard toroidal "square loop" magnetic cores as the basic storage unit or cell. A binary value of 1 is represented in the cell by a condition of magnetic saturation of the same polarity in both cores and a binary 0 by a condition of magnetic saturation of opposite polarity in the two cores.

26,343 WRITE-INTERROGATE MEMORY SYSTEM by E.L. Woods (Ford Motor); U.S. Pat. 3,126,532, Issued Mar. 24, 1964

A nondestructive read magnetic core memory system is described. The memory core element consists of a block with two perpendicular openings. A wire passing through one hole acts as a sensing element. Two wires go through the other. When current is passed through one of the wires a core is shuttled (reversible flux changes) and two voltage pulses are sensed as the magnetic state moves and then is restored. In one remanent state first a positive and then a negative pulse is sensed and in the other remanence the pulses come in the opposite order. This gives non-destructive read-out. In order to write, both wires are simultaneously energized providing a field above the switching threshold. In this case the sensing wire receives only one pulse of a different magnitude. These cores may be arranged in a convenient matrix array; the sensing wires and one write wire set pass through all the cores in a row; and the other write wire set through columns. If words are contained in the columns, an entire word can be read at once by activating the column-write wire.

26,344 AUTOMATIC REGENERATION MEMORY by W.T. Siegle (IBM); U.S. Pat. 3,126,534, Issued Mar. 24, 1964

A non-destructive read magnetic core memory system is described. Magnetic materials have two flux switching thresholds, both static and a pulse threshold which is a function of both the duration and amplitude of the pulse. A magnetic material subjected to a pulse near or above the threshold is put into a sensitized condition. That is, it experiences a lower threshold to subsequent pulses during a definite period of time. Furthermore if the material is in one of the limiting remanence states, its threshold is not lowered as much as when it is in between them. One of the limiting remanence states is made to represent a zero bit and an in-between remanence represents 1. A short duration pulse directed toward the zero state slightly sensitizes a core already in that state. However, if the pulse is not too great it will drive a one-bit only part way to the zero state and leave it in the deeply sensitized condition. Thus a read out is obtained. While the core is in its sensitized state a dc or pulse field of an appropriate magnitude to drive a deeply sensitized core back to its original position is applied to the whole memory matrix. The field is below the threshold for both nonsensitized cores and an affected core in the limiting remanent state. Thus the original condition of the matrix is restored.

26,345 LOW FREQUENCY MAGNETIC CORE STEPPING DEVICE by N.F. Photiades (Minn.-Honeywell); U.S. Pat. 3,127,520, Issued Mar. 31, 1964

A precision low frequency oscillator using a saturable timing core, slightly unbalanced AC current, and improved means of sensing core saturation is described. The saturable timing core is of a type having a substantially rectangular hysteresis loop. An AC current, of sufficient voltage to accomplish a change in flux of the core but of insufficient magnitude to saturate, is superimposed on a DC current of much lower voltage. The resultant unbalanced current slowly drives the core to a state of saturation in a series of minor overlapping hysteresis loops. When saturation of the timing core is reached, the back electromotive force generated within the core is diminished and the resulting increase in current therethrough is used to trigger a bistable switching circuit to reverse the polarity of the applied DC voltage whereupon the core is slowly driven towards the opposite state of saturation to complete one cycle of operation.

26,346 INFORMATION STORAGE ARRANGEMENTS by K. Euler (Siemens and Halske); U.S. Pat. 3,127,590, Issued Mar. 31, 1964

A circuit for temporary storage of binary information which consists of a pulse generator with a plurality of outputs, generating one pulse to each output sequentially in each cycle is described. Each output goes to the write-in winding on one core and to the readout winding on the next core. A bit comes in on the input wire, affecting only the core which is at that time receiving the pulse from the generator. This selectivity can be accomplished either by an AND gate or by arranging the amplitudes so that the input and pulse are each half the amount necessary for saturation. The generator goes through its cycle, storing one bit (one or zero) in each core and reading out the bits previously stored. After one cycle, it begins to read out the bits it has just stored and to store a new number. The time a bit is in this temporary storage is just short of a full cycle by the time from the beginning of one pulse to the beginning of the next. This time can be extended by adding more cores and thus increasing the length of the cycle. Furthermore, several of these storage registers can be run in parallel by a single pulse generator.

26,347 MAGNETIC STORAGE CIRCUITS by E.G. Andrews (Bell Labs.); U.S. Pat. 3,128,452, Issued Apr. 7, 1964

A suggestion is made for a magnetic storage circuit with a form of nondestructive readout. Two parallel matrices of magnetic storage material, such as magnetic cores, are used to store information, with only one of the cores in each respective position being used to store any given bit of information. The cores in each matrix are set and interrogated by conventional coincident-current pulses. An initiator pulse sets the address circuits of both cores at the same time. A readout pulse then causes both the cores at the addressed positions to be interrogated. If a pulse appears on the output line of one of the matrices, indicating that a stored "one" had been found and destroyed, a write-in pulse is sent to the other matrix, the circuits of which still retain the proper address. If no output pulse appears, indicating that both interrogated cores were already in the zero state, no write-in is necessary. In this manner any information destroyed in interrogation of one core is immediately restored in the corresponding core of the other matrix. Provision is also made to write in new information during interrogation.

26,348 PLATED CIRCUIT MAGNETIC CORE ARRAY by R.A. Jones (IBM); U.S. Pat. 3,130,134, Issued Apr. 21, 1964

An improved method for fabricating magnetic core arrays by plating the required components onto the base structure (such as a printed circuit board) is described. An example is given for fabricating one plane of an array with the standard X and Y windings, a winding to reset all cores in the plane, and a

fourth winding with opposite sense on adjacent cores. However, any winding desired may be obtained by the given method. A board of nonconductive material has openings out into it in which the cores are placed. The entire assembly is then coated with an insulating material. The axial surfaces of the cores and places on the upper and lower surfaces on the board, indicated by a template or stencil, are then coated with a conductive material. The assembly is then electroplated, or coated with metal by any other suitable method, in the places indicated by the template. This deposit of metal forms the Y windings. The sections of the winding above the board connect with the sections below the board by the rings, coaxial with the cores, which have been deposited in the openings. Another coat of insulating material is followed by depositing the next winding, and the process is continued until all the desired windings are in place.

26,349 A DIGITAL INTERMITTENT DATA FLOW MAGNETIC TAPE RECORDING SYSTEM by J.R. Kannolt and K.H. Miller (Sandia); *Proc. Natl. Electronics Conf.* 1963, Vol. 19, pp. 295-310

A unique mechanical drive system with associated transistorized circuitry has been developed to allow digital recording on magnetic tape at varying data flow rates. The present system records on command at rates up to 40 characters per second with a packing density of 200 characters per inch. The output is on half-inch magnetic tape in a format compatible with conventional playback equipment. The system provides a direct link between the slow and intermittent outputs of data acquisition equipment and the high-speed input devices of data reduction equipment. The tape transport could also be modified to record or read magnetic tape at either intermittent or continuous rates. Speeds up to 120 characters per second in the intermittent mode are possible.

26,350 MAGNETIC TAPE AND RANDOM ACCESS DEVICES FOR 16 MORE MEDIUM TO LARGE COMPUTERS by Cresup, McCormick and Paget; *Control Engng.*, Vol. 11, pp. 115-120, May 1964

A comparison of magnetic tape units and random access device for 16 medium to large computing systems is presented. The comparison is made by tabulating the performance and capabilities of the magnetic tape units and random access devices used with systems for maintaining data files. The criteria for magnetic tape units are: transfer rate; start/stop time; movement speed; read or write time; simultaneous tape operation; rewind time; maximum number of tape transports; data storage; read or write time sharing, read forward and/or reverse; record search; read checking; and write checking. The criteria for random access devices are: average read or write time; average time sharing; transfer rate; transfer time sharing; maximum number of devices and inquiry stations; number of characters; addressable unit size; dual reading; vertical bit counting, horizontal bit counting; check characters; and write compass.

26,351 A LOW-SPEED MAGNETIC MEMORY DEVICE by W. Chow (ITT); 1964 IEEE Intl. Conv. Rec., Part 5, pp. 262-268, Mar. 23-26

Computer and switching/control systems in use today typically require some type of memory for system operation. The memory, or data store for the system, serves to hold data in storage until it is needed by a cycle of system operation. Relays, flip-flops, punched cards, magnetic tapes, discs, and drums, ferrite cores and matrices represent some of the devices available for this purpose. A new magnetic drum memory that has been developed as a low-cost storage device which does not require ancillary amplification for either input or output functions for switching and control systems is described. This memory device has some features that are characteristic of a digital computer memory, but it does not have the latter's high cost. The new memory device can be used either as a general-purpose bit store, or as the main storage device in switching/control systems.

26,352 ECONOMICAL MAGNETIC MEMORY DEVICE by W. Chow and A.R. Lucas (ITT); in *Okla State U. Papers Presented at the 11th Natl. Conf. on Electromagnetic Relays*, 1963, 23 pp.; *STAR*, Vol. 2, p. 1467(A), June 23, 1964

A new magnetic drum memory that has been developed as a low-cost storage device that does not require ancillary amplification for either input or output functions for switching and control systems is described. This memory device has some features that are characteristic of a digital computer memory, but it does not have the latter's high cost. The new memory device can be used either as a general purpose bit store, or as the main storage device in switching-control systems. The design of the memory and its typical applications are presented.

26,353 TUNNEL DIODE MEMORY by M.M. Kaufman, L. Dillon, and G.G. Ammon (RCA); 1964 IEEE Intl. Conv. Rec., Part 1, pp. 1-11, Mar. 23-26

Tunnel diode memory units applicable to ultra-high-speed computers are described. The memory subsystem used a two-tunnel-device (tunnel diode and tunnel rectifier) memory cell matrix and was completely compatible with a

tunnel-diode logic subsystem. The memory had a full logic gate decoder and addresses were incremented by the logic subsystem. The memory stack was built as 32 words of 5 bits each, and had drive circuits with sufficient power to drive 24-bit words. The decoder was designed as a 32-word portion of a 1,024-word decoder. It was built using the same circuits as those in the logic subsystem with a worst case decode time of 35 nanoseconds. Using the same logic circuits to decode only to one out of 32 words, a 13.8-nanosecond decode time results and the access time is then 23.8 nanoseconds. The estimated storage capacity limit of 256 words of 24 bits is also discussed.

26,354 **ESAKI DIODE MEMORY** by A.A. Henlge, W.L. Lawrence, Jr., J.B. Pace, and H.P. Wolff (IBM); U.S. Pat. 3,134,963, Issued May 26, 1963

An improved storage cell for two and three dimensional memory systems, and an improved read-out or sensing system for a memory array employing tunnel diodes are described. Each storage cell of the memory matrix comprises a tunnel diode having one terminal connected to a reference level and a plurality of voltage sources connected to the other terminal. In the array, predetermined groups of diodes are connected in common to a reference potential, so that a single sensing means may be provided for a large number of diodes.

26,355 **DATA STORAGE SYSTEM** by T.J. Blecher (Westinghouse); U.S. Pat. 3,126,524, Mar. 24, 1964

A digital data storage system using transistor circuits and designed to store sequentially in binary form is described. Data is received at the first or input storage bank and is automatically transferred through the various storage banks to the last vacant one. Data is read out at the last or output storage bank, and following read-out, data in other storage banks automatically drop into the next sequential bank thus always filling the output bank until all information has been read out. The circuitry is highly repetitive and simple and thus is capable of being extended to a very large capacity.

26,356 **ANALYSIS OF SNEAK PATHS AND SENSE-LINE DISTORTION IN AN IMPROVED CAPACITOR READ-ONLY MEMORY** by A. Kaufman (Litton Sys.); *Proc. IEEE*, Vol. 52, p. 634(L), May 1964

The original article of this title (*Proc. IEEE*, Vol. 51, p. 1554, 1963) effectively ignores what is possibly one of the most important parameters limiting the use of two-part memory devices, i.e. sense-address line coupling capacitance. The magnitude of the sense-address line coupling is illustrated and it is pointed out that neglect of this parameter in the original work indicates that the results are of little concern to the practicing computer engineer.

26,357 **HIGH CURRENT PULSE DRIVER USING DARLINGTON CIRCUIT** by M.M. Stern (Sylvania); U.S. Pat. 3,126,490, Issued Mar. 24, 1964

A high speed, high current, transistorized pulse driver useful in the operation of magnetic core memories is described. This circuit has been employed in a magnetic core memory system operating on a one μ sec read write cycle and producing 300 ma pulses with 30 μ sec rise and fall times. The circuit is not only useful in driving an inductive load (a row of memory cores), but may also be used (by changing transistors) in other applications such as the production of wide current pulses with extremely fast rise time.

26,358 **HIGH FREQUENCY BISTABLE TRANSISTOR COUNTER** by S. Yee (Mesne Assignor to U.S.A.); U.S. Pat. 3,131,317, Issued Apr. 28, 1964

A binary, transistor counter capable of counting high frequency square wave pulses without error is described. The previous counting circuits generally applied each pulse to both transistors in, for example, a flip-flop binary counter. Each pulse had the effect of reversing the conductive and non-conductive states existing prior to that time. At high frequencies, however, a pulse might be applied before the change caused by the previous pulse had been completed. In this case it would merely aid in the change already taking place, and thereby not be counted. If the duration of the pulse were longer than the changeover time, the last portion of the pulse might be counted as a separate pulse thus resulting in an addition to the true count. The given circuit uses two transistors in opposite states of conductivity, with a gate to apply incoming pulses only to the conductive one. The gate consists of two other transistors alternately maintained at a reverse bias by capacitors connected to the flip-flop transistors. When a transistor is conductive, the associated gate is open. When the flip-flop is switched, a capacitor charges through a variable resistance and closes the gate when a sufficient voltage is reached. Meanwhile the other gate is closed. The variable resistance is set so the delay in switching is just longer than the maximum duration of the pulses to be counted, thus preventing the errors described above.

26,359 **MATRIX SWITCH** by G. Constantine, Jr. (IBM); U.S. Pat. 3,129,336, Issued Apr. 14, 1964

A matrix switch to control the read-in and read-out of data to and from a magnetic core memory is described. Each core is saturated in one particular

state by current flow in the bias winding. The bias winding is in series with the current source for the signal input winding and a portion of the bias current is used for the signal input winding. The input and bias winding turns relationship is such that the magnetomotive forces of the two windings are equal and opposite. The input current pulse is controlled by a transistor network to make it independent of the input signal amplitude. Thus an input signal variation does not induce a variation in amplitude of the matrix switch output pulse.

26,360 **MAGNETIC ENCODING CIRCUITS** by R.A. Kaenel (Bell Labs.); U.S. Pat. 3,127,600, Issued Mar. 31, 1964

The application of magnetic switching elements to circuits which generate pulse coded modulated output signals is described. Complex information carrying wave forms can be handled in data processing systems with much greater facility if they can be converted to coded groups of discrete signals. The use of solid state devices in encoding circuits should simplify the operation. The encoding circuit described consists of several cores with input and readout windings in series. A constant current conducted through a third series winding drives each core to a certain point on its hysteresis curve. If this bias winding is different, either in polarity or number of turns, on each core, each will be in a different quiescent point on its curve. When the wave form to be encoded appears on the input circuit and a pulse is sent on the readout circuit, the output winding of each core will exhibit an induced pulse of different amplitude. Discriminators can determine which core produced the pulse of greatest amplitude. Each core is representative of a different range of amplitude of the input signal at the time of the readout signal. Narrower ranges can be obtained by increasing the number of cores in the encoding circuit.

26,361 **A TRACTABLE BERNOULLI-SEQUENCE GENERATOR** by C.C. Hoopes (U. Mich.); *Proc. Natl. Electronics Conf.* 1963, Vol. 19, pp. 282-294

The implementation and evaluation of a random-pulse-train generator is discussed. The technique is of special interest and advantage for those testing or working with digital equipment. The generator is a reliable, reproducible, and stable source of Bernoulli sequences with p in the range 10^{-3} to 10^{-1} . The Bernoulli sequence is generated by means of a noise source in conjunction with a shift-register generator; the noise source providing the randomness, the shift-register generator providing the desired probabilities. The features of this random generator are: (1) the system is (other than the random noise source) composed entirely of plug-in type digital equipment, (2) the system principles are easily understood and quickly implemented, and (3) many finely quantized preselected probabilities, in the above range, for the Bernoulli sequence can be obtained.

26,362 **DIODE BRIDGE-GATED STEPPING REGISTER** by J.W. Crownover (Litton); U.S. Pat. 3,130,389, Issued Apr. 21, 1964

A magnetic core stepping register in which diodes inferior to those previously required may be used is described. The register contains a number of magnetic cores, each with an input winding, an output winding, and an advance winding. The cores are connected alternately to one or the other of two pulse sources, through the advance windings of the cores. The input winding of the first core is connected to the input pulse source and, in a recirculating register, to the output of the final core. The input pulses are of proper amplitude either to bring the core to a state of positive remanence, in the case of a one signal; or to leave it at its state of negative remanence, for a zero signal. When the pulse source fires through the advance winding, its polarity is such as to reset the core to the zero state. It then saturates a balanced diode bridge gate to reach the advance winding of the third core down the line, and so on. If the first core had been in the one state, the advance pulse would cause a pulse to be induced in the output winding. Although the polarity of this pulse would be opposed to two of the four diodes in the bridge gate, since they are saturated by the pulse source current they would conduct the induced pulse to the input winding of the second core, bringing it to the one state.

26,363 **VOLTAGE CONTROLLED MAGNETIC SYSTEM** by B.F. Wagner (GE); U.S. Pat. 3,134,966, Issued May 26, 1964

An improved voltage controlled shift register circuit capable of operation with uni-potential voltage pulses and without bias sources is described. The system is designed for maximum flexibility and efficiency with no increased complexity in the pulse source circuit. The output pulse duration may be increased without requiring an increase in input energy. Compact construction is afforded by the fact that the register uses one core per bit and one winding per core.

Ferrite Film Shift Registers - See 25,910

26,364 **SWITCHING CIRCUIT EMPLOYING BISTABLE DEVICES TO SELECTIVELY CONTROL THE CHARGE TIME FOR SWITCHING** by J.W. Lemon Jr., (Robotron); U.S. Pat. 3,129,344, Issued Apr. 14, 1964

A sequence timer where all timing functions are controlled by solid state components is described. The number of timed functions can be increased by adding

additional stages, and the duration of each timing function can be varied. The circuit consists of one or more bistable circuits with a single timing function affected by a combination of states. Thus two bistable circuits will provide four timing functions. Trigger pulses are provided by a unijunction transistor circuit, and timing control is provided by rectifying the line voltage and using an RC network to fire the unijunction transistor.

ANALOG COMPUTER AND OTHER DATA SYSTEMS

26,365 AN ANALOGUE COMPUTER APPLICATION IN OPERATIONS RE-SEARCH by D. Longley (Loughborough Coll. of Tech.); Electronic Engrg., Vol. 36, pp. 378-381, June 1964

The analogue computer is now firmly established as a tool for the control engineer, its flexibility and ease of programming provides a theoretical-cum-experimental approach for the solution of a host of dynamic problems and at the same time it enables the engineer to gain a real insight into the behaviour of the system under study. These techniques may also be extended into the science of operations research where the computer may be used both as a simulator of management control problems and as a fast, flexible 'hill-climbing' device. This article is concerned with the latter application of the analogue computer and examples of the solution of linear and non-linear programming problems are described.

26,366 AN ELECTRONIC ANALOG by C.R. Horney (Ryerson Inst.); I.S.A.J., Vol. 11, pp. 61-68, Feb. 1964

An electronic analog computer for simulating open or closed loop control systems is described. The computer consists basically of dc amplifiers and power supplies. Function generators provide triangular waves for ramp functions and square waves for disturbance functions when investigating the response of process control elements and systems. A waveform generator simulates the changing of the setpoint of a controller as would be done in a time schedule control system. Several experiments performed with the computer are described.

26,367 A TRANSISTOR ANALOG MULTIPLIER [in Italian]; Alta Frequenza, pp. 234-248, Mar. 1964

An analog quarter-square multiplier is described. The parabolic function requested by the two squaring circuits, is approximated by an hyperbolic cosine, being obtained by using two transistors in consequence of the experimental input characteristics. The problem of temperature compensation is considered.

26,368 FAST ANALOGUE MULTIPLIERS WITH FIELD-EFFECT TRANSISTORS by V. Radeka (Brookhaven Lab.); IEEE Trans., Vol. NS-11, pp. 302-307, Jan. 1964

The solution time of analogue multipliers using field-effect transistors is investigated. This time is ultimately limited by the charging time of the field-effect transistor junction. In typical devices suitable for analogue multiplication the charging time is found to be about 10-20 nsec for a multiplication error of less than one percent. A four quadrant pulse amplitude multiplier circuit is described, whose solution time is equal to the field-effect transistor charging time.

26,369 SQUARING CIRCUIT UTILIZING TWO NEGATIVE RESISTANCE DIODES IN SERIES by R.A. Kaenel (Bell Labs.); U.S. Pat. 3,129,342, Issued Apr. 14, 1964

A substantially hysteresis-free squaring circuit using voltage-controlled negative resistance diodes is described. Two tunnel diodes are connected in series-aiding with the upper diode biased at a point on the relatively low positive resistance region of its characteristic curve by a series supply. The lower diode is biased at the peak point of its characteristic curve by a parallel supply. The input signal is applied in series with the diodes with the output taken across the lower diode. As the input signal amplitude increases past the reference level, the lower diode switches followed by the upper diode. For a decreasing amplitude, the lower diode switches first, followed by the upper diode. Switching points are very close to the reference level since the lower diode is biased at its peak.

26,370 RESET OPERATIONAL AMPLIFIER by P. Balaban (Computer Sys.); U.S. Pat. 3,129,326, Issued Apr. 14, 1964

An operational amplifier for use in analog computers is described. A feedback path is provided between output and input, with a second feedback impedance and a reset impedance connected in series between the output and the reset terminal. The junction between the second feedback impedance and the reset impedance forms a reset summing junction for the output signal and the initial condition signal. A T-type switching system between the reset summing junction and the amplifier input provides a reset time in microseconds.

26,371 SERIES CONNECTED TUNNEL-DIODE MULTILEVEL REGISTER by M. Beddoes and C. Salama (U. Brit. Columbia); IEEE Trans., Vol. EC-13, pp. 308-309(L), June 1964

Recent work connecting tunnel diodes in series with a load resistance to form a multistep register is described. Such a circuit has obvious applications to analog-to-digital conversion. The present limitation, however, is the small number of states possible with available tunnel diodes. Information permitting satisfactory operation of a two-diode (GaAs, Ge) register is given. Switching time is found to be critically dependent upon the differences of the valley currents of the two diodes and for worst-case switching time is 12 nsec.

26,372 ANALOG-TO-DIGITAL CONVERTER by S.G. Francisco (IBM); U.S. Pat. 3,135,954, Issued June 2, 1964

A means for converting an analog shift orientation to a digital electrical indication in electrical telemetering apparatus so that it may be transmitted to a remote station through a limited number of electrical conductors is described. Shaft position information on a gimbal mounted platform is transmitted to a relatively remote receiving station by means of a shaft digitizer using discs requiring a small number of conductors and slip rings on the gimbal system.

26,373 HIGH SPEED THRESHOLD LOGIC A/D CONVERTER WITH ERROR CORRECTION by D.S. Schover and M. Stein (Hollcrafters); 1964 IEEE Intl. Conv. Rec., Part 1, pp. 22-29, Mar. 23-26

High performance analog to digital conversion has been achieved by the use of threshold logic with unique error correction and time sharing features. The system is capable of quantizing analog signal information into 12 bit binary coded decimal words at a conversion rate of 200,000 conversions per second and a resolution of 0.1%. The technique used in detecting and correcting encoding errors has made it possible to attain a system resolution and accuracy which is orders of magnitude better than the 1% resolution of the basic threshold element. In order to realize a high overall conversion rate, a time sharing feature has been employed which triples the systems speed without increasing the basic encoder clock rate.

26,374 ANALOG-TO-DIGITAL CONVERTER by R.A. Kaenel (Bell Labs.); U.S. Pat. 3,127,601, Issued Mar. 31, 1964

It is shown that analog signals may be digitally encoded with error amplifiers of narrower bandwidth than those previously considered necessary. The encoding system consists of a reversible binary counter activated by a variable repetition rate bipolar pulse source which response to the polarity and amplitude of the signal from an error amplifier, the error amplifier receives the analog input signal and a feedback signal from the counter. For low amplitude error signals, reflecting small changes in the analog input, the low quality amplifier follows the step-by-step count of the reversible counter and is sufficient to operate in the manner of the conventional converter. For relatively high amplitude error signals, the low quality amplifier is incapable of following the step by step change in the output level of the counter, nevertheless rapid changes in the input analog system can be faithfully encoded by using the amplifier as a stable position servo system during the existence of high amplitude error signals.

Analog-to-Digital Converters - See 26,312

26,375 ELECTROMAGNETIC CODE CONVERSION ARRANGEMENTS by J.B. Clark and P.W. Nicks (AEI, Ltd.); U.S. Pat. 3,129,419, Issued Apr. 14, 1964

An electromagnetic code conversion arrangement by which the numerical value of a digit received in decimal form can be converted to a two-out-of-five code is described. The circuit consists of five electromagnetic devices each having four input windings paired for simultaneous activation. The windings are polarized to cancel the induced flux in unactivated windings to eliminate erroneous signals caused by circulating currents. A different pair of devices will be activated for different decimal values of the input digit.

26,376 BINARY TO TERNARY CONVERTER by K.M. Trampel (IBM); U.S. Pat. 3,126,537, Issued Mar. 24, 1964

A simple three transistor, three diode, binary to ternary (double rail code) converter circuit is described. Output level is independent of input and is well-defined even though input pulses may be distorted. In addition to ternary output the circuit produces an error output pulse for the fourth binary combination not occurring in the double rail code. The first transistor stage of the converter is a conventional NOR circuit. If such a logic is already available in the computer this can be eliminated. The converter with the NCR stage eliminated may also serve to convert any two binary signals into a ternary output.

26,377 CONVERTERS FOR CONVERTING DIGITAL INFORMATION INTO ANALOGUE INFORMATION by R.E. Spencer, R.A. Coil, and F.C. Wolfendale (Electric and Musical Indus., Ltd.); U.S. Pat. 3,136,986, Issued June 9, 1964

An improved means for accurately converting digital information into analogue information, not especially, but no exclusively designed for binary coded decimal digital inputs is presented. Alternating potentials corresponding to representative digits or groups of digits are selected, scaled to a level appropriate to their respective digital places, and then added sequentially. The scaling and adding operations are combined into one unit.

26,378 FERROELECTRIC-PHOTOCONDUCTIVE IMAGE STORAGE by S.C. Requa and J.M.N. Hanlet (Molectro); 1964 IEEE Intl. Conv. Rec., Part 1, pp. 38-46, Mar. 23-26

The principles of an exclusively solid state means of image storage are described. The function is to register an optical image, retain or store said information, and upon command provide a sequential analog voltage representation of said image. The basic device is a sandwich of ferroelectric and photoconductive films between two continuous outer electrodes. Image information is stored in the form of a corresponding polarization pattern in the ferroelectric film. The conversion of image intensity to charge or polarization pattern is accomplished by the photoconductive layer. The photocurrent flow x shutter time product is equal to the charge stored in the ferroelectric film. Storage of image information can be indefinite in duration. High resolution in terms of 10^4 image points per square centimeter is possible. Use of photoconductive rather than photoelectric effect allows the possibility of infrared response.

26,379 BINARY-TO-VIDEO DATA CONVERTER (Hazeltine Tech. Dev. Ctr.); Contract AF30 602 2856, 44 pp., Feb. 1964; U.S. Gov. Res. Rep., Vol. 39, p. 44(A), June 1964 AD 434 759 OTS \$4.60

A study was made of various techniques for a binary-to-video converter suitable for accepting binary information from a computer (or similar type of input) and producing a display on a TV raster. Information to be shown on the display included alpha-numerics, symbols, map data, and similar processed-data readout in the form used for command and control displays. It is concluded that a data converter system capable of storing a digital representation of entire TV rasters would provide the most satisfactory solution. Where a number of different display pictures are to be assembled for simultaneously viewing by different persons at different local areas, a common system with a magnetic drum which provides multiple outputs is recommended. Time sharing most of the common system elements will provide a substantial savings in overall cost.

POWER APPLICATIONS

26,380 SWITCHING POWER SUPPLY REGULATORS FOR GREATER EFFICIENCY by S. Levine (Silicon Transistor Corp.); Electronic Design, Vol. 12, pp. 48-59, June 22, 1964

The design procedure involved in constructing a switching-type voltage regulator to replace a conventional class A power supply regulator, resulting in an increase of supply efficiency from 40% to 90%, and substantial savings in size, weight, and cost is presented. The analysis of operation of the switching regulator is given, and component values with corresponding switching losses are evaluated. It is found that the characteristics of the regulator vary with component selection. A brief procedure for designing the switching regulator is described, and the advantages of increased regulator sensitivity are discussed.

26,381 A SIMPLE, HIGH-PERFORMANCE SERIES STABILIZER by D.J. Collins (Bell and Howell, Ltd.); Electronic Engrg., Vol. 36, pp. 330-331, May 1964

When stable dc voltages are required, the circuit designer has a large variety of circuit configurations from which to choose. His choice is dictated by the basic power parameters, the quality of performance and the allowable cost and whereas the majority of requirements are easily satisfied there occasionally arises a particular problem which requires a special solution. A circuit which was specifically designed to provide an inexpensive, compact, stable voltage source for exciting unbonded strain gauge pressure transducers is described.

26,382 NETWORK FILTERS STABILIZE D-C SUPPLY OVER WIDE RANGE by J.G. Reddie (Aero Service Corp.); Electronics, Vol. 37, p. 83, June 15, 1964

A compact and highly stable dc supply for use in an aerial surveillance system which is able to provide 0-1200 volts at good regulation when set to a particular voltage despite modulation by the aircraft's generators is described.

Regulation is $\pm 0.5\%$ at a maximum output power of 200 mw. The input voltage supply may vary from 22 to 30 volts with up to 5% ripple. The system occupies eight cubic inches of space and is stable over a wide temperature range, having a temperature coefficient of 0.1% of output voltage per $^{\circ}\text{C}$ from -15°C to $+15^{\circ}\text{C}$. Higher output voltages may be obtained by using a full-wave bridge or voltage doubling circuits.

26,383 VOLTAGE REGULATING ARRANGEMENT by J.R. Trenchard; U.S. Pat. 3,124,697, Mar. 10, 1964

A voltage regulator which can act as a sink to absorb power from the load, which protects the load from over-voltage, and which maintains good efficiency under all load conditions is discussed. One variable resistance device comprises a transistor connected in shunt to the load terminals and a control circuit which reduces the resistance of the transistor in the case of over-voltage at the load terminals. The series regulator is also controlled in accordance with voltage fluctuations across the load terminals. With this combination good efficiency may be obtained under all load conditions. At no load or sink loading, negligible current is drawn from the source, and at no load or source loading conditions negligible current need be drawn by the shunt transistor as long as the load voltage does not exceed the nominal value.

26,384 VOLTAGE REGULATING ARRANGEMENT by J.W. Semmer and F.A. Strich; U.S. Pat. 3,124,698, Mar. 10, 1964

A voltage regulator which can act as a sink to absorb power from the load, which protects the load from over-voltage, and which maintains good efficiency under all load conditions is described. One variable resistance device is connected in shunt across the load, and another is connected in series between the source and the load. The resistance of the shunt device is controlled in accordance with the voltage fluctuations across the load terminals, and the resistance of the series device is controlled in accordance with the fluctuations of current through the shunt-regulating device. At no load both the series-regulating device and the shunt-regulating device have relatively high resistance so that very little power is wasted. When the regulator must act as a sink, the resistance of the series-regulating device is further increased, so that negligible power is drawn from the source under this condition. With normal loading, the shunt-regulator resistance is very high, assuring maximum power to the load.

26,385 TRANSISTORIZED POWER SUPPLY by A. Rosenfeld and K. Kupferberg (Forbo Design); U.S. Pat. 3,128,423, Issued Apr. 7, 1964

A transistorized power supply capable of supplying an output voltage much larger than that of any individual transistor is described. A pass transistor arrangement comprising two or more transistors connected in series allows the output voltage to be divided equally among the series connected array. The lead or master pass transistor in each leg of the supply has a control signal applied to it to provide output voltage regulation.

26,386 VOLTAGE REGULATOR by A.M. Iokimidis (ITT); U.S. Pat. 3,130,361, Issued Apr. 26, 1964

A transistorized voltage regulator having automatically controlled reference potentials to provide a greater degree of regulation is described. Two transistor stages automatically regulate the voltage supplied from a transformer-full wave bridge source of current, and supply a constant voltage to the load regardless of changes in load resistance a voltage supplied. The circuit as described does have a limited power handling capacity, but it may be increased by connecting additional transistors in parallel with the output transistor.

26,387 A TRANSISTORIZED HIGH CURRENT STABILIZER AND FIELD SWEEP FOR AN ELECTROMAGNET by J.B. Cook, R.E. George and E.H. Grant (Guy's Hospital Med. School, London); J. Sci. Instr., Vol. 41, pp. 390-392, June 1964

A stabilizer controlling the current of a large electromagnet in a Q-band electron spin resonance spectrometer is described. The maximum field strength of 12,500 g is produced when 13 A flow through the magnet coils. Under normal conditions, after an initial warming up period, a stability of ± 0.25 g or ± 2 parts in 10^5 is attained for main voltage fluctuations of $\pm 5\%$, measured during one hour.

26,388 CONSTANT CURRENT SOURCES IN MEASUREMENTS by G.H. Lechner (Lechner Mfg. Co.); Electronic Products, Vol. 6, pp. 26-27, 120-126, May 1964

The use of constant current sources in measurement applications is discussed. Application criteria are given in terms of best matching to the V-I curve of the device to be investigated, and the three factors of safety, convenience, and accuracy are considered in detail. From a safety viewpoint current testing is much superior to voltage testing when the reverse voltage testing of diodes with avalanche breakdown behavior is attempted. AC and special requirements of a current source are discussed, and the use of a modulated source is described.

26,389 BUCK BOOST TRANSFORMER CONTROLLED BY SILICON CONTROLLED RECTIFIER by A. Lichowsky (Ampex); U.S. Pat. 3,129,380, Issued Apr. 14, 1964

A regulating circuit for an alternating current signal source capable of providing regulation at increased levels of load current utilizing a silicon controlled rectifier is described. The maximum current to the load is not limited by the SCR. The desired value of output voltage may be obtained by suitably adjusting the line voltage. Regulation is provided by a feedback circuit, wherein variations in the output voltage produces a feedback voltage, which, by increasing or decreasing the frequency of an oscillator, triggers the SCR at a corresponding pulse rate, developing the required compensation by means of a back-boost transformer.

26,390 COMPLEMENTARY TRANSISTORS EXPAND CURRENT SUPPLY RANGE by D.L. Boos (Stand. Oil Co.); Electronic Design, Vol. 12, pp. 72-73, June 8, 1964

A wide range current supply using a variable reference voltage given by a mercury battery-attenuator circuit, a reference amplifier, and a complementary power amplifier to control current through a load is described. For one amp to flow through a 1-ohm load resistor, 1.85 v at 50 μ A is required at the input with the transistors specified. Output impedance is 600 ohms.

26,391 A PHASE-LOCKED 4 KC PRIMARY FREQUENCY SUPPLY by W.R. Wysocki (Bell Labs.); 1964 IEEE Intl. Conv. Rec., Part 5, pp. 30-44, Mar. 23-26

A transistorized phase-locked primary frequency supply has been designed to produce an accurate 4 kc base frequency for an L-Type Multiplex carrier and pilot supply. This frequency supply is phase-locked to an incoming pilot frequency. It features digital circuitry, high reliability, high free-running frequency accuracy, and a substantial size reduction over its vacuum tube predecessor. The operational as well as the circuit and equipment design features of this frequency source are reviewed. In addition, an analysis of the phase-lock loop is presented. Finally, mean time to failure and other reliability parameters are calculated.

26,392 THE CLASSIFICATION OF SCR INVERTER CIRCUITS by N.W. Mapham (GE); 1964 IEEE Intl. Conv. Rec., Part 4, pp. 99-105, Mar. 23-26

The reader of silicon controlled rectifier literature is faced by a bewildering nomenclature covering inverter circuits. The object of this paper is to present a method of classifying these circuits and to suggest an arbitrary designation. The basis of the method of classification is to first of all divide the circuits into classes based upon different methods of commutation and then to subdivide the classes into the different circuit configurations. It is convenient to consider the sub-divisions first.

26,393 DC TO AC CONVERSION USING MAGNETORESISTANCE by R. Bechtel, W.W. Grannemann and B.J. Harper (U. New Mexico); Solid-State Electronics, Vol. 7, pp. 357-362, May 1964

The feasibility of using magnetoresistor devices for a dc to ac converter was explored both from the circuit standpoint and the devices themselves. The device study disclosed a geometry with magnetoresistance properties nearly on a par with those of a Corbino disk, but having a higher current capability. An analog computer analysis of a bridge-type converter, using experimentally obtained values for the magnetoresistance parameters, revealed a currently obtainable theoretical efficiency of 75 per cent, neglecting electrical and magnetic circuit losses.

26,394 ONE-STEP CONVERTER FOR EASE OF VOLTAGE CONVERSION by J.A. McLeod (GE); 1964 IEEE Intl. Conv. Rec., Part 7, pp. 241-245, Mar. 23-26

Basic switching problems encountered in variable pulse width (VPW) DC to AC converters are discussed. Switching techniques that have been successfully employed in an inherently stabilized VPW converter DC power supply are described. The effectiveness of this converter in offsetting output voltage variations, caused by input voltage changes and magnetic component drift, is explained. An approach to obtaining optimum output regulation and stability in a VPW converter DC power supply with negative feedback is considered.

26,395 DC INVERTERS USING ADZ11 AND ADZ12 TRANSISTORS by J.R. Nowicki (Mullard Meas. Appl. Labs.); Mullard Tech. Commun., Vol. 7, pp. 305-309, May 1964

Push-pull inverters of the saturating drive transformer type (operating at 400 c/s) and CR-timed type (operating at 2.5 kc/s) have been designed round the Mullard ADZ11 and ADZ12 transistors. For both configurations, outputs of > 300 w were obtained with the ADZ12 and a 28 v supply, and > 120 w with the ADZ11 and a 14 v supply.

26,396 LOW INPUT VOLTAGE CONVERSION by J.T. Lingle (Minn.-Honeywell); Contract DA-36-039-SC-90808, in Army Signal Res. and Dev. Lab. Proc., 17th Ann. Power Sources Conf., 1963, pp. 153-155; STAR, Vol. 2, p. 1084(A), May 9, 1964

A transistor device is described that can convert the output of a single cell (fuel cells, solar cells, thermionic diodes, thermoelectric junctions, etc.); or a minimum number of series-connected cells to one or more usable output voltages. The circuit consists of a starting oscillator, a power amplifier, a rectification circuit, and a filter. For a converter designed to convert 1.5 volts to a 50-watt, 28-volt dc output, it was found that: with a 1.5-volt input, the efficiency was 79.7% at 50 watts, and for a 30-watt load, the efficiency was 82.7%. In a 0.6 to 0.9 input voltage range, maximum efficiencies between 73.5% and 79.5% were obtained. From the performance curves that are presented, it is concluded that transistor converters are a practical and efficient method of converting the low input voltage of newer energy conversion power sources and single-cell electrochemical sources to more usable higher voltages.

26,397 SQUARE WAVE GENERATOR WITH THIRD HARMONIC SUPPRESSOR by D.J. Suda (Automatic Electric Labs.); U.S. Pat. 3,128,438, Issued Apr. 17, 1964

A transistorized inverter circuit that converts direct current supply to alternating current output with controllable frequency and harmonic content is described. The objectionable harmonic of the primary frequencies is removed by the use of a saturable core transformer in the system. The circuit operates from a 48 volt exchange battery and is utilized to provide one of the five frequencies of the decimonic (20, 30, 40, 50 and 60 cycles), of the harmonic ($16^{2/3}$, 25, $33^{1/3}$, 50 and $66^{2/3}$ cycles), or of the synchrononic (20, 30, 4, 2, 54, and 66 cycles) series. Each frequency unit is capable of providing 25 watts of ringing power, and a sufficient amount of ring back tone.

26,398 DC TO AC CONVERTER by W.F. Cormier (Minn.-Honeywell); U.S. Pat. 3,129,379, Issued Apr. 14, 1964

A signal modulator using transistors as active elements for converting a direct current signal to an alternating signal output is described. The circuit configuration features two transistors connected at the base lead, with the collectors attached to either end of the secondary of the output transformer, and the emitters connected together and to one of a pair of input terminals. The input signal is thus applied to the modulator to vary the impedance of the collector-base junction thereby controlling the amplitude of the AC signal supplied to the load. Either PNP or NPN transistor pairs may be used.

26,399 TRANSISTOR VOLTAGE CONVERTER by J.J. Wilting (N. Am. Philips); U.S. Pat. 3,134,948, Issued May 26, 1964

Three figures illustrating different component arrangements of a low-voltage-dc-to-high-voltage-ac transistorized converter are discussed and compared with a previous patent (3,008,068) and other similar ones having certain shortcomings. These disadvantages are generally concerned with the "spread" or non-coincidence of switching feedback pulses inside the oscillating circuit. Improvements are obtained in oscillation efficiency by using additional inductances and other minor configurational changes, especially in collector-emitter and feedback circuits. Such changes also permit using transistors with more widely varying α values. One improvement uses a 30 μ h inductance which helps to prevent almost virtual short-circuiting of the resonant circuit through its capacitance when the transistor conducts; also, base current is smoothed and prolonged by addition of inductance. Another circuit configuration provides, by additional inductance in the base-emitter path, the desired initially inductive load at switch-on time, whereas the reverse pulses fed to the base quickly switch off the transistors, compensating for the fact that discharge in the feedback R-C circuit is very rapid. A feedback circuit using diodes is discussed.

26,400 REGULATED VOLTAGE CONVERTER CIRCUIT by R. Anderson and R. Projain (Bell Labs.); U.S. Pat. 3,135,909, Issued June 2, 1964

A transistorized dc-to-dc voltage converter with reduced hysteresis and eddy current losses, increased output voltage stability for varying loads and low ripple is described. A new control concept is achieved by providing the inductive circuit of the converter circuit with a stable quiescent state after the delivery of electrical energy from the magnetic field of the inductive circuit to the output circuit is complete, and by shortening the duration of the quiescent state as the average output decreases and lengthening the duration of the quiescent state as the average output voltage increases. The exact regulating action of the circuit and its advantages over previous regulation methods are discussed in detail.

26,401 ELECTRICAL SEMICONDUCTOR POWER SUPPLY APPARATUS by J.T. Lingle; U.S. Pat. 3,127,551, Mar. 31, 1964

A dc-to-dc converter applicable to photoflash units is described. A semiconductor oscillator circuit periodically interrupts the low voltage. The resulting pulsating dc is applied to a step-up transformer to produce ac voltage which is then rectified and applied to the capacitor. The components of the oscillator circuit are chosen so that the oscillations decrease in magnitude, finally ceasing when the capacitor is fully charged. The circuit further includes a relaxation oscillator circuit, actuated upon a predetermined drop in capacitor voltage, which is effective to restart the semiconductor oscillatory circuit. Battery life is extended because the converter operates merely long enough to charge the capacitor.

26,402 SWITCH MODULATION TECHNIQUES IN AC TO DC POWER SUPPLIES. Part II by F.C. Schwartz (GE); In *Army Signal Res. and Develop. Lab. Proc.*, 17th Annl. Power Sources Conf., 1963, pp. 167-170; *STAR*, Vol. 2, p. 1085(A), May 8, 1964

The frequency-modulated, self-stabilizing inverter, as used in regulated ac-to-dc power supplies, is discussed. Two experimental models of such power supplies at the 260- and 600-watt levels to provide 26 volts dc and 22 to 30 volts dc respectively, are described.

26,403 DC TO AC CONVERTER WITH NEGATIVE FEEDBACK STABILIZATION by C.M. Hayward; U.S. Pat. 3,127,576, Issued Mar. 31, 1964

Circuits for converting dc to square-wave ac and for converting dc to trapezoidal-wave ac are described. Negative feedback stabilization is employed to make the frequency, amplitude, and wave form of the output largely independent of input variations. In the square-wave converter transistors are employed to alternate the transfer of a direct current across a transformer primary. The base of each transistor is fed by a regenerative and degenerative feedback loop. Initially, the degenerative feedback loop is open because of the presence of a Zener diode. Control of the transistor is left to the regenerative loop, causing decreasing transistor resistance and a rapid output voltage build-up. At maximum amplitude the Zener fires, so that both loops are operative. The relative loop gains are such that the transistor resistance, and therefore the output voltage, are maintained at a constant value. This continues until saturation of the transformer core, at which point the regenerative feedback loop becomes inoperative, and the transistor is switched off. Inductive kick-back turns on the other transistor, which controls the next half-cycle. The trapezoidal-wave converter operates like the square-wave converter, except that additional circuits are provided to alter the waveform. One circuit modifies the leading edge of each half-cycle by controlling the operation of the regenerative feedback loops, thereby introducing a linear ramp in the transistors turn-on. The trailing edge of the half-cycles are initiated and are made linear by providing additional circuitry at the bases of the transistors.

26,404 POWER SUPPLY UTILIZING A MAGNETIC AMPLIFIER FOR DC CONTROL by G.O. Huntzinger (Genl. Motors); U.S. Pat. 3,129,375, Issued Apr. 14, 1964

A power supply for converting ac to dc using a magnetic amplifier to control the dc output voltage, capable of providing a continuous current flow for high loads and a pulse flow for low loads, thus making it suitable as a battery charging device, is described. The magnetic amplifier is controlled by a zener diode network such that the dc voltage will increase with increasing load to a point and then decrease with further increasing load. Load current is never allowed to flow through two rectifiers in series, thus reducing voltage drop across the rectifiers and undesirable heating effects. Line voltage drops are compensated for by the rising voltage characteristic of the supply.

CONTROL APPLICATIONS

26,405 HOW TO DESIGN LOW-COST DIGITAL CONTROLS by R. Centner (Bendix Corp.); *Control Engrg.*, Vol. 11, pp. 75-80, Feb. 1964

The most important step in developing a low cost digital control package is setting the specifications. The criterion suggested by the author is "what minimum performance would customers accept if the cost were low enough?" An approach to determine optimum specifications is given along with choices of storage methods, logics, packages, and peripheral equipment.

26,406 SCR CONTROL IN PAPER MILLS by H. Dooley (English Electric); *Electronics*, Vol. 37, pp. 42-47, June 29, 1964

The application of SCR to control dc paper mill motors to 0.1% is described. SCR control increases efficiency and control response speed and decreases space requirements and maintenance cost. An SCR buck/boost system yields 1/4 speed power factor nearly equal to that of a Ward Leonard control in which a separate dc generator supplies each motor.

26,407 THE SILICON CONTROLLED RECTIFIER AC SWITCH FOR THE CONTROL OF SINGLE-PHASE SERIES AND TRANSFORMER COUPLED LOADS by W. Shepherd and J. Stanway (Royal Mil. Coll. Sci.); *1964 IEEE Intl. Conv. Rec.*, Part 4, pp. 155-163, Mar. 23-26

Performance characteristics, oscillograms and analysis are given for the control of resistive and inductive loads using a pair of silicon controlled rectifiers connected back-to-back. Firing angle adjustment enables the SCR pair to give sensitive continuous control as a series or as a shunt switch or controller.

26,408 THE POLYPHASE INDUCTION MOTOR CONTROLLED BY FIRING ANGLE ADJUSTMENT OF SILICON CONTROLLED RECTIFIERS by W. Shepherd and J. Stanway (Royal Mil. Coll. Sci.); *1964 IEEE Intl. Conv. Rec.*, Part 4, pp. 135-154, Mar. 23-26

The best connection for voltage control of a balanced three-phase load by the use of silicon controlled rectifiers is found to be the delta connection with back-to-back SCR pairs in series with the load impedances. Continuous, stepless control of an induction motor stator voltages is possible by firing-angle control of three SCR pairs. Measured and calculated torque-speed curves have fair agreement. Economic speed control may be possible by the use of SCR pairs shunted across rotor resistors.

26,409 TRANSISTOR AMPLIFIER FOR CONTROLLING SHAFT SPEED by A.W. Wilkerson (Louis Allis Co.); U.S. Pat. 3,131,342, Issued Apr. 28, 1964

A control circuit directly responsive to a broad range of composite control signals, which may be added or deleted without affecting circuit performance using current regulation to provide the control is described. The circuit uses both transistor and magnetic amplification stages and has a low input impedance in both the forward and reverse directions, thus making it well adapted for use with high impedance sources. The control circuit may be used to effect control of driver shaft speed by means of a direct current tachometer attached to the shaft.

26,410 SPEED CONTROL SYSTEM FOR ELECTRIC MOTOR by F. Pisano (US Army); U.S. Pat. 3,135,906, Issued June 2, 1964

A circuit to control the speed of a reversible direct current series wound motor coupled to a mechanical load which is driven by the motor during one cycle of its operation and applies a torque to the motor during another cycle is described. When a direct current series motor is used to lower such a load device, the problem of preventing overheating and excessive speed is encountered. This is solved by using a first field winding of the motor to raise the load, and using a second one to lower the load, the first one used to produce a breaking action during the lowering of the load. This breaking action is accomplished by the control circuit activating a silicon controlled rectifier to short this winding through a resistor and produces a well known electromagnetic breaking force.

26,411 SPEED CONTROL OF WOUND ROTOR INDUCTION MOTOR by P. Miljonic (John Inglic Co., Canada); U.S. Pat. 3,136,937, Issued June 9, 1964

A method of induction motor speed control having superior speed-torque motor characteristics is discussed. Many heavy direct-current motor sets are being used in applications requiring accurate speeds consistent with wide load variations. Previously these characteristics could not be obtained by varying the load resistance of an induction motor; this method permits a continuous or stepwise full variation of motor speed from forward to reverse, while maintaining similar load-torque curves for various speeds. Generally, the method comprises rectification of the variable-frequency, variable voltage rotor output; the dc voltage produced is inverted and fed back to the power supply line over a selectively variable part of its cycle. The rectifier and its choke are bypassed by a variable gate for speed-control which in practice is made selectively variable relative to the supply cycle. Another gate, which in practice is fixed, is connected from the dc bus to the ac mains in at least one phase. Firing points of inverters or gates may be accomplished by commonly known means.

26,412 BRAKING CIRCUIT FOR AC HOIST MOTOR by F.Y. Grepe; U.S. Pat. 3,136,938, Issued June 9, 1964

A speed control system for electric hoists which uses induction motors is described. For raising a load, the speed is controlled by an automatically advancing step which progressively shorts out a resistance across the motor's secondary winding. An automatic cutout breaks the ac stator circuit in case of overhoisting or overload. For slow lowering, speed is controlled by self-induced braking; secondary current depends upon rotor speed and therefore the amount of current returned to the stator. For high speed lowering, current is externally supplied to the stator winding. A brake is used for hoisting which releases only upon current being supplied by the rotor; therefore, the motor must be energized before taking off the brake. Likewise, in lowering,

the friction brake is energized by the same dc current that energizes the stator of the motor to supply the braking torque. Thus, it is impossible to have the friction brake released without having the stator energized with direct current producing the braking torque.

26,413 CORRECTIVE NETWORK PERMITS LATCHING WITH FAST PULSES by K. Kolakowski (Hughes Aircraft); *Electronic Design*, Vol. 12, p. 72, June 8, 1964

A latching relay that can be energized with fast pulses is obtainable by the use of an SCR in conjunction with an RC network. The RC time constant is made equal to the relay equivalent L/R time constant and the values of the two resistors are set equal, thus making the lead of the SCR anode purely resistive of value R.

26,414 A NEW CONCEPT IN SOLID STATE RELAYS by W. Koeffler (Phillips Control Co.); in Okla. State U. Papers Presented at the 11th Natl. Conf. on Electromagnetic Relays, 1963, 16 pp.; *STAR*, Vol. 2, p. 1469(A), June 23, 1964

The use of the silicon-controlled rectifier (SCR) as the basic switching mechanism for electrical currents is discussed. The inherent limitations of the semiconductor are discussed—high contact resistance, low insulation resistance, and vulnerability to high ambient temperature (100°C). Circuits to nullify the forward drop of the SCR to reduce the holding current were tested. The report concluded that the SCR concept best lends itself for switching application with a minimum of associated electronic circuitry.

26,415 TRANSISTORIZED RC TIME DELAY RELAYS by W. Pecota (G-V Controls); in Okla. State U. Papers Presented at the 11th Natl. Conf. on Electromagnetic Relays, 1963, 21 pp.; *STAR*, Vol. 2, p. 1468(A), June 23, 1964

The basic principles of operation of the RC type time-delay relay are presented. This type of device is generally identified by a capacitive network in which the time required for a capacitor to charge or discharge is used to control the conductive state of one or more subsequent networks. The discussion is further restricted to devices with control intervals in the time range of 10 msec to 15 min. Basic circuits are analyzed, and the limitations imposed upon these circuits by available components are investigated. System requirements are discussed and compared to the performance of integrated networks. Special function networks are shown, and their purposes are discussed. Performance characteristics most often encountered and problems frequently faced are also analyzed.

26,416 LIQUID LEVEL CONTROLLER by C.O. Berglund and R.R. Thompson; U.S. Pat. 3,131,335, Issued Apr. 28, 1964

A means of automatically controlling the level of an electrolyte between predetermined upper and lower levels in a vessel, even though a layer of another liquid of unknown height may be present on top of the electrolyte is described. An accompanying proof and support that are operative in an environment of excessive temperatures as well as a corrosive and even explosive atmosphere are employed. The electrical part of the system features a transistorized relay circuit.

26,417 RECIPROCATING MOTOR CONTROL SYSTEM by W. Morgan (Esso Res. Engrg. Co.); U.S. Pat. 3,134,938, Issued May 26, 1964

A solid state power supply and control system for a two coil reciprocating magnetic pump is described. A transistor multivibrator circuit alternates the flow of power to two power coils to reciprocate the piston used to pump fluid through the pump. This circuitry replaces quickly worn-out mechanical switches and noisy cam driver timers. A free-running multivibrator provides base drive for two power transistors, each of which feed one of the power coils. Another transistor controls the current level passing through the coils.

26,418 PROPORTIONAL PULSE SERVO SYSTEM by L.D. Johnson, R.L. Kittrell, and D.E. Meier (Collins Radio); U.S. Pat. 3,131,340, Issued Apr. 28, 1964

An improvement in pulsed servo control systems by which successive application of extremely high prime mover torque may be made to a controlled member producing a proportional control is described. The clutch coupler circuit produces, in response to a servo error signal, an output signal to effect engagement of a magnetic clutch in the form of an output pulse or pulses, the duration and time rate of occurrence of which are each proportional to reduce the clutching duty cycle as a direct function of the servo error signal. Clutch chatter is minimized in this system by utilization of a time interval succeeding each clutching operation.

26,419 LOCK OUT CONTROL CIRCUIT FOR POWER AMPLIFIER by R.E. Morgan (GE); U.S. Pat. 3,128,396, Issued Apr. 7, 1964

A new and improved magnetic controlled power rectifier amplifier utilizing a lock out circuit to prevent misfiring during the commutation of the amplifier and simultaneous conduction of both control rectifiers is described. A commutating circuit is connected across the control rectifier, and consists of a capacitor in series with a saturable reactor. A firing circuit connected to the gate of the control element is operatively coupled to a lock out circuit to prohibit firing during commutating intervals of the control rectifier.

26,420 PROPORTIONAL THERMOREGULATOR USING THYRISTORS by G. Johansson (U. Lund, Sweden); *J. Sci. Instr.*, Vol. 41, p. 382, June 1964

A circuit employing thyristors and operational amplifiers can be used for proportional temperature control. The sensor is a thermistor. The thermoregulator will keep the temperature constant within 0.03°C in an air thermostat with a heat loss of 100 w. The device is easily adapted to temperature programming.

Automobile Air Conditioning Thermostats - See 26,285

26,421 FLASHING LIGHT DEVICE WITH AUTOMATIC DAYTIME SHUTOFF by H.R. Mallory (P.R. Mallory); U.S. Pat. 3,130,349, Issued Apr. 21, 1964

A flashing light device which automatically shuts itself off when the ambient light reaches a selected intensity level without requiring auxiliary circuitry or significant additional current drain from the power source is described. The flashing operation is determined by conduction and nonconduction of a transistor in series with a current supply and the lamp, and control is afforded by a photocell and degenerative and regenerative feedback. Typical values result in a flash rate of sixty flashes per minute where the lamp is on for only 10% of each cycle.

INSTRUMENTATION

26,422 SOLID-STATE ELECTROMETERS WITH INPUT-CAPACITANCE NEUTRALIZATION by H. Fein (Yale U.); *IEEE Trans.*, Vol. BME-11, pp. 13-18, Jan.-Apr. 1964

Two electrometer amplifier circuits employing a unipolar Field-Effect Transistor and an insulated gate Field-Effect Transistor respectively are described. Design and performance criteria are discussed.

26,423 REMOTE METERING DEVICE by R.F. Roe and H. Steinhauer, Jr.; U.S. Pat. 3,127,594, Mar. 31, 1964

An optical remote pickup device for application with existing watt-hour meters is discussed. The pickup device utilizes a light source to direct a small beam of light on the rotating disk of the meter. On the surface of the disk are several equally spaced radially extending reflective segments and black segments. The beam of light is sequentially reflected only by the reflective segments, with the reflected beam being focussed upon a phototransistor pulse generating circuit. A timer-counter circuit totals the pulses. Readings are transferred to a data printer and the counter reset to zero upon monitoring.

26,424 A PORTABLE INSTRUMENT FOR MEASURING THE ELECTRICAL CONDUCTIVITY OF AVIATION FUELS by M.D. Foster and K.J. Marsh (Brit. Petroleum Co. Ltd.); *J. Sci. Instr.*, Vol. 41, pp. 379-381, June 1964

An instrument designed to measure the electrical conductivity of aviation fuels on airfields is described. It is compact, robust and portable, yet its accuracy is almost as good as that of laboratory instruments; the 95% confidence limits of a measurement are ± 0.45 picohm m^{-1} . The principle of operation is to measure the decay of voltage between the plates of a cylindrical condenser whose dielectric is the liquid under test. A radiation dosimeter is modified to act as an electrostatic voltmeter and a clockwork timer provides a fixed sequence of switching operations. Measurements only take a few minutes and can be made by non-technical operators.

26,425 FEEDBACK SAMPLING CHANNEL FOR SAMPLING OSCILLOSCOPES by G. Gilbert (Mullard Lab.); *Mullard Tech. Commun.*, Vol. 7, pp. 293-304, May 1964

Complete circuit details for the sampling channels of a sampling oscilloscope are given. The feedback system used results in excellent linearity, well-defined gain and a constant bandwidth.

Oscilloscope Amplifiers - See 26,174

Hall Effect Magnetometers - See 25,878

26,426 HALL EFFECT DEVICES AS MAGNETOMETERS IN CRYOGENIC APPLICATIONS by T.B. Sanford (Lewis Res. Ctr.); Apr. 1964, 9 pp.; STAR, Vol. 2, p. 1355(A), June 8, 1964 NASA TN D-2272; OTS \$ 0.50

Eight representative samples of commercial Hall effect devices were tested at 4.2°K to determine their utility as magnetometers for cryogenic applications. Although cool-down periods of 10 to 15 min were used in an attempt to reduce the thermal shock, several units failed after one or more immersions in liquid helium. The low-temperature behavior of the tested units differed qualitatively from the room-temperature response in that there were oscillations in the Hall voltage as a function of magnetic field. The procedure for use and the low-temperature response of the devices to magnetic fields up to 70 kilogauss are discussed.

26,427 A TRANSISTORIZED CAPACITOR REFRACTOMETER FOR RADIO-SONDE MEASUREMENTS by T.J. Mohan (Bendix Res. Lab.); Proc. Natl. Electronics Conf. 1963, Vol. 19, pp. 436-443

A transistorized instrument for the dynamic measurement of atmospheric index of refraction is described. Variations in the permittivity of the sample air flowing through a concentric-cylinder sensing capacitor produces changes in a stable oscillator's operating frequency. The output of the sampling oscillator is mixed with the output of a 22-megacycle crystal reference oscillator to produce a difference frequency on the order of 30 kilocycles. After suitable signal conditioning, the difference frequency is reduced by means of a series of cascaded binary stages to a frequency suitable for modulating a radiosonde telemetry transmitter. The sensing capacitor is self-compensated for thermally induced dimensional changes of the low temperature coefficient substrate materials. The Clapp-type oscillator provides a high degree of isolation from transistor and voltage variations. An integrated design concept employed in the oscillator assembly minimizes stray capacitance and inductance and permits close thermal coupling between components. In a stable environment, the refractometer displayed a frequency stability of ± 1 part in 10^6 for a period of 3 hours. The results of performance tests and flight tests indicate a need for better temperature control of the sampling oscillator inductor or the employment of temperature compensation in the oscillator assembly.

26,428 FERROELECTRIC BOLOMETER FOR SPACE RESEARCH by H.C. Ingrao, F.J. Kahn, and D.H. Menzel (Harvard Coll., Observatory); Nov. 1, 1963, 57 pp.; STAR, Vol. 2, p. 838(A), Apr. 8, 1964 NASA CR-55542; OTS: \$5.60 ph, \$1.91 mf

The ferroelectric bolometer is compared with other thermal detectors for use in space instrumentation. Ceramic ferroelectric bolometers were manufactured with Curie points between -10°C and +10°C and dimensions as low as 0.5 mm x 0.5 mm x 50 μ . The performance of a radiation pyrometer with a ferroelectric bolometer 1.0 mm x 1.0 mm x 0.2 mm was measured. With an incident infrared signal of 5.8×10^{-9} watts peak-to-peak chopped at 2.5 cps, and a bandpass $\Delta f = 0.25$ cps at room temperature, the noise level of the system is 4.2×10^{-10} watts rms. Theoretical analyses of the responsivity and minimum detectable power are presented.

26,429 MEASUREMENT OF THE VELOCITY OF SECONDARY FLOW IN TAYLOR'S STABILITY PROBLEM by R.B. Lambert, S.K.F. Karlsson and H.A. Synder (Brown U.); Phys. Lett. (Neth.), Vol. 9, pp. 229-230(L), Apr. 15, 1964

A hot thermistor anemometer for studying hydrodynamic flows is described. A small thermistor (< 0.050 cm in diameter) is embedded in the surface bounding the flow, and a constant amount of power is dissipated in the detector. The steady state temperature of the thermistor is above the free stream temperature. The excess temperature ΔT is proportional to $(dv/dy)^{1/4}$ over the range studied, where y is the coordinate perpendicular to the surface and v is the velocity of the fluid flowing parallel to the surface. The thermistor resistance, which is proportional to its temperature over the range studied, is a measure of dv/dy near the surface. The detector has been used to measure directly the circulation in Taylor's vortices.

26,430 MONITORING CIRCUIT FOR LOGGING INSTRUMENTS by R. Kolb (Shell Oil Co.); U.S. Pat. 3,136,975, Issued June 9, 1964

A system for checking the performance of pressure sensing equipment during its installation in oil wells is described. The system consists of a pulse generator utilizing two four-layer pnpn switches, an isolation network consisting of two diodes, and an audio amplifier. Both the interrogating and return pulses must be heard to indicate satisfactory performance.

26,431 WELL LOGGING APPARATUS HAVING DETECTOR MEANS IN A ROTATABLE CASING MOUNTED WITHIN A DRILL STRING FOR SIMULTANEOUS DRILLING AND LOGGING by R.J. Clements, B.D. Lee, R.B. Stelzer and W.R. McEvers, Jr. (Texaco); U.S. Pat. 3,134,069, Issued May 19, 1964

Improved apparatus used to simultaneously and continuously detect and record the existence and depth of a physical variable in the borehole is described.

The apparatus consists of a cylindrical housing inside a drill stem or string which contains a sealed pressure tight capsule arranged to permit the passage of fluid through the housing. An electric signal is generated in the rotatable inner case and passed up through the shaft to a recording device amplification scheme on the surface.

26,432 ALARM SYSTEM by L.H. Kelly and A.C. La Martina (Am. Dist. Tel. Co., N.J.); U.S. Pat. 3,134,970, Issued May 26, 1964

A vault alarm system insensitive to noise such as jet aircraft and road traffic is discussed. The system utilizes a four-transistor amplifier fed by crystal transducers arranged in parallel. Low frequencies will not activate the alarm but high frequency vibrations may be detected.

26,433 ORDER WIRE AND ALARM CIRCUITS by J.R. Buotte and J.A. Word (Bell Labs.); U.S. Pat. 3,130,277, Issued Apr. 21, 1964

Simplified alarm circuits for use in low cost, light route radio relay systems capable of monitoring the performance of unattended stations to detect failures and service interruptions and, upon detection, substitute an emergency power supply are described. The system consists of an alarm signalling channel forming a loop between master control and the subsidiary stations with provisions at each remote station for breaking or bridging the loop in case of service failure.

26,434 FREQUENCY AND TIME CONTROL by D.L. White (Bell Labs.); U.S. Pat. 3,129,346, Issued Apr. 14, 1964

A frequency and time standard system that utilizes an electro-mechanical, piezoelectric element as a vibrating resonator is described. The element provides high frequencies while maintaining a convenient mechanical thickness by the coupling of an electrical circuit with the fundamental overtone of the element.

26,435 A TUNNEL DIODE TIME MARK GENERATOR by H.W. Lefevre (U. Oregon); IEEE Trans., Vol. NS-11, pp. 426-430, June 1964

A recycling time mark generator has been developed in which the only active element is a shunt connected tunnel diode. The diode is mounted at the junction of a 50 Ω stripline T. Two legs of the T are joined with a length of coaxial cable; the third leg proceeds 2.5 cms to a five port mis-match. This mis-match provides five input-output ports, and its distance from the diode determines the pulse width. Pulse width is about 0.8 ns and recycling periods as short as 3 ns and as long as 160 ns have been used. With a selected diode, up to two hundred pulses can be simultaneously recirculated in a 160 ns RG-8 transmission line indefinitely. Short term instability of circulation period as measured by heating the radiated signal with a quartz crystal is less than 0.05 ps. Bias coefficient of circulation period is 8 ps per mv at 90 mv with a General Electric TD-103 diode, and the tuning range which can be obtained by varying bias is 150 ps. The temperature coefficient of circulation period is 1.5 ps per °C. These measurements were made with a circulation period of 100 ns.

26,436 GAMMA-RAY DETECTION EFFICIENCY AND IMAGE RESOLUTION IN SODIUM IODIDE by H.O. Anger and D.H. Davis (Lawrence Rad.); Rev. Sci. Instr., Vol. 35, pp. 693-697, June 1964

Photoelectric, Compton, and photopeak efficiencies have been calculated at several gamma-ray energies for large flat sodium iodide crystals in which the thickness ranges from 1/8-2 in. Also, the loss of position resolution by gamma-ray scattering within the scintillator is calculated, since this is of interest in the design of gamma-ray imaging devices like the scintillation camera. An examination of the data shows the advantage of using low energy gamma rays for imaging whenever possible. They are efficiently detected by solid sodium iodide scintillators 1/2 in. thick, and there is little loss of resolution due to scattering of gamma rays in the scintillator. In the higher energy range, a choice must be made between a thin scintillator with its relatively good position resolution and low detection efficiency, or a thick crystal with higher detection efficiency and less satisfactory resolution.

26,437 A MULTICRYSTAL GAMMA-RAY SPECTROMETER WITH TIME-OF-FLIGHT REJECTION OF NEUTRON-INDUCED BACKGROUND by R.J. Scroggs, W. Zobel, F.C. Maienschein (Oak Ridge Natl. Lab.); IEEE Trans., Vol. NS-11, pp. 365-373, Jan. 1964

To improve the rejection of neutron-induced background in a multicrystal gamma-ray spectrometer, nanosecond circuitry was designed that exploits the difference in flight times of neutrons and gamma rays produced in a target bombardment with a pulsed beam of monoenergetic protons. This circuitry allows the spectrometer to be gated on for a time (nominally 7 nsec) equal to the pulse width of the proton beam. Only those gamma rays produced during the proton pulse are accepted for energy analysis. These gamma rays arrive at the detector in a time short compared with the flight time of any other secondary radiation produced during that same beam pulse. The system is used as a pair

spectrometer for energies from 1.5 to 11 mev, and as a total absorption spectrometer for energies below 2.5 mev. The energies of the gamma rays produced by 160 mev protons in targets of Be, C, H₂O, Al, Co, and Bi were measured. Spectral data were obtained and the results include determination of essentially all the gamma rays previously described^{1,2,3,4} plus several more at higher energies. The neutron rejection ratio of the spectrometer varied with targets and ranged from 59% for °C to 77% for H₂O.

26,438 GAMMA AMPLIFIER-DISCRIMINATOR by C. Sewell, Jr. (Lawrence Rad.); *IEEE Trans.*, Vol. NS-11, pp. 323-328, Jan. 1964

For applications involving the routine laboratory measurement of gamma radiation, an instrument is described which is simple to operate, versatile, compact, and reliable. It consists of a pulse amplifier with charge-sensitive input and delay-line shaping, a differential discriminator capable of covering the range from 2 kev to 4 mev, a calibration pulser, and a power supply. All controls are calibrated directly in terms of gamma energy. Construction is modular for ease of maintenance, and all circuits use solid-state components.

26,439 SEMICONDUCTOR LITHIUM-ION DRIFT DIODES AS HIGH-RESOLUTION GAMMA-RAY PAIR SPECTROMETERS by A.J. Tavendale (Chalk River Nucl. Labs.); *IEEE Trans.*, Vol. NS-11, pp. 191-200, June 1964

Germanium and silicon p-i-n diodes with active volumes up to 2 cm³ have been fabricated using the lithium-ion drift technique. p-type germanium doped with either gallium or zinc (5-10 ohm-cm) and boron-doped silicon (1100 ohm-cm) were the base materials. Diodes were operated at 77°K in conjunction with a low noise amplifier system (270 RMS electron-holes). They have been used as gamma-ray pair spectrometers, germanium diodes giving a resolution of 7 kev (FWHM) at 2.75 mev gamma-ray energy increasing to 10 kev at 7.64 mev; resolution from a silicon device was slightly inferior. A germanium diode has been used as the central detector in a triple-crystal pair spectrometer incorporating two NaI scintillators. This arrangement improved the ratio of the height of the pair peak to the background below the peak from 7:1 to 150:1 for 2.75 mev gamma-rays from a Na²⁴ source.

26,440 STABILIZATION OF LITHIUM-DRIFTED RADIATION DETECTORS by G. Norgate and R.J. McIntyre (RCA); *IEEE Trans.*, Vol. NS-11, pp. 291-293, June 1964

Ion-pairing occurs in silicon between lithium and acceptor impurities and causes a reduction in the effective diffusivity and drift-mobility of lithium. This effect has been studied experimentally with different acceptor impurities. It appears that the suitable choice of an acceptor may, under certain conditions, result in at least an order of magnitude reduction. This is of interest in connection with lithium-drifted gamma detectors where a constant active volume must be maintained over long periods.

26,441 MEASUREMENT OF X-RAY BEAM QUALITY WITH SOLID-STATE DETECTORS by G. Kramer (Avco); *Rev. Sci. Instr.*, Vol. 35, pp. 607-608, May 1964

The ratio of the currents generated in two solid-state detectors of different lengths by a beam of x-rays parallel to the junction is a measure of the x-ray beam quality. Two detectors with lengths of 0.16 and 1.6 cm, respectively, were used to measure x-radiation varying in quality from a half value layer of 2-7 mm Al.

26,442 A SURVEY OF THE APPLICATIONS AND LIMITATIONS OF VARIOUS TYPES OF DETECTORS IN RADIATION ENERGY MEASUREMENT by F.S. Goulding (Lawrence Rad.); *IEEE Trans.*, Vol. NS-11, pp. 177-190, June 1964

A collection of data relevant to the use of various types of semiconductor detector in nuclear spectroscopy and examples of the use of detectors in specific experimental applications are presented. Basic data on absorption of various kinds of radiation in germanium and silicon are given, and these are related to the characteristics of different types of semiconductor detectors. A brief outline of the optimization procedure for the detector-amplifier system to obtain good energy resolution follows. Included in a brief review of applications of detectors are examples in the fields of α -particle spectrometry, high-energy particle reactions, and low-temperature nuclear alignment studies.

26,443 SILICON P-N JUNCTION RADIATION DETECTORS FOR THE TELSTAR SATELLITE by T.M. Buck, G.H. Wheatley and J.W. Rodgers (Bell Labs.); *IEEE Trans.*, Vol. NS-11, pp. 294-301, June 1964

The development and testing of the silicon p-n junction nuclear particle detectors which have been used in the radiation experiments of the TELSTAR communication satellite, and the Relay and Explorer XV satellites are described. The sensitive element of the detector is a diffused mesa diode of 10,000 to 20,000 ohm-cm p-type silicon. It is encapsulated in a transistor-type can with a thin (0.3 mil) Kovar window. In spite of the encapsulation, surface

reliability was a major development problem. An extensive reliability testing program revealed several types of surface instability. Nevertheless, a high degree of reliability was achieved in most of the detectors, including those which were used on satellites.

26,444 UNIFORM AND STABLE dE/dx P-n JUNCTION PARTICLE DETECTORS by T.C. Madden and W.M. Gibson (Bell Labs.); *IEEE Trans.*, Vol. NS-11, pp. 254-261, June 1964

Solid-state dE/dx-E particle identification systems require thin dE/x detectors having a high degree of thickness uniformity. The lack of this uniformity has been a limiting factor in achieving optimum results with these systems. In addition, reproducible and straightforward fabrication techniques, long term stability, and ruggedness are desired for the routine use of such devices. The use of oxide surface passivation, a planar-etching procedure, and an improved back contact have made possible the reproducible construction of thin, uniform, and stable diffused-junction particle detectors which meet these requirements. The response of these detectors to both penetrating and nonpenetrating particles, and the effects of particle channeling through the crystal lattice are discussed.

26,445 DETERMINATION OF TRANSIENT RESPONSE OF SEMICONDUCTOR DETECTORS BY USE OF A NANOSECOND-PULSE ELECTRON ACCELERATOR by H.M. Mann and I.S. Sherman (Argonne Lab.); *IEEE Trans.*, Vol. NS-11, pp. 271-275, June 1964

An apparatus previously developed and used for determination of scintillator response characteristics has been used for similar studies of the transient response of semiconductor nuclear detectors. With this apparatus a detector pulse as short as 1.2 nsec has been observed. Pulses have been recorded for diffused junction and lithium-drift diodes, in silicon. The effects of depletion-depth, base resistance and electric field intensity in the depletion region are revealed in the shape of the pulse. The experimental method and the application of the apparatus to measurement of detector properties is discussed.

26,446 THE ANOMALY IN THE RESPONSE OF SEMICONDUCTOR DETECTORS by W.R. Dodge, S.R. Domen, A.T. Hirshfield, and D.D. Hoppes (Natl. Bur. Stand.); *IEEE Trans.*, Vol. NS-11, pp. 238-243, June 1964

Preliminary investigation of the response to beta and alpha particles of silicon radiation detectors cooled to temperatures below 77°K has led to the discovery of an anomaly in the pulse height distribution which is a function of detector temperature. The pulse height and resolution of a P-I-N lithium-drift silicon detector shows a rapid decrease in the temperature interval of 40 - 35°K for electric fields up to the maximum of 4200 volts/cm used in this experiment. Lithium-drift detectors of the P+-I-N surface barrier configuration exhibit similar characteristics. Surface barrier detectors of resistivities in the range of 3000 ohm-cm exposed to beta particles exhibit a decrease in pulse height and resolution in the temperature interval of 30 - 15°K. With increasing bias voltage the pulse height tends towards the high temperature values but with degraded resolution. A detailed investigation of the response of a surface barrier detector to alpha particles shows an anomaly of the same characteristics as the beta particle anomaly. In addition, the pulse height decreases at reduced bias voltages below approximately 14°K. A plausible explanation of the primary anomaly based on the analysis of Walter is discussed.

26,447 ELECTRONIC SYSTEM FOR HIGH RESOLUTION PULSE HEIGHT SPECTROSCOPY by L.L. Moon (Lawrence Rad.); *IEEE Trans.*, Vol. NS-11, pp. 329-337, Jan. 1964

A system under development capable of fully utilizing the high resolution capacity of solid state radiation detectors, and featuring excellent over-all stability and low noise is described. The system components, consisting of low noise preamplifiers, a linear amplifier, calibration pulser, and regulated power supply are individually examined. All but the preamplifiers are packaged in one chassis.

26,448 SEMICONDUCTOR RADIATION DETECTOR by D.J. Shombert (Merck); U.S. Pat. 3,131,305, Issued Apr. 28, 1964

A semiconductor radiation detector structure using material of relatively low resistivity and capable of detecting high energy particles with a minimum applied bias is described. The device, constructed of fifteen alternate layers of p and n-type silicon, has a resistivity on the order of 40 ohm-cm and requires a bias across each individual junction of 200 volts. Using twenty layers, each 1.5 mils thick with similar resistivities for P and N, the junction voltage is lowered to 100 volts.

26,449 A LITHIUM DRIFTED SILICON SURFACE BARRIER DETECTOR WITH GUARD RING by L. Wang, M.R. Zatzick, and F.P. Ziemba (Solid State Radiations); *IEEE Trans.*, Vol. NS-11, pp. 314-318, Jan. 1964

A semiconductor nuclear particle detector combining the best features of the lithium ion drift technique, the surface barrier method, and incorporating a guard ring structure is described. Detectors having sensitive depths up to 6 mm with essentially no entrance window have been fabricated by this process and experimental data illustrating some of the properties and applications of these devices are presented.

26,450 CaI_2 AND $\text{CaI}_2(\text{Eu})$ SCINTILLATION CRYSTALS by R. Hofstadter (Stanford U.), E.W. O'Dell and C.T. Schmidt (Harshaw Chem. Co.); IEEE Trans., Vol. NS-11, pp. 12-14, June 1964

Scintillation crystals of CaI_2 and $\text{CaI}_2(\text{Eu})$ have been produced which typically show pulse heights of 180% relative to $\text{NaI}(\text{Tl})$. The emission spectra for both pure and activated materials are well matched to a 5-11 phototube response. Pure CaI_2 has a decay time of 0.55 μsec ; $\text{CaI}_2(\text{Eu})$ has a 0.79 μsec decay time. Though this material is difficult to grow and to package, performance results for obtaining are encouraging.

26,452 A STABILIZED SCINTILLATION COUNTER by P.F. Hinrichsen (Bartol Res. Found.); IEEE Trans., Vol. NS-11, pp. 420-425, June 1964

A gain stabilization system for use with a scintillation counter is described. The system uses a Po^{210} source sandwiched between two 0.020 in. thick discs of plastic phosphor as a reference light source, which is mounted between the $\text{NaI}(\text{Tl})$ crystal and the photomultiplier. This produces a stable Gaussian reference peak in the pulse height distribution, equivalent to 150 kev γ rays. A simple pulse shape discrimination circuit at the photomultiplier anode gates the circuitry such that it only responds to the reference pulses, thus making the system independent of any changes in the γ ray flux.

26,453 FAIL-SAFE CIRCUITS FOR NUCLEAR PROTECTIVE SYSTEMS by T. Businaro, L. Conti, and M. Conti (Naz. Energia Nucl. Div. Tecn.); IEEE Trans., Vol. NS-11, pp. 64-70, Apr. 1964

A new set of fail-safe logic blocks particularly suited to safety systems is described. The input information is normally +5 v; in case of alarm, the input drops to 0 v. Fundamental blocks (AND, OR, NOT, etc.) are pulse-modulated, so as to achieve 0 v output voltage in case of failure. More complex logic function can be synthesized and redundancy can be employed in order to avoid erroneous action.

26,454 A FAST-SLOW COINCIDENCE SYSTEM EMPLOYING A MULTI-CHANNEL TIME DISPLAY by R.B. Tomlinson and R.L. Brown (AE Canada Ltd.); IEEE Trans., Vol. NS-11, pp. 28-38, Apr. 1964

A versatile, solid-state Fast-Slow Coincidence system is described which is used with large $\text{NaI}(\text{Tl})$ scintillators and XP1040 photomultipliers. A multi-channel time display is provided which consists of a time-to-amplitude converter of the star-stop type and a standard 100-channel kicksorter. The calibration of the time analyzer can be varied from 1 nsec to 0.1 nsec per channel. In addition to showing the time spread, the display indicates the coincidence resolving time ($2T_0$) which is variable from 1 to 100 nsec by means of front panel helipot. The electronic time jitter of the system, as measured with a fast pulser is less than 0.2 nsec. A resolving time of 8 nsec gives 95% coincidence efficiency for coincidences between the annihilation radiation photopeaks from Na^{22} .

Tunnel Diode Pulse Height Discriminators - See 26, 259

Pulse:

Height Discriminators - See 26, 258
Discriminators - See 26, 260

Time-to-Pulse Height Converters - See 26, 222, 26, 223

OTHER APPLICATIONS

26,455 DIRECT ENERGY CONVERSION LITERATURE ABSTRACTS (Naval Res. Lab.); Dec. 1963, 156 pp.; U.S. Gov. Res. Rep., Vol. 39, p. 32(A), May 5, 1964 AD 430 693 OTS \$3.00

This is the sixth in a series of bibliographies covering unclassified literature related to the direct conversion of energy. Subject coverage includes thermoelectricity, thermionic emission, photoelectric processes, magnetohydrodynamics, electrochemical processes, energy storage, and energy sources.

26,456 APPLICATION POTENTIALS FOR THERMOELECTRICS AND THERMIONICS by L. Perry (Genl. Dynam.); Machine Des., Vol. 36, pp. 196-200, Feb. 13, 1964

The application of thermoelectrics and thermionics to practical considerations of the production of electricity from heat is discussed. The state of the art is summarized with particular attention being paid to actual efficiency vs theoretical efficiency, reliability, and methods of raising performance specification. Nuclear and solar heat sources are considered.

26,457 SOLAR THERMOELECTRIC GENERATOR by S.J. Loring (United Aircraft); U.S. Pat. 3,130,084, Issued Apr. 21, 1964

A thermoelectric energy conversion scheme that changes solar energy to electric energy by use of an array of reflectors and thermocouples with no moving parts is described. Manufacturing tolerances developed in the fabrication of the array are corrected by directing the reflectors independently in a single assembly operation along the optical axis of the array. The support structure is constructed so that positional variations with temperature are small. The energy conversion scheme is particularly intended for use in space vehicles.

26,458 THERMOELECTRICS FOR POWER - A LOOK AT PRODUCT ENGINEERING POTENTIALS by R.L. Klem (RCA); in RCA, Camden, N.J. Direct Energy Conversion, 1963, pp. 6-7; STAR, Vol. 2, p. 1454(A), June 23, 1964

The basic technical skills, the facilities, the general technology, and the materials required for thermoelectric-device development are discussed. The future of thermoelectric-energy conversion in many applications, including nuclear-reactor thermoelectric systems (such as SNAP-10A) and radioisotope thermoelectric systems, is also discussed.

26,459 THERMOELECTRIC REFRIGERATION, HEATING, TEMPERATURE CONTROL, AND DISTILLATION by P.E. Wright (RCA); in RCA, Camden, N.J. Direct Energy Conversion, 1963, pp. 20-24; STAR, Vol. 2, p. 1454(A), June 23, 1964

Thermoelectrics is unique among the various methods of direct energy conversion because of its dual nature. A thermoelectric circuit can serve as either a generator of electrical energy or as a refrigeration machine. Emphasized are thermoelectric applications other than power generation, e.g., refrigeration, heating, temperature control, dew-point sensing, and distillation.

Laser Applications in:

Continental Drift Measurements - See 26, 072
Speed of Light Measurements - See 26, 068
Light Scattering by Gases - See 26, 070
Acoustic Generation in Liquids - See 26, 069
Metalworking - See 26, 073, 25, 075
Microwelding - See 26, 075

Amplifiers for Radio Astronomy - See 26, 187

Seismic Amplifiers - See 26, 186

SUBJECT INDEX

A

Abraded Surfaces of InSb, Damaged Layers in 25,038
 Absorption, Electric Field Effects on 25,608
 Absorption in:
 Alkali Halides, N-Center 25,620
 B_2F_4 , Infrared 25,628
 BP 25,617
 $CaF_2:Er^{3+}$ 25,625
 Cd Halides 25,627
 CdS 25,618
 CsCl, Color Center 25,624
 CuCl 25,626, 25,665
 Cu-Ni Alloys, X-Ray 25,630, 25,631
 Degenerate Semiconductors 25,205
 EuIG 25,640
 $Fe(CO)_5$, Infrared 25,632
 GaAs 25,613
 GaAs, Infrared 25,615
 GaP 25,614
 GaP,
 Infrared 25,615
 Pressure Effects on 25,145
 GaSb, Infrared 25,615
 Ge 25,611
 Ge, Infrared 25,609
 H_2O (Solid), Infrared 25,636, 25,637
 InP, Infrared 25,615
 KBr,
 Color Center 24,990
 Infrared 25,622
 KCl,
 Color Center 24,990, 25,621
 Infrared 25,622
 KCl:Co 24,959
 LiF, Irradiation-Anneal Effects on 25,752
 $LiH_3(SeO_3)_2$ 25,634
 Mg_2Sn , Infrared 25,633
 $(NH_4)_2SO_4$ 25,634
 Na Azide, Infrared 25,635
 NaBr:Co 24,959
 NaCl 25,623
 NaCl, Irradiation-Anneal Effects on 25,754
 NaCl:Co 24,959
 $NaH_3(SeO_3)_2$ 25,634
 NaI:TI 25,680
 $NaNO_2$, Irradiation Effects on 25,177
 $NaNO_3$, Infrared 25,190
 NiF_2 25,629
 $PbBr_2$ 25,627
 $PbCl_2:Cd$ 25,627
 Pyrene-TCNE 25,638
 RbCl, Color Center 25,624
 $RbHSO_4$ 25,634
 Si 25,611
 Si, Infrared 25,044
 SiC 25,251
 Silicate Glass:Eu 25,639
 Si:Zn 25,612
 $Y_2O_3:Er^{3+}$ 25,671
 ZnS 25,618
 ZnS, Temperature Dependence of 25,707
 Absorption of:
 Eu Chelates in Hosts 25,641
 U(IV) in Octahedral Coordination 25,642
 Absorption Coefficient-Refractive Index Relationship 25,701
 Absorption Coefficients, Determination of 25,607
 Absorption Edge in:
 $CaTaO_6$ 25,650
 CdS, Field Induced Shift in 25,619
 GaP, Pressure Effects on 25,145
 GaS 25,616
 GaSe 25,616
 Ge 25,610
 $Mg_4Nb_2O_9$ 25,650
 Niobates 25,650
 Tantalates 25,650
 $ZnTa_2O_6$ 25,650
 Absorption Isotherms in:
 D-Pt-Pd 24,934
 H-Pt-Pd 24,934

Absorption Line Shape, Theory of 25,606
 AC-to-DC Converters 26,402, 26,404
 Acoustic Absorption, Theory of 25,787
 Acoustic Absorption in Bi 25,788
 Acoustic Amplification, Phonon Maser Picture of 25,792
 Acoustic Attenuation, Theory of 25,779
 Acoustic Propagation in CdS 25,778
 Acoustic Resonance,
 Paramagnetic 25,585
 Selection Rules-Angular Dependence of 25,585
 Acoustic Telephone System, Underwater 26,299
 Acoustic Velocity in Salicylidene Aniline 25,200
 Actinide Metal Superconductors 25,277
 Activation of BiAs Phosphors 25,682
 Activation Energy of SiO_2 , Temperature Variations of 25,237
 Adders 26,324
 Adders,
 Modular 26,340
 TDT 26,334
 Adsorption, Orientation Dependence of 25,112
 Adsorption of:
 Alcohol in InSb 25,267
 Hydrogen on:
 Ag Films 25,125
 Al Films 25,125
 Au Films 25,125
 Adsorption on:
 Cu_2O Films, O and CO 25,384
 Pt, Diffraction Study of 25,124
 Air Conditioning Regulators 26,285
 Aircraft Collision Warning Systems 26,287
 Aircraft Control Systems 26,290
 Alarms 26,432
 Alarms, Radio Relay 26,433
 Alkali Halides,
 Absorption in 25,620
 Fluorescence of 25,663
 Scintillation in 25,679
 Alkali Halides:S, Luminescent Centers in 25,648
 Alkali Metals, Susceptibility of 25,380
 Alkaline Earth Phosphates, Luminescence of 25,649
 Alloys,
 Diffusion in 25,052, 25,057
 Vacancy Migration in 25,057
 Aluminum,
 Crystal Structure of 24,915
 Crystal Substructure of 24,947
 Cyclotron Resonance in 25,355
 Debye Temperature of 25,757
 Diffusion of Mg in 25,988
 Dislocation Densities in 25,008
 Elastic Constants of 25,757
 Fermi Surface of 25,355
 Stress-Wave Propagation in 25,756
 Aluminum Films, Adsorption of Hydrogen on 25,125
 Aluminum Superconducting Films, Transitions in 25,323, 25,324
 Aluminum Superconductors, Transition Temperature of 25,300
 Aluminum-Aluminum Oxide-Aluminum Films,
 Emission from 25,371
 Field Emission from 25,371
 Aluminum Carbide, Heat of Formation of 24,885
 Aluminum Chloride, Heat Capacity of 25,732
 Aluminum-Iron, Magnetoresistivity of 25,343
 Aluminum Iron Cobalt (Al_2FeCo),
 Knight Shift in 25,590
 NMR in 25,590
 Aluminum Iron Nickel (Al_2FeNi),
 Knight Shift in 25,590
 NMR in 25,590
 Aluminum-Magnesium,
 Decomposition of 24,988
 Resistivity of 24,988
 Vacancies in 24,988
 Aluminum-Manganese, Magnetoresistivity of 25,343
 Aluminum Nickel Cobalt (Al_2NiCo),
 Knight Shift in 25,590
 NMR in 25,590
 Aluminum Nitride Whiskers, Growth of 25,110
 Aluminum Oxide,
 Data Sheets on 25,165
 Diffusion of Xe in 25,077
 Dislocation Density in 25,009
 Dislocations in 25,004, 25,770, 25,773
 Fracture of 25,769
 Growth of 25,094
 Heat Capacity of 25,732
 Luminescence of 25,647
 Mechanical Properties of 25,773
 Paramagnetic Resonance Absorption in 25,571
 Twinning in 25,019
 Ultrasonic Absorption in 25,791
 Yield in 25,770
 Aluminum Oxide:Cr,
 Cross Relaxation in 25,564
 Fluorescence of 25,672
 Aluminum Oxide:Cr³⁺,
 Paramagnetic Resonance Line Splitting in 25,557
 Spin Lattice Relaxation in 25,570
 Aluminum Oxide:Fe³⁺, Ultrasonic Attenuation in 25,782
 Aluminum Oxide:Ti³⁺, Paramagnetism of 25,551
 Aluminum Vanadium Technetium,
 Knight Shift in 25,601
 Susceptibility of 25,601
 Aluminum-Zinc, Impurity Clustering in 25,049
 AM/FM Receivers 26,294
 Ammonium Sulfate,
 Absorption in 25,634
 Ferroelectric Transitions in 25,634
 Lattice Vibrations in 25,634
 Amplifier-Multipliers 26,170
 Amplifiers,
 Analysis and Synthesis of 26,157
 Broad Band 26,172-26,176
 Ceramic Triode 26,171
 Complementary 26,166, 26,189
 DC 26,167-26,169, 26,303
 Deflection 26,303
 Differential 26,164
 Feedback 26,166, 26,179
 Hearing Aid 26,181
 High Impedance 26,151
 Hybrid 26,169
 Low Noise 26,151, 26,186
 Low Power 26,181, 26,184, 26,185
 Magnetic 26,191-26,193, 26,419
 Microwave 26,171
 Negative Feedback 26,166
 Operational 26,370
 Oscilloscope 26,174
 Parametric 26,159-26,165, 26,234
 Polarity-Sensing 26,180
 Pulse 26,177-26,179, 26,221
 Seismic 26,186
 Stabilization of 26,158
 Thin Film 26,165
 Transmission Line 26,176
 Tunnel Diode 25,883, 26,173, 26,187
 Amplifiers for Radio Astronomy 26,187
 Analog Computers in:
 Control Systems 26,366
 Operations Research 26,365
 Analog Multipliers 26,367
 Analog Multipliers,
 FET 26,368
 Hall Effect 25,881
 Analog-to-Digital Converters 26,312, 26,372, 26,373, 26,374
 Analog-to-Digital Converters, Tunnel Diode 26,371
 AND Logic Circuits 26,323, 26,327-26,329
 Anemometers 26,429
 Annealing of Noble Metals 24,994
 Annealing Shrinkage of Cu 25,001
 Antenna Matching Circuits 26,295
 Anthracene,
 Crystal Structure of 24,955
 Photocurrents in 25,220, 25,221, 25,691
 Photogeneration in 25,695, 25,696

Anthracene, (Cont'd)
 Segregation of Naphthalene in 24,900
 Susceptibility of 24,955
 Thermal Expansion in 24,955
 Thermally-Induced Currents in 25,221
 Trapping of Holes in 25,220, 25,221
 Antiferroelectrics, Phase Transitions in 25,198
 Antiferromagnetic Anisotropy in Cr_2O_3 25,537
 Antiferromagnetic Linear Chains, Perturbation Calculation of 25,533
 Antiferromagnetic Ordering in:
 CsMnCl_3 25,539
 KMnCl_3 25,539
 RbMnCl_3 25,539
 Antiferromagnetic Properties of YbMnO_3 25,199
 Antiferromagnetic Resonance in:
 Antiferromagnets 25,542
 CoCl_2 25,543
 CsMnCl_3 25,539
 CuF_2 25,413
 $\alpha\text{-Fe}_2\text{O}_3$ 25,544
 FeCl_2 25,543
 KMnCl_3 25,539
 RuMnCl_3 25,539
 Antiferromagnetic Spin Flop in Hematite 25,534
 Antiferromagnetic Structure of:
 ErMn_2 25,407
 Fe_2As 25,540
 MnSO_4 25,541
 TbNi_2 25,407
 TmMn_2 25,407
 Antiferromagnetic Transitions in CuF_2 25,413
 Antiferromagnetism,
 Green Functions in Theory of 25,531
 Molecular Field Theory of 25,532
 Antiferromagnetism of:
 CrCl_2 25,511
 FeBr_2 25,510
 Pd_3Mn_2 25,538
 Rare Earth-Cu Compounds 25,509
 Antiferromagnets,
 Antiferromagnetic Resonance in 25,542
 Phase Transitions in 25,542
 Antimony, Crystallographic Angles of 24,929
 Antimony in Cu, Diffusion of 25,058
 Antimony Sulfide Films, Photovoltaic Effect in 25,698
 Arsenic, Crystallographic Angles of 24,929
 Arsenic Oxide,
 Ultrasonic Attenuation in 25,783
 Ultrasonic Relaxation in 25,783
 Astable Multivibrators 26,152
 Astable Multivibrators, Temperature Compensation of 26,203
 Atmospheric Noise, Tape Recording System for 26,321
 Attenuators,
 Laser 26,051
 Optical 26,051
 Austenite, Lattice Constant of 24,927
 Automobile Air Conditioning Regulators 26,285
 Automobile Electrical Systems, Semiconductors in 26,276-26,278
 Automobile Ignition Systems 26,279-26,283
 Automobile Regulator Systems 26,284
 Automobile Thermostats 26,285
 Autopilots 26,290
 Autopilots, Marine 26,291
 Avalanche Transistor Circuits 26,153
 Avalanche Transistor Circuits, Analysis of 26,154

B

Backward Diode Controlled Rectifiers 25,839, 25,840
 Backward Diode Detectors 26,229
 Backward Diode Modulators 26,229
 Backward Diodes 25,841
 Barium Ferrite Powders, Coercive Force of 25,478
 Barium Fluoride, Refraction in 25,710
 Barium Gold Superconductors, Transition Temperature of 25,298

Barium Oxide,
 Electron Emission from 25,360
 Ion Emission from 25,360
 Barium Phosphate, Luminescence of 25,649
 Barium Potassium Ferrites, Magnetic Anisotropy of 25,495
 Barium-Strontium Titanate,
 Conductivity of 25,250
 Crystal Structure of 25,250
 Thermoelectric Coefficient of 25,250
 Barium Titanate,
 Conductivity of 25,250
 Crystal Structure of 25,090, 25,250
 Dislocations in 25,014
 Domain Motion in 25,193
 Domain Walls in 25,192
 Ferroelectric Properties of 25,090
 Growth of 25,089, 25,090
 Phase Transitions in 24,911
 Thermoelectric Coefficient of 25,250
 Barkhausen Effect in:
 Fe 25,473
 Ni 25,743
 Barrier Detectors 26,449
 bcc Lattices, Lattice Vibrations in 25,156
 bcc Metals, Diffusion in 25,059
 Benzene (Single Crystal), Elastic Constants of 25,763
 Bernoulli Sequence Generators 26,361
 Beryllium,
 Fermi Surface of 25,153
 Lattice Vibrations in 25,162
 Beryllium Fluoride, Heat Capacity of 25,730
 Beryllium Oxide,
 Deformation Properties of 25,775
 Diffusion of Xe in 25,077
 Heat Capacity of 25,732
 Beryllium Titanium,
 Crystal Structure of 24,953
 Phase Transitions in 24,953
 Bias Circuits, Transistor 26,155
 Bicrystals,
 Oxidation of 25,122
 Reduction of 25,122
 Bidirectional Diodes 25,839, 25,840
 Binary-to-Ternary Code Converters 26,376
 Binary-to-Video Converters 26,379
 Biomedical Telemetry 26,271
 Biomedical Transducers 26,270
 Bismuth,
 Acoustic Absorption in 25,788
 Crystallographic Angles of 24,929
 Energy Gap of 25,269
 Negative Resistivity of 25,269
 Nuclear Magnetic Resonance of 25,587
 Resistivity of 25,269
 Thermal Expansion of 25,741
 Ultrasonic Absorption in 25,788
 Bismuth Antimonide Laser Diodes 26,040
 Bismuth-Antimony, Growth of 25,089
 Bismuth Arsenate, Activation of 25,682
 Bismuth Ferrite, Crystal Structure of 24,975
 Bismuth Sulfide,
 Energy Gap of 25,709
 Refractive Index of 25,709
 Bismuth Telluride, Resistivity of 25,260
 Bismuth-Tellurium,
 Electrical Properties of 25,167
 Hall Effect in 25,167
 Resistivity of 25,167
 Bismuth Titanate,
 Dielectric Properties of 25,187
 Growth of 25,187
 Resistivity of 25,187
 Bistable Multivibrators 26,206
 Bistable Switching Circuits 26,216
 Bistable Trigger Circuits 26,215
 Bloch Electron in Magnetic Fields 25,374, 25,375
 Bloch Walls in Cubic Ferromagnetic Lattices 25,502
 Bolometers, Ferroelectric 26,428
 Boron,
 Heat Capacity of 25,732

Boron, (Cont'd)
 Heat of Sublimation of 24,886, 24,887
 Boron in Si 25,044
 Boron Carbide,
 Decomposition of 24,887
 Vaporization of 24,886
 Boron Carbide-Silicon Carbide, Phase Diagram of 24,870
 Boron Nitride, Heat Capacity of 25,732
 Boron Oxide,
 Ultrasonic Attenuation in 25,783
 Ultrasonic Relaxation in 25,783
 Boron Phosphate, Heat Capacity of 25,732
 Boron Phosphide,
 Absorption in 25,617
 Decomposition Pressure of 24,888
 Electroluminescence of 25,617
 Energy Gap in 25,617
 Optical Transitions in 25,617
 Photoelectric Response of 25,617
 Boron Tetrafluoride, Absorption in 25,628
 Boron Trifluoride, Crystal Structure of 24,939
 Breakdown,
 Microplasma 25,331
 Stress Effects in Junction 25,816
 Breakdown in:
 Dielectric Films 25,330
 Ge, Stress Effects on 25,329
 Junctions 25,821
 Junctions, Microplasma 25,331
 Microplasma-Free Junctions 25,232
 Si Junctions 25,822
 SrTiO_3 , Dielectric 25,182
 Transistors 25,852
 Transistors, Secondary 25,853
 Broad Band Amplifiers 26,172-26,176
 Bromine Graphite,
 Magnetoresistivity of 25,339
 Negative Magnetoresistivity of 25,339

C

Cadmium,
 de Haas-van Alphen Effect in 25,605
 Fermi Surface of 25,605
 Cadmium in GaAs, Diffusion of 25,069
 Cadmium Emulsion Grains,
 Ionic Conductivity of 25,214
 Lifetime in 25,214
 Cadmium Antimonide: Au,
 Conductivity of 25,256
 Hall Coefficient of 25,256
 Cadmium Halides, Absorption in 25,627
 Cadmium Palladium Oxide,
 Crystal Structure of 24,977
 Electrical Properties of 24,977
 Resistivity of 24,977
 Cadmium Selenide Thin Film Transistors, Double Pinch off in 25,859
 Cadmium Sulfide,
 Absorption in 25,618
 Absorption Edge in 25,619
 Acoustic Propagation in 25,778
 Cyclotron Resonance in 25,225
 Defect Formation in 24,982
 Defects in 25,003
 Dislocation Direction in 25,007
 Dislocations in 25,003
 Effective Mass in 25,225
 Infrared Emission from 24,982
 NMR in 25,596
 Photoconductivity of 25,687
 Photocurrents in 25,222
 Polaron Effects in 25,225
 Purification of 25,051
 Recombination in 25,222
 Surface Recombination in 25,222
 Tapping Luminescence of 25,687
 Ultrasonic Amplification in 25,794, 25,795
 Ultrasonic Attenuation in 25,780
 Ultrasonic Generation in 25,793
 Ultrasonic Propagation in 25,778

SUBJECT INDEX (Continued)

- Cadmium Sulfide:GaCl₃, Stacking Faults in 25,033
 Cadmium Sulfide:Ni, Susceptibility of 25,385
 Cadmium Sulfide Films,
 Hall Effect in 25,345
 Hail Mobility in 25,345
 Resistivity of 25,345
 Cadmium Sulfide Heterojunctions, Properties and
 Fabrication of 25,843
 Cadmium Sulfide-Type Crystals, Trapping in 25,216
 Cadmium Telluride, Lifetime of Holes in 25,215
 Cadmium Telluride:Cr, Paramagnetic Resonance of
 25,582
 Cadmium Telluride Films, Photo-EMF in 25,697
 Cadmium Telluride-Indium Antimonide,
 Carrier Concentration of 25,169
 Conductivity of 25,169
 Electrical Properties of 25,169
 Hall Constant of 25,169
 Mobility in 25,169
 Thermal Conductivity of 25,169
 Cadmium Telluride-Selenide,
 Conductivity of 25,168
 Crystal Structure of 25,168
 Electrical Properties of 25,168
 Hall Constant of 25,168
 Thermal Conductivity of 25,168
 Thermoelectric Power of 25,168
 Calcite, Phosphorescence in 25,677
 Calcite:Fe, Paramagnetic Resonance Absorption in
 25,573
 Calcium Carbonate, Phosphorescence in 25,677
 Calcium Carbonate:Fe, Paramagnetic Resonance
 Absorption in 25,573
 Calcium Ferrite, Ferromagnetic Resonance in 25,516
 Calcium Fluoride,
 Growth of 25,086
 Phosphorescence in 25,677
 Calcium Fluoride:Dy²⁺ Lasers 26,007
 Calcium Fluoride:Dy²⁺ Lasers, Pumping of 25,944
 Calcium Fluoride:Dy³⁺, Paramagnetic Resonance in
 25,581
 Calcium Fluoride:Er³⁺,
 Absorption of 25,625
 Emission Spectra of 25,625
 Calcium Fluoride:Er³⁺ as Laser Material 25,625
 Calcium Fluoride:Eu²⁺, Faraday Rotation in 25,714
 Calcium Fluoride:Rare Earth,
 Crystal-Field Splitting in 25,556
 Paramagnetic Resonance of 25,556, 25,568
 Spin-Lattice Relaxation in 25,568
 Calcium Fluoride:Sm³⁺, Paramagnetic Resonance in
 25,581
 Calcium Fluoride:Tm²⁺ Lasers 26,007
 Calcium Fluoride:Tm²⁺, Zeeman Splitting in 25,555
 Calcium Fluoride:U³⁺ Lasers 26,008
 Calcium Fluoride:U³⁺, Paramagnetic Resonance of
 26,008
 Calcium Fluoride:Y, Thermoluminescence of 25,661
 Calcium Fluoride-Calcium Hydroxide-Calcium Carbonate, Phase Diagram of
 24,873
 Calcium-Lead Tungstate:Sm, Luminescence of 25,651
 Calcium Molybdate:Nd Lasers 26,009
 Calcium Orthovanadate,
 Crystal Structure of 24,979
 Fluorescence of 24,979
 Calcium Oxide:Eu²⁺, Paramagnetic Resonance of
 25,577
 Calcium Oxide-Aluminum Oxide-Water, Phase Diagram of 24,877
 Calcium Phosphate, Luminescence of 25,649
 Calcium Scandates,
 Crystal Structure of 24,972
 Preparation of 24,972
 Calcium Tantalate,
 Absorption Edge in 25,650
 Luminescence of 25,650
 Photoluminescence of 25,650
 Calcium Tungstate,
 Dislocations in 25,039
 Plastic Deformation of 25,039
 Slip in 25,039
 Calcium Tungstate:Nd Lasers, Cathodoluminescent
 Pumping of 25,945
 Calcium Tungstate:Nd³⁺ Lasers, Oscillations in
 25,956
 Calcium Tungstate:Yb³⁺, Paramagnetic Resonance of
 25,584
 Calorimeters 24,883
 Capacitors,
 SiO₂ Film 25,814
 Ta 25,813
 Ta Foil 25,812
 Carbon,
 Crystal Structure of 24,949
 Elastic Constants of 25,760
 Lattice Vibrations in 24,949
 Thermal Expansion of 24,949
 Carbon in:
 Fe-Co-C, Diffusion of 25,068
 Na 25,045
 Carbon Precipitation in Fe 24,907
 Carbon Monoxide from Mo, Desorption of 25,126
 Carrier Concentration in:
 InSb-CdTe 25,169
 Semiconductors 25,208
 Carrier Density, Calculation of 25,209
 Carrier Diffusion through Junctions 25,820
 Carrier Diffusion Length in Semiconductors 25,213
 Carrier Ionization Rates in Si 25,232
 Carrier Mean Free Path, Spin Wave Scattering Calculations on 25,425
 Carrier Scattering in:
 Graphite 25,257
 Solids 25,229
 Cathodoluminescence of:
 GaAs 25,658
 Zn(PO₃)₂-Cd(PO₃)₂-Mg(PO₃)₂ 24,874
 Ceramic Filters 26,266
 Ceramic Triode Amplifiers 26,171
 Ceramics, Dielectric Properties of 25,185
 Cerium Magnesium (CeMg), Crystal Structure of
 24,937
 Ceric Phosphate Glass,
 Faraday Rotation in 25,715
 Susceptibility of 25,715
 Cesium Chloride,
 Absorption in 25,624
 Lattice Coefficients of 24,941
 Lattice Energies of 24,941
 Lattice Potential of 25,138
 Cesium Iodide:Ti, Fluorescent Decay in 25,667
 Cesium Manganese Chloride (CsMnCl₃),
 Antiferromagnetic:
 Ordering in 25,539
 Resonance in 25,539
 Paramagnetic Resonance in 25,539
 Chemical Analysis, Electron Spectroscopy in 25,040
 Chemical Valence Analysis, Electron Spectroscopy in
 25,040
 Chemisorption on TiO₂, Oxygen 25,688
 Chromium,
 Cracking in 25,037
 Diffusion of N in 25,065
 Nitridation of 25,065
 Spin Waves in 25,430
 Young's Modulus of 25,764
 Chromium in Ni-Cr, Diffusion of 25,066
 Chromium over V-Cr, Vapor Pressure of 24,884
 Chromium Bromide, Dielectric Constant of 25,180
 Chromium Chloride,
 Antiferromagnetism in 25,511
 Metamagnetism in 25,511
 Chromium Nickel, Crystal Structure of 24,954
 Chromium Oxide,
 Antiferromagnetic Anisotropy in 25,537
 Magnetic Structure of 25,398
 Chromium-Silicon Oxide Films, Growth of 25,811
 Chromium Spinel, Paramagnetic Exchange in 25,546
 Chromium Tri-iodide,
 Curie Temperature of 25,439
 Ferromagnetic Resonance of 25,439
 Magnetic Anisotropy of 25,439
 Chromium Tri-iodide, (Cont'd)
 Magnetization of 25,439
 Transmission of 25,439
 Chromium Vanadium,
 Néel Temperature of 25,535
 Nuclear Magnetic Resonance in 25,535
 Circuit Analysis 26,141
 Circuit Reliability 26,142
 Circuits, Radiation Effects on 26,143
 Circulators, Ferrite 25,893, 25,895, 25,896
 Cleaved Surfaces, Etching of 25,127
 Cobalt,
 Crystal Structure of 24,950
 Ferromagnetic Spin Wave Scattering in 25,426
 Cobalt in:
 Ag, Diffusion of 25,061
 Cu, Diffusion of 25,060
 Cobalt Films,
 Hysteresis in 25,460
 Magnetic Anisotropy of 25,460
 Magnetic Properties of 25,437
 Cobalt Aluminum,
 Knight Shift in 25,590
 NMR in 25,590
 Cobalt Chloride,
 Antiferromagnetic Resonance of 25,543
 Metamagnetism of 25,512
 Cobalt Ferrite, Superparamagnetism in 25,552
 Cobalt Ferromagnetic Alloys, Properties of 25,417
 Cobalt Iron, Magnetic Anisotropy Induced by Cold
 Rolling in 25,491
 Cobalt Iron Silicon,
 Electric Properties of 25,166
 Hall Coefficient of 25,166
 Resistivity of 25,166
 Semimetallic Properties of 25,166
 Thermoelectric Power of 25,166
 Cobalt Nickel Ferrite,
 Magnetic Anisotropy of 25,498
 Magnetic Resonance in 25,498
 Cobalt Nickel Ferromagnets, Nuclear Magnetic Relaxation in 25,526
 Cobalt Nickel Films, Coercivity of 25,479
 Cobalt Titanium,
 Knight Shift in 25,590
 NMR in 25,590
 Cobalt Double Sulphates, Lattice Constants of 24,942
 Cobalt-Vanadium,
 Order-Disorder Transitions in 24,905
 Resistivity of 24,905
 Code Converters 26,375
 Code Converters, Binary-to-Ternary 26,376
 Coercive Field in Rochelle Salt 25,197
 Coercive Force of:
 Ba Ferrite Powders 25,478
 FeAl 25,438
 GdIG 25,480
 Coercivity of CoNi Films, Composition Dependence
 of 25,479
 Coherence Time of Pulsed Lasers 25,967
 Coincidence Systems 26,454
 Collision Warning Systems, Aircraft 26,287
 Color Center Absorption in:
 Alkali Halides 25,620
 CsCl 25,624
 KCl 25,621
 RbCl 25,624
 Color Centers, Paramagnetic Resonance of 25,575
 Color Centers in:
 KBr, Bleaching of 24,990
 KCl,
 Bleaching of 24,990, 24,991
 Paramagnetic Resonance of 25,576
 Spin-Lattice Relaxation of 25,567
 KCl:Li, Fluorescence Lifetime of 25,664
 NaCl, Irradiation-Anneal Effects on 25,753
 Coloration of:
 LiF, Irradiation-Anneal Effects on 25,752
 NaCl, Irradiation-Anneal Effects on 25,754
 Colpitts' Oscillators, Analysis of 26,194

SUBJECT INDEX (Continued)

- Communication Systems,
 - Laser 26,061
 - Underwater 26,299
- Comparators 26,218
- Comparators,
 - Tunnel Diode 26,219
 - Voltage 26,152
- Compass,
 - Hall Effect 26,289
 - Magnetic Film 26,288
- Complementary Amplifiers 26,166, 26,189
- Computer Circuits, Modular 260 Mc 26,338
- Conductivity - See also Resistivity; Piezoresistance; Magnetoresistance
- Conductivity of:
 - Ba-Sr TiO₃ 25,250
 - BaTiO₃ 25,250
 - Cd Emulsion Grains, Ionic 25,214
 - CdSb: Au 25,256
 - CdTe-CdSe 25,168
 - FeO, Composition Dependence of 25,264
 - Films 25,239
 - Films, Mechanisms for 25,238
 - Ge, Temperature-Pressure Relationships in 25,265
 - Ge: Au 25,266
 - InSb 25,268, 25,340
 - InSb-CdTe 25,169
 - In₂Te₅ 24,867
 - K Halides 25,255
 - KI, Ionic 25,254
 - NaO₂, Irradiation Effects on 25,177
 - PbS:
 - Films 25,263
 - Layers 25,253
 - TiO₂, Anisotropy of 25,352
 - Tunnel Diodes 25,205
- Conductivity Meters, Liquid 26,424
- Conductivity Tensor of Polycrystalline Materials 25,235, 25,236
- Contacts for Power Transistors 25,874
- Control Systems, Design of 26,405
- Controlled Rectifiers,
 - Fabrication of Si 25,838
 - Properties and Fabrication of Si 25,839, 25,840
- Controls,
 - Flow 26,417
 - Lighting 26,421
 - Liquid Level 26,416
 - Motor 26,406-26,412
 - Temperature 26,420
- Converters,
 - AC-to-DC 26,402, 26,404
 - Analog-to-Digital 26,312, 26,371-26,374
 - Binary-to-Ternary Code 26,376
 - Binary-to-Video 26,379
 - Code 26,375
 - DC-to-AC 26,392-26,399, 26,403
 - DC-to-DC 26,400, 26,401
 - Digital-to-Analog 26,377
 - Energy 26,455-26,458
 - Parametric 26,159, 26,164, 26,233-26,235
 - Thermoelectric 26,083
 - Time-to-Pulse Height 26,222, 26,223
 - Tunnel Diode 26,222
- Coolers,
 - Ettingshausen 26,086
 - Figure of Merit for 26,086
 - Performance Coefficient of 26,077
- Copper,
 - Annealing Shrinkage of 25,001
 - Cyclotron Resonance in 25,356
 - de Haas-van Alphen Effect in 25,603
 - Diffusion of:
 - Ag in 25,060, 25,063
 - Au in 25,060
 - Co in 25,060
 - Ge in 25,060
 - Sb in 25,058
 - Dislocation:
 - Annealing in 25,001
 - Structure of 24,999
 - Etching of 25,128
- Copper, (Cont'd)
 - Fermi Surface of 25,356, 25,603
 - Grain Boundaries in 25,026
 - Growth of Pure 25,083
 - Stacking Faults in 25,032
 - Yield in 25,766
- Copper in Ag, Solubility of 24,897
- Copper:Co⁵⁷,
 - Lattice Dynamics of 25,154
 - Mössbauer Effect in 25,154
- Copper Dendrites, Twins in 25,022, 25,023
- Copper Films, Growth of 25,101
- Copper Solid Solutions, Knight Shift in 25,600
- Copper-Cadmium Ferrite, Magnetization of 25,472
- Copper Chloride,
 - Absorption in 25,626, 25,665
 - Fluorescence of 25,665
 - Spin Flopping Relaxation in 25,520
 - Susceptibility of 25,520
- Copper Fluoride,
 - Antiferromagnetic Resonance in 25,413
 - Antiferromagnetic Transitions in 25,413
 - Ferromagnetic Moments in 25,413
 - Magnetic Properties of 25,413
- Copper Gold (Cu₃Au), Dislocation Stress in 25,015
- Copper Iodide Films, Noise in 25,359
- Copper-Nickel Alloys, Absorption in 25,630, 25,631
- Copper Nickel Cobalt,
 - Magnetic Anisotropy of 25,486
 - Magnetic Annealing of 25,486
- Copper Nickel Iron,
 - Magnetic Anisotropy of 25,486
 - Magnetic Annealing of 25,486
- Copper-Silicon-Zinc, Phase Diagram of 24,869
- Copper-Zinc Ferrites, Susceptibility of 25,381
- Corbino Disks, Magnetoresistivity of 25,338
- Counters 26,358
- Counters,
 - Pulse Rate 26,273
 - Ring 26,152
 - Scintillation 26,451, 26,452
 - TDT 26,334
- Covalency in:
 - Ionic Crystals 25,133
 - (NiF₃)⁴⁻ Complex 25,133, 25,134
- Cracked Dislocations 25,018
- Cracking in:
 - Cr 25,037
 - Mo 25,037
 - W 25,037
- Cracks in MgO 25,036
- Critical Current in:
 - Nb₃Sn:
 - Superconducting Coils 25,290
 - Superconductors, Irradiation Effects of 25,289
 - Nb-Ti Superconducting Coils 25,290
 - Nb-Zr Superconducting Coils 25,290
 - Superconductors 25,287
- Critical Field of:
 - Nb Superconductors 25,292
 - Pb-Tl Superconducting Films, Orientation Dependence of 25,294
 - Pb_{0.5}Tl_{0.5} Superconductors 25,293
 - Sn-Ag Films 25,295
 - Sn In Superconducting Films 25,322
 - Superconductors 25,287, 25,309
- Cross Relaxation, Theory of 25,561-25,563
- Cross Relaxation in Al₂O₃:Cr 25,564
- Crystal-Field Splitting in CaF₂:RE 25,556
- Crystal Ladder Filters 26,267
- Crystal Oscillators 26,195
- Crystal Perfection of Quartz 24,919
- Crystal Structure - See also Lattice Constants; Surface Structure
- Crystal Structure Analysis,
 - Diffraction Aperture Widths in 24,916
 - Electron Micrography in 24,918
 - Infrared Spectrometer in 24,917
 - Neutron Diffraction 24,915
 - X-Ray Dispersion Techniques in 24,913
- Crystal Structure of:
 - Ag Films 24,924
 - Al 24,915
 - Anthracene 24,955
 - Ba-Sr TiO₃ 25,250
 - BaTiO₃ 25,090, 25,250
 - Be-Ti 24,953
 - BF₃ 24,939
 - BiFeO₃ 24,975
 - C 24,949
 - CaPd₃O₄ 24,977
 - CaSc₂O₄ 24,972
 - Ca₃(VO₄)₂ 24,979
 - CdTe-CdSe 25,168
 - CeMg₉ 24,937
 - Co, Electron Diffraction Analysis of 24,950
 - Cr-Ni 24,954
 - Cr₃CoCl₅ 24,961
 - DyAl₃ 24,936
 - Dy₃Al₂ 24,936
 - Dy₃Ge₃ 24,936
 - F (Solid) 24,952
 - Gd₃Al₂ 24,936
 - GdCoO₃ 24,974
 - Gd₅Ge₃ 24,936
 - Ge 24,928
 - Graphite 24,949
 - KCl:Co 24,959
 - K₂O·nTa₂O₅ 24,978
 - KTiNbO₅ 24,976
 - KTi₃NbO₉ 24,976
 - LiBO₂ 24,944
 - Li(N₂H₅)SO₄ 24,956, 24,957
 - Mg Formate Dihydrate 24,970
 - Mn Formate Dihydrate 24,970
 - NaBr 24,958
 - NaBr:Co 24,959
 - NaCd₂ 24,965
 - NaCl:Co 24,959
 - Na₂CO₃ 24,973
 - Na₂H₂P₄O₁₂ 24,971
 - Ne (Solid) 24,951
 - Ni Films, Annealing-Atmosphere Effect on the 24,923
 - O (Solid) 24,952
 - PbTe Films 25,108
 - Pyrene-TCNE 25,638
 - Pyrolytic Graphite, Bragg Reflections in 24,948
 - SeCl₄ 24,960
 - SF₃·BF₄ 24,940
 - Si 24,915, 24,928
 - Si Films 25,105
 - Si₂N₂O 24,945
 - SrSc₂O₄ 24,972
 - Ta₅Ga₃ 24,938
 - Te 24,903
 - TeCl₄ 24,960
 - Th(Al-Mn)₂ 24,967
 - Ti₃Au, Impurity Effects on the 24,920
 - Tl Chalcogenides 24,968
 - UF₄ 24,964
 - U₃O₈ 24,962
 - UO₂(OH)₂ 24,963
 - UO₂MoO₄ 24,943
 - UO₂WO₄ 24,943
 - YAlIG:Bi 24,969
 - ZnSb 24,966
- Crystal Substructure of Al 24,947
- Crystalline Field in GdCl₃·6H₂O 25,137
- Crystallites, X-Ray Diffraction Study of 24,914
- Crystallographic Angles of:
 - As 24,929
 - Bi 24,929
 - Hg 24,929
 - Sb 24,929
- Cubic Lattices, Effective Fields in 25,136
- Cuprous Oxide, Growth of 25,084
- Cuprous Oxide Films,
 - Absorption of O and CO on 25,384
 - Susceptibility of 25,384

SUBJECT INDEX (Continued)

Curie Temperature of:

- Au-Fe 25,450
- CrI₃ 25,439
- Cubic Lattices, Ferromagnetic 25,448
- FeNi, Pressure Effects on 25,445
- Gd 25,449
- NiCu, Pressure Effects on 25,445
- NiSi, Pressure Effects on 25,445
- US 25,333
- Current Density in NbSuperconductors 25,308
- Current Regulators 26,387, 26,388
- Current in Superconducting Sheets 25,453
- Cyclotron Resonance, Fermi-Liquid Effects in 25,354
- Cyclotron Resonance in:
 - Al 25,355
 - CdS 25,225
- Cyclotron Resonance Absorption in PbTe 25,357

D

- Damaged Layers in Abraded Surfaces of InSb 25,038
- Darlington Circuits 26,190
- DC Amplifiers 26,167, 26,169, 26,303
- DC Amplifiers, Drift Compensation in 26,168
- DC-to-AC Converters 26,393-26,399, 26,403
- DC-to-AC Converters, SCR 26,392
- DC-to-DC Converters 26,400, 26,401
- Debye Temperature - See also Specific Heat
- Debye Temperature of:
 - AgI 25,728
 - Al 25,757
- Debye-Waller Factors in NaCl 25,164
- Decoder/Encoders, TDT 26,334
- Decoders, Matrix 26,359
- Decomposition of:
 - Al-Mg 24,988
 - B₂C 24,887
 - MoSi_x 24,864
- Decomposition Pressure of BP 24,888
- Decoration of Vacancies 24,989
- Defect Analysis 24,983
- Defect Annealing, Kinetics of 24,980
- Defect Formation in CdS 24,982
- Defects,
 - Electron Micrographs of 24,983
 - Motion of 24,980
- Defects in:
 - CdS 25,003
 - Fe-C, Computer Analysis of 24,981
 - GaAs, Zn-Induced 24,985
 - GaAs Tunnel Diodes 25,828
 - GaSb 25,042
 - LiF, Electron Irradiation Induced 24,984
 - Si, Mobility of 24,986
- Deflection Amplifiers 26,303
- Deformation of:
 - BeO 25,775
 - Quartz 25,771
 - Zn, Irradiation Effects on 25,774
- Degenerate Semiconductors,
 - Absorption in 25,205
 - Electron-Phonon Interaction in 25,205
 - Energy Levels in 25,205
- de Haas-van Alphen Effect in:
 - Cd 25,605
 - Cu 25,603
 - Fe Whiskers 25,151
 - Ni 25,604
- Delay Circuits, Pulse 26,256, 26,257
- Delay Lines, Superconducting 26,107
- Demodulators,
 - Frequency 26,230
 - High Power 26,232
 - Pulse Width 26,231
- Dendrites - See also Whiskers
- Dendrites,
 - Twins in:
 - Cu 25,022, 25,023
 - Graphite 25,021
- Density of:
 - Diamonds 25,751
 - Sn-In 24,930

Desorption of CO and O⁺ from Mo 25,126

Detectors,

- Backward Diode 26,229
- Barrier 26,449
- Diode 25,841
- γ-Ray 26,437-26,440
- InSb 26,047
- Junction 26,439, 26,440, 26,443-26,446, 26,448
- Laser 26,047, 26,048
- Nuclear Particle 26,449
- Optical 26,047, 26,048
- Photoelectromagnetic 26,047
- Radiation 26,442-26,448
- Video 26,229
- X-Ray 26,441

Deuterium (Solid), Heat Capacity of 25,724

- Deuterium-Platinum-Palladium,
 - Absorption Isotherms in 24,934
 - Lattice Constants of 24,934
 - Phase Boundaries in 24,934

Device Noise Generation, Nomograph on 25,797

Device Operation at Low Temperatures 25,798

Devices,

- Passivation of 25,844
- Radiation Effects on 25,799-25,802
- Reliability of 25,803, 25,804
- Review on Semiconductor 25,796

Diamagnetic Susceptibility of:

- Anthracene 24,955
- Th_{1-x}U_xPd₃ 25,387

Diamonds, Density of Natural 25,751

Diboron Tetrafluoride, Absorption in 25,628

Dichlorobenzene,

- Ultrasonic:
 - Absorption in 25,786
 - Velocity in 25,786

Dielectric Analysis, Resonator Methods for 25,176

Dielectric Breakdown in SrTiO₃ 25,182

Dielectric Coercive Field in Rochelle Salt 25,197

Dielectric Constant Analysis, Immersion Method of 25,178

Dielectric Constant of:

- CrBr₃ 25,180
- Ge 25,144
- K₂O·nTa₂O₅ 24,978
- Se 25,179
- Si 25,144
- Superconductors 25,181
- ZnSe 25,224

Dielectric Domain Motion in BaTiO₃ 25,193

Dielectric Domain Wall Motion in Rochelle Salt 25,197

Dielectric Domain Walls in BaTiO₃ 25,192

Dielectric Films,

- Breakdown in 25,330
- Optical Constant Analysis of 25,703
- Thickness Measurements of 25,703

Dielectric Loss in:

- KCl 25,184
- KCl·CaCl₂, Thermal-Deformation Effects on 25,183

Dielectric Properties of:

- Bi₄Ti₃O₁₂ 25,187
- Ceramics 25,185
- NaNO₂, Irradiation Effects on 25,177
- PbHfO₃-PbTiO₃-PbNb₂O₆ 25,188
- Rb_xK_{1-x}NO₃ 25,189
- Srontium-Bismuth Titanates 25,186

Dielectric Susceptibility of Ge 25,196

Dielectric Transitions in:

- NaNO₃ 25,190
- RbNO₃ 25,191

Dielectrics,

- Electroluminescence of 25,654
- Optical Polarization in 25,713
- Photoconductivity Decay in 25,692
- Properties of 25,185

Differential Amplifiers 26,164

Diffusion,

- Anomalous 25,061
- Ferromagnetic Effects on 25,053

Diffusion, (Cont'd)

Orientation Dependence of 25,056

Two-Step Formulations of 25,054

Diffusion Analysis, Autoradiography in 25,058

Diffusion in:

- Ag,
 - Au 25,060
 - Co 25,061
 - Fe 25,061
 - Ni 26,061
 - Al, Mg 24,988
 - Al₂O₃, Xe 25,077
 - Alloys 25,052
 - Alloys, Activation Energy of 25,057
 - Au,
 - Ag 25,060
 - In 25,062
 - Tl 25,060
 - bcc Metals 25,059
 - BeO, Xe 25,077
 - Cr, N 25,065
 - Cu,
 - Ag 25,060, 25,063
 - Au 25,060
 - Co 25,060
 - Ge 25,060
 - Sb 25,058
 - Dislocation Pipes 25,055
 - Fe, Ni⁶³ 25,067
 - Fe-Co-C Austenites, C 25,068
 - GaAs,
 - Cd 25,069
 - Zn 25,070-25,073
 - GaP, Zn 25,072, 25,073
 - In, Au 25,062
 - InP, Zn 25,074
 - Metals 25,052
 - Metals, Activation Energy of 25,057
 - MgO, Xe 25,077
 - Ni, Ni⁶³ 25,067
 - Ni-Cr, Cr 25,066
 - Pu, Self- 25,076
 - Si, Ga 25,075
 - Solid Solutions, Activation Energy of 25,057
 - Transition Metals, Si 25,064
 - ZrO, Xe 25,077
- ## Diffusion of:
- Ag in:
 - Au 25,060
 - Cu 25,060
 - Cu, Sb Impurity Effects on 25,063
 - Au in:
 - Ag 25,060
 - Cu 25,060
 - In 25,062
 - C in Fe-Co-C Austenites 25,068
 - Cd in GaAs, Dislocation Effects on 25,069
 - Co in:
 - Ag 25,061
 - Cu 25,060
 - Cr in Ni-Cr 25,066
 - Fe in Ag 25,061
 - Ga in Si, Sb Impurity Effects on 25,075
 - Ge in Cu 25,060
 - In in Au 25,062
 - Mg in Al 24,988
 - N in Cr 25,065
 - Ni in Ag 25,061
 - Ni⁶³ in:
 - Fe 25,067
 - Ni 25,067
 - Sb in Cu 25,058
 - Si in Transition Metals 25,064
 - Tl in Au 25,060
 - Xe in:
 - Al₂O₃ 25,077
 - BeO 25,077
 - MgO 25,077
 - ZrO 25,077
 - Zn in:
 - GaAs 25,071, 25,073

SUBJECT INDEX (Continued)

Diffusion of Zn in: (Cont'd)
 GaAs, Concentration Dependence of 25,070,
 25,072
 GaAs Tunnel Diodes 25,828
 GaP 25,073
 GaP, Concentration Dependence of 25,072
 InP 25,074

Diffusion-Induced Dislocations in Si 24,997
 Digital-to-Analog Converters 26,377
 Diode Detectors 25,841
 Diode Harmonic Generators 25,832
 Diode Lasers, Emission Properties of 26,012
 Diode Power Converters 25,835
 Diode Switches 26,208-26,211
 Diodes - See also Junctions 25,837

Diodes,
 Backward 25,841
 Bi-Sb Laser 26,040
 Four Layer 25,842
 GaAs 26,011
 GaAs Laser 26,015-26,032
 GaAs_xP_{1-x} Laser 26,033-26,035
 GaP:

Laser 26,036
 Luminescent 26,036
 GaSb Laser 26,037
 Infrared Laser 26,028, 26,031
 InP Laser 26,038
 InP_xAs_{1-x} Laser 26,039
 Luminescent 26,013, 26,030
 Photovoltaic TiO₂ 25,699
 Point Contact 25,832
 Stress Effects in Tunnel 25,823
 Tunnel - See Tunnel Diodes
 Varactor 25,833, 25,834
 Zener 25,836

Diopside-Nepheline-Albite, Phase Diagram of
 24,876

Discriminators,
 Frequency 26,230
 Pulse 26,260
 Pulse Height 26,258, 26,259

Dislocation Analysis, Etch-Electron Microscope
 24,996

Dislocation Annealing in Cu 25,001
 Dislocation Damping, Thermal Disorder Effects in
 25,012

Dislocation Damping due to Kink Motion 25,011
 Dislocation Distribution in AgCl 25,010
 Dislocation Etch Pits in SiC 25,035
 Dislocation Loops in Mo 25,016
 Dislocation Motion in Metals, Review of 25,005
 Dislocation Multiplication in Zn 24,998
 Dislocation Pipe Diffusion 25,055
 Dislocation Relaxation in Au-Ag Alloys 25,013
 Dislocation Stress in Cu₃Au 25,015
 Dislocation Velocity, Stress Dependence of 25,006

Dislocations,
 Fracture Criteria for 25,018
 Segregation of Interstitials to 24,898
 Thermal Disorder in 25,012
 X-Ray Diffraction Study of 24,995

Dislocations in:

Ag 25,262
 AgCl 25,010
 Al 25,008
 Al₂O₃ 25,004, 25,009, 25,770, 25,773
 BaTiO₃ 25,014
 CaWO₄ 25,039
 CdS 25,003, 25,007
 Cu 24,999, 25,001
 Cu₃Au 25,015
 Fe 25,767
 Ge Films 25,000
 Metals 25,005
 MgO 24,996
 Mo 25,016, 25,017
 Si,
 Diffusion-Induced 24,997
 X-Ray:
 Diffraction Study of 24,995
 Topographs of 25,002

Dislocations in: (Cont'd)

SiFe 25,768
 Zn 24,998
 Display Units, Image 26,378, 26,379
 Ditungsten Pentaboride, Heat Capacity of 25,732
 Dividers,
 Frequency 26,238
 Pulse 26,221

Domain Wall Motion in Rochelle Salt 25,197

Domain Walls in BaTiO₃ 25,192
 Donor Scattering in Ge 25,230
 Doping of Si, Alkali Ion 25,050
 Doppler Radar Systems 26,287
 Drift Velocity in Ge, Hot Carrier 25,231
 Drivers, Pulse 26,357
 Duplexers, Ferrite 25,892, 25,894
 Dynamos, Superconducting 26,103
 Dysprosium,
 Magnetic:

Ordering of 25,408
 Resonance in 25,517
 Transitions in 25,408
 Dysprosium Aluminide, Crystal Structure of 24,936
 Dysprosium Garnet, Faraday Rotation in 25,640
 Dysprosium Germanide, Crystal Structure of 24,936
 Dysprosium Iron Garnet,
 Magnetic Anisotropy of 25,500
 Magnetization of 25,550

E

Edge Effect Suppression in Sn-Ag Films 25,295

Effective Mass in:

CdS 25,225
 Ge 25,144
 PbTe 25,252
 Semiconductors 25,223
 Si 25,144
 ZnSe, Electron 25,224

Elastic Constants of:

Al 25,757
 Benzene (Single Crystal) 25,763
 Carbon, Model for 25,760
 Graphite,
 Irradiation Effects on 25,759
 Model for 25,760
 MgO 25,761
 Salicylidene Aniline 25,200
 Te 25,758
 UCD₁₁ 25,762

Electric Fields in Cubic Lattices 25,136

Electrical Properties of:

Co_{1-x}Fe_xSi 25,166
 Bi-Te 25,167
 CaPd₃O₄ 24,977
 CdTe-CdSe 25,168
 InSb-CdTe 25,169

Electroluminescence of:

BP 25,617
 Dielectrics 25,654
 NaI:TI 25,681
 Organics 25,654
 ZnS:Cu,Al,Cl 25,656
 ZnS:Mn 25,655

Electroluminescent Capacitors, Luminous Efficiency
 of 25,653

Electrometers, FET 26,422

Electron-Atom Scattering 25,170

Electron Beam Heaters in Zone Melting 25,080

Electron Distribution in High Electric Fields 25,207

Electron Emission - See also Photoemission; Secondary
 Emission

Electron Emission from:

BaO 25,360
 NaCl, Photo- 25,364
 W 25,361
 W, Secondary 25,370

Electron Mobility in Ge 25,226

Electron-Phonon Interactions, Bloch Representation
 of 25,204

Electron-Phonon Interactions in:

Degenerate Semiconductors 25,205
 Ge 25,206
 Metals 25,203
 Si 25,206

Electron Spectroscopy Analysis 25,040

Electropolishing of Pyrite 25,130

Emeralds, Surface Structure of 24,922

Emission - See also Photoemission; Secondary Emission;
 Emission,

Secondary 25,367-25,369
 Surface Effect in 25,365

Emission from:

Al-Al₂O₃-Al Films 25,371
 BaO 25,360
 CdS 24,982
 MgCl 25,643
 NaCl, Electron 25,364
 Ta-Ta₂O₅-Ta Films 25,371
 W 25,361-25,363
 W, Cs Ion Induced Secondary 25,370
 Zn 25,366
 ZnS:Cu 25,678

Emission Spectra of CaF₂:Er³⁺ 25,625

Encoders,

Magnetic Core 26,360
 Matrix 26,359
 PCM 26,312

Energy Band Density in Semiconductors 25,149

Energy Band Structure, APW Calculation of 25,140

Energy Band Structure of:

GaP, Pressure Effects on 25,145
 Ge 25,144
 PbTe, Relativistic Effects in 25,142
 Semiconductors 25,141
 Si 25,144
 Sn 25,146
 Transition Metal Compounds 25,143

Energy Converters,

Bibliography on 26,455
 Solar-Electric 26,456, 26,457
 Thermoelectric 26,456, 26,458

Energy Gap of:

BP 25,617
 Bi, Temperature Effects on 25,269
 Bi₂S₃ 25,709
 Ge, Free Carrier Concentration Dependence of
 25,147

NbZr Superconductors 25,286

Sn Superconductors 25,789

Superconductors 25,284, 25,285

Energy Levels in Degenerate Semiconductors 25,205

Energy States in:

Crystals 25,148
 Superconducting Junctions 25,326

Energy Storage Devices, Superconducting 26,100,
 26,101

Energy Transfer in Y₂O₃:Eu³⁺ 25,670

Equivalent Networks, Computer Generation of 26,111

Erbium Cobalt, Magnetic Structure of 25,402

Erbium Iron Garnet,

Magnetic Anisotropy of 25,500
 Magnetization of 25,500

Erbium Manganese (ErMn₂),

Antiferromagnetic Structure of 25,407
 Ferromagnetic Structure of 25,407
 Magnetic Structure of 25,407

Esaki Diodes - See Tunnel Diodes

Etch Pits in:

Ice 25,129
 MgO, Simultaneous Observation of Dislocations
 and 24,996

SiC 25,035

Etching, Field-Induced 24,921

Etching of:

Cu, Thermal 25,128
 Ice, Thermal 25,129
 Topaz Cleavages 25,127
 Tunnel Diodes 25,831
 Vacancies 24,989

Ettingshausen Coolers, Figure of Merit for 26,086

- Europium,
 - Magnetic:
 - Ordering of 25,408
 - Transitions in 25,408
 - Europium Benzoylacetonate, Fluorescence of 25,675
 - Europium Chelates, Fluorescence of 25,675
 - Europium Chelates in Hosts,
 - Absorption of 25,641
 - Fluorescence of 25,641
 - Phosphorescence of 25,641
 - Europium Gallium Garnet, Susceptibility of 25,388
 - Europium Garnet, Faraday Rotation in 25,640
 - Europium Iron Garnet,
 - Absorption in 25,640
 - Ferromagnetic Relaxation in 25,522
 - Europium Orthosilicate, Ferromagnetic Properties of 25,440
 - Europium Sulfide, Heat Capacity of 25,726
 - Eutectic Temperature of MoSi_x 24,864
 - Excess Carrier Concentration in Semiconductors 25,208
 - Exchange Coupling of Magnetic Films 25,483
 - Excitons in Homopolar Crystals 25,202
 - EXCLUSIVE/OR Logic Circuits 26,325, 26,326, 26,328
- F
- F-Centers, Paramagnetic Resonance of 25,575
 - F-Centers in:
 - KCl,
 - Bleaching of 24,991
 - Paramagnetic Resonance of 25,576
 - Spin Lattice Relaxation of 25,567
 - KCl:Li, Fluorescence Lifetime of 25,664
 - Fail-Safe Circuits, Nuclear 26,453
 - Faraday Rotation in:
 - $\text{CaF}_2\text{:Eu}^{2+}$ 25,714
 - $\text{Ce}_2\text{O}_3 \cdot 2.67 \text{P}_2\text{O}_5$ 25,715
 - Dy Garnet 25,640
 - Eu Garnet 25,640
 - Sm Garnet 25,640
 - $\text{SrF}_2\text{:Eu}^{2+}$ 25,714
 - Tb Garnet 25,640
 - ZnSe 25,224
 - Fatigue in Fe 25,767
 - fcc Metals, Vacancy Annihilation at Stacking Faults in 24,993
 - Feedback Amplifiers 26,166, 26,179
 - Fermi Level of:
 - Gallium Arsenide-Phosphide 25,150
 - Group II-VI Semiconductors 25,150
 - Group III-V Semiconductors 25,150
 - Group IV Semiconductors 25,150
 - Metal-Semiconductor Interfaces 25,150
 - Fermi Surface of:
 - Al 25,355
 - Be 25,153
 - Cd 25,605
 - Cu 25,603
 - Graphite 25,257
 - Ni 25,152, 15,604
 - Pb 25,151
 - Ferredes, Operation of 25,906
 - Ferric Oxide, Antiferromagnetic Resonance in 25,544
 - Ferrimagnetic Relaxation in:
 - Permalloy Films 25,524
 - YIG 25,521
 - Ferrimagnetic-to-Antiferromagnetic Transitions in $\text{Mn}_{2-x}\text{Cr}_x\text{Sb}$ 25,405
 - Ferrimagnets,
 - Spin-Wave Instabilities in 25,429
 - Spin Waves in 25,421
 - Ferrite Circulators 25,893, 25,895, 25,896
 - Ferrite Powders, Coercive Force of Ba 25,478
 - Ferrite Core Logic Circuits 26,336, 26,337
 - Ferrite Core Memory Units 26,342-26,344, 26,347, 26,348
 - Ferrite Core Memory Units,
 - Multiaperture 25,907
 - Temperature Variations in 25,915, 25,916
 - Wide Temperature Range 25,914
 - Ferrite Core Stepping Circuits 26,345
 - Ferrite Duplexers 25,892, 25,894
 - Ferrite-Filled:
 - Waveguides 25,899
 - Waveguides, Theory of 25,900
 - Ferrite Film Memory Devices, Control of 25,910
 - Ferrite Film Memory Units,
 - Coupled Biaxial 25,904
 - Digit Current Margins of 25,905
 - Interaction between 25,911
 - Magnetization in 25,912
 - Ferrite Film Shift Registers 25,910
 - Ferrite Harmonic Generators 25,901
 - Ferrite Isolators 25,886, 25,890
 - Ferrite Isolators, Hexagonal 25,885
 - Ferrite Limiters 25,893
 - Ferrite Memory Planes, Fabrication of 25,909
 - Ferrite Memory Units,
 - Electron Beam Fabrication Techniques for 25,917
 - Switching in 25,913
 - Ferrite Phase Shifters 25,888, 25,890, 25,892, 25,897
 - Ferrite Phase Shifters, Materials for 25,891
 - Ferrite Power Dividers 25,897
 - Ferrite Resonators 25,887
 - Ferrite Sheet Memory Units 25,908
 - Ferrite Switches 25,897, 25,898
 - Ferrites,
 - Ferromagnetic Resonance in 25,516
 - Growth of 25,099
 - Magnetic:
 - Anisotropy of: 25,584
 - BaK 25,594
 - Ni-Fe 25,489
 - PbK 25,495
 - SrK 25,495
 - Anomaly in Ni-Fe-Co 25,501
 - Hysteresis Properties of Ni-Mn 25,475
 - Properties of 25,435
 - Magnetization of 25,099
 - Permeability of Ni-Zn 25,452
 - Spin-Wave Theory of 25,419
 - Susceptibility of Cu-Zn 25,381
 - Ferroelectric Bolometers 26,428
 - Ferroelectric Properties of:
 - BaTiO_3 25,090
 - YMnO_3 25,199
 - Ferroelectric Switching in KNO_3 25,195
 - Ferroelectric Transitions in:
 - $\text{LiH}_3(\text{SeO}_3)_2$ 25,634
 - $\text{NaH}_3(\text{SeO}_3)_2$ 25,634
 - $(\text{NH}_4)_2\text{SO}_4$ 25,634
 - RbHSO_4 25,634
 - Ferroelectrics,
 - Bibliography on 25,174
 - Polarization in 25,194
 - Quantum Effects in 25,194
 - Review on 25,175
 - Ferromagnetic Alloys,
 - Properties of:
 - Co 25,417
 - Fe 25,417
 - Ni 25,417
 - Ferromagnetic Au:Fe Foils 25,403
 - Ferromagnetic Curie Temperature in Cubic Lattices 25,448
 - Ferromagnetic Effects on Diffusion 25,053
 - Ferromagnetic Energy Exchange Constant in:
 - Ni Films 25,505
 - NiCu Films 25,505
 - Ferromagnetic EuS 25,726
 - Ferromagnetic Films, Magnetization Variations in 25,447
 - Ferromagnetic Hall Effect 25,353
 - Ferromagnetic Hall Effect, Theory of 25,346
 - Ferromagnetic Lattices, Bloch Walls in 25,502
 - Ferromagnetic Moments in CuF_2 25,413
 - Ferromagnetic Parallel Pumping in Mn-ZnY 25,525
 - Ferromagnetic Properties of Eu_2SiO_4 25,440
 - Ferromagnetic Relaxation in EuIG 25,522
 - Ferromagnetic Resonance, Theory of 25,513
 - Ferromagnetic Resonance in:
 - $\text{CaFe}_2\text{O}_7\text{:Gd}^{3+}$ 25,516
 - CrI_3 25,439
 - NiFe Films 25,514, 25,515
 - Ferromagnetic Spin Wave Scattering in:
 - Co 25,426
 - Ni 25,426
 - Ferromagnetic Structure of:
 - ErMn_2 25,407
 - TbNi_2 25,407
 - TmMn_2 25,407
 - Ferromagnetic Transition Metals, Nuclear Magnetic Relaxation in 25,527
 - Ferromagnetism, Oguchi Transformation in- 25,420
 - Ferromagnetism of Transition Metals 25,434
 - Ferromagnets,
 - Hall Effect in 25,353
 - Magneto-Optical Measurements in 25,353
 - Resistivity of 25,234
 - Spin-Wave Scattering in 25,424
 - Spin-Waves in Heisenberg 25,423
 - Ferrous Bromide,
 - Antiferromagnetism of 25,510
 - Metamagnetism of 25,510
 - Ferrous Chloride, Antiferromagnetic Resonance of 25,543
 - Ferrous Oxide,
 - Conductivity of 25,264
 - Thermal EMF of 25,264
 - Field Effect in PbS Films 25,263
 - Field Effect Mobility in InSb 25,267
 - Field Effect Transistor Amplifiers 26,182, 26,183
 - Field Effect Transistor Analog Multipliers 26,368
 - Field Effect Transistor Circuits 26,151
 - Field Effect Transistor Electrometers 26,422
 - Field Effect Transistor Pulse Generators 26,247
 - Field Effect Transistors,
 - Biasing Formula for 25,865
 - Four Terminal Low Frequency Operation of 25,862
 - Grain Boundary 25,871
 - MOS 25,868
 - Photo- 25,869
 - Pinch Off in 25,863
 - Space Charge Effects in 25,864
 - Surface 25,867
 - Temperature Controlled 25,866
 - Thin Film 25,861, 25,870
 - Field Emission from:
 - Al- Al_2O_3 -Al Films 25,371
 - Ta- Ta_2O_5 -Ta Films 25,371
 - Film Memory Devices, Ferrite 25,910
 - Film Memory Units,
 - Ferrite 25,904, 25,905
 - Interaction between Ferrite 25,911
 - Films,
 - Adsorption of:
 - Hydrogen on:
 - Ag 25,125
 - Al 25,125
 - Au 25,125
 - O and Co on Cu_2O 25,384
 - Breakdown in Dielectric 25,330
 - Coercivity of CoNi 25,479
 - Conduction in 25,239
 - Conduction Mechanisms in 25,238
 - Conductivity of PbS 25,263
 - Critical Field of:
 - Pb-Tl Superconducting 25,294
 - Sn-Ag 25,295
 - Crystal Structure of:
 - Ag 24,924
 - Ni 24,923
 - PbTe 25,108
 - Si 25,105
 - Dislocations in Ge 25,000
 - Edge Effect Suppression in Sn-Ag 25,295
 - Exchange Coupling of Magnetic 25,483
 - Ferrimagnetic Relaxation in Parallel Pumped Permalloy 25,524
 - Ferromagnetic Energy Exchange Constant in:
 - Ni 25,505
 - NiCu 25,505

Films, (Cont'd)

Ferromagnetic Resonance in NiFe 25,514, 25,515
 Field Effect in PbS 25,263
 Field Emission from:
 Al-Al₂O₃-Al 25,371
 Ta-Ta₂O₅-Ta 25,371
 Galvanomagnetic Properties of InSb 25,334
 Growth of: 25,393
 Ag 25,101
 Cr/SiO 25,811
 Cu 25,101
 GaAs-Ge 25,102
 Ga(As-P) 25,102
 GaP-Ge 25,102
 Ge 25,103
 PbS 25,109
 PbTe 25,108
 Si 25,104, 25,105
 SiC 25,106
 SiO₂ 25,814
 Si Oxide 25,107
 Hall Coefficient of PbTe 25,108
 Hall Effect in CdS 25,345
 Hall Effect Device Applications of InSb 25,334
 Hall Mobility in CdS 25,345
 Hall Voltage in:
 Ni 25,342
 Ni-Fe 25,342
 Hysteresis in Co 25,460
 Impurities in Ta 25,041
 Impurity Distribution in Si 25,048
 Lattice Parameters of Ag₂Se 24,909
 Lattice Planes in Au 24,925
 Magnetic Anisotropy of: 25,482, 25,483, 25,492
 Co 25,460, 25,493
 Fe 25,493
 FeCo 25,490
 Ni 25,493
 NiFe 25,488
 Permalloy 25,487, 25,499
 Magnetic Annealing of Permalloy 25,442
 Magnetic Domain Rotation in Permalloy 25,503
 Magnetic Domain Wall Interactions in 25,506
 Magnetic Domain Wall Motion in NiFeCo 25,504
 Magnetic Domain Wall Widths in:
 Ni 25,505
 NiCu 25,505
 Magnetic Domains in: 25,492
 Ni-Fe 25,507
 Magnetic Easy Axis of Permalloy 25,484
 Magnetic Properties of:
 Co 25,437
 Fe 25,437
 Ni 25,436, 25,437
 Permalloy 25,441
 Magnetization Creep in:
 Magnetic 25,482
 Ni-Fe 25,455
 Magnetization of Ferromagnetic 25,447
 Magnetization Ripple in Permalloy 25,456-25,459
 Magnetization Switching in 25,464
 Magnetoelastic Coupling Constant of Magnetic 25,390
 Magnetoresistance of:
 Ni 25,342
 Ni-Fe 25,342
 Magnetostriction in 25,393
 Melting of K 24,894
 Mobility in CdS 25,345
 Noise in:
 CuI 25,359
 In₂O₃ 25,359
 Optical Constant Analysis of:
 Dielectric 25,703
 Semiconductor 25,703
 Penetration Depth in Pb-Tl Superconducting 25,312
 Phase Transitions in Ag₂Se 24,909
 Photo-EMF in CdTe 25,697
 Photovoltaic Effect in 25,698

Films, (Cont'd)

Quantized Vortex Phenomena in Sn Superconducting 25,320
 Reflectivity of SiO:Ag, Au 25,705
 Resistivity of:
 CdS 25,345
 PbTe 25,108
 Spin Wave Resonance in Magnetic 25,523
 Spin Waves in Permalloy 25,427, 25,428, 25,431
 Sputtering Equipment for Fabrication of Ta 25,806
 Stress-Strain Properties of Au 25,765
 Surface States in PbS 25,263
 Susceptibility of Cu₂O 25,384
 Switching in:
 Magnetic 25,465-25,469
 Permalloy 25,468
 Thermal Conductivity of:
 In Superconducting 25,734
 Pb Superconducting 25,734
 Sn Superconducting 25,734
 Thickness Measurements of:
 Au 25,100
 Dielectric 25,703
 Semiconductor 25,703
 Transitions in:
 Al Superconducting 25,323, 25,324
 In Superconducting 25,324
 Pb Superconducting 25,324
 Sn Superconducting 25,324

Filters,

Ceramic 26,266
 Crystal Ladder 26,267
 Design of 26,262-26,264
 High Frequency 26,266
 Low Frequency 26,265
 Low Pass 26,266
 RFI 26,268
 Thin Film 26,269
 Tunable 26,265
 Flashers 26,421
 Flip-Flop Switching Circuits 26,213, 26,214
 Floating Crucible Growth, Capillary Design in 25,082
 Flow Controls 26,417
 Flow Meters 26,429
 Fluorescence of:
 Alkali Halides 25,663
 Al₂O₃:Cr 25,672
 Ca₃(VO₄)₂ 24,979
 CsI:TI, Decay of 25,667
 CuCl 25,665
 Eu Benzoylacetate 25,675
 Eu Chelates 25,675
 Eu Chelates in Hosts 25,641
 Group II-VI Compounds 25,669
 PrCl₃:Nd³⁺, Infrared 25,666
 Silicate Glass:Eu 25,639
 Th₂Ag(PO₄)₃:Cu 25,674
 Th₂Cu(PO₄)₃ 25,674
 Th₂Li(PO₄)₃:Cu 25,674
 Th₃(PO₄)₄:Cu 25,674
 Y₂O₃:Eu³⁺ 25,670, 25,671
 ZnS 25,676

Fluorescence Decay Time Analysis, Equipment for 25,668

Fluorescence Lifetime of F-Centers in KCl:Li 25,664
 Fluorine (Solid), Crystal Structure of 24,952
 Fluorite, Phosphorescence in 25,677
 Flux Flow in Superconductors (II) 25,315
 Flux Jumping in:
 Nb-Zr Superconducting Coils 25,316
 Sn Superconducting Films 25,318
 Ti-V Superconductors 25,317
 Flux Penetration in Superconductors 25,309
 Flux in Superconductors 25,314
 FM Generators 26,228
 FM Receivers 26,294
 Formation Energies of V-Cr 24,884
 Four Layer Diodes, Properties of 25,842
 Four Layer Transistors, Oscillations in 25,856
 Four-Point Probe Resistivity Analysis 25,240, 25,241

Fracture in:

Al₂O₃, Ambient Effects on 25,769
 Quartz 25,771
 SiFe 25,768
 Zn 25,018
 Frequency Discriminators 26,230
 Frequency Dividers 26,238
 Frequency Dividers, Integrated 26,125
 Frequency Modulators 26,228
 Frequency Multipliers 26,237, 26,239, 26,240
 Frequency Multipliers, Parametric 26,236
 Frequency Regulators 26,391
 Frequency Standards 26,434
 Fusibility of Ni-Cr-NiAl 24,896

G

Gadolinium,

Curie Temperature of 25,449
 Lorenz Function of 25,735
 Magnetization of 25,449
 Magnetostriction of 25,395
 Thermal Conductivity of 25,735
 Gadolinium Aluminide, Crystal Structure of 24,936
 Gadolinium Cobalt Oxide, Crystal Structure of 24,974
 Gadolinium Germanide, Crystal Structure of 24,936
 Gadolinium Iron Garnet,
 Coercive Force of 25,480
 Magnetic Anisotropy of 25,500
 Magnetization of 25,500
 NMR in 25,598
 Gadolinium Nitride, Magnetic Properties of 25,415
 Gadolinium Trichloride,
 Crystalline Field in 25,137
 Susceptibility of 25,137
 Gallium in Si, Diffusion of 25,075
 Gallium Antimonide,
 Absorption in 25,615
 Defects in 25,042
 Preparation of 25,042
 Purity Limit in 25,042
 Scattering in 25,615
 Gallium Antimonide Laser Diodes, Pressure Effects on 26,037
 Gallium Arsenide,
 Absorption in 25,613, 25,615
 Cathodoluminescence of 25,658
 Data Sheets on 24,860
 Defects in 24,985, 25,828
 Diffusion of:
 Cd in 25,069
 Zn in 25,070-25,073
 Growth of 24,899, 25,091
 Photoconductivity of 25,690
 Scattering in 25,615
 Segregation of Impurities at Solid-Vapor Interface of 24,899
 Solubility of Zn in 25,073
 Zn Diffusion in 25,828
 Gallium Arsenide:Cr, Photoluminescence of 25,659
 Gallium Arsenide:Mn, Photoluminescence of 25,659
 Gallium Arsenide Diodes,
 Characteristics of 26,032
 Luminescence from 26,030
 Properties of 26,025, 26,026
 Radiation from 25,657
 Recombination Radiation from 25,657
 Gallium Arsenide Laser Diodes 26,022, 26,024, 26,028, 26,030
 Gallium Arsenide Laser Diodes,
 Cooperative Effects in 26,017
 Delay Characteristics of 26,019
 Efficiency of 26,021, 26,023
 Emission Characteristics of 26,032
 V-I Characteristics of 26,020
 Infrared 26,031
 Lasing Characteristics of 26,016
 Modulation of 26,015
 Oscillations in 26,027
 Temperature Effects on 26,018

SUBJECT INDEX (Continued)

- Gallium Arsenide Laser Diodes, (Cont'd)
 Theory of 26,011
 Triangular 26,029
- Gallium Arsenide Tunnel Diodes, Deterioration of
 25,071, 25,828
- Gallium Arsenide Varactor Diodes 25,835
- Gallium Arsenide-Germanium Films,
 Growth of 25,102
 Preparation of 25,102
- Gallium Arsenide-Germanium Heterojunctions,
 Growth of 25,102
 Preparation of 25,102
- Gallium Arsenide-Phosphide,
 Fermi Level of 25,150
 Growth of 25,092
 Resistivity of 25,261
- Gallium Arsenide-Phosphide Films,
 Growth of 25,102
 Preparation of 25,102
- Gallium Arsenide-Phosphide Heterojunctions,
 Growth of 25,102
 Preparation of 25,102
- Gallium Arsenide-Phosphide Laser Diodes 26,033,
 26,034
- Gallium Arsenide-Phosphide Laser Diodes,
 Laser Pumping with 25,944
 Material Selection Techniques in 26,035
- Gallium Iron Oxide, Magnetic Anisotropy of 25,497
- Gallium Phosphide,
 Absorption in 25,145, 25,614, 25,615
 Absorption Edge of 25,145
 Diffusion of Zn in 25,072
 Energy Band Structure of 25,145
 Growth of 25,093
 Junction Growth in 25,093
 Luminescence of 25,614
 Reflectivity of 25,145
 Scattering in 25,615
- Gallium Phosphide Junctions,
 Recombination Radiation from 25,145
 Space-Charge-Limited Current in 25,819
- Gallium Phosphide Laser Diodes, Fabrication of
 26,036
- Gallium Phosphide Luminescent Diodes, Fabrication
 of 26,036
- Gallium Phosphide-Germanium Films,
 Growth of 25,102
 Preparation of 25,102
- Gallium Phosphide-Germanium Heterojunctions,
 Growth of 25,102
- Gallium Selenide, Absorption Edge in 25,616
- Gallium Sulfide, Absorption Edge in 25,616
- Galvanomagnetic Coefficients in Ge 25,332
- Galvanomagnetic Properties of:
 InSb Films 25,334
 US 25,333
- Gamma-Ray Detectors 26,437-26,440
- Gamma-Ray Detectors, NaI 26,436
- Gamma-Ray Spectrometers 26,437, 26,439
- Gating Circuits 26,217
- Gating Devices, Superconducting 26,106
- Generation-Recombination Noise 25,358
- Generators,
 Bernoulli Sequence 26,361
 Ferrite 25,901
 FM 26,228
 Hall Effect 25,877, 25,880
 Harmonic 25,832, 26,241
 Pulse 26,152, 26,242-26,249
 Pulse Pattern 26,245
 Ramp 26,152
 Sawtooth 26,238, 26,251
 Square Wave 26,252
 Staircase 26,152
 Superconducting 26,102
 Sweep 26,250, 26,304
 Thermoelectric 26,078-26,080
 Time Mark 26,435
 Vector Product 25,880
- Germanium,
 Absorption in 25,609, 25,611
- Germanium, (Cont'd)
 Absorption Edge in 25,610
 Breakdown in 25,329
 Carrier Drift Velocity in 25,231
 Conductivity of 25,265
 Crystal Structure of 24,928
 Dielectric Constant of 25,144
 Dielectric Susceptibility of 25,196
 Effective Mass of 25,144
 Electron-Phonon Interactions in 25,206
 Energy Band Structure of 25,144
 Energy Gap of 25,147
 Galvanomagnetic Coefficients in 25,332
 Grüneisen Constant of 25,739
 Lifetime in 25,212
 Lifetime in Irradiated 25,217
 Magnetoresistivity of 25,336, 25,337
 Mobility of Electrons in 25,226
 Optical Properties of 25,144
 Oxidation of 25,122
 Photoelectromagnetic Effect in 25,700
 Piezoresistivity of 25,259
 Reduction of 25,122
 Scattering of Donors in 25,230
 Surface Conductivity of 25,265
 Surface Structure of 24,921
 Susceptibility of 25,196
 Thermal Conductivity of 25,737
 Thermal Expansion of 25,739, 25,740
 Thermoelectric Power of 25,745
 Ultrasonic Wave Propagation in 25,777
- Germanium: Au,
 Conductivity of 25,266
 Negative Resistivity of 25,270
 Resistivity of 25,270
 Surface Conductivity of 25,266
- Germanium in Cu, Diffusion of 25,060
- Germanium Films,
 Dislocations in 25,000
 Growth of 25,103
- Germanium Junctions, Stress Effects in 25,818
- Germanium Dioxide,
 Ultrasonic Attenuation in 25,783
 Ultrasonic Relaxation in 25,783
- Germanium Tetrachloride, Vapor Pressure of 24,890
- Glass,
 Hall Effect in 25,350
 Hall Effect-Seebeck Anomaly in 25,351
 Relaxation in 25,783
 Semiconducting Oxide 25,131
 Ultrasonic Attenuation in 25,783
- Glass:Nd Lasers,
 Hair Trigger Operation of 26,001
 Materials for 26,002
 Modes in 25,999
 Properties of 26,003
 Sun-Pumped 25,998
- Glass:Na³⁺ Lasers 26,004
- Glass:Na³⁺ Lasers, Quenching Effects in 26,000
- Glaze Resistors, Properties of Pd-Ag Glass 25,809
- Glide in Zn, Irradiation Effects on 25,774
- Gold,
 Diffusion of:
 Ag in 25,060
 In in 25,062
 Ti in 25,060
 Stacking Fault Energy of 25,029
 Stacking Fault Tetrahedra in 25,030, 25,031
- Gold:Co⁵⁷,
 Lattice Dynamics of 25,154
 Mössbauer Effect in 25,154
- Gold in:
 Ag, Diffusion of 25,060
 Cu, Diffusion of 25,060
 In, Diffusion of 25,062
- Gold Films,
 Adsorption of Hydrogen on 25,125
 Lattice Planes in 24,925
 Stress-Strain Properties of 25,765
 Thickness Analysis of 25,100
- Gold Wires, Thermoelectric Power of Vacancies in
 25,747
- Gold-Chromium, Magnetic Transitions in 25,404
- Gold:Iron Foils,
 Ferromagnetic 25,403
 Magnetic Ordering in 25,403
 Mössbauer Effect in 25,403
- Gold-Iron,
 Curie Temperature of 25,450
 Magnetic Transitions in 25,404
 Magnetization of 25,450, 25,463
 Remanence of 25,463
- Gold-Manganese, Magnetic Transitions in 25,404
- Gold-Silver, Dislocation Relaxation in 25,013
- Grain Boundaries in:
 Cu 25,026
 LiF, Migration of 25,028
 Mg 25,027
- Graphite,
 Carrier Scattering in 25,257
 Crystal Structure of 24,949
 Crystal Structure of Pyrolytic 24,948
 Elastic Constants of 25,759, 25,760
 Fermi Surface of 25,257
 Hall Coefficient of 25,257
 Lattice Vibrations in 24,949
 Magnetoresistance of 25,257
 Oxidation of Pyrolytic 25,120
 Resistivity of 25,257
 Thermal Expansion of 24,949
 Vacancies in 24,989
 Volume Expansion of 25,755
- Graphite Dendrites, Twins in 25,021
- Graphite Thermocouples 26,082
- Graphite Thermocouples, Performance of 26,081
- Group II-VI Compounds,
 Advances in 24,958
 Fluorescence in 25,669
- Group II-VI Semiconductors, Fermi Level of 25,150
- Group III-V Compounds, Advances in 24,859
- Group III-V Semiconductors, Fermi Level of 25,150
- Group IV Semiconductors, Fermi Level of 25,150
- Growth of - See also Preparation of
- Growth of:
 Ag Films 25,101
 AlN Whiskers 25,110
 Al₂O₃ 25,094
 BaTiO₃ 25,089, 25,090
 Bi-Sb 25,098
 Bi₄Ti₃O₁₂ 25,187
 CaF₂ 25,086
 Cr/SiO Films 25,811
 Cu 25,083
 Cu Films 25,101
 Cu₂O 25,084
 GaAs 24,899, 25,091
 GaAs-Ge Films 25,102
 Ga(As-P) 25,092
 Ga(As-P) Films 25,102
 GaP 25,093
 GaP-Ge Films 25,102
 Ge Films 25,103
 Hexagonal Ferrites 25,099
 HgS 25,088
 Homogeneous Crystals 25,081
 K₂O·nTa₂O₅ 24,978
 LaF₃ 25,096
 LiF 25,085
 Oxides 25,078
 PbS Films 25,109
 PbTe Films 25,108
 Pb(Ti-Zr)O₃ 25,097
 Rb_xK_{1-x}NO₃ 25,189
 Refractories 25,078
 Se Whiskers 25,111
 Si Films 25,104, 25,105
 SiC Films 25,106
 Si Oxide Films 25,107
 SiO₂ Films 25,814
 UC 25,095
 ZnO 25,087
 ZnWO₄ 25,994

SUBJECT INDEX (Continued)

- Grüneisen Parameter - See also Specific Heat
Grüneisen Parameters of:
 Ge 25,739
 Inert Gases (Solid) 25,722
Gyroelectric Crystals, Optical Rotation in 25,716
- H
- Hafnium Carbide, Heat Capacity of 25,732
Hafnium-Carbon Systems,
 Phase Equilibria in 24,865
 Vaporization of 24,865
Hafnium-Plutonium, Lattice Constants of 24,931
Hall Constant of:
 CdSb-Au 25,256
 CdTe-CdSe 25,168
 Co_{1-x}Fe_xSi 25,166
 Graphite 25,257
 InSb 25,340
 InSb-CdTe 25,169
 PbTe 25,348
 PbTe Films 25,108
 Semiconductors 25,233
 US 25,333
Hall Effect,
 Bibliography on 25,344
 Ferromagnetic 25,346
Hall Effect in:
 Bi-Te 25,167
 CdS Films 25,345
 Ferromagnets 25,353
 Nickel Oxide 25,349
 PbS Layers 25,253
 Se 25,347
 Semiconducting Glasses 25,350
 SiC 25,251
 TiO₂, Anisotropy of 25,352
Hall Effect Compass 26,289
Hall Effect Device Applications of InSb Films 25,334
Hall Effect Devices, Bibliography on 25,344
Hall Effect Generators,
 Design of 25,875
 Review on 25,877
Hall Effect Isolators 25,883
Hall Effect Logic Elements, Ternary 25,882
Hall Effect Magnetometers 25,878, 26,426
Hall Effect Multipliers 25,881
Hall Effect Multipliers, Vector Product 25,880
Hall Effect-Seebeck Anomaly in Semiconducting
 Glasses 25,351
Hall Effect Sensors,
 Design and Performance of 25,879
 Development of 25,878
 Noise in 25,876
Hall Effect Vector Product Generators 25,880
Hall Mobility of:
 CdS Films 25,345
 KBr 25,228
 KCl 25,228
 KI 25,228
 NaCl 25,228
 Semiconductors, Minority Carrier 25,227
Hall Voltage in:
 Ni 25,342
 Ni-Fe Films 25,342
Harmonic Generators 26,241
Harmonic Generators,
 Diode 25,832
 Ferrite 25,901
Hearing Aid Amplifiers 26,181
Heat Capacity - See also Specific Heat
Heat Capacity of:
 AlCl₃ 25,732
 Al₂O₃ 25,732
 B 25,732
 BN 25,732
 B₂PO₃ 25,732
 BeF₂ 25,730
 BeO 25,732
 D (Solid) 25,724
 EuS 25,726
 Heat Capacity of: (Cont'd)
 HD 25,725
 HFC 25,732
 LiBO₂ 25,732
 LiCl 25,732
 MnCl₂, Magnetic Field Effects on 25,729
 NaBr 25,727
 NaI 25,727
 NbC 25,732
 P₂O₅ 25,732
 PuC 25,731
 TaC 25,732
 TiB₂ 25,732
 TiN 25,732
 WB 25,732
 W₂B₅ 25,732
 WC 25,732
 ZrB₂ 25,732
 ZrC 25,732
 Heat of Formation of AlC 24,885
 Heat Pumps, Thermoelectric 26,458, 26,459
 Heat of Sublimation of B 24,886, 24,887
 Heisenberg Antiferromagnets, Green Functions in
 Theory of 25,531
 Heisenberg Ferromagnets,
 Spin-Wave Scattering in 25,424
 Spin-Waves in 25,423
 Heisenberg Spin Model 25,372
 Helium in Si 25,043
 Hematite, Antiferromagnetic Spin Flop in 25,534
 Heterojunctions,
 CdS Thin Film 25,843
 GaAs-Ge 25,102
 GaP-Ge 25,102
 Growth of 25,102
 Properties of 25,102
 Hexagonal Ferrites,
 Growth of 25,099
 Magnetization of 25,099
 High Field Effects in Junctions 25,821
 High Frequency Filters 26,266
 High Gain Transistors 25,873
 High Impedance Amplifiers 26,151
 High Power Demodulators 26,232
 High Power Pulse Generators 26,248, 26,249
 Hole Lifetime in CdTe 25,215
 Hole Trapping in Anthracene 25,220, 25,221
 Holmium,
 Magnetic Ordering of 25,408
 Magnetic Transitions in 25,408
 Holmium Cobalt, Magnetic Structure of 25,402
 Holmium Iron Garnet,
 Magnetic Anisotropy of 25,500
 Magnetization of 25,500
 Homogeneous Crystals, Growth of 25,081
 Hot Carrier Drift Velocity in Ge 25,231
 Hot Electron Transistors, Survey of 25,858
 Human Pulse Rate Meters 26,273, 26,274
 Hybrid Amplifiers 26,169
 Hydrogen Deuterium (Solid), Heat Capacity of
 25,725
 Hydrogen-Platinum-Palladium,
 Absorption Isotherms in 24,934
 Lattice Constants of 24,934
 Phase Boundaries in 24,934
 Hypergyroelectric Crystals, Optical Rotation in
 25,716
 Hysteresis, Dynamic Pulse Measurement of 25,474
 Hysteresis in Co Films 25,460
- I
- Ice,
 Absorption in 25,636, 25,637
 Etch Pits on 25,129
 Raman Spectra of 25,645
Ignition Systems 26,279-26,283
Image Display Units 26,378, 26,379
Impurities in Ta Films, Determination of 25,041
Impurity Analysis, Electron Spectroscopy in 25,040
Impurity Clustering in Al-Zn 25,049
Impurity Distribution in:
 Si Films 25,048
 Zone Melting 25,047
Impurity Lines in Si 25,044
Impurity States in Crystals 25,148
INCLUSIVE/OR Logic Circuits 26,328
Indium, Diffusion of Au in 25,062
Indium in Au, Diffusion of 25,062
Indium¹¹⁵ in Pb-In, NMR of 25,588
Indium Superconducting Films,
 Thermal Conductivity of 25,734
 Transitions in 25,324
Indium Antimonide,
 Adsorption of Alcohol in 25,267
 Conductivity of 25,268
 Field Effect Mobility in 25,267
 Inversion Layer on 25,268
 Layer Structure of 25,038
 Photoconductivity of 25,268
 Photoconductivity Oscillations in 25,693
 Photoemission in 25,268
 Surface Conductivity of 25,267, 25,268
 Surface Potential of 25,267
 Vapor Pressure of 24,889
Indium Antimonide Corbino Disks, Magnetoresistivity
 of 25,338
Indium Antimonide Detectors 26,047
Indium Antimonide Films,
 Galvanomagnetic Properties of 25,334
 Hall Effect Device Applications of 25,334
Indium Antimonide-Cadmium Telluride,
 Carrier Concentration of 25,169
 Conductivity of 25,169
 Electrical Properties of 25,169
 Hall Constant of 25,169
 Mobility in 25,169
 Thermal Conductivity of 25,169
Indium Arsenide,
 Conductivity of 25,340
 Hall Constant of 25,340
 Magnetoresistivity of 25,340
 Negative Magnetoresistivity of 25,340
Indium-Lead Superconductors,
 Lattice Parameters of 25,282
 Properties of 25,282
Indium Oxide Films, Noise in 25,359
Indium Phosphide,
 Absorption in 25,615
 Diffusion of Zn in 25,074
 Scattering in 25,615
 Solubility of Zn in 25,074
Indium Phosphide Laser Diodes 26,038
Indium Phosphide Arsenide Laser Diodes 26,039
Indium Telluride (In₂Te₃),
 Conductivity of 24,867
 Phase Transitions in 24,867
Indium-Tellurium,
 Phase Diagram of 24,867
 Phase Transitions in 24,867
Indium-Tin Superconductors,
 Lattice Parameters of 25,282
 Properties of 25,282
Inductors, Microcircuit 26,128
Inert Gases (Solid), Grüneisen Parameters of 25,722
Infrared Absorption in:
 B₂F₄ 25,628
 Fe(CO)₅ 25,632
 GaAs 25,615
 GaP 25,615
 GaSb 25,615
 Ge 25,609
 H₂O (Solid) 25,636, 25,637
 InP 25,615
 KBr 25,622
 KCl 25,622
 Mg₂Sn 25,633
 Na Azide 25,635
 NaNO₃ 25,190
Infrared Emission from CdS 24,982
Infrared Fluorescence of PrCl₃:Nd³⁺ 25,666
Infrared Lasers 25,986, 26,028, 26,031, 26,039

SUBJECT INDEX (Continued)

Infrared Reflectance of:

KMgF₃ 25,708
MgF₂ 25,708
Mg₂Sn 25,633
Semiconductors 25,223
ZnSe 25,224

Infrared Transmittance of:

KMgF₃ 25,708
MgF₂ 25,708

Integrated Circuits,

Design of 26,122-26,124
Review on 26,115, 26,116

Integrated Frequency Dividers 26,125

Internal Field in FePd 25,409

Interstitials to Dislocations, Segregation of 24,898

Interstitials in:

Fe, Kinetics of 24,987
Noble Metals, Migration of 24,994

Inversion Layer on InSb 25,268

Inverters 26,393-26,399, 26,403

Inverters, SCR 26,392

Ion Emission from:

BaO 25,360
W 25,361-25,363

Ionic Conductivity of:

Cd Emulsion Grains 25,214
KI 25,254

Ionic Crystals,

Covalency in 25,133
Luminescence of 25,647
Paramagnetic Relaxation in 25,566
Paramagnetic Resonance in 25,566

Ionization Rates in Si, Carrier 25,232

Iridium:Co⁵⁷,

Lattice Dynamics of 25,154
Mössbauer Effect in 25,154

Iron,

Barkhausen Effect in 25,473
Carbon Precipitation in 24,907
Dislocations in 25,767
Fatigue in 25,767
Interstitials in 24,987

Magnetic After Effect Zones in Neutron Irradiated 25,470

Oxidation of 25,115-25,117
Vacancies in 24,987

Iron in Ag, Diffusion of 25,061

Iron Ferromagnetic Alloys, Properties of 25,417

Iron Films,

Magnetic Anisotropy of 25,492, 25,493
Magnetic Domains in 25,492
Magnetic Properties of 25,437

Iron Whiskers, de Haas-van Alphen Effect in 25,151

Iron Aluminum,

Coercive Force in 25,438
Knight Shift in 25,590
NMR in 25,590
Permeability of 25,438, 25,454
Remanence in 25,438
Resistivity of 25,438

Iron Arsenide (Fe₂As),

Antiferromagnetic Structure of 25,540
Magnetic Structure of 25,540

Iron Carbonate, Absorption in 25,632

Iron-Carbon, Defects in 24,981

Iron Cobalt Films, Magnetic Anisotropy of 25,490

Iron-Cobalt-Carbon, Diffusion of C in 25,068

Iron Formate,

Magnetic Fields in 25,382
Mössbauer Study of 25,382
Susceptibility of 25,382

Iron Germanium, Magnetic Anisotropy of 25,494, 25,496

Iron Nickel,

Curie Temperature of 25,445
Magnetization of 25,445

Iron Nickel Ferromagnets, Nuclear Magnetic Relaxation in 25,526

Iron Palladium,

Internal Field in 25,409
Mössbauer Effect in 25,409

Iron Rhodium,

Magnetic Moments in 25,410
Spin Densities in 25,410

Iron-Rhodium-Transition Metals, Magnetic Properties of 25,416

Iron-Vanadium, Polymorphic Transitions in 24,904

Iron-Zinc Ferrite,

Lattice Constant of 24,946
Phase Boundaries in 24,946

Irradiation Produced Vacancies 24,992

Isolators,

Ferrite 25,885, 25,886, 25,892
Hall Effect 25,883

J

Junction Capacitance Switches, Design of 25,837

Junction Detectors 26,439, 26,440, 26,443-26,446, 26,448

Junction Formation in Si, Alkali Ion 25,050

Junctions - See also Diodes

Junctions,

Breakdown in: 25,331, 25,821
Microplasma-Free 25,232

Si 25,822

Stressed Si 25,816

Carrier Diffusion through 25,820

Current in Stressed Si 25,817

GaP 25,145

High Field Effects in 25,821

High Frequency Properties of Si 25,834

Microplasmas in Si 25,822

Radiation Effects on 25,815

Recombination Radiation from GaP 25,145

Space-Charge-Limited Current in GaP 25,819

Stress Effects in: 25,816

Si 25,817

Superconducting 25,326

Junctions in GaP, Growth of 25,093

K

Knight Shift in:

Ag Solid Solutions 25,600

Al₂FeCo 25,590

Al₂FeNi 25,590

Al₂NiCo 25,590

Al-V-Tc 25,601

CoAl 25,590

CoTi 25,590

Cu Solid Solutions 25,600

FeAl 25,590

NiAl 25,590

Pb Alloys 25,589

Pt 25,602

Superconductors 25,599

Kramers-Kronig Transformation, Computer Program on 25,704

L

Lanthanum Superconductors, Mechanism for 25,283

Lanthanum Aluminate, NMR of La¹³⁹ and Al²⁷ in 25,586

Lanthanum Aluminate:Fe³⁺, Paramagnetic Resonance of 25,586

Lanthanum Cobalt Oxide, Magnetic Properties of 25,414

Lanthanum Fluoride, Growth of 25,096

Lanthanum Tellurides 24,863

Laser - See also Maser

Laser Applications in:

Acoustic Generation in Liquids 26,069
Biology 26,058, 26,060

Communication Systems 26,061

Continental Drift Measurements 26,072

Inertial Guidance 26,066, 26,067

Light Scattering by Gases 26,070

Metalworking 26,073-26,075

Microwelding 26,075, 26,129

Radar 26,318

Laser Applications in: (Cont'd)

Ranging Systems 26,063, 26,064

Rotation Rate Detection 26,066, 26,067

Speed of Light Measurements 26,068

Simulating Meteoroid Impacts 26,071

Laser Attenuators 26,051

Laser Beam Effects 26,058

Laser Beam Effects in Metals 26,073

Laser Blinding 26,059

Laser Detectors 26,047, 26,048

Laser Diodes,

Bi-Sb 26,040

Characteristics of 26,014

Current Dependence of 26,013

Delay Characteristics of 26,019

Efficiency of 26,021, 26,023

V-I Characteristics of 26,020

GaAs 26,011, 26,015-26,032

GaAs_xP_{1-x} 26,033-26,035

GaP 26,036

GaSb 26,037

Infrared 26,028, 26,031

InP 26,038

InP_xAs_{1-x} 26,039

Modulation of 26,015

Laser Heated:

BaO Cathodes, Emission from 25,360

W Cathodes, Emission from 25,361, 25,362

Zn, Photoemission from 25,366

Laser Induced Photocurrents in Anthracene 25,691

Laser Light Source, Xe Flash Tube 26,052

Laser Mixers 26,049

Laser Modulators 26,041-26,046

Laser Output Monitor 26,056

Laser Pumped Microwave Masers 25,992

Laser Pumped Millimeter Wave Masers 25,997

Laser Pumping with GaAs Laser Diodes 25,944

Laser Pumping Source, Xe Flash Tube 26,052

Laser Resonators 26,054, 26,055

Laser Safety Procedures 26,059

Lasers,

Application Parameters of 25,957

Bandwidth of 25,963

Beam Angle of 25,965

Bibliography on 25,918

CaF₂:Dy²⁺ 25,944, 26,007

CaF₂:Er³⁺ 25,625

CaF₂:Tm²⁺ 26,007

CaF₂:U³⁺ 26,008

CaMoO₄:Nd 26,009

Cathodoluminescent Pumping of 25,945

CaWO₄:Nd 25,945

CaWO₄:Nd³⁺ 25,956

Coherence Brightened 25,931

Coherence between Superposed Light Beams in 25,966

Coherence Time of Pulsed 25,967

Conditions for Operation of 25,929

Continuous Wave 25,968

Crystal Quality Effects in 25,941

Distribution of Radiation from 25,964

Double Quantum 25,942

Emission from 25,938, 25,960

Emission at Liquid Nitrogen Temperatures from 25,939

Emission Properties of Diode 26,012

Emission Studies on 25,959

Geometry Effects in 25,964

Glass:Nd 25,998-26,003

Glass:Na³⁺ 26,000, 26,004

Hair Trigger Operation of 26,001

Infrared 25,986, 26,028, 26,031, 26,039

Interference between Beams from 25,972

Interference Effects in 25,971

Inversion in 25,934

Line Splitting in 25,969

Loss in 25,974, 25,975

Mode Beat Detection System for 26,057

Mode Selection in 25,950

Mode Selection System for 26,050

Mode Suppression in 25,951

SUBJECT INDEX (Continued)

Lasers, (Cont'd)

- Modes in 25,949, 25,952-25,954, 25,999
- Modulation of 25,946, 25,947, 26,042
- Multihole Diaphragm 25,937
- Multimoding in 25,948
- Oscillations in 25,926, 26,956
- Output Control of 25,946
- Output Energy of 25,965
- Output Parameters of 25,957
- Photon-Phonon Interactions in 25,970
- Population Density in 25,933
- Population Distributions in 25,922
- Pulse Propagation in 25,976
- Pumping of 25,943, 25,944
- Quenching Effects in 26,000
- Radiation Properties of 25,961
- Raman 25,989
- Relaxation Spikes in 25,928
- Resonator Influence on 25,955
- Review on 25,919, 25,920
- Ruby 25,932, 25,934, 25,938-25,941, 25,952-25,955, 25,959-25,967, 25,969, 25,972, 25,975, 25,982, 25,983, 25,999
- Running Waves in 25,958
- Scattering Losses of 25,973
- Semiconductor 26,010
- Studies on 25,936
- Sun-Pumped 25,998
- Switching of 26,053
- Temperature Effects in 25,938
- Theory of 25,927
- Threshold Populations in 25,932
- Travelling Wave 25,982, 25,983
- X-Ray 25,987
- YAG:Na³⁺ 26,005
- Y₂O₃:Er³⁺ 26,006

Lasers in Refractive Analysis 25,712

Lattice Constants - See also Crystal Structure

Lattice Constants of:

- Ag-Pd, Temperature Dependence of 24,932
- Ag₂Se Films 24,909
- Ag-Zn-Mn 24,933
- Austenite, Low Temperature Effects on 24,927
- Co Double Sulphates 24,942
- CsCl 24,941
- D-Pt-Pd 24,934
- Fe-Zn Ferrite 24,946
- H-Pt-Pd 24,934
- Hf-Pu 24,931
- In-Pb Superconductors 25,282
- In-Sn Superconductors 25,282
- Martensite, Low Temperature Effects on 24,927
- Mo₃Al₂C Superconductors 25,280
- NaCl 24,941
- Rare Earth Orthoferrites 25,412
- Rb_xK_{1-x}NO₃ 25,189
- Sc-Pu 24,931
- Sn-In 24,930
- ThC₂ 24,935
- UC 24,879
- U-Pu 24,931
- Yttrium Orthoferrite 25,412
- Zr-Pu 24,931

Lattice Energies of:

- CsCl 24,941
- NaCl 24,941

Lattice Dynamics of:

- Au:Co⁵⁷ 25,154
- Cu:Co⁵⁷ 25,154
- Ir:Co⁵⁷ 25,154
- Nb 25,160
- Pd:Co⁵⁷ 25,154
- Pt-Co⁵⁷ 25,154
- Rh:Co⁵⁷ 25,154
- SrTiO₃ 25,155
- Ti:Co⁵⁷ 25,154

Lattice Fields, Theory of 25,135

Lattice Planes in Au Films 24,925

Lattice Potential of:

- CsCl 25,138

Lattice Potential of: (Cont'd)

- Cubic Lattices 25,136
- NaCl 25,138
- Lattice Potentials, Calculation of 25,136
- Lattice Structure, Factor Algebra of 24,926
- Lattice Vibrations,
 - Computer Calculation of 25,159
 - Frequency Distribution Function for 25,158
 - Relaxation in 25,157

Lattice Vibrations in:

- bcc Lattices 25,156
- Be 25,162
- C 24,949
- Graphite 24,949
- LiH₃(SeO₃)₂ 25,634
- Metals 24,893
- Mg 25,162
- NaH₃(SeO₃)₂ 25,634
- Ni 25,161
- (NH₄)₂SO₄ 25,634
- Quartz 24,919
- RbHSO₄ 25,634
- Zn 25,162

Layer Structure of InSb 25,038

Lead, Fermi Surface of 25,151

Lead Alloys,

- Knight Shift in 25,589
- NMR in 25,589
- Lead Superconducting Films,
 - Thermal Conductivity of 25,734
 - Transitions in 25,324

Lead Superconducting Junctions,

- Energy States in 25,326
- Tunneling in 25,326

Lead Superconductors, Surface Superconductivity in 25,305

Lead Bromide, Absorption in 25,627

Lead Chloride: Cd, Absorption in 25,627

Lead-Hafnium-Titanium-Tin-Niobium-Oxide Solid Solutions, Dielectric Properties of 25,188

Lead-Indium, NMR of In¹¹⁵ in 25,588

Lead Potassium Ferrites, Magnetic Anisotropy of 25,495

Lead Selenide,

- Data Sheets on 24,861
- Reflectivity of 25,706
- Lead Sulfide, Reflectivity of 25,706

Lead Sulfide Films,

- Conductivity of 25,263
- Field Effect in 25,263
- Growth of 25,109
- Surface States in 25,263

Lead Sulfide Layers,

- Conductivity of 25,253
- Hall Effect in 25,253
- Thermal EMF of 25,253

Lead Telluride,

- Cyclotron Resonance Absorption in 25,357
- Data Sheets on 24,862
- Effective Mass in 25,252
- Energy Band Structure of 25,142
- Hall Constant of 25,348
- Resistivity of 25,252
- Scattering in 25,252
- Seebeck Coefficient of 25,252

Lead Telluride Films,

- Crystal Structure of 25,108
- Growth of 25,108
- Hall Coefficient of 25,108
- Resistivity of 25,108

Lead-Tellurium System, Partial Pressures in the 24,891

Lead-Thallium Superconducting Films,

- Critical Field of 25,294
- Penetration Depth in 25,312

Lead Thallium Superconductors,

- Critical Field of 25,293
- Surface Superconductivity in 25,305
- Upper Critical Field of 25,293

Lead Titanate: Fe³⁺, Paramagnetic Resonance of 25,579

Lead Titanate-Zirconate, Growth of 25,097

Lead Zirconate-Titanate, Pyroelectricity of 25,201.

Lifetime - See also Trapping; Recombination

Lifetime Analysis, Photoelectric 25,212

Lifetime in:

- Cd Emulsion Grains 25,214
- CdTe, Hole 25,215
- Ge 25,212
- Ge, Irradiation Effects on 25,217
- Semiconductors 25,213
- Si 25,212

Lighting Controls 26,421

Limiters, Ferrite 25,893

Liquid Conductivity Meters 26,424

Liquid Flow Controls 26,417

Liquid Level Controls 26,416

Lithium Chloride, Heat Capacity of 25,732

Lithium Fluoride,

- Absorption in 25,752
- Coloration of 25,752
- Defects in 24,984
- Electron Microscope Analysis of 24,984
- Grain Boundary Migration in 25,028
- Growth of 25,085
- Thermoluminescence of 25,662
- Vacancies in 25,752
- Volume Expansion in 25,752

Lithium Fluoride:Mn, NMR in 25,593

Lithium Hydrazinium Sulfate, Crystal Structure of 24,956, 24,957

Lithium Hydrogen Selenate,

- Absorption in 25,634
- Ferroelectric Transitions in 25,634
- Lattice Vibrations in 25,634

Lithium Metaborate,

- Crystal Structure of 24,944
- Heat Capacity of 25,732

Localized States in Crystals 25,148

Logic Circuits - See also Switching Circuits

Logic Circuits,

- AND 26,323, 26,327-26,329
- Design of 26,322
- DTL 26,331, 26,333
- EXCLUSIVE/OR 26,325, 26,326, 26,328
- INCLUSIVE/OR 26,328
- Integrated 26,339
- Magnetic 26,335
- Magnetic Core 26,336, 26,337
- Modular 26,340
- NAND 26,332
- NOR 26,324, 26,332
- NOT 26,327
- OR 26,323, 26,327, 26,329
- RDTL 26,331, 26,332
- Reliability of 26,323
- RTL 26,333
- Safety Circuit for 26,341
- Storage 26,329
- TDTL 26,334
- Ternary 26,329
- Tunnel Diode 26,330

Logic Elements,

- Hall Effect 25,882
- Ternary 25,882

Lorenz Function of Gd 25,735

Low Frequency Filters 26,265

Low Noise Amplifiers 26,151, 26,186

Low Pass Filters 26,266

Low Power Amplifiers 26,181, 26,184, 26,185

Luminescence - See also Electroluminescence; Fluorescence; Phosphorescence; Photoluminescence; Thermoluminescence; Cathodoluminescence, Radioluminescence

Luminescence, Review of 25,646

Luminescence of:

- Alkali Halides: S 25,648
- Alkaline Earth Phosphates 25,649
- Al₂O₃ 25,647
- Ba₂P₂O₇ 25,649
- Ca₂P₂O₇ 25,649

SUBJECT INDEX (Continued)

Luminescence of (Cont'd)

- (Ca-Pb)WO₄:Sm 25,651
- CaTa₂O₆ 25,650
- CdS 25,687
- GaP 25,614
- Ionic Crystals 25,647
- KNO₃ 25,652
- Mg₄Nb₂O₉ 25,650
- Niobates 25,650
- Sr₃(P₃O₁₀)₂:Cu 25,649
- Tantalates 25,650
- ZnTa₂O₆ 25,650
- Luminescent Diodes 26,013
- Luminescent Diodes, GaP 26,036

M

M-Centers in:

- KBr, Bleaching of 24,990
- KCl, Bleaching of 24,990
- Magnesia-Magnesium Fluoride-Germanium-Lithium Fluoride Systems, Thermo-dynamic Data on 24,866

Magnesium,

- Grain Boundary Cavities in 25,027
- Lattice Vibrations in 25,162
- Substructure of 25,027
- Thermal Expansion of 25,741

Magnesium in Al, Diffusion of 24,988

- Magnesium-Aluminum, Magnetoresistivity of 25,343
- Magnesium-Cadmium, Magnetoresistivity of 25,343
- Magnesium Cadmium (Mg₃Cd), Order-Disorder Transitions in 24,906

Magnesium Chloride, Emission from 25,643

- Magnesium Ferrous Ferrite, Magnetic Resonance of 25,518

Magnesium Fluoride,

- Reflectance of 25,708
- Transmittance of 25,708
- Magnesium Formate Dihydrate, Crystal Structure of 24,970

Magnesium-Manganese, Magnetoresistivity of 25,343

Magnesium Niobate,

- Absorption Edge in 25,650
- Luminescence of 25,650
- Photoluminescence of 25,650

Magnesium Oxide,

- Crack Nucleation in 25,036
- Diffusion of Xe in 25,077
- Dislocations in 24,996
- Elastic Constants of 25,761
- Ultrasonic Absorption in 25,791

Magnesium Oxide:Cr³⁺, Paramagnetic Resonance Absorption in 25,572

Magnesium Oxide:Mn⁴⁺, Paramagnetic Resonance of 25,583

Magnesium Oxide-Magnesium Chromium Oxide, Phase Diagram of 24,882

Magnesium Oxide-Vanadium Pentoxide, Phase Diagram of 24,881

Magnesium Oxide-Yttrium Oxide, Thermal Expansion of 25,742

Magnesium Tin,

- Absorption in 25,633
- Reflection of 25,633

Magnetic After Effect Zones in Fe 25,470

Magnetic Amplifiers 26,191-26,193, 26,419

Magnetic Analysis, Balance for 25,377

Magnetic Anisotropy, Green Functions for 25,481

Magnetic Anisotropy of:

- BaK Ferrites 25,495
- Co Films 25,460, 25,493
- CoFe, Cold Roll Induced 25,491
- CoNi Ferrite 25,498
- CrI₃ 25,439
- CuNiCo 25,486
- CuNiFe 25,486
- DyIG 25,500
- ErIG 25,500
- Fe Films 25,492, 25,493

Magnetic Anisotropy of: (Cont'd)

- FeCo Films 25,490
- FeGaO₃ 25,497
- Fe-Ge 25,496
- Fe₃Ge₅ 25,494
- Ferrites 25,485
- GdIG 25,500
- HoIG 25,500
- Magnetic Films 25,482, 25,483
- Ni₃Fe 25,399
- Ni-Fe Ferrites 25,489
- Ni Films 25,493
- NiFe Films, Composition Effects on 25,488
- PbK Ferrites 25,495
- Permalloy Films 25,499
- Permalloy Films, Formation Condition Effects on 25,487

SmIG 25,500

SrK Ferrites 25,495

TbIG 25,500

YbIG 25,500

YIG 25,500

Magnetic Annealing of:

- CuNiCo 25,486
- CuNiFe 25,486
- Ni₃Fe 25,399
- Permalloy Films 25,442

Magnetic Anomaly in Ni-Fe-Co Ferrites 25,501

Magnetic Core Encoders 26,360

Magnetic Core Memory Array 26,348

Magnetic Domain Rotation in Permalloy Films 25,503

Magnetic Domain Wall Interactions in Permalloy 25,506

Magnetic Domain Wall Motion in NiFeCo Films 25,504

Magnetic Domain Wall Widths in:

- Ni Films 25,505
- NiCu Films 25,505

Magnetic Domains in:

- Fe Films 25,492
- Ni Platelets 25,508
- Ni-Fe Films 25,507

Magnetic Drum Memory Units 26,351, 26,352

Magnetic Easy Axis of Permalloy Films 25,484

Magnetic Fields in:

- Fe Formate 25,382
- Ni Formate 25,382
- Superconducting Sheets 25,453

Magnetic Film Compass 26,288

Magnetic Films,

- Exchange Coupling of 25,483
- Magnetic Anisotropy of 25,482, 25,483
- Magnetization Creep in 25,482
- Magnetization Switching in 25,464
- Magnetoelastic Coupling Constant of 25,390
- Spin Wave Resonance in 25,523
- Switching of 25,465, 25,467-25,469

Magnetic Hysteresis Properties of Ni-Mn Ferrites 25,475

Magnetic Layers, Magnetization Coupling between 25,471

Magnetic Logic Circuits 26,335

Magnetic Memory Units, Core Stepping Circuit for 26,345

Magnetic Moments of:

- Fe-Rh 25,410
- Rare Earth-Cu Compounds 25,509
- Rare Earth₃Mn₂₃ 25,411
- YAlIG:Bi 24,969

Magnetic Multivibrators 26,204, 26,205

Magnetic Ordering, High Temperature Expansions of 25,397

Magnetic Ordering of:

- Au:Fe Foils 25,403
- Dy 25,408
- Er 25,408
- Ho 25,408
- Ni₃Fe 25,399
- Rare Earth Alloys 25,408
- Tb 25,408
- Tm 25,408

Magnetic Permeability of:

- FeAl 25,438
- FeAl Alloys, Relaxation of 25,454

Magnetic Properties of:

- Ag-Gd 25,249
- CaCoO₃ 25,414
- Co Films, Deposition Angle Dependence of 25,437
- CuF₂ 25,413
- Fe Films, Deposition Angle Dependence of 25,437
- Fe-Rh-Transition Metals 25,416
- Ferrites, Irradiation Effects on 25,435
- GdCoO₃ 24,974
- GdN 25,415.
- Ni Films,

- Deposition Angle Dependence of 25,437
- Impurity Effects on 25,436

Permalloy Films 25,441

PrN 25,415

Rare Earth Orthoferrites 25,412

TmN 25,415

Y-Ce 25,249

Yttrium Orthoferrites 25,412

Magnetic Recording Systems 26,320

Magnetic Resonance in:

- CoNi Ferrite 25,498
- Dy 25,517
- Mg Ferrous Ferrite 25,518
- Ni Ferrous Ferrite 25,518

Magnetic Spin Waves, Scattering of 25,425

Magnetic Structure,

- Neutron Scattering Techniques for Measuring 25,376
- Space Symmetry in 25,396

Magnetic Structure of:

- Cr₂O₃ 25,398
- ErCo 25,402
- ErMn₂ 25,407
- Fe₂As 25,540
- HoCo 25,402
- Mn-Fe-Sn 25,400
- Mn₅Ge₃ 25,401
- MnSO₄ 25,541
- NdCo 25,402
- Tb (Ag-In) 25,406
- TbCo 25,402
- TbNi₂ 25,407
- Tb (Pd, Ag) 25,406
- TmMn₂ 25,407

Magnetic Susceptibility, Calculations on 25,380

Magnetic Susceptibility Analysis, NMR 25,378

Magnetic Susceptibility of:

- Alkali Metals 25,380
- Al-V-Tc 25,601
- CdS:Ni 25,385
- Ce₂O₃·2.67 P₂O₅ 25,715
- Conduction Electrons 25,379
- CuCl₂·2H₂O 25,520
- Cu₂O Films 25,384
- EuGaG 25,388
- Fe Formate 25,382
- GdCl₃·6H₂O 25,137
- Ni Formate 25,382
- NiNO₃ 25,383
- Pr 25,602
- SmGaG 25,388
- Th_{1-x}U_xPd₃ 25,387
- TiO₂ 25,386
- Transition Metal Superconducting Compounds 25,296

ZnO:Ni 25,385

Magnetic Tape, Fine Particle Interactions in 25,903

Magnetic Tape Memory Units 26,349, 26,350

Magnetic Tape Recording System for Atmospheric Noise 26,321

Magnetic Transitions 25,170

Magnetic Transitions in:

- Au-Cr 25,404
- Au-Fe 25,404
- Au-Mn 25,404
- Dy 25,408
- Er 25,408

SUBJECT INDEX (Continued)

- Magnetic Transitions in: (Cont'd)
 Ho 25,408
 $Mn_{2-x}Cr_xSb$ 25,405
 Tb 25,408
 Tm 25,408
- Magnetic Translation Group Theory 25,374, 25,375
- Magnetism,
 Dyson Method in Theory of 25,373
 Heisenberg Model of 25,372
- Magnetite, Magnetoacoustic Resonance of 25,528
- Magnetization,
 Computer Routine for Calculating 25,443
 Spontaneous 25,444
- Magnetization of:
 Au-Fe 25,450
 $Au_{0.95}Fe_{0.05}$ 25,463
 CrI_3 25,439
 Cu-Cd Ferrite 25,472
 DyIG 25,500
 ErIG 25,500
 FeNi, Pressure Effects on 25,445
 Ferrites 25,099
 Ferromagnetic Films, Variations in 25,447
 Gd 25,449
 GdIG 25,500
 HoIG 25,500
 Nb-Zr Superconducting Cylinders 25,328
 Nb-Zr Superconductors 25,327
 NiCu, Pressure Effects on 25,445
 NiFe Particles 25,446
 Ni-Fe-Nb-Ag 25,476
 NiSi, Pressure Effects on 25,445
 SmIG 25,500
 TbIG 25,500
 YbIG 25,500
 YGaG 25,462
 YIG 25,461, 25,462, 25,500
- Magnetization Analysis, Magnetostatic Modes for 25,462
- Magnetization Coupling between Magnetic Layers 25,471
- Magnetization Creep in:
 Magnetic Films 25,482
 Ni-Fe Films 25,455
- Magnetization Ripple in Permalloy Films 25,456-25,459
- Magnetization Switching in Films 25,464
- Magnetoacoustic Resonance in:
 Magnetite 25,528
 YAG 25,530
 YIG 25,530
- Magnetocaloric Effect in Nb-Zr Superconductors 25,750
- Magnetoelastic Coupling Constant of Magnetic Films 25,390
- Magnetoelastic Resonance in YIG 25,529
- Magnetoelastic Waves in YIG 25,391
- Magnetoelasticity, Theory of 25,389
- Magnetometers, Hall Effect 25,878, 26,624
- Magneto-Optical Measurements in Ferromagnets 25,353
- Magnetoplumbite Ferrites, Spin-Wave Theory of 25,419
- Magnetoresistive Multipliers 25,884
- Magnetoresistivity of:
 Al-Fe 25,343
 Al-Mn 25,343
 Bromine Graphite, Negative 25,339
 Ge 25,336, 25,337
 Graphite 25,257
 InSb 25,340
 InSb Corbino Disks 25,338
 Mg-Al 25,343
 Mg-Cd 25,343
 Mg-Mn 25,343
 Mo 25,341
 Ni Films 25,342
 Ni-Fe Films 25,342
 Pyrolytic Carbon, Negative 25,339
 Si 25,336, 25,337
 Sn, Oscillatory 25,335
- Magnetoresistivity of: (Cont'd)
 US 25,333
 W 25,341
- Magnetostriction Analysis, Device for 25,393
- Magnetostriction of:
 Films 25,393
 Gd 25,395
 Microcrystals 25,392
 Ni 25,394
- Magnetostrictive Films, Growth of 25,393
- Magnets,
 Permanent 25,902
 Superconducting 26,089, 26,093, 26,096, 26,105
- Magnon Drag Contribution to Thermoelectric Power of MnTe 25,746
- Manganese over Mn-Fe-Ni, Partial Pressure of 24,892
- Manganese Chloride, Heat Capacity of 25,729
- Manganese Chromium Antimonide,
 Ferrimagnetic-to-Antiferromagnetic Transitions in 25,405
 Magnetic Transitions in 25,405
- Manganese Chromium Sulfide ($MnCr_2S_4$), Spin Waves in 25,432
- Manganese Fluoride,
 Spin Waves in 25,433
 Ultrasonic Attenuation in 25,781
- Manganese Germanium (Mn_5Ge_3), Magnetic Structure of 25,401
- Manganese Iron Tin, Magnetic Structure of 25,400
- Manganese Oxide, Resistivity of 25,246
- Manganese Oxide: Mn^{55} , NMR in 25,594
- Manganese Sulfate,
 Antiferromagnetic Structure of 25,541
 Magnetic Structure of 25,541
- Manganese Telluride, Thermoelectric Power of 25,746
- Manganese Zinc Yttrium, Ferromagnetic Parallel Pumping in 25,525
- Manganin,
 Piezoresistivity of 25,258
 Resistivity of 25,258
- Manganous Formate Dihydrate, Crystal Structure of 24,970
- Marine Autopilots 26,291
- Martensite, Lattice Constant of 24,927
- Maser - See also Laser
- Maser Applications in:
 Communication Systems 26,062
 Radar 26,065
- Maser Modulators 26,043
- Masers,
 Bibliography on 25,918
 Coupled-Cavity 25,990, 25,991
 Laser Pumped 25,992
 Microwave 25,990-25,992, 25,994
 Millimeter Wave 25,995-25,997
 Multimode Oscillations in 25,925
 Oscillation-Relaxation Relations in 25,924
 Oscillations in 25,926
 Phonon 25,792, 25,988
 Population Distributions in 25,922
 Quantum Fluctuations in 25,923
 Review on 25,919
 Ruby 25,924, 25,979-25,981, 25,993, 25,988, 25,997
 Rutile 25,984
 Rutile:Fe 25,985
 S-Band 25,993
 Superconducting Magnets for 26,089
 Theory of:
 Cavity 25,921
 Semiconductor 26,011
 Three-Level 25,930
 Traveling Wave 25,977-25,981, 25,984, 25,985
 $ZnWO_4$ 25,994
- Matrix Switching Circuits 26,359
- Mechanical Properties of Al_2O_3 25,773
- Mechanical Wave Attenuation in Quartz 25,163
- Medical Electronics:
 Electrometers 26,422
 Larynx 26,275
 Pulse Rate Meters 26,273, 26,274
 Telemetry 26,271, 26,272
 Transducers 26,270
- Melt Stirrers, Electromagnetic 25,081
- Melting of:
 K Films 24,894
 KNO_3 24,895
 Metals, Theory of 24,893
- Melting Point of $MoSi_x$ 24,864
- Memory Planes, Fabrication of 25,909
- Memory Units 26,355
- Memory Units,
 Electron Beam Fabrication Techniques for 25,917
 Ferrite Core 25,907, 25,914-25,916
 Ferrite Film 25,904, 25,905, 25,910-25,912
 Ferrite Sheet 25,908
 Magnetic Core 26,342-26,344, 26,347, 26,348
 Magnetic Drum 26,351, 26,352
 Magnetic Tape 26,349, 26,350
 Multiaperture 25,907
 Sneak Paths and Sense-Line Distortion in 26,356
 Switching in 25,913
 Temperature Variations in 25,915
 Temporary Store 26,346
 Tunnel Diode 26,353, 26,354
- Mercuric Nitrate, Paramagnetic Resonance Absorption in 25,574
- Mercury, Crystallographic Angles of 24,929
- Mercury Sulfide, Growth of 25,088
- Metal Compounds, Energy Band Structure of 25,143
- Metal-Semiconductor Interfaces, Fermi Level of 25,150
- Metal Surfaces, Interactional Energy of Inert Gases with 25,111
- Metal-Oxide-Semiconductor Field Effect Transistors 25,868
- Metals,
 Annealing of Noble 24,994
 Diffusion in 25,052, 25,057, 25,059
 Dislocation Motion in 25,005
 Electron-Phonon Interactions in 25,203
 Ferromagnetism of Transition 25,434
 Interstitial Migration in 24,994
 Lattice Vibrations in 24,893
 Melting of 24,893
 Nuclear Magnetic Relaxation in Ferromagnetic 25,527
 Oxidation of 25,113
 Photoconductivity of 25,684
 Spin Wave Lifetime in 25,422
 Theory of 25,132
 Thermoelectric Power in 25,743
 Vacancy Annihilation at Stacking Faults in 24,993
 Vacancy Migration in 25,057
 Valence States in Transition 25,434
- Metamagnetism of:
 $CoCl_2 \cdot 2H_2O$ 25,512
 $CrCl_3$ 25,511
 $FeBr_2$ 25,510
 Rare Earth-Cu Compounds 25,509
- Meters, Conductivity 26,424
- Microcircuits,
 Connection of 26,130-26,134
 Design of 26,122-26,124
 Electrocompatibility of 26,119
 Feasibility of 26,117, 26,118
 Inductors for 26,128
 Interconnection Techniques for 26,129
 Irradiation Effects on 26,121
 Packaging of 26,138-26,140
 Reliability of 26,120
 Review on 26,115, 26,116
 Substrates for 26,135-26,137
- Microcrystals, Magnetostriction of 25,392
- Microplasma Breakdown, Model for 25,331
- Microplasmas in Si Junctions 25,822
- Micropower Transistors 25,873
- Microwave Amplifiers 26,171

SUBJECT INDEX (Continued)

- Microwave Generators, Ferrite 25,901
 - Microwave Masers 25,990-25,992
 - Microwave Masers,
 - Laser Pumped 25,992
 - Ruby 25,993
 - ZnWO₄ 25,994
 - Microwave Oscillators 26,197
 - Microwave Switching Circuits 26,208-26,211
 - Millimeter Wave Masers 25,996
 - Millimeter Wave Masers,
 - Laser Pumped 25,997
 - Sub- 25,995
 - Mixers,
 - Laser 26,049
 - Optical 26,049
 - Mobility of:
 - CdS Films 25,345
 - Ge, Electron 25,226
 - InSb-CdTe 25,169
 - KBr 25,228
 - KCl 25,228
 - KI 25,228
 - NaCl 25,228
 - Se 25,347
 - Semiconductors, Hall 25,227
 - Modulation of Lasers 25,947
 - Modulators,
 - Backward Diode 26,229
 - Frequency 26,228
 - KDP 26,045
 - Laser 26,041-26,046
 - Maser 26,043
 - Optical 26,041-26,046
 - Piezoelectric 26,041
 - Pulse 26,221, 26,244
 - Pulse Code 26,227, 26,312
 - Pulse Duration 26,226, 26,311
 - Pulse Width 26,224-26,226, 26,242, 26,243
 - RF 26,229
 - Molybdenum,
 - Cracking in 25,037
 - Desorption of CO and O⁺ from 25,126
 - Dislocation Configurations in 25,017
 - Dislocation Loops in 25,016
 - Magnetoresistivity of 25,341
 - Tensile Behavior of Polycrystalline 25,772
 - Molybdenum Aluminum Carbide Superconductors,
 - Lattice Parameters of 25,280
 - Properties of 25,280
 - Molybdenum-Niobium, Resistivity of 25,247
 - Molybdenum Permalloy,
 - Hysteresis Loop of Electron Irradiated 25,477
 - Magnetic Domain Orientation in Electron Irradiated 25,477
 - Molybdenum-Rhenium,
 - Resistivity of 25,247
 - Twinning in 25,020
 - Molybdenum Rhenium Superconductors, Resistance in 25,306
 - Molybdenum Silicon,
 - Decomposition of 24,864
 - Eutectic Temperature of 24,864
 - Melting Point of 24,864
 - Monostable Multivibrators 26,206
 - Mössbauer Effect in:
 - Au:Co⁵⁷ 25,154
 - Au:Fe Foils 25,403
 - Cu:Co⁵⁷ 25,154
 - FePd 25,409
 - Ir:Co⁵⁷ 25,154
 - Pd:Co⁵⁷ 25,154
 - Pt:Co⁵⁷ 25,154
 - Rh:Co⁵⁷ 25,154
 - Ti:Co⁵⁷ 25,154
 - UO₂:Fe 25,673
 - Mössbauer Study of:
 - Fe Formate 25,382
 - Ni Formate 25,382
 - Spin Flop in Hematite 25,534
 - Superparamagnetism in:
 - Co Ferrite 25,552
 - Ni Ferrite 25,552
 - Motor Controls 26,406, 26,409-26,412
 - Motor Controls, SCR 26,407, 26,408
 - Motors, Superconducting 26,104
 - Multiperture Core Memory Units 25,907
 - Multiplexers 26,315-26,317
 - Multiplexers, Time Division 26,316
 - Multiplier-Amplifiers 26,170
 - Multipliers,
 - Analog 26,367
 - Frequency 26,236, 26,237, 26,239, 26,240
 - Hall Effect 25,881
 - Hall Effect Vector Product 25,880
 - Magnetoresistive 25,884
 - Parametric 26,236
 - Pulse 26,221
 - Multivibrators,
 - Astable 26,152, 26,203
 - Bistable 26,206
 - Magnetic 26,204, 26,205
 - Monostable 26,206
 - Negative Resistance 26,206
- N
- N-Center Absorption in Alkali Halides 25,620
 - NAND Logic Circuits 26,332
 - Naphthalene,
 - Ultrasonic Absorption in 25,786
 - Ultrasonic Velocity in 25,786
 - Navigation Systems, Positioning Servo for 26,286
 - Néel Temperature of:
 - Cr-V 25,535
 - Transition Metal Bromides 25,536
 - Transition Metal Chlorides 25,536
 - Transition Metal Iodides 25,536
 - Negative Feedback Amplifiers 26,166
 - Negative Magnetoresistivity of InSb 25,340
 - Negative Resistivity of:
 - Bi, Temperature Effects on 25,269
 - Ge:Au 25,270
 - NbO 25,271
 - Neodymium Cobalt, Magnetic Structure of 25,402
 - Neon (Solid),
 - Crystal Structure of 24,951
 - Specific Heat of 25,723
 - Nernst-Ettingshausen Devices, Theory of 26,084
 - Nernst-Ettingshausen Refrigerators 26,085
 - Networks,
 - Computer Generation of Equivalent 26,113
 - Matrices for 26,109
 - Matrices for Two-Port 26,111
 - Matrix Analysis of Sensitivities of 26,110
 - Synthesis of 26,114
 - Time Domain Approximation of 26,108
 - Topological Test for Realizing N-Port 26,112
 - Neutron Diffraction Crystal Structure Analysis 24,915
 - Nickel,
 - Barkhausen Effect in 25,473
 - de Haas-van Alphen Effect in 25,604
 - Diffusion of Ni⁶³ in 25,067
 - Fermi Surface of 25,152, 25,604
 - Ferromagnetic Spin Wave Scattering in 25,426
 - Lattice Vibrations in 25,161
 - Magnetostriction in 25,394
 - Switching Time of 25,466
 - Nickel in Ag, Diffusion of 25,061
 - Nickel⁶³ in:
 - Fe, Diffusion of 25,067
 - Ni, Diffusion of 25,067
 - Nickel Films,
 - Crystal Structure of 24,923
 - Ferromagnetic Energy Exchange Constant in 25,505
 - Hall Voltage in 24,342
 - Impurity Effects on 25,436
 - Magnetic Anisotropy in 25,493
 - Magnetic Domain Wall Widths in 25,505
 - Magnetic Properties of 25,436, 25,437
 - Magnetoresistance of 25,342
 - Nickel Platelets, Magnetic Domains in 25,508
 - Nickel Wire, Permeability Decrease in 25,451
 - Nickel Aluminum,
 - Knight Shift in 25,590
 - NMR in 25,590
 - Nickel-Chromium, Diffusion of Cr in 25,066
 - Nickel Chromium-Nickel Aluminum, Fusibility of 24,896
 - Nickel Cobalt Ferromagnets, Nuclear Magnetic Relaxation in 25,526
 - Nickel Copper,
 - Curie Temperature of 25,445
 - Magnetization of 25,445
 - Nickel Copper Films,
 - Ferromagnetic Energy Exchange Constant in 25,505
 - Magnetic Domain Wall Widths in 25,505
 - Nickel Ferrite, Superparamagnetism in 25,552
 - Nickel Ferromagnetic Alloys, Properties of 25,417
 - Nickel Ferrous Ferrite, Magnetic Resonance of 25,518
 - Nickel Fluoride, Absorption in 25,629
 - Nickel-Fluorine₆ Complex, Covalency in 25,133, 25,134
 - Nickel-Fluosilicate, NMR in 25,595
 - Nickel Formate,
 - Magnetic Fields in 25,382
 - Mössbauer Study of 25,382
 - Susceptibility of 25,382
 - Nickel Gold, Resistivity of 25,248
 - Nickel Iron - See also Permalloy
 - Nickel Iron,
 - Hysteresis Loop of Electron Irradiated 25,477
 - Magnetic Domain Orientation in Electron Irradiated 25,477
 - Nickel Iron (Ni₃Fe),
 - Magnetic Anisotropy of 25,399
 - Magnetic Annealing of 25,399
 - Magnetic Ordering of 25,399
 - Nickel Iron Films,
 - Ferromagnetic Resonance in 25,514, 25,515
 - Hall Voltage in 25,342
 - Magnetic Anisotropy of 25,488
 - Magnetic Domains in 25,507
 - Magnetization Creep in 25,455
 - Magnetoresistance of 25,342
 - Nickel Iron Particles, Magnetization of 25,446
 - Nickel Iron Cobalt Ferrites, Magnetic Anomaly in 25,501
 - Nickel Iron Cobalt Films, Magnetic Domain Wall Motion in 25,504
 - Nickel Iron Ferrites, Magnetic Anisotropy of 25,489
 - Nickel Iron Niobium Silver, Magnetization of 25,476
 - Nickel Manganese Ferrite Toroids, Magnetic Hysteresis Properties of 25,475
 - Nickel Nitrate, Susceptibility of 25,383
 - Nickel Oxide, Hall Effect in 25,349
 - Nickel Silicon,
 - Curie Temperature of 25,445
 - Magnetization of 25,445
 - Nickel-Zinc Ferrites, Permeability of 25,452
 - Niobates,
 - Absorption Edge in 25,650
 - Luminescence of 25,650
 - Photoluminescence of 25,650
 - Niobium,
 - Lattice Dynamics of 25,160
 - Phase Transitions in 24,902
 - Specific Heat of 25,719, 25,720
 - Niobium Superconductors,
 - Critical Field of 25,291, 25,292
 - Current Density of 25,308
 - Magnetization of 25,291
 - Penetration Depth in 25,310
 - Resistance Transition in 25,308
 - Specific Heat of 25,719, 25,720
 - Upper Critical Field of 25,292
 - Niobium Carbide, Heat Capacity of 25,732
 - Niobium Carbide Superconductors, Transition Temperature of 25,301
 - Niobium-Carbon Systems,
 - Phase Equilibria in 24,865
 - Vaporization of 24,865
 - Niobium Hydrogen, NMR in 25,591

Niobium Oxide,
 Negative Resistivity of 25,271
 Resistivity of 25,271
 Niobium Tin (Nb_3Sn) Superconducting Coils, Critical
 Current in 25,290
 Niobium Tin (Nb_3Sn) Superconducting Wires, Fabri-
 cation of 26,097
 Niobium-Tin Superconductors, Transient Phenomena
 in 25,281
 Niobium Tin (Nb_3Sn) Superconductors, Critical Cur-
 rent of Irradiated 25,289
 Niobium-Titanium Superconducting Coils, Critical
 Current in 25,290
 Niobium Zirconium, Ultrasonic Attenuation in
 25,785
 Niobium-Zirconium Superconducting Coils,
 Critical Current in 25,290
 Flux Jumping in 25,316
 Niobium-Zirconium Superconducting Cylinders,
 Magnetization of 25,328
 Niobium Zirconium Superconductors,
 Energy Gap of 25,286
 Magnetization of 25,327
 Magnetocaloric Effect in 25,750
 Paramagnetic Moments in 25,549
 Resistance in 25,306
 Nitridation of Cr 25,065
 Nitrogen in Cr, Diffusion of 25,065
 Noble Metals,
 Annealing of 24,994
 Interstitial Migration in 24,994
 Optical Constants of 25,702
 Noise, Generation-Recombination 25,358
 Noise in:
 CuI Films, $1/f$ 25,359
 Hall Effect Sensors 25,876
 In_2O_3 Films, $1/f$ 25,359
 SiC Resistors 25,810
 Transistors, $1/f$ 25,855
 Tunnel Diodes 25,826, 25,827
 Noise Generation, Nomograph on Device 25,797
 Noise Suppression in Receivers 26,297
 NOR Logic Circuits 26,324, 26,332
 NOT Logic Circuits 26,327
 Nuclear Fail-Safe Circuits 26,453
 Nuclear Magnetic Relaxation in:
 CoNi Ferromagnets 25,526
 FeNi Ferromagnets 25,526
 Ferromagnetic Metals 25,527
 NiCo Ferromagnets 25,526
 Nuclear Magnetic Resonance in:
 Al_2FeCo 25,590
 Al_2FeNi 25,590
 Al_2NiCo 25,590
 Bi 25,587
 CdS 25,596
 CoAl 25,590
 CoTi 25,590
 Cr-V 25,535
 FeAl 25,590
 GdIG 25,598
 LaAlO_3 , La^{139} and Al^{27} 25,586
 LiF:Mn 25,593
 MnO:Mn⁵⁵ 25,594
 NaCN:Na²³ 24,910
 NaCl, Na and Cl 25,592
 NbH_x 25,591
 NiAl 25,590
 $\text{NiSiF}_6 \cdot 6\text{H}_2\text{O}$ 25,595
 Pb Alloys 25,589
 Pb-In, In^{115} 25,588
 YGaIG 25,597
 Nuclear Particle Detectors 26,449
 Nuclear Quadrupole Coupling of Na²³ in Rochelle
 Salt 25,172
 Nuclear Quadrupole Relaxation in NaI 25,173
 Nuclear Quadrupole Scattering 25,170

O

Oguchi Transformation in Ferromagnetism 25,420

Operational Amplifiers 26,370
 Optical Attenuators 26,051
 Optical Constant Analysis of:
 Dielectric Films 25,703
 Semiconductor Films 25,703
 Optical Constants in:
 Noble Metals 25,702
 the X-Ray Range 25,701
 Optical Detectors 26,047, 26,048
 Optical Mixers 26,049
 Optical Modulators 26,041-26,046
 Optical Modulators, Piezoelectric 26,041
 Optical Polarization in Dielectrics 25,713
 Optical Properties of:
 Ge 25,144
 Si 25,144
 Optical Radar 26,318
 Optical Resonators 26,054, 26,055
 Optical Rotation in:
 Gyroelectric Crystals 25,716
 Hypergyroelectric Crystals 25,716
 Quartz, Pressure Effects on 25,717
 Optical Transitions in:
 BP 25,617
 Noble Metals 25,702
 OR Logic Circuits 26,323, 26,327, 26,329
 Order-Disorder Structure of $\text{Na}_2\text{H}_2\text{P}_4\text{O}_{12}$ 24,971
 Order-Disorder Transitions in:
 Co-V 24,905
 Mg_3Cd 24,906
 Ordering in Ag-Pd 24,932
 Organic Semiconductors,
 Thermal Conductivity of 25,748
 Thermoelectric Power of 25,748
 Organics,
 Electroluminescence of 25,654
 Photoconductivity Decay in 25,692
 Oscillators,
 Colpitts' 26,194
 Crystal 26,195
 Microwave 26,197
 Phase-Locked 26,196
 Relaxation 26,197, 26,198, 26,238
 RF 26,196
 Tunnel Diode 26,198-26,202
 Oscilloscope Amplifiers 26,174
 Oscilloscopes, Sampling Channel Circuits for 26,425
 Oxidation of:
 Bicrystals 25,122
 Fe 25,116, 25,117
 Fe, Orientation Effects on 25,115
 Ge 25,122
 Graphite 25,120
 Metals, Analysis of 25,113
 Si 25,121
 Sn 25,122
 Sn, Orientation Effects on 25,114
 Ti 25,118
 UO_2 25,123
 Zr 25,119
 Oxides, Growth of 25,078
 Oxygen in Ag, Solubility of 24,897
 Oxygen (Solid), Crystal Structure of 24,952
 Oxygen⁺ from Mo, Desorption of 25,126

P

Paging Systems 26,319
 Palladium:Co⁵⁷,
 Lattice Dynamics of 25,154
 Mössbauer Effect in 25,154
 Palladium Manganese (Pd_3Mn_2), Antiferromagnetism
 of 25,538
 Palladium-Silver-Glass Glaze Resistors, Properties
 of 25,809
 Paramagnetic Acoustic Resonance, Selection Rules-
 Angular Dependence of 25,585
 Paramagnetic Curie Temperature of CrI_3 25,439
 Paramagnetic Exchange in:
 Cr Spinel 25,546
 KMnF_3 25,547

Paramagnetic Moments in:
 Nb-Zr Superconductors 25,549
 Sn Superconducting Cylinders 25,548
 Paramagnetic Relaxation - See also Spin Lattice Re-
 laxation; Spin-Spin Relaxation;
 Cross Relaxation
 Paramagnetic Relaxation in Ionic Crystals 25,566
 Paramagnetic Resonance,
 Shape of First Derivative of 25,554
 Transition Processes of 25,553
 Paramagnetic Resonance of:
 $\text{CaF}_2:\text{Dy}^{3+}$ 25,581
 $\text{CaF}_2:\text{RE}$ 25,556, 25,568
 $\text{CaF}_2:\text{Sm}^{3+}$ 25,581
 $\text{CaF}_2:\text{U}^{3+}$ 26,008
 $\text{CaO}:\text{Eu}^{2+}$ 25,577
 $\text{CaWO}_4:\text{Yb}^{3+}$ 25,584
 $\text{CdTe}:\text{Cr}$ 25,582
 CsMnCl_3 25,539
 F-Centers, g-Shift in 25,575
 Ionic Crystals 25,566
 KCl:F Centers 25,576
 KMnCl_3 25,539
 $\text{LaAlO}_3:\text{Fe}^{3+}$ 25,586
 $\text{MgO}:\text{Mn}^{4+}$ 25,583
 NaBrO_3 25,578
 NaClO_3 25,578
 $\text{PbTiO}_3:\text{Fe}^{3+}$ 25,579
 RbMnCl_3 25,539
 Si, Donor Center 25,580
 $\text{SrCl}_2:\text{Mn}^{2+}$ 25,560
 $\text{SrO}:\text{Eu}^{2+}$ 25,577
 Paramagnetic Resonance Absorption in:
 Al_2O_3 25,571
 $\text{CaCO}_3:\text{Fe}$ 25,573
 $\text{Hg}(\text{NO}_3)_2 \cdot 2\text{H}_2\text{O}$ 25,574
 $\text{MgO}:\text{Cr}^{3+}$ 25,572
 Paramagnetic Resonance Line Splitting in $\text{Al}_2\text{O}_3:\text{Cr}^{3+}$
 25,557
 Paramagnetic Susceptibility, Temperature Dependence
 of 25,550
 Paramagnetic Susceptibility of:
 Ta-Nb Superconductors 25,279
 Ta-V Superconductors 25,279
 $\text{Th}_{1-x}\text{U}_x\text{Pd}_3$ 25,387
 Paramagnetism of $\text{Al}_2\text{O}_3:\text{Ti}^{3+}$ 25,551
 Paramagnets, Spin Hamiltonian for 25,545
 Parametric Amplifiers 26,159, 26,162, 26,165,
 26,234
 Parametric Amplifiers,
 Coupling of 26,162
 Idler Circuit for 26,161
 Non-Reciprocal 26,163
 Photo Modulated 26,164
 Theory of 26,160
 Parametric Converters 26,159, 26,233, 26,235
 Parametric Converters, Photo Modulated 26,164
 Parametric Frequency Multipliers 26,236
 Parametric Up-Converters 26,234
 Partial Pressure of Mn over Mn-Fe-Ni 24,892
 Partial Pressures in the Pb-Te System 24,891
 Passivation of Devices 25,844
 Penetration Depth in:
 Nb Superconductors 25,310
 Ta Superconductors 25,311
 V_3Ga Superconductors 25,311
 V_3Ge Superconductors 25,311
 V_3Pt Superconductors 25,311
 V_3Si Superconductors 25,311
 Permalloy - See also Nickel Iron
 Permalloy Films,
 Ferrimagnetic Relaxation in Parallel Pumped
 25,524
 Magnetic Anisotropy of 25,487, 25,499
 Magnetic Annealing of 25,442
 Magnetic Domain Rotation in 25,503
 Magnetic Domain Wall Interactions in 25,506
 Magnetic Easy Axis of 25,484
 Magnetic Properties of 25,441
 Magnetization Ripple in 25,456-25,459
 Spin Waves in 25,427, 25,428, 25,431
 Switching in 25,468

SUBJECT INDEX (Continued)

- Permanent Magnets, Review on 25,902
- Permeability of:
- FeAl 25,438
 - FeAl Alloys, Relaxation of 25,454
 - Ni Wire, Decrease in 25,451
 - Ni-Zn Ferrites 25,452
- Phase Boundaries in:
- D-Pt-Pd 24,934
 - Fe-Zn Ferrite 24,946
 - H-Pt-Pd 24,934
- Phase Diagram of:
- BC-SiC 24,870
 - CaF₂-Ca(OH)₂-CaCO₃ 24,873
 - CaMgSi₂O₆-NaAlSiO₄-NaAlSi₃O₈ 24,876
 - CaO-Al₂O₃-H₂O 24,877
 - Cu-Si-Zn 24,869
 - In-Te 24,867
 - MgO-MgCr₂O₄ 24,882
 - MgO-V₂O₅ 24,881
 - Molybdate-Bi 24,871
 - NaAlF₆-Al₂O₃-SiO₂ 24,875
 - ThO₂-B₂O₃ 24,872
 - U-Al-Fe 24,878
 - U-C-O 24,879
 - UO₂-UO₃-Y₂O₃ 24,880
 - Zn(PO₃)₂-Cd(PO₃)₂ 24,874
 - Zr-S 24,868
- Phase Equilibria in:
- Hf-C 24,865
 - Nb-C 24,865
 - Ta-C 24,865
 - Ti-C 24,865
 - Ti-N 24,865
 - Ti-O 24,865
 - Zr-C 24,865
 - Zr-N 24,865
 - Zr-O 24,865
- Phase-Locked Oscillators 26,196
- Phase Shifters, Ferrite Materials for 25,888-25,892, 25,897
- Phase Transitions in:
- Ag₂Se Films 24,909
 - Antiferroelectrics 25,198
 - Antiferromagnets 25,542
 - BaTiO₃, Tetragonal-to-Cubic 24,911
 - Be-Ti 24,953
 - Co-V 24,905
 - Fe-V 24,904
 - In-Te 24,867
 - In₂Te₅ 24,867
 - Mg₃Cd 24,906
 - NaCN, NMR Study of 24,910
 - Nb, bcc-to-fcc 24,902
 - SrTiO₃ 25,155
 - Tellurium 24,903
 - Ti, β-α 24,901
 - ThSiO₄, Tetragonal-Monoclinic 24,912
- Phonon Attenuation in Quartz 25,163
- Phonon Distribution in High Electric Fields 25,207
- Phonon Drag:
- Contribution to Thermoelectric Power of Ge 25,745
 - Seebeck Effect in Transverse Magnetic Field 25,744
- Phonon Masers 25,792
- Phosphorescence in:
- CaCO₃ 25,677
 - CaF₂ 25,677
- Phosphorescence of Eu Chelates in Hosts 25,641
- Phosphors, Activation of 25,682
- Phosphorus in Si 25,044
- Phosphorus Pentoxide, Heat Capacity of 25,732
- Photoconductive Image Display Units 26,378
- Photoconductivity,
- Basics of 25,683
 - Electron Dependence of Parameters in 25,686
 - Theory of 25,684
- Photoconductivity of:
- CdS 25,687
 - Dielectrics, Decay in 25,692
 - GaAs 25,690
- Photoconductivity of: (Cont'd)
- InSb 25,268
 - InSb, Oscillations in 25,693
 - Metals 25,684
 - Organics, Decay in 25,692
 - Semiconductors 25,685
 - Si 25,689
 - TiO₂, Chemisorption Effects on 25,688
- Photocurrents in:
- Anthracene 25,220, 25,221, 25,691
 - Cd 25,222
- Photoelectric Emission, Surface Effects in 25,365
- Photoelectric Response of BP 25,617
- Photoelectromagnetic Detectors 26,047
- Photoelectromagnetic Effect in Ge 25,700
- Photo-EMF in CdTe Films 25,697
- Photoemission from:
- InSb 25,268
 - NaCl, Electron 25,364
 - Zn 25,366
- Photo-Field Effect Transistors 25,869
- Photogeneration in:
- Anthracene 25,695, 25,696
 - Se 25,694
- Photo-Hall Effect in Se 25,347
- Photoluminescence of:
- CaTa₂O₆ 25,650
 - GaAs:Cr 25,659
 - GaAs:Mn 25,659
 - Mg₄Nb₂O₉ 25,650
 - Niobates 25,650
 - SiC 25,660
 - Tantalates 25,650
 - ZnTa₂O₆ 25,650
- Photo Modulated Parametric Amplifiers 26,164
- Photo Modulated Parametric Converters 26,164
- Photovoltaic Diodes 25,699
- Photovoltaic Effect in:
- Sb₂S₃ Films 25,698
 - TiO₂ 25,699
 - TiO₂, Chemisorption Effects on 25,688
- Piezoelectric Modulators, Optical 26,041
- Piezoelectricity of Salicylidene Aniline 25,200
- Piezoresistivity of:
- Ge 25,259
 - Manganin 25,258
- Planar Transistors, Fabrication of 25,872
- Plastic Deformation of CaWO₄ 25,039
- Platinum,
- Adsorption on 25,124
 - Knight Shift in 25,602
 - Susceptibility of 25,602
- Platinum:Co⁵⁷,
- Lattice Dynamics of 25,154
 - Mössbauer Effect in 25,154
- Plutonium, Diffusion (Self-) in 25,076
- Plutonium Monocarbide, Heat Capacity of 25,731
- Point Contact Diodes 25,832
- Polarity-Sensing Amplifiers 26,180
- Polarization in Ferroelectrics 25,194
- Polaron Effects in CdS 25,225
- Polycrystalline Aggregates, Magnetostriction of 25,392
- Polycrystalline Mixtures, Conductivity Tensor of 25,235, 25,236
- Polymorphic Transitions in Fe-V 24,904
- Population Distributions in Quantum Mechanical Systems 25,922
- Potassium Films, Melting of 24,894
- Potassium Bromide,
- Absorption in 24,990, 25,622
 - Color Center Bleaching in 24,990
 - Hall Mobility of 25,228
 - Mobility of 25,228
- Potassium-Calcium Chloride, Dielectric Loss in 25,183
- Potassium Chloride,
- Absorption in 24,990, 25,622
 - Color Center Absorption in 25,621
 - Color Center Bleaching in 24,990, 24,991
 - Dielectric Loss in 25,184
- Potassium Chloride, (Cont'd)
- Hall Mobility of 25,228
 - Mobility of 25,228
 - Paramagnetic Resonance of F-Centers in 25,576
 - Spin-Lattice Relaxation of F-Centers in 25,567
 - Vacancies in 25,184
- Potassium Chloride:Co,
- Absorption in 24,959
 - Crystal Structure of 24,959
- Potassium Chloride:Li, Fluorescence Lifetime of F-Centers in 25,664
- Potassium Dihydrogen Phosphate Modulators 26,045
- Potassium Dihydrogen Phosphate Q-Switches 26,053
- Potassium Halides, Conductivity of 25,255
- Potassium Iodide,
- Conductivity of 25,254
 - Hall Mobility of 25,228
 - Ionic Conductivity of 25,254
 - Mobility of 25,228
- Potassium Manganese Chloride (KMnCl₃),
- Antiferromagnetic Ordering in 25,539
 - Antiferromagnetic Resonance in 25,539
 - Paramagnetic Resonance in 25,539
- Potassium Manganese Fluoride, Paramagnetic Exchange in 25,547
- Potassium Magnesium Fluoride (KMgF₃),
- Reflectance of 25,708
 - Transmittance of 25,708
- Potassium Nitrate,
- Luminescence of 25,652
 - Melting of 24,895
 - Switching in 25,195
- Potassium-Tantalum Oxide,
- Crystal Structure of 24,978
 - Dielectric Constant of 24,978
 - Growth of 24,978
- Potassium Titanoniobate, Crystal Structure of 24,976
- Power Controls 26,152
- Power Converters, Diode 25,835
- Power Dividers, Ferrite 25,897
- Power Supplies - See Regulators
- Power Supplies, Radio Receiver 26,296
- Power Transistors, Contacts for 25,874
- Praseodymium, Magnetic Properties of 25,415
- Praseodymium Chloride:Nd³⁺, Fluorescence of 25,666
- Preamplifiers 26,186
- Preamplifiers, Field Effect Transistor 26,182, 26,183
- Precipitation in:
- Alloys 24,907
 - Fe, C 24,907
 - NaCl, AgCl 24,908
- Preparation of - See also Growth of
- Preparation of:
- CaSc₂O₄ 24,972
 - GaSb 25,042
 - SeCl₄ 24,960
 - SrSc₂O₄ 24,972
 - TeCl₄ 24,960
 - YAlG:Bi 24,969
 - Zn(PO₃)₂-Cd(PO₃)₂-Mg(PO₃)₂ 24,874
 - ZnS:Cu 25,678
- Pulse Amplifiers 26,221
- Pulse Amplifiers,
- Design of 26,177
 - SCR 26,178
- Pulse Circuits, Avalanche Transistor 26,154
- Pulse Code Modulators 26,227, 26,312
- Pulse Code Modulators, Line Equipment for 26,313
- Pulse Delay Circuits 26,244, 25,256, 26,257
- Pulse Discriminators 26,260
- Pulse Dividers 26,221
- Pulse Drivers 26,357
- Pulse Duration Modulators 26,226, 26,311
- Pulse Forming Circuits 26,255
- Pulse Generators 26,152, 26,242-26,244, 26,247
- Pulse Generators,
- High Power 26,248, 26,249
 - Random Time 26,246
- Pulse-Height Discriminators 26,258, 26,259
- Pulse Modulators 26,221, 26,244
- Pulse Multipliers 26,221

Pulse Pattern Generators 26,245
Pulse Rate Counters 26,273
Pulse Shapers 26,253, 26,254
Pulse Slope Modulators 26,314
Pulse Synchronizers 26,261
Pulse Width Demodulators 26,231
Pulse Width Modulators 26,224-26,226, 26,242, 26,243
Pumps, Magnetic 26,417
Purification of CdS 25,051
Purity Limit in GaSb 25,042
Pyrene-Tetracyanoethylene, Crystal Structure of 25,638
Pyrite, Electropolishing of 25,130
Pyroelectricity of $\text{Pb}(\text{Zr}_{0.95}\text{Ti}_{0.05})\text{O}_3$ 25,201
Pyrolytic Carbon,
Magnetoresistivity of 25,339
Negative Magnetoresistivity of 25,339
Pyrolytic Graphite,
Crystal Structure of 24,948
Oxidation of 25,120
Volume Expansion of 25,755
Pyrolytic Graphite Thermocouples 26,082
Pyrolytic Graphite Thermocouples, Performance of 26,081

Q

Q-Switches, KDP 26,053
Quadrupole Coupling in the Nuclear Magnetic Resonance of Bi 25,587
Quantum Effects in Ferroelectrics 25,194
Quantum Relation 25,157
Quartz,
Crystal Perfection of 24,919
Deformation of 25,771
Fracture in 25,771
Lattice Vibrations in 24,919
Mechanical Wave Attenuation in 25,163
Optical Rotation in 25,717
Phonon Attenuation in 25,163
Ultrasonic Absorption in 25,790
Ultrasonic Attenuation in 25,163

R

Radar,
Masers in 26,065
Optical 26,318
Radar Collision Warning Systems 26,287
Radar Switching Circuits 26,208
Radar Systems, Doppler 26,287
Radiation Detectors 26,442-26,448
Radiation Detectors, γ -Ray 26,436
Radiation Effects on:
Devices 25,799
Junctions 25,815
Transistors 25,802
Radiation from GaAs Diodes 25,657
Radio Astronomy, Amplifiers for 26,187
Radio Frequency Interference Filters 26,268
Radio Receiver Power Supplies 26,296
Radio Receiver Selector System 26,293
Radio Relay Alarms 26,433
Radio Transmitters 26,302
Raman Effects, Higher Order Coherent 25,644
Raman Lasers 25,989
Raman Spectra of:
 H_2O (Solid) 25,645
Na Azide 25,635
Ramp Generators 26,152
Random Time Pulse Generators 26,246
Ranging Systems, Laser 26,063, 26,064
Rare Earth Alloys,
Magnetic Ordering in 25,408
Magnetic Transitions in 25,408
Rare Earth-Copper Compounds,
Antiferromagnetism of 25,509
Magnetic Moments of 25,509
Metamagnetism of 25,509
Rare Earth Manganese (R_2Mn_{23}), Magnetic Moments of 25,411

Rare Earth Orthoferrites,
Lattice Constants of 25,412
Magnetic Properties of 25,412
Rare Earth Salts, Spin-Lattice Relaxation in 25,569
Rare Earths in Zr 25,046
Receiver Power Supplies 26,296
Receiver Selector System 26,293
Receivers,
AM/FM 26,294
Interference Suppression in 26,298
Noise Suppression in 26,297
Recombination - See also Trapping; Lifetime
Recombination,
Analog Computation on 25,211
Statistics of 25,210
Recombination in:
CdS 25,222
Semiconductors 25,213
Si, Oxygen Effects on 25,218
Recombination Radiation from:
GaAs Diodes 25,657
GaP Junctions 25,145
Recording Tape, Fine Particle Interactions in 25,903
Rectifiers, Fabrication of Si Controlled 25,838
Reduction of:
Bicrystals 25,122
Ge 25,122
Sn 25,122
Reflectivity, Computer Program on 25,704
Reflectivity of:
GaP, Pressure Effects on 25,145
 KMgF_3 , Infrared 25,708
 MgF_2 , Infrared 25,708
 Mg_2Sn , Infrared 25,633
PbS 25,706
PbSe 25,706
Semiconductors, Infrared 25,223
 $\text{SiO}_2\text{:Ag, Au}$ Films 25,705
ZnS, Temperature Dependence of 25,707
ZnSe, Infrared 25,224
Refraction in BaF_2 25,710
Refractive Index-Absorption Coefficient Relationship 25,701
Refractive Index Analysis,
Diffraction-Laser 25,712
Interferometric 25,711
Refractive Index of Bi_2S_3 25,709
Refractometers 26,427
Refractories, Growth of 25,078
Refrigerators,
Nernst-Ettingshausen 26,085
Thermoelectric 26,458, 26,459
Registers,
Shift 26,363
Stepping 26,362
Regulators,
Automobile 26,284
Current 26,387-26,390
Frequency 26,391
Voltage 26,380-26,386
Relaxation Oscillators 26,197, 26,238
Relaxation Oscillators, Computer Analysis of 26,198
Relays,
Latching 26,413
SCR 26,414
Time Delay 26,415
Reliability of Devices 25,803, 25,804
Remanence of:
 $\text{Au}_{0.95}\text{Fe}_{0.05}$ 25,463
FeAl 25,438
Resistance Transitions in Nb Superconductors 25,308
Resistivity - See also Conductivity
Resistivity of:
Ag, Deformation Effects on the 25,262
Ag Solid Solutions 25,245
Ag-Gd 25,249
Al-Mg 24,988
Bi, Temperature Effects on the 25,269
Bi-Te 25,167
 Bi_2Te_3 , Pressure Effects on the 25,260
 $\text{Bi}_4\text{Ti}_3\text{O}_{12}$ 25,187

Resistivity of: (Cont'd)
 CaPd_2O_4 24,977
CdS Films 25,345
 $\text{Co}_{1-x}\text{Fe}_x\text{Si}$ 25,166
Co-V, Temperature Dependence of the 24,905
FeAl 25,438
Ferromagnets, Theory of the 25,234
Ga(As-P), Pressure Effects on the 25,261
Ge 25,259
Ge-Au 25,270
Graphite 25,257
Manganin 25,258
 MnO_2 25,246
Mo-Nb 25,247
Mo-Re 25,247
Mo-Re Superconductors 25,306
NbO, Negative 25,271
Nb-Zr Superconductors 25,306
Ni-Au 25,248
PbTe 25,252
PbTe Films 25,108
Se 25,179
SiC 25,251
 SiO_2 , Temperature Variations of the 25,237
US 25,333
W 25,244
Y-Ce 25,249
Resistivity Analysis,
Four-Point Probe 25,240, 25,241
Q Method of 25,243
Thickness Corrections in 25,242
Resistivity Tensor of Semiconductors 25,233
Resistivity-Vacancy Relationships 24,992
Resistors,
Cr/SiO Thin Film 25,811
Evaluation of TaN Film 25,807
Noise in SiC 25,810
Pd-Ag-Glass Glaze 25,809
Properties of TaN Film 25,808
Thin Film 25,805
Resonators,
Ferrite 25,887
Laser 26,054, 26,055
Optical 26,054, 26,055
RF Modulators 26,229
RF Oscillators 26,196
Rhodium: Co^{57} ,
Lattice Dynamics of 25,154
Mössbauer Effect in 25,154
Ring Counters 26,152
Rochelle Salt,
Coercive Field in 25,197
Domain Wall Motion in 25,197
Nuclear Quadrupole Coupling of Na^{23} in 25,172
Rubidium Chloride, Absorption in 25,624
Rubidium Hydrogen Sulfate,
Absorption in 25,634
Ferroelectric Transitions in 25,634
Lattice Vibrations in 25,634
Rubidium Manganese Chloride (RbMnCl_3),
Antiferromagnetic Ordering in 25,539
Antiferromagnetic Resonance in 25,539
Paramagnetic Resonance in 25,539
Rubidium Nitrate,
Dielectric Transitions in 25,191
Thermal Expansion of 25,191
Rubidium Potassium Nitrate,
Dielectric Properties of 25,189
Growth of 25,189
Lattice Parameters of 25,189
Ruby,
Cross Relaxation in 25,564
Dislocation Density in 25,009
Dislocations in 25,004
Fluorescence of 25,672
Luminescence of 25,647
Paramagnetic Resonance Line Splitting in 25,557
Spin-Lattice Relaxation in 25,570
Ruby Lasers,
Bandwidth of 25,963
Beam Angle of 25,965

SUBJECT INDEX (Continued)

Ruby Lasers, (Cont'd)

- Coherence between Superposed Light Beams in 25,966
- Coherence Time of Pulsed 25,967
- Crystal Quality Effects in 25,940, 25,941
- Distribution of Radiation from 25,964
- Emission from 25,938, 25,960
- Emission at Liquid Nitrogen Temperatures from 25,939
- Emission Studies on 25,959
- Interference between Beams from 25,972
- Inversion in 25,934
- Line Splitting in 25,969
- Loss in 25,975
- Modes in 25,952-25,954, 25,999
- Output of 25,962
- Output Energy of 25,965
- Radiation Properties of 25,961
- Resonator Influence on 25,955
- Threshold Populations in 25,932
- Travelling Wave 25,982, 25,983
- Ruby Masers,
 - Microwave 25,993
 - Oscillation-Relaxation Relations in 25,924
 - Travelling Wave 25,980
- Ruby Millimeter Wave Masers, Laser Pumped 25,997
- Ruby Phonon Masers 25,988
- Ruby Travelling Wave Masers,
 - Efficiency of 25,981
 - Intermodulation in 25,979
- Rutile,
 - Chemisorption of Oxygen on 25,688
 - Conductivity of 25,352
 - Hall Effect Anisotropy in 25,352
 - Photoconductivity of 25,688
 - Photovoltaic Effect in 25,688, 25,699
 - Susceptibility of 25,386
- Rutile Diodes, Photovoltaic 25,699
- Rutile Travelling Wave Masers 25,984
- Rutile:Fe Travelling Wave Masers 25,985

S

- S-Band Masers, Ruby 25,993
- Salicylidene Aniline,
 - Acoustic Velocity in 25,200
 - Elastic Constant of 25,200
 - Piezoelectricity of 25,200
- Samarium Gallium Garnet, Susceptibility of 25,388
- Samarium Garnet, Faraday Rotation in 25,640
- Samarium Iron Garnet,
 - Magnetic Anisotropy of 25,500
 - Magnetization of 25,500
- Sapphire,
 - Dislocation Density in 25,009
 - Dislocations in 25,770, 25,773
 - Fracture of 25,769
 - Growth of 25,094
 - Mechanical Properties of 25,773
 - Twinning in 25,019
 - Yield in 25,770
- Saturation Magnetization of:
 - FeNi, Pressure Effects on 25,445
 - NiCu, Pressure Effects on 25,445
 - NiSi, Pressure Effects on 25,445
- Sawtooth Generators 26,238, 26,251
- Scandium-Plutonium, Lattice Constants of 24,931
- Scattering,
 - Electron-Atom 25,170
 - Nuclear Quadrupole 25,170
- Scattering in:
 - GaAs 25,615
 - GaP 25,615
 - GaSb 25,615
 - Ge, Donor 25,230
 - InP 25,615
 - PbTe 25,252
 - Solids 25,229
- Schmitt Trigger Switching Circuits 26,212
- Scintillation in:
 - Alkali Halides 25,679
- Scintillation in: (Cont'd)
 - NaI 25,680
 - NaI:TI 25,681
- Scintillation Counters 26,451, 26,452
- Scintillation Crystals,
 - CaI₂ 26,450
 - CaI₂:Eu 26,450
- Secondary Emission,
 - Calculations on 25,367
 - Surface Effect in 25,365
 - Theory of 25,368, 25,369
- Secondary Emission from W, Cs Ion Induced 25,370
- Seebeck Coefficient of PbTe 25,252
- Seebeck Effect, Phonon Drag 25,744
- Seebeck-Hall Effect Anomaly in Semiconducting Glasses 25,351
- Segregation of:
 - Impurities in GaAs 24,899
 - Interstitials to Dislocations 24,898
 - Naphthalene in Anthracene 24,900
- Seismic Amplifiers 26,186
- Selector System, Receiver 26,293
- Selenium,
 - Dielectric Constant of 25,179
 - Hall Effect in 25,347
 - Mobility in 25,347
 - Photogeneration in 25,694
 - Photo-Hall Effect in 25,347
 - Resistivity of 25,179
 - Thermal Conductivity of 25,738
 - Trapping in 25,694
- Selenium Whiskers, Growth of 25,111
- Selenium Tetrachloride,
 - Crystal Structure of 24,960
 - Preparation of 24,960
- Self-Diffusion in Pu 25,076
- Semiconducting Glasses,
 - Hall Effect in 25,350
 - Hall Effect-Seebeck Anomaly in 25,351
- Semiconducting Oxide Glass, Preparation and Properties of 25,131
- Semiconductor Devices, Review on 25,796
- Semiconductor Films,
 - Optical Constant Analysis of 25,703
 - Thickness Measurements of 25,703
- Semiconductor Lasers, Review on 26,010
- Semiconductor Masers, Theory of 26,011
- Semiconductor-Metal Interfaces, Fermi Level of 25,150
- Semiconductors,
 - Absorption in Degenerate 25,205
 - Advances in Elemental 24,858
 - Carrier Concentration in 25,208
 - Carrier Diffusion Length in 25,213
 - Effective Mass in 25,223
 - Electron-Phonon Interaction in Degenerate 25,205
 - Energy Band Density in 25,149
 - Energy Band Structure of 25,141
 - Energy Levels in Degenerate 25,205
 - Hall Coefficient of 25,233
 - Hall Mobility in 25,227
 - Lifetime in 25,213
 - Photoconductivity in 25,685
 - Reflectivity of 25,223
 - Resistivity Measurements in 25,240
 - Resistivity Tensor of 25,233
 - Surface Recombination in 25,213
 - Thermomagnetic Figure of Merit of 25,749
- Semimetallic Properties of Co_{1-x}Fe_xSi 25,166
- Semimetals, Thermomagnetic Figure of Merit of 25,749
- Sequence Generators, Bernoulli 26,361
- Sequence Timers 26,364
- Servo Systems 26,418
- Shift Registers 26,363
- Shift Registers, Ferrite Film 25,910
- Silica,
 - Activation Energy of 25,237
 - Resistivity of 25,237
- Silicate Glass:Eu,
 - Absorption in 25,639
 - Fluorescence of 25,639

Silicon,

- Absorption in 25,044, 25,611
- Boron in 25,044
- Crystal Structure of 24,915, 24,928
- Defect Mobility in 24,986
- Dielectric Constant of 25,144
- Diffusion of Ga in 25,075
- Diffusion-Induced Dislocations in 24,997
- Dislocation Determination in 24,995
- Dislocations in 24,997, 25,002
- Doping of 25,050
- Effective Mass of 25,144
- Energy Band Structure of 25,144
- He in 25,043
- Impurity Lines in 25,044
- Ionization Rates of Carriers in 25,232
- Junction Formation in 25,050
- Lifetime in 25,212
- Magnetoresistivity of 25,336, 25,337
- Optical Properties of 25,144
- Oxidation of 25,121
- Paramagnetic Resonance in 25,580
- Phosphorus in 25,044
- Photoconductivity of 25,689
- Recombination in 25,218
- Spin Relaxation in 25,559
- Thermal Conductivity of 25,737
- Trapping in 25,219
- Ultrasonic Wave Propagation in 25,777
- Silicon:Zn, Absorption in 25,612
- Silicon in Transition Metals, Diffusion of 25,064
- Silicon Controlled Rectifiers,
 - Fabrication of 25,838
 - Properties and Fabrication of 25,839, 25,840
- Silicon Electron-Phonon Interactions in 25,206
- Silicon Films,
 - Crystal Structure of 25,105
 - Growth of 25,104, 25,105
 - Impurity Distribution in 25,048
- Silicon Junctions,
 - Breakdown in 25,822
 - High Frequency Properties of 25,834
 - Microplasmas in 25,822
 - Stress Effect in 25,816, 25,817
- Silicon Carbide,
 - Absorption in 25,251
 - Dislocation Etch Pits in 25,035
 - Hall Effect in 25,251
 - Photoluminescence of 25,660
 - Resistivity of 25,251
 - Stacking Fault Etch Pits in 25,035
- Silicon Carbide Films, Growth of 25,106
- Silicon Carbide Resistors, Noise in 25,810
- Silicon Carbide Thermistors 25,087
- Silicon Carbide Tunnel Diodes 25,830
- Silicon Dioxide,
 - Ultrasonic Absorption in 25,790
 - Ultrasonic Attenuation in 25,783
 - Ultrasonic Relaxation in 25,783
- Silicon Dioxide:
 - Film Capacitors 25,814
 - Films, Growth of 25,814
- Silicon Iron,
 - Dislocations in 25,768
 - Fracture in 25,768
 - Twinning in 25,768
- Silicon Germanium Thermocouples 26,080
- Silicon Germanium Thermoelectric Generators 26,080
- Silicon Monoxide:Ag,Au Films, Reflectivity of 25,705
- Silicon Oxide Films, Growth of 25,107
- Silicon Oxynitride, Crystal Structure of 24,945
- Silicon Tetrachloride, Vapor Pressure of 24,890
- Silver,
 - Diffusion of:
 - Au in 25,060
 - Co in 25,061
 - Fe in 25,061
 - Ni in 25,061
 - Dislocations in 25,262
 - Resistivity of 25,262

SUBJECT INDEX (Continued)

- Silver, (Cont'd)
 Solubility of:
 Cu in 24,897
 O in 24,897
 Stacking Fault Energy of 25,029
 Vacancies in 25,262
- Silver in:
 Au, Diffusion of 25,060
 Cu, Diffusion of 25,060, 25,063
- Silver Films,
 Adsorption of Hydrogen on 25,125
 Crystal Structure of 24,924
 Growth of 25,101
- Silver Solid Solutions,
 Knight Shift in 25,600
 Resistivity of 25,245
 Thermoelectric Properties of 25,245
- Silver Chloride, Dislocation Distribution in Bent 25,010
- Silver Chloride from NaCl, Precipitation of 24,908
- Silver-Gadolinium,
 Magnetic Properties of 25,249
 Resistivity of 25,249
- Silver Iodide, Debye Temperature of 25,728
- Silver-Palladium,
 Lattice Parameters of 24,932
 Ordering in 24,932
- Silver Selenide Films,
 Lattice Parameters of 24,909
 Phase Transitions in 24,909
- Silver-Zinc-Manganese, Lattice Constants of 24,933
- Single Sideband Transmitters 26,301
- Slip in CaWO_4 25,039
- Smith-Purcell Couplers in Infrared Lasers 25,986
- Sodium,
 Carbon in 25,045
 Spin-Lattice Relaxation in 25,565
 Spin Relaxation in 25,558
- Sodium²³ in:
 NaCN, NMR of 24,910
 Rochelle Salt, Nuclear Quadrupole Coupling of 25,172
- Sodium Aluminum Fluoride-Aluminum Oxide-Silicon Dioxide, Phase Diagram of 24,875
- Sodium Azide,
 Absorption in 25,635
 Raman Spectra of 25,635
- Sodium Bromate, Paramagnetic Resonance in 25,578
- Sodium Bromide,
 Crystal Structure of 24,958
 Heat Capacity of 25,727
- Sodium Bromide:Co,
 Absorption in 24,959
 Crystal Structure of 24,959
- Sodium Cadmium (NaCd_2), Crystal Structure of 24,965
- Sodium Carbonate, Crystal Structure of 24,973
- Sodium Chlorate, Paramagnetic Resonance in 25,578
- Sodium Chloride,
 Absorption in 25,623, 25,754
 Debye-Waller Factors in 25,164
 Color Centers in 25,753
 Coloration of 25,754
 Emission from 25,364
 Hall Mobility of 25,228
 Lattice Coefficients of 24,941
 Lattice Energies of 24,941
 Lattice Potential of 25,138
 Mobility of 25,228
 NMR of Na and Cl in 25,592
 Photoemission from 25,364
 Precipitation of AgCl from 24,908
 Volume Expansion in 25,753, 25,754
- Sodium Chloride:Co,
 Absorption in 24,959
 Crystal Structure of 24,959
- Sodium Cyanide,
 NMR of Na²³ in 24,910
 Phase Transitions in 24,910
- Sodium Hydrogen Selenate,
 Absorption in 25,634
 Ferroelectric Transitions in 25,634
 Lattice Vibrations in 25,634
- Sodium Iodide,
 Absorption in 25,680
 Heat Capacity of 25,727
 Nuclear Quadrupole Relaxation in 25,173
 Scintillation in 25,680
- Sodium Iodide:Ti,
 Absorption in 25,680
 Electroluminescence of 25,681
 Scintillation in 25,680, 25,681
- Sodium Iodide Radiation Detectors, γ -Ray 26,436
- Sodium Nitrate,
 Absorption in 25,190
 Dielectric Transitions in 25,190
- Sodium Nitrite,
 Absorption in 25,188
 Conductivity of 25,177
 Dielectric Properties of 25,177
- Sodium Tetrametaphosphate,
 Crystal Structure of 24,971
 Order-Disorder Structure of 24,971
- Solar-Electric Energy Converters 26,456, 26,457
- Solar Power Supplies 26,296
- Solenoids, Superconducting 26,088, 26,090-26,092, 26,094, 26,095
- Solid Solutions,
 Diffusion in 25,057
 Specific Heat of 25,718
 Vacancy Migration in 25,057
- Solubility in:
 Ag, Cu 24,897
 Ag, O 24,897
 B_2C , SiC 24,870
 GaAs, Zn 25,073
 GaP, Zn 25,073
 InP, Zn 25,074
 SiC, B_2C 24,870
- Soret Diffusion of:
 Ag in Au 25,060
 Ag in Cu 25,060
 Au in Ag 25,060
 Au in Cu 25,060
 Co in Cu 25,060
 Ge in Cu 25,060
 Ti in Au 25,060
- Space-Charge-Limited Current in GaP Junctions 25,819
- Specific Heat - See also Heat Capacity, Debye Temperature; Grüneisen Parameter
- Specific Heat of:
 Nb 25,719, 25,720
 Nb Superconductors 25,719, 25,720
 Ne (Solid) 25,723
 Solid Solutions 25,718
 Ta-Nb Superconductors 25,279
 Ta-V Superconductors 25,279
 Tm 25,721
 Transition Metal Superconducting Compounds 25,296
- Spectrometers, γ -Ray 26,437, 26,439
- Spin Densities in Fe-Rh 25,410
- Spin Flop in Hematite 25,534
- Spin Flopping Relaxation in $\text{CuCl}\cdot 2\text{H}_2\text{O}$ 25,520
- Spin Lattice Relaxation in:
 $\text{Al}_2\text{O}_3\text{:Cr}^{3+}$ 25,570
 $\text{CaF}_2\text{:RE}$ 25,568
 KCl:F-Center 25,567
 Na 25,565
 Rare Earth Salts 25,569
 TmAlG:Yb^{3+} 25,519
 TmGaG:Yb^{3+} 25,519
- Spin Relaxation in:
 Na 25,558
 Si 25,559
- Spin Systems, Free Energy of 25,418
- Spin Wave Resonance in Magnetic Films 25,523
- Spin Wave Scattering in:
 Co, Ferromagnetic 25,426
- Spin Wave Scattering in: (Cont'd)
 Heisenberg Ferromagnets 25,424
 Ni, Ferromagnetic 25,426
- Spin Waves, Scattering of Magnetic 25,425
- Spin Waves in:
 Cr 25,430
 Ferrimagnets 25,421
 Ferrimagnets, Instabilities in 25,429
 Heisenberg Ferromagnets 25,423
 Magnetoplumbite Ferrites, Theory of 25,419
 Metals, Lifetime of 25,422
 MnCr_2S_4 25,432
 MnF_2 25,433
 Permalloy Films 25,427, 25,428, 25,431
- Spontaneous Magnetization, Theory of 25,444
- Sputtering of:
 Ag Films 25,101
 Cu Films 25,101
- Sputtering Equipment for Fabrication of Ta Films 25,806
- Square Wave Generators 26,252
- Squaring Circuits, Tunnel Diode 26,369
- Stabilizers, Current 26,387
- Stacking Fault Etch Pits in SiC 25,035
- Stacking Faults, Vacancy Annihilation of 24,993
- Stacking Faults in:
 Ag 25,029
 Au 25,029-25,031
 CdS:GaCl_3 25,033
 Cu, Hydrogen Content Effects on 25,032
 ZnS 25,034
- Staircase Generators 26,152
- Steel,
 Ultrasonic Attenuation in 25,784
 Ultrasonic Velocity in 25,784
- Stepping Registers 26,362
- Storage Logic Circuits 26,329
- Stress-Strain Properties of Au Films 25,765
- Stress-Wave Propagation in Al 25,756
- Strontium-Bismuth Titanates, Dielectric Properties of 25,186
- Strontium Chloride: Mn^{2+} , Paramagnetic Resonance of 25,560
- Strontium Fluoride: Eu^{2+} , Faraday Rotation in 25,714
- Strontium Oxide: Eu^{2+} , Paramagnetic Resonance of 25,577
- Strontium Phosphate:Cu, Luminescence of 25,649
- Strontium Potassium Ferrites, Magnetic Anisotropy of 25,495
- Strontium Scandates,
 Crystal Structure of 24,972
 Preparation of 24,972
- Strontium Titanate,
 Breakdown in 25,182
 Dielectric Breakdown in 25,182
 Lattice Dynamics of 25,155
 Phase Transitions in 25,155
- Sublimation of B, Heat of 24,886, 24,887
- Sulfur-Boron Fluoride, Crystal Structure of 24,940
- Superconducting Al, Transition Temperature of 25,300
- Superconducting Al Films, Transitions in 25,323, 25,324
- Superconducting Alloys, Prediction of 25,274
- Superconducting Ba-Au, Transition Temperature of 25,298
- Superconducting Binary Transition Metal Compounds,
 Magnetic Susceptibility of 25,296
 Specific Heat of 25,296
 Transition Temperature of 25,296
- Superconducting Cylinders, Trapped Flux in 25,313
- Superconducting Delay Lines 26,107
- Superconducting Dynamos 26,103
- Superconducting Energy Storage Devices 26,100, 26,101
- Superconducting Gating Devices 26,106
- Superconducting Generators 26,102
- Superconducting In Films,
 Thermal Conductivity of 25,734
 Transitions in 25,324

- Superconducting In-Pb,
 - Lattice Parameters of 25,282
 - Properties of 25,282
- Superconducting In-Sn,
 - Lattice Parameters of 25,282
 - Properties of 25,282
- Superconducting La, Mechanism for 25,283
- Superconducting Magnets - See also Superconducting Solenoids
- Superconducting Magnets 26,089, 26,096, 26,105
- Superconducting Magnets, Design of 26,093
- Superconducting $\text{Mo}_3\text{Al}_2\text{C}$,
 - Lattice Parameters of 25,280
 - Properties of 25,280
- Superconducting Mo-Re, Resistance in 25,306
- Superconducting Motors 26,104
- Superconducting Nb,
 - Critical Field of 25,291, 25,292
 - Current Density of 25,308
 - Magnetization of 25,291
 - Penetration Depth in 25,310
 - Resistance Transition in 25,308
 - Specific Heat of 25,719, 25,720
 - Upper Critical Field of 25,292
- Superconducting NbC, Transition Temperature of 25,301
- Superconducting Nb-Sn, Transient Phenomena in 25,281
- Superconducting Nb_3Sn , Critical Current of Irradiated 25,289
- Superconducting Nb_3Sn Coils, Critical Current in 25,290
- Superconducting Nb-Ti Coils, Critical Current in 25,290
- Superconducting NbZr, Energy Gap of 25,286
- Superconducting Nb-Zr,
 - Magnetization of 25,327
 - Magnetocaloric Effect in 25,750
 - Paramagnetic Moments in 25,549
 - Resistance in 25,306
- Superconducting Nb-Zr Coils,
 - Critical Current in 25,290
 - Flux Jumping in 25,316
- Superconducting Nb-Zr Cylinders, Magnetization of 25,328
- Superconducting Pb, Surface Superconductivity in 25,305
- Superconducting Pb Films,
 - Thermal Conductivity of 25,734
 - Transitions in 25,324
- Superconducting Pb Junctions,
 - Energy States in 25,326
 - Tunneling in 25,326
- Superconducting Pb-Tl, Surface Superconductivity in 25,305
- Superconducting Pb-Tl Films,
 - Critical Field of 25,294
 - Penetration Depth in 25,312
- Superconducting $\text{Pb}_{0.5}\text{Tl}_{0.5}$,
 - Critical Field of 25,293
 - Upper Critical Field of 25,293
- Superconducting Sheets,
 - Current in 25,453
 - Magnetic Field in 25,453
 - Magnetization of 25,453
- Superconducting Sn,
 - Energy Gap of 25,285, 25,789
 - Ultrasonic Absorption in 25,789
- Superconducting Sn Cylinders, Paramagnetic Moment in 25,548
- Superconducting Sn Films,
 - Flux in 25,320
 - Flux Jumping in 25,318
 - Quantized Vortex Phenomena in 25,320
 - Thermal Conductivity of 25,734
 - Transitions in 25,324
- Superconducting Sn-Ag Films,
 - Critical Field of 25,295
 - Edge Effect Suppression in 25,295
- Superconducting SnIn Films, Critical Field of 25,321
- Superconducting Solenoids - See also Superconducting Magnets
- Superconducting Solenoids 26,094
- Superconducting Solenoids,
 - Field Calculations for 26,090
 - Field Energy Removal from 26,091
 - Performance of 26,095
 - Review on 26,088
 - Training in 26,092
- Superconducting Switches 26,098, 26,099
- Superconducting Ta,
 - Pair Correlations in 25,278
 - Penetration Depth in 25,311
- Superconducting TaC, Transition Temperature of 25,301
- Superconducting Ta-Nb,
 - Paramagnetic Susceptibility of 25,279
 - Properties of 25,279
 - Specific Heat of 25,279
- Superconducting Ta-V,
 - Paramagnetic Susceptibility of 25,279
 - Properties of 25,279
 - Specific Heat of 25,279
- Superconducting Ti:Mn, Transition Temperature of 25,299
- Superconducting Ti-V, Flux Jumping in 25,317
- Superconducting Transition Metals, Mechanisms for 25,273
- Superconducting Transmission Line Structures, Transitions in 25,288
- Superconducting U, Mechanism for 25,283
- Superconducting V_3Ga , Penetration Depth in 25,311
- Superconducting V_3Ge , Penetration Depth in 25,311
- Superconducting V_3Pt , Penetration Depth in 25,311
- Superconducting V_3Si , Penetration Depth in 25,311
- Superconducting Wires, Fabrication of Nb_3Sn 26,097
- Superconductivity,
 - Model for 25,275, 25,276
 - Theory of 25,272
- Superconductor Rod Systems, Intermediate State in 25,302
- Superconductors,
 - Actinide Metal 25,277
 - Anisotropy Effects on 25,321
 - Critical Current of 25,287
 - Critical Field of 25,309
 - Critical Magnetic Field of 25,309
 - Dielectric Constant of 25,181
 - Dissipation Supercurrents in 25,307
 - Energy Gap of 25,284
 - Flux in 25,314
 - Flux Penetration in 25,309
 - Intermediate State Torque Measurements of 25,304
 - Knight Shift in 25,599
 - Metastable Resistance States on 25,303
 - Quantized Vortex Phenomena in 25,319
 - Thermal Conductivity of 25,733
 - Transition Temperatures of 25,297
 - Tunneling in 25,325
- Superconductors (II), Flux Flow in 25,315
- Superparamagnetism in:
 - Co Ferrite 25,552
 - Ni Ferrite 25,552
- Superregenerative Circuits, Self Quenching in 26,292
- Surface Conductivity of:
 - Ge, Temperature-Pressure Relationships in 25,265
 - Ge:Au 25,266
 - InSb 25,267, 25,268
- Surface Effects on Transistors 25,873
- Surface Field Effect Transistors, Design of 25,867
- Surface Passivation of Devices 25,844
- Surface Potential of InSb 25,267
- Surface Recombination in:
 - CdS 25,222
 - Semiconductors 25,213
- Surface States in PbS Films 25,263
- Surface Structure - See also Crystal Structure
- Surface Structure of:
 - Emeralds 24,922
 - Ge 24,921
- Surfaces,
 - Etching of Topaz 25,127
 - Interactional Energy of Inert Gases with Metal 25,112
- Susceptibility,
 - Magnetic 25,380
 - Paramagnetic 25,550
- Susceptibility of:
 - Alkali Metals 25,380
 - Al-V-Tc 25,601
 - Anthracene 24,955
 - $\text{Ce}_2\text{O}_3 \cdot 2.67 \text{ P}_2\text{O}_5$ 25,715
 - Conduction Electrons 25,379
 - $\text{CuCl}_2 \cdot 2\text{H}_2\text{O}$ 25,520
 - Cu_2O Films, Magnetic 25,384
 - Cu-Zn Ferrites 25,381
 - EuGaG, Magnetic 25,388
 - Fe Formate 25,382
 - $\text{GdCl}_3 \cdot 6\text{H}_2\text{O}$ 25,137
 - Ge, Dielectric 25,196
 - Ni Formate, Magnetic 25,382
 - NiNO_3 , Magnetic 25,383
 - Pt 25,602
 - SmGaG, Magnetic 25,388
 - Ta-Nb Superconductors, Paramagnetic 25,279
 - TaV Superconductors, Paramagnetic 25,279
 - $\text{Th}_{1-x}\text{U}_x\text{Pd}_3$ 25,387
 - TiO_2 25,386
 - Transition Metal Superconducting Compounds 25,296
 - YIG 25,461
- Sweep Generators 26,250, 26,304
- Switches,
 - Ferrite 25,897, 25,898
 - Junction Capacitance 25,837
 - Superconducting 26,098, 26,099
- Switching in:
 - KNO_3 , Ferroelectric 25,195
 - Magnetic Films 25,465, 25,467
 - Magnetic Films, Creep 25,468, 25,469
 - Permalloy Films, Creep 25,468
- Switching Circuits - See also Logic Circuits
- Switching Circuits,
 - Bistable 26,215, 26,216
 - Design and Analysis of 26,207
 - Flip-Flop 26,213, 26,214
 - Gate 26,217
 - Low Impedance 26,220
 - Matrix 26,359
 - Microwave 26,208-26,211
 - Radar 26,208
 - Schmitt Trigger 26,212
- Switching Systems, Telephone 26,306, 26,307
- Switching Time Analysis, MRH 25,466
- Switching Time of Ni 25,466

T

- Tantalates,
 - Absorption Edge in 25,650
 - Luminescence of 25,650
 - Photoluminescence of 25,650
- Tantalum Capacitors, Fabrication of 25,813
- Tantalum Films,
 - Impurities in 25,041
 - Sputtering Equipment for Fabrication of 25,806
- Tantalum Foil Capacitors 25,812
- Tantalum Superconductors,
 - Pair Correlations in 25,278
 - Penetration Depth in 25,311
- Tantalum Carbide, Heat Capacity of 25,732
- Tantalum Carbide Superconductors, Transition Temperature of 25,301
- Tantalum-Carbon Systems,
 - Phase Equilibria in 24,865
 - Vaporization of 24,865
- Tantalum Gallium (Ta_5Ga_3), Crystal Structure of 24,938
- Tantalum-Niobium Superconductors,
 - Paramagnetic Susceptibility of 25,279
 - Properties of 25,279
 - Specific Heat of 25,279
- Tantalum Nitride Film Resistors,
 - Evaluation of 25,807
 - Properties of 25,808

- Tantalum-Tantalum Oxide-Tantalum Films,
Emission from 25,371
Field Emission from 25,371
- Tantalum-Vanadium Superconductors,
Paramagnetic Susceptibility of 25,279
Properties of 25,279
Specific Heat of 25,279
- Tape Recording System for Atmospheric Noise 26,321
- Telemetry,
Multiplexers for 26,315-26,317
PCM for 26,312, 26,313, 26,316, 26,317
PDM for 26,311
PSM for 26,314
- Telemetry for Medical Electronics 26,271, 26,272
- Telephone Handsets 26,305
- Telephone Line Circuits 26,309, 26,310
- Telephone Switching Systems 26,306, 26,307
- Telephone Systems, Underwater 26,299
- Telephone Toll Charge Computers 26,308
- Telephone Traffic Recorders 26,308
- Television Deflection Circuits 26,303
- Television Sweep Generators 26,304
- Tellurides of La 24,863
- Tellurium,
Crystal Structure of 24,903
Elastic Constants of 25,758
Phase Transitions in 24,903
- Tellurium Tetrachloride,
Crystal Structure of 24,960
Preparation of 24,960
- Temperature Controls 26,420
- Tensile Behavior of Mo Polycrystals 25,772
- Terbium,
Magnetic Ordering of 25,408
Magnetic Transitions in 25,408
- Terbium Cobalt, Magnetic Structure of 25,402
- Terbium Garnet, Faraday Rotation in 25,640
- Terbium Iron Garnet,
Magnetic Anisotropy of 25,500
Magnetization of 25,550
- Terbium Nickel ($TbNi_2$),
Antiferromagnetic Structure of 25,407
Ferromagnetic Structure of 25,407
Magnetic Structure of 25,407
- Terbium (Palladium, Silver), Magnetic Structure of 25,406
- Terbium (Silver, Indium), Magnetic Structure of 25,406
- Ternary Logic Circuits 26,329
- Thallium in Au, Diffusion of 25,060
- Thallium Chalcogenides, Crystal Structure of 24,968
- Thermal Conductivity of:
CdTe-CdSe 25,168
Gd 25,735
Ge 25,737
In Superconducting Films 25,734
InSb-CdTe 25,169
Organic Semiconductors 25,748
Pb Superconducting Films 25,734
Se, Temperature Dependence of 25,738
Si 25,737
Sn Superconducting Films 25,734
Superconductors 25,733
Zincblende Structure Crystals 25,736
- Thermal EMF of:
FeO, Composition Dependence of 25,264
PbS Layers 25,253
- Thermal Etching of:
Cu 25,128
Ice 25,129
- Thermal Expansion of:
Anthracene 24,955
Bi 25,741
C 24,949
Ge 25,739, 25,740
Graphite 24,949
Mg 25,741
MgO- Y_2O_3 25,742
RbNO₃ 25,191
Sn 25,741
 Y_2O_3 25,742
Zn 25,741
- Thermal Resistance of Transistors 25,854
- Thermal Resistivity, Spin Wave Scattering Calculations on 25,425
- Thermally-Induced Currents in Anthracene 25,221
- Thermistor Circuits 26,156
- Thermistors, SiC 26,087
- Thermocouples,
Pyrolytic Graphite 26,081, 26,082
Si-Ge 26,080
- Thermoelectric Converters 26,083
- Thermoelectric Coefficient of:
Ba-Sr TiO₃ 25,250
BaTiO₃ 25,250
- Thermoelectric Coolers, Performance Coefficient of 26,077
- Thermoelectric Devices, Review on 26,076
- Thermoelectric Energy Converters 26,456, 26,458
- Thermoelectric Generators 26,078
- Thermoelectric Generators,
Analysis of 26,079
Si-Ge 26,080
- Thermoelectric Heat Pumps 26,458, 26,459
- Thermoelectric Power of:
Au Wires 25,747
CdTe-CdSe 25,168
Co_{1-x}Fe_xSi 25,166
Ge, Phonon Drag Contribution to 25,745
Metals 25,743
MnTe, Magnon Drag Contribution to 25,746
Organic Semiconductors 25,748
SnTe 25,139
- Thermoelectric Properties of Ag Solid Solutions 25,245
- Thermoelectric Refrigerators 26,458, 26,459
- Thermoluminescence of:
CaF₂:Y 25,661
LiF 25,662
- Thermomagnetic Coolers, Figure of Merit for 26,086
- Thermomagnetic Devices,
Review on 26,076
Theory of 26,084
- Thermomagnetic Figure of Merit of:
Semiconductors 25,749
Semimetals 25,749
- Thermomagnetic Refrigerators 26,085
- Thermoregulators 26,420
- Thermostats, Automobile 26,285
- Thickness Analysis of Au Films 25,100
- Thickness Measurements of:
Dielectric Films 25,703
Semiconductor Films 25,703
- Thin Film - See also Films
- Thin Film Amplifiers 26,165
- Thin Film Circuits,
Capacitive Interactions in 26,126
Fabrication of 26,127
Substrates for 26,135, 26,137
- Thin Film Field Effect Transistors 25,870
- Thin Film Filters 26,269
- Thin Film Resistors 25,805
- Thin Film Resistors,
Cr/SiO 25,811
Evaluation of TaN 25,807
Properties of TaN 25,808
- Thin Film Transistor Circuits 26,150
- Thin Film Transistors 25,861
- Thin Film Transistors,
CdSe 25,859
Expressions on 25,870
Survey of 25,858
- Thorium Aluminide-Magnesium, Crystal Structure of 24,967
- Thorium Carbide, Lattice Constants of 24,935
- Thorium Copper Phosphate, Fluorescence of 25,674
- Thorium Lithium Phosphate:Cu, Fluorescence of 25,674
- Thorium Phosphate:Cu, Fluorescence of 25,674
- Thorium Silicate, Phase Transitions in 24,912
- Thorium Silver Phosphate:Cu, Fluorescence of 25,674
- Thorium Uranium Palladium, Susceptibility of 25,387
- Thulium,
Magnetic Ordering of 25,408
Magnetic Transitions in 25,408
Specific Heat of 25,721
- Thulium Aluminum Garnet:Yb³⁺, Spin-Lattice Relaxation in 25,519
- Thulium Gallium Garnet:Yb³⁺, Spin-Lattice Relaxation in 25,519
- Thulium Manganese (TmMn₂),
Antiferromagnetic Structure of 25,407
Ferromagnetic Structure of 25,407
Magnetic Structure of 25,407
- Thulium Nitride, Magnetic Properties of 25,415
- Time Delay Circuits 26,244
- Time Mark Generators, Tunnel Diode 26,435
- Time-to-Pulse Height Converters 26,223
- Time-to-Pulse Height Converters, Tunnel Diode 26,222
- Timers 26,434
- Timers, Sequence 26,364
- Timing Circuits 26,216
- Tin,
Energy Band Structure of 25,146
Magnetoresistivity Oscillations 25,335
Oxidation of 25,114, 25,122
Reduction of 25,122
Thermal Expansion of 25,741
- Tin Superconducting Cylinders, Paramagnetic Moment in 25,548
- Tin Superconducting Films,
Flux in 25,320
Flux Jumping in 25,318
Quantized Vortex Phenomena in 25,320
Thermal Conductivity of 25,734
Transitions in 25,324
- Tin Superconductors,
Energy Gap of 25,285, 25,789
Ultrasonic Absorption in 25,789
- Tin-Indium,
Density of 24,930
Lattice Constants of 24,930
- Tin Indium Superconducting Films, Critical Field of 25,322
- Tin-Silver Superconducting Films,
Critical Field of 24,295
Edge Effect Suppression in 25,295
- Tin Telluride,
Thermoelectric Power of 25,139
Valence Band Model of 25,139
- Titanium,
Oxidation of 25,118
Phase Transitions in 24,901
- Titanium:Co⁵⁷,
Lattice Dynamics of 25,154
Mössbauer Effect in 25,154
- Titanium:Mn Superconductors, Transition Temperature of 25,299
- Titanium-Carbon Systems,
Phase Equilibria in 24,865
Vaporization of 24,865
- Titanium Diboride, Heat Capacity of 25,732
- Titanium Dioxide,
Chemisorption of Oxygen on 25,688
Conductivity of 25,352
Photoconductivity of 25,688
Photovoltaic Effect in 25,699
Susceptibility of 25,386
- Titanium Gold (Ti₃Au), Crystal Structure of 24,920
- Titanium Nitride, Heat Capacity of 25,732
- Titanium-Nitrogen Systems,
Phase Equilibria in 24,865
Vaporization of 24,865
- Titanium-Vanadium Superconductors, Flux Jumping in 25,317
- Topaz Cleavages, Etching of 25,127
- Toroids, Magnetic Hysteresis Properties of Ni-Mn Ferrite 25,475
- Transducers, Biomedical 26,270

SUBJECT INDEX (Continued)

Transistor Bias Circuits 26,155
 Transistor Circuits, Model of 26,149
 Transistor Fabrication, Use of a Two-Step Diffusion Process in 25,054
 Transistors,
 Avalanche 26,154
 Breakdown in 25,852, 25,853
 CdSe 25,859
 Contacts for 25,874
 Current in Stressed 25,849
 DC Parameters of 26,167
 Fabrication of 25,872
 Field Effect 25,861-26,871, 26,151, 26,182, 26,183
 Four Layer 25,856
 High Gain 25,873
 Hot Electron 25,858
 Irradiation Damage in 25,845
 Large Signal Models of 25,850
 Leakage Current in 25,847
 Lumped Model of 26,149
 Micropower 25,873
 Noise in 25,855
 Photo-Field Effect 25,869
 Planar 25,872
 Radiation Effects on 25,802
 Reliability Testing of 25,846
 Stress Effects in 25,849
 Surface Effects on 25,873
 Testing of 25,847
 Thermal Resistance of 25,854
 Thin Film 25,858, 25,859, 25,861, 25,870, 26,150
 Transient Response of 25,851
 UHF Testing of 25,848
 Unijunction 25,857
 Transition Metal Bromides, Néel Temperature of 25,536
 Transition Metal Chlorides, Néel Temperature of 25,536
 Transition Metal Compounds, Energy Band Structure of 25,143
 Transition Metal Iodides, Néel Temperature of 25,536
 Transition Metal Superconducting Compounds,
 Magnetic Susceptibility of 25,296
 Specific Heat of 25,296
 Transition Temperature of 25,296
 Transition Metal Superconductors, Mechanisms for 25,273
 Transition Metals,
 Diffusion of Si in 25,064
 Ferromagnetism of 25,434
 Nuclear Magnetic Relaxation in Ferromagnetic 25,527
 Valence States in 25,434
 Transition Temperature of:
 Al Superconductors, Pressure Effects on 25,300
 Ba-Au Superconductors, Structure Variation of 25,298
 NbC Superconductors 25,301
 Superconductors 25,297
 TaC Superconductors 25,301
 Ti:Mn Superconductors, Concentration Effects on 25,299
 Transitions - See: Dielectric Transitions; Magnetic Transitions; Phase Transitions (Transformations)
 Transmission of CrI₃ 25,439
 Transmission Line Amplifiers 26,176
 Transmission Line Structures, Superconducting Transitions in 25,288
 Transmittance of:
 KMgF₃, Infrared 25,708
 MgF₂, Infrared 25,708
 Transmitters,
 Radio 26,302
 Single Sideband 26,301
 UHF 26,300
 VLF 26,299
 Trapping - See also Recombination

Trapping in:
 Anthracene, Hole 25,220, 25,221
 CdS-Type Crystals 25,216
 Se 25,694
 Si 25,219
 Travelling Wave Lasers, Ruby 25,982, 25,983
 Travelling Wave Masers 25,985
 Travelling Wave Masers,
 Efficiency of 25,981
 Filling Factor for 25,977
 Intermodulation in 25,978, 25,979
 Pulse Propagation in 25,976
 Ruby 25,980
 Rutile 25,984
 Tricesium Pentachlorocobalt, Crystal Structure of 24,961
 Trigger Switching Circuits, Schmitt 26,212
 Tunable Filters 26,265
 Tungsten,
 Cracking in 25,037
 Electron Emission from 25,361-25,363
 Emission from 25,361, 25,362, 25,370
 Ion Emission from 25,361-25,363
 Ion Induced Emission from 25,370
 Magnetoresistivity of 25,341
 Resistivity of 25,244
 Secondary Emission from 25,370
 Tungsten Carbide, Heat Capacity of 25,732
 Tungsten Monoboride, Heat Capacity of 25,732
 Tunnel Diode Amplifiers 26,173, 26,187
 Tunnel Diode Amplifiers,
 Hall Effect Isolators for 25,883
 Operation Beyond Cutoff of 26,188
 Tunnel Diode Analog-to-Digital Converters 26,371
 Tunnel Diode Circuits,
 Stabilization of 26,145-26,148
 Theory of 26,144
 Tunnel Diode Comparators 26,219
 Tunnel Diode Converters, Time-to-Pulse Height 26,222
 Tunnel Diode Logic Circuits 26,330
 Tunnel Diode Memory Units 26,353, 26,354
 Tunnel Diode Oscillators 26,199-26,202
 Tunnel Diode Oscillators, Computer Analysis of 26,198
 Tunnel Diode Pulse Height Discriminators 26,259
 Tunnel Diode Squaring Circuits 26,369
 Tunnel Diode Time Mark Generators 26,435
 Tunnel Diode-Transistor Logic Circuits 26,334
 Tunnel Diodes,
 Conductivity of 25,205
 Deterioration of 25,071
 Deterioration of GaAs 25,828
 Etching of 25,831
 Excess Current in Stressed 25,823
 GaAs 25,071
 Noise in 25,827
 Peak-to-Valley Ratios of 25,829
 Properties of 25,824, 25,825
 SiC 25,830
 Stress Effects in 25,823
 Tunneling in:
 Superconducting Junctions 25,326
 Superconductors 25,325
 Twin Intersections 25,025
 Twin Intersections, Conditions for 25,024
 Twinning in:
 Al₂O₃ 25,019
 Mo-Re 25,020
 Se Whisker Growth 25,111
 SiFe 25,768
 Twins in Cu Dendrites 25,022, 25,023
 Twins in Graphite Dendrites 25,021

U

UHF Transmitters 26,300
 Ultrasonic Absorption, Theory of 25,787
 Ultrasonic Absorption in:
 Al₂O₃ 25,791
 Bi 25,788

Ultrasonic Absorption in: (Cont'd)
 MgO 25,791
 Naphthalene 25,786
 p-Dichlorobenzene 25,786
 Quartz 25,790
 SiO₂ 25,790
 Sn Superconductors 25,789
 Ultrasonic Amplification, Phonon Maser Picture of 25,792
 Ultrasonic Amplification in CdS 25,794, 25,795
 Ultrasonic Amplifiers, CdS 25,794, 25,795
 Ultrasonic Attenuation, Theory of 25,779
 Ultrasonic Attenuation in:
 Al₂O₃:Fe³⁺ 25,782
 As₂O₃ 25,783
 B₂O₃ 25,783
 CdS 25,780
 GeO₂ 25,783
 Glass 25,783
 MnF₂ 25,781
 Nb-Zr 25,785
 Quartz 25,163
 SiO₂ 25,783
 Steel 25,784
 Ultrasonic Attenuation Change due to Dislocation Motion 25,011
 Ultrasonic Generation in CdS 25,793
 Ultrasonic Propagation in CdS 25,778
 Ultrasonic Relaxation in:
 As₂O₃ 25,783
 B₂O₃ 25,783
 GeO₂ 25,783
 Glass 25,783
 SiO₂ 25,783
 Ultrasonic Velocity in:
 Naphthalene 25,786
 p-Dichlorobenzene 25,786
 Steel 25,784
 Ultrasonic Velocity Change due to Dislocation Motion 25,011
 Ultrasonic Wave Propagation 25,776
 Ultrasonic Wave Propagation in:
 Ge 25,777
 Si 25,777
 Unijunction Transistors, Properties of 25,857
 Up-Converters, Parametric 26,234
 Uranium(IV) in Octahedral Coordination, Absorption in 25,642
 Uranium Superconductors, Mechanism for 25,283
 Uranium-Aluminum-Iron, Phase Diagram of 24,878
 Uranium Cadmium (UCd₁₁), Elastic Constants of 25,762
 Uranium Carbide, Lattice Parameters of 24,879
 Uranium-Carbon-Oxygen, Phase Diagram of 24,879
 Uranium Dioxide, Oxidation of 25,123
 Uranium Dioxide:Fe, Mössbauer Effect in 25,673
 Uranium Dioxide-Uranium Trioxide-Yttrium Oxide, Phase Diagram of 24,880
 Uranium Fluoride, Crystal Structure of 24,964
 Uranium-Molybdenum Oxide, Crystal Structure of 24,943
 Uranium Monocarbide, Growth of 25,095
 Uranium Monosulfide,
 Curie Point of 25,333
 Galvanomagnetic Properties of 25,333
 Hall Coefficient of 25,333
 Magnetoresistivity of 25,333
 Resistivity of 25,333
 Uranium Octaoxide, Crystal Structure of 24,962
 Uranium-Plutonium, Lattice Constants of 24,931
 Uranium-Tungsten Oxide, Crystal Structure of 24,943
 Uranyl Dihydroxide, Crystal Structure of 24,963

V

Vacancies,
 Distribution of 24,992
 Irradiation Produced 24,992
 Vacancies in:
 Ag 25,262

Vacancies in: (Cont'd)

- Al-Mg 24,988
- Fe, Kinetics of 24,987
- Graphite, Determination of 24,989
- KCl 25,184
- LiF, Irradiation-Anneal Effects on 25,752
- Vacancy Annihilation in fcc Metals, Stacking Fault 24,993
- Vacancy Clustering in Au 25,030, 25,031
- Vacancy Migration in:
 - Alloys, Activation Energy of 25,057
 - Metals, Activation Energy of 25,057
 - Solid Solutions, Activation Energy of 25,057
- Valence Analysis, Electron Spectroscopy in 25,040
- Valence Band of SnTe, Model of 25,139
- Valence States in Transition Metals 25,434
- Vanadium, Nuclear Quadrupole Moment of 25,171
- Vanadium-Chromium, Formation Energies of 24,884
- Vanadium Gallium (V_3Ga) Superconductors, Penetration Depth in 25,311
- Vanadium Germanium (V_3Ge) Superconductors, Penetration Depth in 25,311
- Vanadium Platinum (V_3Pt) Superconductors, Penetration Depth in 25,311
- Vanadium Silicon (V_3Si) Superconductors, Penetration Depth in 25,311
- Vapor Pressure of:
 - Cr over V-Cr 24,884
 - $GeCl_4$ 24,890
 - InSb 24,889
 - Mn over Mn-Fe-Ni 24,892
 - $SiCl_4$ 24,890
- Vapor Pressures in the Pb-Te System 24,891
- Vaporization of:
 - B_2C 24,886, 24,887
 - Hf-C 24,865
 - Nb-C 24,865
 - Ta-C 24,865
 - Ti-C 24,865
 - Ti-N 24,865
 - Ti-O 24,865
 - Zr-C 24,865
 - Zr-N 24,865
 - Zr-O 24,865
- Varactor Diodes,
 - GaAs 25,835
 - High Frequency Properties of 25,834
 - Impedance of 25,833
- Vector Product Hall Effect Generators 25,880
- Video Detectors 26,229
- VLF Transmitters 26,299
- Voltage Comparators 26,152
- Voltage Converters, DC-to-AC 26,394
- Voltage Regulators 26,380-26,386
- Voltage Sources 26,192
- Volume Expansion in:
 - Graphite 25,755
 - LiF, Irradiation-Anneal Effects on 25,752
 - NaCl, Irradiation-Anneal Effects on 25,753, 25,754

W

- Wattmeters, Remote Pickup 26,423
- Waveguides, Ferrite-Filled 25,899, 25,900
- Well Logging Systems 26,430, 26,431
- Whiskers,
 - de Haas-van Alphen Effect in Fe 25,151
 - Growth of:
 - AlN 25,110
 - Se 25,111

X

- X-Band Maser Communication Systems 26,062
- X-Ray Absorption in Cu-Ni Alloys 25,630, 25,631
- X-Ray Detectors 26,441
- X-Ray Diffraction Study of:
 - Crystallites 24,914
 - Dislocations 24,995
- X-Ray Lasers, Feasibility of 25,987
- X-Ray Topographs of Dislocations in Si 25,002
- Xenon in:
 - Al_2O_3 , Diffusion of 25,077
 - BeO, Diffusion of 25,077
 - MgO, Diffusion of 25,077
 - ZrO, Diffusion of 25,077

Y

- Yield in:
 - Al_2O_3 25,770
 - Cu 25,766
- Young's Modulus of Cr 25,764
- Ytterbium Iron Garnet,
 - Magnetic Anisotropy of 25,500
 - Magnetization of 25,500
- Ytterbium Manganates,
 - Antiferromagnetic Properties of 25,199
 - Ferroelectric Properties of 25,199
- Yttrium Aluminum Garnet, Magnetoacoustic Resonance in 25,530
- Yttrium Aluminum Garnet:Nd³⁺ Lasers 26,005
- Yttrium-Cerium,
 - Magnetic Properties of 25,249
 - Resistivity of 25,249
- Yttrium Gallium Iron Garnet, NMR in 25,597
- Yttrium Iron Aluminum Garnet:Bi,
 - Crystal Structure of 24,969
 - Magnetic Moment of 24,969
 - Preparation of 24,969
- Yttrium Iron Garnet,
 - Ferrimagnetic Relaxation in 25,521
 - Magnetic Anisotropy of 25,500
 - Magnetization of 25,461, 25,462, 25,500
 - Magnetoacoustic Resonance in 25,530
 - Magnetoelastic Resonance in 25,529
 - Magnetoelastic Waves in 25,391
 - Susceptibility of 25,461
- Yttrium Manganates,
 - Antiferromagnetic Properties of 25,199
 - Ferroelectric Properties of 25,199
- Yttrium Orthoferrite,
 - Lattice Constants of 25,412
 - Magnetic Properties of 25,412
- Yttrium Oxide, Thermal Expansion of 25,742
- Yttrium Oxide:Er³⁺,
 - Absorption in 25,671
 - Fluorescence of 25,671
- Yttrium Oxide:Er³⁺ Lasers 26,006
- Yttrium Oxide:Eu³⁺,
 - Energy Transfer in 25,670
 - Fluorescence of 25,670

Z

- Zeeman Splitting in $CaF_2:Tm^{2+}$ 25,555
- Zener Diodes, Fabrication of 25,836
- Zinc,
 - Deformation of 25,774
 - Dislocation Multiplication in 24,998

Zinc, (Cont'd)

- Emission from 25,366
- Fracture of 25,018
- Glide in 25,774
- Lattice Vibrations in 25,162
- Photoemission from 25,366
- Thermal Expansion of 25,741
- Zinc in GaAs,
 - Diffusion of 25,070-25,073
 - Solubility of 25,073
- Zinc in GaAs Tunnel Diodes, Diffusion of 25,828
- Zinc in GaP,
 - Diffusion of 25,072, 25,073
 - Solubility of 25,073
- Zinc in InP,
 - Diffusion of 25,074
 - Solubility of 25,074
- Zinc Antimonide, Crystal Structure of 24,966
- Zinc Oxide, Growth of 25,087
- Zinc Oxide:Ni, Susceptibility of 25,385
- Zinc Phosphate-Cadmium Phosphate, Phase Diagram of 24,874
- Zinc Phosphate-Cadmium Phosphate-Magnesium Phosphate,
 - Cathodoluminescence of 24,874
 - Preparation of 24,874
- Zinc Selenide,
 - Dielectric Constant of 25,224
 - Effective Mass of Electrons in 25,224
 - Faraday Rotation in 25,224
 - Reflectivity of 25,224
- Zinc Sulfide,
 - Absorption in 25,618, 25,707
 - Fluorescence of 25,676
 - Reflectivity of 25,707
 - Stacking Faults in 25,034
- Zinc Sulfide:Cu,
 - Emission of 25,678
 - Preparation of 25,678
- Zinc Sulfide:Cu, Al, Cl, Electroluminescence of 25,656
- Zinc Sulfide:Mn, Electroluminescence of 25,655
- Zinc Tantalate,
 - Absorption Edge in 25,650
 - Luminescence of 25,650
 - Photoluminescence of 25,650
- Zinc Tungstate, Growth of 25,994
- Zinc Tungstate Masers 25,994
- Zincblende Structure Crystals, Thermal Conductivity of 25,736
- Zirconium,
 - Oxidation of 25,119
 - Rare Earths in 25,046
- Zirconium-Carbide, Heat Capacity of 25,732
- Zirconium-Carbon Systems,
 - Phase Equilibria in 24,865
 - Vaporization of 24,865
- Zirconium Diboride, Heat Capacity of 25,732
- Zirconium-Nitrogen Systems,
 - Phase Equilibria in 24,865
 - Vaporization of 24,865
- Zirconium Oxide, Diffusion of Xe in 25,077
- Zirconium-Oxygen Systems,
 - Phase Equilibria in 24,865
 - Vaporization of 24,865
- Zirconium-Plutonium, Lattice Constants of 24,931
- Zirconium-Sulfur, Phase Diagram of 24,868
- Zone Melting,
 - Electron Beam Heaters in 25,080
 - Impurity Distribution in 25,047
- Zone Melting Furnace 25,079

AUTHOR INDEX

- Aagard, R. 25,712
 Abdullaev, G.B. 25,738
 Abe, R. 25,197
 Abe, T. 25,048
 Abraham, D. 25,870
 Acamatu, H. 25,638
 Ackerman, J. 26,056
 Adam, G. 25,837
 Adamowicz, L. 25,532
 Adamson, M.C. 25,953
 Adawi, I. 25,365
 Adler, E. 25,713
 Admiraal, P.S. 26,103
 Aharoni, A. 25,200
 Ahrenkiel, R.K. 25,228
 Ainslie, N. 26,034
 Aitken, E. 24,880
 Aizu, K. 25,716
 Akchurin, R. 26,096
 Akhmedov, S. 26,096
 Akhundov, G.A. 25,616
 Akisue, O. 24,984
 Alberts, L. 25,394
 Alessandrini, E.I. 24,923
 Alexander, D.L. 26,251
 Alexander, F.B. 26,039
 Alexander, L.E. 24,914
 Alexandrov, E.B. 25,558
 Aldred, A.T. 24,884
 Alford, W. 25,009
 Aliev, G.M. 25,738
 Allen, R.J. 25,798
 Allgaier, R.S. 25,139
 Allred, J.C. 25,101
 Alper, A.M. 24,882
 Alperin, H. 25,426
 Alstad, J.K. 25,437
 Amari, H. 25,814
 Ambegaokar, V. 25,733
 Ameen, D.L. 26,098
 Ammen, G. 26,353
 Amos, A.T. 25,148
 Anatychuk, L.I. 25,256
 Anderson, E.E. 25,461
 Anderson, J.R. 25,151
 Anderson, R. 26,400
 Andrew, K. 25,120
 Andrews, E.G. 26,347
 Andrianov, D.G. 25,337
 Anger, H.O. 26,436
 Ansbro, P.M. 26,333
 Antonova, L.I. 24,863
 Apling, A. 25,051
 Appleton, A.S. 25,068
 Arai, T. 25,610
 Arajs, S. 25,735
 Archev, R.J. 25,617
 Arefev, I. 25,634
 Argon, A.S. 25,036
 Ariya, S.M. 25,264
 Arkharov, V.I. 25,056
 Armstrong, A. 25,271
 Armstrong, H. 25,654
 Arnold, D.M. 25,845
 Arrhenius, G. 25,298
 Arthur, Jr., J.R. 24,921
 Artman, J.O. 25,537
 Arzhany, P.M. 25,113
 Asanabe, S. 25,166
 Asawa, C.K. 26,672
 Ashby, A.T. 25,847
 Ashley, W.H. 25,045
 Asnin, V.M. 25,147
 Aso, K. 24,974
 Atabaeva, E.Ya. 26,260
 Aukland, M.F. 25,918
 Ausfresser, H.D. 26,225
 Authier, A. 25,002
 Averbakh, V.S. 25,897
 Awazu, K. 25,583
 Axe, J.D. 25,670
 Azároff, L.V. 25,630
 Azrt, R. 25,790
 Babbo, Jr., S.E. 24,895
 Babenco, A. 24,992
 Babcock, K. 24,979
 Babikova, Yu.F. 25,066
 Bacon, D.J. 24,929
 Boenziger, N. 24,936
 Bai, A.S. 25,118
 Baicker, J.A. 25,658
 Bailey, D. 26,123
 Bainbridge, P.L. 25,810
 Baker, C. 25,759
 Balaban, P. 26,370
 Balberg, J. 25,220
 Baldwin, N. 24,935
 Balk, P. 24,890
 Balkanski, M. 25,629
 Ball, C.J. 24,983
 Baltz, A. 25,459
 Band, H. 26,318
 Bang, W.B. 24,939
 Bapat, Y.N. 26,207
 Bare, D. 24,954
 Bariaux, D. 25,128
 Barker, W.A. 25,922
 Barkinkhoev, K.G. 25,738
 Barnes, R.G. 25,535
 Baro, R. 24,908
 Barrett, H.H. 25,182
 Barros, S. de S. 25,382
 Bartik, W.J. 25,915
 Bartkus, E.A. 25,909
 Barton, P. 25,766
 Bartram, R.H. 25,471
 Bartram, S. 24,880
 Baruch, P. 24,986
 Baskin, H.B. 26,329
 Basu, B. 25,008
 Batdorf, R.L. 25,232
 Bate, G. 25,437
 Bateman, T.B. 25,777
 Batha, H.D. 26,087
 Batterman, B.W. 25,399
 Battin, J. 26,297
 Baudin, J.A. 26,220
 Baugh, C.W. 25,945
 Bean, W. 25,271
 Bechtel, R. 26,393
 Beck, A.J. 25,801
 Becker, J.J. 25,486
 Becker, R.L. 25,496
 Beckman, O. 25,248
 Beddoes, M. 26,371
 Beeler, Jr., J.R. 24,980
 Bell, B.H. 26,153
 Bell, N.W. 26,230
 Bell, R.O. 25,102
 Belland, E.N. 26,325
 Belle, M.L. 25,706
 Bemski, G. 25,409
 Bendik, M.A. 25,069
 Beneteau, P.J. 26,168
 Bennett, L.H. 25,588
 Bennett, S. 25,589
 Beracqua, S. 26,035
 Berge, P. 25,662
 Berger, L. 25,383
 Berger, S.B. 25,715
 Berglund, C.O. 26,416
 Berkeley, D.A. 25,967
 Berko, S. 26,222
 Berlag, R. Ya. 25,253
 Berlan, I.B. 25,668
 Bernan, I. 25,830
 Bernard, W. 25,336
 Bernstein, D. 25,258
 Bernstein, H. 24,865
 Berry, R.W. 25,807
 Bertaut, E.F. 24,926
 Berthel, K.H. 25,244
 Bertie, J.E. 25,636
 Beyer, R.T. 25,786
 Bibby, M.J. 24,901
 Bicknell, R.W. 25,105
 Bidault, M. 25,993
 Bienenstock, A. 25,739
 Bierig, R.W. 25,519
 Bigo, E.H.P. 25,556
 Bir, G.L. 26,330
 Bird, V.R. 25,560
 Birgels, P. 26,339
 Birgeau, R.J. 26,236
 Birks, J.B. 25,161
 Birle, J. 25,541
 Birle, J. 25,130
 Blackwell, G. 25,082
 Blair, R. 25,258
 Blakely, J.M. 25,765
 Blalock, T.V. 26,182
 Blatt, F.J. 25,743
 Blaughner, R.D. 25,317
 Blecher, T.J. 26,355
 Bloch, D. 25,445
 Blum, V.A. 25,857
 Blum, N. 25,534
 Blumenthal, R.H. 26,255
 Bockemuehl, R. 25,869
 Boesch, F.T. 26,109
 Bogdanov, S.V. 25,186
 Bogdanovich, A.S. 25,183
 Boggs, W.E. 25,114
 Bogomolov, V.N. 25,352
 Bojko, I. 25,574
 Bokov, V.A. 25,199
 Boltaks, B.I. 25,075
 Bolton, E.C. 26,321
 Bonyhard, P.I. 25,911
 Boorse, H.A. 25,719
 Boos, D.L. 26,390
 Booth, R. 25,403
 Borg, R.J. 25,053
 Borrego, J.M. 26,079
 Borsa, F. 25,600
 Bosch, S.H. 25,370
 Bortfeld, D. 25,941
 Boutin, H. 25,957
 Bowers, H. 25,366
 Bowman, G.P. 24,871
 Bowness, C. 25,895
 Boyd, G.D. 26,043
 Boyd, R.G. 25,424
 Bozorth, R.M. 25,411
 Brach, B. Ya. 25,264
 Bradshaw, G. 25,872
 Brady, L.E. 25,214
 Braginski, A. 25,501
 Brailsford, A. 25,776
 Bramley, A. 25,970
 Brander, R.W. 25,106
 Braslau, N. 25,942
 Brassart, F. 25,120
 Brauer, W. 25,204
 Braun, J.D. 25,062
 Brebrick, R.F. 24,891
 Brecher, C. 25,675
 Brenol, E. 25,956
 Bridge, N.J. 26,070
 Brixner, L.H. 24,979
 Brodin, M.S. 25,626
 Brophy, V.A. 25,675
 Brosset, C. 24,945
 Brouns, E. 24,973
 Brout, R. 25,433
 Brown, A.C. 25,242
 Brown, D.E. 25,699
 Brown, D.M. 25,098
 Brown, F. 25,090
 Brown, F.C. 25,228
 Brown, G.V. 26,090
 Brown, I.D. 24,956
 Brown, J.E. 26,116
 Brown, J.J. 24,874
 Brown, J.N. 25,704
 Brown, M.C. 25,332
 Brown, N. 24,998
 Brown, P.J. 25,430
 Brown, R.L. 26,454
 Brown, Jr., W.F. 25,389
 Brownlee, L. 24,953
 Brownlow, J.M. 25,909
 Brownword, R. 25,080
 Brumage, W.H. 25,385
 Brust, D. 25,144
 Bruyere, J.C. 25,471
 Bryant, F.J. 24,982
 Bryant, F.R. 26,121
 Bryant, J.I. 25,635
 Bucher, E. 25,296
 Buchhold, T.A. 25,099
 Buchta, G. 25,890
 Buck, R.J. 26,195
 Buck, O. 26,026
 Buck, T.M. 26,443
 Buckingham, A.D. 26,070
 Buckley, T. 26,162
 Budnick, J.I. 25,598
 Buehler, E. 26,097
 Buehler, M.G. 25,227
 Bukke, E.E. 25,656
 Bulabojs, J. 25,959
 Bulaeviskii, L.N. 25,192
 Bullough, R. 25,018
 Buotte, J.R. 26,443
 Burak, N.T. 26,078
 Buras, B. 24,915
 Burckhardt, C.B. 25,338
 Burger, J.P. 25,322
 Burgess, J.P. 25,879
 Burgess, R.E. 25,827
 Burkhalter, J.H. 25,791
 Burley, G. 25,728
 Burns, G. 26,027
 Burns, Jr., H.R. 26,336
 Burrus, C.A. 25,832
 Bushby, T.R.W. 25,804
 Businaro, T. 26,453
 Butera, R.A. 25,729
 Button, M.J. 26,085
 Buyers, W.J.L. 25,164
 Cable, J.W. 25,406
 Calahan, D.A. 26,113
 Calhoun, B.A. 25,577
 Callaway, J. 25,229
 Capana, V.J. 25,424
 Capone, B.R. 25,462
 Caporaso, A.J. 25,087
 Cardona, M. 25,293
 Carleton, H.R. 25,433
 Carlson, O. 24,954
 Carome, E.F. 26,069
 Carpenter, D.R. 26,039
 Carpenter, G.B. 24,939
 Carroll, P.E. 26,087
 Carroll, T.J. 26,042
 Carter, F.L. 24,966
 Carter, J. 24,972
 Casabella, P.A. 25,172
 Caserio, M. 26,278
 Casey, Jr., H.C. 25,074
 Caskey, D.L. 26,001
 Castro, P.S. 26,288
 Centner, R. 26,405
 Chadderton, L.T. 25,034
 Chamberlain, L.L. 24,893
 Chandler, B.S. 25,775
 Chandrasekhar, B.S. 25,316
 Chaney, P.E. 24,895
 Chang, H. 25,468
 Chang, W.S.C. 25,995
 Chapman, F.W. 25,518
 Chappell, G.C. 26,253
 Charig, J.M. 25,105
 Chasmar, R.P. 25,169
 Chen, C.W. 25,393
 Chen, D. 25,712
 Chen, F.S. 25,977
 Chen, T. 25,450
 Cherniack, G. 24,864
 Cherry, W.H. 25,281
 Chiba, S. 25,516
 Chick, B.B. 24,919
 Chi-jen, H. 26,052
 Chikawa, J. 25,007
 Chikazumi, S. 25,507
 Child, H.R. 25,406
 Chiles, W.H. 26,314
 Chin, G.Y. 25,491
 Chin-chi, M. 24,888
 Chizhikova, Z.A. 25,960
 Chow, W. 26,351
 Choyke, W.J. 25,660
 Christie, J. 25,771
 Ciccarello, I.S. 25,790
 Ciszewski, R. 25,401
 Clapsaddle, R.L. 26,119
 Clarebrough, L.M. 25,030
 Clark, B.C. 25,156
 Clark, G. 24,912
 Clark, N.A. 26,069
 Clark, R.C. 26,319
 Clarke, B.H. 25,521
 Clauer, A. 25,764
 Clawson, A. 25,344
 Clements, R.J. 26,431
 Clerc, G. 25,471
 Clogston, A.M. 25,602
 Cockayne, B. 25,039
 Cochran, W. 25,196
 Coffey, H.T. 26,094
 Cogan, E. 25,046
 Coggins, J.L. 25,363
 Cohen, M. 25,115
 Cohen, M.M. 25,116
 Cohen, M.S. 25,829
 Coil, R.A. 25,446
 Cole, J. 26,377
 Coleman, J.A. 26,248
 Coleman, W.E. 25,815
 Coll, J. 25,395
 Collins, D.J. 24,905
 Collins, J.H. 26,381
 Collins, M.F. 25,886
 Collins, S.A. 25,547
 Colombo, R. 26,050
 Colvin, R.V. 25,761
 Comer, J. 25,735
 Comly, J.B. 26,190
 Compton, J.B. 25,524
 Comstock, C.S. 26,126
 Congleton, R.S. 25,503
 Conklin, J.B. 25,934
 Conrad, H. 25,941
 Constantine, Jr., G. 25,142
 Conti, L. 25,019
 Conti, M. 25,770
 Conti, M. 25,772
 Conti, M. 25,773
 Conti, M. 26,359
 Conti, M. 26,453
 Conti, M. 26,453
 Conwell, E.M. 25,207
 Coogan, C.K. 24,910
 Cook, J.B. 26,387
 Cooke, A.H. 25,569
 Cooke, I. 25,680
 Cooper, B.R. 25,517
 Cooper, H.W. 25,121
 Corciovei, A. 24,992
 Cordes, A. 24,960
 Cordes, J. 25,161
 Corelli, J.C. 25,217
 Coren, R.L. 25,456
 Corliss, L.M. 25,398
 Cormier, W.F. 25,407
 Cornwall, J.B. 26,398
 Cotton, J.D. 26,274
 Cottrell, H.E. 25,384
 Cotts, R.M. 25,551
 Court, I.N. 25,591
 Cowley, R.A. 25,935
 Cox, A.F.J. 25,155
 Cox, C.W. 24,982
 Cox, D.E. 26,198
 Cramer, E.M. 25,541
 Crane, L.T. 24,937
 Crapo, W.A. 25,076
 Crawford, B. 25,309
 Crevecoeur, C. 25,909
 Crocker, A. 26,152
 Croft, W.J. 25,189
 Cromer, D.T. 24,968
 Cronin, G. 24,964
 Crowley, M. 25,091
 Crownover, J.W. 24,877
 Crowther, T.S. 26,362
 Cuff, K.F. 25,469
 Cullen, A.L. 25,141
 Cullen, G.W. 26,049
 Culver, W. 25,289
 Culver, W. 25,950

AUTHOR INDEX (Continued)

Cunningham, D.A.	Dodge, W.R.	26,446	Feiner, A.	25,906	Friedlaender, F.J.	24,873	Gruzin, P.L.	25,066
24,883	Dolling, G.	25,158	Felcher, G.P.	25,407	25,288, 25,506	Givens, M.P.	Guentert, O.J.	24,948
Curtis, J.G.	25,161	Feldman, J.	25,943	Frolov, O.S.	25,263	Gladyshevskii, E.I.	Guertin, R.F.	25,136
Cusano, D.A.	Doman, R.C.	24,882	Feltham, P.	25,262	25,819	24,938	Guiliano, M.	25,873
Czekajewski, J.	Domen, S.R.	26,446	Fenichel, H.	25,723	Frost, E.	Glassbrenner, C.J.	Gulbransen, E.	25,120
	Dong, D.	24,890	Fenner, G.E.	25,261	Fryxell, R.	25,737	Guldner, W.G.	25,041
Dahl, J.P.	Donoho, P.L.	25,570	Fensham, P.J.	25,384	25,775	Glasser, M.L.	Gulyaev, Y.	25,149
Dahlberg, R.S.	Dooley, H.	26,406	Fergus, R.W.	26,451	24,950	Glässer, W.	Gupta, R.	25,173
Daintree, E.J.	Dork, R.	25,195	Ferguson, J.	25,708	24,918	26,036	Gurevich, L.E.	25,346
Dalman, G.C.	Dornberger-Schiff, K.	25,360, 24,971	Fesenko, E.G.	25,191	Fujimoto, S.	Glinchuk, M.D.	Guseinova, E.S.	25,616
			Feucht, D.	25,208	Fujita, F.E.	25,202	Gutierrez, W.	25,859
Damask, A.C.	Douglas, T.B.	25,730	Feuerstein, S.	25,772	Fujiwara, H.	Glover, III, R.E.	Gutkin, A.A.	25,657
Damiano, V.	Dove, D.B.	25,484	Fibich, M.	25,325	Fujiwara, K.	Glowacki, J.	Gutowsky, H.S.	24,910
Damon, R.	Dowley, M.W.	26,091	Figgis, B.N.	24,961	26,322	Goedemoed, S.	Gutsche, E.	25,619
Danielson, Jr., G.E.	Downs, N.	26,300	Figielski, T.	25,212	Fullerton, L.D.	Goetzberger, A.	Gutwin, O.A.	25,909
25,946	Doyle, E.F.	26,102	Filipescu, N.	25,641, 24,913	Furuta, N.	Gains, E.	Gutzwiller, M.C.	25,434
Dantsiger, A.Ya.	Doyle, W.D.	25,459, 25,456, 25,450	Finch, C.	24,912	Fushimi, S.	Gold, A.V.	Guyon, E.	25,322
Danzer, P.	Dozier, J.W.	26,241	Finch, R.H.	25,816	24,875	Gold, L.	Gyorgy, E.M.	25,485, 25,530
Das, B.N.	Drazier, J.W.	25,790, 25,791	Fine, S.	26,060	Gaerther, W.W.	Goldberg, C.		
Das, T.P.	Drexford, K.	25,791	Fink, H.J.	25,834	Gagnon, G.P.	Goldberg, N.		
da Silva, X.A.	25,791		Fischer, J.E.	25,217	25,469	25,392		
Date, M.	Dresner, J.	25,347	Fischler, S.	26,085	Gaigher, H.L.	Goldman, A.S.	Haaf, W.R.	24,958
Daughton, J.M.	Drum, C.M.	25,110	Fischman, M.	26,244	25,017	Goldstein, B.	Haas, C.	25,143, 25,746
Dautreppe, D.	Dubrovskii, G.B.	25,611	Fisher, M.E.	25,372	25,579	Golikova, O.A.	Haga, E.	25,615
Davis, D.H.	Dunavan, D.S.	26,332	Fishman, A.J.	26,178	25,960	Golynnya, G.I.	Haggerty, P.E.	26,116
Davis, Jr., D.T.M.	Dungan, R.	25,188	Fistul, V.I.	25,337	26,023	Gomulka, S.	Hagström, S.	25,040
26,067	Durrett, R.H.	25,514	Fitch, D.B.	25,624	Gallagher, P.K.	Gondo, Y.	Hahn, E.L.	25,592
Davis, F.N.	Dvorak, R.F.	26,451	Fitzgerald, A.G.	25,034	25,880	Goodman, A.	Hahn, G.	25,037
Davis, J.I.	Dwight, K.	25,397, 25,432, 25,546	Fitzgerald, T.M.	24,919	25,571	Goodstein, L.	Haistry, R.	25,091
Davis, M.	25,432, 25,546		Flanagan, T.B.	24,934	Gamble, F.T.	Goodwin, F.E.	Haiz, R.H.	25,311, 25,822
Davison, S.G.	Dzhafarov, T.D.	25,075	Flaschen, S.S.	25,121	25,045	Gooves, S.	Hakim, E.B.	25,852, 25,854
Daw, H.A.			Flax, L.	26,090	Gardner, R.D.	Gordon, D.I.	Halaby, S.A.	26,135
Day, J.D.A.	Eagle, F.	26,243	Flicker, H.	25,658, 25,845	25,727	Gordon, E.	Hall, C.	25,188
Dayhoff, E.S.	Earleywine, E.	24,858	Flint, G.W.	26,063	Garland, J.W.	Goswami, K.N.	Hall, R.D.	25,174
Dean, R.T.	Ecklund, W.L.	26,210	Floren, S.	25,006	25,297	Goto, M.	Hall, R.N.	25,092
de Atley, E.R.	Economou, N.A.	25,184	Flournoy, P.	24,979, 26,009	Garlock, G.F.J.	Goto, T.	Hall, W.F.	24,887
De Blois, R.W.	Edgar, A.D.	24,876	Fok, M.V.	25,656	24,982, 25,646	Gottlieb, E.	Hallsted, R.E.	25,669
Decell, R.F.	Edwards, R.	25,849	Folder, W.	26,158	Garret, C.G.B.	Goulding, F.S.	Hamasaki, J.	26,160
De Coster, M.	Edwards, S.	25,149	Follis, L.E.	26,042	25,920	Grabbe, D.	Hamer, F.	25,768
Deigen, M.F.	Effer, D.	25,042	Foner, S.	25,537, 25,544	Gartseva, L.E.	26,132	Hamilton, D.	25,283, 25,850, 25,862
De Jonghe, L.	Ehlers, E.	25,130	Fontaine, G.	25,014	25,218	Gashor, S.	Hamilton, D.J.	26,149
de Jong, M.	Ehrenreich, H.	25,701	Forbes, III, H.L.	25,254	25,368	Gaudios, J.	Hamilton, D.R.	25,660
Dekhtyar, I.Ya.	Elbaum, C.	25,008, 25,011, 25,780	Ford, G.M.	26,279	25,628	Gayles, J.N.	Hamilton, J.F.	25,214
de Klerk, D.	Elfant, R.F.	25,909	Forlani, F.	25,330	25,302	Gazey, B.K.	Hamilton, P.M.	24,859
De Lange, O.E.	Eliseev, A.A.	24,863	Forsyth, J.B.	25,430	26,299	Gazis, D.C.	Hamilton, S.	25,893
Delves, R.T.	Elleman, T.S.	25,077	Forsythe, J.G.	26,009	25,156	Geilikman, B.T.	Hamilton, W.	24,913
De Maria, A.J.	Elliott, A.G.	24,864	Fortgang, M.M.	26,202	25,321	Geissinger, E.L.	Hamme, J.	24,879
25,947	Elliott, D.W.	25,763	Forty, E.	25,914	25,806	Geller, M.	Hammer, K.E.	26,305
Dembinski, S.T.	Ely, B.W.	25,051	Foster, G.M.	25,307	25,941	Geller, S.	Hammond, Jr., J.H.	26,303
de Micheli, S.M.	Emmons, R.B.	26,048	Foster, K.	25,438	24,961	George, R.E.	Hancock, J.	25,654
Demos, J.R.	Engeler, W.E.	26,022	Foster, M.D.	26,424	26,387	Gerharz, R.	Hanlet, J.M.N.	26,378
de Planta, T.	Ergonist, R.D.	26,129	Foster, R.J.	25,916	26,051	Gerlach, M.	Hanned, B.	26,048
Dero, V.E.	Ergon, J.E.	25,085	Fowler, A.	26,017, 26,027	24,961	Germain, J.	Hanton, J.P.	25,480
DeSavage, B.F.	Epstein, M.	25,876, 25,878	Fox, A.J.	25,986	26,297	Gershenson, E.M.	Hanus, J.	25,423
Desilets, B.	Ergun, S.	24,914	Fox, D.K.	26,094	25,231	Gertsriken, S.D.	Happ, W.W.	26,126
DeSorbo, W.	Ernst, L.J.	26,166	Foy, P.W.	25,819	25,052	Gesi, K.	Harman, T.C.	26,085
Detert, K.	Espinosa, G.P.	24,969	Fraleux, J.	25,824	25,177, 25,190	Geusic, J.E.	Harmon, E.F.	26,133
Deutsch, T.	Esposito, R.J.	25,704	Francisco, S.G.	26,372	25,983, 26,005	26,005	Harper, B.J.	26,393
Deutscher, G.	Essmann, U.	25,026	Franklin, A.R.	26,021	26,240	Geyer, W.A.	Harris, L.	24,912
Dever, J.A.	Etter, P.J.	25,042	Franks, J.	25,678	24,924	Ghez, R.	Harrison, F.W.	25,500
DeVries, A.J.	Euler, K.	26,346	Frantsvog, D.J.	25,503	25,851, 26,276, 26,277	Giacoletto, L.J.	Harrison, J.E.R.	26,196
DeVries, R.	Evitts, H.C.	25,121	Fraser, D.B.	25,530	25,729	Giacoletto, L.J.	Harrison, S.E.	25,692
Dewald, J.F.	Evthuv, V.	25,952	Frazier, B.C.	25,541	24,954	Giauque, W.F.	Hart, T.	26,242
de Wolff, P.	Ewald, A.W.	25,335	Free, J.	25,954	26,444	Gibson, E.	Harte, K.J.	25,465
D'Haenens, I.J.	25,992		Freeborn, J.C.	26,204	24,954	Gibson, W.M.	Hartlin, E.M.	25,324
			Freedman, L.A.	26,304	25,158	Giger, A.J.	Hartman, P.	24,942
Dicke, R.H.	Fokan, J.C.	26,105	Freedman, M.S.	25,681	25,037	Gilat, C.	Hartman, R.L.	25,230
Dietrich, J.	Falge, Jr., R.L.	25,299	Freedman, N.S.	26,093, 26,105	26,425	Gilbert, A.	Hasegawa, K.	25,691
Dijkstra, J.	Fanslow, G.E.	26,165	Freeman, A.J.	25,134, 25,534	24,886	Gilbert, B.	Hashimoto, F.	25,049
Dill, H.G.	Farr, J.	25,080	Freeman, J.F.	25,436	24,953	Gilles, P.W.	Hässner, A.	25,067
Dill, J.G.	Farrell, G.	25,168	Fried, D.L.	26,041	25,571	Gilliam, E.	Hastings, J.M.	25,398, 25,407
Dillon, Jr., J.F.	Farrell, J.J.	25,502	Friedberg, S.A.	25,382, 25,383	25,414	Gilliam, O.R.	Hasty, T.E.	25,431, 25,515
Dillon, L.	Faulkner, T.A.	26,277			26,185	Gillmore, R.	Harkin, L.	25,929
Divito, E.L.	Fawcett, E.	25,152, 25,341			25,709	Gilson, R.A.		
Dixon, Jr., S.	Fechner, B.	25,550			25,949	26,184		
Dobrot, B.E.	Feigelson, R.	24,972				Ginsburg, N.		
Dobrov, W.I.	Fein, H.	26,422				Giordmaine, J.A.		
Dodd, R.						25,949		

AUTHOR INDEX (Continued)

Haubenreissen, W.	25,481	Hoopes, C.C.	26,361	Jarnagin, R.C.	25,220	Kazmierowicz, C.W.	25,333	Knowles, C.H.	26,116	Kucza, J.A.	25,096
Haverbusch, M.	25,378	Hopfield, J.J.	25,225	Jarrett, H.S.	25,405	Kchadavoj, V.A.	25,558	Kobayashi, H.	25,512	Kuglin, C.D.	25,141
Hayes, A.R.	26,280	Hoppes, D.D.	26,446		25,448	Kear, B.H.	25,015	Kobayashi, J.	25,193	Kuhlmann-Wilsdorf, D.	
Haynes, J.L.	26,316	Hora, H.	25,964	Jauvris, H.I.	25,504	Kearns, D.R.	25,696	Koc, S.	25,265		25,005
Hayward, C.M.	26,403	Horn, L.	25,829	Jennings, D.A.	25,989	Keating, J.D.	25,922	Koch, J.F.	25,356	Kulevsky, L.A.	25,939
Healey, III, D.J.	26,195	Horn, W.E.	25,945	Jenny, A.L.	25,812	Keating, P.N.	26,013	Kochneva, N.S.	25,614		25,982
Heard, H.	25,771	Horney, C.R.	26,366	Jense, M.	25,283	Kechin, V.V.	25,257	Koeffler, W.	26,414	Kulp, B.A.	25,687
Heckscher, F.	24,929	Houston, B.B.	25,139	Jensen, R.A.	26,212	Kedzie, R.W.	25,539	Koehler, W.C.	25,402, 25,406, 25,408	Kultkowski, J.	25,501
Hedgcock, F.T.	25,343	Hovi, V.	24,906	Jérôme, D.	25,580	Keesom, P.H.	25,720			Kulyupin, Yu.A.	25,652
Heffner, H.	26,054	Howard, D.F.	24,871	Jervis, E.R.	26,120	Keezer, R.	25,688	Koester, C.J.	26,000	Kume, K.	25,595
Hegenbarth, J.	24,936	Howard, R.C.	26,232	Jeynes, G.F.	26,253		25,699	Kohane, T.	25,529	Kunze, H.	25,964
Hegner, H.R.	25,847	Howson, D.P.	26,233	Jezewski, M.	25,178	Keiha, F.G.	24,882	Koikeda, T.	25,507	Kunzler, J.	26,097
Heiche, G.	25,443		26,234, 26,235	Joenk, R.J.	25,413	Keillor, J.H.	26,311	Kokado, H.	25,221	Kupferberg, K.	26,385
Heijne, L.	25,683	Hoy, G.R.	25,382	Johansson, G.	26,420	Keister, F.Z.	26,129	Kolakovski, K.	26,413	Kupsky, G.	25,835
Heinemann, H.M.	25,957	Huang, J.S.T.	26,154	Johari, O.	24,999	Keister, G.L.	25,799	Kolb, E.D.	25,087	Kurihara, K.	25,516
Heiniger, F.	25,279	Huebener, R.P.	25,747	Johnson, A.	25,766	Keldysh, L.V.	25,205	Kolb, R.	26,430	Kurkjian, C.R.	25,639
	25,296	Huelsman, L.P.	26,110	Johnson, G.W.	25,252		25,609	Kolbinger, J.	26,310	Kurada, H.	25,638
Heinz, W.W.	25,893	Huggins, R.A.	24,898	Johnson, L.D.	26,418	Kelllett, E.A.	24,949	Kolesnik, L.I.	25,700	Kurov, G.A.	25,000
Heiter, G.L.	25,901		25,032, 25,593	Johnson, L.E.	25,142	Kellington, C.M.	25,940	Komada, T.	24,925	Kushida, T.	25,596
Hejhall, R.C.	26,301	Hughes, E.	25,766	Johnson, R.A.	24,981	Kelly, A.	25,759	Kondo, Y.	26,298	Kuskevics, G.	25,370
Helfrich, W.	24,930	Hughes, F.	25,575		24,987	Kelly, B.T.	25,760	Konev, V.N.	25,065	Kuznetsov, A.	25,705
Helszajn, J.	25,888	Hughes, K.L.	26,159	Johnson, Q.C.	24,937	Kemanis, G.	25,429	Konigstein, J.	26,005	Kyhl, R.L.	25,564
Helliwell, B.S.	26,313		26,233	Johnston, J.	25,280	Kemp, M.	24,960	Konjukhov, V.K.	25,939		
Hemenger, P.M.	25,505	Hughes, T.P.	25,953	Jones, E.D.	25,594	Kenan, R.P.	25,421	Konnerth, K.	26,019	Lade, R.	25,209
Hemphill, R.B.	25,570	Hughes, W.E.	25,996	Jones, H.	25,718, 25,889	Kennedy, D.	25,054	Konorov, P.P.	25,253	LaFuse, H.G.	26,314
Hempstead, C.F.	25,315	Hull, D.	25,768	Jones, J.D.	26,104	Kennedy, K.	25,280	Kontos, J.	26,226	Lagunova, T.S.	25,340
Henderson, B.	24,933	Hulm, J.K.	26,094	Jones, R.A.	26,348		25,301	Kontsevoi, Yu.A.	25,700	Lainer, D.I.	25,118
Henderson, J.C.	24,995	Hummel, F.A.	24,874	Jones, R.V.	25,524	Kennedy, L.Z.	25,201	Kooi, C.F.	25,882	Laisley, F.H.	26,169
Hendricks, R.	24,908	Humphrey, F.B.	25,490	Jordan, T.	24,952	Keough, D.D.	25,258	Kopaev, Yu.V.	25,205	Lakatos, E.	26,287
Heng, T.M.	25,886	Hunt, G.R.	25,708	Jorgensen, C.K.	25,642	Kerns, Q.A.	26,260	Kopp, E.H.	26,111	Lalevic, B.	25,303
	25,899	Hunter, N.	26,285	Joseph, A.S.	25,312	Kessel', A.R.	25,553	Koppel, J.U.	25,162	Lam, D.J.	25,601
Henley, E.M.	25,284	Huntzinger, G.O.	26,404		25,603, 25,604	Kessler, H.K.	26,016	Kopville, U.Kh.	25,606	LaMartina, A.C.	26,432
Henning, G.R.	24,989		26,404	Joseph, M.	25,667	Kestigian, M.	25,539	Kornilov, B.V.	25,612	Lamb, Jr., W.E.	25,927
Henning, H.B.	26,163	Hurihara, K.	25,440	Joshi, S.K.	25,173	Kettunen, P.	25,767	Kornilov, I.I.	24,896	Lambert, Jr., L.M.	26,215
Henry, W.E.	25,463	Hussey, R.J.	25,119	Joyce, B.A.	25,105	Keyes, R.J.	26,032	Korobkin, V.V.	25,960	Lambert, R.B.	26,429
Heppner, R.	25,428	Hutchings, T.J.	25,514	Judge, J.S.	25,479	Keyes, R.W.	25,745	Korolkov, V.S.	25,554	La Mori, P.	25,771
Herman, F.	25,141	Hutchinson, R.I.	25,027	Juenke, E.	24,943	Khachatryan, Y.M.	25,381	Korolyuk, A.P.	25,788	Lampathakis, K.E.	26,340
Hertzberg, A.	26,071		24,880	Jung, W.	25,180		25,381	Korostoff, E.	25,442	Lane, C.T.	25,313
Heseltine, J.C.W.	25,763	Ibers, J.	24,913	Jura, G.	25,269	Kholuyanov, G.F.	25,251	Korpel, A.	25,954	Lane, G.	24,872
Heumann, F.K.	25,098	Ibuki, S.	25,583		26,298	Klotsman, C.M.	25,063	Korsun, V.	25,655	Lang, A.R.	25,002
Hewitt, R.R.	25,587	Ichikawa, A.	26,298	Kabalkin, S.S.	24,903	Kiefer, J.E.	25,991	Kortum, R.L.	25,141	Lang, G.K.	25,550
Hewson, A.C.	25,531	Ichinose, N.	25,516	Kabell, L.J.	26,228	Kikuchi, A.	25,978	Koschel, H.	25,846	Lange, H.	25,619
Higgins, V.J.	26,211	Idrestedt, I.	24,945	Kachik, R.H.	25,114	Kilby, J.S.	26,117	Koshelev, V.V.	25,898	Langer, J.S.	25,272
Hildenbrand, D.L.	24,887	Ihantola, H.K.J.	25,867	Kadenoff, L.P.	25,203	Kim, P.H.	25,965	Kosicki, B.	26,037	Lanza, C.	26,019
		Iida, S.	25,103	Kadanel, R.A.	26,360	Kim, Y.B.	25,314, 25,315	Kostylev, S.	25,655	Larson, A.C.	24,963
Hildish, L.	25,003	Ikedate, T.	25,097	Kagan, M.R.	25,641	Kimura, H.	25,031	Koteva, Y.	25,651		24,964
Hill, F.	26,327	Ikezawa, M.	24,990	Kagan, M.R.	25,641		25,615		25,682	Larson, A.H.	24,868
Hills, M.E.	24,959	Iliff, R.L.	26,064	Kaganov, M.I.	25,684	Kinbara, A.	25,100	Kouvel, J.S.	25,400	Larson, D.	25,428
Hilsum, C.	26,010	Im, H.B.	25,475		25,787	King, B.G.	25,826	Kovacs, I.	25,262	Larson, R.L.	26,284
Hindin, H.J.	26,202	Ingle, L.V.	25,803	Kahan, A.	25,607	King, D.D.	26,241	Kovalchenko, M.S.	25,064	Lasher, G.J.	26,024
Hinkley, E.D.	25,335	Ingrao, H.C.	26,428	Kahn, F.J.	26,428	King, J.	26,335	Kovalev, O.V.	25,396		26,025, 26,026
Hinrichsen, P.F.	26,452	Isborn, C.	26,213	Kahn, M.	26,114	King, P.G.R.	26,066	Kowalewski, L.	25,419	Lashkarev, V.E.	25,222
Hirsch, A.	25,466	Ishiguro, T.	25,794	Kalnajs, J.	25,751	Kinoshita, A.	25,084	Koyama, R.Y.	25,617	Latham, D.C.	25,862
Hirshfeld, A.T.	26,446	Ishihara, Y.	25,695	Kanal, L.N.	26,112	Kip, A.F.	25,356	Koyama, R.Y.	25,084	Laudise, R.A.	25,087
Hitt, J.	25,943	Ishii, K.	26,197	Kanamoto, J.R.	25,417	Kip, A.K.	25,355	Kozlov, M.M.	25,657	Laves, F.	24,920
Hodges, J.A.	25,572	Ismailov, F.I.	25,616	Kanter, M.A.	25,333	Kirby, P.L.	26,137	Kozlovskii, V.Kh.	25,194, 25,198	Lavine, J.M.	25,858
Hoemi, J.	25,866	Itskevich, E.S.	25,260	Kaplan, R.A.	25,957	Kirk, R.D.	25,648	Krag, W.E.	25,332	Lawley, A.	25,017
Hoffins, C.	26,239	Ivanov, G.A.	25,167	Kaplan, T.A.	25,397	Kirov, K.	25,216	Krainov, B.N.	25,421	Lawrence, P.E.	25,510
Hoffman, H.	25,457	Ivanov, O.S.	24,878		25,546	Kisako, S.	25,088		25,472		25,543
Hofstadter, R.	26,450	Izatt, J.R.	25,933	Karasik, V.	26,096	Kiselev, A.A.	25,623	Kramer, G.	26,441	Lawrence, T.R.	25,520
Hogan, C.L.	26,115	Izumi, K.	24,984	Karlsson, S.K.F.	26,429	Kiser, K.M.	25,359	Kraus, K.	26,156	Lawrence, Jr., W.L.	26,354
	26,116			Karmin, I.	26,257	Kisluk, P.	25,671	Kresin, V.Z.	25,321	Lax, M.	25,157
Hohl, J.H.	26,337	Jaccarino, V.	25,602	Karpovich, I.A.	25,698	Kiss, W.F.	26,184	Kressel, H.	25,835	Lazarus, A.J.	25,667
Holden, S.J.	25,125	Kasper, J.S.	24,928		25,928		26,185	Krinchik, G.S.	25,353	Leakey, D.	26,307
Holley, J.H.	26,129	Katoaka, S.	25,884	Kass, Z.J.	26,007	Kiss, Z.J.	26,007		25,640	LeBlanc, M.A.R.	25,327
Hollox, G.E.	25,039	Kato, T.	25,048	Kittrell, R.L.	26,418	Kizhaev, S.A.	25,199	Krishnan, R.	25,498		25,549
Holmes, D.	25,208	Katoh, J.E.	25,748	Kizhaev, S.A.	25,199	Klapp, S.	26,141	Krochuk, A.S.	25,626	Leclerc, P.	25,841
	25,929	Katrich, G.A.	25,266	Kleimack, J.J.	25,232	Klein, C.A.	26,081	Kroemer, H.	25,883	Le Crow, R.C.	25,522
Holmes, L.	25,388	Katsuraki, H.	25,540	Klein, E.	26,060	Klein, M.	25,764	Kroger, H.	25,778		25,530
Holonyak, Jr., N.	26,035	Katzman, M.	25,940	Klein, E.	25,764	Kleinman, D.	25,951	Kronast, B.	25,964	Lee, B.D.	26,431
		Kaufman, A.	26,356	Klein, M.	25,951	Klem, R.L.	26,458	Kruger, O.L.	25,731	Lee, C.A.	25,232
Holshouser, D.F.	26,055	Kaufman, L.	24,865	Kleimann, D.	25,951	Klugmann, E.	25,451	Kruh, R.	24,960	Lee, H.	25,835
Holt, A.G.J.	25,810	Kaufman, M.M.	26,353	Klein, E.	25,764	Knight, H.T.	25,246	Krupke, W.F.	25,671	Lefevre, H.W.	26,435
Honig, J.M.	26,084	Kawabe, U.	25,189	Klein, E.	25,764	Knight, W.D.	25,323	Krueger, O.L.	25,731	Leichner, G.H.	26,388
	26,085	Kawajii, S.	25,267	Klein, E.	25,764			Kryzhanovskii, V.	26,334	Leinkram, C.	25,873
Honig, W.	26,072	Kay, J.R.	26,171	Klein, E.	25,764				25,705	Leipold, M.	25,742
				Klein, E.	25,764			Kucherenko, I.V.	25,329	Leite, R.C.C.	26,012
				Klein, E.	25,764					Lemaire, H.P.	25,914

AUTHOR INDEX (Continued)

LeMay, C.Z.	25,070	Lykken, G.I.	25,487	Maxfield, B.W.	25,310	Misezhnikov, G.S.	25,095	Nadler, H.	25,095	Ogland, J.W.	25,945
Lemon, Jr., J.W.	26,364	Lynch, D.W.	25,254	Maycock, J.N.	25,255,	25,981	25,171	Nagasawa, H.	25,171	Oguchi, T.	25,533
Lempicki, A.	25,675	Lynch, F.J.	26,223	25,620	Mayer, S.E.	25,104	25,606	Nagibarov, V.P.	25,606	Ogurtani, T.O.	25,593
Lenk, H.	26,292				Mayo, E.S.	26,009	26,157	Nagorny, L.Ya.	26,157	Ohlwiler, R.W.	25,175
Lenotvitch, A.M.	25,960	MacAvoy, T.C.	26,135		Mazelsky, R.	24,966	25,262	Nagy, E.	25,262	Ohta, M.	25,049
		Macek, W.M.	26,067		Mazur, J.	24,927	25,414	Naiman, C.S.	25,414	Ohta, T.	25,744
Lentz, N.	26,218	MacElroy, D.E.	26,140		Mazzolai, F.M.	25,013	25,520	Nakada, I.	25,695	Ohtani, K.	25,084
Lepie, M.P.	26,081	MacFarlane, I.P.	26,145		McAvoy, N.	25,641	25,618	Nakado, M.	25,583	Okuda, T.	25,084
Lepoff, J.	26,173	Mackenzie, J.D.	25,131		McCabe, C.L.	24,892	24,974	Nakagawa, Y.	25,160	Okwit, S.	25,893
Lessoff, H.	25,914	MacKenzie, L.A.	25,361		McCaig, M.	25,902	24,978	Nakai, Y.	24,970	Oliver, R.W.	25,781
Leupold, H.A.	25,719				McCaldin, J.	25,050	26,209	Nakano, T.	25,193	Ol'khov, O.A.	25,513
Levi, L.	25,129	Madden, T.C.	26,444		McComas, R.	25,941	24,889	Nakamura, T.	25,084	Olson, C.E.	25,439
Levine, S.	26,380	Madden, R.	25,020,		McCormick, G.R.	24,866	25,093	Nakano, T.	25,193	Olsen, J.L.	25,300
Levitt, R.S.	26,038	25,031			McCreary, H.J.	26,308	25,629	Nambiar, K.K.	26,112	Olson, A.L.	25,455
Levy, M.	25,300	Maeland, A.	24,934		McCumber, D.E.	25,921,	25,319,	Nannichi, Y.	26,020	Olthius, Jr., R.W.	26,067
Levy, P.M.	25,137,	Maestre, N.E.	26,231		25,932		25,320	Narasimham, M.A.	25,101	O'Malley, T.F.	25,170
25,571		Magee, R.M.	25,802		McDermott, P.S.	26,039	24,947		25,511	O'Meara, T.R.	25,990
Levy, P.W.	25,571	Magleby, K.B.	26,254		McDonald, R.A.	25,732	26,069		25,850	Oredson, H.N.	25,488
Liben, W.	25,243	Mah, A.D.	24,885		McDonald, R.A.	25,732	26,427		25,340,	Oran, M.	25,021
Lichowsky, A.	26,389	Mahan, G.D.	25,225		McEvers, Jr., W.R.	26,431	25,003		25,690	Orowan, E.	25,036
Liebmann, W.	25,035	Maienschein, F.C.	26,437		McEvoy, Jr., J.P.	25,328	25,867		26,027,	Orton, J.W.	26,089
Lifshitz, I.M.	25,684				25,328		25,809		26,029, 26,030,	Osaki, K.	24,970
Likhter, A.I.	25,257	Maier, L.C.	26,116		McGuigan, J.H.	26,342	25,757		26,031	Otto, G.	25,712
Lilja, R.	25,179	Maiman, T.H.	25,919		McGuire, T.	25,440	25,471		25,398,	Overmeyer, J.	25,577
Lin, C.C.	25,385	Maine, R.W.	26,245		McIntyre, R.J.	26,440	26,447		25,410, 25,430,	Owen, A.E.	25,107
Lindholm, F.A.	25,850,	Makarov, V.P.	25,555		McKay, S.	25,755	25,402		25,547		
25,862		Makino, Y.	25,108		McLachlan, Jr., D.	24,893	25,674		25,790	Paalassalo, P.	24,906
Lindsay, A.	26,170	Makram, H.	25,498		McLean, W.L.	24,310	25,233		26,283	Paccard, D.	25,471
Lingle, J.T.	26,396,	Malgrange, J.L.	25,758		McLeod, J.A.	26,394	25,905		26,295	Pace, J.B.	26,354
26,401		Malhotra, G.L.	24,909		McLouski, R.	25,873	26,290		26,295	Pafomova, L.	25,705
Linz, A.	25,414	Malitson, I.H.	25,710		McNally, R.N.	24,882	26,419		26,295	Pajot, B.	25,044
Lipscomb, W.	24,952	Malkin, B.Z.	25,647		Mead, C.A.	25,150	26,417		25,614	Paladino, A.E.	26,085
Lipsett, M.S.	25,963,	Mallick, G.T.	25,316,		26,092		25,814		25,471	Palais, J.C.	25,900
25,966		26,092			Mallory, H.R.	26,421	25,527		25,952	Palser, R.	25,680
Lipson, H.G.	25,633	Mallory, W.R.	25,973		Mandell, L.	25,963,	25,937		25,781	Pandarese, F.	26,259
Litchman, W.S.	26,061	Mandel, L.	25,963,		25,966, 25,972		25,707		25,932	Pandiscio, A.A.	26,154
Litovchenko, N.M.	25,219	Manenkov, A.A.	25,557		Manley, G.W.	26,039	25,734		25,932	Pankove, J.	25,944
		Manin, H.M.	26,445		26,185		25,734		24,860,	Pantell, R.H.	25,948
Little, W.	25,278	Mannam, M.	24,984		Meiseles, M.	26,195	25,985		24,862	Papadakis, E.P.	25,784
Lityak-Gorskaya, L.B.	25,231	Manteuffel, E.W.	26,192		Meister, R.	25,782	25,480		24,860,	Pappalardo, R.	25,642
		Mapham, N.W.	26,392		Melchior, H.	25,853	25,077		25,079	Paretzkin, B.	25,023
Liu, B.	26,108	Mapyar, G.	25,972		Melchior, H.	25,853	25,437		25,785	Paris, D.T.	25,176
Liu, S.H.	25,234	Marccone, N.	24,905		Mendelson, K.S.	25,012	25,479		24,908	Parisi, G.I.	25,807
Loejejenicz, J.	24,915	Marcus, I.R.	26,203		Mengali, O.J.	25,881	25,178		26,248	Parker, E.	25,280
Loebner, E.E.	25,617	Marinace, J.	26,029		Menna, A.A.	25,102	25,061		26,014	Parker, J.R.	25,845
Loewenstern, L.R.	25,709	Maringer, R.E.	25,454,		Men'shikov, A.Z.	25,065	24,940		26,021	Parks, R.D.	25,319,
		25,764			Menyuk, N.	25,397,	25,371		26,021	25,320	
Logan, R.A.	25,232,	Maris, H.J.	25,163		25,432, 25,546		25,470		25,934	Parr, J.G.	24,901
25,819		Markiv, V.Ya.	24,938		Menzel, D.H.	26,428	25,991		25,798	Parzen, P.	26,044
Long, T.R.	25,484	Marlow, J.J.	26,193		Mercereau, J.E.	25,309	25,489		25,522	Pasechnik, Yu.A.	25,263
Longley, D.	26,365	Marple, D.T.F.	25,224		Merriam, M.F.	25,282,	25,769		25,994	Pashinin, P.P.	25,982
Loopstra, B.O.	24,962	Marples, J.A.C.	24,931		25,754		25,699		25,213	Pasotti, G.	26,095
Loos, K.R.	25,632	Marriage, A.J.	25,887		Merz, M.	25,811	25,268		25,427	Patel, A.R.	25,127
Lorenz, M.R.	25,215,	Marsh, K.J.	26,424		Mewissen, L.	25,673	25,377		25,048	Patrick, L.	25,660
25,582		Marshall, J.M.	25,756		Meyers, L.	25,278	25,378		25,476,	Paul, W.	25,145, 25,146
Lores, T.R.	24,904	Marshall, R.	25,618,		Michel, A.	26,029,	Mulhern, Jr., J.E.		25,576	Pauli, S.	26,205
Loring, S.J.	26,457	25,678			26,030, 26,031		25,336		25,195	Pauphinet, R.	25,445
Lotkova, E.	24,917	Marshall, S.A.	25,572,		Michel, R.E.	25,518	25,345,		25,464	Pavlovic, A.S.	25,395
Loucks, T.L.	25,153	25,573			25,165		25,843		25,040	Pavlovic, D.	25,438
Lounasmaa, O.V.	25,721	Masocchi, V.A.	25,342		25,421		25,296		26,440	Paxton, H.W.	24,892,
Lourens, J.A.J.	25,394	Martinet, A.	25,322		26,411		25,610		26,004	25,059	
Love, G.R.	25,055	Mascarenhas, S.	25,752,		25,985		26,168		26,130	Pearson, A.	25,351
Lovisell, W.H.	25,923	25,753			26,134		25,054		25,289	Pearson, A.D.	26,004
Low, W.	25,581	Masens, R.	26,147		26,349		26,303		25,697	Pearson, G.L.	25,072,
Lowde, R.D.	25,376	Mason, D.R.	24,867		25,172		25,537		26,395	25,073	
Lubart, L.	25,129	Mason, R.	24,955,		25,435		25,975		26,116	Pearson, J.D.	26,161
Lubell, M.S.	25,316,	24,961			25,421		25,769		25,357	Pearson, J.J.	25,447
26,092		Mason, W.P.	25,777		25,421					Peck, Jr., W.F.	25,350
Luborsky, F.E.	25,495	Mossenet, O.	25,471		25,677					Pecota, W.	26,415
Lucas, A.R.	26,352	Masters, J.	25,975		25,703					Peddle, J.G.	26,382
Lucas, R.C.	25,617	Matkura, Y.	25,818		25,021					Peek, Jr., R.L.	25,906
Lucovsky, G.	26,048	Matlow, S.	25,836		25,330					Peel, M.E.	26,131
Ludwig, G.W.	25,582	Matsumi, A.	24,900		24,896					Peibst, H.	25,003
Lunt, K.D.	26,161	Matthei, W.G.	26,164		25,622					Peiser, H.	25,023
Lüscher, J.	25,839,	Matthews, P.W.	26,104		25,067					Pekerman, F.M.	25,653
25,840		Matukura, Y.	25,817							Pellissier, G.E.	25,114
Lutes, O.S.	25,404									Peloke, J.R.	26,039
Lyashenko, S.	25,703									P'eng-nien, C.	24,888
Lyden, H.A.	25,223									Pensak, L.	25,227

AUTHOR INDEX (Continued)

Penslet, A.	25,128	Quade, C.R.	25,551	Rogachev, A.A.	25,147	Sawaguchi, E.	24,978	Serway, R.A.	25,572	Slack, G.A.	25,737
Pentina, A.A.	25,056	Queisser, H.J.	24,997	Rogers, J.	26,335	Sawyer, J.A.	25,367	Sery, R.S.	25,477	Slater, J.C.	25,140
Peretto, P.	25,470	Quentin, G.	25,758	Rogers, J.L.	26,106	Saxer, R.K.	24,871	Sevin, L.J.	25,865	Slater, L.E.	26,270
Perry, C.H.	25,708	Quinn, H.F.	26,039	Rolfe, J.	25,663	Scanlan, J.O.	26,188	Sewall, Jr., C.	26,438	Sleeswyk, A.W.	25,025
Perry, L.	26,456	Quinn, H.P.	26,282	Roof, Jr., R.B.	24,963	Schafer, A.H.	25,807	Sewell, P.B.	25,115	Slobodchikov, S.V.	25,690
Peschanskii, V.G.	25,787	Quinn, J.	25,779	Roulston, J.	24,964	Schaffer, P.S.	25,094	Shackleton, J.R.	26,075	Slusher, R.E.	25,592
		Quinzio, G.	26,168	Rooksby, H.	24,953	Schapink, F.	24,993	Shadrin, V.S.	25,259	Smakula, A.	25,751
Petoshina, L.N.	25,653	Quist, T.M.	26,032	Rooksby, H.P.	24,949	Schelleng, J.H.	25,497	Shafer, M.	25,045	Smeltzer, W.W.	25,119
Petrusevich, R.L.	25,069			Root, C.D.	25,868	Schenk, H.L.	25,290	Shagen, J.L.	26,326	Smit, W.	26,341
Petschauer, R.J.	25,905	Raag, V.	26,080	Ropp, R.C.	25,649	Schenk, M.	24,911	Shahbender, R.A.	25,917	Smith, A.D.	26,203
Pettit, G.D.	25,659	Radeko, V.	26,151	Rosenberg, H.	26,320	Schieber, M.	25,388	Shaifer, T.R.	25,847	Smith, B.R.	26,264
Pezirtzoglou, E.	26,262			Rosenblum, B.	25,293			Shalimova, K.V.	25,707	Smith, D.O.	25,499
Philipp, H.R.	25,701	Rae, W.J.	26,071			Schiffres, P.	26,268	Shaltiel, D.	25,387	Smith, F.W.	25,980
Phillips, A.B.	26,122	Rajnak, K.	25,135	Rosenfeld, A.	26,385	Schineller, E.R.	25,957	Shane, J.R.	25,539	Smith, G.S.	24,937
Phillips, J.C.	25,196	Ramamoorthy, C.V.	26,334	Rosenthal, J.A.	26,221	Schlechten, A.W.	24,868	Shaner, J.W.	25,534	Smith, H.W.	24,952
Photiades, N.F.	26,345			Ross, R.G.	25,085	Schlicke, H.M.	26,266	Shapira, Y.	25,785	Smith, J.	25,762
Pickart, S.J.	25,426	Ramasastri, C.	25,578	Ross, T.C.	26,247	Schlomann, E.	25,529	Sharpe, G.E.	25,826	Smith, J.H.	24,892
Pickus, M.	25,301	Ramer, C.E.	25,101	Rossing, T.D.	25,428	Schmeckenbecher, A.	25,912	Sharma, S.K.	24,909	Smith, L.	26,286
Pierce, J.F.	26,183	Rand, J.L.	25,756	Rossington, D.R.	25,125	Schmidt, W.F.	25,674	She, C.Y.	26,054	Smith, N.W.	25,986
Pierrorini, G.J.	24,941	Ranon, U.	25,584	Rossol, F.C.	25,517	Schmidt, C.T.	26,450	Sheftel', I.T.	25,250	Smith, P.H.	24,867
Pilat, I.M.	25,256	Rao, B.D.N.	25,564	Roth, H.	25,336	Schmidt, P.F.	25,107	Sheinkman, M.K.	25,222	Smith, R.B.	25,833
Pilkun, M.H.	26,018	Rao, C.N.	24,932	Roth, W.L.	25,495	Shmidt, V.V.	25,287	Shekhotov, N.A.	25,856	Smith, T.	25,164
	26,033, 26,034	Rao, G.N.	25,750	Rothstein, J.	26,074	Schmit, J.L.	25,404	Shelykh, A.I.	25,349	Smolenskii, G.A.	25,199
Pinto, J.J.	26,167	Rao, K.K.	24,932	Rothwarf, F.	25,704	Schmitt, G.A.	24,867	Shen, Y.R.	25,174	Smoluchowski, R.	25,752
Pisano, F.	26,410	Rao, P.T.	25,643	Roulston, D.J.	26,237	Schmitz, A.	26,144	Shen, Y.R.	25,174		25,753, 25,754
Pitzalis, O.	26,184	Rao, V.S.	25,643	Rowland, T.J.	25,600	Schnabel, P.	25,241	Shepard, M.	25,762	Smortchkov, V.N.	25,960
	26,185	Rase, D.E.	24,872	Rowntree, R.F.	25,995	Schneider, J.R.	26,067	Shepelev, A.G.	25,789	Sneath, O.B.	26,293
Piuz, F.	24,924	Rausch, W.V.	25,905	Rozkwitalski, Z.	26,271	Schneider, W.G.	25,221	Shepherd, W.	26,407	Snitz, E.	25,263
Platzman, P.M.	25,354	Raven, L.J.	26,284	Rubens, S.M.	25,393	Schnettler, F.J.	25,485	Sherman, I.S.	25,681	Snodgrass, R.J.	25,588
Pleshko, P.	26,330	Read, W.S.	26,041	Rubin, S.	25,994		25,530		26,445		25,589
Plotnikov, A.F.	25,689	Ready, J.	25,956	Rubinstein, C.B.	25,715	Schoeffler, J.D.	26,267	Sherwood, R.C.	24,969	Snyder, H.A.	26,429
Pocsik, G.	25,275	Redhead, P.A.	25,126	Rudee, M.L.	24,898	Scholz, H.	26,036		25,387, 25,509	Sobel, F.	26,241
Podgurski, H.H.	24,897	Redlien, H.W.	25,957	Rudee, M.L.	25,032	Schönemeyer, H.	26,306		25,536	Sobhanadri, J.	25,578
Poehler, T.O.	25,243	Reed, W.A.	25,152	Ruffa, A.R.	25,386	Schover, D.S.	26,373	Shevchenko, A.K.	25,997	Sochava, L.S.	25,560
	25,870		25,341	Rupperecht, H.	24,985	Schrader, E.R.	26,105			Soden, R.R.	24,967
Pohm, A.V.	25,503	Reed-Hill, R.E.	25,024		25,070, 26,018,	Schraivogel, R.	26,224	Shewmon, P.G.	26,060	Soga, R.	25,249
Pollack, S.A.	25,625	Reese, W.E.	25,613		26,033, 26,034	Schreiber, D.S.	25,323	Shibata, A.	25,071	Sollertinskaya, E.S.	25,069
Pollard, A.J.	24,881	Regensburger, P.J.	25,694	Russell, J.E.	26,317	Schooler, R.B.	25,109	Shilliday, T.S.	25,881	Solomon, A.	25,835
Pollack, D.B.	26,041			Russell, V.A.	25,861	Schott, J.J.	25,081	Shilova, M.V.	25,698	Soltys, T.J.	25,092
Pollock, D.D.	25,245	Reggia, F.	25,889	Ryskin, A. Ya.	25,555	Schubring, N.	25,195	Shinoda, D.	25,166	Sooy, W.R.	25,934
Poncellet, C.	25,209	Reich, B.	25,852			Schuele, W.J.	25,552				25,941, 25,962
Poplawsky, R.P.	25,518	Reid, C.	25,037	Sacchetti, N.	26,095	Schulman, J.H.	25,648	Shirane, G.	25,398	Sorokin, P.P.	25,942
Papova, S.V.	25,260	Remeika, J.P.	25,522			Schulz, R.B.	26,119		25,410, 25,426,	Southgate, P.D.	25,012
Pops, H.	24,869		25,530	Sacerdoti, G.	26,095	Schulz-Du Bois, E.O.	25,541	Shockley, W.	25,871	Sovers, P.C.	25,269
Porter, F.T.	25,681	Renouf, T.J.	25,058	Safronov, B.V.	25,856		25,978, 25,979	Shockley, W.L.	25,806	Spain, R.J.	25,504
Porto, S.P.S.	26,004	Requa, S.C.	26,378	Saito, F.	25,924	Schumacher, D.P.	25,415	Shombert, D.J.	26,448	Span, R.E.	26,094
	26,008	Reshina, I.I.	25,622	Saito, N.	25,492	Schumacher, R.T.	25,565	Shtrikman, S.	25,552	Spector, H.	25,792
Post, B.	24,977	Revuz, J.	26,146	Saito, T.	25,814	Schuringa, T.M.	26,341	Shudra, D.	26,142	Speich, G.	24,946
Post, F.L.	25,907	Reynolds, H.K.	25,101	Saitoh, M.	25,100	Schuster, S.	25,017	Shulenan, B.M.	24,903	Speliotis, D.E.	25,437
Potapovich, A.K.	25,554	Reynolds, J.M.	25,750	Sakson, P.J.	26,291	Schwarz, F.C.	26,402	Shulman, R.G.	25,629	Spencer, R.E.	26,377
Poultny, S.K.	25,940	Reynolds, W.T.	26,094	Sakurai, S.	25,814	Schwartz, N.	25,808	Shumate, M.S.	25,711	Spinedi, P.	25,122
Powell, G.J.	26,311	Rice, L.	25,772	Salama, C.	26,371	Schwindenhammer, M.	26,237	Shustov, A.	24,917	Spinks, A.H.	26,311
Powell, G.W.	25,062	Richards, S.M.	24,928	Salama, K.	25,757			Sie, C.H.	25,474	Spitzer, W.G.	25,150
Powers, J.K.	26,048	Riemenschneider, A.L.	26,198	Samaonov, G.V.	25,064	Schwutke, G.H.	24,985	Siegbahn, K.	25,040	Sprackling, M.T.	25,010
Pracht, D.W.	25,601			Samelson, H.	25,675	Sconl, H.E.D.	25,983	Siegel, K.	25,893	Stablein, P.F.	24,996
Prakash, V.	25,086	Riemersma, H.	25,453	Samson, S.	24,965	Scott, T.	25,006	Siegle, W.T.	25,483	Stachowiak, H.	25,235
Prange, R.E.	25,181	Rigby, G.A.	26,174	Samuels, L.E.	25,038	Scovil, H.E.D.	26,005		26,344		25,236
	25,203	Rigg, R.N.	26,229	Sanford, T.B.	26,426	Scroggs, R.J.	26,437	Sigety, E.A.	25,639	Stafeev, V.I.	25,270
Prather, W.	26,272	Riley, L.	25,941	Sanna, G.	26,095	Searcy, A.W.	25,057	Sikorskii, Yu.A.	25,183	Stamper, J.A.	25,233
Pratt, Jr., G.W.	25,142	Riley, R.J.	26,039	Sapozhnikov, D.	25,566	Seber, B.E.	26,338	Silber, L.M.	25,896	Stanley, H.E.	25,397
Presland, A.E.B.	25,027	Rimai, L.	25,519	Sarachik, M.P.	25,207	Sedov, V.E.	25,657	Silva, L.F.	25,506	Stannard, Jr., C.R.	
Presland, M.	25,678	Rimus, A.I.	25,557	Saraga, W.	25,880	Seeger, A.	24,994	Silver, A.H.	25,596		25,693
Price, P.J.	25,230	Rind, E.	26,121	Sarbei, O.G.	25,266		25,029	Silver, M.	25,220	Stanway, J.	26,407
Pritchard, W.M.	26,077	Rindner, W.	25,823	Sard, E.W.	25,893	Seelbach, W.C.	26,340	Silverman, B.D.	25,566		26,408
Privorotskii, I.A.	25,599	Ring, J.	26,075	Sarney, A.	24,865	Seemann, D.F.	26,309	Simanek, E.	25,133	Stark, A.	25,188
Prohovsky, E.	25,778	Rischall, H.	25,426	Sasaki, H.	25,088	Segall, R.L.	25,030	Simphony, M.	25,220	Starr, A.T.	26,227
Prokhorov, A.M.	25,939	Riste, T.	26,168	Sasaki, Y.	25,166	Segall, B.	25,669	Simon, R.	25,749	Starr, H.	26,296
	25,997	Riva, G.M.	25,704			Sehr, R.	26,040	Simons, D.G.	26,272	Stead, R.C.T.	25,925
Prokhorov, E.D.	25,856	Robbins, R.M.	25,248	Sass, A.R.	25,288	Selber, F.	26,312	Simpson, G.R.	25,998	Stefanelli, R.	26,367
Prophet, H.	25,732	Roberts, L.D.	25,543	Sastry, S.B.S.	25,578	Self, J.	25,628	Sinclair, D.	26,068	Stein, M.	26,373
Prosen, R.J.	25,441	Roberts, S.	24,886	Sato, N.	25,116	Selling, T.V.	26,187	Sinclair, W.R.	25,639	Stein, S.J.	25,805
Proshko, G.P.	25,069	Robson, H.E.	26,049	Sato, Y.	25,190	Sekine, T.	25,651	Sirota, N.N.	25,381	Steingraber, O.J.	25,668
Prosser, T.F.	25,797	Roddick, R.G.	26,223	Saunders, G.A.	25,339	Sekine, T.	25,682	Sivertsen, J.	25,450	Steinhauer, Jr., H.	26,423
Provotorov, B.N.	25,513	Rode, V.E.	25,472	Savage, H.	25,731	Semmer, J.W.	26,384	Skaggs, C.W.	26,127	Steinschleiger, V.B.	
Puff, H.	25,368	Rodgers, J.W.	26,443	Savage, R.O.	25,099	Serafin, F.A.	25,641	Skorikov, V.M.	25,187		25,981
Pugh, E.N.	25,038	Rodolakis, A.	25,318		25,525	Serin, B.	25,723			Stelzer, R.B.	26,431
Pulfer, J.	26,170	Roe, R.F.	26,423								
Pure, S.	26,216										
Purton, R.F.	26,315										

LIST OF SUBJECTS COVERED BY CAMBRIDGE COMMUNICATIONS CORPORATION'S CUMULATIVE ABSTRACTS IN BOOK FORM

For an announcement of these books see overleaf

METALLURGY

Thermodynamics
(Phase Diagrams, etc.)
Crystal Structure
Crystal Growth
Crystal Processing
and Environmental Effects

SOLID STATE PHYSICS

Crystal Physics
(Band Structure, etc.)
Dielectrics
Carrier Properties
Conductivity
Superconductivity
Ferro- and Ferrimagnetism
Paramagnetism
Magnetoelectricity
Optical Properties
Thermal Properties
Mechanical Properties

SOLID STATE DEVICES

Diodes and Transistors
Masers and Lasers
Thin Films

SOLID STATE ELECTRONICS

Amplifiers and Oscillators
Switches and Converters
Communications
Instrumentation

COMPUTERS

Logic and Switching Theory
Digital Systems

COMPUTERS (Continued)

Computer Hardware
Digital Storage and
Input-Output
Computer Programming
Mechanical Translation and
Documentation
Pattern Recognition and
Artificial Intelligence
Computer Mathematics
Operations Research and
Information Theory
Computer Applications
Analog and Hybrid Computers
Real Time Systems and Automatic
Control

AEROSPACE

Electric Power in Space
Guidance and Attitude Control
Telecommunications
Instrumentation (Telemetry)
Environmental Control
Carrier Structures
Carrier Propulsion
Payload Structures
Payload Propulsion
Unmanned Payloads
Manned Payloads
Manned Flight Factors
Terrestrial Vehicles
Lunar Vehicles
Planetary Vehicles
Extraterrestrial Installations
Ground Support

ANNOUNCING...

CUMULATIVE ABSTRACTS IN BOOK FORM

A new series of 51 volumes of extraordinary value to:

**METALLURGISTS,
PHYSICISTS,
ELECTRONICS ENGINEERS,
COMPUTER and AEROSPACE SPECIALISTS**

Incorporating A Major Advance in the Selective Dissemination of Information

Each volume contains hundreds (in some cases thousands) of abstracts of papers and reports on a selected subject, the abstracts arranged by topic according to a detailed classification system.

The contents of each volume will be **replaced annually** by a new cumulative issue. In addition each volume has associated with it a supplement of current abstracts which will be **replaced bimonthly** by a new cumulative issue. Current awareness searches are facilitated by a separate printing of the abstracts most recently added to the current cumulative issue.

Now every scientist and engineer working in the fields covered by these books can have a **continuously updated literature survey** of his own specialty, right at his own desk.

For a list of subjects covered, see overleaf.

For complete descriptions and prices, write to:

CAMBRIDGE COMMUNICATIONS CORPORATION
238 MAIN STREET, CAMBRIDGE, MASSACHUSETTS, U.S.A.